Factors that contribute to B cell oncogenesis in people living with HIV

Anna Shmakova

▶ **To cite this version:**

Anna Shmakova. Factors that contribute to B cell oncogenesis in people living with HIV. Cancer. Université Paris-Saclay, 2023. English. NNT : 2023UPASL095 . tel-04287460

HAL Id: tel-04287460
https://theses.hal.science/tel-04287460

Submitted on 15 Nov 2023

HAL is a multi-disciplinary open access archive for the deposit and dissemination of scientific research documents, whether they are published or not. The documents may come from teaching and research institutions in France or abroad, or from public or private research centers.

L'archive ouverte pluridisciplinaire **HAL**, est destinée au dépôt et à la diffusion de documents scientifiques de niveau recherche, publiés ou non, émanant des établissements d'enseignement et de recherche français ou étrangers, des laboratoires publics ou privés.

THÈSE DE DOCTORAT

NNT: 2023UPASL095

université PARIS-SACLAY

Factors that contribute to B cell oncogenesis in people living with HIV

Facteurs qui contribuent à l'oncogenèse des lymphocytes B chez les personnes vivant avec le VIH

Thèse de doctorat de l'université Paris-Saclay

École doctorale n°582 : cancérologie : biologie, médecine, santé (CBMS)
Spécialité de doctorat : Sciences du Cancer
Graduate School : Sciences de la vie et santé. Référent : Faculté de médecine

Thèse préparée dans l'unité de recherche **Aspects métaboliques et systémiques de l'oncogénèse pour de nouvelles approches thérapeutiques (Université Paris-Saclay, CNRS, Institut Gustave Roussy)**, sous la direction de **Yegor VASSETZKY**, directeur de thèse

Thèse soutenue à Paris-Saclay, le 24 Octobre 2023, par

Anna SHMAKOVA

Composition du Jury

Membres du jury avec voix délibérative

Stéphanie BURY-MONE Professeure, CNRS, Université Paris-Saclay, I2BC	Présidente
Eugenia BASYUK Directrice de recherche, CNRS, Université de Bordeaux, MFP UMR 5234	Rapporteur & Examinatrice
Sergei NEKHAI Professeur, Howard University	Rapporteur & Examinateur
Alexander ISHOV Professeur, University of Florida	Examinateur

Acknowledgements

I would like to express my gratitude to my supervisor, Dr. Yegor VASSETZKY, who guided me throughout this project with unwavering support. I am grateful for his style of supervision which develops an independent and open mindset, curiosity and scientific courage. His mentorship has been a source of inspiration, and I am fortunate to have had the opportunity to work under his guidance.

I would also like to thank the members of my dissertation committee, Pr. Stéphanie BURY MONE, Dr. Eugenia BASYUK, Pr. Sergei NEKHAI, Pr. Alexander ISHOV, for their thoughtful feedback and constructive criticism. Their expertise in the field has been a valuable resource in shaping my research questions and methodology.

I am deeply grateful to the entire research unit UMR 9018, led by the remarkable Dr. Catherine BRENNER and Pr. Karim BENIHOUD, and the invaluable assistance of Isabelle CROQUISON and Anne TAN, I extend my heartfelt appreciation. Their competence and collaboration have been instrumental in the successful and timely conduct of our research projects. I am forever indebted to each one of you for your dedication and collaboration. I would also like to express my sincere gratitude to the previous research unit UMR 8126, under the guidance of Dr. Joelle WIELS, whose expertise has laid a strong foundation for this work, and I am grateful for the valuable insights and knowledge shared by your team.

I appreciate the help of my colleagues that guided me through the years of my thesis, helped to master various methods and techniques, assisted with experiments, and discussed with me the results I obtained: Dr. Diego GERMINI, Anna SCHWAGER (KARPUKHINA), Dr. Yana KOZHEVNIKOVA, Dr. Fatimata BINTOU SALL, Dr. Reynand CANOY, Coline HUGOT, Dr. Ivan TSIMAILO, Emile CLERF, Dr. Florian DARESSY, Zhenrui PAN, Dr. Yahir Alberto LOISSEL BALTAZAR, Leslie VALLET, Romain FERNANDES, Enzo GAUTREAU.

I would like to thank our scientific collaborators, who provided us with invaluable assistance with reagents, experimental models, and study participants and offered critical insights into the research design: Dr. Eugene SHEVAL, Dr. David BOUTBOUL, Dr. Laurence GERARD, Pr. Emmanuel DROUET, Dr. Bruno BEAUMELLE, Nikolai LOMOV, Dr. Alexander ISCHENKO, Dr. Murat SAPARBAEV, Dr. Regina GROISMAN. Their contributions have been essential to the success of my research.

I am grateful to Paris-Saclay University for providing me with the resources and facilities necessary to conduct my research. The help and opportunities

for intellectual growth and professional development afforded by CBMS Cancerology, Biology, Medicine, Health with Professor Eric DEUTSCH as a director and Léa POISOT as an administrative and pedagogical assistant have been invaluable. I would like to express my sincere gratitude to the members of my mid-term thesis committees, Dr. Sébastien APCHER, Dr. Alexander ISHCHENKO, Pr. Emmanuel DROUET, whose guidance and insights have been invaluable throughout the development of this research.

I owe a debt of gratitude to my family, Dr. Olga SHMAKOVA, Andrey SHMAKOV and Aleksei SHMAKOV, my husband, Dr. Ivan TSIMAILO, and my friends (Dr. Rakhil BORSHCHEVSKAYA, Dr. George KOTSOEV, Dr. Alexandra KUTOVAYA, Dr. Alisa LOBACH, Dr. Nina ROZINA, Bogdan SULDIN), who have provided me with unwavering love and support throughout my graduate studies. Their encouragement, understanding, and patience have been a constant source of inspiration and motivation.

Finally, I would like to thank my former scientific supervisors, Dr. Lubov ANDROSOVA and Dr. Ekaterina SEMINA, for their guidance and support during my early research career that cultivated my passion for science. Their patience, insights and encouragement were invaluable, and I am grateful for their mentorship.

CONTENTS

Acknowledgements **5**
Contents **7**
List of abbreviations **10**
List of figures **16**
List of tables **18**
Summary **19**
Synthèse **20**
1 Introduction **23**
1.1 HIV 23
Article 1. Review "HIV-1, HAART and cancer: A complex relationship" 28
1.2 EBV 43
1.2.1 EBV genome structure 43
1.2.2 EBV life cycle 47
1.3 EBV infection in people living with HIV (epidemiological and immunological aspects) 49
1.3.1 Antibody responses to EBV in people living with HIV 49
1.3.2 EBV viral load in people living with HIV 51
1.3.3 EBV-specific T cell response in people living with HIV 54
1.4 B cell lymphomas in people living with HIV 56
1.4.1 Chromosomal translocations in B cell lymphomas 58
Article 2. Review "Factors That Affect the Formation of Chromosomal Translocations in Cells" 60
1.4.2 EBV-associated B cell lymphomas in people living with HIV 80
1.5 HIV "interaction" with EBV and B cells: the role of cell-penetrating viral proteins 83
1.5.1 HIV-1 Tat 84
1.5.2 EBV Zta 94
Article 3. Review "Oncogenic Properties of the EBV ZEBRA Protein" 95
2 Hypothesis, aim, research questions and objectives of the study **123**
3 Results and discussion **125**
3.1 The contribution of HIV, EBV and antiretroviral therapy to genome instability and lymphoma-associated chromosomal translocations 125
3.1.1 Some antiretroviral drugs might increase the frequency of Burkitt's-lymphoma-associated t(8;14) translocation in B cells 125
Article 4. Research paper "Cell models with inducible oncogenic

translocations allow to evaluate the potential of drugs to favor secondary translocations"..... 126
3.1.2 EBV reactivation promotes Burkitt's-lymphoma-associated t(8;14) translocation in B cells..... 150
Article 5. Research paper "Epstein−Barr virus reactivation induces *MYC*-*IGH* spatial proximity and t(8;14) in B cells"..... 154
3.1.3 Exposure to HIV-1 Tat Inhibits DNA Damage Sensing and Repair in B cells..... 188
Article 6. Research paper "Exposure to HIV-1 Tat inhibits DNA damage sensing and repair in B cells"..... 189
3.2 The contribution of HIV-1 Tat and EBV Zta to the immune evasion of EBV-infected B cells..... 219
3.2.1 Detection of circulating HIV-1 Tat in the serum of people living with HIV-1 with effective viral suppression..... 219
Article 7. Research paper "HIV-1 Tat is present in the serum of people living with HIV-1 despite viral suppression"..... 219
3.2.2 HIV-1 Tat modifies gene expression in B cells..... 233
Article 8. Research paper "Ectopic expression of HIV-1 Tat modifies gene expression in cultured B cells: implications for the development of B-cell lymphomas in HIV-1-infected patients"..... 236
3.2.3 HIV-1 Tat downregulates the expression of HLA-DR genes in B cells and impairs EBV-specific CD4+ T cell response..... 276
Article 9. Research paper "Chronic HIV-1 Tat action induces HLA-DR downregulation in B cells: a mechanism for lymphoma immune escape in people living with HIV"..... 278
3.2.4 Comparative analysis of transcriptomes between Tat-expressing B cells and B cells from people living with HIV..... 368
3.2.5 Interaction between HIV-1 Tat and EBV Zta favours immune escape of B cells by suppressing HLA-ABC..... 371
Article 10. Research paper "Interaction between HIV-1 Tat and EBV Zta favours immune escape of B cells by downregulating HLA-ABC expression"..... 374
3.2.6 Comparison of our data with published Tat and Zta transcriptomes in T and B cells..... 431
4 Materials and methods..... 434
4.1 Antibodies, enzymes, recombinant proteins..... 434
4.2 Blood plasma collection and primary B cell isolation..... 437
4.3 Cell lines, cell culture and cell treatments..... 438
4.4 Generation of EBV-specific cytotoxic CD8+ T cell lines..... 440
4.5 Generation of EBV-specific CD4+ T cell line and the analysis of their

reactivity.....441
4.6 Generation of RPMI8866-based cell lines with inducible translocations.....444
4.7 Drug treatment of RPMI8866-based cell lines with inducible translocations.....444
4.8 Analysis of RPMI8866 Tat^{i} cell sensitivity to cisplatin, oxaliplatin and doxorubicin.....447
4.9 Cell transfection.....447
4.10 Lentivirus production and lentiviral transduction.....448
4.11 Flow cytometry analysis.....449
4.12 Immunofluorescent staining and microscopy.....450
4.13 3D-fluorescence in situ hybridization (FISH).....451
4.14 Image analysis.....453
4.15 Cell lysate preparation.....455
4.16 Western Blot.....456
4.17 Immunoprecipitation and co-immunoprecipitation (Co-IP).....456
4.18 In vitro binding assay.....456
4.19 HIV-1 Tat ELISA in human serum samples.....457
4.20 HIV p24 ELISA in human serum samples.....457
4.21 EBV Zta ELISA in human serum samples.....458
4.22 Plasmid cloning, synthesis, extraction.....458
4.23 PCR.....467
4.24 RNA extraction, sequencing, RNA-seq data processing and analysis 469
4.25 RNA extraction, reverse transcription and quantitative PCR (qPCR)..472
4.26 qPCR for translocation quantification.....472
4.27 DNA extraction and dot blot for cisplatin-specific DNA damage.....473
4.28 Chromatin immunoprecipitation quantitative real-time PCR (ChIP-qPCR).....475
4.29 Statistical analysis.....477
Conclusions.....477
Major publications related to the topic of PhD thesis.....481
Participation in the conferences.....482
Annexes.....485
Article 11. Review "CRISPR/Cas: History and Perspectives".....485
Article 12. Research paper "Specificity of cancer-related chromosomal translocations is linked to proximity after the DNA double-strand break and subsequent selection".....497
References.....527

List of abbreviations

ABC, abacavir
ACV, acyclovir
ADC, AIDS-defining cancer
AF, Alexa Fluor
AICDA, activation-induced cytidine deaminase
AID, activation-induced cytidine deaminase
AIDS, acquired immunodeficiency syndrome
Akt, protein kinase B
AML, acute myeloid leukemia
aNHEJ, alternative non-homologous end joining
ANKRD6, ankyrin repeat domain 6
ANOVA, analysis of variance
AP-1, activator protein 1
APC, allophycocyanin
ART, antiretroviral therapy
ATAC-seq, assay for transposase-accessible chromatin using sequencing
ATM, ataxia-telangiectasia mutated
ATR, ATM- and Rad3-related protein
AZT, azidothymidine (zidovudine)
BCA, bicinchoninic acid
BCL-xL, B-cell lymphoma-extra large
BFP, blue fluorescent protein
BL, Burkitt's lymphoma
BSA, bovine serum albumin
cART, combination antiretroviral therapy
Cas9, CRISPR-associated protein 9
CCR5, CC-chemokine receptor 5
CD, cluster of differentiation
CDK9, cyclin-dependent kinase 9
cDNA, complementary DNA
CFP, Cyan Fluorescent Protein
ChIP, chromatin immunoprecipitation
cHL, classical Hodgkin lymphoma
CIITA, class II major histocompatibility complex transactivator
CMV, cytomegalovirus
CNS, central nervous system
Cp, C promoter
CPD, cell penetration domain
CpG, cytosine-phosphate-guanine
CPP, cell-penetrating peptide
CRISPR, clustered regularly interspaced short palindromic repeats

CTD, C-terminal domain
CtIP, CtBP-interacting Protein
CTLs, cytotoxic T lymphocytes
CXCR4, CXC-chemokine receptor 4
Cy5, Cyanine 5
DAPI, 4',6-Diamidino-2-Phenylindole
DC, dendritic cells
DEGs, differentially expressed genes
DLBCL, diffuse large B cell lymphoma
DMSO, Dimethyl Sulfoxide
DNA, deoxyribonucleic acid
DNA-PK, DNA-dependent protein kinase
dNTP, deoxynucleotide Triphosphate
Dox, doxycycline
DSB, double-strand break
EA-D, early antigen-diffuse
EBER, Epstein-Barr early RNA
EBNA, Epstein-Barr nuclear antigen
EBV, Epstein-Barr virus
EDTA, ethylenediaminetetraacetic acid
EGFP, enhanced green fluorescent protein
eIF2, eukaryotic translation initiation factor 2
ELISA, enzyme-linked immunosorbent assay
ENIT, engineered nuclease-induced translocations
EPOCH, etoposide, prednisone, vincristine, cyclophosphamide, and doxorubicin
ERGIC-53, Endoplasmic Reticulum-Golgi Intermediate Compartment Protein 53
ERK1, Extracellular Signal-Regulated Kinase 1
FACS, Fluorescence-Activated Cell Sorter
FACT, facilitates chromatin transcription
FASLG, Fas Ligand
FBS, Fetal Bovine Serum
Fc, Fragment, Crystallizable (part of an antibody)
FISH, fluorescence in situ hybridization
FITC, Fluorescein Isothiocyanate
FL, Follicular Lymphoma
FTC, emtricitabine
G4, G-quadruplexes
GC, germinal centre
GEO, Gene Expression Omnibus
GFP, green fluorescent protein
GO, Gene Ontology
GO BP, gene ontology biological process

GRCh38.p10, Genome Reference Consortium Human Build 38, patch release 10
gRNA, guide RNA
GSEA, gene set enrichment analysis
HEK, Human Embryonic Kidney
HHV-4, human herpesvirus 4
HIAR, heat-Induced antigen retrieval
HISAT2, hierarchical indexing for spliced alignment of transcripts 2
HIV, human immunodeficiency virus
HIV-1, human immunodeficiency virus type 1
HL, Hodgkin lymphoma
HLA, human leukocyte antigen
HLA-ABC, human leukocyte antigen ABC
HLA-DR, human leukocyte antigen DR
HR, homologous recombination
HRP, Horseradish peroxidase
HSP, heat shock protein
HSV, herpes simplex virus
HVEM, herpesvirus entry mediator
IC50, half-maximal inhibitory concentration
IE, immediate early
IFI44L, interferon induced protein 44 Like
IFI6, interferon alpha inducible protein 6
IFN, interferon
IFNγ, interferon gamma
Ig, immunoglobulin
IgG, immunoglobulin G
IGH, immunoglobulin heavy chain gene
IGK, immunoglobulin kappa light-chain gene
IGL, immunoglobulin lambda light chain
IgM, immunoglobulin M
Igκ, immunoglobulin kappa light-chain
Igλ, immunoglobulin lambda light-chain
IKK, IκB kinase
IL, interleukin
JAK, Janus Kinase
kbp, kilobase pairs
KEGG, Kyoto encyclopedia of genes and genomes
LB, Luria-Bertani (medium)
LCL, lymphoblastoid cell line
LEDGF/p75, lens epithelium-derived growth factor/p75
Lig1/Lig3, DNA ligase 1/3
Lig4, DNA ligase 4
LMB, Leptomycin B

LMP, latent membrane protein
LTR, long terminal repeat
mART, monotherapy antiretroviral therapy
MCS, multiple cloning site
MHC, major histocompatibility complex
miRNA, microRNA
MNAse, micrococcal nuclease
MOPS, 3-(N-morpholino)propanesulfonic acid
MRE11, meiotic recombination 11 homolog A
mTORC1, mechanistic target of rapamycin complex 1
MTT, methylthiazolyltetrazolium
MW, molecular weight
MYO5B, Myosin VB
NaB, Sodium Butyrate
NADC, non-AIDS-defining cancer
NF-κB, nuclear factor kappa B
NHEJ, non-homologous end joining
NHL, non-Hodgkin lymphoma
NIH, National Institute of Health
NK, natural killer cells
NLS, nuclear localization signal
NP40, Nonidet P-40
NPC, nasopharyngeal carcinoma
NR4A1, nuclear receptor subfamily 4 group A member 1 (Nur77)
NRTIs, nucleoside reverse transcriptase inhibitors
OHL, oral hairy leukoplakia
OR, odds ratio
ORA, Overrepresentation Analysis
oriLyt, lytic replication origin
oriP, latency-associated origin of replication
p24, capsid protein p24
P2A, porcine teschovirus-1 2A sequence
PBL, plasmablastic lymphoma
PBMC, peripheral blood mononuclear cells
PBS, phosphate-buffered saline
PCNSL, primary central nervous system lymphoma
PCR, polymerase chain reaction
PD-L1, programmed death-ligand 1
PE, phycoerythrin
PECAM1, platelet and endothelial cell adhesion molecule 1 (CD31)
PE-Cy5, phycoerythrin-cyanine 5
PEL, primary effusion lymphoma
PerCP, peridinin chlorophyll protein
PI, propidium iodide

PI(4,5)P2, phosphatidylinositol-4,5-bisphosphate
PI3K, phosphoinositide 3-kinase
PLWH, people living with HIV
PMA, phorbol myristate acetate
PML, promyelocytic leukemia
Pol II, RNA-polymerase II
P-TEFb, positive transcription elongation factor b
PTLD, post-transplant lymphoproliferative disorder
PVDF, polyvinylidene fluoride
Qp, Q promoter
qPCR, quantitative polymerase chain reaction
qRT-PCR, quantitative reverse transcription polymerase chain reaction
RFP, red fluorescent protein
RNA, ribonucleic acid
RNAi, RNA interference
RNA Pol II, RNA polymerase II
RNAse, Ribonuclease
RNA-seq, RNA sequencing
ROI, regions of interest
ROS, reactive oxygen species
RPA, replication protein A
Rpl32, ribosomal protein L32
RPMI, Roswell Park Memorial Institute
rtTA, reverse tetracycline transactivator
SDS, sodium dodecyl sulfate
SDS-PAGE, sodium dodecyl sulfate-polyacrylamide gel electrophoresis
SEM, standard error of the mean
shRNA, short hairpin RNA
SLAMF1, signaling lymphocytic activation molecule family member 1
SP-1, specificity protein 1
STAT1, signal transducer and activator of transcription 1
STAT3, signal transducer and activator of transcription 3
SULF2, sulfatase 2
TAK, Tat-associated kinase
TAR, trans-activation response element
Tat, transactivator of transcription
TBST, tris-buffered saline and 0.1% Tween-20
TF, transcription factor
TFEC, transcription factor EC
Tfh, follicular B helper T cells
TGFβ, transforming growth factor beta
TIMD4, T Cell Immunoglobulin and Mucin Domain Containing 4
TNFRSF, tumor necrosis factor receptor superfamily
TNFSF10, tumor necrosis factor superfamily member 10 (TRAIL)

TPA, 12-O-tetradecanoylphorbol 13-acetate
TR, terminal repeat
TRITC, tetramethylrhodamine
TRRUST, transcriptional regulatory relationships unraveled by sentence-based text mining
UNAIDS, joint United Nations programme on HIV/AIDS
UPR, unfolded protein response
V(D)J, Variable, diversity, and joining (gene segments)
VCA, viral capsid antigen
WHO, World health organization
Wp, W promoter
XRCC5, X-Ray repair cross complementing 5
XRCC6, X-Ray repair cross complementing 6
YFP, yellow fluorescent protein
ZRE, Zta response element
Zta, Epstein-Barr virus immediate-early transactivator protein

List of figures

Figure 1. An overview of the HIV genome structure and life cycle.
Figure 2. An overview of EBV genome structure and life cycle.
Figure 3. Factors that affect the formation of chromosomal translocations.
Figure 4. The pathogenesis of EBV-associated lymphoma in people living with HIV, influenced by host-mediated and viral factors.
Figure 5. Domain structure of HIV-1 Tat.
Figure 6. The mechanism of Tat-mediated transactivation of HIV transcription.
Figure 7. An overview of the experimental setup for inducing oncogenic *AML1-ETO* and *MYC-IGH* translocations in B cells.
Figure 8. DSB repair pathways involved in chromosomal translocation formation.
Figure 9. The effect of antiretroviral drugs on t(8;14) formation rate.
Figure 10. Correlation analyses of EBV reactivation in a cohort of asymptomatic people with HIV patients under cART.
Figure 11. Latent EBV-positive RPMI8866 were treated with sodium butyrate (NaB) and/or acyclovir (ACV) for 48h or left untreated.
Figure 12. The proposed model of how EBV reactivation promotes Burkitt's lymphoma.
Figure 13. The effect of B cell activation and EBV reactivation on MYC-IGH colocalization in primary B cells.
Figure 14. HIV-1 Tat significantly suppressed the expression of multiple genes involved in DNA damage sensing and repair pathways in B cells.
Figure 15. HIV-1 Tat decreased the expression of genes involved in DNA damage repair in B cells.
Figure 16. Forest plot of multivariable logistic regression model for factors associated with HIV-1 Tat detection in serum of HIV-positive individuals above 2.5 ng/ml.
Figure 17. HIV-1 Tat regulates gene expression in B cells. RPMI8866 cells expressing HIV-1 Tat or its transactivation-deficient mutant (TatC22G) were used to study the effects of HIV-1 Tat on B cell transcriptome.
Figure 18. Enrichment analysis of differentially expressed genes negatively regulated by Tat in RPMI8866 cells.
Figure 19. HIV-1 Tat decreases HLA-DR expression in B cells.
Figure 20. Chronic exposure to Tat, which can be secreted from infected CD4+ T cells and penetrate into non-infected cells, led to the downregulation of HLA-DR expression in B cells, impairing their recognition by CD4+ T cells.
Figure 21. Proposed model for gene regulation by Tat and TatC22G in B cells.
Figure 22. A comparison of transcriptomes of Tat-expressing B cells and B cells from people living with HIV.

Figure 23. Zta presence in the serum of people living with HIV.
Figure 24. YFP reconstitution technique.
Figure 25. Transcriptome comparison of T cells, expressing Tat, and B cells, treated with Tat.
Figure 26. Transcriptome comparison of Akata B cells, expressing Zta, and B cells, treated with Zta.
Figure 27. The confirmation of the purity of recombinant Zta protein.
Figure 28. The penetration of Zta in the cells.
Figure 29. Representative flow cytometry contour plots showing CD3 and CD4 and respective isotype control antibody staining of BLAS-reactive, BLYaK-reactive and BLIT-reactive EBV-specific CD4+ T cell lines.
Figure 30. The derivation of the % of specific lysis formula used in the study.
Figure 31. Flow cytometry gating strategy as shown on RPMI8866 cells (untransfected and unstained) and RPMI8866 cells transfected with YFP and stained with PE-Cy5 anti-HLA-ABC antibodies.
Figure 32. The illustration of the functioning of a plugin developed for matching nuclear and cellular ROIs.
Figure 33. The analysis of the transactivation capacity of BFP-Tat in RPMI8866 cells stably expressing HIV-1 3′-LTR-TurboRFP reporter and transfected with BFP or BFP-Tat.
Figure 34. Confirmation of Tat and Zta successful cloning in pcDNA3-YFP1 and pcDNA3-YFP2 plasmids by PC, Western blot and immunofluorescent staining.
Figure 35. Confirmation of Tat and Zta mutants successful cloning in pcDNA3-YFP1 and pcDNA3-YFP2 plasmids by PCR and restriction analysis.
Figure 36. Confirmation of the functionality of the created NF-κB-mCherry reporter plasmid.
Figure 37. A Western blot analysis of Tat and Zta accumulation in B cells.
Figure 38. Cell penetration efficiency might affect gene expression levels in the bulk population.
Figure 39. The effect of DNA denaturation on the detection of cisplatin-specific DNA damages.
Figure 40. Chromatin sonication analysis by agarose gel electrophoresis.

List of tables

Table 1. Antibody responses to EBV in people living with HIV compared to the HIV-negative population.
Table 2. B cell lymphomas in people living with HIV.
Table 3. Tat effects on the immune cells.
Table 4. Oncogenic properties of HIV Tat.
Table 5. Characteristics of asymptomatic cART-treated people with HIV.
Table 6. Characteristics of patients with HIV-negative EBV-related lymphoproliferative disorders.
Table 7. Treatments of RPMI8866-based cell lines with inducible translocations.
Table 8. Electrotransfection conditions for different cell lines used in the study.
Table 9. Primers and oligonucleotides used in the study for cloning.
Table 10. gRNA sequences.
Table 11. Primers used for PCR and qPCR.

SUMMARY

People living with human immunodeficiency virus (HIV) are at an elevated risk of developing B cell lymphomas, especially those associated with Epstein-Barr Virus (EBV), compared to the general population. Although immune suppression has been implicated in this increased risk, the specific mechanisms through which HIV infection in the era of combination antiretroviral therapy (cART) contributes to B cell malignancies remain unclear. To address this knowledge gap, we conducted a comprehensive study to investigate factors beyond immune deficiency that may play a role in B cell lymphomagenesis in individuals living with HIV.

We assessed the potential impact of specific antiretroviral drugs on the occurrence of chromosomal translocations in B cells. Using CRISPR/Cas9-based experimental models, we identified certain antiretroviral drugs as potential contributors to lymphomagenesis in HIV-infected individuals. We then focused on EBV reactivation, a common phenomenon in people living with HIV, and its implications in B cell lymphomagenesis. We demonstrated that EBV reactivation induces increased proximity between potential translocation partners, *MYC* and *IGH* loci, promoting chromosomal translocation and thereby promoting B cell lymphomas. We next investigated the impact of HIV-1 Tat, a viral transcriptional activator protein with cell-penetration capacities that can be secreted from infected cells, circulate in the blood of people living with HIV and penetrate non-infected cells. HIV-1 Tat was found to disrupt DNA damage sensing and repair in B cells and to downregulate major histocompatibility complex class II (MHC class II) expression in B cells, leading to accumulated DNA lesions and impaired recognition by CD4+ T cells, respectively, thus creating an environment conducive to lymphomagenesis. Finally, we investigated the interaction between HIV-1 Tat and EBV Zta, another viral transcriptional activator, in B cells. The two proteins were found to directly interact in B cells and in the blood serum of individuals with HIV. This interaction led to the downregulation of MHC class I molecules in B cells, favouring immune evasion of B cells from CD8+ T cell response.

Overall, our study sheds light on the complex interplay between HIV, EBV, and B cell lymphomagenesis, providing mechanistic insights into the development of B cell malignancies in people living with HIV. Understanding these underlying biological factors and molecular pathways may pave the way for novel therapeutic strategies and targeted interventions to mitigate lymphoma risk in this population. Further clinical and epidemiological studies are warranted to validate and expand upon these findings.

Keywords: HIV, EBV, HIV-1 Tat, EBV Zta, chromosomal translocations, immune evasion.

SYNTHÈSE

Le virus de l'immunodéficience humaine (VIH) infecte 38,4 millions de personnes dans le monde, avec deux types : le VIH-1 et le VIH-2, le premier étant le plus répandu. Cette étude se concentre principalement sur le VIH-1. Le VIH pénètre dans les cellules susceptibles par l'intermédiaire des récepteurs CD4 et des co-récepteurs CCR5 ou CXCR4, puis s'intègre dans le génome des cellules de l'hôte, conduisant à la réplication virale et à l'épuisement éventuel des lymphocytes T CD4+, ce qui entraîne une immunodéficience sévère (SIDA). La thérapie antirétrovirale combinée (cART) peut supprimer la réplication virale, mais un réservoir latent de VIH persiste. Les personnes vivant avec le VIH présentent un risque élevé de développer des lymphomes à cellules B, en particulier ceux associés au virus d'Epstein-Barr (EBV), par rapport à la population générale. Bien que la suppression immunitaire ait été impliquée dans ce risque accru, les mécanismes spécifiques par lesquels l'infection par le VIH à l'ère de la cART contribue aux malignités à cellules B restent flous. Pour combler cette lacune de connaissance, nous avons mené une étude approfondie pour étudier les facteurs au-delà du déficit immunitaire qui pourraient jouer un rôle dans la lymphomagenèse à cellules B chez les individus vivant avec le VIH.

L'EBV est un facteur potentiel contribuant aux lymphomes à cellules B chez les personnes vivant avec le VIH. Il co-infecte la quasi-totalité des personnes vivant avec le VIH en raison de sa prévalence élevée, mais il a reçu peu d'attention. L'EBV est associé à divers cancers, dont les lymphomes à cellules B, et maintient un cycle de vie complexe impliquant des phases latentes et lytiques. L'EBV infecte principalement les cellules B et établit une infection latente à vie dans les cellules B mémoire. Les personnes vivant avec le VIH présentent des taux de séropositivité à l'EBV plus élevés, une réactivation accrue de l'EBV, des niveaux élevés d'anticorps contre les antigènes lytiques de l'EBV et des niveaux élevés de charges virales de l'EBV dans la salive et le sang. L'EBV joue un rôle dans divers lymphomes chez les personnes vivant avec le VIH, notamment le lymphome de Burkitt, le lymphome Hodgkinien classique, le lymphome diffus à grandes cellules B et la maladie lymphoproliférative B associée au VIH. La relation entre le VIH et l'EBV est complexe et va au-delà de l'immunosuppression. La charge virale de l'EBV tend à être plus élevée chez les personnes vivant avec le VIH, même sous cART, et n'est pas toujours corrélée directement aux taux de lymphocytes T CD4+. Les réponses des lymphocytes T CD4+ et CD8+ spécifiques de l'EBV sont essentielles pour contrôler l'infection par l'EBV, mais l'infection par le VIH peut altérer ces réponses, ce qui pourrait contribuer à des charges virales de l'EBV

plus élevées et à des risques oncogènes. Comprendre l'interaction entre l'EBV et le VIH est essentiel pour comprendre l'origine de certains cancers associés au VIH, en particulier les lymphomes à cellules B, chez les personnes vivant avec le VIH.

Nous avons évalué l'impact potentiel de médicaments antirétroviraux spécifiques sur l'apparition de translocations chromosomiques dans les cellules B. En utilisant des modèles expérimentaux basés sur CRISPR/Cas9, nous avons identifié certains médicaments antirétroviraux comme des contributeurs potentiels à la lymphomagenèse chez les personnes infectées par le VIH. Ensuite, nous nous sommes concentrés sur la réactivation de l'EBV, un phénomène courant chez les personnes vivant avec le VIH, et ses implications dans la lymphomagenèse à cellules B. Nous avons démontré que la réactivation de l'EBV induit une proximité accrue entre les partenaires potentiels de translocation, les loci *MYC* et *IGH*, favorisant ainsi la translocation chromosomique et la promotion des lymphomes à cellules B. Ensuite, nous avons étudié l'impact du Tat du VIH-1, une protéine activateur transcriptionnel virale avec des capacités de pénétration cellulaire qui peut être sécrétée par des cellules infectées, circuler dans le sang des personnes vivant avec le VIH et pénétrer dans les cellules non infectées. On a découvert que le Tat du VIH-1 perturbait la détection et la réparation des dommages de l'ADN dans les cellules B et régulait à la baisse l'expression du complexe majeur d'histocompatibilité de classe II (CMH de classe II) dans les cellules B, entraînant respectivement l'accumulation de lésions de l'ADN et une reconnaissance altérée par les cellules T CD4+, créant ainsi un environnement propice à la lymphomagenèse. Enfin, nous avons étudié l'interaction entre le Tat du VIH-1 et le Zta de l'EBV, un autre activateur transcriptionnel viral, dans les cellules B. Les deux protéines ont été trouvées en interaction directe dans les cellules B et dans le sérum sanguin des individus atteints du VIH. Cette interaction a entraîné la régulation à la baisse des molécules du CMH de classe I dans les cellules B, favorisant ainsi l'évasion immunitaire des cellules B par la réponse des cellules T CD8+.

Dans l'ensemble, notre étude met en lumière l'interaction complexe entre le VIH, l'EBV et la lymphomagenèse à cellules B, fournissant des éclaircissements mécanistiques sur le développement des malignités à cellules B chez les personnes vivant avec le VIH. La compréhension de ces facteurs biologiques sous-jacents et des voies moléculaires pourrait ouvrir la voie à de nouvelles stratégies thérapeutiques et à des interventions ciblées pour atténuer le risque de lymphome dans cette population. Des études cliniques et épidémiologiques supplémentaires sont nécessaires pour valider et étendre ces résultats.

Mots-clés : VIH, EBV, Tat du VIH-1, Zta de l'EBV, translocations chromosomiques, évasion immunitaire

1 INTRODUCTION

1.1 HIV

Human immunodeficiency virus (HIV) currently infects 38.4 million people worldwide (http://www.who.int/hiv/en/) (WHO fact sheet 2022). HIV exists in two types: HIV-1 and HIV-2 (Nyamweya et al. 2013). HIV-1 infection is widespread worldwide, while HIV-2 infection is mainly restricted to West Africa and related communities and is estimated to affect 1-2 million people (although accurate HIV-2 prevalence is difficult to estimate since HIV-1/HIV-2 typing is not always performed and there is no formal surveillance system for HIV-2 by WHO or UNAIDS) (Gottlieb et al. 2018). Compared with HIV-1, HIV-2 infection typically presents slower clinical progression, increased asymptomatic period, reduced transmission risk, and lower mortality (Campbell-Yesufu & Gandhi 2011; Gottlieb et al. 2018). In the current study, we mostly focused on HIV-1 infection.

HIV is a lentivirus from the *Retroviridae* family, whose genome is represented by two identical positive single-stranded RNAs of ~10 kb (Sükösd et al. 2015). HIV's basic genomic structure comprises three genes encoding the structural proteins (*gag*, *pol,* and *env*); two genes encoding the regulatory proteins (*tat* and *rev*); four genes encoding the accessory proteins (*vpu*, *vpr*, *vif*, *nef*); genes are flanked by the long-terminal repeats (LTR) that contain viral promoters, enhancers and binding sites for the host regulatory factors (**Figure 1A**). To infect susceptible cells, the viral envelope binds to the cell surface CD4 receptor, expressed on T cells, monocytes, macrophages, and dendritic cells, and either CC-chemokine receptor 5 (CCR5) or CXC-chemokine receptor 4 (CXCR4) as a co-receptor (**Figure 1B**). This interaction triggers the fusion of the viral and cellular membranes, allowing the release of the viral core into the host cytoplasm (Chen 2019). The viral RNA genome is then reverse-transcribed into double-stranded DNA; HIV completes reverse-transcription and uncoating (the viral core disassembly) in the host nucleus, as was recently shown by several landmark papers (Burdick et al. 2020; Dharan et al. 2020; Müller et al. 2021). Unintegrated viral DNAs predominate during the early post-infection period as well as during untreated chronic infection, while integrated viral DNAs only make up a small portion of reverse-transcribed genomes (Sloan & Wainberg 2011; Thierry et al. 2016). To effectively integrate viral DNA, HIV-1 integrase associates with the nucleosomes in host chromatin through histone tails (Benleulmi et al. 2017). A histone chaperone complex FACT (FAcilitates Chromatin Transcription) partially disassembles nucleosomes, which increases chromatin accessibility and stimulates HIV-1 integration (Matysiak et al. 2017). HIV integration preferentially occurs in transcriptionally active genomic regions (Schröder et al. 2002), which is partly attributed to HIV-1 integrase interaction with host transcriptional activator lens epithelium-derived growth

factor (LEDGF)/p75 (Christ & Debyser 2013; Ciuffi et al. 2005; Llano et al. 2006; McNeely et al. 2011; Shun et al. 2008). Viral DNA, integrated into the host cell genome (provirus), serves as the blueprint for viral gene expression and subsequent production of new viral particles. Transcription of the proviral DNA leads to the synthesis of viral RNA and the production of viral proteins, which are then assembled into immature viral particles at the plasma membrane (Freed 2015). Viral genomic RNAs are dimerized in the cytosol and packaged into virions (Ferrer et al. 2016). Finally, the virions bud from the infected cell, acquiring an envelope derived from the host cell membrane (Freed 2015). During this process (concomitant with or soon after budding), the viral protease enzyme cleaves precursor proteins to generate mature infectious virions (Engelman & Cherepanov 2012). The released virions are now capable of infecting new target cells, perpetuating the HIV life cycle and ensuring its persistence within the host (Deeks et al. 2015). Intrinsic mechanisms, such as reverse-transcriptase errors, and viral recombination, contribute to high HIV genome diversity (Taylor et al. 2008). HIV-1 has more non-synonymous mutations retained by positive selection than other viruses and mammalian cells (Lin et al. 2019).

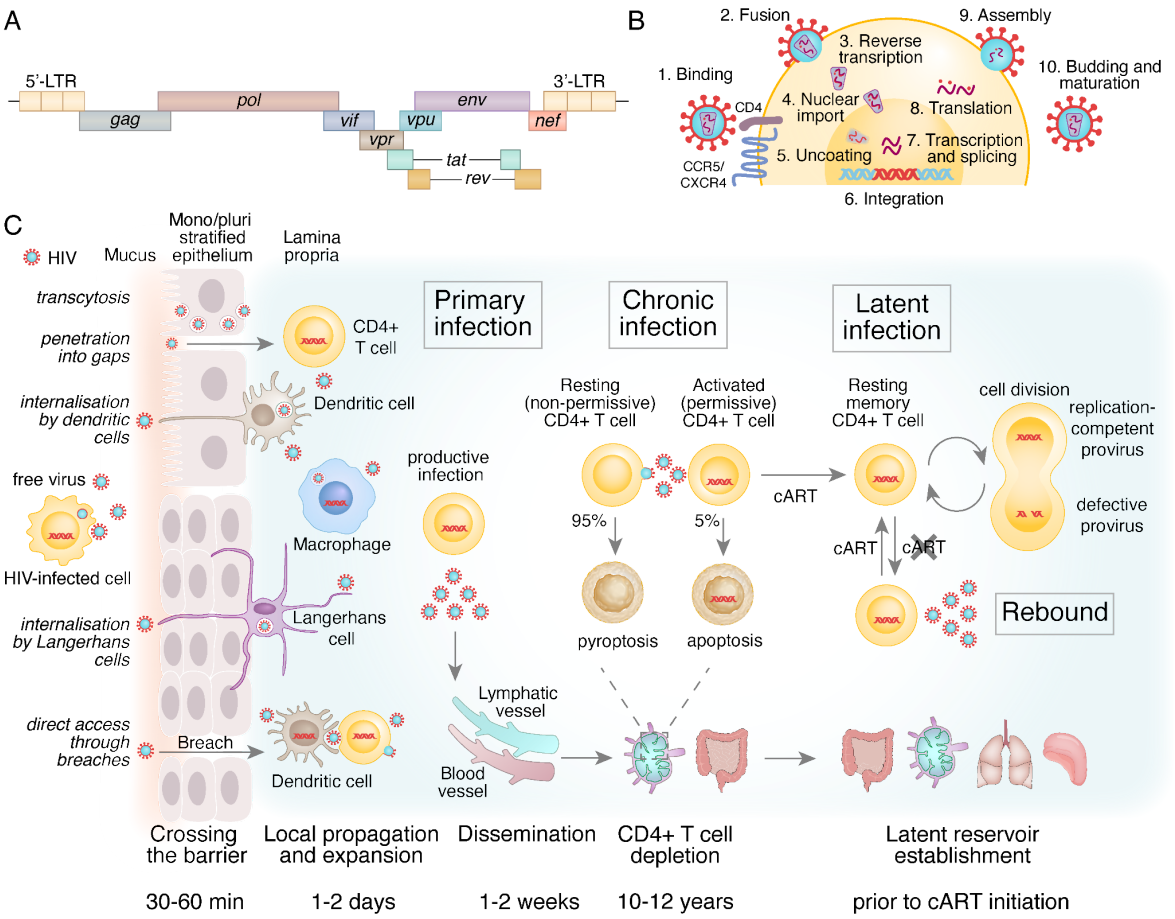

Figure 1. An overview of the HIV genome structure and life cycle. (A) The simplified genome structure of HIV-1. The HIV-1 genome is approximately 10 kb in length and encompasses several genes encoding crucial viral proteins: the structural proteins include Gag, Pol (polymerase), and Env (envelope); the regulatory proteins

comprise Tat (transactivator of transcription) and Rev (regulatory for expression of viral proteins), while the accessory proteins consist of Vpu (viral protein u), Vpr (viral protein r), Vif (viral infectivity factor), and Nef (negative factor). The genome structure is flanked by long terminal repeats (LTRs), which are important for viral gene expression and integration into the host genome. (B) Key steps of the HIV life cycle. HIV engages CD4 and chemokine receptors (CCR5 or CXCR4), fusing viral and cellular membranes and allowing the release of the viral core into the host cytoplasm. HIV core then enters the host nucleus, where it completes the reverse transcription of viral RNA into DNA and uncoating. The synthesised viral DNA then integrates into the host genome, leading to the establishment of proviral DNA. Exploiting the host cellular machinery, viral genes are expressed from the proviral DNA, initiating the process of RNA synthesis, splicing and subsequent production of viral proteins. Assembled viral proteins form immature particles, which undergo maturation to yield infectious virions. Ultimately, the mature virions bud from the infected cell, ready to infect new target cells and perpetuate the HIV life cycle. (C) HIV host invasion, dissemination, and formation of viral reservoirs. The mechanisms of HIV transmission at mucosal sites involve the trapping of free HIV virions or HIV-infected donor cells in mucus, resulting in the penetration of the free virions into gaps between epithelial cells or the attachment of HIV-infected donor cells to the luminal surface of the mucosa, followed by the internalisation of virions by Langerhans cells within the epithelium. Additionally, HIV can fuse with the surface of intraepithelial CD4+ T cells, resulting in productive infection of these cells. Further, infected donor cells or free virions can migrate along physical abrasions of the epithelium into the mucosal stroma, where they can be taken up by lymphatic or venous microvessels and transported to local lymph nodes or into the bloodstream, or they can make contact with stromal dendritic cells, T cells, and macrophages. Virions can also transcytose through epithelial cells near or within the basal layer of the squamous epithelium, infect basal epithelial cells, be internalised into endocytic compartments, or penetrate between epithelial cells. Abbreviations: cART, combination antiretroviral therapy; LTR, long terminal repeat.

HIV is transmitted through contact of infected body fluids with mucosal tissue, blood, or broken skin, i.e. by blood transfusions, mother-to-child (vertical) transmission, unprotected sexual intercourse, and injection drug use with shared equipment (Deeks et al. 2015). The risk of HIV transmission through sexual intercourse increases with high plasma and semen HIV RNA levels (Attia et al. 2009; Baeten et al. 2011). Upon initial exposure at mucosal sites, HIV virions, that are initially free, or those that are released from infected cells, interact with epithelial cells and traverse the epithelial barrier through various pathways, including transcytosis, penetration through gaps between epithelial cells, and direct internalisation of intraepithelial Langerhans cells and dendritic cells with subsequent exit underneath in the lamina propria (**Figure 1C**) (Hladik & McElrath 2008). The crossing of the epithelial barrier occurs rapidly, within 30-60 minutes, allowing for the infection of susceptible immune cells in the lamina propria, such as activated CD4+ T cells, dendritic cells and macrophages. Subsequently, within a few days after contact with the virus, the productive infection of subepithelial CD4+ T lymphocytes causes local viral propagation and expansion, leading to subsequent dissemination through the draining lymph nodes, followed by distal lymph nodes and bloodstream,

ultimately establishing a systemic infection and the formation of viral reservoirs in secondary lymphoid organs shortly after infection (Chun et al. 1998; Hladik & McElrath 2008).

Secondary lymphoid tissues (lymph nodes, spleen) and lymphoid structures within gut mucosa serve as major sites for HIV replication and CD4+ T cell depletion during chronic infection (Estes et al. 2017). There, HIV infects activated CD4+ T cells (~5% of the total CD4+ T cell population), initiating a productive infection, which ultimately results in cell death through caspase-mediated apoptosis. In contrast, when the virus infects a resting CD4+ T cell, which constitutes the majority (~95%) of the CD4+ T cell population, the virus encounters an abortive infection, triggering pyroptosis (an inflammatory form of programmed cell death) (Doitsh & Greene 2016; Doitsh et al. 2010). As a consequence, HIV leads to a gradual depletion of CD4+ T cells and eventually, if left untreated, HIV infection evolves into a severe immune deficiency (CD4+ T cell count of <200 cells per µl), associated with opportunistic infections or specific cancers, which defines acquired immune deficiency syndrome (AIDS) (Doitsh & Greene 2016). Only a small fraction of people, known as elite controllers, that acquired HIV infection, are able to spontaneously establish control over the virus. Such people differ in the host immune response (Woldemeskel et al. 2020). For others, immune activity determines the degree of HIV control and disease progression (Gonzalo-Gil et al. 2017).

CD4+ T cell depletion is reversed by cART that inhibits active HIV replication and cell-to-cell transmission by targeting viral entry, reverse transcription, integration, or viral protein cleavage (Deeks et al. 2015). Since the advent of cART in 1996, the overall survival rates of people with HIV/AIDS have significantly improved. But despite this major advance, antiretroviral therapy is still not worldwide accessible: the global antiretroviral therapy coverage is estimated at 75%, while in different countries it ranges from 10% to 98% (Global Health Observatory data repository 2022). Among people treated with antiretroviral therapy, especially those in middle- and low-income countries, not all achieve complete viral suppression due to a lack of adherence programs, routine viral load testing, and accessibility of different therapy regimens. Thus, HIV remains one of the leading causes of global mortality and disability (Roth et al. 2018; Vos et al. 2020).

Upon cART, a small proportion of HIV-infected activated CD4+ T cells that haven't undergone apoptosis turn into resting (or, quiescent) memory CD4+ T cells, where HIV persists in the form of transcriptionally silent proviral DNA (latency) resulting in a lifelong infection (Cohn et al. 2020). A direct infection of resting CD4+ T cells was also described (Chavez et al. 2015). The cells and tissues that continue to harbour HIV under effective cART are described as “HIV reservoir”. This latent HIV reservoir is formed just prior to cART initiation

and is not eradicated by cART (Abrahams et al. 2019; Siliciano et al. 2003). The latent HIV reservoir is maintained and clonally expanded through the proliferation of CD4+ T cells, which can be either homeostatic (Chomont et al. 2009) or driven by HIV integration or antigenic stimulation (Cohn et al. 2020). Notably, co-infection with EBV can stimulate antigen-driven proliferation of CD4+ T cells latently infected with HIV (Henrich et al. 2017), which will be discussed further. Latently infected CD4+ T cells are enriched in tissues abundant in lymphoid structures, such as the gut mucosa, spleen, lung, and lymph nodes, particularly, among CD4+ follicular B helper T cells (Tfh) within B cell follicles (Banga et al. 2016; Yu et al. 2020).

Upon cART, only a small proportion of latently infected CD4+ T cells still may harbour replication-competent provirus, while >95% of infected cells carry defective forms of HIV proviral DNA (e.g. with large internal deletions or lethal mutations). Cells with the defective provirus are unable to generate infectious viral particles, however, they may contain open reading frames for viral proteins that keep being produced by infected cells and could potentially contribute to the development of HIV-associated diseases (Imamichi et al. 2016, 2020). The development of HIV transcriptional inhibitors is a promising therapeutic target in the treatment of HIV-related chronic diseases (Alanazi et al. 2021).

cART interruption or ineffective viral suppression may cause viral rebound from cells with intact replication-competent proviruses. This occurs typically within 2-8 weeks after cART cession (Li et al. 2016, 2022). Different cellular and anatomical compartments may serve as a source of viral rebound (De Scheerder et al. 2019). Eventually, infected cells with replication-competent proviruses rapidly repopulate tissues throughout the body (Chaillon et al. 2020a).

cART provides complete suppression of HIV replication and immune restoration (HIV-CAUSAL Collaboration et al. 2010); despite this fact, people living with HIV are at higher risk of developing certain comorbidities as compared to the general population, such as cardiovascular diseases (So-Armah et al. 2020), neurocognitive disorders (Saylor et al. 2016), certain cancers (Hernández-Ramírez et al. 2017; Shmakova et al. 2020), and other diseases are more common in this population. People living with HIV diagnosed with cancer have a more severe clinical course and lower survival rates compared to the non-infected population (Coghill et al. 2015; Marcus et al. 2015; Powles et al. 2009). They also experience excess mortality that exceeds the expected mortality from the simple combination of HIV and cancer (Coghill et al. 2017). Cancers in people living with HIV are traditionally divided into AIDS-defining cancers (ADCs: Kaposi's sarcoma, non-Hodgkin's lymphoma (NHL), invasive cervical cancer) and others, referred to as non-AIDS-defining cancers (NADCs) (Berretta et al. 2016). The incidence of

AIDS-defining cancers, though decreased in the cART era, is still largely elevated, while the incidence of non-AIDS-defining cancers is rising in the cART era and is expected to continue to rise (Hernández-Ramírez et al. 2017; Shiels et al. 2018). Understanding the reasons for these trends and finding the causative agents is a vital need and a rising challenge for public health (Shmakova et al. 2020). See review **Article 1** for more detail on HIV-1 and cancer relationship in the cART era.

To conclude, cART has significantly improved survival rates but cannot completely eradicate the virus, leading to a lifelong infection with a latent HIV reservoir. The presence of HIV increases the risk of developing certain cancers, including AIDS-defining and non-AIDS-defining cancers. Understanding the underlying causes of these trends is an essential challenge for public health.

Article 1. Review "HIV-1, HAART and cancer: A complex relationship"

Check for updates

uicc global cancer control

IJC
International Journal of Cancer

HIV-1, HAART and cancer: A complex relationship

Anna Shmakova [1,2,3], Diego Germini[1,2] and Yegor Vassetzky [1,2,4]

[1]UMR 8126, CNRS, Univ. Paris-Sud, Institut Gustave Roussy, Université Paris Saclay, Édouard-Vaillant, Villejuif, France
[2]LIA 1066 LFR2O French-Russian Joint Cancer Research Laboratory, Édouard-Vaillant, Villejuif, France
[3]Laboratory of Gene and Cell Technologies, Faculty of Medicine, Lomonosov Moscow State University, Moscow, Russia
[4]Koltzov Institute of Developmental Biology, Moscow, Russia

Review

HIV infected people are at higher risk of developing cancer, although it is globally diminished in the era of highly active antiretroviral treatment (HAART). Recently, antioncogenic properties of some HAART drugs were discovered. We discuss the role of HAART in the prevention and improvement of treatment outcomes of cancers in HIV-infected people. We describe different trends in HAART–cancer relationships: cancer-predisposing as well as cancer-preventing. We cover the roles of particular drug regimens in cancer prevention. We also describe the causes of cancer treatment with HAART drugs in HIV-negative people, including ongoing clinical studies that may directly point to a possible independent anti-oncogenic activity of HAART drugs. We conclude that despite potent antioncogenic activities of every class of HAART drugs reported in preclinical models, the evidence to date indicates that their independent clinical impact in HIV-infected people is limited. Improved cancer prevention strategies besides HAART are needed to reduce HIV-cancer-related mortality.

Introduction

The introduction of highly active antiretroviral therapy (HAART) in 1996 has profoundly modified the overall survival rates of people with HIV/AIDS. HAART suppresses viral replication, restores the immunity and reduces mortality,[1] but even in the era of HAART, HIV-infected individuals still have a higher risk of developing cancer compared to healthy individuals. They also have a more severe clinical course of cancer and lower survival rate compared to the noninfected population.[2,3] In HIV+ patients, 10–20% of all deaths are attributable to cancer.[4,5]

Key words: HIV-1, AIDS, cancer, HAART, anticancer drugs

Abbreviations: AIDS: acquired immune deficiency syndrome; CCR5: C-C chemokine receptor type 5; EBV: Epstein–Barr virus; HAART: highly active antiretroviral therapy; HBV: hepatitis B virus; HCV: hepatitis C virus; HHV: human herpes virus; HIV: human immunodeficiency virus; HPV: human papillomavirus; INSTI: HIV-integrase strand transfer inhibitor; KS: Kaposi sarcoma; LINE-1: long interspersed nuclear element-1; MMP: matrix metalloproteinases; NHL: non-Hodgkin lymphoma; NNRTI: non-nucleoside reverse transcriptase inhibitor; NRTI: nucleoside reverse transcriptase inhibitor; PI: HIV-protease inhibitor; PI3K: phosphatidylinositol 3-kinase; PSA: prostate-specific antigen; VEGF: vascular endothelial growth factor

Conflict of interest: The authors declare that they have no conflict of interests.

Grant sponsor: Agence Nationale de Recherches sur le Sida et les Hepatites Virales; **Grant sponsor:** ITMO Cancer;
Grant number: Enviburkitt

DOI: 10.1002/ijc.32730

History: Received 10 May 2019; Accepted 2 Oct 2019; Online 11 Oct 2019

Correspondence to: Dr Yegor Vassetzky, E-mail: yegor.vassetzky@cnrs.fr

Given the higher risks for HIV-positive population, developing cancer control strategies for this group is a rising challenge to public health. To provide the context for further research, we will discuss clinical aspects related to the cancer burden in patients with HIV-infection and highlight details on the role of antiretroviral drugs in the development of cancer, which is not limited to viral suppression. Preclinical studies have shown that many antiretroviral drugs could exert antitumor effects independently of their capacity to suppress viral replication and reconstitute the immune system. Understanding the role of HAART in HIV-cancer relationship is important to optimize cancer prevention strategies, screening and clinical management of people with HIV infection. The present review also discusses the clinical impact of antiretroviral treatment in terms of cancer.

Search Strategy and Selection Criteria

The review is based on the works referenced in MEDLINE, EBSCO OpenDissertations, Cochrane Library, Web of Science, Scopus, Embase, ScienceDirect and Google scholar from January 1, 1996 to December 1, 2018. We also analyzed registers of clinical trials (Cochrane Central Register of Controlled Trials [CENTRAL]; ClinicalTrials.gov), abstracts of scientific meetings related to cancer and reference lists of included studies relevant to the subject of the review. The search terms were "highly active antiretroviral therapy", "HIV protease inhibitors", "HIV reverse transcriptase inhibitors", "CCR5 receptor antagonists", "HIV integrase inhibitors" and "cancer/neoplasms". The language of records was limited to English. The final reference list was generated on the basis of originality and relevance to the broad scope of this Review.

HIV and Cancer Risks in the HAART Era

HAART contributed to a slight reduction in overall cancer rates in HIV-infected people.[6–8] Nevertheless, nowadays people

living with HIV still have a 1.6–1.7-fold greater overall risk of cancer development relative to the general population,[8,9] and the risk is rising with age.[10] This fact can be explained by predisposing factors such as immunosuppression combined with chronic inflammation due to virus persistence.[11,12] HIV-infected population is also more susceptible to cancer risk behavior (men who have sex with men, intravenous drug use, heavy alcohol consumption and smoking) than general population and is prone to frequent coinfection with other oncogenic viruses (Epstein Barr Virus [EBV], Human Herpesvirus Virus 8 [HHV-8], Human Papilloma Virus [HPV], Hepatitis B and C Viruses [HBV, HCV]) exacerbated by loss of immune control.[11,12] This results in a cumulative greater probability of cancer development. Some of these risk factors are modifiable. Highly active antiretroviral therapy (HAART) restores the immunity and suppresses viral replication,[1] it was also shown to possess preclinical antioncogenic activity, which will be discussed below (Fig. 1).

Prevalence of these risk factors among people with HIV infection indicates a vital need for risk factor reduction efforts,[13] including a possible pharmacological intervention. Indeed, a combination of HIV and cancer produces a synergistic effect on mortality rates, which become significantly higher than mortality rates for each disease taken separately.[3]

AIDS-defining cancers (ADCs: Kaposi's sarcoma, non-Hodgkin's lymphoma [NHL], invasive cervical cancer) are traditionally distinguished in HIV-infected patients; other cancers are referred to as non-AIDS defining cancers (NADCs).[14] NADCs, in turn, are usually classified into virus-related cancers (HPV-, EBV- and HCV-related cancers) and virus-unrelated cancers.

AIDS-defining cancers

HAART contributed to a significant decline in the incidence of ADCs, the outcome of such cancers has improved and mortality has decreased.[8,15–18] However, the risks for developing all ADCs are still largely elevated in HIV-infected people; this risk is proportional to the HIV load and inversely proportional to the CD4 cell count (Fig. 1).[19,20] Immunosuppression is a strong predictor for ADCs. For Burkitt's lymphoma, albeit, immune reconstitution is supposed to be, at certain CD4 cell counts, a risk factor for the development of lymphoma, indicating a more complex relationship with the immune status.[21–23] Consistently, it was shown that the incidence of Burkitt's lymphoma is either rising in the HAART era,[24,25] or remains stable over time[9,23] as opposed to other NHLs; the proportion of Burkitt's lymphoma among NHLs is growing.[26]

Non-AIDS defining cancers

The number of all non-AIDS defining cancers (NADCs) is increasing since 1996 compared to the pre-HAART era and is expected to continue to rise.[27,28] Both virus-related and virus-unrelated cancers contribute to this trend.[29] NADCs represent approximately 2/3 of all cancers in HIV-patients; they are two times more frequent than ADCs.[9,11] The rise of NADCs in the HAART era is in part linked to the overall aging of people with HIV, this provides more time for cancer to evolve.[11,29] Contrary to ADCs, the association of risk of NADCs and CD4 counts or HIV load remains a matter of discussion, as some researchers suppose they are not related,[30] while others have shown that immunodeficiency was a risk factor associated with NADCs incidence.[31–34] It appears that low CD4 cell count is a specific risk factor exclusively for virus-related NADCs, but

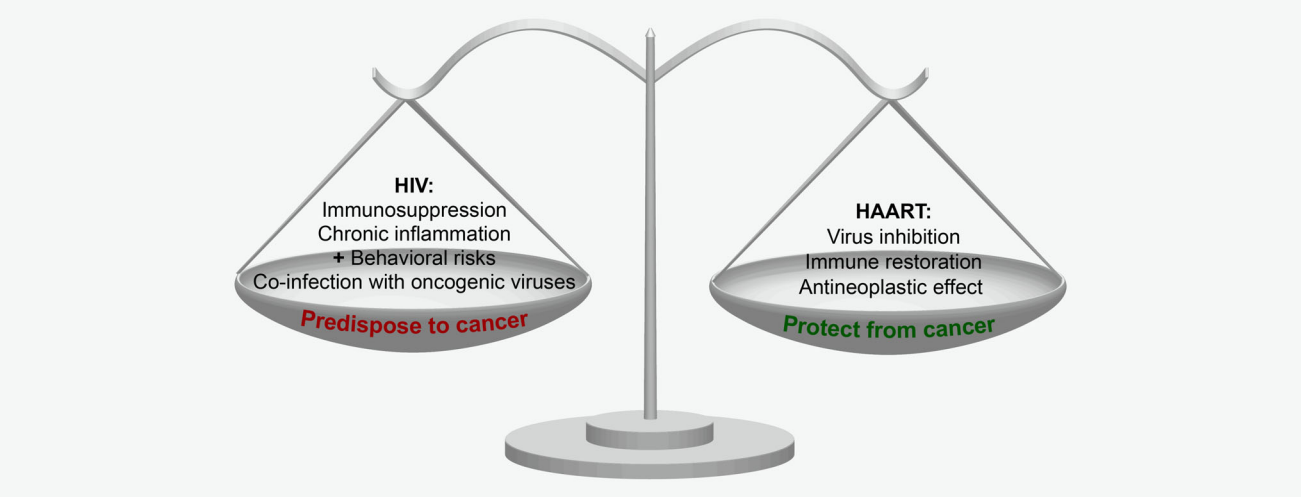

Figure 1. Factors influencing the risk of cancer in HIV-infected people. Cancer risk factors are represented on the left. Immunosuppression and chronic inflammation, caused by HIV infection, predispose to tumorigenesis. Besides, HIV-infected population is more susceptible to cancer risk behavior (smoking, men who have sex with men, intravenous drug use, alcohol consumption) and coinfection with other oncogenic viruses. Some of these risk factors are modifiable. Factors that reduce cancer risk are represented on the right. Highly active antiretroviral therapy (HAART) restores the immunity and suppresses viral replication, it was also shown to possess preclinical antioncogenic activity; however, the clinical relevance of this activity remains to be elucidated. [Color figure can be viewed at wileyonlinelibrary.com]

not for virus-unrelated ones,[34] for example, CD4 counts are significantly higher in HIV+ patients that develop prostate cancer compared to HIV+ patients without cancer, indicating that lower CD4 counts are possibly associated with less prostate cancer risk.[35]

The overall incidence of NADCs in HIV-positive individuals was shown to be up to two times higher compared to the general population and it remains basically unchanged during the HAART era.[2,8,9] This elevated incidence is mainly due to virus-related NADCs, which are five times more frequent in HIV-infected people: Hepatitis B Virus (HBV)/HCV-related hepatocellular carcinoma, HPV-related oropharyngeal cancers, HPV-related anal cancer, EBV-related classical Hodgkin lymphoma and others.[9] Some virus-unrelated NADCs: lung, larynx, nasal cavity cancers also occur more frequently in HIV-infected people[9]; this effect can be partially explained by the prevalence of smokers.[36,37] Smoking cessation should be discussed with patients to reduce cancer risk (Fig. 1).[38]

Interestingly, for some reasons, some cancers are significantly more rare in HIV-infected patients compared to the general population.[9] They include stomach, colorectal, kidney, uterus, prostate, breast, brain and thyroid cancers.[9,39–41] This cannot be solely explained by targeted cancer screening for these types of cancer (mammography, colon/sigmoidoscopy, PSA test)[39] or hormone levels alteration due to HIV infection.[42] Overweight/obesity is less prevalent in people living with HIV than in general population, and that is a proposed risk factor for gastrointestinal tract tumors, breast, endometrial and renal cancers.[13,43] This requires further investigation with a direct comparison of HIV-infected people with body mass index-matched uninfected people. These trends may also be due to viral-host interaction. It is a common knowledge that HIV induces T-cell apoptosis.[44–46] Several studies have shown that HIV-1 and its molecules (gp120, Nef) can also mediate neuroblastoma,[47] breast,[48] colorectal,[49,50] prostate[51] cancer cell growth inhibition and apoptosis. An interesting possibility, explaining lower frequency of several cancers in HIV-infected persons, is that the HAART drugs can possess cancer-prevention or antineoplastic activity. Below we shall consider recent data on this subject.

HIV and Cancer Treatment in the HAART Era

During the HAART era, cancer-contributable mortality is higher in patients with HIV compared to noninfected population even when clinical features are similar, and HIV-infected people diagnosed with cancer experience excess mortality that exceeds the expected mortality from a simple combination of HIV and cancer.[3,52–54] Cancer treatment in people living with HIV/AIDS is challenging due to the absence of clinical recommendations or established protocols and lack of clinical experience.[55] A significantly higher proportion of HIV-infected individuals does not receive treatment for diffuse large B-cell lymphoma, lung cancer, Hodgkin's lymphoma, prostate cancer and colorectal cancer. HIV infection is associated with a lack of standard treatment modality for local-stage diffuse large B-cell lymphoma, nonsmall-cell lung cancer and colon cancer.[55]

AIDS-defining cancers

The introduction of HAART has significantly improved survival rates for ADCs,[56] nevertheless, HIV infection seems to remain a factor increasing the risk of death in patients with ADCs. The overall survival of HIV-infected patients with NHLs and cervical cancer is significantly lower than in HIV-negative population.[57,58]

ADCs give better responses to treatment with the HAART + chemotherapy/radiotherapy combination rather than HAART alone or chemotherapy/radiotherapy alone,[59–63] therefore, HAART use is recommended for patients with ADCs.[14] No difference was found between PI-based HAART *vs*. other regimens in treatment outcomes of Kaposi's sarcoma[64] and NHL[65,66] in a combination with chemotherapy. Even HAART treatment alone without chemotherapy can lead to positive outcomes of Kaposi's sarcoma,[67–70] NHLs,[71–74] oncogenic cervical squamous intraepithelial lesions.[75,76] Nonetheless, a further clinical study proved that HAART + chemotherapy combination gave a better response than HAART alone, albeit no difference in the survival rate was revealed.[77] At the same time, a PI-based regimen was revealed to be associated with higher toxicity during chemotherapy of lymphomas.[66] Patients with lymphomas receiving PI-based HAART had a significantly lower 1-year survival compared to NNRTI-based HAART probably due to toxicity.[78] Burkitt's lymphoma is again a puzzling exception among NHLs, since its outcome remains rather poor in the HAART era.[79,80]

Non-AIDS defining cancers

In the HAART era, survival rates for HLs and anal cancer improved considerably.[56] The overall 3-year survival of HIV-infected patients with HLs is significantly lower than in HIV-negative population,[57] which might be due to treatment disparities.[81] For solid tumors, such as lung, liver, anal cancer 5-year survival is comparable to that in general population.[56,82]

Promising results were obtained in several reports of NADCs treatment in HIV-infected people with HAART-drugs alone or in combination with chemotherapy, which resulted in a good clinical response.[83–87]

Combination of HAART and chemotherapy

HIV-infected people are generally excluded from clinical trials; therefore, data on toxicity, outcomes and possible drug interactions during cancer treatment are limited. Despite the increased toxicity and drug–drug interactions, HAART withdrawal during chemotherapy is unfavorable in HIV-patients with cancer and can lead to a poorer outcome[88]; therefore, in general, any HAART interruption is not advisable during cancer treatment.[38] Possible drug–drug interactions should be therefore carefully assessed when treating cancer in HIV-infected patients. Drug–drug interactions rely on many

factors, such as the route of elimination, the effect on enzymes and transporters involved in drug metabolism. Both HAART and antioneoplastic drugs can be metabolized by CYP450 enzyme family and serve as CYP450 inhibitors, which can lead to drug accumulation and potential toxicity, or as CYP450 inducers, which leads to drug elimination and decreased efficacy, except for active metabolites of several drugs.[38,89] As an example, ritonavir*, a PI and a potent CYP3A4 inhibitor, was reported to be associated with more severe toxicity in combination with chemotherapy compared to nonritonavir-based HAART.[88] On the contrary, NNRTIs are mainly CYP3A inducers.[89] HAART regimen should be modified when facing undesirable drug–drug interactions or elevated toxicity.[38] In this case, preference can be given to the INSTI-based regimen, which is supposed to be relatively safe.[38,90] Both NNRTIs and INSTIs are superior to PIs in terms of viral suppression in HIV-infected patients with malignancies.[90] Regarding the complexity of multidrug interaction, if a patient is HAART-naive, it is recommended to start HAART more than a week before or after the cancer treatment in order to differentiate between adverse effects.[38] It is also recommended that clinicians consult major reviews dedicated to the topic of potential drug–drug interactions between HAART and chemotherapeutic drugs,[89,91,92] treatment guidelines[38] and refer to available resources such as http://www.hiv-druginteractions.org to optimize clinical management of HIV-infected patients with cancer and increase therapeutic benefit.

An individual pharmacogenetic profile is another factor that influences patients' response to drug combinations. A promising strategy is to evaluate personalized pharmacogenomic profile to predict efficacy and undesirable adverse effects of the therapeutic agents when planning HAART and chemotherapy regimens.[93]

Thus, cancer treatment in people with HIV requires both an adequate control of HIV infection by HAART and an individual drug–drug interaction assessment.

HAART and cancer prevention

HAART is defined as the use of several (at least three, rarely two) antiretroviral drugs and has different regimens: two nucleoside reverse transcriptase inhibitors (NRTIs) in combination with a third drug from one of three drug classes: HIV-integrase strand transfer inhibitors (INSTIs), non-nucleoside reverse transcriptase inhibitors (NNRTI) or HIV-protease inhibitors (PIs) are currently recommended.[94]

In HIV-infected people, HAART use is definitely associated with lower cancer incidence over no treatment for most cancers and particularly for ADCs.[7,95,96] Whether this effect is based on immune reconstitution and virus suppression, or it is an independent protective factor, remains unclear. HAART use is considered to be a strong factor responsible for the decreased ADCs occurrence in HIV-infected people and the greater cumulative exposure to HAART, the lower the risk of ADCs is.[97] The protective effect of HAART is mainly explained by virus inhibition and immune restoration. Although at first it was thought that HAART had an additional protective effect independent of CD4 cell count and viral load,[19,98–100] the latter studies did not detect any independent effect of HAART on Kaposi sarcoma incidence after adjusting for more variables and in a larger cohort.[20,101]

HAART was first reported to be protective for NADCs,[102] or to have no effect[6]; nowadays, the use of HAART is associated with a higher rate of NADCs over no treatment and long cumulative exposure to HAART is a predictor of NADCs risk.[33,96,97,100] This effect is mainly driven by virus-related cancers, as their incidence was significantly higher in people treated with antiretrovirals compared to no antiretroviral treatment, while there was no change in virus-unrelated cancer rates between HIV-infected people with or without antiretroviral therapy.[100] Improved survival of HIV-positive individuals during the HAART era may allow for sufficient time for virus-associated lesions to develop into malignancies. For Hodgkin's lymphoma, though, HAART use was not associated with higher cancer risk in large European cohort studies.[103–105] The absence of HAART was not proven to be an independent risk factor for NADCs.[19] HAART exposure did not play any role in lung cancer staging.[106] No association was shown between HAART use and the risk of lung cancer.[107,108] The opposite trend is observed in prostate cancer, where the cumulative antiretroviral exposure decreases cancer risk, though no difference was observed between people with or without antiretroviral therapy.[100] The role of HAART in anal cancer prevention is ambiguous. HAART is associated with a lower prevalence of anal intraepithelial neoplasia,[109] and it takes more time for anal cancer development in HAART era than before,[110] but treatment duration does not reduce anal cancer risk,[111] and HAART is considered to be a risk factor for relapse of anal cancer.[112]

A lack of specific and independent protective effect of HAART on cancer incidence, regardless of their potent antitumor effect observed in preclinical studies (see below), may be explained by low doses, sufficient for viral suppression, but insufficient for cancer prevention. These relationships are further complicated by various factors. For example, the hepatotoxicity of HAART may amplify the carcinogenic effect of HBV and HCV.[113] NRTIs, a mandatory component of main HAART regimens, were also considered to be genotoxic and carcinogenic.[114] However, large prospective cohort studies of HIV-negative children, perinatally exposed to any drug of NRTI class, revealed no change in cancer incidence compared to nonexposed ones and to the general population.[115–118] They found, albeit, that the risk of cancer development was significantly higher in those exposed to didanosine-lamivudine combination than to zidovudine monotherapy.[115] Later, it was

*Ritonavir is currently recommended to improve the pharmacokinetic profiles of other antiretroviral drugs (pharmacokinetic booster), not as an independent HAART component.[94,198]

found that didanosine exposure in HIV-negative children was oncogenic and accounted for higher cancer risk.[117,118] Didanosine use is not currently recommended.[94]

Comparison between HAART Regimens in Terms of Cancer Prevention

As HAART drugs have various mechanisms of action additionally to their main antiretroviral activity, their efficiency in cancer prevention can vary. Below we shall consider the association between HAART regimens and cancer risk.

AIDS-defining cancers

PI and NNRTI-based HAART were reported to have a similar protective effect on ADC incidence (Table 1).[97,100,119] Ritonavir-based, indinavir†-based or nelfinavir*-based therapy confers no advantages compared to other PI- or NNRTI-based regimens in the prevention of ADCs.[95,96,120] This is in line with the fact that the HAART impact on the decrease of ADCs is mainly connected with improvement in immune function and viral load.[20] At the same time, some studies showed potential advantages of PI-based HAART in ADCs prevention over other regimens. Only PI-containing HAART significantly reduces the frequency of HHV-8 detection compared to HAART-naïve patients.[121] In patients with low immune activity, PI-based therapy is more efficient at inducing complete response than NNRTI–HAART.[122] NNRTI-based HAART was shown to be associated with Kaposi's sarcoma relapse in a case series study ($n = 5$)[123] and in a small prospective cohort study ($n = 45$),[124] though the opposite was shown in another case series study ($n = 24$).[125] NNRTIs were shown to be more potent in reducing the risk of NHL.[97] The regimens other than PI- or NNRTI-based are less studied, however, there were two case report of human herpesvirus 8 (HHV8) viremia and Kaposi's sarcoma relapse after switching from a PI- to an INSTI-based HAART and rapid remission of Kaposi's sarcoma after returning back to PI-based therapy.[126,127] A recent large cohort study found no evidence that INSTIs were associated with increased cancer risk.[128] Treatment with the CCR5 antagonist (vicriviroc‡) can be associated with the increased risk of developing cancers, including lymphomas,[129] but later studies showed that the cancer incidence was similar between vicriviroc and placebo[130]; maraviroc from the same class was also confirmed to be relatively safe.[131]

Non-AIDS defining cancers

Several large cohort studies reported no difference between PI- and NNRTI-based regimens in cancer prevention in all cancers except anal cancer (Table 1).[95,96,100,132] One study showed NNRTI association with an increased risk of NADCs and precisely Hodgkin's lymphoma,[2] and controversially, another study showed that overall NADCs incidence was higher in people receiving PI-based HAART.[97] Moreover, the latter study reported that PI-based regimen did not decrease the risk of Hodgkin lymphoma, while NNRTI-based HAART did.[97]

PI-based HAART may be associated with an increased risk of anal cancer, whereas NNRTI use has no association with anal cancer or is associated with a decreased risk.[96,97,100,133,134] Interestingly, nelfinavir-based HAART was not associated with a higher risk of anal cancer as opposed to other PI-based regimens.[96] It was recently reported that adjustment for both CD4 cell count and cumulative NRTI exposure abolished the association of PI-based regimen with anal cancer risk in a case–control study.[135] On the other hand, PI use was associated with a lower risk of prostate cancer,[100] which is consistent with the overall lower incidence of prostate cancer in HIV-infected people compared to the general population. These trends remain difficult to explain.

In conclusion, currently, there is no evidence for any particular HAART regimen being more or less associated with cancer risk for ADCs and virus-unrelated NADCs, except for a lower risk of prostate cancer with a PI-based HAART. Regarding virus-unrelated NADCs, PI-based HAART is estimated to be associated with an increased risk of anal cancer and probably of Hodgkin lymphoma.

Preclinical Antineoplastic Activity of HAART Drugs

Recent preclinical studies showed that HAART drugs from different classes possessed potent antioncogenic activity. The proposed mechanisms of their action are summarized in Figure 2.

HIV-PIs have pleiotropic pharmacological properties besides their antiretroviral activity. They have been reported to inhibit the growth of various cancer cell lines *in vitro* as well as tumors in *in vivo* xenografts models.[136–139] PIs induce cell growth arrest, endoplasmic reticulum stress, caspase-dependent apoptosis, autophagy (for review see[140–142]). Moreover, PIs are known for their antiangiogenic and radiosensitizing effects.[141,143] PIs action is associated with inhibition of phosphatidylinositol 3-kinase (PI3K)/Akt pathway; one of the possible mechanisms is binding to Hsp90 and inhibiting its chaperone function followed by decreased PI3K/Akt signaling.[137,138] Together and independently of each other, PI3K and its downstream kinase Akt regulate various cell processes such as growth, proliferation, survival, migration, apoptosis and their hyperactivation is a cancer hallmark.[144,145] PI3K/Akt signaling in cancer inhibits apoptotic enzymes; promotes activation of mTOR and NF-κB axes that regulate transcription, increase cell growth, survival, proliferation, increase matrix metalloproteinases (MMPs) and vascular endothelial growth factor (VEGF) expression, associated with migration and angiogenesis, respectively; causes chemo/radiotherapy resistance by misregulation of DNA damage response.[143,146–149] Akt, VEGF, MMPs and other important cancer-phenotype proteins are partners of Hsp90, the latter works as a molecular chaperone and guarantees correct folding of its substrates.[150] Hsp90

†Both indinavir and nelfinavir are no longer recommended accordingly to the latest guidelines of HIV treatement.[94]

‡Phase III clinical trials were discontinued and vicriviroc was not approved for HIV treatment.[94,198]

Table 1. A comparison of regimens based on non-nucleoside reverse transcriptase inhibitors, protease inhibitors or integrase strand transfer inhibitors in preventing cancers in HIV-infected persons

Type of cancer	Study design	Cohort size	Conclusion	References
ADCs				
ADCs, Kaposi's sarcoma alone, NHL alone	Prospective cohort study	42,006	Nelfinavir = non-Nelfinavir-PI = NNRTI in cancer prevention	96
ADCs, Kaposi's sarcoma alone	Prospective cohort study	41,762	PI = NNRTI in cancer prevention	97
NHL alone			NNRTI, but not PI, is associated with a lower risk	
Kaposi's sarcoma	Prospective cohort study	4,480	Ritonavir = non-Ritonavir-PI = NNRTI in cancer prevention	120
Kaposi's sarcoma	Prospective cohort study	1,204	PI = NNRTI in cancer prevention	119
Kaposi's sarcoma	Prospective cohort study	45	Kaposi's sarcoma relapse after switch from PI to NNRTI	124
ADCs, Kaposi's sarcoma alone, NHL alone	Retrospective cohort study	12,872	PI = NNRTI in cancer prevention	100
ADCs	Retrospective cohort study	2,499	Nelfinavir = Indinavir = other regimens in cancer prevention	95
Kaposi's sarcoma	Retrospective cohort study	91	PI = NNRTI in cancer incidence and clinical course	194
Kaposi's sarcoma	Case series	24	No Kaposi's sarcoma relapse after switching from PI to NNRTI	125
Kaposi's sarcoma	Case series	5	Kaposi's sarcoma relapse after switch from PI to NNRTI	123
Kaposi's sarcoma	Case report	1	PI switch to INSTI leaded to HHV8 viremia and sarcoma relapse	127
Kaposi's sarcoma	Case report	1	PI switch to INSTI led to HHV8 viremia, while INSTI switch back to PI resulted in a remission	126
NADCs				
Anal cancer	Prospective cohort study	72,355	PI monotherapy, opposite to other antiretroviral therapy, is associated with increased cancer risk	134
NADCs, anal cancer alone	Prospective cohort study	42,006	PI = NNRTI in cancer prevention, except for higher risk of anal cancer with longer non-Nelfinavir PI, but not Nelfinavir or NNRTI	96
NADCs, anal cancer alone, HL alone	Prospective cohort study	41,762	PI but not NNRTI, use is associated with increased cancer risk	97
Lung cancer, head and neck cancers			PI = NNRTI in cancer prevention	
NADCs, HL alone	Prospective cohort study	5,076	NNRTI but not PI or NRTI therapy was associated with an increased risk of NADCs	2
NADCs	Prospective cohort study	3,158	Initial PI = NNRTI = NRTI in cancer prevention	132
Virus-related, virus-unrelated NADCs	Retrospective cohort study	12,872	PI = NNRTI in cancer prevention, except for higher risk of anal cancer with longer PI, but not NNRTI	100
NADCs	Retrospective cohort study	2,499	Nelfinavir = Indinavir = other regimens in cancer prevention	95
All cancers				
All cancers	Prospective cohort study	7,971	Raltegravir (INSTI) is not associated with an increased risk of cancer compared to other treatment strategies	128

Abbreviations: INSTI, HIV-integrase strand transfer inhibitor-based antiretroviral therapy; NNRTI, non-nucleoside reverse transcriptase inhibitor-based antiretroviral therapy; PI, HIV-protease inhibitor-based antiretroviral therapy.

inhibition leads not only to targeted destabilization of key oncogenic proteins but also to misfolded protein aggregation, endoplasmic reticulum stress and apoptotic death or autophagy.[151,152]

Detailed docking analysis has shown that PIs can be potent Hsp90 inhibitors; their binding capacity to Hsp90 decreases in the following order: Nelfinavir, Indinavir, Saquinavir, Ritonavir, Lopinavir, Tipranavir, Darunavir and Amprenavir[§].[153] Indeed, among all PIs, nelfinavir seems to have the highest anticancer activity.[141] It is noteworthy that a longitudinal study of antitumor effects of PIs and especially, nelfinavir, is nuanced by the fact that in 2007 Roche's Viracept (nelfinavir mesylate) was discovered to be contaminated by a mutagenic compound.[154] Importantly, PIs can also directly inhibit the replication of human herpesvirus 8 (HHV8), the etiological agent of Kaposi's sarcoma.[121,155]

Though at first nucleoside reverse transcriptase inhibitors (NRTIs) were supposed to be genotoxic, mutagenic and oncogenic due to their ability to incorporate into nuclear DNA and directly inhibit cellular DNA polymerases,[114,117,156,157] the subsequent clinical studies have shown no clear correlation between NRTIs and cancer (see above). In fact, *in vitro* studies have shown, that NRTIs might also possess anticancer activity,[158–160] which is probably associated with their capacity to inhibit DNA repair,[161] induce mitochondrial toxicity,[162] apoptosis, modulate activity and expression of endogenous reverse transcriptase encoded by the long interspersed nuclear element-1 (LINE-1).[158] LINE-1 propagation throughout the DNA may play a role in genome instability, mutagenesis and contribute to carcinogenesis.[163]

Another HAART class, non-nucleoside reverse transcriptase inhibitors (NNRTIs) were also demonstrated to inhibit the growth of cancer cell lines and xenografts in rodents,[157,164–166] among them, efavirenz is supposed to have the highest anticancer potential.[167] NNRTIs can act on cancer cells through the induction of DNA damage,[157] apoptosis,[168] oxidative stress[165] and downregulation of LINE-1 expression.[169] Similarly to PIs, exposure to NNRTIs was associated with the radiosensitizing effect.[165,170]

HIV-integrase strand transfer inhibitors (INSTIs) may cause aberrant HIV-integration and rearrangements in the host DNA when used in low doses.[171,172] Low-dose INSTI may create the

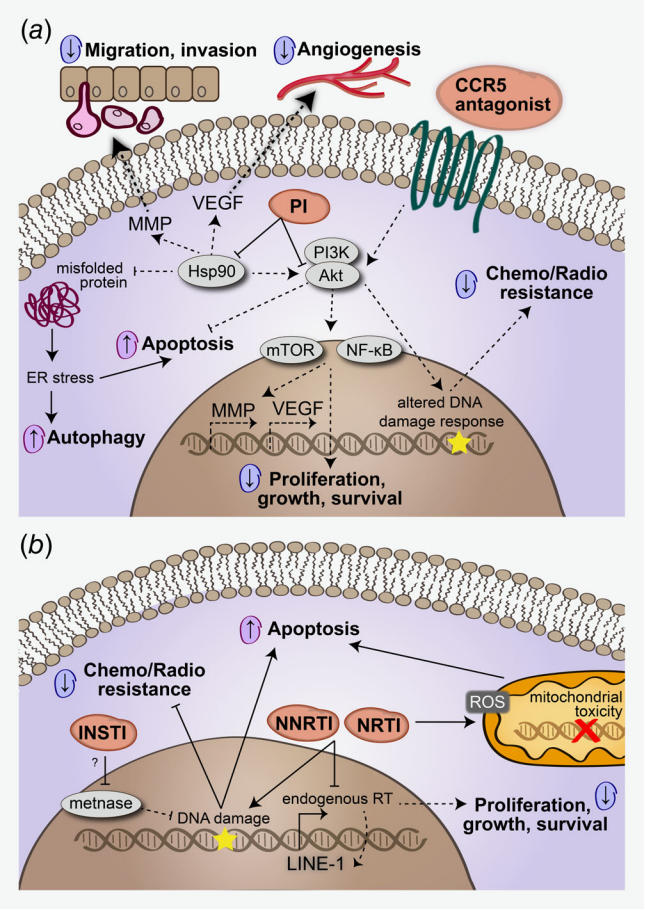

Figure 2. Legend on next column.

Figure 2. Potential mechanisms of the antineoplastic effects of different classes of HAART drugs. (*a*) PI3K/Akt pathway regulates growth, proliferation, survival, migration and apoptosis. In cancer, PI3K/Akt activation inhibits apoptotic enzymes; promotes transcription regulation that increases growth, survival, proliferation, increases MMPs (migration, invasion and metastasis) and VEGF (angiogenesis) expression *via* mTOR and NF-κB axes; causes chemo/radiotherapy resistance by deregulation of DNA damage response. PIs inhibit the PI3K/Akt pathway, possibly through binding to Hsp90 and inhibiting its chaperone function. MMPs and VEGF are also Hsp90 clients destabilized by chaperone inhibition; overall, Hsp90 inhibition leads to misfolded protein aggregation, ER stress, apoptosis and autophagy. CCR5 receptor promotes pro-oncogenic cascades as it also activates the PI3K/Akt pathway, thus CCR5 antagonists are also antioncogenic effectors. Other pathways implicated in CCR5 downstream signaling include phospholipase C-γ, Rac/CDC42/RhoA, JAK–STAT pathways (data not shown).[197] (*b*) NRTIs and NNRTIs interfere with nuclear DNA integrity, mitochondrial DNA maintenance and oxidative stress, retrotransposon LINE-1 expansion, which makes them potential anticancer agents. LINE-1 promotes genome instability and contributes to carcinogenesis. INSTIs also inhibit the DNA-repair enzyme menace involved in chemotherapy resistance. Abbreviations: CCR5, C-C chemokine receptor type 5; ER, endoplasmic reticulum; INSTI, HIV-integrase strand transfer inhibitor; LINE-1, long interspersed nuclear element-1; MMPs, matrix metalloproteinases; NNRTI, non-nucleoside reverse transcriptase inhibitor; NRTI, nucleoside reverse transcriptase inhibitor; PI, HIV-protease inhibitor; PI3K, phosphatidylinositol 3-kinase; ROS, reactive oxygen species; RT, reverse transcriptase; VEGF, vascular endothelial growth factor. ➤—promoting downstream effect; ⊣—inhibiting downstream effect; ▬▬—active pathway under the action of drugs; ▬ ▬ ▬—suppressed pathway under the action of drugs, ↳—gene transcription; ⇅—resulting effects of drugs on critical cellular cancer-related processes (activation and suppression, respectively). [Color figure can be viewed at wileyonlinelibrary.com]

[§]Amprenavir production was discontinued, a prodrug fosamprenavir is available and approved.[94,198]

Table 2. Clinical trials of antiretroviral drugs in non-HIV related cancer treatment

NCT number	Drug	Condition	Phase	Actual enrollment	Start date
HIV-protease inhibitors					
NCT00233948	Nelfinavir	Liposarcoma	I/II	29	March 2006
NCT01445106	Nelfinavir	Solid Tumors	I	28	December 2006
NCT00589056	Nelfinavir	Stage III Nonsmall Cell Lung Cancer	I/II	55	June 2007
NCT01068327	Nelfinavir	Locally Advanced Pancreatic Cancer	I	46	November 2007
NCT00704600	Nelfinavir	Rectal Cancer	I/II	15	September 2008
NCT00694837	Nelfinavir	Glioblastoma	I/II	6	March 2009
NCT00915694	Nelfinavir	Glioblastoma Multiforme	I	23	April 2009
NCT01020292	Nelfinavir	Grade IV Glioma	I	31	April 2009
NCT01086332	Nelfinavir	Pancreatic Cancer	I	7	May 2009
NCT01079286	Nelfinavir	Advanced Cancers	I	18	June 2009
NCT01065844	Nelfinavir	Adenoid Cystic Cancer of the Head and Neck	II	15	October 2009
NCT01108666	Nelfinavir	Inoperable Stage III Nonsmall Cell Lung Cancer	I	72	March 2010
NCT01164709	Nelfinavir	Relapsed or Progressive Advanced Hematologic Cancer	I	18	July 2010
NCT01485731	Nelfinavir	Cervical Cancer	I	8	January 2012
NCT01555281	Nelfinavir	Progressive Multiple Myeloma	I/II	33	February 2012
NCT01925378	Nelfinavir	Cervical Intraepithelial Neoplasia	II	10	July 2012
NCT01728779	Nelfinavir	Oligometastases	II	40	June 2013
NCT01959672	Nelfinavir	Locally Advanced Pancreatic Cancer	II	12	September 2013
NCT02207439	Nelfinavir	Squamous Cell Carcinoma of the Oral Cavity, Oropharynx, Larynx, or Hypopharynx	II	28	July 2014
NCT02188537	Nelfinavir	Proteasome Inhibitor-nonresponsive Myeloma	II	34	December 2014
NCT02363829	Nelfinavir	Locally Advanced Cervical Cancer	I	6	February 2015
NCT02024009	Nelfinavir	Advanced Localized Pancreatic Cancer	I/II	289	March 2016
NCT03050060	Nelfinavir	Advanced Melanoma, Lung or Kidney Cancer	II	120	June 2017
NCT03256916	Nelfinavir	Locally Advanced Carcinoma of Cervix	III	0	September 2017
NCT00637637	Ritonavir/Indinavir	Brain Metastases	II	60	September 2007
NCT01095094	Ritonavir/Lopinavir	Progressive or Recurrent High-Grade Glioma	II	19	January 2009
NCT01009437	Ritonavir	Breast Cancer	I/II	28	May 2010
NCT03066154	ModraDoc006/r (oral docetaxel with ritonavir)	High-risk Prostate Cancer	I	24	September 2016
NCT02770378	Ritonavir	Recurrent Glioblastoma	I	10	November 2016
NCT03136640	ModraDoc006/r (oral docetaxel with ritonavir)	Castration-resistant Prostate Cancer	I	20	April 2017
NCT03150368	ModraDoc006/r (oral docetaxel with ritonavir)	Advanced Solid Tumors	I	22	May 2017
NCT03383692	Ritonavir	Advanced Solid Malignant Tumors	I	40	January 2018
Nucleoside reverse transcriptase inhibitors					
NCT03144804	Lamivudine	p53 Mutant Metastatic Colorectal Cancer	II	32	October 2017
Non-nucleoside reverse transcriptase inhibitors					
NCT00964002	Efavirenz	Metastatic Prostate Cancer	II	60	May 2008
NCT00964171	Efavirenz	Metastatic Pancreatic Cancer	II	72	August 2008
NCT01878890	Efavirenz	Solid Tumors or NHL	I	30	June 2011
Integrase strand transfer inhibitors					

(Continues)

Table 2. Clinical trials of antiretroviral drugs in non-HIV related cancer treatment (Continued)

NCT number	Drug	Condition	Phase	Actual enrollment	Start date
NCT01275183	Raltegravir	Squamous Cell Carcinoma of Head and Neck	I	5	December 2010
CCR5 antagonist					
NCT01736813	Maraviroc	Metastatic Colorectal Cancer	I	12	November 2012
NCT03274804	Maraviroc	Metastatic Colorectal Cancer	I	20	April 2018

The studies on AIDS-, EBV-, HBV-, HCV- and HTLV-related cancers are excluded.

situation when strand transfer reaction is blocked at only one of two ends of viral DNA, which subsequently leads to mutation-prone integration of a blocked end *via* the host enzymes.[171] Thus, these drugs are potentially mutagenic and carcinogenic; however, there is no evidence for increased cancer risk in patients exposed to INSTIs. INSTIs were also shown to inhibit a metnase enzyme associated with chemotherapy resistance[173]; thus, they can be potentially applied together with antineoplastic drugs to increase their efficacy.

Finally, recent studies have shown that CCR5 antagonists are also potent antioncogenic and antimetastatic effectors for various cancer cell lines and xenografts.[174–178] CCR5 blockade results in a decreased invasion, migration, metastatic potential cell proliferation and leads to proapoptotic signaling.[174,176,179]

Thus, the preclinical data on HAART components point to its protective effect against cancer for virtually every class of drug, which is very promising in terms of drug repositioning. Still, it is important to reveal the causal impact of these drugs on humans who undergo HIV and/or cancer treatment.

Antiretroviral Drugs and Cancer Treatment in HIV-Negative Patients

As many *in vitro* studies have shown the anticancer activity of HAART drugs, they were proposed for use in cancer treatment. In addition, the use of antiretroviral drugs in HIV-negative people with cancer can help us evaluate a possible protective effect of HAART, independent of its antiretroviral activity *per se*. The favorable treatment outcome of HIV-negative patients with Kaposi's sarcoma treated with indinavir (PI) points to its direct antioncogenic properties in ADCs.[180] At present, several clinical trials of antiretroviral drugs in cancer are underway. They are summarized in Table 2. However, the data addressing this question are still limited, and the results obtained from clinical trials are often inconclusive.

Promising results were obtained for nelfinavir (PI) as monotherapy or combined with chemoradiotherapy in phase I clinical trials: in locally advanced pancreatic cancer,[181] in locally advanced nonsmall cell lung cancer,[182] in locally advanced rectal cancer,[183] in multiple myeloma,[184] in neuroendocrine tumors of the midgut or pancreatic origin[185] and in glioblastoma multiforme,[186] where the level of response was higher than reported before and the toxicity was acceptable. A phase II clinical trial of nelfinavir added to bortezomib and dexamethasone in the proteasome inhibitor-refractory multiple myeloma showed exceptional response rates (~65%).[184] A phase II clinical trial of nelfinavir combined with chemoradiation in locally advanced inoperable pancreatic cancer showed improved tumor oxygenation and perfusion, which might lead to better treatment response, however, the study was discontinued because of the unavailability of nelfinavir in Europe.[187] Data from a phase I clinical trial of maraviroc (CCR5 antagonist) in advanced colorectal cancer with hepatic metastases showed a partial response in patients with previously refractory disease.[179] Lopinavir/Ritonavir combination (PIs) was successfully used for the treatment of HPV-positive high grade squamous intraepithelial lesions in HIV-negative women.[188] There was also a case report of successful thyroid papillary carcinoma treatment

Table 3. Summary of the role of HAART in HIV–cancer relationship

			NADCs	
Parameter	All cancers	ADCs	Virus-related	Virus-unrelated
Cancer incidence compared to the general population in the pre-HAART era	↑↑	↑↑↑	↑	=[1]
Cancer incidence compared to the general population in the HAART era	↑	↑↑	↑	↓
Cancer incidence in the HAART era compared to the pre-HAART era	↓	↓↓↓[2]	↑	↑
The risk of cancer with HAART use compared to no treatment	↓	↓↓↓	↑	=

Sources[195,196]: and other articles cited in the text.
[1]Due to a small cohort size and a large 95% confidence interval.
[2]Except Burkitt's lymphoma.

with a combination of Nevirapine (NNRTI) and radioiodine, resulting in re-induction of cell differentiation, better drug uptake and sensitivity to treatment, slower progression of the disease.[189,190] However, definite conclusions cannot be drawn at this stage due to a small number of patients, possible patient selection bias and lack of control groups.

Some studies point to the absence of the antitumor activity of antiretroviral drugs. No meaningful improvement in clinical outcomes was reported among patients with recurrent adenoid cystic carcinomas and nelfinavir (PI) monotherapy in a phase II clinical trial.[191] The use of efavirenz (NNRTI) also did not improve the nonprogression rate of castration-resistant prostate cancer in a phase II clinical trial.[192] A phase II clinical trial of ritonavir/lopinavir (PIs) combination in patients with progressive or recurrent high-grade gliomas did not reveal a potent clinical activity either.[193] These results can be explained by low effectivity of these drugs as monotherapy, by low plasma concentrations of drugs, or their low tissue concentrations due to poor access to the tumor. Therefore, even though some results concerning the use of antiretroviral drugs in cancer treatment are promising, further studies, investigating higher dosage of the drugs and combinations with chemoradiotherapy, are necessary to assess their effectiveness in the treatment of different types of cancer and will provide insight into optimal oncological doses of HAART drugs.

Conclusions

HIV-associated cancers are a serious health problem leading to rising mortality in an HIV-infected population, therefore cancer prevention and cancer control strategies are required. The main trends in cancer incidence relative to HAART treatment are summarized in Table 3. The main protective effect of HAART in HIV-infected people is related to ADCs and may be explained by immune reconstitution and viral suppression. The effect of HAART in NADCs is more complex and nuanced. Interestingly, the difference between HAART regimens in cancer prevention is observed only for virus-related cancers, where PI-based HAART is less favorable than other regimens. The role of HAART during cancer treatment is positive, though it may be complicated by drug–drug interactions. The later should be carefully assessed by clinicians when planning the cancer treatment in HIV-infected people. Doctors should also take measures to reduce risk behavior in people with HIV (smoking and alcohol consumption cessation), as a cancer prevention strategy and during cancer treatment. PI-based HAART is not preferred during cancer treatment as well, because of suboptimal viral suppression in patients with HIV and cancer.

Antiretroviral drugs that are in use for many years were recently shown to be potentially antineoplastic and therefore may present an elegant solution for cancer control in this population. The plethora of published articles studied their effects in primary cells, tumor cell lines and tumor xenografts models; however, their effect on cancer prevention, treatment and outcome in humans remains poorly understood. Here, we summarized and discussed all potential clinical aspects related to the impact of antiretroviral treatment on cancer.

Finally, several reports of HAART use in cancer treatment in the HIV-negative population may help answer the question about an antioncogenic activity of HAART, but to date, the data from clinical studies are still limited. It is possible that some modifications or optimizations of HAART regimens are required in order to observe antioncogenic and cancer-protective properties of these drugs in clinical practice.

Many epidemiological studies exploring HIV-cancer relationships have a common limitation: they lack the information on antiretroviral therapy, thus a potentially promising question about the relationships between HAART and cancer risks and outcomes remains unanswered. The absence of clinical recommendations, together with a lack of experience regarding cancer prevention or simultaneous treatment of HIV and cancer and substandard cancer care, indicates an urgent need for large-scale epidemiological studies addressing the question about the effect of particular HAART drugs and their dosage on cancer prevention. Furthermore, the inclusion of people with HIV in clinical trials of antineoplastic treatments should be encouraged.

Acknowledgements

This work was supported by grants from Plan Cancer (ENVIBURKITT), ANRS and LNCC to YV. AS was supported by a short-term fellowship from the Boehringer Ingelheim Fonds. These funding sources had no role in the writing of the manuscript or the decision to submit it for publication. YV confirms having full access to all the data in the study and having final responsibility for the decision to submit for publication.

References

1. HIV-CAUSAL Collaboration, Ray M, Logan R, et al. The effect of combined antiretroviral therapy on the overall mortality of HIV-infected individuals. *AIDS* 2010;24:123–37.
2. Powles T, Robinson D, Stebbing J, et al. Highly active antiretroviral therapy and the incidence of non–AIDS-defining cancers in people with HIV infection. *J Clin Oncol* 2009;27:884–90.
3. Coghill AE, Shiels MS, Suneja G, et al. Elevated cancer-specific mortality among HIV-infected patients in the United States. *J Clin Oncol* 2015;33:2376–83.
4. Engels EA, Yanik EL, Wheeler W, et al. Cancer-attributable mortality among people with treated human immunodeficiency virus infection in North America. 2017;65:636–43.
5. Goehringer F, Bonnet F, Salmon D, et al. Causes of death in HIV-infected individuals with immunovirologic success in a National Prospective Survey. *AIDS Res Hum Retroviruses* 2017;33:187–93.
6. Crum-Cianflone N, Hullsiek KH, Marconi V, et al. Trends in the incidence of cancers among HIV-infected persons and the impact of antiretroviral therapy: a 20-year cohort study. *AIDS* 2009;23:41–50.
7. Franceschi S, Lise M, Clifford GM, et al. Swiss HIV cohort Study the SHC. Changing patterns of cancer incidence in the early- and late-HAART periods: the Swiss HIV cohort Study. *Br J Cancer* 2010;103:416–22.
8. Park LS, Tate JP, Sigel K, et al. Time trends in cancer incidence in persons living with HIV/AIDS in the antiretroviral therapy era: 1997-2012. *AIDS* 2016;30:1795–806.

9. Hernández-Ramírez RU, Shiels MS, Dubrow R, et al. Cancer risk in HIV-infected people in the USA from 1996 to 2012: a population-based, registry-linkage study. *Lancet HIV* 2017;4: e495–504.
10. Hasse B, Ledergerber B, Furrer H, et al. Morbidity and aging in HIV-infected persons: the Swiss HIV cohort Study. *Clin Infect Dis* 2011;53: 1130–9.
11. Robbins HA, Pfeiffer RM, Shiels MS, et al. Excess cancers among HIV-infected people in the United States. *JNCI J Natl Cancer Inst* 2015; 107:dju503.
12. Hart BB, Nordell AD, Okulicz JF, et al. INSIGHT SMART and ESPRIT groups. Inflammation related morbidity and mortality among HIV-positive adults. JAIDS. *J Acquir Immune Defic Syndr* 2017;77:1.
13. Park LS, Hernández-Ramírez RU, Silverberg MJ, et al. Prevalence of non-HIV cancer risk factors in persons living with HIV/AIDS: a meta-analysis. *AIDS* 2016;30:273–91.
14. Berretta M, Di Francia R, Stanzione B, et al. New treatment strategies for HIV-positive cancer patients undergoing antiblastic chemotherapy. *Expert Opin Pharmacother* 2016;17:2391–403.
15. Franceschi S, Maso LD, Rickenbach M, et al. Kaposi sarcoma incidence in the Swiss HIV cohort Study before and after highly active antiretroviral therapy. *Br J Cancer* 2008;99:800–4.
16. Polesel J, Clifford GM, Rickenbach M, et al. Non-Hodgkin lymphoma incidence in the Swiss HIV cohort Study before and after highly active antiretroviral therapy. *AIDS* 2008;22:301–6.
17. Clifford GM, Polesel J, Rickenbach M, et al. Swiss HIV Cohort. Cancer risk in the Swiss HIV cohort Study: associations with immunodeficiency, smoking, and highly active antiretroviral therapy. *J Natl Cancer Inst* 2005;97:425–32.
18. Shiels MS, Engels EA. Evolving epidemiology of HIV-associated malignancies. *Curr Opin HIV AIDS* 2017;12:6–11.
19. Guiguet M, Boué F, Cadranel J, et al. Clinical epidemiology group of the FHDH-ANRS CO4 cohort. Effect of immunodeficiency, HIV viral load, and antiretroviral therapy on the risk of individual malignancies (FHDH-ANRS CO4): a prospective cohort study. *Lancet Oncol* 2009;10: 1152–9.
20. Dubrow R, Qin L, Lin H, et al. Association of CD4+ T-cell count, HIV-1 RNA viral load, and antiretroviral therapy with Kaposi sarcoma risk among HIV-infected persons in the United States and Canada. *J Acquir Immune Defic Syndr* 2017;75:382–90.
21. Guech-Ongey M, Simard EP, Anderson WF, et al. AIDS-related Burkitt lymphoma in the United States: what do age and CD4 lymphocyte patterns tell us about etiology and/or biology? *Blood* 2010;116:5600–4.
22. Sabattini E, Bacci F, Sagramoso C. WHO classification of tumours of haematopoietic and lymphoid tissues in 2008: an overview. *Pathologica* 2010;102:83–7.
23. Gibson TM, Morton LM, Shiels MS, et al. Risk of non-Hodgkin lymphoma subtypes in HIV-infected people during the HAART era: a population-based study. *AIDS* 2014;28:2313–8.
24. Howlader N, Shiels MS, Mariotto AB, et al. Contributions of HIV to non-Hodgkin lymphoma mortality trends in the United States. *Cancer Epidemiol Biomarkers Prev* 2016;25: 1289–96.
25. Hishima T, Oyaizu N, Fujii T, et al. Decrease in Epstein–Barr virus-positive AIDS-related lymphoma in the era of highly active antiretroviral therapy. *Microbes Infect* 2006;8:1301–7.
26. Gopal S, Patel MR, Yanik EL, et al. Temporal trends in presentation and survival for HIV-associated lymphoma in the antiretroviral therapy era. *J Natl Cancer Inst* 2013;105:1221–9.
27. Shiels MS, Islam JY, Rosenberg PS, et al. Projected Cancer incidence rates and burden of incident Cancer cases in HIV-infected adults in the United States through 2030. *Ann Intern Med* 2018;168:866–73.
28. Nicolè S, Mengoli C, Marini G, et al. Characteristics of AIDS-related and non-AIDS-related cancers in an Italian cohort of HIV patients in the period 1996–2018. *J Int AIDS Soc* 2018;21 (S8):124.
29. Cobucci RNO, Lima PH, de Souza PC, et al. Cornetta M da C de M, Fernandes JV, Gonçalves AK. Assessing the impact of HAART on the incidence of defining and non-defining AIDS cancers among patients with HIV/AIDS: a systematic review. *J Infect Public Health* 2015; 8:1–10.
30. Schmidt C. The Cancer-HIV/AIDS treatment conundrum. *JNCI J Natl Cancer Inst* 2010;102: 1615–7.
31. Silverberg MJ, Chao C, Leyden WA, et al. HIV infection, immunodeficiency, viral replication, and the risk of Cancer. *Cancer Epidemiol Biomarkers Prev* 2011;20:2551–9.
32. Baker JV, Peng G, Rapkin J, et al. Terry Beirn community programs for clinical research on AIDS (CPCRA). CD4+ count and risk of non-AIDS diseases following initial treatment for HIV infection. *AIDS* 2008;22:841–8.
33. Monforte A, Abrams D, Pradier C, et al. Data collection on adverse events of anti-HIV drugs (D:a:D) Study group. HIV-induced immunodeficiency and mortality from AIDS-defining and non-AIDS-defining malignancies. *AIDS* 2008;22: 2143–53.
34. Kesselring A, Gras L, Smit C, et al. Immunodeficiency as a risk factor for non-AIDS-defining malignancies in HIV-1-infected patients receiving combination antiretroviral therapy. *Clin Infect Dis* 2011;52:1458–65.
35. Bedimo RJ, McGinnis KA, Dunlap M, et al. Incidence of non-AIDS-defining malignancies in HIV-infected versus noninfected patients in the HAART era: impact of immunosuppression. *J Acquir Immune Defic Syndr* 2009;52:203–8.
36. Engels EA, Brock MV, Chen J, et al. Elevated incidence of lung Cancer among HIV-infected individuals. *J Clin Oncol* 2006;24:1383–8.
37. Shiels MS, Cole SR, Mehta SH, et al. Lung Cancer incidence and mortality among HIV-infected and HIV-uninfected injection drug users. *JAIDS J Acquir Immune Defic Syndr* 2010;55:510–5.
38. Reid E, Suneja G, Ambinder RF, et al. Cancer in people living with HIV, version 1.2018, NCCN clinical practice guidelines in oncology. *J Natl Compr Cancer Netw* 2018;16:986–1017.
39. Coghill AE, Engels EA, Schymura MJ, et al. Risk of breast, prostate, and colorectal Cancer diagnoses among HIV-infected individuals in the United States. *J Natl Cancer Inst* 2018;110: 959–66.
40. Patel P, Hanson DL, Sullivan PS, et al. Incidence of types of cancer among HIV-infected persons compared with the general population in the United States, 1992-2003. *Ann Intern Med* 2008; 148:728–36.
41. Dauby N, De Wit S, Delforge M, et al. Characteristics of non-AIDS-defining malignancies in the HAART era: a clinico-epidemiological study. *J Int AIDS Soc* 2011;14:16.
42. Marcus JL, Chao CR, Leyden WA, et al. Prostate Cancer incidence and prostate-specific antigen testing among HIV-positive and HIV-negative men. *JAIDS J Acquir Immune Defic Syndr* 2014; 66:495–502.
43. Stone TW, McPherson M, Gail Darlington L. Obesity and Cancer: existing and new hypotheses for a causal connection. *EBioMedicine* 2018; 30:14–28.
44. Trushin SA, Algeciras-Schimnich A, Vlahakis SR, et al. Glycoprotein 120 binding to CXCR4 causes p38-dependent primary T cell death that is facilitated by, but does not require cell-associated CD4. *J Immunol* 2007;178:4846–53.
45. Anand AR, Ganju RK. HIV-1 gp120-mediated apoptosis of T cells is regulated by the membrane tyrosine phosphatase CD45. *J Biol Chem* 2006;281:12289–99.
46. Cummins NW, Badley AD. Mechanisms of HIV-associated lymphocyte apoptosis: 2010. *Cell Death Dis* 2010;1:e99.
47. Liu Z, Qiao L, Zhang Y, et al. ASPP2 plays a dual role in gp120-induced autophagy and apoptosis of neuroblastoma cells. *Front Neurosci* 2017;11:150.
48. Endo M, Inatsu A, Hashimoto K, et al. Human immunodeficiency virus-induced apoptosis of human breast cancer cells via CXCR4 is mediated by the viral envelope protein but does not require CD4. *Curr HIV Res* 2008;6:34–42.
49. Bumpers HL, Huang M-B, Powell M, et al. Effects of HIV-1 Nef, a cytotoxic viral protein, on the growth of primary colorectal cancer. *Cancer Biol Ther* 2005;4:72–6.
50. Harrington W, Bond V, Huang MB, et al. HIV Nef-M1 effects on colorectal Cancer growth in tumor-induced spleens and hepatic metastasis. *Mol Cell Pharmacol* 2009;1:85–91.
51. Singh S, Bond VC, Powell M, et al. CXCR4-gp120-IIIB interactions induce caspase-mediated apoptosis of prostate cancer cells and inhibit tumor growth. *Mol Cancer Ther* 2009;8: 178–84.
52. Marcus JL, Chao C, Leyden WA, et al. Survival among HIV-infected and HIV-uninfected individuals with common non-AIDS-defining cancers. *Cancer Epidemiol Biomarkers Prev* 2015;24:1167–73.
53. Coghill AE, Pfeiffer RM, Shiels MS, et al. Excess mortality among HIV-infected individuals with Cancer in the United States. *Cancer Epidemiol Biomarkers Prev* 2017;26:1027–33.
54. Zucchetto A, Virdone S, Taborelli M, et al. Non-AIDS-defining Cancer mortality. *JAIDS J Acquir Immune Defic Syndr* 2016;73:190–6.
55. Suneja G, Shiels MS, Angulo R, et al. Cancer treatment disparities in HIV-infected individuals in the United States. *J Clin Oncol* 2014;32:2344–50.
56. Hleyhel M, Belot A, Bouvier A-M, et al. Trends in survival after cancer diagnosis among HIV-infected individuals between 1992 and 2009. Results from the FHDH-ANRSCO4 cohort. *Int J Cancer* 2015;137:2443–53.

57. Cingolani A, Cozzi Lepri A, Teofili L, et al. Survival and predictors of death in people with HIV-associated lymphoma compared to those with a diagnosis of lymphoma in general population. *PLoS One* 2017;12:e0186549.
58. Dryden-Peterson S, Bvochora-Nsingo M, Suneja G, et al. HIV infection and survival among women with cervical cancer. *J Clin Oncol* 2016;34:3749–57.
59. Leitch H, Trudeau M, Routy J-P. Effect of protease inhibitor-based highly active antiretroviral therapy on survival in HIV-associated advanced Kaposi's sarcoma patients treated with chemotherapy. *HIV Clin Trials* 2003;4:107–14.
60. Hoffmann C, Tabrizian S, Wolf E, et al. Survival of AIDS patients with primary central nervous system lymphoma is dramatically improved by HAART-induced immune recovery. *AIDS* 2001; 15:2119–27.
61. Castillo JJ, Echenique IA. Rituximab in combination with chemotherapy versus chemotherapy alone in HIV-associated non-Hodgkin lymphoma: a pooled analysis of 15 prospective studies. *Am J Hematol* 2012;87:330–3.
62. Uldrick TS, Pipkin S, Scheer S, et al. Risk factors for death and temporal trends in overall survival in patients with AIDS-associated primary central nervous system lymphoma (AIDS-PCNSL). *Infect Agent Cancer* 2012;7(S1):O18.
63. Vaccher E, Spina M, di Gennaro G, et al. Concomitant cyclophosphamide, doxorubicin, vincristine, and prednisone chemotherapy plus highly active antiretroviral therapy in patients with human immunodeficiency virus-related, non-Hodgkin lymphoma. *Cancer* 2001;91:155–63.
64. Martinez V, Caumes E, Gambotti L, et al. Remission from Kaposi's sarcoma on HAART is associated with suppression of HIV replication and is independent of protease inhibitor therapy. *Br J Cancer* 2006;94:1000–6.
65. Wong AYJ, Marcotte S, Laroche M, et al. Safety and efficacy of CHOP for treatment of diffuse large B-cell lymphoma with different combination antiretroviral therapy regimens: SCULPT study. *Antivir Ther* 2013;18:699–707.
66. Ibrahim K, Milliken S. Protease Inhibitor vs. non-protease inhibitor based antiretroviral therapy in HIV-infected patients with Hodgkin and non-Hodgkin lymphoma receiving chemotherapy. *Blood* 2013;122:3843.
67. Cattelan AM, Calabrò ML, Gasperini P, et al. Acquired immunodeficiency syndrome-related Kaposi's sarcoma regression after highly active antiretroviral therapy: biologic correlates of clinical outcome. *J Natl Cancer Inst Monogr* 2001; (28): 44–49
68. Pinto-Almeida T, Torres T, Rosmaninho A, et al. Letter: Penile Kaposi sarcoma: a case of complete resolution with highly active antiretroviral therapy alone. *Dermatol Online J* 2011;17:12.
69. Kumarasamy N, Venkatesh KK, Devaleenol B, et al. Regression of Kaposi's sarcoma lesions following highly active antiretroviral therapy in an HIV-infected patient. *Int J STD AIDS* 2008;19: 786–8.
70. Leder HA, Galor A, Peters GB, et al. Resolution of conjunctival Kaposi sarcoma after institution of highly active antiretroviral therapy alone. *Br J Ophthalmol* 2008;92:151.
71. Hallit RR, Afridi M, Sison R, et al. AIDS-related lymphoma: resolution with antiretroviral therapy alone. *J Int Assoc Provid AIDS Care* 2014;13: 313–5.
72. Lim DH, Rhee J-Y, Park KW. Stage IV advanced diffuse large B-cell lymphoma in human immunodeficiency virus infection with achieving cure by using highly active antiretroviral therapy alone: a case report. *Int J STD AIDS* 2017;28:932–6.
73. Travi G, Ferreri AJM, Cinque P, et al. Long-term remission of HIV-associated primary CNS lymphoma achieved with highly active antiretroviral therapy alone. *J Clin Oncol* 2012;30:e119–21.
74. Katsidzira L, Ramsay A, Makunike-Mutasa R, et al. Complete regression of early diffuse B-cell lymphoma in an HIV-positive patient on antiretroviral therapy alone. *Int J STD AIDS* 2011;22: 409–10.
75. Heard I, Schmitz V, Costagliola D, et al. Early regression of cervical lesions in HIV-seropositive women receiving highly active antiretroviral therapy. *AIDS* 1998;12:1459–64.
76. Blitz S, Baxter J, Raboud J, et al. Canadian Women's HIV Study group. Evaluation of HIV and highly active antiretroviral therapy on the natural history of human papillomavirus infection and cervical cytopathologic findings in HIV-positive and high-risk HIV-negative women. 2013;208.
77. Mosam A, Shaik F, Uldrick TS, et al. A randomized controlled trial of highly active antiretroviral therapy versus highly active antiretroviral therapy and chemotherapy in therapy-naive patients with HIV-associated Kaposi sarcoma in South Africa. *JAIDS J Acquir Immune Defic Syndr* 2012;60:150–7.
78. Sombogaard F, Franssen EJF, Terpstra WE, et al. Outcome effects of antiretroviral drug combinations in HIV-positive patients with chemotherapy for lymphoma: a retrospective analysis. *Int J Clin Pharmacol* 2018;40:1402–8.
79. Lim ST, Karim R, Nathwani BN, et al. AIDS-related Burkitt's lymphoma versus diffuse large-cell lymphoma in the pre-highly active antiretroviral therapy (HAART) and HAART eras: significant differences in survival with standard chemotherapy. *J Clin Oncol* 2005;23:4430–8.
80. Simcock M, Blasko M, Karrer U, et al. Swiss HIV cohort Study. Treatment and prognosis of AIDS-related lymphoma in the era of highly active antiretroviral therapy: findings from the Swiss HIV cohort Study. *Antivir Ther* 2007;12:931–9.
81. Olszewski AJ, Castillo JJ. Outcomes of HIV-associated Hodgkin lymphoma in the era of antiretroviral therapy. *AIDS* 2016;30:787–96.
82. Chiao EY, Giordano TP, Richardson P, et al. Human immunodeficiency virus-associated squamous cell cancer of the anus: epidemiology and outcomes in the highly active antiretroviral therapy era. *J Clin Oncol* 2008;26:474–9.
83. Kato T, Ieki R, Saito E, et al. A long-term survival case of small cell lung cancer in an HIV-infected patient. *Jpn J Clin Oncol* 2005;35: 349–52.
84. Modest GA, Cooley TP, Zacks JF. HIV and refractory anemia with excess blasts (RAEB). *Am J Hematol* 2002;70:318–9.
85. Leng LK, Pancharoen C, Bunupuradah T, et al. Regression of a cervical spinal mass following highly active antiretroviral therapy (HAART) in child with advanced human immunodeficiency virus (HIV) disease. *J Med Assoc Thai* 2007;90: 1937–42.
86. Vilchez RA, Finch CJ, Jorgensen JL, et al. The clinical epidemiology of Hodgkin lymphoma in HIV-infected patients in the highly active antiretroviral therapy (HAART) era. *Medicine (Baltimore)* 2003;82:77–81.
87. Lavolé A, Chouaïd C, Baudrin L, et al. Effect of highly active antiretroviral therapy on survival of HIV infected patients with non-small-cell lung cancer. *Lung Cancer* 2009;65:345–50.
88. Rudek MA, Moore PC, Mitsuyasu RT, et al. A phase 1/pharmacokinetic study of sunitinib in combination with highly active antiretroviral therapy in human immunodeficiency virus-positive patients with cancer: AIDS malignancy consortium trial AMC 061. *Cancer* 2014;120:1194–202.
89. Berretta M, Caraglia M, Martellotta F, et al. Drug-drug interactions based on pharmacogenetic profile between highly active antiretroviral therapy and Antiblastic chemotherapy in Cancer patients with HIV infection. *Front Pharmacol* 2016;7:71.
90. Torres HA, Rallapalli V, Saxena A, et al. Efficacy and safety of antiretrovirals in HIV-infected patients with cancer. *Clin Microbiol Infect* 2014;20:O672–9.
91. Mounier N, Katlama C, Costagliola D, et al. Drug interactions between antineoplastic and antiretroviral therapies: implications and management for clinical practice. *Crit Rev Oncol Hematol* 2009;72:10–20.
92. Deeken JF, Pantanowitz L, Dezube BJ. Targeted therapies to treat non-AIDS-defining cancers in patients with HIV on HAART therapy: treatment considerations and research outlook. *Curr Opin Oncol* 2009;21:445–54.
93. Di Francia R, Fierro C, Di Paolo M. Selected pharmacogenetic panel test for toxicity prevention of drug-drug interactions between highly active antiretroviral therapy (HAART) and antiblastic. *World Cancer Res J* 2015;2:e492.
94. Department of Health and Human Services. Panel on antiretroviral guidelines for adults and adolescents. *Guidelines for the use of antiretroviral agents in adults and adolescents with HIV*. Washington, DC: Department of Health and Human Services, 2019.
95. Crum-Cianflone NF, Hullsiek KH, Marconi V, et al. The impact of nelfinavir exposure on cancer development among a large cohort of HIV-infected patients. *J Acquir Immune Defic Syndr* 2009;51:305–9.
96. Boettiger DC, Sabin CA, Grulich A, et al. Data collection on adverse events of anti-HIV drugs (D:a:D) study group. Is nelfinavir exposure associated with cancer incidence in HIV-positive individuals? *AIDS* 2016;30:1629–37.
97. Bruyand M, Ryom L, Shepherd L, et al. Cancer risk and use of Protease Inhibitor or non-nucleoside reverse transcriptase Inhibitor–based combination antiretroviral therapy. *JAIDS J Acquir Immune Defic Syndr* 2015;68: 568–77.
98. Bohlius J, Valeri F, Maskew M, et al. Kaposi's sarcoma in HIV-infected patients in South Africa: multicohort study in the antiretroviral therapy era. *Int J Cancer* 2014;135:2644–52.
99. Mocroft A, Kirk O, Clumeck N, et al. The changing pattern of Kaposi sarcoma in patients with HIV, 1994-2003. *Cancer* 2004;100:2644–54.
100. Chao C, Leyden WA, Xu L, et al. Exposure to antiretroviral therapy and risk of cancer in HIV-infected persons. *AIDS* 2012;26:2223–31.

101. Lodi S, Guiguet M, Costagliola D, et al. CASCADE collaboration the C. Kaposi sarcoma incidence and survival among HIV-infected homosexual men after HIV seroconversion. *J Natl Cancer Inst* 2010;102:784–92.
102. Burgi A, Brodine S, Wegner S, et al. Incidence and risk factors for the occurrence of non-AIDS-defining cancers among human immunodeficiency virus-infected individuals. *Cancer* 2005; 104:1505–11.
103. Clifford GM, Rickenbach M, Lise M, et al. Hodgkin lymphoma in the Swiss HIV cohort Study. *Blood* 2009;113:5737–42.
104. Bohlius J, Schmidlin K, Boué F, et al. Collaboration of Observational HIV Epidemiological Research Europe. HIV-1-related Hodgkin lymphoma in the era of combination antiretroviral therapy: incidence and evolution of $CD4^+$ T-cell lymphocytes. *Blood* 2011;117:6100–8.
105. Lanoy E, Rosenberg PS, Fily F, et al. HIV-associated Hodgkin lymphoma during the first months on combination antiretroviral therapy. *Blood* 2011;118:44–9.
106. Cheng Z, Shan F, Liu J, et al. Clinical and computed tomography findings in Chinese lung cancer patients with HIV infection: a multi-center study. *Thorac cancer* 2017;8:238–45.
107. Bruyand M, Le Marec F, Lavole A, et al. Protease inhibitors exposure is not related to lung cancer risk in HIV smoker patients: a nested case-control study. *AIDS* 2015;29:1105–9.
108. Kirk GD, Merlo C, O'Driscoll P, et al. HIV infection is associated with an increased risk for lung cancer, independent of smoking. *Clin Infect Dis* 2007;45:103–10.
109. van der Snoek EM, van der Ende ME, den Hollander JC, et al. Use of highly active antiretroviral therapy is associated with lower prevalence of anal intraepithelial neoplastic lesions and lower prevalence of human papillomavirus in HIV-infected men who have sex with men. *Sex Transm Dis* 2012;39:495–500.
110. Duncan KC, Chan KJ, Chiu CG, et al. HAART slows progression to anal cancer in HIV-infected MSM. *AIDS* 2015;29:305–11.
111. Crum-Cianflone NF, Hullsiek KH, Marconi VC, et al. Infectious disease clinical research program HIV working group. Anal cancers among HIV-infected persons: HAART is not slowing rising incidence. *AIDS* 2010;24:535–43.
112. Pappou EP, Magruder JT, Fu T, et al. Prognostic and predictive clinicopathologic factors of squamous Anal Canal Cancer in HIV-positive and HIV-negative patients: does HAART influence outcomes? *World J Surg* 2018;42:876–83.
113. Sahasrabuddhe VV, Shiels MS, McGlynn KA, et al. The risk of hepatocellular carcinoma among individuals with acquired immunodeficiency syndrome in the United States. *Cancer* 2012;118:6226–33.
114. Olivero OA. Mechanisms of genotoxicity of nucleoside reverse transcriptase inhibitors. *Environ Mol Mutagen* 2007;48:215–23.
115. Benhammou V, Warszawski J, Bellec S, et al. Incidence of cancer in children perinatally exposed to nucleoside reverse transcriptase inhibitors. *AIDS* 2008;22:2165–77.
116. Brogly S, Williams P, Seage GR, et al. In utero nucleoside reverse transcriptase inhibitor exposure and cancer in HIV-uninfected children: an update from the pediatric AIDS clinical trials group 219 and 219C cohorts. *J Acquir Immune Defic Syndr* 2006;41:535–6.
117. Hleyhel M, Goujon S, Delteil C, et al. ANRS French perinatal cohort Study group. Risk of cancer in children exposed to didanosine in utero. *AIDS* 2016;30:1245–56.
118. Hleyhel M, Goujon S, Sibiude J, et al. Risk of cancer in children exposed to antiretroviral nucleoside analogues *in utero*: the French experience. *Environ Mol Mutagen* 2017;60:404–9.
119. Portsmouth S, Stebbing J, Gill J, et al. A comparison of regimens based on non-nucleoside reverse transcriptase inhibitors or protease inhibitors in preventing Kaposi's sarcoma. *AIDS* 2003; 17:F17–22.
120. Stebbing J, Portsmouth S, Nelson M, et al. The efficacy of ritonavir in the prevention of AIDS-related Kaposi's sarcoma. *Int J Cancer* 2004;108:631–3.
121. Gantt S, Cattamanchi A, Krantz E, et al. Reduced human herpesvirus-8 oropharyngeal shedding associated with protease inhibitor-based antiretroviral therapy. *J Clin Virol* 2014;60:127–32.
122. Gill J, Bourboulia D, Wilkinson J, et al. Prospective study of the effects of antiretroviral therapy on Kaposi sarcoma-associated herpesvirus infection in patients with and without Kaposi sarcoma. *J Acquir Immune Defic Syndr* 2002;31: 384–90.
123. Bani-Sadr F, Fournier S, Molina JM. Relapse of Kaposi's sarcoma in HIV-infected patients switching from a protease inhibitor to a non-nucleoside reverse transcriptase inhibitor-based highly active antiretroviral therapy regimen. *AIDS* 2003;17:1580–1.
124. Paparizos VA, Kyriakis KP, Kourkounti S, et al. The influence of a HAART regimen on the expression of HIV-associated Kaposi sarcoma. *J Acquir Immune Defic Syndr* 2008;49:111.
125. Ridolfo AL, Corbellino M, Tosca N, et al. Is switching protease inhibitor-based effective antiretroviral therapy safe in patients with AIDS-associated Kaposi's sarcoma? *AIDS* 2004;18: 1224–6.
126. Philibert P, Chiche L, Caillères S, et al. HHV8 and Kaposi's sarcoma: should we really give up protease inhibitors in all HIV-infected patients? *AIDS* 2017;31:2167–9.
127. Simonetti FR, Ricaboni D, Cattaneo D, et al. Relapse of Kaposi's sarcoma and HHV-8 viremia in an HIV-infected patient switching from protease inhibitor to integrase inhibitor-based antiretroviral therapy. *J Clin Virol* 2016;74:75–7.
128. Cozzi-Lepri A, Zangerle R, Machala L, et al. Incidence of cancer and overall risk of mortality in individuals treated with raltegravir-based and non-raltegravir-based combination antiretroviral therapy regimens. *HIV Med* 2018;19:102–17.
129. Gulick RM, Su Z, Flexner C, et al. Phase 2 Study of the safety and efficacy of Vicriviroc, a CCR5 Inhibitor, in HIV-1–infected, treatment-experienced patients: AIDS Clinical Trials Group 5211. *J Infect Dis* 2007;196:304–12.
130. Caseiro MM, Nelson M, Diaz RS, et al. Vicriviroc plus optimized background therapy for treatment-experienced subjects with CCR5 HIV-1 infection: final results of two randomized phase III trials. *J Infect* 2012;65:326–35.
131. Gulick RM, Fatkenheuer G, Burnside R, et al. Five-year safety evaluation of maraviroc in HIV-1-infected treatment-experienced patients. *J Acquir Immune Defic Syndr* 2014;65:78–81.
132. Krishnan S, Schouten JT, Jacobson DL, et al. Incidence of non-AIDS-defining cancer in antiretroviral treatment-naïve subjects after antiretroviral treatment initiation: an ACTG longitudinal linked randomized trials analysis. *Oncology* 2011;80:42–9.
133. Mbang PA, Kowalkowski MA, Amirian ES, et al. Association between time on Protease inhibitors and the incidence of squamous cell carcinoma of the anus among U.S. male veterans. *PLoS One* 2015;10:e0142966.
134. Lusivika-Nzinga C, Selinger-Leneman H, Grabar S, et al. Performance of the marginal structural cox model for estimating individual and joined effects of treatments given in combination. *BMC Med Res Methodol* 2017;17:160.
135. Grabar S, Selinger-Leneman H, Abramowitz L, et al. Anal cancer risk and use of a protease inhibitor: a nested case-control study within the ANRS CO4-FHDH cohort. *J Int AIDS Soc* 2018; 21(S8):121–2.
136. Gills JJ, LoPiccolo J, Tsurutani J, et al. Nelfinavir, a Lead HIV Protease Inhibitor, is a broad-Spectrum, anticancer agent that induces endoplasmic reticulum stress, autophagy, and apoptosis in vitro and in vivo. *Clin Cancer Res* 2007;13:5183–94.
137. Srirangam A, Mitra R, Wang M, et al. Effects of HIV protease inhibitor ritonavir on Akt-regulated cell proliferation in breast cancer. *Clin Cancer Res* 2006;12:1883–96.
138. Shim JS, Rao R, Beebe K, et al. Selective inhibition of HER2-positive breast Cancer cells by the HIV Protease Inhibitor nelfinavir. *JNCI J Natl Cancer Inst* 2012;104:1576–90.
139. Soprano M, Sorriento D, Rusciano MR, et al. Oxidative stress mediates the antiproliferative effects of nelfinavir in breast cancer cells. *PLoS One* 2016;11:e0155970.
140. Koltai T. Nelfinavir and other protease inhibitors in cancer: mechanisms involved in anticancer activity. *F1000Research* 2015;4:9.
141. Maksimovic-Ivanic D, Fagone P, McCubrey J, et al. HIV-protease inhibitors for the treatment of cancer: repositioning HIV protease inhibitors while developing more potent NO-hybridized derivatives? *Int J Cancer* 2017;140:1713–26.
142. Bernstein WB, Dennis PA. Repositioning HIV protease inhibitors as cancer therapeutics. *Curr Opin HIV AIDS* 2008;3:666–75.
143. Goda J, Pachpor T, Basu T, et al. Targeting the AKT pathway: repositioning HIV protease inhibitors as radiosensitizers. *Indian J Med Res* 2016; 143:145–59.
144. Faes S, Dormond O. PI3K and AKT: unfaithful Partners in Cancer. *Int J Mol Sci* 2015;16: 21138–52.
145. Radisavljevic Z. AKT as locus of cancer phenotype. *J Cell Biochem* 2015;116:1–5.
146. Martini M, De Santis MC, Braccini L, et al. PI3K/AKT signaling pathway and cancer: an updated review. *Ann Med* 2014;46:372–83.
147. Polivka J, Janku F. Molecular targets for cancer therapy in the PI3K/AKT/mTOR pathway. *Pharmacol Ther* 2014;142:164–75.
148. Zheng H-C. The molecular mechanisms of chemoresistance in cancers. *Oncotarget* 2017;8: 59950–64.
149. Farrand L, Oh S-W, Song YS, et al. Phytochemicals: a multitargeted approach to gynecologic cancer therapy. *Biomed Res Int* 2014;2014: 890141.

150. Miyata Y, Nakamoto H, Neckers L. The therapeutic target Hsp90 and cancer hallmarks. *Curr Pharm Des* 2013;19:347–65.
151. Kim JG, Lee SC, Kim O-H, et al. HSP90 inhibitor 17-DMAG exerts anticancer effects against gastric cancer cells principally by altering oxidant-antioxidant balance. *Oncotarget* 2017;8: 56473–89.
152. Manalo RVM, Medina PMB. The endoplasmic reticulum stress response in disease pathogenesis and pathophysiology. *Egypt J Med Hum Genet* 2018;19:59–68.
153. Arodola O, Soliman M. Could the FDA-approved anti-HIV PR inhibitors be promising anticancer agents? An answer from enhanced docking approach and molecular dynamics analyses. *Drug Des Dev Ther* 2015;9:6055.
154. Lutz WK. The Viracept (nelfinavir)–ethyl methanesulfonate case: a threshold risk assessment for human exposure to a genotoxic drug contamination? *Toxicol Lett* 2009;190:239–42.
155. Gantt S, Carlsson J, Ikoma M, et al. The HIV Protease Inhibitor nelfinavir inhibits Kaposi's sarcoma-associated herpesvirus replication in vitro. *Antimicrob Agents Chemother* 2011;55: 2696–703.
156. Brown JA, Pack LR, Fowler JD, et al. Pre-steady-state kinetic analysis of the incorporation of anti-HIV nucleotide analogs catalyzed by human X- and Y-family DNA polymerases. *Antimicrob Agents Chemother* 2011;55:276–83.
157. Perna A, Lucariello A, Sellitto C, et al. Different cell cycle modulation in SKOV-3 ovarian Cancer cell line by anti-HIV drugs. *Oncol Res Featur Preclin Clin Cancer Ther* 2017;25:1617–24.
158. Carlini F, Ridolfi B, Molinari A, et al. The reverse transcription inhibitor abacavir shows anticancer activity in prostate cancer cell lines. 2010;5:e14221.
159. Landriscina M, Spadafora C, Cignarelli M, et al. Anti-tumor activity of non-nucleosidic reverse transcriptase inhibitors. *Curr Pharm Des* 2007; 13:737–47.
160. Brüning A, Burger P, Gingelmaier A, et al. The HIV reverse transcriptase inhibitor tenofovir induces cell cycle arrest in human cancer cells. *Invest New Drugs* 2012;30:1389–95.
161. Crespan E, Garbelli A, Amoroso A, et al. Exploiting the nucleotide substrate specificity of repair DNA polymerases to develop novel anticancer agents. *Molecules* 2011;16:7994–8019.
162. Young MJ. Off-target effects of drugs that disrupt human mitochondrial DNA maintenance. *Front Mol Biosci* 2017;4:74.
163. Xiao-Jie L, Hui-Ying X, Qi X, et al. LINE-1 in cancer: multifaceted functions and potential clinical implications. *Genet Med* 2016;18:431–9.
164. Mangiacasale R, Pittoggi C, Sciamanna I, et al. Exposure of normal and transformed cells to nevirapine, a reverse transcriptase inhibitor, reduces cell growth and promotes differentiation. *Oncogene* 2003;22:2750–61.
165. Hecht M, Harrer T, Korber V, et al. Cytotoxic effect of Efavirenz in BxPC-3 pancreatic cancer cells is based on oxidative stress and is synergistic with ionizing radiation. *Oncol Lett* 2017;15: 1728–36.
166. Landriscina M, Bagalà C, Piscazzi A, et al. Nevirapine restores androgen signaling in hormone-refractory human prostate carcinoma cells both in vitro and in vivo. *Prostate* 2009;69:744–54.
167. Hecht M, Erber S, Harrer T, et al. Efavirenz has the highest anti-proliferative effect of non-nucleoside reverse transcriptase inhibitors against pancreatic cancer cells. *PLoS One* 2015; 10:e0130277.
168. Brüning A, Jückstock J, Kost B, et al. Induction of DNA damage and apoptosis in human leukemia cells by efavirenz. *Oncol Rep* 2017;37:617–21.
169. Sciamanna I, Landriscina M, Pittoggi C, et al. Inhibition of endogenous reverse transcriptase antagonizes human tumor growth. *Oncogene* 2005;24:3923–31.
170. Ulrike K, Markus H, Thomas H, et al. NNRTI-based antiretroviral therapy may increase risk of radiation induced side effects in HIV-1-infected patients. *Radiother Oncol* 2015;116:323–30.
171. Varadarajan J, McWilliams MJ, Hughes SH. Treatment with suboptimal doses of raltegravir leads to aberrant HIV-1 integrations. *Proc Natl Acad Sci USA* 2013;110:14747–52.
172. Varadarajan J, McWilliams MJ, Mott BT, et al. Drug resistant integrase mutants cause aberrant HIV integrations. *Retrovirology* 2016;13:71.
173. Williamson EA, Damiani L, Leitao A, et al. Targeting the transposase domain of the DNA repair component Metnase to enhance chemotherapy. *Cancer Res* 2012;72:6200–8.
174. Pervaiz A, Zepp M, Mahmood S, et al. CCR5 blockage by maraviroc: a potential therapeutic option for metastatic breast cancer. *Cell Oncol* 2018;42:93–106.
175. Casagrande N, Borghese C, Visser L, et al. CCR5 antagonism by maraviroc inhibits Hodgkin lymphoma microenvironment interactions and xenograft growth. *Haematologica* 2018;104: 564–75.
176. Velasco-Velazquez M, Jiao X, De La Fuente M, et al. CCR5 antagonist blocks metastasis of basal breast Cancer cells. *Cancer Res* 2012;72:3839–50.
177. Tanabe Y, Sasaki S, Mukaida N, et al. Blockade of the chemokine receptor, CCR5, reduces the growth of orthotopically injected colon cancer cells via limiting cancer-associated fibroblast accumulation. *Oncotarget* 2016;7:48335–45.
178. Sicoli D, Jiao X, Ju X, et al. CCR5 receptor antagonists block metastasis to bone of v-Src oncogene-transformed metastatic prostate cancer cell lines. *Cancer Res* 2014;74:7103–14.
179. Halama N, Zoernig I, Berthel A, et al. Tumoral immune cell exploitation in colorectal cancer metastases can be targeted effectively by anti-CCR5 therapy in Cancer patients. *Cancer Cell* 2016;29:587–601.
180. Monini P, Sgadari C, Grosso MG, et al. Clinical course of classic Kaposi's sarcoma in HIV-negative patients treated with the HIV protease inhibitor indinavir. *AIDS* 2009;23:534–8.
181. Brunner TB, Geiger M, Grabenbauer GG, et al. Phase I trial of the human immunodeficiency virus protease inhibitor nelfinavir and chemoradiation for locally advanced pancreatic cancer. *J Clin Oncol* 2008;26:2699–706.
182. Rengan R, Mick R, Pryma D, et al. A phase I trial of the HIV protease inhibitor nelfinavir with concurrent chemoradiotherapy for unresectable stage IIIA/IIIB non-small cell lung cancer: a report of toxicities and clinical response. *J Thorac Oncol* 2012;7:709–15.
183. Buijsen J, Lammering G, Jansen RLH, et al. Phase I trial of the combination of the Akt inhibitor nelfinavir and chemoradiation for locally advanced rectal cancer. *Radiother Oncol* 2013; 107:184–8.
184. Driessen C, Muller R, Novak U, et al. The HIV protease inhibitor nelfinavir in combination with bortezomib and dexamethasone (NVd) has excellent activity in patients with advanced, proteasome inhibitor-refractory multiple myeloma: a multicenter phase II trial (SAKK 39/13). 58th Annual Meeting of the American Society of Hematology, ASH 2016. December 3–6, 2016; 128
185. Blumenthal GM, Gills JJ, Ballas MS, et al. A phase I trial of the HIV protease inhibitor nelfinavir in adults with solid tumors. *Oncotarget* 2014;5:8161–72.
186. Alonso-Basanta M, Fang P, Maity A, et al. A phase I study of nelfinavir concurrent with temozolomide and radiotherapy in patients with glioblastoma multiforme. *J Neurooncol* 2014;116:365–72.
187. Wilson JM, Fokas E, Dutton SJ, et al. ARCII: a phase II trial of the HIV protease inhibitor nelfinavir in combination with chemoradiation for locally advanced inoperable pancreatic cancer. *Radiother Oncol* 2016;119:306–11.
188. Hampson L, Maranga IO, Masinde MS, et al. A Single-arm, proof-of-concept trial of Lopimune (Lopinavir/ritonavir) as a treatment for HPV-related pre-invasive cervical disease. *PLoS One* 2016; 11: e0147917.
189. Modoni S, Landriscina M, Fabiano A, et al. Reinduction of cell differentiation and 131I uptake in a poorly differentiated thyroid tumor in response to the reverse transcriptase (RT) inhibitor nevirapine. *Cancer Biother Radiopharm* 2007;22:289–95.
190. Landriscina M, Modoni S, Fabiano A, et al. Cell differentiation and iodine-131 uptake in poorly differentiated thyroid tumour in response to nevirapine. *Lancet Oncol* 2006;7:877–9.
191. Hoover AC, Milhem MM, Anderson CM, et al. Efficacy of nelfinavir as monotherapy in refractory adenoid cystic carcinoma: results of a phase II clinical trial. *Head Neck* 2015;37:722–6.
192. Houede N, Pulido M, Mourey L, et al. A phase II trial evaluating the efficacy and safety of efavirenz in metastatic castration-resistant prostate cancer. *Oncologist* 2014;19:1227–8.
193. Ahluwalia MS, Patton C, Stevens G, et al. Phase II trial of ritonavir/lopinavir in patients with progressive or recurrent high-grade gliomas. *J Neurooncol* 2011;102:317–21.
194. Mani D, Neil N, Israel R, et al. A retrospective analysis of AIDS-associated Kaposi's sarcoma in patients with undetectable HIV viral loads and CD4 counts greater than 300 cells/mm^3. *J Int Assoc Physicians AIDS Care (Chic)* 2009;8:279–85.
195. Engels EA, Biggar RJ, Hall HI, et al. Cancer risk in people infected with human immunodeficiency virus in the United States. *Int J Cancer* 2008;123:187–94.
196. van Leeuwen MT, Vajdic CM, Middleton MG, et al. Continuing declines in some but not all HIV-associated cancers in Australia after widespread use of antiretroviral therapy. *AIDS* 2009; 23:2183–90.
197. Wu Y, Yoder A. Chemokine coreceptor signaling in HIV-1 infection and pathogenesis. *PLoS Pathog* 2009;5:e1000520.
198. European AIDS Clinical Society. *EACS guidelines 9.1*. Brussels: European AIDS Clinical Society, 2018.

1.2 EBV

Since the introduction of cART in 1996 which blocks HIV replication and restores CD4+ T cell counts, people living with HIV experienced marked improvements in terms of mortality and quality of life. Nevertheless, the high prevalence of certain types of malignancies even after the successful introduction of cART suggests the possible role of factors other than immune suppression in the pathogenesis of HIV-associated neoplasms. One of these potentially contributing factors is the Epstein-Barr virus (EBV).

More than 90% of the human adult population is infected with Epstein-Barr virus (EBV) (Balfour et al. 2013; Levin et al. 2010; Smatti et al. 2017). People living with HIV are almost inevitably co-infected with EBV as well (Gianella et al. 2020; O'Sullivan et al. 2002; Ouedraogo et al. 2014), but due to the ubiquitous nature of EBV infection, the effect of EBV contribution to HIV pathology remains underseen and under-evaluated. Both EBV and HIV establish chronic persistent infection and regardless of integration (for HIV) or non-integration (for EBV) in the host genome, two viruses are exceedingly difficult to eradicate.

EBV has a strong association with human cancers (1-2% of human cancers) (Cohen 2000; Cohen et al. 2011; Tsurumi et al. 2005). After primary infection, EBV establishes a life-long latency in B cells and a very stable virus-host relationship with the possibility to reactivate following specific stimuli (Murata 2014). EBV is an established etiological factor for diseases of B and epithelial cells: infectious mononucleosis, Burkitt lymphoma (BL), Hodgkin's lymphomas (HL), nasopharyngeal (NPC) and gastric carcinoma, and post-transplant lymphoproliferative disorder (PTLD) (Pattle & Farrell 2006). EBV is also associated with diseases involving cells not directly targeted by the virus: breast and hepatocellular carcinoma, leiomyosarcoma and follicular dendritic sarcoma, T-cell malignancies and multiple autoimmune diseases, including multiple sclerosis (Cao et al. 2021; Kutok & Wang 2006; Levin et al. 2010; Robinson & Steinman 2022).

1.2.1 EBV genome structure

Also referred to as human herpesvirus 4 (HHV-4), EBV is a γ-herpesvirus, containing a double-stranded linear DNA genome of 170-175 kbp. The EBV genome exhibits a highly complex organisational structure, characterised by the presence of at least 85 viral genes, many of which are generated by alternative splicing of transcripts (**Figure 2A**). The EBV life cycle encompasses two distinct phases, latency and lytic replication and its gene products are typically classified as either latent or lytic, depending on the predominant phase of expression. EBV encodes for 10 latent proteins: six nuclear antigen proteins (Epstein-Barr nuclear antigen (EBNA) leader peptide (EBNA-LP), EBNA1, EBNA2, EBNA3A, EBNA3B, EBNA3C), three latent membrane proteins

(latent membrane protein 1 (LMP1), LMP2A, LMP2B) and one anti-apoptotic BHRF1 (the EBV Bcl2 homologue) (Amon & Farrell 2005; Kelly et al. 2009). During latency, the expression of EBNA genes is regulated by three distinct promoters, Cp, Wp, or Qp, while separate promoters drive LMP1 and LMP2A,2B transcription. One of two promoters, Cp or Wp, directs the transcription of all EBNA genes in a long primary transcript, which is subsequently processed into mature EBNA transcripts through alternative splicing (Bodescot & Perricaudet 1986; Woisetschlaeger et al. 1990). The expression of a single EBNA1 transcript is directed by the Qp promoter. In addition to latent proteins, two small non-coding RNAs, EBER1 and 2, are expressed during all forms of EBV latency and also during the lytic cycle (Skalsky & Cullen 2015). The non-coding RNAs expressed by EBV also include 25 pre-miRNAs that are clustered in the BHRF1 region (3 pre-miRNAs, located upstream and downstream of the BHRF1 protein-coding region) and BART region (22 pre-miRNAs) and give rise to at least 44 miRNAs (Münz 2019; Skalsky & Cullen 2015). Again, BART miRNAs are expressed in all forms of latency and during the lytic cycle; BHRF1 miRNAs are expressed during latency III, Wp-restricted latency, and partially during the lytic cycle (Amoroso et al. 2011; Kelly et al. 2009; Münz 2019; Skalsky & Cullen 2015; Xing & Kieff 2011).

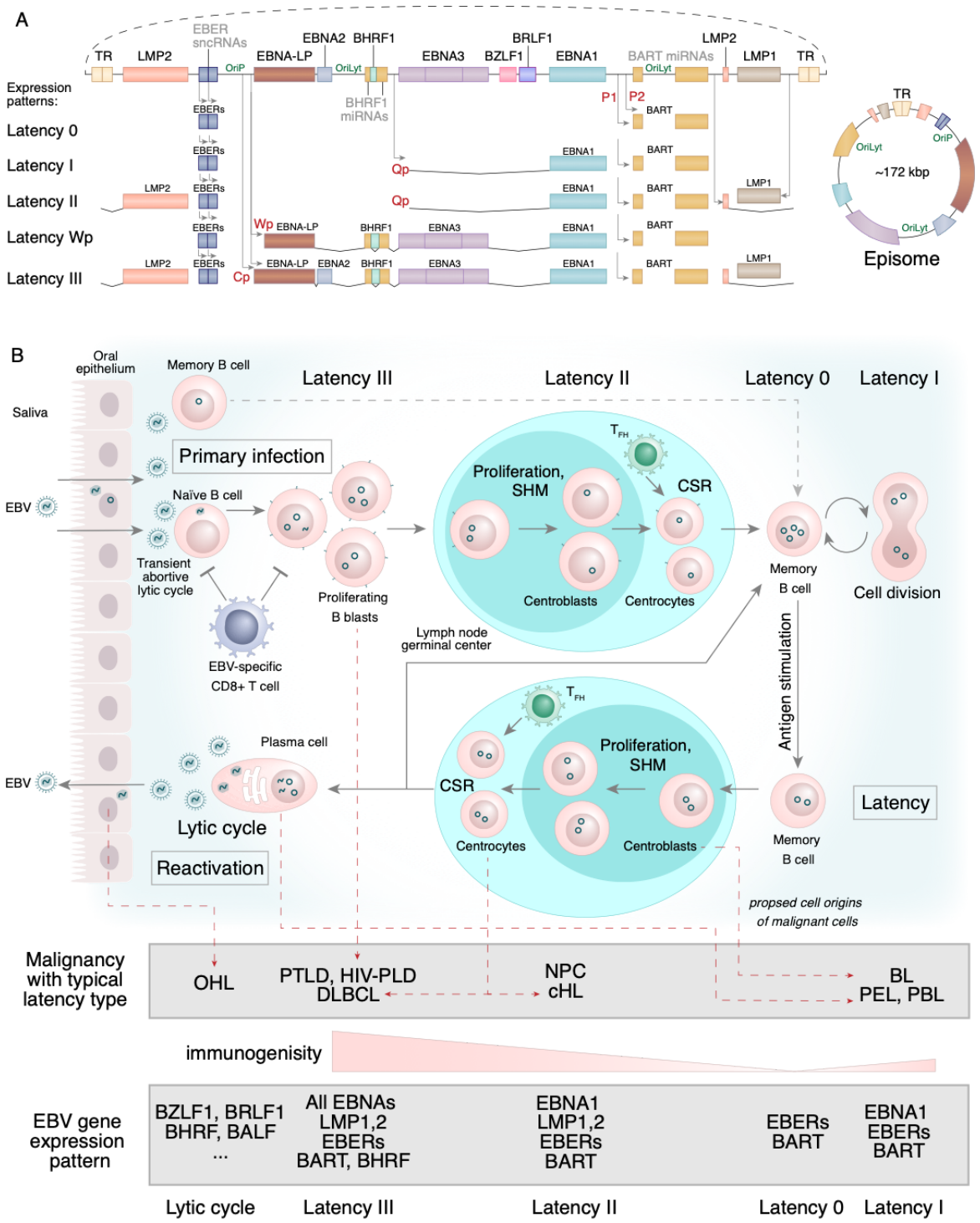

Figure 2. An overview of EBV genome structure and life cycle. **(A)** A simplified depiction of the ~172-kbp Epstein-Barr virus (EBV) genome showing the location of genes encoding the latent proteins (EBNA-LP, EBNA2, EBNA3 [A,B,C], LMP1, LMP2 [A,B], BHRF1), non-coding small RNAs (EBER1,2), miRNA regions (BHRF1 and BART) and the immediate early lytic proteins (BZLF1 and BRLF1). The arrows indicate gene promoters and the direction in which the genes are transcribed. EBNA gene promoters, Cp, Wp, or Qp, BART region promoters, P1 and P2, and the resulting transcripts characteristic for each latency type are shown. When transcribed from Cp or Qp promoters, the individual EBNAs mRNAs are generated by alternative splicing of the long primary transcript. The individual EBNA1 transcript originates from the Qp promoter. LMP2A and LMP2B are composed of several exons, which are located on either side of the terminal repeat (TR) region; they are brought

together after the circularization of the linear DNA to produce the viral episome. The origins of latent (OriP) and lytic replication (OriLyt) are shown in green. Expression patterns typical for each EBV latency are shown. In latency 0 no viral proteins are expressed, the only transcribed EBV genes are two non-coding small RNAs, EBER1 and 2, and BART miRNAs. Conventional latency I expresses a single protein EBNA1 transcribed from a Qp viral promoter, non-coding small RNAs, EBER1 and 2, and BART miRNAs. In latency II, LMP1 and LMP2A/B proteins are expressed in addition to Qp-driven EBNA1, EBER1, EBER2, BART, and none of the other EBNAs is expressed. Wp-restricted latency is characterised by the presence of an EBNA2-deleted EBV genome and expression of truncated EBNA-LP, EBNA1, EBNA3 (A,B,C), and BHRF1 from a Wp viral promoter, along with two non-coding small RNAs, EBER1 and 2, BHRF1 and BART miRNAs. In latency III, all EBNAs (1, 2, 3A, 3B, 3C, and -LP) are expressed from a Cp viral promoter, accompanied by the expression of LMPs 1, 2A, and 2B from their own promoters and low levels of BHRF1 protein (presumably, from weakly active Wp promoter (Kelly et al. 2009)), along with the expression of two non-coding small RNAs, EBER1 and 2, BART and BHRF1 miRNAs. **(B)** An overview of the EBV life cycle: primary infection, latency establishment, and reactivation from latency. During primary infection, EBV infects naïve B cells of the oropharyngeal mucosa, and after the initial replicative (lytic) phase of infection, the EBV genome circularises to be maintained as an episome. Infected naïve B cells turn into proliferative blasts (latency III), that are pushed to migrate into the germinal centre (GC) of secondary lymphoid organs, where they switch to latency II. In GC EBV-infected cells progressively differentiate into centroblasts, centrocytes, and, finally, memory B cells circulating in peripheral blood (latency 0). The homeostatic division of memory B cells shortly switches them to latency I. EBV has the ability to spontaneously reactivate and go through periods of lytic replication and particle shedding. Following antigenic stimulation and recruitment to GC, activated memory B cells differentiate into plasma cells, which reactivate the virus from latency and the EBV undergoes a productive lytic cycle. In some scenarios, EBV may be also able to infect a memory B cell subtype without the requirement for a GC reaction. Latency programs differ by expression patterns of specific viral proteins. Latency type 0 is characterised by the expression of two EBV-encoded small RNAs, EBER-1 and EBER-2. Latency type I is characterised by the expression of the viral nuclear antigen EBNA1. Latency type II is characterised by the expression of EBNA1 and latent membrane proteins LMP1 and LMP2. Latency type III is characterised by the expression of six nuclear antigens (EBNA1, EBNA2, EBNA3A, EBNA3B, EBNA3C, and EBNA-LP), three latent membrane proteins (LMP1, LMP2A, and LMP2B) and transcripts from the miRNA cluster BamHI-A region (BARTs). Abbreviations: BL, Burkitt's lymphoma; cHL, classical Hodgkin lymphoma; CSR, class-switch recombination; DLBCL, diffuse large B cell lymphoma; EBER, Epstein-Barr virus-encoded small RNAs; EBNA, Epstein-Barr nuclear antigen; LMP, latent membrane protein; NPC, nasopharyngeal carcinoma; OHL, oral hairy leukoplakia; oriLyt, the lytic replication origin; oriP, the latency-associated origin of episomal replication; PBL, plasmablastic lymphoma; PEL, primary effusion lymphoma; PTLD, post-transplant lymphoproliferative disorder; SHM, somatic hypermutation; sncRNA, small noncoding RNA.

In its linear form, the genome is flanked by terminal direct repeats that allow the circularization of EBV DNA upon host cell infection, leading to the establishment of a stable intracellular viral episome (Zimmermann & Hammerschmidt 1995). The promoter region and exons of LMP2 are located

at opposite ends of the linear genome and they are brought together after genome circularization, which allows the expression of both LMP2A and LMP2B isoforms (Laux et al. 1988; Sample et al. 1989) (**Figure 2A**). During latency, EBV genome replication occurs *via* the latency-associated origin of episomal replication, oriP (Hammerschmidt & Sugden 2013). Various stimuli can trigger EBV reactivation from latency, which will lead to a sequential expression of immediate-early, early, and late EBV lytic genes in a temporally regulated manner (lytic gene cascade of more than 80 viral genes). Two immediate early transcription factors (BZLF1 and BRLF1) jointly trigger the EBV lytic gene transcription, which eventually results in the production of new virions and lysis of infected cells (complete lytic cycle) or only in early lytic viral gene expression without virion production (abortive lytic cycle) (Schepers et al. 1993; Zalani et al. 1996). During lytic replication, the circular EBV genome is amplified *via* two lytic-associated origins of replication, oriLyt, giving rise to long head-to-tail concatemers of the genome that are subsequently processed within the TR region into linear unit-length EBV genomes and packaged into virion particles (Hammerschmidt & Sugden 2013; Schepers et al. 1993; Zimmermann & Hammerschmidt 1995).

1.2.2 EBV life cycle

EBV is mainly transmitted by oral transfer, the virus is extensively shed in saliva months/years after primary infection, and upon establishing life-long latency the virus continues to be shed intermittently at low levels (Dunmire et al. 2018). Primary infection is usually asymptomatic when it happens in early childhood or causes infectious mononucleosis when it happens in adolescence and young adulthood (Dunmire et al. 2018). Clinical manifestations of primary EBV infection can differ in children with HIV (Slyker et al. 2013).

In its life cycle, EBV efficiently exploits and mimics the natural pathway of antigen-activated B cell differentiation, eventually settling in the resting memory B cells for the lifetime of the host (Thorley-Lawson 2001). Each step of the EBV life cycle is characterised by the specific pattern of EBV gene expression (of both proteins and non-coding RNAs); these patterns are denoted as latency types or programs (**Figure 2B**). In primary infection, EBV infects naïve B cells of the oropharyngeal mucosa, possibly after the initial infection of oropharyngeal epithelial cells. B cell infection depends on CD21 or CD35 receptors (also known as complement receptor type 2 or type 1) and MHC class II as a co-receptor, while the epithelial cell infection presumably occurs via virus binding to ephrin receptor A2 and integrins (αVβ5, αVβ6, and αVβ8) and non-muscle myosin heavy chain IIA as cofactors (Chen et al. 2018; Li et al. 1997; Ogembo et al. 2013; Tanner et al. 1987; Zhang et al. 2018a). After the initial replicative (lytic) phase of infection, the EBV genome circularises to be maintained as a multicopy episome. Infected naïve B cells turn into proliferative blasts (latency III or the growth programme, analogous to that of

B cells transformed *in vitro* by EBV), and the stimulation of B blasts proliferation expands the pool of EBV-infected cells. Latency type III is characterised by the Cp-controlled expression of six nuclear antigens (EBNA1, EBNA2, EBNA3A, EBNA3B, EBNA3C, and EBNA-LP), Wp-controlled low-level expression of BHRF1 protein and the expression three latent membrane proteins (LMP1, LMP2A, and LMP2B) from their own promoters. Latency type III is typical for EBV-positive PTLD and DLBCL. Part of these cells migrates into the germinal centre (GC) of secondary lymphoid organs and switches to latency II (the default program). In latency II, Cp/Wp promoters are shut down, decreasing the panel of expressed EBV antigens to LMP1,2A,2B, and EBNA1 (expressed from Qp promoter). The latency type II program is typical for EBV-positive cHL. In GC, antigen-activated B cells undergo proliferation, class switch recombination and somatic hypermutation. EBV proteins LMP1 and LMP2, expressed in latency II, have been shown to possess the CD40 and B-cell receptor (BCR) signalling functions, respectively, and thus assist the survival of EBV-infected B cells in the GC (Mohamed et al. 2014). In GC EBV-infected cells progressively differentiate into centroblasts, centrocytes, and, finally, memory B cells circulating in peripheral blood. According to the current paradigm of persistent asymptomatic EBV infection, during primary infection, EBV-positive proliferative blasts are forced to develop into resting memory B cells, which shut down viral protein expression and evade immune monitoring. Thus, during primary infection, EBV-positive proliferative blasts are forced to develop into resting memory B cells, which shut down viral protein expression and evade immune surveillance.

Throughout life, EBV resides mainly in the long-lived memory B cells, and EBV viral load in memory B cells is much higher than that found in GC B cells isolated from the same donors (Chaganti et al. 2009). EBV-infected memory B cells express a minimal amount of EBV genes (latency 0, with only EBER and BART non-coding RNAs expressed) and are invisible to EBV-specific immune cells. The homeostatic division of memory B cells switches them to latency I, where EBNA1 is expressed, which permits EBV replication and the segregation of viral episomes to daughter cells. Latency type I is typical for EBV-positive BL. Additionally, a distinct so-called Wp-restricted latency pattern in BL was recently revealed: ~15% of BL carry mutant EBV genomes with EBNA2 deletions and employ the latency III-associated W promoter (Wp), expressing EBNA3A, 3B, 3C, and BHRF1 proteins and in some cases a truncated EBNA-LP in addition to EBNA1 (Kelly et al. 2002, 2009). Following antigenic stimulation and recruitment to GC, activated memory B cells differentiate into plasma cells, which reactivate the virus from latency and EBV undergoes a productive lytic cycle, re-infecting new naïve B cells (Germini et al. 2020; Vockerodt et al. 2015). In some scenarios, EBV may be also able to infect a memory B cell subtype without the requirement for a GC reaction (Vockerodt et al. 2015). Despite a clearly established correlation between the stage of B cell

development and EBV gene expression pattern, the mechanisms responsible for the switch between EBV latency types remain largely unknown.

Rarely EBV-positive cells can be detected undergoing LMP1/2-independent expansion in GC, forming a condition called lymphoid hyperplasia with EBV-positive GCs, this condition is typical for immunosuppressed individuals as people living with HIV (Martín et al. 2011; Mohamed et al. 2014; Vockerodt et al. 2015).

The interplay between EBV and HIV may play a crucial role in the development of certain cancers, especially B cell lymphomas, in individuals living with HIV. Investigating the involvement of EBV in HIV-associated neoplasms could provide valuable insights into the underlying mechanisms of their development.

1.3 EBV infection in people living with HIV (epidemiological and immunological aspects)

HIV infection is associated with EBV reactivation and increases EBV viral loads in saliva and blood (Ling et al. 2003; Rahman et al. 1991; Yan et al. 2018). EBV is involved in lymphomagenesis in people living with HIV: HIV-associated BL is EBV positive in 30-40% of cases, classical HL – ~100% of EBV+ cases, diffuse large B-cell lymphoma (DLBCL) is EBV positive in 30-40% and HIV-associated B-lymphoproliferative disease consists of ~100% of EBV+ cases (Shannon-Lowe et al. 2017; Yan et al. 2018). In humanised mice, EBV superinfection with HIV leads to increased tumour formation as compared to solo virus infection independently of CD8+ T cell response (McHugh et al. 2020). Immune deficiency cannot fully explain the increased incidence of certain EBV-related malignancies in people living with HIV, which remains still increased in the cART era (Shmakova et al. 2020). These aspects point to a complex relationship between HIV and EBV, which is not straightforwardly linked to immunosuppression and lack of EBV control. A detailed understanding of the mechanisms and consequences of viral coexistence at the molecular level is required for novel strategies of targeted cancer therapy.

1.3.1 Antibody responses to EBV in people living with HIV

EBV viral proteins elicit both antibody and cell-mediated immune responses. EBV seroprevalence is often evaluated in clinical settings as an important indicator of overall immune status: anti-EBV IgG positivity reflects chronic latent (so-called "past") EBV infection, while anti-EBV IgM positivity is a marker of primary EBV infection or EBV reactivation (De Paschale & Clerici 2012). The presence and the levels of antibodies to the specific EBV antigens are analysed; detectable antibodies are typically specific for EBV latent antigens (EBNAs) or EBV lytic antigens (viral capsid antigen (VCA), early antigen-diffuse

(EA-D), BZLF1) (Johannsen & Kaye 2020). The designations of the lytic antigenic complexes, VCA and EA, first uncovered by serological methods, remain in use today, despite the knowledge that these antigens consist of a number of discrete viral proteins. The serologic profile of the healthy virus carrier consists of positive anti-VCA IgG, positive anti-EBNA1 IgG, weak/negative anti-EBNA2 IgG, and negative anti-VCA IgM (Taylor et al. 2015). In the general population, IgG seropositivity to VCA is found in 83% of individuals, to EBNA-1 in 71%, and to EA-D in 1% (Sallah et al. 2020). The increase in the levels of IgG and IgA antibodies directed against EBV lytic antigens is another marker of EBV reactivation (De Paschale & Clerici 2012).

Compared to the general population, people living with HIV are more likely to be seropositive for EBV (Sallah et al. 2020; Yan et al. 2018). In a recent cohort study, HIV infection was associated with IgG seropositivity to EBV with an OR 2.22 [1.32−3.73] (Sallah et al. 2020). Moreover, people living with HIV more often present EBV reactivation, which is detectable by anti-EBV IgM seropositivity, higher titers of IgG antibodies directed against EBV lytic antigens (**Table 1**) and an increase in circulating EBV DNA levels (Burbelo et al. 2013; Sallah et al. 2020). HIV infection is associated with higher levels of IgG antibodies to EBV lytic antigens VCA and EA-D (OR 1.37 [1.27−1.47]), but not the latent antigen EBNA-1 (Quesnel et al. 1992; Rahman et al. 1989; Sallah et al. 2020; Stevens et al. 2002). Higher anti-VCA IgG levels and lower anti-EBNA-1 IgG levels are associated with higher EBV DNA levels in people living with HIV (Stevens et al. 2002). A significantly higher proportion of cART-controlled individuals are positive for EBV IgM as compared to the uninfected population, although the reported frequencies seem quite high (Yan et al. 2018).

Table 1. Antibody responses to EBV in people living with HIV compared to the HIV-negative population. Data from (Burbelo et al. 2013; Sallah et al. 2020; Yan et al. 2018). Abbreviations: EA-D, early antigen-diffuse; EBNA, EBV nuclear antigen; EBV, Epstein-Barr virus; ND, not determined; OR, odds ratio; VCA, virus capsid antigen.

Anti-EBV antibodies	Frequency of positive serostatus compared to HIV-negative population	Antibody levels compared to HIV-negative population
anti-EBV IgM (primary infection or reactivation)	↑	ND
anti-EBV IgG (latent infection)	↑ OR 2.22 [1.32−3.73]	↑
anti-EBNA-1 IgG	= OR 1.17 [0.88-1.54]	= OR 1.06 [0.98-1.15]

anti-VCA IgG	↑ OR 2.95 [1.88-4.64]	↑ OR 1.37 [1.27-1.47]
anti-EA-D IgG	↑ OR 8.9 [4.7-16.87]	↑ OR 1.23 [1.17-1.29]

Not surprisingly, the uncontrolled HIV infection is even more associated with EBV reactivation: a higher proportion of cART-uncontrolled patients are positive for EBV IgM compared to cART-controlled ones (Hernández et al. 2018; Yan et al. 2018), anti-BZLF1 IgG are detectable in untreated HIV carriers and in AIDS patients (Joab et al. 1991). CD4+ T cell count inversely correlates with anti-VCA IgG level (Keramat et al. 2019). The initiation of cART has been associated with an increase in the titers of EBNA and EA anti-EBV antibodies (O'Sullivan et al. 2002) as well as a rise in overall anti-EBV antibody breadth (i.e. the number of unique epitopes targeted), potentially reflecting immune reconstitution (Eshleman et al. 2019).

It is important to note that cases of primary HIV infection presenting with false-positive EBV IgM test results have been reported, indicating the need for clinicians to consider testing for primary HIV infection in cases of positive anti-EBV IgM and low EBV viral loads in the blood (Post et al. 2011; Robertson et al. 2003; Vidrih et al. 2001).

1.3.2 EBV viral load in people living with HIV

EBV is impeccably sensitive to changes in the immune status and EBV DNA detection in peripheral blood is relevant, although not well-standardised, marker of immune function with a potential prognostic significance in haematological malignancies. EBV DNA is detectable in cell-associated (peripheral blood mononuclear cells (PBMCs), whole blood) and cell-free (plasma, serum) blood fractions. The increase in cell-associated EBV DNA might reflect either the increase in the number of latently infected cells or an increase in the viral copies in an infected cell due to the lytic viral replication (Babcock et al. 1999). On the contrary, cell-free EBV DNA is almost absent in chronic latent infection, since it mostly comes from virions secreted by lytically infected cells and/or from fragmented DNA of apoptotic cells mainly during primary EBV infection or EBV reactivation (De Paschale & Clerici 2012). After primary infection, EBV DNA rapidly drops in plasma and slowly decreases in PBMCs (Kimura et al. 2008). Thus, the plasma/serum EBV DNA load is a marker of primary EBV infection or EBV reactivation. The growing body of evidence suggests that the quantification of circulating cell-free EBV DNA represents a more sensitive marker of a broad range of EBV-related diseases than the

quantification of cell-associated EBV DNA (Kanakry et al. 2016; Lee et al. 2021; Tsai et al. 2015).

In its latent phase, EBV is prevented from reactivating through efficient EBV-specific CD8+ cytotoxic T cellular response assisted by CD4+ T cells, while immunodeficiency (triggered by various stimuli, including stress) is known to facilitate EBV reactivation (Kerr 2019). In humanised mice (immunodeficient mice reconstituted with human hematopoietic stem cells) selective depletion of either CD4+ or CD8+ T cells followed by EBV infection leads to a 3- or 5-fold increase in EBV viral loads, respectively, and the concomitant depletion of CD4+ and CD8+ T cells increases viral titers ~20 times (Strowig et al. 2009). In healthy humans, EBV DNA is present in 5-10 cells in 1-50 copies per 10^6 peripheral blood B cells, while in immunosuppressed patients up to 160 infected cells per 10^6 B cells can be detected, in both cases, EBV is stringently restricted to resting memory B cells (Babcock et al. 1999; Birx et al. 1986; Miyashita et al. 1997; Wagner et al. 1992). Immunosuppressed patients tend to have higher EBV DNA viral burden due to both EBV reactivation (lytically infected cells with high EBV genome copy numbers) and expansion of latently infected cells (Babcock et al. 1999).

In general, even under cART treatment people living with HIV tend to have higher levels of EBV DNA in their blood (Fellner et al. 2007; Richard et al. 2010), PBMC (Fellner et al. 2007; Legoff et al. 2004; Ling et al. 2003; Piriou et al. 2004), saliva (Byrne et al. 2021; Ling et al. 2003; Yan et al. 2018) and semen (Lisco et al. 2012; Morris et al. 2017) as compared to HIV-negative individuals. The long-term effect of cART treatment on high EBV DNA levels in HIV-positive individuals remains to be fully estimated. At the beginning of the XXI century, several early studies found that despite cART treatment and recovery of CD4+ T cell counts, EBV viral loads remained high and didn't change compared to EBV viral loads before treatment initiation, and no clear correlations between EBV viral loads and HIV viral loads decline after cART were found (Bekker et al. 2006; Kostense et al. 2002; Piriou et al. 2005a). At that time, no significant difference in EBV viral loads in people with HIV was found between the pre-cART and post-cART eras (Stevens et al. 2002). This formulated the hypothesis that EBV viral load was irreversibly altered after HIV seroconversion: primary HIV infection can lead to B cell activation, EBV reactivation from latency, expansion and persistence of EBV-infected cells, leading to a higher EBV load that remained unchanged despite cART (Piriou et al. 2004, 2005a). Moreover, it was hypothesized that peripheral immune reconstitution (CD4+ T cell count increase) during cART without a reduction in HIV-1 replication (a.k.a. immunological response) may increase B cell stimulation and the number of EBV-infected B cells as well as EBV viral load in PBMCs (Burighel et al. 2006; Righetti et al. 2002). Nevertheless, more recent studies demonstrate that EBV DNA is, in fact, decreasing in people living with HIV upon cART treatment, and people with undetectable HIV RNA and higher

CD4+ T cell counts (e.g. > 500 cells/µl) tend to have lower levels of EBV DNA (Legoff et al. 2004; Petrara et al. 2013). Initially high (~500 copies/10^6 PBMC), EBV DNA declines (~25 copies/10^6 PBMC) in people living with HIV undertaking cART, but not monotherapy (mART) within almost 2 years of observation (Petrara et al. 2017). Thus, upon cART treatment high EBV DNA levels tend to decrease in people living with HIV.

Despite that, the relationship between EBV viral load and CD4+ T cell counts as a measure of immune function in people living with HIV is not straightforward. cART interruption results in EBV DNA rebound despite the absence of a pronounced CD4+ T cell decrease (Petrara et al. 2013). Furthermore, despite the fact that numerous studies have demonstrated that people living with HIV with low CD4+ T cell counts typically have higher levels of EBV DNA, no linear correlation is detected between these two parameters (Fellner et al. 2007; Legoff et al. 2004; Petrara et al. 2013; Silva et al. 2015). This suggests that uncontrolled HIV infection affects EBV immune control through mechanisms that are not limited to global CD4+ T cell depletion.

Vice versa, EBV contribution to the control of HIV infection and virus rebound was also suggested, although most of these observations remain correlative. In an early phase of suppressive cART initiation, higher EBV DNA levels were associated with higher levels of HIV DNA and unspliced HIV RNA, lower CD4+/CD8+ T cell ratio, and higher CD8+ T cell counts (Gianella et al. 2016; Smith et al. 2016). A positive correlation between EBV salivary shedding and plasma HIV-1 RNA levels was found (Griffin et al. 2008). Finally, a periodical sequencing of the HIV *env* gene in a cohort of 37 people living with HIV followed for a period of two years showed that HIV viral diversity under suppressive cART over time significantly correlates with the presence of high-level EBV DNA in peripheral blood cells (Chaillon et al. 2020b). Together this data suggests that high EBV DNA might be associated with or is a marker of worse HIV control upon cART.

As HIV infection often affects adults, most people establish latent EBV infection prior to HIV infection and little is known about the reverse cases. A few studies of HIV-seropositive children have demonstrated that primary EBV infection in children with HIV is associated with higher peak EBV DNA loads in plasma or PBMCs than in HIV-negative children, and the absence of its decline months after first EBV detection, suggesting a poor immune control over EBV in children with HIV (Brandt et al. 1998; Slyker et al. 2013). Even after latency establishment, EBV DNA loads are increased in HIV-positive children compared to HIV-negative children with either latent or acute EBV infection (Bekker et al. 2006).

1.3.3 EBV-specific T cell response in people living with HIV

Cell-mediated EBV-specific immune responses seem to be essential throughout each step of the virus-host interaction, functioning both to manage the primary infection and to prevent the reactivation of latently infected cells. CD8+ T cells (also referred to as cytotoxic T cells or lymphocytes) orchestrate the central axis of anti-EBV adaptive cellular response, but CD4+ T cells are also implicated in the immune response to EBV infection, although to a lesser extent (reviewed in (Hislop et al. 2007; Rickinson et al. 2014; Taylor et al. 2015)). Of note, in addition to classical cytokine-secreting capacity, EBV-specific CD4+ T cells are capable of cytotoxic cell lysis (at least in vitro) (Khanolkar et al. 2001; Long et al. 2009). Both CD8+ and CD4+ T cells can be specific for EBV lytic (BZLF1, BRLF1, BMRF1, BMLF1) or latent (EBNAs, LMPs) antigens. Lytic antigen-specific CD8+ T cells dominate in acute infection, while the establishment of the pool of latently infected cells elicits latent antigen-specific CD8+ and CD4+ T cell response (Hislop et al. 2007; Rickinson et al. 2014). However, even during persistent infection, most EBV-specific CD8+ T cells are directed against lytic epitopes (Taylor et al. 2015), which is also true for people living with HIV (Legoff et al. 2004; van Baarle et al. 2001). This suggests that lytic antigen-specific CD8+ T cells play a major role in controlling EBV reactivation by eliminating virus-producing cells at an early stage.

While it may appear evident that HIV-mediated immune suppression can exhaust the immune response to other viruses, early studies claimed that HIV-1 progression was not necessarily paralleled with a loss of EBV-specific cytotoxic T cells (Carmichael et al. 1993; Geretti et al. 1996; Kersten et al. 1997; Piriou et al. 2004, 2005c). Preserved quantity, however, does not equal quality. van Baarle et al. examined EBV-specific CD8+ T cell response in people living with HIV at an early stage of infection and HIV-negative individuals. While no difference was observed in the percentage of EBV-specific CD8+ T cells between the two groups, a smaller proportion of EBV-specific CD8+ T cells produced IFNγ in response to EBV antigens in people living with HIV compared to HIV-negative individuals, indicating that EBV-specific CD8+ T cells from people living with HIV were less functionally active (van Baarle et al. 2001). This formulated the hypothesis of the dysfunctionality of EBV-specific CD8+ T cells in people living with HIV, which could contribute to an increased EBV viral load and EBV-driven oncogenesis. The latter studies confirmed that EBV-specific CD8+ T cell responses were less intense and showed reduced polyclonality in people living with HIV, especially in those with low CD4+ T cell counts, when compared to HIV-negative individuals (Legoff et al. 2004). The loss of functional EBV-specific CD8+ T cells correlated with higher EBV DNA viral loads and lower CD4+ T cell counts (Legoff et al. 2004; van Baarle et al. 2001); on the contrary, antiretroviral treatment was able to restore the functionality of EBV-specific CD8+ T cells in parallel with CD4+ T cell counts increase (Dalod et al. 1999; Kostense et al. 2002; van Baarle et al. 2001).

A decrease in the function of EBV-specific CD8+ T cells in people living with HIV may be due to the continuous depletion of EBV-specific CD4+ T cell help. Notably, it was shown that untreated HIV infection can lead to a decline in EBNA1-specific CD4+ T cell responses that are restored by cART (Piriou et al. 2005a,c). IL-2, IFNγ and TNF-α-producing cytokine responses of EBV-specific CD4+ T cells are less frequent in people living with HIV (Hernández et al. 2018; Smith et al. 2013). An inverse trend was observed for lytic antigen-specific T cells: the level of BZLF1-specific CD4+ T cells decreased after initiation of cART and long-term treated individuals have lower amounts of BZLF1-specific CD4+ and CD8+ T cells than HIV-negative individuals (Piriou et al. 2005a).

In the absence of treatment, active HIV-1 replication induces immune activation of "bystander" non-productively infected CD4+ T cells, eventually leading to their death, which represents one of the major mechanisms for CD4+ T cell depletion in people living with HIV (Bangs et al. 2006; Doitsh & Greene 2016; Doitsh et al. 2014). Haas et al. recently discovered that bystander activation of HIV-uninfected CD4+ T cells is non-random and occurs specifically in herpes-virus-specific CD4+ T cells, among which are EBV-specific CD4+ T cells (Haas et al. 2010). The authors suggested that HIV replication upon cART cessation, combined with the low-level presence of cognate herpes virus antigens, may stimulate CD4+ T cells through the activation of dendritic cells, assuming that later could, in turn, allow for more effective presentation of low-level persistent antigens to CD4+ T cells (Haas et al. 2010). In another study, untreated people living with HIV were found to exhibit elevated activation profiles of EBV-specific cytokine-producing CD4+ T cells (measured by CD38 and HLA-DR co-expression) without clinical evidence for EBV reactivation as compared to HIV-negative people (Smith et al. 2013). The level of the CD4+ T activation did not correlate with total CD4+ T cell counts (Smith et al. 2013) or EBV DNA levels in PBMCs (Christensen-Quick et al. 2019). Whether this "bystander" activation can lead to the depletion of EBV-specific CD4+ T cells remains to be elucidated.

Thus, CD8+ and CD4+ T cell-mediated immune responses are essential for managing EBV infection and preventing the reactivation of latently infected cells, but HIV infection can lead to a decline in EBV-specific CD4+ T cells and impair the functionality of EBV-specific CD8+ T cells, which may contribute to increased EBV viral load and oncogenesis in people living with HIV. It is important to note that the studies concerning EBV-specific CD4+ and CD8+ T cell responses in people living with HIV are quite scarce and most of them were conducted early in the HIV/AIDS epidemic; more recent research is warranted. Additionally, the complexity of the interaction between HIV and EBV is not solely attributed to immunosuppression and we emphasise the importance of understanding the mechanisms and consequences of their coexistence at the molecular level.

1.4 B cell lymphomas in people living with HIV

Lymphomas that develop in the setting of immunosuppression, particularly those in people living with HIV, differ from lymphomas that develop in immunocompetent patients both clinically and biologically. Due to this fact, the World Health Organization (WHO) classification of Haematolymphoid Tumours (4th edition) has designated lymphoid proliferations and lymphomas associated with immune deficiency and dysregulation as a separate classification, amongst which are lymphomas associated with HIV infection (Alaggio et al. 2022; Swerdlow et al. 2017) (**Table 2**). Aggressive B cell non-Hodgkin lymphomas (NHL): diffuse large B cell lymphoma (DLBCL), Burkitt's lymphoma (BL), primary central nervous system lymphoma (PCNSL)[1], primary effusion lymphoma (PEL), plasmablastic lymphoma (PBL)[1], are also generally embedded into the case definition of AIDS (AIDS-defining cancers) (Yarchoan & Uldrick 2018). With this regard, patients presenting with aggressive B cell lymphomas should be routinely tested for HIV (Hwang et al. 2015). While PCNSL and PEL occur in severely immunocompromised individuals (Gopal et al. 2013; Hernández-Ramírez et al. 2019), classical Hodgkin lymphoma (cHL) and BL are more common among people living with HIV with higher CD4+ T cell counts (Besson et al. 2015; Guech-Ongey et al. 2010).

Table 2. B cell lymphomas in people living with HIV. Based on the WHO Classification of Tumours of Haematopoietic and Lymphoid Tissues (4th edition) (Swerdlow et al. 2017). Abbreviations: BL, Burkitt lymphoma; cHL, classical Hodgkin lymphoma; DLBCL, diffuse large B-cell lymphoma; EBV, Epstein-Barr virus; ND, not determined; PBL, plasmablastic lymphoma; PCNSL, primary central nervous system lymphoma; PEL, primary effusion lymphoma; WHO, world health organisation.

Lymphoma	Standardised incidence ratios [95% CI][†]	% of EBV association[‡] in people living with HIV	% of cases among lymphomas in people living with HIV	Degree of immune deficiency	Survival rate[§]
Lymphomas also occurring in immunocompetent patients					
BL	20.2 [8.4-22.2]	30-50% (Arvey et al. 2015; Kersten et al. 1998;	10-15% (Gibson et al. 2014; Olszewski et al. 2016)	Mild to moderate	70-80%

[1] PCNSL and PBL are subtypes of DLBCL

		Swerdlow et al. 2017)			
DLBCL	10.3 [9.89-10.7]	30-80% (Arvey et al. 2015; Swerdlow et al. 2017)	40-50% (Antel et al. 2019; Gibson et al. 2014; Olszewski et al. 2016; Schommers et al. 2015)	Moderate to severe	70-80%
PBL	ND	60-100% (Arvey et al. 2015; Bailly et al. 2022; Delecluse et al. 1997; Loghavi et al. 2015; Swerdlow et al. 2017)	2-15% (Antel et al. 2019; Castillo et al. 2015; Schommers et al. 2015)	Severe	75%
cHL	7.70 [7.20-8.23]	80-100% (Herndier et al. 1993; Swerdlow et al. 2017; Tirelli et al. 1995)	5%	Moderate	80-90%
Lymphomas occurring more specifically in HIV-positive patients					
PEL	ND	100% 86% (Arvey et al. 2015)	1-5% (Olszewski et al. 2016; Schommers et al. 2015)	Severe	40%
PCNSL	153 [140-167]	100% (MacMahon et al. 1991)	9% (Olszewski et al. 2016)	Severe	60%

† The information in this column is based on 1996–2012 data from (Hernández-Ramírez et al. 2017);
‡ As identified by the expression of EBER or other EBV genes in lymphoma cells;
§ The information in this column is based on data from (Noy 2019).

People living with HIV are at a higher risk of developing aggressive NHLs and cHL, and their prognosis is poorer than the general population (Coghill et al. 2019; Engels et al. 2008; Luo et al. 2022). Moreover, when compared with immunosuppressed transplant recipients, people living with HIV still have a higher incidence of both cHL and NHL (Grulich et al. 2007), again pointing to the fact that apart from immune deficiency, other factors might play a role in lymphomagenesis in people living with HIV. Lymphomas in people with HIV are often diagnosed at an advanced stage, and despite the success of cART, lymphomas are still the main cause of death due to cancer among people living with HIV (5-25% of AIDS-related death causes) (Gopal et al. 2013; Luo et al. 2022; Morlat et al. 2014; Simard & Engels 2010). While the incidence of DLBCL and PCNSL has dropped significantly after the widespread availability of cART, the incidence of BL, cHL and PBL has not decreased in the era of cART (Powles et al. 2009; van Leeuwen et al. 2009; Vaughan et al. 2021).

1.4.1 Chromosomal translocations in B cell lymphomas

Chromosomal translocations are recurrent genetic events in B cell lymphomas, often characterised by a reciprocal exchange of genetic material between two non-homologous chromosomes. A prominent feature of these translocations is their preference for immunoglobulin (Ig) genes, particularly the immunoglobulin heavy chain (*IGH*) gene located on human chromosome 14 and strongly expressed in B cells. Less frequently, the Igκ and Igλ light-chain genes (*IGK* on chromosome 2 and *IGL* on chromosome 22) are also implicated in these rearrangements (Robbiani & Nussenzweig 2013). The genes translocated near immunoglobulin genes typically encode protooncogenes that become overexpressed and disrupt crucial cellular processes, leading to uncontrolled proliferation, evasion of apoptosis, and tumorigenesis. For instance, the t(8;14)(q24;q32) translocation in BL induces overexpression of the *MYC* oncogene positioned next to the immunoglobulin heavy chain locus (*IGH*); the t(14;18)(q32;q21) translocation results in the overexpression of anti-apoptotic *BCL2* protein in follicular lymphoma; the t(11;14)(q13;q32) in mantle cell lymphoma results in the overexpression of cell cycle regulator Cyclin D1 (*CCND1*); whereas the t(3;14)(q27;q32) translocation in DLBCL involves a transcriptional repressor gene *BCL6* (Dalla-Favera et al. 1982; Godon et al. 2003; Jain & Wang 2022; López et al. 2022; Ye et al. 1993, 1995).

The generation of chromosomal translocation involves two major steps: the formation of specific double-strand breaks (DSBs) and their erroneous repair *via* non-homologous end joining (NHEJ) (Lieber 2010a). DSBs originate from either extrinsic factors (ionising radiation, UV light, genotoxic drugs, e.g. chemotherapy) or intrinsic factors (e.g. cellular activities that involve DNA-cutting or DNA-modifying enzymes). Throughout the cell cycle DSBs are mostly repaired by error-prone NHEJ, which can proceed in a more accurate

classical variant (classical NHEJ, c-NHEJ) or, in the cases when c-NHEJ is abrogated, in a less accurate alternative variant (alternative NHEJ, a-NHEJ) (Iliakis et al. 2015; Lieber et al. 2010). The faithful repair based on the homologous template provided by the sister chromatid is only ensured by the homologous recombination (HR) pathway, which occurs in 15-20% of DNA lesions and only after the S phase of the cell cycle (Jasin & Rothstein 2013; Shibata et al. 2011).

Genome instability and DSBs present a major risk factor for the development of oncogenic chromosomal translocations. In B cells, lymphomogenic DSBs arise from exogenous factors (ionising radiation, genotoxic substances, i.e. alkylating agents and topoisomerase inhibitors) or endogenous factors (programmed DNA damages *via* lymphocyte-specific enzymes Rag1/2 (during V(D)J recombination) and activation-induced deaminase (AID) (during somatic hypermutation and class switch recombination) (Nickoloff et al. 2008; Nussenzweig & Nussenzweig 2010). The principal source of DSBs in the *IGH* and other "bystander" loci is AID, an enzyme that in physiological conditions creates DSBs, regulating immunoglobulin gene somatic hypermutation and class switch recombination in B cells in the germinal centre of lymph nodes (Chaudhuri et al. 2007; Di Noia & Neuberger 2007; Honjo et al. 2002; Xu et al. 2007). In addition to being indispensable for the production of affine antibodies to different antigens, *IGH* rearrangements increase the risk of chromosomal translocations (Dorsett et al. 2007; Ramiro et al. 2004; Sall et al. 2018). In the context of HIV infection, both the virus per se and antiretroviral or other drugs can promote genome instability (Ellwanger et al. 2023). Noteworthy, both chemotherapeutic and cART drugs in different models can interfere with DNA integrity or DNA repair enzymes (Annovazzi et al. 2017; Koczor & Lewis 2010; Lewis et al. 2001; Xie et al. 2016), which might influence the translocation formation.

Understanding the mechanisms underlying chromosomal instability and chromosomal translocations in people living with HIV is essential for developing targeted therapies and diagnostic tools in the context of cancer and other diseases associated with genomic instability. See review **Article 2** which highlights the mechanistic insights into chromosomal translocation formation (**Figure 3**).

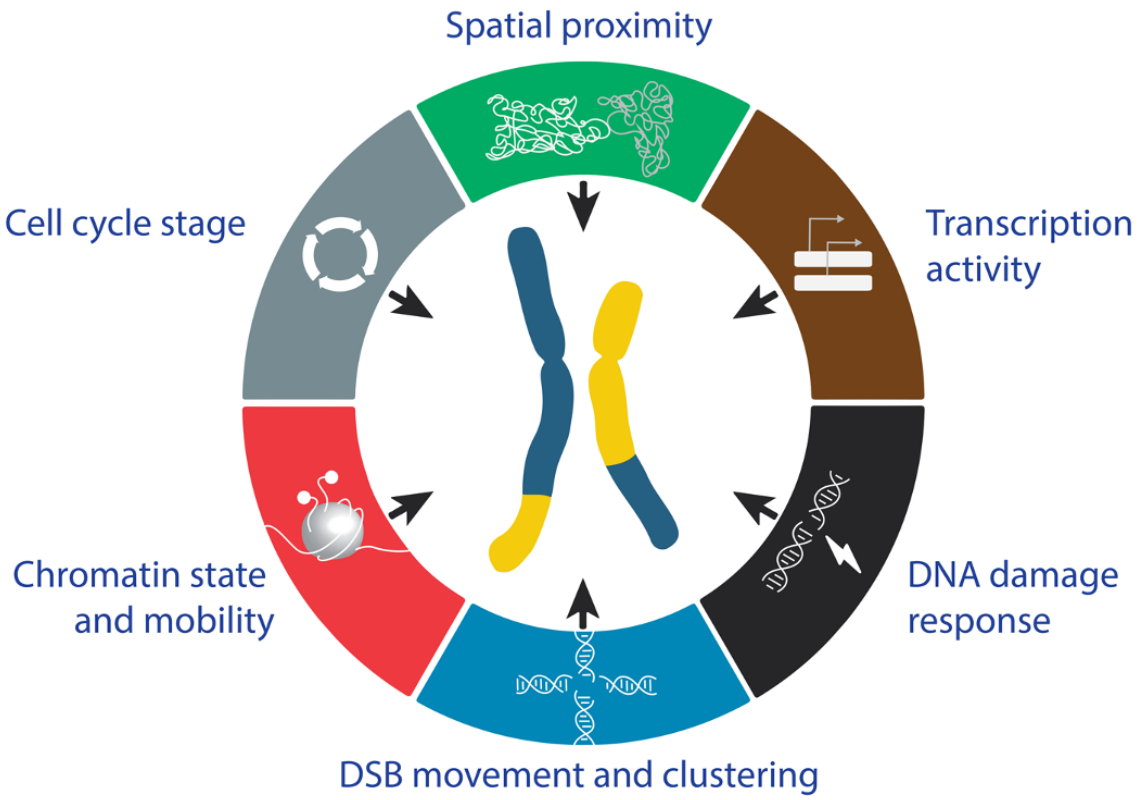

Figure 3. Factors that affect the formation of chromosomal translocations. Recent evidence suggests that the formation of chromosomal translocations is influenced by the spatial proximity of gene loci that are potential partners for translocation; transcriptional activity of gene loci that are potential partners for translocation; DNA damage sensing and choice of DNA repair pathway; chromatin state and chromatin motion; the movement of double-strand breaks (DSBs) and their clustering in common repair centres; and cell cycle stage, which might influence all the factors mentioned above.

I contributed to this review by writing chapters about the role of DNA damage response, transcription activity and cell cycle in translocation formation, creating illustrations, and manuscript review and editing.

Article 2. Review "Factors That Affect the Formation of Chromosomal Translocations in Cells"

cancers

MDPI

Review

Factors That Affect the Formation of Chromosomal Translocations in Cells

Reynand Jay Canoy [1,2,3], Anna Shmakova [1,4], Anna Karpukhina [1,4], Mikhail Shepelev [5], Diego Germini [1,*] and Yegor Vassetzky [1,4,*]

1 UMR 9018, CNRS, Université Paris Saclay, Institut Gustave Roussy, F-94805 Villejuif, France
2 Institute of Human Genetics, National Institutes of Health, University of the Philippines Manila, Manila 1000, Philippines
3 Scilore Asia-Pacific Corporation, Ayala-Alabang, Muntinlupa City 1780, Philippines
4 Koltzov Institute of Developmental Biology, 117334 Moscow, Russia
5 Institute of Gene Biology, 117334 Moscow, Russia
* Correspondence: germinidiego@gmail.com (D.G.); yegor.vassetzky@cnrs.fr (Y.V.)

Simple Summary: Chromosomal translocations are products of the erroneous repair of DNA double-strand breaks that result in the illegitimate joining of the two broken chromosomal ends from non-homologous chromosomes. Chromosomal translocations have been linked to aneuploidy, infertility, mental retardation, cancer and other diseases. Here we discuss how chromosomal translocations are formed and explore how different cellular factors contribute to their formation.

Abstract: Chromosomal translocations are products of the illegitimate repair of DNA double-strand breaks (DSBs). Their formation can bring about significant structural and molecular changes in the cell that can be physiologically and pathologically relevant. The induced changes may lead to serious and life-threatening diseases such as cancer. As a growing body of evidence suggests, the formation of chromosomal translocation is not only affected by the mere close spatial proximity of gene loci as potential translocation partners. Several factors may affect formation of chromosomal translocations, including chromatin motion to the potential sources of DSBs in the cell. While these can be apparently random events, certain chromosomal translocations appear to be cell-type-specific. In this review, we discuss how chromosomal translocations are formed and explore how different cellular factors contribute to their formation.

Keywords: chromosomal translocation; cancer; translocation formation; spatial proximity

check for updates

Citation: Canoy, R.J.; Shmakova, A.; Karpukhina, A.; Shepelev, M.; Germini, D.; Vassetzky, Y. Factors That Affect the Formation of Chromosomal Translocations in Cells. *Cancers* **2022**, *14*, 5110. https://doi.org/10.3390/cancers14205110

Academic Editor: Frederic Chibon

Received: 28 September 2022
Accepted: 17 October 2022
Published: 18 October 2022

Publisher's Note: MDPI stays neutral with regard to jurisdictional claims in published maps and institutional affiliations.

Copyright: © 2022 by the authors. Licensee MDPI, Basel, Switzerland. This article is an open access article distributed under the terms and conditions of the Creative Commons Attribution (CC BY) license (https://creativecommons.org/licenses/by/4.0/).

1. Introduction

Chromosomal translocations are the products of an illegitimate proximity-based repair of DNA double-strand breaks (DSBs), where the proximity of DNA ends from different non-homologous chromosomes can result in their erroneous joining. The appearance of a chromosomal translocation results in substantial structural and molecular alterations in the cell and may have perilous pathological consequences. The mechanisms of chromosomal translocation generation, as well as their contribution to human diseases, were extensively reviewed before (e.g., [1–4]). Still, it is currently unknown why certain chromosomal translocations are observed in specific cell types. In the current review we aim to summarize cellular factors that contribute to the formation of chromosomal translocations and that, among other things, could explain the specificity of the occurrence of certain chromosomal translocations.

1.1. History of Chromosomal Translocations in Cancer

The link between an aberrant number of chromosomes and cancer was first described by Theodor Boveri, who postulated that "growth stimulatory chromosomes" triggered

the unlimited growth of tumor cells [5,6]. Then, in 1960, the Philadelphia chromosome, which appeared to be smaller than chromosomes 21 and 22, was described in patients with chronic myeloid leukemia (CML) [7]. However, it was not until 1973 that Janet Rowley showed that this chromosome is the truncated derivative of chromosome 22 fused to the fragment of chromosome 9 [8–10]. This report was the first to demonstrate that the novel chromosomes, which were usually reported to be present in tumor cells, were actually the products of chromosomal translocations.

1.2. Types of Chromosomal Translocations

Chromosomal translocations are generated when non-homologous chromosomes exchange their parts with each other. A few types of chromosomal translocations have been described [11,12]. Chromosomal translocations are considered reciprocal (Figure 1A) if the exchange between chromosomes is bidirectional. Non-reciprocal chromosomal translocations result from the unidirectional transfer of one chromosomal part to another chromosome (Figure 1B). Chromosomal translocations can also be classified as balanced (no net loss or gain of genomic material) or unbalanced if genetic material is lost or amplified. In reciprocal translocations, one of the three sets of possible derivative chromosomes can be produced [13]:

(1) Two chromosomes produce monocentric derivative chromosomes with one centromere (Figure 1A);

(2) Two chromosomes produce a derivative chromosome with two centromeres (dicentric) and a derivative chromosome without a centromere (acentric) (Figure 1A);

(3) Two acrocentric chromosomes fuse at the centromere (Figure 1C) (Robertsonian translocation; [14,15]). The remnants of the short p arms of the two chromosomes also fuse and the small reciprocal product are usually lost, which may not be deleterious for the cell [16].

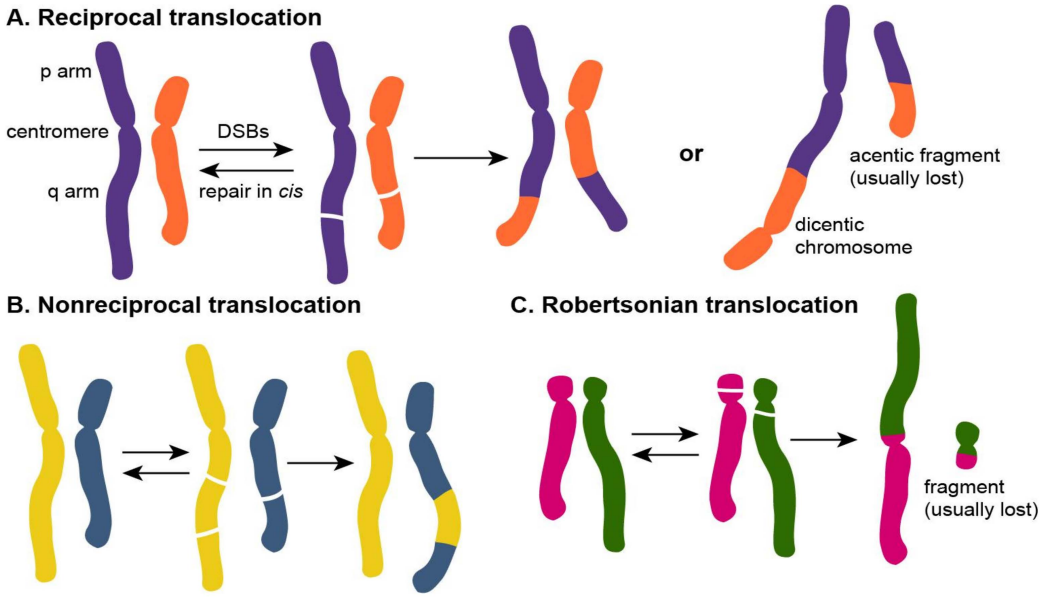

Figure 1. Types of chromosomal translocations. The illegitimate repair of the two DSBs in two non-homologous chromosomes can produce (**A**) reciprocal translocations if the exchange between two translocating chromosomes is bidirectional or (**B**) non-reciprocal translocations if the exchange is unidirectional. (**C**) Robertsonian translocations occur between two acrocentric chromosomes that are fused at the centromere.

The dicentric and acentric chromosomes are often lost after several rounds of cell divisions as they are either lethal or unstable [11], while Robertsonian translocations may persist in meiosis and even produce gametes [12].

1.3. Chromosomal Translocations Affect the Normal Cell Functions

The mere rearrangement of chromosome parts can cause significant consequences in the cell. Chromosomal translocations have been linked to aneuploidy, infertility, mental retardation, cancer, and other diseases [17–22]. Chromosomal translocations may result in the formation of fusion proteins (Figure 2A) with unique or atypical functions or activity, as in the case of the BCR-ABL fusion protein in CML [23–25]. In addition, they can result in the aberrant expression (upregulation or downregulation) of an otherwise normal gene if it is positioned next to the new cis-regulatory elements (Figure 2B). Usually these aberrantly expressed genes are proto-oncogenes that are controlled by a potent gene promoter or enhancer after the translocation. Either of these two can significantly affect the cell and can lead to its transformation and malignancy. This is exemplified by Burkitt's lymphoma, where the *MYC* gene on chromosome 8 is translocated next to the *IGH* locus on chromosome 14; this triggers its overexpression [26–30]. Recently, large-scale changes in the nuclear organization have also been attributed to chromosomal translocations, further expanding our understanding of the consequences of chromosomal translocations for the cell [11,31–36].

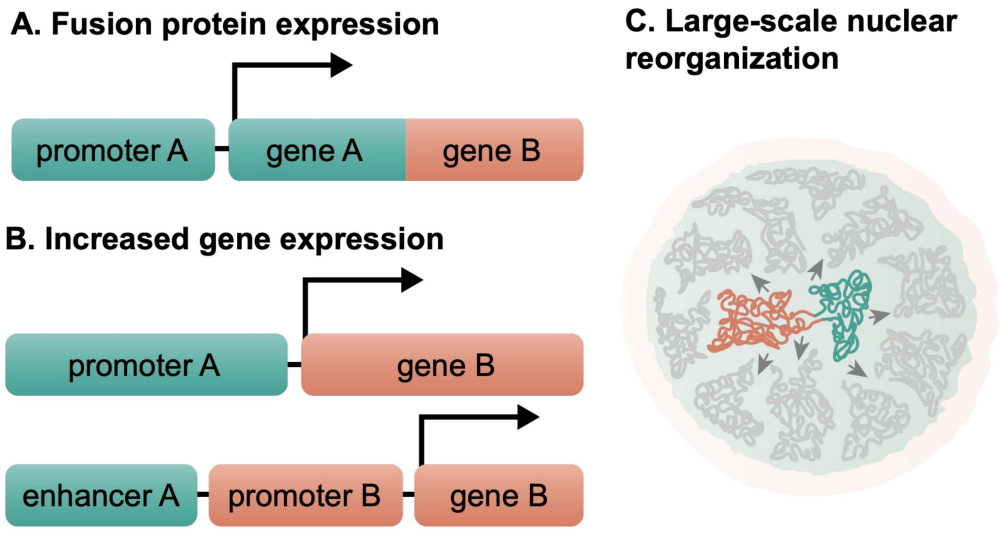

Figure 2. Molecular and functional consequences of chromosomal translocations. Chromosomal translocations can bring about the formation of fusion protein (**A**) or the (**B**) aberrant expression of an otherwise normal gene as well as (**C**) large-scale changes in the nuclear organization have also been attributed to chromosomal translocations.

Chromosomal translocations are characteristic for many types of cancer [37,38], including carcinomas [39,40], lymphomas, leukemias [19,37], and soft tissue sarcomas [20,41,42]. The Mitelman Database of Chromosome Aberrations and Gene Fusions in Cancer (https://mitelmandatabase.isb-cgc.org/ (accessed on 27 September 2022)) contains exhaustive data related to chromosomal aberrations, including translocations and cancer [43].

2. Sources of DSBs In Vivo and Their Experimental Modeling for Studying Translocations

2.1. Sources of DSBs

The sources of DSBs can be grouped into extrinsic and intrinsic ones. The former include environmental factors such as the ionizing radiation of X-rays and alpha particles [44–49], UV light, or exposure to genotoxic chemical agents (e.g., chemotherapy). Cellular activities that involve DNA-cutting enzymes or produce nonspecific DNA damage, are the potential intrinsic sources of DSBs. In meiotic recombination, DSBs are induced mainly by SPO11 [50,51] during the segregation of chromosomes to convert the cell from diploid to haploid [52,53]. DSBs are consequently produced in lymphocytes during the V(D)J recombination in maturing B and T cells [54–56]. Furthermore, DSBs are also formed during the somatic hypermutation (SHM) and the immunoglobulin class switching or class switch recombination (CSR) in mature B cells [57,58]. The breaks in V(D)J recombination are initiated by the recombination-activating gene (RAG) 1/2 complex [59], while the breaks in SHM and CSR are initiated by the activation-induced deaminase (AID) [60]. Although AID has a special affinity for immunoglobulin genes, it is able to target a large number of other genes (~25% of all expressed genes in B cells) [61]. This programmed DNA damage is considered as a major contributing factor to the susceptibility of B-cells to chromosomal translocations [1]. On the other hand, there are cellular activities that unintentionally produce DSBs such as gene transcription [62–67], DNA replication [68,69] and oxidative metabolism [70,71].

Apparently, different sources of DSB and the chromosome regions targeted by these DSBs differently affect the formation of chromosomal translocations; different sources of DSBs might also determine which factors influence the formation of translocations and thus, translocation specificity, which is discussed below. For instance, CRISPR/Cas9 mostly induce DSBs independently of the chromatin context, which makes the generation of CRISPR/Cas9-induced translocations dependent on the spatial proximity of DNA ends and the choice of DSB repair pathway [72–74]. This should also be taken into account when modeling chromosomal translocations by various methods of DSB induction.

2.2. Experimental Models of Chromosomal Translocations

Translocations can be induced either randomly (e.g., by treatment with γ-rays or H_2O_2) or specifically (e.g., by engineered programmed nucleases) [75]. The advent of engineered nucleases provided a new opportunity to precisely study translocations by introducing DSBs in the regions of interest. Specific chromosomal translocations can now be generated from precisely induced DSBs using programmed nucleases such as zinc finger nucleases (ZFN), transcription activator-like effector nucleases (TALEN), and clustered regularly interspaced short palindromic repeats (CRISPR) [76–84]. A more sophisticated way to induce chromosomal translocations in cells would be to use proteins that naturally induce DNA damage and are known to be implicated in chromosomal translocations, reviewed in [85,86]. In B cells, the chromosome breaks are usually caused by either AID, involved in class switch recombination and somatic hypermutation, or RAG endonuclease, essential for V(D)J recombination together with its RAG2 cofactor. Consequently, physiological or aberrant activation of these genes may induce DSBs and chromosomal translocations. These translocations can then be identified by next-generation sequencing [87,88]. A subset of chromosomal translocations in hematological and solid tumors are driven by DNA topoisomerse II (TOP2) [89]. TOP2 poisons, such as the anticancer agent etoposide, which trap DNA-TOP2 complexes, can be used to induce and identify chromosomal translocations [90]. The factors favoring chromosomal translocations (Figure 3) identified in these and other studies are considered below.

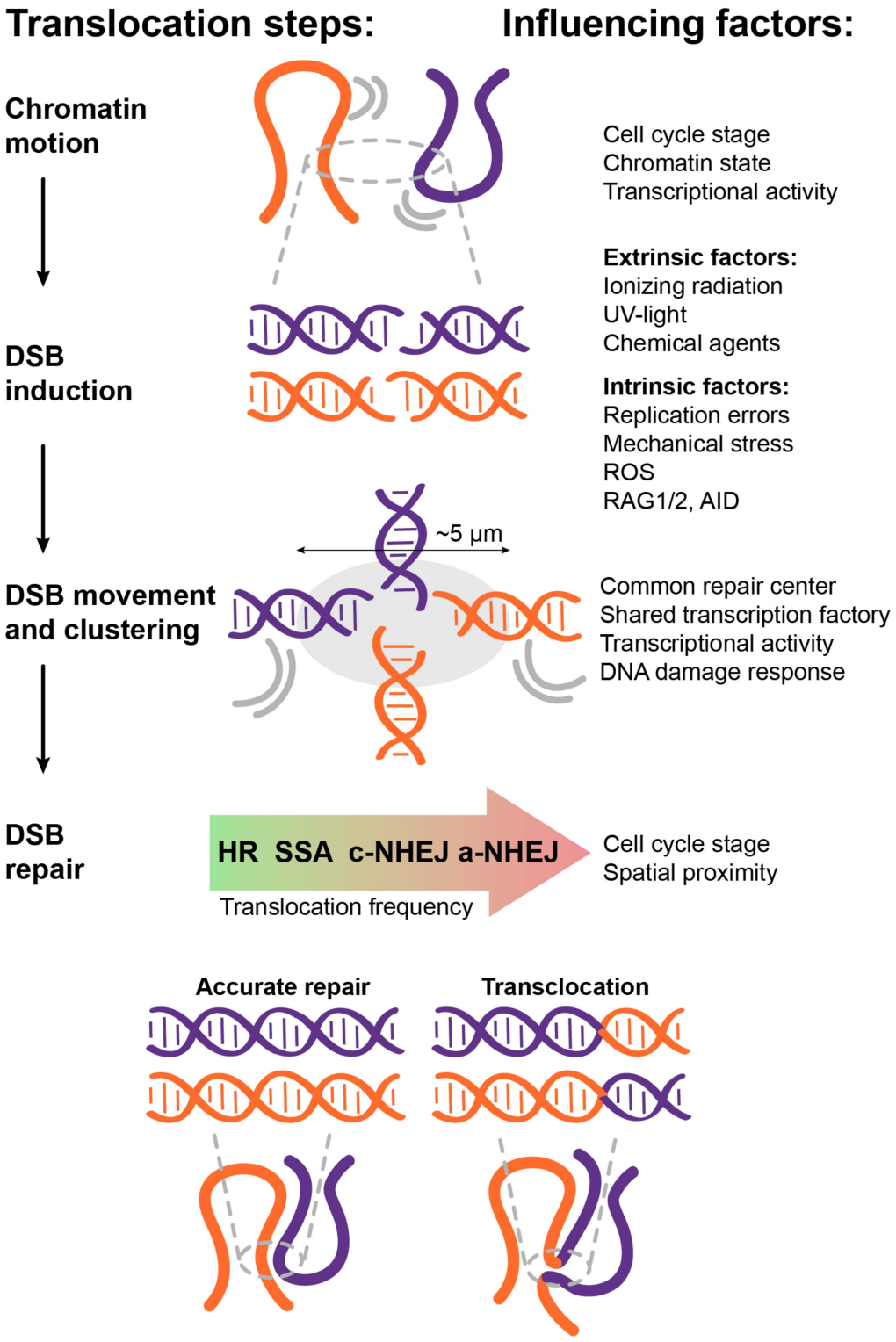

Figure 3. Different factors affect the formation of chromosomal translocations. These cellular factors are not mutually exclusive and can influence each other to affect the multiple stages of chromosomal translocation formation.

3. How Do the Different Factors Affect the Formation of Chromosomal Translocations?

3.1. Spatial Proximity

The erroneous repair of DSBs on different non-homologous chromosomes can result in their joining; this mechanism of chromosomal translocation generation largely relies on

the spatial proximity of DNA ends. However, whether the potential translocation partners should be initially proximally close when the breaks occur or they can move in the nuclear space after the break to get closer is still an open question. In this regard, the "contact first" and "break first" models of translocation formation have been proposed, which assume that the movement of intact chromatin or the movement of DSBs, respectively, contribute to the eventual proximity of DNA ends and translocation [3,75,91,92].

In the nuclear landscape of mammalian cells, chromosomes are organized into spatially distinct territories where they interact with each other more than with those belonging to the other different territories [93]. The term chromosome territory (CT) was actually first introduced by Boveri in the early 1900s in his studies on the blastomere stages of horse roundworms [94,95]. These CTs are composed of chromatin fibers [96]. Different types of cells and tissues have been observed to have different patterns of CTs in their nuclei [97,98]. The proximity of translocation-prone loci (e.g., *MYC/IGH* or *IGH/BCL6*) is largely determined by the higher order chromosome territory positioning [99]. In contrast to higher eukaryotes, yeasts do not exhibit this manner of organization of their chromosomes [100].

The nuclear genome architecture can be visualized using fluorescence in situ hybridization (FISH) using conventional or high-resolution microscopy, or it can be inferred using chromosome conformation structure (3C) and its spin-offs [101,102]. Using FISH, it was found that the gene loci that are commonly involved in oncogenic chromosomal translocation are already proximal to each other in pre-cancerous cells, supporting the "contact first" model of translocation formation. This was the case of the *ABL-BCR* translocation involving chromosomes 9 and 22 in CML [103], the *PML-RARA* translocation involving chromosomes 15 and 17 in acute promyelocytic leukemia [104], and the translocations of *MYC* in chromosome 8 with either of the three of the immunoglobulin genes: *IGH* in chromosome 14, *IGL* in chromosome 22, and *IGK* in chromosome 2 in Burkitt's lymphoma [99]. The *MYC* gene has been often found to be close to the *IGH* gene locus compared with the *IGL* and *IGK* gene loci, which may explain why the *MYC-IGH* translocation is observed in around 80% of Burkitt's lymphoma cases while the remaining *MYC-IGK* and *MYC-IGL* translocations occupy the rest [105]. Interestingly, the specific chromosomal position of the *MYC* gene, but not its sequence, was proven to affect its involvement in translocations, since the replacement with *MYCN* sequence does not affect its role as a translocation partner [106].

With the advent of advanced staining and imaging technologies, the preservation of the overall 3D structure of the nucleus and the 3D imaging of the whole chromosome have become possible. Using the technology of 3D structured illumination microscopy (3D-SIM) with pan-chromosome-specific paints, Sathitruangsak et al. investigated the positioning of chromosomes 4, 9, 11, 14, 16, 18, 19, and 22 in normal lymphocytes and myeloma cells from treatment-naïve patients with monoclonal gammopathy of undetermined significance or multiple myeloma [107]. They calculated the overlap between five chromosomal pairs and found out that the pair of chromosomes 18 and 19, which does not usually engage in chromosomal translocation in multiple myeloma, has up to 50% less overlap compared to the remaining pairs, which are usually involved in translocations, both in normal and malignant nuclei. The chromosomal pair which has less overlap has fewer chances of physical interaction or proximity, which can then negatively affect translocation formation.

FISH methods examine the distance between and the relative position of specific gene loci in the nucleus while Hi-C methods determine the interactions of the gene loci with each other on the genome-wide scale. In this line, Zhang et al. demonstrated the positive correlation between inter-chromosomal contacts and translocation frequency [108]. They built a high resolution Hi-C spatial organization map of G1-arrested mouse pro-B cells and used high-throughput translocation sequencing to detect the translocations after DSB induction by ionizing radiation. They found that in the condition when DNA damage is random (i.e., DSBs happen with the same frequency in different sites), the spatial proximity between loci is the main factor contributing to translocation formation (Figure 3).

To further demonstrate the role of spatial proximity in oncogenic translocations, the publicly available Hi-C datasets on genome-wide interaction maps of a lymphoblastoid cell line (GM06990) and an erythroleukemic cell line (K562) were analyzed along with the collections of 1533 chromosomal translocations from cancer and germline genomes [91]. They observed that the gene loci that are usually involved in oncogenic translocations, such as *MYC-IGH* and *BCR-ABL*, have high Hi-C contact frequencies in normal cells. With these findings, the authors were able to show that the high contact interaction between any two gene loci can influence translocation formation if DSBs are formed in them.

To conclude, the overall nuclear genome architecture has been shown to have a significant influence on the formation of chromosomal translocation by virtue of spatial proximity, which can be analyzed by measuring the physical distance or calculating the contact frequency between potential translocation partners.

3.2. Transcriptional Activity

Transcriptional activity can influence the genome's vulnerability to DNA damage and its access to the cellular repair machinery. Endogenous DSBs or DSBs caused by DNA replication inhibitors favorably occur in transcriptionally active genomic regions [87,109,110], which could be explained by transcription-induced DNA damage or the collision of transcriptional and replication forks in S phase. Transcriptionally active chromatin is also more vulnerable to DSB formation induced by ionizing radiation [111]. Consistently, it was observed that genetic rearrangements such as chromosomal translocations preferentially occur in coding regions and in actively transcribed genes compared to the intergenic regions and transcriptionally silent genes [88]. Active gene transcription can cause DNA damage in several ways. Transcription produces short DNA–RNA hybrids called R loops that leave the non-template DNA single strand susceptible to mutagenic activities, including DSBs [63,64,112–115]. In B cells, AID was observed to bind R loops formed at the *MYC* and *IGH* gene loci and to produce DSBs [116–118]. Moreover, AID, through its interaction with Spt5, can be recruited to gene promoters occupied by stalled RNA polymerase II, which explains the prevalence of AID-mediated damages within transcription start sites [119,120].

DNA topoisomerase III beta (TOPB3) has been found to relax the negative supercoiled DNA, reducing the transcription-generated R loops and *MYC-IGH* translocation in mammalian cells [121]. Recent studies have shown that other repair factors suppress chromosomal translocations by modulating the R loop formation [115]. In particular, ATM is a known suppressor of the *MYC-IGH* translocation in vivo [122], and it can also prevent the formation of R loops in proliferating cells [123]. BRCA2, which plays a key role in the HR pathway by recruiting Rad51 to the DSBs, has also been found to prevent R loop formation [124]. The R loop suppression activity of BRCA2 could be part of the coordinated roles between BRCA1 and BRCA2 in the HR pathway, or it could be part of the Fanconi anemia pathway to protect the replication fork [115,125].

However, in the study of mutations in different cancers, euchromatin had a lower mutation rate due to transcription-coupled repair, while heterochromatin and nucleosomal DNA were less accessible to repair machinery and had a higher cancer mutation rate [126]. Meanwhile, a relationship between transcriptional activity and chromatin movement was observed in HeLa cells, where inhibition of transcription with actinomycin D abolished increased transcriptional chromatin mobility and configurational changes during early S phase [127]. Moreover, actively transcribed genes are recruited into shared transcription factories, which increases their spatial proximity and promotes translocation in case DSBs occur among them [128]. This was shown for the genes that are usually involved in chromosomal translocations that cause Burkitt's lymphoma: *MYC*, *IGH*, *IGL*, and *IGK*, where they share a common translocation factory [129]. The correlation between high gene transcription, their spatial proximity within the nuclear space, and chromosomal translocation appearance have also been observed in diffuse large B-cell lymphoma [130], anaplastic cell lymphoma [131], and prostate cancer [132].

3.3. DNA Damage Response

Eukaryotic cells have evolved complex and tightly regulated mechanisms that coordinate the detection, signaling, and repair of DNA damage [133]. These mechanisms are not always efficient, and the formation of chromosomal translocations is one example when the DNA repair machinery incorrectly repairs DSBs. Chromosome translocations are normally found in peripheral blood cells and the non-neoplastic tissues of healthy individuals [134–139], which indicates that their formation should not be seen as a pathological cellular event but rather as an inevitable outcome of DNA repair activities. Only when the chromosomal translocation results in molecular and functional consequences that can disrupt the normal physiological processes and then confer selective survival advantage to the cell does it become pathologically relevant.

DNA breaks are repaired either by homologous recombination (HR) or the non-homologous end joining (NHEJ). The HR pathway is mostly used during S phase of the cell cycle. HR uses the homologous template from the unbroken strand to repair the breakage with high fidelity [140,141]. The NHEJ pathway is cell cycle-independent; it ligates the broken ends together and does not require an extended homology template [142,143]. The DNA ends can be either resected during S/G2 stages or suppressed in the G1 stage; this affects the choice of the repair pathway [144]. The resected DNA produces 3′ overhangs coated with Rad51, forming the nucleoprotein filament that is essential in the strand invasion of a homologous template to start the repair [145]. If the homologous template is provided by the sister chromatid, then faithful repair is performed by the HR pathway as opposed to the protected ends in NHEJ [144]. In the absence of a homologous template from a sister chromatid, the resected DNA end can then be repaired by the alternative NHEJ pathway (a-NHEJ) that uses a microhomology of around less than 100 bp, thus requiring limited resection [146]. Additionally, resected DNA ends can be repaired by single-strand annealing (SSA), but this needs annealing of repeats that are more than 100 bp, thus requiring extensive resection [147,148]. Because of the absence of a repair template, the NHEJ pathway results in erroneous repair, ranging from the small indels or mutations at the broken ends up to the relocation of the broken segments leading to chromosomal rearrangements [149]. Whichever pathway the cell utilizes, the repair usually takes from minutes to hours [150]. Both the HR and NHEJ pathways can compete for or even collaborate in DSB repair [151]. DNA repair initiated by the HR pathway can be completed by the NHEJ pathway in some cases [152–154], but when it comes to translocation formation, NHEJ is the most proficient, followed by the SSA pathway [149].

Translocations result from erroneous DNA repair mediated by one of the three different DNA damage response and repair (DDR) pathways: the classical NHEJ (cNHEJ; mediated by DNA-PKcs and Lig4); alternative NHEJ (aNHEJ; mediated by CtIP, Parp1 and Lig1/Lig3); and the single-strand annealing (SSA; mediated by Rad-52) pathway. Chromosome translocations in rodent and human cells are mainly formed by the alternative NHEJ pathway [155–158]. SSA-mediated translocations occur predominantly within repetitive DNA elements [159]. The choice of these pathways depends on several factors.

Kinetic aspect. The cNHEJ pathway proceeds very fast (within 2–4 h) [160,161], which makes it the cellular "first-line therapy" of DSBs. Fast kinetics explains the low frequency of translocation formation with cNHEJ [156]: right after the lesion, DSBs are situated close to each other and their direct joining is favored. Consistently, when cNHEJ is slowed down in G1 (a related process known as Artemis- or resection-dependent cNHEJ), the probability of translocation formation is increased [160,162]. An impairment or slow progression of cNHEJ allows aNHEJ to manifest as a backup process [156,161]. The HR pathway proceeds slower than the NHEJ pathway [163] and has a priority over NHEJ in G2 in repairing DSBs situated in heterochromatin regions, complex, or slow-to-repair lesions [163–165]. Abrogated or stalled HR can be rescued by the aNHEJ pathway [161].

Spatial aspect. Different types of DNA repair have a spatial selectivity as well, which is influenced by the chromatin context. In the study of CRISPR/Cas9-induced DSBs, cNHEJ was found to largely comprise the main DNA repair mechanism both for euchromatin and

heterochromatin, while aNHEJ participates in a small proportion of DSBs repair, although its contribution to DSB repair increases in heterochromatin regions [74]. Another study has shown that the DSBs induced by CRISPR/Cas9 in pericentric heterochromatin are immobile and repaired by NHEJ in G1, while in S/G2 they move to the periphery of heterochromatin and are repaired by HR [166]. In addition, the centromeric DSBs that are majorly peripheral recruit both NHEJ and HR factors throughout the cell cycle [166].

Cell type aspect. The demand for sister chromatids as repair templates restricts HR to S/G2 phase; thus, NHEJ is considered as the dominant repair pathway in most of the human cells. There are, however, some notable exceptions. DSB repair in human embryonic stem cells is largely dependent on HR due to the prolonged S phase, which facilitates the accurate repair of DNA breaks [167]. The differentiation of human embryonic stem cells decreases DNA repair through HR [168]. In some cases, cell differentiation accompanied by chromatin condensation may even completely suppress DSB repair response [169]. Cancer cells often grow in hypoxic conditions, which may also preferentially inhibit HR and contribute to increased rates of mutation [170].

3.4. Chromatin State and Mobility

The DNA in eukaryotic cells is packaged into nucleosomes and then further compacted into denser chromatin [171]. Each nucleosome is composed of around 150 bp DNA that is wrapped around a set of histone octamer [172] containing two copies of H2A, H2B, H3, and H4 [173,174]. The realization of the highly dynamic nature of chromatin has uncovered various regulatory mechanisms that affect different cellular activities such as cell division, DNA replication, DNA repair, and gene expression [175,176]. Chromatin contains epigenetic marks which consist of histone modifications, histone variants, and regions of open chromatin whose distribution and activity are shown to be different in different cell types and diseases [177,178]. The combination of these marks in their spatial context constitutes the chromatin state that encompasses genomic elements such as promoters, enhancers and different regions which are either transcribed, repressed or repetitive [179,180]. Using live cell tracking of chromosome loci tagged with either GFP or fluorescent topoisomerase II, scientists were able to show in yeasts and in Drosophila that the chromatin moves in a suggestive Brownian motion, right into a confined subregion of the nucleus [181]. This constrained motion of chromatin was also observed in bacteria and mammalian cells whose chromatin movement ranges from 10^{-4} to 10^{-3} $\mu m^2/s$ [182]. However, chromatin movement does not fully follow the Brownian motion. Chromatin movement has been shown to be dependent on ATP levels and is affected by temperature [183–185]. It was also shown that movement of the intact chromatin can be affected by the cell cycle [127,186–190], transcription activity [184,191–193], and chromatin condensation [184,194,195]. Physiological chromatin movements occurring within the cell nucleus many times a day can predispose to the chromosomal translocation formation; however, other events should take place to produce translocations.

The chromatin state was shown to affect the chromatin mobility as chromatin decondensation without changes in transcription activity resulted in the repositioning of genes [195] in a manner similar to that of the transcription-induced chromosomal repositioning [191]. In yeasts, actin-dependent increase of chromatin mobility [194] was observed after targeting the nucleosome remodeling complex INO80 and INO80-dependent nucleosome remodeling [184]. On the other hand, a 30–40% reduction in chromatin density in mammalian cells was observed after DSB induction [196]. In Drosophila, the DSBs located in the heterochromatic region move out from their original domain to be repaired [197]. Specifically, the DSBs in yeasts and mammalian cells were found to move out into the periphery of the heterochromatin [198,199], and this was independent of chromatin state, at least in mammalian cells [166]. However, DSBs associated with the nuclear lamina were observed be repaired differently compared to relocated DSBs [200]. On the other hand, an increase in condensin II activity was found to promote chromatin condensation, spatial

separation of CTs, decreased CT contacts and intermixing, and, as a result, decreased translocation frequency after DSBs induction in Drosophila cells [201].

3.5. DSB Movement and Clustering

Upon DNA damage, repair factors flock the sites of breakage and form the microscopically-detectable DNA repair foci [202]. The movement of DSBs is usually investigated using time-lapse microscopy on fluorescently tagged DNA repair foci. Upon DSB induction, the resulting chromosomal breaks in yeast and mammals were observed to remain physically close to each other and were positionally stable over time [203–205].

In yeasts, DSBs were observed to group together in common repair centers [206]. In contrast in mammalian cells, live cell tracking of several DSBs revealed that DSBs did not group together or form clusters, although there were instances when they did, but they were only transient and were observed to be reversible [196,207]. The DNA repair foci after induction of up to four DSBs were also tracked and were found to remain separated [92,205]; they only came together or clustered to a common repair focus if they were to be translocated [92]. The DSBs in mammalian cells were only observed to cluster in common repair foci in case of induction of multiple DSBs (around 100 per cell) [208]. The clustering of multiple DSBs in common repair foci in mammalian cells could be due to the random motion of the breaks, increasing the probability that they meet and group together, or it could be due to the overall control mechanism, as placing the DSBs together in common repair foci can increase the chances that they be illegitimately joined and produce oncogenic translocations [182]. Another possibility is that there are just a limited number of repair foci which the cell can form, thus DSBs are driven to these repair foci similarly to genes recruited into shared transcription factories [128]. The nucleolus is a hub for many nuclear functions [209] formed by rDNA genes located on acrocentric chromosomes. Acrocentric chromosomes are actively involved in chromosomal translocations [210] and several derivative chromosomes remain associated with the nucleolus; this affects expression of proto-oncogenes [31]. Recently, genes whose transcription was inhibited by DSBs were shown to cluster in the vicinity of the nucleolus [211,212]; this potentially increases the probability of translocation, including those with the acrocentric chromosomes.

In mammalian cells, DSBs exhibit similar mobility with that of intact chromatin with a mean displacement of around 1 $\mu m^2/h$ [182,196,207]. This includes DSBs formed after exposure to ultrasoft X-rays [213] and DSBs induced by endonucleases [205]. On the other hand, large-scale DNA damage from exposure to α-particles resulted in an extensive movement and clustering of DSB-containing chromosome domains [214]. This was also the case after exposure to γ irradiation, where DSB mobility was observed to be at least twice as high as that of the intact loci [186]. γ Irradiation was shown to induce repositioning of *ABL* and *BCR* genes in the nuclear center of lymphocytes [103]. When breaks were induced by I-SceI endonuclease, the translocating DSBs were observed to exhibit higher mobility compared to the non-translocating DSBs; 5% of the translocating DSBs were capable of traveling long distance (up to 5 μm) [92]. This observation supported the notion that DSBs do search and move to find their respective translocation partner, supporting the "breakage first" model of translocation formation.

In yeasts, breakage induced by I-SceI resulted in the increased mobility of both the induced DSBs and the intact chromatin [215–218]. The increased DSB mobility in yeasts was shown to be dependent on the homologous recombination factors such as Rad51 [215,217,219–222] as yeasts do not have other repair pathways than the HR pathway and DSBs need to search the entire nucleus for homology [140].

3.6. Cell Cycle

Cell cycle stage determines the state of cellular chromatin and how it is repaired when DSBs occur. As such, it can potentially affect translocation formation. Chromatin mobility has been observed to be different across cell stages, with the highest mobility observed during the early G1 phase and thereafter, the chromosome territories remain quite stable

from mid G1 to late G2 [187,189]. During the S phase, the highest mobility can be observed in the early S phase [127]. However in a study where the entire cell cycle phases were considered, no significant differences in chromatin movement were observed between cells in G1, S, and G2 [190]. Nonetheless, the chromatin movement can lead to distancing or approaching of specific gene loci during the cell cycle. Namely, it was shown that the spatial proximity between *ABL-BCR* and *PML-RARA* pairs increases in the period from late S to G2 in hematopoietic precursors and lymphoid cells [104]. The "natural" mobility of intact chromatin does not always reflect the mobility of DSBs that occurs throughout the cell cycle. It was shown that DSBs, induced by ionizing radiation, had decreased mobility during S phase compared with G1/G2 [186]. In contrast, DSBs induced by CRISPR/Cas9 in pericentric heterochromatic regions were shown to be positionally stable in G1 and then move towards the periphery in G2 [166].

How the cell decides which DNA repair pathway to utilize to repair DSBs can be affected by its cell cycle stage: the accurate HR pathway takes place in late S and G2, while the NHEJ pathway is active throughout the cell cycle [140,164]. However in centromeric heterochromatin regions, it was shown that the HR pathway is active both in G1 and S/G2 [166]. Surprisingly, the HR pathway does not have a priority over NHEJ in repairing DSBs during G2 and only accounts for the repair of ~15% of ionizing radiation-induced DSBs [163]. The NHEJ pathway has the highest activity observed in the G1 phase, while the HR pathway has its highest activity in S phase [223]. Although the S/G2 phase requires accurate DNA repair to maintain genomic stability, chromosomal translocations can still be generated at any time as the NHEJ pathway is active all throughout the cell cycle. However, experimentally, no changes in DSB pairing and translocation formation were detected at different cell cycle stages after ISceI-induced DSBs in NIH3T3duo cells [92]. Perhaps this observation could be due to site- and cell-specific conditions, and extrapolating this to the general conclusion about the role of cell cycle stage on translocation formation is still premature.

4. Conclusions

Spatial proximity of the potential translation partners primarily affects translocation formation, perhaps largely because chromosomal translocation is a product of a proximity-based DSB misrepair. However, several other factors come into play and influence each other to affect multiple stages in chromosomal translocation formation (Figure 3), highlighting the sheer complexity of this potentially serious and life-threatening occurrence.

Author Contributions: Writing—original draft preparation, R.J.C., A.S., A.K. and M.S.; writing—review and editing, D.G. and Y.V. All authors have read and agreed to the published version of the manuscript.

Funding: This study was supported by Ministry of Science and Higher Education of the Russian Federation (075-15-2020-773). RJC was a recipient of the CHED-PhilFrance Scholarship Programme.

Conflicts of Interest: The authors declare no conflict of interest. The funders had no role in the design of the study; in the collection, analyses, or interpretation of data; in the writing of the manuscript; or in the decision to publish the results.

References

1. Nussenzweig, A.; Nussenzweig, M.C. Origin of Chromosomal Translocations in Lymphoid Cancer. *Cell* **2010**, *141*, 27–38. [CrossRef] [PubMed]
2. Ramsden, D.A.; Nussenzweig, A. Mechanisms Driving Chromosomal Translocations: Lost in Time and Space. *Oncogene* **2021**, *40*, 4263–4270. [CrossRef] [PubMed]
3. Roukos, V.; Misteli, T. The Biogenesis of Chromosome Translocations. *Nat. Cell Biol.* **2014**, *16*, 293–300. [CrossRef] [PubMed]
4. Zheng, J. Oncogenic Chromosomal Translocations and Human Cancer (Review). *Oncol. Rep.* **2013**, *30*, 2011–2019. [CrossRef] [PubMed]
5. Balmain, A. Cancer Genetics: From Boveri and Mendel to Microarrays. *Nat. Rev. Cancer* **2001**, *1*, 77–82. [CrossRef] [PubMed]
6. Boveri, T. Concerning the Origin of Malignant Tumours by Theodor Boveri. Translated and Annotated by Henry Harris. *J. Cell Sci.* **2008**, *121*, 1–84. [CrossRef] [PubMed]

7. Nowell, P.C.; Hungerford, D.A. Chromosome Studies on Normal and Leukemic Human Leukocytes. *J. Natl. Cancer Inst.* **1960**, *25*, 85–109. [CrossRef]
8. Levan, A. Some Current Problems of Cancer Cytogenetics. *Hereditas* **1967**, *57*, 343–355. [CrossRef]
9. Rowley, J.D. A New Consistent Chromosomal Abnormality in Chronic Myelogenous Leukaemia Identified by Quinacrine Fluorescence and Giemsa Staining. *Nature* **1973**, *243*, 290–293. [CrossRef]
10. Rowley, J.D. Identification of a Translocation with Quinacrine Fluorescence in a Patient with Acute Leukemia. *Ann. De Genet.* **1973**, *16*, 109–112.
11. Bohlander, S.K.; Kakadiya, P.M.; Coysh, A. Chromosome Rearrangements and Translocations. In *Encyclopedia of Cancer*, 3rd ed.; Boffetta, P., Hainaut, P., Eds.; Academic Press: Oxford, UK, 2019; pp. 389–404. ISBN 978-0-12-812485-7.
12. Morin, S.J.; Eccles, J.; Iturriaga, A.; Zimmerman, R.S. Translocations, Inversions and Other Chromosome Rearrangements. *Fertil. Steril.* **2017**, *107*, 19–26. [CrossRef]
13. Barra, V.; Fachinetti, D. The Dark Side of Centromeres: Types, Causes and Consequences of Structural Abnormalities Implicating Centromeric DNA. *Nat. Commun.* **2018**, *9*, 4340. [CrossRef]
14. Robertson, W.R.B. Chromosome Studies. I. Taxonomic Relationships Shown in the Chromosomes of Tettigidae and Acrididae: V-Shaped Chromosomes and Their Significance in Acrididae, Locustidae, and Gryllidae: Chromosomes and Variation. *J. Morphol.* **1916**, *27*, 179–331. [CrossRef]
15. Matveevsky, S.; Tretiakov, A.; Kashintsova, A.; Bakloushinskaya, I.; Kolomiets, O. Meiotic Nuclear Architecture in Distinct Mole Vole Hybrids with Robertsonian Translocations: Chromosome Chains, Stretched Centromeres, and Distorted Recombination. *Int. J. Mol. Sci.* **2020**, *21*, 7630. [CrossRef]
16. Spinner, N.B.; Conlin, L.K.; Mulchandani, S.; Emanuel, B.S. Chapter 45—Deletions and Other Structural Abnormalities of the Autosomes. In *Emery and Rimoin's Principles and Practice of Medical Genetics*, 6th ed.; Rimoin, D., Pyeritz, R., Korf, B., Eds.; Academic Press: Oxford, UK, 2013; pp. 1–37. ISBN 978-0-12-383834-6.
17. Eykelenboom, J.E.; Briggs, G.J.; Bradshaw, N.J.; Soares, D.C.; Ogawa, F.; Christie, S.; Malavasi, E.L.V.; Makedonopoulou, P.; Mackie, S.; Malloy, M.P.; et al. A t(1;11) Translocation Linked to Schizophrenia and Affective Disorders Gives Rise to Aberrant Chimeric DISC1 Transcripts That Encode Structurally Altered, Deleterious Mitochondrial Proteins. *Hum. Mol. Genet.* **2012**, *21*, 3374–3386. [CrossRef]
18. Fraccaro, M.; Maraschio, P.; Pasquali, F.; Tiepolo, L.; Zuffardi, O.; Giarola, A. Male Infertility and 13–14 Translocation. *Lancet* **1973**, *1*, 488. [CrossRef]
19. Mitelman, F.; Johansson, B.; Mertens, F. Mitelman Database of Chromosome Aberrations and Gene Fusions in Cancer. Available online: https://mitelmandatabase.isb-cgc.org (accessed on 5 July 2021).
20. Nakano, K.; Takahashi, S. Translocation-Related Sarcomas. *Int. J. Mol. Sci.* **2018**, *19*, 3784. [CrossRef]
21. Prasher, V.P. Presenile Dementia Associated with Unbalanced Robertsonian Translocation Form of Down's Syndrome. *Lancet* **1993**, *342*, 686–687. [CrossRef]
22. Zhang, H.-G.; Wang, R.-X.; Pan, Y.; Zhang, H.; Li, L.-L.; Zhu, H.-B.; Liu, R.-Z. A Report of Nine Cases and Review of the Literature of Infertile Men Carrying Balanced Translocations Involving Chromosome 5. *Mol. Cytogenet* **2018**, *11*, 10. [CrossRef]
23. Daley, G.Q.; Baltimore, D. Transformation of an Interleukin 3-Dependent Hematopoietic Cell Line by the Chronic Myelogenous Leukemia-Specific P210(Bcr/Abl) Protein. *Proc. Natl. Acad. Sci. USA* **1988**, *85*, 9312–9316. [CrossRef]
24. Daley, G.Q.; Van Etten, R.A.; Baltimore, D. Induction of Chronic Myelogenous Leukemia in Mice by the P210 Bcr/Abl Gene of the Philadelphia Chromosome. *Science* **1990**, *247*, 824–830. [CrossRef]
25. Gishizky, M.L.; Johnson-White, J.; Witte, O.N. Efficient Transplantation of BCR-ABL-Induced Chronic Myelogenous Leukemia-like Syndrome in Mice. *Proc. Natl. Acad. Sci. USA* **1993**, *90*, 3755–3759. [CrossRef]
26. Adams, J.M.; Harris, A.W.; Pinkert, C.A.; Corcoran, L.M.; Alexander, W.S.; Cory, S.; Palmiter, R.D.; Brinster, R.L. The C-Myc Oncogene Driven by Immunoglobulin Enhancers Induces Lymphoid Malignancy in Transgenic Mice. *Nature* **1985**, *318*, 533–538. [CrossRef]
27. Ar-Rushdi, A.; Nishikura, K.; Erikson, J.; Watt, R.; Rovera, G.; Croce, C.M. Differential Expression of the Translocated and the Untranslocated C-Myc Oncogene in Burkitt Lymphoma. *Science* **1983**, *222*, 390–393. [CrossRef]
28. Dalla-Favera, R.; Bregni, M.; Erikson, J.; Patterson, D.; Gallo, R.C.; Croce, C.M. Human C-Myc Onc Gene Is Located on the Region of Chromosome 8 That Is Translocated in Burkitt Lymphoma Cells. *Proc. Natl. Acad. Sci. USA* **1982**, *79*, 7824–7827. [CrossRef]
29. Taub, R.; Kirsch, I.; Morton, C.; Lenoir, G.; Swan, D.; Tronick, S.; Aaronson, S.; Leder, P. Translocation of the C-Myc Gene into the Immunoglobulin Heavy Chain Locus in Human Burkitt Lymphoma and Murine Plasmacytoma Cells. *Proc. Natl. Acad. Sci. USA* **1982**, *79*, 7837–7841. [CrossRef]
30. Zech, L.; Haglund, U.; Nilsson, K.; Klein, G. Characteristic Chromosomal Abnormalities in Biopsies and Lymphoid-cell Lines from Patients with Burkitt and Non-burkitt Lymphomas. *Int. J. Cancer* **1976**, *17*, 47–56. [CrossRef]
31. Allinne, J.; Pichugin, A.; Iarovaia, O.; Klibi, M.; Barat, A.; Zlotek-Zlotkiewicz, E.; Markozashvili, D.; Petrova, N.; Camara-Clayette, V.; Ioudinkova, E.; et al. Perinucleolar Relocalization and Nucleolin as Crucial Events in the Transcriptional Activation of Key Genes in Mantle Cell Lymphoma. *Blood* **2014**, *123*, 2044–2053. [CrossRef]
32. Bickmore, W.A.; van Steensel, B. Genome Architecture: Domain Organization of Interphase Chromosomes. *Cell* **2013**, *152*, 1270–1284. [CrossRef]

33. Harewood, L.; Schutz, F.; Boyle, S.; Perry, P.; Delorenzi, M.; Bickmore, W.A.; Reymond, A. The Effect of Translocation-Induced Nuclear Reorganization on Gene Expression. *Genome Res.* **2010**, *20*, 554–564. [CrossRef]
34. Meaburn, K.J. Spatial Genome Organization and Its Emerging Role as a Potential Diagnosis Tool. *Front. Genet.* **2016**, *7*, 134. [CrossRef] [PubMed]
35. Pannunzio, N.R.; Lieber, M.R. Concept of DNA Lesion Longevity and Chromosomal Translocations. *Trends Biochem. Sci.* **2018**, *43*, 490–498. [CrossRef] [PubMed]
36. Zheng, H.; Xie, W. The Role of 3D Genome Organization in Development and Cell Differentiation. *Nat. Rev. Mol. Cell Biol.* **2019**, *20*, 535–550. [CrossRef] [PubMed]
37. Mitelman, F.; Johansson, B.; Mertens, F. The Impact of Translocations and Gene Fusions on Cancer Causation. *Nat. Rev. Cancer* **2007**, *7*, 233–245. [CrossRef]
38. Robbiani, D.F.; Nussenzweig, M.C. Chromosome Translocation, B Cell Lymphoma, and Activation-Induced Cytidine Deaminase. *Annu. Rev. Pathol. Mech. Dis.* **2013**, *8*, 79–103. [CrossRef]
39. Bray, F.; Ferlay, J.; Soerjomataram, I.; Siegel, R.L.; Torre, L.A.; Jemal, A. Global Cancer Statistics 2018: GLOBOCAN Estimates of Incidence and Mortality Worldwide for 36 Cancers in 185 Countries. *CA A Cancer J. Clin.* **2018**, *68*, 394–424. [CrossRef]
40. Ferlay, J.; Colombet, M.; Soerjomataram, I.; Mathers, C.; Parkin, D.M.; Piñeros, M.; Znaor, A.; Bray, F. Estimating the Global Cancer Incidence and Mortality in 2018: GLOBOCAN Sources and Methods. *Int. J. Cancer* **2019**, *144*, 1941–1953. [CrossRef]
41. Lobato, M.N.; Metzler, M.; Drynan, L.; Forster, A.; Pannell, R.; Rabbitts, T.H. Modeling Chromosomal Translocations Using Conditional Alleles to Recapitulate Initiating Events in Human Leukemias. *JNCI Monogr.* **2008**, *2008*, 58–63. [CrossRef]
42. Nambiar, M.; Raghavan, S.C. How Does DNA Break during Chromosomal Translocations? *Nucleic Acids Res.* **2011**, *39*, 5813–5825. [CrossRef]
43. Mitelman, F.; Johansson, B.; Mertens, F. Mitelman Database Chromosome Aberrations and Gene Fusions in Cancer. Available online: https://mitelmandatabase.isb-cgc.org/about (accessed on 28 January 2020).
44. Cannan, W.J.; Pederson, D.S. Mechanisms and Consequences of Double-Strand DNA Break Formation in Chromatin. *J. Cell. Physiol.* **2016**, *231*, 3–14. [CrossRef]
45. Georgakilas, A.G. Processing of DNA Damage Clusters in Human Cells: Current Status of Knowledge. *Mol. BioSystems* **2008**, *4*, 30–35. [CrossRef]
46. Sax, K. Chromosome Aberrations Induced by X-Rays. *Genetics* **1938**, *23*, 494–516. [CrossRef]
47. Shikazono, N.; Noguchi, M.; Fujii, K.; Urushibara, A.; Yokoya, A. The Yield, Processing, and Biological Consequences of Clustered DNA Damage Induced by Ionizing Radiation. *J. Radiat Res.* **2009**, *50*, 27–36. [CrossRef]
48. Sutherland, B.M.; Bennett, P.V.; Sutherland, J.C.; Laval, J. Clustered DNA Damages Induced by X Rays in Human Cells. *Rare* **2002**, *157*, 611–616. [CrossRef]
49. Ward, J.F. DNA Damage Produced by Ionizing Radiation in Mammalian Cells: Identities, Mechanisms of Formation, and Reparability. In *Progress in Nucleic Acid Research and Molecular Biology*; Cohn, W.E., Moldave, K., Eds.; Academic Press: Cambridge, MA, USA, 1988; Volume 35, pp. 95–125.
50. Cao, L.; Alani, E.; Kleckner, N. A Pathway for Generation and Processing of Double-Strand Breaks during Meiotic Recombination in S. Cerevisiae. *Cell* **1990**, *61*, 1089–1101. [CrossRef]
51. Keeney, S.; Giroux, C.N.; Kleckner, N. Meiosis-Specific DNA Double-Strand Breaks Are Catalyzed by Spo11, a Member of a Widely Conserved Protein Family. *Cell* **1997**, *88*, 375–384. [CrossRef]
52. De Massy, B. Initiation of Meiotic Recombination: How and Where? Conservation and Specificities Among Eukaryotes. *Annu. Rev. Genet.* **2013**, *47*, 563–599. [CrossRef]
53. Paigen, K.; Petkov, P. Mammalian Recombination Hot Spots: Properties, Control and Evolution. *Nat. Rev. Genet.* **2010**, *11*, 221–233. [CrossRef]
54. Cobb, R.M.; Oestreich, K.J.; Osipovich, O.A.; Oltz, E.M. Accessibility Control of V(D)J Recombination. In *Advances in Immunology*; Academic Press: Cambridge, MA, USA, 2006; Volume 91, pp. 45–109.
55. Davis, M.M.; Bjorkman, P.J. T-Cell Antigen Receptor Genes and T-Cell Recognition. *Nature* **1988**, *334*, 395–402. [CrossRef]
56. Krangel, M.S. Mechanics of T Cell Receptor Gene Rearrangement. *Curr. Opin. Immunol.* **2009**, *21*, 133–139. [CrossRef]
57. Chaudhuri, J.; Basu, U.; Zarrin, A.; Yan, C.; Franco, S.; Perlot, T.; Vuong, B.; Wang, J.; Phan, R.T.; Datta, A.; et al. Evolution of the Immunoglobulin Heavy Chain Class Switch Recombination Mechanism. In *Advances in Immunology*; AID for Immunoglobulin Diversity; Academic Press: Cambridge, MA, USA, 2007; Volume 94, pp. 157–214.
58. Di Noia, J.M.; Neuberger, M.S. Molecular Mechanisms of Antibody Somatic Hypermutation. *Annu. Rev. Biochem.* **2007**, *76*, 1–22. [CrossRef]
59. Schatz, D.G.; Baltimore, D. Uncovering the V(D)J Recombinase. *Cell* **2004**, *116*, S103–S108. [CrossRef]
60. Honjo, T.; Kinoshita, K.; Muramatsu, M. Molecular Mechanism of Class Switch Recombination: Linkage with Somatic Hypermutation. *Annu. Rev. Immunol.* **2002**, *20*, 165–196. [CrossRef]
61. Liu, M.; Duke, J.L.; Richter, D.J.; Vinuesa, C.G.; Goodnow, C.C.; Kleinstein, S.H.; Schatz, D.G. Two Levels of Protection for the B Cell Genome during Somatic Hypermutation. *Nature* **2008**, *451*, 841–845. [CrossRef] [PubMed]
62. Helmrich, A.; Stout-Weider, K.; Hermann, K.; Schrock, E.; Heiden, T. Common Fragile Sites Are Conserved Features of Human and Mouse Chromosomes and Relate to Large Active Genes. *Genome Res.* **2006**, *16*, 1222–1230. [CrossRef] [PubMed]

63. Helmrich, A.; Ballarino, M.; Tora, L. Collisions between Replication and Transcription Complexes Cause Common Fragile Site Instability at the Longest Human Genes. *Mol. Cell* **2011**, *44*, 966–977. [CrossRef] [PubMed]
64. Huertas, P.; Aguilera, A. Cotranscriptionally Formed DNA:RNA Hybrids Mediate Transcription Elongation Impairment and Transcription-Associated Recombination. *Mol. Cell* **2003**, *12*, 711–721. [CrossRef]
65. Iannelli, F.; Galbiati, A.; Capozzo, I.; Nguyen, Q.; Magnuson, B.; Michelini, F.; D'Alessandro, G.; Cabrini, M.; Roncador, M.; Francia, S.; et al. A Damaged Genome's Transcriptional Landscape through Multilayered Expression Profiling around in Situ -Mapped DNA Double-Strand Breaks. *Nat. Commun.* **2017**, *8*, 15656. [CrossRef]
66. Le Tallec, B.; Dutrillaux, B.; Lachages, A.-M.; Millot, G.A.; Brison, O.; Debatisse, M. Molecular Profiling of Common Fragile Sites in Human Fibroblasts. *Nat. Struct. Mol. Biol.* **2011**, *18*, 1421–1423. [CrossRef]
67. Sutherland, G.R. Heritable Fragile Sites on Human Chromosomes II. Distribution, Phenotypic Effects, and Cytogenetics. *Am. J. Hum. Genet.* **1979**, *31*, 136–148.
68. Pfeiffer, P.; Goedecke, W.; Obe, G. Mechanisms of DNA Double-Strand Break Repair and Their Potential to Induce Chromosomal Aberrations. *Mutagenesis* **2000**, *15*, 289–302. [CrossRef]
69. Syeda, A.H.; Hawkins, M.; McGlynn, P. Recombination and Replication. *Cold Spring Harb Perspect Biol.* **2014**, *6*, a016550. [CrossRef]
70. Fraga, C.G.; Shigenaga, M.K.; Park, J.W.; Degan, P.; Ames, B.N. Oxidative Damage to DNA during Aging: 8-Hydroxy-2'-Deoxyguanosine in Rat Organ DNA and Urine. *Proc. Natl. Acad. Sci. USA* **1990**, *87*, 4533–4537. [CrossRef]
71. Lindahl, T.; Nyberg, B. Rate of Depurination of Native Deoxyribonucleic Acid. *Biochemistry* **1972**, *11*, 3610–3618. [CrossRef]
72. Jain, S.; Shukla, S.; Yang, C.; Zhang, M.; Fatma, Z.; Lingamaneni, M.; Abesteh, S.; Lane, S.T.; Xiong, X.; Wang, Y.; et al. TALEN Outperforms Cas9 in Editing Heterochromatin Target Sites. *Nat. Commun.* **2021**, *12*, 606. [CrossRef]
73. Mitrentsi, I.; Soutoglou, E. CRISPR/Cas9-Induced Breaks in Heterochromatin, Visualized by Immunofluorescence. *Methods Mol. Biol.* **2021**, *2153*, 439–445. [CrossRef]
74. Schep, R.; Brinkman, E.K.; Leemans, C.; Vergara, X.; van der Weide, R.H.; Morris, B.; van Schaik, T.; Manzo, S.G.; Peric-Hupkes, D.; van den Berg, J.; et al. Impact of Chromatin Context on Cas9-Induced DNA Double-Strand Break Repair Pathway Balance. *Mol. Cell* **2021**, *81*, 2216–2230.e10. [CrossRef]
75. Iarovaia, O.V.; Rubtsov, M.; Ioudinkova, E.; Tsfasman, T.; Razin, S.V.; Vassetzky, Y.S. Dynamics of Double Strand Breaks and Chromosomal Translocations. *Mol. Cancer* **2014**, *13*, 249. [CrossRef]
76. Brunet, E.; Simsek, D.; Tomishima, M.; DeKelver, R.; Choi, V.M.; Gregory, P.; Urnov, F.; Weinstock, D.M.; Jasin, M. Chromosomal Translocations Induced at Specified Loci in Human Stem Cells. *Proc. Natl. Acad. Sci. USA* **2009**, *106*, 10620–10625. [CrossRef]
77. Germini, D.; Saada, Y.B.; Tsfasman, T.; Osina, K.; Robin, C.; Lomov, N.; Rubtsov, M.; Sjakste, N.; Lipinski, M.; Vassetzky, Y. A One-Step PCR-Based Assay to Evaluate the Efficiency and Precision of Genomic DNA-Editing Tools. *Mol. Ther. Methods Clin. Dev.* **2017**, *5*, 43–50. [CrossRef]
78. Piganeau, M.; Ghezraoui, H.; De Cian, A.; Guittat, L.; Tomishima, M.; Perrouault, L.; René, O.; Katibah, G.E.; Zhang, L.; Holmes, M.C.; et al. Cancer Translocations in Human Cells Induced by Zinc Finger and TALE Nucleases. *Genome Res.* **2013**, *23*, 1182–1193. [CrossRef]
79. Torres, R.; Martin, M.C.; Garcia, A.; Cigudosa, J.C.; Ramirez, J.C.; Rodriguez-Perales, S. Engineering Human Tumour-Associated Chromosomal Translocations with the RNA-Guided CRISPR–Cas9 System. *Nat. Commun.* **2014**, *5*, 3964. [CrossRef]
80. Vanoli, F.; Jasin, M. Generation of Chromosomal Translocations That Lead to Conditional Fusion Protein Expression Using CRISPR-Cas9 and Homology-Directed Repair. *Methods* **2017**, *121–122*, 138–145. [CrossRef]
81. Shmakova, A.A.; Germini, D.; Vassetzky, Y.S. Exploring the Features of Burkitt's Lymphoma-Associated t(8;14) Translocations Generated via a CRISPR/Cas9-Based System. *Biopolym. Cell* **2019**, *35*, 232–233. [CrossRef]
82. Canoy, R.J.; André, F.; Shmakova, A.; Wiels, J.; Lipinski, M.; Vassetzky, Y.; Germini, D. Easy and Robust Electrotransfection Protocol for Efficient Ectopic Gene Expression and Genome Editing in Human B Cells. *Gene Ther.* **2020**, 1–5. [CrossRef]
83. Shmakova, A.A.; Lomov, N.; Viushkov, V.; Tsfasman, T.; Kozhevnikova, Y.; Sokolova, D.; Pokrovsky, V.; Syrkina, M.; Germini, D.; Rubtsov, M.; et al. Cell Models with Inducible Oncogenic Translocations Allow to Evaluate the Potential of Drugs to Favor Secondary Translocations. *Cancer Commun.* **2022**, in press. [CrossRef]
84. Shmakova, A.A.; Shmakova, O.P.; Karpukhina, A.A.; Vassetzky, Y.S. CRISPR/Cas: History and Perspectives. *Russ. J. Dev. Biol.* **2022**, *53*, 272–282. [CrossRef]
85. Byrne, M.; Wray, J.; Reinert, B.; Wu, Y.; Nickoloff, J.; Lee, S.-H.; Hromas, R.; Williamson, E. Mechanisms of Oncogenic Chromosomal Translocations. *Ann. New York Acad. Sci.* **2014**, *1310*, 89–97. [CrossRef]
86. Lieber, M.R. Mechanisms of Human Lymphoid Chromosomal Translocations. *Nat. Rev. Cancer* **2016**, *16*, 387–398. [CrossRef]
87. Chiarle, R.; Zhang, Y.; Frock, R.L.; Lewis, S.M.; Molinie, B.; Ho, Y.J.; Myers, D.R.; Choi, V.W.; Compagno, M.; Malkin, D.J.; et al. Genome-Wide Translocation Sequencing Reveals Mechanisms of Chromosome Breaks and Rearrangements in B Cells. *Cell* **2011**, *147*, 107–119. [CrossRef]
88. Klein, I.A.; Resch, W.; Jankovic, M.; Oliveira, T.; Yamane, A.; Nakahashi, H.; Di Virgilio, M.; Bothmer, A.; Nussenzweig, A.; Robbiani, D.F.; et al. Translocation-Capture Sequencing Reveals the Extent and Nature of Chromosomal Rearrangements in B Lymphocytes. *Cell* **2011**, *147*, 95–106. [CrossRef]
89. Haffner, M.C.; Aryee, M.J.; Toubaji, A.; Esopi, D.M.; Albadine, R.; Gurel, B.; Isaacs, W.B.; Bova, G.S.; Liu, W.; Xu, J.; et al. Androgen-Induced TOP2B-Mediated Double-Strand Breaks and Prostate Cancer Gene Rearrangements. *Nat. Genet.* **2010**, *42*, 668–675. [CrossRef]

90. Canela, A.; Maman, Y.; Huang, S.N.; Wutz, G.; Tang, W.; Zagnoli-Vieira, G.; Callen, E.; Wong, N.; Day, A.; Peters, J.-M.; et al. Topoisomerase II-Induced Chromosome Breakage and Translocation Is Determined by Chromosome Architecture and Transcriptional Activity. *Mol. Cell* **2019**, *75*, 252–266.e8. [CrossRef]
91. Engreitz, J.M.; Agarwala, V.; Mirny, L.A. Three-Dimensional Genome Architecture Influences Partner Selection for Chromosomal Translocations in Human Disease. *PLoS ONE* **2012**, *7*, e44196. [CrossRef]
92. Roukos, V.; Voss, T.C.; Schmidt, C.K.; Lee, S.; Wangsa, D.; Misteli, T. Spatial Dynamics of Chromosome Translocations in Living Cells. *Science* **2013**, *341*, 660–664. [CrossRef]
93. Cremer, T.; Cremer, M.; Dietzel, S.; Müller, S.; Solovei, I.; Fakan, S. Chromosome Territories—A Functional Nuclear Landscape. *Curr. Opin. Cell Biol.* **2006**, *18*, 307–316. [CrossRef]
94. Boveri, T. Die Blastomerenkerne von Ascaris Megalocephala Und Die Theorie Der Chromosomenindividualität. *Arch. Zellforsch* **1909**, *3*, 181–268.
95. Cremer, T.; Cremer, M. Chromosome Territories. *Cold Spring Harb Perspect Biol.* **2010**, *2*, a003889. [CrossRef]
96. Belmont, A.S.; Bruce, K. Visualization of G1 Chromosomes: A Folded, Twisted, Supercoiled Chromonema Model of Interphase Chromatid Structure. *J. Cell Biol.* **1994**, *127*, 287–302. [CrossRef]
97. Marella, N.V.; Bhattacharya, S.; Mukherjee, L.; Xu, J.; Berezney, R. Cell Type Specific Chromosome Territory Organization in the Interphase Nucleus of Normal and Cancer Cells. *J. Cell. Physiol.* **2009**, *221*, 130–138. [CrossRef]
98. Parada, L.A.; McQueen, P.G.; Misteli, T. Tissue-Specific Spatial Organization of Genomes. *Genome Biol.* **2004**, *5*, R44. [CrossRef]
99. Roix, J.J.; McQueen, P.G.; Munson, P.J.; Parada, L.A.; Misteli, T. Spatial Proximity of Translocation-Prone Gene Loci in Human Lymphomas. *Nat. Genet.* **2003**, *34*, 287–291. [CrossRef]
100. Haber, J.E.; Leung, W.-Y. Lack of Chromosome Territoriality in Yeast: Promiscuous Rejoining of Broken Chromosome Ends. *Proc. Natl. Acad. Sci. USA* **1996**, *93*, 13949–13954. [CrossRef]
101. Fraser, J.; Williamson, I.; Bickmore, W.A.; Dostie, J. An Overview of Genome Organization and How We Got There: From FISH to Hi-C. *Microbiol. Mol. Biol. Rev.* **2015**, *79*, 347–372. [CrossRef]
102. Fritz, A.J.; Barutcu, A.R.; Martin-Buley, L.; van Wijnen, A.J.; Zaidi, S.K.; Imbalzano, A.N.; Lian, J.B.; Stein, J.L.; Stein, G.S. Chromosomes at Work: Organization of Chromosome Territories in the Interphase Nucleus. *J. Cell. Biochem.* **2016**, *117*, 9–19. [CrossRef]
103. Lukášová, E.; Kozubek, S.; Kozubek, M.; Kjeronská, J.; Rýznar, L.; Horáková, J.; Krahulcová, E.; Horneck, G. Localisation and Distance between ABL and BCR Genes in Interphase Nuclei of Bone Marrow Cells of Control Donors and Patients with Chronic Myeloid Leukaemia. *Hum. Genet.* **1997**, *100*, 525–535. [CrossRef]
104. Neves, H.; Ramos, C.; da Silva, M.G.; Parreira, A.; Parreira, L. The Nuclear Topography of ABL, BCR, PML, and RARalpha Genes: Evidence for Gene Proximity in Specific Phases of the Cell Cycle and Stages of Hematopoietic Differentiation. *Blood* **1999**, *93*, 1197–1207. [CrossRef]
105. Boxer, L.M.; Dang, C.V. Translocations Involving C- Myc and c- Myc Function. *Oncogene* **2001**, *20*, 5595–5610. [CrossRef]
106. Gostissa, M.; Ranganath, S.; Bianco, J.M.; Alt, F.W. Chromosomal Location Targets Different MYC Family Gene Members for Oncogenic Translocations. *Proc. Natl. Acad. Sci. USA* **2009**, *106*, 2265–2270. [CrossRef]
107. Sathitruangsak, C.; Righolt, C.H.; Klewes, L.; Chang, D.T.; Kotb, R.; Mai, S. Distinct and Shared Three-Dimensional Chromosome Organization Patterns in Lymphocytes, Monoclonal Gammopathy of Undetermined Significance and Multiple Myeloma. *Int. J. Cancer* **2017**, *140*, 400–410. [CrossRef]
108. Zhang, Y.; McCord, R.P.; Ho, Y.-J.; Lajoie, B.R.; Hildebrand, D.G.; Simon, A.C.; Becker, M.S.; Alt, F.W.; Dekker, J. Spatial Organization of the Mouse Genome and Its Role in Recurrent Chromosomal Translocations. *Cell* **2012**, *148*, 908–921. [CrossRef]
109. Crosetto, N.; Mitra, A.; Silva, M.J.; Bienko, M.; Dojer, N.; Wang, Q.; Karaca, E.; Chiarle, R.; Skrzypczak, M.; Ginalski, K.; et al. Nucleotide-Resolution DNA Double-Strand Breaks Mapping by next-Generation Sequencing. *Nat. Methods* **2013**, *10*, 361–365. [CrossRef]
110. Lensing, S.V.; Marsico, G.; Hänsel-Hertsch, R.; Lam, E.Y.; Tannahill, D.; Balasubramanian, S. DSBCapture: In Situ Capture and Sequencing of DNA Breaks. *Nat. Methods* **2016**, *13*, 855–857. [CrossRef]
111. Falk, M.; Lukásová, E.; Kozubek, S. Chromatin Structure Influences the Sensitivity of DNA to Gamma-Radiation. *Biochim. Biophys. Acta* **2008**, *1783*, 2398–2414. [CrossRef]
112. Aguilera, A. The Connection between Transcription and Genomic Instability. *EMBO J.* **2002**, *21*, 195–201. [CrossRef]
113. Ginno, P.A.; Lott, P.L.; Christensen, H.C.; Korf, I.; Chédin, F. R-Loop Formation Is a Distinctive Characteristic of Unmethylated Human CpG Island Promoters. *Mol. Cell* **2012**, *45*, 814–825. [CrossRef]
114. Santos-Pereira, J.M.; Aguilera, A. R Loops: New Modulators of Genome Dynamics and Function. *Nat. Rev. Genet.* **2015**, *16*, 583–597. [CrossRef]
115. Stirling, P.C.; Hieter, P. Canonical DNA Repair Pathways Influence R-Loop-Driven Genome Instability. *J. Mol. Biol.* **2017**, *429*, 3132–3138. [CrossRef] [PubMed]
116. Boerma, E.G.; Siebert, R.; Kluin, P.M.; Baudis, M. Translocations Involving 8q24 in Burkitt Lymphoma and Other Malignant Lymphomas: A Historical Review of Cytogenetics in the Light of Todays Knowledge. *Leukemia* **2009**, *23*, 225–234. [CrossRef] [PubMed]
117. Duquette, M.L.; Pham, P.; Goodman, M.F.; Maizels, N. AID Binds to Transcription-Induced Structures in c- MYC That Map to Regions Associated with Translocation and Hypermutation. *Oncogene* **2005**, *24*, 5791–5798. [CrossRef]

118. Yu, K.; Chedin, F.; Hsieh, C.-L.; Wilson, T.E.; Lieber, M.R. R-Loops at Immunoglobulin Class Switch Regions in the Chromosomes of Stimulated B Cells. *Nat. Immunol.* **2003**, *4*, 442–451. [CrossRef]
119. Pavri, R.; Gazumyan, A.; Jankovic, M.; Di Virgilio, M.; Klein, I.; Ansarah-Sobrinho, C.; Resch, W.; Yamane, A.; Reina San-Martin, B.; Barreto, V.; et al. Activation-Induced Cytidine Deaminase Targets DNA at Sites of RNA Polymerase II Stalling by Interaction with Spt5. *Cell* **2010**, *143*, 122–133. [CrossRef]
120. Yamane, A.; Resch, W.; Kuo, N.; Kuchen, S.; Li, Z.; Sun, H.; Robbiani, D.F.; McBride, K.; Nussenzweig, M.C.; Casellas, R. Deep-Sequencing Identification of the Genomic Targets of the Cytidine Deaminase AID and Its Cofactor RPA in B Lymphocytes. *Nat. Immunol.* **2011**, *12*, 62–69. [CrossRef]
121. Yang, Y.; McBride, K.M.; Hensley, S.; Lu, Y.; Chedin, F.; Bedford, M.T. Arginine Methylation Facilitates the Recruitment of TOP3B to Chromatin to Prevent R Loop Accumulation. *Mol. Cell* **2014**, *53*, 484–497. [CrossRef]
122. Ramiro, A.R.; Jankovic, M.; Callen, E.; Difilippantonio, S.; Chen, H.-T.; McBride, K.M.; Eisenreich, T.R.; Chen, J.; Dickins, R.A.; Lowe, S.W.; et al. Role of Genomic Instability and P53 in AID-Induced c-Myc—Igh Translocations. *Nature* **2006**, *440*, 105–109. [CrossRef]
123. Yeo, A.J.; Becherel, O.J.; Luff, J.E.; Cullen, J.K.; Wongsurawat, T.; Jenjaroenpoon, P.; Kuznetsov, V.A.; McKinnon, P.J.; Lavin, M.F. R-Loops in Proliferating Cells but Not in the Brain: Implications for AOA2 and Other Autosomal Recessive Ataxias. *PLoS ONE* **2014**, *9*, e90219. [CrossRef]
124. Bhatia, V.; Barroso, S.I.; García-Rubio, M.L.; Tumini, E.; Herrera-Moyano, E.; Aguilera, A. BRCA2 Prevents R-Loop Accumulation and Associates with TREX-2 MRNA Export Factor PCID2. *Nature* **2014**, *511*, 362–365. [CrossRef]
125. Schlacher, K.; Wu, H.; Jasin, M. A Distinct Replication Fork Protection Pathway Connects Fanconi Anemia Tumor Suppressors to RAD51-BRCA1/2. *Cancer Cell* **2012**, *22*, 106–116. [CrossRef]
126. Roberts, S.A.; Gordenin, D.A. Hypermutation in Human Cancer Genomes: Footprints and Mechanisms. *Nat. Rev. Cancer* **2014**, *14*, 786–800. [CrossRef]
127. Pliss, A.; Malyavantham, K.; Bhattacharya, S.; Zeitz, M.; Berezney, R. Chromatin Dynamics Is Correlated with Replication Timing. *Chromosoma* **2009**, *118*, 459–470. [CrossRef]
128. Osborne, C.S.; Chakalova, L.; Brown, K.E.; Carter, D.; Horton, A.; Debrand, E.; Goyenechea, B.; Mitchell, J.A.; Lopes, S.; Reik, W.; et al. Active Genes Dynamically Colocalize to Shared Sites of Ongoing Transcription. *Nat. Genet.* **2004**, *36*, 1065–1071. [CrossRef]
129. Osborne, C.S.; Chakalova, L.; Mitchell, J.A.; Horton, A.; Wood, A.L.; Bolland, D.J.; Corcoran, A.E.; Fraser, P. Myc Dynamically and Preferentially Relocates to a Transcription Factory Occupied by Igh. *PLoS Biol.* **2007**, *5*, e192. [CrossRef]
130. Barlow, J.; Faryabi, R.B.; Callen, E.; Wong, N.; Malhowski, A.; Chen, H.T.; Gutierez-Cruz, G.; Sun, H.-W.; McKinnon, P.; Wright, G.; et al. A Novel Class of Early Replicating Fragile Sites That Contribute to Genome Instability in B Cell Lymphomas. *Cell* **2013**, *152*, 620–632. [CrossRef]
131. Mathas, S.; Kreher, S.; Meaburn, K.J.; Jöhrens, K.; Lamprecht, B.; Assaf, C.; Sterry, W.; Kadin, M.E.; Daibata, M.; Joos, S.; et al. Gene Deregulation and Spatial Genome Reorganization near Breakpoints Prior to Formation of Translocations in Anaplastic Large Cell Lymphoma. *Proc. Natl. Acad. Sci. USA* **2009**, *106*, 5831–5836. [CrossRef]
132. Lin, C.; Yang, L.; Tanasa, B.; Hutt, K.; Ju, B.; Ohgi, K.; Zhang, J.; Rose, D.; Fu, X.-D.; Glass, C.K.; et al. Nuclear Receptor-Induced Chromosomal Proximity and DNA Breaks Underlie Specific Translocations in Cancer. *Cell* **2009**, *139*, 1069–1083. [CrossRef]
133. Ciccia, A.; Elledge, S.J. The DNA Damage Response: Making It Safe to Play with Knives. *Mol. Cell* **2010**, *40*, 179–204. [CrossRef]
134. Janz, S.; Potter, M.; Rabkin, C.S. Lymphoma- and Leukemia-Associated Chromosomal Translocations in Healthy Individuals. *Genes Chromosomes Cancer* **2003**, *36*, 211–223. [CrossRef]
135. Rabkin, C.S.; Hirt, C.; Janz, S.; Dölken, G. T(14;18) Translocations and Risk of Follicular Lymphoma. *J. Natl. Cancer Inst. Monogr.* **2008**, *39*, 48–51. [CrossRef]
136. Schüler, F.; Hirt, C.; Dölken, G. Chromosomal Translocation t(14;18) in Healthy Individuals. *Semin. Cancer Biol.* **2003**, *13*, 203–209. [CrossRef]
137. Bäsecke, J.; Griesinger, F.; Trümper, L.; Brittinger, G. Leukemia- and Lymphoma-Associated Genetic Aberrations in Healthy Individuals. *Ann. Hematol.* **2002**, *81*, 64–75. [CrossRef]
138. Brassesco, M.S.; Montaldi, A.P.; Gras, D.E.; de Paula Queiroz, R.G.; Martinez-Rossi, N.M.; Tone, L.G.; Sakamoto-Hojo, E.T. MLL Leukemia-Associated Rearrangements in Peripheral Blood Lymphocytes from Healthy Individuals. *Genet. Mol. Biol.* **2009**, *32*, 234–241. [CrossRef] [PubMed]
139. Nambiar, M.; Raghavan, S.C. Chromosomal Translocations among the Healthy Human Population: Implications in Oncogenesis. *Cell Mol. Life Sci.* **2013**, *70*, 1381–1392. [CrossRef] [PubMed]
140. Jasin, M.; Rothstein, R. Repair of Strand Breaks by Homologous Recombination. *Cold Spring Harb Perspect Biol.* **2013**, *5*, a012740. [CrossRef] [PubMed]
141. Prakash, R.; Zhang, Y.; Feng, W.; Jasin, M. Homologous Recombination and Human Health: The Roles of BRCA1, BRCA2, and Associated Proteins. *Cold Spring Harb Perspect Biol.* **2015**, *7*, a016600. [CrossRef]
142. Boboila, C.; Alt, F.W.; Schwer, B. Chapter One—Classical and Alternative End-Joining Pathways for Repair of Lymphocyte-Specific and General DNA Double-Strand Breaks. In *Advances in Immunology*; Alt, F.W., Ed.; Academic Press: Cambridge, MA, USA, 2012; Volume 116, pp. 1–49.
143. Lieber, M.R. The Mechanism of Double-Strand DNA Break Repair by the Nonhomologous DNA End-Joining Pathway. *Annu. Rev. Biochem.* **2010**, *79*, 181–211. [CrossRef]

144. Symington, L.S.; Gautier, J. Double-Strand Break End Resection and Repair Pathway Choice. *Annu. Rev. Genet.* **2011**, *45*, 247–271. [CrossRef]
145. Moynahan, M.E.; Jasin, M. Mitotic Homologous Recombination Maintains Genomic Stability and Suppresses Tumorigenesis. *Nat. Rev. Mol. Cell Biol.* **2010**, *11*, 196–207. [CrossRef]
146. Sfeir, A.; Symington, L.S. Microhomology-Mediated End Joining: A Back-up Survival Mechanism or Dedicated Pathway? *Trends Biochem. Sci.* **2015**, *40*, 701–714. [CrossRef]
147. Brunet, E.; Jasin, M. Induction of Chromosomal Translocations with CRISPR-Cas9 and Other Nucleases: Understanding the Repair Mechanisms That Give Rise to Translocations. In *Chromosome Translocation*; Zhang, Y., Ed.; Advances in Experimental Medicine and Biology; Springer: Singapore, 2018; pp. 15–25. ISBN 9789811305931.
148. Stark, J.M.; Pierce, A.J.; Oh, J.; Pastink, A.; Jasin, M. Genetic Steps of Mammalian Homologous Repair with Distinct Mutagenic Consequences. *Mol. Cell. Biol.* **2004**, *24*, 9305–9316. [CrossRef]
149. Weinstock, D.M.; Richardson, C.A.; Elliott, B.; Jasin, M. Modeling Oncogenic Translocations: Distinct Roles for Double-Strand Break Repair Pathways in Translocation Formation in Mammalian Cells. *DNA Repair* **2006**, *5*, 1065–1074. [CrossRef]
150. Ghosh, R.; Das, D.; Franco, S. The Role for the DSB Response Pathway in Regulating Chromosome Translocations. In *Chromosome Translocation*; Zhang, Y., Ed.; Advances in Experimental Medicine and Biology; Springer: Singapore, 2018; pp. 65–87. ISBN 9789811305931.
151. Kass, E.M.; Jasin, M. Collaboration and Competition between DNA Double-Strand Break Repair Pathways. *FEBS Lett.* **2010**, *584*, 3703–3708. [CrossRef]
152. Costantino, L.; Sotiriou, S.K.; Rantala, J.K.; Magin, S.; Mladenov, E.; Helleday, T.; Haber, J.E.; Iliakis, G.; Kallioniemi, O.P.; Halazonetis, T.D. Break-Induced Replication Repair of Damaged Forks Induces Genomic Duplications in Human Cells. *Science* **2014**, *343*, 88–91. [CrossRef]
153. Johnson, R.D.; Jasin, M. Sister Chromatid Gene Conversion Is a Prominent Double-Strand Break Repair Pathway in Mammalian Cells. *EMBO J.* **2000**, *19*, 3398–3407. [CrossRef]
154. Richardson, C.; Jasin, M. Coupled Homologous and Nonhomologous Repair of a Double-Strand Break Preserves Genomic Integrity in Mammalian Cells. *Mol. Cell. Biol.* **2000**, *20*, 9068–9075. [CrossRef]
155. Soni, A.; Siemann, M.; Pantelias, G.E.; Iliakis, G. Marked Contribution of Alternative End-Joining to Chromosome-Translocation-Formation by Stochastically Induced DNA Double-Strand-Breaks in G2-Phase Human Cells. *Mutat. Res./Genet. Toxicol. Environ. Mutagen.* **2015**, *793*, 2–8. [CrossRef]
156. Simsek, D.; Jasin, M. Alternative End-Joining Is Suppressed by the Canonical NHEJ Component Xrcc4-Ligase IV during Chromosomal Translocation Formation. Available online: https://pubmed.ncbi.nlm.nih.gov/20208544/ (accessed on 29 November 2020).
157. Zhang, Y.; Jasin, M. An Essential Role for CtIP in Chromosomal Translocation Formation through an Alternative End-Joining Pathway. *Nat. Struct. Mol. Biol.* **2011**, *18*, 80–84. [CrossRef]
158. Boboila, C.; Jankovic, M.; Yan, C.T.; Wang, J.H.; Wesemann, D.R.; Zhang, T.; Fazeli, A.; Feldman, L.; Nussenzweig, A.; Nussenzweig, M.; et al. Alternative End-Joining Catalyzes Robust IgH Locus Deletions and Translocations in the Combined Absence of Ligase 4 and Ku70. *Proc. Natl. Acad. Sci. USA* **2010**, *107*, 3034–3039. [CrossRef]
159. Elliott, B.; Richardson, C.; Jasin, M. Chromosomal Translocation Mechanisms at Intronic Alu Elements in Mammalian Cells. *Mol. Cell* **2005**, *17*, 885–894. [CrossRef]
160. Löbrich, M.; Jeggo, P. A Process of Resection-Dependent Nonhomologous End Joining Involving the Goddess Artemis. *Trends Biochem. Sci.* **2017**, *42*, 690–701. [CrossRef]
161. Iliakis, G.; Murmann, T.; Soni, A. Alternative End-Joining Repair Pathways Are the Ultimate Backup for Abrogated Classical Non-Homologous End-Joining and Homologous Recombination Repair: Implications for the Formation of Chromosome Translocations. *Mutat. Res./Genet. Toxicol. Environ. Mutagen.* **2015**, *793*, 166–175. [CrossRef]
162. Biehs, R.; Steinlage, M.; Barton, O.; Juhász, S.; Künzel, J.; Spies, J.; Shibata, A.; Jeggo, P.A.; Löbrich, M. DNA Double-Strand Break Resection Occurs during Non-Homologous End Joining in G1 but Is Distinct from Resection during Homologous Recombination. *Mol. Cell* **2017**, *65*, 671–684.e5. [CrossRef]
163. Beucher, A.; Birraux, J.; Tchouandong, L.; Barton, O.; Shibata, A.; Conrad, S.; Goodarzi, A.A.; Krempler, A.; Jeggo, P.A.; Löbrich, M. ATM and Artemis Promote Homologous Recombination of Radiation-Induced DNA Double-Strand Breaks in G2. *EMBO J.* **2009**, *28*, 3413–3427. [CrossRef]
164. Kakarougkas, A.; Jeggo, P.A. DNA DSB Repair Pathway Choice: An Orchestrated Handover Mechanism. *Br. J. Radiol.* **2014**, *87*, 20130685. [CrossRef]
165. Shibata, A.; Conrad, S.; Birraux, J.; Geuting, V.; Barton, O.; Ismail, A.; Kakarougkas, A.; Meek, K.; Taucher-Scholz, G.; Löbrich, M.; et al. Factors Determining DNA Double-Strand Break Repair Pathway Choice in G2 Phase. *EMBO J.* **2011**, *30*, 1079–1092. [CrossRef]
166. Tsouroula, K.; Furst, A.; Rogier, M.; Heyer, V.; Maglott-Roth, A.; Ferrand, A.; Reina-San-Martin, B.; Soutoglou, E. Temporal and Spatial Uncoupling of DNA Double Strand Break Repair Pathways within Mammalian Heterochromatin. *Mol. Cell* **2016**, *63*, 293–305. [CrossRef]
167. Choi, E.-H.; Yoon, S.; Koh, Y.E.; Seo, Y.-J.; Kim, K.P. Maintenance of Genome Integrity and Active Homologous Recombination in Embryonic Stem Cells. *Exp. Mol. Med.* **2020**, *52*, 1220–1229. [CrossRef] [PubMed]

168. Mujoo, K.; Pandita, R.K.; Tiwari, A.; Charaka, V.; Chakraborty, S.; Singh, D.K.; Hambarde, S.; Hittelman, W.N.; Horikoshi, N.; Hunt, C.R.; et al. Differentiation of Human Induced Pluripotent or Embryonic Stem Cells Decreases the DNA Damage Repair by Homologous Recombination. *Stem Cell Rep.* **2017**, *9*, 1660–1674. [CrossRef] [PubMed]
169. Lukášová, E.; Kořistek, Z.; Klabusay, M.; Ondřej, V.; Grigoryev, S.; Bačíková, A.; Řezáčová, M.; Falk, M.; Vávrová, J.; Kohútová, V.; et al. Granulocyte Maturation Determines Ability to Release Chromatin NETs and Loss of DNA Damage Response; These Properties Are Absent in Immature AML Granulocytes. *Biochim. Biophys. Acta* **2013**, *1833*, 767–779. [CrossRef] [PubMed]
170. Bristow, R.G.; Hill, R.P. Hypoxia and Metabolism. Hypoxia, DNA Repair and Genetic Instability. *Nat. Rev. Cancer* **2008**, *8*, 180–192. [CrossRef]
171. Lee, J.Y.; Orr-Weaver, T.L. Chromatin. In *Encyclopedia of Genetics*; Brenner, S., Miller, J.H., Eds.; Academic Press: New York, NY, USA, 2001; pp. 340–343. ISBN 978-0-12-227080-2.
172. Thomas, J.O.; Kornberg, R.D. An Octamer of Histones in Chromatin and Free in Solution. *Proc. Natl. Acad. Sci. USA* **1975**, *72*, 2626–2630. [CrossRef]
173. Arents, G.; Burlingame, R.W.; Wang, B.C.; Love, W.E.; Moudrianakis, E.N. The Nucleosomal Core Histone Octamer at 3.1 A Resolution: A Tripartite Protein Assembly and a Left-Handed Superhelix. *Proc. Natl. Acad. Sci. USA* **1991**, *88*, 10148–10152. [CrossRef]
174. Luger, K.; Mäder, A.W.; Richmond, R.K.; Sargent, D.F.; Richmond, T.J. Crystal Structure of the Nucleosome Core Particle at 2.8 Å Resolution. *Nature* **1997**, *389*, 251–260. [CrossRef]
175. Campos, E.I.; Reinberg, D. Histones: Annotating Chromatin. *Annu. Rev. Genet.* **2009**, *43*, 559–599. [CrossRef]
176. Misteli, T. The Cell Biology of Genomes: Bringing the Double Helix to Life. *Cell* **2013**, *152*, 1209–1212. [CrossRef]
177. Ernst, J.; Kheradpour, P.; Mikkelsen, T.S.; Shoresh, N.; Ward, L.D.; Epstein, C.B.; Zhang, X.; Wang, L.; Issner, R.; Coyne, M.; et al. Mapping and Analysis of Chromatin State Dynamics in Nine Human Cell Types. *Nature* **2011**, *473*, 43–49. [CrossRef]
178. Maurano, M.T.; Humbert, R.; Rynes, E.; Thurman, R.E.; Haugen, E.; Wang, H.; Reynolds, A.P.; Sandstrom, R.; Qu, H.; Brody, J.; et al. Systematic Localization of Common Disease-Associated Variation in Regulatory DNA. *Science* **2012**, *337*, 1190–1195. [CrossRef]
179. Ernst, J.; Kellis, M. Discovery and Characterization of Chromatin States for Systematic Annotation of the Human Genome. *Nature Biotechnology* **2010**, *28*, 817–825. [CrossRef]
180. Ernst, J.; Kellis, M. Chromatin-State Discovery and Genome Annotation with ChromHMM. *Nat. Protoc.* **2017**, *12*, 2478–2492. [CrossRef]
181. Marshall, W.F.; Straight, A.; Marko, J.F.; Swedlow, J.; Dernburg, A.; Belmont, A.; Murray, A.W.; Agard, D.A.; Sedat, J.W. Interphase Chromosomes Undergo Constrained Diffusional Motion in Living Cells. *Curr. Biol.* **1997**, *7*, 930–939. [CrossRef]
182. Gothe, H.J.; Minneker, V.; Roukos, V. Dynamics of Double-Strand Breaks: Implications for the Formation of Chromosome Translocations. In *Chromosome Translocation*; Zhang, Y., Ed.; Advances in Experimental Medicine and Biology; Springer: Singapore, 2018; pp. 27–38. ISBN 9789811305931.
183. Heun, P.; Laroche, T.; Shimada, K.; Furrer, P.; Gasser, S.M. Chromosome Dynamics in the Yeast Interphase Nucleus. *Science* **2001**, *294*, 2181–2186. [CrossRef]
184. Neumann, F.R.; Dion, V.; Gehlen, L.R.; Tsai-Pflugfelder, M.; Schmid, R.; Taddei, A.; Gasser, S.M. Targeted INO80 Enhances Subnuclear Chromatin Movement and Ectopic Homologous Recombination. *Genes Dev.* **2012**, *26*, 369–383. [CrossRef] [PubMed]
185. Weber, S.C.; Spakowitz, A.J.; Theriot, J.A. Nonthermal ATP-Dependent Fluctuations Contribute to the in Vivo Motion of Chromosomal Loci. *Proc. Natl. Acad. Sci. USA* **2012**, *109*, 7338. [CrossRef] [PubMed]
186. Krawczyk, P.M.; Borovski, T.; Stap, J.; Cijsouw, T.; ten Cate, R.; Medema, J.P.; Kanaar, R.; Franken, N.a.P.; Aten, J.A. Chromatin Mobility Is Increased at Sites of DNA Double-Strand Breaks. *J. Cell Sci.* **2012**, *125*, 2127–2133. [CrossRef] [PubMed]
187. Thomson, I.; Gilchrist, S.; Bickmore, W.A.; Chubb, J.R. The Radial Positioning of Chromatin Is Not Inherited through Mitosis but Is Established De Novo in Early G1. *Curr. Biol.* **2004**, *14*, 166–172. [CrossRef] [PubMed]
188. Vazquez, J.; Belmont, A.S.; Sedat, J.W. Multiple Regimes of Constrained Chromosome Motion Are Regulated in the Interphase Drosophila Nucleus. *Curr. Biol.* **2001**, *11*, 1227–1239. [CrossRef]
189. Walter, J.; Schermelleh, L.; Cremer, M.; Tashiro, S.; Cremer, T. Chromosome Order in HeLa Cells Changes during Mitosis and Early G1, but Is Stably Maintained during Subsequent Interphase Stages. *J. Cell Biol.* **2003**, *160*, 685–697. [CrossRef]
190. Wiesmeijer, K.; Krouwels, I.M.; Tanke, H.J.; Dirks, R.W. Chromatin Movement Visualized with Photoactivable GFP-Labeled Histone H4. *Differentiation* **2008**, *76*, 83–90. [CrossRef]
191. Chuang, C.-H.; Carpenter, A.E.; Fuchsova, B.; Johnson, T.; de Lanerolle, P.; Belmont, A.S. Long-Range Directional Movement of an Interphase Chromosome Site. *Curr. Biol.* **2006**, *16*, 825–831. [CrossRef]
192. Dundr, M.; Ospina, J.K.; Sung, M.-H.; John, S.; Upender, M.; Ried, T.; Hager, G.L.; Matera, A.G. Actin-Dependent Intranuclear Repositioning of an Active Gene Locus in Vivo. *J. Cell Biol.* **2007**, *179*, 1095–1103. [CrossRef]
193. Tumbar, T.; Belmont, A.S. Interphase Movements of a DNA Chromosome Region Modulated by VP16 Transcriptional Activator. *Nat. Cell Biol.* **2001**, *3*, 134–139. [CrossRef]
194. Spichal, M.; Brion, A.; Herbert, S.; Cournac, A.; Marbouty, M.; Zimmer, C.; Koszul, R.; Fabre, E. Evidence for a Dual Role of Actin in Regulating Chromosome Organization and Dynamics in Yeast. *J. Cell Sci.* **2016**, *129*, 681–692. [CrossRef]
195. Therizols, P.; Illingworth, R.S.; Courilleau, C.; Boyle, S.; Wood, A.J.; Bickmore, W.A. Chromatin Decondensation Is Sufficient to Alter Nuclear Organization in Embryonic Stem Cells. *Science* **2014**, *346*, 1238–1242. [CrossRef]

196. Kruhlak, M.J.; Celeste, A.; Dellaire, G.; Fernandez-Capetillo, O.; Müller, W.G.; McNally, J.G.; Bazett-Jones, D.P.; Nussenzweig, A. Changes in Chromatin Structure and Mobility in Living Cells at Sites of DNA Double-Strand Breaks. *J. Cell Biol.* **2006**, *172*, 823–834. [CrossRef]
197. Chiolo, I.; Minoda, A.; Colmenares, S.U.; Polyzos, A.; Costes, S.V.; Karpen, G.H. Double-Strand Breaks in Heterochromatin Move Outside of a Dynamic HP1a Domain to Complete Recombinational Repair. *Cell* **2011**, *144*, 732–744. [CrossRef]
198. Jakob, B.; Splinter, J.; Conrad, S.; Voss, K.-O.; Zink, D.; Durante, M.; Löbrich, M.; Taucher-Scholz, G. DNA Double-Strand Breaks in Heterochromatin Elicit Fast Repair Protein Recruitment, Histone H2AX Phosphorylation and Relocation to Euchromatin. *Nucleic Acids Res.* **2011**, *39*, 6489–6499. [CrossRef]
199. Kim, J.-A.; Kruhlak, M.; Dotiwala, F.; Nussenzweig, A.; Haber, J.E. Heterochromatin Is Refractory to γ-H2AX Modification in Yeast and Mammals. *J. Cell Biol.* **2007**, *178*, 209–218. [CrossRef]
200. Lemaître, C.; Grabarz, A.; Tsouroula, K.; Andronov, L.; Furst, A.; Pankotai, T.; Heyer, V.; Rogier, M.; Attwood, K.M.; Kessler, P.; et al. Nuclear Position Dictates DNA Repair Pathway Choice. *Genes Dev.* **2014**, *28*, 2450–2463. [CrossRef]
201. Rosin, L.F.; Crocker, O.; Isenhart, R.L.; Nguyen, S.C.; Xu, Z.; Joyce, E.F. Chromosome Territory Formation Attenuates the Translocation Potential of Cells. *eLife* **2019**, *8*, e49553. [CrossRef]
202. Lukas, J.; Lukas, C.; Bartek, J. More than Just a Focus: The Chromatin Response to DNA Damage and Its Role in Genome Integrity Maintenance. *Nat. Cell Biol.* **2011**, *13*, 1161–1169. [CrossRef]
203. Kaye, J.A.; Melo, J.A.; Cheung, S.K.; Vaze, M.B.; Haber, J.E.; Toczyski, D.P. DNA Breaks Promote Genomic Instability by Impeding Proper Chromosome Segregation. *Curr. Biol.* **2004**, *14*, 2096–2106. [CrossRef]
204. Lobachev, K.; Vitriol, E.; Stemple, J.; Resnick, M.A.; Bloom, K. Chromosome Fragmentation after Induction of a Double-Strand Break Is an Active Process Prevented by the RMX Repair Complex. *Curr. Biol.* **2004**, *14*, 2107–2112. [CrossRef]
205. Soutoglou, E.; Dorn, J.F.; Sengupta, K.; Jasin, M.; Nussenzweig, A.; Ried, T.; Danuser, G.; Misteli, T. Positional Stability of Single Double-Strand Breaks in Mammalian Cells. *Nat. Cell Biol.* **2007**, *9*, 675–682. [CrossRef]
206. Lisby, M.; Mortensen, U.H.; Rothstein, R. Colocalization of Multiple DNA Double-Strand Breaks at a Single Rad52 Repair Centre. *Nat. Cell Biol.* **2003**, *5*, 572–577. [CrossRef]
207. Jakob, B.; Splinter, J.; Durante, M.; Taucher-Scholz, G. Live Cell Microscopy Analysis of Radiation-Induced DNA Double-Strand Break Motion. *Proc. Natl. Acad. Sci. USA* **2009**, *106*, 3172–3177. [CrossRef]
208. Caron, P.; Choudjaye, J.; Clouaire, T.; Bugler, B.; Daburon, V.; Aguirrebengoa, M.; Mangeat, T.; Iacovoni, J.S.; Álvarez-Quilón, A.; Cortés-Ledesma, F.; et al. Non-Redundant Functions of ATM and DNA-PKcs in Response to DNA Double-Strand Breaks. *Cell Rep.* **2015**, *13*, 1598–1609. [CrossRef]
209. Iarovaia, O.V.; Minina, E.P.; Sheval, E.V.; Onichtchouk, D.; Dokudovskaya, S.; Razin, S.V.; Vassetzky, Y.S. Nucleolus: A Central Hub for Nuclear Functions. *Trends Cell Biol.* **2019**, *29*, 647–659. [CrossRef]
210. Lin, C.-Y.; Shukla, A.; Grady, J.P.; Fink, J.L.; Dray, E.; Duijf, P.H.G. Translocation Breakpoints Preferentially Occur in Euchromatin and Acrocentric Chromosomes. *Cancers (Basel)* **2018**, *10*, 13. [CrossRef] [PubMed]
211. Yasuhara, T.; Xing, Y.-H.; Bauer, N.C.; Lee, L.; Dong, R.; Yadav, T.; Soberman, R.J.; Rivera, M.N.; Zou, L. Condensates Induced by Transcription Inhibition Localize Active Chromatin to Nucleoli. *Mol. Cell* **2022**, *82*, 2738–2753.e6. [CrossRef]
212. Ramanand, S.G.; Mani, R.S. Stress and the CITI. *Mol. Cell* **2022**, *82*, 2730–2731. [CrossRef]
213. Nelms, B.E.; Maser, R.S.; MacKay, J.F.; Lagally, M.G.; Petrini, J.H.J. In Situ Visualization of DNA Double-Strand Break Repair in Human Fibroblasts. *Science* **1998**, *280*, 590–592. [CrossRef]
214. Aten, J.A.; Stap, J.; Krawczyk, P.M.; van Oven, C.H.; Hoebe, R.A.; Essers, J.; Kanaar, R. Dynamics of DNA Double-Strand Breaks Revealed by Clustering of Damaged Chromosome Domains. *Science* **2004**, *303*, 92–95. [CrossRef] [PubMed]
215. Dion, V.; Kalck, V.; Horigome, C.; Towbin, B.D.; Gasser, S.M. Increased Mobility of Double-Strand Breaks Requires Mec1, Rad9 and the Homologous Recombination Machinery. *Nat. Cell Biol.* **2012**, *14*, 502–509. [CrossRef]
216. Dion, V.; Kalck, V.; Seeber, A.; Schleker, T.; Gasser, S.M. Cohesin and the Nucleolus Constrain the Mobility of Spontaneous Repair Foci. *EMBO Rep.* **2013**, *14*, 984–991. [CrossRef] [PubMed]
217. Miné-Hattab, J.; Rothstein, R. Increased Chromosome Mobility Facilitates Homology Search during Recombination. *Nat. Cell Biol.* **2012**, *14*, 510–517. [CrossRef] [PubMed]
218. Saad, H.; Gallardo, F.; Dalvai, M.; Tanguy-le-Gac, N.; Lane, D.; Bystricky, K. DNA Dynamics during Early Double-Strand Break Processing Revealed by Non-Intrusive Imaging of Living Cells. *PLoS Genet.* **2014**, *10*, e1004187. [CrossRef] [PubMed]
219. Forget, A.L.; Kowalczykowski, S.C. Single-Molecule Imaging of DNA Pairing by RecA Reveals a Three-Dimensional Homology Search. *Nature* **2012**, *482*, 423–427. [CrossRef]
220. Ragunathan, K.; Liu, C.; Ha, T. RecA Filament Sliding on DNA Facilitates Homology Search. *eLife* **2012**, *1*, e00067. [CrossRef]
221. Renkawitz, J.; Lademann, C.A.; Kalocsay, M.; Jentsch, S. Monitoring Homology Search during DNA Double-Strand Break Repair In Vivo. *Mol. Cell* **2013**, *50*, 261–272. [CrossRef]
222. Seeber, A.; Dion, V.; Gasser, S.M. Checkpoint Kinases and the INO80 Nucleosome Remodeling Complex Enhance Global Chromatin Mobility in Response to DNA Damage. *Genes Dev.* **2013**, *27*, 1999–2008. [CrossRef]
223. Mao, Z.; Bozzella, M.; Seluanov, A.; Gorbunova, V. DNA Repair by Nonhomologous End Joining and Homologous Recombination during Cell Cycle in Human Cells. *Cell Cycle* **2008**, *7*, 2902–2906. [CrossRef]

Studying and modelling chromosomal translocations presents several challenges due to two main factors. Firstly, spontaneous translocations are infrequent events, and for certain types, they may occur only once in the entire organism and can survive and multiply only if the translocation provides a growth advantage within the cell population, which is not always the case in proliferating cells in culture. Secondly, the breakpoints of naturally occurring translocations are dispersed over a wide genomic range, ranging from kilobases to hundreds of kilobases apart. Detecting these breakpoints requires advanced and sophisticated techniques such as long-range polymerase chain reaction (PCR), fluorescence in situ hybridization (FISH), next-generation sequencing, and others (Busch et al. 2007; Kovalchuk et al. 2012).

In contrast, an artificial system that induces DSBs with high efficiency and always at precisely the same loci, like a well-known "gold standard" CRISPR/Cas9 system, makes it much simpler to detect and quantify translocations using PCR. CRISPR/Cas9 system allows to specifically simulate the formation of these DSBs in a manner that is less dependent on cellular chromatin context (Jain et al. 2021; Mitrentsi & Soutoglou 2021) to study factors that contribute to translocation formation. Additionally, the repair of DSBs after Cas9 cleavage is error-prone, which prevents the re-cutting of the same locus (Brinkman et al. 2018).

1.4.2 EBV-associated B cell lymphomas in people living with HIV

Lymphomas in people living with HIV are more frequently associated with EBV, i.e. EBV is found in lymphoma cells of HIV-positive patients more frequently than in the same lymphoma subtypes in HIV-negative patients (Arvey et al. 2015). There are several indications that failing EBV control prior to the oncological disease is an important step for its development in people living with HIV (**Figure 4**). The impairment of CD4+ and CD8+ T cell immunity permits EBV reactivation from latency and expansion of the pool of EBV-infected B cells; the latter increases the chances of a subsequent malignant transformation of EBV-infected B cells and is often detectable in people living with HIV as an increased EBV viral load. This hypothesis is supported by the observation that in HIV-progressors the appearance of NHL is preceded by a decrease in EBV-specific CD8+ T cell response and an increase in the number of EBV-infected B cells (Kersten et al. 1997). EBV-positive DLBCL typically arises in people living with HIV with lower CD4+ T count at the time of diagnosis, when compared to EBV-negative DLBCL cases in the same population (Chapman et al. 2021). CD4+ T cells are indispensable for maintaining the proper functional capacity of CD8+ T cells, including EBV-specific CD8+ T cells, and their loss (either general or EBV-specific) correlates with the disease onset. In an early study of people living with HIV progressing to AIDS-related DLBCL, a significant drop in the functional activity of EBV-specific CD8+ T cells (as measured by IFNγ production), paralleled with CD4+ T cell loss, was found

right before lymphoma diagnosis, without any significant changes in the total amount of EBV-specific CD8+ T cells; this decline in IFNγ-producing EBV-specific CD8+ T cells was not observed in a group people living with HIV of progressing to AIDS-related opportunistic infections or in HIV-positive long-term asymptomatics with high CD4+ T-cell counts (van Baarle et al. 2001). Later on, the authors confirmed that the loss of EBV-specific CD8+ T cells indeed correlated with the discrete loss of EBNA1-specific memory CD4+ T cells in patients progressing to AIDS-related NHL (Piriou et al. 2005b). A decline in tumour-infiltrating CD4+ T cells and activated (granzyme B+) CD8+ cytotoxic T cells was described in cHL patients with HIV compared to HIV-negative cHL counterparts (Bosch Príncep et al. 2005).

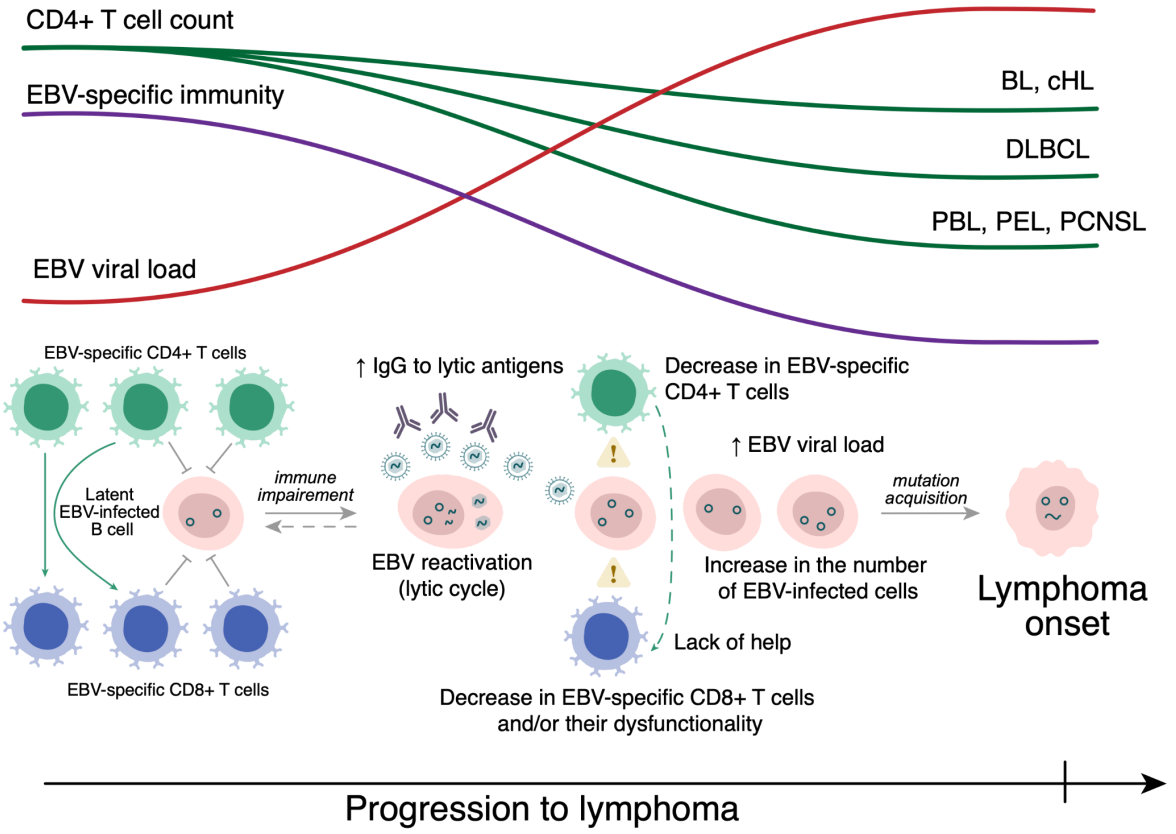

Figure 4. The pathogenesis of EBV-associated lymphoma in people living with HIV, influenced by host-mediated and viral factors. The impairment of CD4+ and CD8+ T cell immunity permits EBV reactivation from latency and expansion of the pool of EBV-infected B cells; the latter increases the chances of a subsequent malignant transformation of EBV-infected B cells and is often detectable in people living with HIV as an increased EBV viral load. Abbreviations: BL, Burkitt lymphoma; cHL, classical Hodgkin lymphoma; DLBCL, diffuse large B-cell lymphoma; EBV, Epstein-Barr virus; PBL, plasmablastic lymphoma; PCNSL, primary central nervous system lymphoma; PEL, primary effusion lymphoma.

EBV can both promote the malignant transformation of B cells and support the survival of malignantly transformed B cells at the early stages of lymphoma development. Intriguingly, host differentially expressed genes in HIV-related lymphomas show a certain degree of overlap across different

lymphoma subtypes, supporting a consistent role for EBV across multiple HIV-related malignancies (Arvey et al. 2015). Latent EBV infection was long assumed to be the main contributor to lymphomagenesis, however, an increasing amount of recent data supports the contribution of EBV reactivation to oncogenesis mainly at its initiation or through the abortive lytic cycle and the expansion of the pool of EBV-infected B cells (Germini et al. 2020; Sall et al. 2023). The contribution of EBV reactivation to the expansion of the pool of EBV-infected B cells during lymphomagenesis is supported by the fact that levels of IgG to lytic antigen VCA, but not to latent EBNA, are increased in people living with HIV prior to the diagnosis of PCNSL compared to matched HIV-infected controls without lymphomas (Gasser et al. 2007b). People living with HIV with lymphomas more frequently had detectable EBV DNA load at lymphoma diagnosis than either HIV-negative patients with the same lymphoma type or people living with HIV without lymphoma (Muncunill et al. 2019). High plasma EBV DNA levels at diagnosis are associated with decreased overall survival in HL and NHL in people living with HIV, but not in HIV-negative patients (Montgomery et al. 2019; Muncunill et al. 2019). In a cohort study with mixed NHL lymphoma subtypes, however, EBV detection in plasma or whole blood showed no significant correlation with NHL survival in people living with HIV, which could be due to the small sample size (Lupo et al. 2021); in HIV-related HL plasma or whole blood EBV DNA detection also does not predict the outcome (Lupo et al. 2019; Ul-Haq et al. 2018). Thus, compromised EBV-specific CD4+ and CD8+ T cell immunity precedes the development of EBV-associated lymphomas in people living with HIV and presumably results in the EBV reactivation and expansion of the pool of EBV-infected B cells, creating a higher risk for their malignant transformation.

Surprisingly, the loss of EBV immune surveillance might not always be related to the overall immune status, but to the isolated defects in EBV-specific reactions in people living with HIV. It was found that people living with HIV progressing to B cell subtype PCNSL lack EBV-specific CD4+ T cells irrespective of their absolute CD4+ T cell counts (Gasser et al. 2007a). No clear correlation is found between EBV viral load and CD4+ T cell count or HIV viral load in patients with or without HIV-related lymphomas (Fan et al. 2005; Richard et al. 2010).

With a certain proportion of B cell lymphomas in people living with HIV being EBV-negative, one cannot exclude the virus's contribution to lymphomagenesis through the so-called "hit-and-run" mechanism (Scott 2017), i.e. EBV enables cellular transformation ("hit") followed by malignancy expansion and loss of viral genome ("run"). This is supported by the fact that EBV is detectable in rare tumour cells of B cell lymphomas (BL, DLBCL, cHL), classified as EBV-negative by conventional methods (Mundo et al. 2020). Moreover, the detection of EBV plasma DNA might have a prognostic significance in lymphomas regardless of tumour EBV status (Tisi et al. 2016).

Additionally, HIV infection is believed to contribute to EBV-related B cell lymphomagenesis by chronically stimulating B cells expanding EBV reservoir in B cells (either by stimulating infected B cell division or by stimulating EBV reactivation) and immune senescence (Righetti et al. 2002). Both of these factors persist in people living with HIV despite successful viral suppression with cART.

EBV DNA viral load and anti-EA IgG antibody titer decrease following chemotherapy for EBV-related lymphomas (Lupo et al. 2021; Muncunill et al. 2019). EBV infection might also contribute to the HIV-1 reservoir persistence after chemotherapy. In a pilot study by Henrich et al., the reconstitution of CD4+ T cells, a major HIV-1 reservoir, in people living with HIV following chemotherapy was examined. Although systemic chemotherapies transiently decrease CD4+ T cell counts, Henrich et al. found that the mean level of HIV-1 RNA and DNA increased following chemotherapy cessation and that the HIV-1 reservoir resided almost exclusively in clonally-expanded HIV-1 infected CD4+ T cells responsive to EBV and/or cytomegalovirus (CMV) (Henrich et al. 2017). It is plausible that EBV or CMV antigen exposure caused the proliferation of EBV/CMV-responsive CD4+ T cells that harbour HIV-1.

Targeting EBV latency in HIV&EBV-related lymphomas was considered a promising therapeutic approach since EBV reactivation from latency in infected cells could induce their lysis. Nevertheless, the supplementation of standard EPOCH (etoposide, prednisone, vincristine, cyclophosphamide, and doxorubicin) regimen with the oral histone deacetylase inhibitor vorinostat, which disrupts EBV latency, has demonstrated no efficacy in the treatment of HIV-associated NHLs in a randomised clinical trial (Ramos et al. 2020).

To conclude, lymphomas in people with HIV are closely associated with EBV infection, which is found more frequently in lymphoma cells of HIV-positive patients compared to HIV-negative patients. The impairment of EBV-specific CD4+ and CD8+ T cell immunity allows EBV reactivation and expansion of infected B cells, increasing the risk of malignant transformation. Understanding the mechanisms responsible for the impairment of EBV-specific immunity in people living with HIV is crucial for improved diagnosis and treatment of EBV-associated lymphomas in this population.

1.5 HIV "interaction" with EBV and B cells: the role of cell-penetrating viral proteins

Mechanisms underlying B cell lymphoma formation in people living with HIV remain obscure, as HIV is believed not to infect B cells. A few articles, most of them being published in late 80s and 90s, report that B cells can be infected with HIV-1 (majorly those that are transformed with EBV) (Blumberg et al.

1987; Dahl et al. 1990; Goldblum et al. 1990; McHugh et al. 2020; Monroe et al. 1988; Montagnier et al. 1984; Rodriguez-Alfageme et al. 1998; Shepherd et al. 1992; Tozzi et al. 1989; Tremblay & Wainberg 1989; Tremblay et al. 1988, 1990), which seems to be a rare event in real life. A single case report was published that described AIDS-related B cell lymphoma with HIV-1 genome integration, which caused 3'-LTR-driven STAT3 overexpression (Katano et al. 2007). In another study, HIV-1 DNA was detected in 2 out of 21 HIV-1 and EBV-associated DLBCL (Lazzi et al. 2002). The rare, if even possible, B cell infection with HIV does not mean that HIV can not influence B cell pathology and "interact" with EBV *in vivo* through indirect mechanisms.

The cellular targets of HIV are CD4+ T cells, monocytes/macrophages, and dendritic cells, EBV mainly infects B cells and epithelial cells, and the infected cells can meet within the circulatory and lymphatic systems. Notably, CD4+ follicular B helper T cells (Tfh) within B cell follicles of lymphoid tissues are thought to be the main HIV reservoir upon cART (Aid et al. 2018). In the B cell follicle niche, Tfh cells might reside in the vicinity of EBV-infected B cells. Moreover, antiretroviral drug penetration into the lymphoid tissues was reported to be insufficient to suppress HIV-1 transcription and replication (Fletcher et al. 2014). Finally, defective HIV proviruses (and most of the proviruses that persist in CD4+ T-cells of people living with HIV upon cART use are defective (>95%)) are not transcriptionally silent and are able to produce viral proteins (Imamichi et al. 2016, 2020).

Since HIV-associated B cell lymphomas affect cells not targeted by the virus, a direct oncogenic effect of HIV-1 could be mediated by viral proteins that have the property of being secreted by the infected cell and entering other non-infected cells (Isaguliants et al. 2021). With this regard, we draw our attention to viral transactivator proteins with cell penetration capacities. It is known that viruses evolved different strategies to manipulate host cell defence programs (Agol & Gmyl 2010; Xu et al. 2011). Many of these strategies are governed by viral transcriptional activator proteins that above sustaining transcription of viral genomes alter existing cellular programs in a way that promotes viral propagation (Liu et al. 2020) and can potentially target neighbouring cells. Of note, cell penetration domains (CPDs) are present in different proteins of different viruses: Tat protein of HIV (Rayne et al. 2010b), L2 protein of the human papillomavirus (Zhang et al. 2018b), hemagglutinin of H5N1 highly pathogenic avian influenza virus (Kajiwara et al. 2020), Zta of Epstein-Barr virus (Rothe et al. 2010), X-protein of hepatitis B virus (Montrose et al. 2013), however, their role for viruses remains insufficiently investigated.

1.5.1 HIV-1 Tat

Among HIV-1 proteins, an interesting protein in the context of B cell lymphoma development is the HIV-1 transactivator of transcription (Tat). HIV-1

Tat is a 12 kDa basic protein that exists predominantly in two different lengths – 86 residues or 101 residues, with the most common form consisting of 101 residues (Campbell & Loret 2009). Tat's primary sequence consists of six domains: a proline-rich acidic N-terminus (residues 1-21), a cysteine-rich region (residues 22-37), a hydrophobic core region (residues 38-48), an arginine-rich basic domain (residues 49-57), glutamine-rich domain (residues 58-72) and a C-terminal domain (residues 73-86/101, encoded by the second exon) (**Figure 5**). The first exon is endowed with a full transactivation activity (Kurnaeva et al. 2019). Tat domains concatenate several functions within a limited number of residues. A small arginine-rich basic domain of Tat (residues 49-57 of HIV-1 Group M Subtype B Tat) is responsible for three functions at once: trans-activation response element (TAR)-binding, nuclear targeting (nuclear localization signal, NLS) and cell penetration (CPD) (Kurnaeva et al. 2019; van der Kuyl et al. 2018). N-terminal 48 residues of HIV-1 Tat contain the binding site for the cyclin T1, a component of the positive transcription elongation factor (P-TEFb) (Clark et al. 2017). The interaction between Tat and cyclin T1 requires zinc ions (Zn^{2+}) as well as cysteine residues in both HIV-1 Tat (cysteine-rich domain and C22 in particular) and cyclin T1 (C261) (Garber et al. 1998). Additionally, phosphorylation of Ser15 regulates Tat's binding to cyclin T1 (Ivanov et al. 2018). Tat is an intrinsically disordered protein that provides conformational flexibility and hence the ability to bind a large variety of partners; this property determines the diversity of Tat's functions (Shojania & O'Neil 2006; Xue et al. 2012).

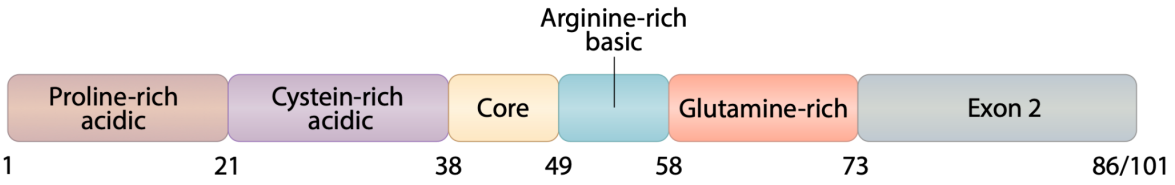

Figure 5. Domain structure of HIV-1 Tat.

Tat sequence varies between viral subtypes and isolates, which affects protein functioning and clinical outcome (Hutto et al. 1996; Roy et al. 2015; van der Kuyl et al. 2018). Even one amino acid substitution can drastically affect the functions of Tat: R75S mutation in the BD (characteristic for HIV-1 group M subtype C) drastically decreases transactivation and cell penetration (Ruiz et al. 2019). C22S mutation in HIV-1 Oyi strain results in loss of transactivation activity and in long-term non-progressive infection (Opi et al. 2002). HIV-1 Tat from the E subtype selectively inhibits *TNF* gene transcription by interfering with histone acetyltransferase P/CAF recruitment to the *TNF* promoter and chromatin remodelling due to F32W mutation (Ranjbar et al. 2006).

HIV-1 Tat plays a crucial role in activating HIV-1 transcription (**Figure 6**), binding to nascent viral RNA element (TAR, transactivation-responsive region) and recruiting transcriptional factors to viral promoter, which leads to

increased viral transcript synthesis and facilitates viral propagation (Brigati et al. 2003; Kao et al. 1987; Mancebo et al. 1997; Ne et al. 2018; Raha et al. 2005; Romani et al. 2010). In the absence of Tat, HIV-1 proviral promoter is incompetent for elongation: shortly after transcription initiation, RNA Pol II is stalled due to the presence of an inactive form of positive transcription elongation factor b (P-TEFb) composed of CDK9, cyclin T1 or T2,[2] and inhibitory 7SK small nuclear ribonucleoprotein complex (containing 7SK RNA and HEXIM1) (D'Orso & Frankel 2010; Kao et al. 1987; Sedore et al. 2007). Tat is able to relieve this repressed state by binding to the TAR-like sequence in 7SK snRNA and displacing HEXIM1 from cyclin T1, which disrupts the 7SK-P-TEFb negative transcriptional regulatory complex and releases active P-TEFb (Barboric et al. 2007; Muniz et al. 2010; Pham et al. 2018; Sedore et al. 2007). This ability of Tat depends on Tat C22 residue within the activation domain (Barboric et al. 2007). It was also recently shown that Tat exploits ubiquitin ligase UBE2O to ubiquitinate HEXIM1, which leads to its retention in the cytoplasm and consequently frees P-TEFb from its inhibitory state within the 7SK complex (Faust et al. 2018). Tat then recruits the active P-TEFb complex (consisting of CDK9, cyclin T1 or T2) and other transcriptional coactivators to the TAR RNA element at the 5' end of stalled nascent HIV-1 transcripts to relieve stalled RNA Pol II (He et al. 2010; Nekhai & Jeang 2006). Additional host factors that further stimulate HIV-1 transcription include AFF4, ENL, AF9, and ELL2, which together with P-TEFb form the so-called super elongation complex (He & Zhou 2011; He et al. 2010; Sobhian et al. 2010). The time during which CDK9 remains bound to nascent HIV-1 RNAs is significantly increased in the presence of HIV-1 Tat (71s vs 11s without Tat) (Molle et al. 2007). P-TEFb phosphorylates the C-terminal domain (CTD) of Pol II, which enables the assembly and operation of factors involved in transcript elongation (Zhou & Yik 2006). Along with the CTD of Pol II, P-TEFb phosphorylates DRB sensitivity inducing factor (DSIF, composed of Spt4 and Spt5) and negative elongation factor (NELF) to counteract their inhibitory effects, causing Pol II to be released from promoter-proximal pausing (Ott et al. 2011). Tat participates in Pol II CTD phosphorylation by engaging CDK2, which requires Tat's C22 residue (Deng et al. 2002). Additionally, Tat may also enhance the initiation of viral transcription (Raha et al. 2005). Tat can be expressed even from unintegrated viral DNA at levels sufficient to induce the expression of latent integrated viral DNA (Thierry et al. 2016). Tat can also promote transcription from unintegrated HIV cDNAs (Burdick et al. 2020). Inhibiting Tat interaction with TAR elements to block HIV

[2] When first described by Herrmann and Rice in relation to HIV-1 Tat-mediated viral transcription, it was originally named Tat-associated kinase (TAK) (Herrmann & Rice 1993, 1995). TAK was shown to hyperphosphorylate CTD of RNA Pol II to promote viral transcript elongation (Herrmann & Rice 1995). It was later established that TAK was actually composed of CDK9 (formerly known as PITALRE) (Yang et al. 1997) and its regulatory partner, cycling T1, was soon identified (Wei et al. 1998).

transcription is a promising therapeutic approach for chronic HIV infection (Alanazi et al. 2021; Nekhai & Jeang 2009).

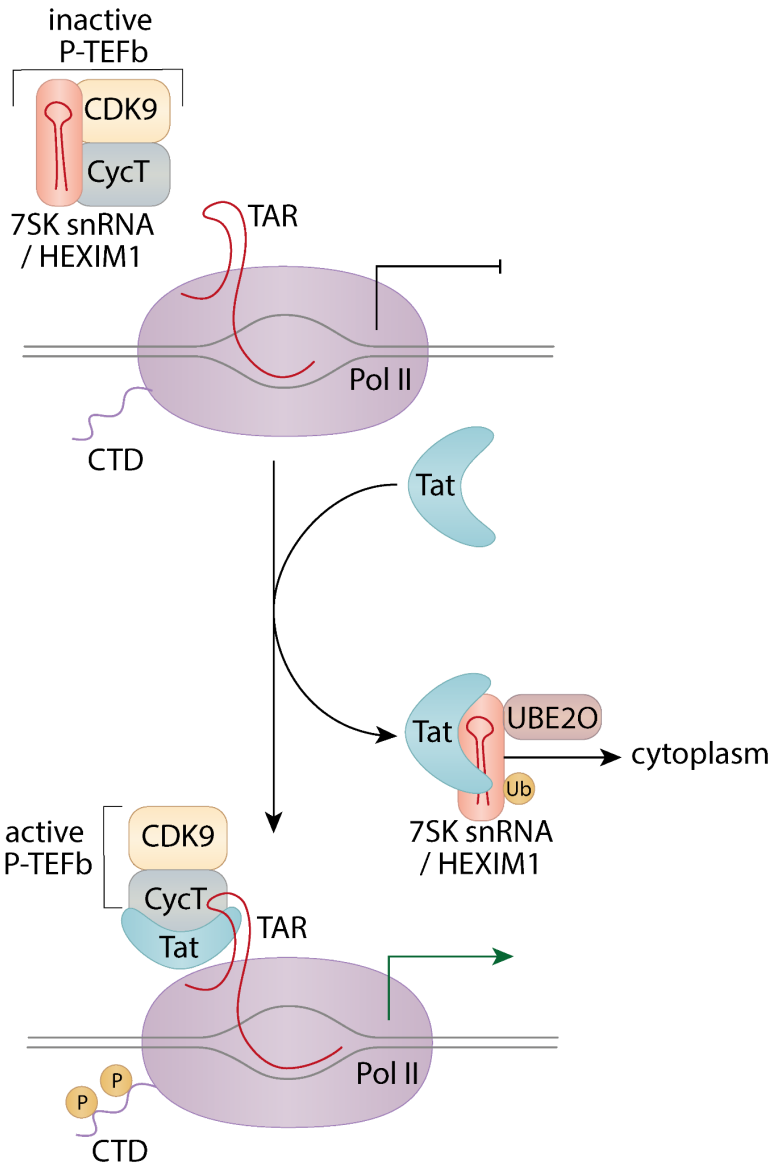

Figure 6. The mechanism of Tat-mediated transactivation of HIV transcription. In the absence of Tat, RNA Pol II is stalled on HIV-1 proviral promoter shortly after transcription initiation due to the presence of an inactive form of positive transcription elongation factor b (P-TEFb) composed of CDK9, cyclin T1 or T2, and inhibitory 7SK small nuclear ribonucleoprotein complex (containing 7SK RNA and HEXIM1). Tat is able to relieve this repressed state by binding to the TAR-like sequence in 7SK snRNA and displacing HEXIM1 from cyclin T1, which disrupts the 7SK-P-TEFb negative transcriptional regulatory complex and releases active P-TEFb. Tat also exploits ubiquitin ligase UBE2O to ubiquitinate HEXIM1, which leads to its retention in the cytoplasm and consequently frees P-TEFb from its inhibitory state within the 7SK complex. Tat then recruits the active P-TEFb complex (consisting of CDK9, cyclin T1 or T2) and other transcriptional coactivators to the TAR RNA element at the 5′ end of stalled nascent HIV-1 transcripts to relieve stalled RNA Pol II. P-TEFb phosphorylates the C-terminal domain (CTD) of Pol II, which enables transcript elongation. Abbreviations: 7SK snRNA, 7SK small nuclear RNA; CDK9, cyclin-dependent kinase 9; CTD, C-terminal

domain; HIV, human immunodeficiency virus; P-TEFb, positive transcription elongation factor b; Pol II, RNA Polymerase II; TAR, trans-activation response element; Tat, trans-activator of transcription; UBE2O, ubiquitin-conjugating enzyme E2O.

Surprisingly, a recent finding suggests that RNA Pol II promoter-proximal pausing in the absence of HIV-1 Tat is rather stochastic than an obligatory event, with only a small fraction of polymerases undergoing long-term pausing (Tantale et al. 2021). This stochastic pausing may lead to bursts in viral transcription in latent cells even in the absence of Tat, which facilitates latency exit of infected cells and might explain the stochasticity of viral rebounds (Tantale et al. 2021). The transcription of latent proviruses in the absence of Tat (particularly, transcription initiation) is regulated by host transcription factors, such as SP1 and NF-κB (Perkins et al. 1993; Suñé & García-Blanco 1995; Williams et al. 2007), that interact directly with specific sites in viral promoters. Several restriction factors that inhibit viral transcription were also described. Notably, DNA topoisomerase I, an enzyme that regulates the topological state of DNA, was shown to repress viral promoter activity (Lista et al. 2023). This occurs *via* DNA topoisomerase I binding to secondary structures folded in G-rich motifs of HIV-1 promoter, so-called G-quadruplexes (G4) (Lista et al. 2023). Targeting G4 is a promising strategy for antiviral therapy (Ruggiero & Richter 2023). FACT (facilitates chromatin transcription) complex, which was shown to facilitate HIV-1 integration (Matysiak et al. 2017), silences HIV transcription by assembling nucleosomes along the proviral DNA (Gallastegui et al. 2011; Huang et al. 2015a).

Tat is also capable of controlling the expression of host genes, which occurs via modulation of RNA-polymerase II recruitment to host gene promoters (stimulation of transcription initiation) and decrease of RNA-polymerase II promoter-proximal pausing (stimulation of transcription elongation) (Marban et al. 2011; Reeder et al. 2015). In addition to binding to host genes, HIV-1 Tat also interacts with a subset of human cellular mRNA transcripts that have a stem-loop structural element, this interaction is associated with an increase in mRNA abundance (Bouwman et al. 2014). Besides transcriptional regulation, Tat is able to bind cellular proteins, including host transcription factors, affecting their functioning (Jean et al. 2017).

HIV-1 Tat is actively released by infected cells (Rayne et al. 2010b), can be found in the bloodstream (at concentrations ranging from 10 ng/ml to 550 ng/ml) (Germini et al. 2017b; Poggi et al. 2004) and in the cerebrospinal fluid (at concentrations ranging from 200 pg/ml to 6.5 ng/ml) (Henderson et al. 2019) in people living with HIV under cART. Tat secretion was shown to increase in four out of five patients after cART initiation, which indicates that Tat secretion is not inhibited by cART (Henderson et al. 2019). Tat presence at high levels was detected in HIV-1-associated B cell lymphomas (BL, DLBCL) (Alves de Souza Rios et al. 2021; Lazzi et al. 2002; Luzzi et al. 2014). CPD

ensures Tat secretion by infected cells, its tissue accumulation, circulation in the bloodstream and penetration in non-infected bystander cells, including the immune cells (Ensoli et al. 1993; Marchiò et al. 2005; Rayne et al. 2010a,b; Xiao et al. 2000). Tat also penetrates the brain blood barrier (Banks et al. 2005). Tat efficient secretion is mediated by basic domain (CPD) binding to phosphatidylinositol-4,5-bisphosphate ($PI(4,5)P_2$) on cell plasma membrane (Rayne et al. 2010a), while its extracellular accumulation and cellular uptake is mediated by heparan sulphate proteoglycans binding (Albini et al. 1996a; Chang et al. 1997; Rusnati et al. 1997; Urbinati et al. 2009). Thus, local concentrations of Tat in the mucosal (e.g. at the primary site of infection), lymphoid tissues and the endothelium surface can be much higher than detected in the serum of HIV-infected patients. Upon binding with $PI(4,5)P_2$ Tat protein undergoes secondary structure changes that enable the membrane insertion of Tat Trp11 and Tat organisation into membrane-inserted oligomers, which leads to the formation of membrane pores, facilitating Tat secretion (Debaisieux et al. 2012; Zeitler et al. 2015). According to recent data, Tat can also be released extracellularly within exosomes (Rahimian & He 2016).

Due to this property, Tat is considered to play a role in several HIV-associated pathologies, such as HIV-associated neurocognitive disorder, substance use disorder, cardiovascular complications, accelerated ageing, B cell lymphomas, including BL, and others (Ferrell & Giunta 2014; Cirino & McLaughlin 2021; Jiang et al. 2018; Germini et al. 2017b; Akbay et al. 2020; Bagashev & Sawaya 2013; Fields et al. 2015a,b; Cohen & Torres 2017; Zhao et al. 2020). Extracellular Tat is able to interact with components of the extracellular matrix and cell surface, thereby influencing lymphocyte functions, promoting cell migration, and inducing cytopathic effects on leukocytes and neural cells (Clark et al. 2017). However, the majority of its functions rely on Tat's absorbance by bystander cells. Tat has various binding sites on the cell surface, including ubiquitous endocytic receptors, such as the lipoprotein receptor-related protein, CXCR4 and heparan sulphate proteoglycans, which allow Tat internalisation in several cell types (Debaisieux et al. 2012). There are two proposed pathways of Tat endocytosis: caveolar (Fittipaldi et al. 2003) or clathrin/AP-2 dependent (Vendeville et al. 2004); it seems that the choice of pathway depends on the target cell type. Following endosomal uptake, Tat goes through a Rab5-dependent pathway to late endosomes/lysosomes, where it is exposed to low pH (<6). Acidification triggers Tat insertion into the endosomal membrane, followed by Tat translocation to cytoplasm catalysed by the cytosolic chaperone Hsp90 (Debaisieux et al. 2012). Once in the cytoplasm, Tat can translocate to the nucleus to influence host cell gene expression and trigger various cell responses (Musinova et al. 2016). Transactivation capacity of extracellular Tat is strongly enhanced by chloroquine, which is thought to act by de-acidification of endolysosomes and

prevention of Tat degradation (Frankel & Pabo 1988; Khan et al. 2019; Kolson et al. 1994; Vendeville et al. 2004).

One can hypothesise that changes in cellular gene expression under Tat action provide a favourable environment for virus propagation, which requires further investigation, especially in tissues not directly targeted by the virus. Secreted Tat was shown to affect immune cell functioning, in a way that may contribute to viral spread (**Table 3**). It contributes to the impaired functioning of natural killer cells (Poggi & Zocchi 2006; Poggi et al. 2002; Zocchi et al. 1998) and CD8+ T cells (Chiozzini et al. 2014), important components of anti-HIV immunity (Alter & Altfeld 2009; Collins et al. 2020). HIV-1 Tat reprograms dendritic cells in a way that they secrete more chemokines that recruit activated T cells and macrophages, facilitating the expansion of HIV infection (Izmailova et al. 2003). Finally, on uninfected CD4+ T cells and macrophages, extracellular HIV-1 Tat upregulates the expression of HIV entry receptors (CXCR4, CCR5), thus enhancing infectivity (Huang et al. 1998; Secchiero et al. 1999). The changes caused by Tat protein alone correlate with the immune cell dysregulations seen in people living with HIV (Altfeld et al. 2011; Herbein et al. 2010; Shen & Tomaras 2011). The presence of anti-Tat cellular and humoral immune responses correlates with the control of HIV infection, which confirms the pathogenicity of Tat and suggests its use as a target for vaccination (Cafaro et al. 2019; Kulkarni et al. 2017). Immune selective pressure might have influenced the optimisation of cell-penetrating properties of Tat.

Table 3. Tat effects on the immune cells. Abbreviations: DC, dendritic cells; IL, interleukin; NK, natural killer cells; TGFβ, transforming growth factor beta.

Cell type	Tat effect	References
Natural killer cells (NK)	impairs NK activation, cytotoxic activity, prevents degranulation, decreases the number of contacts with target cell	(Poggi et al. 2004; Zocchi et al. 1998)
	inhibits NK cell-mediated lysis of DC	(Tasca et al. 2003)
	NK cell apoptosis *via* TGFβ	(Poggi & Zocchi 2006)
Uninfected CD4+ T cells	induces CXCR4, thus enhances infectivity	(Huang et al. 1998; Secchiero et al. 1999)
	induces apoptosis	(Li et al. 1995a; Westendorp et al. 1995; Zauli et al.

		1996)
CD8+ T cells	contributes to the CD8+ T cell hyperactivation and dysfunctionality	(Nicoli et al. 2013)
	IL7 receptor (CD127) downregulation, impaired proliferation and cytolytic potential	(Faller et al. 2006, 2009)
Dendritic cells (DCs)	induces PD-L1 expression, functionally compromises the ability to stimulate T cells	(Planès et al. 2014)
	induces the production of proinflammatory cytokines	(Haij et al. 2015)
	increases chemokine expression that recruit activated T cells and macrophages	(Izmailova et al. 2003)
Monocytes / macrophages	inhibits the phagocytosis	(Debaisieux et al. 2015)
	induces the production of proinflammatory cytokines	(Haij et al. 2015)
	promotes chemotaxis and invasive behaviour	(Lafrenie et al. 1996)
	stimulates production of TGFβ	(Zauli et al. 1992)
	inhibits production of IL12	(Ito et al. 1998)
B cells	inhibits the proliferation of naive and memory B cells	(Lefevre et al. 1999)
	induces hyperactivation, upregulates Fas	(Huang et al. 1997)
	induces DNA damage *via* mitochondrial ROS production	(El-Amine et al. 2018)

	induces *AICDA* expression, somatic hypermutation and genome instability	(Akbay et al. 2021; Sall et al. 2019; Wang et al. 2018)

Oncogenic properties of Tat have been already proposed in different cancers (Altavilla et al. 2000; Corallini et al. 1996; Huynh et al. 2007; Vogel et al. 1995). Tat is supposed to be a tumour promoter that accelerates tumour development under the action of cancer agents (carcinogens, viruses) (Altavilla et al. 2000, 2004; Chen et al. 2009; Vogel et al. 1995). It modulates cell cycling, DNA repair mechanisms, and decreases apoptosis (Cantaluppi et al. 2001; Colombrino et al. 2004; Nunnari et al. 2008; Nyagol et al. 2006). Tat promotes vascular permeability, worsens the oncogenic properties of cancer cells and accelerates tumour development in animal xenograft models (Huynh et al. 2007; Toschi et al. 2001). Tat-transgenic mice are prone to the development of tumours of various origins, including B cell lymphomas (Altavilla et al. 1999, 2004; Corallini et al. 1993; Kundu et al. 1999). Different oncogenic properties of HIV-1 Tat are summarised in **Table 4**.

Table 4. Oncogenic properties of HIV Tat. Abbreviations: MHC, Major Histocompatibility Complex; ROS, reactive oxygen species; VEGF, vascular endothelial growth factor.

Tat effect	Description	References
Promoting cell survival and proliferation	growth factor for Kaposi's sarcoma cells	(Barillari et al. 1993; Ensoli et al. 1990)
	upregulates *BCL2* expression	(Zauli et al. 1995; Zheng et al. 2007)
	inhibits pRb2/p130	(De Falco et al. 2003; Lazzi et al. 2002)
Genomic instability	inhibits *TP53* expression	(Li et al. 1995b)
	upregulates *RAG1* expression	(Germini et al. 2017b)
	upregulates *AICDA* expression	(Akbay et al. 2021; Sall et al. 2019)
	stimulates ROS production	(El-Amine et al. 2018)
	upregulates DNA polymerase β expression	(Srivastava et al. 2001)

Angiogenesis and metastasis	binds and activates VEGF receptors	(Albini et al. 1996b; Scheidegger et al. 2001)
	retrieves into a soluble form extracellular basic fibroblast growth factor	(Barillari et al. 1999a,b)
	promotes epithelial-to-mesenchymal transition and invasion by interacting with TIP30	(Liu et al. 2018)
Inflammation and immune evasion	targets IL-7R for proteasomal degradation in CD8+ T cells and impairs their proliferation and function	(Faller et al. 2010, 2014)
	induces the production of proinflammatory cytokines by dendritic cells and monocytes/macrophages through TLR4 pathway	(Ben Haij et al. 2013; Haij et al. 2015)
	downregulates MHC I expression	(Howcroft et al. 1993; Weissman et al. 1998)
	induces of C chemokine XCL1 expression	(Kim et al. 2004)

The role of Tat in the B cell lymphoma development has been described only partially. Tat expression in EBV-transformed B cells was shown to cause Bcl-2 downregulation and increased apoptosis rate upon serum starvation, at the same time, a portion of EBV-transformed B cells with Tat retained proliferative capacity as opposed to control cells upon serum starvation (Colombrino et al. 2004). Exogenous Tat induces DNA damage in B cells through reactive oxygen species (ROS) production promoting genetic instability and malignant transformation (El-Amine et al. 2018). Another study showed that Tat activates the transcription of the nuclease-encoding RAG1 gene in B cells, which leads to DSBs, including DSBs in the *MYC* gene locus, which, in turn, promotes *MYC* gene locus colocalization with the *IGH* gene locus after DSBs in B cells, resulting in BL-specific t(8;14) chromosomal translocation (Germini et al. 2017a). Tat also activates the expression of the *AICDA* gene through Akt/mTORC1 pathway activation and inhibition of the *AICDA* transcriptional repressors c-Myb and E2F8; *AICDA* gene encodes the activation-induced

cytidine deaminase (AID), an enzyme that in physiological conditions creates DSBs for immunoglobulin class-switch recombination and immunoglobulin gene maturation in B cells. Overexpression of AID leads to increased DSBs within the *IGH* and potentially *MYC* gene loci, favouring the formation of t(8;14) translocation (Akbay et al. 2021; Sall et al. 2019). Tat expression in EBV-transformed B cells was shown to cause Bcl-2 downregulation and increased apoptosis rate upon serum starvation, at the same time, a portion of EBV-transformed B cells with Tat retained proliferative capacity as opposed to control cells upon serum starvation (Colombrino et al. 2004). Additionally, Tat can increase the expression of *MYC* in B cells by binding to its promoter (Alves de Souza Rios et al. 2021). Thus, Tat protein is a potentially important factor contributing to B cell lymphomagenesis in people living with HIV.

1.5.2 EBV Zta

Another viral transcriptional activator, EBV Zta has several features functionally homologous to HIV-1 Tat: it is a transcriptional activator, it can be released from infected cells, penetrates other cells, where being transported into a nucleus regulates viral and host gene transcription (Germini et al. 2017b; Kurnaeva et al. 2022; Rayne et al. 2010b; Rothe et al. 2010).

EBV Zta (also known as ZEBRA, Z, BZLF1, or EB-1) is a 35 kDa protein, encoded by the *BZLF1* gene of EBV (Germini et al. 2020). Zta is a key factor in switching from latency to lytic cycle (Countryman & Miller 1985; Feederle et al. 2000). The Zta promoter zone (Zp) shows a low basal activity and is efficiently activated by transcriptional inducers of the lytic cycle (e.g. SP-1, SP-3, AP-1), switching EBV-infected B cells from latent infection to virus replication (Liu et al. 1997; Speck et al. 1997). Zp contains sites that bind Zta with high affinity, creating a positive feedback loop, where Zta enhances its own expression (Speck et al. 1997). Zta is a basic leucine zipper transcription factor (Petosa et al. 2006) with a cell penetration domain (Rothe et al. 2010). In contrast to HIV-1 Tat which binds gene promoters, Zta majorly binds distal enhancer regions of the host genes (Liu et al. 2020; Ramasubramanyan et al. 2015). Zta has a special affinity and selectivity for CpG-methylated binding sites (Bergbauer et al. 2010; Dickerson et al. 2009; Flower et al. 2011). EBV reactivation from latency is a rather rare event, possibly because Zta expression needs to overcome a certain threshold. When Zta expression is low, transactivator protein will bind only high affinity methylated ZRE, while oriLyt (origin of replication), for example, requires a higher Zta concentration for binding (Bergbauer et al. 2010; Buschle & Hammerschmidt 2020; Buschle et al. 2019). This threshold can be overcome by a positive feedback loop, whereby Zta stimulates its own expression (Flemington & Speck 1990). Zta also binds various cellular transcription factors (p53, p65, c/EBP, Pax5, Oct2, NFAT, IRF-7) and hence influences the expression of their target genes (Germini et al. 2020).

Zta was also shown to disrupt promyelocytic leukemia (PML) nuclear bodies by inhibiting SUMO-1 modification of PML (Adamson & Kenney 2001), similar activity was previously reported for the ICP0 protein of herpes simplex virus 1 (HSV-1) (Ahn et al. 1998; Everett et al. 2006) and immediate early (IE) gene product IE1 protein of CMV (Korioth et al. 1996). PML nuclear bodies are nuclear membrane-less organelles with a diameter of 0.1–1 μm containing macromolecular multiprotein complexes, including concentrated tumour suppressor PML protein - the main organizer of PML nuclear bodies (Corpet et al. 2020; Hirose et al. 2023; Lallemand-Breitenbach & de Thé 2010). SUMO-1 modification of PML is essential for its proper positioning and functioning (Ishov et al. 1999). PML nuclear bodies are considered to be an important frontier of host antiviral defence (Tavalai & Stamminger 2008); they are involved in the regulation of MHC class I expression (Zheng et al. 1998), interferon-mediated cellular response to viral infections (Doucas et al. 1996; Regad & Chelbi-Alix 2001), stress response (Maul et al. 1995) and apoptosis (Takahashi et al. 2004). The parental genomes and replication complexes of several DNA viruses (HSV-1, adenoviruses, papovaviruses) were found to preferentially localize in close association with PML bodies (Everett 2001; Ishov & Maul 1996; Maul et al. 1996), suggesting that PML nuclear bodies might be implicated in the inhibition of viral replication (Scherer & Stamminger 2016) and in the chromatinization of viral genomes (Corpet et al. 2020).

There is growing evidence concerning Zta implication in EBV-driven oncogenesis (Dorothea et al. 2023; Germini et al. 2020; Rosemarie & Sugden 2020). Zta is detected in serum samples from humanized mice developing lymphomas and correlates with tumour mass (Ma et al. 2012). Zta high expression was shown in post-transplant lymphoproliferative disorder (PTLD) samples, HL, DLBCL, BL, nasopharyngeal carcinoma (NPC) and breast cancer (Cohen et al. 2018; Huang et al. 2003; Ramayanti et al. 2017; Xue et al. 2000, 2002). The mechanisms of Zta contribution to cancer development include Zta-induced tumour-promoting inflammation, genome instability, immune evasion, stimulation of growth and proliferation and resistance to apoptosis (Germini et al. 2020). See review **Article 3** for more detail on the oncogenic properties of EBV Zta protein.

I contributed to this review by writing chapters about EBV Zta structure, domain organisation, post-translational modification, and EBV Zta functioning in host cells (transcriptional regulation, binding to the replication origin in EBV lytic replication and interaction with other cellular proteins).

Article 3. Review "Oncogenic Properties of the EBV ZEBRA Protein"

cancers

MDPI

Review

Oncogenic Properties of the EBV ZEBRA Protein

Diego Germini [1], Fatimata Bintou Sall [1,2,†], Anna Shmakova [1,†], Joëlle Wiels [1], Svetlana Dokudovskaya [1], Emmanuel Drouet [3] and Yegor Vassetzky [1,4,*]

1 CNRS UMR9018, Université Paris-Saclay, Institut Gustave Roussy, 94805 Villejuif, France; germinidiego@gmail.com (D.G.); fabisall3007@gmail.com (F.B.S.); anyashm@gmail.com (A.S.); wiels@igr.fr (J.W.); svetlana.dokudovskaya@gustaveroussy.fr (S.D.)
2 Laboratory of Hematology, Aristide Le Dantec Hospital, Cheikh Anta Diop University, Dakar 12900, Senegal
3 CIBB-IBS UMR 5075 Université Grenoble Alpes, 38044 Grenoble, France; Emmanuel.Drouet@ibs.fr
4 Koltzov Institute of Developmental Biology, 117334 Moscow, Russia
* Correspondence: yegor.vassetzky@cnrs.fr
† These authors contributed equally to this work as co-second authors.

Received: 19 May 2020; Accepted: 4 June 2020; Published: 5 June 2020

Abstract: Epstein Barr Virus (EBV) is one of the most common human herpesviruses. After primary infection, it can persist in the host throughout their lifetime in a latent form, from which it can reactivate following specific stimuli. EBV reactivation is triggered by transcriptional transactivator proteins ZEBRA (also known as Z, EB-1, Zta or BZLF1) and RTA (also known as BRLF1). Here we discuss the structural and functional features of ZEBRA, its role in oncogenesis and its possible implication as a prognostic or diagnostic marker. Modulation of host gene expression by ZEBRA can deregulate the immune surveillance, allow the immune escape, and favor tumor progression. It also interacts with host proteins, thereby modifying their functions. ZEBRA is released into the bloodstream by infected cells and can potentially penetrate any cell through its cell-penetrating domain; therefore, it can also change the fate of non-infected cells. The features of ZEBRA described in this review outline its importance in EBV-related malignancies.

Keywords: EBV; ZEBRA; Zta; BZLF1; lytic cycle; viral-host interaction; oncogenesis; transcription; transactivation

1. Introduction

Epstein-Barr Virus (EBV) or Human Herpesvirus 4, is a γ-herpesvirus that predominantly infects B-lymphocytes, and, to a lesser extent, epithelial, T and Natural Killers (NK) cells [1,2]. Discovered in 1964 as the first human oncogenic virus, EBV is one of the most widespread human viruses, affecting nearly 90% of the world's population [3,4]. After an initial infection, it persists as an episome in B cells for the rest of the host's life. In the vast majority of cases, EBV infection is asymptomatic, but in some individuals, it causes infectious mononucleosis. Furthermore, EBV is associated with various types of malignancies, including Burkitt lymphoma (BL), Hodgkin lymphomas (HL), nasopharyngeal and gastric carcinoma, and post-transplant lymphoproliferative disorder (PTLD). Indeed, EBV was classified as a class I carcinogen by World Health Organization (WHO) [5] and the evidence for EBV-associated oncogenesis have been recently reviewed and updated [6]. The pathogenic and oncogenic effects of EBV are mediated by several EBV proteins and non-coding RNAs. Here we will describe the role of one of EBV immediate early (IE) proteins, ZEBRA, in the viral life cycle and in regulation of the host genome and the consequences thereof.

1.1. EBV Life Cycle

EBV life cycle involves a latency phase and a lytic cycle, each associated with specific gene transcription and translation programs. These phases are summarized in Figure 1.

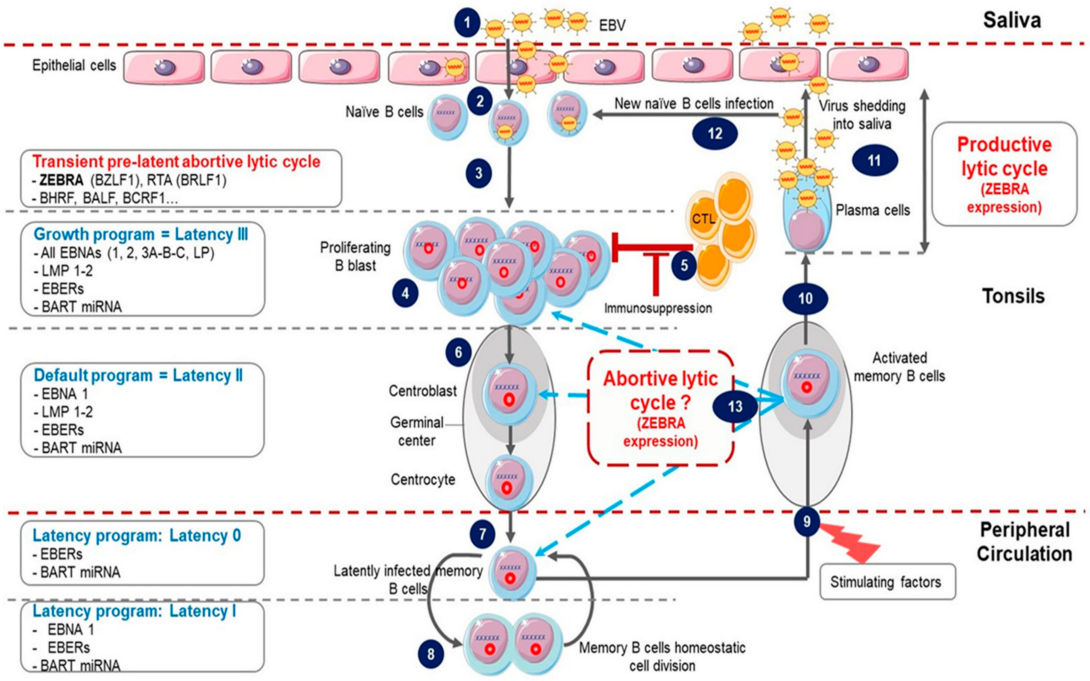

Figure 1. Epstein-Barr Virus (EBV) life cycle. (**1**) Infection occurs after the contact with an infected saliva. (**2**) After initial infection of oropharyngeal epithelial cells, the virus passes into the underlying lymphoid tissue where it infects naive B cells. (**3**) This immediately triggers the transient pre-latent lytic cycle with expression of ZEBRA and other lytic genes involved in resistance to apoptosis and evasion from the immune system. (**4**) Infected naive B cells become proliferating B blasts through the growth program (latency III) where all latency proteins are expressed. (**5**) Cytotoxic T lymphocytes (CTL) trigger a strong immune response (which is impaired during immunodeficiency) to eliminate EBV-infected B cells. (**6**) Proliferating B blasts migrate into the germinal center (GC) and activate the default transcription program (latency II) where latency protein expression is restricted to EBNA1, LMP1 and LMP2. They differentiate into centroblasts and then centrocytes. (**7**) Centrocytes leave the GC and differentiate into memory B cells circulating in peripheral blood. These cells have turned off the expression of all viral proteins (latency 0). (**8**) Occasionally, circulating EBV-positive memory B cells express EBNA1 during homeostatic cell division to ensure viral genome replication and segregation into daughter cells. (**9**) Following stimulation, latently infected memory B cells can be recruited into GC. (**10**) Activated EBV-positive memory B cells can differentiate into plasma cells, reactivate the virus and undergo productive lytic cycle that leads to (**11**) viral shedding into saliva and (**12**) new naive B cells infection. (**13**) Activated EBV-positive memory B cells reintegrate the pool of memory B cells. It is not clear whether in vivo stimulated EBV-positive memory B cells which have not differentiated into plasma cells undergo an abortive lytic cycle (ZEBRA and early gene expression without viral production) before reintegrating the pool of memory cells. It is also not clear whether these cells successively re-express different latency programs in the GC in vivo before reintegrating the pool of memory cells.

1.1.1. Latency

Following contamination via saliva, primary lytic infection occurs in the epithelial cells of the oropharynx [7] through virus binding to αvβ integrins and the ephrin A2 receptor [8,9]. EBV also infects naïve B cells by interaction with complement receptors 1 and 2 (CR1/CD35 and CR2/CD21)

as well as major histocompatibility complex (MHC) class II as a co-receptor [10,11]; this leads to latency establishment and lifelong EBV persistence. Latency can be divided into three successive programs [7,12,13].

The first, called the "growth program" or latency III is characterized by the expression of nine latency proteins (six nuclear proteins: Epstein Barr Nuclear Antigen (EBNA) 1, 2, 3A, 3B, 3C and LP, and three membrane proteins: Latent Membran Protein (LMP) 1, 2A and 2B); two Epstein Barr virus-encoded small non-coding RNAs (EBER1 and 2), BHRF1 miRNA and BamHI-A fragment rightward transcript (BART) transcripts [14,15]. EBV-infected B cells are activated and differentiate into proliferating B blasts. This phase triggers a powerful immune T cell cytotoxic response; however, it is usually insufficient to eliminate all infected B cells [12].

Remaining B blasts migrate to the tonsil germinal center (GC) where the second program, called the "default program" or latency II, occurs. Infected cells turn off the expression of all latency proteins except EBNA1 and LMP1 and 2. These proteins are thought to promote B blasts differentiation into centroblasts and then centrocytes [16].

The last program is named the "latency program" or latency 0. Centrocytes differentiate into resting memory B cells which leave the GC and circulate in peripheral blood without any latency protein expression [17]. Finally, during latency I, cell division of infected memory B cells occurs, the weakly immunogenic EBNA1 is expressed to ensure latent viral genome replication and its persistence within daughter cells [18].

1.1.2. Lytic Cycle

Occasionally, following stimulation, infected memory B cells may be recruited into GC and then either reintegrate the memory cell reservoir or differentiate into plasma cells and reactivate the EBV lytic cycle. In healthy carriers, lytic reactivation is observed only in plasma cells [19]. It is characterized by sequential expression of lytic cycle proteins resulting in production of new infectious viruses and lysis of infected cells [7,13].

Studies of the defective EBV genome helped to identify a transcription factor encoded by the EBV *BZLF1* gene as the key actor in switching from latency to lytic phase [20]. This protein, named ZEBRA, Zta, Z, BZLF1 or EB-1, when expressed in latently infected cells, activates the entire EBV lytic cycle cascade [21]. ZEBRA also activates transcription of the second IE gene *BRLF1* coding for the RTA transcription factor. ZEBRA and RTA function synergistically to activate the early genes involved in metabolism and viral DNA replication and the late genes encoding for EBV structural proteins [4].

Thus, EBV has two tightly regulated latent and lytic phases characterized by specific gene expression patterns. However, there is evidence that both latent and lytic gene expression may be simultaneously present within the same cell. *BZLF1* expression in freshly infected B cells starts as early as 1.5 h post-infection and lasts for several days. In these cells, transcription of the late gene *BLLF1* was not detected suggesting a partial activation of the lytic cycle [22]. This stage, characterized by IE and early gene expression without production of new virions or cell lysis, is commonly referred to as an abortive lytic cycle [23,24] or transient pre-latent abortive lytic cycle when it occurs immediately after infection [25]. Only a minority of EBV-infected B lymphocytes from healthy carriers completes the lytic cycle after stimulation, the vast majority generating an abortive lytic cycle [26]. However, how this abortive lytic cycle takes place in vivo remains unclear.

1.2. EBV-Related Oncogenesis

Despite its asymptomatic persistence in most of the adult population worldwide, in a minority of individuals, EBV is strongly associated with several non-malignant diseases such as infectious mononucleosis, chronic active infection, hemophagocytic lymphohistiocytosis, oral hairy leukoplakia and autoimmune diseases [2,27]. The vast majority of EBV-associated diseases are however represented by cancers occurring both in immunocompetent hosts (Table 1) and in patients with primary or acquired immunodeficiency (Table 2). They are mostly B cell malignancies (BL, HL, PTLD, diffuse large B

cell lymphoma (DLBCL)), nasopharyngeal carcinoma (NPC) or, less frequently, T cell malignancies, gastric, breast and hepatocellular carcinomas, leiomyosarcoma and follicular dendritic sarcoma [1,2,28]. Many mechanisms of EBV related oncogenesis have been proposed and a possible role for different EBV components has been described (reviewed in [7,27,29–32]). Nevertheless, even if great progress has been made in understanding the EBV links to cancers, many aspects of EBV-related oncogenesis are still unknown and represent a major challenge in cancer research.

Table 1. EBV-associated malignancies in immunocompetent hosts and corresponding EBV association frequency and latent gene expression pattern.

Diseases	% EBV Association	Latency Type [a]
B-cells malignancies		
Burkitt Lymphoma		
• *Endemic BL*	>95%	I
• *Sporadic BL*	20–80%	I
Classical Hodgkin Lymphoma	20–90%	II
Diffuse Large B Cells Lymphoma (DLBCL)		
• *EBV+ DLBCL Not Otherwise Specified (NOS)*	100%	III
• Pyothorax associated Lymphoma (PAL)	100%	III
T/NK cells malignancies		
Extranodal NK/T-cell lymphoma, nasal type	>95%	I/II
Virus-associated hemophagocytic syndrome T-cell lymphoma	100%	I/II
Angioimmunoblastic T-cell Lymphoma (AITL) [b]	>80%	I/II
Hepatosplenic T-cell lymphoma		
Non-hepatosplenic γδ T-cell lymphomas		
Enteropathy-type T-cell Lymphoma		
Epithelial malignancies		
Undifferentiated Nasopharyngeal carcinoma	100%	II
Gastric carcinoma	10%	II
Lymphoepithelioma-like carcinoma (salivary gland, tonsils, larynx, thymus, lungs, skin, uterus cervix, bladder, stomach)		
Breast carcinoma		
Hepatocellular carcinoma		
Mesenchymal malignancies		
Follicular dendritic cell sarcoma		

[a] Latency type: Latency I = EBNA1, EBER 1 and 2, BART miRNA; Latency II = EBNA1, LMP1, 2A and 2B, EBER1 and 2, BART miRNA; Latency III = All EBNAs, LMPs, EBERs and BART miRNA. [b] In AITL there is no EBV in tumor cells but EBV is nearly always present in tumor B cells, suggesting an indirect role of EBV [6,33]. Blank spaces indicate the missing data.

Table 2. EBV-associated malignancies in immunodeficient hosts and corresponding EBV association frequency and latent gene expression pattern.

Diseases	% EBV Association	Latency Type [a]
Acquired Immunodeficiency		
AIDS-associated B cell lymphomas		
• *BL*	30–50%	I
• *Hodgkin Lymphoma*	100%	II
• *DLBCL*		
○ Immunoblastic	70–100%	II/III
○ Non Immunoblastic	10–30%	II/III
○ Central Nervous System lymphoma (CNS)	>95%	II/III
○ Primary Effusion Lymphoma (PEL)	70–90%	I
○ Plasmablastic lymphoma	60–75%	I
Post-transplantation lymphoproliferative disorder	>90%	III
Lymphomatoid granulomatosis		
Methotrexate-associated B cell lymphoma		
Leiomyosarcoma		

Table 2. *Cont.*

Diseases	% EBV Association	Latency Type [a]
Congenital immunodeficiency		
Severe combined immunodeficiency–associated B cell lymphoma		
Wiskott-Aldrich syndrome–associated B cell lymphomas		
X-linked lymphoproliferative disorder–associated B cell lymphomas		

[a] Latency type: Latency I = EBNA1, EBER 1 and 2, BART miRNA; Latency II = EBNA1, LMP1, 2A and 2B, EBER1 and 2, BART miRNA; Latency III = All EBNAs, LMPs, EBERs and BART miRNA. Blank spaces indicate the missing data.

EBV genome contains approximately a hundred genes coding for latency and lytic cycle proteins and many small non-coding RNAs expressed to ensure the normal life cycle of the virus. Expression of some proteins and RNAs have been correlated with development of EBV-associated malignancies. The oncogenic properties of each EBV latent protein has been extensively explored (reviewed in [1,2,7]); however the involvement of EBV lytic cycle in oncogenesis is no less important than the contribution of individual proteins. Even though the lytic cycle was long assumed to inhibit tumorigenesis due to final lysis of the infected cells, an increasing amount of data support its contribution to oncogenesis mainly at its initiation or through the abortive lytic cycle and/or autocrine or paracrine effects of EBV IE proteins [27,34,35]. ZEBRA could thus be seen as an important player in EBV-driven oncogenesis, in collaboration with other viral and cellular proteins since it induces the lytic cycle. Additionally, ZEBRA can exit EBV-infected cells either by secretion or after cell lysis and potentially penetrate other cells through its cell penetration domain (CPD) [36]. In EBV-infected cells, ZEBRA alone can switch EBV from latency to lytic cycle; therefore, it may transduce reactivation signals between infected cells. ZEBRA can also reactivate transcriptionally silent host genes due to its affinity to methylated promoters [37] and thus affect key cellular pathways implicated in oncogenesis, control of cell cycle, proliferation and apoptosis.

We will next discuss the structural and biological properties of ZEBRA to provide insights into its potential oncogenic activity and clinical applications.

2. ZEBRA Structure and Functions

2.1. ZEBRA Domain Organisation

ZEBRA is encoded by the EBV *BZLF1* gene, transcribed to a mRNA composed of three exons and translated into a 27 kDa protein containing 245 amino acids (Figure 2A).

ZEBRA belongs to the family of basic leucine zipper (bZIP) transcription factors. Its bZIP domain (residues 175–221) consists of the central basic DNA binding domain (DBD, residues 178–194) and the C-terminal coiled-coil dimerization domain (DD, residues 195–221) [38,39]. ZEBRA homodimer grasps DNA via its two long helices, with the DBD contacting the major groove and DD forming a coiled coil. A185 and S186 of ZEBRA directly interact with methylated cytosines in DNA [37].

Unlike eukaryotic bZIP factors, ZEBRA lacks a classical heptad repeat of the leucine zipper motif [40], but its bZIP domain is additionally stabilized by the C-terminal tail, which makes a turn and runs antiparallel to the coiled coil [39]. Residues 167–177 are considered as the "regulatory domain" and their phosphorylation can modulate ZEBRA activity [38,41].

In the N-terminal transactivation domain (TAD, residues 1–166), the residues 52–64 and 77–86 are rather unstructured and amorphic [42,43] (Figure 2A). The basic region within TAD (residues 157–161) is considered to be important for recognition and high affinity binding to methylated DNA [44].

ZEBRA can exit and enter cells and nuclei due to its CPD situated within the bZIP domain between residues 170 and 220 [36]. This CPD was successfully used to transduce human cells in vitro [36,45]. CPDs are short sequences with a composition that enables them (and the adjacent protein) to penetrate cells either via endocytotic entry followed by endosomal escape, or by directly penetrating the cell

membrane. Their composition is usually either cationic (with a high number of positively charged residues) or amphipathic (with hydrophilic and hydrophobic regions of residues) [46]. ZEBRA CPD is rich in positively charged residues (seven lysines and seven arginines), mostly within DBD (basic region) (Figure S1A in blue), whereas hydrophobic amino acids (one valine, five alanines, seven leucines) of CPD are mostly within DD (leucine zipper) (Figure S1B in red) [36]. In another protein possessing the CPD, human immunodeficiency virus (HIV)-1 Tat, the CPD region is also multifunctional [47]. Presumably, the cationic part serves for interaction with the negatively charged phosphate groups of membrane phospholipids as well as on DNA, while hydrophobic residues interact with the hydrophobic part of the phospholipid membrane and participate in ZEBRA's dimerization (Figure S1C).

When entering cells, ZEBRA is targeted to the nucleus and has a pan-nuclear localization, with the exception of the nucleolus [48]. Substitution of several amino acids within DBD can alter subnuclear localization from pan-nuclear to focal [49]. The bipartite nuclear localization sequence of ZEBRA is located within DBD (residues 178-194), but a small region within TAD (residues 157-162) is also important for the nuclear import [50].

To summarize, ZEBRA structure accounts for its important functions because the chromatin-binding capacity via its DBD and DD and its ability to act as a transcriptional activator thanks to its TAD allows it to regulate expression of both viral and host genes [36,51]. ZEBRA also possesses a CPD that allows it to penetrate into uninfected cells [36].

2.2. Posttranslational Modifications of ZEBRA

ZEBRA is prone to posttranslational modifications. It is constitutively phosphorylated in vivo at multiple sites mostly clustered within TAD and the regulatory domain [52]. Phosphorylation of S173 and to a lesser extent S167 within the regulatory domain is important for DNA binding [41,53]. Constitutive phosphorylation may also explain why ZEBRA's apparent mass on gel electrophoresis is 35 kDa [40] instead of the predicted 27 kDa [54].

ZEBRA also has a sustained N-terminal M1 acetylation [55]. K12 of ZEBRA is a substrate of partial and reversible SUMOylation [56,57] that affects neither protein stability nor its subcellular localization but significantly decreases ZEBRA transactivation activity by inhibiting its binding to CBP (CREB-binding protein) (see below) [57,58]. SUMOylation is diminished in DD-deficient ZEBRA [57]; EBV-encoded protein kinase also reduces ZEBRA's SUMOylation, and this effect is not related to S209 phosphorylation, conventional site of ZEBRA modification by this kinase [59].

Thus, ZEBRA is extensively and mostly constitutively modified after translation, presumably by certain viral and host enzymes. The regulation of posttranslational modifications, their role and possible regulatory potential for ZEBRA activity and the EBV status remain to be elucidated.

2.3. ZEBRA Functioning in Host Cells

ZEBRA functions in host cells rely on its capacity to bind specific DNA motifs and interact with other proteins. DBD of ZEBRA binds to heptamer DNA motifs, named ZEBRA response elements (ZREs). ZREs are present within both viral and host gene promoters. At present, two types of ZREs are identified: an activator protein 1 (AP-1)-like recognition elements (non-CpG-containing) [40] and CpG-containing recognition elements [60] (Figure 2B). Binding to CpG-ZREs depends on DNA methylation [60,61]. During latency, EBV genome becomes heavily methylated to suppress its transcription, however, ZEBRA binds methylated promoters with high affinity and activates gene transcription to initiate lytic cascade [44]. ZEBRA's selectivity and preference for methylated DNA is a key to hijacking host epigenetic silencing, which is important for EBV latency reversal, oncogenesis, control of cell cycle, proliferation and apoptosis [37]. Ten-eleven translocation methylcytosine dioxygenase that reduces ZEBRA binding to methylated promoters [37] can be considered as ZEBRA host restriction factor.

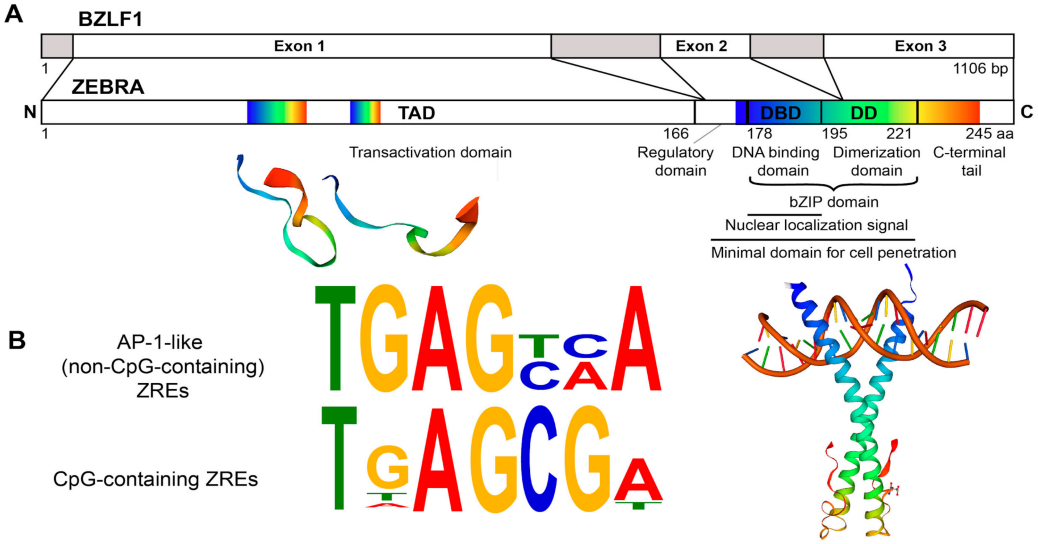

Figure 2. Structure of the ZEBRA protein. (**A**) ZEBRA structure. ZEBRA is encoded by the *BZLF1* gene containing three exons. ZEBRA protein has an N-terminal transactivation domain (TAD, residues 1-166), a regulatory domain (residues 167–177), a bZIP domain, which consists of a central basic DNA binding domain (DBD, residues 178-194) and a C-terminal coiled-coil dimerization domain (DD, residues 195–221). The minimal domain for cell penetration is located between residues 170-220. Three available partial 3D structures were imported from the SWISS-MODEL Repository [62] (accession number P03206) and are based on crystal structure data published by [39,42,43]. They are shown below the respective primary sequence. Rainbow color code is used to map approximate residue position concordance between primary and tertiary (or quaternary) structure. (**B**) ZEBRA-response elements (ZREs). Sequences of ZEBRA DNA binding sites (ZREs) of two types: AP-1-like (non-CpG-containing) ZREs and CpG-containing ZREs are depicted as sequence logos, adapted from [51,60].

2.3.1. Transcriptional Regulation

ZEBRA can both activate and downregulate transcription of viral and host genes. Transcriptomic analysis of B cells with ectopic expression of ZEBRA revealed 2263 deregulated genes (74% upregulated, 26% downregulated) [49]. Upregulated genes include those involved in cell adhesion, morphogenesis, projection and response to hormones, while downregulated genes are involved in the immune response, induction of apoptosis and lymphocyte activation [49]. In total, 12% of these genes (207 upregulated and 71 downregulated) are directly regulated by ZEBRA which binds to their promoters, as identified by chromatin immunoprecipitation followed by sequencing (ChIP-seq).

During activation of lytic cycle, ZEBRA binds promoters of early lytic viral genes and host genes and, via its TAD, interacts with basal transcription factors IID [63] and IIA [64] (TFIID and TFIIA); this leads to sequential recruitment of other basal transcription factors and RNA polymerase II (Figure 3A). In addition, ZEBRA binds the transcriptional coactivator and histone acetyltransferase CBP (CREB binding protein) which increases ZEBRA transactivation properties [65]. Direct binding to the Transducer of Regulated CREB coactivator enhances ZEBRA-mediated transcription [66].

Transcriptional repression by ZEBRA is related to its specific binding to cellular transcription factors mainly via its bZIP or TAD. In most cases, such interaction mutually impedes their function as transcription factors and results in repression of target genes for both ZEBRA and the associated transcription factors [67,68].

Direct binding to p53 [69,70], p65 [71] and c/EBP family of transcription factors [68] inhibits their transcriptional activity. ZEBRA directly binds B cell specific transcription factors Pax5 and Oct2 via bZIP domain; this inhibits ZEBRA activity, however, the reciprocal inhibition was proven only for Pax5 [72,73]. Unidirectional inactivation of the family of nuclear factor of activated T cells (NFAT) transcription factors, involved in calcium signal transduction, by direct interaction with ZEBRA was

also reported [74]. Presumably, the same mechanism related to ZEBRA inhibitory binding to host transcriptional factor is involved in the class II transactivator (CIITA) repression, however, it involves the TAD and a transcriptional factor inhibited by ZEBRA was not identified [67]. ZEBRA also binds to interferon regulatory factor 7 (IRF-7) through its TAD, decreasing the transcription of interferon (*IFN*) *α4*, *IFNβ*, and antigen presentation 2 (*Tap-2*) [75]. Finally, SUMOylation of ZEBRA appears to be important for transcriptional repression since it promotes recruitment of histone deacetylases to responsive promoters [57] (Figure 3B).

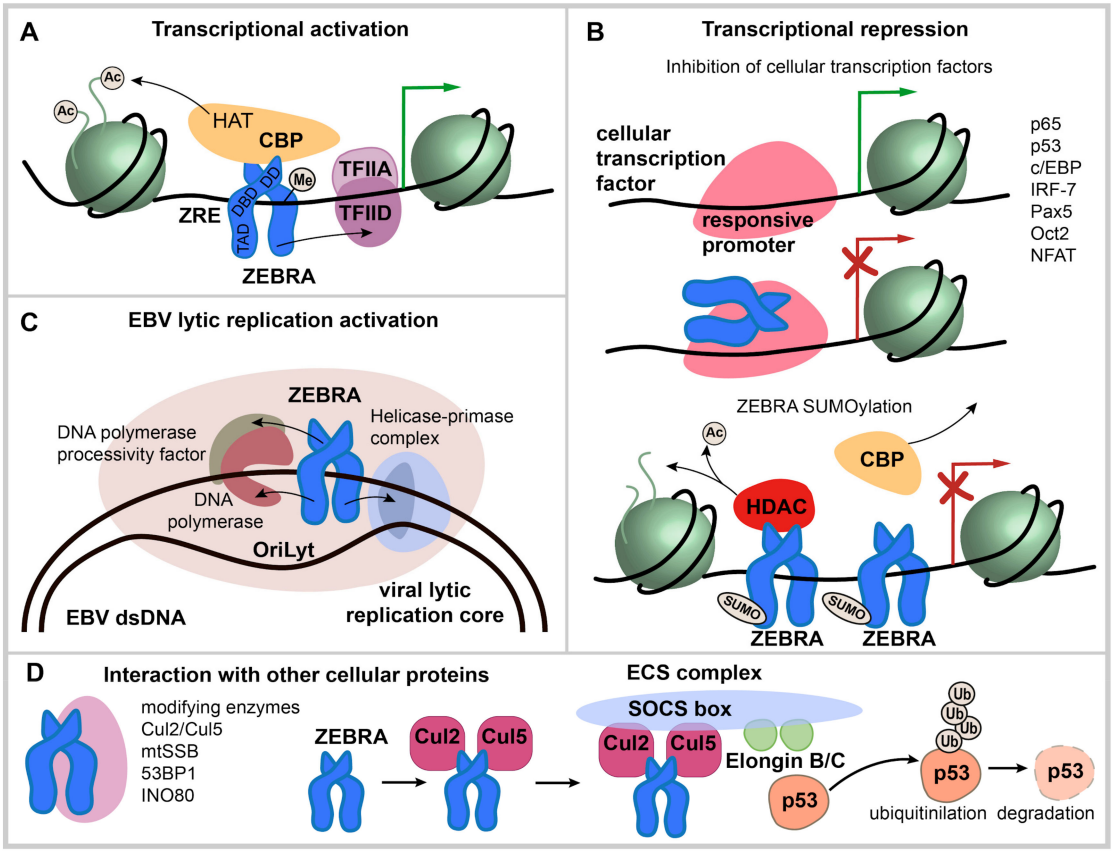

Figure 3. ZEBRA functions. (**A**) transcriptional activation by ZEBRA. ZEBRA is shown as a homodimer, relative positions of transactivation domain (TAD), DNA binding domain (DBD) and dimerization domain (DD) are indicated. ZEBRA binds to specific ZEBRA response elements (ZREs) within promoters of viral and host genes with a preference to methylated-CpG DNA. ZEBRA binding leads to sequential recruitment of basal transcription factors and RNA polymerase II. In addition, ZEBRA binds transcriptional coactivator CREB binding protein (CBP). (**B**) transcriptional repression via ZEBRA binding to cellular transcription factors and by SUMOylated ZEBRA. Transcription factors that interact directly with ZEBRA are listed. The interaction occurs mainly via ZEBRA's bZIP domain and mutually impedes the function of both ZEBRA and bound transcription factor and results in repression of targeted genes. SUMOylated ZEBRA has a low transactivation activity related to decreased CBP binding and the ability to recruit histone deacetylases (HDAC) to responsive promoters. (**C**) activation of EBV lytic replication. ZEBRA recognizes the EBV lytic origin (oriLyt), serves as the origin binding protein and recruits viral core replication enzymes to initiate lytic replication of EBV. (**D**) interaction with cellular proteins not directly involved in transcriptional regulation. ZEBRA interaction partners are listed. ZEBRA interaction with Cul2/Cul5 induces the formation of multimolecular ECS complex (Elongin B/C-Cul2/5-SOCS-box protein) with the ubiquitin ligase activity that targets p53 for proteasomal degradation.

2.3.2. Binding to the Replication Origin in EBV Lytic Replication

During the lytic cycle, ZEBRA binds EBV lytic origin (oriLyt) and recruits viral core replication enzymes to initiate replication [76,77] (Figure 3C). In contrast to latent replication, EBV lytic replication relies on virally encoded replication enzymes, whose expression is induced during the lytic cycle: helicase (*BBLF4*), primase (*BSLF1*), primase-associated factor (*BBLF2/3*), DNA polymerase (*BALF5*), DNA polymerase processivity factor (*BMRF1*), and single-stranded DNA binding protein (*BALF2*) [41]. This function is mediated by the TAD (residues 11–25), which interacts with the viral helicase, primase and DNA polymerase [78,79]; and by the bZIP domain which interacts with the DNA polymerase processivity factor [41]. S173 phosphorylation within the regulatory domain is essential for ZEBRA action as a replication factor [41].

2.3.3. Interaction with Other Cellular Proteins

ZEBRA also interacts with proteins other than transcription factors (Figure 3D). For example, ZEBRA interaction with Cul2 and Cul5 induces the formation of the multimolecular ECS complex (Elongin B/C-Cul2/5-SOCS-box protein) that ubiquitinates p53 for proteasomal degradation [80].

Other ZEBRA cellular partners include mitochondrial single-stranded DNA binding protein (mtSSB) [81], nuclear protein 53BP1, a component of the ATM DNA damage response pathway [82], INO80 chromatin remodeler ATPase [83]; these interactions are important for EBV lytic cycle reactivation and replication.

In summary, ZEBRA binds specific DNA motifs and/or interacts with other proteins, either recruiting them to DNA binding sites or altering their activity. However, ZEBRA direct interactions with many other cellular proteins [74] are much less studied as compared to interaction with chromatin-binding proteins.

3. EBV-Related Diseases and Oncogenic Properties of ZEBRA

3.1. ZEBRA Implication in EBV-Related Malignancies

Increasing evidence supports that *BZLF1* gene expression could contribute, directly or indirectly, to EBV-induced tumorigenesis. ZEBRA protein and mRNA were detected in more than 80% of biopsies from 44 PTLD patients [84]. Lymphoblastoid cell lines (LCLs) derived with wild-type (WT) EBV are more prone to induce a lymphoproliferative disorder when injected into Severe Combined Immunodeficient (SCID) mice than LCLs derived with *BZLF1*-KO EBV [85]. Interestingly, the same results were observed after acyclovir treatment, which inhibits viral DNA replication but not *BZLF1* expression. These data suggest that ZEBRA, and not the production of infectious viral particles, is required for tumor formation in SCID mice [85]. These results were also confirmed in a humanized mouse model where both human fetal CD34+ hematopoietic stem cells and human thymus/liver tissues were transplanted. Indeed, in this model, the development of CD20+ DLBCL was more frequent in mice infected with WT EBV as compared to *BZLF1*-KO EBV [86]. Soluble ZEBRA can be detected in the serum of PTLD patients at concentrations up to 4 µg/mL and it is significantly higher in PTLD patients compared to transplanted patients without PTLD [87]. ZEBRA is also present in serum samples from immunocompromised humanized mice developing lymphoma, with a correlation with tumor mass [35]. The presence of ZEBRA protein or its mRNA was also reported in tumor cells or in tumor tissue biopsies in other types of EBV-induced lymphomas, such as HL, DLBCL and BL [88–91].

In some EBV-associated lymphoma, there is also evidence for indirect action of ZEBRA. *BHRF1* and *BALF1*, two EBV early lytic genes whose expression is induced by ZEBRA, are found highly expressed in DLBCL [89]. The products of these two genes are the viral Bcl-2 homologs required for B cells immortalization [92]. Moreover, EBV cofactors for endemic BL (*Plasmodium falciparum*, *Euphorbia tirucalli* and potentially Aflatoxin B1) are all able to reactivate EBV in vitro and in vivo [93–95].

High ZEBRA expression at mRNA or protein level was also reported in NPC biopsies [96,97] and in breast carcinoma [98]. High anti-ZEBRA IgG titers in sera correlate with poorer clinical outcome in

patients [99,100]. The presence of anti-ZEBRA antibody has a high diagnostic accuracy for early-stage NPC [101]. More generally, EBV replication and expression of some early lytic cycle genes were detected in EBV-induced epithelial malignancies including NPC [102,103]. In addition, EBV-infected individuals with elevated titers of IgA antibodies against EBV lytic viral capsid antigen (VCA) have a higher risk of NPC [104]. A subset of EBV-associated gastric carcinoma and some NPC cells also express early lytic genes such as *BHRF1*, *BALF1*, *BARF1* and *BGLF5* [105–108]. A specific EBV strain isolated from NPC and gastric carcinoma has an enhanced capacity for spontaneous lytic replication and therefore ZEBRA expression [109,110].

3.2. ZEBRA Oncogenic Properties

In this section, we will discuss the mechanism by which ZEBRA contributes to acquisition of cancer hallmarks by cells (Figure 4).

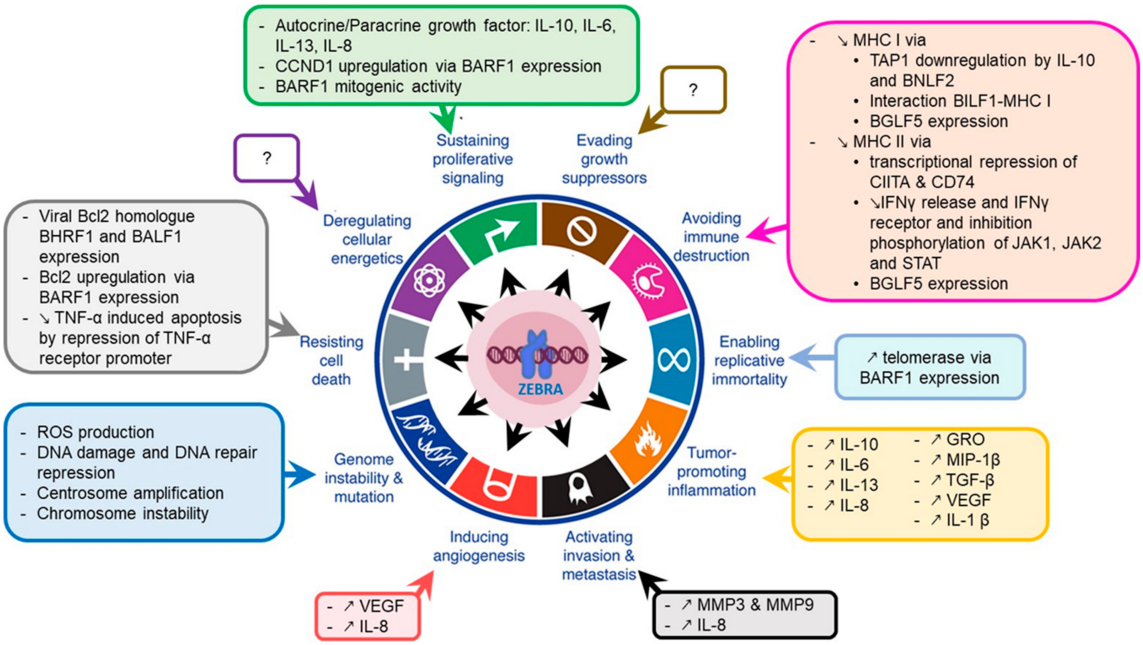

Figure 4. ZEBRA oncogenic properties. ZEBRA directly, or through its target genes, contributes to the acquisition of cancer hallmarks by cells including sustained proliferative signaling, evading or altering the immune response, resisting cell death, enabling replicative immortality, inducing angiogenesis and activating tumor invasion and metastasis. A part of these effects is mediated by genome instability and tumor-promoting inflammation that induce an environment favorable to cancer development and progression. Adapted from [111].

3.2.1. Genome Instability

Genome instability (GI), one of the major factors of oncogenic transformation, may result in random mutations and chromosomal rearrangements which can confer selective advantage to certain cells through oncogene activation, downregulation or loss of tumor suppressor genes [111]. GI can occur through different mechanisms: (1) DNA damage production with incapacity to detect damaged DNA; (2) DNA damage with defects in DNA repair; (3) defects in preventing the action of potential mutagens [112–114].

Although ZEBRA can interact with proteins implicated in DNA damage response (e.g., 53BP1, a component of the ATM pathway) [82], not much data exist in support of a direct relationship between GI and ZEBRA. However, some events such as oxidative stress that lead to GI occur following EBV reactivation and can thus be related to ZEBRA expression [115,116]. Oxidative stress was also described in purified B cells and epithelial cells at an early stage of EBV infection when ZEBRA is expressed [117].

Furthermore, several early lytic proteins induced by ZEBRA may participate in GI. For example, BMRF1 induces centrosome amplification and chromosome instability in B cells in vitro and in vivo in a mouse model [118]. BGLF4 directly or indirectly induces DNA damage by retarding cellular S-phase progression or inducing premature chromosome condensation associated with a high risk of chromosomal breaks at common fragile sites [119–121]. EBV DNase was also found to induce GI in human epithelial cells through DNA damage induction and DNA repair repression [122]. BALF3 has also been linked to DNA strand breaks induction, resulting in copy number aberrations accumulation in NPC cells [123]. Recurrent chemical reactivation of EBV in NPC cells appears to induce GI [124]. EBV reactivation in LCLs induces global nuclear architecture remodeling that could enhance formation of chromosomal translocations [125].

3.2.2. Tumor-Promoting Inflammation

Inflammation favors tumor development and progression. This could be related to high levels of cytokines, chemokines and growth factors observed upon EBV reactivation, including interleukin (IL)-8, IL-10, IL-6, IL-13, Transforming Growth Factor-beta (TGF-β) [25]. ZEBRA can also directly transactivate *IL-8* promoter through its two ZREs, resulting in *IL-8* upregulation in NPC cells [126]. ZEBRA expression in NPC is also associated with upregulation of growth related oncogene and macrophage inflammatory protein-1β [126].

ZEBRA can also bind directly to the human IL-10 (*hIL-10*) minimal promoter to induce transcription of *hIL-10* during the early phase of the lytic cycle in EBV-infected B cells [127]. IL-10 is upregulated in breast cancer and NPC [127–129]. A viral analog of the hIL-10 (vIL-10) encoded by the *BCRF1* gene can be produced during the lytic cycle [130].

Other interleukin genes contain ZREs in their promoters [25] and IL-6 and IL-13 production can be directly activated by ZEBRA in infected cells [131–133]. ZEBRA also increases expression of the genes coding for *TGF-β* [134] and the Vascular Endothelial Growth Factor (*VEGF*) [135] in B cells undergoing lytic cycle. Finally, ZEBRA can also induce inflammatory cytokines through expression of the early lytic gene *BLLF3,* which can activate NF-κB and induce secretion of pro-inflammatory cytokines (tumor necrosis factor (TNF)-α, IL-1β, IL-6, IL-8 and IL-10) in human monocyte-derived macrophages [136,137].

3.2.3. Immune Evasion

ZEBRA-induced viral and human IL-10 production protects infected cells from immune recognition and elimination. Indeed, IL-10 interferes with antiviral cytokines and NK/NKT cell-mediated lysis [130]. Moreover, IL-10 downregulates transporter proteins associated with TAP1 and consequently induces a reduction of surface MHC I molecules on infected B lymphocytes [138]. IL-10 also inhibits IFNγ release which plays a central role in resistance of the host to infection [139].

ZEBRA also promotes immune evasion by disrupting cell signaling pathways activated by IFNγ such as the JAK-STAT pathway. It decreases IFNγ receptor expression and inhibits phosphorylation of Jak1, Jak2 and STAT1 molecules consequently downregulating their downstream target genes, including *MHC II* [140]. ZEBRA can also directly thwart surface expression of MHC II molecules by transcriptional repression of *CIITA*, a main regulator of human leukocyte antigen (HLA) class II genes [141] and *CD74*, the invariant chain of MHC II that facilitates its transport to the cell surface [142].

The immunomodulatory effects can be induced by three EBV lytic cycle proteins called immunoevasins (*BILF1*, *BNLF2a* and *BGLF5*). They interfere with host antigen processing pathways and consequently allow EBV-infected cells to escape from immune system action. BILF1 reduces MHC I molecules on the cell surface by physical interaction and inhibits CD8+ T cell recognition of endogenous target antigens [143,144]. BNLF2, a TAP inhibitor, impairs peptide loading onto HLA class I molecules thus blocking antigen presentation to cytotoxic T cells [130,145]. BGLF5, the EBV alkaline exonuclease, downregulates HLA class I and II impairing antigen recognition by immune cells [146].

It is noteworthy that the described immunomodulatory effects induced by ZEBRA are associated not only with cancer progression but also with development of autoimmune diseases, e.g., systemic lupus erythematosus [147].

3.2.4. Cell Proliferation and Growth

ZEBRA-induced IL-10 enhances the viability of resting B lymphocytes and supports growth and differentiation of EBV-infected cells [127,139]. Both IL-6 and IL-13 promote proliferation of EBV-infected cells and long term growth of LCLs [131,133]. In agreement with this, growth of both LCLs and EBV-induced B cells after primary infection can be inhibited by treatment with an anti-IL-13 antibody [133]. Treatment with an anti-IL-6 antibody led to remission of B-lymphoproliferative disorder in eight out of 12 patients studied [148].

ZEBRA-induced IL-8 may be used by some tumor cells as an autocrine growth factor [149]. The early lytic gene *BARF1* also possesses an autocrine mitogenic activity and is an in vivo growth factor [150]. *BARF1* is associated with Cyclin D1 overexpression in EBV-associated gastric cancer [151].

3.2.5. Resistance to Cell Death

The most common anti-apoptotic effect following ZEBRA expression is through activation of the two viral Bcl-2 homologs *BHRF1* and *BALF1*. Another EBV early lytic gene, *BARF1*, can activate the cellular anti-apoptotic protein Bcl-2 in fibroblasts [152]. *BARF1* expression leads to an increased Bcl-2 and Bax ratio and decreased PARP cleavage in gastric carcinoma cells [153].

BZLF1-KO LCLs showed a significant increase in the percentage of dead cells, reversible after *BZLF1* expression, whereas no difference was observed between *BRLF1*-KO and WT LCLs, thus suggesting a direct ZEBRA-mediated anti-apoptotic effect [85]. ZEBRA also downregulates the expression of tumor necrosis factor receptor 1 (TNFR1) by direct binding to its promoter [68,154]. This prevents TNF-α activation and consequently TNF-α induced apoptosis.

3.2.6. Other Oncogenic Effects

ZEBRA can positively affect tumor progression by inducing the expression of *VEGF* and *IL-8*, both associated with angiogenesis, tumor development, metastasis and resistance to chemotherapy [135,155,156]. Moreover, expression of ZEBRA by tumor cells from NPC patients correlates with advanced lymph node metastasis, and this effect has been related to direct transactivation of the Matrix Metalloproteinase (*MMP9*) promoter by ZEBRA [157]. In addition to *MMP9*, ZEBRA can also induce *MMP3* upregulation in epithelial cells by binding to the ZRE in the *MMP3* promoter. Both MMP3 and MMP9 act in synergy to promote tumor invasion and metastasis [158]. The oncogenic early lytic gene *BARF1* enables replicative immortality through induced activation of telomerase in primary epithelial cells [159].

ZEBRA, through its bZIP domain, can also directly interact with cancer-associated transcription factors: p53, RAR, CBP, and C/EBPα [160–163]. These interactions have a functional importance for EBV life cycle, but a direct demonstration for their role in human disease is still lacking even if these ZEBRA targets are often deregulated in cancers [164,165].

Interestingly, ZEBRA has a functional homology with another viral protein: the HIV-1 transactivator protein Tat. Like ZEBRA, Tat can be secreted into the bloodstream by HIV-1 infected T cells and, through its cell penetration domain, can enter uninfected cells, including B cells. Tat protein is potentially oncogenic in B cells since it induces a relocation in the nuclear space of the *MYC* locus close to the *IGH* gene in circulating B-cells [166] and an overexpression of the *AICDA* gene coding for the Activation-induced Deaminase (AID) [167]. These two events promote formation of BL-specific translocations and could at least partly account for the high frequency of BL in HIV-infected patients. Tat also promotes mitochondrial production of reactive oxygen species (ROS) and thus DNA damage and genome instability in B cells [168]. Interestingly, ZEBRA and Tat can be present in a cell at the same time in the blood of HIV-infected individuals and possibly interact. This hypothetical interaction could have an antagonistic or synergistic effect on their oncogenic activity.

4. ZEBRA in Diagnosis and Therapy

Many articles report the presence of EBV lytic cycle in tumor cells from HL [169], NPC [99,170–174], in transplant patients [175], and in breast tumors [98]. Clinical studies on EBV lytic proteins including ZEBRA in patients with PTLD or HIV-associated non-Hodgkin lymphoma NHL are mostly related to the role of these proteins in neoplastic tissues [84,89,176,177]. Both high EBV copy number and strong *BZLF1* mRNA expression in the peripheral blood lymphocytes (PBL) of patients are sensitive markers of EBV-related PTLD [178]. ZEBRA was expressed in 5% of whole peripheral blood mononuclear cells from a patient with a lymphoproliferative disease who underwent non-myeloablative allogeneic stem cell transplantation [179]. Moreover, the number of EBV-infected cells in the peripheral blood increases after immunosuppression: on average, 1.6 latently-infected cells per 10^4 B lymphocytes [180] vs. 12.5 per 10^6 B cells in persistently infected healthy individuals [181].

Soluble ZEBRA concentrations of >100 ng/mL detected by an enzyme-linked immunosorbent assay (ELISA) in serum of patients after solid organ or hematopoietic stem cell transplant were predictive of PTLD in 80% of the cases within three weeks [87]. Interestingly, the circulating ZEBRA could be detected during periods in which the viral DNA was not detectable by qPCR. For example, in two patients, ZEBRA was detected at 2 and 6 weeks, respectively, prior to the PTLD episode and before an increase in qPCR signals. Thus, ZEBRA testing in serum could help identify patients likely to develop severe outcomes during the critical posttransplant period and serve as a potential diagnostic marker for EBV follow-up in immunocompromised patients.

The relevance of EBV lytic cycle to human pathology prompted researchers to target certain lytic proteins with therapeutic aims. Adenovirus vectors expressing BZLF1 or BRLF1 were used to treat EBV-positive tumors [182]. On the other hand, Food and Drug Administration (FDA)-approved leflunomide, which targets EBV replication, was shown to inhibit the earliest step of lytic EBV reactivation (*BZLF1* and *BMRF1* expression) and prevented the development of EBV-induced lymphomas in both a humanized mouse model and a xenograft model [183]. More recently, duvelisib (a molecule inhibiting the PI3K/AKT signaling pathway, and B cell receptor (BCR) signaling) was shown to reduce cell growth and expression of EBV lytic genes *BZLF1* and *gp350/220* in EBV-positive cell lines [184]. The histone deacetylase (HDAC) and DNA methyltransferase inhibitors are also possible avenues to suppress the ZEBRA expression and the entire lytic cascade [185].

Immunotherapeutic approaches, such as vaccination against IE proteins or IE-specific therapeutic monoclonal antibodies also represent a promising approach. A recent study demonstrated that vaccination of hu-PBL-SCID mice against ZEBRA could enhance specific cellular immunity and significantly delay the development of the lethal EBV-related lymphoproliferative disease [186].

5. Conclusions and Remaining Questions

The role of ZEBRA in EBV infection, lytic cycle and oncogenesis has been extensively studied, but numerous questions remain:

Abortive lytic cycle: ZEBRA can affect host cells by inducing the abortive lytic cycle in B cells (production of early EBV lytic proteins without cell lysis); however the fate of these cells remains unclear: they may reintegrate the memory cell reservoir after the abortive lytic cycle, return to latency 0 profile or restart the latency cycle as for the primary infection (Figure 1). Another remaining question is whether some stimuli are more prone than others to specifically induce the abortive lytic cycle. *In vitro*, EBV reactivation stimuli such as stress inducing agents, ROS, anticancer drugs or hypoxia [14,187] directly reactivate the virus in EBV-positive cell lines. Thus, in vivo, the abortive lytic cycle may occur after stimulation by these stress-induced agents, instead of an immunological stimulation which mainly leads to a productive lytic cycle in plasma cells.

A role of ZEBRA in oncogenesis: ZEBRA upregulates the transcription of host cell genes coding for cytokines involved in inflammation, angiogenesis, metastasis and cell proliferation. ZEBRA downregulates the expression of MHC II class genes thus promoting the immune evasion and genes related to apoptosis thus inducing cell death resistance. ZEBRA also interacts with cancer-related

cellular proteins altering their activity. The net cellular effect of these interactions is quite complex and depends on protein localization, concentration, nuclear architecture, nature of promoters involved. Indeed, for p53 signaling pathway, both inhibitory and stimulatory effects of ZEBRA have been described [69,164,165]. This activity of ZEBRA needs additional studies.

A role of ZEBRA in non-infected cells: ZEBRA is released into the bloodstream by infected cells and, due to its CPD, can potentially penetrate into uninfected cells and alter their transcriptional program either directly or via interaction with cellular proteins. These potentially oncogenic effects of ZEBRA in non-infected cells are worth investigating and could link EBV to other as yet unidentified pathologies, independently of EBV presence in cells, thus potentially expanding the spectrum of EBV-associated diseases.

ZEBRA interaction with other proteins: the cellular interactome of ZEBRA needs further investigation to explain the functional significance of ZEBRA interaction network [74]. ZEBRA is extensively modified in vivo [52], however, the enzymes (viral and cellular) and signaling pathways involved in its post-translational modifications are largely unknown, as well as the effect of these modifications on ZEBRA activity. A splicing variant of ZEBRA was also described but its functional role is poorly understood [188]. Some EBV strains as well as sequence variations in the *BZLF1* gene may have an enhanced ability to reactivate the lytic cycle [109,110,189]. A better characterization of the variations in the structure of the ZEBRA protein produced by these different virus strains could be relevant.

The relevance of the lytic cycle and the role of ZEBRA in lymphomagenesis is a new paradigm pertaining to the prevention and treatment strategies for EBV-associated cancers. It is therefore important to investigate the lytic EBV infection in immunocompromised patients, such as organ transplant recipients, who are highly prone to developing EBV-associated malignancies. More efforts should be invested to examine the potential of drugs that target EBV lytic proteins, including ZEBRA.

ZEBRA as a biomarker (mRNA, anti-ZEBRA IgG and soluble ZEBRA concentration in blood) has mainly been studied in PTLD. It would be important to test whether circulating ZEBRA could serve as a biomarker for other EBV-associated diseases, especially those with the lytic cycle involvement, e.g., endemic BL.

A better understanding of the mechanisms underlying ZEBRA activity in cells will shed light on its role in oncogenesis and open perspectives in early diagnosis and treatment of EBV-related cancers.

Supplementary Materials: The following are available online at http://www.mdpi.com/2072-6694/12/6/1479/s1, Figure S1: ZEBRA cell penetration domain.

Funding: The work in the laboratory was supported by INCa, ANRS, INSERM (ENVIBURKITT), the Presidium of RAS and the state program of fundamental scientific research of IDB RAS.

Conflicts of Interest: The authors declare no conflict of interest.

Abbreviations

AID	activation-induced deaminase
AIDS	acute immunodeficiency syndrome
AITL	angioimmunoblastic T cell lymphoma
AP-1	activator protein 1
ATM	ataxia telangiectasia mutated
BALF	BamHI-A fragment leftward open reading frame
BARF	BamHI-A fragment rightward open reading frame
BART	BamHI-A fragment rightward transcript
BGLF	BamHI-G fragment leftward open reading frame
BHRF	BamHI-H fragment rightward open reading frame
BILF	BamHI-I fragment leftward open reading frame
BL	Burkitt's lymphoma
BLLF	BamHI-L fragment leftward open reading frame

BMRF	BamHI-M fragment rightward open reading frame
BNLF	BamHI-N fragment leftward open reading frame
bZIP	basic leucine zipper
BRLF	BamHI-R fragment leftward open reading frame
BZLF	BamH1-Z fragment leftward open reading frame
CNS	central nervous system
CPB	CREB binding protein
CPD	cell penetration domain
CR	complement receptors
DBD	DNA binding domain of ZEBRA
DD	dimerization domain of ZEBRA
DLBCL	diffuse large B cell lymphoma
EBER	EBV-encoded small RNA
eBL	endemic Burkitt's lymphoma
EBNA	EBV nuclear antigen
EBV	Epstein-Barr Virus
ECS	Elongin B/C-Cul2/5-SOCS-box protein
GC	germinal center
GI	genome instability
HDAC	histone deacetylases
hIL	human interleukin
HIV	human immunodeficiency virus
HL	Hodgkin lymphoma
HLA	human leukocyte antigen
IARC	international agency for research on cancer
IE	immediate early
IFN	interferon
IGH	immunoglobulin heavy chain
IL	interleukin
LCL	lymphoblastoid cell lines
LMP	latent membrane protein
MHC	major histocompatibility complex
MMP	matrix metalloproteinase
MYC	myelocytoma
NF-κB	nuclear factor kappa B
NFAT	nuclear factor activated T cells
NHL	non-hodgkin lymphoma
NK	natural killers
NLS	nuclear localization sequence
NOS	DLBCL not otherwise specified
NPC	nasopharyngeal carcinoma
PAL	pyothorax associated lymphoma
PBL	peripheral blood lymphocytes
PEL	primary effusion lymphoma
PTLD	post-transplant lymphoproliferative disorders
ROS	reactive oxygen species
SCID	severe combined immunodeficiency
SUMO-1	small ubiquitin-related modifier 1
TAD	transactivation domain of ZEBRA
TAP	transporter associated with antigen processing
TGF-β	tumor growth factor β
TNF	tumor necrosis factor
TNFR	tumor necrosis factor receptor

VEGF	vascular endothelial growth factor
vIL	viral interleukin
WT	wild type
ZRE	ZEBRA response elements

References

1. Dolcetti, R.; Dal Col, J.; Martorelli, D.; Carbone, A.; Klein, E. Interplay among viral antigens, cellular pathways and tumor microenvironment in the pathogenesis of EBV-driven lymphomas. *Semin. Cancer Biol.* **2013**, *23*, 441–456. [CrossRef] [PubMed]
2. Kutok, J.L.; Wang, F. Spectrum of Epstein-Barr Virus–Associated Diseases. *Annu. Rev. Pathol. Mech. Dis.* **2006**, *1*, 375–404. [CrossRef]
3. Cohen, J.I. Epstein-Barr virus infection. *N. Engl. J. Med.* **2000**, *343*, 481–492. [CrossRef] [PubMed]
4. Tsurumi, T.; Fujita, M.; Kudoh, A. Latent and lytic Epstein-Barr virus replication strategies. *Rev. Med. Virol.* **2005**, *15*, 3–15. [CrossRef] [PubMed]
5. IARC. Proceedings of the IARC Working Group on the Evaluation of Carcinogenic Risks to Humans. Epstein-Barr Virus and Kaposi's Sarcoma Herpesvirus/Human Herpesvirus 8. Lyon, France, 17-24 June 1997. *IARC Monogr. Eval. Carcinog. Risks Hum.* **1997**, *70*, 1–492.
6. International Agency for Research on Cancer; Weltgesundheitsorganisation (Eds.) *IARC Monographs on the Evaluation of Carcinogenic Risks to Humans, Volume 100 B, Biological Agents: This Publication Represents The Views And Expert Opinions of an IARC Working Group on the Evaluation of Carcinogenic Risks to Humans, Which Met in Lyon, 24 February–03 March 2009*; IARC: Lyon, France, 2012; ISBN 978-92-832-1319-2.
7. Saha, A.; Robertson, E.S. Mechanisms of B-Cell Oncogenesis Induced by Epstein-Barr Virus. *J. Virol.* **2019**, *93*. [CrossRef]
8. Hutt-Fletcher, L.M. The Long and Complicated Relationship between Epstein-Barr Virus and Epithelial Cells. *J. Virol.* **2017**, *91*. [CrossRef]
9. Zhang, H.; Li, Y.; Wang, H.-B.; Zhang, A.; Chen, M.-L.; Fang, Z.-X.; Dong, X.-D.; Li, S.-B.; Du, Y.; Xiong, D.; et al. Author Correction: Ephrin receptor A2 is an epithelial cell receptor for Epstein-Barr virus entry. *Nat. Microbiol.* **2018**, *3*, 1075. [CrossRef]
10. Hutt-Fletcher, L.M. Epstein-Barr Virus Entry. *J. Virol.* **2007**, *81*, 7825–7832. [CrossRef]
11. Haan, K.M.; Kwok, W.W.; Longnecker, R.; Speck, P. Epstein-Barr Virus Entry Utilizing HLA-DP or HLA-DQ as a Coreceptor. *J. Virol.* **2000**, *74*, 2451–2454. [CrossRef]
12. Nijland, M.; Kersten, M.J.; Pals, S.; Bemelman, F.; ten Berge, I. Epstein-Barr Virus–Positive Posttransplant Lymphoproliferative Disease After Solid Organ Transplantation: Pathogenesis, Clinical Manifestations, Diagnosis, and Management. *Transplant. Direct* **2016**, *2*, e48. [CrossRef]
13. Thorley-Lawson, D.A.; Gross, A. Persistence of the Epstein-Barr virus and the origins of associated lymphomas. *N. Engl. J. Med.* **2004**, *350*, 1328–1337. [CrossRef]
14. Thorley-Lawson, D.A. EBV Persistence–Introducing the Virus. *Curr. Top. Microbiol. Immunol.* **2015**, *390*, 151–209. [CrossRef]
15. Xing, L.; Kieff, E. Epstein-Barr Virus BHRF1 Micro- and Stable RNAs during Latency III and after Induction of Replication. *J. Virol.* **2007**, *81*, 9967–9975. [CrossRef]
16. Babcock, G.J.; Hochberg, D.; Thorley-Lawson, A.D. The expression pattern of Epstein-Barr virus latent genes in vivo is dependent upon the differentiation stage of the infected B cell. *Immunity* **2000**, *13*, 497–506. [CrossRef]
17. Babcock, G.J.; Decker, L.L.; Volk, M.; Thorley-Lawson, D.A. EBV persistence in memory B cells in vivo. *Immunity* **1998**, *9*, 395–404. [CrossRef]
18. Hochberg, D.; Middeldorp, J.M.; Catalina, M.; Sullivan, J.L.; Luzuriaga, K.; Thorley-Lawson, D.A. Demonstration of the Burkitt's lymphoma Epstein-Barr virus phenotype in dividing latently infected memory cells in vivo. *Proc. Natl. Acad. Sci. USA* **2004**, *101*, 239–244. [CrossRef]
19. Laichalk, L.L.; Thorley-Lawson, D.A. Terminal differentiation into plasma cells initiates the replicative cycle of Epstein-Barr virus in vivo. *J. Virol.* **2005**, *79*, 1296–1307. [CrossRef]

20. Countryman, J.; Miller, G. Activation of expression of latent Epstein-Barr herpesvirus after gene transfer with a small cloned subfragment of heterogeneous viral DNA. *Proc. Natl. Acad. Sci. USA* **1985**, *82*, 4085–4089. [CrossRef]
21. Grogan, E.; Jenson, H.; Countryman, J.; Heston, L.; Gradoville, L.; Miller, G. Transfection of a rearranged viral DNA fragment, WZhet, stably converts latent Epstein-Barr viral infection to productive infection in lymphoid cells. *Proc. Natl. Acad. Sci. USA* **1987**, *84*, 1332–1336. [CrossRef]
22. Wen, W.; Iwakiri, D.; Yamamoto, K.; Maruo, S.; Kanda, T.; Takada, K. Epstein-Barr virus BZLF1 gene, a switch from latency to lytic infection, is expressed as an immediate-early gene after primary infection of B lymphocytes. *J. Virol.* **2007**, *81*, 1037–1042. [CrossRef]
23. Chiu, Y.-F.; Sugden, B. Epstein-Barr Virus: The Path from Latent to Productive Infection. *Annu. Rev. Virol.* **2016**, *3*, 359–372. [CrossRef]
24. Ersing, I.; Nobre, L.; Wang, L.W.; Soday, L.; Ma, Y.; Paulo, J.A.; Narita, Y.; Ashbaugh, C.W.; Jiang, C.; Grayson, N.E.; et al. A Temporal Proteomic Map of Epstein-Barr Virus Lytic Replication in B Cells. *Cell Rep.* **2017**, *19*, 1479–1493. [CrossRef]
25. Morales-Sánchez, A.; Fuentes-Panana, E. The Immunomodulatory Capacity of an Epstein-Barr Virus Abortive Lytic Cycle: Potential Contribution to Viral Tumorigenesis. *Cancers* **2018**, *10*, 98. [CrossRef]
26. Al Tabaa, Y.; Tuaillon, E.; Bollore, K.; Foulongne, V.; Petitjean, G.; Seigneurin, J.-M.; Duperray, C.; Desgranges, C.; Vendrell, J.-P. Functional Epstein-Barr virus reservoir in plasma cells derived from infected peripheral blood memory B cells. *Blood* **2009**, *113*, 604–611. [CrossRef]
27. Münz, C. Latency and Lytic Replication in Epstein–Barr Virus-Associated Oncogenesis. *Nat. Rev. Microbiol.* **2019**, *17*. [CrossRef]
28. Shannon-Lowe, C.; Rickinson, A.B.; Bell, A.I. Epstein-Barr virus-associated lymphomas. *Philos. Trans. R. Soc. Lond. B. Biol. Sci.* **2017**, *372*. [CrossRef]
29. Yin, H.; Qu, J.; Peng, Q.; Gan, R. Molecular mechanisms of EBV-driven cell cycle progression and oncogenesis. *Med. Microbiol. Immunol. Berl.* **2019**, *208*, 573–583. [CrossRef]
30. Raab-Traub, N. Novel mechanisms of EBV-induced oncogenesis. *Curr. Opin. Virol.* **2012**, *2*, 453–458. [CrossRef]
31. Jha, H.C.; Pei, Y.; Robertson, E.S. Epstein–Barr Virus: Diseases Linked to Infection and Transformation. *Front. Microbiol.* **2016**, *7*. [CrossRef]
32. El-Sharkawy, A.; Al Zaidan, L.; Malki, A. Epstein–Barr Virus-Associated Malignancies: Roles of Viral Oncoproteins in Carcinogenesis. *Front. Oncol.* **2018**, *8*, 265. [CrossRef]
33. Zhou, Y.; Attygalle, A.D.; Chuang, S.-S.; Diss, T.; Ye, H.; Liu, H.; Hamoudi, R.A.; Munson, P.; Bacon, C.M.; Dogan, A.; et al. Angioimmunoblastic T-cell lymphoma: Histological progression associates with EBV and HHV6B viral load. *Br. J. Haematol.* **2007**, *138*, 44–53. [CrossRef]
34. Drouet, E. The Role of the Epstein-Barr Virus Lytic Cycle in Tumor Progression: Consequences in Diagnosis and Therapy. In *Human Herpesvirus Infection—Biological Features, Transmission, Symptoms, Diagnosis and Treatment*; Luis Thomasini, R., Ed.; IntechOpen: London, UK, 2020; ISBN 978-1-83881-158-7.
35. Ma, S.-D.; Yu, X.; Mertz, J.E.; Gumperz, J.E.; Reinheim, E.; Zhou, Y.; Tang, W.; Burlingham, W.J.; Gulley, M.L.; Kenney, S.C. An Epstein-Barr Virus (EBV) Mutant with Enhanced BZLF1 Expression Causes Lymphomas with Abortive Lytic EBV Infection in a Humanized Mouse Model. *J. Virol.* **2012**, *86*, 7976–7987. [CrossRef] [PubMed]
36. Rothe, R.; Liguori, L.; Villegas-Mendez, A.; Marques, B.; Grunwald, D.; Drouet, E.; Lenormand, J.L. Characterization of the cell-penetrating properties of the Epstein-Barr virus ZEBRA trans-activator. *J. Biol. Chem.* **2010**, *285*, 20224–20233. [CrossRef]
37. Hong, S.; Wang, D.; Horton, J.R.; Zhang, X.; Speck, S.H.; Blumenthal, R.M.; Cheng, X. Methyl-dependent and spatial-specific DNA recognition by the orthologous transcription factors human AP-1 and Epstein-Barr virus Zta. *Nucleic Acids Res.* **2017**, *45*, 2503–2515. [CrossRef]
38. Heston, L.; El-Guindy, A.; Countryman, J.; Dela Cruz, C.; Delecluse, H.-J.; Miller, G. Amino Acids in the Basic Domain of Epstein-Barr Virus ZEBRA Protein Play Distinct Roles in DNA Binding, Activation of Early Lytic Gene Expression, and Promotion of Viral DNA Replication. *J. Virol.* **2006**, *80*, 9115–9133. [CrossRef]
39. Petosa, C.; Morand, P.; Baudin, F.; Moulin, M.; Artero, J.B.; Müller, C.W. Structural basis of lytic cycle activation by the Epstein-Barr virus ZEBRA protein. *Mol. Cell* **2006**, *21*, 565–572. [CrossRef]

40. Chang, Y.N.; Dong, D.L.; Hayward, G.S.; Hayward, S.D. The Epstein-Barr virus Zta transactivator: A member of the bZIP family with unique DNA-binding specificity and a dimerization domain that lacks the characteristic heptad leucine zipper motif. *J. Virol.* **1990**, *64*, 3358–3369. [CrossRef]
41. El-Guindy, A.S.; Heston, L.; Delecluse, H.-J.; Miller, G. Phosphoacceptor Site S173 in the Regulatory Domain of Epstein-Barr Virus ZEBRA Protein Is Required for Lytic DNA Replication but Not for Activation of Viral Early Genes. *J. Virol.* **2007**, *81*, 3303–3316. [CrossRef]
42. Liu, Y.C.; Chen, Z.; Burrows, S.R.; Purcell, A.W.; McCluskeys, J.; Rossjohn, J.; Gras, S. The energetic basis underpinning T-cell receptor recognition of a super-bulged peptide bound to a major histocompatibility complex class I molecule. *J. Biol. Chem.* **2012**, *287*, 12267–12276. [CrossRef]
43. Tynan, F.E.; Elhassen, D.; Purcell, A.W.; Burrows, J.M.; Borg, N.A.; Miles, J.J.; Williamson, N.A.; Green, K.J.; Tellam, J.; Kjer-Nielsen, L.; et al. The immunogenicity of a viral cytotoxic T cell epitope is controlled by its MHC-bound conformation. *J. Exp. Med.* **2005**, *202*, 1249–1260. [CrossRef] [PubMed]
44. Weber, E.; Buzovetsky, O.; Heston, L.; Yu, K.-P.; Knecht, K.M.; El-Guindy, A.; Miller, G.; Xiong, Y. A Noncanonical Basic Motif of Epstein-Barr Virus ZEBRA Protein Facilitates Recognition of Methylated DNA, High-Affinity DNA Binding, and Lytic Activation. *J. Virol.* **2019**, *93*. [CrossRef] [PubMed]
45. Mahot, S.; Fender, P.; Vivès, R.R.; Caron, C.; Perrissin, M.; Gruffat, H.; Sergeant, A.; Drouet, E. Cellular uptake of the EBV transcription factor EB1/Zta. *Virus Res.* **2005**, *110*, 187–193. [CrossRef]
46. Váňová, J.; Hejtmánková, A.; Kalbáčová, M.H.; Španielová, H. The Utilization of Cell-Penetrating Peptides in the Intracellular Delivery of Viral Nanoparticles. *Materials* **2019**, *12*, 2671. [CrossRef] [PubMed]
47. Kurnaeva, M.A.; Sheval, E.V.; Musinova, Y.R.; Vassetzky, Y.S. Tat basic domain: A "Swiss army knife" of HIV-1 Tat? *Rev. Med. Virol.* **2019**. [CrossRef]
48. Cai, M.; Liao, Z.; Chen, T.; Wang, P.; Zou, X.; Wang, Y.; Xu, Z.; Jiang, S.; Huang, J.; Chen, D.; et al. Characterization of the subcellular localization of Epstein-Barr virus encoded proteins in live cells. *Oncotarget* **2017**, *8*, 70006–70034. [CrossRef] [PubMed]
49. Park, R.; Heston, L.; Shedd, D.; Delecluse, H.J.; Miller, G. Mutations of amino acids in the DNA-recognition domain of Epstein-Barr virus ZEBRA protein alter its sub-nuclear localization and affect formation of replication compartments. *Virology* **2008**, *382*, 145–162. [CrossRef]
50. Mikaélian, I.; Drouet, E.; Marechal, V.; Denoyel, G.; Nicolas, J.C.; Sergeant, A. The DNA-binding domain of two bZIP transcription factors, the Epstein-Barr virus switch gene product EB1 and Jun, is a bipartite nuclear targeting sequence. *J. Virol.* **1993**, *67*, 734–742. [CrossRef]
51. Ramasubramanyan, S.; Osborn, K.; Al-Mohammad, R.; Naranjo Perez-Fernandez, I.B.; Zuo, J.; Balan, N.; Godfrey, A.; Patel, H.; Peters, G.; Rowe, M.; et al. Epstein–Barr virus transcription factor Zta acts through distal regulatory elements to directly control cellular gene expression. *Nucleic Acids Res.* **2015**, *43*, 3563–3577. [CrossRef]
52. El-Guindy, A.S.; So, Y.P.; Countryman, J.; Miller, G. Identification of constitutive phosphorylation sites on the Epstein-Barr virus ZEBRA protein. *J. Biol. Chem.* **2006**, *281*, 3085–3095. [CrossRef]
53. Kolman, J.L.; Taylor, N.; Marshak, D.R.; Miller, G. Serine-173 of the Epstein-Barr virus ZEBRA protein is required for DNA binding and is a target for casein kinase II phosphorylation. *Proc. Natl. Acad. Sci. USA* **1993**, *90*, 10115–10119. [CrossRef] [PubMed]
54. Kinoshita, E.; Kinoshita-Kikuta, E.; Koike, T. Phosphate-Affinity Gel Electrophoresis Using a Phos-Tag Molecule for Phosphoproteome Study. *Curr. Proteom.* **2012**, *6*, 104–121. [CrossRef]
55. Traylen, C.; Ramasubramanyan, S.; Zuo, J.; Rowe, M.; Almohammad, R.; Heesom, K.; Sweet, S.M.M.; Matthews, D.A.; Sinclair, A.J. Identification of Epstein-Barr virus replication proteins in Burkitt's lymphoma cells. *Pathogens* **2015**, *4*, 739–751. [CrossRef] [PubMed]
56. Adamson, A.L. Effects of SUMO-1 upon Epstein-Barr virus BZLF1 function and BMRF1 expression. *Biochem. Biophys. Res. Commun.* **2005**, *336*, 22–28. [CrossRef]
57. Murata, T.; Hotta, N.; Toyama, S.; Nakayama, S.; Chiba, S.; Isomura, H.; Ohshima, T.; Kanda, T.; Tsurumi, T. Transcriptional repression by sumoylation of Epstein-Barr virus BZLF1 protein correlates with association of histone deacetylase. *J. Biol. Chem.* **2010**, *285*, 23925–23935. [CrossRef] [PubMed]
58. Adamson, A.L.; Kenney, S. Epstein-Barr Virus Immediate-Early Protein BZLF1 Is SUMO-1 Modified and Disrupts Promyelocytic Leukemia Bodies. *J. Virol.* **2001**, *75*, 2388–2399. [CrossRef] [PubMed]

59. Hagemeier, S.R.; Dickerson, S.J.; Meng, Q.; Yu, X.; Mertz, J.E.; Kenney, S.C. Sumoylation of the Epstein-Barr Virus BZLF1 Protein Inhibits Its Transcriptional Activity and Is Regulated by the Virus-Encoded Protein Kinase. *J. Virol.* **2010**, *84*, 4383–4394. [CrossRef]
60. Flower, K.; Thomas, D.; Heather, J.; Ramasubramanyan, S.; Jones, S. Epigenetic Control of Viral Life-Cycle by a DNA-Methylation Dependent Transcription Factor. *PLoS ONE* **2011**, *6*, 25922. [CrossRef]
61. Dickerson, S.J.; Xing, Y.; Robinson, A.R.; Seaman, W.T.; Gruffat, H.; Kenney, S.C. Methylation-dependent binding of the epstein-barr virus BZLF1 protein to viral promoters. *PLoS Pathog.* **2009**, *5*. [CrossRef]
62. Bienert, S.; Waterhouse, A.; de Beer, T.; Tauriello, G.; Studer, G.; Bordoli, L.; Schwede, T. The SWISS-MODEL Repository: New features and functionalities. *Nucleic Acids Res.* **2017**, *45*, D313–D319. [CrossRef]
63. Lieberman, P.M.; Berk, A.J. The Zta trans-activator protein stabilizes TFIID association with promoter DNA by direct protein-protein interaction. *Genes Dev.* **1991**, *5*, 2441–2454. [CrossRef] [PubMed]
64. Lieberman, P.M.; Ozer, J.; Gürsel, D.B. Requirement for transcription factor IIA (TFIIA)-TFIID recruitment by an activator depends on promoter structure and template competition. *Mol. Cell. Biol.* **1997**, *17*, 6624–6632. [CrossRef] [PubMed]
65. Chen, C.J.; Deng, Z.; Kim, A.Y.; Blobel, G.A.; Lieberman, P.M. Stimulation of CREB binding protein nucleosomal histone acetyltransferase activity by a class of transcriptional activators. *Mol. Cell. Biol.* **2001**, *21*, 476–487. [CrossRef] [PubMed]
66. Murata, T.; Sato, Y.; Nakayama, S.; Kudoh, A.; Iwahori, S.; Isomura, H.; Tajima, M.; Hishiki, T.; Ohshima, T.; Hijikata, M.; et al. TORC2, a Coactivator of cAMP-response Element-binding Protein, Promotes Epstein-Barr Virus Reactivation from Latency through Interaction with Viral BZLF1 Protein. *J. Biol. Chem.* **2009**, *284*, 8033–8041. [CrossRef] [PubMed]
67. Balan, N.; Osborn, K.; Sinclair, A.J. Repression of CIITA by the Epstein–Barr virus transcription factor Zta is independent of its dimerization and DNA binding. *J. Gen. Virol.* **2016**, *97*, 725–732. [CrossRef] [PubMed]
68. Bristol, J.A.; Robinson, A.R.; Barlow, E.A.; Kenney, S.C. The Epstein-Barr Virus BZLF1 Protein Inhibits Tumor Necrosis Factor Receptor 1 Expression through Effects on Cellular C/EBP Proteins. *J. Virol.* **2010**, *84*, 12362–12374. [CrossRef]
69. Dreyfus, D.H.; Nagasawa, M.; Kelleher, C.A.; Gelfand, E.W. Stable expression of Epstein-Barr virus BZLF-1-encoded ZEBRA protein activates p53-dependent transcription in human Jurkat T-lymphoblastoid cells. *Blood* **2000**, *96*, 625–634. [CrossRef]
70. Sato, Y.; Shirata, N.; Kudoh, A.; Iwahori, S.; Nakayama, S.; Murata, T.; Isomura, H.; Nishiyama, Y.; Tsurumi, T. Expression of Epstein–Barr virus BZLF1 immediate-early protein induces p53 degradation independent of MDM2, leading to repression of p53-mediated transcription. *Virology* **2009**, *388*, 204–211. [CrossRef]
71. Morrison, T.E.; Kenney, S.C. BZLF1, an Epstein-Barr virus immediate-early protein, induces p65 nuclear translocation while inhibiting p65 transcriptional function. *Virology* **2004**, *328*, 219–232. [CrossRef]
72. Raver, R.M.; Panfil, A.R.; Hagemeier, S.R.; Kenney, S.C. The B-Cell-Specific Transcription Factor and Master Regulator Pax5 Promotes Epstein-Barr Virus Latency by Negatively Regulating the Viral Immediate Early Protein BZLF1. *J. Virol.* **2013**, *87*, 8053–8063. [CrossRef]
73. Robinson, A.R.; Kwek, S.S.; Kenney, S.C. The B-Cell Specific Transcription Factor, Oct-2, Promotes Epstein-Barr Virus Latency by Inhibiting the Viral Immediate-Early Protein, BZLF1. *PLoS Pathog.* **2012**, *8*. [CrossRef] [PubMed]
74. Zhou, Y.; Heesom, K.; Osborn, K.; AlMohammed, R.; Sweet, S.M.; Sinclair, A.J. Identifying the Cellular Interactome of Epstein-Barr Virus Lytic Regulator Zta Reveals Cellular Targets Contributing to Viral Replication. *J. Virol.* **2020**, *94*. [CrossRef] [PubMed]
75. Hahn, A.M.; Huye, L.E.; Ning, S.; Webster-Cyriaque, J.; Pagano, J.S. Interferon regulatory factor 7 is negatively regulated by the Epstein-Barr virus immediate-early gene, BZLF-1. *J. Virol.* **2005**, *79*, 10040–10052. [CrossRef] [PubMed]
76. Gao, Z.; Krithivas, A.; Finan, J.E.; Semmes, O.J.; Zhou, S.; Wang, Y.; Hayward, S.D. The Epstein-Barr virus lytic transactivator Zta interacts with the helicase-primase replication proteins. *J. Virol.* **1998**, *72*, 8559–8567. [CrossRef] [PubMed]
77. Rennekamp, A.J.; Wang, P.; Lieberman, P.M. Evidence for DNA Hairpin Recognition by Zta at the Epstein-Barr Virus Origin of Lytic Replication. *J. Virol.* **2010**, *84*, 7073–7082. [CrossRef]

78. Sarisky, R.T.; Gao, Z.; Lieberman, P.M.; Fixman, E.D.; Hayward, G.S.; Hayward, S.D. A replication function associated with the activation domain of the Epstein-Barr virus Zta transactivator. *J. Virol.* **1996**, *70*, 8340–8347. [CrossRef]
79. Schepers, A.; Pich, D.; Hammerschmidt, W. Activation of oriLyt, the lytic origin of DNA replication of Epstein-Barr virus, by BZLF1. *Virology* **1996**, *220*, 367–376. [CrossRef]
80. Sato, Y.; Kamura, T.; Shirata, N.; Murata, T.; Kudoh, A.; Iwahori, S.; Nakayama, S.; Isomura, H.; Nishiyama, Y.; Tsurumi, T. Degradation of Phosphorylated p53 by Viral Protein-ECS E3 Ligase Complex. *PLOS Pathog.* **2009**, *5*, e1000530. [CrossRef]
81. Wiedmer, A.; Wang, P.; Zhou, J.; Rennekamp, A.J.; Tiranti, V.; Zeviani, M.; Lieberman, P.M. Epstein-Barr virus immediate-early protein Zta co-opts mitochondrial single-stranded DNA binding protein to promote viral and inhibit mitochondrial DNA replication. *J. Virol.* **2008**, *82*, 4647–4655. [CrossRef]
82. Bailey, S.G.; Verrall, E.; Schelcher, C.; Rhie, A.; Doherty, A.J.; Sinclair, A.J. Functional interaction between Epstein-Barr virus replication protein Zta and host DNA damage response protein 53BP1. *J. Virol* **2009**, *83*, 11116–11122. [CrossRef]
83. Schaeffner, M.; Mrozek-Gorska, P.; Buschle, A.; Woellmer, A.; Tagawa, T.; Cernilogar, F.M.; Schotta, G.; Krietenstein, N.; Lieleg, C.; Korber, P.; et al. BZLF1 interacts with chromatin remodelers promoting escape from latent infections with EBV. *Life Sci. Alliance* **2019**, *2*. [CrossRef] [PubMed]
84. Montone, K.T.; Hodinka, R.L.; Salhany, K.E.; Lavi, E.; Rostami, A.; Tomaszewski, J.E. Identification of Epstein-Barr virus lytic activity in post-transplantation lymphoproliferative disease. *Mod. Pathol. Off. J. U. S. Can. Acad. Pathol. Inc.* **1996**, *9*, 621–630.
85. Hong, G.K.; Gulley, M.L.; Feng, W.-H.; Delecluse, H.-J.; Holley-Guthrie, E.; Kenney, S.C. Epstein-Barr virus lytic infection contributes to lymphoproliferative disease in a SCID mouse model. *J. Virol.* **2005**, *79*, 13993–14003. [CrossRef] [PubMed]
86. Ma, S.-D.; Hegde, S.; Young, K.H.; Sullivan, R.; Rajesh, D.; Zhou, Y.; Jankowska-Gan, E.; Burlingham, W.J.; Sun, X.; Gulley, M.L.; et al. A New Model of Epstein-Barr Virus Infection Reveals an Important Role for Early Lytic Viral Protein Expression in the Development of Lymphomas. *J. Virol.* **2011**, *85*, 165–177. [CrossRef] [PubMed]
87. Habib, M.; Buisson, M.; Lupo, J.; Agbalika, F.; Socié, G.; Germi, R.; Baccard, M.; Imbert-Marcille, B.-M.; Dantal, J.; Morand, P.; et al. Lytic EBV infection investigated by detection of Soluble Epstein-Barr virus ZEBRA in the serum of patients with PTLD. *Sci. Rep.* **2017**, *7*, 10479. [CrossRef] [PubMed]
88. Brousset, P.; Knecht, H.; Rubin, B.; Drouet, E.; Chittal, S.; Meggetto, F.; Saati, T.A.; Bachmann, E.; Denoyel, G.; Sergeant, A. Demonstration of Epstein-Barr virus replication in Reed-Sternberg cells of Hodgkin's disease. *Blood* **1993**, *82*, 872–876. [CrossRef]
89. Cohen, M.; Vistarop, A.G.; Huaman, F.; Narbaitz, M.; Metrebian, F.; De Matteo, E.; Preciado, M.V.; Chabay, P.A. Epstein-Barr virus lytic cycle involvement in diffuse large B cell lymphoma. *Hematol. Oncol.* **2018**, *36*, 98–103. [CrossRef]
90. Xue, S.; Labrecque, L.G.; Lu, Q.-L.; Ong, S.K.; Lampert, I.A.; Kazembe, P.; Molyneux, E.; Broadhead, R.L.; Borgstein, E.; Griffin, B.E. Promiscuous expression of Epstein-Barr virus genes in Burkitt's lymphoma from the central African country Malawi. *Int. J. Cancer* **2002**, *99*, 635–643. [CrossRef]
91. Xue, S.A.; Lu, Q.L.; Poulsom, R.; Karran, L.; Jones, M.D.; Griffin, B.E. Expression of two related viral early genes in Epstein-Barr virus-associated tumors. *J. Virol.* **2000**, *74*, 2793–2803. [CrossRef]
92. Altmann, M.; Hammerschmidt, W. Epstein-Barr virus provides a new paradigm: A requirement for the immediate inhibition of apoptosis. *PLoS Biol.* **2005**, *3*, e404. [CrossRef]
93. Accardi, R.; Gruffat, H.; Sirand, C.; Fusil, F.; Gheit, T.; Hernandez-Vargas, H.; Le Calvez-Kelm, F.; Traverse-Glehen, A.; Cosset, F.L.; Manet, E.; et al. The mycotoxin aflatoxin B1 stimulates Epstein-Barr virus-induced B-cell transformation in in vitro and in vivo experimental models. *Carcinogenesis* **2015**, *36*, 1440–1451. [CrossRef] [PubMed]
94. Chêne, A.; Donati, D.; Guerreiro-Cacais, A.O.; Levitsky, V.; Chen, Q.; Falk, K.I.; Orem, J.; Kironde, F.; Wahlgren, M.; Bejarano, M.T. A molecular link between malaria and Epstein-Barr virus reactivation. *PLoS Pathog.* **2007**, *3*, 0826–0834. [CrossRef] [PubMed]
95. Mannucci, S.; Luzzi, A.; Carugi, A.; Gozzetti, A.; Lazzi, S.; Malagnino, V.; Simmonds, M.; Cusi, M.G.; Leoncini, L.; Van Den Bosch, C.A.; et al. EBV reactivation and chromosomal polysomies: Euphorbia tirucalli as a possible cofactor in endemic Burkitt lymphoma. *Adv. Hematol.* **2012**. [CrossRef] [PubMed]

96. Martel-Renoir, D.; Grunewald, V.; Touitou, R.; Schwaab, G.; Joab, I. Qualitative analysis of the expression of Epstein-Barr virus lytic genes in nasopharyngeal carcinoma biopsies. *J. Gen. Virol.* **1995**, *76*, 1401–1408. [CrossRef]
97. Ramayanti, O.; Juwana, H.; Verkuijlen, S.A.M.W.; Adham, M.; Pegtel, M.D.; Greijer, A.E.; Middeldorp, J.M. Epstein-Barr virus mRNA profiles and viral DNA methylation status in nasopharyngeal brushings from nasopharyngeal carcinoma patients reflect tumor origin. *Int. J. Cancer* **2017**, *140*, 149–162. [CrossRef]
98. Huang, J.; Chen, H.; Hutt-Fletcher, L.; Ambinder, R.F.; Hayward, S.D. Lytic viral replication as a contributor to the detection of Epstein-Barr virus in breast cancer. *J. Virol.* **2003**, *77*, 13267–13274. [CrossRef]
99. Dardari, R.; Menezes, J.; Drouet, E.; Joab, I.; Benider, A.; Bakkali, H.; Kanouni, L.; Jouhadi, H.; Benjaafar, N.; El Gueddari, B.; et al. Analyses of the prognostic significance of the Epstein-Barr virus transactivator ZEBRA protein and diagnostic value of its two synthetic peptides in nasopharyngeal carcinoma. *J. Clin. Virol.* **2008**, *41*, 96–103. [CrossRef]
100. Marrão, G.; Habib, M.; Paiva, A.; Bicout, D.; Fallecker, C.; Franco, S.; Fafi-Kremer, S.; Simões da Silva, T.; Morand, P.; Freire de Oliveira, C.; et al. Epstein-Barr virus infection and clinical outcome in breast cancer patients correlate with immune cell TNF-α/IFN-γ response. *BMC Cancer* **2014**, *14*, 665. [CrossRef]
101. Zhang, G.; Li, Z.; Zhou, Q. Utility of Serum EB Virus Zta Antibody in the Diagnostic of Nasopharyngeal Carcinoma: Evidences From 2126 Cases and 15,644 Controls. *Front. Oncol.* **2019**, *9*, 1391. [CrossRef]
102. Trumper, P.A.; Epstein, M.A.; Giovanella, B.C.; Finerty, S. Isolation of infectious EB virus from the epithelial tumour cells of nasopharyngeal carcinoma. *Int. J. Cancer* **1977**, *20*, 655–662. [CrossRef]
103. Henle, G.; Henle, W. Epstein-Barr virus-specific IgA serum antibodies as an outstanding feature of nasopharyngeal carcinoma. *Int. J. Cancer* **1976**, *17*, 1–7. [CrossRef] [PubMed]
104. Chien, Y.C.; Chen, J.Y.; Liu, M.Y.; Yang, H.I.; Hsu, M.M.; Chen, C.J.; Yang, C.S. Serologic markers of Epstein-Barr virus infection and nasopharyngeal carcinoma in Taiwanese men. *N. Engl. J. Med.* **2001**, *345*, 1877–1882. [CrossRef] [PubMed]
105. Borozan, I.; Zapatka, M.; Frappier, L.; Ferretti, V. Analysis of Epstein-Barr Virus Genomes and Expression Profiles in Gastric Adenocarcinoma. *J. Virol.* **2018**, *92*. [CrossRef] [PubMed]
106. Sbih-Lammali, F.; Berger, F.; Busson, P.; Ooka, T. Expression of the DNase encoded by the BGLF5 gene of Epstein-Barr virus in nasopharyngeal carcinoma epithelial cells. *Virology* **1996**, *222*, 64–74. [CrossRef] [PubMed]
107. Seto, E.; Yang, L.; Middeldorp, J.; Sheen, T.-S.; Chen, J.-Y.; Fukayama, M.; Eizuru, Y.; Ooka, T.; Takada, K. Epstein-Barr virus (EBV)-encoded BARF1 gene is expressed in nasopharyngeal carcinoma and EBV-associated gastric carcinoma tissues in the absence of lytic gene expression. *J. Med. Virol.* **2005**, *76*, 82–88. [CrossRef]
108. Zur Hausen, A.; Brink, A.A.; Craanen, M.E.; Middeldorp, J.M.; Meijer, C.J.; van den Brule, A.J. Unique transcription pattern of Epstein-Barr virus (EBV) in EBV-carrying gastric adenocarcinomas: Expression of the transforming BARF1 gene. *Cancer Res.* **2000**, *60*, 2745–2748.
109. Tsai, M.-H.; Raykova, A.; Klinke, O.; Bernhardt, K.; Gärtner, K.; Leung, C.S.; Geletneky, K.; Sertel, S.; Münz, C.; Feederle, R.; et al. Spontaneous Lytic Replication and Epitheliotropism Define an Epstein-Barr Virus Strain Found in Carcinomas. *Cell Rep.* **2013**, *5*, 458–470. [CrossRef]
110. Tsai, M.-H.; Lin, X.; Shumilov, A.; Bernhardt, K.; Feederle, R.; Poirey, R.; Kopp-Schneider, A.; Pereira, B.; Almeida, R.; Delecluse, H.-J. The biological properties of different Epstein-Barr virus strains explain their association with various types of cancers. *Oncotarget* **2017**, *8*, 10238–10254. [CrossRef]
111. Hanahan, D.; Weinberg, R.A. Hallmarks of Cancer: The Next Generation. *Cell* **2011**, *144*, 646–674. [CrossRef]
112. Chatterjee, N.; Walker, G.C. Mechanisms of DNA damage, repair, and mutagenesis: DNA Damage and Repair. *Environ. Mol. Mutagen.* **2017**, *58*, 235–263. [CrossRef]
113. Friedberg, E.C.; Aguilera, A.; Gellert, M.; Hanawalt, P.C.; Hays, J.B.; Lehmann, A.R.; Lindahl, T.; Lowndes, N.; Sarasin, A.; Wood, R.D. DNA repair: From molecular mechanism to human disease. *DNA Repair* **2006**, *5*, 986–996. [CrossRef]
114. Ciccia, A.; Elledge, S.J. The DNA Damage Response: Making It Safe to Play with Knives. *Mol. Cell* **2010**, *40*, 179–204. [CrossRef]
115. Gargouri, B.; Van Pelt, J.; El Feki, A.E.F.; Attia, H.; Lassoued, S. Induction of Epstein-Barr virus (EBV) lytic cycle in vitro causes oxidative stress in lymphoblastoid B cell lines. *Mol. Cell. Biochem.* **2009**, *324*, 55–63. [CrossRef]

116. Gargouri, B.; Nasr, R.; ben Mansour, R.; Lassoued, S.; Mseddi, M.; Attia, H.; El Feki, A.e.F.; Van Pelt, J. Reactive Oxygen Species Production and Antioxidant Enzyme Expression after Epstein–Barr Virus Lytic Cycle Induction in Raji Cell Line. *Biol. Trace Elem. Res.* **2011**, *144*, 1449–1457. [CrossRef]
117. Lassoued, S.; Ben Ameur, R.; Ayadi, W.; Gargouri, B.; Ben Mansour, R.; Attia, H. Epstein-Barr virus induces an oxidative stress during the early stages of infection in B lymphocytes, epithelial, and lymphoblastoid cell lines. *Mol. Cell. Biochem.* **2008**, *313*, 179–186. [CrossRef]
118. Shumilov, A.; Tsai, M.-H.; Schlosser, Y.T.; Kratz, A.-S.; Bernhardt, K.; Fink, S.; Mizani, T.; Lin, X.; Jauch, A.; Mautner, J.; et al. Epstein-Barr virus particles induce centrosome amplification and chromosomal instability. *Nat. Commun.* **2017**, *8*, 14257. [CrossRef]
119. Lee, C.-P.; Chen, J.-Y.; Wang, J.-T.; Kimura, K.; Takemoto, A.; Lu, C.-C.; Chen, M.-R. Epstein-Barr virus BGLF4 kinase induces premature chromosome condensation through activation of condensin and topoisomerase II. *J. Virol.* **2007**, *81*, 5166–5180. [CrossRef]
120. Moquin, S.A.; Thomas, S.; Whalen, S.; Warburton, A.; Fernandez, S.G.; McBride, A.A.; Pollard, K.S.; Miranda, J.L. The Epstein-Barr Virus Episome Maneuvers between Nuclear Chromatin Compartments during Reactivation. *J. Virol.* **2018**, *92*. [CrossRef]
121. Chang, Y.-H.; Lee, C.-P.; Su, M.-T.; Wang, J.-T.; Chen, J.-Y.; Lin, S.-F.; Tsai, C.-H.; Hsieh, M.-J.; Takada, K.; Chen, M.-R. Epstein-Barr virus BGLF4 kinase retards cellular S-phase progression and induces chromosomal abnormality. *PloS ONE* **2012**, *7*, e39217. [CrossRef]
122. Wu, C.-C.; Liu, M.-T.; Chang, Y.-T.; Fang, C.-Y.; Chou, S.-P.; Liao, H.-W.; Kuo, K.-L.; Hsu, S.-L.; Chen, Y.-R.; Wang, P.-W.; et al. Epstein-Barr virus DNase (BGLF5) induces genomic instability in human epithelial cells. *Nucleic Acids Res.* **2010**, *38*, 1932–1949. [CrossRef]
123. Chiu, S.-H.; Wu, C.-C.; Fang, C.-Y.; Yu, S.-L.; Hsu, H.-Y.; Chow, Y.-H.; Chen, J.-Y. Epstein-Barr virus BALF3 mediates genomic instability and progressive malignancy in nasopharyngeal carcinoma. *Oncotarget* **2014**, *5*, 8583–8601. [CrossRef]
124. Fang, C.-Y.; Lee, C.-H.; Wu, C.-C.; Chang, Y.-T.; Yu, S.-L.; Chou, S.-P.; Huang, P.-T.; Chen, C.-L.; Hou, J.-W.; Chang, Y.; et al. Recurrent chemical reactivations of EBV promotes genome instability and enhances tumor progression of nasopharyngeal carcinoma cells. *Int. J. Cancer* **2009**, *124*, 2016–2025. [CrossRef]
125. Sall, F.B.; Germini, D.; Shmakova, A.; Diouf, P.M.D.; Wiels, J.; Ndour, M.; Touré, A.O.; Vassetzky, Y. Role of Epstein-Barr Virus Zebra protein in induction of t(8;14) translocation. *Biopolym. Cell* **2019**, *35*, 230–231. [CrossRef]
126. Hsu, M.; Wu, S.-Y.; Chang, S.-S.; Su, I.-J.; Tsai, C.-H.; Lai, S.-J.; Shiau, A.-L.; Takada, K.; Chang, Y. Epstein-Barr virus lytic transactivator Zta enhances chemotactic activity through induction of interleukin-8 in nasopharyngeal carcinoma cells. *J. Virol.* **2008**, *82*, 3679–3688. [CrossRef]
127. Mahot, S.; Sergeant, A.; Drouet, E.; Gruffat, H. A novel function for the Epstein-Barr virus transcription factor EB1/Zta: Induction of transcription of the hIL-10 gene. *J. Gen. Virol.* **2003**, *84*, 965–974. [CrossRef]
128. Lee, C.-H.; Yeh, T.-H.; Lai, H.-C.; Wu, S.-Y.; Su, I.-J.; Takada, K.; Chang, Y. Epstein-Barr virus Zta-induced immunomodulators from nasopharyngeal carcinoma cells upregulate interleukin-10 production from monocytes. *J. Virol.* **2011**, *85*, 7333–7342. [CrossRef]
129. Sheikhpour, E.; Noorbakhsh, P.; Foroughi, E.; Farahnak, S.; Nasiri, R.; Neamatzadeh, H. A Survey on the Role of Interleukin-10 in Breast Cancer: A Narrative. *Rep. Biochem. Mol. Biol.* **2018**, *7*, 30–37.
130. Jochum, S.; Moosmann, A.; Lang, S.; Hammerschmidt, W.; Zeidler, R. The EBV immunoevasins vIL-10 and BNLF2a protect newly infected B cells from immune recognition and elimination. *PLoS Pathog.* **2012**, *8*, e1002704. [CrossRef]
131. Jones, R.J.; Seaman, W.T.; Feng, W.-H.; Barlow, E.; Dickerson, S.; Delecluse, H.-J.; Kenney, S.C. Roles of lytic viral infection and IL-6 in early versus late passage lymphoblastoid cell lines and EBV-associated lymphoproliferative disease. *Int. J. Cancer* **2007**, *121*, 1274–1281. [CrossRef]
132. Katsumura, K.R.; Maruo, S.; Takada, K. EBV lytic infection enhances transformation of B-lymphocytes infected with EBV in the presence of T-lymphocytes. *J. Med. Virol.* **2012**, *84*, 504–510. [CrossRef]
133. Tsai, S.-C.; Lin, S.-J.; Chen, P.-W.; Luo, W.-Y.; Yeh, T.-H.; Wang, H.-W.; Chen, C.-J.; Tsai, C.-H. EBV Zta protein induces the expression of interleukin-13, promoting the proliferation of EBV-infected B cells and lymphoblastoid cell lines. *Blood* **2009**, *114*, 109–118. [CrossRef] [PubMed]

134. Cayrol, C.; Flemington, E.K. Identification of cellular target genes of the Epstein-Barr virus transactivator Zta: Activation of transforming growth factor beta igh3 (TGF-beta igh3) and TGF-beta 1. *J. Virol.* **1995**, *69*, 4206–4212. [CrossRef] [PubMed]
135. Hong, G.K.; Kumar, P.; Wang, L.; Damania, B.; Gulley, M.L.; Delecluse, H.-J.; Polverini, P.J.; Kenney, S.C. Epstein-Barr virus lytic infection is required for efficient production of the angiogenesis factor vascular endothelial growth factor in lymphoblastoid cell lines. *J. Virol.* **2005**, *79*, 13984–13992. [CrossRef] [PubMed]
136. Ariza, M.-E.; Glaser, R.; Kaumaya, P.T.P.; Jones, C.; Williams, M.V. The EBV-encoded dUTPase activates NF-kappa B through the TLR2 and MyD88-dependent signaling pathway. *J. Immunol. Baltim. Md. 1950* **2009**, *182*, 851–859. [CrossRef]
137. Waldman, W.J.; Williams, M.V.; Lemeshow, S.; Binkley, P.; Guttridge, D.; Kiecolt-Glaser, J.K.; Knight, D.A.; Ladner, K.J.; Glaser, R. Epstein-Barr virus-encoded dUTPase enhances proinflammatory cytokine production by macrophages in contact with endothelial cells: Evidence for depression-induced atherosclerotic risk. *Brain Behav. Immun.* **2008**, *22*, 215–223. [CrossRef]
138. Zeidler, R.; Eissner, G.; Meissner, P.; Uebel, S.; Tampé, R.; Lazis, S.; Hammerschmidt, W. Downregulation of TAP1 in B lymphocytes by cellular and Epstein-Barr virus-encoded interleukin-10. *Blood* **1997**, *90*, 2390–2397. [CrossRef]
139. Swaminathan, S.; Hesselton, R.; Sullivan, J.; Kieff, E. Epstein-Barr virus recombinants with specifically mutated BCRF1 genes. *J. Virol.* **1993**, *67*, 7406–7413. [CrossRef]
140. Morrison, T.E.; Mauser, A.; Wong, A.; Ting, J.P.; Kenney, S.C. Inhibition of IFN-gamma signaling by an Epstein-Barr virus immediate-early protein. *Immunity* **2001**, *15*, 787–799. [CrossRef]
141. Li, D.; Qian, L.; Chen, C.; Shi, M.; Yu, M.; Hu, M.; Song, L.; Shen, B.; Guo, N. Down-regulation of MHC class II expression through inhibition of CIITA transcription by lytic transactivator Zta during Epstein-Barr virus reactivation. *J. Immunol.* **2009**, *182*, 1799–1809. [CrossRef]
142. Zuo, J.; Thomas, W.A.; Haigh, T.A.; Fitzsimmons, L.; Long, H.M.; Hislop, A.D.; Taylor, G.S.; Rowe, M. Epstein-Barr virus evades CD4+ T cell responses in lytic cycle through BZLF1-mediated downregulation of CD74 and the cooperation of vBcl-2. *PLoS Pathog.* **2011**, *7*, e1002455. [CrossRef]
143. Zuo, J.; Currin, A.; Griffin, B.D.; Shannon-Lowe, C.; Thomas, W.A.; Ressing, M.E.; Wiertz, E.J.H.J.; Rowe, M. The Epstein-Barr virus G-protein-coupled receptor contributes to immune evasion by targeting MHC class I molecules for degradation. *PLoS Pathog.* **2009**, *5*, e1000255. [CrossRef] [PubMed]
144. Zuo, J.; Quinn, L.L.; Tamblyn, J.; Thomas, W.A.; Feederle, R.; Delecluse, H.-J.; Hislop, A.D.; Rowe, M. The Epstein-Barr virus-encoded BILF1 protein modulates immune recognition of endogenously processed antigen by targeting major histocompatibility complex class I molecules trafficking on both the exocytic and endocytic pathways. *J. Virol.* **2011**, *85*, 1604–1614. [CrossRef] [PubMed]
145. Horst, D.; van Leeuwen, D.; Croft, N.P.; Garstka, M.A.; Hislop, A.D.; Kremmer, E.; Rickinson, A.B.; Wiertz, E.J.H.J.; Ressing, M.E. Specific targeting of the EBV lytic phase protein BNLF2a to the transporter associated with antigen processing results in impairment of HLA class I-restricted antigen presentation. *J. Immunol. Baltim. Md. 1950* **2009**, *182*, 2313–2324. [CrossRef] [PubMed]
146. Zuo, J.; Thomas, W.; van Leeuwen, D.; Middeldorp, J.M.; Wiertz, E.J.H.J.; Ressing, M.E.; Rowe, M. The DNase of gammaherpesviruses impairs recognition by virus-specific CD8+ T cells through an additional host shutoff function. *J. Virol.* **2008**, *82*, 2385–2393. [CrossRef]
147. Draborg, A.H.; Duus, K.; Houen, G. Epstein-Barr Virus in Systemic Autoimmune Diseases. *Clin. Dev. Immunol.* **2013**, *2013*, 1–9. [CrossRef]
148. Haddad, E.; Paczesny, S.; Leblond, V.; Seigneurin, J.M.; Stern, M.; Achkar, A.; Bauwens, M.; Delwail, V.; Debray, D.; Duvoux, C.; et al. Treatment of B-lymphoproliferative disorder with a monoclonal anti-interleukin-6 antibody in 12 patients: A multicenter phase 1-2 clinical trial. *Blood* **2001**, *97*, 1590–1597. [CrossRef]
149. Masood, R.; Cai, J.; Tulpule, A.; Zheng, T.; Hamilton, A.; Sharma, S.; Espina, B.M.; Smith, D.L.; Gill, P.S. Interleukin 8 is an autocrine growth factor and a surrogate marker for Kaposi's sarcoma. *Clin. Cancer Res. Off. J. Am. Assoc. Cancer Res.* **2001**, *7*, 2693–2702.
150. Sall, A.; Caserta, S.; Jolicoeur, P.; Franqueville, L.; de Turenne-Tessier, M.; Ooka, T. Mitogenic activity of Epstein-Barr virus-encoded BARF1 protein. *Oncogene* **2004**, *23*, 4938–4944. [CrossRef]

151. Wiech, T.; Nikolopoulos, E.; Lassman, S.; Heidt, T.; Schöpflin, A.; Sarbia, M.; Werner, M.; Shimizu, Y.; Sakka, E.; Ooka, T.; et al. Cyclin D1 expression is induced by viral BARF1 and is overexpressed in EBV-associated gastric cancer. *Virchows Arch. Int. J. Pathol.* **2008**, *452*, 621–627. [CrossRef]
152. Sheng, W.; Decaussin, G.; Sumner, S.; Ooka, T. N-terminal domain of BARF1 gene encoded by Epstein-Barr virus is essential for malignant transformation of rodent fibroblasts and activation of BCL-2. *Oncogene* **2001**, *20*, 1176–1185. [CrossRef]
153. Wang, Q.; Tsao, S.W.; Ooka, T.; Nicholls, J.M.; Cheung, H.W.; Fu, S.; Wong, Y.C.; Wang, X. Anti-apoptotic role of BARF1 in gastric cancer cells. *Cancer Lett.* **2006**, *238*, 90–103. [CrossRef] [PubMed]
154. Morrison, T.E.; Mauser, A.; Klingelhutz, A.; Kenney, S.C. Epstein-Barr virus immediate-early protein BZLF1 inhibits tumor necrosis factor alpha-induced signaling and apoptosis by downregulating tumor necrosis factor receptor 1. *J. Virol* **2004**, *78*, 544–549. [CrossRef] [PubMed]
155. Waugh, D.J.J.; Wilson, C. The Interleukin-8 Pathway in Cancer. *Clin. Cancer Res.* **2008**, *14*, 6735–6741. [CrossRef] [PubMed]
156. Duffy, A.M.; Bouchier-Hayes, D.J.; Harmey, J.H. Vascular Endothelial Growth Factor (VEGF) and Its Role in Non-Endothelial Cells: Autocrine Signalling by VEGF. In *VEGF and Cancer*; Springer: Boston, MA, USA, 2004; pp. 133–144. ISBN 978-1-4613-4810-8.
157. Yoshizaki, T.; Sato, H.; Murono, S.; Pagano, J.S.; Furukawa, M. Matrix metalloproteinase 9 is induced by the Epstein-Barr virus BZLF1 transactivator. *Clin. Exp. Metastasis* **1999**, *17*, 431–436. [CrossRef] [PubMed]
158. Lan, Y.-Y.; Yeh, T.-H.; Lin, W.-H.; Wu, S.-Y.; Lai, H.-C.; Chang, F.-H.; Takada, K.; Chang, Y. Epstein-Barr Virus Zta Upregulates Matrix Metalloproteinases 3 and 9 That Synergistically Promote Cell Invasion In Vitro. *PLoS ONE* **2013**, *8*. [CrossRef] [PubMed]
159. Jiang, R.; Cabras, G.; Sheng, W.; Zeng, Y.; Ooka, T. Synergism of BARF1 with Ras Induces Malignant Transformation in Primary Primate Epithelial Cells and Human Nasopharyngeal Epithelial Cells. *Neoplasia* **2009**, *11*, 964–973. [CrossRef] [PubMed]
160. Sista, N.D.; Barry, C.; Sampson, K.; Pagano, J. Physical and functional interaction of the Epstein-Barr virus BZLF1 transactivator with the retinoic acid receptors RAR alpha and RXR alpha. *Nucleic Acids Res.* **1995**, *23*, 1729–1736. [CrossRef]
161. Wu, F.Y.; Chen, H.; Wang, S.E.; apRhys, C.M.J.; Liao, G.; Fujimuro, M.; Farrell, C.J.; Huang, J.; Hayward, S.D.; Hayward, G.S. CCAAT/Enhancer Binding Protein Interacts with ZTA and Mediates ZTA-Induced p21CIP-1 Accumulation and G1 Cell Cycle Arrest during the Epstein-Barr Virus Lytic Cycle. *J. Virol.* **2003**, *77*, 1481–1500. [CrossRef]
162. Zerby, D.; Chen, C.J.; Poon, E.; Lee, D.; Shiekhattar, R.; Lieberman, P.M. The amino-terminal C/H1 domain of CREB binding protein mediates zta transcriptional activation of latent Epstein-Barr virus. *Mol. Cell Biol.* **1999**, *19*, 1617–1626. [CrossRef]
163. Zhang, Q.; Gutsch, D.; Kenney, S. Functional and physical interaction between p53 and BZLF1: Implications for Epstein-Barr virus latency. *Mol. Cell Biol.* **1994**, *14*, 1929–1938. [CrossRef]
164. Cayrol, C.; Flemington, E.K. The Epstein-Barr virus bZIP transcription factor Zta causes G0/G1 cell cycle arrest through induction of cyclin-dependent kinase inhibitors. *EMBO J.* **1996**, *15*, 2748–2759. [CrossRef] [PubMed]
165. Mauser, A.; Saito, S.; Appella, E.; Anderson, C.W.; Seaman, W.T.; Kenney, S. The Epstein-Barr Virus Immediate-Early Protein BZLF1 Regulates p53 Function through Multiple Mechanisms. *J. Virol.* **2002**, *76*, 12503–12512. [CrossRef] [PubMed]
166. Germini, D.; Tsfasman, T.; Klibi, M.; El-Amine, R.; Pichugin, A.; Iarovaia, O.V.; Bilhou-Nabera, C.; Subra, F.; Bou Saada, Y.; Sukhanova, A.; et al. HIV Tat induces a prolonged MYC relocalization next to IGH in circulating B-cells. *Leukemia* **2017**, *31*, 2515–2522. [CrossRef] [PubMed]
167. Sall, F.B.; El Amine, R.; Markozashvili, D.; Tsfasman, T.; Oksenhendler, E.; Lipinski, M.; Vassetzky, Y.; Germini, D. HIV-1 Tat protein induces aberrant activation of AICDA in human B-lymphocytes from peripheral blood. *J. Cell. Physiol.* **2019**. [CrossRef]
168. El-Amine, R.; Germini, D.; Zakharova, V.V.; Tsfasman, T.; Sheval, E.V.; Louzada, R.A.N.; Dupuy, C.; Bilhou-Nabera, C.; Hamade, A.; Najjar, F.; et al. HIV-1 Tat protein induces DNA damage in human peripheral blood B-lymphocytes via mitochondrial ROS production. *Redox Biol.* **2018**, *15*, 97–108. [CrossRef]

169. Drouet, E.; Brousset, P.; Fares, F.; Icart, J.; Verniol, C.; Meggetto, F.; Schlaifer, D.; Desmorat-Coat, H.; Rigal-Huguet, F.; Niveleau, A.; et al. High Epstein-Barr virus serum load and elevated titers of anti-ZEBRA antibodies in patients with EBV-harboring tumor cells of Hodgkin's disease. *J. Med. Virol.* **1999**, *57*, 383–389. [CrossRef]
170. Chan, K.H.; Gu, Y.L.; Ng, F.; Ng, P.S.P.; Seto, W.H.; Sham, J.S.T.; Chua, D.; Wei, W.; Chen, Y.L.; Luk, W.; et al. EBV specific antibody-based and DNA-based assays in serologic diagnosis of nasopharyngeal carcinoma. *Int. J. Cancer* **2003**, *105*, 706–709. [CrossRef]
171. Dardari, R.; Hinderer, W.; Lang, D.; Benider, A.; El Gueddari, B.; Joab, I.; Benslimane, A.; Khyatti, M. Antibody responses to recombinant Epstein-Barr virus antigens in nasopharyngeal carcinoma patients: Complementary test of ZEBRA protein and early antigens p54 and p138. *J. Clin. Microbiol.* **2001**, *39*, 3164–3170. [CrossRef]
172. Joab, I.; Nicolas, J.C.; Schwaab, G.; de-Thé, G.; Clausse, B.; Perricaudet, M.; Zeng, Y. Detection of anti-Epstein-Barr-virus transactivator (ZEBRA) antibodies in sera from patients with nasopharyngeal carcinoma. *Int. J. Cancer* **1991**, *48*, 647–649. [CrossRef]
173. Mathew, A.; Cheng, H.M.; Sam, C.K.; Joab, I.; Prasad, U.; Cochet, C. A high incidence of serum IgG antibodies to the Epstein-Barr virus replication activator protein in nasopharyngeal carcinoma. *Cancer Immunol. Immunother. CII* **1994**, *38*, 68–70. [CrossRef]
174. Yip, T.T.; Ngan, R.K.; Lau, W.H.; Poon, Y.F.; Joab, I.; Cochet, C.; Cheng, A.K. A possible prognostic role of immunoglobulin-G antibody against recombinant Epstein-Barr virus BZLF-1 transactivator protein ZEBRA in patients with nasopharyngeal carcinoma. *Cancer* **1994**, *74*, 2414–2424. [CrossRef]
175. Drouet, E.B.; Chapuis-Cellier, C.; Garnier, J.L.; Touraine, J.L. Early detection of EBV infection and meaning in transplant patients. In *Cancer in Transplantation: Prevention and Treatment*; Touraine, J.L., Traeger, J., Bétuel, H., Dubernard, J.M., Revillard, J.P., Dupuy, C., Eds.; Springer: Dordrecht, The Netherlands, 1996; pp. 201–207. ISBN 978-94-010-6563-4.
176. Fink, S.E.K.; Gandhi, M.K.; Nourse, J.P.; Keane, C.; Jones, K.; Crooks, P.; Jöhrens, K.; Korfel, A.; Schmidt, H.; Neumann, S.; et al. A comprehensive analysis of the cellular and EBV-specific microRNAome in primary CNS PTLD identifies different patterns among EBV-associated tumors. *Am. J. Transplant. Off. J. Am. Soc. Transplant. Am. Soc. Transpl. Surg.* **2014**, *14*, 2577–2587. [CrossRef]
177. Rea, D.; Fourcade, C.; Leblond, V.; Rowe, M.; Joab, I.; Edelman, L.; Bitker, M.O.; Gandjbakhch, I.; Suberbielle, C.; Farcet, J.P. Patterns of Epstein-Barr virus latent and replicative gene expression in Epstein-Barr virus B cell lymphoproliferative disorders after organ transplantation. *Transplantation* **1994**, *58*, 317–324. [CrossRef]
178. Vajro, P.; Lucariello, S.; Migliaro, F.; Sokal, E.; Gridelli, B.; Vegnente, A.; Iorio, R.; Smets, F.; Quinto, I.; Scala, G. Predictive value of Epstein-Barr virus genome copy number and BZLF1 expression in blood lymphocytes of transplant recipients at risk for lymphoproliferative disease. *J. Infect. Dis.* **2000**, *181*, 2050–2054. [CrossRef] [PubMed]
179. Imbert-Marcille, B.M.; Coste-Burel, M.; Robillard, N.; Foucaud-Gamen, J.; Billaudel, S.; Drouet, E. Sequential use of paraformaldehyde and methanol as optimal conditions for the direct quantification of ZEBRA and rta antigens by flow cytometry. *Clin. Diagn. Lab. Immunol.* **2000**, *7*, 206–211. [CrossRef] [PubMed]
180. Babcock, G.J.; Decker, L.L.; Freeman, R.B.; Thorley-Lawson, D.A. Epstein-barr virus-infected resting memory B cells, not proliferating lymphoblasts, accumulate in the peripheral blood of immunosuppressed patients. *J. Exp. Med.* **1999**, *190*, 567–576. [CrossRef]
181. Miyashita, E.M.; Yang, B.; Lam, K.M.; Crawford, D.H.; Thorley-Lawson, D.A. A novel form of Epstein-Barr virus latency in normal B cells in vivo. *Cell* **1995**, *80*, 593–601. [CrossRef]
182. Feng, W.; Westphal, E.; Mauser, A.; Raab-Traub, N.; Gulley, M.L.; Busson, P.; Kenney, S.C. Use of adenovirus vectors expressing Epstein-Barr virus (EBV) immediate-early protein BZLF1 or BRLF1 to treat EBV-positive tumors. *J. Virol.* **2002**, *76*, 10951–10959. [CrossRef]
183. Bilger, A.; Plowshay, J.; Ma, S.; Nawandar, D.; Barlow, E.A.; Romero-Masters, J.C.; Bristol, J.A.; Li, Z.; Tsai, M.-H.; Delecluse, H.-J.; et al. Leflunomide/teriflunomide inhibit Epstein-Barr virus (EBV)- induced lymphoproliferative disease and lytic viral replication. *Oncotarget* **2017**, *8*, 44266–44280. [CrossRef]
184. Kawada, J.-I.; Ando, S.; Torii, Y.; Watanabe, T.; Sato, Y.; Ito, Y.; Kimura, H. Antitumor effects of duvelisib on Epstein-Barr virus-associated lymphoma cells. *Cancer Med.* **2018**, *7*, 1275–1284. [CrossRef]
185. Daskalogianni, C.; Pyndiah, S.; Apcher, S.; Mazars, A.; Manoury, B.; Ammari, N.; Nylander, K.; Voisset, C.; Blondel, M.; Fåhraeus, R. Epstein-Barr virus-encoded EBNA1 and ZEBRA: Targets for therapeutic strategies against EBV-carrying cancers. *J. Pathol.* **2015**, *235*, 334–341. [CrossRef]

186. Hartlage, A.S.; Liu, T.; Patton, J.T.; Garman, S.L.; Zhang, X.; Kurt, H.; Lozanski, G.; Lustberg, M.E.; Caligiuri, M.A.; Baiocchi, R.A. The Epstein-Barr Virus Lytic Protein BZLF1 as a Candidate Target Antigen for Vaccine Development. *Cancer Immunol. Res.* **2015**, *3*, 787–794. [CrossRef]
187. Kenney, S.C.; Mertz, J.E. Regulation of the latent-lytic switch in Epstein-Barr virus. *Semin. Cancer Biol.* **2014**, *26*, 60–68. [CrossRef] [PubMed]
188. Needham, J.; Adamson, A.L. BZLF1 transcript variants in Epstein–Barr virus-positive epithelial cell lines. *Virus Genes* **2019**, *55*, 779–785. [CrossRef]
189. Bristol, J.A.; Djavadian, R.; Albright, E.R.; Coleman, C.B.; Ohashi, M.; Hayes, M.; Romero-Masters, J.C.; Barlow, E.A.; Farrell, P.J.; Rochford, R.; et al. A cancer-associated Epstein-Barr virus BZLF1 promoter variant enhances lytic infection. *PLOS Pathog.* **2018**, *14*, e1007179. [CrossRef]

© 2020 by the authors. Licensee MDPI, Basel, Switzerland. This article is an open access article distributed under the terms and conditions of the Creative Commons Attribution (CC BY) license (http://creativecommons.org/licenses/by/4.0/).

Supplemental Materials: Oncogenic Properties of the EBV ZEBRA Protein

Diego Germini, Fatimata Bintou Sall, Anna Shmakova, Joelle Wiels, Svetlana Dokudovskaya, Emmanuel Drouet and Yegor Vassetzky

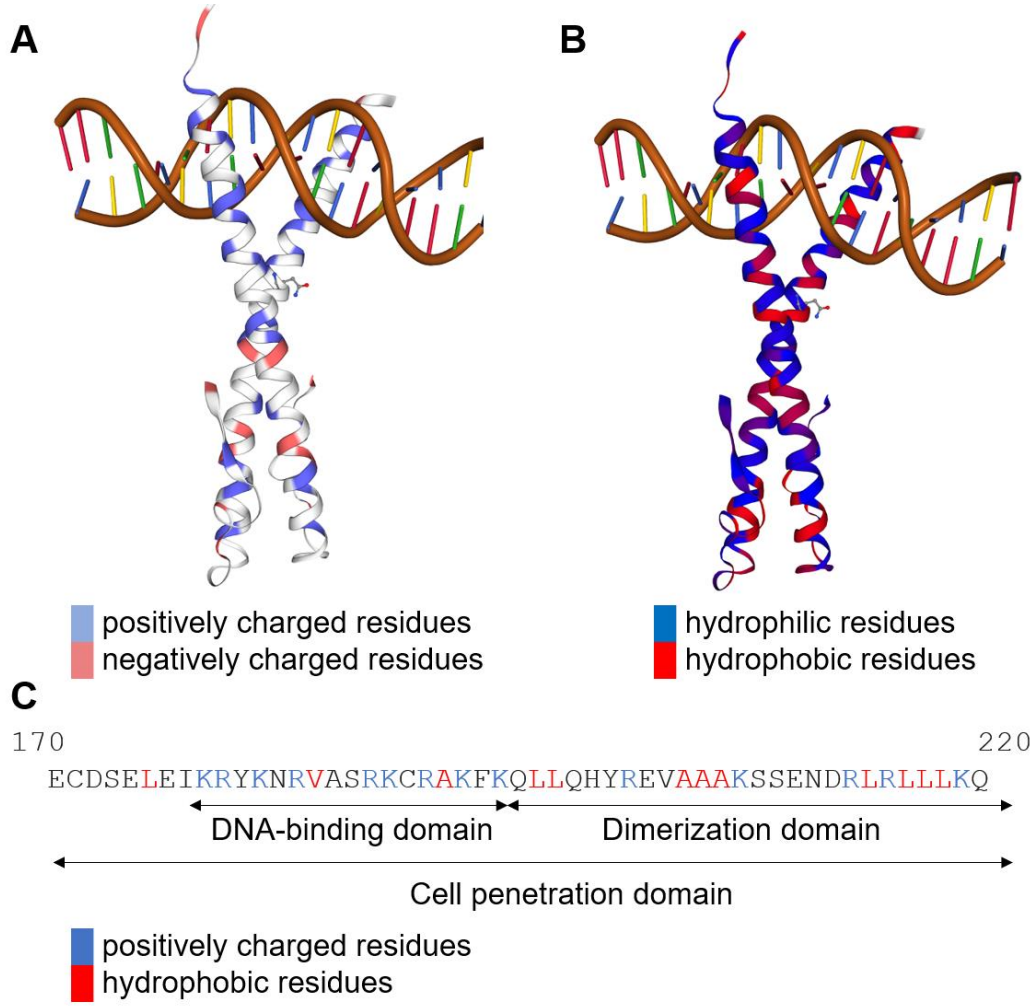

Figure 1. ZEBRA cell penetration domain. **(A)** positions of positively (blue) and negatively (red) charged residues in ZEBRA structure. Residues from 175 (top) to 236 (bottom) were characterized by X-ray crystallography [38] and are available at the SWISS-MODEL Repository [188]. **(B)** the same ZEBRA structure, positions of hydrophilic (blue) and hydrophobic (red) residues are shown. **(C)** primary structure of ZEBRA cell penetration domain (residues 170-220). Positively charged amino acids (seven lysines and seven arginines) are shown in blue, whereas hydrophobic amino acids (seven leucines, five alanines, one valine) are shown in red [35].

© 2020 by the authors. Licensee MDPI, Basel, Switzerland. This article is an open access article distributed under the terms and conditions of the Creative Commons Attribution (CC BY) license (http://creativecommons.org/licenses/by/4.0/).

2 Hypothesis, aim, research questions and objectives of the study

People living with HIV are at a higher risk of developing B cell lymphomas, especially EBV-associated B cell lymphomas, than the general population (Coghill et al. 2019; Engels et al. 2008; Luo et al. 2022). Moreover, when compared with immunosuppressed transplant recipients, people living with HIV still have a higher incidence of B cell lymphomas (Grulich et al. 2007). HIV infection is also more frequently associated with EBV reactivation (Ling et al. 2003; Rahman et al. 1991; Yan et al. 2018). This has prompted us to investigate the potential implications of HIV and EBV infection in the process of B cell lymphomagenesis. The specific mechanisms through which HIV infection in the cART era may contribute to the development of B cell malignancies are not fully understood. We **hypothesize** that HIV infection might promote B cell lymphomagenesis not exclusively through immune suppression. Thus, the **aim** of the current study was to investigate factors and specific mechanisms, other than immune deficiency, that might play a role in B cell lymphomagenesis in people living with HIV. By understanding the underlying biological factors and molecular pathways involved in B cell lymphomagenesis in this population, we seek to shed light on the complex interplay between HIV, EBV and B cell lymphomagenesis, which may pave the way for novel therapeutic strategies and targeted interventions to mitigate lymphoma risk in people living with HIV.

The **research questions** we addressed in this study were:

1. Could the usage of certain cART drugs in people living with HIV affect the incidence of translocation-caused lymphomas/leukaemias?
2. How does EBV reactivation, common for people living with HIV, contribute to B cell lymphomagenesis?
3. Can HIV-1 Tat perturb DNA damage sensing and repair pathways in B cells, leading to potential genome instability and increased risk of lymphomagenesis?
4. How does HIV-1 Tat regulate the expression of major histocompatibility complex class II (MHC class II) in B cells, and what is the impact of this regulation on immune evasion of B cells from CD4+ T cell response?
5. Is there a direct interaction between HIV-1 Tat and EBV Zta proteins in B cells, and what are the functional consequences of this interaction?

The specific **objectives** of the study included:

1. To investigate the contribution of cART to B cell lymphomagenesis, particularly, the impact of common cART drugs on the frequency of Burkitt's-lymphoma-associated t(8;14) translocation in B cells;

2. To examine the effect of EBV reactivation on B cell pathology, particularly its effect on the spatial localization of *MYC* and *IGH* loci to understand how EBV reactivation may promote *MYC-IGH* chromosomal translocation and contribute to Burkitt's lymphoma development;
3. To assess the influence of HIV-1 Tat on DNA damage sensing and repair pathways in B cells, elucidating the mechanisms through which Tat may disturb DNA repair and promote genome instability, potentially leading to lymphomagenesis;
4. To analyze the role of HIV-1 Tat in the regulation of MHC class II expression in B cells, examining its potential impact on immune evasion and the development of EBV-associated B cell lymphomas in people living with HIV;
5. To investigate the potential interaction between HIV-1 Tat and EBV Zta proteins in B cells in order to elucidate the functional consequences of this interaction and its potential role in promoting immune evasion and B cell growth advantage, crucial hallmarks of malignancies.

Through these objectives, we sought to uncover novel insights into the complex interplay between HIV, EBV, and B cell lymphomagenesis, and gain a comprehensive understanding of the underlying biological factors and molecular pathways that contribute to B cell lymphomagenesis in people living with HIV. Overall, we aimed to contribute to the advancement of knowledge in the field and provide a basis for future studies to improve the management and prevention of B cell malignancies in this population.

3 Results and discussion

3.1 The contribution of HIV, EBV and antiretroviral therapy to genome instability and lymphoma-associated chromosomal translocations

3.1.1 Some antiretroviral drugs might increase the frequency of Burkitt's-lymphoma-associated t(8;14) translocation in B cells

Chromosomal translocations, which are caused by DSBs and their incorrect repair *via* NHEJ, play important in the development of B cell lymphomas (Canoy et al. 2022). Oncogenic chromosomal translocations can occur as a result of DSBs brought on by genotoxic drugs. The risk factors affecting translocation-prone DSB repair, however, are still largely unknown. The formation of chromosomal rearrangements at this stage can be influenced by chromatin state, DSB movement, DNA damage sensing and repair mechanisms (Canoy et al. 2022) or even the presence of particular transcripts, such as long non-coding RNAs that share homology regions for two different loci (Demin et al. 2022; Shmakova & Vassetzky 2023).

Studying chromosomal translocations is difficult for two reasons. First, spontaneous translocations are rare events. In some cases, only a single translocation occurs in the entire organism, and cells with translocations can only survive and grow if the translocation gives them an advantage over other cells in the population. This survival advantage does not always manifest in cells that are growing in culture. Second, the location of breakpoints in spontaneous translocations can vary by kilobases to hundreds of kilobases. This requires elaborated methods, such as long-range PCR, FISH, and sequencing, to detect them (Busch et al. 2007; Kovalchuk et al. 2012). In contrast, the translocation can be easily identified and measured by PCR in an artificial system where DSBs are produced efficiently and consistently at the same loci (Germini et al. 2017a). We created two CRISPR/Cas9-based experimental human B cell-based models for the t(8;14) *MYC-IGH* chromosomal translocation, a feature of BL, and the t(8;21) *AML1-ETO* chromosomal translocation, a feature of acute myeloid leukaemia (AML), to study lymphomagenic and leukemogenic chromosomal translocations (**Figure 7**). These models were applied to investigate DNA repair pathways and drugs affecting the frequency of oncogenic chromosomal translocations (see **Article 4**).

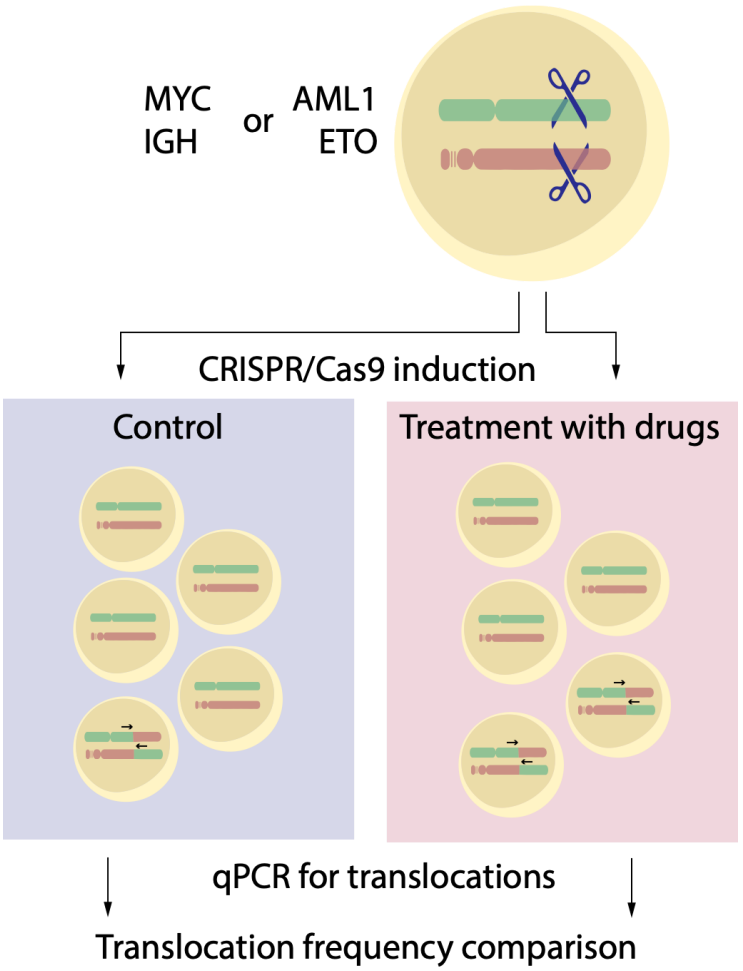

Figure 7. An overview of the experimental setup for inducing oncogenic *AML1-ETO* and *MYC-IGH* translocations in B cells. The models reproduce the generation of specific DSBs in the two loci *via* inducible Cas9 and guide RNAs (gRNAs) expression, which stimulates the formation of either t(8;14) or t(8;21) translocations at a high and stable rate in the cell culture and allows their detection by qPCR. Abbreviations: qPCR, quantitative polymerase chain reaction.

Article 4. Research paper "Cell models with inducible oncogenic translocations allow to evaluate the potential of drugs to favor secondary translocations"

Received: 25 May 2022 | Revised: 21 July 2022 | Accepted: 2 October 2022

DOI: 10.1002/cac2.12370

CANCER COMMUNICATIONS Open Access

LETTER TO THE EDITOR

Cell models with inducible oncogenic translocations allow to evaluate the potential of drugs to favor secondary translocations

Dear Editor,

Chromosomal translocations result from the interchange of genetic material between non-homologous chromosomes. Chromosomal translocations are formed by erroneous repair of double-stranded breaks (DSBs) via non-homologous end joining (NHEJ) [1]. Some genotoxic drugs produce DSBs and thus present a major risk factor for the development of oncogenic chromosomal translocations. The risk factors that interfere with translocation-prone DSB repair, once DSBs are already formed, are obscure, and potential effects of drugs on translocation formation during this step have never been explored.

The study of chromosomal translocations is complicated since naturally occurring translocations are rare, and the localization of breakpoints varies from kilobases to hundreds of kilobases, which complicates their detection. In contrast, when DSBs are generated at precise loci, the translocation can be easily detected by PCR. In the present work, we developed two experimental human B cell-based models to study lymphomagenic t(8;14) *MYC-IGH* and leukemogenic t(8;21) *AML1-ETO* translocations, characteristic for Burkitt's lymphoma (BL) [2] and acute myeloid leukemia (AML), respectively [3]. We used these systems to study pathways and drugs that affect the probability of oncogenic translocations. BL often arises in people living with human immunodeficiency virus (HIV, PLWH) who are treated with combination antiretroviral therapy regimen [4], while chemotherapy is a risk factor for secondary AML [3]; therefore, we tested common antiretroviral and chemotherapeutic drugs for their ability to influence the rate of translocation formation in our systems.

Two experimental systems for the targeted generation of DSBs in either the *AML1* and *ETO* (iAML1-ETO cell line) or *MYC* and *IGH* loci (iMYC-IGH cell line) were created. The models were derived from the RPMI8866 lymphoblastoid cell line with the stable integration of the *Cas9* gene, expressed under the control of a doxycycline (Dox)-inducible promoter and two guide RNA genes (targeting either *AML1-ETO* or *MYC-IGH* loci) (Figure 1A, Supplementary Figure S1). The DSB loci in the *AML1-ETO* model were similar to breakpoints in patients with therapy-related AML and cells treated with etoposide; the DSB loci in the *MYC-IGH* model were similar to breakpoints in patients with sporadic and HIV-induced BL (see Supplementary Methods for further information). The addition of Dox activated Cas9 expression after 4 hours (Figure 1B, Supplementary Figure S2) and stimulated the formation of DSBs in the selected loci (data not shown). The generated t(8;14) or t(8;21) translocations were detectable by qPCR using the primers that surrounded the translocation breakpoint (Figure 1C-D, Supplementary Figure S3). Translocations peaked after 48 hours for iMYC-IGH and 96 hours for iAML1-ETO (data not shown), and these timepoints were selected for further experiments. Without Dox treatment, chromosomal translocations were undetectable.

To get insight into the mechanisms of the translocation generation in our system, we used several inhibitors of DSB

List of abbreviations: 17-AAG, 17-N-allylamino-17-demethoxygeldanamycin; 3TC, Lamivudine; ABC, abacavir; AML, acute myeloid leukemia; a-NHEJ, alternative NHEJ; ANOVA, analysis of variance; ATM, ataxia telangiectasia mutated; AZT, azidothymidine; BL, Burkitt's lymphoma; Cas9, CRISPR associated protein 9; CCR5, C-C Motif Chemokine Receptor 5; c-NHEJ, classical NHEJ; CRISPR/Cas9, Clustered regularly interspaced short palindromic repeats/CRISPR-associated nuclease9; DNA-Pk, DNA-dependent protein kinase; Dox, doxycycline; DSB, Double-strand break; ENIT, Engineered nuclease-induced translocations; FTC, emtricitabine; HIV, human immunodeficiency virus; IC_{10}, 10% inhibitory concentration; IC_{50}, half-maximal inhibitory concentration; iMYC-IGH, RPMI8866-derived cell line that inducibly express CRISPR/Cas9 and guide RNAs, targeting both *MYC* and *IGH* loci; iAML1-ETO, RPMI8866-derived cell line that inducibly express CRISPR/Cas9 and guide RNAs, targeting both *AML1* and *ETO* loci; HR, homologous recombination; NHEJ, Non-homologous end-joining; PARP, poly(ADP-ribose) polymerase; PCR, Polymerase chain reaction; PLWH, people living with HIV.

This is an open access article under the terms of the Creative Commons Attribution-NonCommercial-NoDerivs License, which permits use and distribution in any medium, provided the original work is properly cited, the use is non-commercial and no modifications or adaptations are made.
© 2022 The Authors. *Cancer Communications* published by John Wiley & Sons Australia, Ltd. on behalf of Sun Yat-sen University Cancer Center.

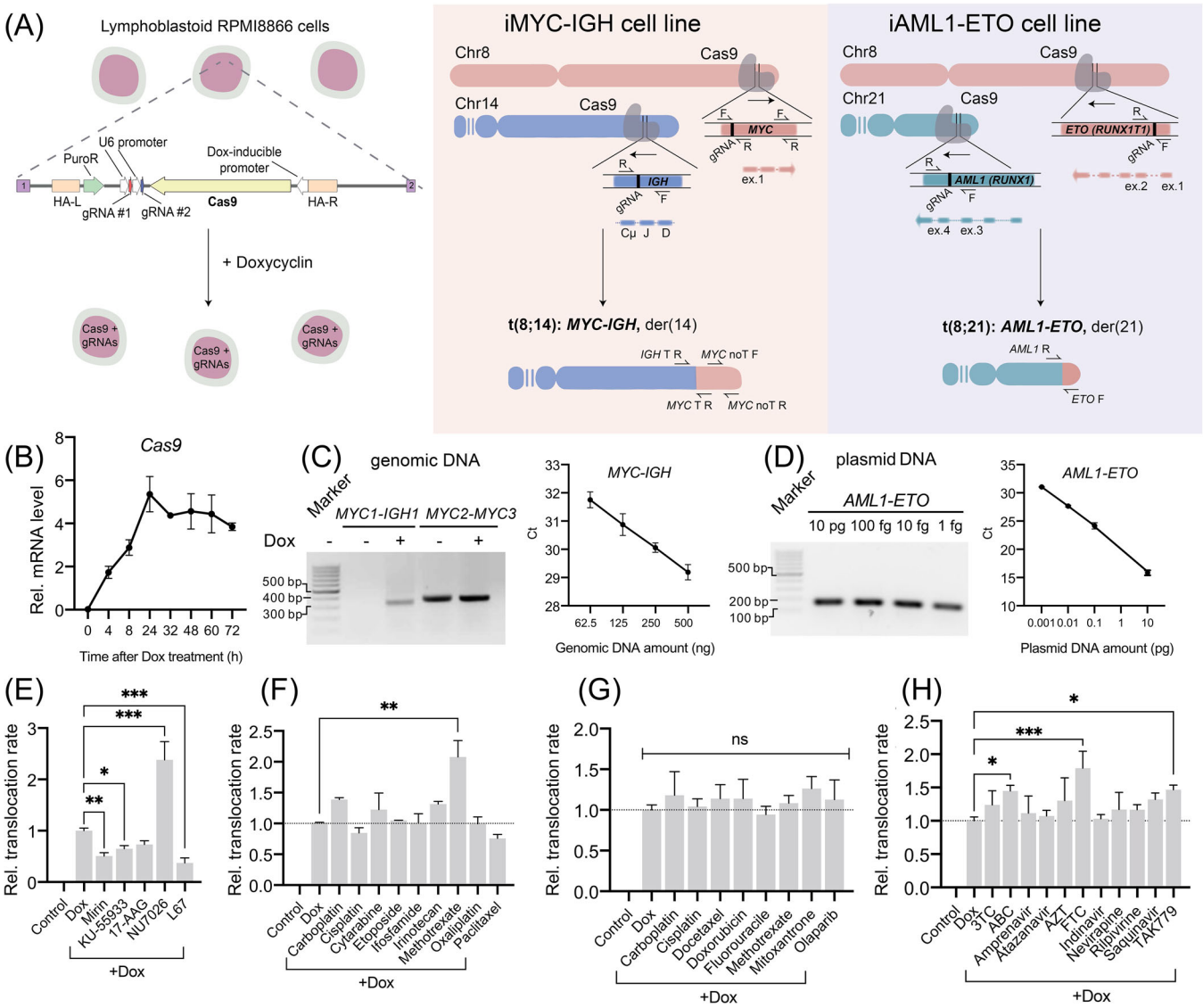

FIGURE 1 RPMI8866-based iMYC-IGH and iAML1-ETO cell models to induce and detect specific chromosomal translocations. (A) General overview of the experimental setup. HA-L and HA-R homology arms were used for the homology-directed genome knock-in of Cas9 and guide RNA genes in the AAVS1 loci on chromosome 19. PuroR, puromycin resistance gene. (B) Kinetics of *Cas9* expression as analyzed by RT-qPCR. The mRNA level was normalized to *GAPDH* expression. (C) Detection of *MYC-IGH* translocations by qPCR: a representative image of agarose gel electrophoresis of PCR products amplified with *MYC1-IGH1* (translocation primers) and *MYC2-MYC3* (primers ~6.8 kbp downstream the breakpoint in *MYC*) from genomic DNA with and without Dox induction (left panel) and the analysis of primer efficiency by plotting the cycle threshold value (Ct) against the dilution of the genomic DNA sample (right panel). (D) Detection of *AML1-ETO* translocations by qPCR: a representative image of agarose gel electrophoresis of *AML1-ETO* PCR products amplified from 10 pg, 100 fg, 10 fg or 1 fg of plasmid DNA (left panel) and the analysis of primer efficiency by plotting the cycle threshold value (Ct) against the dilution of the plasmid DNA sample (right panel). Due to the lower rate of *AML1-ETO* translocations, pUC18-based plasmid containing *AML1-ETO* PCR product was created for the quantification of translocation rate and for the amplification efficiency determination with the standard curve. (E) Effect of DNA repair inhibitors on the *MYC-IGH* translocation rate in iMYC-IGH cells. Cells were simultaneously treated with Dox and the indicated inhibitor or left untreated (control) for 48 h, and translocations were detected by qPCR. Fold changes of t(8;14) translocation rate were calculated relative to that in Dox-treated cells, set as 1. (F) The effect of chemotherapeutic drugs on t(8;21) translocation rate. iAML1-ETO cells were simultaneously treated either with Dox alone to induce the expression of Cas9 and guide RNAs targeting *AML1* and *ETO*, or with chemotherapeutic drugs and Dox, or left untreated (control). Chemotherapeutic drugs were added at a non-lethal 10% inhibitory concentration. At 96 hours later, DNA was collected, and the t(8;21) translocation rate was measured by qPCR. Fold changes of t(8;21) translocation rate were calculated relative to that in Dox-treated cells, set as 1. (G) The effect of chemotherapeutic drugs on t(8;14) translocation rate. iMYC-IGH cells were simultaneously treated either with Dox alone or with chemotherapeutic drugs and Dox, or left untreated (control). At 48 hours later, DNA was collected, and the t(8;14) translocation rate was measured by qPCR. Fold changes of t(8;14) translocation rate were calculated relative to that in Dox-treated cells, set as 1. (H) The effect of antiretroviral drugs on t(8;14) translocation

repair pathways. iMYC-IGH cells were simultaneously treated with Dox and either Mirin (an MRE11 inhibitor), KU-55933 [(an ataxia telangiectasia mutated (ATM) inhibitor)], 17-N-allylamino-17-demethoxygeldanamycin [17-AAG, an Hsp90 inhibitor that inhibits homologous recombination (HR) repair by destabilizing Rad51], NU7026 [a DNA-dependent protein kinase (DNA-PK) inhibitor, classical NHEJ, (c-NHEJ)], or L67 [an inhibitor of DNA ligase I and III, alternative NHEJ (a-NHEJ)]. Treatment with Mirin, KU-55933 or L67 significantly decreased, whereas treatment with NU7026 significantly increased the *MYC-IGH* translocation rate (Figure 1E). Presumably, the inhibition of MRE11 and ATM, involved in the early steps of DNA damage detection and response, resulted in DSB repair defects [5] and ultimately cell cycle arrest or death, which decreased the overall translocation rates. ATM also promotes the clustering of DSBs into large repair foci [5], which might contribute to DSB proximity and translocations. The inhibition of c-NHEJ increased the translocation rate, while the inhibition of the a-NHEJ pathway decreased the translocation rate, which were in agreement with a previous studies [1]. The increase in the translocation rate when c-NHEJ is abrogated is due to the slow kinetics of DNA repair via a-NHEJ, which permits the free movement of unrepaired DNA ends and increases the chance of meeting their translocation partner in the nuclear space [1].

We next tested whether some chemotherapeutic drugs could influence the translocation formation and thus contribute to the formation of secondary neoplasms, e.g., therapy-related AML. We used drugs of different classes: platinum-based antineoplastics (carboplatin, cisplatin, oxaliplatin), topoisomerase inhibitors (doxorubicin, etoposide, irinotecan, mitoxantrone), antimetabolites (cytarabine, fluorouracil, methotrexate), poly(ADP-ribose) polymerase (PARP) inhibitor (olaparib), an alkylating agent (ifosfamide), and cytoskeletal drugs (docetaxel, paclitaxel). To exclude the effects related to cytotoxicity and cell death, we chose the non-lethal 10% inhibitory concentration (IC_{10}) of the above drugs (Supplementary Table S3, Supplementary Figure S4). iAML1-ETO cells were simultaneously treated with Dox and chemotherapeutic drugs, and the level of t(8;21) translocations was measured and compared to those in Dox-treated cells. We found that the addition of methotrexate increased more than two-fold the rate of *AML1-ETO* translocations (Figure 1F). No significant differences were found for other drugs, which was further confirmed in iMYC-IGH cells with five other chemotherapeutic drugs used at IC_{10}. No significant differences were found between the translocation rate in Dox-treated and Dox+drug-treated iMYC-IGH cells (Figure 1G). These results indicated that in the iMYC-IGH model, chemotherapeutic drugs did not interfere with the DSB repair once DSBs were formed. Thus, methotrexate use can increase the risk of secondary therapy-related AML, and patients treated with methotrexate should be monitored for the development of AML. Noteworthy, the development of therapy-related myelodysplastic syndrome/AML with t(8;21) and t(3;21) translocations was described in patients following low-dose treatment with methotrexate for rheumatoid arthritis [6].

We next tested whether antiretroviral drugs could influence the level of *MYC-IGH* translocations since BL is a common neoplasm in PLWH. We used drugs from different classes, such as nucleoside reverse transcriptase inhibitors (NRTIs) [abacavir (ABC), azidothymidine (AZT), emtricitabine (FTC), lamivudine (3TC)], non-NRTIs (nevirapine, rilpivirine), protease inhibitors (amprenavir, atazanavir, indinavir, saquinavir), and C-C motif chemokine receptor 5 (CCR5) antagonist (TAK779). The drugs were added simultaneously with Dox to the iMYC-IGH cell medium at the reported IC_{50} for virus inhibition. The chosen concentrations were not toxic for the cells (Supplementary Figure S4C). We found that two NRTIs, ABC and FTC, and CCR5 antagonist TAK779 significantly increased the rate of *MYC-IGH* translocations (Figure 1H). NTRIs are known to be incorporated into nuclear DNA by certain DNA polymerases during DNA repair, and they can act as chain terminators and directly inhibit cellular DNA polymerases by binding to their catalytic site [7]. Compromised DNA damage response may delay the classical repair machinery and engage translocation-prone a-NHEJ. Furthermore, mitochondrial toxicity of NRTIs could affect nuclear

rate. iMYC-IGH cells were simultaneously treated either with Dox alone or with antiretroviral drugs and Dox, or left untreated (control). At 48 hours later, DNA was collected, and the t(8;14) translocation rate was measured by qPCR. Fold changes of t(8;14) translocation rate were calculated relative to that in Dox-treated cells, set as 1. All data are plotted as mean ± SEM. ns, non-significant; *$P < 0.05$; ** $P < 0.01$; *** $P < 0.001$ as compared by ANOVA, Dunnett's post-test relative to Dox-treated cells. The experiments were carried out in at least three biological replicates. Abbreviations: 17-AAG, 17-N-allylamino-17-demethoxygeldanamycin; 3TC, Lamivudine; ABC, abacavir; AML, acute myeloid leukemia; AZT, azidothymidine; CRISPR/Cas9, Clustered regularly interspaced short palindromic repeats/CRISPR-associated nuclease 9; Dox, doxycycline; FTC, emtricitabine; gRNA, guide RNA; HA, homology arms; iMYC-IGH, RPMI8866-derived cell line that inducibly express CRISPR/Cas9 and guide RNAs, targeting both *MYC* and *IGH* loci; iAML1-ETO, RPMI8866-derived cell line that inducibly express CRISPR/Cas9 and guide RNAs, targeting both *AML1* and *ETO* loci; kbp, kilobase pairs; PCR, Polymerase chain reaction; PuroR, puromycin resistance gene.

DNA integrity through reactive oxygen species production and imbalanced deoxynucleoside triphosphate pools [8]. CCR5 governs DNA damage repair (HR and single-strand annealing); consequently, CCR5 inhibitors were shown to sensitize cells to DNA-damaging agents [9]. Defects in HR and c-NHEJ repair mechanisms can result in chromosomal translocations [1]. A phase II clinical study of vicriviroc, a CCR5 antagonist, showed that vicriviroc treatment was associated with an increased risk of developing lymphomas [10]. Vicriviroc was not approved for HIV treatment.

To conclude, we developed CRISPR/Cas9-based cell models with inducible *AML1-ETO* and *MYC-IGH* translocations to evaluate the potential of drugs to favor secondary translocations. In our screen, we identified four drugs, methotrexate, ABC, FTC and TAK779, that increased the rate of chromosomal translocations.

DECLARATIONS

AUTHOR CONTRIBUTIONS

A.S. and N.L. performed the following experiments: cell line creation and characterization, experimental setup, translocation rate analysis, survival analysis, RT-qPCR, western blotting, analyzed data and wrote the paper; D.S. and V.P. performed the following experiments: translocation rate and survival analysis and contributed new reagents; V.V., T.T., D.G. and Y.K. performed the following experiments: translocation rate analysis, RT-qPCR, western blotting; M.S. and M.R. analyzed data; Y.V. designed research, analyzed data and wrote the paper.

ACKNOWLEDGMENTS

This study was supported by Cancéropole IdF, the Koltzov Institute of Developmental Biology, Russian Academy of Sciences Government basic research programs (0088-2021-0007) and the Ministry of Science and Higher Education grants (075-15-2021-1075 to YV and 075-15-2021-1062 and 075-15-2021-1060 to MR); Russian Foundation for Basic Research (19-54-16002) and by the Interdisciplinary Scientific and Educational School of Moscow University «Molecular Technologies of the Living Systems and Synthetic Biology» to MR. AS was supported by the Travel Grant from Boehringer Ingelheim Fonds in 2018.

COMPETING INTERESTS

The authors declare that they have no competing interests

AVAILABILITY OF DATA AND MATERIALS

Methods and materials are available in the supplementary file. All data generated or analyzed during this study are included in this published article and its supplementary information files.

ETHICS APPROVAL AND CONSENT TO PARTICIPATE

Not applicable

CONSENT FOR PUBLICATION

Not applicable

Anna Shmakova[1,2,4]
Nikolai Lomov[1,3]
Vladimir Viushkov[3]
Tatyana Tsfasman[1]
Yana Kozhevnikova[1,5]
Darina Sokolova[6,7,8]
Vadim Pokrovsky[6,7,8]
Marina Syrkina[3]
Diego Germini[1]
Mikhail Rubtsov[3,9]
Yegor Vassetzky[1,2]

[1]*UMR9018, Université Paris-Saclay, Centre national de la recherche scientifique, Gustave Roussy, Villejuif 94805, France*
[2]*Koltzov Institute of Developmental Biology, Russian Academy of Sciences, Moscow 119334, Russia*
[3]*Department of Molecular Biology, Faculty of Biology, Lomonosov Moscow State University, Leninskie Gory, Moscow 119991, Russia*
[4]*Institute of Experimental Cardiology, National Medical Research Centre of Cardiology, Moscow 121552, Russia*
[5]*Faculty of Medicine, Lomonosov Moscow State University, Moscow 119991, Russia*
[6]*Laboratory of Combined Treatment, Blokhin Cancer Research Center, Moscow 115478, Russia*
[7]*Department of Biochemistry, Peoples' Friendship University of Russia, Moscow 117198, Russia*
[8]*Center of Genetics and Life Sciences, Sirius University of Science and Technology, Federal Territory Sirius, Sochi 354340, Russia*
[9]*Department of Biochemistry, Center for Industrial Technologies and Entrepreneurship, Sechenov First Moscow State Medical University, Moscow 119991, Russia*

Correspondence
Yegor Vassetzky, UMR9018, Université Paris-Saclay, Centre national de la recherche scientifique, Gustave Roussy, Villejuif 94805, France.
Email: yegor.vassetzky@cnrs.fr

Anna Shmakova and Nikolai Lomov contributed equally to this paper

ORCID

Anna Shmakova https://orcid.org/0000-0001-7162-074X
Nikolai Lomov https://orcid.org/0000-0003-2101-3479
Yegor Vassetzky https://orcid.org/0000-0003-3101-7043

REFERENCES

1. Lieber MR. NHEJ and Its Backup Pathways: Relation to Chromosomal Translocations. Nat Struct Mol Biol. 2010;17(4):393–5.
2. Saleh K, Michot JM, Camara-Clayette V, Vassetzky Y, Ribrag V. Burkitt and Burkitt-like lymphomas: a systematic review. Curr Oncol Rep. 2020;22(4):33
3. De Kouchkovsky I, Abdul-Hay M. Acute myeloid leukemia: a comprehensive review and 2016 update. Blood Cancer J. 2016;6(7):e441.
4. Shmakova A, Germini D, Vassetzky Y. HIV-1, HAART and cancer: A complex relationship. Int J Cancer. 2020;146(10):2666–79.
5. Scully R., Panday A, Elango R, Willis NA. DNA double-strand break repair-pathway choice in somatic mammalian cells. Nat Rev Mol Cell Biol. 2019;20:698–714.
6. Tanaka K, Oshikawa G, Akiyama H, Ishida S, Nagao T, Yamamoto M, et al. Acute myeloid leukemia with t(3;21)(q26.2;q22) developing following low-dose methotrexate therapy for rheumatoid arthritis and expressing two AML1/MDS1/EVI1 fusion proteins: A case report. Oncology Lett. 2017;14(1):97–102.
7. Olivero OA. Mechanisms of genotoxicity of nucleoside reverse transcriptase inhibitors. Environ Mol Mutagen. 2007;48(3-4):215–23.
8. Koczor CA, Lewis W. Nucleoside reverse transcriptase inhibitor toxicity and mitochondrial DNA. Expert Opin Drug Metab Toxicol. 2010;6(12):1493–1504.
9. Jiao X, Velasco-Velázquez MA, Wang M, Li Z, Rui H, Peck AR, et al. CCR5 Governs DNA Damage Repair and Breast Cancer Stem Cell Expansion. Cancer Res. 2018;78(7):1657–71.
10. Tsibris AMN, Paredes R, Chadburn A, Su Z, Henrich TJ, Krambrink A, et al. Lymphoma diagnosis and plasma Epstein-Barr virus load during vicriviroc therapy: results of the AIDS Clinical Trials Group A5211. Clin Infect Dis. 2009;48(5):642–9.

SUPPORTING INFORMATION

Additional supporting information can be found online in the Supporting Information section at the end of this article.

Cell models with inducible oncogenic translocations allow to evaluate the potential of drugs to favor secondary translocations

Anna Shmakova[1,2,4]*, Nikolai Lomov[1,3]*, Vladimir Viushkov[3], Tatyana Tsfasman[1], Yana Kozhevnikova[1,5], Darina Sokolova[6-8], Vadim S. Pokrovsky[6-8], Marina Syrkina[3], Diego Germini[1], Mikhail Rubtsov[3,9], Yegor Vassetzky[1,2#]

[1]UMR9018, Université Paris-Saclay, Centre national de la recherche scientifique (CNRS), Gustave Roussy, Villejuif 94805, France

[2]Koltzov Institute of Developmental Biology, Russian Academy of Sciences, Moscow 119334, Russia

[3]Department of Molecular Biology, Faculty of Biology, Lomonosov Moscow State University, Leninskie Gory, Moscow 119991, Russia

[4]Laboratory of Molecular Endocrinology, Institute of Experimental Cardiology, Federal State Budgetary Organization National Cardiology Research Center Ministry of Health of the Russian Federation, Moscow 121552, Russia

[5]Faculty of Medicine, Lomonosov Moscow State University, Moscow 119991, Russia

[6]Laboratory of Combined Treatment, N.N. Blokhin Cancer Research Center, Kashirskoe Shosse 24, 115478 Moscow, Russia

[7]Department of Biochemistry, Peoples' Friendship University of Russia, Miklukho-Maklaya Street 6, 117198 Moscow, Russia

[8]Center of Genetics and Life Sciences, Sirius University of Science and Technology, Federal Territory Sirius, 1 Olimpiisky Prospect, 354340 Sochi, Russia

[9]Department of Biochemistry, Center for Industrial Technologies and Entrepreneurship Sechenov First Moscow State Medical University (Sechenov University), Trubetskaya, Moscow 119991, Russia.

*Both authors contributed equally to this paper

[#]Corresponding author: yegor.vassetzky@cnrs.fr

Supplementary materials and methods

1. Plasmids and cloning

The DSB loci in the *AML1-ETO* model were similar to breakpoints in patients with therapy-related AML [1] and in cells treated with etoposide [2]. The DSB loci in the *MYC-IGH* model were similar to breakpoints in patients with sporadic and HIV-induced forms of BL [3,4]. Guide RNAs (gRNAs) targeting *MYC*, *IGH*, *ETO* and *AML1* genes were designed using the online CRISPR Design tool (http://crispr.mit.edu, Zhang Lab, Massachusetts Institute of Technology [5]) (**Supplementary Table S1**) and cloned into the phU6-gRNA plasmid (Addgene, Watertown, Massachusetts, #53188, [6]) digested by the BstV2I restriction enzyme. Cas9/gRNAs DNA cutting efficacy was confirmed by the ENIT method based on detection of translocatoins as described previously [7]. gRNA genes from phU6-gRNA plasmids were amplified by PCR (primer sequences are listed in **Supplementary Table S2**) and were subsequently cloned into Puro-Cas9 donor plasmid (Addgene #58409, [8]) with puromycin resistance gene in the SalI restriction site. Plasmids were assembled using Gibson Assembly Master Mix kit (NEB, Ipswich, Massachusetts, USA). Primers for insert amplification were designed according to the NEB Gibson Assembly protocol. PCR products were purified using NucleoSpin® Gel or PCR Clean-up PCR kit (Macherey-Nagel, Düren, Germany).

2. Cell lines

Human Epstein-Barr virus (EBV)-transformed lymphoblastoid cell line RPMI8866 (American Type Culture Collection) was used in the study. RPMI8866 cells were cultured in RPMI 1640, supplemented with 10% certified tetracycline-free fetal bovine serum (Takara, Tokyo, Japan), 2 mmol/L-Glutamine, 1 mmol/L sodium pyruvate, 20 mmol/L glucose, 100 U/mL penicillin and 100 μg/mL streptomycin (all reagents except Tet-free FBS are from Gibco®, Thermo Fisher Scientific, Waltham, Massachusetts, USA).

RPMI8866 cells were co-electrotransfected with the Puro-Cas9-gRNA plasmid, containing puromycin resistance, Tet-inducible Cas9 and gRNAs genes, and homology arms for AAVS1 site, AAVS1-Neo-M2rtTA plasmid containing neomicin resistance and tetracycline transactivator (TA) genes and homology arms for AAVS1 site

(Addgene, #60843) and two TALEN plasmids for cutting in the safe-harbor AAVS1 site (AAVS1-TALEN-L+ AAVS1-TALEN-R) (Addgene # 59025 and # 59026) using a protocol developed in our laboratory [9]. RPMI8866 cells with inducible Cas9 expression and gRNAs to *MYC* and *IGH* (iMYC-IGH cell line) or *AML1* and *ETO* loci (iAML1-ETO cell line) were created. The cells were maintained in the RPMI 1640 medium, supplemented with 10% certified tetracycline-free fetal bovine serum (Takara), 100 U/mL penicillin, 100 μg/mL streptomycin, and 800 μg/mL G418 antibiotic for 10 days. The cells were subsequently transferred into the medium with 0.3 μg/mL puromycin (Sigma-Aldrich, Burlington, MA, USA) and were cultured for 4 days. Resistant cells were cloned via finite dilution technique in a 96-well plate. Clones and bulk lines were grown with and without 1 μg/mL doxycycline (Dox, Sigma-Aldrich) for 48h and then tested for the presence of specific translocations.

3. Drug treatment

To assess the effect of various drugs on translocation formation, drugs were added to the cell medium simultaneously with the induction of Cas9 expression (Dox treatment). Since the peak of translocation rate was 48 hours for *MYC-IGH* cell line and 96 hours for *AML1-ETO* cell line (data not shown), *MYC-IGH* cells were treated for 48 hours, *AML1-ETO* cells were treated for 96 hours. After indicated times cells were collected, DNA was extracted and tested for the presence of specific translocations by qPCR. In each experiment negative control (non-treated with Dox cells) and cells treated with Dox only were present. The translocation rate in drug+Dox-treated cells was normalized to the translocation rate in Dox-treated cells within the same experiment in at least 3 biological replicates. The list of drugs and their concentrations is presented in **Supplementary Table S3**. Antiretroviral therapy (ART) drugs were used at the concentrations that correspond to IC_{50} for virus inhibition, chemotherapeutic drugs were used at the concentrations that correspond to IC_{10} to ensure that cells survive the treatment. ART drugs were obtained through the National Institutes of Health (NIH) HIV Reagent Program, Division of Acquired immunodeficiency syndrome (AIDS), National Institute of Allergy and Infectious Diseases (NIAID), NIH. Chemotherapeutic agents were purchased from Accord (Lille, France), Sigma-Aldrich, Veropharm (Moscow, Russia), Teva (Petah Tikva, Israel), Bristol-Myers Squibb (New York, New York, USA), EBEWE Pharma (Unterach am Attersee, Austria), AstraZeneca (Cambridge, United Kingdom), Sanofi (Paris, France) (**Supplementary Table S3**).

4. Cell survival analysis

Cytotoxic activity of the drugs and cell survival was evaluated by cell counting using TC 20^{TM} Automated Cell Counter (Bio-Rad, Hercules, California, USA) and methylthiazolyltetrazolium (MTT) test as described earlier [10]. Briefly, cells were seeded at equal densities and treated with different drugs. After treatment (48 hours for iMYC-IGH line and 96 hours for iAML1-ETO line, which corresponds to the peak of detected translocations) 100 µL of cell suspension was incubated with 0.1 mg of MTT (5 mg/mL, Merck Millipore, Manassas, Virginia, United States, USA) for 2 hours at 37°C in the dark and then lysed in 100 µL of lysing buffer (25 mmol/L HCl, 2% acetic acid, 3% dimethylformamide (DMF), 5% sodium dodecyl sulfate (SDS), pH 4.7). The absorbance at 570 nm was measured using plate reader Infinite F200 PRO (Life Sciences, Tecan, Germany). Each sample was tested in two technical replicates and the mean absorbance was taken into consideration. The cell survival was calculated relative to non-treated cells.

5. Quantitative PCR for translocation quantitation

Genomic DNA was extracted using the Nucleospin® Tissue kit (Macherey-Nagel) according to the manufacturer's protocol. To detect *MYC-IGH* translocation, qPCR amplification was performed using the PowerUp SYBR Green Master Mix (Thermo Fisher Scientific) with the following cycling conditions: 1 cycle of 50°C (2min), 95°C (2min); 40 cycles 95°C (15s), annealing at 60°C or 64°C (1min), 72°C (1min); 1 cycle 72°C (10min). Genomic DNA (500 ng) was used for the reaction, all reactions were performed in triplicates. Primers surrounding the translocation breakpoint were designed to detect *MYC-IGH* translocation (MYC1 and IGH1); primers that target MYC region ~6.8 kbp away from the translocation breakpoint (MYC2 and MYC3) were used as a control of DNA load. Primer sequences are listed in **Supplementary Table S2**. The $2^{-\Delta\Delta Ct}$ method was used for the quantification of translocation rate.

To detect *AML1-ETO* translocation, qPCR amplification was performed using the TaqMan probe with the following cycling conditions: 1 cycle of 95°C (5min); 40 cycles includes melting at 95°C (30s), annealing at 58°C (1min), elongation at 72°C (15 s); 1 µg of genomic DNA measured by Qubit Fluorometer (Thermo Fisher Scientific) was used in 25 µL reaction, all reactions were performed in triplicates. Primers surrounding

the translocation breakpoint were designed to detect *AML1-ETO* translocation (AML1 and ETO1) and TaqMan probe (FAM—CCCAGCAGAATAGGCCCACTGGAGCCCA—BHQ1). pUC18-based plasmid containing *AML1-ETO* PCR product was created for the quantification of translocation rate and for the amplification efficiency determination with the standard curve method.

6. RNA extraction, cDNA synthesis and RT-qPCR

In cases when both DNA and RNA are isolated from the cells, extraction was performed with TRIzol reagent according to the manufacturer's protocol (Invitrogen, Thermo Fisher Scientific, Waltham, Massachusetts, USA). Prior to reverse transcription, DNA impurities were removed from RNA using DNase I (Thermo Fisher Scientific). Reverse transcription was performed using reverse transcriptase RevertAid H minus (Thermo Fisher Scientific) according to the manufacturer's protocol.

For RT-qPCR, Maxima SYBR Green qPCR Master mix and PowerUp SYBR Green Master Mix (Thermo Fisher Scientific) were used. qPCR was performed using the CFX96 instrument (Bio-Rad Laboratories, Hercules, California, USA) was used. As an additional check of specificity, reaction products were analyzed by agarose gel electrophoresis. The primer sequences used for qPCR are shown in **Supplementary Table S2**. qPCR was performed according to the following protocol: 95°C for 10 min, 40 cycles of 95°C 15s, 60°C 20s, 72°C 30 s. Primer amplification efficiencies were first determined as described in [11]. They were 1.93 for Cas9 F+R and 1.89 for TA F+R. The expression of Cas9 and TA genes was normalized to the expression of the *GAPDH* gene. Each reaction was set in triplicate. All experiments were carried out in three biological replicates. Expression analysis was carried out in accordance with the method described in [11].

7. Protein extraction, electrophoresis and Western blotting

Cells were harvested from culture dishes and centrifuged at 4°C for 10 minutes at 800 g, supernatant was discarded, and cell pellets were washed with ice-cold phosphate-buffered saline (PBS, Sigma). PBS was then aspirated and cells were lysed in 150 µL of ice-cold NETN buffer (NaCl 150 mmol/L, ethylenediaminetetraacetic acid (EDTA) 1 mmol/L, Tris pH 7.5 50 mmol/L, NP40 0.5%, 1× protease inhibitor cocktail; Roche, Basel, Switzerland). The lysates were sonicated 10 seconds at 30% of intensity to completely lyse cells using a Vibra Cell sonicator (SONICS & MATERIALS, Inc.,

Newtown, CT, USA), incubated on ice for 30 minutes and centrifuged at 4°C for 20 minutes at 16,000 g. The supernatant was transferred into a new pre-cooled microcentrifuge tube and the cell pellet was discarded. The supernatant (5 µL) diluted 1:10 was used for quantification of protein concentration by BCA assay (Thermo Fisher Scientific). Finally, after measuring the concentration, the lysates were dissolved in the 6× Laemmli buffer with dithiothreitol (DTT) and heated at 95°C for 10 min.

Proteins (20 µg) were resolved in 10% SDS-polyacrylamide gel electrophoresis (SDS-PAGE) gels and transferred to polyvinylidene fluoride (PVDF) membrane (GE Healthcare, Chicago, Illinois, USA) in a transfer buffer (25 mmol/L Tris, 192 mmol/L glycine, 20% ethanol). PageRuler Prestained PLus Protein Ladder (Thermo Fisher Scientific) was used as a molecular weight marker. Nonspecific binding was blocked in 5% non-fat dried milk diluted in Tris-buffered saline (TBS), containing 0.1% Tween-20 at 4°C overnight. Proteins were probed with the following primary antibodies: mouse anti-Cas9 (1:200 dilution, #sc-517386, Santa Cruz, Dallas, Texas), mouse anti-FLAG M2 (1:200 dilution, # F3165, Sigma-Aldrich), mouse anti-β-actin (1:1000 dilution, control of protein load, #sc-81178, Santa Cruz), for 2h at 22 °C. First, the membranes were washed with TBS, containing 0.1% Tween-20, incubated with appropriate peroxidase-conjugated secondary antibodies (Invitrogen) (in 1:2000 dilution) at 22 °C for 2h, and washed in TBS afterwards (containing 0.1% Tween-20). Proteins were visualized using Immobilon Western Chemiluminescent HRP Substrate (Millipore) and ImageQuant LAS 4000 mini (GE Healthcare) for Western blotting imaging and analysis.

8. Statistical analyses

The data presented in the study are based on results from at least three independent experiments with three technical replicates for each. All statistical tests were performed using the Graphpad Prism 9 software (GraphPad software Inc., La Jolla, CA, USA). The inhibitory concentrations IC_{50}, IC_{25} and IC_{10} were calculated by nonlinear regression curve. One-way analysis of variance (ANOVA) test followed by Dunnett's post-hoc test was used to compare averages between different groups relative to the Dox-treated group. Data are presented as mean ± standard error of mean (SEM).

References

[1] Smith KA, Cowell IG, Zhang Y, Sondka Z, Austin CA. The role of topoisomerase II beta on breakage and proximity of RUNX1 to partner alleles RUNX1T1 and EVI1. *Genes Chromosomes Cancer*. 2014; **53**(2): 117– 28.

[2] Kantidze OL, Razin SV. Chemotherapy-related secondary leukemias: A role for DNA repair by error-prone non-homologous end joining in topoisomerase II - Induced chromosomal rearrangements. *Gene*. 2007; **391**(1-2): 76– 9.

[3] Blum KA, Lozanski G, Byrd JC. Adult Burkitt leukemia and lymphoma. *Blood*. 2004; **104**(10): 3009– 20.

[4] Gibson TM, Morton LM, Shiels MS, Clarke CA, Engels EA. Risk of non-Hodgkin lymphoma subtypes in HIV-infected people during the HAART era: a population-based study. *AIDS*. 2014; **28**(15): 2313– 8.

[5] Hsu PD, Scott DA, Weinstein JA, Ran FA, Konermann S, Agarwala V, et al. DNA targeting specificity of RNA-guided Cas9 nucleases. *Nat Biotechnol*. 2013; **31**(9):827- 32.

[6] Kabadi AM, Ousterout DG, Hilton IB, Gersbach CA. Multiplex CRISPR/Cas9-based genome engineering from a single lentiviral vector. *Nucleic Acids Res*. 2014; **42**(10):e147.

[7] Germini D, Bou Saada Y, Tsfasman T, Osina K, Robin C, Lomov N et al. A One-Step PCR-Based Assay to Evaluate the Efficiency and Precision of Genomic DNA-Editing Tools. *Mol Ther Methods Clin Dev*. 2017; **5**: 43–50.

[8] González F, Zhu Z, Shi Z, Lelli K, Verma N, Li QV, et al. An iCRISPR platform for rapid, multiplexable, and inducible genome editing in human pluripotent stem cells. *Cell Stem Cell*. 2014; **15**(2):215- 26.

[9] Canoy RJ, André F, Shmakova A, Wiels J, Lipinski M, Vassetzky Y et al. Easy and robust electrotransfection protocol for efficient ectopic gene expression and genome editing in human B cells. *Gene Ther*. 2020. doi:10.1038/s41434-020-00194-x.

[10] van Meerloo J, Kaspers GJL, Cloos J. Cell sensitivity assays: the MTT assay. *Methods Mol Biol*. 2011; **731**: 237– 45.

[11] Pfaffl MW. A new mathematical model for relative quantification in real-time RT-PCR. *Nucleic Acids Res*. 2001; **29**(9): e45.

Supplementary Tables

Supplementary Table S1. gRNA sequences.

Target loci	**Sequence 5'→3'**	**Position**
AML1 (RUNX1)	GACTCCCCCATGTACCCCTA	intron 5
ETO (RUNX1T1)	GATGTAAGAGGAAGCAGCTT	intron 1
IGH	GAGAACATACCAAGCCCCAC	4.8 kb upstream *IGH* constant μ locus
MYC	TGCACCTCGGACGCTCCTGC	1.4 kb upstream 1 exon

Abbreviations: gRNA: guide RNA.

Supplementary Table S2. List of primer sequences used in the study.

Target gene	**Sequence 5'->3'**	**Annealing temperature (°C)**
Primers for gRNA genes amplification from phU6-gRNA plasmids		
gRNA_U6-f	TGGTATGGCTGATTATGATCCTC TAGAGATATCGAGGGCCTATTTC CCATGATTCCTTC	64
gRNA_U6-r	CGCGTGCTAGCGCGGCCGCATC GATAAGCTTGAAAAAAAGCACC GACTCGGTGCCAC	64
gRNA_fus-f	AAGTGGCACCGAGTCGGTGCTT TTTTTGAGGGCCTATTTCCCATG ATTCCTTCATATTTG	64
gRNA_fus-r	GAAGGAATCATGGGAAATAGGC CCTCAAAAAAAGCACCGACTCG GTGCCACTTTTTCAAG	64
Primers for translocation detection		
MYC1 (translocation primer)	GCGTTCAGGTTTGCGAAAGTA	64
IGH1 (translocation primer)	TCCCCTCCCTTCTGAGTCTGC	64
MYC2 (~6.8 kbp downstream the breakpoint)	AAGGTCAGAGTCTGGATCAC	60

MYC3 (~6.8 kbp downstream the breakpoint)	TAACTACCTTGGGGGCCTTT	60
ETO1	TGCATGAACATAAACAGGCACTC	58
AML1	GAAGCTCACCAGATAGGCTGTA	58
Primers for RT-qPCR		
Cas9 F	CCGAAGAGGTCGTGAAGAAG	60
Cas9 R	GCCTTATCCAGTTCGCTCAG	60
TA F	AAATCAGCTCGCGTTCCTGT	60
TA R	CGCTTTCGCACTTTAGCTGT	60
GAPDH F	CAAGGTCATCCATGACAACTTTG	60
GAPDH R	GTCCACCACCCTGTTGCTGTAG	60

Abbreviations: gRNA: guide RNA; RT-qPCR: reverse transcription – quantitative PCR.

Supplementary Table S3. Cell treatments.

Drug	**Company**	**Mechanism of action**	**Working concentration**
ART			
Abacavir (ABC)	NIH ARP	NRTI	6 µmol/L
Amprenavir	NIH ARP	PI	0.4 µmol/L
Atazanavir sulfate	NIH ARP	PI	5 nmol/L
AZT	NIH ARP	NRTI	0.4 µmol/L
Emtricitabine (FTC)	NIH ARP	NRTI	0.64 µmol/L
Indinavir sulfate	NIH ARP	PI	100 nmol/L

Lamivudine (3TC)	NIH ARP	NRTI	15 µmol/L
Nevirapine	NIH ARP	NNRTI	100 nmol/L
Rilpivirine	NIH ARP	NNRTI	9.2 µmol/L
Saquinavir	NIH ARP	PI	30 nmol/L
TAK-779	NIH ARP	CCR5 antagonist	200 nmol/L
Chemotherapy			
Carboplatin	Accord	DNA crosslinks and lesions	For iMYC-IGH: 15 µmol/L For iAML-ETO: 270 nmol/L
Cisplatin	Accord	DNA crosslinks and lesions	For iMYC-IGH: 0.1 µmol/L For iAML-ETO: 24 nmol/L
Cytarabine	Sigma	Antimetabolite and nucleoside analog	0.01 nmol/L
Docetaxel	Accord	Microtubule suppression	0.1 nmol/L
Doxorubicin	Teva	DNA intercalation, topoisomerase II inhibitor	3 nmol/L
Etoposide	Teva	Topoisomerase II inhibitor	2 nmol/L
Fluorouracil	Accord	Antimetabolite, thymidylate synthase inhibitor	3 µmol/L
Ifosfamide	Veropharm	Alkylating agent and nitrogen mustard	35.6 µmol/L

Irinotecan	Veropharm	Topoisomerase I inhibitor	15.5 nmol/L
Methotrexate	EBEWE PHARMA	Antimetabolite of the antifolate type	2.9 nmol/L
Mitoxantrone	Accord	Topoisomerase II inhibitor	5 nmol/L
Olaparib	AstraZeneca	PARP inhibitor	3 µmol/L
Oxaliplatin	Sanofi	DNA crosslinks and lesions	7 nmol/L
Paclitaxel	Bristol-Myers Squibb	Cytoskeletal drug (tubulin)	4.7 pmol/L
Inhibitors			
Mirin	Calbiochem	MRE11 inhibitor	25 µmol/L
NU7026	Sigma Aldrich	DNA-Pk inhibitor	20 µmol/L
17-AAG	Apexbio	Hsp90 inhibitor	10 µmol/L
L67	Sigma Aldrich	DNA ligase I and III inhibitor	25 µmol/L
KU-55933	Sigma Aldrich	ATM inhibitor	10 µmol/L

Abbreviations: 3TC: lamivudine; ABC: abacavir; ART: antiretroviral therapy; ATM: ataxia telangiectasia mutated; AZT: azidothymidine; CCR5: C-C Motif Chemokine Receptor 5; DNA-Pk: DNA-dependent protein kinase; FTC: emtricitabine; Hsp90: heat shock protein 90; iAML1-ETO: RPMI8866-derived cell line that inducibly express CRISPR/Cas9 and gRNAs, targeting both AML1 and ETO loci; iMYC-IGH: RPMI8866-derived cell line that inducibly express CRISPR/Cas9 and gRNAs, targeting both MYC and IGH loci; MRE11: meiotic recombination 11; NIH ARP: NIH AIDS Reagent Program; NNRTI: non-nucleoside reverse transcriptase inhibitors; NRTI: nucleoside analog reverse-transcriptase inhibitors; PARP: poly (ADP-ribose) polymerase; PI: protease inhibitors.

Supplementary figures

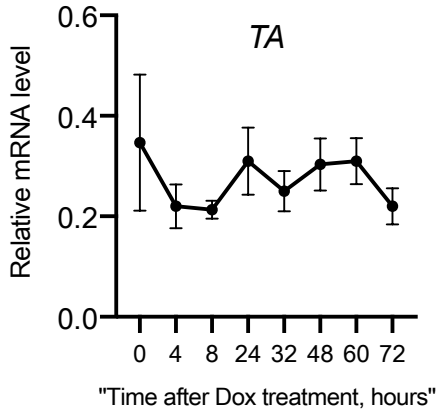

Supplementary Figure S1. Kinetics of tetracycline activator (TA) expression as analyzed by RT-qPCR. The mRNA level was normalized to *GAPDH* expression as a housekeeping gene. Data are plotted as mean±SEM.

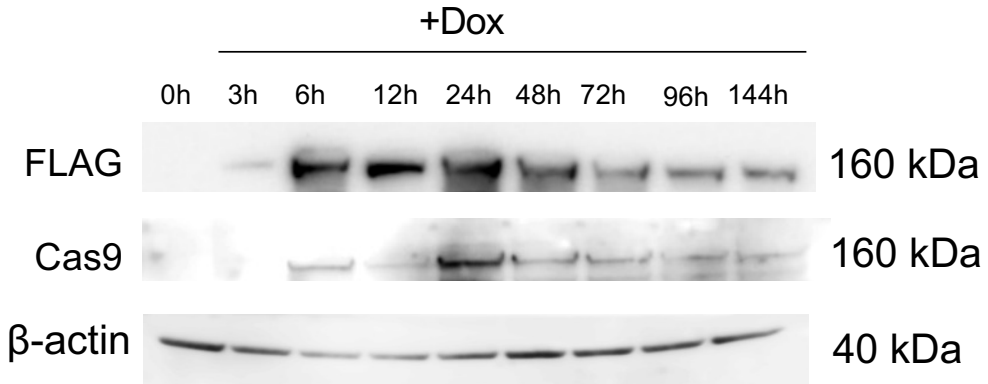

Supplementary figure S2. Kinetics of Cas9 expression as analyzed by Western blottting and revealed by either FLAG or anti-Cas9 antibodies. β-actin was used as a control of protein load. The experiments were carried out in triplicate. A representative result is presented.

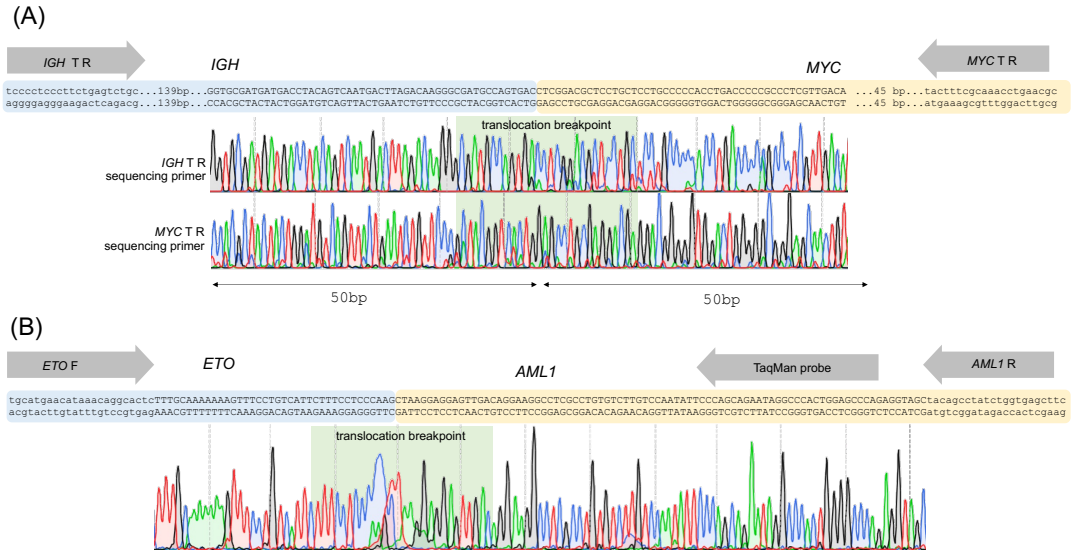

Supplementary figure S3. Sanger sequencing of *MYC-IGH* (A) and *AML1-ETO* (B) translocation regions amplified by PCR and their alignment to respective genes.

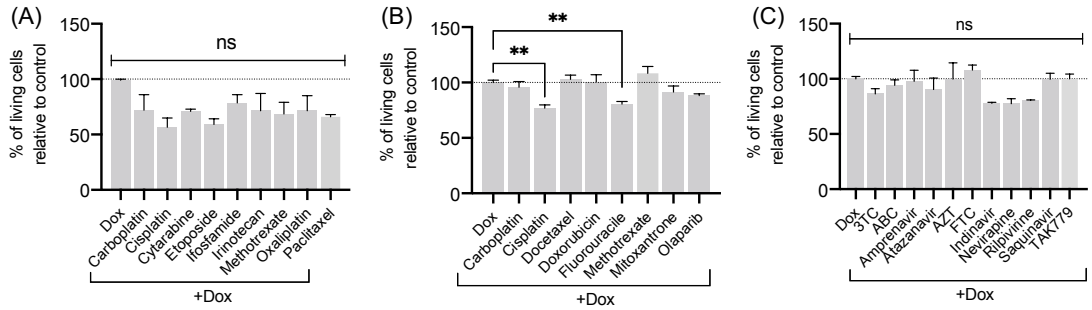

Supplementary figure S4. Cell survival 48 hours after indicated treatments relative to control (Dox-treated) cells. (A) iAML1-ETO or (B-C) iMYC-IGH cells cells were simultaneously treated either with Dox to induce the expression of Cas9 and gRNAs, or with (A-B) chemotherapeutic or (C) ART drugs and Dox. Chemotherapeutic drugs were added at IC_{10} concentration. ns, non-significant; $^{**}p<0.01$; as compared by ANOVA, Tukey's post-test. The experiments were carried out in at least two biological replicates.

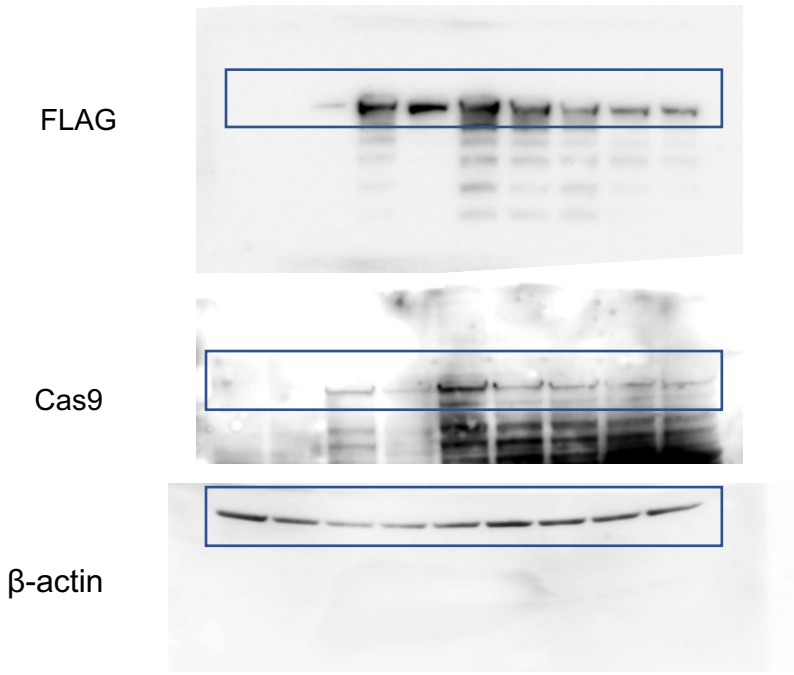

Supplementary figure S5. Original Western blotting images.

BL is an aggressive B cell non-Hodgkin lymphoma. 80% cases of BL are associated with a specific chromosomal translocation t(8;14) (q24;q32) which relocates the oncogene *MYC* (8q24) near regulatory regions of the immunoglobulin heavy chain gene locus (*IGH*; 14q32) resulting in *MYC* overexpression (Boerma et al. 2009). In Europe and the US, BL is sporadic or associated with HIV, and people living with HIV develop BL 20 times more often than the general population even in the era of cART (Hernández-Ramírez et al. 2017; Shmakova et al. 2020).

The secondary effects of drugs in provoking cancer-related translocations are quite elusive, due to the delay between drug application and tumour detection. Screening of drugs for their potential translocation-inducing activity *in vitro* or *ex vivo* is next to impossible due to the sporadic and rare nature of translocations. In the current study, we devised experimental CRISPR/Cas9-based screening systems to reveal drugs that could stimulate or prevent the occurrence of AML- and BL-like translocations. The system is based on the lymphoblastoid cell line RPMI8866 with the inducible expression of Cas9 and gRNAs that target either *AML1* and *ETO* or *MYC* and *IGH* loci. gRNAs were chosen to target the gene regions that correspond to actual breakage points in patients with AML and BL. Following Cas9 and gRNAs induction, DSBs were introduced in target loci; this initiated the formation of specific *AML1-ETO* or *MYC-IGH* chromosomal translocations in a part of cells that could easily be detected and quantified by qPCR.

NHEJ and HR represent two conceptually different pathways for repairing DSBs. NHEJ is the major DSB repair pathway active all throughout the cell cycle whereas HR is only essential for the repair of ~15-20% of DSBs in the S/G2 cell cycle phase (Jasin & Rothstein 2013; Shibata et al. 2011). Both the c-NHEJ (dependent on DNA-dependent protein kinase (DNA-PK) and ligase 4 (Lig4)) and a-NHEJ (mediated by the CtBP-interacting protein (CtIP), poly[ADP-ribose] polymerase 1 (PARP1), and ligase 1/3 (Lig1/Lig3)) repair pathways can result in translocation formation; precise repair of DSBs that restores original DNA structure is only ensured by Rad51-mediated HR (Iliakis et al. 2015; Jasin & Rothstein 2013; Lieber et al. 2010). In our model, the inhibition of MRE11 and ataxia-telangiectasia mutated (ATM), involved in the early steps of DNA damage detection and response within NHEJ and HR (Lee & Paull 2021; Stracker & Petrini 2011), results in a significant decrease in translocation formation (**Figure 8**). Presumably, the inhibition of MRE11 exonuclease activity by mirin and ATM kinase activity by KU-55933 results in DSB repair defect (Frit et al. 2014; Shibata et al. 2014; Zhang et al. 2015) and ultimately cell cycle arrest or death, which decreases the overall yield of translocations. ATM also promotes the clustering of DSBs into large repair foci (Caron et al. 2015), which might contribute to DSB proximity and translocations. We have recently shown that loci proximity after DSB is a key factor driving the formation of chromosomal translocations (Canoy et al. 2023). c-NHEJ is a predominant DSB

repair pathway throughout the cell cycle and it largely suppresses genome instability. In turn, blockade or delay in c-NHEJ results in the manifestation of a backup a-NHEJ that often mediates the illegitimate repair, joining different chromosomes to generate chromosomal translocations (Boboila et al. 2012). In our model, the inhibition of DNA-PK (c-NHEJ pathway) significantly increased the frequency of translocations, while the inhibition of DNA ligase I and III (a-NHEJ pathway) significantly decreased the frequency of translocations (**Figure 8**), which is in agreement with the previous studies that reported that in rodent and human cells, chromosome translocations are mainly formed by the a-NHEJ pathway (Boboila et al. 2010; Simsek & Jasin 2010; Soni et al. 2015; Zhang & Jasin 2011). Although, several studies suggest that a subset of chromosomal translocations may be generated through the c-NHEJ pathway (Ghezraoui et al. 2014; Zagelbaum et al. 2023). The increased frequency of translocations, when c-NHEJ is abrogated, can be explained by the slow kinetics of DNA repair *via* a-NHEJ, which is ~10-fold slower than c-NHEJ. This permits the free movement of unrepaired DNA ends, increasing the chance to meet their translocation partner in the 3D-nuclear space (Lieber 2010b). This was recently confirmed by Zagelbaum et al., who observed that the inhibition of DNA-PK drastically increases DSB clustering upon DNA damage (Zagelbaum et al. 2023).

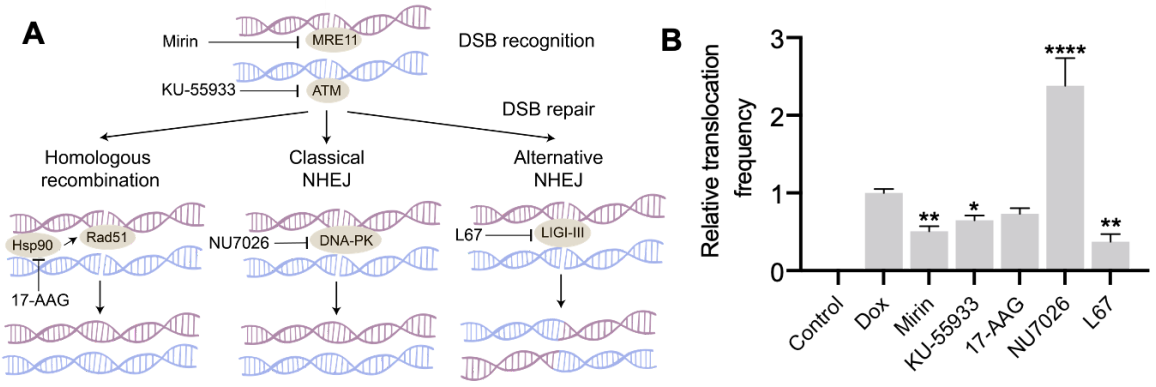

Figure 8. DSB repair pathways involved in chromosomal translocation formation. (A) General overview of DSB repair pathways and targets of the inhibitors used in the study. (B) Effect of DNA repair inhibitors on the *MYC-IGH* translocation rate in iMYC-IGH cells. Cells were simultaneously treated with doxycycline (Dox) and the indicated inhibitor or left untreated (control) for 48h and translocations were detected by qPCR. t(8;14) rate fold changes are calculated after normalisation to the *MYC* gene in comparison to the t(8;14) level in Dox-treated cells, set as 1. All data are plotted as mean±SEM. ns, non-significant; *p<0.05; **p<0.01; ***p<0.001; ****p<0.0001 as compared by ANOVA, Dunnetts's post-hoc test relative to Dox-treated cells. The experiments were carried out in at least three biological replicates. Abbreviations: Dox, doxycycline; DSB, double-strand break; NHEJ, non-homologous end joining.

We next proceeded with the analysis of whether some of the commonly used antiretroviral drugs might influence the frequency of *MYC-IGH* chromosomal

translocations in our cellular systems. We found that two nucleoside/nucleotide reverse transcriptase inhibitor (NRTI) drugs, abacavir (ABC) and emtricitabine (FTC), as well as CCR5 antagonist TAK-779, significantly increased the frequency of *MYC-IGH* translocations (**Figure 9**). The precise mechanisms through which these drugs may impact the formation of *MYC-IGH* chromosomal translocations following the induction of DSBs are yet to be fully understood. NTRIs are known to be incorporated into nuclear DNA by certain DNA polymerases during DNA repair and can act as chain terminators; they can also directly inhibit cellular DNA polymerases by binding in their catalytic site (Brown et al. 2011; Crespan et al. 2011; Olivero 2007). Compromised DNA damage response may result in delays of classical repair machinery and engage translocation-prone a-NHEJ. Furthermore, mitochondrial toxicity of NRTIs could affect nuclear DNA integrity through ROS production and imbalanced deoxynucleotide triphosphate (dNTP) pools (Brinkman et al. 1998; Koczor & Lewis 2010; Lewis et al. 2001; Lu et al. 2009; Macchi & Mastino 2002). CCR5 governs DNA damage repair (HR and single-strand annealing), consequently, CCR5 inhibitors were shown to sensitise cells to DNA-damaging agents (Jiao et al. 2018). Defects in HR and c-NHEJ repair mechanisms can result in DNA lesions, including chromosomal translocations (Richardson & Jasin 2000). Notably, a phase II clinical study of vicriviroc, a CCR5 antagonist, has shown that vicriviroc treatment can be associated with the increased risk of developing lymphomas (two cases of Hodgkin lymphoma and two cases of diffuse large B cell lymphoma were observed in vicriviroc group, genetic lesions were not characterised) (Gulick et al. 2007; Tsibris et al. 2009). Later studies, however, showed that the malignancy incidence was not increased in the vicriviroc group (Caseiro et al. 2012). Vicriviroc was not approved for HIV treatment.

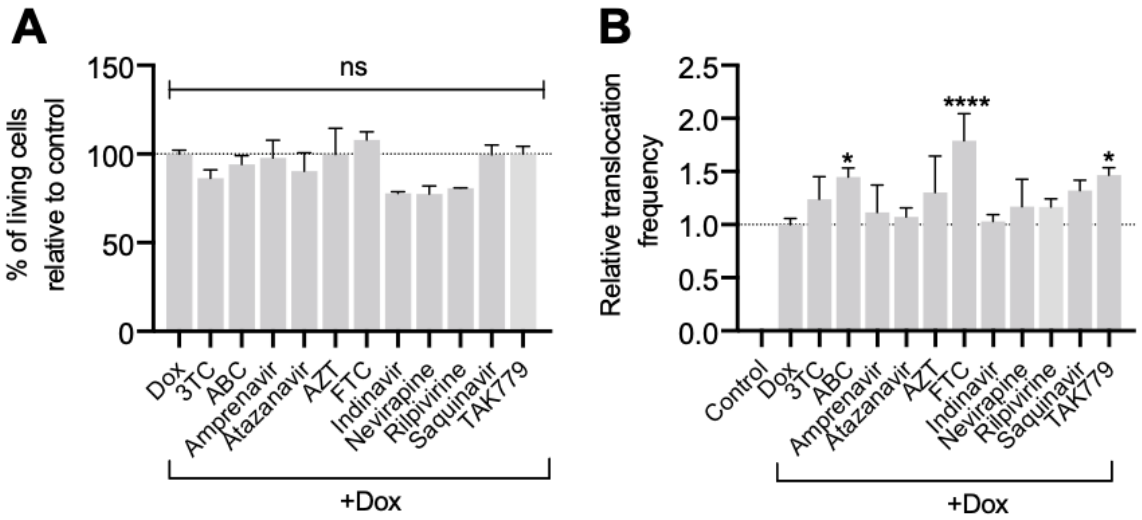

Figure 9. The effect of antiretroviral drugs on t(8;14) formation rate. (A) Cell survival 48 hours after indicated treatments relative to control (non-treated) cells. (B)

iMYC-IGH cells were simultaneously treated either with doxycycline (Dox) to induce the expression of Cas9 and gRNAs targeting *MYC* and *IGH*, or with chemotherapeutic drugs and Dox, or left untreated (control). 48 hours later DNA was collected and the frequency of t(8;14) was measured by qPCR. t(8;14) rate fold changes are calculated by the $2^{-\Delta\Delta Ct}$ method after normalisation to the *MYC* gene (~6.8 kbp downstream the translocation breakpoint) and relative to t(8;14) level in Dox-treated cells, set as 1. All data are plotted as mean±SEM. ns, non-significant; *p<0.05; **p<0.01; ***p<0.001; ****p<0.0001 as compared by ANOVA, Dunnetts's post-hoc test relative to Dox-treated cells. The experiments were carried out in at least three biological replicates. Abbreviations: 3TC, lamivudine; ABC, abacavir; AZT, azidothymidine; Dox, doxycycline; FTC, emtricitabine; gRNA, guide RNA.

People living with HIV develop BL 20 times more often than the general population, and the incidence of BL has not decreased in the era of cART (Hernández-Ramírez et al. 2017; Shmakova et al. 2020). An intriguing possibility is that the usage of certain cART drugs in people living with HIV might indeed affect the incidence of BL and other translocation-caused lymphomas/leukaemias. Many epidemiological studies exploring cancer incidence in people living with HIV have a common limitation: they lack the precise information on antiretroviral therapy used by people living with HIV to address the question about the effect of particular cART drug and their dosage on cancer incidence, this requires further exploration.

This CRISPR/Cas9-based system opens new avenues for systematically identifying other drugs that could potentially heighten the risk of chromosomal translocation formations. Equally promising is the system's capability to function as a screening tool for identifying drugs that possess the ability to decrease the frequency of chromosomal translocation formation. Thus, it can be used as a platform for discovering compounds with translocation-inhibiting properties.

To conclude, in the current study, we developed CRISPR/Cas9-based cell models with inducible *AML1-ETO* and *MYC-IGH* translocations. We examined whether common antiretroviral drugs could influence translocation formation. Two NRTIs, ABC and FTC, CCR5 antagonist TAK779, were found to significantly increase the rate of *MYC-IGH* translocations. In addition to antiretroviral therapy, chemotherapy is a risk factor for secondary AML. Among the chemotherapeutic drugs tested, methotrexate was found to increase the rate of *AML1-ETO* translocations.

In summary, factors contributing to B cell lymphomagenesis in people living with HIV may include the use of specific antiretroviral drugs (ABC, FTC, and TAK779) and methotrexate as part of chemotherapy for other conditions. Understanding these factors can help identify individuals at higher risk and guide personalised treatment strategies to minimise lymphoma development in people living with HIV. Certainly, further clinical and epidemiological studies

are required to assess the incidence of BL and AML in patients exposed to these medications.

3.1.2 EBV reactivation promotes Burkitt's-lymphoma-associated t(8;14) translocation in B cells

EBV reactivation is a common phenomenon observed in people living with HIV, and it is associated with an increase in EBV viral loads in both saliva and blood (Ling et al. 2003; Rahman et al. 1991; Yan et al. 2018). To corroborate this data, we analyzed the dynamics of EBV reactivation in a cohort of asymptomatic individuals living with HIV who were under cART (n = 15, **Table 5**). The average age was 58±3.26 years, 5/15 (33%) individuals were female. The patient cohort exhibited a mean CD4+ T-cell count of 557.9±47.48 cells/mm^3 and only 3/15 (20%) individuals had detectable levels of HIV plasma RNA (mean of 12.13 ± 7.742 copies per ml), indicating a robust immune profile and effective control of HIV infection exerted by cART for the majority of individuals in the studied cohort. Notably, EBV reactivation, evidenced by detectable PCR EBV, was observed in 8/15 (53%) of asymptomatic individuals living with HIV treated with cART with a mean log value of 2.949± 0.156 among individuals with detectable EBV PCR and 1.573±0.401 in the whole cohort. Thus, EBV reactivation may be common in asymptomatic individuals with HIV under cART. Strikingly, no correlation was found between EBV reactivation and CD4+ T-cell counts (r = 0.1545, p = 0.5787) or HIV viral loads (r = 0.4768, p = 0.1223) (**Figure 10**), indicating that EBV reactivation does not correlate with immune suppression in patients with controlled HIV infection. These findings challenge the notion that EBV reactivation solely arises in the context of compromised immunity associated with HIV infection and suggest that other factors might play a role in EBV reactivation from latency. This prompted us to investigate the potential consequences of EBV reactivation for B cell pathology.

Table 5. Characteristics of asymptomatic cART-treated people with HIV.

Patient	Age	Sex	CD4+ T cells (/mm^3)	Plasma HIV RNA (Log_{10} copies/ml)	cART start date	Log PCR EBV in whole blood
1	69	M	656	108	1997	3.2
2	47	M	816	<20	2015	<2,18
3	48	M	727	<20	2012	3.07
4	69	F	391	<20	2015	<2,18
5	29	F	563	<20	2020	<2,18
6	70	F	757	<20	2008	<2,18

7	47	F	644	<20	2010	2.61
8	57	M	336	51	2014	3.18
9	69	M	366	<20	1995	<2,26
10	77	M	374	<20	2003	<2,26
11	59	M	499	23	1995	2.33
12	46	F	475	<20	2008	<2,26
13	61	M	359	<20	2011	2.86
14	59	M	905	<20	2021	3.73
15	63	M	500	<20	2000	2.61

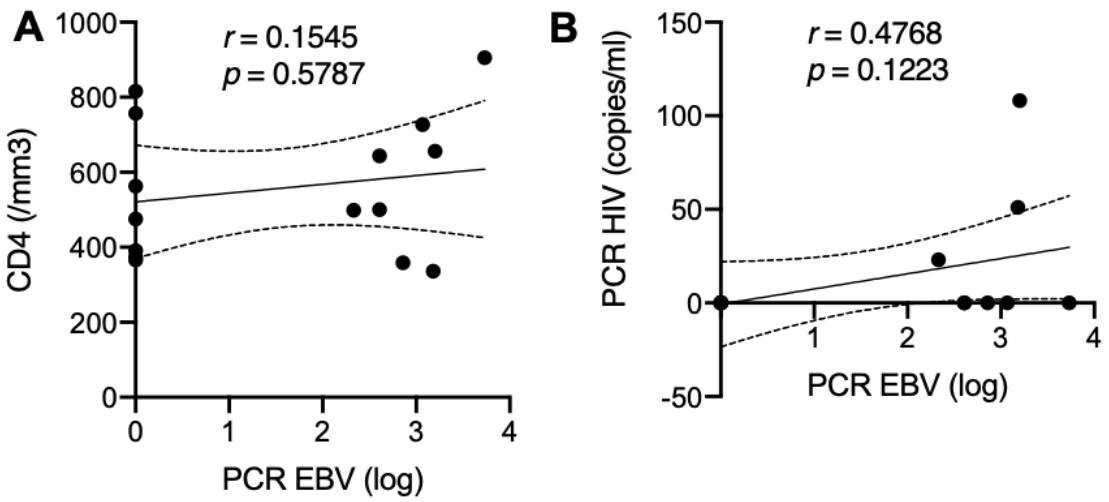

Figure 10. Correlation analyses of EBV reactivation in a cohort of asymptomatic people with HIV patients under cART. (A) Correlation plot illustrating the relationship between EBV reactivation, quantified as detectable PCR EBV (log), and CD4+ T-cell counts (cells/mm^3). (B) Correlation plot depicting the association between EBV reactivation (detectable PCR EBV, log scale) and HIV plasma RNA levels (copies per ml). The Spearman correlation coefficient and p-values as well as the results of simple linear regression with 95%-confidence intervals (dotted lines) are depicted.

Latent EBV infection was previously considered the primary contributor to lymphomagenesis, however, recent data increasingly support the involvement of EBV reactivation in oncogenesis, particularly the initiation of EBV lytic cycle might have profound effects on B cell state (Germini et al. 2020; Rosemarie & Sugden 2020; Sall et al. 2023). While the complete lytic cycle leads to infected cell lysis and release of new infectious virions, EBV reactivation from latency rarely leads to cell lysis and oftentimes an abortive lytic cycle takes place, characterized by the expression of immediate early and early lytic proteins

without genome replication or cell lysis (Al Tabaa et al. 2009; Robinson et al. 2018). We also observed that in cultured EBV-positive RPMI886 B cells, when we reactivated EBV by treatment with sodium butyrate (NaB) or Zta protein with or without blocking viral DNA replication with 0.1 mM acyclovir (ACV, an inhibitor of viral DNA polymerase), we did not observe differences in EBV DNA quantity, which points to the absence of active EBV genome replication (**Figure 11A**). Additionally, we did not observe significant differences in the expression of the *BLLF1* EBV late gene in the same situation, which points to the absence of active late gene transcription induction upon EBV reactivation in our system (**Figure 11B**). We also observed that acyclovir treatment did not impede EBV early reactivation as evidenced by *BZLF1* transcription (**Figure 11C**). Thus, we are able to model an abortive lytic cycle by reactivating EBV in RPMI8866 cells, which results in immediate early and early lytic protein expression (see **Article 5**) but does not result in genome replication or cell lysis of B cells. This reactivation of EBV has implications in the development of lymphomas, e.g. EBV-associated BL, although the exact mechanisms of how EBV reactivation might promote BL were previously unknown.

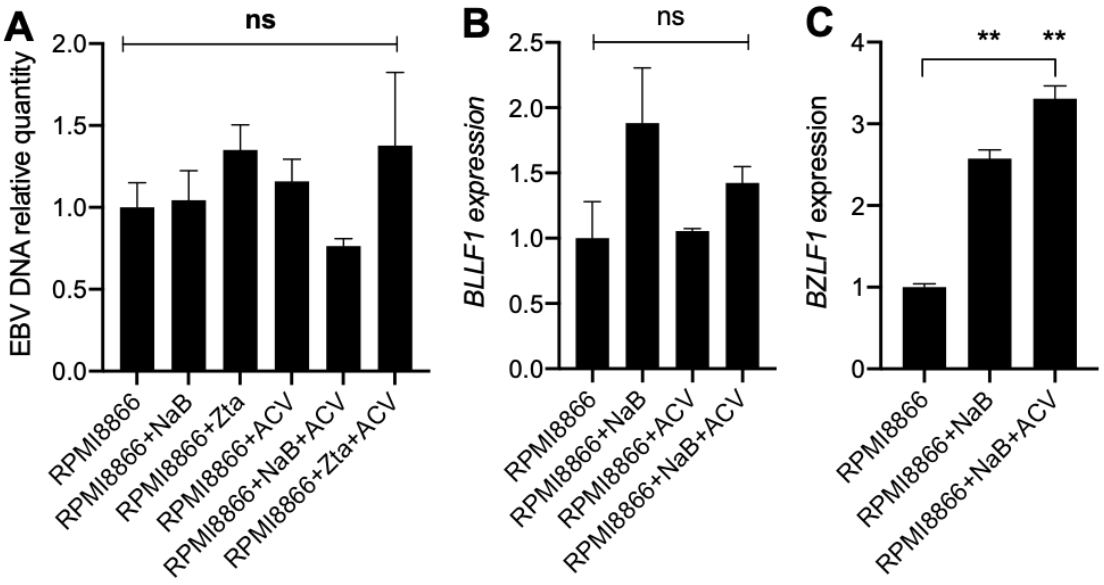

Figure 11. Latent EBV-positive RPMI8866 were treated with sodium butyrate (NaB) and/or acyclovir (ACV) for 48h or left untreated. (A) The relative quantity of EBV DNA measured by qPCR as *EBER1* gene level normalized to the *MYC* gene level, the relative *EBER1* quantity was set as 1 in non-treated RPMI8866 cells. (B) Analysis of the expression of *BLLF1* by qRT-PCR in RPMI886 cells. Expression is presented, after normalisation with *GAPDH* expression, as fold change in comparison to the untreated RPMI8866, set as 1. (C) Analysis of the expression of *BZLF1* by qRT-PCR in RPMI886 cells. Expression is presented, after normalisation with *GAPDH* expression, as fold change in comparison to the untreated RPMI8866, set as 1. ns, non-significant; *p<0.05; **p<0.01; ***p<0.001; ****p<0.0001 as compared by ANOVA, Bonferroni's post-test. Abbreviations: ACV, acyclovir; NaB, sodium butyrate.

We investigated the impact of EBV reactivation on the spatial localization of *MYC* and *IGH* loci in lymphoblastoid cell lines (LCLs). *MYC* and *IGH* are the genes involved in chromosomal translocation found in BL and we hypothesised that EBV reactivation could affect the nuclear localization of these loci. We found that EBV reactivation led to an increased colocalization of *MYC* and *IGH* loci within the 3D-nuclear space (**Figure 12**). Further experiments indicated that EBV-reactivation-induced DNA damage specifically within the *MYC* locus was essential for the increased *MYC-IGH* proximity induced by EBV reactivation. Additionally, the expression of the *MRE11* gene, which is involved in DNA repair and chromatin movement, increased during EBV reactivation. Inhibiting MRE11 led to a reduction in *MYC-IGH* colocalization, suggesting that MRE11 might be responsible for *MYC* displacement towards *IGH* following lytic cycle induction. To explore the relationship between EBV-reactivation-induced *MYC-IGH* proximity and the *MYC-IGH* translocation, we utilised the cell line with the inducible expression of Cas9 and gRNAs that target *MYC* and *IGH*, described above (**Figure 7**). We observed an increased translocation rate between the two loci following prior EBV reactivation and DNA damage induction, suggesting that increased spatial proximity facilitates the occurrence of chromosomal translocation.

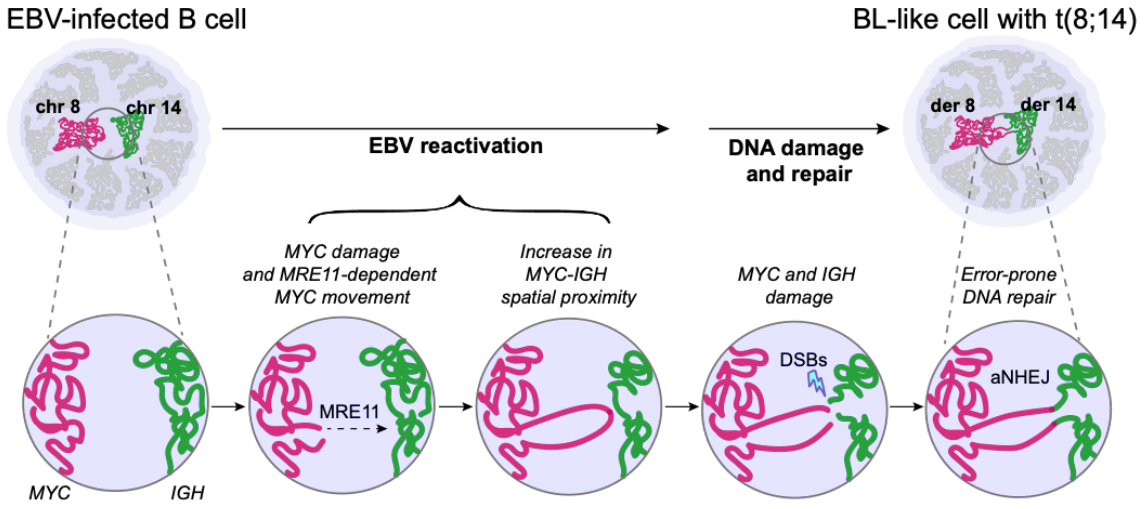

Figure 12. The proposed model of how EBV reactivation promotes Burkitt's lymphoma. Epstein-Barr virus (EBV)-associated Burkitt's lymphoma (BL) is characterised by a t(8;14) chromosomal translocation involving the *MYC* oncogene and the immunoglobulin heavy chain gene (*IGH*). We provide experimental evidence that EBV reactivation increases proximity between *MYC* and *IGH* loci, leading to higher t(8;14) translocation frequency. Specific DNA damage in the *MYC* locus, induced by EBV reactivation, and MRE11-dependent repair contribute to this process. Abbreviations: aNHEJ, alternative non-homologous end joining; BL, Burkitt's lymphoma; DSB, double-strand break.

Overall, the study provides evidence that EBV reactivation induces *MYC-IGH* colocalization, potentially increasing the likelihood of *MYC-IGH* chromosomal translocation and promoting BL (see **Article 5**). This finding contributes to a

better understanding of the molecular mechanisms underlying EBV-associated lymphomagenesis.

I participated in this study by processing patients' samples and analyzing *MYC-IGH* colocalisation in patients' samples and activated B cells, by analyzing EBV reactivation in B cells by BMRF1 staining and its link to *MYC-IGH* colocalisation, by creating illustrations, and by manuscript reviewing and editing.

Article 5. Research paper "Epstein–Barr virus reactivation induces *MYC*-*IGH* spatial proximity and t(8;14) in B cells"

Check for updates

Received: 4 August 2022 | Accepted: 16 February 2023

DOI: 10.1002/jmv.28633

RESEARCH ARTICLE

JOURNAL OF MEDICAL VIROLOGY WILEY

Epstein–Barr virus reactivation induces *MYC-IGH* spatial proximity and t(8;14) in B cells

Fatimata Bintou Sall[1,2] | **Anna Shmakova**[1,3,4] | **Anna Karpukhina**[1,4] | **Tatyana Tsfasman**[1] | **Nikolai Lomov**[1,5] | **Reynand Jay Canoy**[1] | **David Boutboul**[6] | **Eric Oksenhendler**[6] | **Awa Oumar Toure**[2] | **Marc Lipinski**[1] | **Joëlle Wiels**[1] | **Diego Germini**[1] | **Yegor Vassetzky**[1,4]

[1]UMR9018, Université Paris-Saclay, CNRS, Gustave Roussy, Villejuif, France

[2]Faculty of Medicine, Pharmacy and Odontology, Cheikh Anta Diop University of Dakar, Dakar, Senegal

[3]Laboratory of Molecular Endocrinology, Institute of Experimental Cardiology, Federal State Budgetary Organization National Cardiology Research Center Ministry of Health of the Russian Federation, Moscow, Russia

[4]Koltzov Institute of Developmental Biology, Russian Academy of Sciences, Moscow, Russia

[5]Faculty of Biology, State University of Moscow, Moscow, Russia

[6]Service d'Immunopathologie Clinique, Hôpital St Louis, APHP, Paris, France

Correspondence

Diego Germini, CNRS UMR9018, Institut Gustave Roussy, 39, rue Camille-Desmoulins, 94805 Villejuif, France.
Email: germinidiego@gmail.com

Yegor Vassetzky, CNRS UMR9018, Institut Gustave Roussy, 39, rue Camille-Desmoulins, 94805 Villejuif, France.
Email: yegor.vassetzky@cnrs.fr

Funding information

Agence Nationale de Recherches sur le Sida et les Hépatites Virales

Abstract

Burkitt lymphoma (BL) is a B cell malignancy associated with the Epstein–Barr virus (EBV). Most BL cases are characterized by a t(8;14) chromosomal translocation involving the *MYC* oncogene and the immunoglobulin heavy chain gene (*IGH*). The role of EBV in promoting this translocation remains largely unknown. Here we provide the experimental evidence that EBV reactivation from latency leads to an increase in the proximity between the *MYC* and *IGH* loci, otherwise located far away in the nuclear space both in B-lymphoblastoid cell lines and in patients' B-cells. Specific DNA damage within the *MYC* locus, followed by the MRE11-dependent DNA repair plays a role in this process. Using a CRISPR/Cas9-based B cell model to induce specific DNA double strand breaks in *MYC* and *IGH* loci, we have shown that the *MYC-IGH* proximity induced by EBV reactivation leads to an increased t(8;14) translocation frequency.

KEYWORDS

EBV; Burkitt lymphoma, lymphomagenesis; CRISPR/Cas9; MRE11; t(8;14)

Abbreviations: AMLETOC9, RPMI8866-derived cell line that inducibly express CRISPR/Cas9 and gRNAs, targeting both *AML* and *ETO* loci; aNHEJ, alternative NHEJ; ANOVA, analysis of variance; BL, Burkitt's lymphoma; BLLF, BamHI-L fragment leftward open reading frame; BMRF, BamHI-M fragment rightward open reading frame; BRLF, BamHI-R fragment leftward open reading frame; BZLF, BamH1-Z fragment leftward open reading frame; Cas9, CRISPR associated protein 9; cNHEJ, classical NHEJ; CRISPR, clustered regularly interspaced short palindromic repeats; Dox, doxycycline; DSB, double strand break; EBV, Epstein–Barr virus; FISH, fluorescence in situ hybridization; gRNA, guide RNA; HIV, human immunodeficiency virus; HR, homologous recombination; IGH, immunoglobulin heavy chain; IGHC9, RPMI8866-derived cell line that inducibly express CRISPR/Cas9 and gRNA, targeting both *IGH* locus; LCL, lymphoblastoid cell line; MYCC9, RPMI8866-derived cell line that inducibly express CRISPR/Cas9 and gRNA, targeting both *MYC* locus; MYCIGHC9, RPMI8866-derived cell line that inducibly express CRISPR/Cas9 and gRNAs, targeting both *MYC* and *IGH* loci; NaB, sodium butyrate; NHEJ, nonhomologous end-joining.

This is an open access article under the terms of the Creative Commons Attribution-NonCommercial-NoDerivs License, which permits use and distribution in any medium, provided the original work is properly cited, the use is non-commercial and no modifications or adaptations are made.
© 2023 The Authors. *Journal of Medical Virology* published by Wiley Periodicals LLC.

1 | INTRODUCTION

Burkitt lymphoma (BL) is an extremely aggressive non-Hodgkin B cell malignancy with a geographically variable incidence and features. In Europe and United States, BL is sporadic or associated with human immunodeficiency virus (HIV), while in African regions, it's endemic and nearly always associated with Epstein–Barr virus (EBV).[1–5]

EBV, the first described human oncovirus, is a γ-herpesvirus infecting mainly B lymphocytes. Its life cycle is composed of two distinct phases: the lytic phase when viral particles are produced and the latent phase when the viral genome persists as an extrachromosomal episome in the host cell nucleus.[6–9] The switch from latency to lytic cycle is mainly triggered by the *BZLF1* and *BRLF1* genes encoding for the transcriptional activators Zebra (or Zta) and Rta, respectively. Both are expressed at the onset of the lytic cycle and are often used as markers of lytic cycle activation.[10–13] The complete lytic cycle involves viral genome replication, infected cell lysis, and release of new infectious virions while an abortive lytic cycle is characterized by the expression of immediate early and early lytic proteins without genome replication or cell lysis.[14] EBV replication rarely leads to cell lysis and the virus is secreted from live cells, through the secretory pathway.[15] Moreover, only a minority of EBV-infected memory B cells from healthy carriers complete a productive lytic cycle after stimulation.[14] EBV-associated diseases display various types of EBV latency but there is a growing number of reports showing that the lytic phase, both complete and abortive, could contribute to the process of oncogenesis (reviewed in[11,16]).

BL cells always display chromosomal translocations involving the *MYC* (HGNC:7553) oncogene on chromosome 8 and one of the genes coding for the immunoglobulin heavy (*IGH*, HGNC:5477) or light chains (*IGK*, HGNC:5715, or *IGL*, HGNC:5853) on chromosomes 14, 2, and 22, respectively; the t(8;14) translocation is found in more than 80% of cases.[17–20] So far, specific mechanisms leading to the t(8;14) translocation in BL remain largely unknown.

To be generated, a translocation requires simultaneous DNA double strand breaks (DSBs) on the two partner chromosomes, DSB repair through the error-prone nonhomologous end-joining (NHEJ) pathway and the spatial proximity between the two partners.[21–24] The activation-induced deaminase (AID), implicated in somatic hypermutation and class switch recombination in B cells in the germinal center of lymph nodes, is the primary source of DSBs in the *MYC* and *IGH* loci.[25–27] The *IGH* rearrangements are required to produce specific affine antibodies, but they also incidentally predispose to t(8;14).[28–30] To translocate after DSBs, *MYC* and *IGH* have to be spatially proximal. EBV, in both its life cycle phases, can interact with chromatin remodeling complexes or lead to epigenetic alterations, DNA damage and, consequently, to B cell nuclear remodeling (reviewed in[28]). These effects can predispose to chromosomal translocations. Nevertheless, there is still no direct evidence for EBV implication in the BL t(8;14) translocation.

Here, we investigated the role of EBV in t(8;14) generation. Modeling the role of EBV in the BL is challenging, since the translocation formation results from the combination of very rare events in B cells: DSBs formation at *MYC* and *IGH* loci, their proximity and erroneous repair. Moreover, only a minority of primary B cells from blood are EBV positive (1–50 out of 10^6 during latency[31]). That is why we used an experimental system for specific induction of t(8;14) in EBV-transformed B cells, and we provided the first direct evidence that EBV reactivation led to an increased rate of the *MYC-IGH* colocalization which promoted a higher rate of the t(8;14). This newly acquired *MYC-IGH* proximity was triggered by a specific DNA damage at *MYC* locus and driven by the subsequent MRE11-dependent DNA repair. Our findings were confirmed in vivo in B-cells of patients with EBV-related lymphoproliferative disorders.

2 | MATERIALS AND METHODS

2.1 | Cells

Human RPMI8866 and PRIESS, marmoset M81 and rMSHJ EBV-transformed lymphoblastoid cell lines (LCLs) were used in this study (Supporting Information: Table 1). M81 and rMSHJ are LCLs generated with recombinant M81 and MSHJ EBV strains, respectively isolated from a Chinese Nasopharyngeal Carcinoma and a German Stem Cell Transplant recipient.[32] Human cell lines (RPMI8866 and PRIESS) have been authenticated using STR profiling (Supporting Information: File 1, Supporting Information: Table 2). We also created RPMI8866-derived cell lines that inducibly expressed CRISPR/Cas9 and guide RNAs (gRNAs), targeting both *MYC* and *IGH*; *MYC* only; *IGH* only or both *AML* and *ETO* loc as previously described.[33] These RMPI8866-derived cell lines were named MYCIGHC9, MYCC9, IGHC9, and AMLETOC9, respectively. Cells were transfected and gRNAs efficiency was tested exploiting techniques and protocols developed in the laboratory.[34,35] The sequences of gRNAs are listed in Supporting Information: Table 3. Primary human B cells were isolated from blood of healthy donors by negative selection from total PBMCs. Cells were treated as described in Supporting Information: Table 4. See Supporting Information: Materials and Methods for details.

2.2 | Patients

Three patients were included in the study after obtaining an informed consent and a review by the local ethic committee (IMMUNOLYMPH protocol, CLEA-2020-113). All patients were diagnosed with HIV-negative EBV-related lymphoproliferative disorders. Detailed information on patients' history can be found in Table 1 and Supporting Information: Material and Methods section.

2.3 | Western blot

Cell pellets were resuspended in the NETN buffer and sonicated. Proteins (30 µg) were resolved on 4%–12% SDS-PAGE gels,

TABLE 1 Patients' characteristics.

Patient	Diagnosis	Treatment	Age	Gender	Log PCR EBV in whole blood	% of B cells with *MYC-IGH* loci colocalization (*n* of cells analyzed)	*p* Value compared to healthy donor B cells
P1	Severe posttransplant primary EBV infection	Steroids, rituximab, etoposide	74	M	6	21.46 (*n* = 460)	<0.0001****
P2	Cerebral EBV+ polymorphic lymphoproliferative disorder related to prolonged iatrogenic immunosuppression (systemic lupus erythematosus)	Rituximab, cytarabine	43	F	3	16.67 (*n* = 132)	0.0012**
P3	Severe infectious mononucleosis with hemophagocytic lympho-histiocytosis	Steroids, etoposide, cyclosporin	23	F	8	11.63 (*n* = 86)	ns

Note: All patients were diagnosed with HIV-negative EBV-related lymphoproliferative disorders. **$p < 0.01$, ****$p < 0.0001$ as compared by ANOVA, Bonferroni's post-test.

Abbreviations: EBV, Epstein–Barr virus; HIV, human immunodeficiency virus; IGH, immunoglobulin heavy.

transferred onto a PVDF membrane and probed with the following primary antibodies: mouse anti-Cas9; mouse anti-Zebra; rabbit anti-α-tubulin and mouse anti-β-actin (Supporting Information: Table 1). Secondary HRP-conjugated antibodies were used to reveal bands. Western blot band intensity quantification was performed using the ImageJ software. The band intensity of a target protein was normalized to the band intensity of the indicated loading control protein.

2.4 | Quantitative PCR and RT-PCR

Total DNA was extracted using Nucleospin® Tissue DNA purification kit (Macherey-Nagel) according to the manufacturer's protocol. Five hundred ng genomic DNA was amplified using primers specific for the t(8;14) translocation and control primers designed ~6.5 kbp downstream of the breakpoint sequence in the *MYC* gene locus. For RT-PCR, total RNA was extracted using Nucleospin® RNA II purification kit (Macherey-Nagel) according to the manufacturer's protocol. cDNA synthesis was performed as previously described.[36] PCR amplification was performed using the PowerUp SYBR Green Master Mix (Thermo Fisher Scientific) following the manufacturer's protocol. The $2^{-\Delta\Delta C_t}$ method was used for quantification. Primer sequences are listed in Supporting Information: Table 5.

2.5 | 3D-fluorescence in situ hybridization (FISH), immuno-3D FISH, microscope image acquisition, and analysis

Cells were processed for 3D-FISH or immuno-3D-FISH as previously described.[37] Nuclei were counterstained with DAPI. Images were acquired using a multiphoton SP8 confocal microscope (Leica Microsystems). Imaris software (Bitplane) was used to analyze gene localization. The LEICA Application Suite X (Leica Microsystems) software was used to evaluate the percentage of cells that have γH2AX foci colocalized with *MYC* and/or *IGH*. Mean BMRF1 nuclear intensity was analyzed in ImageJ (see Supporting Information: Methods).

2.6 | Statistics

All statistical tests were performed using the Graphpad Prism 5 software (GraphPad software Inc.). One-way analysis of variance (ANOVA) test followed by Bonferroni's posttest or Student's *t*-test was used to compare averages between different groups. For binary comparisons of colocalization rate χ^2 test was also used, odds ratio (OR) [95% confidence interval], χ^2 value, and *p*-value are provided. Two-way ANOVA followed by Bonferroni's posttest was used to compare averages for multiple-group comparisons with two factors (cell cycle and proliferation data). Data are presented as mean ± standard error of mean.

3 | RESULTS

3.1 | EBV reactivation leads to *MYC-IGH* colocalization in LCLs

Chromosomal translocations are induced by the NHEJ, a proximity-based mechanism,[38] but in human naive B cells, *MYC* and *IGH* loci are separated in the nuclear space.[37,39] As EBV infection and reactivation are accompanied by large-scale modifications in the nuclear architecture,[40–42] we hypothesized that this could affect the nuclear localization of the *MYC* and *IGH* loci.

To study the effect of EBV reactivation on *MYC* and *IGH* spatial localization within the nuclear space, we first determined the optimal virus reactivation conditions in RPMI8866 and PRIESS LCLs (see Supporting Information: Figure 1). We observed a high level of virus

reactivation in RPMI8866 cells treated with sodium butyrate (NaB) or Zebra protein (Supporting Information: Figure 1a,b,f). Thus, for the following experiments, we used Zebra protein and NaB to induce the lytic cycle in RPMI8866 cells.

We next analyzed the localization of the *MYC* and *IGH* loci in the tridimensional nuclear space of primary B cells, RPMI8866 and PRIESS cell lines (treated or not with EBV lytic cycle inducers) using 3D-FISH. *MYC* and *IGH* loci were considered as colocalized when the centers of their fluorescent foci were 1 µm or less from each other (Figure 1A). In naive B cells from healthy donors, *MYC* and *IGH* loci were colocalized in 5.80 ± 0.57% cells ($n = 180$ cells); in latent nontreated RPMI8866 and PRIESS cells, *MYC* and *IGH* loci colocalization was also low (4.55 ± 0.88% and 2.78 ± 0.78%, respectively; $n \geq 100$ cells; Figure 1B and Supporting Information: Figure 1d). EBV lytic cycle induction in RPMI8866 cells increased the *MYC-IGH* colocalization twofold (8.7 ± 0.56% in NaB treated cells and 9.52 ± 0.25% in Zebra-treated cells vs. 4.55 ± 0.88% in latent RPMI8866 cells; $p < 0.001$; $n \geq 100$ cells; Figure 1A,B). Lytic cycle activation in PRIESS cells also increased twofold the colocalization between the *MYC* and *IGH* loci (Supporting Information: Figure 1d). Thus, EBV reactivation led to a significant increase in *MYC-IGH* colocalization rate in LCLs. Importantly, EBV reactivation did not cause cell cycle arrest in our model (Supporting Information: Figure 2a,b).

We next tested whether the *MYC-IGH* colocalization observed upon EBV reactivation could be directly induced by the Zebra protein. Indeed, Zebra interacts with host genes and may thus affect their expression and, consequently, spatial localization (reviewed in[11]). We treated B lymphocytes from healthy donors with the recombinant Zebra protein for various times. Zebra was detectable in B cells 6 h after treatment, peaked at 24 h and remained in the cells at 48 h (Figure 1C). No difference in *MYC-IGH* colocalization rate was detected in Zebra-treated naive or activated B cells as compared to the untreated controls (Figure 1D,E). Zebra treatment did not affect B cell cycle (Supporting Information: Figure 2c). The increase in *MYC-IGH* colocalization rate in activated B cells relative to nonactivated B cells is consistent with previous reports.[43] Zebra alone is therefore not sufficient to induce *MYC-IGH* proximity in EBV-negative B cells.

3.2 | LCLs with spontaneous EBV lytic cycle show an increased spatial proximity between the *MYC* and *IGH* loci

To confirm that EBV lytic cycle affects the proximity of the *MYC* and *IGH* loci, we used two additional LCLs, M81 and rMSHJ, with a high spontaneous lytic activity.[32,44] Their spontaneous lytic activity was confirmed by expression of EBV immediate early (*BZLF1* and *BRLF1)* and late (*BDRF1* and *BLLF1*) genes and BMRF1 protein (Figure 1F,G; Supporting Information: Figure 1e,g;3a,b).

Both M81 and rMSHJ cells presented a significantly higher *MYC-IGH* colocalization rate than non-stimulated RPMI8866 (14.98 ± 1.59% in M81 cells and 15.54 ± 1.77% in rMSHJ cells vs. 4.56 ± 0.62% in RPMI8866; $p < 0.05$; $n \geq 200$ cells Figure 1H). Moreover, using immunofluorescent staining for EBV early protein BMRF1 (whose transcription is activated by the Zebra) in M81 cells, we found that *MYC-IGH* colocalization was significantly higher in BMRF1-positive cells as compared to BMRF1-negative ones (43.89 ± 3.70% vs. 7.77 ± 3.30%; $p < 0.0001$; OR: 6.376 [2.396–15.96], $\chi^2 = 16.79$, $p < 0.0001$; $n \geq 60$ cells, Figure 1I,J). These results reinforce our conclusion that EBV reactivation induces the proximity between the *MYC* and *IGH* loci in the nuclear space.

3.3 | B cells from individuals with EBV-related lymphoproliferative disorders and immune suppression present an increased spatial proximity between the *MYC* and *IGH* loci

We next assessed the proximity of the *MYC* and *IGH* loci in B cells from three patients (P1–P3) with EBV-related lymphoproliferative disorders (Table 1). Case history can be found in the Supporting Information: Materials. B cells from P1 and P2 with EBV-related lymphoproliferative disorders and immune suppression had a significantly elevated *MYC-IGH* colocalization rate compared to B cells isolated from healthy donors (Table 1). A trend to increased *MYC-IGH* colocalization rate was observed in P3 with a severe infectious mononucleosis, although very few circulating B cells in P3 blood did not allow larger sampling to obtain statistical significance.

To confirm that *MYC-IGH* colocalization can be driven by EBV reactivation, we focused on a unique case of primary EBV infection on the background of immune suppression caused by kidney transplant from EBV + donor into an EBV-recipient (P1). PBMCs obtained from P1 were spontaneously transformed in culture (Supporting Information: Figure 4). As mentioned above, B cells from P1 presented a significantly higher *MYC-IGH* colocalization rate than B cells from healthy donors (Table 1). Moreover, EBV-infected B cells were undergoing a lytic cycle as observed by BMRF1 staining (Figure 2A). We found that *MYC-IGH* colocalization was significantly higher in BMRF1-positive cells as compared to all B cells from P1 (34.60 ± 2.203% vs. 21.46 ± 2.363%; $n \geq 50$ cells; $p < 0.01$; Figure 2B,C). These results demonstrate that EBV reactivation is associated with the increased proximity between the *MYC* and *IGH* loci in vivo.

3.4 | Development and characterization of the MYCIGHC9 cell line to induce and detect the *MYC-IGH* translocation

In B cells from healthy individuals, spontaneous translocations are exceedingly rare, occurring in approximately 1×10^{-6} cells,[45] and thus undetectable by standard cytogenetic techniques. In addition, endemic BL translocations occur over large chromosomal regions, making these translocations impossible to analyze by standard PCR techniques. To experimentally prove that *MYC-IGH* spatial proximity favors generation of a translocation between the two loci, we created an experimental system for targeted generation of DSBs in the *MYC* and *IGH* loci: an RPMI8866-derived MYCIGHC9 cell line containing the *Cas9* gene and gRNAs targeting the *MYC* and *IGH* loci under the

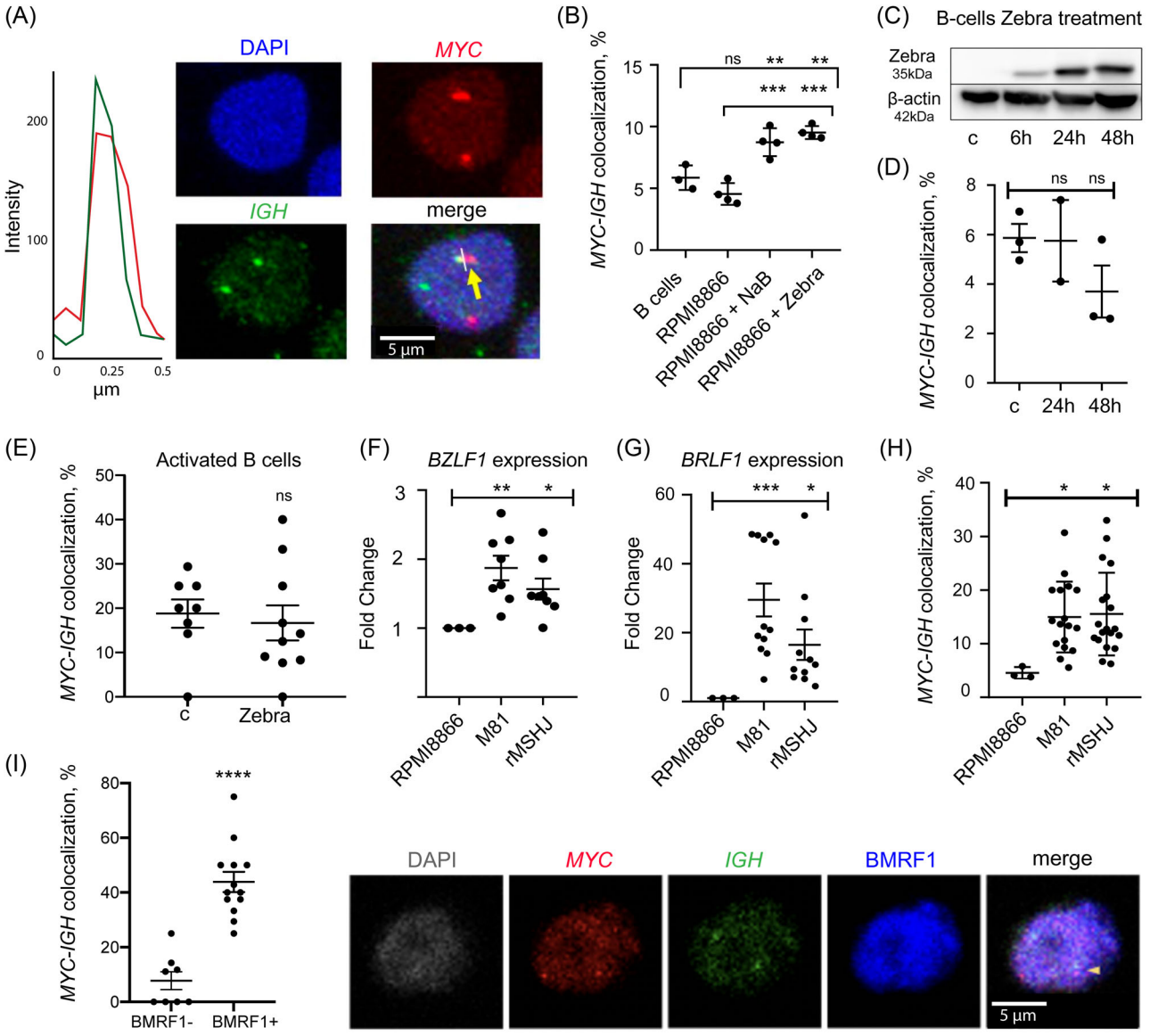

FIGURE 1 EBV reactivation in RPMI8866 induces *MYC-IGH* colocalization. (A) Representative optic section of a 3D-FISH image of RPMI8866 cells treated with the EBV lytic cycle inducer Zebra for 48 h. Nuclei stained with DAPI are represented in blue, *MYC* and *IGH* gene loci stained with specific fluorescent probes are represented in red and green, respectively. Colocalization between the *MYC* and *IGH* loci is highlighted by the yellow arrow. Scale bar = 5 µm. The right panel shows *MYC* (red curve) and *IGH* (green curve) signal intensities along the white bar drawn in the MERGE picture. (B) The percentage of cells with colocalized *MYC-IGH* signals (i.e., cells where the distance between the centers of corresponding 3D-FISH signals was equal or less than 1 µm) in B cells purified from healthy donors (B cells), latent EBV-positive RPMI8866 untreated or treated with sodium butyrate (NaB) or Zebra recombinant protein to induce lytic cycle. 3D-FISH was performed 48 h after treatment. A minimum of 100 cells from at least two different experiments and two technical replicates were analyzed. (C) Western blot analysis of Zebra protein cell entry into primary B cells purified from healthy donors and treated with 1 µg/mL recombinant Zebra for the indicated time. Control, untreated B cells. (D) *MYC-IGH* colocalization rate in B cells purified from healthy donors and treated with the recombinant Zebra protein for the indicated times. 3D-FISH was performed 24 and 48 h after treatment. A minimum of 180 cells from at least two different experiments and two technical replicates were analyzed. (E) *MYC-IGH* colocalization in primary B cells purified from healthy donors, activated with a cocktail of reagents (recombinant human IL4 + human CD40 monoclonal antibody + anti-human IgM monoclonal antibody) and treated or not with the recombinant Zebra protein for 48 h. A minimum of 60 cells were analyzed. (F, G) Analysis of the expression of *BZLF1* (F) and *BRLF1* (G) by qRT-PCR in M81 and rMSHJ cell lines with spontaneous EBV lytic activity. Expression is presented, after normalization with *GAPDH* expression, as fold change in comparison to the unstimulated RPMI8866, set as 1. Data are from three experiments and two technical replicates. (H) *MYC-IGH* colocalization rate in M81 and rMSHJ cells with spontaneous lytic activity, in comparison to RPMI8866. A minimum of 200 cells from at least two different experiments and two technical replicates were analyzed. (I) *MYC-IGH* colocalization in BMRF1 positive and BMRF1 negative M81 cells. M81 cells were processed for 3D-FISH targeting *MYC* and *IGH* loci and cells undergoing lytic cycle were identified by immunofluorescence staining of the EBV early lytic protein BMRF1. $n > 70$ cells analyzed per condition. (J) A representative immuno-3D FISH image of *MYC-IGH* colocalization occuring in a BMRF1 positive M81 cell. All data are plotted as individual values, mean ± SEM. *$p < 0.05$, **$p < 0.01$, ***$p < 0.001$, ****$p < 0.0001$ as compared by ANOVA, Bonferroni's posttest for more than two groups or *t*-test for two groups. ANOVA, analysis of variance; EBV, Epstein–Barr virus; FISH, fluorescence in situ hybridization; IGH, immunoglobulin heavy; SEM, standard error of mean.

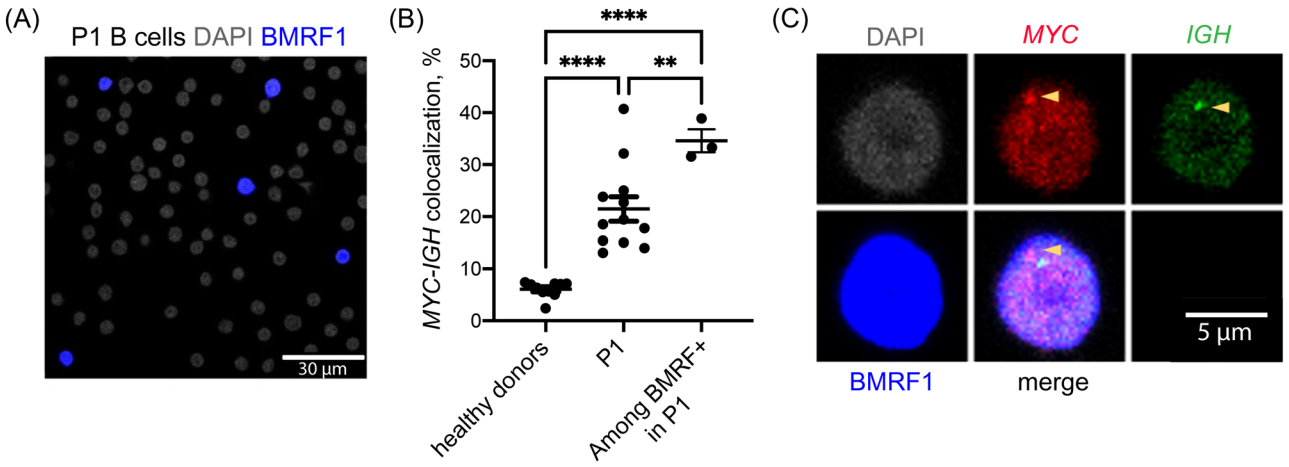

FIGURE 2 EBV reactivation in a patient with severe posttransplant primary EBV infection is associated with *MYC-IGH* colocalization. (A) Representative image of immunofluorescent staining of the EBV early lytic protein BMRF1 in patient #1 B cells (P1). Nuclei stained with DAPI are represented in gray, BMRF1 in blue. Scale bar = 30 µm. (B) The percentage of cells with colocalized *MYC-IGH* signals (i.e., cells where the distance between the centers of corresponding 3D-FISH signals was equal or less than 1 µm) in B cells purified from healthy donors, in B cells purified from patient #1 with severe posttransplant primary EBV infection (P1) and in among BMRF1 positive (BMRF1+) B cells from patient #1. $n > 50$ cells analyzed per condition. Data are plotted as individual values, mean ± SEM. $^{**}p < 0.01$, $^{****}p < 0.0001$ as compared by ANOVA, Bonferroni's posttest. (C) A representative immuno-3D FISH image of *MYC-IGH* colocalization occuring in a BMRF1 positive B cell. ANOVA, analysis of variance; EBV, Epstein–Barr virus; FISH, fluorescence in situ hybridization; IGH, immunoglobulin heavy; SEM, standard error of mean.

control of a Doxycycline (Dox)-inducible promoter (see Section 2). In the presence of Dox, DSBs are specifically generated in the *MYC* and *IGH* loci. In some cells, erroneous repair of these DSBs by NHEJ generates the t(8;14) translocation. This translocation can then be detected and quantified by qPCR using a forward *MYC* primer and a reverse *IGH* primer, surrounding the chromosomal break[35] (Supporting Information: Figure 5).

Cas9 expression started 3 h after Dox treatment (Figure 3A). Specific induction of DSBs was confirmed by colocalization between *MYC* and *IGH* loci and γH2AX foci (3D-FISH followed by γH2AX immunostaining). The damage in both loci peaked at 6 h post-Dox treatment (Figure 3B,C). We detected t(8;14) translocations by end-point PCR starting from 24 h after Dox treatment (Figure 3D). The more sensitive quantitative PCR was then applied to quantify the translocation rate. t(8;14) appeared already at 12 h after Dox treatment ($0.8 \pm 0.24 \times 10^{-3}$ cells), then the translocation rate increased at 24 h ($7.2 \pm 0.54 \times 10^{-3}$ cells; Figure 3E) and peaked at 48 h ($1.08 \pm 0.03 \times 10^{-2}$ cells; Figure 3E).

To get insight into the mechanism of the translocation generation in our system, we next used classical and alternative NHEJ (cNHEJ and aNHEJ, respectively) inhibitors. MYCIGHC9 cells treated with Dox were simultaneously incubated with either Mirin, an inhibitor of MRE11 (HR and NHEJ pathways) or NU7026 DNA-PK inhibitor (cNHEJ pathway) or L67 DNA ligase I and III inhibitor (aNHEJ pathway) and the t(8;14) translocation rate was measured by qPCR. Treatment with Mirin or L67 significantly decreased the t(8;14) translocation rate (fold change 0.60 ± 0.02; $p < 0.05$ for Mirin and 0.28 ± 0.10; $p < 0.01$ for L67; Figure 3F) whereas treatment with NU7026 significantly increased the translocation frequency (fold change 3.68 ± 0.13; $p < 0.0001$; Figure 3F). These results indicate that only inhibition of the aNHEJ pathway negatively impacts the t(8;14) translocation process and therefore suggests that, in our model, aNHEJ is a major pathway favouring the occurrence of translocations; this is consistent with previous results.[46,47]

3.5 | EBV reactivation-induced *MYC-IGH* spatial proximity increases the probability of t(8;14)

Using the MYCIGHC9 cell line, we next investigated whether an increased *MYC-IGH* proximity resulted in a higher t(8;14) translocation frequency. To this aim, MYCIGHC9 cells were first treated with either the recombinant Zebra protein or NaB for 48 h to increase *MYC-IGH* proximity via EBV reactivation and then Cas9 and gRNAs expression was induced by addition of Dox. After additional 24 h, cells were collected for t(8;14) quantification by qPCR (Figure 4A). EBV reactivation with Zebra and NaB leads to the spatial proximity between the *MYC* and *IGH*, followed by a 2.07 ± 0.28 and 3.72 ± 0.56 fold increase in the translocation rate, respectively ($p < 0.01$ and $p < 0.001$; Figure 4B). These data provide the first experimental proof that gene proximity increases the probability of a chromosome translocation upon DSB induction.

3.6 | Specific DNA damage within the MYC locus and MRE11 protein are involved in EBV-induced *MYC-IGH* spatial proximity

The increase in the colocalization rate between the *MYC* and *IGH* loci observed after EBV reactivation (Figure 1B) could be a consequence

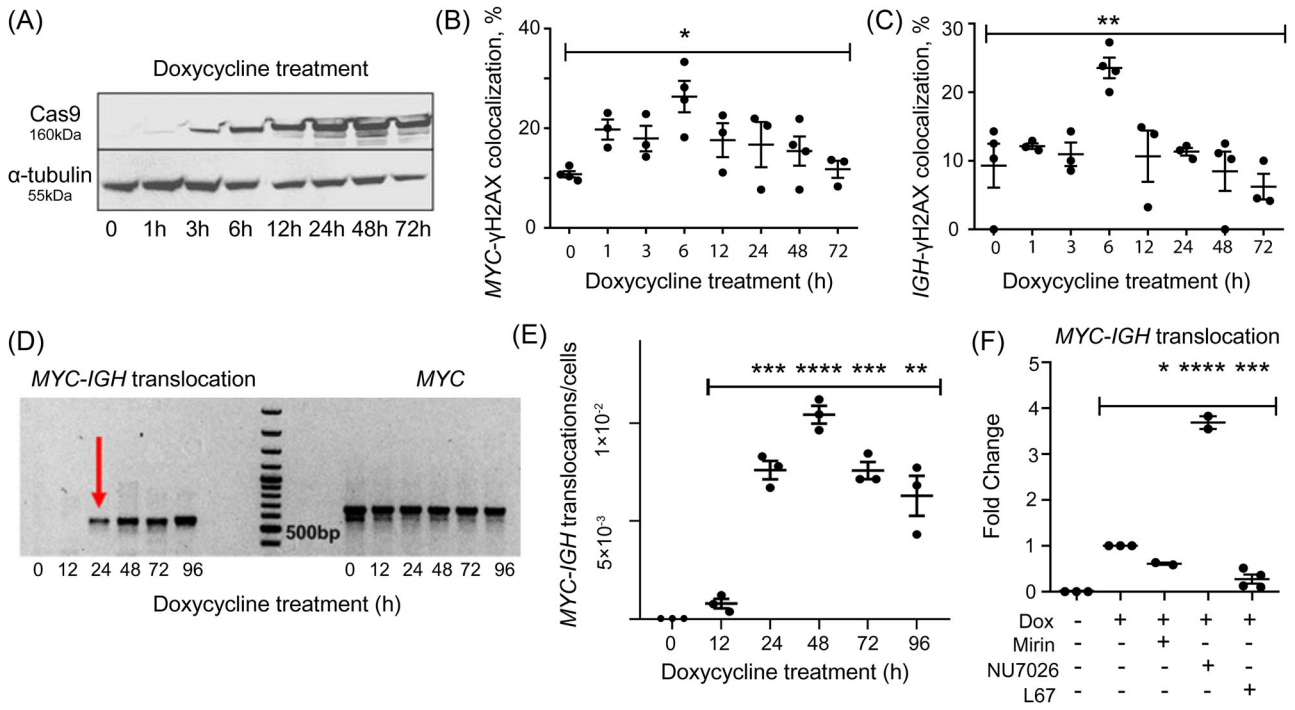

FIGURE 3 Induction of the t(8;14) in the MYCIGHC9 cell line. (A) Representative image of western blot kinetic analysis of Dox-induced Cas9 expression. α-tubulin was used as a protein loading control. (B, C) Induction of DNA damage within the *MYC* and *IGH* loci after Cas9 and gRNAs expression. Cells were treated with Dox for the indicated times and 3D-FISH was performed with *MYC* and *IGH* probes followed by γH2AX immunofluorescence staining. Percentage of cells with γH2AX foci colocalized with the *MYC* (B) or *IGH* loci (C) were obtained from at least two independent experiments where at least 150 cells were examined for each condition. (D, E) Kinetics of *MYC-IGH* translocation formation after Dox treatment. Cells were treated with Dox for the indicated times and collected for DNA extraction. End-point PCR followed by electrophoresis on agarose gel (D) or quantitative PCR (E) were performed. t(8;14) rates in (E) are calculated according to the following formula: translocation rate = $2 \times 2^{-\Delta C_t \text{ of MYC-IGH and MYC amplicon}}$ translocations per cell. The data represent results from three independent experiments and two technical replicates for each. (F) Effect of DNA repair inhibitors on the *MYC-IGH* translocation rate. Cells were simultaneously treated with Dox and the indicated inhibitor or left untreated for 24 h and translocations were detected by qPCR. t(8;14) rate fold changes are calculated after normalization to the *MYC* gene in comparison to t(8;14) level in Dox-treated cells, set as 1. The data represent results from three independent experiments with two technical replicates for each. All data are plotted as individual values, mean ± SEM. ns, nonsignificant; $^{*}p < 0.05$, $^{**}p < 0.01$, $^{***}p < 0.001$, $^{****}p < 0.0001$ as compared by ANOVA, Bonferroni's posttest. ANOVA, analysis of variance; FISH, fluorescence in situ hybridization; IGH, immunoglobulin heavy; SEM, standard error of mean.

of a displacement of one or both of these loci. Since DNA damage induction is one of the factors that can lead to loci movement within the nuclear space,[21] we next analyzed the proximity between the *IGH* and *MYC* loci in different conditions using several experimental systems.

We first used the MYCIGHC9 line to study *MYC* and *IGH* relative positioning following specific DSBs. We observed a significantly increased colocalization between these loci 48 h after the DSB induction by Dox treatment (10.20 ± 1.67% in Dox treated cells vs. 4.65 ± 0.34% in the control; $p < 0.05$; OR: 2.672 [1.063–7.052], $\chi^2 = 4.862$, $p = 0.0275$; $n \geq 120$ cells, Figure 4C). To test whether the observed *MYC-IGH* colocalization occurring after the introduction of DSBs within the *MYC* and *IGH* loci was gene-specific (i.e., concerned only *MYC* and *IGH* loci) and not related to the overall increased genome mobility or particularly enhanced *IGH* DSB movement, we analyzed the *IGH* colocalization with another of its known translocation partners, *CCND1*[48] located on chromosome 11 (HGNC:1582). Although a slight increase in the colocalization rate between the *CCND1* and *IGH* was observed 48 h after Dox treatment of the MYCIGHC9 line, it was not statistically significant (9.23 ± 1.7% in Dox treated cells vs. 6.54 ± 0.76% in the control; $p < 0.05$; OR: 1.319 [0.5525–3.082], $\chi^2 = 0.3739$, $p = 0.5409$; $n \geq 120$ cells, Figure 4D). We thus conclude that the *MYC-IGH* colocalization induced by specific DSBs in the respective loci occurred with gene-specificity.

We next tested whether induction of a single DSB in either *MYC* or *IGH* locus would affect the proximity between the two genes by using the IGHC9 or MYCC9 cell lines where DSBs are induced only within the *IGH* or *MYC* loci, respectively. In Dox-treated IGHC9 cells we did not observe any increase in the *MYC-IGH* colocalization rate (3.86 ± 1.32% vs. 4.28 ± 0.49% in the control; OR: 1.129 [0.3778–3.330], $\chi^2 = 0.04843$, $p = 0.8258$; $n \geq 160$ cells, Figure 4E) whereas in MYCC9 cells, a significant increase in the *MYC-IGH* colocalization rate was detected (5.90 ± 0.11% vs. 3.60 ± 0.06%; $p < 0.01$; OR: 2.701 [1.161–6.514], $\chi^2 = 5.099$, $p = 0.0239$; $n \geq 85$ cells Figure 4F) suggesting that the DBS induction in the *MYC* locus triggers the colocalization.

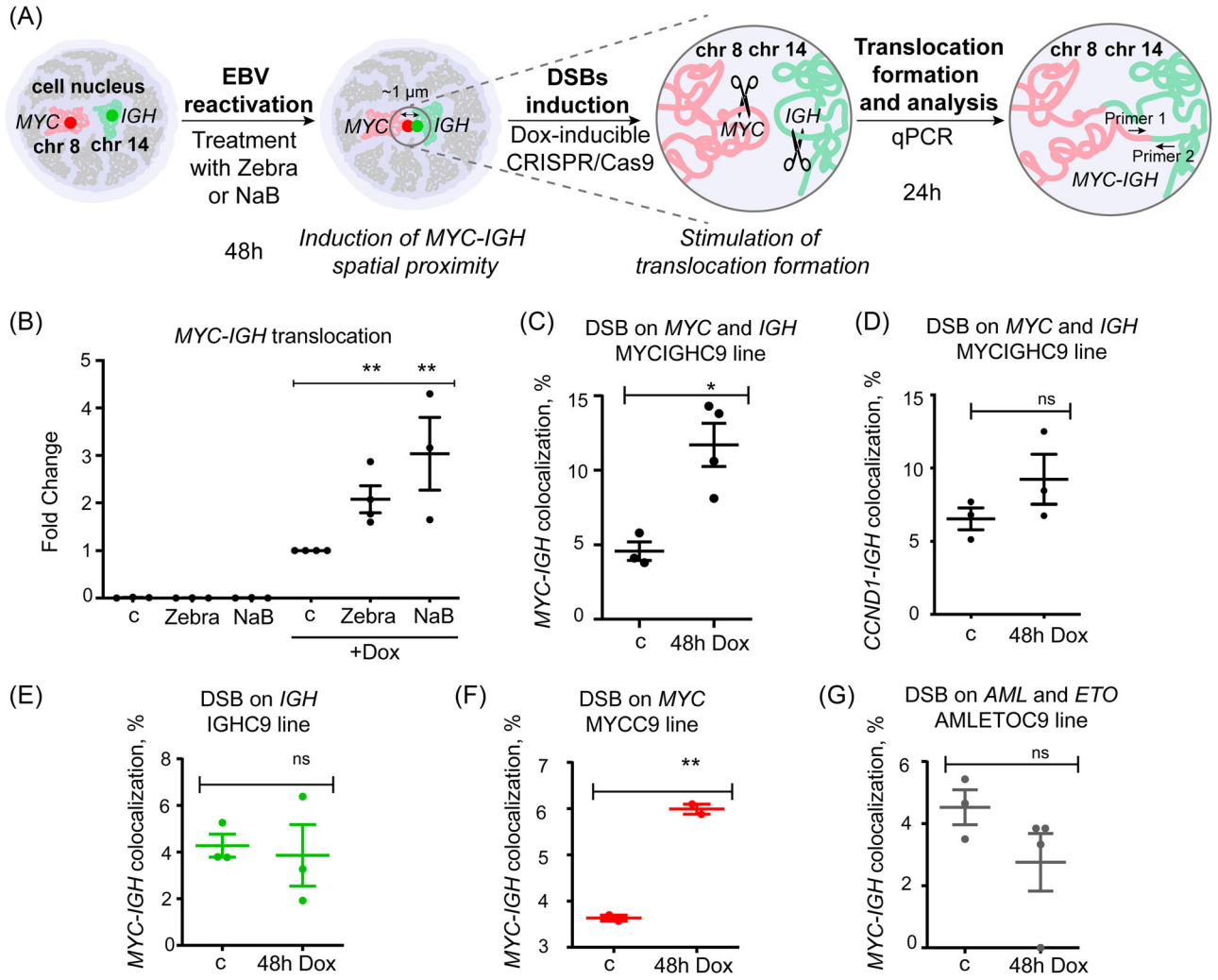

FIGURE 4 EBV reactivation-induced *MYC-IGH* spatial proximity is favored by specific DNA damage in the *MYC* locus and increases the t (8;14) rate upon DSB induction within the *MYC* and *IGH* loci. (A) Experimental design. MYCIGHC9 line cells were treated or not with recombinant Zebra protein or sodium butyrate (NaB) for 48 h to induce EBV reactivation and the consequent *MYC-IGH* proximity followed by Dox treatment for 24 h and qPCR for *MYC-IGH* translocation detection. (B) qPCR for *MYC-IGH* translocation in Dox-treated cells after Zebra or NaB treatment. Fold changes in t(8;14) levels are calculated after normalization to the *MYC* gene in comparison to translocation rate in cells treated only with Dox, set as 1. The data represent results from three independent experiments with two technical replicates for each. (C) *MYC-IGH* colocalization rate in the MYCIGHC9 cell line. Cells were treated by Dox for 48 h to induce the expression of Cas9 and gRNA targeting *MYC* and *IGH*. 3D-FISH was performed to evaluate the *MYC-IGH* spatial proximity. (D) *CCND1-IGH* colocalization rate in the MYCIGHC9 line after Cas9-induced DSBs in the *MYC* and *IGH* loci. The same cells as in (C) were used to evaluate the *IGH* proximity with the *CCND1* locus by 3D-FISH. (E) *MYC-IGH* colocalization rate in IGHC9 line after Cas9 induced DSB on *IGH* locus. (F) *MYC-IGH* colocalization rate in the *MYCC9* line after Cas9 induced DSB on *MYC* locus. (G) *MYC-IGH* colocalization in the AMLETOC9 line after simultaneous Cas9 induced DSB within the *AML* and *ETO* loci. A minimum of 85 cells from at least one experiment and at least three technical replicates were analyzed for each 3D FISH experiment. All data are plotted as individual values, mean ± SEM. ns, nonsignificant; $^{*}p < 0.05$, $^{**}p < 0.01$ as compared by ANOVA, Bonferroni's posttest (B) or by *t*-test (C–G). ANOVA, analysis of variance; DSBs, double strand breaks; EBV, Epstein–Barr virus; FISH, fluorescence in situ hybridization; IGH, immunoglobulin heavy; SEM, standard error of mean.

To test whether DSB induction outside the target loci would affect the proximity between *MYC* and *IGH*, we have used the AMLETOC9 cell line with inducible expression of Cas9 and gRNA targeting the *ETO* and *AML* loci located on chromosomes 8 and 21, respectively. Induction of DSBs in these loci led to a slight decrease in the colocalization between the *MYC* and *IGH* loci (2.76 ± 0.92% in Dox treated cells vs. 5.04 ± 0.39% in the control; OR: 0.4449 [0.1229–1.661], $\chi^2 = 1.391$, $p = 0.2383$; $n \geq 100$ cells, Figure 4G).

Taken together, all these results suggest that in our experimental system, specific DNA damage within *MYC* locus, rather than within *IGH* locus is required for the *MYC-IGH* proximity to occur and as a consequence, it is quite likely that *MYC*, when damaged, moves toward the *IGH* locus.

Since the induction of EBV lytic cycle triggers DNA damage response in B cells (reviewed in[49]), and DNA damage within the *MYC* loci is an important factor for inducing *MYC-IGH* proximity, we next

wanted to understand whether lytic cycle induction in RPMI8866 cells caused DNA damage within the *MYC* locus. We induced EBV lytic cycle by treating cells with the recombinant Zebra protein and quantified the percentage of cells showing specific DNA damage within at least one *MYC* locus by measuring the colocalization between *MYC* loci and γH2AX foci using immuno-3D FISH. DNA damage within the *MYC* loci was also analyzed in the M81 and rMSHJ cell lines that present spontaneous EBV reactivation. Both induced and spontaneous EBV reactivation were associated with an increased level of DNA damage within the *MYC* locus (27.48 ± 4.01% in Zebra-treated RPMI8866 cells; 23.99 ± 2.30% in M81 cells; 19.00 ± 1.37% in rMSHJ cells vs. 9.41 ± 2.23% in RPMI8866 unstimulated cells; $p < 0.01$; $p < 0.001$; $p < 0.01$, respectively; $n \geq 380$ cells Figures 5A,B). As simultaneous DNA damage in the *MYC* and *IGH* loci is required to generate the t(8;14) translocation, we also checked for the presence of DNA damage within the *IGH* locus in the same cells. After EBV reactivation, we observed a higher rate of DNA damage within the *IGH* locus as compared to the control RPMI8866 (data not shown). Simultaneous DNA damage within the *MYC* and *IGH* loci when they are located close to each other was also detected and even if this observation is not statistically significant, it illustrates the fact that DSBs can occur simultaneously within both loci when they are in

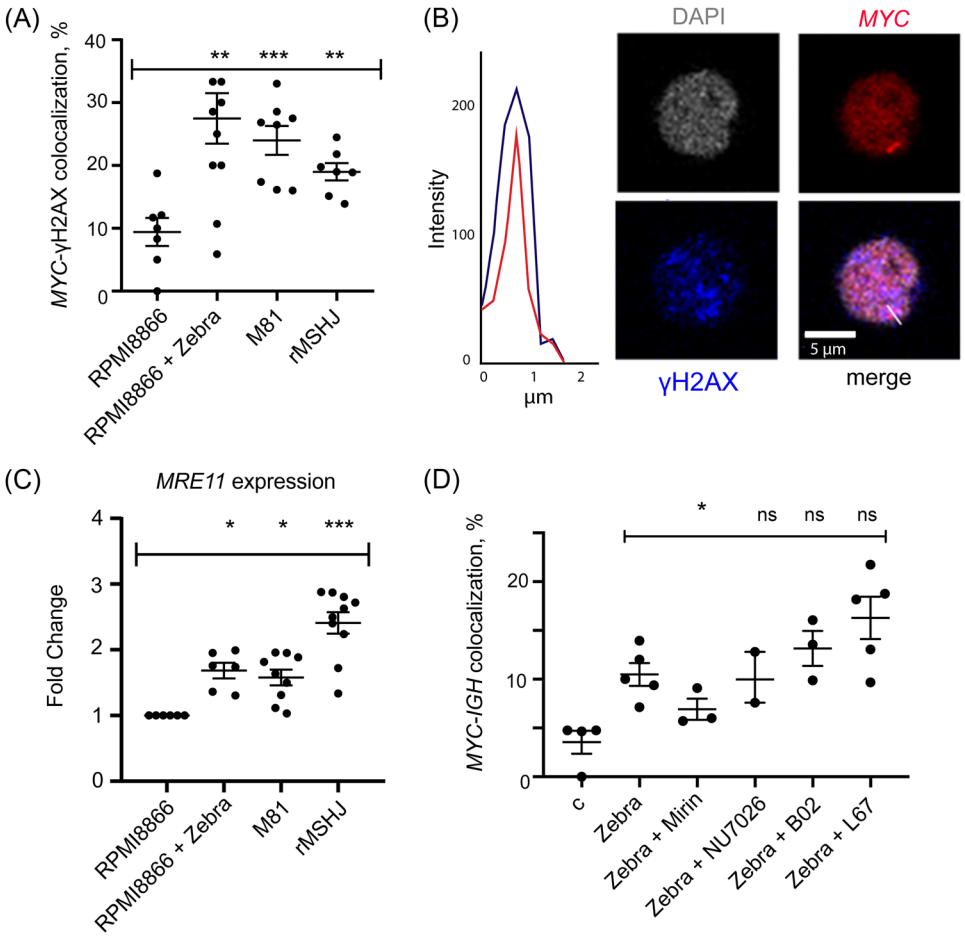

FIGURE 5 EBV reactivation induces DNA damage within the *MYC* locus and MRE11 is involved in *MYC* relocalization next to *IGH*. (A) DNA damage within the *MYC* locus in LCLs with the induced (RPMI8866 + Zebra) or spontaneous (M81 and rMSHJ) lytic activity. Cells were processed for 3D-FISH followed by immunostaining for γH2AX. *Y*-axis, percentage of cells with γH2AX foci colocalized with the *MYC* locus. A minimum of 380 cells from two experiments and at least three technical replicates were analyzed. (B) Representative slice-section of an immuno-3D-FISH image with colocalized γH2AX foci (represented in blue) and the *MYC* locus (in red). Scale bar = 5 μm. The right panel illustrates *MYC* (red curve) and γH2AX (blue curve) colocalization (*x*-axis) along the white bar drawn in the MERGE picture, with the respective peak intensities (*y*-axis), Scale bar = 5 μm. (C) *MRE11* expression analyzed by qRT-PCR in LCLs with induced (RPMI8866 + Zebra) or spontaneous (M81 and rMSHJ) lytic activity. *MRE11* expression fold changes upon EBV reactivation are calculated after normalization with *GAPDH* expression in comparison with *MRE11* expression in RPMI8866, set as 1. (D) *MYC-IGH* colocalization in RPMI8866 treated or not with recombinant Zebra protein for 48 h, in association or not with the MRE11 inhibitor Mirin or the DNA-PK inhibitor NU7026 or the Rad51 inhibitor B02 or the DNA Ligase III inhibitor L67. A minimum of 100 cells from two experiments and at least three technical replicates were analyzed. All data are plotted as individual values, mean ± SEM. ns, nonsignificant; $^{*}p < 0.05$, $^{**}p < 0.01$, $^{***}p < 0.001$, as compared by ANOVA, Bonferroni's posttest. ANOVA, analysis of variance; EBV, Epstein–Barr virus; FISH, fluorescence in situ hybridization; IGH, immunoglobulin heavy; LCLs, lymphoblastoid cell lines; SEM, standard error of mean.

close proximity. This may increase the risk of chromosomal translocations. Representative images of simultaneous DNA damage within the *MYC* and *IGH* loci following EBV reactivation are shown in Supporting Information: Figure 6.

MRE11, one of the components of the DNA repair machinery, was shown to be involved in the movement of chromatin loci.[37,50] We next explored a potential role of MRE11 in loci displacement in our model. First, we showed that EBV reactivation was accompanied by an increase in *MRE11* gene (HGNC:7230) expression measured by qRT-PCR (fold change 1.68 ± 0.11 in Zebra-treated RPMI8866 cells; 1.57 ± 0.11 in M81 cells and 2.40 ± 0.16 in rMSHJ cells vs. unstimulated RPMI8866 cells; $p < 0.001$; $p < 0.01$; and $p < 0.0001$, respectively; Figure 5C). We also observed that MRE11 inhibition by Mirin blocked the increase in *MYC-IGH* proximity induced by EBV reactivation (6.93 ± 1.08% in Zebra + Mirin treated cells vs. 10.49 ± 1.16% in Zebra treated cells) (Figure 5D). In contrast, inhibition of DNA-PK (involved in the cNHEJ) by NU7026, of Rad51 (involved in homologous recombination) by B02 or of Ligase III (involved in aNHEJ) by L67 did not affect the *MYC-IGH* colocalization (10.2 ± 2.6% in Zebra + NU7026 treated cells; 13.16 ± 1.79% in Zebra + B02-treated cells; 16.28 ± 2.16% in Zebra + L67-treated cells vs. 10.49 ± 1.16% in Zebra-treated cells, $n \geq 100$ cells) (Figure 5D). We also demonstrated that Mirin reduced the *MYC-IGH* colocalization rate in the MYCIGHC9 cells upon DNA damage induction in the *MYC* and *IGH* loci (5.42 ± 0.92% in Dox + Mirin treated cells vs. 8.87 ± 0.89% in Dox treated cells, $n \geq 90$ cells) (Supporting Information: Figure 7). Taken together, these data suggest that MRE11 could drive *MYC* displacement toward *IGH* following lytic cycle induction.

4 | DISCUSSION

The productive EBV lytic cycle increases the pool of infected B cells, but its intrinsic oncogenic effect is hardly conceivable due to the ensuing cell death[51]; however an abortive (incomplete) lytic cycle which does not lead to the cell lysis[14,52–55] may be involved in EBV-associated cancers (reviewed in[11,55]). During latency, EBV latent proteins induce *MYC* expression through a reconfiguration of the DNA loop domains formed by *MYC* and its specific enhancers.[56,57] Upon reactivation, the Zebra lytic protein blocks *MYC* expression[58] and the level of MYC protein controls the switch from latency to lytic cycle by negatively regulating *BZLF1*.[59] Therefore, *MYC* down-regulation required for lytic cycle activation might involve suppression of the DNA loops between *MYC* locus and its enhancers and could explain the *MYC* locus movement suggested in our study. However, the reason why specific DNA damage within the *MYC* locus occurs during EBV reactivation remains an open question.

BL is one of the most common EBV-related diseases. Here we provide the first direct experimental evidence that EBV lytic cycle predisposes to the appearance of the BL-specific t(8;14) chromosomal translocation. We found that both spontaneous and induced EBV reactivation led to a significant increase in the proportion of B cells showing the proximity between the *MYC* and *IGH* loci, otherwise located distantly in the nuclear space (Figure 1B,G; Supporting Information: Figure 1d). We also characterized here a rare case of primary EBV infection in an elderly patient caused by a kidney transplant from an EBV + donor into the EBV- recipient (P1, Table 1). In this patient, B cells undergoing EBV lytic cycle had a prominent increase in *MYC-IGH* colocalization (Figure 2). The development of BL is a possible scenario in posttransplant settings; these BLs have a high frequency of EBV positivity and a high mortality rate.[60–63]

MYC and *IGH* spatial proximity and simultaneous DSBs on the two loci are prerequisites for t(8;14) generation; however it has never been experimentally shown that their proximity leads to translocation. We for the first time developed a cell line where simultaneous breaks within the *MYC* and the *IGH* loci can be induced, leading to t(8;14) detectable and measurable by qPCR. In this model, by inducing *MYC-IGH* proximity through EBV reactivation before DSBs, we were able to provide the first direct experimental proof that increased *MYC-IGH* proximity leads to an increased t(8;14) rate (Figure 4).

We next demonstrated that specific DNA damage within the *MYC* locus could be a driving factor for the *MYC-IGH* proximity (Figure 5). Consistently, we showed that EBV reactivation significantly increased the rate of DNA damage within the *MYC* locus. (Figure 5A). Finally, our results point to a role for the DNA repair protein MRE11 in the *MYC* locus displacement. The *MRE11* gene is overexpressed upon EBV reactivation (Figure 5C) and MRE11 inhibition after EBV reactivation or induced-DSB on *MYC* locus almost halved the *MYC-IGH* proximity (Figure 5D and Supporting Information: Figure 7). These results are in agreement with data from other studies implicating MRE11 in the relocation of damaged DNA loci.[37,50,64,65]

Several other factors might contribute to increased *MYC-IGH* proximity in B cells. B cell activation was previously linked to *MYC* preferential relocation next to IGH,[43] and our results confirm this finding (Figure 1D,E). We have previously demonstrated that HIV-1 transactivator protein Tat may play a role in the development of B cell lymphomas and induce *MYC-IGH* proximity in primary B cells in vitro and in vivo.[37,66] Unlike Zebra, the presence of Tat alone is able to promote *MYC-IGH* proximity; but despite this difference, the generation of DNA damage within the *MYC* locus and its MRE11-dependent relocalization in the nucleus are observed in both cases. Consistently, DNA DSBs have already been linked to chromatin movement,[21,67,68] either for the search of a recombination partner[69,70] or to join the DNA repair centers.[64,71] The increased chromatin movement following DSBs may lead to translocations.[65]

In our system, DSBs were artificially generated by CRISPR/Cas9. In B cells, the main source of DSBs in the *MYC* and *IGH* loci is the AID involved in somatic hypermutation and class switch recombination.[25–27] Although AID has a specific affinity for immunoglobulin genes, it is also able to target a large number of other genes (~25% of all expressed genes in B-cells).[72] AID was observed to associate with the *MYC* and *IGH* loci and to produce DSBs.[73–75] Importantly, AID is localized in B cells in a discrete "recombination compartment" where it colocalizes with the *IGH*

locus.[76] Thus, colocalization of the *MYC* and *IGH* loci that we observed upon EBV reactivation might increase the probability of simultaneous AID-induced DSBs and thus t(8;14).

The role of EBV lytic cycle in the development of described genomic features points toward its causative role in endemic BL. Indeed, EBV contribution to *MYC-IGH* colocalisation can be correlated with the fact that African children with an EBV-reactivated serological profile are more likely to develop endemic BL.[77] Moreover, endemic EBV cofactors (*Plasmodium falciparum*, *Euphorbia tirucalli*, and aflatoxin B1) induce EBV reactivation.[78–80] Children living in EBV endemic areas and exposed to these cofactors, undergo repeated EBV reactivation with a subsequent increase in *MYC-IGH* proximity in their B cells. The oncogenic t(8;14) could then occur upon simultaneous DNA damage, for example, by AID.[29,30,81] As a matter of fact, *P. falciparum* is known to induce AID expression in B cells.[20,82] Monitoring and targeting EBV reactivation concomitantly with avoiding endemic EBV cofactors in this population may serve as a promising therapeutic approach to reduce the burden of endemic BL. EBV reactivation should be also monitored in posttransplant settings. Although currently there are no licensed drugs for the treatment of EBV reactivation, several therapeutic options are under development.[83]

In summary, we provide the first experimental evidence that EBV reactivation triggered *MYC* and *IGH* spatial proximity in vitro and in patients; this proximity increased the t(8;14) rate after DSB induction in the *MYC* and *IGH* loci. Finally, we suggested a role for the MRE11 protein in the *MYC* locus displacement next to the *IGH* locus.

AUTHOR CONTRIBUTIONS

Conceptualization: Yegor Vassetzky. *Data curation*: Fatimata Bintou Sall, Anna Shmakova, Anna Karpukhina, and Diego Germini. *Formal analysis*: Awa Oumar Toure, Marc Lipinski, and Joëlle Wiels. *Funding acquisition*: Yegor Vassetzky. *Investigation*: Fatimata Bintou Sall, Anna Shmakova, Diego Germini, Tatyana Tsfasman, Nikolai Lomov, Anna Karpukhina, and Reynand Jay Canoy. *Methodology*: Fatimata Bintou Sall and Diego Germini. *Project administration*: Diego Germini and Yegor Vassetzky. *Resources*: David Boutboul, Eric Oksenhendler, and Yegor Vassetzky. *Software*: Fatimata Bintou Sall, Anna Shmakova, Anna Karpukhina, and Diego Germini. *Supervision*: Diego Germini and Yegor Vassetzky. *Validation*: Anna Shmakova, Diego Germini, Anna Karpukhina, and Reynand Jay Canoy. *Visualization*: Fatimata Bintou Sall, Anna Shmakova, Anna Karpukhina, and Diego Germini. *Writing—original draft*: Fatimata Bintou Sall. *Writing—review & editing*: Anna Shmakova, Diego Germini, Joëlle Wiels, and Yegor Vassetzky.

ACKNOWLEDGMENTS

M81 and rMSHJ are a kind gift from Henri-Jacques Delecluse (DKFZ, Heidelberg, Germany). The authors thank Tudor Manoliu, Gustave Roussy Cancer Campus, Plateforme Imagerie et Cytométrie—UMS 23/3655—Université Paris Saclay, Villejuif, France for technical help. This study was supported by grants from the INSERM (ENVIBUR-KITT), La Ligue Contre le Cancer (M27231), and the IDB RAS government basic research program 0088-2021-0007. F. B. S. was a recipient of the grants from the Institut Servier and Service de coopération et d'action culturelle de l'Ambassade de France au Sénégal. A. K. is a recipient of the Eiffel Fellowship from Campus France. This study was supported by a grant from TA2019 and TA2021, Univ. Paris Sud, université Paris Saclay, France.

CONFLICT OF INTEREST STATEMENT

The authors declare no conflict of interest.

DATA AVAILABILITY STATEMENT

The data that support the findings of this study are available from the corresponding author upon reasonable request. All data generated or analyzed during this study are included in this published article and its additional files. No unique code or sequencing data was generated during the study. A semiautomatic macro for ImageJ is available at https://github.com/AnnaK135/sall2021_bmrf1.git.

ETHICS STATEMENT

Three patients were included in the study after obtaining an informed consent and a review by the local ethic committee (IMMUNOLYMPH protocol, CLEA-2020-113). Consent for publication has been obtained from the patients.

ORCID

Anna Shmakova http://orcid.org/0000-0001-7162-074X
Yegor Vassetzky http://orcid.org/0000-0003-3101-7043

REFERENCES

1. Brady G, MacArthur GJ, Farrell PJ. Epstein-Barr virus and Burkitt lymphoma. *Postgrad Med J*. 2008;84(12):372-377. doi:10.1136/jcp.2007.047977
2. Bornkamm GW. Epstein-Barr virus and the pathogenesis of Burkitt's lymphoma: more questions than answers. *Int J Cancer*. 2009;124(8):1745-1755. doi:10.1002/ijc.24223
3. Moormann AM, Bailey JA. Malaria—how this parasitic infection aids and abets EBV-associated Burkitt lymphomagenesis. *Current Opinion in Virology*. 2016;20:78-84. doi:10.1016/j.coviro.2016.09.006
4. Mawson AR, Majumdar S. Malaria, Epstein-Barr virus infection and the pathogenesis of Burkitt's lymphoma: malaria, EBV infection and the pathogenesis of Burkitt's lymphoma. *Int J Cancer*. 2017;141(9):1849-1855. doi:10.1002/ijc.30885
5. Shmakova A, Germini D, Vassetzky Y. HIV-1, HAART and cancer: a complex relationship. *Int J Cancer*. 2020;146(10):2666-2679. doi:10.1002/ijc.32730
6. Amon W, Farrell PJ. Reactivation of Epstein-Barr virus from latency. *Rev Med Virol*. 2005;15(3):149-156. doi:10.1002/rmv.456
7. Cohen JI. Epstein-Barr virus infection. *N Engl J Med*. 2000;343(7):481-492. doi:10.1056/NEJM200008173430707
8. Epstein MA, Henle G, Achong BG, Barr YM. Morphological and biological studies on a virus in cultured lymphoblasts from Burkitt's lymphoma. *J Exp Med*. 1965;121:761-770. doi:10.1084/jem.121.5.761
9. Tsurumi T, Fujita M, Kudoh A. Latent and lytic Epstein-Barr virus replication strategies. *Rev Med Virol*. 2005;15(1):3-15. doi:10.1002/rmv.441
10. Countryman J, Miller G. Activation of expression of latent Epstein-Barr herpesvirus after gene transfer with a small cloned subfragment of heterogeneous viral DNA. *Proc Natl Acad Sci*. 1985;82(12):4085-4089. doi:10.1073/pnas.82.12.4085

11. Germini D, Sall FB, Shmakova A, et al. Oncogenic properties of the EBV ZEBRA protein. *Cancers*. 2020;12(6):1479. doi:10.3390/cancers12061479
12. Grogan E, Jenson H, Countryman J, Heston L, Gradoville L, Miller G. Transfection of a rearranged viral DNA fragment, WZhet, stably converts latent Epstein-Barr viral infection to productive infection in lymphoid cells. *Proc Natl Acad Sci*. 1987;84(5):1332-1336. doi:10.1073/pnas.84.5.1332
13. Murata T, Tsurumi T. Switching of EBV cycles between latent and lytic states. *Rev Med Virol*. 2014;24(3):142-153. doi:10.1002/rmv.1780
14. Al Tabaa Y, Tuaillon E, Bollore K, et al. Functional Epstein-Barr virus reservoir in plasma cells derived from infected peripheral blood memory B cells. *Blood*. 2009;113(3):604-611. doi:10.1182/blood-2008-02-136903
15. Robinson M, Schor S, Barouch-Bentov R, Einav S. Viral journeys on the intracellular highways. *Cell Mol Life Sci*. 2018;75(20):3693-3714. doi:10.1007/s00018-018-2882-0
16. Rosemarie Q, Sugden B. Epstein-Barr virus: how its lytic phase contributes to oncogenesis. *Microorganisms*. 2020;8(11):1824. doi:10.3390/microorganisms8111824
17. Allday MJ. How does Epstein-Barr virus (EBV) complement the activation of Myc in the pathogenesis of Burkitt's lymphoma? *Sem Cancer Biol*. 2009;19(6):366-376. doi:10.1016/j.semcancer.2009.07.007
18. Molyneux EM, Rochford R, Griffin B, et al. Burkitt's lymphoma. *Lancet*. 2012;379(9822):1234-1244. doi:10.1016/S0140-6736(11)61177-X
19. Saleh K, Michot JM, Camara-Clayette V, Vassetsky Y, Ribrag V. Burkitt and Burkitt-like lymphomas: a systematic review. *Curr Oncol Rep*. 2020;22(4):33. doi:10.1007/s11912-020-0898-8
20. Torgbor C, Awuah P, Deitsch K, Kalantari P, Duca KA, Thorley-Lawson DA. A multifactorial role for *P. falciparum* malaria in endemic Burkitt's lymphoma pathogenesis. *PLoS Pathog*. 2014;10(5):e1004170. doi:10.1371/journal.ppat.1004170
21. Iarovaia OV, Rubtsov M, Ioudinkova E, Tsfasman T, Razin SV, Vassetzky YS. Dynamics of double strand breaks and chromosomal translocations. *Mol Cancer*. 2014;13:249. doi:10.1186/1476-4598-13-249
22. Roix JJ, McQueen PG, Munson PJ, Parada LA, Misteli T. Spatial proximity of translocation-prone gene loci in human lymphomas. *Nature Genet*. 2003;34(3):287-291. doi:10.1038/ng1177
23. Roukos V, Burman B, Misteli T. The cellular etiology of chromosome translocations. *Curr Opin Cell Biol*. 2013;25(3):357-364. doi:10.1016/j.ceb.2013.02.015
24. Canoy RJ, Shmakova A, Karpukhina A, Shepelev M, Germini D, Vassetzky Y. Factors that affect the formation of chromosomal translocations in cells. *Cancers*. 2022;14(20):5110. doi:10.3390/cancers14205110
25. Honjo T, Kinoshita K, Muramatsu M. Molecular mechanism of class switch recombination: linkage with somatic hypermutation. *Annu Rev Immunol*. 2002;20:165-196. doi:10.1146/annurev.immunol.20.090501.112049
26. Chaudhuri J, Basu U, Zarrin A, et al. Evolution of the immunoglobulin heavy chain class switch recombination mechanism. *Adv Immunol*. 2007;94:157-214. doi:10.1016/S0065-2776(06)94006-1
27. Di Noia JM, Neuberger MS. Molecular mechanisms of antibody somatic hypermutation. *Annu Rev Biochem*. 2007;76:1-22. doi:10.1146/annurev.biochem.76.061705.090740
28. Sall FB, Germini D, Kovina AP, et al. Effect of environmental factors on nuclear organization and transformation of human B lymphocytes. *Biochemistry*. 2018;83(4):402-410. doi:10.1134/S0006297918040119
29. Dorsett Y, Robbiani DF, Jankovic M, Reina-San-Martin B, Eisenreich TR, Nussenzweig MC. A role for AID in chromosome translocations between c-myc and the IgH variable region. *J Exp Med*. 2007;204(9):2225-2232. doi:10.1084/jem.20070884
30. Ramiro AR, Jankovic M, Eisenreich T, et al. AID is required for c-myc/IgH chromosome translocations in vivo. *Cell*. 2004;118(4):431-438. doi:10.1016/j.cell.2004.08.006
31. Nijland ML, Kersten MJ, Pals ST, Bemelman FJ, ten Berge IJM. Epstein-Barr virus–positive posttransplant lymphoproliferative disease after solid organ transplantation: pathogenesis, clinical manifestations, diagnosis, and management. *Transplant Direct*. 2016;2(1):e48. doi:10.1097/TXD.0000000000000557
32. Delecluse S, Poirey R, Zeier M, et al. Identification and cloning of a new western Epstein-Barr virus strain that efficiently replicates in primary B cells. *J Virol*. 2020;94(10):e01918-19. doi:10.1128/JVI.01918-19
33. Shmakova A, Lomov N, Viushkov V, et al. Cell models with inducible oncogenic translocations allow to evaluate the potential of drugs to favor secondary translocations. *Cancer Commun*. 2022;43:154-158. doi:10.1002/cac2.12370
34. Canoy RJ, André F, Shmakova A, et al. Easy and robust electrotransfection protocol for efficient ectopic gene expression and genome editing in human B cells. *Gene Therapy*. 2020;30:167-171. doi:10.1038/s41434-020-00194-x
35. Germini D, Bou Saada Y, Tsfasman T, et al. A one-step PCR-based assay to evaluate the efficiency and precision of genomic DNA-editing tools. *Mol Therapy—Methods Clin Development*. 2017;5:43-50. doi:10.1016/j.omtm.2017.03.001
36. Sall FB, El Amine R, Markozashvili D, et al. HIV-1 Tat protein induces aberrant activation of *AICDA* in human B-lymphocytes from peripheral blood. *J Cell Physiol*. 2019;234(9):15678-15685. doi:10.1002/jcp.28219
37. Germini D, Tsfasman T, Klibi M, et al. HIV Tat induces a prolonged MYC relocalization next to IGH in circulating B-cells. *Leukemia*. 2017;31(11):2515-2522. doi:10.1038/leu.2017.106
38. Pannunzio NR, Watanabe G, Lieber MR. Nonhomologous DNA end-joining for repair of DNA double-strand breaks. *J Biol Chem*. 2018;293(27):10512-10523. doi:10.1074/jbc.TM117.000374
39. Sklyar I, Iarovaia OV, Gavrilov AA, et al. Distinct patterns of colocalization of the CCND1 and CMYC genes with their potential translocation partner IGH at successive stages of B-cell differentiation. *JCB*. 2016;117(7):1506-1510. doi:10.1002/jcb.25516
40. Kim KD, Tanizawa H, De Leo A, et al. Epigenetic specifications of host chromosome docking sites for latent Epstein-Barr virus. *Nat Commun*. 2020;11(1):877. doi:10.1038/s41467-019-14152-8
41. Li C, Shi Z, Zhang L, et al. Dynamic changes of territories 17 and 18 during EBV-infection of human lymphocytes. *Mol Biol Rep*. 2010;37(5):2347-2354. doi:10.1007/s11033-009-9740-y
42. Moquin SA, Thomas S, Whalen S, et al. The Epstein-Barr virus episome maneuvers between nuclear chromatin compartments during reactivation. *J Virol*. 2018;92(3):e01417. doi:10.1128/JVI.01413-17
43. Osborne CS, Chakalova L, Mitchell JA, et al. Myc dynamically and preferentially relocates to a transcription factory occupied by Igh. *PLoS Biol*. 2007;5(8):e192. doi:10.1371/journal.pbio.0050192
44. Tsai MH, Raykova A, Klinke O, et al. Spontaneous lytic replication and epitheliotropism define an Epstein-Barr virus strain found in carcinomas. *Cell Rep*. 2013;5(2):458-470. doi:10.1016/j.celrep.2013.09.012
45. Küppers R, Dalla-Favera R. Mechanisms of chromosomal translocations in B cell lymphomas. *Oncogene*. 2001;20(40):5580-5594. doi:10.1038/sj.onc.1204640
46. Simsek D, Jasin M. Alternative end-joining is suppressed by the canonical NHEJ component Xrcc4-ligase IV during chromosomal translocation formation. *Nat Struct Mol Biol*. 2010;17(4):410-416. doi:10.1038/nsmb.1773

47. Soni A, Siemann M, Pantelias GE, Iliakis G. Marked contribution of alternative end-joining to chromosome-translocation-formation by stochastically induced DNA double-strand-breaks in G2-phase human cells. *Mutation Res/Genetic Toxicol Environmental Mutag*. 2015;793:2-8. doi:10.1016/j.mrgentox.2015.07.002
48. Vogt N, Dai B, Erdmann T, Berdel WE, Lenz G. The molecular pathogenesis of mantle cell lymphoma. *Leuk Lymphoma*. 2017;58(7):1530-1537. doi:10.1080/10428194.2016.1248965
49. Hau P, Tsao S. Epstein–Barr virus hijacks DNA damage response transducers to orchestrate its life cycle. *Viruses*. 2017;9(11):341. doi:10.3390/v9110341
50. Caridi CP, D'Agostino C, Ryu T, et al. Nuclear F-actin and myosins drive relocalization of heterochromatic breaks. *Nature*. 2018;559(7712):54-60. doi:10.1038/s41586-018-0242-8
51. Münz C. Latency and lytic replication in Epstein–Barr virus-associated oncogenesis. *Nat Rev Microbiol*. 2019;17(11):691-700. doi:10.1038/s41579-019-0249-7
52. Arvey A, Tempera I, Tsai K, et al. An atlas of the Epstein-Barr virus transcriptome and epigenome reveals host-virus regulatory interactions. *Cell Host Microbe*. 2012;12(2):233-245. doi:10.1016/j.chom.2012.06.008
53. Chiu YF, Sugden B. Epstein-Barr virus: the path from latent to productive infection. *Annual Rev Virol*. 2016;3(1):359-372. doi:10.1146/annurev-virology-110615-042358
54. Ersing I, Nobre L, Wang LW, et al. A temporal proteomic map of Epstein-Barr virus lytic replication in B cells. *Cell Rep*. 2017;19(7):1479-1493. doi:10.1016/j.celrep.2017.04.062
55. Morales-Sánchez A, Fuentes-Panana E. The immunomodulatory capacity of an Epstein-Barr virus abortive lytic cycle: potential contribution to viral tumorigenesis. *Cancers*. 2018;10(4):98. doi:10.3390/cancers10040098
56. Wood CD, Veenstra H, Khasnis S, et al. MYC activation and BCL2L11 silencing by a tumour virus through the large-scale reconfiguration of enhancer-promoter hubs. *eLife*. 2016;5:e18270. doi:10.7554/eLife.18270
57. Jiang S, Zhou H, Liang J, et al. The Epstein-Barr virus regulome in lymphoblastoid cells. *Cell Host Microbe*. 2017;22(4):561-573.e4. doi:10.1016/j.chom.2017.09.001
58. Rodriguez A, Jung EJ, Yin Q, Cayrol C, Flemington EK. Role of c-myc regulation in Zta-mediated induction of the cyclin-dependent kinase inhibitors p21 and p27 and cell growth arrest. *Virology*. 2001;284(2):159-169. doi:10.1006/viro.2001.0923
59. Guo R, Jiang C, Zhang Y, et al. MYC controls the Epstein-Barr virus lytic switch. *Mol Cell*. 2020;78(4):653-669. doi:10.1016/j.molcel.2020.03.025
60. Ferreiro JF, Morscio J, Dierickx D, et al. Post-transplant molecularly defined Burkitt lymphomas are frequently MYC-negative and characterized by the 11q-gain/loss pattern. *Haematologica*. 2015;100(7):e275-e279. doi:10.3324/haematol.2015.124305
61. Djokic M, Le Beau MM, Swinnen LJ, et al. Post-transplant lymphoproliferative disorder subtypes correlate with different recurring chromosomal abnormalities. *Genes Chromosom Cancer*. 2006;45(3):313-318. doi:10.1002/gcc.20287
62. Picarsic J, Jaffe R, Mazariegos G, et al. Post-transplant Burkitt lymphoma is a more aggressive and distinct form of post-transplant lymphoproliferative disorder. *Cancer*. 2011;117(19):4540-4550. doi:10.1002/cncr.26001
63. Akar Özkan E, Özdemir BH, Akdur A, Deniz EE, Haberal M. Burkitt lymphoma after transplant: an aggressive lymphoproliferative disease. *Exp Clin Transplant*. 2014;12(Suppl 1):136-138.
64. Aten JA, Stap J, Krawczyk PM, et al. Dynamics of DNA double-strand breaks revealed by clustering of damaged chromosome domains. *Science*. 2004;303(5654):92-95. doi:10.1126/science.1088845
65. Roukos V, Voss TC, Schmidt CK, Lee S, Wangsa D, Misteli T. Spatial dynamics of chromosome translocations in living cells. *Science*. 2013;341(6146):660-664. doi:10.1126/science.1237150
66. Valyaeva AA, Tikhomirova MA, Potashnikova DM, et al. Ectopic expression of HIV-1 Tat modifies gene expression in cultured B cells: implications for the development of B-cell lymphomas in HIV-1-infected patients. *PeerJ*. 2022;10:e13986. doi:10.7717/peerj.13986
67. Krawczyk PM, Borovski T, Stap J, et al. Chromatin mobility is increased at sites of DNA double-strand breaks. *J Cell Sci*. 2012;125(Pt 9):2127-2133. doi:10.1242/jcs.089847
68. Kruhlak MJ, Celeste A, Dellaire G, et al. Changes in chromatin structure and mobility in living cells at sites of DNA double-strand breaks. *J Cell Biol*. 2006;172(6):823-834. doi:10.1083/jcb.200510015
69. Miné-Hattab J, Chiolo I. Complex chromatin motions for DNA repair. *Front Genet*. 2020;11:800. doi:10.3389/fgene.2020.00800
70. Miné-Hattab J, Rothstein R. Increased chromosome mobility facilitates homology search during recombination. *Nature Cell Biol*. 2012;14(5):510-517. doi:10.1038/ncb2472
71. Neumaier T, Swenson J, Pham C. Evidence for formation of DNA repair centers and dose-response nonlinearity in human cells. *Proc Natl Acad Sci*. 2012;109(2):443-448. doi:10.1073/pnas.1117849108
72. Liu M, Duke JL, Richter DJ. Two levels of protection for the B cell genome during somatic hypermutation. *Nature*. 2008;451(7180):841-845. doi:10.1038/nature06547
73. Boerma EG, Siebert R, Kluin PM, Baudis M. Translocations involving 8q24 in Burkitt lymphoma and other malignant lymphomas: a historical review of cytogenetics in the light of todays knowledge. *Leukemia*. 2009;23(2):225-234. doi:10.1038/leu.2008.281
74. Duquette ML, Pham P, Goodman MF, Maizels N. AID binds to transcription-induced structures in c-MYC that map to regions associated with translocation and hypermutation. *Oncogene*. 2005;24(38):5791-5798. doi:10.1038/sj.onc.1208746
75. Yu K, Chedin F, Hsieh CL, Wilson TE, Lieber MR. R-loops at immunoglobulin class switch regions in the chromosomes of stimulated B cells. *Nature Immunol*. 2003;4(5):442-451. doi:10.1038/ni919
76. Pichugin A, Iarovaia OV, Gavrilov A. The IGH locus relocalizes to a "recombination compartment" in the perinucleolar region of differentiating B-lymphocytes. *Oncotarget*. 2017;8(25):40079-40089. doi:10.18632/oncotarget.16941
77. Coghill AE, Proietti C, Liu Z, et al. The association between the comprehensive Epstein-Barr virus serologic profile and endemic burkitt lymphoma. *Cancer Epidemiol Biomarkers Prevent*. 2020;29(1):57-62. doi:10.1158/1055-9965.EPI-19-0551
78. Accardi R, Gruffat H, Sirand C. The mycotoxin aflatoxin B1 stimulates Epstein-Barr virus-induced B-cell transformation in in vitro and in vivo experimental models. *Carcinogenesis*. 2015;36(11):1440-1451. doi:10.1093/carcin/bgv142
79. Chêne A, Donati D, Guerreiro-Cacais AO. A molecular link between malaria and Epstein-Barr virus reactivation. *PLoS Pathog*. 2007;3(6):e80. doi:10.1371/journal.ppat.0030080
80. MacNeil A, Sumba OP, Lutzke ML, Moormann A, Rochford R. Activation of the Epstein-Barr virus lytic cycle by the latex of the plant *Euphorbia tirucalli*. *Br J Cancer*. 2003;88(10):1566-1569. doi:10.1038/sj.bjc.6600929
81. Robbiani DF, Bothmer A, Callen E, et al. AID is required for the chromosomal breaks in c-myc that lead to c-myc/IgH translocations. *Cell*. 2008;135(6):1028-1038. doi:10.1016/j.cell.2008.09.062
82. Robbiani DF, Deroubaix S, Feldhahn N, et al. Plasmodium infection promotes genomic instability and AID-dependent B cell lymphoma. *Cell*. 2015;162(4):727-737. doi:10.1016/j.cell.2015.07.019

83. Kerr JR. Epstein-Barr virus (EBV) reactivation and therapeutic inhibitors. *J Clin Pathol*. 2019;72(10):651-658. doi:10.1136/jclinpath-2019-205822

SUPPORTING INFORMATION

Additional supporting information can be found online in the Supporting Information section at the end of this article.

How to cite this article: Sall FB, Shmakova A, Karpukhina A, et al. Epstein–Barr virus reactivation induces *MYC-IGH* spatial proximity and t(8;14) in B cells. *J Med Virol*. 2023;95:e28633. doi:10.1002/jmv.28633

Supplementary Material and Methods

EBV-positive B cell lines

RPMI8866 and PRIESS are human EBV-transformed lymphoblastoid cell lines (LCLs). M81 and rMSHJ are LCLs with an enhanced spontaneous EBV lytic activity. EBV M81 strain was isolated from a Chinese patient with nasopharyngeal carcinoma. The rMSHJ cell line was generated by infection of common marmoset peripheral B cells with an EBV virus isolated from a German stem cell transplant recipient with increased EBV load [1,2]. All LCLs were cultured in RPMI 1640, supplemented with 10% fetal bovine serum, 2mM L-Glutamine, 1mM sodium pyruvate, 20mM glucose, 100 U/ml penicillin and 100 μg/ml streptomycin (all reagents for cell culture were from Gibco®, Thermofisher scientific).

RPMI8866 cell lines inducibly expressing CRISPR/Cas9 and guide RNAs targeting specific gene loci

RPMI8866 cell lines inducibly expressing CRISPR/Cas9 were created as follows. First, the guide RNAs (gRNAs) targeting *MYC*, *IGH, ETO* and *AML* genes were designed and cloned into the phU6-gRNA plasmid (Addgene #53188). gRNAs efficacy was confirmed by the ENIT method [3]. The sequences of the selected gRNAs are listed in **Supplementary table 1.** Then the gRNAs were amplified, purified and cloned by the SalI restriction enzyme site into Puro_Cas9 donor plasmid (Addgene #58409). The final plasmids containing the cassette of the selected gRNA(s), the Cas9 gene and the puromycin resistance gene (Puro-Cas9_gRNA(s) plasmid), were assembled using Gibson Assembly Master Mix kit (NEB, USA).

The RPMI8866 cells were co-electrotransfected with the generated Puro-Cas9_gRNA(s) plasmid, a Tet-inducible Cas9 gene + AAVS1-Neo-M2rtTA plasmid (Addgene, #60843) and two TALEN plasmids for cutting in the safe-harbor site (AAVS1-TALEN-L+ AAVS1-TALEN-R) (Addgene # 59025 and # 59026) using a protocol developed in our laboratory [4]. Then the cells were maintained in the RPMI 1640 medium, supplemented with 10% certified tetracycline-free fetal bovine serum (Takara, Japan), 100 U/ml penicillin, 100 μg/ml streptomycin, and 800 µg/ml G418 antibiotic. Resistant cells were cloned *via* finite dilution technique in a 96-well plate. Clones and bulk lines were grown with and without 1 μg/ml doxycycline (Dox) for 48h and then tested for the presence of specific translocations.

Using this technology, we generated four different cell lines expressing gRNAs targeting both *MYC* and *IGH*; *MYC* only; *IGH* only and both *AML* and *ETO* loci named MYCIGHC9, MYCC9, IGHC9 and AMLETOC9, respectively. All cells were cultured as described above.

Primary human B cell isolation and activation

Whole blood samples from healthy donors of different sex and age were obtained from the “Etablissment Français du Sang”, Hôpital Saint-Louis, Paris, France. In agreement with French law, the study was registered as a non-interventional study at the Agence Nationale de Sécurité du Médicament (2016-A01316-45) and an informed consent was obtained from all subjects. B cells were purified from peripheral blood by negative selection using the Magnisort B cell enrichment kit II (Invitrogen, Thermo Fisher Scientific, Carlsbad, CA) after PBMC isolation by Ficoll density gradient centrifugation. These B cells were considered as EBV-negative B cells as even in case of EBV-positive healthy donors, the probability of encountering an EBV positive circulating B cell is extremely low: 1-50/10^6 cells during latency or 1-10/10^3 cells during lytic phase [5]. At most 400 B cells were analysed for 3D-FISH.

Primary B cells plated at 10^6 cells/mL were activated by addition of a cocktail of reagents composed of recombinant human IL4 (Proteintech, 10 ng/mL), an anti-human CD40 monoclonal antibody (Sigma, 1 µg/mL) and an anti-human IgM monoclonal antibody

(eBioscience, 20 µg/mL) in complete medium and left in culture for 48 hours. Cells were then treated or not with Zebra for 48 hours as described later. B cell purity and activation were verified by double staining with a phycoerythrin (PE)-conjugated anti-CD19 antibody (Biolegend, dilution 1:200) and a fluorescein isothiocyanate (FITC)-coupled anti-CD23 antibody (BD Pharmingen, dilution 1:200) for 30 minutes (data not shown).

Patients' history

P1 was a 74 y.o. male admitted for deterioration of general status, fever and enlarged lymph nodes 4 months after receiving a kidney transplant for end-stage obstructive nephropathy. Conditioning regimen associated with anti-Thymoglobulin, Mycophenolate mofetil (MMF), tacrolimus and steroids. There was a mismatched EBV status with an EBV+ donor and an EBV- recipient. Biological evaluation performed at M4 post transplantation showed emergence of anti-VCA IgM and IgG with high whole blood EBV replication (6 log). Lymph node biopsy showed pathological aspects compatible with infectious mononucleosis. MMF was stopped and a 4-weekly course of rituximab was administered with an unfavorable course. The patient died from refractory hemophagocytic lympho-histiocytosis (HLH).

P2 is a 43 y.o. female admitted with a recent aphasia revealing multifocal brain lesions. She had been diagnosed with systemic lupus erythematosus 20 years earlier and recurrent flares required prolonged heavy immunosuppression. She had been immunized against EBV for more than 10 years. Stereotactic biopsy of one lesion showed cerebral EBV+ polymorphic B-cell lymphoproliferative disorder related to acquired severe immunosuppression. No extracerebral lesion was noted, with a low whole blood EBV replication (3 log). She received combined immuno-chemotherapy (4 cycles of rituximab + cytarabine) with obtention of a complete remission.

P3 is a 23 y.o. female with no past medical history, admitted in the ICU for severe HLH. Enlarged lymph nodes, liver and spleen were present at admission but severe coagulation disorders related to HLH precluded lymph nodes or liver sampling. Peripheral blood workup showed positivity for anti-VCA IgM and IgG, negativity for anti-EBNA, very few circulating B cells and high whole blood EBV replication (8 log). Severe infectious mononucleosis was diagnosed and she received steroids, etoposide and cyclosporin with a favorable outcome.

Cell treatment

Cells were treated or not with specific substances at concentrations listed in **Supplementary Table 2** for indicated times before being collected and processed for the different experiments.

Western Blot

Approximately 10^7 cells were collected at indicated time points by centrifugation (10 minutes 1000 x g). Cell pellet was then resuspended in 150 μl of NETN buffer (NaCl 150mM, EDTA 1mM, Tris pH 7.5 50mM, NP40 0.5%, protease inhibitor cocktail (Roche)). Resuspended cells were then sonicated 10 seconds at 30% of intensity to completely lyse cells using a Vibra Cell sonicator (Newtown, CT, USA) and incubated on ice for 30 minutes. Cell lysates were then centrifuged at 4° at maximum speed for 10 minutes. Supernatants were aliquoted and stored at -80°C. Proteins were quantified using the Pierce™ BCA Protein Assay Kit and the Nanodrop (Thermo scientific).

Thirty micrograms (µg) of protein were loaded onto a 4-12% SDS-PAGE precast gel (Invitrogen) in the MOPS running buffer (Invitrogen), run at 80V for 30 minutes and then 120V for 75 minutes and transferred onto a PVDF membrane (GE healthcare, USA) at 90V at 4° for 2 hours in transfer buffer (0.025M Tris, 0.192M Glycine, 20% ethanol). The membrane was then blocked with 5% milk in 1X TBST buffer (Tris-buffered saline, 0.1% Tween-20) for 1h at room temperature (RT) before an overnight incubation with specific primary antibodies at 4°C.

The following day membranes were washed with 1X TBST buffer three times (5 minutes each) and incubated for 1h at RT with a secondary HRP-conjugated antibody. After three washes with 1X TBST, the membrane was incubated with Immobilon® Western Chemiluminescent HRP substrate (Merck-Millipore, USA) reagent before exposure and revelation. Western blot band intensity quantification was performed using ImageJ software. The band intensity of the target protein was always normalized to the band intensity of the loading control protein. The following primary antibodies were used: mouse anti-Cas 9 (Santa Cruz) at a concentration of 1:200; mouse anti-Zebra (a kind gift from Emmanuel Drouet, Université Grenoble Alpes, France) at a concentration of 1:1000, rabbit anti-α-tubulin (Santa Cruz) at a concentration of 1:1000 and mouse anti-β-actin (Santa Cruz) at a concentration of 1:1000. Anti-rabbit or anti-mouse HRP-conjugated secondary antibodies were used at a concentration of 1:2500 (Invitrogen).

Cell cycle analysis

The cell cycle was analysed as follows: cells were washed with PBS and fixed in 70% ice-cold ethanol overnight. RNA was digested with RNAse A (100 µg/ml) and cells were stained with propidium iodide (10 µg/ml). The fluorescence was analyzed using BD Accuri C6 Plus Flow Cytometer (BD Biosciences, USA) and BD Accuri C6 software, the same gating was applied to all samples within one experiment.

Quantitative RT-PCR

Total RNA was extracted using Nucleospin® RNA II purification kit (Macherey-Nagel) according to the manufacturer's protocol. cDNA synthesis was performed as previously described [6]. QPCR amplification was performed using the PowerUp SYBR Green Master Mix (Thermo Scientific) with the following cycling conditions: 1 cycle of 50°C (2mn) + 95°C (2mn); 40 cycles 95°C (15s) + 60°C (1mn) + 72°C (1mn) and 1 cycle 72°C (10mn). Primer sequences are listed in **Supplementary Table 3**. The $2^{-\Delta\Delta Ct}$ method was used for comparative expression analysis of target genes with normalization to *GAPDH*. Comparison of expression was done between untreated RPMI8866 cells (control) and treated ones; or between RPMI8866 cells and M81 and rMSHJ cells. RPMI8866 gene expression levels were set to 1.

Quantitative PCR

Total DNA was extracted using Nucleospin® Tissue DNA purification (MACHEREY-NAGEL) according to the manufacturer's protocol. DNA was quantified by Nanodrop (Thermo scientific). Five hundred ng of genomic DNA were amplified using *MYC* and *IGH* specific primers designed surrounding the DNA breakpoints for translocation detection and, as a control, specific *MYC* primers designed ~6.5 kbp downstream from the breakpoint sequence. PCR amplification was performed using the PowerUp SYBR Green Master Mix (Thermo Scientific) using the following program: 1 cycle of 50°C (2mn) + 95°C (2mn); 40 cycles 95°C (15s) + 60°C (1mn) + 72°C (1mn) and 1 cycle 72°C (10mn). Primer sequences are listed in **Supplementary Table 3**. PCR products were loaded on 1% agarose gel and migrated by electrophoresis for amplicon visualization. For quantification of the translocation rate, the $2^{-\Delta\Delta Ct}$ method was used. Translocation expression was first normalized to *MYC* expression and then compared to 12h post Dox treatment time point for Dox kinetics experiment and cells treated only with Dox when studying the translocation level variation after EBV reactivation. Translocation level was set to 1 for all controls.

Estimation of the CRISPR/Cas9-induced t(8;14) rate

The rate of the CRISPR/Cas9-induced t(8;14) was estimated after Dox treatment by ΔCt of *MYC-IGH* and *MYC* amplicons. If $\Delta Ct = X$, the value gave us a rough estimation that per each *MYC* locus there are 2^{-X} specific *MYC-IGH* translocations or 2×2^{-X} per 1 cell. The estimation assumes that all cells are in G1, each cell has 2 *MYC* loci, and that primers' efficiencies are equal to 2.

3D-FISH and Immuno-3D FISH

Hybridization and staining of human chromosome loci 8q24 (*MYC* gene locus), 14q32 (*IGH* gene locus) and 11q13 (*CCND1* gene locus) were performed using “RainbowFISH" probes (Empire Genomics, Buffalo, NY, USA). *MYC* and *CCND1* were labelled with SpectrumOrange and *IGH* with SpectrumGreen. 3D-FISH was performed as previously described [27]. For immuno-3D-FISH, cells were immuno-stained after 3D-FISH with rabbit anti-histone H2AX phospho-Ser139 (γH2AX) (Active Motif, diluted 1:500) or mouse anti-BMRF1 (Sigma, diluted 1:100). Alexa-633 anti-rabbit antibody or Alexa-647 anti-mouse antibody (Invitrogen) were used as a secondary antibody diluted 1:200. Nuclei were counterstained with DAPI diluted 1:1000 in the Vectashield mounting medium (Vector Laboratories, Burlingame, CA, USA).

Image acquisition and analysis

Multiphoton SP8 confocal microscope (Leica Microsystems, Berlin, Germany) with a 63X oil immersion objective was used for 3D-FISH and Immuno-3D FISH images acquisition. Z-stacks were acquired using a frame size of 1024 × 1024, and 0.5 µm z-steps, with sequential multitrack scanning using the 405, 488, 543, 633 nm laser wavelengths. For *MYC-IGH* and *CCND1-IGH* colocalization, Imaris software (Bitplane) was used. The colocalization rate corresponded to the percentage of cells where at least one *MYC* or *CCND1* locus was located 1 μm or less from one *IGH* locus. The LEICA Application Suite X (Leica Microsystems) software was used to evaluate the percentage of cells that have colocalized γH2AX foci with *MYC* and/or *IGH*.
The abundance of the EBV early lytic protein BMRF1 was assessed in ImageJ using a semi-automatic macro (https://github.com/AnnaK135/sall2021_bmrf1.git). For each field, mean nuclear BMRF1 fluorescence intensity was measured and the background fluorescence of BMRF1-negative nuclei from the same field was subtracted). 2-6 fields (67-120 nuclei per field) were analysed in 2-3 biological replicates.

Statistics

All statistical tests were performed using the Graphpad Prism 5 software (GraphPad software Inc., La Jolla, CA). One-way analysis of variance (ANOVA) test followed by Bonferroni's post-test or Student’s t-test was used to compare averages between different groups. For binary comparisons of colocalization rate χ^2 test was also used, odds ratio (OR) [95% confidence interval], χ^2 value and p-value are provided. Two-way ANOVA followed by Bonferroni's post-test was used to compare averages for multiple-group comparisons with two factors (cell cycle and proliferation data). Data are presented as mean ± standard error of mean (SEM).

References

1. Delecluse, S.; Poirey, R.; Zeier, M.; Schnitzler, P.; Behrends, U.; Tsai, M.-H.; Delecluse, H.-J. Identification and Cloning of a New Western Epstein-Barr Virus Strain That Efficiently Replicates in Primary B Cells. J Virol 2020, 94, doi:10.1128/JVI.01918-19.

2. Tsai, M.-H.; Raykova, A.; Klinke, O.; Bernhardt, K.; Gärtner, K.; Leung, C.S.; Geletneky, K.; Sertel, S.; Münz, C.; Feederle, R.; et al. Spontaneous Lytic Replication and Epitheliotropism Define an Epstein-Barr Virus Strain Found in Carcinomas. Cell Rep 2013, 5, 458–470, doi:10.1016/j.celrep.2013.09.012.

3. Germini, D.; Bou Saada, Y.; Tsfasman, T.; Osina, K.; Robin, C.; Lomov, N.; Rubtsov, M.; Sjakste, N.; Lipinski, M.; Vassetzky, Y. A One-Step PCR-Based Assay to Evaluate the Efficiency and Precision of Genomic DNA-Editing Tools. Mol Ther Methods Clin Dev 2017, 5, 43–50, doi:10.1016/j.omtm.2017.03.001.

4. Canoy, R.J.; André, F.; Shmakova, A.; Wiels, J.; Lipinski, M.; Vassetzky, Y.; Germini, D. Easy and Robust Electrotransfection Protocol for Efficient Ectopic Gene Expression and Genome Editing in Human B Cells. Gene Ther 2020, doi:10.1038/s41434-020-00194-x.

5. Nijland, M.; Kersten, M.J.; Pals, S.; Bemelman, F.; ten Berge, I. Epstein-Barr Virus–Positive Posttransplant Lymphoproliferative Disease After Solid Organ Transplantation: Pathogenesis, Clinical Manifestations, Diagnosis, and Management. Transplantation Direct 2016, 2, e48, doi:10.1097/TXD.0000000000000557.

6. Sall, F.B.; El Amine, R.; Markozashvili, D.; Tsfasman, T.; Oksenhendler, E.; Lipinski, M.; Vassetzky, Y.; Germini, D. HIV-1 Tat Protein Induces Aberrant Activation of AICDA in Human B-lymphocytes from Peripheral Blood. J Cell Physiol 2019, 234, 15678–15685, doi:10.1002/jcp.28219.

Supplementary figure legends

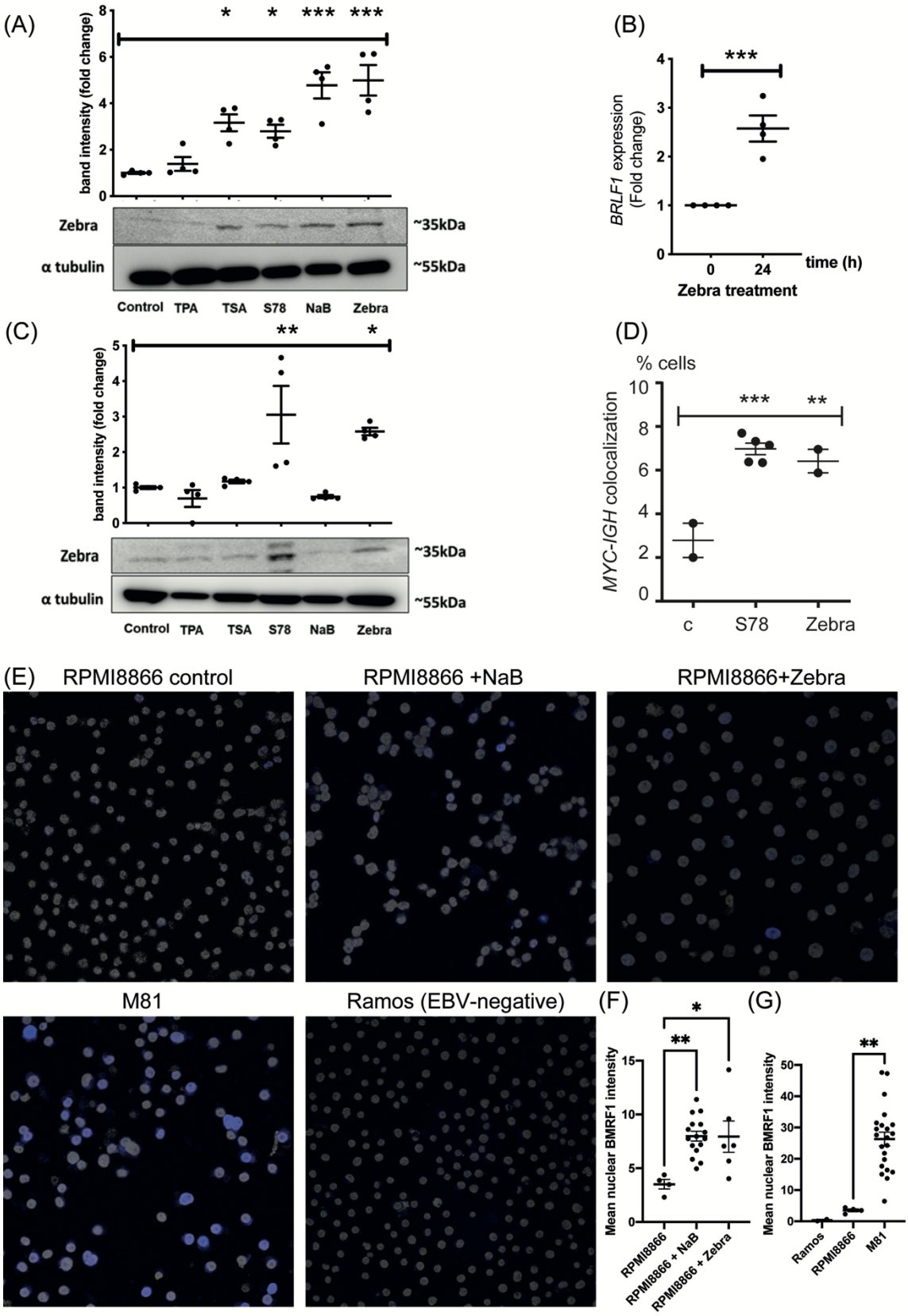

Supplementary Fig. 1. EBV lytic cycle induction in RPMI8866 and PRIESS cells. (a) RPMI8866 cells were treated with different EBV lytic cycle inducers (TPA: 12-O-tetradecanoylphorbol-13-acetate; TSA: trichostatin A; S78: histone deacetylase inhibitor Abexinostat; NaB: sodium

butyrate) for 24h and protein extracts were analyzed by western blot for detection of EBV immediate early protein Zebra expression. Alpha tubulin was used as a loading control (Bottom panel). Zebra specific bands were quantified by densitometry and normalized to α-tubulin bands intensity. Results are represented as a fold change of the intensity in treated cells compared with the intensity in untreated cells (control), set as 1 (upper panel). A representative western blot image is shown below the graph. (b) EBV immediate early *BRLF1* gene expression analysis by qRT-PCR in cells treated with recombinant Zebra protein for 24h. Fold change expression is in comparison with *BRLF1* gene expression level after normalization to *GAPDH* expression in untreated RPMI8866, set as 1. Data are plotted as mean ± SEM. **p*<0.05; ****p*<0.001 as compared by ANOVA, Bonferroni's post-test (a) or t-test (b). Results of three independent experiments are presented. EBV lytic cycle induction in lymphoblastoid cell line PRIESS. (c) EBV immediate early protein Zebra expression detected by western blot (bottom panels) after PRIESS cells treatment with different EBV lytic cycle inducers for 24h. Zebra bands intensity (top panels) of three replicates were quantified and normalized to α-tubulin. Fold change of band intensity are compared to band intensity of untreated cells (Control), set as 1. (d) *MYC-IGH* colocalization in PRIESS untreated or treated with S78 or Zebra recombinant protein to induce lytic cycle. 3D-FISH was performed 48h after treatment. A minimum of 100 cells from at least two different experiments were analysed. TPA: 12-O-tetradecanoylphorbol-13-acetate; TSA: trichostatin A; S78: histone deacetylase inhibitor Abexinostat; NaB: sodium butyrate. Data are plotted as mean ± SEM. **p*<0.05; ***p*<0.01; ****p*<0.001 as compared by ANOVA, Bonferroni's post-test. (e) Representative images of immunofluorescent staining of the EBV early lytic protein BMRF1 in RPMI8866 control and sodium butyrate (NaB) treated cells (48 hours of treatment), in spontaneously EBV reactivating M81 line and Ramos EBV-negative line as a control for the specificity of immunostaining. Nuclei stained with DAPI are represented in gray, BMRF1 in blue. (f,g) The abundance of the EBV early lytic protein BMRF1 as assessed by mean nuclear BMRF1 fluorescence intensity normalised by subtracting the background fluorescence of BMRF1-negative nuclei from the same field. 2-6 fields (67-120 nuclei per field) were analysed in 2-3 biological replicates. Data are plotted as individual values, mean ± SEM. **p*<0.05; ***p*<0.01 as compared by ANOVA, Bonferroni's post-test.

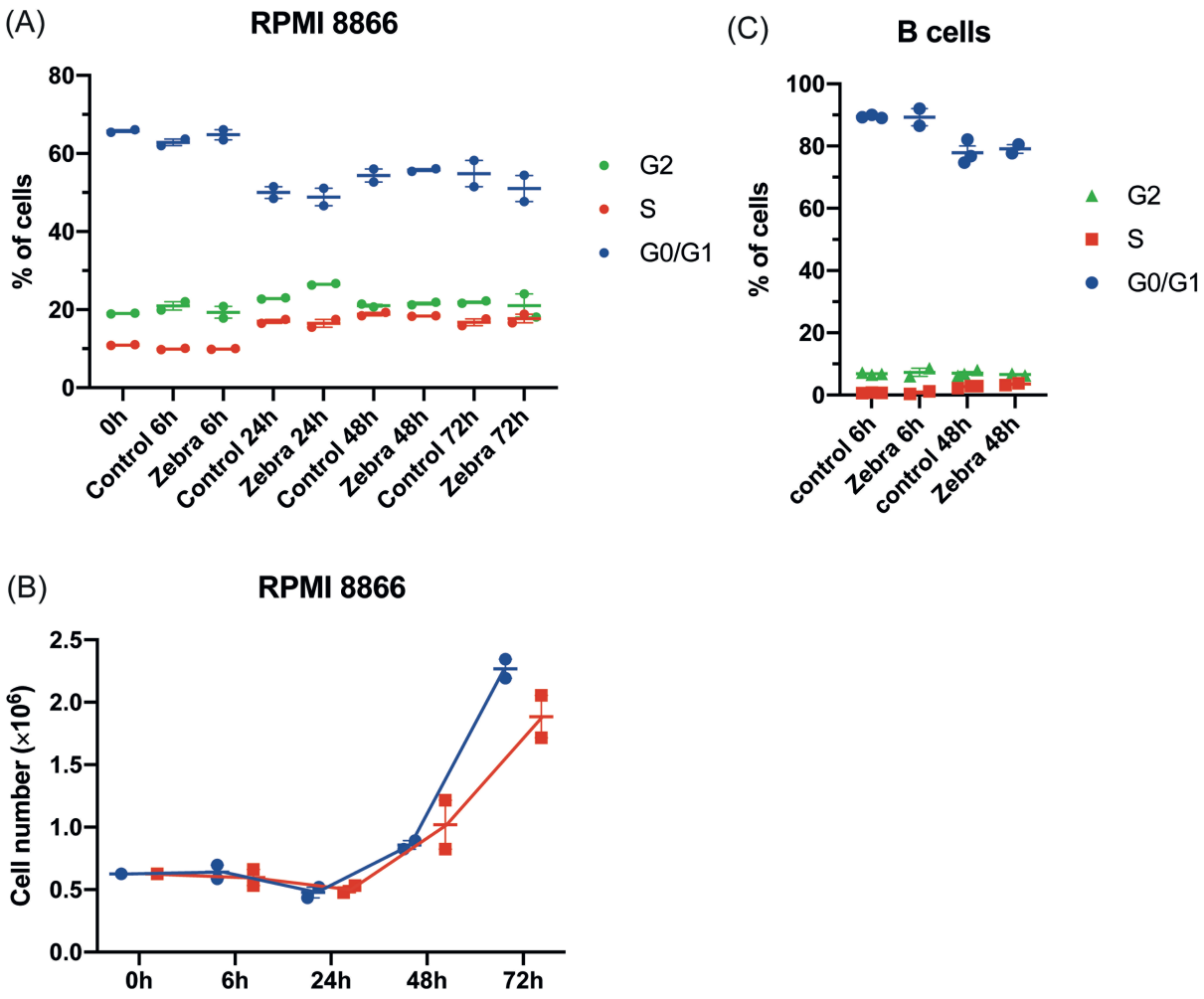

Supplementary Fig. 2. The analysis of cell cycle and proliferation in RPMI8866 cells and cell cycle in primary B cells, treated with Zebra. (a) RPMI8866 cells were treated with Zebra for indicated times and the cell cycle was analyzed by PI staining, non-treated cells were used as a control. Percentages of cells in G0/G1, S, and G2 cycle phases are represented. Data are presented as mean ± SEM. No significant changes were found between Zebra-treated and control cells for each time period analysed (two-way ANOVA, Bonferroni's post-test). (b) RPMI8866 cells were seeded at $0.5x10^5$ cells/well and were treated with Zebra or left untreated. The cell number was calculated at indicated time points using Automated Cell Counter (Biorad) and the proliferation curves were plotted based on the obtained data. Data are presented as mean ± SEM. No significant changes were found between the number of Zebra-treated and control cells for each time period analysed (two-way ANOVA, Bonferroni's post-test). (c) Primary B cells were treated with Zebra for indicated times and the cell cycle was analyzed by PI staining, non-treated cells were used as a control. Percentages of cells in G0/G1, S, and G2 cycle phases are represented. Data are presented as individual values, mean ± SEM. No significant changes were found between Zebra-treated and control cells for each time period analysed (two-way ANOVA, Bonferroni's post-test).

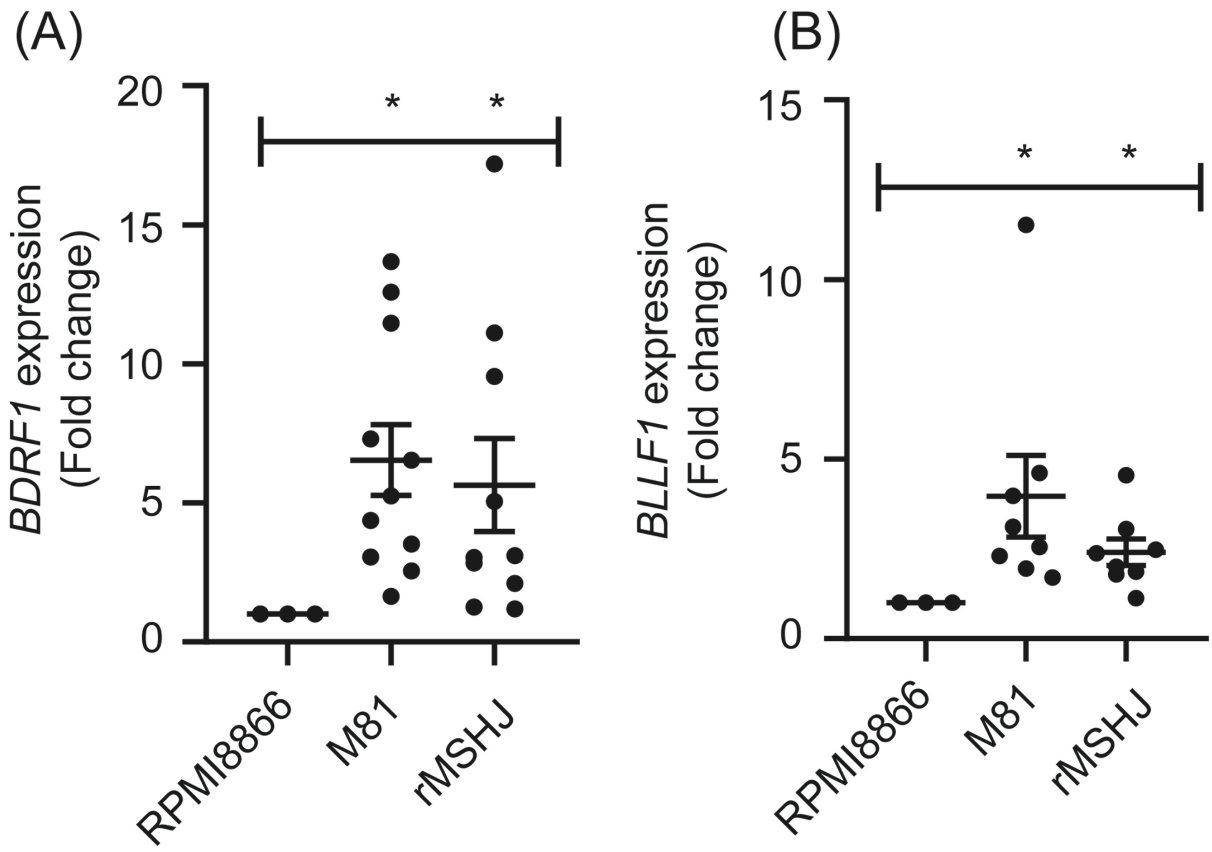

Supplementary Fig. 3. M81 and rMSHJ cells show a spontaneous EBV lytic activity. qRT-PCR analysis of expression of two EBV late genes, *BDRF1* (a) and *BLLF1* (b) in cells with spontaneous EBV lytic activity M81 and rMSHJ. Fold changes of gene expression of M81 and rMSHJ cells are calculated after normalization to *GAPDH* expression in comparison to expression in RPMI8866, set as 1. Results from three independent experiments and two technical replicates are presented. Data are plotted as individual values, mean ± SEM. **p*<0.05; as compared by ANOVA, Bonferroni's post-test.

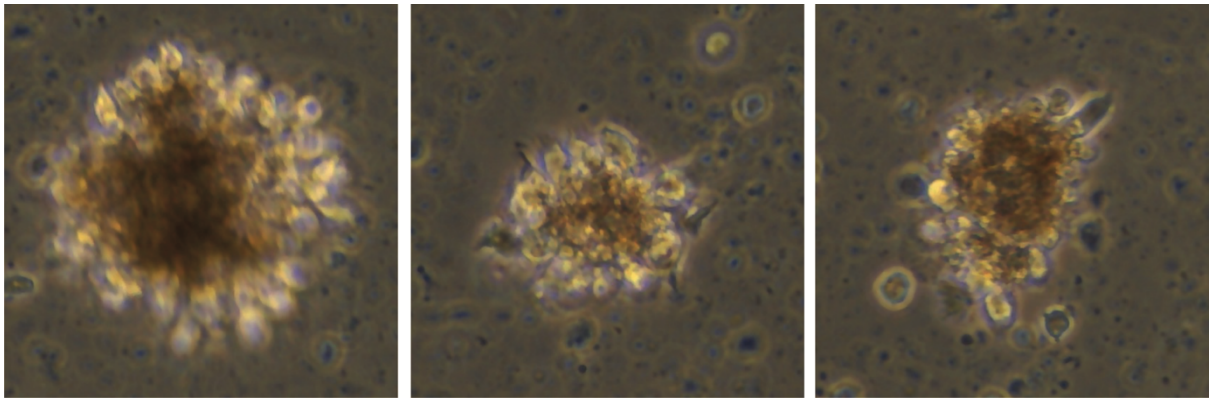

Supplementary Fig. 4. Representative images of proliferating lymphoblastoid cells spontaneously formed from peripheral blood mononuclear cells of P1 after several weeks in culture. The image was obtained using EVOS XL Core Imaging System (Thermo Fisher) at 40x magnification.

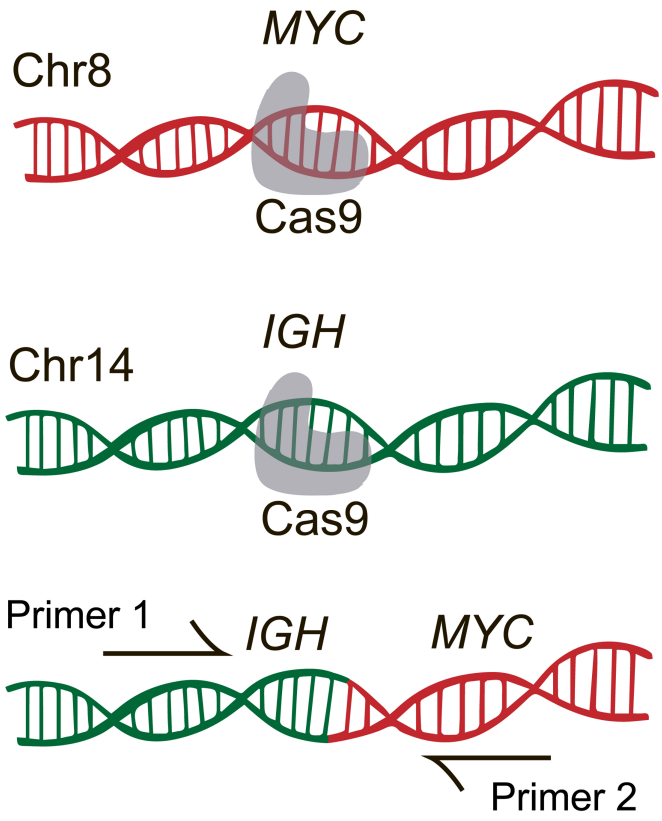

Supplementary Fig. 5. Generation of chromosomal translocations in the the MYCIGHC9 cell line: RPMI8866-derived MYCIGHC9 cell line harbours genes coding for Cas9 (represented by scissors) coupled with two guide RNA targeting specifically *MYC* on chromosome 8 (red) and *IGH* on chromosome 14 (green). Cas9 and gRNA expression can be induced by Dox and then leads to the appearance of DSBs in the *MYC* and *IGH* loci. This leads to appearance in some cells of the *MYC-IGH* translocation that can be detected by qPCR using specific primer pairs surrounding the breakpoint.

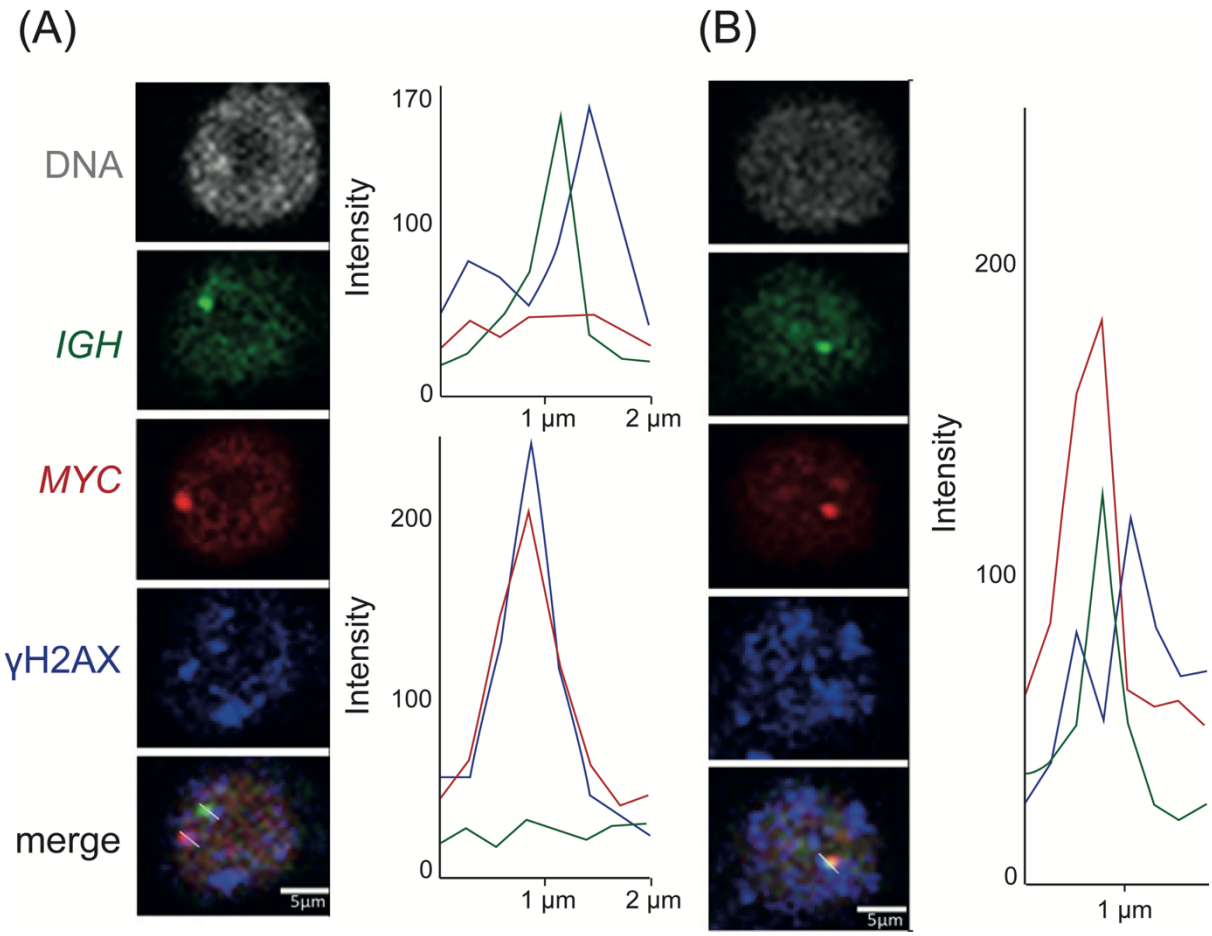

Supplementary Fig. 6. EBV reactivation promotes simultaneous *MYC-IGH* double strand breaks in the same cell. (a) Representative slice-section of an immuno-3D-FISH image of *IGH* (green), *MYC* (red) and γH2AX foci (blue) colocalization. *IGH*-γH2AX and *MYC*-γH2AX colocalization are separate. The right are shown illustrates graphs *IGH* (green curve) and γH2AX (blue curve) colocalization (top, x-axis) and *MYC* (red curve) and γH2AX (blue curve) colocalization (bottom, x-axis) along the white bar drawn in the MERGE picture, with the respective peak intensities (y-axis). Scale bar = 5μm. (b) Triple colocalization *MYC* (red), *IGH* (green) and γH2AX (blue) with the corresponding illustrative graph (right panel). Scale bar = 5μm.

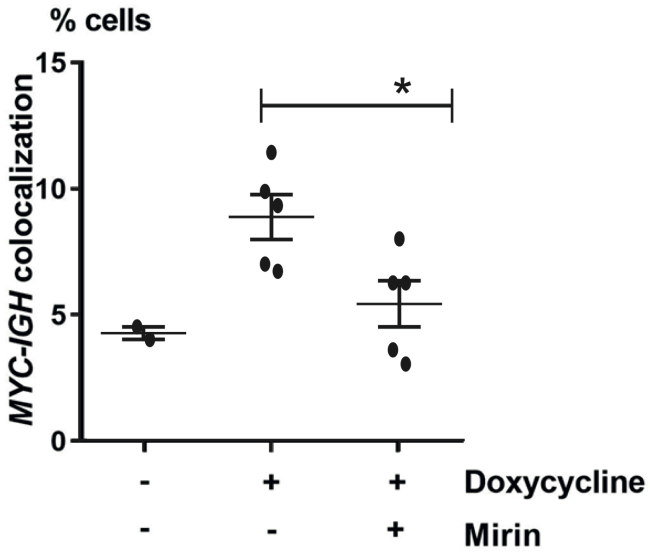

Supplementary Fig. 7. *MYC-IGH* colocalization in MYCIGHC9 line obtained by 3D-FISH analysis treated or not with Dox for 48h, in association or not with the MRE11 inhibitor Mirin. A minimum of 90 cells from at least two different experiments were analysed. Data are plotted as individual values, mean ± SEM. *p<0.05 as compared by ANOVA, Bonferroni's post-test.

Supplementary tables

Supplementary Table 1. List of key resources used in the study.

Reagent or resource	Source	Identifier
Antibodies		
Alexa-633 anti-rabbit	Invitrogen	Cat. # A21070; RRID:AB_2535731
Alexa-647 anti-mouse	Invitrogen	Cat. # A21235; RRID:AB_2535804
anti-mouse HRP-conjugated	Invitrogen	Cat. # 31430; RRID:AB_228307
anti-rabbit HRP-conjugated	Invitrogen	Cat. # 31460; RRID:AB_228341
FITC mouse anti-Human CD23	BD	Cat. # 561146; RRID:AB_10611730
IgM monoclonal antibody (SA-DA4)	eBioscience, Invitrogen	Cat. # 14-9998-82; RRID:AB_468683
mouse anti-BMRF1	Sigma	Cat. # MAB8186; RRID:AB_95286
mouse anti-Cas 9	Santa Cruz	Cat. # sc-517386; RRID:AB_2800509
mouse anti-CD40	Sigma	Cat. # WH0000958M1; RRID:AB_1840567
mouse anti-Zebra	a kind gift from Emmanuel Drouet, Université Grenoble Alpes, France	N/A
mouse anti-β-actin	Santa Cruz	Cat. # sc-81178; RRID:AB_2223230
PE mouse anti-CD19	Biolegend	Cat. # 302208; RRID:AB_314238
rabbit anti-histone H2AX phospho-Ser139 (γH2AX)	Active Motif	Cat. # 39118
rabbit anti-α-tubulin	Santa Cruz	Cat. # sc-398103; RRID:AB_2832217
Cell lines		
M81	a kind gift from Henri-Jacques Delecluse (DKFZ, Heidelberg, Germany)	N/A
PRIESS		RRID:CVCL_E813
rMSHJ	a kind gift from Henri-Jacques Delecluse (DKFZ, Heidelberg, Germany)	N/A
RPMI8866		RRID:CVCL_1668
Chemicals and recombinant proteins		
100 mM sodium pyruvate	Gibco	11360-070

10000 U/ml penicillin and 10000 µg/ml streptomycin	Gibco	15140-122
12-O tetradecanoylphorbol-13-acetate	Sigma Aldrich	P3766
200 mM L-Glutamine	Gibco	25030-024
4-12% SDS-PAGE precast gel	Invitrogen	NP0322BOX
B02	Calbiochem	553525
Doxycycline	Sigma Aldrich	D3447
Fetal bovine serum	Gibco	10270-106
G418	Euromedex	EU0600
Gibson Assembly Master Mix kit	NEB	E2611L
Glucose	Thermo scientific	A11090
HumanKine recombinant human IL-4 protein	Proteintech	HZ-1004
Immobilon® Western Chemiluminescent HRP substrate	Merck-Millipore	WBKLS0500
L67	Sigma Aldrich	SML1797
Magnisort B cell enrichment kit II	Invitrogen	8804-6867-74
Mirin	Calbiochem	475954
MOPS running buffer	Invitrogen	NP0001
MycoAlert® Mycoplasma Detection Kit	Lonza	LT07-318
NU7026	Sigma Aldrich	N1537
Nucleospin® RNA II purification kit	Macherey-Nagel	740955.5
Nucleospin® Tissue DNA purification	Macherey-Nagel	740952.5
Pancoll human	PAN-Biotech	P04-601000
Pierce™ BCA Protein Assay Kit	Thermo Scientific	23227
PowerUp SYBR Green Master Mix	Thermo Scientific	A25742
Protease inhibitor cocktail	Roche	11697498001
RCPI-11 346I20 Green (*IGH*)	Empire genomics	N/A
RCPI-11 440N18 Orange (*MYC*)	Empire genomics	N/A
Recombinant Zebra protein	BiologicsCorp, USA	N/A
RP-11 300I6 Orange (*CCND1*)	BlueGnome	N/A
RPMI 1640 Medium, GlutaMAX™ Supplement	Gibco	61870-010
Sodium Butyrate	Sigma-Aldrich	B5887
Tetracycline-free fetal bovine serum	Takara	631107
Trichostatin A	Calbiochem	647925

Vectashield mounting medium	Vector laboratories	H-1000
Plasmids		
AAVS1-Neo-M2rtTA	Addgene	Cat. #60843; RRID:Addgene_60843
AAVS1-TALEN-L	Addgene	Cat. #59025; RRID:Addgene_59025
AAVS1-TALEN-R	Addgene	Cat. #59026; RRID:Addgene_59026
Puro_Cas9 donor	Addgene	Cat. #58409; RRID:Addgene_58409
phU6-gRNA	Addgene	Cat. #53188; RRID:Addgene_53188
Software		
BD Accuri C6	BD Biosciences	RRID:SCR_019591
Graphpad Prism 5	GraphPad software Inc., La Jolla, CA	RRID:SCR_002798
ImageJ	National Institutes of Health, Bethesda, MA, USA	RRID:SCR_003070
Imaris	Bitplane	RRID:SCR_007370
LEICA Application Suite X	Leica Microsystems	RRID:SCR_013673

Supplementary Table 2. STR profile of human cell lines used in the study.

Loci	RPMI-8866	PRIESS
AMEL	X,X	X,X
CSF1PO	11,11	12,13
D13S317	10,14	9,13
D16S539	11,11	9,12
D18S51	12,14	14,18
D19S433	12,13	14,15
D21S11	28,30	31,31.2
D2S1338	20,25	17,20
D3S1358	15,16	14,15
D5S818	12,12	11,11
D7S820	11,12	7,11
D8S1179	12,14	11,13
FGA	22,23	24,26
TH01	9.3,9.3	6,6
TPOX	8,11	8,11
vWA	14,16	16,17

Supplementary Table 3. List of gRNA sequences used in the study.

Target	Sequence 5'->3'
AML	GACTCCCCCATGTACCCCTA
ETO	GATGTAAGAGGAAGCAGCTT
IGH	GAGAACATACCAAGCCCCAC
MYC	TGCACCTCGGACGCTCCTGC

Supplementary Table 4. Cell treatments.

Substance	Function	Used for	Working concentration
Recombinant Zebra protein (obtained from BiologicsCorp, USA)	EBV immediate early protein	EBV reactivation in LCLs	1 µg/ml
Sodium Butyrate (NaB), Sigma-Aldrich	HDAC inhibitor		2.5 µM
Trichostatin A (TSA), Calbiochem			6.6 µM
Abexinostat (S78)			100 nM
12-O tetradecanoylphorbol-13- acetate (TPA), Sigma Aldrich	Activator of the cellular protein kinase C		8 nM
Mirin, Calbiochem	MRE11 inhibitor	DNA repair inhibition	25 µM
NU7026, Sigma Aldrich	DNA-PK inhibitor	Classical NHEJ inhibition	20 µM
B02, Calbiochem	Rad51 inhibitor	Homologous recombination inhibition	6.25 µM
L67, Sigma Aldrich	DNA ligase I and III inhibitor	Alternative NHEJ inhibition	25 µM
Doxycycline, Sigma Aldrich	Activator of doxycycline-inducible promoter	CRISPR/Cas9 and gRNAs expression induction	1 µg/ml

Supplementary Table 5. Primer sequences. HGNC - The HUGO Gene Nomenclature Committee accession ID.

Target gene	Sequence 5'->3'	Annealing temperature (°C)
MYC (translocation primer) (HGNC:7553)	AGGAGGTGGCTGGAAACTTGT	60
IGH (translocation primer) (HGNC:5477)	TCCCCTCCCTTCTGAGTCTGC	
MYC F (~6.5 kbp downstream the breakpoint) (HGNC:7553)	AAGGTCAGAGTCTGGATCAC	

MYC R (~6.5 kbp downstream the breakpoint) (HGNC:7553)	TAACTACCTTGGGGGCCTTT	
BZLF1-b F	AAATTTAAGAGATCCTCGTGTAAAACATC	
BZLF1-b R	CGCCTCCTGTTGAAGCAGAT	
BRLF1-b F	CAAACAGACGCAGATGAGGC	
BRLF1-b R	GCGGTGCCTGGTGGCAGG	
BDRF1 F	CGGAGTGGCTCAGTCTAAGG	
BDRF1 R	AGGTGGGCTGACACAGACTT	
BLLF1 F	AGAATCTGGGCTGGGACGTT	
BLLF1 R	ACATGGAGCCCGGACAAGT	
MRE11 F (HGNC:7230)	CCAGAGAAGCCTCTTGTACG	
MRE11 R	TTCCACCTCTTCGACCTCTTC	
GAPDH F (HGNC:4141)	CTGCACCACCAACTGCTTAG	
GAPDH R	AGGTCCACCACTGACACGTT	

Thus, one of the potential mechanisms that link HIV infection and B cell lymphomas is EBV reactivation. Being a more common event in people living with HIV as compared to the general population (Ling et al. 2003; Rahman et al. 1991; Yan et al. 2018), EBV reactivation induces DNA damage in *MYC* locus and is associated with an increase in *MYC*-*IGH* proximity in B cells, which are risk factors for chromosomal translocation involving *MYC* and *IGH*. It is important to note that B cells from people living with HIV were previously shown to have an increased frequency of *MYC*-*IGH* colocalization, when compared with healthy donors (Germini et al. 2017b).

Several other factors are known to contribute to the increased proximity between *MYC* and *IGH* in B cells, which might explain an increased frequency of *MYC*-*IGH* colocalization in people living with HIV. Previous research has connected B cell activation with the relocation of the *MYC* locus close to *IGH* (Osborne et al. 2007), and our findings support and confirm this observation (**Figure 13**, clinical data for HIV-negative patients with EBV reactivation P1-3 depicted in Figure 13 is shown in **Table 6**). HIV perturbs B cell homeostasis both directly and on the systemic level (Moir & Fauci 2017). Persistent HIV infection can be associated with chronic B cell activation (Moir & Fauci 2017). Microbial translocation in the gut can also contribute to B cell activation during HIV infection (Marks et al. 2013).

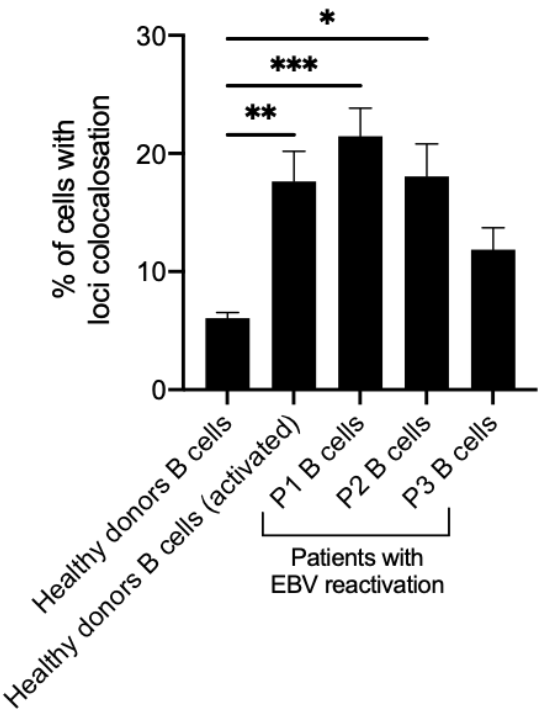

Figure 13. The effect of B cell activation and EBV reactivation on MYC-IGH colocalization in primary B cells. The percentage of cells with colocalized MYC-IGH signals (i.e., cells where the distance between the centres of corresponding 3D-FISH signals was equal or less than 1 µm) in B cells purified from healthy donors, activated or not with a cocktail of reagents (recombinant human IL4 + human CD40 monoclonal antibody + anti-human IgM monoclonal antibody) and in B cells purified from

patients with EBV reactivation (P1, P2, P3). n > 50 cells analysed per condition. Data are plotted as mean ± SEM. **p < 0.01, ****p < 0.0001 as compared by ANOVA, Tukey's post-hoc test. ANOVA, analysis of variance; EBV, Epstein−Barr virus; FISH, fluorescence in situ hybridization; IGH, immunoglobulin heavy; SEM, standard error of the mean.

Table 6. Characteristics of patients with HIV-negative EBV-related lymphoproliferative disorders.

Patient	Diagnosis	Treatment	Age	Gender	Log PCR EBV in whole blood	% of B cells with *MYC-IGH* loci colocalization (n of cells analysed) and P value compared to healthy donor B cells
P1	Severe post-transplant primary EBV infection	Steroids, rituximab, etoposide	74	M	6	21.46 (n=460) <0.0001 ****
P2	Cerebral EBV+ polymorphic lymphoproliferative disorder related to prolonged iatrogenic immunosuppression (systemic lupus erythematosus)	Rituximab, cytarabine	43	F	3	16.67 (n=132) 0.0012 **
P3	Severe infectious mononucleosis with hemophagocytic lymphohistiocytosis	Steroids, etoposide, cyclosporin	23	F	8	11.63 (n=86) ns

In addition to B cell activation, it has also been shown that the HIV-1 transactivator protein Tat could play a role in the development of B cell lymphomas. HIV-1 Tat induces genomic instability, promotes DNA damage through increased ROS production and promotes *MYC-IGH* proximity in primary B cells *in vitro* and *in vivo* (El-Amine et al. 2018; Germini et al. 2017b; Valyaeva et al. 2022). The association between DNA damage and chromatin movement has been previously established (Aten et al. 2004; Iarovaia et al. 2014; Krawczyk et al. 2012; Kruhlak et al. 2006; Miné-Hattab & Chiolo 2020; Miné-Hattab & Rothstein 2012; Neumaier et al. 2012). The increased chromatin movement following DSBs may ultimately lead to chromosomal translocations (Roukos et al. 2013). We have also recently shown that DSBs in

MYC and *IGH* loci increase their co-localisation, which correlates with increased translocation frequency (Canoy et al. 2023).

In conclusion, the available evidence to date strongly suggests that there is a link between HIV infection and B cell lymphomas, with EBV reactivation being one of the potential mechanisms involved. EBV reactivation leads to DNA damage in the *MYC* locus and increased proximity between *MYC* and *IGH* loci in B cells. This increased proximity is associated with a higher risk of chromosomal translocation involving *MYC* and *IGH*, a known driver of BL. Factors such as B cell activation, which is stimulated by HIV infection, and the presence of the HIV-1 transactivator protein Tat in B cells, may also contribute to genomic instability and *MYC*-*IGH* proximity in B cells. Moreover, certain antiretroviral drugs might increase the frequency of *MYC*-*IGH* translocation in the presence of DSBs in *MYC* and *IGH* loci. These findings shed light on the complex interplay between HIV and EBV contribution to the development of B cell lymphomas in the era of cART. Further research in this area may provide valuable insights into potential therapeutic interventions that could disrupt these disease-promoting factors and reduce the risk of B cell lymphomas in individuals living with HIV.

3.1.3 Exposure to HIV-1 Tat Inhibits DNA Damage Sensing and Repair in B cells

Among HIV-1 Tat effects on non-infected cells is the disturbance of DNA damage repair pathways. It has been shown that Tat increases the expression of DNA polymerase beta, a key component of the DNA base-excision repair pathway, by interacting with cellular transcription factors in B cells, which affects genome stability and can promote lymphomagenesis (Srivastava et al. 2001). Tat also influences DSB repair by reducing the nonhomologous end-joining in cells treated with DNA-damaging agents (Chipitsyna et al. 2004). Tat-expressing rhabdomyosarcoma cells showed decreased capacity to repair radiation-induced DNA DSBs (Sun et al. 2006). Thus, we decided to analyse whether Tat can perturb DNA damage sensing and repair in B cells (**see Article 6**).

We utilised a B lymphoblastoid cell line (RPMI8866) that inducibly expressed HIV-1 Tat (Gorbacheva et al. 2019). By analysing the gene expression profiles of B cells with or without Tat exposure using RNA sequencing, we sought to unravel the mechanisms underlying Tat-induced lymphomagenesis in people living with HIV. The results of this study demonstrated that HIV-1 Tat significantly suppressed the expression of numerous genes involved in DNA damage sensing and repair pathways in B cells. Consequently, Tat-expressing B cells displayed impaired DNA damage sensing and repair when exposed to the DNA-damaging drug cisplatin: an increase in cisplatin-specific DNA adducts was observed in Tat-expressing B cells. Upon treatment with cisplatin,

Tat-expressing B cells demonstrated a decrease in the levels of γH2AX and the phosphorylated form of p53, which are involved in DNA damage recognition and repair, supporting the disruption of DNA repair processes. Intriguingly, despite the impairment of DNA repair pathways, Tat-expressing B cells maintained their viability, indicating that these cells survive at the same level as control cells even in the presence of accumulated DNA lesions (**Figure 14**). This preservation of cell viability, coupled with the accumulation of DNA damage, could create a conducive environment for the progression of B cells toward lymphoma in people living with HIV.

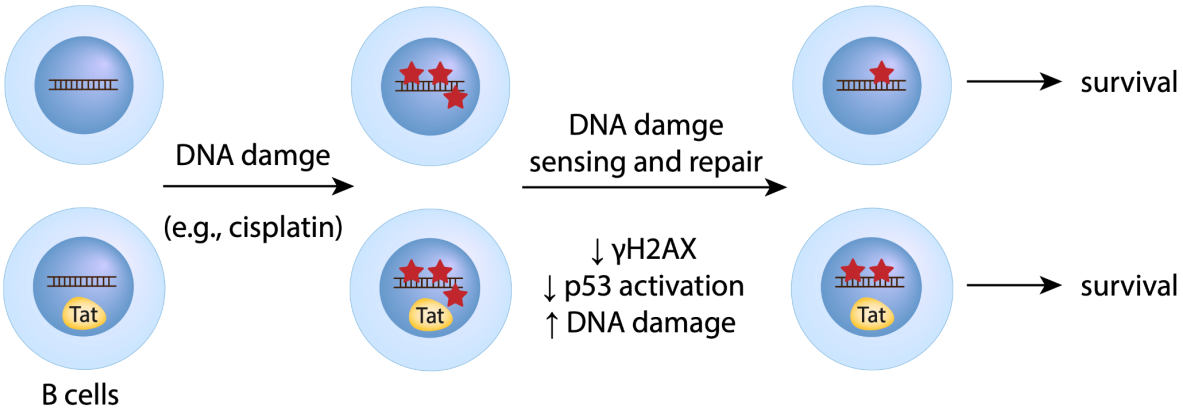

Figure 14. HIV-1 Tat significantly suppressed the expression of multiple genes involved in DNA damage sensing and repair pathways in B cells. As a consequence, Tat-expressing B cells displayed impaired DNA damage sensing and repair when exposed to cisplatin, leading to a decrease in the levels of two crucial markers of DNA damage recognition and repair, namely, γH2AX and phosphorylated p53, and an increase in cisplatin-specific DNA adducts in these cells. Despite the impaired DNA repair pathways, Tat-expressing B cells demonstrated no substantial decrease in viability compared to control cells, indicating that they maintain their survival capacity even in the presence of accumulated DNA lesions.

I contributed to this study by designing and planning experiments, guiding the project, RNA-sequencing processing and analysis, statistical analysis, manuscript reviewing and editing.

Article 6. Research paper "Exposure to HIV-1 Tat inhibits DNA damage sensing and repair in B cells"

Exposure to HIV-1 Tat inhibits DNA damage sensing and repair in B cells *(manuscript in preparation)*

Yana Kozhevnikova[1], Anna Schwager (Karpukhina)[1,2], Ivan Tsimailo[1], Anna Valyaeva[3,4], Eugene V. Sheval[3,4], Yegor Vassetzky[1,2,]*, Anna Shmakova[1,2]*

[1]*CNRS, UMR 9018, Université Paris-Saclay, Institut Gustave Roussy, 94800 Villejuif, France;*
[2]*Koltzov Institute of Developmental Biology, 119334 Moscow, Russia;*
[3]*Belozersky Institute of Physico-Chemical Biology, Lomonosov Moscow State University, 119991 Moscow, Russia;*
[4]*Department of Cell Biology and Histology, School of Biology, Lomonosov Moscow State University, 119991 Moscow, Russia*
*Corresponding authors: yegor.vassetzky@cnrs.fr; anyashm@gmail.com

Abstract

Despite the remarkable success of combination antiretroviral therapy (cART), people living with HIV continue to face an increased risk of B cell malignancies compared to the general population. In the HIV setting, B cell physiology is altered by co-existence with HIV-infected cells and the action of secreted viral proteins, e.g., HIV-1 Tat that, once released, efficiently penetrates non-infected cells. HIV-1 Tat has been demonstrated to promote DNA damage and contribute to the development of HIV-associated diseases. In this study, we aimed to investigate the specific effects of acute HIV-1 Tat action on B cells, elucidating potential mechanisms underlying lymphomagenesis in people living with HIV. We employed a B lymphoblastoid cell line that inducibly expressed HIV-1 Tat and performed an RNA-sequencing analysis to compare the expression profiles of B cells with or without Tat exposure. Our findings revealed that Tat significantly suppressed the expression of numerous genes involved in critical DNA repair pathways. Upon exposure to the DNA-damaging drug cisplatin, Tat-expressing B cells had decreased levels of γH2AX and phosphorylated p53, pivotal markers of DNA damage sensing and repair. Moreover, we identified an increase in cisplatin-specific DNA adducts in Tat-expressing B cells, further confirming the disruption of DNA repair processes. Intriguingly, despite the impairment of DNA repair pathways by Tat, there was no substantial increase in apoptosis or decreased viability of B cells. This preservation of cell viability, even in the presence of genomic alterations, may establish a favorable environment for the progression of B cells towards lymphoma in people living with HIV. In conclusion, our study highlights the role of HIV-1 Tat in promoting B cell lymphomagenesis by disturbing DNA repair pathways, leading to the accumulation of DNA damage and genomic instability in B cells.

Introduction

Human immunodeficiency virus (HIV) currently infects 38.4 million people worldwide (http://www.who.int/hiv/en/). HIV infection increases the risk of development of certain cancers, and among the most common malignancies in people living with HIV (people living with HIV) are B-cell lymphomas [1]. Since the introduction of combination antiretroviral therapy (cART) the incidence of most cancers in people living with HIV has significantly decreased, however, some lymphoma subtypes, including Burkitt lymphoma (BL) and Hodgkin lymphoma (HL), became more frequent despite cART use [2]. Mechanisms underlying B-cell lymphoma formation in people living with HIV remain obscure, as HIV-1 does not directly infect B cells. It was previously thought that the main factors contributing to lymphomagenesis are those related to immunosuppression, co-infection with oncogenic viruses, chronic B cell activation, and impaired immune surveillance [3]; but these factors cannot fully explain the persistence of incidence of certain lymphoma subtypes in people using cART that blocks HIV replication and restores CD4+ T cell counts [4]. It has been suggested that HIV can directly contribute to lymphomagenesis through the production of viral proteins, such as gp120, p17, and Tat [5]. Most of the proviruses that persist in CD4+ T-cells of people living with HIV upon cART use are defective (>95%), and recent studies suggest that these proviruses are not transcriptionally silent and are able to produce viral proteins [6]. In HIV patients receiving cART, HIV-1 structural proteins p24, p17 and envelope glycoproteins gp120/gp41 persist in germinal centers of lymph nodes in the absence of detectable virus replication [7]. Among HIV-1 proteins, the most interesting in the context of B cell lymphoma development is Tat, which is secreted by infected CD4+ cells, is present in sera of people living with HIV even during cART use and can penetrate into non-infected cells due to its cell-penetration domain [8–10]. Tat expression in transgenic mice can cause the growth of several types of neoplasms, including B cell lymphomas [11].

Tat, or transactivator of transcription, is a small basic and intrinsically disordered protein which provides conformational flexibility and hence the ability to bind a large variety of partners; this property determines the diversity of Tat's functions [12]. Tat's main function is regulation of the transcription of the integrated HIV provirus. In the absence of Tat protein, elongation of HIV transcript is abortive: the presence of an inactive large form of P-TEFb leads to stalling of RNA polymerase II shortly after the beginning of transcription. Tat protein rescues stalled HIV transcription by releasing P-TEFb from its inactive state and recruiting active P-TEFb to viral transactivation response (TAR) RNA, enabling RNA polymerase II elongation of the viral transcript [13]. Tat protein also regulates the expression of host cell genes to promote effective viral production and spread. For example, Tat helps evade antiviral interferon(IFN)-modulated cell response by binding to and blocking the IFN-induced, dsRNA-dependent serine/threonine protein kinase (PKR) [14]. Due to the ability of Tat to be secreted from host cells and enter bystander non-infected cells, it is considered to play a role in several HIV-associated pathologies, such as HIV-associated neurocognitive disorder, substance use disorder, cardiovascular

complications, BL and others [15–17,9]. The process of Tat secretion is efficient and does not follow the conventional endoplasmic reticulum/Golgi pathway, but occurs directly through the plasma membrane [18]. Tat secretion is driven by Tat's basic domain high affinity binding to phosphatidylinositol-4,5-bisphosphate ($PI(4,5)P_2$) and phosphatidylserine on the plasma membrane [19,20]. Upon binding with $PI(4,5)P_2$ Tat protein undergoes secondary structure changes that enable the membrane insertion of Tat Trp11 and Tat organization into membrane-inserted oligomers, which leads to the formation of membrane pores, facilitating Tat secretion [21].

Extracellular Tat is able to interact with components of the extracellular matrix and cell surface, thereby influencing lymphocyte functions, promoting cell migration, and inducing cytopathic effects on leukocytes and neural cells [22]. However, the majority of its functions rely on Tat's absorbance by bystander cells. Tat has various binding sites on the cell surface, including ubiquitous endocytic receptors, such as the lipoprotein receptor-related protein, CXCR4 and heparan sulfate proteoglycans, which allow Tat internalization in several cell types [23]. There are two proposed pathways of Tat endocytosis: caveolar [24] or clathrin/AP-2 dependent [25]; it seems that the choice of pathway depends on the target cell type. Following endosomal uptake, Tat goes through a rab5-dependent pathway to late endosomes/lysosomes, where it is exposed to low pH (<6). Acidification triggers Tat insertion into the endosomal membrane, followed by Tat translocation to cytoplasm catalyzed by the cytosolic chaperone Hsp90 [23]. Once in the cytoplasm, Tat can translocate to the nucleus to influence host cell gene expression and trigger various cell responses.

The role of Tat in B cell lymphoma development has been described only partially. In B cells, Tat increases the expression of oncogenic transcriptional factor *MYC* [26]; activation‑induced cytidine deaminase (*AICDA*) [27,28]; nuclease *RAG1* [9] and DNA polymerase beta [29], which affects genome stability and can promote lymphomagenesis. Exogenous Tat induces DNA damage in B cells through reactive oxygen species (ROS) production promoting genetic instability [30]. Tat also promotes *MYC* gene locus colocalization with *IGH* gene locus after DSBs in B cells, resulting in BL-specific t(8;14) chromosomal translocation [9]. It has been recently demonstrated by transcriptomic analysis that stable expression of Tat in B cells leads to substantial modifications of gene expression and genome instability of B cells, facilitating oncogenic transformation [31]. Thus, Tat protein is an important factor contributing to B-cell lymphomagenesis in people living with HIV.

The transcription level of HIV-1 can quickly increase in several situations, including cART resistance, discontinuation of therapy or administration of latency-reversing agents that aim for latent HIV reactivation while maintaining cART in order to kill latently infected cells and prevent new infection events ("shock and kill" strategy) [32]. During these events, expression and secretion levels of Tat may rise, resulting in acute action on bystander cells. In this study, we aimed to assess the effect of acute HIV-1 Tat action on DNA damage, DNA repair and B cell survival after treatment with DNA-damaging drugs. For that

purpose, we chose a B lymphoblastoid cell line RPMI8866 with an inducible expression of HIV-1 Tat. We demonstrated that HIV-1 Tat decreased the ability of B cells to repair DNA damage and enhanced DNA damage in B cells after treatment with cisplatin, but did not substantially influence B cell survival.

Materials and Methods

Cell culture

Human Epstein-Barr virus (EBV)-transformed B lymphoblastoid cell line RPMI8866 (ECACC General Cell Collection) with inducible expression of HIV-1 Tat protein (RPMI8866 Tat^{i} line) was produced by the Sleeping beauty transposon system as previously described [33]. Tat gene was inserted into pSBtet-GP plasmid (Addgene, #60495), which allows doxycycline-induced Tat protein expression and stable EGFP protein expression (**Figure 1A**).

Cells were cultured at 37℃ in the RPMI 1640 medium supplemented with 10% FBS, 2% glucose, 2 mM L-Glutamine, 1 mM Pyruvate and 1000 units/mL of penicillin and 1000 µg/mL of streptomycin antibiotics (all from Gibco, Thermo Fisher Scientific, Waltham, Massachusetts, USA). The induction of HIV-1 Tat expression was performed with doxycycline (Sigma, St. Louis, Missouri, USA) in the concentration of 1 µg/ml for 16 hours unless otherwise specified (RPMI8866 Tat^{i} + Dox); cells from the same line without Tat induction with doxycycline served as control (RPMI8866 Tat^{i} control).

MTT survival test

MTT test was performed to evaluate the viability of RPMI8866 Tat^{i} cells with or without induction of HIV-1 Tat expression. Cells were seeded in complete medium in 96-well plates at 0.1×10^{6} / 100 µl concentration; the expression of HIV-1 Tat was induced by doxycycline treatment for 16 hours, followed by treatment with either cisplatin (Mylan), oxaliplatin (Accord) or doxorubicin (Teva) in different concentrations. For survival experiments, we used the following concentrations: 0, 1, 5, 10, 20, 30, 40, 50, 100, 200 or 300 µM of cisplatin; 0, 0.05, 0.1, 0.5, 1, 5, 10 or 50 µM of oxaliplatin; 0, 0.1, 0.2, 0.3, 0.4, 0.5, 1, 2, 5, 10 or 20 µM of doxorubicin. 24 hours after the treatment cells were incubated with 0.1 mg of MTT (Merck Millipore, Burlington, MA, USA) for 2 hours at 37 °C and then lysed in 100 µL per well of lysing buffer (25 mM HCl, 2% acetic acid, 3% DMF, 5% SDS, pH 4.7) at room temperature overnight. The next day the absorbance at 570 nm was measured using a plate reader Infinite F200 PRO (Life Sciences, Tecan, Grodig, Austria). Acquired data was analyzed using Excel software. For all experiments, six technical repeats of each dose were analyzed for each of at least three biological replicates.

Cell staining and flow cytometry for Annexin V apoptosis test

For apoptosis tests, RPMI8866 Tat^{i} cells were treated or not with doxycycline for 16 hours to induce HIV-1 Tat expression, and then treated with 0, 10, 50, 100 or 300 µM of cisplatin,

0, 0.1, 1, 10 or 100 µM of oxaliplatin or 0, 0.2, 20, or 200 µM of doxorubicin for 24 hours. 0.5×10^6 cells were collected by centrifugation for 5 minutes at 800g, washed with PBS and resuspended in 300 µL of Annexin buffer (100 mM Hepes pH 7.4, 150 mM NaCl, and 2.5 mM $CaCl_2$). 3 µL of APC Annexin V (Biolegend, cat. #640941) and 3 µL of propidium iodide (PI) (Sigma-Aldrich, cat. #P4170-10MG) were added to each sample and incubated for 5 minutes in the dark. Fluorescence was acquired using BD Accuri C6 Plus Flow Cytometer (BD Biosciences, USA), and the data were analyzed using FlowJo software (version 10.4), the same gating was applied to all samples within one experiment, the compensation was performed with single-stained controls. For all experiments, two technical repeats of each dose were analyzed for each of at least three biological replicates.

The cell cycle was analysed as follows: cells were washed with PBS and fixed in 70% ice-cold ethanol overnight. RNA was digested with RNase A (100 µg/ml) and cells were stained with propidium iodide (10 µg/ml). The fluorescence was analyzed using BD Accuri C6 Plus Flow Cytometer (BD Biosciences, USA) and BD Accuri C6 software, the same gating was applied to all samples within one experiment.

RNA extraction, RNA sequencing, reverse transcription and quantitative polymerase chain reaction

For the assessment of Tat mRNA expression kinetics, RPMI8866 Tat^i cells were treated with doxycycline and incubated for 0, 1, 3, 6, 16, 24, 48 or 72 hours to induce HIV-1 Tat expression and then collected for quantitative polymerase chain reaction (qPCR). For other qPCR experiments and RNA sequencing, RPMI8866 Tat^i cells were treated or not with doxycycline for 16 hours to induce HIV-1 Tat expression. Then 3×10^6 cells were pelleted by centrifugation for 5 minutes at 800g. RNA was extracted by Quick-RNA Miniprep Kit (Zymo Research) following the manufacturer's protocol. The quantity and quality of total RNA samples were measured on a NanoDrop 2000C Spectrophotometer (Thermo Scientific, Waltham, MA, USA). For RNAseq, RNA samples were sent to Novogene company for the NGS library preparation and sequencing.

For qPCR, 1 µg of total RNA was reverse-transcribed using Maxima™ H Minus cDNA Synthesis Master Mix (Thermo Scientific, USA) following the manufacturer's protocol. The human cDNA primers (**Table 1**) were obtained from Eurofins Genomics, Germany; primer specificity was evaluated using NCBI PrimerBlast. cDNA samples were amplified using the PowerUp SYBR Green Master Mix (Thermo Scientific) with the following program: a 2-minute denaturation step at 50°C, a 2-minute denaturation step at 95°C followed by 40 amplification cycles consisting of 15 seconds of denaturation at 95°C, 1 minute of annealing at 60°C and 1 minute of elongation at 72°C, followed by a final step 10 minute elongation at 72°C. qPCR for each sample was performed in three technical replicates on each of the three biological replicates. The no-template controls (included on each plate) were reliably negative. A relative transcript level was calculated using the Pfaffl method [34] and the geometric averaging of the relative quantities of the *RPL32* and *GAPDH* reference genes; normalization was done assuming as 1 the mean level of each

transcript in the control group. The analysis of primer efficiency was performed by plotting the cycle threshold value (Ct) against the serial 1:10 dilution of the cDNA sample using the equation $E = 10^{-\frac{1}{the\ slope\ value}}$.

Table 1. Primers used in this study

RPL32 F	CATCTCCTTCTCGGCATCA
RPL32 R	AACCCTGTTGTCAATGCCTC
GAPDH F	CTGCACCACCAACTGCTTAG
GAPDH R	AGGTCCACCACTGACACGTT
SSBP1 F	CAAAAGACAACATGGCACAGAA
SSBP1 R	TGTTGCTTGTCGCCTCACATTA
UNG F	CCACACCAAGTCTTCACCTGGA
APEX1 R	TGAGGTCTCCACACAGCACAA
POLE3 F	GACGGTGTCAACATCTCCAAGG
POLE3 R	ATGGCTGAGAGCACATCACTGG
POLD2 F	ACTGACCCGTTCATCTTCCCAG
POLD2 R	CAACAGCACTGTCTGGTCCTCA
GTF2H2 F	TCTTTAGCAGCCTTACAACTTGCG
GTF2H2 R	CAGTGCAAACGCGAACTTCTGC
Tat F	CTAGACTAGAGCCCTGGAAGCA
Tat R	TGAGGAGGTCTTCGTCGCT

RNA-seq data processing and analysis

The cDNA libraries were constructed and sequenced by Novogene, UK. The raw sequencing reads were mapped to the human genome (assembly GRCh38.p10) using HISAT2 (version 2.0.5). Read counting was performed using featureCounts (ver 2.0.1) in a strand-specific mode. GENCODE v26 gene annotation (ALL) was used. Features with a low total count number (< N counts across all samples, where N is the number of replicates in each condition) were discarded. Differential expression analysis was performed using the DESeq2 R package (version 1.30.1). The genes meeting the criteria p value adjusted (p.adjust) by the Benjamini-Hochberg procedure < 0.05, $|\log_2$ fold change$| > 0.5$ were considered differentially expressed.

clusterProfiler R package (version 4.4.4) was used to conduct gene set enrichment analysis (GSEA) on a pre-ranked list of genes ordered by the stat column of DESeq2 results. Gene sets of biological processes and pathways were obtained from the Gene Ontology resource

(R package org.Hs.eg.db, version 3.15.0) (The Gene Ontology Consortium, 2017) and the Kyoto Encyclopedia of Genes and Genomes (KEGG) database (release 104.0) (Kanehisa and Goto, 2000). An adjusted p-value cutoff of 0.05 was used to select statistically significant activated or suppressed pathways; redundant terms were removed with the simplify() function of the same package (cutoff parameter of 0.7). Heatmap visualization and sample clustering were performed with the ComplexHeatmap R package (version 2.12.1) (Gu, 2022). Three biological replicates were sequenced for each cell line, with a mean of 25 million 55 nt reads generated per sample.

Protein extraction, SDS-PAGE and western blotting

For the assessment of Tat expression kinetics, RPMI8866 Tat^{i} cells were treated with doxycycline and incubated for 0, 1, 3, 6, 16, 24, 48 or 72 hours to induce HIV-1 Tat expression and then collected for western blotting. For the measuring of phosphorylated p53 levels, RPMI8866 Tat^{i} cells (with or without prior induction of HIV-1 Tat expression for 16 hours) were treated with 300 μM cisplatin for 24 hours and then collected for western blotting.

For Western blotting, 3×10^{6} cells for each sample were pelleted by centrifugation for 5 minutes at 800g and resuspended in NETN lysis buffer (150 mM NaCl, 1 mM EDTA, 50 mM Tris pH 7.5, 0.5% NP-40, protease inhibitor cocktail). Lysates were sonicated for 15 sec at 30% amplitude in a Vibra Cell sonicator (SONICS & MATERIALS, Inc., USA), incubated on ice for 30 minutes and centrifuged for 10 minutes at 16000g at 4°C. Protein quantification was performed using the PierceTM BCA Protein Assay Kit (Thermo Scientific, USA) on a NanoDrop 2000C Spectrophotometer (Thermo Scientific, USA). After measuring the concentration, cell lysates were supplemented with Laemmli buffer and 0.1 M DTT and then heated at 95℃ for 10 minutes. Protein samples and prestained molecular weight markers (PageRulerTM Prestained Plus Protein Ladder; Thermo Scientific, USA) were separated on precast SDS-PAGE gels (NuPAGE™ 4-12% Bis-Tris sodium dodecyl sulfate-polyacrylamide gel electrophoresis gels, Invitrogen) in MOPS Running Buffer (NuPage). Proteins were transferred onto a 0.45 mm polyvinylidene fluoride (PVDF) membrane (GE Healthcare, USA) in a transfer buffer (25 mM Tris, 192 mM glycine, 20% ethanol) at 90V at 4℃ for 2 hours. Nonspecific binding was blocked in 5% nonfat dried milk in Tris-buffered saline (20 mM Tris, 150 mM NaCl) and 0.1% Tween-20 (TBST) at room temperature for 30 minutes.

The following primary antibodies were used: mouse anti-HIV-1 Tat antibodies (1:200, Santa Cruz, cat. #sc65912), mouse anti-β-actin antibodies (1:1000, Santa Cruz, cat. #sc81178), rabbit anti-p53 antibodies (1:200, Santa Cruz, cat. #sc-6243), rabbit anti-phospho-p53 (Ser15) antibodies (1:1500, Cell Signaling Technology, cat. #9284). Membranes were washed 3 times for 5 minutes in TBST and stained with appropriate peroxidase-conjugated secondary antibodies at room temperature for 2 hours: goat anti-mouse IgG (ThermoFisher Scientific, cat. #31432), goat-anti-rabbit IgG (Pierce, cat. #1858415). After washing 3 times for 5 minutes in TBST, membranes were revealed using

Immobilon Western Chemiluminescent HRP Substrate (Millipore, Burlington, MA, USA) and ImageQuant LAS 4000 mini (GE Healthcare, Chicago, IL, USA). Images were analyzed using ImageJ software.

DNA extraction and dot blot for DNA damage

To analyze the accumulation of cisplatin-induced DNA damages, RPMI8866 Tat^{i} cells were seeded at a concentration of 1×10^6 / ml, treated or not with doxycycline for 16 hours to induce HIV-1 Tat expression, then treated with 50 µM or 300 µM of cisplatin and incubated for 2 and 4 hours. 3×10^6 cells were pelleted by centrifugation for 5 minutes at 800g, washed with phosphate-buffered saline (PBS, Sigma) and pelleted again. To collect chromatin fraction, cell pellets were resuspended in 150 µL of cold MNAse buffer (20 mM Tris pH 7.5, 2.5 mM $CaCl_2$, 5 mM NaCl) with protease inhibitor cocktail and subjected to lysis by freezing them at −80 °C overnight. After defrosting, lysed cells were centrifuged for 5 minutes at 16000g at 4℃ and the supernatant was removed. To release chromatin-bound proteins and shear chromatin, pellets were treated with 2U of micrococcal nuclease (MNase) from Staphylococcus aureus (Sigma-Aldrich, USA, cat. #N3755) in 100 µL of MNase buffer and incubated on ice for 10 minutes. Samples were then centrifuged for 5 minutes at 16000g at 4℃, and pellets were washed with 100 µL of 10X TBS buffer (200 mM Tris, 1500 mM NaCl) followed by washing with 200 µL of 1X TBS buffer; supernatants from three centrifugations were combined to obtain chromatin fraction.

To isolate DNA from chromatin fraction, phenol-chloroform extraction was used. Briefly, 150 µL of chromatin fraction was treated with 2 µL of RNAse A 10mg/mL (ThermoFisher Scientific, cat. #EN0531) for 1 hour at 37℃, followed by treatment with 150 µl of Proteinase K 5 mg/ml (Macherey-Nagel, cat. #740506) in Proteinase Buffer (10 mM Tris pH 8; 20 mM EDTA pH 8; 10 mM NaCl, 1% SDS) for 1 hour at 56℃. Samples were supplemented with 300 µL of Phenol-Chloroform-Isoamyl solution (25:24:1, Biosolve Chemicals, France) and centrifuged for 5 minutes at 16000g; the upper phase was transferred to the new tube. After the addition of 1 volume of chloroform, samples were centrifuged and the upper phase was separated with the addition of 10% of 3 M Sodium acetate buffer solution and 3 volumes of cold 100% ethanol. Samples were incubated on dry ice for 40 minutes and then centrifuged for 30 minutes at 16000g at 4°C. The supernatant was aspirated and 1 mL of cold 70% ethanol was added to the pellet, followed by centrifugation for 20 minutes at 16000g. After aspiration of ethanol, pellets were dried and dissolved in 12 µL of water. DNA concentration was measured on a NanoDrop 2000C Spectrophotometer (Thermo Scientific, USA).

Each sample was diluted to the concentration of 100 ng/µL and 3 µL of each sample were loaded on 0.45 µm nylon membrane (Amersham Hybond-N+, GE Healthcare, cat. #RPN203B). The membrane was dried and crosslinked with 254-nm UV, 120 mJ/cm2 on UV Stratalinker 2400™ (Stratagene). Then the membrane was incubated in 1:10000 SYBR Gold (Invitrogen, cat. #S11494) in TBST for 30 minutes in the dark and washed with 20%

ethanol for 20 minutes. ImageQuant LAS 4000 mini (GE Healthcare, USA) was used to detect DNA loading. The membrane was then blocked in 5% milk in TBST for 30 minutes at room temperature and incubated for 2 hours at room temperature in primary rat antibodies to Cisplatin-modified DNA [CP9/19] (Abcam, cat. #ab103261). The membrane was then washed 3 times for 5 minutes in TBST and incubated for 2 hours at room temperature with secondary goat-anti-rat antibodies (Sigma-Aldrich, cat. # AP136P). After washing 3 times for 5 minutes in TBST, the membrane was revealed using Immobilon Western Chemiluminescent HRP Substrate (Millipore, USA) and ImageQuant LAS 4000 mini (GE Healthcare, USA). Images were analyzed using ImageJ software.

Immunofluorescent staining, microscopy and image analysis

For immunofluorescent staining, RPMI8866 Tat^{i} cells were treated or not with doxycycline for 16 hours to induce HIV-1 Tat expression, then treated with 10 μM of cisplatin and incubated for 2, 6 and 24 hours. 0.5×10^{6} cells were collected by centrifugation for 5 minutes at 800g, washed with PBS and resuspended in 70 μl of the RPMI 1640 medium. Suspension cells were attached to coverslips covered with poly-D-lysine (0.1 mg/ml, Merck Millipore, cat. #A-003-E). Cells were washed with PBS, fixed in 4% paraformaldehyde (Electron Microscopy Sciences, cat. # 15710) for 10 minutes, washed with PBS 3 times for 5 minutes and permeabilized with 2% Triton X-100 for 10 minutes. Nonspecific binding was blocked in 1% bovine serum albumin (BSA) with normal goat serum (JacksonImmunoResearch cat. #005-000-121) at 37℃ for 1h. Cells were stained with anti-H2A.X Phospho (Ser139) antibody (1:200 in 1% BSA in 1X PBS, BioLegend, cat. #613412) for 1 hour at 37℃, followed by staining with secondary antibodies Alexa Fluor 647 Goat anti-mouse IgG H+L (1:200 in 1% BSA in 1X PBS, Thermo Fisher Scientific, cat. #A-21235) for 45 minutes at 37℃. Coverslips were mounted on slides with Fluoroshield mounting medium with DAPI (Abcam, cat. # ab104139). Fluorescent images were acquired using Leica TCS SP8 Multiphoton Microscope (Leica Microsystems). All images within the experiment were captured with the same laser intensity, gain and exposure settings.

To analyze the nuclear fluorescence intensity of γH2AX, confocal images were processed using a semi-automatic macro in Fiji (ImageJ version 2.1.0/1.53c, Java version 1.8.0). Briefly, to create nuclear cell masks, the nuclear regions of interest (ROIs) were detected on the images with the DAPI-staining, the "Moments" threshold method implemented in Fiji was used. The masks were split to detect single nuclei. The area and circularity of detected ROIs were measured, and mean fluorescence intensity in nuclear ROIs was measured in the γH2AX channel. Nuclear ROIs with area <10 μm^2 (debris) or >60 μm^2 (doublets), irregular nuclei (ROIs circularity <0.3) were removed. At least five fields and at least 200 cells were analyzed per biological replicate and images from at least two independent experiments were analyzed. The plugin is available on request.

Statistical analysis

Data were analyzed using GraphPad Prism 9 software (GraphPad Software Inc.). The unit of analysis was a single biological replicate. Student's unpaired t-tests were used to compare data between two groups. Two-way analysis of variance (ANOVA) followed by Sidak post-hoc test was used to determine differences between two or more groups that involved two factors. Data are presented as a mean ± standard error of the mean (SEM). The level of significance was set at $p < 0.05$.

Results

Acute HIV-1 Tat induced transcriptome changes in B cells

To study the effects of HIV-1 Tat protein on B cells, a RPMI8866 cell line with doxycycline-induced expression of HIV-1 Tat protein (RPMI8866 Tat^{i} line, **Figure 1A**) was used. To assess the kinetics of Tat mRNA and protein production after the expression induction in this newly established line we incubated cells with doxycycline (Dox) for 1, 3, 6, 16, 24 and 48 and performed qPCR and western blotting, respectively. Non-treated cells (Dox 0h) were used as a specificity control. We observed a gradual increase of Tat mRNA and protein levels from 1 hour up to 48 hours after the induction (**Figure 1B, 1C**).

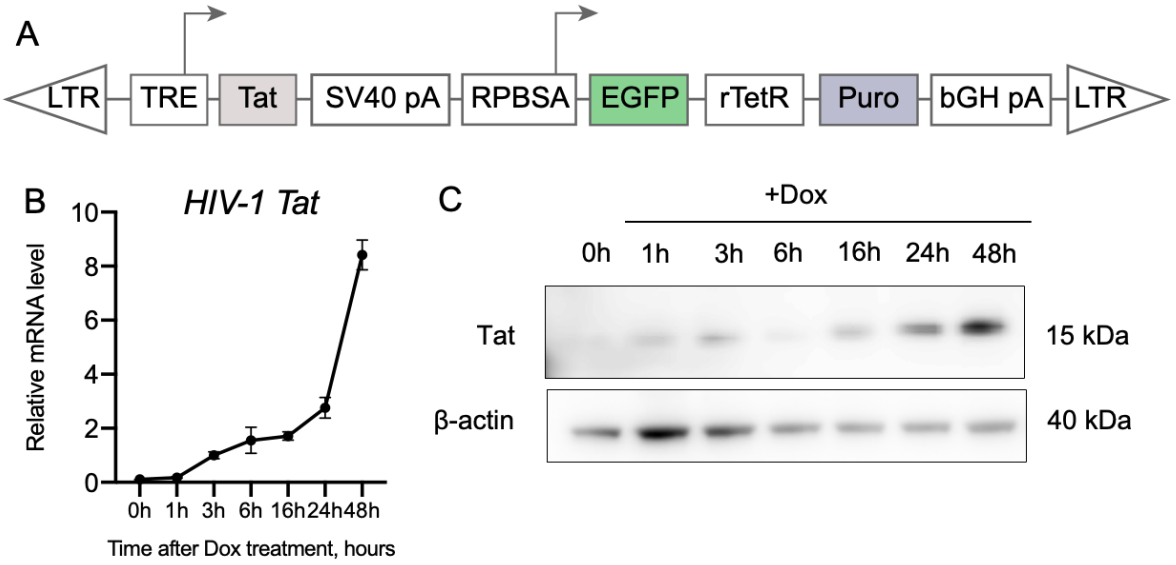

***Figure 1**. HIV-1 Tat was expressed in the RPMI8866 Tat^{i} cell line after induction with doxycycline. (A) Schematic depiction of the pSBtet derivative construct enabling inducible expression of Tat and stable expression of EGFP in RPMI8866 Tat^{i} cell line. bGH pA, Bovine growth hormone polyadenylation signal; EGFP, Enhanced green fluorescent protein; LTR, Long terminal repeat; Puro, Puromycin resistance gene; RPBSA, constitutive promoter; rTetR, reverse tetracycline repressor (transactivator); SV40 pA, Simian virus 40 polyadenylation signal; TRE, Tetracycline response element (promoter). Adapted from [33]. (B) The level of Tat mRNA expression in RPMI8866 Tat^{i} cell line at different time points; mRNA level was normalized to GAPDH and RPL32 expression as housekeeping genes. Data are presented as mean ± SEM. (C) Western blotting of Tat protein content in RPMI8866 Tat^{i} cell line at different time points; β-actin was used as a loading control.*

To detect possible changes in B cell physiology caused by acute HIV-1 Tat action that might contribute to oncogenic hallmark acquisition, we performed a genome-wide analysis of cellular gene expression (RNA-sequencing) in RPMI8866 Tat^{i} cell line with or without Tat induction with doxycycline. Differentially expressed genes (DEGs) were defined as genes with p.adjust < 0.05 and |$\log_2$ fold change| >0.5 as compared to the RPMI8866 Tat^{i} control cell line. Our analysis revealed 1495 DEGs in RPMI8866 Tat^{i} + Dox *vs* RPMI8866 Tat^{i} control cells; 864 genes were upregulated, and 631 genes were downregulated (**Figure 2A, 2B**). Among detected DEGs, the majority were protein-coding genes (808 upregulated and 590 downregulated) but differentially expressed non-coding RNAs were also identified (45 upregulated and 22 downregulated) (**Figure 2B**).

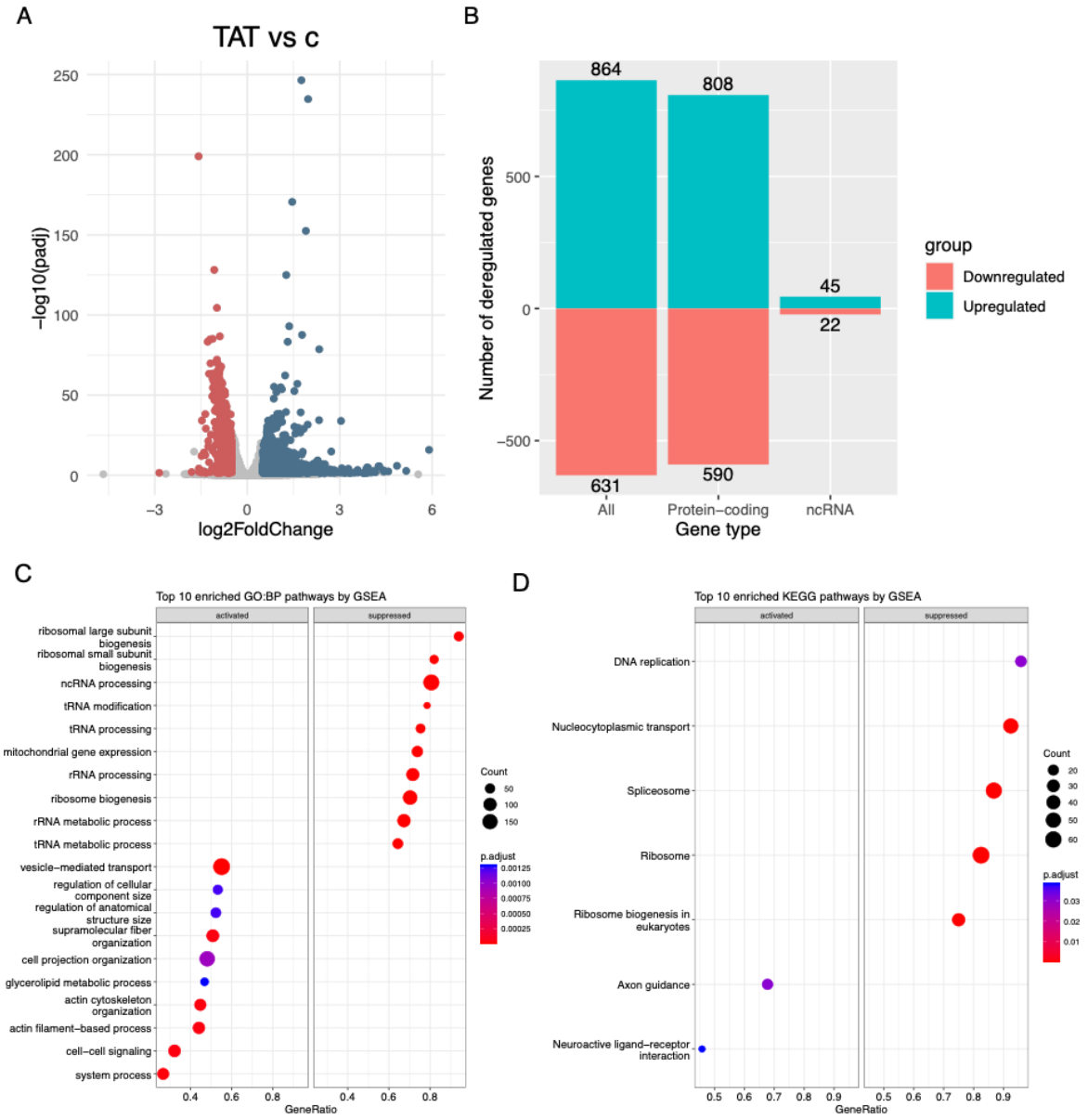

***Figure 2**. Acute HIV-1 Tat protein action affected the gene expression profile of B cells. (A) Volcano plot of differentially expressed genes (DEGs) between RPMI8866 Tat^{i} + Dox and RPMI8866 Tat^{i} control cells. (B) The number of all DEGs, protein-coding DEGs or DEGs*

encoding non-coding RNAs in RPMI8866 Tat^{i} + Dox vs RPMI8866 Tat^{i} control cells. (C) Gene set enrichment analysis (GSEA) for functional categories defined by the Gene Ontology Biological Process (GO BP) enriched among DEGs between RPMI8866 Tat^{i} + Dox and RPMI8866 Tat^{i} control cells; activated pathways are shown on the left, suppressed pathways are shown on the right; top 10 significantly enriched GO BP pathways are shown. (D) GSEA for functional categories defined by the Kyoto Encyclopedia of Genes and Genomes (KEGG) enriched among DEGs between RPMI8866 Tat^{i} + Dox and RPMI8866 Tat^{i} control cells; activated pathways are shown on the left, suppressed pathways are shown on the right; 7 significantly enriched KEGG pathways are shown. c, control; padj, adjusted p-value.

Next, we performed gene set enrichment analysis (GSEA) to search for activated and suppressed functional categories defined by the Gene Ontology Biological Process (GO BP) and the Kyoto Encyclopedia of Genes and Genomes (KEGG) databases (**Figure 2C, 2D**). The transcriptomic changes caused by the inducible Tat expression had a negative effect on several important cellular processes: the *DNA replication* (p.adjust = 3.1×10^{-4}), *ribosome biogenesis processes* (p.adjust = 3.14×10^{-8}), *ncRNA processing (*p.adjust = $3.1 \times 10^{-8)}$, *rRNA processing*, (p.adjust = 3.14×10^{-8}), *tRNA processing*, (p.adjust = 3.14×10^{-8}), *mitochondrial gene expression* (p.adjust = 3.14×10^{-8}) and others. The gene sets with an elevated expression included *vesicle-mediated transport* (p.adjust = 9.24×10^{-8}), *regulation of cellular component size* (p.adjust = 1.24×10^{-4}), *supramolecular fiber organization* (p.adjust = 3.47×10^{-5}), *cell projection organization* (p.adjust = 9.5×10^{-4}), *glycerolipid metabolic process* (p.adjust = 1.29×10^{-3}), *actin cytoskeleton organization* (p.adjust = 2.77×10^{-5}), *actin filament-based process* (p.adjust = 3.24×10^{-5}), cell-cell signaling (p.adjust = 3.35×10^{-5}) and others.

Acute HIV-1 Tat action reduced DNA damage repair in B cells

Among significantly suppressed GO BP functional categories were DNA repair (p.adjust = 1.36×10^{-3}) and signal transduction by p53 class mediator (p.adjust = 3.26×10^{-3}), which contained multiple genes, whose expression was downregulated by the action of HIV-1 Tat (**Figure 3A, 3B**). We next confirmed the Tat-induced downregulation of DNA repair genes by qPCR (**Figure 3C**): the mRNA levels of *POLE3* (0.831 ± 0.044 vs 1.000 ± 0.029, p = 0.0133; t-test), *UNG* (0.749 ± 0.085 vs 1.000 ± 0.033, p = 0.0249; t-test), *GFT2H2* (0.833 ± 0.035 vs 1.000 ± 0.030, p = 0.0069; t-test) were significantly decreased in RPMI8866 Tat^{i} + Dox cell line compared to non-induced controls. The mRNA levels of *APEX1* (0.917 ± 0.025 vs 1.000 ± 0.035, p = 0.0902; t-test), *POLD2* (0.914 ± 0.041 vs 1.000 ± 0.025, p = 0,1085; t-test) and *SSBP1* (0.934 ± 0.028 vs 1.000 ± 0.029, p = 0,1440; t-test) in RPMI8866 Tat^{i} + Dox cells also showed a trend towards decrease compared to control cells, although did not reach statistical significance.

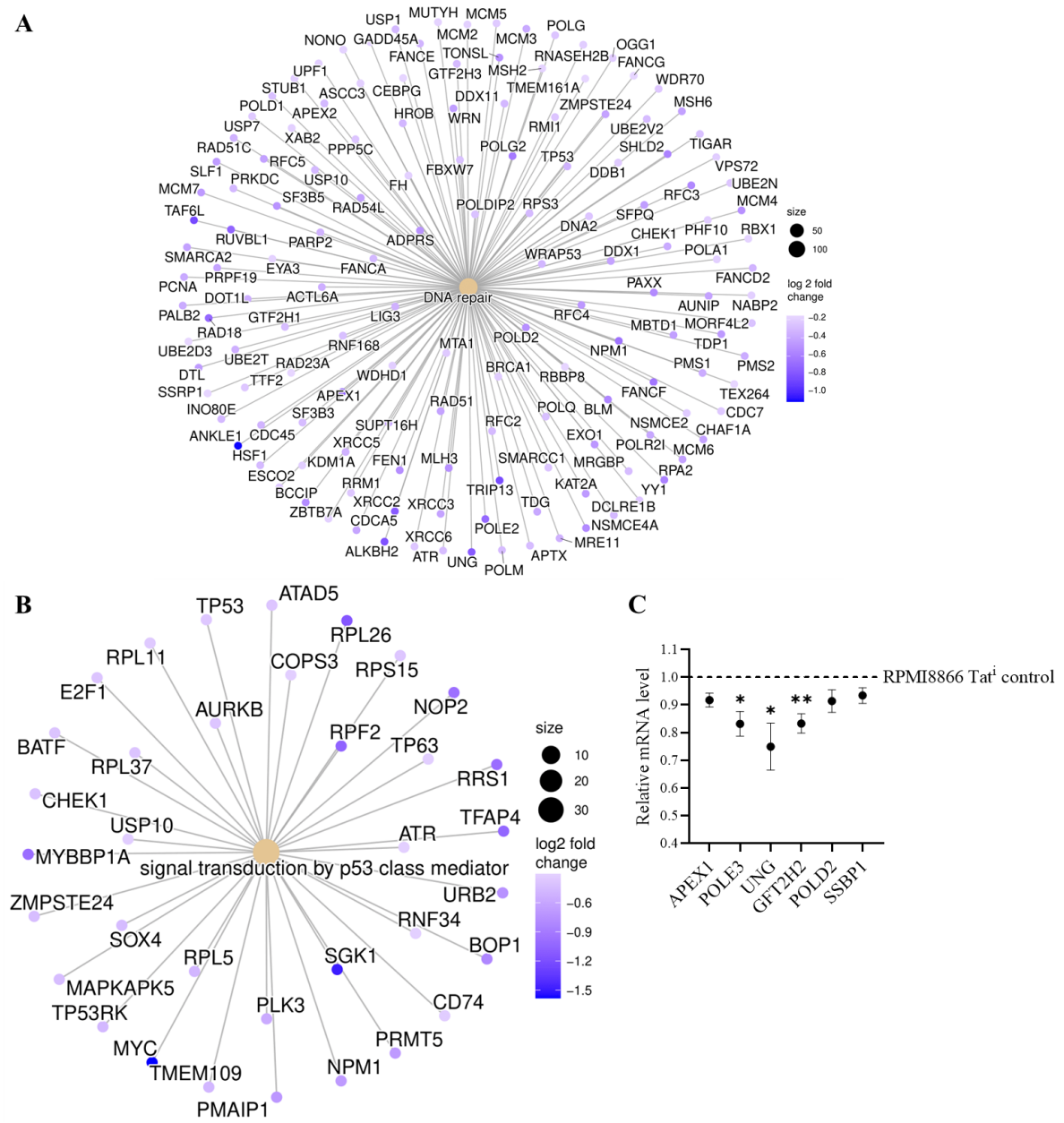

Figure 3. *HIV-1 Tat decreased the expression of genes involved in DNA damage repair in B cells. (A-B) Selected GO BP terms pathways, enriched among significantly downregulated genes in RPMI8866 Tat^{i} + Dox vs RPMI8866 Tat^{i} control comparison and associated DEGs: DNA repair (A) and signal transduction by p53 class mediator (B). (C) The level of APEX1, POLE3, UNG, GFT2H2, POLD2 and SSBP1 mRNA expression in RPMI8866 Tat^{i} + Dox cells. mRNA level was normalized to GAPDH and RPL32 expression as housekeeping genes; the normalization was done assuming the mean level of transcript in RPMI8866 Tat^{i} control cells to be 1. Data are presented as mean ± SEM. * $p < 0.05$, ** $p < 0.01$ relative to RPMI8866 Tat^{i} control cells, t-test.*

To further investigate the effect of Tat on DNA repair and DNA damage accumulation, we incubated RPMI8866 Tat^{i} cells with a DNA-damaging agent and a chemotherapeutic drug, cisplatin. We first analyzed the accumulation of cisplatin-induced DNA damages after 2

and 4 hours of incubation with 50 µM or 300 µM cisplatin in RPMI8866 Tat^{i} cells with or without prior induction of Tat expression for 16 hours. For this purpose, we used a dot blot technique with specific antibodies to platinum-DNA adducts. We observed that DNA damage in RPMI8866 Tat^{i} + Dox cells was higher than in control cells 4 hours after 50 µM cisplatin treatment compared to cells without Tat expression (3.447 ± 0.790 vs 1.4523 ± 0.262, p = 0.0199, 2-way ANOVA, Šídák's post-hoc test) (**Figure 4A-C**). Our results indicated that the acute action of HIV-1 Tat on B cells led to an increased accumulation of cisplatin-DNA adducts as compared to that of control cells, which is in agreement with RNA-seq data indicating that Tat decreased the expression of genes involved in DNA damage sensing and repair (**Figure 3A, 3B**).

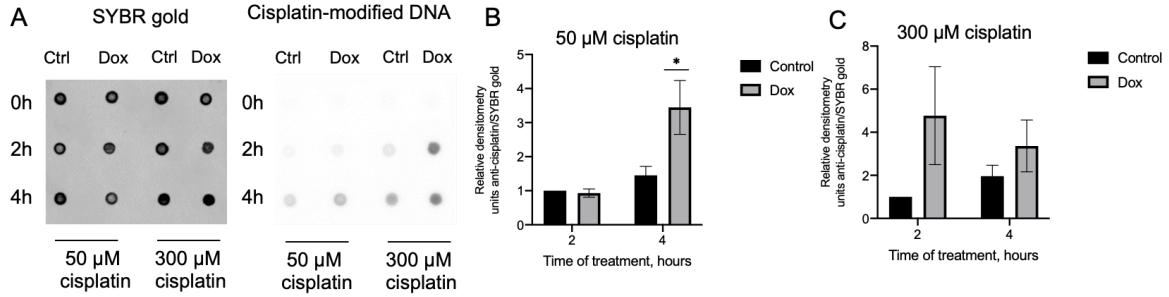

***Figure 4**. HIV-1 Tat increased the accumulation of specific DNA damage. (A) Dot blot analysis of cisplatin-modified DNA levels in RPMI8866 Tat^{i} cells after 50 µM or 300 µM cisplatin treatment. SYBR gold was used as DNA loading control. (B-C) Levels of cisplatin-modified DNA in RPMI8866 Tat^{i} cells after 50 µM (B) or 300 µM (C) cisplatin treatment. The cisplatin-modified DNA level was normalized to SYBR gold as loading control; the normalization was done assuming the mean level of cisplatin-modified DNA in RPMI8866 Tat^{i} control cells 2 hours after treatment to be 1. Data are presented as mean ± SEM. * p < 0.05, relative to RPMI8866 Tat^{i} control cells, 2-way ANOVA, Sidak post-hoc test.*

Cisplatin-induced interstrand crosslinks (~5% of cisplatin-induced DNA lesions) promote DSB formation during replication and/or repair processes [35] and γH2AX foci are formed in cells following cisplatin exposure as a component of DNA damage response [36]. We thus next assessed DNA damage recognition and repair by analyzing the presence of γH2AX marker in RPMI8866 Tat^{i} cells treated or not with 10 µM cisplatin for 2, 6 or 24 hours with or without prior induction of Tat expression for 16 hours. γH2AX is a form of histone H2AX that becomes phosphorylated near DNA damage sites in the early stages of DNA repair [37]. We evaluated the kinetics of γH2AX levels by immunofluorescent staining and confocal microscopy. The results demonstrated that γH2AX level was significantly decreased in RPMI8866 Tat^{i} + Dox cells compared to control cells at 2, 6 and 24 hours after cisplatin treatment (**Figure 5A, 5B**). Lower γH2AX levels were not linked to decreased replication in RPMI8866 Tat^{i} + Dox cells, since no changes in the cell cycle were observed between RPMI8866 Tat^{i} + Dox cells and RPMI8866 Tat^{i} control cells (**Supplementary figure 1**). Consequently, these data suggest lower DNA damage

recognition after cisplatin treatment in RPMI8866 Tat^{i} + Dox cells. Of note, H2AX mRNA levels were unchanged by RNA-sequencing analysis.

At the core of DNA damage response and repair is the tumour suppressor protein p53, which undergoes post-translational modifications (e.g. phosphorylation), leading to its activation upon sensing DNA damage [38]. To analyze the effect of HIV-1 Tat on p53 activation upon cisplatin treatment of B cells, we performed a western blotting analysis of RPMI8866 Tat^{i} cells 24 hours after treatment with 300 µM cisplatin with or without prior induction of Tat expression for 16 hours. The expression and phosphorylation of p53 were low in B cells without cisplatin treatment regardless of Tat expression (**Figure 5C-E**). Upon cisplatin treatment, both the level of p53 and its phosphorylated form peaked compared to the non-treated control (**Figure 5C-E**). However, the activation of p53 upon cisplatin treatment (as assessed by the level of phospho-p53) was significantly decreased in RPMI8866 Tat^{i} + Dox cells compared to RPMI8866 Tat^{i} control (1.520±0.028 vs 1.137±0.057, p = 0.0262) (**Figure 5E**), pointing again to lower activation of DNA damage response.

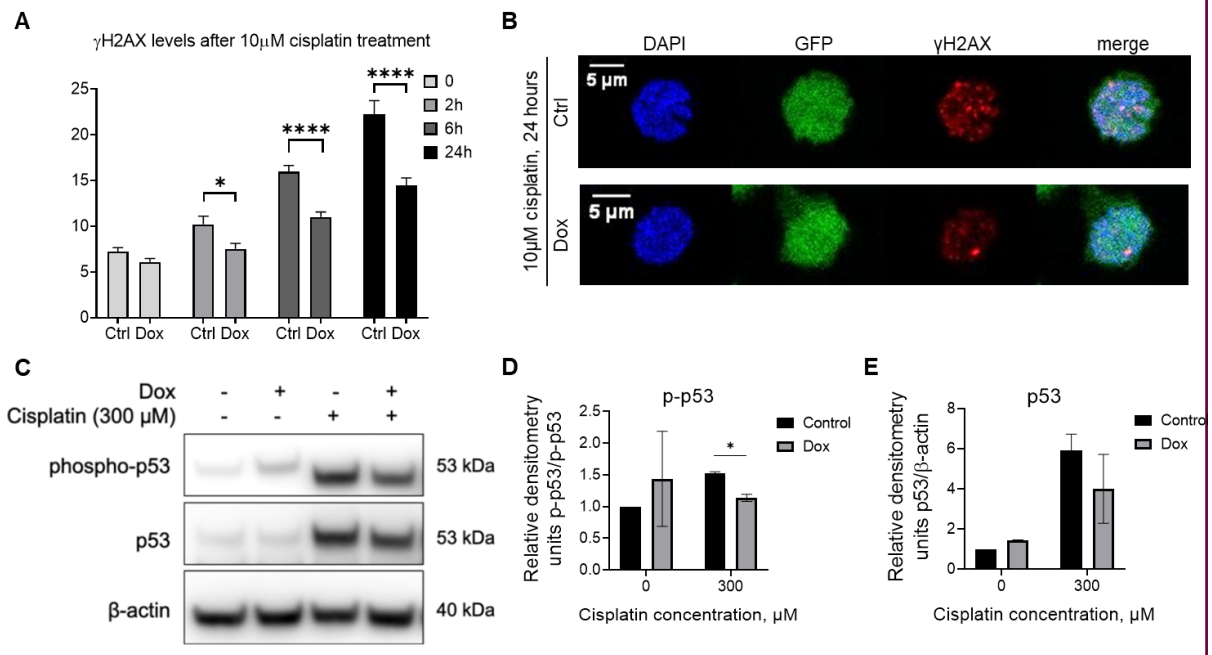

***Figure 5**. HIV-1 Tat decreased DNA damage repair in B cells. (A) The mean nuclear fluorescence intensity of γH2AX in RPMI8866 Tat^{i} cells after 2, 6 or 24 hours of treatment with 10 µM cisplatin. * $p < 0.05$, **** $p < 0.0001$ relative to RPMI8866 Tat^{i} control cells, 2-way ANOVA, Sidak post-hoc test. (B) A representative confocal image of RPMI8866 Tat^{i} cells stained with antibodies to γH2AX (red) after 24 hours of treatment with 10µM cisplatin. Nuclei were counterstained with DAPI (blue) and GFP fluorescence (green) in cells was detected since RPMI8866 Tat^{i} cells stably express EGFP. Scale bar 5 µm. (C) Western blotting analysis of phospho-p53 protein level after the treatment with 300 µM cisplatin. (D) Densitometry analysis of phospho-p53 level after the treatment with 300 µM cisplatin, normalized to p53; the normalization was done assuming the mean level of*

*phospho-p53 in RPMI8866 Tat^{i} control cells without cisplatin treatment to be 1. * $p < 0.05$, two-way ANOVA, Sidak post-hoc test. (E) Densitometry analysis of p53 level after the treatment with 300 μM cisplatin, normalized to β-actin; the normalization was done assuming the mean level of p53 in RPMI8866 Tat^{i} control cells without cisplatin treatment to be 1. Data are presented as mean ± SEM. Ctrl, RPMI8866 Tat^{i} control cells; Dox, RPMI8866 Tat^{i} + Dox cells (with doxycycline induced Tat expression).*

Thus, HIV-1 Tat can contribute to the elevated accumulation of cisplatin-specific DNA damages by decreasing the expression of DNA repair genes, which leads to defects in DNA damage sensing and repair as shown by decreased γH2AX levels and decreased p53 activation upon cisplatin treatment in B cells.

Acute HIV-1 Tat action did not substantially influence B cell sensitivity to DNA-damaging drugs

Having shown that the acute presence of HIV-1 Tat protein in B cells can exert a significant impact on the heightened accumulation of cisplatin-induced DNA damages by means of compromised DNA damage sensing and repair mechanisms, we next decided to test whether this can have an impact on B cell survival and apoptosis induction upon chemotherapy treatment. To evaluate the viability of RPMI8866 Tat^{i} cells with or without prior induction of HIV-1 Tat expression for 16 hours followed by treatment with DNA damaging drugs treatment with DNA-damaging drugs, we performed MTT tests. We incubated cells with various concentrations of cisplatin (1, 5, 10, 20, 30, 40, 50, 100, 200 or 300 μM), oxaliplatin (0.05, 0.1, 0.5, 1, 5, 10 or 50 μM) or doxorubicin (0.1, 0.2, 0.3, 0.4, 0.5, 1, 2, 5, 10 or 20 μM) for 24 hours. Cell viability was analyzed by MTT assay and compared to the viability of non-treated RPMI8866 Tat^{i} control which was assumed to be 100%. In most cases, there was no statistically significant difference between RPMI8866 Tat^{i} + Dox cells and RPMI8866 Tat^{i} control cells (**Figure 6A-C**). We observed a decrease of viability of RPMI8866 Tat^{i} + Dox cells in comparison with control cells after treatment with 0.05 μM oxaliplatin (82.875 ± 2.448 *vs* 95.650 ± 1.160, $p = 0.0001$; two-way ANOVA), 0.1 μM oxaliplatin (76.997 ± 2.141 *vs* 95.617 ± 1.274, $p < 0.0001$; two-way ANOVA) or 0.5 μM oxaliplatin (73.830 ± 2.757 *vs* 82.617 ± 2.029, $p = 0.0219$; two-way ANOVA) (**Figure 6B)**. At high oxaliplatin concentrations (1 μM, 5 μM, 10 μM, 50 μM), however, no significant differences were found between RPMI8866 Tat^{i} + Dox and RPMI8866 Tat^{i} control cells.

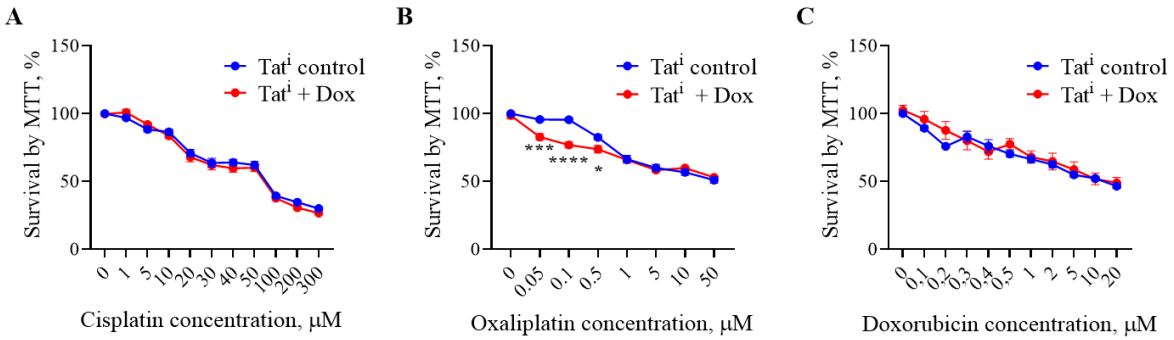

***Figure 6**. Acute HIV-1 Tat action did not substantially influence the survival of B cells after treatment with DNA-damaging drugs. (A-C) Relative viability of RPMI8866 Tat^{i} + Dox and RPMI8866 Tati control cells after 24 hours of treatment with different concentrations of cisplatin (A), oxaliplatin (B) or doxorubicin (C). The normalization was done assuming the mean level of viability in RPMI8866 Tat^{i} control cells without any treatment to be 100%. Data are presented as mean ± SEM. * $p < 0.05$; *** $p < 0.001$; **** $p < 0.0001$, two-way ANOVA, Sidak post-hoc test.*

To investigate the effect of acute Tat action on B cell apoptosis, we performed Annexin V/PI staining of RPMI8866 Tat^{i} cells with or without prior induction of HIV-1 Tat expression for 16 hours followed by treatment with DNA-damaging drugs. Cells were treated with different concentrations of cisplatin (10, 50, 100 or 300 μM), oxaliplatin (0.1, 1, 10 or 100 μM) or doxorubicin (0.2, 20, or 200 μM) for 24 hours. We detected early and late apoptotic cells by staining with Annexin V, which binds to phosphatidylserine at the outer leaflet of the plasma membrane of early and late apoptotic cells, and propidium iodide (PI), which penetrates in cells with damaged membrane (only late apoptotic cells) and binds to DNA. Thus, early apoptotic cells were defined as Annexin V-positive and PI-negative, and late apoptotic cells were defined as Annexin V-positive and PI-positive. For samples treated with doxorubicin, we were able to access only the total level of apoptosis (Annexin V-positive cells) without discrimination into early and late apoptosis as the fluorescence of doxorubicin overlapped with that of PI.

Our results showed that in the majority of cases, there was no significant difference in early, late or total apoptosis levels between RPMI8866 Tat^{i} + Dox cells and RPMI8866 Tat^{i} control cells (**Figure 7**). The significant increase of apoptosis level in RPMI8866 Tati + Dox cells compared to control cells was revealed only after treatment with 300 μM cisplatin (**Figure 7A, 7C**): 29.213 ± 2.475% cells were early apoptotic in RPMI8866 Tat^{i} + Dox cells *vs* 21.663 ± 1.478% in RPMI8866 Tat^{i} control ($p = 0.001$, two-way ANOVA); 62.417 ± 5.041% cells were apoptotic in RPMI8866 Tat^{i} + Dox cells *vs* 50.400 ± 4.555% in RPMI8866 Tat^{i} control ($p = 0.0287$; two-way ANOVA). Taking together the results of MTT tests for cell viability and Annexin V test for apoptosis, we concluded that Tat did not substantially influence the chemosensitivity of B cells to DNA-damaging drugs.

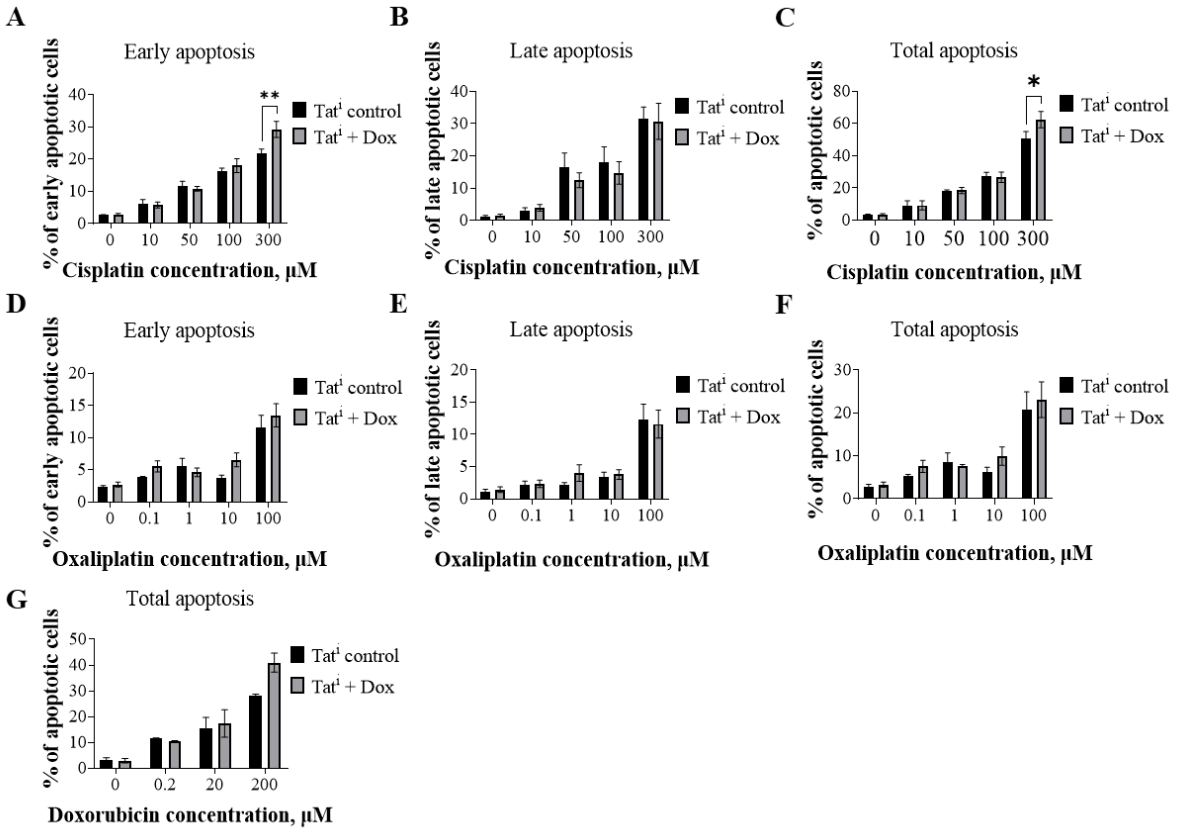

***Figure** 7. Acute HIV-1 Tat action did not influence the apoptosis level of B cells after treatment with DNA-damaging drugs. (A-C) The percentage of RPMI8866 Tat^{i} + Dox and RPMI8866 Tati control cells in early (A), late (B) and total (C) apoptosis after 24 hours of treatment with different concentrations of cisplatin. * $p < 0.05$; *** $p < 0.001$; **** $p < 0.0001$, two-way ANOVA, Sidak post-hoc test. (D-F) The percentage of RPMI8866 Tati + Dox and RPMI8866 Tati control cells in early (D), late (E) and total (F) apoptosis after 24 hours of treatment with different concentrations of oxaliplatin. (G) The percentage of RPMI8866 Tat^{i} + Dox and RPMI8866 Tat^{i} control cells in apoptosis after 24 hours of treatment with different concentrations of doxorubicin. Early apoptotic cells were defined as Annexin V-positive and PI-negative, late apoptotic cells were defined as Annexin V-positive and PI-positive, and total apoptotic cells were defined as Annexin V-positive. Data are presented as mean ± SEM.*

Discussion

cART has reshaped HIV infection from an almost inevitably lethal disease to a manageable chronic infection for the majority of infected individuals. Nevertheless, HIV infection remains incurable and, despite suppression of viral replication and immune restoration, people living with HIV still have an increased risk of B cell malignancies [4]. In the current study, we aimed to identify mechanisms that could contribute to B cell lymphomagenesis in people living with HIV. B cells are not infected by HIV, although they can be affected by HIV indirectly, e.g. through the acute action of secreted viral proteins produced by the cells bearing both normal and defective HIV proviruses [6]. Likewise, HIV-1 Tat, a crucial

regulator of HIV transcription, is efficiently exported from infected cells and uptaken by neighbouring non-infected cells [23,25]. Due to its cell-penetrating property, as well as its intrinsic disorder allowing it to interact with various partners in non-infected cells, Tat is believed to contribute to the development of multiple HIV-related diseases, including BL [9].

To study the effects of acute HIV-1 Tat action on B cells, we used an EBV-immortalized lymphoblastoid B cell line RPMI8866 with an inducible expression HIV-1 Tat (RPMI8866 Tat^{i} cell line, **Figure 1**). We performed a genome-wide analysis of cellular gene expression (RNA-sequencing analysis) of the RPMI8866 Tat^{i} cell line and revealed that Tat regulated the expression of hundreds of genes that included protein-coding genes (**Figure 2**). Among them, many genes involved in DNA repair and replication were suppressed (**Figure 3**). Whether the Tat acts as a transcriptional regulator of these genes or through indirect interactions with other transcriptional factors requires further investigation. HIV-1 Tat was shown to downregulate DNA-PKcs (*PRKDC*) expression by directly binding to its promoter [39]. We have recently shown that HIV-1 Tat decreases NF-κB activation in B cells (*unpublished data*). NF-κB is activated upon genotoxic stress and regulates the transcription of multiple DNA repair genes [40]. Tat also was previously shown to downregulate *TP53* expression [41], which is confirmed by our RNA-sequencing data, and which might have resulted in the downregulation of *TP53*-regulated transcription of DNA repair genes [40]. B cells are intrinsically prone to programmed DNA damage events throughout their lifespan, primarily occurring during key processes of B cell maturation such as V(D)J recombination, somatic hypermutation and the immunoglobulin class switch recombination [42]. Disruption of DNA repair pathways in B cells can lead to the accumulation of DNA damage, promoting genome instability and mutations (a hallmark of cancer [43]) and eventually contributing to the development of B cell lymphomas in people living with HIV. Thus, in our study, we focused on this aspect of Tat action on B cells.

HIV-1 Tat was previously reported to induce DNA damage through ROS production in B cells [30]. Tat increases the expression of DNA polymerase beta, a key component of the DNA base-excision repair pathway, by interacting with cellular transcription factors in B cells, which affects genome stability and can promote lymphomagenesis [29]. Tat also influences DSB repair by reducing the nonhomologous end-joining in cells treated with DNA-damaging agents [44]. It also increases DNA damage accumulation in rhabdomyosarcoma cells after exposure to ionizing radiation [45]. Here we used common chemotherapeutic drugs to model DNA damages in B cells and evaluate the effect of Tat on the accumulation of specific DNA damages and their sensing and repair. We showed that HIV-1 Tat can promote specific DNA damage accumulation induced by cisplatin in B cells (**Figure 4**), which is consistent with its role in downregulating multiple genes involved in DNA repair. The specificity of this effect was confirmed by dot blot with anti-cisplatin modified DNA, which showed an accumulation of cisplatin-specific DNA damage in Tat-expressing B cells (**Figure 4**), suggesting that we did not detect Tat contribution to general DNA damage (such as through the production of ROS), but rather found that it hinders the repair process, leading to the accumulation of specific DNA damage. Further

supporting our findings, we employed immunofluorescence microscopy to assess γH2AX levels, a widely recognized marker of DNA damage site recognition DNA damage in the early stages of DNA repair [37]. Our results revealed a significant decrease in γH2AX levels in B cells expressing Tat (**Figure 5A,B**). The diminished γH2AX signal supports the notion that Tat impedes the proper recognition and signaling of DNA damage in B cells. Additionally, we evaluated the phosphorylation status of p53, a critical transcription factor involved in DNA repair and cell cycle regulation [38]. Western blotting analysis demonstrated a notable decrease in phospho-p53 levels in B cells expressing Tat (**Figure 5C-E**), which suggests that Tat may disrupt the activation of p53 and subsequent downstream signaling, further compromising the DNA repair process. Therefore, Tat expression in B cells led to a decrease in DNA repair capacity and an accumulation of cisplatin-induced DNA damage.

Next, we assessed whether Tat-induced disruption of DNA repair leads to an increased level of apoptosis in B cells (**Figure 7**). The effect of Tat on apoptosis of bystander non-infected CD4+ T cells leading to HIV-associated CD4+ T cell depletion is well known [46]. Tat was found to use different pathways to induce apoptosis in bystander cells. One of them requires Tat binding to tubulin/microtubules, facilitated by pro-apoptotic protein Bim, leading to the activation of a mitochondria-dependent apoptotic pathway [47]. Tat also promotes apoptosis in bystander cells through unfolded protein response (UPR): Tat action on Jurkat cells results in overexpression of UPR markers, an increase in levels of downstream mediators and proapoptotic factors, which leads to apoptosis [48]. Unlike bystander non-infected CD4+ T cells, productively infected cells are able to escape apoptosis and survive, and this process is also regulated by Tat. It has been shown that Tat downregulates caspase-10 and up-regulates cFLIP and thus protects acutely HIV-infected CD4+ cells from apoptosis [49]. Upregulation of microRNAs by Tat may also contribute to protection against apoptosis in HIV-infected CD4+ T cells [50]. Therefore, Tat exhibits both pro- and apoptotic effects on CD4+ cells.

The effect of Tat on apoptosis in other types of cells is less studied. Some studies show the promotion of apoptosis by Tat. For example, Tat induces apoptosis of neurons by disrupting neuronal calcium homeostasis [51]. Tat action also promotes apoptosis of human enterocytes through oxidative stress [52]. However, there is evidence of anti-apoptotic action of Tat on other cell types. For example, Tat increases Bcl-2 expression in monocytes which leads to the inhibition of apoptosis [53]. Tat was also found to protect cells from chemical-induced death: in cells of Kaposi's sarcoma, Tat functions as a protecting agent from vincristine-induced apoptosis by upregulating anti-apoptotic protein Bcl-X(L) expression, which induces a decrease in caspase-3 activity [54]. It was shown that Tat is able to induce the polyubiquitination and degradation of Tip60, which plays a critical role in controlling the cell response to genotoxic treatments. Thus, Tat-mediated degradation of Tip60 protects cells against the Tip60-dependent apoptotic cell response to DNA damage [55]. Nevertheless, the impact of Tat on apoptosis in different cell types and conditions requires further investigation.

Here we studied the acute effect of HIV-1 Tat on the survival and apoptosis of B cells after treatment with DNA-damaging drugs. For this purpose, we treated RPMI8866 Tat^{i} cells with or without Tat induction with cisplatin, oxaliplatin and doxorubicin in different concentrations. We did not observe any substantial elevation or decrease of cell viability and apoptosis (**Figure 6, 7**). Only treatment with high doses of cisplatin resulted in increased apoptosis in RPMI8866 Tat^{i} cells with Tat induction (**Figure 7A, C**); treatment with oxaliplatin in small concentrations resulted in the decrease of cell viability in RPMI8866 Tat^{i} cells with Tat induction compared to control (**Figure 6B**). The preservation of cell viability in the face of increased genomic instability is a notable observation from this study. It suggests that HIV-1 Tat may possess a dual function, allowing B cells to accumulate genetic lesions without rendering them susceptible to the detrimental effects of these changes. This ability to maintain cell viability despite the presence of genomic alterations may provide a favourable environment for the progression of B cells towards lymphoma.

In conclusion, our research provides evidence that acute Tat action on B cells leads to a decrease in DNA repair capacity and an accumulation of DNA damage. However, we did not observe a substantial increase in apoptosis levels or a decrease in cell survival in Tat-expressing B cells upon treatment with DNA-damaging drugs such as cisplatin, oxaliplatin and doxorubicin. These results suggest that Tat-mediated impairment of DNA repair mechanisms may contribute to genomic instability without directly influencing cell viability, which can potentially lead to the malignant transformation of B cells in people living with HIV.

Abbreviations

AID, activation‐induced cytidine deaminase
ANOVA, analysis of variance
BL, Burkitt lymphoma
BSA, bovine serum albumin
cART, combination antiretroviral therapy
CCR5, CC-chemokine receptor 5
CXCR4, CXC-chemokine receptor 4
DEGs, differentially expressed genes
Dox, doxycycline
DSB, double-strand break
EBV, Epstein-Barr virus
eIF2α, translation initiation factor 2
GO BP, Gene Ontology Biological Process
GSEA, gene set enrichment analysis
HIV, human immunodeficiency virus
HL, Hodgkin lymphoma
IFN, interferon
KEGG, Kyoto Encyclopedia of Genes and Genomes

PBS, phosphate-buffered saline
PI, propidium iodide
PI(4,5)P_2, phosphatidylinositol-4,5-bisphosphate
PKR, interferon-induced, dsRNA-dependent serine/threonine protein kinase
p-TEFb, positive transcription elongation factor
PVDF, polyvinylidene fluoride
qPCR, quantitative polymerase chain reaction
ROIs, nuclear regions of interest
ROS, reactive oxygen species
SEM, standard error of the mean
TAR, transactivation response
Tat, transactivator of transcription
TBST, Tris-buffered saline and 0.1% Tween-20

References

1. Hernández-Ramírez, R.U.; Shiels, M.S.; Dubrow, R.; Engels, E.A. Spectrum of Cancer Risk among HIV-Infected People in the United States during the Modern Antiretroviral Therapy Era: A Population-Based Registry Linkage Study. *Lancet HIV* **2017**, *4*, e495–e504, doi:10.1016/S2352-3018(17)30125-X.
2. Carbone, A.; Vaccher, E.; Gloghini, A. Hematologic Cancers in Individuals Infected by HIV. *Blood* **2022**, *139*, 995–1012, doi:10.1182/blood.2020005469.
3. Epeldegui, M.; Vendrame, E.; Martínez-Maza, O. HIV-Associated Immune Dysfunction and Viral Infection: Role in the Pathogenesis of AIDS-Related Lymphoma. *Immunol. Res.* **2010**, *48*, 72–83, doi:10.1007/s12026-010-8168-8.
4. Shmakova, A.; Germini, D.; Vassetzky, Y. HIV-1, HAART and Cancer: A Complex Relationship. *Int. J. Cancer* **2020**, *146*, 2666–2679, doi:10.1002/ijc.32730.
5. Dolcetti, R.; Gloghini, A.; Caruso, A.; Carbone, A. A Lymphomagenic Role for HIV beyond Immune Suppression? *Blood* **2016**, *127*, 1403–1409, doi:10.1182/blood-2015-11-681411.
6. Imamichi, H.; Smith, M.; Adelsberger, J.W.; Izumi, T.; Scrimieri, F.; Sherman, B.T.; Rehm, C.A.; Imamichi, T.; Pau, A.; Catalfamo, M.; et al. Defective HIV-1 Proviruses Produce Viral Proteins. *Proc. Natl. Acad. Sci. U. S. A.* **2020**, *117*, 3704–3710, doi:10.1073/pnas.1917876117.
7. Popovic, M.; Tenner-Racz, K.; Pelser, C.; Stellbrink, H.-J.; van Lunzen, J.; Lewis, G.; Kalyanaraman, V.S.; Gallo, R.C.; Racz, P. Persistence of HIV-1 Structural Proteins and Glycoproteins in Lymph Nodes of Patients under Highly Active Antiretroviral Therapy. *Proc. Natl. Acad. Sci. U. S. A.* **2005**, *102*, 14807–14812, doi:10.1073/pnas.0506857102.
8. Mediouni, S.; Darque, A.; Baillat, G.; Ravaux, I.; Dhiver, C.; Tissot-Dupont, H.; Mokhtari, M.; Moreau, H.; Tamalet, C.; Brunet, C.; et al. Antiretroviral Therapy Does Not Block the Secretion of the Human Immunodeficiency Virus Tat Protein. *Infect. Disord. Drug Targets* **2012**, *12*, 81–86, doi:10.2174/187152612798994939.
9. Germini, D.; Tsfasman, T.; Klibi, M.; El-Amine, R.; Pichugin, A.; Iarovaia, O.V.; Bilhou-Nabera, C.; Subra, F.; Bou Saada, Y.; Sukhanova, A.; et al. HIV Tat Induces a Prolonged MYC Relocalization next to IGH in Circulating B-Cells. *Leukemia* **2017**, *31*, 2515–2522, doi:10.1038/leu.2017.106.
10. Poggi, A.; Carosio, R.; Fenoglio, D.; Brenci, S.; Murdaca, G.; Setti, M.; Indiveri, F.;

Scabini, S.; Ferrero, E.; Zocchi, M.R. Migration of Vδ1 and Vδ2 T Cells in Response to CXCR3 and CXCR4 Ligands in Healthy Donors and HIV-1-Infected Patients: Competition by HIV-1 Tat. *Blood* **2004**, *103*, 2205–2213, doi:10.1182/blood-2003-08-2928.
11. Altavilla, G.; Trabanelli, C.; Merlin, M.; Caputo, A.; Lanfredi, M.; Barbanti-Brodano, G.; Corallini, A. Morphological, Histochemical, Immunohistochemical, and Ultrastructural Characterization of Tumors and Dysplastic and Non-Neoplastic Lesions Arising in BK Virus/Tat Transgenic Mice. *Am. J. Pathol.* **1999**, *154*, 1231–1244, doi:10.1016/S0002-9440(10)65375-8.
12. Xue, B.; Mizianty, M.J.; Kurgan, L.; Uversky, V.N. Protein Intrinsic Disorder as a Flexible Armor and a Weapon of HIV-1. *Cell. Mol. Life Sci.* **2012**, *69*, 1211–1259, doi:10.1007/s00018-011-0859-3.
13. Sedore, S.C.; Byers, S.A.; Biglione, S.; Price, J.P.; Maury, W.J.; Price, D.H. Manipulation of P-TEFb Control Machinery by HIV: Recruitment of P-TEFb from the Large Form by Tat and Binding of HEXIM1 to TAR. *Nucleic Acids Res.* **2007**, *35*, 4347–4358, doi:10.1093/nar/gkm443.
14. Endo-Munoz, L.; Warby, T.; Harrich, D.; McMillan, N.A.J. Phosphorylation of HIV Tat by PKR Increases Interaction with TAR RNA and Enhances Transcription. *Virol. J.* **2005**, *2*, 17, doi:10.1186/1743-422X-2-17.
15. Ferrell, D.; Giunta, B. The Impact of HIV-1 on Neurogenesis: Implications for HAND. *Cell. Mol. Life Sci. CMLS* **2014**, *71*, 4387–4392, doi:10.1007/s00018-014-1702-4.
16. Cirino, T.J.; McLaughlin, J.P. Mini Review: Promotion of Substance Abuse in HIV Patients: Biological Mediation by HIV-1 Tat Protein. *Neurosci. Lett.* **2021**, *753*, 135877, doi:10.1016/j.neulet.2021.135877.
17. Jiang, Y.; Chai, L.; Fasae, M.B.; Bai, Y. The Role of HIV Tat Protein in HIV-Related Cardiovascular Diseases. *J. Transl. Med.* **2018**, *16*, 121, doi:10.1186/s12967-018-1500-0.
18. Rayne, F.; Debaisieux, S.; Bonhoure, A.; Beaumelle, B. HIV-1 Tat Is Unconventionally Secreted through the Plasma Membrane. *Cell Biol. Int.* **2010**, *34*, 409–413, doi:10.1042/CBI20090376.
19. Rayne, F.; Debaisieux, S.; Yezid, H.; Lin, Y.-L.; Mettling, C.; Konate, K.; Chazal, N.; Arold, S.T.; Pugnière, M.; Sanchez, F.; et al. Phosphatidylinositol-(4,5)-Bisphosphate Enables Efficient Secretion of HIV-1 Tat by Infected T-Cells. *EMBO J.* **2010**, *29*, 1348–1362, doi:10.1038/emboj.2010.32.
20. Ghanam, R.H.; Eastep, G.N.; Saad, J.S. Structural Insights into the Mechanism of HIV-1 Tat Secretion from the Plasma Membrane. *J. Mol. Biol.* **2023**, *435*, 167880, doi:10.1016/j.jmb.2022.167880.
21. Zeitler, M.; Steringer, J.P.; Müller, H.-M.; Mayer, M.P.; Nickel, W. HIV-Tat Protein Forms Phosphoinositide-Dependent Membrane Pores Implicated in Unconventional Protein Secretion. *J. Biol. Chem.* **2015**, *290*, 21976–21984, doi:10.1074/jbc.M115.667097.
22. Clark, E.; Nava, B.; Caputi, M. Tat Is a Multifunctional Viral Protein That Modulates Cellular Gene Expression and Functions. *Oncotarget* **2017**, *8*, 27569–27581, doi:10.18632/oncotarget.15174.
23. Debaisieux, S.; Rayne, F.; Yezid, H.; Beaumelle, B. The Ins and Outs of HIV-1 Tat. *Traffic* **2012**, *13*, 355–363, doi:10.1111/j.1600-0854.2011.01286.x.
24. Fittipaldi, A.; Ferrari, A.; Zoppé, M.; Arcangeli, C.; Pellegrini, V.; Beltram, F.; Giacca, M. Cell Membrane Lipid Rafts Mediate Caveolar Endocytosis of HIV-1 Tat Fusion Proteins. *J. Biol. Chem.* **2003**, *278*, 34141–34149,

doi:10.1074/jbc.M303045200.
25. Vendeville, A.; Rayne, F.; Bonhoure, A.; Bettache, N.; Montcourrier, P.; Beaumelle, B. HIV-1 Tat Enters T Cells Using Coated Pits before Translocating from Acidified Endosomes and Eliciting Biological Responses. *Mol. Biol. Cell* **2004**, *15*, 2347–2360, doi:10.1091/mbc.e03-12-0921.
26. Alves de Souza Rios, L.; Mapekula, L.; Mdletshe, N.; Chetty, D.; Mowla, S. HIV-1 Transactivator of Transcription (Tat) Co-Operates With AP-1 Factors to Enhance c-MYC Transcription. *Front. Cell Dev. Biol.* **2021**, *9*, 693706, doi:10.3389/fcell.2021.693706.
27. Sall, F.B.; El Amine, R.; Markozashvili, D.; Tsfasman, T.; Oksenhendler, E.; Lipinski, M.; Vassetzky, Y.; Germini, D. HIV-1 Tat Protein Induces Aberrant Activation of AICDA in Human B-Lymphocytes from Peripheral Blood. *J. Cell. Physiol.* **2019**, *234*, 15678–15685, doi:10.1002/jcp.28219.
28. Akbay, B.; Germini, D.; Bissenbaev, A.K.; Musinova, Y.R.; Sheval, E.V.; Vassetzky, Y.; Dokudovskaya, S. HIV-1 Tat Activates Akt/mTORC1 Pathway and AICDA Expression by Downregulating Its Transcriptional Inhibitors in B Cells. *Int. J. Mol. Sci.* **2021**, *22*, 1588, doi:10.3390/ijms22041588.
29. Srivastava, D.K.; Tendler, C.L.; Milani, D.; English, M.A.; Licht, J.D.; Wilson, S.H. The HIV-1 Transactivator Protein Tat Is a Potent Inducer of the Human DNA Repair Enzyme Beta-Polymerase. *AIDS Lond. Engl.* **2001**, *15*, 433–440, doi:10.1097/00002030-200103090-00001.
30. El-Amine, R.; Germini, D.; Zakharova, V.V.; Tsfasman, T.; Sheval, E.V.; Louzada, R.A.N.; Dupuy, C.; Bilhou-Nabera, C.; Hamade, A.; Najjar, F.; et al. HIV-1 Tat Protein Induces DNA Damage in Human Peripheral Blood B-Lymphocytes via Mitochondrial ROS Production. *Redox Biol.* **2018**, *15*, 97–108, doi:10.1016/j.redox.2017.11.024.
31. Valyaeva, A.A.; Tikhomirova, M.A.; Potashnikova, D.M.; Bogomazova, A.N.; Snigiryova, G.P.; Penin, A.A.; Logacheva, M.D.; Arifulin, E.A.; Shmakova, A.A.; Germini, D.; et al. Ectopic Expression of HIV-1 Tat Modifies Gene Expression in Cultured B Cells: Implications for the Development of B-Cell Lymphomas in HIV-1-Infected Patients. *PeerJ* **2022**, *10*, e13986, doi:10.7717/peerj.13986.
32. Ait-Ammar, A.; Kula, A.; Darcis, G.; Verdikt, R.; De Wit, S.; Gautier, V.; Mallon, P.W.G.; Marcello, A.; Rohr, O.; Van Lint, C. Current Status of Latency Reversing Agents Facing the Heterogeneity of HIV-1 Cellular and Tissue Reservoirs. *Front. Microbiol.* **2019**, *10*, 3060, doi:10.3389/fmicb.2019.03060.
33. Gorbacheva, M.A.; Tikhomirova, M.A.; Potashnikova, D.M.; Akbay, B.; Sheval, E.V.; Musinova, Y.R. Production of Stable Cell Lines on the Basis of the Cultured RPMI 8866 B-Cells with Constant and Inducible Expression of the Human Immunodeficiency Virus Tat Protein. *Russ. J. Dev. Biol.* **2019**, *50*, 275–280, doi:10.1134/s1062360419050060.
34. Pfaffl, M.W. A New Mathematical Model for Relative Quantification in Real-Time RT–PCR. *Nucleic Acids Res.* **2001**, *29*, e45.
35. Rocha, C.R.R.; Silva, M.M.; Quinet, A.; Cabral-Neto, J.B.; Menck, C.F.M. DNA Repair Pathways and Cisplatin Resistance: An Intimate Relationship. *Clinics* **2018**, *73*, e478s, doi:10.6061/clinics/2018/e478s.
36. Olive, P.L.; Banáth, J.P. Kinetics of H2AX Phosphorylation after Exposure to Cisplatin. *Cytometry B Clin. Cytom.* **2009**, *76B*, 79–90, doi:10.1002/cyto.b.20450.
37. Kuo, L.J.; Yang, L.-X. Gamma-H2AX - a Novel Biomarker for DNA Double-Strand Breaks. *Vivo Athens Greece* **2008**, *22*, 305–309.
38. Shieh, S.Y.; Ikeda, M.; Taya, Y.; Prives, C. DNA Damage-Induced Phosphorylation of

P53 Alleviates Inhibition by MDM2. *Cell* **1997**, *91*, 325–334, doi:10.1016/s0092-8674(00)80416-x.
39. Zhang, S.-M.; Zhang, H.; Yang, T.-Y.; Ying, T.-Y.; Yang, P.-X.; Liu, X.-D.; Tang, S.-J.; Zhou, P.-K. Interaction between HIV-1 Tat and DNA-PKcs Modulates HIV Transcription and Class Switch Recombination. *Int. J. Biol. Sci.* **2014**, *10*, 1138–1149, doi:10.7150/ijbs.10366.
40. Christmann, M.; Kaina, B. Transcriptional Regulation of Human DNA Repair Genes Following Genotoxic Stress: Trigger Mechanisms, Inducible Responses and Genotoxic Adaptation. *Nucleic Acids Res.* **2013**, *41*, 8403–8420, doi:10.1093/nar/gkt635.
41. Luzzi, A.; Morettini, F.; Gazaneo, S.; Mundo, L.; Onnis, A.; Mannucci, S.; Rogena, E.A.; Bellan, C.; Leoncini, L.; De Falco, G. HIV-1 Tat Induces DNMT over-Expression through microRNA Dysregulation in HIV-Related Non Hodgkin Lymphomas. *Infect. Agent. Cancer* **2014**, *9*, 41, doi:10.1186/1750-9378-9-41.
42. Canoy, R.J.; Shmakova, A.; Karpukhina, A.; Shepelev, M.; Germini, D.; Vassetzky, Y. Factors That Affect the Formation of Chromosomal Translocations in Cells. *Cancers* **2022**, *14*, 5110, doi:10.3390/cancers14205110.
43. Hanahan, D. Hallmarks of Cancer: New Dimensions. *Cancer Discov.* **2022**, *12*, 31–46, doi:10.1158/2159-8290.CD-21-1059.
44. Chipitsyna, G.; Slonina, D.; Siddiqui, K.; Peruzzi, F.; Skorski, T.; Reiss, K.; Sawaya, B.E.; Khalili, K.; Amini, S. HIV-1 Tat Increases Cell Survival in Response to Cisplatin by Stimulating Rad51 Gene Expression. *Oncogene* **2004**, *23*, 2664–2671, doi:10.1038/sj.onc.1207417.
45. Sun, Y.; Huang, Y.-C.; Xu, Q.-Z.; Wang, H.-P.; Bai, B.; Sui, J.-L.; Zhou, P.-K. HIV-1 Tat Depresses DNA-PK(CS) Expression and DNA Repair, and Sensitizes Cells to Ionizing Radiation. *Int. J. Radiat. Oncol. Biol. Phys.* **2006**, *65*, 842–850, doi:10.1016/j.ijrobp.2006.02.040.
46. Li, C.J.; Friedman, D.J.; Wang, C.; Metelev, V.; Pardee, A.B. Induction of Apoptosis in Uninfected Lymphocytes by HIV-1 Tat Protein. *Science* **1995**, *268*, 429–431, doi:10.1126/science.7716549.
47. Chen, D.; Wang, M.; Zhou, S.; Zhou, Q. HIV-1 Tat Targets Microtubules to Induce Apoptosis, a Process Promoted by the pro-Apoptotic Bcl-2 Relative Bim. *EMBO J.* **2002**, *21*, 6801–6810, doi:10.1093/emboj/cdf683.
48. Campestrini, J.; Silveira, D.B.; Pinto, A.R. HIV-1 Tat-Induced Bystander Apoptosis in Jurkat Cells Involves Unfolded Protein Responses. *Cell Biochem. Funct.* **2018**, *36*, 377–386, doi:10.1002/cbf.3357.
49. Gibellini, D.; Re, M.C.; Ponti, C.; Vitone, F.; Bon, I.; Fabbri, G.; Grazia Di Iasio, M.; Zauli, G. HIV-1 Tat Protein Concomitantly down-Regulates Apical Caspase-10 and up-Regulates c-FLIP in Lymphoid T Cells: A Potential Molecular Mechanism to Escape TRAIL Cytotoxicity. *J. Cell. Physiol.* **2005**, *203*, 547–556, doi:10.1002/jcp.20252.
50. Sánchez-Del Cojo, M.; López-Huertas, M.R.; Díez-Fuertes, F.; Rodríguez-Mora, S.; Bermejo, M.; López-Campos, G.; Mateos, E.; Jiménez-Tormo, L.; Gómez-Esquer, F.; Díaz-Gil, G.; et al. Changes in the Cellular microRNA Profile by the Intracellular Expression of HIV-1 Tat Regulator: A Potential Mechanism for Resistance to Apoptosis and Impaired Proliferation in HIV-1 Infected CD4+ T Cells. *PloS One* **2017**, *12*, e0185677, doi:10.1371/journal.pone.0185677.
51. Haughey, N.J.; Mattson, M.P. Calcium Dysregulation and Neuronal Apoptosis by the HIV-1 Proteins Tat and Gp120. *J. Acquir. Immune Defic. Syndr. 1999* **2002**, *31 Suppl 2*, S55-61, doi:10.1097/00126334-200210012-00005.

52. Buccigrossi, V.; Laudiero, G.; Nicastro, E.; Miele, E.; Esposito, F.; Guarino, A. The HIV-1 Transactivator Factor (Tat) Induces Enterocyte Apoptosis through a Redox-Mediated Mechanism. *PloS One* **2011**, *6*, e29436, doi:10.1371/journal.pone.0029436.
53. Zheng, L.; Yang, Y.; Guocai, L.; Pauza, C.D.; Salvato, M.S. HIV Tat Protein Increases Bcl-2 Expression in Monocytes Which Inhibits Monocyte Apoptosis Induced by Tumor Necrosis Factor-Alpha-Related Apoptosis-Induced Ligand. *Intervirology* **2007**, *50*, 224–228, doi:10.1159/000100565.
54. Cantaluppi, V.; Biancone, L.; Boccellino, M.; Doublier, S.; Benelli, R.; Carlone, S.; Albini, A.; Camussi, G. HIV Type 1 Tat Protein Is a Survival Factor for Kaposi's Sarcoma and Endothelial Cells. *AIDS Res. Hum. Retroviruses* **2001**, *17*, 965–976, doi:10.1089/088922201750290087.
55. Col, E.; Caron, C.; Chable-Bessia, C.; Legube, G.; Gazzeri, S.; Komatsu, Y.; Yoshida, M.; Benkirane, M.; Trouche, D.; Khochbin, S. HIV-1 Tat Targets Tip60 to Impair the Apoptotic Cell Response to Genotoxic Stresses. *EMBO J.* **2005**, *24*, 2634–2645, doi:10.1038/sj.emboj.7600734.

Supplementary figures

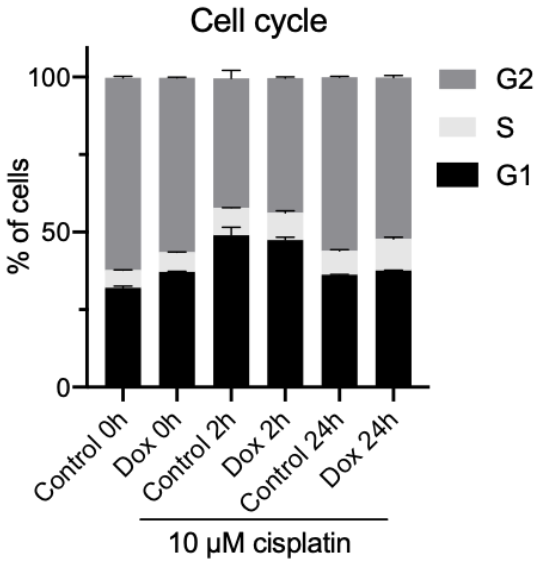

Supplementary figure 1. The analysis of cell cycle in RPMI8866 Tat^{i} cells treated or not with 10 µM cisplatin for 2 or 24 hours with or without prior induction of Tat expression for 16 hours.

Cisplatin-induced DNA damage includes inter- (on opposite strands) and intrastrand (on the same strand) DNA crosslinks, which are mainly repaired by nucleotide excision repair (Rocha et al. 2018). In the nucleotide excision repair process DNA damage that distorts normal DNA structure is recognized and excised; the excised region is then resynthesized and ligated (Martin et al. 2008). However, since crosslinks promote other types of DNA damage, other mechanisms of DNA repair, such as mismatch repair, NHEJ, and HR, are also engaged in removing cisplatin-induced DNA damage (Rocha et al. 2018). H2AX phosphorylation is an early step in the response to DNA damage and DSBs in particular (Mah et al. 2010). Interstrand crosslinks (~5% of cisplatin-induced DNA lesions) promote DSB formation during replication and/or repair processes (Rocha et al. 2018) and γH2AX foci are formed in cells following cisplatin exposure (Olive & Banáth 2009). H2AX phosphorylation is an early step in the response to DNA damage and DSBs in particular(Mah et al. 2010). ATM and DNA-PK act as the sensors of DSBs and they both phosphorylate histone family member X (H2AX) by its Ser139 residue to form γH2AX (Stiff et al. 2004). ATM- and Rad3-Related (ATR) protein was also shown to initiate γH2AX formation upon DNA damage. A serine/threonine protein kinase ATM is activated and recruited to DSBs by the MRE11-RAD50-NBS1 (MRN) complex (Blackford & Jackson 2017). A serine/threonine protein kinase DNA-PK is a complex of a catalytic subunit (DNA-PKcs, *PRKDC* gene) and a Ku heterodimer composed of the Ku70 (*XRCC6* gene) and Ku80 (*XRCC5* gene) subunits (Mohiuddin & Kang 2019). Ku heterodimer attracts DNA-PKcs to DSBs, which activates DNA-PKcs. Interestingly, Ku heterodimer also plays an important role in HIV-1 infection: it promotes early transcription from the HIV-1 promoter and limits the establishment of viral latency (Manic et al. 2013). Finally, ATR is the serine/threonine protein kinase that is recruited to single-stranded DNA covered with replication protein A (RPA, heterotrimer of three subunits encoded by *RPA1*, *RPA2*, and *RPA3* gens), thus, it responds to a large spectrum of DNA damages, including single-strand DNA breaks, stalled DNA replication forks, interstrand crosslinks, and DSBs (Blackford & Jackson 2017; Maréchal & Zou 2013).

The expression of multiple genes involved in the aforementioned DNA damage-sensing mechanisms was downregulated by HIV-1 Tat in B cells upon its acute action (**Figure 15**). Albeit significant, the fold changes in Tat-downregulated DNA repair genes are not remarkably high, which suggests a potential "fine-tuning" effect. Rather than inducing drastic changes in gene expression, HIV-1 Tat might subtly modulate the levels of these genes to maintain a delicate balance in the DNA repair process. The purpose of this fine-tuning effect could be to avoid triggering a strong cellular response that may lead to the clearance of infected cells or cells, penetrated by Tat, by the immune system. Although the individual fold changes in gene expression are not substantial, the cumulative effect of downregulating multiple DNA repair

genes has significant consequences for the overall DNA repair capacity of cells exposed to HIV-1 Tat: upon cisplatin treatment, which models DNA damage, we observe an accumulation of cisplatin-induced DNA adducts and decrease in their recognition (decrease of γH2AX and phosphorylated p53).

Decreased expression of key DNA repair genes may impact the cell's ability to sense DNA damage accurately and render B cells more vulnerable to DNA damage induced by various endogenous and exogenous factors, including oxidative stress, chemical agents, radiation, and endogenous nucleases. Consequently, this could lead to the accumulation of DNA lesions, which might promote genomic instability and potentially increase the risk of oncogenic transformation of B cells in people living with HIV.

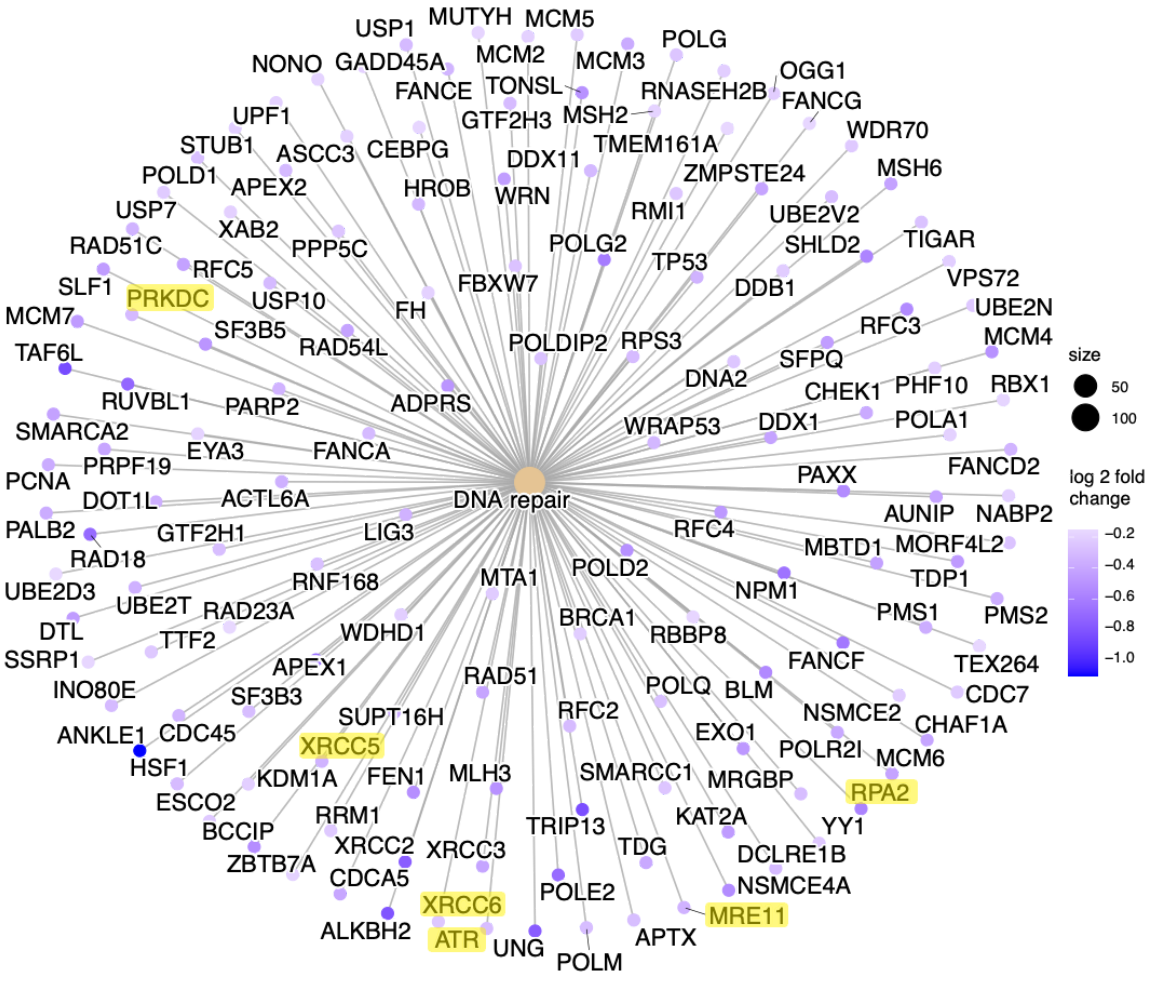

Figure 15. HIV-1 Tat decreased the expression of genes involved in DNA damage repair in B cells. GO:BP term "DNA repair" pathway, enriched among significantly downregulated genes in RPMI8866 Tat^{i} + Dox vs RPMI8866 Tat^{i} control comparison and associated differentially expressed genes. Several genes involved in DNA damage sensing are highlighted in yellow. GO:BP, Gene ontology: Biological processes.

3.2 The contribution of HIV-1 Tat and EBV Zta to the immune evasion of EBV-infected B cells

3.2.1 Detection of circulating HIV-1 Tat in the serum of people living with HIV-1 with effective viral suppression

Despite the fact that HIV-1 does not directly infect B cells, there is an increased incidence of B cell lymphomas in these patients, suggesting a potential indirect role of viral proteins such as Tat, which can be secreted by infected cells and penetrate into non-infected cells due to its cell-penetration capacity.

Several studies have shown that Tat can circulate in the blood of people living with HIV (Germini et al. 2017b; Poggi et al. 2004; Westendorp et al. 1995; Xiao et al. 2000). To corroborate previous reports in patients with long-term cART treatment, we performed an HIV-1 Tat ELISA assay in cART-treated people with HIV (n = 63, **Article 7**). Among them, 16 out of 63 (25.4%) displayed HIV-1 Tat concentrations above the established specificity cut-off (> 2.5 ng/ml). The mean concentration of HIV-1 Tat in this subgroup was 5.553 ± 0.785 ng/ml, with a range of 11.03 ng/ml (minimum value: 2.97 ng/ml, maximum value: 14.00 ng/ml). Moreover, no association between HIV replication or CD4+ T cell levels and high levels of circulating HIV-1 Tat was found.

Article 7. Research paper "HIV-1 Tat is present in the serum of people living with HIV-1 despite viral suppression"

HIV-1 Tat is present in the serum of people living with HIV-1 despite viral suppression

(manuscript in preparation)

Anna Shmakova[1,2], Ivan Tsimailo[1], Yana Kozhevnikova[1], Laurence Gerard[3], David Boutboul[3], Eric Oksenhendler[3], Edouard Tuaillon[4], Diego Germini[1], Bruno Beaumelle[5] *, Yegor Vassetzky[1,2,] *

[1]CNRS, UMR 9018, Université Paris-Saclay, Institut Gustave Roussy, 94800 Villejuif, France;
[2]Koltzov Institute of Developmental Biology, 119334 Moscow, Russia;
[3]Service d'Immunopathologie Clinique, Hôpital St Louis, APHP, 75012 Paris, France;
[4]Pathogenesis and Control of Chronic and Emerging Infections, Montpellier University, INSERM U1058, Montpellier University Hospital, Montpellier, France
[5]Institut de Recherche en Infectiologie de Montpellier, Université de Montpellier, CNRS UMR 9004, Montpellier, France

*Corresponding authors: bruno.beaumelle@irim.cnrs.fr, yegor.vassetzky@cnrs.fr. These authors share the last authorship.

Highlights

- 25% of cART-treated HIV-positive individuals with effective viral suppression had detectable Tat levels
- The Tat seric levels were not influenced by immune suppression or HIV replication.

Abstract

Background

Despite successful human immunodeficiency virus (HIV) control with combination antiretroviral therapy (cART), individuals with HIV still face health risks, including cardiovascular diseases, neurocognitive issues, and cancers. HIV-1 Tat, a viral protein, is potentially involved in these HIV-related diseases. Previous studies have shown circulating Tat in the blood of untreated people with HIV. Here, we measured Tat levels in the serum of cART-treated people with HIV to examine the effect of cART on Tat production.

Methods

Serum samples from 63 HIV-positive individuals and 20 HIV-seronegative individuals were analysed using an ELISA assay that detected Tat concentrations above 2.5 ng/ml.

Results

Among HIV-positive individuals, the mean Tat level was 1.676 ± 0.353 ng/ml, ranging from 0 to 14 ng/ml. 25.4% (16 out of 63) exceeded the 2.5 ng/ml cut-off, with a mean HIV-1 Tat level 5.553 ± 0.785 ng/ml. There was no correlation between Tat levels and CD4+ T cell counts or serum HIV RNA or p24 antigen levels.

Discussion

Despite successful viral suppression with cART, circulating HIV-1 Tat persists and may contribute to HIV-related diseases. This emphasizes the need for further research to elucidate the mechanisms of Tat action on non-infected cells in which it can penetrate upon circulation in the blood.

Keywords: HIV, cART, HIV-1 Tat, ELISA

Introduction

Human immunodeficiency virus (HIV) infection affects ~38.4 million people worldwide (http://www.who.int/hiv/en/). The implementation of combination antiretroviral therapy (cART) in the late nineties dramatically decreased mortality and prolonged the lifespan of individuals with HIV [1]. However, people with HIV still face increased risks of comorbidities, including cardiovascular diseases, neurocognitive disorders, some cancers, tuberculosis, and others [2–6]. cART effectively controls viral replication but does not eliminate latent HIV-infected cells, posing challenges in achieving a cure [7]. Moreover, cART inhibits several steps of the HIV-1 cycle, but neither viral gene transcription nor translation is affected. Recent research indicates that even cells with defective proviral DNA can produce viral proteins, potentially contributing to HIV-associated diseases [8,9]. Both Nef [10] and p24 [11] were detected in the sera of virally suppressed individuals.

HIV Tat is needed for viral transcription and pathogenesis [12,13]. Beyond its classical role in transcriptional activation, Tat is efficiently secreted from HIV-infected cells [14,15] and can penetrate into non-infected cells through endocytosis [16]. Emerging evidence suggests that Tat is involved in various aspects of HIV pathogenesis, including cardiovascular and neurocognitive diseases, accelerated ageing and B cell pathology [17–25].

Tat circulates in the blood of people with HIV [25–29]. Pre-cART era reports indicated Tat seric concentrations from 0.1 to 40 ng/ml [28,29]. In individuals with low to undetectable viral loads (<40 copies/ml), one study reported high seric Tat levels, in the 250 to 550 ng/ml range [27], while we observed 0.2-9 ng/ml seric Tat in 13 people living with HIV [25]. To clarify this issue, this multi-centre study aimed to quantify Tat serum concentrations in a larger cohort of cART-treated people with HIV using a quantitative enzyme-linked immunosorbent assay (ELISA).

Materials and methods

Blood collection

Blood samples from individuals who signed a written informed consent were collected at the Hôpital Saint-Louis, Paris, France, or Montpellier University Hospital Center, Montpellier, France, in accordance with French legislation (agreements 2016-A01316-45 [25], 14/EFS/033, VIHEBV for Paris and 233-2018-SR for Montpellier).

ELISA

HIV-1 Tat concentration in the sera was determined by ELISA as described previously [30], with minor modifications. Tat concentrations above 2.5 ng/ml were detected. HIV-1 p24 concentration was determined using an HIV-antigen mAB ELISA kit (Innotest, cat.#80564), following the manufacturer's instructions, detecting p24 concentrations above 5 pg/ml. The standard p24 antigen was prepared as described previously [31].

Statistical analysis

Tat and p24 concentrations were calculated from linear standard curves using reference dilutions. Data are presented as individual values, mean ± standard error of the mean (SEM).

Results

We quantified circulating HIV-1 Tat in the serum of cART-treated people with HIV (n=63). To establish a specificity cut-off for the Tat ELISA, we also analyzed the serum samples from HIV-seronegative individuals (n=20). Most individuals with HIV had viral levels <20 HIV RNA copies/ml (**Table 1**). To confirm this lack of circulating virus, we performed a p24 ELISA test. Capsid protein p24 is a viral antigen, widely used to assess HIV infection and disease progression, and treatment efficacy in HIV clinical monitoring [11,32,33], although p24 ELISA is generally less sensitive than qRT-PCR of viral RNA. Only one HIV-positive individual (1.6%) had detectable p24 antigen in the serum (5.91 pg/ml) (**Fig. 1A**), confirming that the majority of the cohort achieved effective viral suppression. As expected, HIV-seronegative individuals showed no detectable p24 antigen in their serum (**Fig. 1A**).

The HIV-1 Tat ELISA was performed to evaluate the levels of circulating HIV-1 Tat protein in these human serum samples (**Fig. 1B**). In the HIV-seronegative group, 10 (50%) subjects had undetectable HIV-1 Tat levels (0 ng/ml), as expected. For 10 others, the range of background Tat concentrations spanned from 0.280 to 2.290 ng/ml with a mean of 0.633±0.190 ng/ml. Based on the HIV-seronegative group's values, a specificity cut-off of 2.5 ng/ml was chosen for the test.

In the HIV-positive group, the mean concentration of HIV-1 Tat was found to be 1.676±0.353 ng/ml, ranging from 0 (for 31 subjects) to 14 ng/ml (**Fig. 1B**). Among the HIV-positive individuals, 16 (25.4%) displayed Tat concentrations above the established specificity cut-off (>2.5 ng/ml). The mean concentration of Tat in this subgroup was 5.553±0.785 ng/ml, with a minimum of 2.97 ng/ml and a maximum of 14.00 ng/ml. The individual showing a high p24 level in the serum had a low level of circulating Tat. A weak negative correlation was observed between levels of circulating Tat and age (**Fig. 1C**). Moreover, no association between levels of circulating Tat and either CD4+ T cell concentration or HIV RNA seric levels was found (**Fig. 1D-1F**). Weak positive correlations between levels of circulating Tat and the percentage of CD4+ T cells and CD4/CD8 T cell ratio, but not the percentage of CD8+ T cells were found (**Fig. 1G-1I**). In multiple linear regression of different factors that could affect HIV-1 Tat levels, only age remained significantly associated with the level of HIV-1 Tat ($p = 0.001$, **Table 2**).

Discussion

The present study investigated the presence and concentration of circulating HIV-1 Tat protein in the serum of cART-treated individuals with HIV (n = 63). The majority of individuals with HIV had low levels of HIV replication (<20 HIV RNA copies/ml, **Table 1**). We found that 16 out of 63 (25.4%) people living with HIV displayed HIV-1 Tat concentrations above the established specificity cut-off (>2.5 ng/ml) with the mean concentration of HIV-1 Tat 5.553±0.785 ng/ml (**Fig. 1B**). Tat seric level was apparently not influenced by immune suppression, as assessed by CD4+ T cell counts, or HIV replication, as assessed by HIV RNA and p24 blood levels (**Fig. 1C-1F**). These findings thus suggest that, despite the successful control of viral replication and the restoration of immune function through cART, HIV-1 Tat is still produced, as observed earlier for other viral proteins, e.g. Nef [10] and p24 [11]. The chronic secretion of HIV-1 Tat may play a contributory role in the development of HIV-associated pathologies. It is noteworthy that even low Tat concentrations (10-15 ng/ml) produce significant biological effects, e.g. oxidative stress, DNA damage and genome reorganization in B cells [23,25].

The Tat concentrations we detected align with levels observed in the blood of HIV-positive individuals before cART (0.1-10 ng/ml) [28], during early cART (2-40 ng/ml) [29] or late cART era (0.2-9.0 ng/ml) [25]. We found that ~25% of people with HIV had detectable Tat levels, similar to the ~29% reported by Westendorp et al. in a similar-sized group (n=41) [28]. Moreover, Tat concentrations in the same range (0.2-6.5 ng/ml) were reported in the cerebrospinal fluid of 37% of people with HIV who were virologically controlled with long-term cART [34]. Altogether, these observations suggest that cART and viral suppression do not significantly affect the Tat production. The observed prevalence of circulating Tat also aligns with reported rates of anti-Tat antibody-mediated immune responses in people with HIV (~20%) [35]. The potential correlation between these two phenomena warrants further investigation.

Conversely, Poggi et al. reported notably higher HIV-1 Tat levels in the sera of both untreated and cART-treated people with HIV, ranging from 150 to 550 ng Tat/ml [27]. This difference with our study could stem from variations in assay specificities, sensitivities, and the studied population. Furthermore, our ELISA used a monoclonal antibody targeting the N-terminus of Tat from the most prevalent HIV-1 B-subtype (HXB2). This region of Tat, while relatively conserved, may vary across viral subtypes [36], potentially causing our assay to underestimate Tat levels in individuals with other viral subtypes. This limitation was also reported for Nef concentration assays [10].

Together with data from the pre-ART period [28], our findings suggest that HIV-1 Tat circulation in the blood of people with HIV is weakly affected by cART. The high Tat concentrations in cART-treated individuals may arise from Tat production by the HIV reservoir that includes various latently infected cells, such as T cells, macrophages, and microglial cells that are not entirely transcriptionally silent and are capable of producing viral proteins [37–39]. It is indeed well established that HIV LTR promoter is never entirely silent [40,41].

In conclusion, our study demonstrated the presence of circulating Tat in cART-treated individuals with effective viral suppression. It highlights the need for research on Tat implications in HIV-associated clinical disorders and on potential therapeutic approaches to inhibit Tat secretion or penetration in cells, for instance through the use of endocytosis inhibitors [42].

Acknowledgements

We thank all study participants who agreed to provide blood samples for this study. This study was supported by grants from ANRS, the IDB RAS Government basic research program (0088-2021-0007), the Russian Science Foundation (grant 21-74-20134 to EVS) and the Ministry of Science and Higher Education grants 075-15-2020-773 to YV and Sidaction to BB. IT is a recipient of the French Government scholarship awarded by the Ministry of Foreign Affairs from Campus France.

Figures

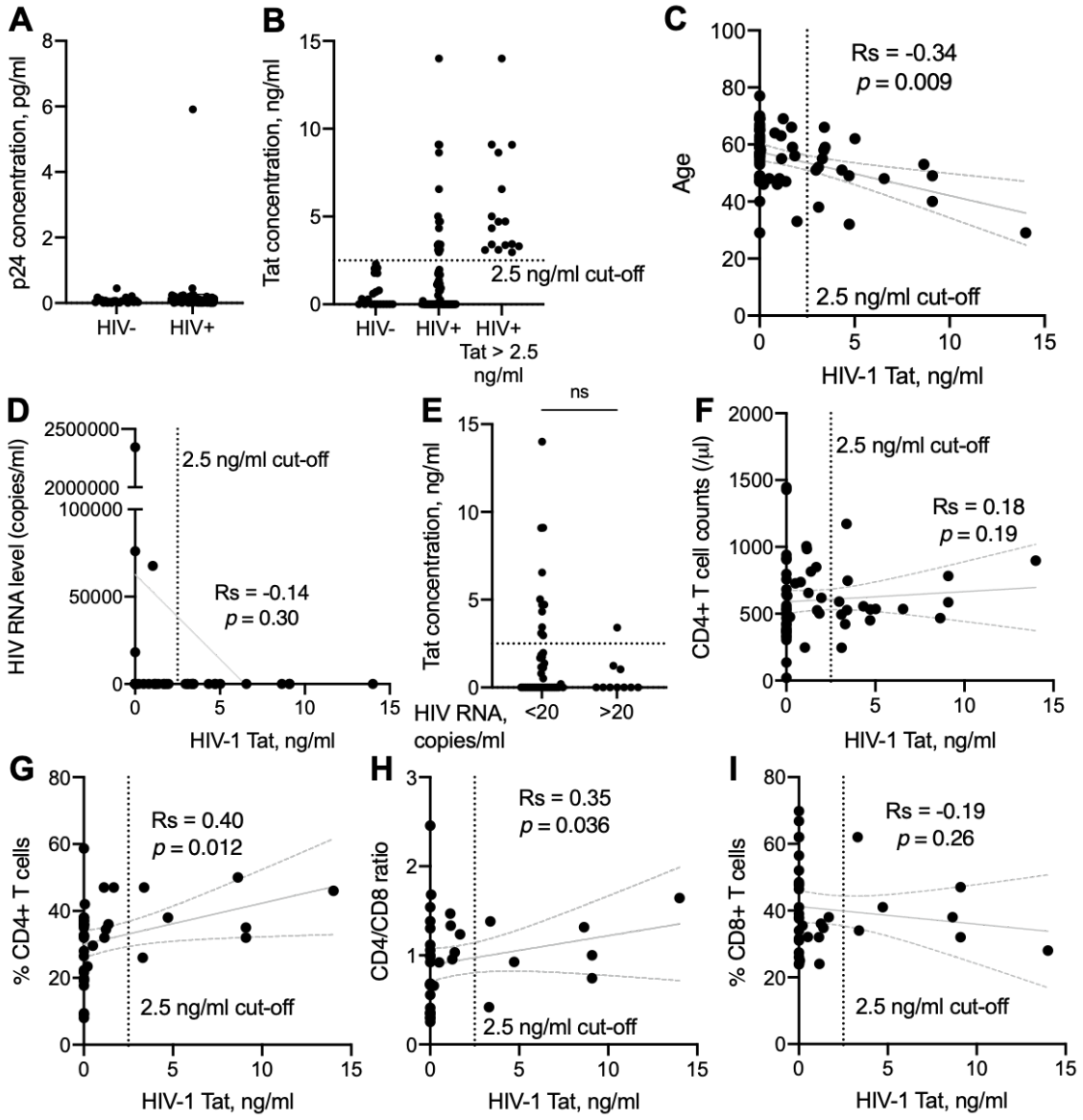

Fig. 1. HIV-1 Tat and p24 antigen levels in the serum of cART-treated HIV-positive individuals. (A) Serum levels of capsid protein p24 were assessed using ELISA in cART-treated people living with HIV (n = 63) and HIV-seronegative people (n = 20). (B) HIV-1 Tat serum levels were measured in the same two cohorts using ELISA. An established specificity cut-off of 2.5 ng/ml is shown with a black dotted line. Data are presented as individual values. (C) Correlation between age and HIV-1 Tat serum levels in HIV-positive individuals; the grey solid line represents a linear regression. The Spearman correlation coefficient (Rs) and its corresponding p-value are shown. (D) Correlation between HIV RNA levels and HIV-1 Tat serum levels in HIV-positive individuals. (E) HIV-1 Tat protein serum levels in HIV-positive individuals with HIV RNA below and above 20 copies/ml. ns - non-significant, t-test. (F) Correlation between CD4+ T cell counts and HIV-1 Tat serum levels in HIV-positive individuals. The grey dashed lines

represent 95% confidence intervals for linear regression (grey solid line). The Spearman correlation coefficient (Rs) and its corresponding p-value are shown. (G) Correlation between the percentage of CD4+ T cells and HIV-1 Tat serum levels in HIV-positive individuals. The grey dashed lines represent 95% confidence intervals for linear regression (grey solid line). The Spearman correlation coefficient (Rs) and its corresponding p-value are shown. (H) Correlation between the CD4/CD8 T cell ratio and HIV-1 Tat serum levels in HIV-positive individuals. The grey dashed lines represent 95% confidence intervals for linear regression (grey solid line). The Spearman correlation coefficient (Rs) and its corresponding p-value are shown. (I) Correlation between the percentage of CD8+ T cells and HIV-1 Tat serum levels in HIV-positive individuals. The grey dashed lines represent 95% confidence intervals for linear regression (grey solid line). The Spearman correlation coefficient (Rs) and its corresponding p-value are shown. cART, combination antiretroviral therapy, ELISA, enzyme-linked immunosorbent assay.

Tables

Table 1. Demographic and clinical characteristics of HIV-positive individuals enrolled in the study. Data are presented as n (%) or median [interquartile range]. NA - not available.

Characteristic	HIV-positive individuals (n = 63)
Age	56 [48-77]
Female Male	17 (27%) 46 (73%)
CD4+ T cell count/µl in plasma	535.5 [423.5 - 754.5]
HIV viral load copies/ml NA <20 >20	 7 (11%) 46 (73%) 10 (16%); 93.50 [48.50 - 69731]*

*Only four individuals had viremia above 150 HIV RNA copies/ml (Fig. 1D).

Table 2. Multiple linear regression of different factors potentially associated with serum levels of HIV-1 Tat in people with HIV. Observations (complete cases) n = 36, R^2 / R^2 adjusted = 0.4654 / 0.3317. CI, 95% confidence intervals. *P*-value < 0.05 is denoted in bold.

	HIV-1 Tat level		
Predictors	*Estimates*	*CI*	*p-value*
Sex (male vs. female)	2.481	-0.007 — 4.968	0.051

Age	-0.157	**-0.245 — -0.069**	**0.001**
CD4+ T cell counts	-0.002	-0.006 — 0.002	0.356
HIV RNA level (>20 copies/ml vs. <20 copies/ml)	-0.617	-3.648 — 2.414	0.680
%CD4	0.069	-0.188 — 0.327	0.585
%CD8	-0.004	-0.161 — 0.153	0.960
CD4/CD8 ratio	1.021	-6.496 — 8.538	0.783

References

[1] S.G. Deeks, J. Overbaugh, A. Phillips, S. Buchbinder, HIV infection, Nat. Rev. Dis. Primer. 1 (2015) 1–22. https://doi.org/10.1038/nrdp.2015.35.

[2] K. So-Armah, L.A. Benjamin, G.S. Bloomfield, M.J. Feinstein, P. Hsue, B. Njuguna, M.S. Freiberg, HIV and cardiovascular disease, Lancet HIV. 7 (2020) e279–e293. https://doi.org/10.1016/S2352-3018(20)30036-9.

[3] D. Saylor, A.M. Dickens, N. Sacktor, N. Haughey, B. Slusher, M. Pletnikov, J.L. Mankowski, A. Brown, D.J. Volsky, J.C. McArthur, HIV-associated neurocognitive disorder — pathogenesis and prospects for treatment, Nat. Rev. Neurol. 12 (2016) 234–248. https://doi.org/10.1038/nrneurol.2016.27.

[4] R.U. Hernández-Ramírez, M.S. Shiels, R. Dubrow, E.A. Engels, Cancer risk in HIV-infected people in the USA from 1996 to 2012: a population-based, registry-linkage study, Lancet HIV. 4 (2017) e495–e504. https://doi.org/10.1016/S2352-3018(17)30125-X.

[5] A. Shmakova, D. Germini, Y. Vassetzky, HIV-1, HAART and cancer: A complex relationship, Int. J. Cancer. 146 (2020) 2666–2679. https://doi.org/10.1002/ijc.32730.

[6] P.Y. Khan, T.A. Yates, M. Osman, R.M. Warren, Y. van der Heijden, N. Padayatchi, E.A. Nardell, D. Moore, B. Mathema, N. Gandhi, V. Eldholm, K. Dheda, A.C. Hesseling, V. Mizrahi, R. Rustomjee, A. Pym, Transmission of drug-resistant tuberculosis in HIV-endemic settings, Lancet Infect. Dis. 19 (2019) e77–e88. https://doi.org/10.1016/S1473-3099(18)30537-1.

[7] L.B. Cohn, N. Chomont, S.G. Deeks, The Biology of the HIV-1 Latent Reservoir and Implications for Cure Strategies, Cell Host Microbe. 27 (2020) 519–530. https://doi.org/10.1016/j.chom.2020.03.014.

[8] H. Imamichi, M. Smith, J.W. Adelsberger, T. Izumi, F. Scrimieri, B.T. Sherman, C.A. Rehm, T. Imamichi, A. Pau, M. Catalfamo, A.S. Fauci, H.C. Lane, Defective HIV-1 proviruses produce viral proteins, Proc. Natl. Acad. Sci. U. S. A. 117 (2020) 3704–3710. https://doi.org/10.1073/pnas.1917876117.

[9] H. Imamichi, R.L. Dewar, J.W. Adelsberger, C.A. Rehm, U. O'Doherty, E.E. Paxinos, A.S. Fauci, H.C. Lane, Defective HIV-1 proviruses produce novel protein-coding RNA species in HIV-infected patients on combination antiretroviral therapy, Proc.

Natl. Acad. Sci. U. S. A. 113 (2016) 8783–8788. https://doi.org/10.1073/pnas.1609057113.
[10] J. Ferdin, K. Goričar, V. Dolžan, A. Plemenitaš, J.N. Martin, B.M. Peterlin, S.G. Deeks, M. Lenassi, Viral protein Nef is detected in plasma of half of HIV-infected adults with undetectable plasma HIV RNA, PloS One. 13 (2018) e0191613. https://doi.org/10.1371/journal.pone.0191613.
[11] C. Passaes, H.M. Delagreverie, V. Avettand-Fenoel, A. David, V. Monceaux, A. Essat, M. Müller-Trutwin, D. Duffy, N. De Castro, L. Wittkop, C. Rouzioux, J.-M. Molina, L. Meyer, C. Delaugerre, A. Sáez-Cirión, Ultrasensitive Detection of p24 in Plasma Samples from People with Primary and Chronic HIV-1 Infection, J. Virol. 95 (2021) e00016-21. https://doi.org/10.1128/JVI.00016-21.
[12] N. He, M. Liu, J. Hsu, Y. Xue, S. Chou, A. Burlingame, N.J. Krogan, T. Alber, Q. Zhou, HIV-1 Tat and host AFF4 recruit two transcription elongation factors into a bifunctional complex for coordinated activation of HIV-1 transcription, Mol. Cell. 38 (2010) 428–438. https://doi.org/10.1016/j.molcel.2010.04.013.
[13] S. Nekhai, K.-T. Jeang, Transcriptional and post-transcriptional regulation of HIV-1 gene expression: role of cellular factors for Tat and Rev, Future Microbiol. 1 (2006) 417–426. https://doi.org/10.2217/17460913.1.4.417.
[14] Y.R. Musinova, E.V. Sheval, C. Dib, D. Germini, Y.S. Vassetzky, Functional roles of HIV-1 Tat protein in the nucleus, Cell. Mol. Life Sci. 73 (2016) 589–601. https://doi.org/10.1007/s00018-015-2077-x.
[15] F. Rayne, S. Debaisieux, A. Bonhoure, B. Beaumelle, HIV-1 Tat is unconventionally secreted through the plasma membrane, Cell Biol. Int. 34 (2010) 409–413. https://doi.org/10.1042/CBI20090376.
[16] A. Vendeville, F. Rayne, A. Bonhoure, N. Bettache, P. Montcourrier, B. Beaumelle, HIV-1 Tat Enters T Cells Using Coated Pits before Translocating from Acidified Endosomes and Eliciting Biological Responses, Mol. Biol. Cell. 15 (2004) 2347–2360. https://doi.org/10.1091/mbc.E03-12-0921.
[17] Y. Jiang, L. Chai, M.B. Fasae, Y. Bai, The role of HIV Tat protein in HIV-related cardiovascular diseases, J. Transl. Med. 16 (2018) 121. https://doi.org/10.1186/s12967-018-1500-0.
[18] A. Bagashev, B.E. Sawaya, Roles and functions of HIV-1 Tat protein in the CNS: an overview, Virol. J. 10 (2013) 358. https://doi.org/10.1186/1743-422X-10-358.
[19] J. Fields, W. Dumaop, S. Elueteri, S. Campos, E. Serger, M. Trejo, K. Kosberg, A. Adame, B. Spencer, E. Rockenstein, J.J. He, E. Masliah, HIV-1 Tat Alters Neuronal Autophagy by Modulating Autophagosome Fusion to the Lysosome: Implications for HIV-Associated Neurocognitive Disorders, J. Neurosci. 35 (2015) 1921–1938. https://doi.org/10.1523/jneurosci.3207-14.2015.
[20] J.A. Fields, W. Dumaop, L. Crews, A. Adame, B. Spencer, J. Metcalf, J. He, E. Rockenstein, E. Masliah, Mechanisms of HIV-1 Tat Neurotoxicity via CDK5 Translocation and Hyper-Activation: Role in HIV-Associated Neurocognitive Disorders, Curr. HIV Res. 13 (2015) 43–54.
[21] J. Cohen, C. Torres, HIV-associated cellular senescence: A contributor to accelerated aging, Ageing Res. Rev. 36 (2017) 117–124. https://doi.org/10.1016/j.arr.2016.12.004.
[22] X. Zhao, Y. Fan, P.H. Vann, J.M. Wong, N. Sumien, J.J. He, Long-term HIV-1 Tat Expression in the Brain Led to Neurobehavioral, Pathological, and Epigenetic Changes Reminiscent of Accelerated Aging, Aging Dis. 11 (2020) 93–107. https://doi.org/10.14336/AD.2019.0323.
[23] R. El-Amine, D. Germini, V.V. Zakharova, T. Tsfasman, E.V. Sheval, R.A.N.

Louzada, C. Dupuy, C. Bilhou-Nabera, A. Hamade, F. Najjar, E. Oksenhendler, M. Lipinski, B.V. Chernyak, Y.S. Vassetzky, HIV-1 Tat protein induces DNA damage in human peripheral blood B-lymphocytes via mitochondrial ROS production, Redox Biol. 15 (2018) 97–108. https://doi.org/10.1016/j.redox.2017.11.024.

[24] A. Valyaeva, M. Tikhomirova, D. Potashnikova, A. Bogomazova, G. Snigiryova, A. Penin, M. Logacheva, E. Arifulin, A. Shmakova, D. Germini, A. Kachalova, A. Saidova, A. Zharikova, Y. Musinova, A. Mironov, Y. Vassetzky, E.V. Sheval, Ectopic expression of HIV-1 Tat modifies gene expression in cultured B cells: Implications for the development of B-cell lymphomas in HIV-1-infected patients, PeerJ. in press (2022).

[25] D. Germini, T. Tsfasman, M. Klibi, R. El-Amine, A. Pichugin, O.V. Iarovaia, C. Bilhou-Nabera, F. Subra, Y. Bou Saada, A. Sukhanova, D. Boutboul, M. Raphaël, J. Wiels, S.V. Razin, S. Bury-Moné, E. Oksenhendler, M. Lipinski, Y.S. Vassetzky, HIV Tat induces a prolonged MYC relocalization next to IGH in circulating B-cells, Leukemia. 31 (2017) 2515–2522. https://doi.org/10.1038/leu.2017.106.

[26] S. Mediouni, A. Darque, G. Baillat, I. Ravaux, C. Dhiver, H. Tissot-Dupont, M. Mokhtari, H. Moreau, C. Tamalet, C. Brunet, P. Paul, F. Dignat-George, A. Stein, P. Brouqui, S.A. Spector, G.R. Campbell, E.P. Loret, Antiretroviral therapy does not block the secretion of the human immunodeficiency virus tat protein., Infect. Disord. Drug Targets. 12 (2012) 81–6.

[27] A. Poggi, R. Carosio, D. Fenoglio, S. Brenci, G. Murdaca, M. Setti, F. Indiveri, S. Scabini, E. Ferrero, M.R. Zocchi, Migration of Vδ1 and Vδ2 T cells in response to CXCR3 and CXCR4 ligands in healthy donors and HIV-1-infected patients: Competition by HIV-1 Tat, Blood. 103 (2004) 2205–2213. https://doi.org/10.1182/blood-2003-08-2928.

[28] M.O. Westendorp, R. Frank, C. Ochsenbauer, K. Stricker, J. Dhein, H. Walczak, K.-M. Debating, P.H. Krammer, Sensitization of T cells to CD95-mediated apoptosis by HIV-1 Tat and gp120, Nature. 375 (1995) 497–500. https://doi.org/10.1038/375497a0.

[29] H. Xiao, C. Neuveut, H.L. Tiffany, M. Benkirane, E.A. Rich, P.M. Murphy, K.T. Jeang, Selective CXCR4 antagonism by Tat: implications for in vivo expansion of coreceptor use by HIV-1, Proc. Natl. Acad. Sci. U. S. A. 97 (2000) 11466–11471. https://doi.org/10.1073/pnas.97.21.11466.

[30] F. Rayne, S. Debaisieux, A. Tu, C. Chopard, P. Tryoen-Toth, B. Beaumelle, Detecting HIV-1 Tat in Cell Culture Supernatants by ELISA or Western Blot, Methods Mol. Biol. Clifton NJ. 1354 (2016) 329–342. https://doi.org/10.1007/978-1-4939-3046-3_22.

[31] M. Schatz, L. Marty, C. Ounadjela, P.B.V. Tong, I. Cardace, C. Mettling, P.-E. Milhiet, L. Costa, C. Godefroy, M. Pugnière, J.-F. Guichou, J.-M. Mesnard, M. Blaise, B. Beaumelle, A Tripartite Complex HIV-1 Tat-Cyclophilin A-Capsid Protein Enables Tat Encapsidation That Is Required for HIV-1 Infectivity, J. Virol. 97 (2023) e0027823. https://doi.org/10.1128/jvi.00278-23.

[32] J. Schüpbach, Measurement of HIV-1 p24 antigen by signal-amplification-boosted ELISA of heat-denatured plasma is a simple and inexpensive alternative to tests for viral RNA, AIDS Rev. 4 (2002) 83–92.

[33] J. Schüpbach, Z. Tomasik, D. Nadal, B. Ledergerber, M. Flepp, M. Opravil, J. Böni, Use of HIV-1 p24 as a sensitive, precise and inexpensive marker for infection, disease progression and treatment failure, Int. J. Antimicrob. Agents. 16 (2000) 441–445. https://doi.org/10.1016/s0924-8579(00)00272-7.

[34] L.J. Henderson, T.P. Johnson, B.R. Smith, L.B. Reoma, U.A. Santamaria, M. Bachani,

C. Demarino, R.A. Barclay, J. Snow, N. Sacktor, J. Mcarthur, S. Letendre, J. Steiner, F. Kashanchi, A. Nath, Presence of Tat and transactivation response element in spinal fluid despite antiretroviral therapy, AIDS Lond. Engl. 33 Suppl 2 (2019) S145–S157. https://doi.org/10.1097/QAD.0000000000002268.

[35] A. Tripiciano, O. Picconi, S. Moretti, C. Sgadari, A. Cafaro, V. Francavilla, A. Arancio, G. Paniccia, M. Campagna, M.R. Pavone-Cossut, L. Sighinolfi, A. Latini, V.S. Mercurio, M.D. Pietro, F. Castelli, A. Saracino, C. Mussini, G.D. Perri, M. Galli, S. Nozza, F. Ensoli, P. Monini, B. Ensoli, Anti-Tat immunity defines CD4+ T-cell dynamics in people living with HIV on long-term cART., EBioMedicine. 66 (2021) 103306. https://doi.org/10.1016/j.ebiom.2021.103306.

[36] S. Debaisieux, F. Rayne, H. Yezid, B. Beaumelle, The ins and outs of HIV-1 Tat, Traffic Cph. Den. 13 (2012) 355–363. https://doi.org/10.1111/j.1600-0854.2011.01286.x.

[37] C. Dufour, P. Gantner, R. Fromentin, N. Chomont, The multifaceted nature of HIV latency, J. Clin. Invest. 130 (2020) 3381–3390. https://doi.org/10.1172/JCI136227.

[38] M.E. Wong, A. Jaworowski, A.C. Hearps, The HIV Reservoir in Monocytes and Macrophages, Front. Immunol. 10 (2019) 1435. https://doi.org/10.3389/fimmu.2019.01435.

[39] C. Wallet, M. De Rovere, J. Van Assche, F. Daouad, S. De Wit, V. Gautier, P.W.G. Mallon, A. Marcello, C. Van Lint, O. Rohr, C. Schwartz, Microglial Cells: The Main HIV-1 Reservoir in the Brain, Front. Cell. Infect. Microbiol. 9 (2019) 362. https://doi.org/10.3389/fcimb.2019.00362.

[40] K. Tantale, E. Garcia-Oliver, M.-C. Robert, A. L'Hostis, Y. Yang, N. Tsanov, R. Topno, T. Gostan, A. Kozulic-Pirher, M. Basu-Shrivastava, K. Mukherjee, V. Slaninova, J.-C. Andrau, F. Mueller, E. Basyuk, O. Radulescu, E. Bertrand, Stochastic pausing at latent HIV-1 promoters generates transcriptional bursting, Nat. Commun. 12 (2021) 4503. https://doi.org/10.1038/s41467-021-24462-5.

[41] S.A. Yukl, P. Kaiser, P. Kim, S. Telwatte, S.K. Joshi, M. Vu, H. Lampiris, J.K. Wong, HIV latency in isolated patient CD4+ T cells may be due to blocks in HIV transcriptional elongation, completion, and splicing, Sci. Transl. Med. 10 (2018) eaap9927. https://doi.org/10.1126/scitranslmed.aap9927.

[42] O.K. Szewczyk-Roszczenko, P. Roszczenko, A. Shmakova, N. Finiuk, S. Holota, R. Lesyk, A. Bielawska, Y. Vassetzky, K. Bielawski, The Chemical Inhibitors of Endocytosis: From Mechanisms to Potential Clinical Applications, Cells. 12 (2023) 2312. https://doi.org/10.3390/cells12182312.

Supplementary Materials and Methods

Blood collection

Blood samples from HIV-positive individuals who signed written informed consent for the study and were treated at the Department of Clinical Immunology, Hôpital Saint-Louis, Paris, France, or Montpellier CHU, Montpellier, France, were collected in accordance with French legislation (agreements 2016-A01316-45, VIHEBV for Paris and 233-2018-SR for Montpellier). The clinical characteristics of HIV-positive individuals are summarized in Table 1. HIV status was analyzed by immunoassay of anti-HIV-1/2 antibodies IgM and IgG and antigen p24 in venous blood samples. Positive tests were confirmed twice. Whole blood samples from anonymous healthy donors of different sex and age were obtained from the "Etablissement Français du Sang", either at the Saint-Louis Hospital, Paris, France or at Montpellier University Hospital Center (CHU), in accordance with the French legislation (agreements 14/EFS/033 for Paris and 233-2018-SR for Montpellier).

Tat ELISA

Recombinant Tat (Tat86, HXB2) was produced in E. coli and purified as described previously [16]. HIV-1 Tat concentration in human serum samples was determined as described previously [30] with minor modifications. Briefly, 96-well plates (Sarstedt, cat. # 82.1581200) were coated with rabbit polyclonal anti-Tat HXB2 antibodies (a kind gift from Erwann Loret) at a dilution of 1:1000 in a 0.2 M carbonate buffer (pH 9.6). After overnight incubation at 4°C, plates were washed twice in PCBST (0.015 M Na2HPO4, 0.015 M sodium citrate, 0.140 M NaCl, 0.05% Tween-20), then saturated with 8% milk in PBST (PBS/0.05% Tween-20) for 2 hours at room temperature, followed by three washes with PCBST. Reference dilutions of recombinant HXB2 Tat protein prepared as described in [16] and resuspended in uninfected serum / PBS (1/1) and serum samples (1/1 with PBS) were loaded onto the plate (100 µl/well) and incubated for 4 hours at room temperature. The plates were then washed five times with PCBST and incubated overnight at 4°C with mouse monoclonal anti-Tat antibodies (Santa-Cruz, sc-65912) diluted 1:100 in 8% milk in PCBST. The plates were then washed five times with PCBST and incubated for 2.5 hours at room temperature with peroxidase-conjugated goat anti-mouse antibodies (Jackson Immunoresearch) diluted 1:2000 in 8% milk in PBST, followed by five washes with PCBST. Peroxidase substrate (3,3′,5,5′ Tetramethylbenzidine, TMB, Sigma, cat. # T8665) was then added (100 µl/well) for 15-20 minutes and the reaction was stopped using 0.5 M H_2SO_4 (50 µl/well). The Absorbance at 450 nm was measured using a Tecan plate reader. This assay detected Tat concentrations above 2.5 ng/ml.

HIV p24 ELISA in human serum samples

HIV-1 p24 concentration in human serum samples was determined using an HIV Antigen mAB ELISA kit (Innotest, cat. # 80564) following the manufacturer's instructions. The standard p24 antigen was recombinant p24 prepared as described previously [31]. This assay detected p24 concentrations above 5 pg/ml.

Statistical analysis

The resulting HIV-1 Tat concentrations were extrapolated from the linear standard curves based on reference dilutions of recombinant Tat protein. All samples were analysed in triplicates and the mean value was calculated for each sample. Student's unpaired t-test was used to compare HIV-1 Tat levels between two groups. For the correlation analysis, the Spearman correlation between the HIV-1 Tat level and different predictors was performed. Data are presented as individual values, mean ± standard error of the mean (SEM). To identify the independent factors associated with HIV-1 Tat levels, multivariable linear regression was performed using the lm() function in R (R version 4.2.1), with age, sex, CD4+ T cell counts, HIV RNA level (>20 copies/ml vs. <20 copies/ml), percentage of CD4+ and CD8+ T cells and CD4/CD8 ratio as independent variables and HIV-1 Tat level as the dependent variable. The level of significance was set at $p < 0.05$.

These findings demonstrate that HIV-1 Tat is circulating in the blood of people living with HIV on cART despite effective viral suppression. In ¼ of such individuals, the levels of circulating HIV-1 Tat are detectable at levels higher than the specificity cut-off of our ELISA test (2.5 ng/ml). In a multiple logistic regression analysis of different factors that could affect the prevalence of HIV-1 Tat detection in serum, only age (categorised as >55 years old and ≤ 55 years old) was significantly associated with the detection of HIV-1 Tat above the specificity cut-off (odds ratio 0.22 [0.05-0.82], p = 0.0306, **Figure 16**). The detected concentrations are in line with the reports on HIV-1 Tat presence in the sera of people living with HIV prior to cART (Westendorp et al. 1995), in early cART (from 2 ng/ml to 40 ng/ml) (Xiao et al. 2000) or late cART era (from 0.2 ng/ml to 9.0 ng/ml) (Germini et al. 2017b). Tat levels can be substantially higher in lymphoid tissues, where both latent reservoir and productively infected cells can be present, and in neighbouring cells (e.g., B cells), due to its effective cell-penetration capacities, than those detected in the serum of people living with HIV.

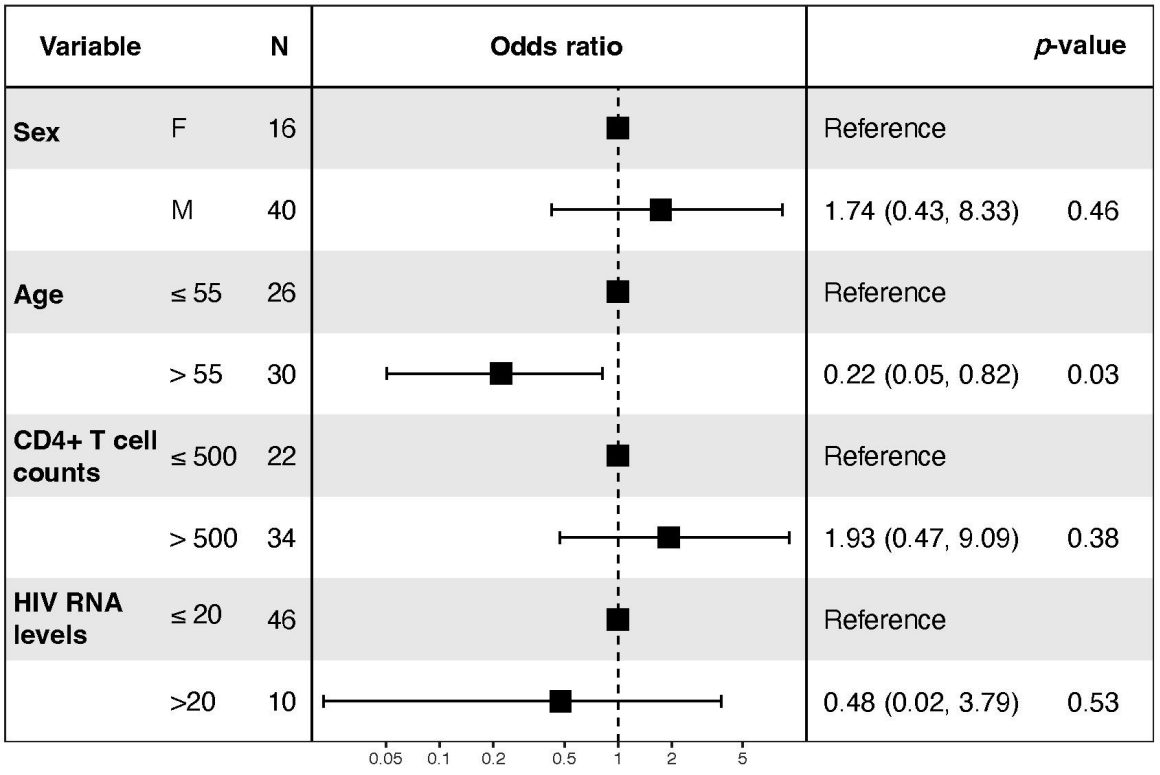

Figure 16. Forest plot of multivariable logistic regression model for factors associated with HIV-1 Tat detection in serum of HIV-positive individuals above 2.5 ng/ml. The horizontal lines correspond to the odds ratio [95% confidence intervals] of >2.5 ng/ml vs. <2.5 ng/ml Tat serum levels for each variable included in the association study.

3.2.2 HIV-1 Tat modifies gene expression in B cells

To simulate the prolonged systemic effect of HIV-1 Tat on B cells, which can be seen in chronically infected individuals, we used a model of HIV-1 Tat ectopic

stable expression in cultured B cells, immortalized with EBV. While working with primary B cells is challenging, using cultured B cells immortalized with EBV serves as a close-to-physiological condition, as many B cell lymphomas in people living with HIV are associated with EBV infection. HIV-1 Tat is a transcriptional activator that can regulate the expression of host genes. However, its effect on host gene transcription in human cells was previously described mostly in T cells (Menon et al. 2020; Reeder et al. 2015). This experimental model allowed us to study the effects of HIV-1 Tat on B cell transcriptome and provided valuable insights into the molecular mechanisms underlying the prolonged systemic effects of HIV-1 Tat on B cells, which may have implications for the B cell lymphomagenesis in people living with HIV (see **Article 8** for model description).

In this study, a genome-wide analysis of cellular gene expression (RNA-seq) of RPMI8866 cells stably expressing HIV-1 Tat or its mutant, deprived of transactivation activity, fused with EGFP (RPMI8866^{Tat} or RPMI8866^{TatC22G}) was conducted to assess the impact of Tat on B cell transcriptome, aiming to understand the role of this protein in the development of B cell lymphomas in people living with HIV. The results showed that long-term exposure to Tat led to the differential expression of approximately 1000 genes in B cells (**Figure 17**). Functional analysis of these gene expression changes indicated the activation of pathways involved in cellular antiviral reactions and the suppression of various metabolic pathways. HIV-1 Tat was found to induce the expression of pro-inflammatory cytokines, including IL-6, which may contribute to the observed gene expression pattern. Comparing the effects of HIV-1 Tat with its transactivation-deficient mutant (TatC22G), we identified that some genes regulated by Tat's transactivator activity in B cells and other genes are influenced by protein-protein interactions involving Tat. Moreover, Tat interaction with host proteins appeared to be the primary mechanism of its chronic action in B cells, since most of the deregulated genes were common between Tat and TatC22G.

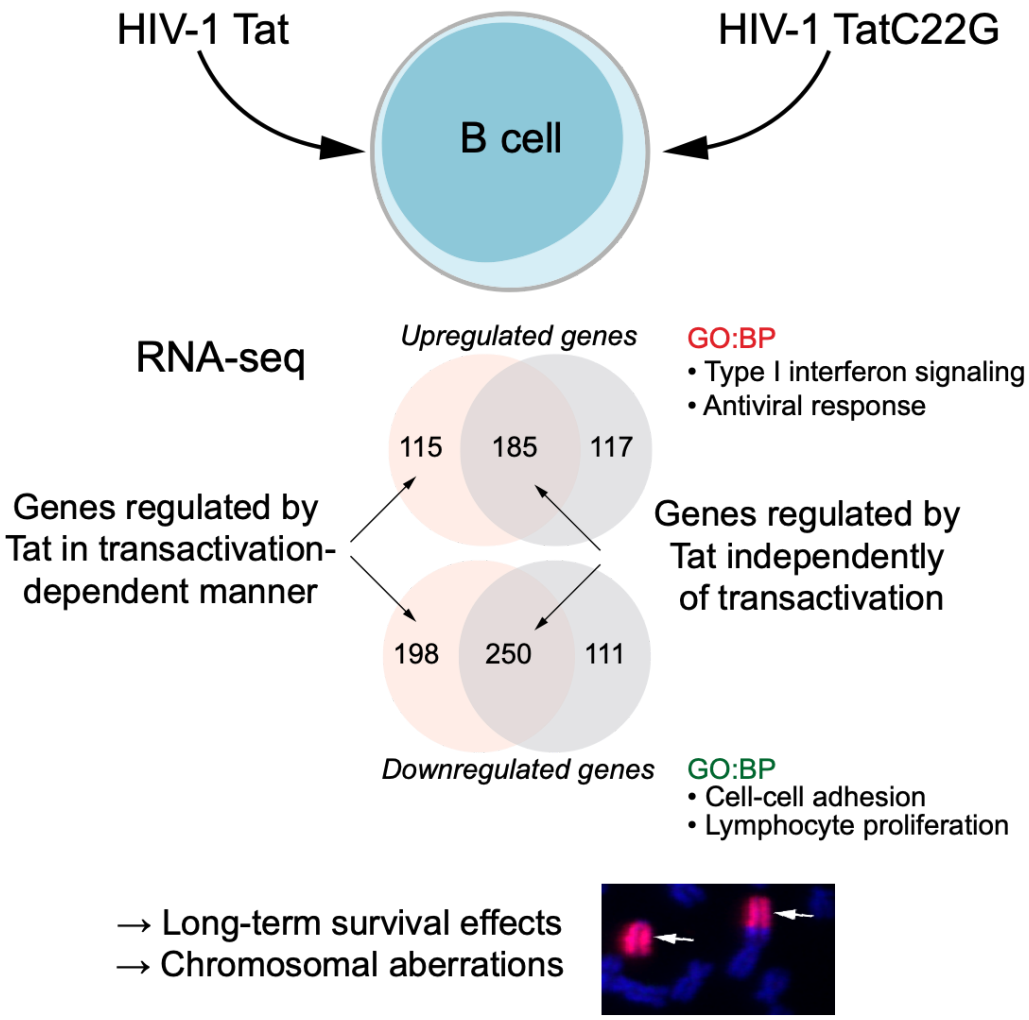

Figure 17. HIV-1 Tat regulates gene expression in B cells. RPMI8866 cells expressing HIV-1 Tat or its transactivation-deficient mutant (TatC22G) were used to study the effects of HIV-1 Tat on B cell transcriptome. Tat exposure led to the differential expression of 1038 genes, 748 of which were protein-coding genes. The analysis of modified biological processes (GO:BP) revealed activation of Type I interferon signalling and antiviral pathways and suppression of proliferation and cell-cell adhesion pathways. The deregulated genes were of two types: dependent on Tat's transactivator activity (i.e. deregulated only by Tat) and genes regulated independently of Tat's transactivator activity, presumably through protein-protein interactions (i.e. deregulated by both Tat and TatC22G). Prolonged Tat exposure slightly inhibited cell growth and promoted chromosome aberrations, potentially promoting oncogenic transformation in B cells. GO:BP, Gene ontology: Biological processes.

Physiological analysis of the Tat-expressing B cells revealed an increased occurrence of chromosome aberrations. This observation suggests that prolonged exposure to HIV-1 Tat can modify cellular physiology and genome stability, potentially promoting oncogenic transformation in B cells, which is in agreement with our previous observation that HIV-1 Tat downregulates the expression of genes involved in DNA damage sensing and repair (**Figure 15**) and can contribute to the accumulation of DNA damages without significant reduction in cell viability.

I contributed to this study by cell line characterization (analysis of HIV-1 Tat expression in stable cell lines) and by participation in manuscript review and editing.

Article 8. Research paper "Ectopic expression of HIV-1 Tat modifies gene expression in cultured B cells: implications for the development of B-cell lymphomas in HIV-1-infected patients"

Ectopic expression of HIV-1 Tat modifies gene expression in cultured B cells: implications for the development of B-cell lymphomas in HIV-1-infected patients

Anna A. Valyaeva[1,2,3], Maria A. Tikhomirova[1,4], Daria M. Potashnikova[3], Alexandra N. Bogomazova[5,6], Galina P. Snigiryova[7], Aleksey A. Penin[8], Maria D. Logacheva[2,9], Eugene A. Arifulin[2], Anna A. Shmakova[4,10], Diego Germini[10], Anastasia I. Kachalova[3], Aleena A. Saidova[3,11], Anastasia A. Zharikova[1,2], Yana R. Musinova[2,4], Andrey A. Mironov[1,8], Yegor S. Vassetzky[4,10] and Eugene V. Sheval[1,2,3]

[1] School of Bioengineering and Bioinformatics, Lomonosov Moscow State University, Moscow, Russia
[2] Belozersky Institute of Physico-Chemical Biology, Lomonosov Moscow State University, Moscow, Russia
[3] Department of Cell Biology and Histology, School of Biology, Lomonosov Moscow State University, Moscow, Russia
[4] Koltzov Institute of Developmental Biology, Moscow, Russia
[5] Federal Research and Clinical Center of Physical-Chemical Medicine, Moscow, Russia
[6] Center for Precision Genome Editing and Genetic Technologies for Biomedicine, Federal Research and Clinical Center of Physical-Chemical Medicine of Federal Medical Biological Agency, Moscow, Russia
[7] Burdenko National Medical Research Center of Neurosurgery, Moscow, Russia
[8] Institute for Information Transmission Problems, Moscow, Russia
[9] Skolkovo Institute of Science and Technology, Moscow, Russia
[10] UMR9018 (CNRS – Institut Gustave Roussy – Université Paris Saclay), Centre National de Recherche Scientifique, Villejuif, France, France
[11] Center for Precision Genome Editing and Genetic Technologies for Biomedicine, Engelhardt Institute of Molecular Biology, Moscow, Russia

Submitted 12 May 2022
Accepted 11 August 2022
Published 18 October 2022

Corresponding authors
Yegor S. Vassetzky,
yegor.vassetzky@cnrs.fr
Eugene V. Sheval,
sheval_e@belozersky.msu.ru

Academic editor
Ravi Tandon

Additional Information and Declarations can be found on page 20

DOI **10.7717/peerj.13986**

Copyright
2022 Valyaeva et al.

Distributed under
Creative Commons CC-BY 4.0

OPEN ACCESS

ABSTRACT

An increased frequency of B-cell lymphomas is observed in human immunodeficiency virus-1 (HIV-1)-infected patients, although HIV-1 does not infect B cells. Development of B-cell lymphomas may be potentially due to the action of the HIV-1 Tat protein, which is actively released from HIV-1-infected cells, on uninfected B cells. The exact mechanism of Tat-induced B-cell lymphomagenesis has not yet been precisely identified. Here, we ectopically expressed either Tat or its TatC22G mutant devoid of transactivation activity in the RPMI 8866 lymphoblastoid B cell line and performed a genome-wide analysis of host gene expression. Stable expression of both Tat and TatC22G led to substantial modifications of the host transcriptome, including pronounced changes in antiviral response and cell cycle pathways. We did not find any strong action of Tat on cell proliferation, but during prolonged culturing, Tat-expressing cells were displaced by non-expressing cells, indicating that Tat expression slightly inhibited cell growth. We also found an increased frequency of chromosome aberrations in cells expressing Tat. Thus, Tat can modify gene expression in cultured B cells, leading to subtle modifications in

How to cite this article Valyaeva AA, Tikhomirova MA, Potashnikova DM, Bogomazova AN, Snigiryova GP, Penin AA, Logacheva MD, Arifulin EA, Shmakova AA, Germini D, Kachalova AI, Saidova AA, Zharikova AA, Musinova YR, Mironov AA, Vassetzky YS, Sheval EV. 2022. Ectopic expression of HIV-1 Tat modifies gene expression in cultured B cells: implications for the development of B-cell lymphomas in HIV-1-infected patients. **PeerJ 10:e13986 DOI 10.7717/peerj.13986**

cellular growth and chromosome instability, which could promote lymphomagenesis over time.

Subjects Cell Biology, Molecular Biology, Virology, HIV, Oncology
Keywords HIV-1 Tat, B cells, Virus-cell interactions, Gene expression, RNA-seq

INTRODUCTION

In the second part of the 20th century, human immunodeficiency virus-1 (HIV-1) has rapidly spread throughout the world and caused high mortality due to its high evolution rate. HIV-1 preferentially infects CD4^{+} T cells, macrophages, and microglial cells, leading to a damaged immune system and the development of acquired immunodeficiency syndrome (AIDS). Combined antiretroviral therapy (cART) stops the virus from making copies of itself in the body and may slow down the development of AIDS (*Autran et al., 1997*; *HIV-CAUSAL Collaboration et al., 2010*). However, even after the introduction of cART, individuals infected with HIV-1 are at significantly higher risk of developing non-AIDS-related comorbidities, including the development of neurocognitive disorders (*Mateen et al., 2012*; *Marino et al., 2020*), cardiovascular diseases (*Wang et al., 2015*; *Jiang et al., 2018*), adipose tissue senescence (*Gorwood et al., 2020*), and cancer (*Shmakova, Germini & Vassetzky, 2020*).

Despite the improved control of HIV-1 infection achieved by cART, B-cell lymphomas are still elevated in HIV-1-infected patients and are the most frequent cause of death in these patients (*Noy, 2020*; *Shmakova, Germini & Vassetzky, 2020*; *Hübel, 2020*). However, even more surprising is the fact that HIV-1-infected patients have an increased incidence of specific B-cell lymphomas, namely Burkitt lymphoma and diffuse large B-cell lymphoma (*Gloghini, Dolcetti & Carbone, 2013*; *Besson et al., 2017*; *Atallah-Yunes, Murphy & Noy, 2020*). Only a few articles report that B cells can be infected with HIV-1 (*Fritsch et al., 1998*; *Lazzi et al., 2002*; *Katano et al., 2007*), and it seems that this is an extremely rare/artifactual event. One of the most likely mechanisms of the development of HIV-1-associated B-cell lymphomas in HIV-1-infected patients may be an action of viral proteins on uninfected B cells (*Dolcetti et al., 2016*).

HIV-1 produces a small nuclear transcriptional activator protein known as transactivator of transcription (Tat) which regulates viral transcription (*Ali et al., 2021*). In the absence of Tat, HIV-1 proviral promoter is incompetent for elongation: shortly after transcription initiation, RNA Pol II is stalled due to the presence of inactive form of positive transcription elongation factor b (P-TEFb) composed of CDK9, cyclin T1 or T2, and inhibitory 7SK small nuclear ribonucleoprotein complex (containing 7SK RNA and HEXIM1) (*Kao et al., 1987*; *Sedore et al., 2007*; *D'Orso & Frankel, 2010*). Tat is able to relieve this repressed state by binding to the TAR-like sequence in 7SK snRNA and displacing HEXIM1 from cyclin T1, which disrupts the 7SK-P-TEFb negative transcriptional regulatory complex and releases active P-TEFb (*Barboric et al., 2007*; *Sedore et al., 2007*; *Muniz et al., 2010*; *Pham et al., 2018*). This ability of Tat depends on Tat C22 residue within the activation domain (*Barboric et al., 2007*). Tat then recruits the

active P-TEFb complex (consisting of CDK9, cyclin T1 or T2) and other transcriptional coactivators to the TAR RNA element at the 5′ end of stalled nascent HIV-1 transcripts to relieve stalled RNA Pol II (*Nekhai & Jeang, 2006*; *He et al., 2010*). Simultaneously, HIV-1 Tat modulates cellular processes by interacting with different cellular structures, particularly nuclear components (*Musinova et al., 2016*; *Ali et al., 2021*).

Expression of HIV-1 Tat alone in mice leads to development of different neoplasms, including lymphomas (*Vogel et al., 1988*, *1991*; *Corallini et al., 1993*; *Altavilla et al., 1999*; *Kundu et al., 1999*), suggesting that Tat protein participates in oncogenesis in HIV-1-infected patients. Tat is actively released from HIV-1-infected cells (*Ensoli et al., 1990*; *Nath, 2015*) and is detectable in the serum of HIV-1-infected individuals (*Westendorp et al., 1995*; *Xiao et al., 2000*; *Poggi et al., 2004*; *Germini et al., 2017*). Exogenous HIV-1 Tat can enter uninfected cells, and in particular, HIV-1 Tat is present within tumor cells of HIV-1-associated B-cell lymphomas (*Lazzi et al., 2002*; *Alves de Souza Rios et al., 2021*). Some other HIV-1 proteins might also affect cells not infectable by HIV-1, *e.g.*, HIV-1 Nef, which can be secreted in a form of extracellular vesicles and released into circulation (*Raymond et al., 2011*; *Pushkarsky et al., 2022*).

The mechanisms of Tat-dependent lymphomagenesis in HIV-1-infected patients have been described only partially. Incubation of B cells from healthy donors with recombinant HIV-1 Tat *ex vivo* led to the convergence of chromosomal loci that are usually involved in t (8;14) translocation, which is common in Burkitt lymphoma (*Germini et al., 2017*). These data indicate that exogenous viral proteins can induce global rearrangement of nuclear organization and that these changes can promote lymphomagenesis. Additionally, HIV-1 Tat can modify the chromatin organization and gene expression of host cells, particularly T cells (*Marban et al., 2011*; *Reeder et al., 2015*) and macrophages (*Carvallo et al., 2017*), and it seems that Tat can induce a chain of similar events in B cells. Indeed, Tat can affect the expression of several genes in B cells, including *AICDA*, a gene that encodes the activation-induced cytidine deaminase that participates in immunoglobulin gene maturation (*Sall et al., 2019*; *Akbay et al., 2021*). Additionally, HIV-1 Tat enhances *c-MYC* transcription by binding to the *c-MYC* promoter, which can contribute to a more aggressive lymphoma phenotype (*Lazzi et al., 2002*; *Alves de Souza Rios et al., 2021*). Thus, HIV-1 Tat present in blood may affect gene expression in B cells, and these changes can promote lymphomagenesis. However, the effect of Tat on B cells has never been studied on a genome-wide level. Here, we ectopically expressed HIV-1 Tat in the lymphoblastoid B cell line (RPMI 8866) and analyzed host gene expression by RNA-seq. We found that the expression of HIV-1 Tat led to substantial modifications of gene expression and induced cellular antiviral reactions. Ectopic Tat expression also resulted in modification of cellular proliferation and genome stability, thus promoting changes that could facilitate lymphomagenesis.

MATERIALS AND METHODS

Cell culture

RPMI 8866 cells (Sigma, St. Louis, MI, USA) were grown at 37 °C in RPMI 1640-GlutaMax medium (Gibco, Waltham, MA, USA) supplemented with 10% fetal bovine serum

(HyClone, Logan, UT, USA), sodium pyruvate (PanEco, Singapore), and an antibiotic and antimycotic solution (Gibco, Waltham, MA, USA).

HeLa cells with integrated LTR-TurboRFP (*Kurnaeva et al., 2022*) were grown in Dulbecco's modified Eagle's medium supplemented with alanyl-glutamine (Paneco, Singapore), 10% fetal calf serum (HyClone, Logan, UT, USA) and an antibiotic and antimycotic solution (Gibco, Waltham, MA, USA). The transactivation assay based on fast-maturing TurboRFP protein was described elsewhere (*Kurnaeva et al., 2022*). The expression of EGFP and TurboRFP was analyzed using a FACS Aria SORP instrument (BD Biosciences, San Jose, CA, USA).

Plasmids and cell lines

The pGST-Tat 1 86R plasmid was obtained through the NIH AIDS Reagent Program, Division of AIDS, NIAID, from Dr. Andrew Rice (*Herrmann & Rice, 1993*, *1995*; *Rhim et al., 1994*).

Plasmids for EGFP, Tat-EGFP and TatC22G-EGFP expression and lentiviral particles were constructed by Evrogen (Moscow, Russia). EGFP-, Tat-EGFP- or TatC22G-EGFP-expressing cells were collected using a FACSAria SORP cell sorter (BD Biosciences, San Jose, CA, USA). The excitation wavelength for EGFP was 488 nm, and the emission was detected by a 505LP and 515/20BP set of filters. Sorting was performed with an 85 µm nozzle and the corresponding custom pressure parameters. The sorted cells were grown, then frozen in the complete medium in the presence of DMSO, and stored in liquid nitrogen. To achieve better reproducibility of experiments, cells were used for no more than one month after thawing (excluding the experiments on long-term culture).

Cell lysate preparation, SDS-PAGE and western blotting

Cells were collected by centrifugation for 10 min at 800 g. Cell pellets were washed with PBS and resuspended in NETN buffer (150 mM NaCl, 1 mM EDTA, 50 mM Tris pH 7.5, 0.5% NP 40, protease inhibitor cocktail), sonicated, incubated on ice for 30 min and centrifuged at 4 °C at 12,000 g for 10 min. Protein quantification was performed using the Pierce™ BCA Protein Assay Kit (Thermo Scientific, Waltham, MA, USA) on a NanoDrop 2000C (Thermo Scientific, Waltham, MA, USA). After measuring the concentration, cell lysates were supplemented with Laemmli buffer and 0.1 M DTT and then heated at 95 °C for 10 min.

Protein samples (20 µg) and prestained molecular weight markers (PageRuler™ Prestained Plus Protein Ladder; Thermo Scientific, Waltham, MA, USA) were resolved on 15-well precast SDS–PAGE gels (4–12%) (NuPage) in MOPS Running Buffer (NuPage). Proteins were transferred onto a 0.45 µm PVDF membrane (GE Healthcare, Chicago, IL, USA) in transfer buffer (0.025 M Tris, 0.192 M glycine, 20% ethanol) at 90 V at 4 °C for 2 h. Nonspecific binding was blocked in 5% nonfat dried milk in Tris-buffered saline and 0.1% Tween-20 (TBST) at room temperature for 1 h.

Proteins were probed at 4 °C overnight with the following primary antibodies: anti-Tat (1:200, cat. #sc-65912; Santa Cruz, CA, USA), anti-GFP (1:1,000, Roche, cat. #11814460001), anti-β-actin (1:1,000, control of protein load, cat. #sc-81178; Santa Cruz,

CA, USA). The membranes were washed with TBST and incubated with goat anti-mouse IgG-HRP (cat. # sc-2005; Santa Cruz, CA, USA) secondary antibodies at a 1:2,000 dilution at room temperature for 1.5 h, followed by washing in TBST. Proteins were visualized using Immobilon Western Chemiluminescent HRP Substrate (Millipore, Burlington, MA, USA) and ImageQuant LAS 4000 mini (GE Healthcare, Chicago, IL, USA) for western blotting imaging and analysis.

RNA extraction and sequencing

Cells were collected and stored in RNALater (Qiagen, Hilden, Germany). Total RNA was extracted using a RNeasy Mini RNA isolation kit (Qiagen, Hilden, Germany) following the Qiagen protocol, with the following modifications: (1) lysis time was increased up to 40 min; (2) on-column DNase I treatment was performed. RNA sample quality was assessed using a capillary electrophoresis Bioanalyzer 2100 (Agilent, Santa Clara, CA, USA), and all samples had RIN >8. The cDNA libraries were constructed using the NEBNext Ultra II Directional RNA Library Prep Kit for Illumina (NEB) following the manufacturer's recommendations. RNA was fragmented for 5 min. Thereafter, the constructed libraries were sequenced on an Illumina HiSeq 2000 with a single-end 51 bp read length. Basecalling was performed using bcl2fastq v2.17.1.14.

RNA-seq data processing and analysis

Read quality control was performed using FastQC (version 0.11.7) (http://www.bioinformatics.babraham.ac.uk/projects/fastqc/). Due to the good quality of the reads, no filtering or adapter removal was performed. The reads were then aligned to the human genome assembly GRCh38.p10 using HISAT2 (version 2.0.5) (*Kim, Langmead & Salzberg, 2015*). Read counting was performed in strand-specific mode by the htseq-count script from Python library HTSeq (version 0.12.4) (*Anders, Pyl & Huber, 2015*) using GENCODE v26 gene annotation (ALL). Genes with no counts for all samples, as well as highly expressed ribosomal genes, were filtered out, resulting in the expression set of 32,120 genes across 12 samples.

Principal component analysis (PCA) was performed on the rlog-transformed count data, and the first two principal components were extracted with the corresponding percentage of explained variance. Differential expression analysis was performed with the R package DESeq2 (version 1.30.1) (*Love, Huber & Anders, 2014*). We declared the gene to be differentially expressed if padj (*p* value adjusted by the Benjamini-Hochberg procedure) was smaller than 0.05 and the fold change was larger than 1.5 in any direction (Table S1). The statistical power for protein-coding genes (with median 80 aligned reads) was calculated with R package RNASeqPower (version 1.30.0) and was 0.91. Each group of samples consisted of three biological replicates.

Overrepresentation analysis (ORA) and gene set enrichment analysis (GSEA) (*Subramanian et al., 2005*) were performed with the R package clusterProfiler (version 3.18.1) (*Yu et al., 2012*). GSEA was performed on a preranked list of genes ordered by the *stat* column of DESeq2 results. The KEGG (release 99) (*Kanehisa & Goto, 2000*) and GO biological process (*Ashburner et al., 2000*; *The Gene Ontology Consortium, 2017*) databases

were used as the sources of gene sets for ORA and GSEA. GO annotation was obtained from the R package org.Hs.eg.db (version 3.12.0). An adjusted *p* value cutoff of 0.05 was used to select statistically significant categories. REVIGO (*Supek et al., 2011*) with a cutoff parameter of 0.4 was used to remove redundant GO terms.

To assess the possible additional activation of EBV genes due to Tat protein expression in RPMI^{Tat} cells, the same pipeline for differential expression analyses was used. The EBV gene annotation file in GTF format was obtained from GenBank file NC_007605.1 using a custom Python script. Raw reads were aligned to combined human and viral genomes. The EBV GTF annotation file was used to obtain counts for viral genes, and previously obtained human gene counts were used to estimate size factors for all samples. Subsequent differential expression analysis was performed for viral genes.

RNA extraction and qRT-PCR assays

Total RNA from RPMI 8866 cells was isolated using the RNeasy Mini Kit (Qiagen, Hilden, Germany). The RNA concentration was measured with a NanoPhotometer (Implen, Westlake Village, CA, USA). Reverse transcription was performed with an iScript Advanced cDNA Synthesis Kit (BioRad, Hercules, CA, USA) according to the manufacturer's instructions, and qPCR was performed in technical triplicates using a SYBR Green kit (Syntol) in a CFX96 Real-Time PCR Detection System (BioRad, Hercules, CA, USA). Melting curve analyses were performed to verify the amplification specificity. Experiments were performed in biological triplicates, and error bars represent the SEM as indicated in all figure legends. The HPRT, YWHAZ and UBC2 genes were used as references. The primers used for qRT-PCR analysis are listed in Table S2.

Electron microscopy

The cells were fixed in 4.0% glutaraldehyde in 0.1 M cacodylate buffer for 8 h, postfixed with 1% osmium tetroxide for 1 h, dehydrated in ethanol and acetone (70% ethanol containing 2% uranyl acetate), and embedded in Spi-pon 812 epoxy resin (SPI Inc., Albany, NY, USA). Ultrathin sections were cut using an Ultracut E. Ultratome (Reichert Jung), stained with lead citrate, and photographed using a JEM-1400 electron microscope (Jeol, Tokyo, Japan).

Analysis of the cell cycle

Cells were incubated in the presence of 1 µg/ml EdU for 15 min at 37 °C, washed in PBS, fixed with 3.7% paraformaldehyde for 10 min and permeabilized in 0.5% Triton X-100. EdU was labeled using a Click-iT EdU Cell Proliferation Kit for Imaging, Alexa Fluor 555 dye (Thermo Fisher Scientific, Waltham, MA, USA), according to the manufacturer's instructions. DNA was stained with 1 µg/ml Hoechst 33342 (Thermo Fisher Scientific, Waltham, MA, USA). Cells were analyzed using a FACSAria SORP cell sorter (BD Biosciences, San Jose, CA, USA). The detection parameters were as follows: Ex. 405 nm, Em. 450/50 BP for Hoechst 33342 and Ex. 561 nm, Em. 585/15 BP for EdU-Alexa Fluor 555.

For Ki-67 staining, cells were fixed with 1% paraformaldehyde for 10 min, washed in PBS, permeabilized in 0.01% Triton X-100 for 10 min, washed in PBS and stained with anti-Ki-67 PE-conjugated antibodies (BD Pharmingen, San Diego, CA, USA) according to the manufacturer's instructions. Cells were analyzed using a FACSAria SORP cell sorter (BD Biosciences, San Jose, CA, USA). PE fluorescence was detected at Ex. 561 nm, Em. 585/15 BP.

Analysis of apoptosis

Cell death was analyzed by flow cytometry using a FACSAria SORP instrument (BD Biosciences, San Jose, CA, USA). Cells were simultaneously stained with 1 µg/ml Hoechst 33342 (Thermo Fisher Scientific, Waltham, MA, USA), 100 nM TMRE (tetramethylrhodamine, ethyl ester, perchlorate, Thermo Fisher Scientific, Waltham, MA, USA) and annexin V-Alexa Fluor 647 (Thermo Fisher Scientific, Waltham, MA, USA) according to the manufacturer's instructions. Thus, the DNA content, mitochondrial membrane potential and phosphatidylserine externalization were analyzed together for each sample. The detection parameters were as follows: Ex. 405 nm, Em. 450/50 BP for Hoechst 33342; Ex. 561 nm, Em. 585/15 BP for TMRE and Ex. 647 nm, Em. 640/14 BP for annexin V-Alexa Fluor 647. Additionally, the cells were stained with anti-caspase 3 PE-conjugated antibodies (PE active caspase-3 apoptosis kit; BD Biosciences, San Jose, CA, USA). Cell fixation, permeabilization and staining were performed according to the manufacturer's instructions. Active caspase 3-PE was detected at Ex. 561 nm, Em. 585/15 BP using a FACSAria SORP cell sorter (BD Biosciences, San Jose, CA, USA).

Chromosome preparations, FISH and cytogenetic analysis

For metaphase chromosome preparations, colcemid (Invitrogen, Waltham, MA, USA) was added to cultivation media at a final concentration of 0.1 µg/ml. Cells were collected 3 h after the addition of colcemid. Hypotonic treatment (0.075 M KCl) was performed for 15 min at 37 °C. Cells were fixed with an ice-cold mix of methanol and glacial acetic acid (3:1). Metaphase slides were made according to standard procedures and used for FISH one day after preparation. FISH was performed according to the manufacturer's recommendation with a mix of DNA probes specific to whole human chromosomes 1, 2 and 4 (Metasystems, Altlußheim, Germany). The DNA probes to human chromosomes 1, 2 and 4 were labeled by fluorochromes of red, green and both colors, respectively.

Metaphase identification and image acquisition were performed with the slide scanning platform Metafer (v.3.11.8, Metasystems, Altlußheim, Germany) installed on an upright light microscope (Axioscope A1, Carl Zeiss, Germany). For image processing, the Isis FISH imaging system (v5.5, release 5.5.10, Metasystems, Altlußheim, Germany) was used. The number of metaphases scored per sample in each replicate varied from 1,091 to 1,592.

We used Fisher's exact test to estimate the statistical significance of differences in the level of chromosomal aberrations. Differences were considered statistically significant at a significance level of $p < 0.01$.

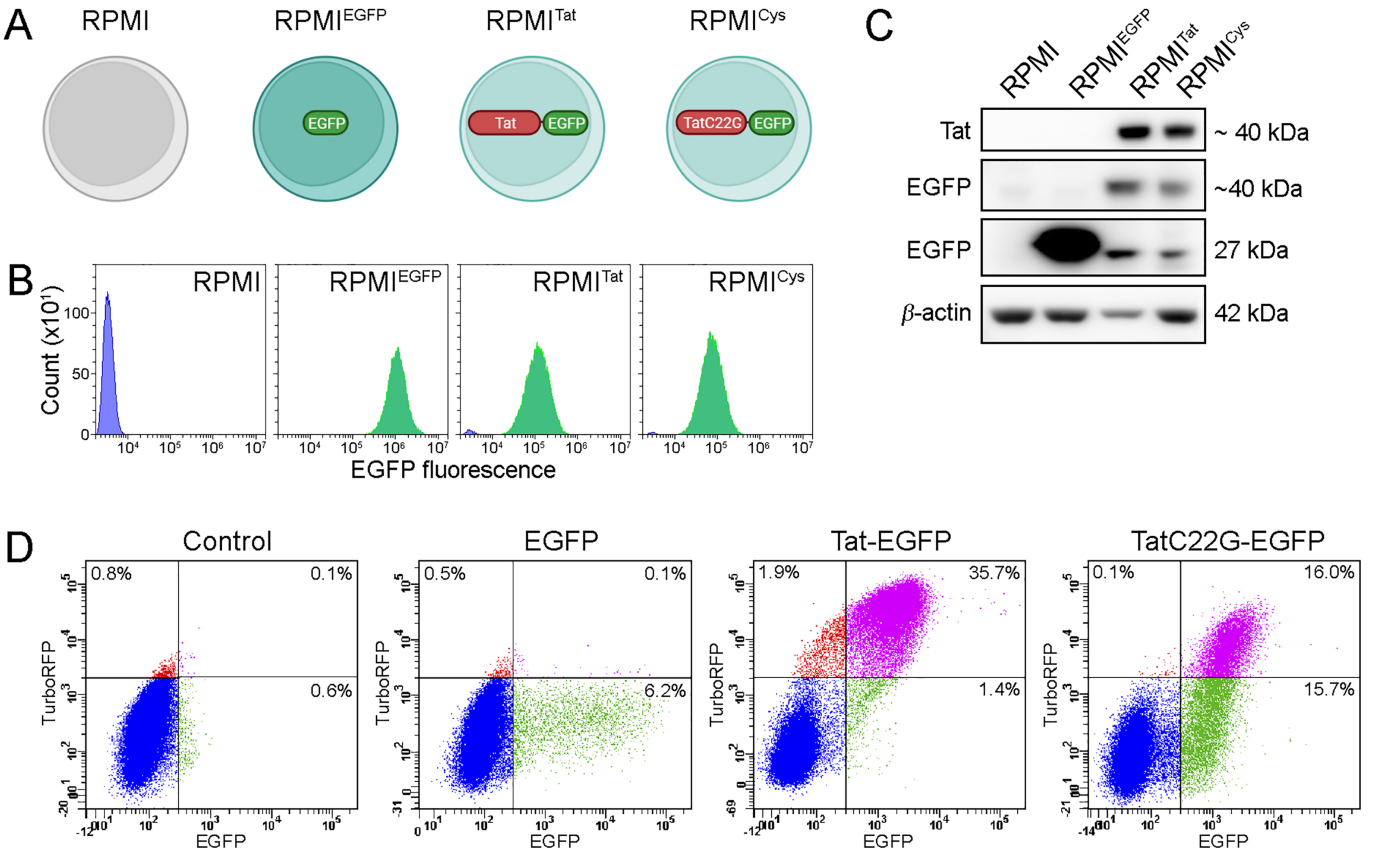

Figure 1 Cell lines that were used to analyze HIV-1 Tat action of cultured B cells. (A) Four cell lines that were used in this study. Created with BioRender.com. (B) EGFP fluorescence of demonstrated high purity and homogeneity of the obtained cell lines (cells without EGFP fluorescence are colored blue, and those with EGFP fluorescence are colored green). (C) Western blot analysis of EGFP, Tat-EGFP and TatC22G-EGFP expression in the cell lines. (D) The transactivation ability of Tat-EGFP in HeLa cells with integrated LTR-TurboRFP (flow cytometry, a representative experiment). TurboRFP fluorescence was clearly detected after the expression of Tat-EGFP but not in nontransduced cells (control) or after the expression of EGFP.
Full-size DOI: 10.7717/peerj.13986/fig-1

RESULTS

Generation of cell lines for the analysis of HIV-1 Tat action in B cells

To analyze the effect of HIV-1 Tat on B cells, we developed RPMI 8866-based cell lines stably expressing Tat protein fused with EGFP (hereafter referred to as RPMI^{Tat}) (Fig. 1A). As controls, we constructed cell lines expressing either EGFP (RPMI^{EGFP}) or TatC22G-EGFP, a mutant Tat protein deprived of transactivation capacity (RPMI^{Cys}).

Stable lines were obtained by transduction of cells with pseudoviral particles, and cells expressing the proteins of interest were selected using a fluorescence-activated sorter (FACS) (Fig. 1B). Flow cytometry demonstrated high purity and homogeneity of the obtained cell lines. Of note, there was an admixture of nonfluorescent cells in the RPMI^{Tat} and RPMI^{Cys} cell lines. Tat-EGFP and TatC22G-EGFP expression was confirmed by western blotting (Fig. 1C). Tat-EGFP and TatC22G-EGFP were partially proteolysed, and as a result, additional bands at ~27 kDa were visible (nonprocessed images are presented in

Fig. S1). As the EGFP tag could have interfered with Tat activity, we analyzed the transactivation capacity of Tat-EGFP and TatC22G-EGFP using an *in vitro* assay based on the fast-maturing fluorescent protein TurboRFP. TurboRFP expression in HeLa cells was controlled by a fragment of the HIV-1 3′ LTR (*Kurnaeva et al., 2022*). We transduced EGFP, Tat-EGFP, or TatC22G-EGFP into these HeLa cells and found that the expression of Tat-EGFP substantially increased TurboRFP fluorescence compared to EGFP, which did not cause an increase in TurboRFP expression (Fig. 1D). TatC22G had a ~17 fold decreased transactivation activity as compared to Tat (the median fluorescence intensity of TurboRFP in Tat-expressing cells was 34601, the median fluorescence intensity in TatC22G-expressing cells was 2009, and the median fluorescence intensity in EGFP-expressing cells was 309 in the representative experiment shown in Fig. 1D). Hence, the transactivation activity of the Tat protein was not perturbed by its fusion with EGFP.

HIV Tat protein affects the gene expression profile of RPMI 8866 cells

To determine the genes regulated by HIV-1 Tat, total RNA from RPMI 8866, RPMI^{EGFP}, RPMI^{Tat} and RPMI^{Cys} cell lines was collected, and RNA-seq was performed. Three biological replicates were sequenced for each cell line. From 16 to 24 million 51 nt sequencing reads were generated for the RPMI^{Tat}, RPMI^{Cys}, RPMI^{EGFP} and RPMI samples. On average, 67.17% of reads in every sample were uniquely aligned to the reference genome GRCh38, and 78.93% of them were nonambiguously mapped to the GENCODE gene annotation (Fig. S2). To assess variability between replicates and between cell lines, rlog-transformed filtered count data were visualized by principal component analysis (Fig. S3A). Biological replicates proved to be highly alike by clustering tightly according to sample type. RPMI^{Tat} samples tended to cluster with RPMI^{Cys} samples, implying similar effects of Tat-EGFP and TatC22G-EGFP on gene expression. This finding was also confirmed by Spearman correlation of normalized gene expression profiles (Fig. S3B).

To identify changes in gene expression induced by Tat protein in RPMI 8866 cells, we performed differential expression analysis for each cell line. We qualified differentially expressed genes (DEGs) with p.adj < 0.05 and fold change >1.5 in any direction.

Comparison of the control RPMI^{EGFP} against the RPMI cell line demonstrated that the impact of EGFP on gene expression could be neglected, as the analysis revealed only 17 upregulated and 36 downregulated DEGs, implying that the gene expression profiles of RPMI^{EGFP} and RPMI samples were highly similar (Fig. 2A). Therefore, we further used RPMI cells as the control and their gene expression level as the baseline to identify genes regulated by Tat or TatC22G proteins.

Out of 32,120 genes with detectable expression, 1,038 genes were differentially expressed between RPMI^{Tat} and RPMI cells. A comparable number of DEGs (902 genes) were identified in the comparison RPMI^{Cys} *vs* the control (Fig. 2A). Among the detected DEGs, slightly more genes were downregulated (60% or 55%) than upregulated in the presence of Tat or TatC22G protein, respectively. The majority of genes whose expression was affected were protein-coding genes. We validated the expression of several DEGs using quantitative real-time polymerase chain reaction (qRT-PCR) assays, thus confirming the reliability of RNA-seq (Fig. 2B).

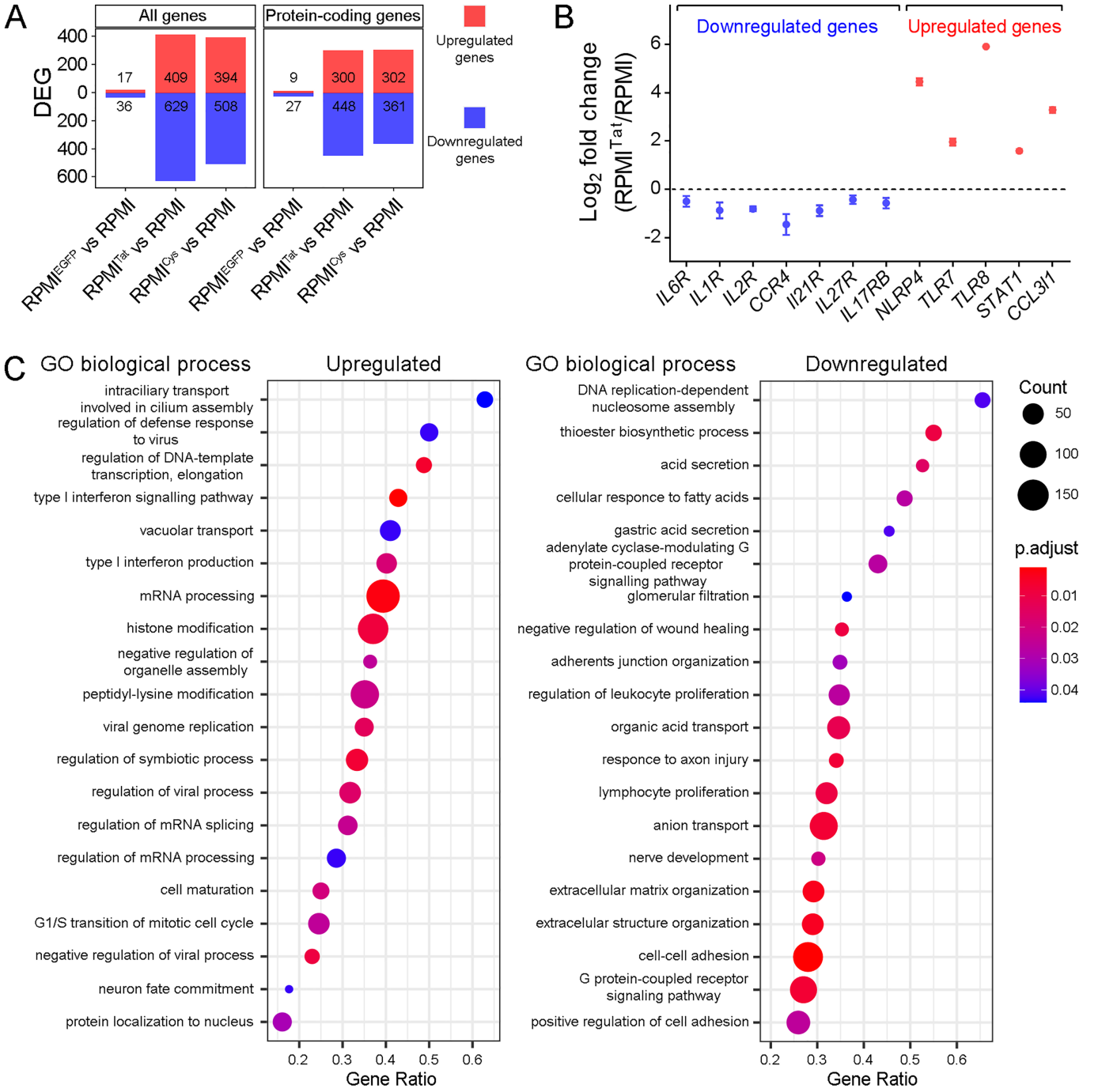

Figure 2 Differentially expressed genes (DEGs) in RPMI cells expressing EGFP, EGFP-Tat or EGFP-TatC22G. (A) The number of all DEGs (left) and protein-coding DEGs (right) found in three comparisons: RPMI^{EGFP} *vs* RPMI, RPMI^{Tat} *vs* RPMI, and RPMI^{Cys} *vs* RPMI. (B) Validation of the RNA-seq dataset using qRT-PCR on the indicated upregulated and downregulated genes (mean ± SEM; n = 3). (C) Upregulated (left) and downregulated (right) GO BP terms affected by Tat identified by GSEA (RFPI^{Tat} cells *vs* RPMI cells). Only significantly enriched (adjusted p value < 0.05) and nonredundant GO BP terms are shown (the top 20). Full-size DOI: 10.7717/peerj.13986/fig-2

RPMI 8866 is an EBV-positive B-lymphoblastoid cell line derived from a patient with chronic myelogenous leukemia (*McCune, Fu & Kunkel, 1981*). RPMI 8866 cells express EBNA1, -2, -3A, -3B, -3C, and LMP-1, -2A, and -2B proteins and several noncoding RNAs. To explore the possibility that changes in gene expression were a result of Tat-induced changes in the expression of EBV genes, we performed differential gene expression analysis of the EBV transcriptome and found no evidence of Tat or TatC22G protein impact on the expression of viral genes in $RPMI^{Tat}$ or $RPMI^{Cys}$ cells (Fig. S4); thus we concluded that we observed a direct effect of Tat or TatC22G on the host cell.

Next, we performed gene set enrichment analysis (GSEA) and overrepresentation analysis (ORA) to search for activated or suppressed functional gene groups and molecular pathways as defined by the GO Biological Process (GO BP) and KEGG databases.

The analysis of modified biological processes (GO BP) was performed by GSEA with subsequent removal of redundant GO terms with REVIGO (Fig. 2C). Comparison of $RPMI^{Tat}$ cells with the control RPMI cells showed that genes whose expression was upregulated in the presence of Tat protein were enriched for antiviral responses, including *Regulation of defense response to virus* (p.adjust = 4.3×10^{-2}), *Type I interferon production* (p.adjust = 1.9×10^{-2}), *Type I interferon signaling pathway* (p.adjust = 1.1×10^{-3}), *Viral genome replication* (p.adjust = 1.4×10^{-2}), *Regulation of viral process* (p.adjust = 1.6×10^{-2}), and *Negative regulation of viral processes* (p.adjust = 9.2×10^{-3}) (Fig. 2C, left panel). In addition to the activation of pathways associated with antiviral responses, the activation of *Regulation of DNA-template transcription, elongation* (p.adjust = 5.9×10^{-3}), *mRNA processing* (p.adjust = 2.2×10^{-3}), *Regulation of mRNA processing* (p.adjust = 4.3×10^{-2}), and *G1/S phase transition of mitotic cell cycle* (p.adjust = 2.5×10^{-2}) was also observed in $RPMI^{Tat}$ cells. These changes may be either part of the global antiviral response or the result of the action of a viral protein (proviral reaction). Among the downregulated pathways, pathways associated with cell adhesion (*Adherens junction organization* (p.adjust = 3.1×10^{-2}), *Cell-cell adhesion* (p.adjust = 2.6×10^{-6}), *Positive regulation of cell adhesion* (p.adjust = 2.5×10^{-2})), and multiple metabolic and biosynthetic pathways were detected (Fig. 2C, right panel). Notably, genes involved in the regulation of cellular proliferation were downregulated (*Regulation of leukocyte proliferation* (p.adjust = 2.5×10^{-2}), *Lymphocyte proliferation* (p.adjust = 8.4×10^{-3})).

We additionally analyzed changes in signaling pathways, for which overrepresentation analysis (ORA) using KEGG databases was performed (Fig. 3). Analysis of up- and downregulated DEGs revealed activation of innate immunity pathways, such as *Toll-like receptor signaling pathways* (hsa04620; p.adjust = 3.1×10^{-2}) and *NOD-like receptor signaling pathways* (hsa04621; p.adjust = 3.1×10^{-2}), as well as the *Influenza A* (hsa05164; p.adjust = 3.1×10^{-2}) pathway, which was highly overlapping with the former two. *Herpes simplex virus 1 infection* pathway (hsa05168; p.adjust = 3.1×10^{-2}) seems to be related to the antiviral response (Fig. 3A). Several zinc finger proteins (ZNFs) were annotated as related to this pathway. Notably, several genes of the JAK-STAT signaling pathway (*JAK1* and *STAT1*) were general for all detected pathways (Fig. 3B). Secreted interferon-I induces IFN-stimulated genes through the JAK-STAT pathway (*Ivashkiv & Donlin, 2014*). Some ZNFs regulate the transcription of interferon-stimulated genes (*Wang & Zheng, 2021*), but

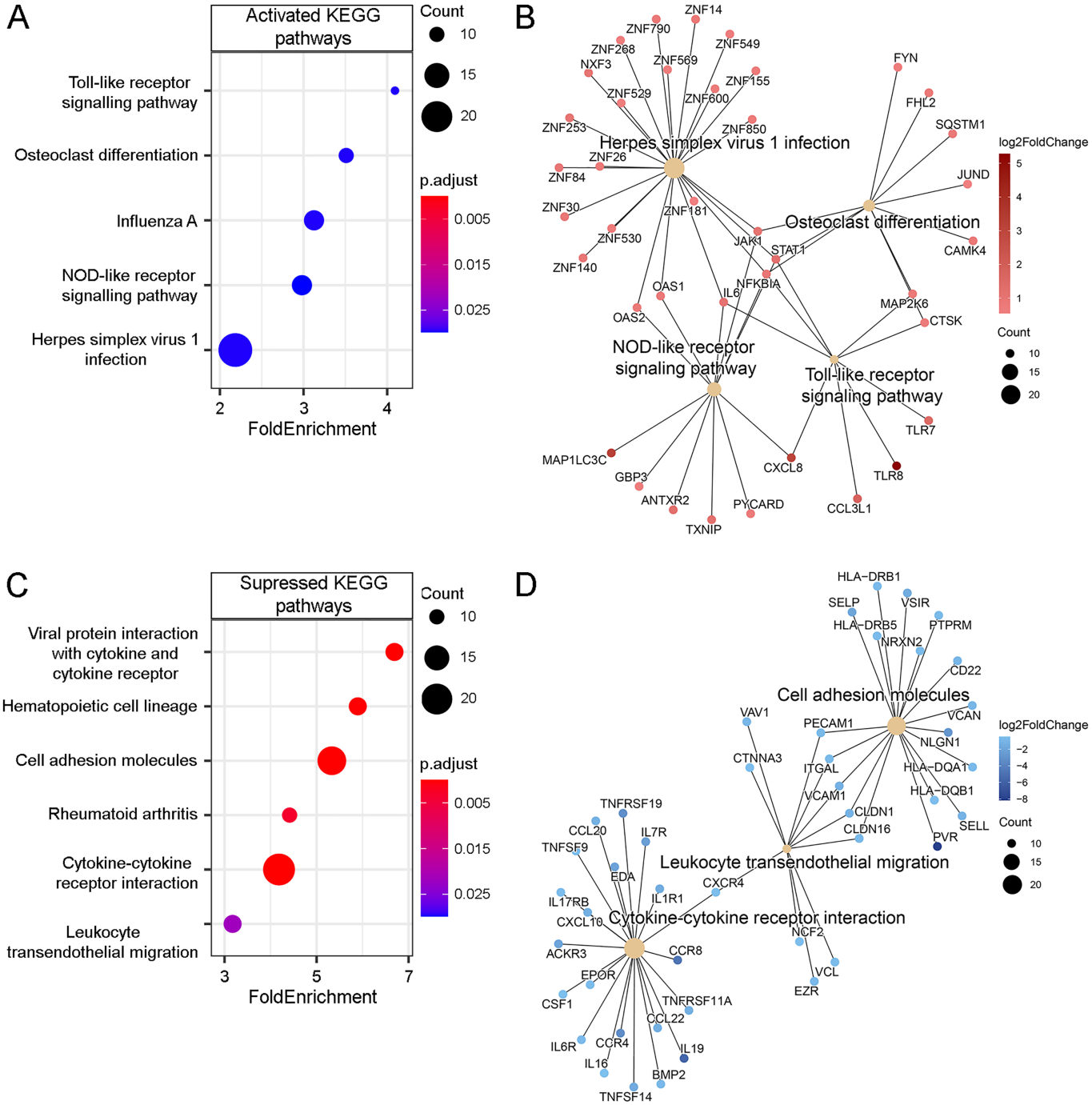

Figure 3 **Enrichment analysis of Tat-affected DEGs (RPMI^{Tat} *vs* RPMI).** (A) KEGG pathways positively regulated by Tat, identified by ORA of protein-coding DEGs. Only significantly enriched (adjusted *p* value < 0.05) KEGG pathways are shown. (B) Activated KEGG pathways (hsa04620, hsa04380, hsa04621, and hsa05168) and associated DEGs after filtering overlapping gene sets. (C) KEGG pathways negatively regulated by Tat, identified by overrepresentation analysis of protein-coding DEGs. Only significantly enriched (adjusted *p* value < 0.05) KEGG pathways are shown. (D) Suppressed KEGG pathways (hsa04514, hsa04060, and hsa04670) and associated DEGs after filtering overlapping gene sets.

Full-size DOI: 10.7717/peerj.13986/fig-3

among ZNF genes detected by RNA-seq, there was only one well-investigated protein: ZNF268 (Table S3). ZNF268 was described as chronic lymphocytic leukemia (CLL)-associated antigen (*Krackhardt et al., 2002*), its aberrant alternative splicing was detected in human hematological malignancies (*Zhao et al., 2008*). ZNF268 also contributes to cervical carcinogenesis through the NF-κB signaling pathway (*Wang et al., 2012*).

Downregulated DEGs were enriched for *Cytokine-cytokine receptor interaction* pathway (hsa04060; *p*.adjust = 2.0×10^{-6}) and overlapped with *Viral protein interaction with cytokine and cytokine receptor* pathway (hsa04061; *p*.adjust = 2.9×10^{-5}), reflecting possible inhibition of the proinflammatory response (Fig. 3C). The downregulated genes of these pathways included several cytokines (*IL16*, *IL19*, *TNFSF9*, *CCL20*, *CCL22*, *CFS1*, *etc.*) and receptors of cytokines (*IL1R1*, *IL6R*, *IL7R*, *CCR4*, *CCR8*, *TNFRSF19*, *TNFRSF11A*, *etc.*) (Fig. 3D). At the same time, some proinflammatory cytokines were upregulated (for example, *IL6*, FC 2.12). Additionally, pathways associated with *cell adhesion molecules* (hsa04514; *p*.adjust = 8.0×10^{-7}), and *Leukocyte transendothelial migration* (hsa04670; *p*.adjust = 2.2×10^{-2}) were also suppressed in $RPMI^{Tat}$ cells, indicating possible inhibition of cell adhesion (Fig. 3C). Among the genes of *cell adhesion molecules* pathway, several genes (*HLA-DQA1*, *HLA-DQB1*, *HLA-DRB1*, and *HLA-DRB5*) coding an MHC class II cell surface receptor were suppressed, which might affect the T cell receptor signaling pathway (Fig. 3D).

Additionally, we analyzed the expression of different transcription factors because such changes can lead to pronounced effects. We found that the expression of 12 transcription factors was upregulated (*ASCL1*, *ATF5*, *FOXO3*, *NR2F2*, *PBX1*, *PRDM5*, *REL*, *SIX1*, *STAT1*, *TFCP2*, *ZNF268*, *ZNF740*), and 13 were downregulated (*DMRT2*, *FLI1*, *HOXB7*, *JUN*, *KDM3A*, *MYCN*, *NR1H4*, *SOX5*, *SOX6*, *SSX1*, *ZC3H6*, *ZNF358*, *ZNF613*); thus, the action of Tat (direct or indirect) may be at least partially connected with the regulation of transcription factor expression.

In addition to differentially expressed protein coding genes, the expression levels of 154 long non-protein coding RNAs (lncRNAs) were altered by HIV-1 Tat expression (54 and 100 lncRNAs were upregulated and downregulated, respectively). Differentially expressed lncRNAs accounted for 14.8% of all DEGs between $RPMI^{Tat}$ and control cells. These lncRNAs are poorly characterized, but two genes of lncRNAs among the identified DEGs are well known. The MALAT1 lncRNA involved in transcriptional regulation and alternative splicing (*West et al., 2014*) was upregulated 2.44-fold in $RPMI^{Tat}$ over the control (the elevated expression was additionally confirmed by qRT-PCR, Fig. S5A). MALAT1 is upregulated in HIV-1-infected $CD4^+$ T cells (*Qu et al., 2019*) and in the peripheral blood of HIV-1-infected patients (*Jin et al., 2016*). NEAT1 lncRNA forms the core structural component of paraspeckle bodies and is known for its contribution to HIV replication (*Zhang et al., 2013*). We observed a 1.66-fold increase in *NEAT1* expression in the $RPMI^{Tat}$ B cell line (see also Fig. S5B), indicating that NEAT1 may play an important role in the development of cell responses induced by the Tat protein.

We also analyzed other DE lncRNAs. The complete list of DE lncRNAs is presented in Table S4, and, since the level of some of these lncRNAs was extremely low, we additionally analyzed ten most expressed DE lncRNAs (Table 1). Some of DE lncRNAs, which were

Table 1 Upregulated and downregulated long non-coding RNAs (PPMI^{Tat} *vs* RPMI cells) with the highest expression (top 10).

EnsID	Gene name	padj	log2FC	FC	Mean count	Functions and possible involvement in oncogenesis	Reference
Upregulated genes							
ENSG00000251562	MALAT1	9.9E−22	1.28	2.44	34,783.28	Table S5	
ENSG00000245532	NEAT1	2.2E−08	0.73	1.66	3,039.09	Table S5	
ENSG00000260658	RP11-368L12.1	7.0E−05	0.67	1.59	1,545.91	Co-expressed with gene module of actively proliferating pre-B cells	(*Petri et al., 2015*)
ENSG00000248837	RP11-412P11.1	9.5E−08	0.99	1.99	859.73	–	
ENSG00000230448	LINC00276	2.6E−04	0.59	1.50	517.66	–	
ENSG00000234663	LINC01934	1.4E−09	0.90	1.86	516.91	Downregulated in thyroid carcinoma	(*Zhang et al., 2019*)
ENSG00000226965	AC003088.1	2.3E−11	1.19	2.29	319.39	Upregulated in breast cancer line	(*Li et al., 2021*)
ENSG00000238129	RP3-410C9.2	8.2E−15	0.86	1.82	307.45	–	
ENSG00000235385	LINC02154	8.5E−79	2.43	5.40	272.56	Upregulated in Laryngeal Squamous Cell Carcinoma and renal cell carcinoma, and can be used as a prognostic feature; promotes the proliferation and metastasis of hepatocellular carcinoma	(*Zuo et al., 2018*; *Gong et al., 2020*; *Yue et al., 2022*)
ENSG00000249645	RP11-552M14.1	2.0E−22	1.19	2.28	261.05	–	
Downregulated genes							
ENSG00000253377	RP11-566H8.3	6.4E−07	−0.86	0.55	1,751.51	Produces non-canonical cancer/testis antigen	(*Chong et al., 2020*)
ENSG00000254119	RP11-705O24.1	9.9E−16	−1.40	0.38	1,623.69	Potential prognostic feature in esophageal cancer	(*Fan & Liu, 2016*)
ENSG00000251381	LINC00958	9.4E−23	−0.68	0.62	1,003.09	Canonical lncRNA in human cancer progression (overexpressed in many cancers)	(*Li et al., 2022*)
ENSG00000267761	CTD-2130O13.1	4.5E−08	−1.13	0.46	895.69	Potential cancer-specific biomarker	(*Mohammed et al., 2017*)
ENSG00000271955	RP11-444A22.1	3.4E−79	−3.03	0.12	803.23	Involved in acute myeloid leukemia cell differentiation	(*Cozzi et al., 2022*)
ENSG00000231772	RP1-154K9.2	8.3E−53	−9.37	0.00	726.17	–	
ENSG00000227681	RP11-307P5.1	4.5E−10	−1.17	0.44	621.53	–	
ENSG00000251088	RP11-325B23.2	1.5E−04	−0.63	0.65	454.27	–	
ENSG00000185904	LINC00839	2.5E−62	−1.88	0.27	332.95	Downregulated in gastric cancer with *H. pilori* infection; upregulated in chemoresistant breast cancer	(*Zhong et al., 2018*; *Chen et al., 2020*)
ENSG00000242741	LINC02005	1.6E−20	−1.44	0.37	324.00	–	

Note:
The full list of DE lncRNAs is presented in Table S4.

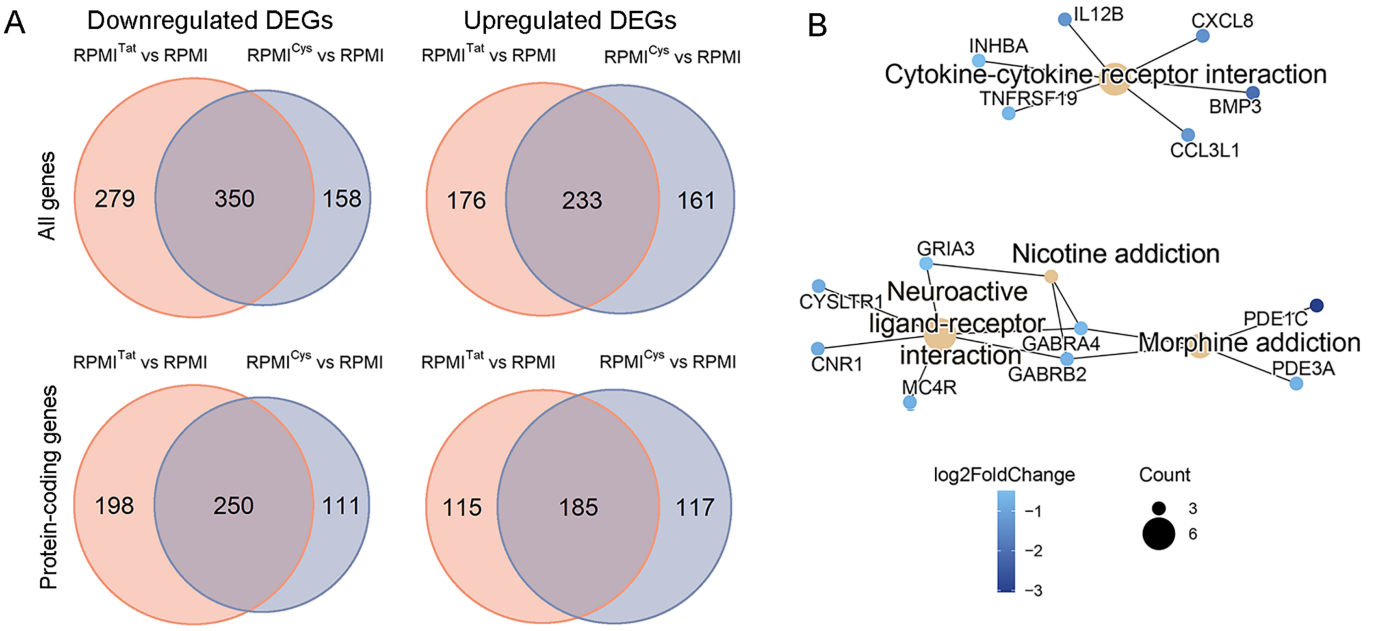

Figure 4 Comparison of gene expression between RPMI^{Tat} and RPMI^{Cys} cells. (A) Venn diagrams demonstrated that approximately half of the DEGs overlapped, indicating similar but not identical modifications induced by EGFP-Tat and its mutated form EGFP-TatC22G. (B) Suppressed KEGG pathways (hsa04060, hsa04080, hsa05033, and hsa05032) and associated DEGs when comparing RPMI^{Cys} against RPMI^{Tat} cells.
Full-size DOI: 10.7717/peerj.13986/fig-4

differentially expressed in RPMI^{Tat} cells, are also differentially expressed in different tumors and might be involved in development of these tumors. The most known examples are *MALAT1* and *NEAT1* expressed in different neoplasms, including B-cell lymphomas and leukemias (Table S5).

Comparison of Tat- and TatC22G-induced effects

HIV-1 Tat can modify host gene expression by several nonrelated mechanisms. Tat can transactivate host genes by binding to TAR-like sequences in their nascent mRNAs, *e.g.*, IL6 mRNA (*Ambrosino et al., 1997*) or TNF-β mRNA (*Buonaguro et al., 1994*). Tat can also associate with chromatin and control RNA polymerase II recruitment and pause release (*Reeder et al., 2015*). Additionally, HIV-1 Tat interacts with hundreds of nuclear proteins (*Gautier et al., 2009*), and this interaction may also modify the expression of host genes.

Transactivation of transcription by the mutant TatC22G protein was significantly weaker than that by Tat (Fig. 1D), but it could still bind to chromatin and interact with other proteins. Both Tat and TatC22G proteins modulate the expression of similar and overlapping sets of genes (Fig. 4A). Comparison of the transcriptome profiles of the RPMI^{Tat} and RPMI^{Cys} cell lines revealed 201 protein-coding DEGs (p.adj < 0.05; fold change >1.5 in any direction).

Overrepresentation analysis against the KEGG database also demonstrated little gene set enrichment, reflecting relatively small differences between RPMI^{Cys} and RPMI^{Tat} cells

(Fig. 4B). Notably, the *Cytokine-cytokine receptor interaction* pathway (hsa04060) downregulated by HIV-1 Tat was further suppressed by mutant TatC22G protein in $RPMI^{Cys}$ cells compared to $RPMI^{Tat}$ cells.

The pathological effects of Tat expression

Our RNA-seq analysis identified several pathways affected by Tat. We next experimentally analyzed key characteristics of RPMI 8866, $RPMI^{EGFP}$, $RPMI^{Tat}$, and $RPMI^{Cys}$ cell lines to identify how Tat affected B cells.

Electron microscopy demonstrated that the expression of EGFP, Tat-EGFP or TatC22G-EGFP did not lead to any substantial changes in cellular organization (Fig. 5A). To ascertain whether changes in the expression of several genes involved in the G_1/S phase transition and cell proliferation (Fig. 2C) affected cell cycle progression in Tat-expressing cells, we analyzed the proportion of G_1/G_0, S, and G_2/M cells in the total population of $RPMI^{Tat}$ cells using flow cytometry. We could not detect any significant changes in the proportions of cells at different stages of the cell cycle using this approach (Figs. 5B, 5C). We also detected S-phase cells using incorporation of EdU and did not observe any difference between different cell lines (Fig. 5D). Finally, we analyzed fractions of cycling (non-G_0) cells using antibodies against the proliferation marker Ki-67, and again, no difference was found (Fig. 5E).

Cell death can also influence the dynamics of cell populations; therefore we analyzed apoptosis in $RPMI^{Tat}$ cells. We did not observe any statistically significant changes in the content of sub-G_1 cells (dead cells), cells with reduced mitochondrial potential (TMRE staining, which allowed for marker cells during very early stages of apoptosis), proportion of annexin V-positive, or caspase 3-positive cells (markers of apoptotic cells) (Fig. 5F).

Thus, stable expression of Tat did not produce strong effects that could be detected using standard analysis of cellular proliferation and apoptosis. At the same time, subtle, but persistent changes (if they exist) could potentially influence the dynamics of cell growth. Therefore, we cultured cells for three months and found that the percentage of cells expressing Tat-EGFP was gradually reduced (Figs. 6A, 6B). Such replacement of Tat-expressing cells by non-expressing cells was not detected in cells expressing either TatC22G-EGFP or EGFP, clearly indicating that this effect was a consequence of Tat protein *per se*.

To detect possible mutagenic effects of HIV-1 Tat expression, we performed cytogenetic analysis. We scored chromosome aberrations involving chromosomes 1, 2 and 4 revealed by fluorescence *in situ* hybridization with whole chromosome paints (Fig. 6C). The images of metaphases were automatically acquired, and then metaphases were analyzed for the presence of structural chromosomal aberrations, including translocations, dicentrics, acentrics, and deletions. Numerical chromosomal abnormalities, such as polyploidy and aneuploidy, were also taken into consideration. We observed a reproducible increase in the frequency of translocations as well as in the total yield of structural aberrations in cells expressing either Tat-EGFP or TatC22G-EGFP (Fig. 6D; Table S6).

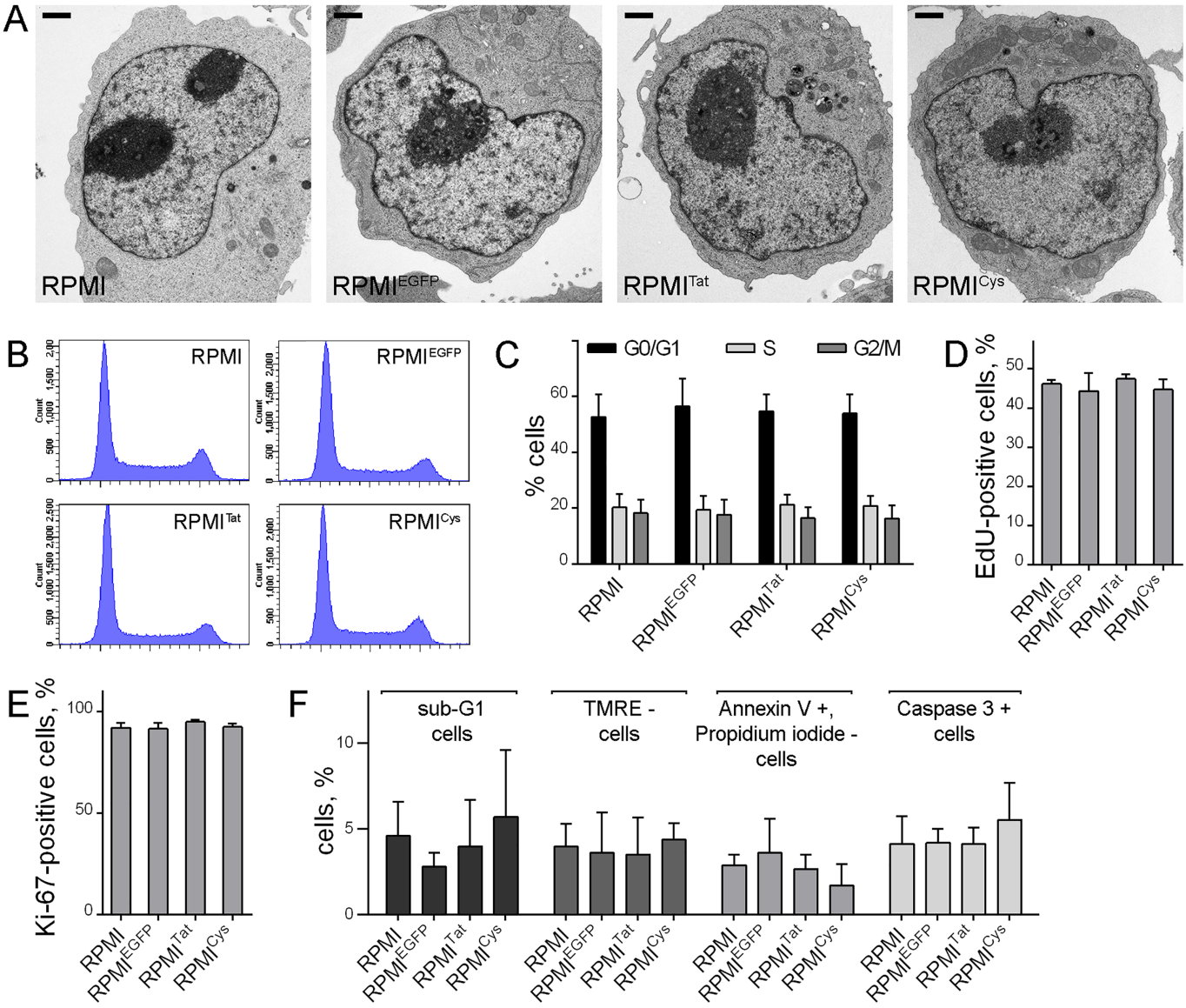

Figure 5 EGFP, Tat-EGFP or TatC22G-EGFP expression does not affect the morphology or proliferative potential of RPMI 8866 cells. (A) Representative cells of RPMI, RPMI^{EGFP}, RPMI^{Tat}, and RPMI^{Cys} lines under electron microscopy. Bars = 1 µm. (B) Cell cycle distribution of RPMI, RPMI^{EGFP}, RPMI^{Tat}, and RPMI^{Cys} cells (representative experiment) and (C) estimation of cell proportions at the G0/G1, S, and G2/M stages (mean ± SD, n = 3). (D) Estimation of S-phase cells using incorporation of synthetic nucleotides (EdU) (mean ± SD, n = 3). (E) Estimation of cycling cells (Ki-67-positive) (mean ± SD, n = 3). (F) Estimation of the content of apoptotic cells in RPMI, RPMI^{EGFP}, RPMI^{Tat}, and RPMI^{Cys} lines using four independent methods (mean ± SD, n = 3). In C–F, all differences between control cells (RPMI) and cells expressing different proteins (RPMI^{EGFP}, RPMI^{Tat}, and RPMI^{Cys}) were insignificant (Kruskal–Wallis test, $p > 0.05$; n = 3). Full-size DOI: 10.7717/peerj.13986/fig-5

DISCUSSION

To identify the mechanisms potentially leading to the development of B-cell lymphomas in HIV-infected patients, we investigated the effect of Tat protein on gene expression in cultured B cells. Upon long-term exposure of B-cells to Tat, the effects could accumulate and potentially provoke an oncogenic transformation. Therefore, we did not use either an

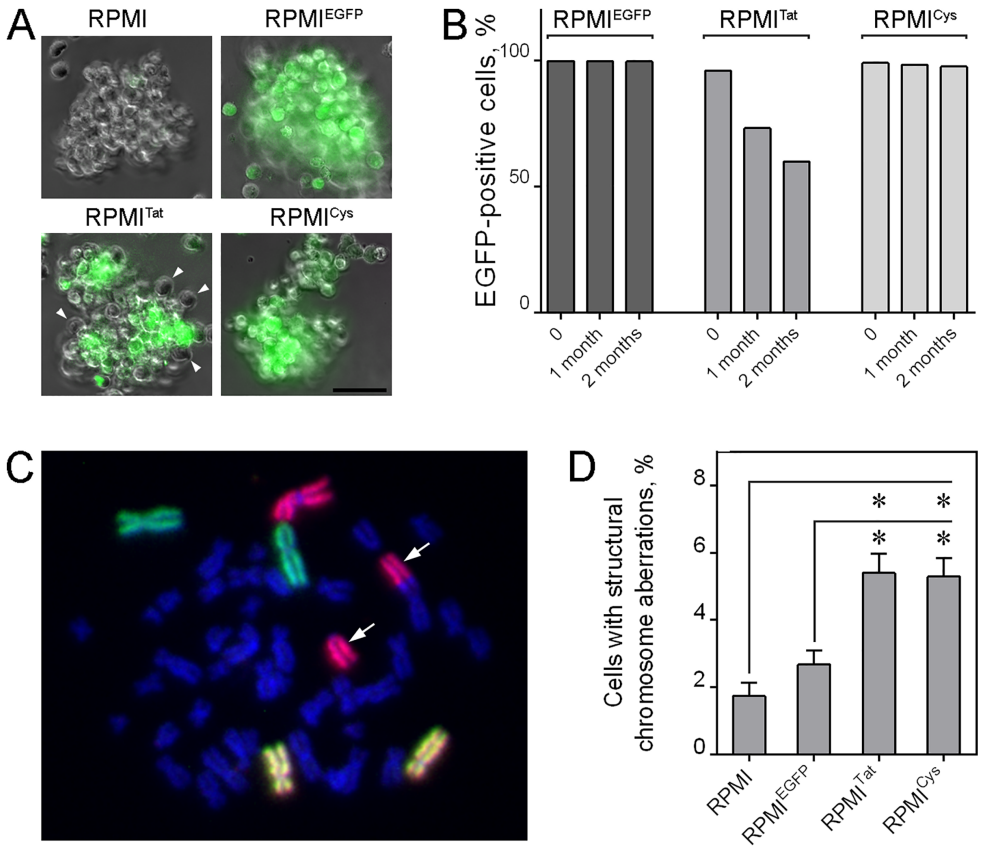

Figure 6 HIV-1 Tat influences cellular dynamics and chromosome organization upon prolonged cultivation. (A) Phase contrast images and EGFP fluorescence (merged) in RPMI, RPMI^{EGFP}, RPMI^{Tat}, and RPMI^{Cys} after 3 months of cultivation (representative images). In the RPMI^{Tat} line, there are ~40% cells without EGFP fluorescence (arrowheads). (B) The proportion of EGFP-positive cells was decreased during prolonged cultivation of RPMI^{Tat} but not RPMI^{EGFP} and RPMI^{Cys} cells (a representative experiment). (C) Representative image of a metaphase plate with detected chromosomes 1 (red), 2 (green) and 4 (orange). The chromosome with a translocation is marked with an arrow. (D) Cells expressing Tat-EGFP or TatC22G-EGFP contained a significantly higher proportion of chromosomes with aberrations (see Table S6 for a detailed description of chromosome aberrations). The comparison was performed using Fisher's exact test. An asterisk (*) indicates differences were considered statistically significant at $p < 0.01$. Full-size DOI: 10.7717/peerj.13986/fig-6

ex vivo experimental model, in which lymphocytes isolated from the blood of healthy donors were incubated in the presence of Tat protein (for example, (*Germini et al., 2017*)), or a model with the expression of HIV-1 controlled by an inducible promoter (for example, (*Reeder et al., 2015*)). These experimental systems are more likely to simulate an acute infection situation, but they do not allow for the study of weak long-term effects of protein and compensatory reactions of the cell. In the current study, we obtained the B lymphoid cell line RPMI 8866 stably expressing HIV-1 Tat fused with EGFP and used these cells to simulate a prolonged systemic effect of the presence of Tat in blood of chronically infected patients.

To detect possible changes provoked by chronic exposure of B-cells to Tat, we performed a genome-wide analysis of cellular gene expression (RNA-seq). Tat protein induces differential expression of approximately 1,000 genes (p.adj < 0.05 and fold change of ≥1.5 in any direction). To predict the effects of these changes, the analysis of metabolic and signaling pathways (GO BP and KEGG analysis) was performed. GO BP analysis demonstrated the activation of pathways involved in cellular antiviral reactions, and suppression of different metabolic pathways and proliferation. KEGG analysis also demonstrated activation of innate immunity pathways involved in antiviral reactions: *toll-like receptor signaling* and *NOD-like receptor signaling* pathways. We observed an increase in *JAK1* and *STAT1* expression, indicating that Tat may affect these pathways *via* the JAK-STAT signaling. Additionally, we found the reduction of Cytokine-cytokine receptor interaction pathway. Downregulation of this pathway (and downregulation of metabolic pathways and proliferation) may result from direct HIV-1 Tat action (proviral reactions). It should be noted however that not all cytokines and their receptors were downregulated. HIV-1 Tat induces the expression of several proinflammatory cytokines, mainly IL-6 in several cell types (*Ambrosino et al., 1997*; *Nookala & Kumar, 2014*; *Ben Haij et al., 2015*). Our results also confirm the upregulation of pro-inflammatory IL6 gene in Tat-expressing B cells. Thus, the gene expression pattern we observed in Tat-expressing B cells probably resulted from a combination of Tat action *per se* and cellular antiviral reactions.

We also analyzed the lncRNA expression. Differentially expressed lncRNAs accounted for 14.8% of all DEGs between $RPMI^{Tat}$ and the control cells. While functions of the majority of identified lncRNA are poorly studied, some of them (*e.g.*, NEAT1 and MALAT1) play a role in development of B-cell neoplasms (Table S5). In Tat-expressing RPMI 8866 cells, both of these lncRNAs were upregulated. It is possible that these or some other DE lncRNAs can be involved in the development of B-cell lymphomas in HIV-1-infected patients, but this requires further study.

Another important observation on the mode of action of Tat in host cells came from the comparison of the action of Tat and its TatC22G mutant with the reduced transactivation activity. In our experiments, 313 protein-coding genes were regulated by Tat only (115 upregulated and 198 downregulated, respectively), 228 genes were regulated by TatC22G only (117 upregulated and 111 downregulated genes), while the most genes (435) were regulated both by Tat and TatC22G (185 upregulated and 250 downregulated genes) (Fig. 4). HIV-1 Tat can modify cellular processes *via* different mechanisms. It can transactivate host genes by binding to TAR-like sequences (for example, this mechanism seems to regulate the transcription of *IL6* in T cells (*Ambrosino et al., 1997*) and *TNF-b* in B cells (*Buonaguro et al., 1994*)). Tat can also interact with chromatin and RNA-polymerase II (*Reeder et al., 2015*) as well as with hundreds of other cellular and nuclear proteins (*Gautier et al., 2009*). Therefore, to distinguish between the two potential modes of action of Tat, we compared the effects of HIV-1 Tat and that with the C22G mutation possessing a significantly decreased transactivation activity. We hypothesized that genes differentially expressed between $RPMI^{Tat}$ and $RPMI^{Cys}$ cells would be associated with the transactivator activity of this protein while genes similarly regulated would rather be affected by

protein-protein interactions involving Tat. The RNA-seq results demonstrated that most of the effects of EGFP-Tat and EGFP-TatC22G were similar, and hence, the main mechanism of prolonged Tat action on B-cells seems to be due to Tat interaction with host proteins.

We next analyzed some physiological parameters of RPMI^{Tat} cells. We could not find any manifested changes in cellular morphology, proliferation, or apoptosis. At the same time, we observed an effect of prolonged cultivation, *i.e.*, a decrease in EGFP-Tat-expressing cells, indicating that Tat inhibited cell growth. Thus, although there were no strong effects of EGFP-Tat expression, a weak effect, which manifested itself only in situations of long observation, was induced. Additionally, we found that chromosome aberrations occurred more frequently in cell lines expressing EGFP-Tat and EGFP-TatC22G. These observations are consistent with published data obtained using an *ex vivo* model (*El-Amine et al., 2018*). Modification of cell cycle progression and chromosome aberrations may both promote lymphomagenesis.

Thus, the presence of HIV-1 Tat can in the long run modify the cellular physiology and genome stability of cultured B cells and, as a result, may promote oncogenic transformation. The precise mechanisms of these effects will be the subject of our future work.

ACKNOWLEDGEMENTS

We are grateful to A.V. Lazarev for technical support. The following reagent was obtained through the NIH AIDS Reagent Program, Division of AIDS, NIAID, NIH: HIV-1 HXB2 GST-Tat Expression Vector (GST-Tat 1 (86R)) from Dr. Andrew Rice. This work was carried out within the framework of the International Research Network (IRN) ONCO3D and the IDB RAS Government basic research program (0088-2021-0007). The flow cytometry facility became available in the framework of the Moscow State University Development Program.

ADDITIONAL INFORMATION AND DECLARATIONS

Funding

This research was funded by the Russian Science Foundation (grant 21-74-20134 to Eugene V. Sheval) and the Russian Foundation for Basic Research (PhD student grant 20-34-90156 to Maria A. Tikhomirova). The funders had no role in study design, data collection and analysis, decision to publish, or preparation of the manuscript.

Grant Disclosures

The following grant information was disclosed by the authors:
Russian Science Foundation: 21-74-20134.
Russian Foundation for Basic Research: 20-34-90156.

Competing Interests

Yegor S. Vassetzky is an Academic Editor for PeerJ.

Author Contributions

- Anna A. Valyaeva performed the experiments, analyzed the data, prepared figures and/or tables, authored or reviewed drafts of the article, and approved the final draft.
- Maria A. Tikhomirova performed the experiments, analyzed the data, prepared figures and/or tables, authored or reviewed drafts of the article, and approved the final draft.
- Daria M. Potashnikova performed the experiments, prepared figures and/or tables, and approved the final draft.
- Alexandra N. Bogomazova performed the experiments, prepared figures and/or tables, authored or reviewed drafts of the article, and approved the final draft.
- Galina P. Snigiryova performed the experiments, prepared figures and/or tables, resources contribution, and approved the final draft.
- Aleksey A. Penin performed the experiments, analyzed the data, prepared figures and/or tables, and approved the final draft.
- Maria D. Logacheva performed the experiments, prepared figures and/or tables, and approved the final draft.
- Eugene A. Arifulin performed the experiments, prepared figures and/or tables, and approved the final draft.
- Anna A. Shmakova performed the experiments, analyzed the data, prepared figures and/or tables, authored or reviewed drafts of the article, and approved the final draft.
- Diego Germini performed the experiments, prepared figures and/or tables, and approved the final draft.
- Anastasia I. Kachalova performed the experiments, prepared figures and/or tables, and approved the final draft.
- Aleena A. Saidova performed the experiments, prepared figures and/or tables, and approved the final draft.
- Anastasia A. Zharikova performed the experiments, analyzed the data, prepared figures and/or tables, and approved the final draft.
- Yana R. Musinova performed the experiments, prepared figures and/or tables, and approved the final draft.
- Andrey A. Mironov conceived and designed the experiments, analyzed the data, prepared figures and/or tables, authored or reviewed drafts of the article, and approved the final draft.
- Yegor S. Vassetzky conceived and designed the experiments, analyzed the data, prepared figures and/or tables, authored or reviewed drafts of the article, and approved the final draft.
- Eugene V. Sheval conceived and designed the experiments, performed the experiments, analyzed the data, prepared figures and/or tables, authored or reviewed drafts of the article, and approved the final draft.

DNA Deposition

The following information was supplied regarding the deposition of DNA sequences:

GSE182538

Data Availability

The following information was supplied regarding data availability:

Original blot pictures are available in the Supplemental Files.

Supplemental Information

Supplemental information for this article can be found online at http://dx.doi.org/10.7717/peerj.13986#supplemental-information.

REFERENCES

Akbay B, Germini D, Bissenbaev AK, Musinova YR, Sheval EV, Vassetzky Y, Dokudovskaya S. 2021. HIV-1 Tat activates Akt/mTORC1 pathway and AICDA expression by downregulating its transcriptional inhibitors in B cells. *International Journal of Molecular Sciences* **22(4)**:1588 DOI 10.3390/ijms22041588.

Ali A, Mishra R, Kaur H, Chandra Banerjea A. 2021. HIV-1 Tat: an update on transcriptional and non-transcriptional functions. *Biochimie* **190**:24–35 DOI 10.1016/j.biochi.2021.07.001.

Altavilla G, Trabanelli C, Merlin M, Caputo A, Lanfredi M, Barbanti-Brodano G, Corallini A. 1999. Morphological, histochemical, immunohistochemical, and ultrastructural characterization of tumors and dysplastic and non-neoplastic lesions arising in BK virus/Tat transgenic mice. *The American Journal of Pathology* **154(4)**:1231–1244 DOI 10.1016/S0002-9440(10)65375-8.

Alves de Souza Rios L, Mapekula L, Mdletshe N, Chetty D, Mowla S. 2021. HIV-1 transactivator of transcription (Tat) co-operates with AP-1 factors to enhance c-MYC transcription. *Frontiers in Cell and Developmental Biology* **9**:161 DOI 10.3389/fcell.2021.693706.

Ambrosino C, Ruocco MR, Chen X, Mallardo M, Baudi F, Trematerra S, Quinto I, Venuta S, Scala G. 1997. HIV-1 Tat induces the expression of the interleukin-6 (IL6) gene by binding to the IL6 leader RNA and by interacting with CAAT enhancer-binding protein beta (NF-IL6) transcription factors. *The Journal of Biological Chemistry* **272(23)**:14883–14892 DOI 10.1074/jbc.272.23.14883.

Anders S, Pyl PT, Huber W. 2015. HTSeq—a Python framework to work with high-throughput sequencing data. *Bioinformatics* **31(2)**:166–169 DOI 10.1093/bioinformatics/btu638.

Ashburner M, Ball CA, Blake JA, Botstein D, Butler H, Cherry JM, Davis AP, Dolinski K, Dwight SS, Eppig JT, Harris MA, Hill DP, Issel-Tarver L, Kasarskis A, Lewis S, Matese JC, Richardson JE, Ringwald M, Rubin GM, Sherlock G. 2000. Gene ontology: tool for the unification of biology. The gene ontology consortium. *Nature Genetics* **25(1)**:25–29 DOI 10.1038/75556.

Atallah-Yunes SA, Murphy DJ, Noy A. 2020. HIV-associated Burkitt lymphoma. *The Lancet Haematology* **7(8)**:e594–e600 DOI 10.1016/S2352-3026(20)30126-5.

Autran B, Carcelain G, Li TS, Blanc C, Mathez D, Tubiana R, Katlama C, Debré P, Leibowitch J. 1997. Positive effects of combined antiretroviral therapy on CD4+ T cell homeostasis and function in advanced HIV disease. *Science* **277(5322)**:112–116 DOI 10.1126/science.277.5322.112.

Barboric M, Yik JHN, Czudnochowski N, Yang Z, Chen R, Contreras X, Geyer M, Matija Peterlin B, Zhou Q. 2007. Tat competes with HEXIM1 to increase the active pool of P-TEFb for HIV-1 transcription. *Nucleic Acids Research* **35(6)**:2003–2012 DOI 10.1093/nar/gkm063.

Ben Haij N, Planès R, Leghmari K, Serrero M, Delobel P, Izopet J, BenMohamed L, Bahraoui E. 2015. HIV-1 Tat protein induces production of proinflammatory cytokines by human dendritic cells and monocytes/macrophages through engagement of TLR4-MD2-CD14 complex and activation of NF-κB pathway. *PLOS ONE* **10(6)**:e0129425 DOI 10.1371/journal.pone.0129425.

Besson C, Lancar R, Prevot S, Algarte-Genin M, Delobel P, Bonnet F, Meyohas M-C, Partisani M, Oberic L, Gabarre J, Goujard C, Boue Fçois, Coppo P, Costello R, Hendel-Chavez H, Mekerri N, Dos Santos G, Recher C, Delarue R, Casasnovas R-O, Taoufik Y, Mounier N, Costagliola D. 2017. Outcomes for HIV-associated diffuse large B-cell lymphoma in the modern combined antiretroviral therapy era. *AIDS* **31(18)**:2493–2501 DOI 10.1097/QAD.0000000000001652.

Buonaguro L, Buonaguro FM, Giraldo G, Ensoli B. 1994. The human immunodeficiency virus type 1 Tat protein transactivates tumor necrosis factor beta gene expression through a TAR-like structure. *Journal of Virology* **68(4)**:2677–2682 DOI 10.1128/JVI.68.4.2677-2682.1994.

Carvallo L, Lopez L, Fajardo JE, Jaureguiberry-Bravo M, Fiser A, Berman JW. 2017. HIV-Tat regulates macrophage gene expression in the context of neuroAIDS. *PLOS ONE* **12(6)**:e0179882 DOI 10.1371/journal.pone.0179882.

Chen Q, Shen H, Zhu X, Liu Y, Yang H, Chen H, Xiong S, Chi H, Xu W. 2020. A nuclear lncRNA Linc00839 as a Myc target to promote breast cancer chemoresistance via PI3K/AKT signaling pathway. *Cancer Science* **111(9)**:3279–3291 DOI 10.1111/cas.14555.

Chong C, Müller M, Pak H, Harnett D, Huber F, Grun D, Leleu M, Auger A, Arnaud M, Stevenson BJ, Michaux J, Bilic I, Hirsekorn A, Calviello L, Simó-Riudalbas L, Planet E, Lubiński J, Bryśkiewicz M, Wiznerowicz M, Xenarios I, Zhang L, Trono D, Harari A, Ohler U, Coukos G, Bassani-Sternberg M. 2020. Integrated proteogenomic deep sequencing and analytics accurately identify non-canonical peptides in tumor immunopeptidomes. *Nature Communications* **11(1)**:1293 DOI 10.1038/s41467-020-14968-9.

Corallini A, Altavilla G, Pozzi L, Bignozzi F, Negrini M, Rimessi P, Gualandi F, Barbanti-Brodano G. 1993. Systemic expression of HIV-1 tat gene in transgenic mice induces endothelial proliferation and tumors of different histotypes. *Cancer Research* **53**:5569–5575.

Cozzi E, Neddermeyer A, Miliara S, Lennartsson A, Lehmann S. 2022. Identification of long non-coding RNAs involved in leukemogenesis and venetoclax response in acute myeloid leukemia through functional CRISPR-dCas9 interference screens. *Available at http://urn.kb.se/resolve?urn=urn:nbn:se:uu:diva-469815*.

Dolcetti R, Gloghini A, Caruso A, Carbone A. 2016. A lymphomagenic role for HIV beyond immune suppression? *Blood* **127(11)**:1403–1409 DOI 10.1182/blood-2015-11-681411.

D'Orso I, Frankel AD. 2010. RNA-mediated displacement of an inhibitory snRNP complex activates transcription elongation. *Nature Structural & Molecular Biology* **17(7)**:815–821 DOI 10.1038/nsmb.1827.

El-Amine R, Germini D, Zakharova VV, Tsfasman T, Sheval EV, Louzada RAN, Dupuy C, Bilhou-Nabera Cèle, Hamade A, Najjar F, Oksenhendler E, Lipinski Mc, Chernyak BV, Vassetzky YS. 2018. HIV-1 Tat protein induces DNA damage in human peripheral blood B-lymphocytes via mitochondrial ROS production. *Redox Biology* **15**:97–108 DOI 10.1016/j.redox.2017.11.024.

Ensoli B, Barillari G, Salahuddin SZ, Gallo RC, Wong-Staal F. 1990. Tat protein of HIV-1 stimulates growth of cells derived from Kaposi's sarcoma lesions of AIDS patients. *Nature* **345(6270)**:84–86 DOI 10.1038/345084a0.

Fan Q, Liu B. 2016. Identification of a RNA-seq based 8-long non-coding RNA signature predicting survival in esophageal cancer. *Medical Science Monitor* **22**:5163–5172 DOI 10.12659/MSM.902615.

Fritsch L, Marechal V, Schneider V, Barthet C, Rozenbaum W, Moisan-Coppey M, Coppey J, Nicolas JC. 1998. Production of HIV-1 by human B cells infected in vitro: characterization of an EBV genome-negative B cell line chronically synthetizing a low level of HIV-1 after infection. *Virology* **244(2)**:542–551 DOI 10.1006/viro.1998.9120.

Gautier VW, Gu L, O'Donoghue N, Pennington S, Sheehy N, Hall WW. 2009. In vitro nuclear interactome of the HIV-1 Tat protein. *Retrovirology* **6(1)**:47 DOI 10.1186/1742-4690-6-47.

Germini D, Tsfasman T, Klibi M, El-Amine R, Pichugin A, Iarovaia OV, Bilhou-Nabera C, Subra F, Bou Saada Y, Sukhanova A, Boutboul D, Raphaël M, Wiels J, Razin SV, Bury-Moné S, Oksenhendler E, Lipinski M, Vassetzky YS. 2017. HIV Tat induces a prolonged MYC relocalization next to IGH in circulating B-cells. *Leukemia* **31**:2515–2522 DOI 10.1038/leu.2017.106.

Gloghini A, Dolcetti R, Carbone A. 2013. Lymphomas occurring specifically in HIV-infected patients: from pathogenesis to pathology. *Seminars in Cancer Biology* **23(6)**:457–467 DOI 10.1016/j.semcancer.2013.08.004.

Gong S, Xu M, Zhang Y, Shan Y, Zhang H. 2020. The prognostic signature and potential target genes of six long non-coding RNA in laryngeal squamous cell carcinoma. *Frontiers in genetics* **11**:413 DOI 10.3389/fgene.2020.00413.

Gorwood J, Ejlalmanesh T, Bourgeois C, Mantecon M, Rose C, Atlan M, Desjardins D, Le Grand R, Fève B, Lambotte O, Capeau J, Béréziat V, Lagathu C. 2020. SIV infection and the HIV proteins Tat and nef induce senescence in adipose tissue and human adipose stem cells, resulting in adipocyte dysfunction. *Cells* **9(4)**:854 DOI 10.3390/cells9040854.

He N, Liu M, Hsu J, Xue Y, Chou S, Burlingame A, Krogan NJ, Alber T, Zhou Q. 2010. HIV-1 Tat and host AFF4 recruit two transcription elongation factors into a bifunctional complex for coordinated activation of HIV-1 transcription. *Molecular Cell* **38(3)**:428–438 DOI 10.1016/j.molcel.2010.04.013.

Herrmann CH, Rice AP. 1993. Specific interaction of the human immunodeficiency virus Tat proteins with a cellular protein kinase. *Virology* **197(2)**:601–608 DOI 10.1006/viro.1993.1634.

Herrmann CH, Rice AP. 1995. Lentivirus Tat proteins specifically associate with a cellular protein kinase, TAK, that hyperphosphorylates the carboxyl-terminal domain of the large subunit of RNA polymerase II: candidate for a Tat cofactor. *Journal of Virology* **69(3)**:1612–1620 DOI 10.1128/jvi.69.3.1612-1620.1995.

HIV-CAUSAL Collaboration, Ray M, Logan R, Sterne JAC, Hernández-Díaz S, Robins JM, Sabin C, Bansi L, van Sighem A, de Wolf F, Costagliola D, Lanoy E, Bucher HC, von Wyl V, Esteve A, Casbona J, del Amo J, Moreno S, Justice A, Goulet J, Lodi S, Phillips A, Seng R, Meyer L, Pérez-Hoyos S, García de Olalla P, Hernán MA. 2010. The effect of combined antiretroviral therapy on the overall mortality of HIV-infected individuals. *AIDS* **24(1)**:123–137 DOI 10.1097/QAD.0b013e3283324283.

Hübel K. 2020. The changing landscape of lymphoma associated with HIV infection. *Current Oncology Reports* **22(11)**:111 DOI 10.1007/s11912-020-00973-0.

Ivashkiv LB, Donlin LT. 2014. Regulation of type I interferon responses. *Nature Reviews Immunology* **14(1)**:36–49 DOI 10.1038/nri3581.

Jiang Y, Chai L, Fasae MB, Bai Y. 2018. The role of HIV Tat protein in HIV-related cardiovascular diseases. *Journal of Translational Medicine* **16(1)**:121 DOI 10.1186/s12967-018-1500-0.

Jin C, Peng X, Xie T, Lu X, Liu F, Wu H, Yang Z, Wang J, Cheng L, Wu N. 2016. Detection of the long noncoding RNAs nuclear-enriched autosomal transcript 1 (NEAT1) and metastasis associated lung adenocarcinoma transcript 1 in the peripheral blood of HIV-1-infected patients. *HIV Medicine* **17(1)**:68–72 DOI 10.1111/hiv.12276.

Kanehisa M, Goto S. 2000. KEGG: Kyoto Encyclopedia of Genes and Genomes. *Nucleic Acids Research* **28(1)**:27–30 DOI 10.1093/nar/28.1.27.

Kao SY, Calman AF, Luciw PA, Peterlin BM. 1987. Anti-termination of transcription within the long terminal repeat of HIV-1 by Tat gene product. *Nature* **330(6147)**:489–493 DOI 10.1038/330489a0.

Katano H, Sato Y, Hoshino S, Tachikawa N, Oka S, Morishita Y, Ishida T, Watanabe T, Rom WN, Mori S, Sata T, Weiden MD, Hoshino Y. 2007. Integration of HIV-1 caused STAT3-associated B cell lymphoma in an AIDS patient. *Microbes and Infection/Institut Pasteur* **9(14–15)**:1581–1589 DOI 10.1016/j.micinf.2007.09.008.

Kim D, Langmead B, Salzberg SL. 2015. HISAT: a fast spliced aligner with low memory requirements. *Nature Methods* **12(4)**:357–360 DOI 10.1038/nmeth.3317.

Krackhardt AM, Witzens M, Harig S, Hodi FS, Zauls AJ, Chessia M, Barrett P, Gribben JG. 2002. Identification of tumor-associated antigens in chronic lymphocytic leukemia by SEREX. *Blood* **100(6)**:2123–2131 DOI 10.1182/blood-2002-02-0513.

Kundu RK, Sangiorgi F, Wu LY, Pattengale PK, Hinton DR, Gill PS, Maxson R. 1999. Expression of the human immunodeficiency virus-Tat gene in lymphoid tissues of transgenic mice is associated with B-cell lymphoma. *Blood* **94(1)**:275–282 DOI 10.1182/blood.V94.1.275.413a30_275_282.

Kurnaeva MA, Zalevsky AO, Arifulin EA, Lisitsyna OM, Tvorogova AV, Shubina MY, Bourenkov GP, Tikhomirova MA, Potashnikova DM, Kachalova AI, Musinova YR, Golovin AV, Vassetzky YS, Sheval EV. 2022. Molecular coevolution of nuclear and nucleolar localization signals inside the basic domain of HIV-1 Tat. *Journal of Virology* **96(1)**:e0150521 DOI 10.1128/JVI.01505-21.

Lazzi S, Bellan C, De Falco G, Cinti C, Ferrari F, Nyongo A, Claudio PP, Tosi GM, Vatti R, Gloghini A, Carbone A, Giordano A, Leoncini L, Tosi P. 2002. Expression of RB2/p130 tumor-suppressor gene in AIDS-related non-Hodgkin's lymphomas: implications for disease pathogenesis. *Human Pathology* **33(7)**:723–731 DOI 10.1053/hupa.2002.125372.

Li H, An X, Li Q, Yu H, Li Z. 2021. Construction and analysis of competing endogenous RNA network of MCF-7 breast cancer cells based on the inhibitory effect of 6-thioguanine on cell proliferation. *Oncology Letters* **21(2)**:104 DOI 10.3892/ol.2020.12365.

Li H, Gao J, Liu L, Zhang S. 2022. LINC00958: A promising long non-coding RNA related to cancer. *Biomedicine & Pharmacotherapy* **151(9)**:113087 DOI 10.1016/j.biopha.2022.113087.

Love MI, Huber W, Anders S. 2014. Moderated estimation of fold change and dispersion for RNA-seq data with DESeq2. *Genome Biology* **15(12)**:550 DOI 10.1186/s13059-014-0550-8.

Marban C, Su T, Ferrari R, Li B, Vatakis D, Pellegrini M, Zack JA, Rohr O, Kurdistani SK. 2011. Genome-wide binding map of the HIV-1 Tat protein to the human genome. *PLOS ONE* **6(11)**:e26894 DOI 10.1371/journal.pone.0026894.

Marino J, Maubert ME, Mele AR, Spector C, Wigdahl B, Nonnemacher MR. 2020. Functional impact of HIV-1 Tat on cells of the CNS and its role in HAND. *Cellular and Molecular Life Sciences* **77(24)**:5079–5099 DOI 10.1007/s00018-020-03561-4.

Mateen FJ, Shinohara RT, Carone M, Miller EN, McArthur JC, Jacobson LP, Sacktor N, For the Multicenter AIDS Cohort Study (MACS) Investigators. 2012. Neurologic disorders incidence

in HIV+ vs HIV- men: multicenter AIDS Cohort Study, 1996–2011. *Neurology* **79(18)**:1873–1880 DOI 10.1212/WNL.0b013e318271f7b8.

McCune JM, Fu SM, Kunkel HG. 1981. J chain biosynthesis in pre-B cells and other possible precursor B cells. *Journal of Experimental Medicine* **154(1)**:138–145 DOI 10.1084/jem.154.1.138.

Mohammed A, Biegert G, Adamec J, Helikar T. 2017. Identification of potential tissue-specific cancer biomarkers and development of cancer versus normal genomic classifiers. *Oncotarget* **8(49)**:85692–85715 DOI 10.18632/oncotarget.21127.

Muniz L, Egloff S, Ughy B, Jády BE, Kiss T. 2010. Controlling cellular P-TEFb activity by the HIV-1 transcriptional transactivator Tat. *PLOS Pathogens* **6(10)**:e1001152 DOI 10.1371/journal.ppat.1001152.

Musinova YR, Sheval EV, Dib C, Germini D, Vassetzky YS. 2016. Functional roles of HIV-1 Tat protein in the nucleus. *Cellular and Molecular Life Sciences* **73(3)**:589–601 DOI 10.1007/s00018-015-2077-x.

Nath A. 2015. Eradication of human immunodeficiency virus from brain reservoirs. *Journal of NeuroVirology* **21(3)**:227–234 DOI 10.1007/s13365-014-0291-1.

Nekhai S, Jeang K-T. 2006. Transcriptional and post-transcriptional regulation of HIV-1 gene expression: role of cellular factors for Tat and Rev. *Future Microbiology* **1(4)**:417–426 DOI 10.2217/17460913.1.4.417.

Nookala AR, Kumar A. 2014. Molecular mechanisms involved in HIV-1 Tat-mediated induction of IL-6 and IL-8 in astrocytes. *Journal of Neuroinflammation* **11(1)**:214 DOI 10.1186/s12974-014-0214-3.

Noy A. 2020. HIV lymphoma and burkitts lymphoma. *The Cancer Journal* **26(3)**:260–268 DOI 10.1097/PPO.0000000000000448.

Petri A, Dybkær K, Bøgsted M, Thrue CA, Hagedorn PH, Schmitz A, Bødker JS, Johnsen HE, Kauppinen S. 2015. Long noncoding RNA expression during human B-Cell development. *PLOS ONE* **10(9)**:e0138236 DOI 10.1371/journal.pone.0138236.

Pham VV, Salguero C, Khan SN, Meagher JL, Brown WC, Humbert N, de Rocquigny H, Smith JL, D'Souza VM. 2018. HIV-1 Tat interactions with cellular 7SK and viral TAR RNAs identifies dual structural mimicry. *Nature Communications* **9(1)**:4266 DOI 10.1038/s41467-018-06591-6.

Poggi A, Carosio R, Fenoglio D, Brenci S, Murdaca G, Setti M, Indiveri F, Scabini S, Ferrero E, Zocchi MR. 2004. Migration of V delta 1 and V delta 2 T cells in response to CXCR3 and CXCR4 ligands in healthy donors and HIV-1-infected patients: competition by HIV-1 Tat. *Blood* **103(6)**:2205–2213 DOI 10.1182/blood-2003-08-2928.

Pushkarsky T, Ward A, Ivanov A, Lin X, Sviridov D, Nekhai S, Bukrinsky MI. 2022. Abundance of Nef and p-Tau217 in brains of individuals diagnosed with HIV-associated neurocognitive disorders correlate with disease severance. *Molecular Neurobiology* **59(2)**:1088–1097 DOI 10.1007/s12035-021-02608-2.

Qu D, Sun W-W, Li L, Ma L, Sun L, Jin X, Li T, Hou W, Wang J-H. 2019. Long noncoding RNA MALAT1 releases epigenetic silencing of HIV-1 replication by displacing the polycomb repressive complex 2 from binding to the LTR promoter. *Nucleic Acids Research* **47(6)**:3013–3027 DOI 10.1093/nar/gkz117.

Raymond AD, Campbell-Sims TC, Khan M, Lang M, Huang MB, Bond VC, Powell MD. 2011. HIV Type 1 Nef is released from infected cells in CD45(+) microvesicles and is present in the plasma of HIV-infected individuals. *AIDS Research and Human Retroviruses* **27(2)**:167–178 DOI 10.1089/aid.2009.0170.

Reeder JE, Kwak Y-T, McNamara RP, Forst CV, D'Orso I. 2015. HIV Tat controls RNA Polymerase II and the epigenetic landscape to transcriptionally reprogram target immune cells. *eLife* **4**:e08955 DOI 10.7554/eLife.08955.048.

Rhim H, Echetebu CO, Herrmann CH, Rice AP. 1994. Wild-type and mutant HIV-1 and HIV-2 Tat proteins expressed in Escherichia coli as fusions with glutathione S-transferase. *Journal of Acquired Immune Deficiency Syndromes* **7**:1116–1121.

Sall FB, El Amine R, Markozashvili D, Tsfasman T, Oksenhendler E, Lipinski M, Vassetzky Y, Germini D. 2019. HIV-1 Tat protein induces aberrant activation of AICDA in human B-lymphocytes from peripheral blood. *Journal of Cellular Physiology* **234(9)**:15678–15685 DOI 10.1002/jcp.28219.

Sedore SC, Byers SA, Biglione S, Price JP, Maury WJ, Price DH. 2007. Manipulation of P-TEFb control machinery by HIV: recruitment of P-TEFb from the large form by Tat and binding of HEXIM1 to TAR. *Nucleic Acids Research* **35(13)**:4347–4358 DOI 10.1093/nar/gkm443.

Shmakova A, Germini D, Vassetzky Y. 2020. HIV-1, HAART and cancer: a complex relationship. *International Journal of Cancer* **146(10)**:2666–2679 DOI 10.1002/ijc.32730.

Subramanian A, Tamayo P, Mootha VK, Mukherjee S, Ebert BL, Gillette MA, Paulovich A, Pomeroy SL, Golub TR, Lander ES, Mesirov JP. 2005. Gene set enrichment analysis: a knowledge-based approach for interpreting genome-wide expression profiles. *Proceedings of the National Academy of Sciences of the United States of America* **102(43)**:15545–15550 DOI 10.1073/pnas.0506580102.

Supek F, Bošnjak M, Škunca N, Šmuc T. 2011. REVIGO summarizes and visualizes long lists of gene ontology terms. *PLOS ONE* **6(7)**:e21800 DOI 10.1371/journal.pone.0021800.

The Gene Ontology Consortium. 2017. Expansion of the Gene Ontology knowledgebase and resources. *Nucleic Acids Research* **45(D1)**:D331–D338 DOI 10.1093/nar/gkw1108.

Vogel J, Hinrichs SH, Napolitano LA, Ngo L, Jay G. 1991. Liver cancer in transgenic mice carrying the human immunodeficiency virus tat gene. *Cancer Research* **51**:6686–6690.

Vogel J, Hinrichs SH, Reynolds RK, Luciw PA, Jay G. 1988. The HIV tat gene induces dermal lesions resembling Kaposi's sarcoma in transgenic mice. *Nature* **335(6191)**:606–611 DOI 10.1038/335606a0.

Wang W, Guo M, Hu L, Cai J, Zeng Y, Luo J, Shu Z, Li W, Huang Z. 2012. The zinc finger protein ZNF268 is overexpressed in human cervical cancer and contributes to tumorigenesis via enhancing NF-κB signaling. *The Journal of biological chemistry* **287(51)**:42856–42866 DOI 10.1074/jbc.M112.399923.

Wang T, Yi R, Green LA, Chelvanambi S, Seimetz M, Clauss M. 2015. Increased cardiovascular disease risk in the HIV-positive population on ART: potential role of HIV-Nef and Tat. *Cardiovascular Pathology* **24(5)**:279–282 DOI 10.1016/j.carpath.2015.07.001.

Wang G, Zheng C. 2021. Zinc finger proteins in the host-virus interplay: multifaceted functions based on their nucleic acid-binding property. *FEMS Microbiology Reviews* **45(3)**:17 DOI 10.1093/femsre/fuaa059.

West JA, Davis CP, Sunwoo H, Simon MD, Sadreyev RI, Wang PI, Tolstorukov MY, Kingston RE. 2014. The long noncoding RNAs NEAT1 and MALAT1 bind active chromatin sites. *Molecular Cell* **55(5)**:791–802 DOI 10.1016/j.molcel.2014.07.012.

Westendorp MO, Frank R, Ochsenbauer C, Stricker K, Dhein J, Walczak H, Debatin KM, Krammer PH. 1995. Sensitization of T cells to CD95-mediated apoptosis by HIV-1 Tat and gp120. *Nature* **375(6531)**:497–500 DOI 10.1038/375497a0.

Xiao H, Neuveut C, Tiffany HL, Benkirane M, Rich EA, Murphy PM, Jeang KT. 2000. Selective CXCR4 antagonism by Tat: implications for in vivo expansion of coreceptor use by HIV-1.

Proceedings of the National Academy of Sciences of the United States of America **97(21)**:11466–11471 DOI 10.1073/pnas.97.21.11466.

Yu G, Wang L-G, Han Y, He Q-Y. 2012. clusterProfiler: an R package for comparing biological themes among gene clusters. *OMICS: A Journal of Integrative Biology* **16(5)**:284–287 DOI 10.1089/omi.2011.0118.

Yue H, Wu K, Liu K, Gou L, Huang A, Tang H. 2022. LINC02154 promotes the proliferation and metastasis of hepatocellular carcinoma by enhancing SPC24 promoter activity and activating the PI3K-AKT signaling pathway. *Cellular Oncology* **45(3)**:447–462 DOI 10.1007/s13402-022-00676-7.

Zhang Q, Chen C-Y, Yedavalli VSR, Jeang K-T. 2013. NEAT1 long noncoding RNA and paraspeckle bodies modulate HIV-1 posttranscriptional expression. *mBio* **4(1)**:e00596 DOI 10.1128/mbio.00596-12.

Zhang Y, Jin T, Shen H, Yan J, Guan M, Jin X. 2019. Identification of long non-coding RNA expression profiles and co-expression genes in thyroid carcinoma based on the cancer genome atlas (TCGA) database. *Medical Science Monitor* **25**:9752–9769 DOI 10.12659/MSM.917845.

Zhao Z, Wang D, Zhu C, Shao H, Sun C, Qiu H, Xue L, Xu J, Guo M, Li W. 2008. Aberrant alternative splicing of human zinc finger gene ZNF268 in human hematological malignancy. *Oncology Reports* **20**:1243–1248 DOI 10.3892/or_00000136.

Zhong F, Zhu M, Gao K, Xu P, Yang H, Hu D, Cui D, Wang M, Xie X, Wei Y, Zhang H, Du H. 2018. Low expression of the long non-coding RNA NR_026827 in gastric cancer. *American Journal of Translational Research* **10**:2706–2711.

Zuo S, Wang L, Wen Y, Dai G. 2018. Identification of a universal 6-lncRNA prognostic signature for three pathologic subtypes of renal cell carcinoma. *Journal of Cellular Biochemistry* **120(5)**:7375–7385 DOI 10.1002/jcb.28012.

Supplementary Figures

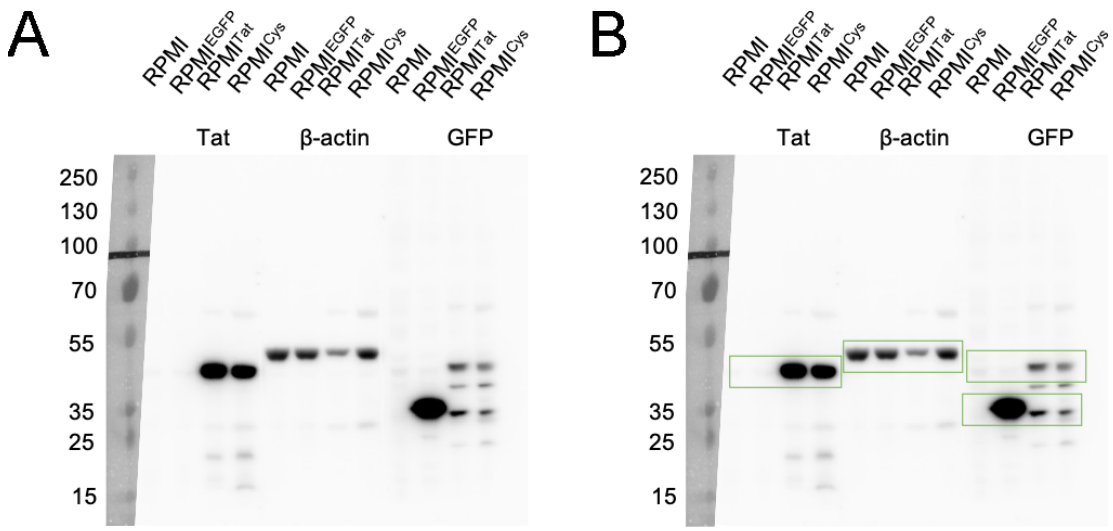

Figure S1. Nonprocessed images of the western blot experiment presented in Fig. 1C. (A) Nonprocessed image. (B) Image with the cropped regions of interest, which are presented in Fig. 1C.

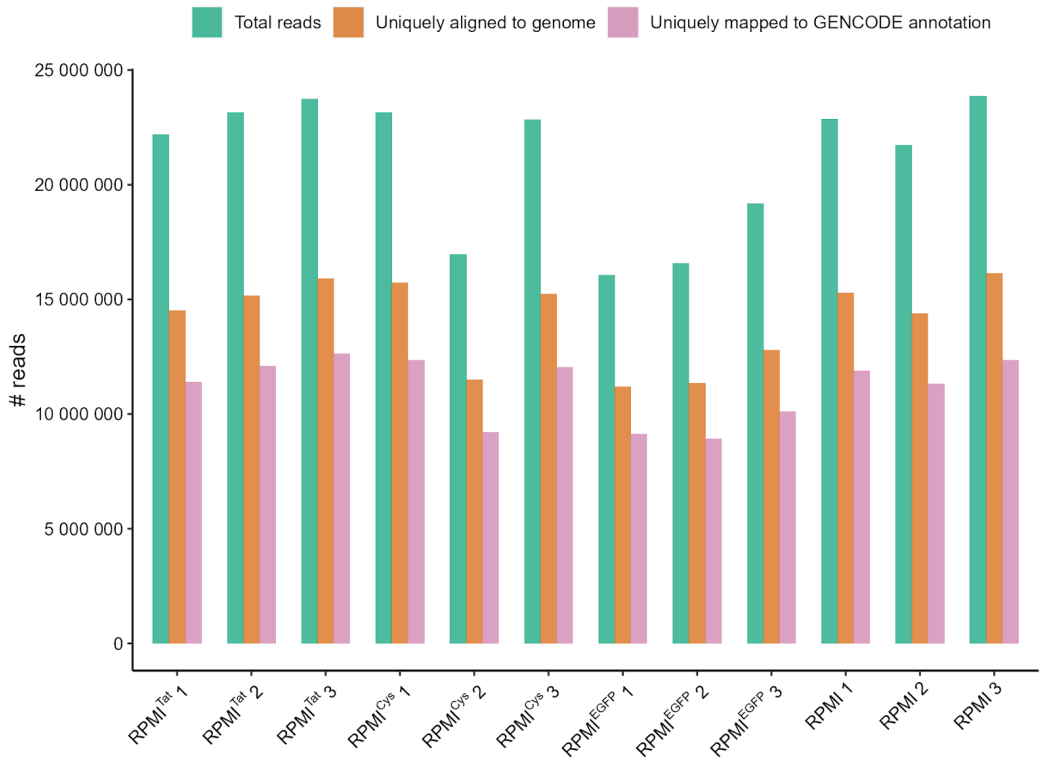

Figure S2. The number of reads at different stages of RNA-seq analysis: total reads obtained from RNA sequencing, reads that were uniquely aligned to the reference human genome GRCh38.p10, and reads that were unambiguously mapped to the GENCODE v26 gene annotation.

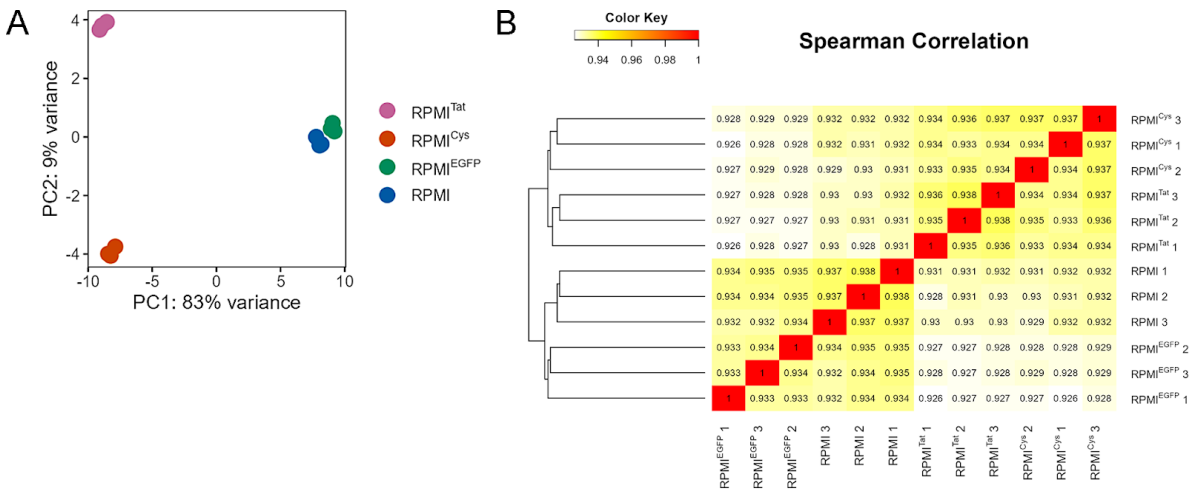

Figure S3. Quality control of the RNA-seq replicates. (A) PCA performed on regularized log-transformed filtered count data. (B) Heatmap of Spearman correlation coefficients between DESeq2-normalized gene expression profiles.

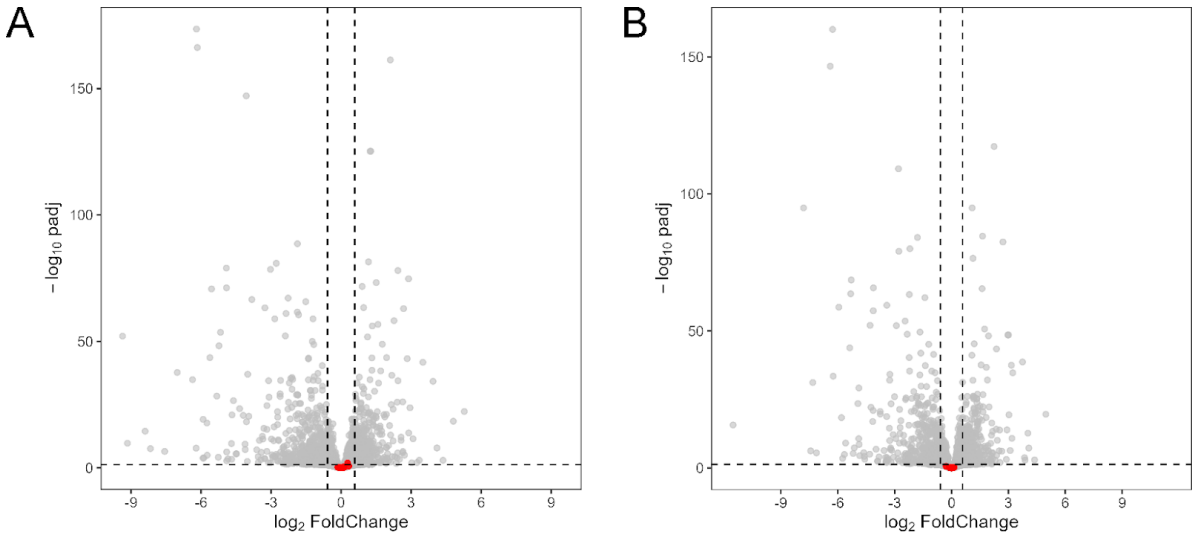

Figure S4. Tat protein had no impact on the expression of EBV genes in RPMI^{Tat} cells. The volcano plot shows the logarithm of the fold change in gene expression (along the X-axis) and the significance of the gene expression change (along the Y-axis). EBV genes are highlighted in red, and human genes are shown as gray dots. (A) RPMI^{Tat} cells. (B) RPMI^{Cys} cells.

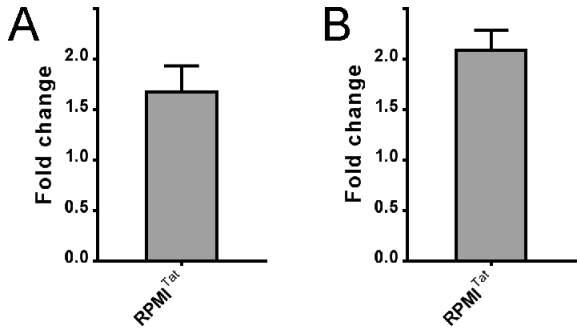

Figure S5. Validation of the RNA-seq dataset using qRT-PCR (mean ± SEM; n = 3). (A) MALAT1 gene. (B) NEAT1 gene.

Table S2. Primers used in this study.

NEAT 1_2	5'-GCTTATCCCACAGCACACAC-3' 5'-CTAAGTCCCAACCTGCCGAT-3'
MALAT1	5'-GACGGAGGTTGAGATGAAGC-3' 5'-ATTCGGGGCTCTGTAGTCCT-3'
UBC	5'-GTCGCAGCCGGGATTTGGGT-3' 5'-GTCAGACAGGGTGCGCCCAT-3'
YWHAZ	5'-ACTTTTGGTACATTGTGGCTTCAA-3' 5'-CCGCCAGGACAAACCAGTAT-3'
HPRT1	5'-TGTAATGACCAGTCAACAGGGGACA-3' 5'-TCCAACACTTCGTGGGGTCCT-3'
IL6R	5'-CTCCTGCCAGTTAGCAGTCC-3' 5'-TCTTGCCAGGTGACACTGAG-3'
IL2RB	5'-GCCCCCATCTCCCTCCAAGT-3' 5'-AGGGGAAGGGCGAAGAGAGC-3'
CCR4	5'-TGTTCACTGCTGCCTTAATCCCATC-3' 5'-TGGACTGCGTGTAAGATGAGCTGG-3'
IL1R	5'-CCTGCTATGATTTTCTCCCAATAAA-3' 5'- AACACAAAAATATCACAGTCAGAGGTAGAC-3'
IL21R	5'-GTGTGGATTCTCACCCCAGGC-3' 5'-TGCCTCATCTTCTGTTTCGGCT-3'
IL27R	5'-GTCTGCATGAATGTGAGTGGC-3' 5'-AACAGGAACAAGCCCCACAA-3'
IL17R	5'-GAGAGCCGACCGTTCAATGT-3' 5'-CTTCAACAAGCGGATGCTGG-3'
TLR8	5'-TGGGAAAGGAGACTAAAAAGGAAA-3' 5'-TCTGGTGCTGTACATTGGGG-3'

NLRP4	5’-CCTGGTATACCTGATGTTGGCT-3’ 5’-TCTCCGATTTCATTGCACCCA-3’
CCL3L1	5’-AGGTCCTCTCTGCACCACTT-3’ 5’-CTCTCTTGGTTAGGAAGATGACACT-3’
TLR7	5’-TGCCATCAAGAAAGTTGATGCTAT-3’ 5’-CAGAGTGACATCACAGGGCA-3’
STAT1	5’-GAACGGAGGCGAACCTGACT-3’ 5’-GCAAGGCTGGCTTGAGGTT-3’

Table S5

Differential expression of MALAT1 and NEAT1 lncRNAs in B-cell-derived neoplasms (Lnc2cancer 3.0 database, http://bio-bigdata.hrbmu.edu.cn/lnc2cancer/).

LncRNA	Cancer name	Expression pattern	Reference
MALAT1	chronic lymphocytic leukemia	up-regulated	(Ahmadi et al., 2018)
	mantle cell lymphoma	up-regulated	(Wang et al., 2016)
	myeloma	up-regulated	(Li et al., 2014; Cho et al., 2014; Ronchetti et al., 2016; Gao et al., 2017; Liu et al., 2017, 2020; Handa et al., 2017; Gu, Xiao & Yang, 2017; Hu et al., 2018; Sun et al., 2019)
		down-regulated	(Isin et al., 2014)
	diffuse large B-cell lymphoma	up-regulated	(Li et al., 2017)
NEAT1	chronic lymphocytic leukemia	up-regulated	(Blume et al., 2015; Ronchetti et al., 2020)
	multiple myeloma	up-regulated	(Wu & Wang, 2018; Taiana et al., 2020)
	diffuse large B-cell lymphoma	up-regulated	(Qian et al., 2020)
	Burkitt's lymphoma	up-regulated	(Blume et al., 2015)

References

Ahmadi A, Kaviani S, Yaghmaie M, Pashaiefar H, Ahmadvand M, Jalili M, Alimoghaddam K, Eslamijouybari M, Ghavamzadeh A. 2018. Altered expression of MALAT1 lncRNA in chronic lymphocytic leukemia patients, correlation with cytogenetic findings. *Blood research* **53:**320–324. DOI: 10.5045/br.2018.53.4.320.

Blume CJ, Hotz-Wagenblatt A, Hüllein J, Sellner L, Jethwa A, Stolz T, Slabicki M, Lee K, Sharathchandra A, Benner A, Dietrich S, Oakes CC, Dreger P, te Raa D, Kater AP, Jauch A, Merkel O, Oren M, Hielscher T, Zenz T. 2015. p53-dependent non-coding RNA networks in chronic lymphocytic leukemia. *Leukemia* **29:**2015–2023. DOI: 10.1038/leu.2015.119.

Cho S-F, Chang YC, Chang C-S, Lin S-F, Liu Y-C, Hsiao H-H, Chang J-G, Liu T-C. 2014. MALAT1 long non-coding RNA is overexpressed in multiple myeloma and may serve as a marker to predict disease progression. *BMC cancer* **14:**809. DOI: 10.1186/1471-2407-14-809.

Gao D, Lv A-E, Li H-P, Han D-H, Zhang Y-P. 2017. LncRNA MALAT-1 Elevates HMGB1 to Promote Autophagy Resulting in Inhibition of Tumor Cell Apoptosis in Multiple Myeloma. *Journal of cellular biochemistry* **118:**3341–3348. DOI: 10.1002/jcb.25987.

Gu Y, Xiao X, Yang S. 2017. LncRNA MALAT1 acts as an oncogene in multiple myeloma through sponging miR-509-5p to modulate FOXP1 expression. *Oncotarget* **8:**101984–101993. DOI: 10.18632/oncotarget.21957.

Handa H, Kuroda Y, Kimura K, Masuda Y, Hattori H, Alkebsi L, Matsumoto M, Kasamatsu T, Kobayashi N, Tahara K-I, Takizawa M, Koiso H, Ishizaki T, Shimizu H, Yokohama A, Tsukamoto N, Saito T, Murakami H. 2017. Long non-coding RNA MALAT1 is an inducible stress response gene associated with extramedullary spread and poor prognosis of multiple myeloma. *British journal of haematology* **179:**449–460. DOI: 10.1111/bjh.14882.

Hu Y, Lin J, Fang H, Fang J, Li C, Chen W, Liu S, Ondrejka S, Gong Z, Reu F, Maciejewski J, Yi Q, Zhao J-J. 2018. Targeting the MALAT1/PARP1/LIG3 complex induces DNA damage and apoptosis in multiple myeloma. *Leukemia* **32:**2250–2262. DOI: 10.1038/s41375-018-0104-2.

Isin M, Ozgur E, Cetin G, Erten N, Aktan M, Gezer U, Dalay N. 2014. Investigation of circulating lncRNAs in B-cell neoplasms. *Clinica chimica acta; international journal of clinical chemistry* **431:**255–259. DOI: 10.1016/j.cca.2014.02.010.

Li L-J, Chai Y, Guo X-J, Chu S-L, Zhang L-S. 2017. The effects of the long non-coding RNA MALAT-1 regulated autophagy-related signaling pathway on chemotherapy resistance in diffuse large B-cell lymphoma. *Biomedicine & pharmacotherapy = Biomedecine & pharmacotherapie* **89:**939–948. DOI: 10.1016/j.biopha.2017.02.011.

Li B, Chen P, Qu J, Shi L, Zhuang W, Fu J, Li J, Zhang X, Sun Y, Zhuang W. 2014. Activation of LTBP3 gene by a long noncoding RNA (lncRNA) MALAT1 transcript in mesenchymal stem cells from multiple myeloma. *The Journal of biological chemistry* **289:**29365–29375. DOI: 10.1074/jbc.M114.572693.

Liu N, Feng S, Li H, Chen X, Bai S, Liu Y. 2020. Long non-coding RNA MALAT1 facilitates the tumorigenesis, invasion and glycolysis of multiple myeloma via miR-1271-5p/SOX13 axis. *Journal of cancer research and clinical oncology* **146:**367–379. DOI: 10.1007/s00432-020-03127-8.

Liu H, Wang H, Wu B, Yao K, Liao A, Miao M, Li Y, Yang W. 2017. Down-regulation of long non-coding RNA MALAT1 by RNA interference inhibits proliferation and induces apoptosis in multiple myeloma. *Clinical and experimental pharmacology & physiology* **44:**1032–1041. DOI: 10.1111/1440-1681.12804.

Qian C-S, Li L-J, Huang H-W, Yang H-F, Wu D-P. 2020. MYC-regulated lncRNA NEAT1 promotes B cell proliferation and lymphomagenesis via the miR-34b-5p-GLI1 pathway in diffuse large B-cell lymphoma. *Cancer cell international* **20:**87. DOI: 10.1186/s12935-020-1158-6.

Ronchetti D, Agnelli L, Taiana E, Galletti S, Manzoni M, Todoerti K, Musto P, Strozzi F, Neri A. 2016. Distinct lncRNA transcriptional fingerprints characterize progressive stages of multiple myeloma. *Oncotarget* **7:**14814–14830. DOI: 10.18632/oncotarget.7442.

Ronchetti D, Favasuli V, Monti P, Cutrona G, Fabris S, Silvestris I, Agnelli L, Colombo M, Menichini P, Matis S, Gentile M, Nurtdinov R, Guigó R, Baldini L, Fronza G, Ferrarini M, Morabito F, Neri A, Taiana E. 2020. NEAT1 Long Isoform Is Highly Expressed in Chronic Lymphocytic Leukemia Irrespectively of Cytogenetic Groups or Clinical Outcome. *Non-coding RNA* **6:**11. DOI: 10.3390/ncrna6010011.

Sun Y, Jiang T, Jia Y, Zou J, Wang X, Gu W. 2019. LncRNA MALAT1/miR-181a-5p affects the proliferation and adhesion of myeloma cells via regulation of Hippo-YAP signaling pathway. *Cell cycle* **18:**2509–2523. DOI: 10.1080/15384101.2019.1652034.

Taiana E, Favasuli V, Ronchetti D, Todoerti K, Pelizzoni F, Manzoni M, Barbieri M, Fabris S, Silvestris I, Gallo Cantafio ME, Platonova N, Zuccalà V, Maltese L, Soncini D, Ruberti S, Cea M, Chiaramonte R, Amodio N, Tassone P, Agnelli L, Neri A. 2020. Long non-coding RNA NEAT1 targeting impairs the DNA repair machinery and triggers anti-tumor activity in multiple myeloma. *Leukemia* **34:**234–244. DOI: 10.1038/s41375-019-0542-5.

Wang X, Sehgal L, Jain N, Khashab T, Mathur R, Samaniego F. 2016. LncRNA MALAT1 promotes development of mantle cell lymphoma by associating with EZH2. *Journal of translational medicine* **14:**346. DOI: 10.1186/s12967-016-1100-9.

Wu Y, Wang H. 2018. LncRNA NEAT1 promotes dexamethasone resistance in multiple myeloma by targeting miR-193a/MCL1 pathway. *Journal of biochemical and molecular toxicology* **32.** DOI: 10.1002/jbt.22008.

Another notable observation from this study was the downregulation of genes encoding the components MHC class II receptor (*HLA-DRB1*, *HLA-DRB5*, *HLA-DQA1*, and *HLA-DQB1*) by HIV-1 Tat in B cells (**Figure 18**). We further confirmed that this downregulation was observed on the protein level by analyzing the population of RPMI8866^{Tat} cells by immunofluorescent staining of HLA-DR. Although these lines are stable, Tat expression was quite heterogeneous in the cells. A representative image of cells with different Tat expression levels is presented in **Figure 19A**. We analyzed the mean fluorescence intensity of Tat in each cell nucleus in a cell population and compared it with the mean fluorescence intensity of HLA-DR on the cell surface. Cells were then divided into two distinct groups: "Tat^{low}" and "Tat^{high}" according to the mean fluorescence intensity of Tat in each nucleus. The mean fluorescence intensity of HLA-DR was significantly lower in "Tat^{high}" cells relative to "Tat^{low}" cells (p = 0.0463, t-test, **Figure 19B**). Thus, HIV-1 Tat presence decreases HLA-DR expression in B cells.

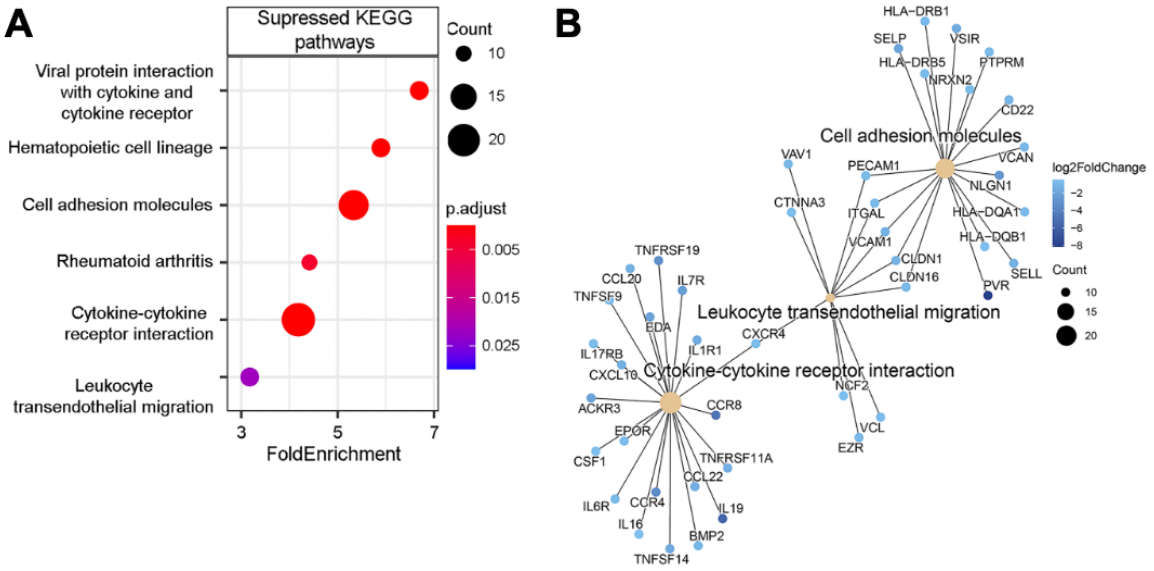

Figure 18. Enrichment analysis of differentially expressed genes negatively regulated by Tat in RPMI8866 cells. (A) KEGG pathways negatively regulated by Tat, identified by overrepresentation analysis of protein-coding differentially expressed genes. Only significantly enriched (adjusted p-value < 0.05) KEGG pathways are shown. (B) Suppressed KEGG pathways (hsa04514, hsa04060, and hsa04670) and associated differentially expressed genes after filtering overlapping gene sets. Figure from (Valyaeva et al. 2022).

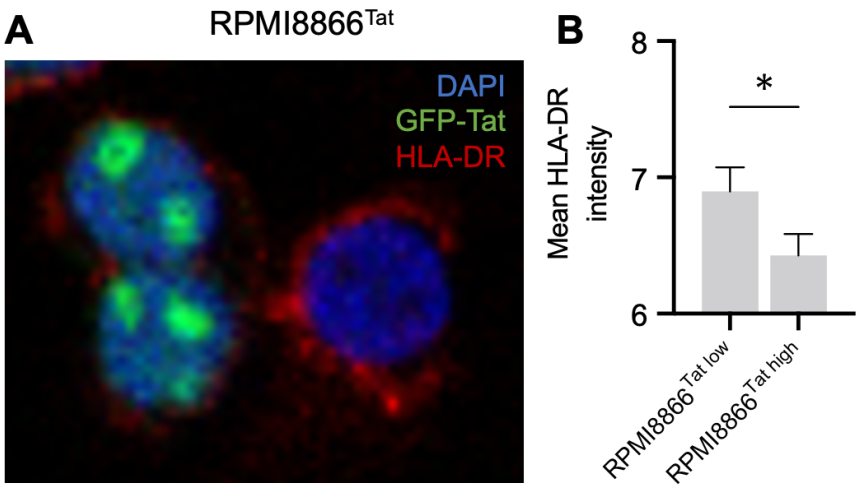

Figure 19. HIV-1 Tat decreases HLA-DR expression in B cells. (A) A representative confocal image of cells with different Tat expression levels in RPMI8866^{Tat} cell line (green fluorescence). Immunofluorescent staining with antibodies against HLA-DR (red fluorescence). Nuclei were counterstained with DAPI (blue fluorescence). (H) The mean fluorescence intensity of HLA-DR around the cell nucleus (cell surface) in "Tat^{high}" and "Tat^{low}" cells (n > 600 cells). Cells were divided by half into two groups according to the mean fluorescence intensity of Tat in each nucleus. * $p < 0.05$, t-test.

The MHC class II receptor mediates antigen presentation to CD4+ T cells by antigen-presenting cells (DCs, macrophages, and B cells), and thus plays a crucial role in initiating an adaptive immune response (Roche & Furuta 2015). By binding antigenic peptides produced from the proteolysis of both self and non-self proteins in endosomes and lysosomes, MHC class II presents these antigens to antigen-specific CD4+ T cells (Roche & Furuta 2015). Together with antibody production, these are the two primary functions of B cells in the immune system. Altered antigen processing and presentation is a common feature of B cell malignancies (McShane & Malinova 2022). The downregulation of MHC class II genes in B cells by HIV-1 Tat could have significant implications for the immune response and may contribute to immune evasion of EBV-infected B cells or malignantly transformed B cells in individuals with HIV. The findings of this study underscore the complex and multifaceted impact of HIV-1 Tat on B cell physiology and immune responses.

3.2.3 HIV-1 Tat downregulates the expression of HLA-DR genes in B cells and impairs EBV-specific CD4+ T cell response

Understanding the mechanisms through which Tat influences MHC class II expression and whether it might have some functional consequences for immune evasion may provide insights into the pathogenesis of HIV-associated B cell lymphomas. We thus proceeded with a more detailed analysis of the role of HIV-1 Tat in the regulation of HLA-DR expression in B cells (**Article 9**).

In order to simulate the chronic presence of Tat in B cells, we used two EBV-immortalized lymphoblastoid B cell lines (RPMI8866 and BLAS, a B lymphoblastoid cell line recently immortalized from a healthy donor) and ectopically expressed HIV-1 Tat. We also used a mutant form of Tat (HIV-1 TatC22G) that lacks transactivation activity. We next used RNA-sequencing analysis to examine the modifications brought about by Tat expression in B cells. The findings demonstrated that HIV-1 Tat affected the expression of hundreds of genes in B cells, including the downregulation of a subset of MHC class II-related genes. Tat suppressed *HLA-DRB1* and *HLA-DRB5* gene expression, which reduced the surface expression of HLA-DR molecules on B cells. This effect was replicated when we co-cultured B cells with Jurkat T cells that expressed Tat. We also looked at a group of HIV-positive individuals to validate their findings. *HLA-DRB1* downregulation was discovered in B cells from HIV-positive individuals. Using IFNγ production analysis and cytotoxicity assay, we also assessed the effect of Tat on the CD4+ T cell EBV-specific. Tat-induced downregulation of HLA-DR in B cells impaired CD4+ T cells' ability to recognize EBV-transformed B cells (reduced IFNγ production and cytotoxic cell lysis), which might result in immune evasion and a higher risk of developing B cell lymphoma in HIV-positive individuals.

In conclusion, we propose that long-term HIV-1 Tat exposure modifies the physiology of B cells by inhibiting the expression of HLA-DR, which confers protection against CD4+ T cell identification (**Figure 20**). In HIV-positive individuals, this compromised immune response may help to promote the growth of EBV-associated B-cell lymphomas. It may be possible to develop new treatment approaches to prevent or treat B-cell malignancies in this population by comprehending the molecular mechanisms driving these interactions.

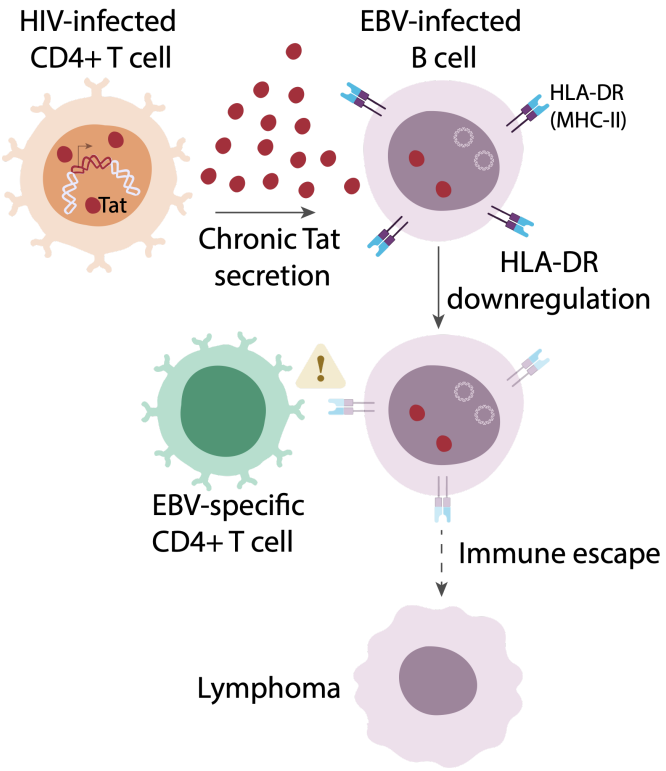

Figure 20. Chronic exposure to Tat, which can be secreted from infected CD4+ T cells and penetrate into non-infected cells, led to the downregulation of HLA-DR expression in B cells, impairing their recognition by CD4+ T cells. This could potentially promote immune evasion and increase the risk of B-cell lymphoma in people living with HIV.

Article 9. Research paper "Chronic HIV-1 Tat action induces HLA-DR downregulation in B cells: a mechanism for lymphoma immune escape in people living with HIV"

Chronic HIV-1 Tat action induces HLA-DR downregulation in B cells: a mechanism for lymphoma immune escape in people living with HIV

(manuscript in preparation)

Anna Shmakova[1,2], Coline Hugot[1†], Yana Kozhevnikova[1†], Anna Schwager (Karpukhina)[1,2], Ivan Tsimailo[1], Laurence Gerard[3], David Boutboul[3], Eric Oksenhendler[3], Olga Szewczyk-Roszczenko[4], Piotr Roszczenko[5], Kamila Buzun[5], Eugene V. Sheval[7,8], Bruno Beaumelle[6], Diego Germini[1], Yegor Vassetzky[1,2,*]

[1]CNRS, UMR 9018, Université Paris-Saclay, Institut Gustave Roussy, 94800 Villejuif, France;

[2]Koltzov Institute of Developmental Biology, 119334 Moscow, Russia;

[3]Service d'Immunopathologie Clinique, Hôpital St Louis, APHP, 75012 Paris, France;

[4]Department of Synthesis and Technology of Drugs, Medical University of Bialystok, 15-089 Bialystok, Poland;

[5]Department of Biotechnology, Medical University of Bialystok, 15-089 Bialystok, Poland;

[6]Institut de Recherche en Infectiologie de Montpellier Université de Montpellier, CNRS UMR 9004, Montpellier, France;

[7]Belozersky Institute of Physico-Chemical Biology, Lomonosov Moscow State University, 119991 Moscow, Russia;

[8]Department of Cell Biology and Histology, School of Biology, Lomonosov Moscow State University, 119991 Moscow, Russia

*Corresponding author: yegor.vassetzky@cnrs.fr

†These authors contributed equally

Abstract

Background. Despite the success of combination antiretroviral therapy (cART), people living with HIV still have an increased risk of EBV-associated B-cell malignancies. In the HIV setting, B cell physiology is altered by co-existence with HIV-infected cells and the chronic action of secreted viral proteins, *e.g.* HIV-1 Tat that, once released, efficiently penetrates non-infected cells. We hypothesized that the chronic action of HIV-1 Tat on B cells can contribute to B cell lymphomagenesis.

Methods. We modelled the chronic action of HIV-1 Tat on B cells by ectopically expressing Tat or its mutant version TatC22G deprived of transactivation activity in two EBV-immortalized lymphoblastoid B cell lines and analysed the induced changes *via* an RNA-sequencing analysis, RT-qPCR, western blotting and immunofluorescent staining. A cohort of people with HIV was analysed to confirm the results. EBV-specific CD4+ T cell response was evaluated using IFNγ production analysis and cytotoxicity assay.

Results. The RNA-sequencing analysis revealed that Tat regulated the expression of hundreds of genes in B cells, including the downregulation of a subset of genes related to MHC class II. Tat-induced transcriptional downregulation of *HLA-DRB1* and *HLA-DRB5* genes was accompanied by a decrease in HLA-DR surface expression; this effect could be reproduced by co-culturing B cells with Tat-expressing T cells. Notably, *HLA-DRB1* expression in B cells was also decreased in people living with HIV. Chronic Tat presence decreased the NF-κB pathway activity; this downregulated NF-κB-dependent

transcriptional targets, including MHC class II genes. Tat-induced HLA-DR downregulation in B cells also impaired EBV-specific CD4+ T cell response, which contributed to the escape from immune surveillance and could eventually promote B cell lymphomagenesis.

Conclusions. HIV-1 Tat transcriptionally downregulated the HLA-DR expression in B cells, which led to a decrease in CD4+ T cells recognition of EBV-transformed B cells, leading to immune evasion and B cell lymphoma predisposition in people living with HIV.

Keywords: HIV-1, EBV, Tat, MHC class II, B cells, CD4+ T cells, NF-κB pathway RNA-sequencing.

Background

Over 38 million people worldwide are infected with the human immunodeficiency virus (HIV) (http://www.who.int/hiv/en/) [1]. People living with HIV experience marked improvements in terms of mortality and quality of life since the introduction of combination antiretroviral therapy (cART) in 1996 that blocks HIV replication and restores CD4+ T cell counts [2]. Nevertheless, the high prevalence of certain types of malignancies, such as B cell lymphomas [3], even after the successful introduction of cART suggests a possible role of factors other than immune suppression in the pathogenesis of HIV-associated cancers.

Compared to the general population, people living with HIV are 12 times more likely to be diagnosed with B cell non-Hodgkin lymphomas, including diffuse large B-cell lymphoma (DLBCL) and Burkitt lymphoma (BL), and eight times more likely to be diagnosed with Hodgkin lymphoma [4]. The molecular mechanisms of these lymphomas are quite different, which implies that there might be a common B cell

lymphoma-predisposing factor in people with HIV. It was recently shown that even defective HIV proviruses (>95% of proviruses in the peripheral blood of people living with HIV under cART are defective, i.e. incapable of virus production) still produce viral proteins [5]. Among them, the HIV transactivator of transcription (Tat) protein is particularly interesting, since it is actively released by infected cells [6], can be found in the bloodstream (at concentrations ranging from 10 ng/ml to 550 ng/ml) [7,8] and in the cerebrospinal fluid (at concentrations ranging from 200 pg/ml to 6.5 ng/ml) [9] in PWLH under cART. Due to its cell-penetration capacities, Tat efficiently penetrates neighbouring cells [6]. Tat presence at high levels was detected in HIV-1-associated B cell lymphomas (BL, DLBCL) [10–12].

In infected cells, Tat activates HIV transcription through the release of a positive transcription elongation factor b (P-TEFb) from its inactive state bound to the inhibitory 7SK small nuclear ribonucleoprotein complex and recruitment of active P-TEFb to the HIV trans-activation response (TAR) RNA element at the 5' end of stalled nascent HIV-1 transcripts [13–15]. This transactivation activity of Tat depends on cysteine at position 22 (C22 residue) [14]. The underlying mechanisms of Tat effects in non-infected cells, including B cells, are much less studied, although it is estimated that up to 2/3 of Tat is exported from infected cells and is efficiently uptaken by neighbouring cells *via* endocytosis while remaining transactivationally active [6,16]. We have recently shown that the acute action of Tat induced oxidative stress and DNA damage in B cells within the first 6 hours and promoted genetic instability and chromosomal aberrations [17] as well as *MYC* relocalization next to the *IGH* locus (potential translocation partners, characteristic for BL) [8]. The long-term effects of Tat action on B cells remain elusive.

In the current study, we unravelled the effects of chronic HIV-1 Tat action on B

cells. We found that Tat was able to transcriptionally downregulate the expression of HLA-DR by inhibiting the NF-κB pathway activity, which led to a decrease in CD4+ T cells recognition of EBV-transformed B cells, thus leading to the acquisition of the cancer hallmark of immune evasion and B cell lymphoma predisposition in people living with HIV.

Materials and methods

Blood collection, peripheral blood mononuclear cells and primary B cell isolation

Blood samples from HIV-positive individuals who signed a written informed consent for the study and were treated at the Department of Clinical Immunology, Hôpital Saint-Louis, Paris, France, were collected in accordance with French legislation. The first patient cohort, which was analysed for *HLA-DRB1* and *HLA-DRB5* mRNA expression in B cells, was recruited in the frame of a non-interventional study registered at the Agence Nationale de Sécurité du Médicament (2016-A01316-45) [8,17]. The clinicopathological characteristics of HIV-positive individuals from the first cohort are summarized in **Table 1**. The second patient cohort, which was analysed for HLA-DR surface expression in B cells, was recruited in the frame of a non-interventional study organised by CNRS UMR9018 - Institut Gustave Roussy (agreement VIHEBV). The clinicopathological characteristics of HIV-positive individuals from the second cohort are summarized in **Table 2**. HIV status was analyzed by immunoassay of anti-HIV-1/2 antibodies IgM and IgG and antigen p24 in venous blood samples. Positive tests were confirmed twice. Tat concentrations in sera from HIV-positive individuals were determined using both a dot blotting assay and an enzyme-linked immunosorbent assay as described previously [8,18]. Whole blood samples from anonymous age- and sex-matched healthy donors were obtained from the "Establissement Français du Sang", Hôpital Saint-Louis, Paris, France in accordance with

the French legislation (agreement number № 14/EFS/033) at the same time periods as samples from HIV-positive individuals for each cohort separately.

Peripheral blood mononuclear cells (PBMCs) were purified by Pancoll (PAN biotech) density gradient centrifugation. B lymphocytes were obtained by negative cell selection using the MagniSort Human B cell Enrichment Kit (Thermo, cat. # 8804-6867-74) according to the manufacturer's protocol.

Plasmids and cloning

An LTR-TurboRFP plasmid that contained the HIV-1 3' LTR fragment upstream to the promoter-less red fluorescent protein TurboRFP gene cloned in pTurboRFP-PRL plasmid (Evrogen, Moscow, Russia) was described previously [19].

An NF-κB-mCherry reporter plasmid consisted of five repeats of the NF-κB response elements (5′-TGGGGACTTTCCGC-3'), a minimal promoter (5′-TAGAGGGTATATAATGGAAGCTCGACTTCCAG-3') and red fluorescent protein mCherry2 as a reporter gene. The construct was cloned into mCherry2-C1 plasmid (Addgene, # 54563) through the removal of CMV enhancer and CMV promoter fragments. For this, the plasmid was digested by the PciI and BmtI restriction enzymes (New England Biolabs) and dephosphorylated using shrimp alkaline phosphatase (Fermentas) prior to ligation. Single-stranded DNA oligos encoding NF-κB response elements and minimal promoter sequences were purchased from Eurofins Genomics, Germany (**Table S1**), annealed, phosphorylated using T4 polynucleotide kinase (Thermo Fisher Scientific) and sequentially ligated into the mCherry2-C1 plasmid upstream to the mCherry2 gene using T4 DNA ligase (Thermo Fisher Scientific): NF-κB response elements were inserted at the PciI and BmtI restriction sites, the minimal promoter was inserted at the AgeI restriction site (Thermo Fisher Scientific). The sequence of the resulting plasmid was confirmed using

Sanger sequencing.

shRNA targeting the human *CIITA* gene was designed using the GPP Web Portal (the RNAi Consortium, https://portals.broadinstitute.org/gpp/public/, date of accession 13.03.2023). Scrambled shRNA sequence was imported from Addgene plasmid #1864, [20]. shRNAs were cloned into the pLKO.1 plasmid with puromycin resistance gene (Addgene, #8453 [21]) as described previously [22]. Briefly, single-stranded DNA oligos encoding shRNA sequences were purchased from Eurofins Genomics, Germany (**Table S1**), annealed, phosphorylated using T4 polynucleotide kinase (Thermo Fisher Scientific) and ligated into the pLKO.1 plasmid using T4 DNA ligase (Thermo Fisher Scientific). The plasmid was digested by the AgeI and EcoRI restriction enzymes (New England Biolabs) and dephosphorylated using shrimp alkaline phosphatase (Fermentas) prior to ligation. The sequence of resulting plasmids encoding CIITA shRNA (pLKO.1-shCIITA) or scrambled shRNA (pLKO.1-scrambled-shRNA) was confirmed using Sanger sequencing.

Cell lines

Human Epstein-Barr virus (EBV)-transformed B lymphoblastoid cell line RPMI8866 (ECACC General Cell Collection), freshly EBV-transformed B lymphoblastoid cell line from healthy donor AS and IT (BLAS and BLIT, established by EBV (B95-8) immortalization of mature B cells and characterized by Genethon (Evry, France)), human immortalized T cell line Jurkat (American Type Culture Collection), Jurkat that stably expresses HIV-1 Tat (Jurkat-Tat, obtained through the NIH HIV Reagent Program, Division of AIDS, NIAID, NIH, ARP-1399, contributed by Dr. Antonella Caputo, Dr. William Haseltine and Dr. Joseph Sodroski), human EBV-negative Burkitt's lymphoma cell line Ramos (obtained through the NIH HIV Reagent Program, Division of AIDS, NIAID, ARP-9938, contributed by Drs. Li Wu and Vineet N. Kewal Ramani), monocytic

THP-1 cell line (American Type Culture Collection), neuroblastoma SH-SY5Y cell line (American Type Culture Collection), human embryonic kidney (HEK) 293T cell line (American Type Culture Collection) and their derivatives were used in the study. RPMI8866^{GFP}, RPMI8866^{Tat}, RPMI8866^{TatC22G}, BLAS^{GFP}, BLAS^{Tat}, BLAS^{TatC22G}, Ramos^{Tat} and THP-1^{Tat} cell lines that stably expressed enhanced green fluorescent protein (EGFP), EGFP-Tat or EGFP-TatC22G (Tat defective in transactivation) were produced through lentiviral transduction as described previously [23].

Lymphoblastoid B-cell lines RPMI8866, Ramos, BLAS, BLIT, a monocytic THP-1 cell line and their derivatives were cultured in RPMI 1640 medium supplemented with 10% fetal bovine serum (FBS), 2% glucose, 2 mM L-Glutamine, 1 mM Pyruvate and 1× penicillin/streptomycin antibiotics (all from Gibco, Thermo Fisher Scientific, Waltham, Massachusetts, USA). Jurkat T cells were cultured in RPMI 1640 medium supplemented with 10% FBS, 1% D-glucose, 1M HEPES Buffer solution, 100 mM sodium pyruvate, 1× penicillin/streptomycin antibiotics (all from Gibco). Jurkat-Tat were cultured with the addition of 800 µg/ml G418 (Sigma-Aldrich, Burlington, MA, USA). SH-SY5Y and HEK293T cell lines were cultured in DMEM medium (Gibco, Thermo Fisher Scientific) supplemented with 10% FBS, 1× penicillin/streptomycin antibiotics. Cells were maintained at 37 °C with 5% CO_2 in a humidified incubator.

Cell treatments

For the experiments with a fluorescently-labelled Tat-derived cell-penetrating peptide GRKKRRQRRRPPQ-Cy5 (Tat CPP-Cy5, SB-PEPTIDE, Saint Egreve, France), SH-SY5Y cells were seeded in 4-chamber Labtek plates (0.0925×10^6 cells / well in 500 µl of DMEM medium supplemented with 10% FBS and 1× penicillin/streptomycin). On the day of assay, the cell medium was changed to a fresh one and cells were pre-treated or

not (control) with 100 μM genistein (MedChemExpress, cat. # HY-14596) for one hour and then 1 μM Tat CPP-Cy5 was added to cell medium. After 30 minutes of incubation with Tat CPP-Cy5, cells were washed three times with PBS and then fixed in 4% paraformaldehyde (Electron Microscopy Sciences, cat. # 15710) for 10 minutes followed by another three washes with PBS and nuclear counterstaining with cell-permeant nuclear dye Hoechst 33342 (1 μg/ml, Invitrogen, cat. #H3570).

For the experiments with NF-κB pathway inhibition, RPMI8866 and BLAS cells were treated for 24 hours with 1 μM Bay 11-7082 (MedChemExpress, Monmouth Junction, NJ, USA), for 24 hours with 40 μg/ml SN52 (MedChemExpress), or for 6 hours with 20 μM MG132 (Selleckchem, Houston, TX, US). After indicated times, cells were collected for HLA-DR expression analysis by flow cytometry or western blotting. For the experiments of endocytosis inhibition, co-cultured Jurkat and BLAS^{GFP} cells (mixed 1:1 at day 0 in normal lymphoblastoid B-cell line medium) were treated with 100 μM genistein (MedChemExpress) at day 3.

For the experiments with nuclear export inhibition, RPMI8866 cells were treated for 2 hours with 5 ng/ml Lemptomycin B (LMB) from *Streptomyces sp*. (Sigma-Aldrich, L2913). Cells were then washed with PBS and fixed in 4% paraformaldehyde (Electron Microscopy Sciences, cat. # 15710) for 10 minutes followed by immunofluorescent staining as described below.

Cell transfections for reporter assays

The transactivation assay based on HIV-1 3′ long terminal repeat (LTR)-driven expression of fast-maturing TurboRFP protein from LTR-TurboRFP plasmid was described previously [19]. RPMI8866, BLAS, Ramos and THP-1 cells and their derivatives were electrotransfected in 4-mm electroporation cuvettes (Cell Projects) using Cliniporator™

(Igea) following previously established protocol [24] with the parameters listed in **Table S2**. 400 µl electrotransfection mixture was composed of 50% of the Minimum Essential Medium Eagle with Spinner Modification (S-MEM, Sigma Aldrich), water and 50 µg LTR-TurboRFP plasmid (dissolved in water). TurboRFP fluorescence was evaluated 24 h after electrotransfection. When analysing NF-κB activity, RPMI8866 cells and their derivatives were electrotransfected with the NF-κB-mCherry reporter plasmid as described above and mCherry fluorescence was evaluated 24 h after electrotransfection. In some experiments, phorbol myristate acetate (PMA, 1-3 µg/ml, Sigma Aldrich) was added to RPMI8866 cells 24 h after electrotransfection; mCherry fluorescence was evaluated 48 h after electrotransfection.

Lentivirus production and lentiviral transduction

HEK 293 T cells were used for lentivirus packaging and production. Cells were seeded in T-175 flask 24 h before transfection to achieve 80% confluency on the day of transfection. HEK 293 T cells were transfected with second-generation lentiviral packaging plasmid psPAX2 (Addgene, # 12260), VSV-G envelope expressing plasmid pMD2.G (Addgene, # 12259) and transfer plasmid (EGFP, EGFP-Tat, EGFP-TatC22G, pLKO.1-scrambled-shRNA, or pLKO.1-shCIITA) at 15:6:20 ratio using Turbofect transfection reagent (Thermo Fisher Scientific, USA) according to the manufacturer's instructions (20 µg of plasmid DNA and 40 µl of Turbofect transfection reagent were premixed in 2 ml of OptiMEM medium (Gibco) and added to 20 ml of DMEM/10% FBS cell medium in T-175 flask). Cell medium was changed to DMEM/0%FBS 24 hours after transfection and lentiviral supernatant was collected 48 hours after transfection, centrifuged to remove cell debris and filtered through a 0.45-µm filter.

RPMI8866^{GFP}, RPMI8866^{Tat}, RPMI8866^{TatC22G}, BLAS^{GFP}, BLAS^{Tat}, BLAS^{TatC22G},

Ramos^{Tat} and THP-1^{Tat} cell lines that stably expressed enhanced green fluorescent protein (EGFP), EGFP-Tat or EGFP-TatC22G (Tat defective in transactivation) were produced through lentiviral transduction as described previously [23]. Briefly, 2 × 10^6 cells (plated in six-well plates) diluted in 1 ml of normal medium were transduced with 1 ml of lentiviral supernatant, GFP expression was confirmed 72 hours after transduction and GFP$^+$ cells were sorted using ARIA Fusion-UV cell sorter (BD Biosciences). RPMI8866 cell lines that stably expressed scrambled shRNA or CIITA-shRNA were produced through lentiviral transduction of 2 × 10^6 cells with 1 ml of lentiviral supernatant and subsequent selection with 1 μg/ml puromycin for at least five weeks. Cells were maintained in normal RPMI8866 cell medium with 1 μg/ml puromycin and subjected to the second round of lentiviral transduction to produce RPMI8866 cell lines that stably expressed scrambled shRNA or CIITA-shRNA and EGFP or EGFP-Tat.

Generation of EBV-specific CD4+ T cell line and the analysis of their reactivity

EBV-specific polyclonal human CD4+ T cell line was derived as previously described [25] with modifications. Briefly, PBMCs from healthy donor AS were depleted in CD8+ T cells using human CD8 magnetic beads (Proteintech, cat. # MS0044-100) following the manufacturer's instructions. CD8-depleted PBMCs (1 × 10^6/ml) were then co-cultured with autologous irradiated (40 Gy) EBV-transformed BLAS (2.5 × 10^4/ml) at 40:1 responder-to-stimulator ratio in 24-well plates in RPMI 1640 medium supplemented with 10% human AB serum (Sigma) and 1× penicillin/streptomycin antibiotics. After 9 to 11 days, T cells (1 × 10^6/ml) were restimulated with irradiated BLAS (2.5 × 10^5/ml) at 4:1 responder-to-stimulator ratio. Recombinant human IL-2 (50 ng/ml; Proteintech, cat. # HZ-1015) was added to the cultures at this time. T-cell lines were subsequently maintained by restimulation with irradiated BLAS every 14 days, with interim half-changes of fresh medium plus IL-2 every 3 to 4 days. After seven restimulation cycles, the T cell line was

>90% CD4+ by flow cytometric analysis (see **Figure 5B**). Phenotype analysis was performed by flow cytometry with immunofluorescent staining specific for CD3 (APC), CD8 (FITC), and CD4 (PerCP).

For IFNγ production analysis, the generated CD4+ T cell line or PBMCs (5×10^5/well) from autologous donor were co-cultured with BLAS, $BLAS^{GFP}$, $BLAS^{Tat}$ or $BLAS^{TatC22G}$ (1.25×10^4/well) at 40:1 E/T ratio for 18 hours in 48-well plates in RPMI 1640 medium supplemented with 10% human AB serum (Sigma) and 1× penicillin/streptomycin antibiotics followed by CD4 and IFNγ staining as described below.

For cytotoxicity assays, a non-radioactive method comparable to the conventional ^{51}Cr release assay was used [26] with modifications. Briefly, sensitive BLAS and control RPMI8866 target cells were labelled with 5- (and 6-) carboxyfluorescein diacetate succinimydyl ester (CFSE, Biolegend, cat. #423801) as follows: 1×10^6 cells were washed once with PBS and resuspended in 1% FBS/PBS to a concentration 1×10^6 cells/ml. For sensitive targets (BLAS), 1 µl of 5 mM CFSE solution was added to 1 ml of cell suspension; for control targets (RPMI8866), 0.5 µl of 500 µM CFSE solution was added to 1 ml of cell suspension; cells were incubated for 4 min at room temperature under shading. After incubation, 9 ml of 5% FBS/PBS was added to stop the labelling reaction. Then, cells were washed once with 5% FBS/PBS and resuspended with 400 µl of RPMI 1640 medium supplemented with 10% human AB serum (Sigma) and 1× penicillin/streptomycin antibiotics at a final concentration (2.5×10^6 cells/ml). CD4+ T cell line effector cells were washed once with PBS and resuspended in RPMI 1640 medium supplemented with 10% human AB serum (Sigma) and 1× penicillin/streptomycin antibiotics to a final concentration of 1×10^6 cells/ml. For sensitive reactions, 5×10^4 BLAS target cells (20 µl) and various numbers of effector cells (0, 1.25×10^5, 2.5×10^5, 5×10^5) were mixed in a 48-well plate at a final volume of 520 µL to yield various effector/target (E/T) ratios (0:1,

2.5:1, 5:1, 10:1). For each sensitive reaction, a respective control reaction was also separately prepared: 5×10^4 RPMI8866 target cells (20 µl) and the same number of effector cells were mixed in a 48-well plate at a final volume of 520 µL. The plate was centrifuged at 200g for 1 min and then incubated at 37°C for 4 h. After incubation, wells with the sensitive target cells were mixed 1:1 with the respective control target cells with the same E/T ratio in one tube, washed once with PBS and fixed in 4% PFA/PBS for 10 minutes. The % of specific lysis was calculated as follows:

$$\%\ of\ specific\ lysis\ =\ \frac{a-b}{a-ab}\ *\ 100\%,$$

where a - the fraction of sensitive cells among target cells in E/T 0:1 sample, and b - the fraction of sensitive cells among target cells in E/T X:1 sample. The derivation of the % of specific lysis formula is explained in **Supplementary Figure 1**.

Cell surface and intracellular staining, flow cytometry analysis

The following anti-human fluorescently-labelled antibodies were used: FITC anti-CD8 (Biolegend, cat. #344704), PE/Cy5 anti-HLA-DR (Biolegend, cat. #307608), APC anti-CD3 (Biolegend, cat. #300312), PerCP anti-IFNγ (Biolegend, cat. #502524), PerCP anti-CD4 (Biolegend, cat. #300528), APC anti-CD4 (Biolegend, cat. #300514), PerCP Mouse IgG1, κ isotype control (Biolegend, cat. # 400148), APC Mouse IgG2a, κ isotype control (Biolegend, cat. #400220). Immunophenotyping of PBMCs from healthy donors and people living with HIV from the second cohort was performed with the following antibodies: APC/Cyanine7 anti-CD4 (Biolegend, cat. # 300517), Pacific Blue anti-CD27 (Biolegend, cat. # 356413), PE anti-CD19 (Biolegend, cat. # 302208), PE/Cyanine5 anti-HLA-DR (Biolegend, cat. # 307608), FITC anti-CD8 (Biolegend, cat. # 344704), APC anti-HLA-ABC (Biolegend, cat. # 311410). For antibody staining of surface molecules, 0.3 × 10^6/test cells were harvested, washed with PBS and resuspended in 1% BSA/PBS. For

intracellular staining of CD4 and IFNγ, 0.5 × 10^6/test cells were harvested, washed with PBS and fixed and permeabilized using Cyto-Fast™ Fix/Perm Buffer Set (Biolegend, cat. # 426803) according to the manufacturer's instructions. For B cells (including lymphoblastoid cell lines), Fc receptor binding was blocked by Fc block (Miltenyi Biotec Inc., cat. # 130-059-901 or Biolegend, cat. #422302) according to the manufacturer's instructions. Cells were then incubated on ice with fluorescently-labelled antibodies for 30 minutes followed by 3 washes with PBS.

Fluorescence was acquired using BD Accuri C6 Plus Flow Cytometer (BD Biosciences, USA) and the data were analyzed using FlowJo software (version 10.4), the same gating was applied to all samples within one experiment. If several fluorescent channels were analyzed, the compensation was performed with single-stained controls.

Immunofluorescent staining and microscopy

For immunofluorescent staining, suspension cells were attached to coverslips covered with poly-D-lysine (Merck Millipore, cat. # A-003-E, 50 μg/ml). Cells were washed with PBS, fixed in 4% paraformaldehyde (Electron Microscopy Sciences, cat. # 15710) and permeabilized with 2% Triton X-100 (in case of intracellular staining). When analyzing RelA and NFKB1 expression and localization, cells were stained with anti-RelA (1:100, Santa Cruz, cat. # sc-8008) and anti-NFKB1 (1:200, Proteintech, cat. # 14220-1-AP) antibodies, followed by staining with secondary antibodies AF546 Goat anti-rabbit IgG H+L (1:200, Invitrogen, cat. # A11010) and AF647 Goat anti-mouse IgG H+L (1:200, Invitrogen, cat. # A21235). When analyzing RelB expression and localization, cells were stained with anti-RelB (1:100, Proteintech, cat. # 25027-1-AP) antibodies, followed by staining with secondary antibodies AF647 Goat anti-rabbit IgG H+L (1:200, Invitrogen, cat. # A21245). Coverslips were mounted on slides with Fluoroshield mounting medium

with DAPI (Abcam, cat. # ab104139). When analyzing RelA localization upon LMB treatment, cells were stained with anti-RelA (1:100, Santa Cruz, cat. # sc-8008) and anti-actin (1:200, Sigma, cat. # A2103) antibodies (since RelA was almost entirely translocated to the nucleus upon LMB treatment, we stained for actin to mark cytoplasm), followed by staining with secondary antibodies AF546 Goat anti-rabbit IgG H+L (1:200, Invitrogen, cat. # A11010) and AF647 Goat anti-mouse IgG H+L (1:200, Invitrogen, cat. # A21235). All antibodies were diluted in 1% BSA in 1× PBS.

Fluorescent images were acquired using Leica TCS SP8 Multiphoton Microscope (Leica Microsystems). All images within the experiment were captured with the same laser intensity, gain and exposure settings.

Image analysis

To analyze the total and nuclear fluorescence intensity of RelA, RelB and NFKB1, confocal images were processed using a semi-automatic macro in Fiji (ImageJ version 2.1.0/1.53c, Java version 1.8.0). Briefly, to create nuclear and total cell masks, the nuclear regions of interest (ROIs) were detected on the images with the DAPI-staining, the total cellular ROIs were detected on the images with the RelA- or RelB-staining; in both cases, the "Huang dark" threshold method implemented in Fiji was used. The masks were split to detect single nuclei and single cells. The area, circularity and X and Y centre coordinates of detected ROIs were measured, and total fluorescence intensity (integrated density in Fiji) in nuclear and cellular ROIs was measured in RelA and NFKB1 channels. An algorithm in R (version 4.2.1) was created to process the results. Nuclear ROIs with area <10 μm^2 (debris) or >55 μm^2 (doublets), irregular nuclei (ROIs circularity < 0.3), cellular ROIs with area <20 μm^2 or >95 μm^2 and circularity < 0.3 were automatically removed. A provisional cellular radius (r_{cell}) was calculated as follows: $r_{cell} = \sqrt{\frac{Area}{\pi}}$; nuclear ROIs

that met the condition $(Xnuc - Xcell)^2 + (Ynuc - Ycell)^2 < r_{cell}^2$ were matched with respective cellular ROIs; unmatched nuclear or cellular ROIs or cellular ROIs where >1 nuclei matched were removed from the analysis. The total fluorescence intensity in the nuclear ROI was then divided by the respective total fluorescence intensity in the total cellular ROI for each cell. At least five fields were analyzed per biological replicate and images from at least two independent experiments were analyzed. The plugin is available on request.

To analyse the nuclear penetration of Tat CPP-Cy5, confocal images were processed using a semi-automatic macro in Fiji that detected nuclear ROIs on the images with the Hoechst 33342-staining as described above. Mean Cy5 fluorescence intensity in the nuclear ROI was analysed for each cell individually.

Cell lysate preparation, SDS-PAGE and western blotting

Cells were harvested from culture dishes and centrifuged at 4°C for 10 minutes at 800 g, the supernatant was discarded, and cell pellets were washed with ice-cold phosphate-buffered saline (PBS, Sigma). PBS was then aspirated and for whole cell extracts, cells were lysed in 150 µL of ice-cold NETN buffer (NaCl 150 mM, ethylenediaminetetraacetic acid (EDTA) 1 mM, Tris pH 7.5 50 mmol/L, NP40 0.5%, 1× protease inhibitor cocktail; Roche, Basel, Switzerland). The lysates were sonicated in a Vibra Cell sonicator (SONICS & MATERIALS, Inc., Newtown, CT, USA) for 10 seconds at 30% of intensity to completely lyse cells, incubated on ice for 30 minutes and centrifuged at 4°C for 20 minutes at 16000 g. The supernatant was transferred into a new pre-cooled microcentrifuge tube and the cell pellet was discarded. When preparing cytoplasmic and nuclear extracts, cells and nuclei were lysed using NE-PER Nuclear and

Cytoplasmic Extraction Reagents (ThermoFisher) according to the manufacturer's instructions. The lysates (whole cell, cytoplasmic or nuclear) (5 µl) were used for quantification of protein concentration by BCA assay (Thermo Fisher Scientific). Finally, after measuring the concentration, the lysates were dissolved in the 6× Laemmli buffer with dithiothreitol (DTT) and heated at 95°C for 10 min.

Proteins (20 µg) were resolved in NuPAGE™ 4-12% Bis-Tris sodium dodecyl sulfate-polyacrylamide gel electrophoresis (SDS-PAGE) gels (Invitrogen) and transferred to polyvinylidene fluoride (PVDF) membrane (GE Healthcare, Chicago, Illinois, USA) in a transfer buffer (25 mM Tris, 192 mM glycine, 20% ethanol). PageRuler Prestained Plus Protein Ladder (Thermo Fisher Scientific) was used as a molecular weight marker. Nonspecific binding was blocked in 5% non-fat dried milk diluted in Tris-buffered saline (TBS), containing 0.1% Tween-20 at 4°C overnight. Proteins were probed with the following primary antibodies: mouse anti-Tat (1:200, Santa Cruz, cat. #sc-65912), anti-GFP (1:1000, Roche, cat. #11814460001), mouse anti-HLA-DR (1:1000; Santa Cruz, cat. # sc-6262), mouse anti-RelA (1:1000, Santa Cruz, cat. # sc-8008), rabbit anti-NFKB1 (p105, p50, 1:1000, Proteintech, cat. # 14220-1-AP), mouse anti-IκBα (1:1000, Santa Cruz, cat. # sc-371), rabbit anti-pIκBα (1:1000, R&D Systems, cat. # AF4809), rabbit anti-RelB (1:1000, Proteintech, cat. # 25027-1-AP), rabbit anti-NFKB2 (p100, p52, 1:1000, Proteintech, cat. # 15503-1-AP), mouse anti-β-actin (1:1000, control of protein load in whole cell extracts, #sc-81178, Santa Cruz), rabbit anti-GAPDH (1:1000, control of protein load in cytoplasmic extracts, Cell Signaling Technology, cat. #2118), rabbit anti-H2A (1:1000, control of protein load in nuclear extracts, Abcam, cat. # ab116677), rabbit anti-topoisomerase IIb (1:1000, control of protein load in nuclear extracts, Santa Cruz, cat. # sc-13059) for 2h at 22 °C. First, the membranes were washed with TBS, containing 0.1%

Tween-20, incubated with appropriate peroxidase-conjugated secondary antibodies (Invitrogen) (in 1:2000 dilution) at 22 °C for 2h, and washed in TBS afterwards (containing 0.1% Tween-20). Proteins were visualized using Immobilon Western Chemiluminescent HRP Substrate (Millipore) and ImageQuant LAS 4000 mini (GE Healthcare) for Western blotting imaging and analysis. Densitometric analysis of blots at non-saturating exposures was performed using ImageJ. The original uncropped western blotting images are presented in **Supplementary Figure 2**.

RNA extraction, sequencing, RNA-seq data processing and analysis

For the BLAS cell lines, RNA-seq experiments were performed in the framework of this study. Raw RNA-seq data as well as processed data (gene counts) are deposited in the GEO database with an accession number GSE212499. For the RPMI8866 cell lines, raw sequencing data was downloaded from GSE182538 and processed as described below.

3×10^6 cells were collected by centrifugation (5 minutes, 800 x g), cell pellets were then processed immediately. Total RNA from BLAS cells was isolated using the NucleoSpin RNA kit (Macherey-Nagel, Düren, Germany) following the manufacturer's instructions. The quantity and quality of total RNA were measured using NanoDrop2000C Spectrophotometer (Thermo Fisher Scientific). The cDNA libraries were constructed and sequenced by Novogene, UK. The raw sequencing reads were mapped to the human genome (assembly GRCh38.p10) using HISAT2 (version 2.0.5). Read counting was performed using featureCounts (ver 2.0.1) in a strand-specific mode. GENCODE v26 gene annotation (ALL) was used. Features with a low total count number (< N counts across all samples, where N is the number of replicates in each condition) were discarded. Differential expression analysis was performed using the DESeq2 R package (version 1.30.1). The genes meeting the criteria p value adjusted (p.adjust) by the

Benjamini-Hochberg procedure < 0.05, $|\log_2$ fold change$|$ > 0.5 were considered differentially expressed. The list of differentially expressed genes can be found in **Table S3**.

Overrepresentation analysis (ORA) was performed with an R package clusterProfiler (version 4.4.4) [27] on a list of genes that overlapped between the following comparisons: RPMI8866^{Tat} *vs* RPMI8866 and BLAS^{Tat} *vs* BLAS. Benjamini-Hochberg p.adjust cutoff of 0.05 and q-value cutoff of 0.05 were used to select statistically significant categories, redundant terms were removed with the simplify() function of the same package (cutoff parameter of 0.7). The Gene Ontology (GO) biological process and Kyoto Encyclopedia of Genes and Genomes (KEGG) databases were used for annotation. Transcription factor (TF)-target enrichment was performed based on the TRRUST TF-target database (2019) [28] *via* an R-based interface accessing the Enrichr server [29] with a p.adjust cutoff of 0.05.

RNA extraction, reverse transcription and quantitative polymerase chain reaction

Approximately 3×10^6 cells were collected by centrifugation (5 minutes, 800 x g). Cell pellets were then processed immediately or quickly frozen and stored at -80°C for less than a month prior to total RNA extraction. Total RNA was isolated using the NucleoSpin RNA kit (Macherey-Nagel, Düren, Germany) following the manufacturer's instructions and RNA samples were treated with DNase. The quantity and quality of total RNA were measured using NanoDrop2000C Spectrophotometer (Thermo Fisher Scientific). 1% agarose gel with ethidium bromide was used to assess RNA integrity. 1.0 µg of total RNA was reverse-transcribed using Maxima™ H Minus cDNA Synthesis Master Mix (Thermo Scientific, USA) with oligo $(dT)_{18}$ and random hexamer primers. Quantitative polymerase chain reaction (qPCR) was carried out using Powerup SYBR Green Mastermix

(ThermoFisher) on a StepOnePlus Real-Time PCR System machine (Applied Biosystems). The human cDNA primers (**Table S4**) were obtained from Eurofins Genomics, Germany; primer specificity was evaluated using NCBI PrimerBlast. The thermal cycling program was as follows: a 2-minute denaturation step at 50°C, a 2-minute denaturation step at 95°C followed by 40 amplification cycles consisting of 15 seconds of denaturation at 95°C, 1 minute of annealing at 60°C and 1 minute of elongation at 72°C, followed by a final step 10-minute elongation at 72°C. qPCRs for each sample were performed in triplicates (technical replicates). The no-template controls (included on each plate) were reliably negative. A relative transcript level was calculated using the Pfaffl method [30] and the geometric averaging of the relative quantities of the *RPL32 and GAPDH* reference genes as described previously [31,32]; normalization was done assuming as 1 the mean level of each transcript in the control group. The analysis of primer efficiency was performed by plotting the cycle threshold value (Ct) against the serial 1:10 dilution of the cDNA sample using the equation $E = 10^{-\frac{1}{the\ slope\ value}}$.

Polymerase chain reaction

Approximately 3×10^6 cells were collected by centrifugation (5 minutes, 800 x g). Cell pellets were then processed immediately or quickly frozen and stored at -80°C for less than a month prior to total DNA extraction. Total genomic DNA was extracted using Nucleospin® Tissue DNA purification (Macherey-Nagel) according to the manufacturer's protocol. DNA was quantified by Nanodrop (Thermo Fisher Scientific). The quantity and quality of total DNA were measured using NanoDrop 2000c Spectrophotometer (Thermo Fisher Scientific). 100 ng of genomic DNA were amplified with StepOnePlus™ Real-Time PCR System (Applied Biosystems) using the PowerUp SYBR Green Master Mix (Thermo Scientific) with the following program: a 2-minute denaturation step at 50°C, a 2-minute

denaturation step at 95°C followed by 40 amplification cycles consisting of 15 seconds denaturation at 95°C, 1 minute of annealing at 60°C and 1 minute of elongation at 72°C, followed by a final step 10-minute elongation at 72°C. The human genomic DNA primers (**Table S4**) were obtained from Eurofins Genomics, Germany; primer specificity was evaluated using NCBI PrimerBlast. PCR products were loaded on 1% agarose gel and migrated by electrophoresis for amplicon visualisation.

Chromatin immunoprecipitation quantitative real-time PCR (ChIP-qPCR)

Chromatin immunoprecipitation (ChIP) was performed as described previously [33]. Briefly, to perform ChIP-qPCR, 2 × 10^7 RPMI8866, RPMI8866^{GFP} and RPMI8866^{Tat} cells were collected, centrifuged (800g, 5 min), and resuspended in 10 ml of culture medium. Formaldehyde (37%) was added drop-wise to a final concentration of 1%, followed by gentle rotation for 10 minutes at room temperature for cross-linking. The fixation was halted by adding glycine (2.5 M) to a final concentration of 125 mM and incubating with rotation for 5 minutes at room temperature. After washing the cells three times with ice-cold PBS, the cell pellet was resuspended in 1 ml of cytoplasm lysis buffer (10mM Tris-HCl pH 8, 150mM NaCl, 0.5mM EDTA, 0.5% NP-40, 1× protease inhibitor cocktail, 0.5mM PMSF) and dounced 10 times in dounce homogenizer. The nuclei were then pelleted, and the supernatant (cytoplasm) was removed. The nuclei were resuspended in 350 µl of nuclear lysis buffer (50mM Tris-HCl pH 8, 10mM EDTA, 1% SDS, 1× protease inhibitor cocktail, 1mM PMSF). The chromatin was sonicated using Covaris sonicator, and specific parameters (Power Peak: 200; Duty Factor: 20; Cycles/Burst: 200; 20 min) were set to achieve an average fragment size of 200-1000 bp. After sonication, debris was pelleted by centrifugation for 10 min, 4°C, 15000 g, and the supernatant was transferred to a new tube. A 25 µl aliquot was taken to determine DNA concentration and fragment size. For DNA concentration and fragment size determination, 20 µl of 2M NaCl,

145 µl of water, and 3 µl of RNase A (10 mg/ml) were added to the aliquot, followed by overnight incubation at 65°C. On the next day, 3 µl of proteinase K (20 mg/ml) was added, and the mixture was incubated with shaking at 60°C for 1 hour. DNA was purified using a PCR clean-up kit (Marchery-Nagel, Germany). For immunoprecipitation, a pre-clearing step was performed by adding 10 µl of Protein G Dynabeads (Invitrogen) to the 20 µg of sonicated chromatin and incubating for 2 hours with gentle rotation at 4°C. ChIP was carried out overnight at 4°C with 5 µl of the rabbit monoclonal anti-RelA antibody (Cell Signalling, cat. #8242) or 5 µl of normal rabbit IgG antibody (Cell Signalling, cat. #2729) and 10 µg of chromatin per reaction in ChIP buffer (16.7 mM Tris-HCl pH 8, 167 mM NaCl, 1.2 mM EDTA, 0.01% SDS, 1.1% Triton X-100, supplemented with protease inhibitors). An aliquot of the chromatin sample (200 ng, 2%) was kept as a ChIP input. The next day, the bead/chromatin mixture was placed on a magnetic rack, and the supernatant was removed. The beads were washed successively with Low-salt Wash Buffer (150 mM NaCl, 20 mM Tris-HCl pH 8, 2 mM EDTA, 0.1% SDS, 1% Triton X-100, supplemented with protease inhibitors), High-salt Wash Buffer (500 mM NaCl, 20 mM Tris-HCl pH 8, 2 mM EDTA, 0.1% SDS, 1% Triton X-100), LiCl Wash Buffer (250 mM LiCl, 10 mM Tris HCl pH 8, 1 mM EDTA, 1% Nonidet P-40, 1% Na-Deoxycholate), and twice with TE Wash Buffer (10 mM Tris HCl pH 8, 1 mM EDTA). DNA was eluted with 200 µl of ChIP elution buffer (100 mM sodium bicarbonate, 1% SDS). ChIP input and the eluted DNA were incubated with 8 µl of 5M NaCl and 3 µl of RNase A (10 mg/ml) at 65°C with shaking overnight, followed by the addition of 3 µl of proteinase K (20 mg/ml) and incubation with shaking at 60°C for 1 hour. DNA purification using a PCR clean-up kit (Marchery-Nagel, Germany) was performed and DNA concentration was measured with a Nanodrop.

RelA binding to *HLA-DRB1* and *HLA-DRB5* promoter sequences was measured by qPCR with StepOnePlus™ Real-Time PCR System (Applied Biosystems) using PowerUp SYBR Green Master Mix (Thermo Scientific) with the following program: a 2-minute denaturation step at 50°C, a 2-minute denaturation step at 95°C followed by 40 amplification cycles consisting of 15 seconds denaturation at 95°C, 1 minute of annealing at 60°C and 1 minute of elongation at 72°C, followed by a final step 10-minute elongation at 72°C. For qPCR analysis, 5% of the immunoprecipitated and input DNA were used. The human genomic DNA primers for ChIP-qPCR (**Table S4**) were obtained from Eurofins Genomics, Germany. Primers for *HLA-DRB1* and *HLA-DRB5* promoter sequences were chosen based on data of RelA binding from ReMap 2022 (4th release, https://remap.univ-amu.fr/, accession date: 12 January 2023), a database of transcriptional regulators peaks derived from curated ChIP-seq, ChIP-exo, DAP-seq experiments in human [34] (**Supplementary figure 3**). Primers for *ACTB* were imported from [35], *ACTB* PCR product sequence did not overlap with RelA peaks from ReMap 2022 (data not shown) and severed as a control. For each sample, values were normalized to input DNA and reported as % of input.

Statistical analysis

Data were analyzed using GraphPad Prism 9 software (GraphPad Software Inc.). The unit of analysis was a single biological replicate. Student's unpaired t-tests were used to compare data between two groups. One-way analysis of variance (ANOVA), followed by Tukey's post-hoc test was used to determine differences between more than two groups that involved one factor. Two-way ANOVA followed by Tukey's post hoc test was used to determine differences between two or more groups that involved two factors. Data are

presented as a mean ± standard error of the mean (SEM). The level of significance was set at $p < 0.05$.

Results

HIV-1 Tat decreased HLA-DR expression in B cells of people living with HIV

To analyze the effects of chronic HIV-1 Tat presence on B cells, we have established an RPMI8866 lymphoblastoid B cell line ectopically expressing either Tat or TatC22G (Tat deprived of transactivation capacity), RPMI8866^{Tat} or RPMI8866^{TatC22G}, respectively; both proteins were coupled to EGFP (hereafter referred to as GFP) [23]. We also used a new lymphoblastoid B cell line from a healthy donor (BLAS), which was established by immortalization of mature B cells with EBV (B95-8). We constructed BLAS cells expressing Tat or TatC22G, hereafter referred to as BLAS^{Tat} or BLAS^{TatC22G}. Cells expressing GFP (RPMI8866^{GFP} or BLAS^{GFP}) and initial cell lines (RPMI8866 or BLAS) were used as controls (**Figure 1A**). The expression of Tat and GFP in these cell lines was confirmed by western blotting (**Figure 1B,1C**). The transactivation capacity of cell lines with Tat and TatC22G and respective controls was assessed using HIV-1 3′-LTR-TurboRFP reporter plasmid as described previously [19]. Tat expression led to substantially increased TurboRFP fluorescence compared to TatC22G, GFP or the control, confirming that fusion with GFP did not perturb the transactivation functions of wild-type Tat, while the transactivation function of TatC22G was decreased (**Supplementary Figure 4**).

To detect possible changes in B cell physiology caused by chronic HIV-1 Tat presence that might contribute to oncogenic hallmark acquisition, we performed a genome-wide analysis of cellular gene expression (RNA-sequencing) in BLAS cell lines

and compared the results with the previously published transcriptomes of RPMI8866 cell lines (GSE182538) [23]. Differentially expressed genes (DEGs) were defined as genes with p.adjust < 0.05 and $|\log_2$ fold change| >0.5 as compared to the initial cell lines (RPMI8866 or BLAS). As expected, we confirmed that GFP expression did not alter significantly the transcriptome profile of RPMI8866 cells: only 20 upregulated and 60 downregulated genes were identified. Thus, the effect of GFP on gene expression in B cells could be neglected, therefore, for the BLAS line the RNA-sequencing of $BLAS^{Tat}$, $BLAS^{TatC22G}$ and BLAS cells was performed (**Figure 1D**). Our analysis revealed that 1372 genes (578 upregulated and 794 downregulated) were differentially expressed in $RPMI8866^{Tat}$ *vs* RPMI8866 cells, and 4424 genes (2121 upregulated and 2303 downregulated) were differentially expressed in $BLAS^{Tat}$ *vs* BLAS cells (**Figure 1D**). Comparable results were observed in cells expressing TatC22G: 1198 genes (526 upregulated and 672 downregulated) were differentially expressed in $RPMI8866^{TatC22G}$ *vs* RPMI8866 cells, and 3486 genes (1542 upregulated and 1944 downregulated) were differentially expressed in $BLAS^{TatC22G}$ *vs* BLAS cells (**Figure 1D**). Thus, among the detected DEGs, a slightly higher proportion of genes were downregulated in the presence of either Tat or TatC22G. Among these genes, the majority were protein-coding genes (**Figure 1E**), but differentially expressed lncRNAs were also identified (**Figure 1F**). A considerably higher number of DEGs in BLAS cells can be explained by the fact that these cells were freshly immortalized and carried a normal genome of primary B cells, and thus were more sensitive to any changes in their state, including viral protein expression. In culture, BLAS cells proliferated considerably slower than RPMI8866 cells and were more sensitive to culture conditions (data not shown).

To explore whether genes regulated by Tat action in B cells have any common biological functions, we next performed overrepresentation analysis (ORA) and searched for activated and suppressed functional categories defined by the gene ontology biological process (GO BP) and KEGG databases. GO BP terms significantly enriched in the set of 84 upregulated DEGs overlapped between RPMI8866^{Tat} *vs* RPMI8866 and BLAS^{Tat} *vs* BLAS comparisons (**Figure 1G**) included: regulation of neuron projection development and positive regulation of cell projection organisation (**Figure 1I**). No significantly enriched KEGG pathways were revealed for the same gene set. GO BP terms significantly enriched in the set of 146 downregulated DEGs overlapped between RPMI8866^{Tat} *vs* RPMI8866 and BLAS^{Tat} *vs* BLAS comparisons (**Figure 1H**) included: leukocyte cell-cell adhesion, positive regulation of T cell activation, T cell receptor signalling pathway, peptide antigen assembly with the major histocompatibility complex (MHC) class II protein complex, antigen processing and presentation of exogenous peptide antigen *via* MHC class II (**Figure 1J, 1K**). The same gene set was significantly enriched in the following KEGG pathways: cell adhesion molecules, intestinal immune network for IgA production, hematopoietic cell lineage, viral myocarditis, and TNF signalling pathway (**Figure 1L, 1M**). To conclude, both in RPMI8866 and BLAS cells, Tat downregulated a subset of MHC class II genes (*HLA-DRB1*, *HLA-DRB5*, *HLA-DQA1*, *HLA-DQB1*) and thus Tat could potentially decrease CD4+ T cell activation in response to EBV-infected cells. As *HLA-DRB1* and *HLA-DRB5* were more markedly downregulated by Tat (log2 fold changes -0.92 and -1.08, respectively in BLAS^{Tat} cells) compared to *HLA-DQA1* and *HLA-DQB1* (log2 fold changes -0.73 and -0.85, respectively in BLAS^{Tat} cells), we further focused on HLA-DR expression regulation.

We next confirmed the Tat-induced downregulation of HLA-DR genes by qPCR: *HLA-DRB1* mRNA expression was significantly decreased both in RPMI8866^{Tat} and RPMI8866^{TatC22G} as compared to RPMI8866 (0.7068 ± 0.038 and 0.763 ± 0.056 vs 1.000 ± 0.028, $p = 0.0004$ and $p = 0.0111$, ANOVA, Tukey's posthoc test, respectively, **Figure 2A**). *HLA-DRB5* mRNA expression was also significantly decreased both in RPMI8866^{Tat} and RPMI8866^{TatC22G} as compared to RPMI8866 (0.590 ± 0.047 and 0.610 ± 0.058 vs 1.000 ± 0.019, $p = 0.0001$ and $p = 0.0021$, ANOVA, Tukey's posthoc test, respectively, **Figure 2B**). Accordingly, *HLA-DRB1* mRNA expression was significantly decreased both in BLAS^{Tat} and BLAS^{TatC22G} as compared to BLAS (0.490 ± 0.072 and 0.332 ± 0.102 vs 1.000 ± 0.047, $p = 0.0008$ and $p < 0.0001$, ANOVA, Tukey's posthoc test, respectively, **Figure 2C**). *HLA-DRB5* mRNA expression was significantly decreased both in BLAS^{Tat} and BLAS^{TatC22G} as compared to BLAS (0.348 ± 0.089 and 0.425 ± 0.122 vs 1.000 ± 0.017, $p = 0.0247$ and $p = 0.0366$, ANOVA, Tukey's post-hoc test, respectively, **Figure 2D**). Both *HLA-DRB1* and *HLA-DRB5* mRNAs were upregulated in RPMI8866^{GFP} *vs* RPMI8866 ($p = 0.0006$ and $p = 0.0002$, ANOVA, Tukey's posthoc test, respectively, **Figure 2A, 2B**).

This result was further confirmed by the analysis of HLA-DR surface expression by flow cytometry: we observed that HLA-DR surface expression was decreased both in RPMI8866^{Tat} and RPMI8866^{TatC22G} compared to RPMI8866 ($p = 0.032$ and $p = 0.0295$, ANOVA, Tukey's posthoc test, respectively, **Figure 2E, 2F**) and in BLAS^{Tat} and BLAS^{TatC22G} compared to BLAS ($p = 0.0024$ and $p < 0.0001$, ANOVA, Tukey's posthoc test, respectively, **Figure 2G, 2H**). Thus, HIV-1 Tat presence decreased HLA-DR expression in B cells.

As a control, we also established a Burkitt's lymphoma cell line Ramos and a monocytic cell line THP-1 that ectopically expressed HIV-1 Tat (**Supplementary figure**

5). To ensure that the effect of Tat on HLA-DR surface expression was not limited to cells infected with EBV, we analysed HLA-DR surface expression in EBV-negative Ramos cells (**Supplementary figure 5A, 5B**) that stably expressed Tat (**Supplementary figure 5C**) and found that *HLA-DRB5* mRNA level, HLA-DR surface and total expression were significantly decreased in Ramos^{Tat} cells compared to Ramos (**Supplementary figure 5E-5I**). On the contrary, Tat expression had no effect on the HLA-DR surface expression level in the monocytic THP-1 cells, where the overall HLA-DR expression level was low (**Supplementary figure 5D, 5J-5L**). Tat, however, increased the *HLA-DRB5* mRNA level and the percentage of HLA-DR-positive THP-1 cells (**Supplementary figure 5M**). This indicates that HIV-1 Tat-dependent decrease in HLA-DR expression was specific to B cells and was not dependent on EBV infection.

HLA-DR surface expression is decreased in B cells from people with HIV [36]; this can be attributed to the chronic secretion of Tat protein from infected cells. To support this hypothesis, we decided to test whether HLA-DR expression was also decreased on the mRNA level in people living with HIV. We analyzed *HLA-DRB1* and *HLA-DRB5* gene expression in B cells isolated from the peripheral blood of 11 HIV-negative healthy individuals (control) and 10 people living with HIV; their clinicopathological characteristics are summarized in **Table 1**. We found that the expression of *HLA-DRB1* was indeed decreased (0.64 ± 0.12 in people living with HIV *vs* 1.00 ± 0.12 in the control group, $p = 0.0463$, t-test, **Figure 2I**), while *HLA-DRB5* expression remained unchanged (1.10 ± 0.20 in people living with HIV *vs* 1.00 ± 0.12 in the control group, $p = 0.6889$, t-test, **Figure 2J**); this might indicate differential transcriptional regulation of these genes. Thus, the decrease in HLA-DR surface expression in people with HIV could result from a transcriptional downregulation of *HLA-DRB1* and could be due to the action of Tat protein

secreted from infected CD4+ T cells. We decided to confirm this by co-cultivating BLAS cells with CD4+ T cells that expressed Tat (Jurkat-Tat) and a respective control (Jurkat) (**Figure 2K, 2L**). Jurkat-Tat cells were previously shown to efficiently secrete Tat protein [6]. Briefly, $BLAS^{GFP}$ cells were mixed with the Jurkat cells and co-cultured for 7 days to allow for long-term effects of Tat to manifest, HLA-DR expression was then measured in GFP+ B cells (**Figure 2K**). The proposed approach to evaluate the long-term effects of Tat on B cells allows to overcome the difficulties related to the use of recombinant Tat protein (susceptibility to oxidation, quick degradation). We found that HLA-DR expression in $BLAS^{GFP}$ cells co-cultured with Jurkat-Tat cells decreased significantly as compared to $BLAS^{GFP}$ cells co-cultured with Jurkat cells (0.586 ± 0.053 vs 1.000 ± 0.014, $p < 0.0001$, ANOVA, Tukey's post-hoc test, **Figure 2M**).

It has been previously demonstrated that Tat is taken up by cells mainly through endocytosis [16,37–39]. To confirm this, a fluorescently labelled Tat-derived cell-penetrating peptide (Tat CPP-Cy5) was used. Cells were first pre-treated or not (control) for 1 hour with genistein, an inhibitor of endocytosis [40], and then Tat CPP-Cy5 was added to cell medium for 30 minutes followed by extensive cell wash and subsequent analysis of Tat CPP-Cy5 cellular and nuclear penetration (**Supplementary figure 6**). The addition of genistein drastically inhibited Tat CPP-Cy5 penetration in cells (**Supplementary figure 6**). We next treated an aliquot of co-cultivated cells with genistein as a control that HLA-DR downregulation was induced by Tat penetration into B cells in our co-culture experiments, (**Figure 2K**). When Tat entry in B cells was blocked by genistein, no decrease in HLA-DR expression in $BLAS^{GFP}$ cells co-cultured with Jurkat-Tat cells as compared to $BLAS^{GFP}$ cells co-culutred with Jurkat cells was observed (**Figure 2M**). These results confirm our RNA-seq data and demonstrate for the first time that

chronic HIV-1 Tat secretion from infected CD4+ T cells can induce HLA-DR downregulation in B cells.

Chronic HIV-1 Tat decreased classical NF-κB activation in B cells

We next studied the mechanism of action of HIV-1 Tat in B cells that led to HLA-DR downregulation. HIV-1 Tat reprograms host gene expression both directly through chromatin binding and transactivation/repression by controlling RNA polymerase II recruitment to target genes and indirectly, *e.g.* through protein-protein interaction with host transcription factors (TFs) [41,42]. The mutation of C22 in the transactivation domain largely disrupts Tat interaction with chromatin and direct regulation of gene expression (both stimulation and downregulation), favouring the indirect effects of Tat [41]. Our results demonstrated that in B cells, a high proportion of the genes were regulated by Tat indirectly, sharing a significant overlap with TatC22G-regulated genes (**Figure 1G, 1H, Supplementary Figure 8**). This included *HLA-DR* genes, downregulated by both Tat and TatC22G (**Figure 2**). Consequently, we assumed that *HLA-DR* downregulation could be caused by Tat interaction with the TFs regulating MHC class II gene expression. HIV-1 Tat was previously shown to inhibit class II, major histocompatibility complex, transactivator (CIITA), a transcriptional regulator of MHC class II molecules, by competing for the binding to cyclin T1, a component of P-TEFb complex [43]. The interaction between HIV-1 Tat and human cyclin T1, however, requires C22 residue and TatC22G mutant can not bind cyclin T1 [44], and thus can not compete with CIITA. Our results indicated that both Tat and TatC22G decreased the expression of HLA-DR genes in B cells (**Figure 2**). Moreover, when we knocked down the expression of *CIITA* in RPMI8866 cells *via* shRNA, Tat was still able to downregulate HLA-DR expression as compared to GFP (0.529 ± 0.061 in $RPMI8866^{Tat}$ vs 1.493 ± 0.178 in $RPMI8866^{GFP}$ with stable

CIITA-shRNA expression, $p < 0.0001$, ANOVA, Tukey's post-hoc test) (**Supplementary figure 7**). This indicates that the downregulation of HLA-DR expression by HIV-1 Tat in B cells is not exclusively dependent on CIITA and might involve interaction with other TFs.

The presence of Tat could either lead to activation of TFs that downregulate target gene expression or inhibition of TFs that upregulate target gene expression. To test this hypothesis, we performed TF-target enrichment analysis to predict potential TFs that could regulate the expression of a subset of downregulated genes common between RPMI8866^{Tat} and BLAS^{Tat} (**Figure 3**). We found that the highest overlap with the downregulated target gene set was for RelA and NFKB1 TFs of the NF-κB pathway (**Figure 3A**). Since indirect gene regulation in Tat-expressing cells is not dependent on C22 residue, we also performed the enrichment for DEGs common between Tat- and TatC22G-expressing RPMI8866 and BLAS cells. Again, RelA and NFKB1 were significantly enriched with the highest overlap for the target gene set when considering the union (**Figure 3B**) and intersection (**Figure 3C**) for two cell lines. Thus, the gene downregulation in response to Tat or its mutant was potentially linked to a decrease in NF-κB pathway activity, since an enrichment for NF-κB-regulated targets was observed among downregulated genes. Interestingly, both RelA and NFKB1 are confirmed Tat-interacting partners identified in at least two different proteome datasets [42].

We next decided to confirm that HLA-DR expression was regulated by the NF-κB pathway in B lymphoblastoid cells. To do so, we treated RPMI8866 and BLAS cells with the inhibitors of NF-κB activation: the inhibitor of IκB kinase (IKK) Bay 11-7082, which inhibited both NF-κB1 (classical) and NF-κB2 (alternative) pathways [45], proteasome inhibitor MG132 that prevented pIκB and p100 degradation and thus also inhibited both NF-κB1 (classical) and NF-κB2 (alternative) pathways [46,47], and inhibitor of RelB:p52

nuclear import SN52, which specifically inhibited NF-κB2 (alternative) pathway [48]. We then analyzed surface and total HLA-DR expression by flow cytometry and western blotting. We found that treatment with Bay 11-7082, MG132 or SN52 decreased ~2-fold both surface and total HLA-DR expression in RPMI8866 B lymphoblastoid cells (**Figure 3D-3O**). The same results were observed in BLAS cells (**Supplementary figure 9**). Thus, HLA-DR was regulated by the NF-κB pathway in B lymphoblastoid cells.

We next tested whether NF-κB activation decreased in lymphoblastoid cells expressing Tat. To measure NF-κB activation, we analyzed the cytosolic and nuclear content of key proteins of the NF-κB signalling pathway: inhibitory protein IκBα and its phosphorylated form p-IκBα, transactivation-competent components RelA and RelB, and their partners p50 (NFKB1) and p52 (NFKB2) as well as their precursors (p105 and p100) (**Figure 4A-4G, Supplementary figure 10**). When NF-κB is activated, IκBα in the cytoplasm is phosphorylated and degraded, which permits RelA/p50 (classical) or RelB/p52 (alternative) dimer translocation from the cytoplasm into the nucleus where they regulate gene expression [49]. The presence of Tat or TatC22G in cells led to an increased IκBα phosphorylation and a decrease in total IκBα content in the cytoplasm of RPMI8866 cells (**Figure 4A, 4B, Supplementary figure 10A, 9B**) while RelA accumulated in the cytoplasm of Tat- or TatC22G-expressing cells and decreased in the nuclear compartment, which confirmed our *in silico* predicted decrease in the NF-κB activity (**Figure 4A, 4C**). No significant changes in RelB, NFKB1 and NFKB2 cytoplasmic/nuclear presence were detected (**Supplementary figure 10A, 10C, 10D, Figure 4A, 4D)** while an increase in nuclear p-IκBα in Tat expressing cells was observed (**Supplementary figure 10A, 10B**).

To corroborate the observed results, we also performed immunofluorescent staining of RelA and NFKB1 in RPMI8866 cells; to detect nuclear translocation of RelA and

NFKB1, nuclei were counterstained with DAPI (**Figure 4E-4F**). While in RPMI8866 and RPMI8866^{GFP} cells RelA showed mostly nuclear staining, in RPMI8866^{Tat} and RPMI8866^{TatC22G} cells, RelA was sequestered in the cytoplasm (**Figure 4F**), which indicated lower classical NF-κB activation in Tat-expressing B cells. This was further confirmed when we calculated the ratio of nuclear to total cellular RelA fluorescence in individual cells: the mean ratio of RelA was significantly lower in RPMI8866^{Tat} and RPMI8866^{TatC22G} cells as compared to RPMI8866 and RPMI8866^{GFP} cells (0.688 ± 0.010, 0.707 ± 0.010, 0.746 ± 0.011, 0.768 ± 0.025, respectively, $p < 0.01$ and $p < 0.05$ compared to RPMI8866 cells, ANOVA, Tukey's posthoc test, **Figure 4E**). No significant changes in NFKB1 nuclear to total ratio were observed between studied cell lines, which was in accordance with western blotting results (**Figure 4E**). Additionally, no significant changes in RelB distribution were observed between studied cell lines (**Supplementary figure 11**). In BLAS^{Tat} and BLAS^{TatC22G} cells, RelA was also more present in the cytoplasm when compared to BLAS and BLAS^{GFP} cells (**Supplementary figure 12**), which confirmed lower classical NF-κB activation in Tat-expressing B cells.

Finally, to confirm that the observed RelA sequestration in the cytoplasm of B cells was associated with the decrease in NF-κB-mediated gene transcription, we generated an NF-κB-mCherry reporter plasmid, which consisted of five repeats of the NF-κB response elements, a minimal promoter and red fluorescent protein mCherry2 as a reporter gene (**Figure 4G**). RPMI8888 cell transfection with this plasmid led to a detectable expression of mCherry2, which was significantly higher upon NF-κB activation with PMA (**Figure 4H, 4I**). In the next step, we analysed the NF-κB reporter activity in RPMI8866, RPMI8866^{GFP}, RPMI8866^{Tat} and RPMI8866^{TatC22G} cells (**Figure 4J, 4K**). mCherry expression was significantly lower in RPMI8866^{Tat} and RPMI8866^{TatC22G} cells when

compared to RPMI8866 and RPMI8866^{GFP} cells (0.605 ± 0.079 in RPMI8866^{Tat} and 0.509 ± 0.041 in RPMI8866^{TatC22G} vs 1.000 ± 0.053 in RPMI8866 cells and 1.037 ± 0.066 in RPMI8866^{GFP} cells, p = 0.0009 and p <0.0001 relative to RPMI8866, respectively, ANOVA, Tukey's posthoc test). No significant differences in mCherry fluorescence level were found between RPMI8866^{GFP} and RPMI8866 (1.037 ± 0.066 in RPMI8866^{GFP} vs 1.000 ± 0.053 in RPMI8866 cells, p = 0.9793, ANOVA, Tukey's posthoc test). Additionally, the NF-κB reporter activity was decreased by ~10% in BLAS^{GFP} cells co-cultured with Jurkat-Tat cells for 7 days (0.9142 ± 0.012 vs 1.000 ± 0.007, p = 0.0001, t-test, **Supplementary figure 13B**), while the NF-κB reporter activity in Jurkat-Tat cells was higher than in Jurkat cells (2.811 ± 0.119 vs 1.000 ± 0.020, p < 0.0001, t-test, **Supplementary figure 13C**), which is in agreement with previous reports [35,50]. These results confirmed that HIV-1 Tat presence induced a decrease in classical NF-κB activation in lymphoblastoid B cells.

In our subsequent analysis, we proceeded to verify whether the Tat-induced sequestration of the active component of the NF-κB pathway, RelA, within the cytoplasm was dependent on the functionality of the nuclear export. To accomplish this, we treated cells with the nuclear export inhibitor leptomycin B (LMB) and examined the distribution pattern of RelA with or without treatment (**Figure 4L**). Our observations revealed that the inhibition of nuclear export cancelled the effect of HIV-1 Tat and TatC22G on RelA subcellular localisation (**Figure 4L, 4M**). As a result of nuclear export inhibition, RelA in RPMI8866^{Tat} and RPMI8866^{TatC22G} cells transitioned from cytoplasmic to primarily nuclear localization similar to what was observed in RPMI8866 cells. These findings demonstrate that Tat promotes the nuclear export of RelA (rather than inhibits RelA nuclear import), as

evidenced by the restoration of RelA accumulation within the nucleus upon nuclear export inhibition.

In order to further substantiate our findings regarding the nuclear export of RelA by HIV-1 Tat and its implications for MHC class II gene regulation, we conducted a chromatin immunoprecipitation assay followed by a quantitative polymerase chain reaction (ChIP-qPCR). Specifically, we performed ChIP using antibodies targeting RelA and focused on RelA binding to the promoters of the *HLA-DRB1* and *HLA-DRB5* genes. Our results demonstrated a significant decrease in the binding of RelA to the promoters of both *HLA-DRB1* and *HLA-DRB5* genes in Tat-expressing cells compared to the control cells (**Figure 4N**). In the *HLA-DRB1* promoter, RelA binding was significantly reduced in RPMI8866^{Tat} cells compared to RPMI8866^{GFP} (% input 0.387 ± 0.112 vs. 1.241 ± 0.419, p = 0.0303, two-way ANOVA, Tukey's posthoc test) and was lower compared to RPMI8866 cells (0.946 ± 0.155), although did not reach the statistical significance. Similarly, at the *HLA-DRB5* promoter, RelA binding was notably decreased in RPMI8866^{Tat} compared to RPMI8866 and RPMI8866^{GFP} (0.474 ± 0.060 vs 1.366 ± 0.081 and 2.439 ± 0.294, p = 0.0069 and $p < 0.0001$, respectively, two-way ANOVA, Tukey's posthoc test) cells. No significant differences for the RelA binding to the control *ACTB* promoter in RPMI8866, RPMI8866^{GFP} and RPMI8866^{Tat} cells were found. This reduction in NF-κB binding to the promoters of MHC class II genes corroborates our earlier observations of Tat-induced cytoplasmic sequestration of RelA and provides mechanistic insights into the downregulation of HLA-DR expression.

HIV-1 Tat presence in B cells reduced EBV-specific CD4+ T cell response

The expression of cell surface HLA-DR is downregulated during B cell lymphomagenesis decreasing the efficacy of functional immune responses and worsening

the prognosis [51,52]. MHC class II-restricted CD4+ T cell response is also responsible for the control of EBV infection and EBV-induced B cell proliferation [53]. To confirm that Tat-induced HLA-DR downregulation could impair CD4+ T cell response and contribute to the escape from the immune surveillance, we generated a BLAS-reactive EBV-specific CD4+ T cell line. Briefly, PBMCs from healthy donor AS were depleted in CD8+ T cells and stimulated with autologous irradiated BLAS cells which caused their *in vitro* expansion (**Figure 5A**). After seven restimulation cycles, the T cell line was >90% CD4+ by flow cytometric analysis (see **Figure 5B**).

To study EBV-specific CD4+ T cell responses, we co-cultured BLAS cells with autologous PBMCs or the generated CD4+ T cell lines and analyzed the percentage of activated IFNγ+/CD4+ cells in response to antigen stimulation (**Figure 5C**). As expected, a small proportion of PBMCs were responsive to BLAS without any preceding stimulation (**Figure 5D**). On the contrary, the co-culture of the CD4+ T cell line with BLAS led to a significant increase in the percentage of activated IFNγ+/CD4+ cells (**Figure 5D**). Notably, this percentage was significantly lower when CD4+ T cell line was co-cultured with $BLAS^{Tat}$ or $BLAS^{TatC22G}$ compared to BLAS or $BLAS^{GFP}$ (24.70 ± 0.200, 23.35 ± 0.450, 27.60 ± 0.438, 31.00 ± 0.473, respectively, $p < 0.0001$, 2-way ANOVA, Tukey's post-hoc test), confirming the functional significance of Tat-downregulated HLA-DR expression in lymphoblastoid cells (**Figure 5D**).

EBV-specific CD4+ T cells are also capable of inducing lymphoblastoid cell cytotoxic lysis that necessitates MHC class II-restricted recognition [25,54]; therefore we decided to measure the cytotoxic activity of the generated BLAS-reactive CD4+ T cell line. The cytotoxicity was assessed as the percentage of specific lysis. Briefly, sensitive target lymphoblastoid cells (BLAS) and control target lymphoblastoid cells (RPMI8866)

were labelled with CFSE at two different concentrations to allow their differentiation between each other and with CD4+ T cells (**Figure 5E**). The effector (E, CD4+ T cell line) and target cells (T, BLAS or RPMI8866) were mixed at various E/T ratios and incubated for 4 hours; the percentage of specific lysis was derived from the decrease in the sensitive target population (**Figure 5F**). We found that $BLAS^{Tat}$ or $BLAS^{TatC22G}$ cells were much less susceptible to cytotoxic cell lysis by CD4+ T cells as compared to BLAS cells, e.g., at E/T ratio 10:1 the percentage of specific lysis was 19.52 ± 4.632 in $BLAS^{Tat}$ cells and 20.08 ± 4.510 in $BLAS^{TatC22G}$ cells compared to 42.04 ± 3.806 in BLAS cells ($p < 0.0001$, 2-way ANOVA, Tukey's posthoc test, **Figure 5G**). Taken together, we provide compelling evidence that Tat-induced HLA-DR expression downregulation contributes to the immune escape of EBV-infected lymphoblastoid B cells.

HIV-1 Tat presence in the serum of people living with HIV was linked to decreased HLA-DR surface expression in B cells

To confirm the observed role of HIV-1 Tat in the regulation of HLA-DR expression in B cells and EBV-specific immunity, we analysed HLA-DR surface expression in people living with HIV from an independent cohort. PBMC from 6 HIV-negative healthy individuals (control) and 17 people living with HIV, whose clinicopathological characteristics are summarized in **Table 2**, were immunophenotyped and analysed by flow cytometry. B cells in people with HIV exhibited a tendency to have lower HLA-DR expression compared to HIV-uninfected controls (0.828 ± 0.0494 vs. 1.000 ± 0.051, $p = 0.0677$, t-test, **Figure 6A**). This observation was consistent across both memory (0.7938 ± 0.051 vs. 1.000 ± 0.053, $p = 0.0352$, t-test, **Figure 6B**) and naïve B cells (0.8047 ± 0.049 vs. 1.000 ± 0.06661, $p = 0.0451$, t-test, **Figure 6C**). Furthermore, among PLWH, those with seric Tat concentrations exceeding 2.5 ng/ml demonstrated significantly diminished

HLA-DR surface expression compared to PLWH with lower Tat concentrations (0.656 ± 0.182 vs 0.882 ± 0.184, p = 0.0478, t-test, **Figure 6D**). Moreover, EBV reactivation as detected by PCR EBV DNA levels surpassing 2.26 log had a tendency to be associated with reduced HLA-DR expression in B cells (0.729 ± 0.145 vs. 0.9170 ± 0.214, p = 0.0543, t-test, **Figure 6E**). Collectively, these findings underscore a link between HIV-1 Tat presence and decreased HLA-DR expression on B cells, highlighting potential implications for EBV-specific immune response modulation in people living with HIV.

Discussion

cART has reshaped HIV infection from an almost inevitably lethal disease to a manageable chronic infection for the majority of infected individuals. Nevertheless, HIV infection remains incurable and, despite suppression of viral replication and immune restoration, people living with HIV still have an increased risk of B cell malignancies [3]. In the current study, we identified some mechanisms that contributed to B cell lymphomagenesis in this population. B cells are not infected by HIV, although they can be affected by HIV indirectly, *e.g.* through co-existence with HIV-infected cells and the chronic action of secreted viral proteins produced by the cells bearing both normal and defective HIV proviruses [5]. Likewise, HIV-1 Tat, a crucial regulator of HIV transcription, is efficiently exported from infected cells and uptaken by neighbouring non-infected cells [6,16]. The chronic presence of HIV-1 Tat in people with HIV is estimated to alter the physiology of multiple cells not infected by HIV [55,56] and contribute to neurocognitive [57,58], cardiovascular disorders [59], and adipose tissue senescence [60]. To study the effects of chronic HIV-1 Tat presence on B cells, we used lymphoblastoid B cell lines that ectopically expressed HIV-1 Tat or its mutant TatC22G, deprived of transactivation capacity. The proposed approach to evaluate the long-term effects of Tat on B cells allows

to overcome the difficulties related to the use of recombinant Tat protein (susceptibility to oxidation, quick *ex vivo* degradation).

We performed a genome-wide analysis of cellular gene expression (RNA-sequencing analysis) of two EBV-immortalized lymphoblastoid cell lines (RPMI88666 and a freshly immortalized BLAS cell line) that expressed Tat and revealed that Tat regulated the expression of hundreds of genes that included protein-coding genes and lncRNAs (**Figure 1D-1F**). More precisely, Tat-downregulated genes were enriched for the GO BP terms: leukocyte cell-cell adhesion, positive regulation of T cell activation, T cell receptor signalling pathway, peptide antigen assembly with MHC class II protein complex, antigen processing and presentation of exogenous peptide antigen *via* MHC class II; and KEGG pathways: cell adhesion molecules, intestinal immune network for IgA production, hematopoietic cell lineage, viral myocarditis, TNF signalling pathway (**Figure 1J-1M**). Therefore, Tat downregulated a subset of genes related to MHC class II (including *HLA-DRB1* and *HLA-DRB5*) and could potentially decrease CD4+ T cell activation in response to B cells infected by EBV.

EBV is a γ-herpesvirus that infects more than 90% of the human adult population [61,62]. Compared to the general population, people living with HIV are more likely to be seropositive to EBV and more often present EBV reactivation [63,64]. Not surprisingly, B cell lymphomas in people living with HIV are more frequently associated with EBV [65]. Failing EBV control and EBV reactivation prior to the oncological disease are important steps for oncogenesis and poor prognosis in people with HIV regardless of their immune status [66–69]. Notably, HIV-positive people progressing to B cell subtype primary central nervous system lymphoma were recently found to lack EBV-specific CD4+ T cells irrespective of their absolute CD4+ T cell counts [70]. A critical role for EBV-specific

CD4+ T cells in coordinating an immune response to Burkitt's lymphoma was previously shown: unlike EBNA-1 specific CD8+ T cells, EBNA-1 specific CD4+ T cells were necessary and sufficient for tumor growth inhibition in mice [71].

Our results suggest that HIV-1 Tat protein can contribute to B cell immune escape by transcriptionally downregulating *HLA-DRB1* and *HLA-DRB5*, which led to a decrease in the surface HLA-DR expression (**Figure 2A-2H**). HLA-DR surface expression was previously shown to be decreased in B cells from people with HIV [36]. Here we confirmed that both memory and naïve B cells from HIV-positive individuals exhibited consistently lower HLA-DR surface expression compared to the controls (**Figure 6A-6C**). Remarkably, people with HIV with higher seric Tat concentrations displayed a significantly decreased HLA-DR (**Figure 6D**). In an independent cohort, we demonstrated that *HLA-DRB1* expression in B cells from people with HIV was decreased on the mRNA level (**Figure 2I**), which can be attributed to the chronic secretion of Tat protein from infected cells. Additionally, prolonged co-culture of lymphoblastoid cells with CD4+ T cells that express Tat led to a significant decrease in HLA-DR expression in lymphoblastoid cells; this effect was blocked when Tat entry in cells was inhibited by genistein, an inhibitor of endocytosis (**Figures 2K-2M**).

The observed effect of HIV-1 Tat on HLA-DR expression in lymphoblastoid B cells was not dependent on Tat C22 residue (**Figure 2A-2H**), which suggests that the mechanism of Tat action on HLA-DR expression was indirect, probably through protein-protein interaction with host proteins. The mutation of C22 in the transactivation domain largely disrupts Tat interaction with chromatin and prevents direct regulation of gene expression (both stimulation and downregulation), favouring the indirect effects of Tat [41]. The effect of Tat on HLA-DR expression in B cells was also not dependent on

CIITA (**Supplementary figure 7**). Tat action might have inhibited other TFs that normally upregulate their targets, leading to the appearance of the downregulated gene subset. We performed TF-target enrichment analysis to predict potential TFs that regulated the expression of downregulated genes, common between Tat and TatC22G and found that the highest overlap with the downregulated target gene set was for RelA and NFKB1 TFs of NF-κB pathway (**Figure 3A-3C**). RelA and NFKB1 (p50) are the key components of the classical NF-κB pathway: upon activation, RelA:p50 dimer translocates into the nucleus, where it regulates gene expression; thus, NF-κB activation can be assessed by RelA nuclear translocation [49].

Using a set of inhibitors of NF-κB activation, we confirmed that HLA-DR expression was indeed regulated by the NF-κB pathway in B lymphoblastoid cells (**Figures 3D-3O, Supplementary figure 9**), and as predicted *in silico*, we found that Tat or TatC22G chronic presence in B cells led to increased RelA sequestration in the cytoplasm, indicating reduced NF-κB activity (**Figure 4**). RelA sequestration in the cytoplasm, induced by HIV-1 Tat, relied on nuclear export and was accompanied by a decrease in NF-κB-mediated transcription and decreased RelA association with the promoters of *HLA-DRB1* and *HLA-DRB5* genes (**Figure 4**). Thus, HLA-DR downregulation in response to Tat or its mutant TatC22G was linked to a decrease in NF-κB pathway activity. Notably, an NF-κB inhibitory effect was previously shown for another viral protein: EBV Zta (*BZLF1* gene) [72], a protein that has similar activities as HIV-1 Tat (transcriptional regulation, host chromatin binding, cell penetration) [73].

It was previously shown that the acute action of Tat (treatment with recombinant protein or expression induction) was, in fact, associated with the activation of the NF-κB pathway [17,35,74]. The mechanism of NF-κB activation was related to Tat interaction

with the inhibitory protein IκBα and Tat-induced IκBα degradation; this was demonstrated in Jurkat T cells, monocytes/macrophages and astrocytes [35,74,75]. We found that Tat presence led to an increased IκBα phosphorylation and a decrease in total IκBα cytoplasmic content in lymphoblastoid B cells (**Figure 4A-4B, Supplementary figure 10A, 10B**), which is in agreement with previous results. However, we also found that the phosphorylated IκBα was accumulated in the nucleus of Tat-expressing B cells (**Supplementary figure 10A, 10B**). The presence of nuclear IκB promotes NF-κB nuclear export and decreases the NF-κB-dependent gene transcription [76–78], including a decrease in Tat-induced NF-κB-dependent LTR activation [79]. In our case, the transactivation-active component of NF-κB signalling, RelA, was more present in the cytoplasm and decreased in the nuclear compartment in Tat-expressing cells. This might be associated with an increase in nuclear p-IκBα in Tat-expressing cells. To our knowledge, little is known about the role of the phosphorylated form of IκBα in the nucleus (although both IκBα and its kinases IKK are present in the nucleus), but chronic action of Tat may lead to an increased NF-κB nuclear export through p-IκBα accumulation/stabilisation in the nucleus, which should be further explored. The inhibition of nuclear export restored the accumulation of RelA in the nuclei of Tat-expressing B cells (**Figure 4L, 4M**), reinforcing the proposed model of Tat's role in promoting the nuclear export of RelA. Apart from IκB, other proteins that interact with RelA and shuttle between the nucleus and cytoplasm (e.g., p28) may also promote RelA export from the nucleus [80]. HIV-1 Tat directly interacts with both RelA and NFKB1 components of the NF-κB pathway [35,42] and is able to shuttle between the nucleus and cytoplasm [81], which may constitute another potential mechanism of Tat-induced NF-κB pathway inactivation in B cells.

MHC class II-restricted CD4+ T cell response controls EBV infection and

EBV-induced B cell proliferation [53] and the loss of cell surface HLA-DR promotes B cell lymphomagenesis by decreasing the efficacy of functional immune response [51,52]. Of note, a recent large genome-wide association study found that anti-EBV antibody response presents a strong association with *HLA-DRA*, *HLA-DQA1* and *HLA-DQB1* loci [63], which confirms the importance of MHC class II-restricted response for the immune control of EBV. We demonstrated that EBV-infected B cells that expressed Tat were less responsive to EBV-specific CD4+ T cell-mediated cytotoxic lysis compared to WT cells and to a smaller degree stimulated EBV-specific CD4+ T cell activation as evidenced by IFNγ production (**Figure 5**). Consequently, Tat-induced HLA-DR downregulation could impair CD4+ T cell response and contribute to the escape from immune surveillance of EBV-infected B cells. Notably, we observed a trend linking EBV reactivation, denoted by elevated PCR EBV DNA levels, with reduced HLA-DR expression in people living with HIV (**Figure 6E**).

Besides antigen presentation, MHC class II is a signalling molecule that regulates B cell activation, proliferation, differentiation and promotes antibody production during cognate CD4+ T cell-B cell interaction [82]. B cell activation is triggered by the antigen binding to the B cell receptor (BCR), which initiates a cascade of intracellular signalling, including NF-κB activation, and stimulates B cell differentiation into antibody-producing B cells [83,84]. A potential consequence of reduced NF-κB pathway activity and MHC class II expression, induced by HIV-1 Tat in B cells, is impaired B cell activation, leading to a compromised ability to initiate an effective immune response against pathogens, including HIV itself. It is known that despite its circulation in the blood and effective cell penetration, HIV-1 Tat is able to elicit an antibody-mediated immune response only in ~20% of people living with HIV [85]. HIV-1 Tat-mediated downregulation of MHC class

II genes in B cells might contribute to the defects in B cell activation and antibody response.

MHC class II also serves as a co-receptor for EBV entry by interacting with EBV membrane glycoprotein 42 (gp42, encoded by *BZLF2* gene) during B cell infection [86]. Upon EBV reactivation, the interaction of newly produced gp42 with the MHC class II complex targets gp42 for degradation, which leads to the release of gp42-depleted viral particles that preferentially target epithelial cells [87]. This results in the switch of EBV tropism from B cells to epithelial cells and may limit the direct EBV spread from reactivating B cells to other B cells [87]. In general, even under cART treatment people living with HIV tend to have higher levels of EBV DNA in their blood [88,89] and in PBMCs [88,90–92] as compared to HIV-negative individuals. Our data demonstrate that despite the effective control of HIV infection exerted by cART for the majority of HIV-positive individuals in the studied cohort (**Table 2**), 8/17 of them (47%) had high levels of EBV DNA in the whole blood (**Table 2**). The expansion of the pool of EBV-infected B cells in people living with HIV (and hence higher EBV load) might partly arise from HIV-1 Tat penetration in EBV-infected cells, which decreases MHC class II expression and might increase the production of gp42-enriched viral particles that would target B cells, which requires further studies.

Conclusions

In conclusion, HIV-1 Tat chronic presence can contribute to immune evasion of B cells *via* HLA-DR downregulation, thus leading to the acquisition of a cancer hallmark and B cell lymphoma predisposition in people living with HIV. Targeting HIV-1 Tat secretion by infected cells or its penetration in non-infected cells is a promising therapeutic strategy.

List of abbreviations

ANOVA, analysis of variance;

BL, Burkitt lymphoma;

cART, combination antiretroviral therapy;

CFSE, carboxyfluorescein diacetate succinimydyl ester;

DEGs, differentially expressed genes;

DLBCL, diffuse large B-cell lymphoma;

DTT, dithiothreitol;

EBV, Epstein-Barr virus;

E/T, effector/target;

GFP, green fluorescent protein;

GO, gene ontology;

GO BFP, gene ontology biological process;

HIV, Human immunodeficiency virus;

KEGG, Kyoto Encyclopedia of Genes and Genomes;

LTR, long terminal repeat;

MHC, major histocompatibility complex;

ORA, overrepresentation analysis;

PBMC, peripheral blood mononuclear cells;

PBS, phosphate-buffered saline;

P-TEFb, positive transcription elongation factor b;

qPCR, quantitative polymerase chain reaction;

TAR, trans-activation response;

SDS, sodium dodecyl sulfate;

SEM, standard error of the mean;

SDS-PAGE, SDS-polyacrylamide gel electrophoresis;

TBS, Tris-buffered saline;

TF, transcription factor.

Declarations

Ethics approval and consent to participate

Blood samples from HIV-positive individuals who signed a written informed consent for the study and were treated at the Department of Clinical Immunology, Hôpital Saint-Louis, Paris, France, were collected in accordance with the French legislation. This study was registered as a non-interventional study at the Agence Nationale de Sécurité du Médicament (2016-A01316-45).

Consent for publication

Consent for publication has been obtained from the patients.

Availability of data and materials

The dataset supporting the conclusions of this article (raw RNA-seq data as well as processed data (gene counts)) is available in the GEO repository, accession number GSE212499, https://www.ncbi.nlm.nih.gov/geo/query/acc.cgi?acc=GSE212499.

Competing interests

The authors report there are no competing interests to declare.

Funding

This study was supported by Cancéropole IdF, the IDB RAS Government basic research program (0088-2021-0007), the Russian Science Foundation (grant 21-74-20134 to EVS) and the Ministry of Science and Higher Education grants 075-15-2020-773 to YV. AK is a recipient of the Eiffel Fellowship from Campus France. IT is a recipient of the French Government scholarship awarded by the Ministry of Foreign Affairs from Campus France.

Authors' contributions

A.S. performed research, analyzed data and wrote the paper; C.H., Y.K., A.K., I.T., K.B., O.S.R., P.R. and D.G. performed research and analyzed data; B.B. and E.V.S. performed research and contributed new reagents; L.G., D.B. and E.O. provided samples from patients and clinical data; Y.V. designed research, analyzed data and wrote the paper. All authors read and approved the final manuscript.

Acknowledgements

The authors thank Tudor Manoliu, Flavien Berthou and Cyril Catelain, Gustave Roussy Cancer Campus, Plateforme Imagerie et Cytométrie - UMS 23/3655 - Université Paris Saclay, Villejuif, France for technical help.

Tables

Table 1. The main clinicopathological features of people living with HIV from the first cohort investigated in this study. cART - combination antiretroviral therapy.

#	Age	Sex	CD4+ T cells ($\times 10^6$/l)	Plasma HIV RNA ($\log_{10}$ copies/ml)	cART	Effective cART duration (months)	Seric Tat concentration (ng/ml)	*HLA-DRB1* relative expression in B cells	*HLA-DRB5* relative expression in B cells
1	69	M	20	6.37	No	0	0.34	0.01	0.00
2	48	M	247	4.83	No	0	5.72	1.07	0.95
3	51	F	556	<1.3	Yes	102	0.21	0.10	0.73
4	49	M	683	<1.3	Yes	19	0.67	0.44	1.42
5	64	M	737	<1.3	Yes	203	0.78	0.81	0.54
6	59	M	747	<1.3	Yes	66	1.14	1.20	0.79
7	48	F	535	<1.3	Yes	59	1.55	0.82	1.67
8	56	F	502	<1.3	Yes	100	2.83	0.76	1.06
9	62	F	536	<1.3	Yes	73	9.02	0.60	2.20
10	66	M	527	1.78	Yes	98	1.7	0.55	1.63

Table 2. The main clinicopathological features of people living with HIV from the second cohort investigated in this study. cART - combination antiretroviral therapy.

#	Age	Sex	CD4+ T cells ($\times 10^6$/l)	Plasma HIV RNA (copies/ml)	Whole blood EBV PCR (log)	cART start date	Seric Tat concentration (ng/ml)	Relative HLA-DR surface expression
1	69	M	656	108	3.2	1997	6.04	0.75
2	47	M	816	<20	<2.18	2015	6.29	0.80
3	48	M	727	<20	3.07	2012	4.63	0.39
4	69	F	391	<20	<2.18	2015	<2.5	0.62

5	29	F	563	<20	<2.18	2020	<2.5	1.01
6	70	F	757	<20	<2.18	2008	<2.5	0.91
7	47	F	644	<20	2.61	2010	<2.5	0.86
8	57	M	336	51	3.18	2014	<2.5	0.79
9	69	M	366	<20	<2.26	1995	<2.5	1.31
10	77	M	374	<20	<2.26	2003	<2.5	1.08
11	59	M	499	23	2.33	1995	<2.5	0.83
12	46	F	475	<20	<2.26	2008	4.02	0.68
13	61	M	359	<20	2.86	2011	<2.5	0.75
14	59	M	905	<20	3.73	2021	<2.5	0.75
15	63	M	500	<20	2.61	2000	<2.5	0.71
16	62	F	1428	41	<2.26	1993	<2.5	1.02
17	55	M	468	76100	<2.26	1997	<2.5	0.82

Figures

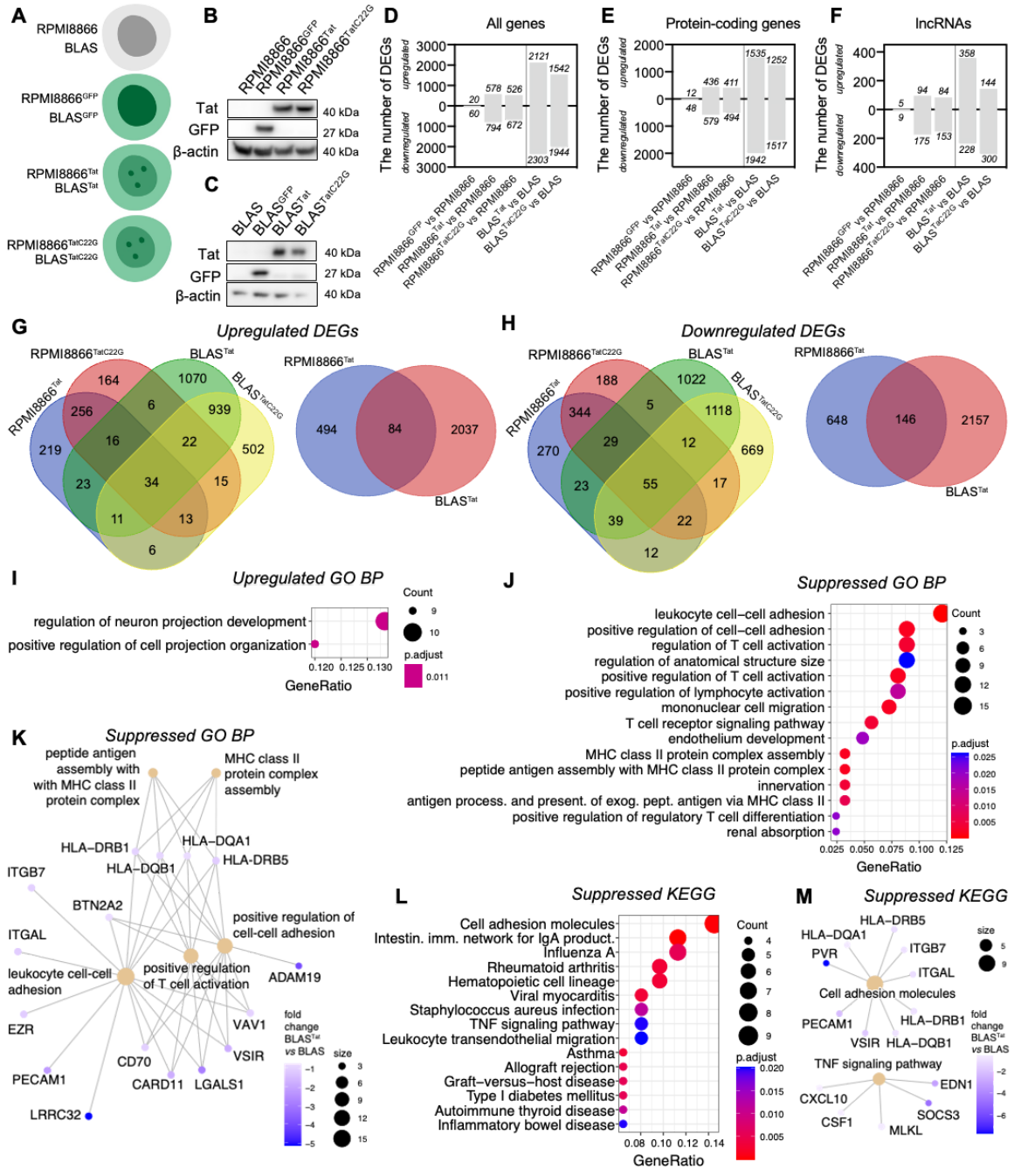

Figure 1. HIV-1 Tat protein presence affects the gene expression profile of lymphoblastoid B cells. (A) Cell lines that were used to analyze the action of HIV-1 Tat on cultured B cells: human EBV-transformed B lymphoblastoid cell line RPMI8866 and freshly

EBV-transformed B lymphoblastoid cell line from healthy donor AS (BLAS, established by EBV (B95-8) immortalization of mature B cells), which were used as a negative control; cells expressing EGFP (RPMI8866^{GFP} and BLAS^{GFP}), which were used as a control of the possible effects of vector integration and the fluorescent tag; cells expressing HIV-1 Tat fused with EGFP (RPMI8866^{Tat} and BLAS^{Tat}); and cells expressing mutated HIV-1 TatC22G deprived of transactivation activity fused with EGFP (RPMI8866^{TatC22G} and BLAS^{TatC22G}). (B) Western blotting analysis of Tat and GFP expression in RPMI8866 cell lines. β-actin was used as a loading control. (C) Western blotting analysis of Tat and GFP expression in BLAS cell lines. β-actin was used as a loading control. (D) The number of all differentially expressed genes (DEGs) found in comparisons: RPMI8866^{GFP} *vs* RPMI8866, RPMI8866^{Tat} *vs* RPMI8866, RPMI8866^{TatC22G} *vs* RPMI8866, BLAS^{Tat} *vs* BLAS, BLAS^{TatC22G} *vs* BLAS. The RPMI8866^{GFP} vs RPMI8866 comparison revealed only small amount of DEGs, implying that the WT cell lines (RPMI8866 and BLAS) could be used as control cell lines without taking into account the effect of EGFP on gene expression. (E) The number of protein-coding DEGs found in comparisons: RPMI8866^{GFP} *vs* RPMI8866, RPMI8866^{Tat} *vs* RPMI8866, RPMI8866^{TatC22G} *vs* RPMI8866, BLAS^{Tat} *vs* BLAS, BLAS^{TatC22G} *vs* BLAS. (F) The number of DEGs encoding long non-coding RNAs (lncRNAs) found in comparisons: RPMI8866^{GFP} *vs* RPMI8866, RPMI8866^{Tat} *vs* RPMI8866, RPMI8866^{TatC22G} *vs* RPMI8866, BLAS^{Tat} *vs* BLAS, BLAS^{TatC22G} *vs* BLAS. (G) Venn diagrams demonstrating the overlap of upregulated DEGs between RPMI8866^{Tat} *vs* RPMI8866, RPMI8866^{TatC22G} *vs* RPMI8866, BLAS^{Tat} *vs* BLAS, and BLAS^{TatC22G} *vs* BLAS (left panel) and separately between RPMI8866^{Tat} *vs* RPMI8866 and BLAS^{Tat} *vs* BLAS (right panel). (H) Venn diagrams demonstrating the overlap of downregulated DEGs between RPMI8866^{Tat} *vs* RPMI8866, RPMI8866^{TatC22G} *vs* RPMI8866, BLAS^{Tat} *vs* BLAS, and BLAS^{TatC22G} *vs* BLAS (left panel) and separately between RPMI8866^{Tat} *vs* RPMI8866

and BLAS^{Tat} *vs* BLAS (right panel). (I) Overrepresentation analysis of Tat-upregulated DEGs (overlap between RPMI8866^{Tat} *vs* RPMI8866 and BLAS^{Tat} *vs* BLAS), significantly enriched and nonredundant GO BP terms are shown. (J) Overrepresentation analysis of Tat-downregulated DEGs (overlap between RPMI8866^{Tat} *vs* RPMI8866 and BLAS^{Tat} *vs* BLAS), top 15 significantly enriched and nonredundant GO BP terms are shown. (K) Selected suppressed GO BP terms pathways and associated DEGs. (L) Overrepresentation analysis of Tat-downregulated DEGs (overlap between RPMI8866^{Tat} *vs* RPMI8866 and BLAS^{Tat} *vs* BLAS), top 15 significantly enriched KEGG pathways are shown. (M) Selected suppressed KEGG pathways (hsa04514 and hsa04668) and associated DEGs.

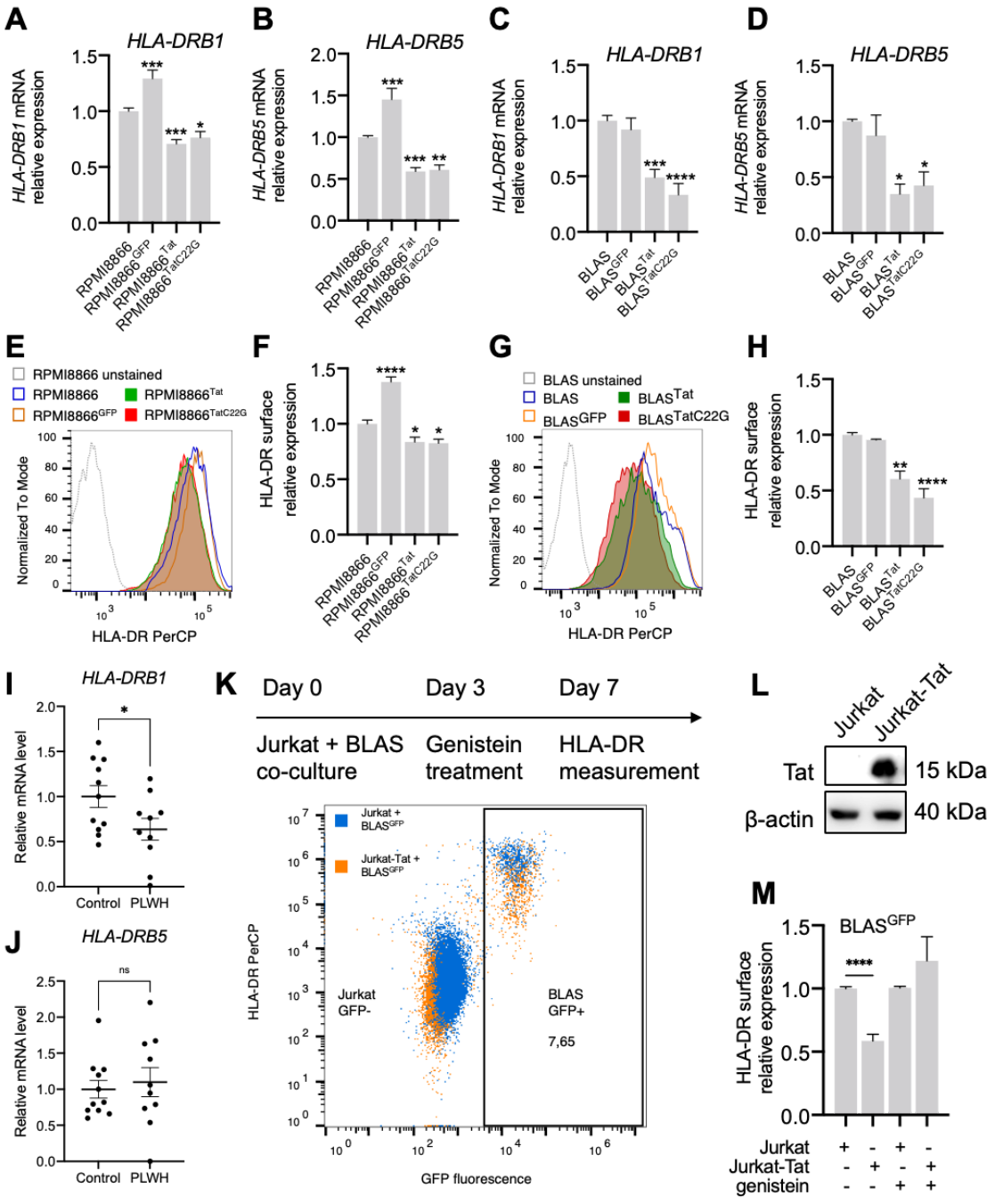

Figure 2. HIV-1 Tat decreases HLA-DR expression in B cells. (A-B) The level of *HLA-DRB1* (A) and *HLA-DRB5* (B) mRNA expression in RPMI8866, RPMI8866^{GFP}, RPMI8866^{Tat} and RPMI8866^{TatC22G} cells. (C-D) The level of *HLA-DRB1* (C) and *HLA-DRB5* (D) mRNA expression in BLAS, BLAS^{GFP}, BLAS^{Tat} and BLAS^{TatC22G} cells. (A-D) The mRNA level of *HLA-DRB1* or *HLA-DRB5* was normalized to *RPL32* and

GAPDH expression as housekeeping genes; the normalization was done assuming the mean level of transcript in WT cells to be 1. * $p < 0.05$, ** $p < 0.01$, *** $p < 0.001$, **** $p < 0.0001$ relative to WT cells, ANOVA, Tukey post-hoc. (E) A representative histogram for flow cytometry analysis of HLA-DR surface staining in RPMI8866 (blue), RPMI8866^{GFP} (orange), RPMI8866^{Tat} (green) and RPMI8866^{TatC22G} (red) cells. The negative control sample is shown for comparison (gray dotted line). (F) The level of HLA-DR surface expression in RPMI8866, RPMI8866^{GFP}, RPMI8866^{Tat} and RPMI8866^{TatC22G} cells as analyzed by flow cytometry. (G) A representative histogram for flow cytometry analysis of HLA-DR surface staining in BLAS (blue), BLAS^{GFP} (orange), BLAS^{Tat} (green) and BLAS^{TatC22G} (red) cells. The negative control sample is shown for comparison (gray dotted line). (H) The level of HLA-DR surface expression in BLAS, BLAS^{GFP}, BLAS^{Tat} and BLAS^{TatC22G} cells as analyzed by flow cytometry. (E-F) HLA-DR surface relative expression was calculated as the median fluorescence intensity in the sample normalized relative to the median fluorescence intensity in the control, averaged data from at least three biologically independent experiments are shown. * $p < 0.05$, ** $p < 0.01$, **** $p < 0.0001$, ANOVA, Tukey post-hoc. (G) A representative confocal image of cells with different Tat expression levels in RPMI8866^{Tat} cell line (green fluorescence). Immunofluorescent staining with antibodies against HLA-DR (red fluorescence). Nuclei were counterstained with DAPI (blue fluorescence). (H) The mean fluorescence intensity of HLA-DR around the cell nucleus (cell surface) in "Tat^{high}" and "Tat^{low}" cells (n > 600 cells). Cells were divided by half into two groups according to the mean fluorescence intensity of Tat in each nucleus. * $p < 0.05$, t-test. (I-J) The level of *HLA-DRB1* (I) and *HLA-DRB5* (J) mRNA expression in B cells isolated from peripheral blood of people living with HIV (PLWH) and HIV-uninfected control individuals (control). The mRNA level of *HLA-DRB1* or *HLA-DRB5* was normalized to *RPL32* and *GAPDH* expression as

housekeeping genes; the normalization was done assuming the mean level of transcript in control to be 1. ns - non-significant, * $p < 0.05$, t-test. (K) An experimental setup for the experiment of $BLAS^{GFP}$ co-culture with Jurkat or Jurkat expressing Tat (Jurkat-Tat) cells. Briefly, $BLAS^{GFP}$ cells were mixed with Jurkat or Jurkat-Tat cells and co-cultivated for 7 days, HLA-DR expression was measured in GFP+ cells. As a control, at day 3 an aliquot of co-cultivated cells was taken and 100 μM genistein, an inhibitor of endocytosis, was added to the culture medium. A representative dot-plot for flow cytometry analysis of HLA-DR surface staining in $BLAS^{GFP}$ cells (GFP+), co-cultured with Jurkat (blue) or Jurkat-Tat (orange) cells. (L) Western blotting analysis of Tat expression in Jurkat and Jurkat-Tat cell lines. β-actin was used as a loading control. (M) The level of HLA-DR surface expression in $BLAS^{GFP}$ cells co-cultured with Jurkat or Jurkat expressing Tat (Jurkat-Tat) cells as analyzed by flow cytometry. HLA-DR surface relative expression was calculated as the median fluorescence intensity in the sample normalized relative to the median fluorescence intensity in the control, averaged data from at least three biologically independent experiments are shown. **** $p < 0.0001$, ANOVA, Tukey post-hoc. Data are presented as mean ± SEM.

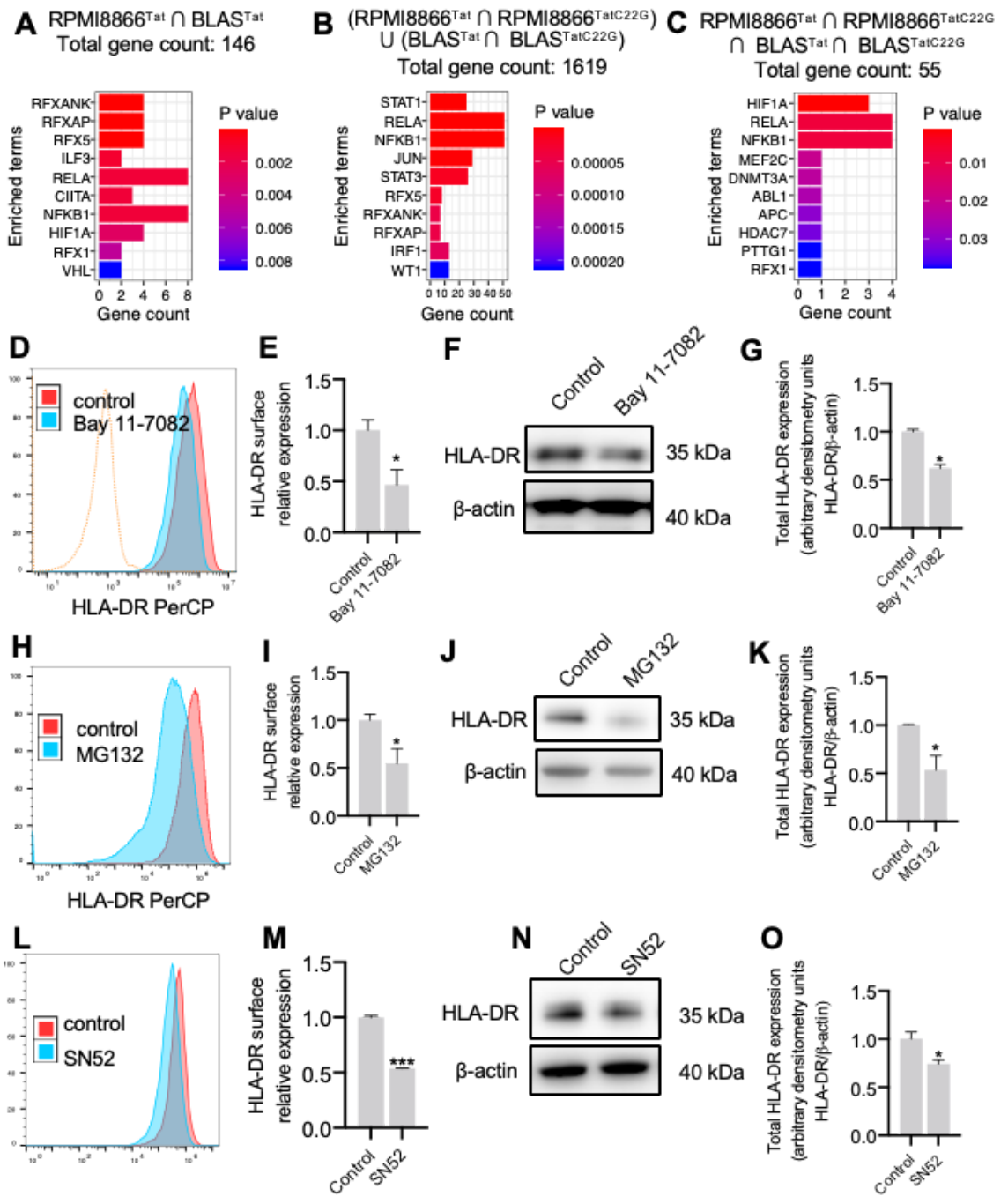

Figure 3. NF-κB pathway regulates HLA-DR expression in B cells. (A) Barplot visualizing the top 10 significantly enriched (p.adjust < 0.05) transcription factors potentially regulating downregulated genes, common between RPMI8866^{Tat} and BLAS^{Tat}, based on TRRUST TF-target database (2019). (B) Barplot visualizing the top 10 significantly enriched (p.adjust < 0.05) transcription factors potentially regulating

downregulated genes, common between RPMI8866^{Tat} and RPMI8866^{TatC22G}, or BLAS^{Tat} and BLAS^{TatC22G}, based on TRRUST TF-target database (2019). (C) Barplot visualizing the top 10 significantly enriched (p.adjust < 0.05) transcription factors potentially regulating downregulated genes, common between RPMI8866^{Tat}, RPMI8866^{TatC22G}, BLAS^{Tat} and BLAS^{TatC22G}, based on TRRUST TF-target database (2019). (D-G) RPMI8866 cells were treated for 24 hours with 1 μM Bay 11-7082 or left untreated (control), HLA-DR expression was then analyzed by flow cytometry analysis and western blotting. (D) A representative histogram for flow cytometry analysis of HLA-DR surface staining in control RPMI8866 cells (red) and cells, treated with 1 μM Bay 11-7082 (blue). A negative control sample is shown for comparison (orange dotted line). (E) HLA-DR surface relative expression was calculated as the median fluorescence intensity in the sample normalized relative to the median fluorescence intensity in the control, averaged data from at least three biologically independent experiments are shown. (F) Western blotting analysis of HLA-DR content in RPMI8866 cells. β-actin was used as a loading control. A reproducible result is presented. (G) Densitometry analysis of HLA-DR content normalized to β-actin. (H-K) RPMI8866 cells were treated for 6 hours with 20 μM MG132 or left untreated (control), HLA-DR expression was then analyzed by flow cytometry analysis and western blotting. (H) A representative histogram for flow cytometry analysis of HLA-DR surface staining in control RPMI8866 cells (red) and cells, treated with 20 μM MG132 (blue). (I) HLA-DR surface relative expression was calculated as the median fluorescence intensity in the sample normalized relative to the median fluorescence intensity in the control, averaged data from at least three biologically independent experiments are shown. (J) Western blotting analysis of HLA-DR content in RPMI8866 cells. β-actin was used as a loading control. A reproducible result is presented. (K) Densitometry analysis of HLA-DR content normalized to β-actin. (L-O) RPMI8866 cells were treated for 24 hours with 40

μg/ml SN52 or left untreated (control), HLA-DR expression was then analyzed by flow cytometry analysis and western blotting. (L) A representative histogram for flow cytometry analysis of HLA-DR surface staining in control RPMI8866 cells (red) and cells, treated with 40 μg/ml SN52 (blue). (M) HLA-DR surface relative expression was calculated as the median fluorescence intensity in the sample normalized relative to the median fluorescence intensity in the control, averaged data from at least three biologically independent experiments are shown. (N) Western blotting analysis of HLA-DR content in RPMI8866 cells. β-actin was used as a loading control. A reproducible result is presented. (O) Densitometry analysis of HLA-DR content normalized to β-actin. Data are presented as mean ± SEM, * $p < 0.05$, ** $p < 0.01$, *** $p < 0.001$, t-test.

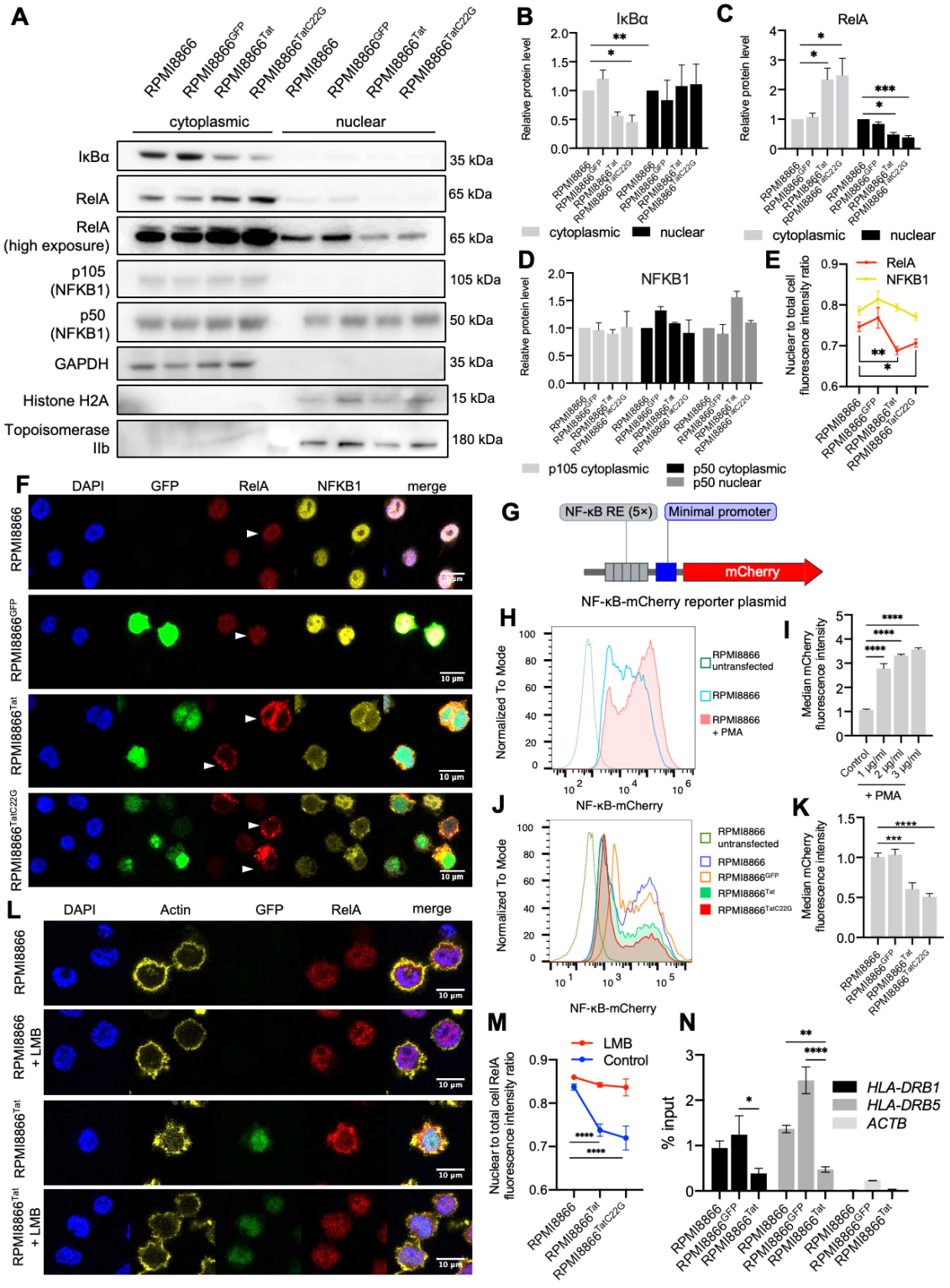

Figure 4. HIV-1 Tat expression reduced classical NF-κB activation in B cells. (A) Western blotting analysis of IκBα, RelA, NFKB1 (p105 and p50) cytoplasmic and nuclear content in RPMI8866, RPMI8866^{GFP}, RPMI8866^{Tat} and RPMI8866^{TatC22G} cells. GAPDH

was used as a loading control for cytoplasmic extracts; histone H2A and topoisomerase IIb were used as loading controls for nuclear extracts. A reproducible result is presented. (B-D) Densitometry analysis of IκBα (B), RelA (C), NFKB1 (D), cytoplasmic and nuclear content normalized to respective cytosolic or nuclear control of protein load. (E-F) Immunofluorescent staining with antibodies to RelA and to NFKB1 (p105 and p50) in RPMI8866, RPMI8866^{GFP}, RPMI8866^{Tat} and RPMI8866^{TatC22G} cells. (E) The ratio of total fluorescence intensity of RelA (red) or NFKB1 (yellow) in the nucleus divided by the respective total cellular fluorescence intensity for each cell. (F) A representative confocal image of RPMI8866, RPMI8866^{GFP}, RPMI8866^{Tat} and RPMI8866^{TatC22G} cells, stained with antibodies to RelA (red) and to NFKB1 (p105 and p50, yellow). Nuclei were counterstained with DAPI (blue) and GFP fluorescence in cells expressing GFP, Tat-GFP or TatC22G-GFP was detected (green). White arrows indicate RelA sequestration in the nucleus or cytoplasm. Scale bar 10 μm. (G) Schematic illustration of NF-κB-mCherry reporter plasmid that consisted of five repeats of the NF-κB response elements, a minimal promoter and red fluorescent protein mCherry2 as a reporter gene. (H) A representative histogram for flow cytometry analysis of RPMI8866 cells transfected with the NF-κB-mCherry reporter plasmid and treated (red) or not (blue) with 1 μg/ml PMA for 24 h. Untransfected RPMI8866 cells served as negative control (green dotted line). (I) The effect of different concentrations of PMA on mCherry expression in RPMI8866 cells after transfection with the NF-κB-mCherry reporter plasmid calculated as the median fluorescence intensity in the sample normalized relative to the median fluorescence intensity in the control (untreated RPMI8866 cells after transfection with the NF-κB-mCherry reporter plasmid), averaged data from at least three biologically independent experiments are shown. (J) A representative histogram for flow cytometry analysis of RPMI8866, RPMI8866^{GFP}, RPMI8866^{Tat} and RPMI8866^{TatC22G} cells transfected

with the NF-κB-mCherry reporter plasmid. Untransfected RPMI8866 cells served as negative control (green dotted line). (K) The effect of HIV-1 Tat on the activity of the NF-B pathway analysed by the reporter assay. RPMI8866, RPMI8866^{GFP}, RPMI8866^{Tat} and RPMI8866^{TatC22G} cells were transfected with the NF-κB-mCherry reporter plasmid and mCherry expression level was calculated as the median fluorescence intensity in the sample normalized relative to the median fluorescence intensity in the control RPMI8866 cells, averaged data from at least three biologically independent experiments are shown. (L-M) Immunofluorescent staining with antibodies to RelA and to actin (cytoplasm marker) in RPMI8866, RPMI8866^{Tat} and RPMI8866^{TatC22G} cells treated or not with 5 ng/ml Lemptomycin B (LMB), an inhibitor of nuclear export. (L) A representative confocal image of RPMI8866, and RPMI8866^{Tat} cells (treated or not with LMB), stained with antibodies to RelA (red) and to actin (yellow). Nuclei were counterstained with DAPI (blue) and GFP fluorescence in cells expressing Tat-GFP was detected (green). Scale bar 10 μm. (M) The ratio of total fluorescence intensity of RelA in the nucleus divided by the respective total cellular fluorescence intensity for each cell in cells treated with LMB (red) or not (blue). (N) . Data are presented as mean ± SEM, * $p < 0.05$, ** $p < 0.01$, *** $p < 0.001$, **** $p < 0.0001$, ANOVA, Tukey's post-hoc test.

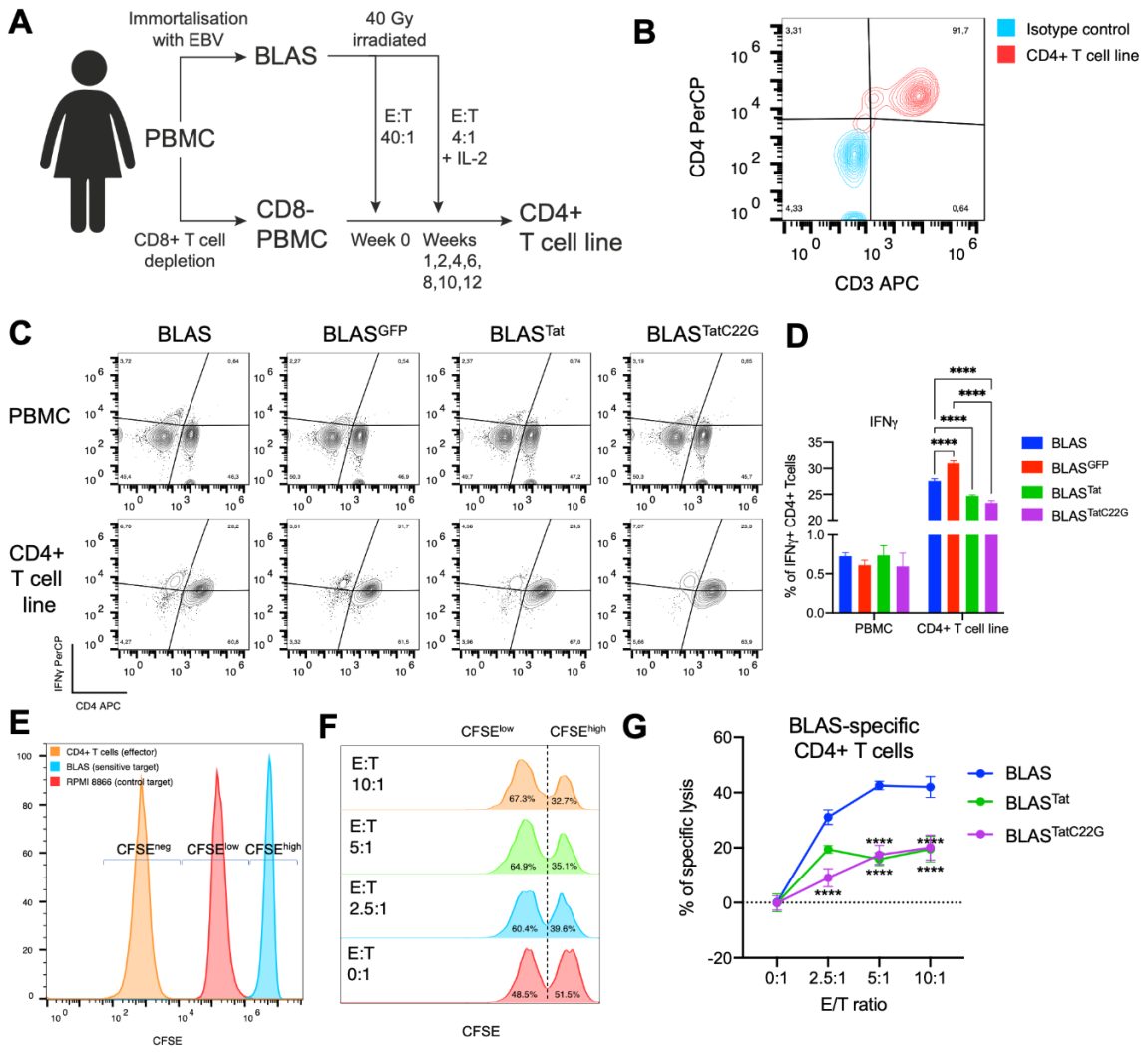

Figure 5. HIV-1 Tat expression in B cells reduces EBV-specific CD4+ T cell response. (A) An overview of the experimental setup for the generation of BLAS-reactive EBV-specific CD4+ T cell line. (B) Representative flow cytometry contour plots showing CD3 and CD4 and respective isotype control antibody staining of BLAS-reactive EBV-specific CD4+ T cell line. (C) Representative flow cytometry contour plots showing CD4 and IFNγ intracellular staining in non-stimulated PBMC population and BLAS-reactive CD4+ T cell line, co-cultured for 18 hours with different BLAS cells at E/T ratio 40:1. Outliers are shown as dots. (D) The percentage of IFNγ+/CD4+ cells in the population of non-stimulated PBMC or BLAS-reactive CD4+ T cell line cells, co-cultured for 18 hours

with different BLAS cells at E/T ratio 40:1. (E) A representative histogram for flow cytometry analysis of CFSE fluorescence (FITC channel) in unstained CD4+ T cells ($CFSE^{neg}$), stained with low concentration CFSE control target cells RPMI8866 ($CFSE^{low}$) and stained with high concentration CFSE sensitive target cells BLAS ($CFSE^{high}$). (F) Representative histograms for flow cytometry analysis of CFSE fluorescence in the target cell population (CFSE positive gating) after co-cultivating with BLAS-reactive EBV-specific CD4+ T cell line at various E/T ratios for 4h, two populations are visualized: $CFSE^{low}$, which are control target cells RPMI886, and $CFSE^{high}$, which are sensitive target cells BLAS that gradually decrease with the increasing E/T ratio. (G) Percentage of specific lysis of different BLAS cells after co-cultivation with BLAS-reactive EBV-specific CD4+ T cell line at various E/T ratios for 4h. Data are presented as mean ± SEM, **** $p < 0.0001$, 2-way ANOVA, Tukey's post-hoc test. PBMC - peripheral blood mononuclear cells.

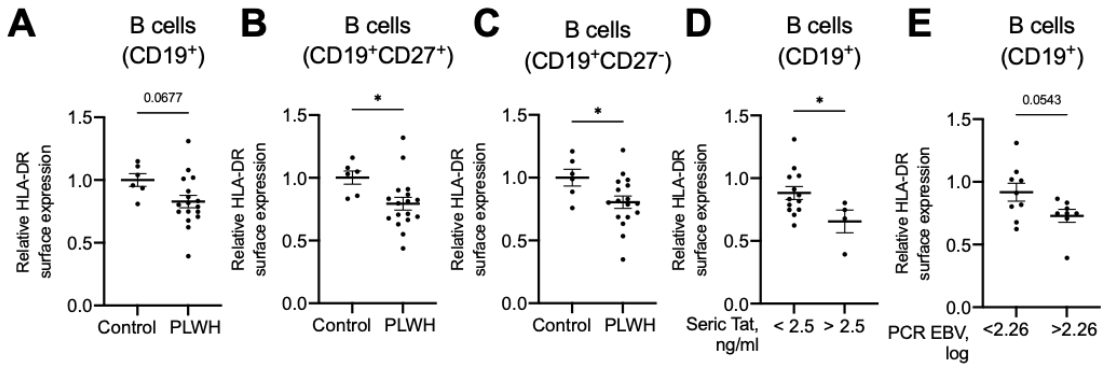

Figure 6. The analysis of HLA-DR surface expression on B cells from people living with HIV and HIV-uninfected controls. PLWH - people living with HIV. (A) The level of HLA-DR surface expression in B cells (gated as $CD19^{+}$) as analyzed by flow cytometry. (B) The level of HLA-DR surface expression in memory B cells (gated as $CD19^{+}CD27^{+}$) as analyzed by flow cytometry. (C) The level of HLA-DR surface expression in naïve B

cells (gated as $CD19^{+}CD27^{-}$) as analyzed by flow cytometry. (D) The level of HLA-DR surface expression in B cells (gated as $CD19^{+}$) as analyzed by flow cytometry in people living with HIV with seric Tat concentration below and above 2.5 ng/ml cut-off. (E) The level of HLA-DR surface expression in B cells (gated as $CD19^{+}$) as analyzed by flow cytometry in people living with HIV with PCR EBV DNA in whole blood below and above 2.26 log cut-off. * $p < 0.05$, t-test.

References

1. WHO fact sheet. HIV/AIDS [Internet]. https://www.who.int/. 2022 [cited 2022 Jul 16]. Available from: https://www.who.int/news-room/fact-sheets/detail/hiv-aids
2. HIV-CAUSAL Collaboration, Ray M, Logan R, Sterne JAC, Hernández-Díaz S, Robins JM, et al. The effect of combined antiretroviral therapy on the overall mortality of HIV-infected individuals. AIDS. 2010;24:123–37.
3. Shmakova A, Germini D, Vassetzky Y. HIV-1, HAART and cancer: A complex relationship. International Journal of Cancer. 2020;146:2666–79.
4. Hernández-Ramírez RU, Shiels MS, Dubrow R, Engels EA. Spectrum of cancer risk among HIV-infected people in the United States during the modern antiretroviral therapy era: a population-based registry linkage study. Lancet HIV. 2017;4:e495–504.
5. Imamichi H, Smith M, Adelsberger JW, Izumi T, Scrimieri F, Sherman BT, et al. Defective HIV-1 proviruses produce viral proteins. Proc Natl Acad Sci U S A. 2020;117:3704–10.
6. Rayne F, Debaisieux S, Yezid H, Lin Y-L, Mettling C, Konate K, et al. Phosphatidylinositol-(4,5)-bisphosphate enables efficient secretion of HIV-1 Tat by infected T-cells. EMBO J. 2010;29:1348–62.
7. Poggi A, Carosio R, Fenoglio D, Brenci S, Murdaca G, Setti M, et al. Migration of Vδ1 and Vδ2 T cells in response to CXCR3 and CXCR4 ligands in healthy donors and HIV-1-infected patients: Competition by HIV-1 Tat. Blood. 2004;103:2205–13.
8. Germini D, Tsfasman T, Klibi M, El-Amine R, Pichugin A, Iarovaia OV, et al. HIV Tat induces a prolonged MYC relocalization next to IGH in circulating B-cells. Leukemia. 2017;31:2515–22.
9. Henderson LJ, Johnson TP, Smith BR, Reoma LB, Santamaria UA, Bachani M, et al. Presence of Tat and transactivation response element in spinal fluid despite antiretroviral therapy. AIDS. 2019;33 Suppl 2:S145–57.
10. Lazzi S, Bellan C, De Falco G, Cinti C, Ferrari F, Nyongo A, et al. Expression of RB2/p130 tumor-suppressor gene in AIDS-related non-Hodgkin's lymphomas: implications for disease pathogenesis. Hum Pathol. 2002;33:723–31.
11. Alves de Souza Rios L, Mapekula L, Mdletshe N, Chetty D, Mowla S. HIV-1 Transactivator of Transcription (Tat) Co-operates With AP-1 Factors to Enhance c-MYC Transcription. Front Cell Dev Biol. 2021;9:693706.
12. Luzzi A, Morettini F, Gazaneo S, Mundo L, Onnis A, Mannucci S, et al. HIV-1 Tat induces DNMT over-expression through microRNA dysregulation in HIV-related non Hodgkin lymphomas. Infectious Agents and Cancer. 2014;9:41.
13. Nekhai S, Jeang K-T. Transcriptional and post-transcriptional regulation of HIV-1 gene expression: role of cellular factors for Tat and Rev. Future Microbiol. 2006;1:417–26.
14. Barboric M, Yik JHN, Czudnochowski N, Yang Z, Chen R, Contreras X, et al. Tat competes with HEXIM1 to increase the active pool of P-TEFb for HIV-1 transcription. Nucleic Acids Res. 2007;35:2003–12.
15. Muniz L, Egloff S, Ughy B, Jády BE, Kiss T. Controlling cellular P-TEFb activity by the HIV-1 transcriptional transactivator Tat. PLoS Pathog. 2010;6:e1001152.
16. Johnson TP, Patel K, Johnson KR, Maric D, Calabresi PA, Hasbun R, et al. Induction of IL-17 and nonclassical T-cell activation by HIV-Tat protein. Proceedings of the National Academy of Sciences of the United States of America. 2013;110:13588–93.
17. El-Amine R, Germini D, Zakharova VV, Tsfasman T, Sheval EV, Louzada RAN, et al. HIV-1 Tat protein induces DNA damage in human peripheral blood B-lymphocytes via mitochondrial ROS production. Redox Biology. 2018;15:97–108.

18. Rayne F, Debaisieux S, Tu A, Chopard C, Tryoen-Toth P, Beaumelle B. Detecting HIV-1 Tat in Cell Culture Supernatants by ELISA or Western Blot. Methods Mol Biol. 2016;1354:329–42.
19. Kurnaeva MA, Zalevsky AO, Arifulin EA, Lisitsyna OM, Tvorogova AV, Shubina MY, et al. Molecular Coevolution of Nuclear and Nucleolar Localization Signals inside the Basic Domain of HIV-1 Tat. Journal of Virology. 2022;96:e01505-21.
20. Sarbassov DD, Guertin DA, Ali SM, Sabatini DM. Phosphorylation and regulation of Akt/PKB by the rictor-mTOR complex. Science. 2005;307:1098–101.
21. Stewart SA, Dykxhoorn DM, Palliser D, Mizuno H, Yu EY, An DS, et al. Lentivirus-delivered stable gene silencing by RNAi in primary cells. RNA. 2003;9:493–501.
22. Shmakova AA, Popov VS, Romanov IP, Khabibullin NR, Sabitova NR, Karpukhina AA, et al. Urokinase System in Pathogenesis of Pulmonary Fibrosis: A Hidden Threat of COVID-19. Int J Mol Sci. 2023;24:1382.
23. Valyaeva A, Tikhomirova M, Potashnikova D, Bogomazova A, Snigiryova G, Penin A, et al. Ectopic expression of HIV-1 Tat modifies gene expression in cultured B cells: Implications for the development of B-cell lymphomas in HIV-1-infected patients. PeerJ. 2022;in press.
24. Canoy RJ, André F, Shmakova A, Wiels J, Lipinski M, Vassetzky Y, et al. Easy and robust electrotransfection protocol for efficient ectopic gene expression and genome editing in human B cells. Gene Therapy. 2020;
25. Long HM, Zuo J, Leese AM, Gudgeon NH, Jia H, Taylor GS, et al. CD4+ T-cell clones recognizing human lymphoma-associated antigens: generation by in vitro stimulation with autologous Epstein-Barr virus–transformed B cells. Blood. 2009;114:807–15.
26. Nakagawa Y, Watari E, Shimizu M, Takahashi H. One-step simple assay to determine antigen-specific cytotoxic activities by single-color flow cytometry. Biomed Res. 2011;32:159–66.
27. Wu T, Hu E, Xu S, Chen M, Guo P, Dai Z, et al. clusterProfiler 4.0: A universal enrichment tool for interpreting omics data. Innovation (Camb). 2021;2:100141.
28. Han H, Cho J-W, Lee S, Yun A, Kim H, Bae D, et al. TRRUST v2: an expanded reference database of human and mouse transcriptional regulatory interactions. Nucleic Acids Research. 2018;46:D380–6.
29. Kuleshov MV, Jones MR, Rouillard AD, Fernandez NF, Duan Q, Wang Z, et al. Enrichr: a comprehensive gene set enrichment analysis web server 2016 update. Nucleic Acids Res. 2016;44:W90-97.
30. Pfaffl MW. A new mathematical model for relative quantification in real-time RT-PCR. Nucleic Acids Res. 2001;29:e45.
31. Vandesompele J, De Preter K, Pattyn F, Poppe B, Van Roy N, De Paepe A, et al. Accurate normalization of real-time quantitative RT-PCR data by geometric averaging of multiple internal control genes. Genome Biol. 2002;3:research0034.1-research0034.11.
32. Hellemans J, Mortier G, De Paepe A, Speleman F, Vandesompele J. qBase relative quantification framework and software for management and automated analysis of real-time quantitative PCR data. Genome Biol. 2007;8:R19.
33. Holliday H, Khoury A, Swarbrick A. Chromatin immunoprecipitation of transcription factors and histone modifications in Comma-Dβ mammary epithelial cells. STAR Protoc. 2021;2:100514.
34. Hammal F, de Langen P, Bergon A, Lopez F, Ballester B. ReMap 2022: a database of Human, Mouse, Drosophila and Arabidopsis regulatory regions from an integrative analysis of DNA-binding sequencing experiments. Nucleic Acids Research. 2022;50:D316–25.

35. Fiume G, Vecchio E, De Laurentiis A, Trimboli F, Palmieri C, Pisano A, et al. Human immunodeficiency virus-1 Tat activates NF-κB via physical interaction with IκB-α and p65. Nucleic Acids Res. 2012;40:3548–62.
36. Ginaldi L, De Martinis M, D'Ostilio A, Marini L, Quaglino D. Changes in antigen expression on B lymphocytes during HIV infection. Pathobiology. 1998;66:17–23.
37. Ferrari A, Pellegrini V, Arcangeli C, Fittipaldi A, Giacca M, Beltram F. Caveolae-mediated internalization of extracellular HIV-1 tat fusion proteins visualized in real time. Mol Ther. 2003;8:284–94.
38. Vendeville A, Rayne F, Bonhoure A, Bettache N, Montcourrier P, Beaumelle B. HIV-1 Tat Enters T Cells Using Coated Pits before Translocating from Acidified Endosomes and Eliciting Biological Responses. Molecular Biology of the Cell. 2004;15:2347–60.
39. Fittipaldi A, Giacca M. Transcellular protein transduction using the Tat protein of HIV-1. Advanced Drug Delivery Reviews. 2005;57:597–608.
40. Vercauteren D, Vandenbroucke RE, Jones AT, Rejman J, Demeester J, De Smedt SC, et al. The Use of Inhibitors to Study Endocytic Pathways of Gene Carriers: Optimization and Pitfalls. Mol Ther. 2010;18:561–9.
41. Reeder JE, Kwak Y-TT, McNamara RP, Forst CV, D'Orso I, D'Orso I. HIV Tat controls RNA Polymerase II and the epigenetic landscape to transcriptionally reprogram target immune cells. eLife. 2015;4:e08955–e08955.
42. Jean MJ, Power D, Kong W, Huang H, Santoso N, Zhu J. Identification of HIV-1 Tat-Associated Proteins Contributing to HIV-1 Transcription and Latency. Viruses. 2017;9:E67.
43. Kanazawa S, Okamoto T, Peterlin BM. Tat competes with CIITA for the binding to P-TEFb and blocks the expression of MHC class II genes in HIV infection. Immunity. 2000;12:61–70.
44. Garber ME, Wei P, KewalRamani VN, Mayall TP, Herrmann CH, Rice AP, et al. The interaction between HIV-1 Tat and human cyclin T1 requires zinc and a critical cysteine residue that is not conserved in the murine CycT1 protein. Genes Dev. 1998;12:3512–27.
45. Rauert-Wunderlich H, Siegmund D, Maier E, Giner T, Bargou RC, Wajant H, et al. The IKK inhibitor Bay 11-7082 induces cell death independent from inhibition of activation of NFκB transcription factors. PLoS One. 2013;8:e59292.
46. Nakajima S, Kato H, Takahashi S, Johno H, Kitamura M. Inhibition of NF-κB by MG132 through ER stress-mediated induction of LAP and LIP. FEBS Letters. 2011;585:2249–54.
47. Xiao G, Harhaj EW, Sun SC. NF-kappaB-inducing kinase regulates the processing of NF-kappaB2 p100. Mol Cell. 2001;7:401–9.
48. Xu Y, Fang F, St Clair DK, Sompol P, Josson S, St Clair WH. SN52, a novel nuclear factor-kappaB inhibitor, blocks nuclear import of RelB:p52 dimer and sensitizes prostate cancer cells to ionizing radiation. Mol Cancer Ther. 2008;7:2367–76.
49. Hoesel B, Schmid JA. The complexity of NF-κB signaling in inflammation and cancer. Molecular Cancer. 2013;12:86.
50. Scala G, Ruocco MR, Ambrosino C, Mallardo M, Giordano V, Baldassarre F, et al. The expression of the interleukin 6 gene is induced by the human immunodeficiency virus 1 TAT protein. J Exp Med. 1994;179:961–71.
51. Momburg F, Herrmann B, Moldenhauer G, Möller P. B-cell lymphomas of high-grade malignancy frequently lack HLA-DR, -DP and -DQ antigens and associated invariant chain. Int J Cancer. 1987;40:598–603.
52. Higashi M, Tokuhira M, Fujino S, Yamashita T, Abe K, Arai E, et al. Loss of HLA-DR expression is related to tumor microenvironment and predicts adverse outcome in diffuse large B-cell lymphoma. Leuk Lymphoma. 2016;57:161–6.

53. Nikiforow S, Bottomly K, Miller G. CD4+ T-Cell Effectors Inhibit Epstein-Barr Virus-Induced B-Cell Proliferation. J Virol. 2001;75:3740–52.
54. Khanolkar A, Yagita H, Cannon MJ. Preferential utilization of the perforin/granzyme pathway for lysis of Epstein-Barr virus-transformed lymphoblastoid cells by virus-specific CD4+ T cells. Virology. 2001;287:79–88.
55. Akbay B, Shmakova A, Vassetzky Y, Dokudovskaya S. Modulation of mTORC1 Signaling Pathway by HIV-1. Cells. 2020;9:E1090.
56. Ajasin D, Eugenin EA. HIV-1 Tat: Role in Bystander Toxicity. Front Cell Infect Microbiol. 2020;10:61.
57. Dickens AM, Yoo SW, Chin AC, Xu J, Johnson TP, Trout AL, et al. Chronic low-level expression of HIV-1 Tat promotes a neurodegenerative phenotype with aging. Sci Rep. 2017;7:7748.
58. Qrareya AN, Mahdi F, Kaufman MJ, Ashpole NM, Paris JJ. HIV-1 Tat promotes age-related cognitive, anxiety-like, and antinociceptive impairments in female mice that are moderated by aging and endocrine status. GeroScience. 2020;43:309–27.
59. Kovacs L, Bruder-Nascimento T, Greene L, Kennard S, Belin de Chantemèle EJ. Chronic Exposure to HIV-Derived Protein Tat Impairs Endothelial Function via Indirect Alteration in Fat Mass and Nox1-Mediated Mechanisms in Mice. Int J Mol Sci. 2021;22:10977.
60. Gorwood J, Ejlalmanesh T, Bourgeois C, Mantecon M, Rose C, Atlan M, et al. SIV Infection and the HIV Proteins Tat and Nef Induce Senescence in Adipose Tissue and Human Adipose Stem Cells, Resulting in Adipocyte Dysfunction. Cells. 2020;9:E854.
61. Balfour HH Jr, Sifakis F, Sliman JA, Knight JA, Schmeling DO, Thomas W. Age-Specific Prevalence of Epstein–Barr Virus Infection Among Individuals Aged 6–19 Years in the United States and Factors Affecting Its Acquisition. The Journal of Infectious Diseases. 2013;208:1286–93.
62. Levin LI, Munger KL, O'Reilly EJ, Falk KI, Ascherio A. Primary infection with the Epstein-Barr virus and risk of multiple sclerosis. Ann Neurol. 2010;67:824–30.
63. Sallah N, Miley W, Labo N, Carstensen T, Fatumo S, Gurdasani D, et al. Distinct genetic architectures and environmental factors associate with host response to the γ2-herpesvirus infections. Nat Commun. 2020;11:3849.
64. Yan Y, Ren Y, Chen R, Hu J, Ji Y, Yang J, et al. Evaluation of Epstein-Barr Virus Salivary Shedding in HIV/AIDS Patients and HAART Use: A Retrospective Cohort Study. Virologica Sinica. 2018;33:227–33.
65. Shindiapina P, Ahmed EH, Mozhenkova A, Abebe T, Baiocchi RA. Immunology of EBV-Related Lymphoproliferative Disease in HIV-Positive Individuals. Front Oncol. 2020;10:1723.
66. Kersten MJ, Klein MR, Holwerda AM, Miedema F, van Oers MH. Epstein-Barr virus-specific cytotoxic T cell responses in HIV-1 infection: different kinetics in patients progressing to opportunistic infection or non-Hodgkin's lymphoma. J Clin Invest. 1997;99:1525–33.
67. Gasser O, Wolbers M, Steffen I, Hirsch HH, Battegay M, Hess C, et al. Increased Epstein–Barr virus-specific antibody-levels in HIV-infected individuals developing primary central nervous system lymphoma. AIDS. 2007;21:1664–6.
68. Muncunill J, Baptista M-J, Hernandez-Rodríguez Á, Dalmau J, Garcia O, Tapia G, et al. Plasma Epstein-Barr Virus Load as an Early Biomarker and Prognostic Factor of Human Immunodeficiency Virus-related Lymphomas. Clin Infect Dis. 2019;68:834–43.
69. Montgomery ND, Randall C, Painschab M, Seguin R, Kaimila B, Kasonkanji E, et al. High pretreatment plasma Epstein‐Barr virus (EBV) DNA level is a poor prognostic marker in HIV‐associated, EBV‐negative diffuse large B‐cell lymphoma in Malawi.

Cancer Med. 2019;9:552–61.
70. Gasser O, Bihl FK, Wolbers M, Loggi E, Steffen I, Hirsch HH, et al. HIV Patients Developing Primary CNS Lymphoma Lack EBV-Specific CD4+ T Cell Function Irrespective of Absolute CD4+ T Cell Counts. PLoS Med. 2007;4:e96.
71. Fu T, Voo KS, Wang R-F. Critical role of EBNA1-specific CD4+ T cells in the control of mouse Burkitt lymphoma in vivo. J Clin Invest. 2004;114:542–50.
72. Dreyfus DH, Nagasawa M, Pratt JC, Kelleher CA, Gelfand EW. Inactivation of NF-kappaB by EBV BZLF-1-encoded ZEBRA protein in human T cells. J Immunol. 1999;163:6261–8.
73. Germini D, Sall FB, Shmakova A, Wiels J, Dokudovskaya S, Drouet E, et al. Oncogenic properties of the ebv zebra protein. Cancers. 2020;12:1–26.
74. Akhtar L, Qin H, Muldowney M, Yanagisawa L, Kutsch O, Clements J, et al. Suppressor of Cytokine Signaling 3 Inhibits Antiviral IFN- Signaling To Enhance HIV-1 Replication in Macrophages. Journal of immunology (Baltimore, Md : 1950). 2010;185:2393–404.
75. Youn GS, Kwon D-J, Ju SM, Rhim H, Bae YS, Choi SY, et al. Celastrol ameliorates HIV-1 Tat-induced inflammatory responses via NF-kappaB and AP-1 inhibition and heme oxygenase-1 induction in astrocytes. Toxicology and Applied Pharmacology. 2014;280:42–52.
76. Arenzana-Seisdedos F, Turpin P, Rodriguez M, Thomas D, Hay RT, Virelizier JL, et al. Nuclear localization of I kappa B alpha promotes active transport of NF-kappa B from the nucleus to the cytoplasm. J Cell Sci. 1997;110 (Pt 3):369–78.
77. Aguilera C, Fernández-Majada V, Inglés-Esteve J, Rodilla V, Bigas A, Espinosa L. Efficient nuclear export of p65-IkappaBalpha complexes requires 14-3-3 proteins. J Cell Sci. 2006;119:3695–704.
78. Wuerzberger-Davis SM, Chen Y, Yang DT, Kearns JD, Bates PW, Lynch C, et al. Nuclear Export of the NF-κB Inhibitor IκBα Is Required for Proper B Cell and Secondary Lymphoid Tissue Formation. Immunity. 2011;34:188–200.
79. Coiras M, López-Huertas MR, Rullas J, Mittelbrunn M, Alcamí J. Basal shuttle of NF-κB/IκBα in resting T lymphocytes regulates HIV-1 LTR dependent expression. Retrovirology. 2007;4:56.
80. Chen Y, Li HH, Fu J, Wang XF, Ren YB, Dong LW, et al. Oncoprotein p28GANK binds to RelA and retains NF-κB in the cytoplasm through nuclear export. Cell Res. 2007;17:1020–9.
81. Stauber RH, Pavlakis GN. Intracellular trafficking and interactions of the HIV-1 Tat protein. Virology. 1998;252:126–36.
82. Katikaneni DS, Jina L. B cell MHC class II signaling: A story of life and death. Hum Immunol. 2019;80:37–43.
83. Treanor B. B-cell receptor: from resting state to activate. Immunology. 2012;136:21–7.
84. Guldenpfennig C, Teixeiro E, Daniels M. NF-kB's contribution to B cell fate decisions. Front Immunol. 2023;14:1214095.
85. Tripiciano A, Picconi O, Moretti S, Sgadari C, Cafaro A, Francavilla V, et al. Anti-Tat immunity defines CD4+ T-cell dynamics in people living with HIV on long-term cART. EBioMedicine. 2021;66:103306.
86. Li Q, Spriggs MK, Kovats S, Turk SM, Comeau MR, Nepom B, et al. Epstein-Barr virus uses HLA class II as a cofactor for infection of B lymphocytes. J Virol. 1997;71:4657–62.
87. Borza CM, Hutt-Fletcher LM. Alternate replication in B cells and epithelial cells switches tropism of Epstein-Barr virus. Nat Med. 2002;8:594–9.
88. Fellner MD, Durand K, Correa RM, Redini L, Yampolsky C, Colobraro A, et al.

Circulating Epstein–Barr virus (EBV) in HIV-infected patients and its relation with primary brain lymphoma. International Journal of Infectious Diseases. 2007;11:172–8.
89. Richard Y, Amiel C, Jeantils V, Mestivier D, Portier A, Dhello G, et al. Changes in Blood B Cell Phenotypes and Epstein-Barr Virus Load in Chronically Human Immunodeficiency Virus—Infected Patients before and after Antiretroviral Therapy. The Journal of Infectious Diseases. 2010;202:1424–34.
90. Legoff J, Amiel C, Calisonni O, Fromentin D, Rajoely B, Abuaf N, et al. Early impairment of CD8+ T cells immune response against Epstein-Barr virus (EBV) antigens associated with high level of circulating mononuclear EBV DNA load in HIV infection. J Clin Immunol. 2004;24:125–34.
91. Ling PD, Vilchez RA, Keitel WA, Poston DG, Peng RS, White ZS, et al. Epstein-Barr Virus DNA Loads in Adult Human Immunodeficiency Virus Type 1-Infected Patients Receiving Highly Active Antiretroviral Therapy. Clinical Infectious Diseases. 2003;37:1244–9.
92. Piriou ER, van Dort K, Nanlohy NM, Miedema F, van Oers MH, van Baarle D. Altered EBV viral load setpoint after HIV seroconversion is in accordance with lack of predictive value of EBV load for the occurrence of AIDS-related non-Hodgkin lymphoma. J Immunol. 2004;172:6931–7.

Supplementary information for

Chronic HIV-1 Tat action induces HLA-DR downregulation in B cells: a mechanism for lymphoma immune escape in people living with HIV

Supplementary tables

Table S1. DNA sequences used for cloning.

DNA oligo	Sequence (5' → 3')
NFκB_RE_1_F	CATGTTGGGGACTTTCCGCTGGGGACTTTCCGCTGGG
NFκB_RE_2_F	GACTTTCCGCTGGGGACTTTCCGCTGGGGACTTTCCGCGCTAG
NFκB_RE_1_R	AGTCCCCAGCGGAAAGTCCCCAGCGGAAAGTCCCCAA
NFκB_RE_2_R	CGCGGAAAGTCCCCAGCGGAAAGTCCCCAGCGGAA
Min_promoter_F	CCGGTTAGAGGGTATATAATGGAAGCTCGACTTCCAGA
Min_promoter_R	CCGGTCTGGAAGTCGAGCTTCCATTATATACCCTCTAA
shRNA_CIITA_F	CCGGCATACGTGATGCGCTACTTTGCTCGAGCAAAGTAGCGCATCACGTATGTTTTTG
shRNA_CIITA_R	AATTCAAAAACATACGTGATGCGCTACTTTGCTCGAGCAAAGTAGCGCATCACGTATG
scrambled shRNA F	CCGGCCTAAGGTTAAGTCGCCCTCGCTCGAGCGAGGGCGACTTAACCTTAGGTTTTTG
scrambled shRNA R	AATTCAAAAACCTAAGGTTAAGTCGCCCTCGCTCGAGCGAGGGCGACTTAACCTTAGG

Table S2. Electrotransfection conditions for different cell lines used in the study.

Cell line	Cuvette size	Cell quantity	Voltage	Number of pulses	Pulse frequency
RPMI8866	4-mm	8×10^6	520 V	8	100 µs at 1 Hz
Ramos	4-mm	8×10^6	520 V	8	100 µs at 1 Hz
BLAS	4-mm	8×10^6	520 V	4	100 µs at 1 Hz
THP-1	4-mm	8×10^6	520 V	4	100 µs at 1 Hz

Table S3. The list of differentially expressed genes.

Due to the large size, the table can be found here :

https://osf.io/chqa4/?view_only=ebb54bbab066401ba0cd442a79a565dc

Table S4. The human cDNA and gDNA primers used in the study. cDNA, coding DNA; gDNA, genomic DNA.

Primer	Sequence (5' → 3')	Primer efficiency	Reference
Primers for cDNA			
RPL32 F	CATCTCCTTCTCGGCATCA	2.023	
RPL32 R	AACCCTGTTGTCAATGCCTC		
GAPDH F	CTGCACCACCAACTGCTTAG	2.010	[1]
GAPDH R	AGGTCCACCACTGACACGTT		
HLA-DRB1 F	GGGTGGAGGGGTTCATAGTT	2.026	[2]
HLA-DRB1 R	CTCCAGGGAGCTTCAGACAC		
HLA-DRB5 F	CACAGTGGAATGGAGAGCACAGTC	2.079	[3]
HLA-DRB5 R	GAGCAGGCCCAGCACAAAGC		
Primers for gDNA			
GAPDH F	CCCATCACCATCTTCCAGGAG	2.246	[4]
GAPDH R	GTTGTCATGGATGACCTTGGC		
ACTB F	GCCAGCTGCAAGCCTTGG	2.542	[4]
ACTB R	GCCACTGGGCCTCCATTC		
EBER1 F	AGGACCTACGCTGCCCTA		[5]
EBER1 R	AAAACATGCGGACCACCA		
Primers for ChIP-qPCR			
HLA-DRB1 i F	GCTGGAGAACAGGACAGGAC	2.403	
HLA-DRB1 i R	TTACCCAACCCAGGAGCAAG		
HLA-DRB5 i F	TGCTTTACTGCTATCACCCTGT	2.419	
HLA-DRB5 i R	CCACTCCCACTTCCCAAACC		
HLA-DRB5 ii F	GTGTCACTGTCAGCTTTGCC	2.369	
HLA-DRB5 ii R	TGGTCCTGTCCTGTTCTCCA		
ACTB F	GCCAGCTGCAAGCCTTGG	2.542	[4]
ACTB R	GCCACTGGGCCTCCATTC		

Supplementary figures

Typical output of flow cytometry analysis:

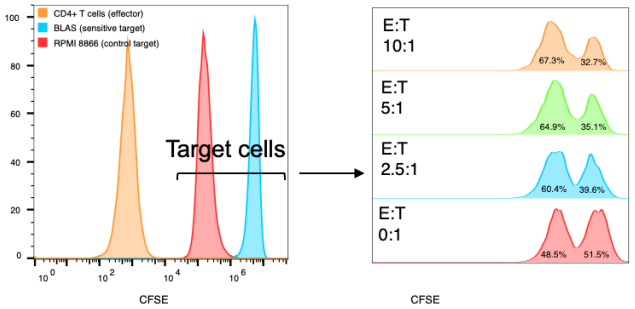

Fraction of sensitive cells:

0.327	b_{10}
0.351	b_5
0.396	$b_{2.5}$
0.515	a

Let a be a fraction of sensitive cells among target cells in E/T 0:1 sample, b be the fraction of sensitive cells among target cells in E/T 10:1 sample, x be the total number of sensitive target cells before the cytotoxic lysis, y be the total number of control target cells before the cytotoxic lysis, and z be the total number of sensitive target cells lysed by the cytotoxic lysis.

Knowing that control and target cells were mixed at the same quantity for all samples, then the fraction of sensitive cells among target cells in E/T 0:1 sample can be expressed as the fraction of sensitive target cells before the cytotoxic lysis and the fraction of sensitive cells among target cells in E/T 10:1 sample can be expressed as the fraction of sensitive target cells after the cytotoxic lysis:

$$a = \frac{x}{x+y} \text{ and } b = \frac{x-z}{x-z+y}$$

Then the percentage of specific lysis can be expressed as the total number of sensitive target cells lysed by the cytotoxic lysis relative to the the total number of sensitive target cells before the cytotoxic lysis:

$$\%\ of\ specific\ lysis = \frac{z}{x} * 100\%$$

If we express x and z through a and b and substitute it in the above formula, it turns out that:

$$a = \frac{x}{x+y} \Rightarrow$$
$$(x+y)a = x \Rightarrow$$
$$xa + ya = x \Rightarrow$$
$$ya = x(1-a) \Rightarrow$$
$$y = \frac{x(1-a)}{a}$$

$$b = \frac{x-z}{x-z+y} \Rightarrow$$
$$b(x-z+y) = x-z \Rightarrow$$
$$bx - bz + by = x - z \Rightarrow$$
$$z - bz = x - bx - by \Rightarrow$$
$$z(1-b) = x(1-b) - by \Rightarrow$$
$$z = x - \frac{b}{1-b} * y \Rightarrow$$
$$z = x - \frac{b}{1-b} * \frac{x(1-a)}{a} \Rightarrow$$
$$z = x\left(1 - \frac{b}{1-b} * \frac{1-a}{a}\right)$$

$$\frac{z}{x} = \frac{x\left(1 - \frac{b}{1-b} * \frac{1-a}{a}\right)}{x} \Rightarrow$$
$$\frac{z}{x} = 1 - \frac{b}{1-b} * \frac{1-a}{a} \Rightarrow$$
$$\frac{z}{x} = \frac{(1-b)a - b(1-a)}{(1-b)a} \Rightarrow$$
$$\frac{z}{x} = \frac{a - ab - b + ab}{a - ab} \Rightarrow$$
$$\frac{z}{x} = \frac{a-b}{a-ab}$$

Thus, the $\%\ of\ specific\ lysis = \frac{a-b}{a-ab} * 100\%$

and for the above example at E/T 10:1 $\%\ of\ specific\ lysis = \frac{0.515-0.327}{0.515-0.515*0.327} * 100\% = 54\%$, which can be illustrated like this:

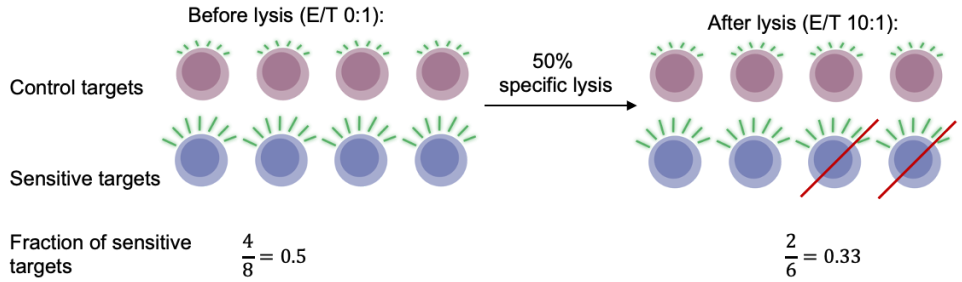

Supplementary Figure 1. The derivation of the % of specific lysis formula used in the study.

Supplementary Figure 2. The original uncropped western blotting images.

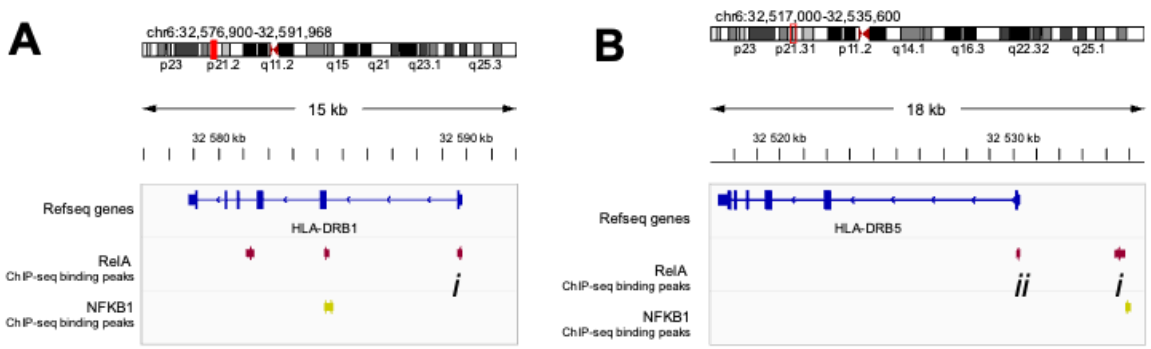

Supplementary Figure 3. RelA and NFKB1 DNA-binding peaks in the vicinity of *HLA-DRB1* (A) and *HLA-DRB5* (B) genes imported from ReMap 2022 (4th release, https://remap.univ-amu.fr/, accession date: 12 January 2023), a database of transcriptional regulators peaks derived from curated ChIP-seq, ChIP-exo, DAP-seq experiments in human [33]. Data were visualized and figures were made using the Integrative Genomics Viewer (version 2.15.2). Non-redundant RelA and NFKB1 peaks are shown. *i* and *ii* indicate the peaks in the vicinity or upstream of *HLA-DRB1* (A) and *HLA-DRB5* (B) genes transcription start sites that were chosen for primer search in these regions for ChIP-qCR. Genomic positions are indicated in GRCH38/hg38 coordinates.

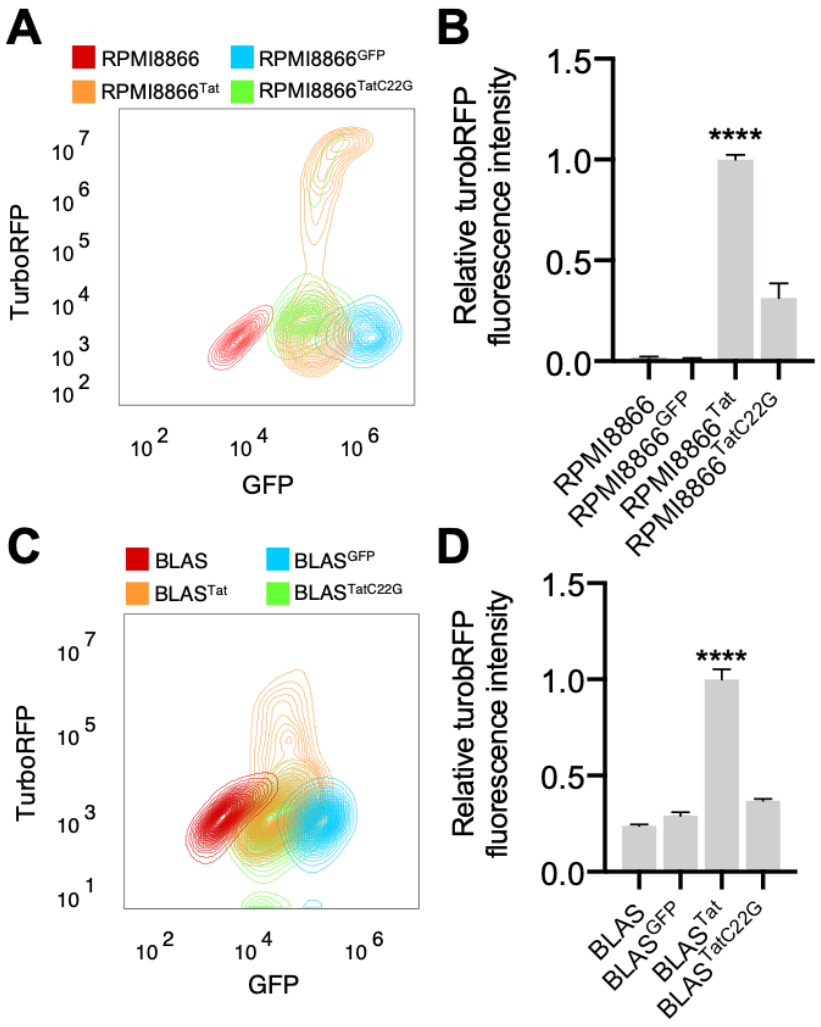

Supplementary figure 4. The analysis of transactivation capacity of Tat-EGFP in RPMI8866 cells transfected with LTR-TurboRFP. (A) Representative flow cytometry contour plots showing GFP and TurobRFP fluorescence in RPMI8866-derived cell lines. (B) Relative TurboRFP fluorescence intensity in RPMI8866-derived cell lines was calculated as the median fluorescence intensity in the sample normalized relative to the median fluorescence intensity in the RPMI8866^{Tat} sample, averaged data from at least three biologically independent experiments are shown. (C) Representative flow cytometry contour plots showing GFP and TurobRFP fluorescence in BLAS-derived cell lines. (D) Relative TurboRFP fluorescence intensity in BLAS-derived cell lines was calculated as the median fluorescence intensity in the sample normalized relative to the median fluorescence

intensity in the BLAS^{Tat} sample, averaged data from at least three biologically independent experiments are shown. Data are presented as mean ± SEM, **** $p < 0.0001$, ANOVA, Tukey's post-hoc test.

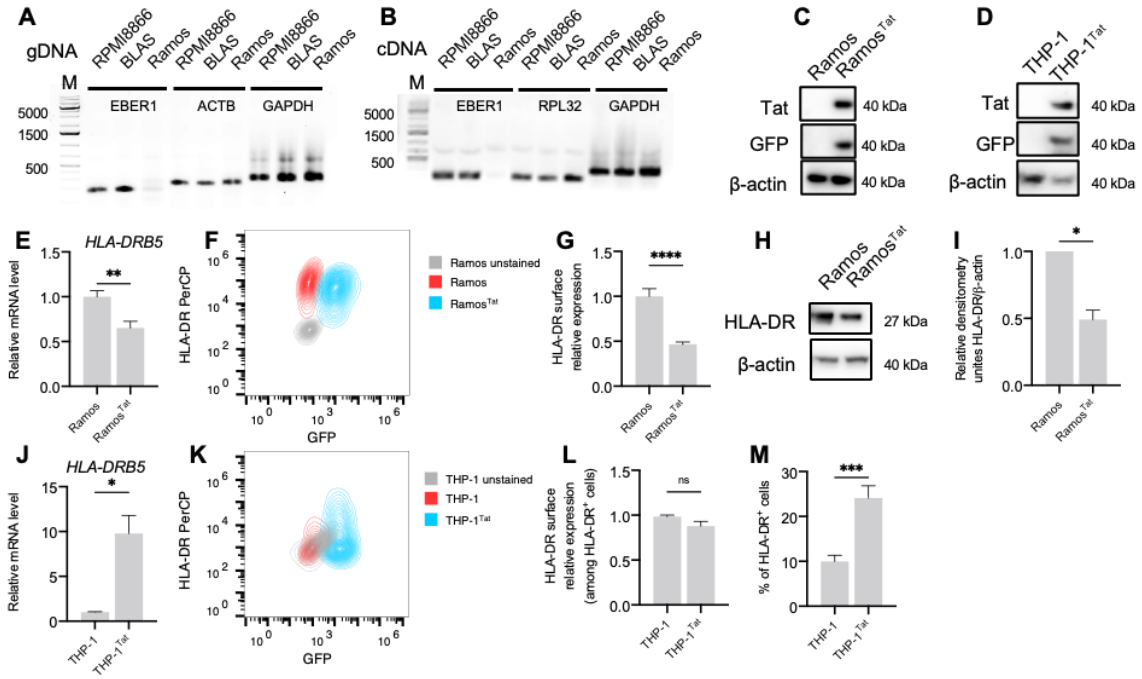

Supplementary figure 5. HIV-1 Tat decreases HLA-DR expression in B cells, but not in monocytes. (A) A representative agarose gel electrophoresis image of end-point PCR to detect *EBER1*, *ACTB* and *GAPDH* gene amplification in genomic DNA (gDNA) samples from RPMI8866, BLAS and Ramos cells. M – markers of molecular weight (bp). (B) A representative agarose gel electrophoresis image of end-point RT-PCR to detect *EBER1*, *RPL32* and *GAPDH* transcript amplification in coding DNA (cDNA) samples from RPMI8866, BLAS and Ramos cells. M – markers of molecular weight (bp). (C) Western blotting analysis of Tat and GFP expression in Ramos and Ramos^{Tat} cell lines. β-actin was used as a loading control. (D) Representative flow cytometry contour plots showing GFP expression and HLA-DR staining of Ramos (red) and Ramos^{Tat} (blue) cell lines. Unstained Ramos cells are shown in grey. (E) HLA-DR surface relative expression in Ramos and

Ramos^{Tat} cell lines calculated as the median fluorescence intensity in the sample normalized relative to the median fluorescence intensity in the control, averaged data from at least three biologically independent experiments are shown. (F) Western blotting analysis of Tat and GFP expression in THP-1 and THP-1^{Tat} cell lines. β-actin was used as a loading control. (G) Representative flow cytometry contour plots showing GFP expression and HLA-DR staining of THP-1 (red) and THP-1^{Tat} (blue) cell lines. Unstained THP1 cells are shown in grey. (H) HLA-DR surface relative expression in THP-1 and THP-1^{Tat} cell lines calculated as the median fluorescence intensity in the sample normalized relative to the median fluorescence intensity in the control, averaged data from at least three biologically independent experiments are shown. Data are presented as mean ± SEM. ** $p < 0.01$, t-test.

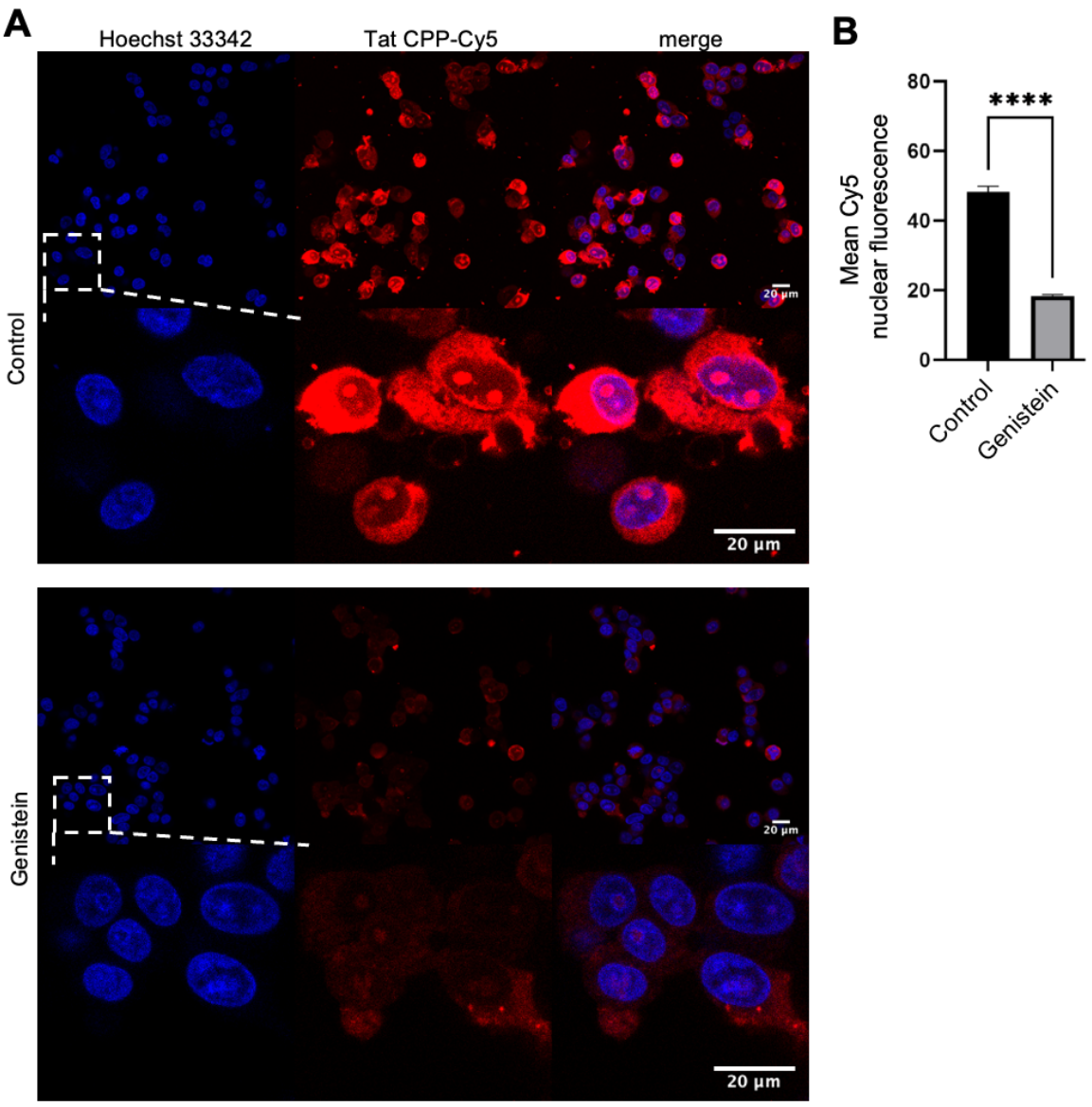

Supplementary figure 6. Genistein, an inhibitor of clathrin-mediated endocytosis, blocks cellular penetration of a fluorescently-labelled Tat-derived cell-penetrating peptide (Tat CPP-Cy5). SH-SY5Y cells were pre-treated or not (control) for 1 hour with 100 µM genistein and then 1 µM Tat CPP-Cy5 was added to cell medium for 30 minutes followed by extensive cell wash, fixation and subsequent analysis of Tat CPP-Cy5 cellular and nuclear penetration using a Leica TCS SP8 Multiphoton confocal Microscope (Leica Microsystems). (A) A representative confocal image of control and genistein-treated SH-SY5Y cells, Tat CPP-Cy5 fluorescence (red) is detected in cells and Tat CPP nucleolar

accumulation can be observed. Nuclei were counterstained with Hoechst 33342 (blue). Scale bar 20 μm. (B) The mean intensity of Tat CPP-Cy5 in the nucleus. Data are presented as mean ± SEM, **** – $p < 0.0001$, ANOVA.

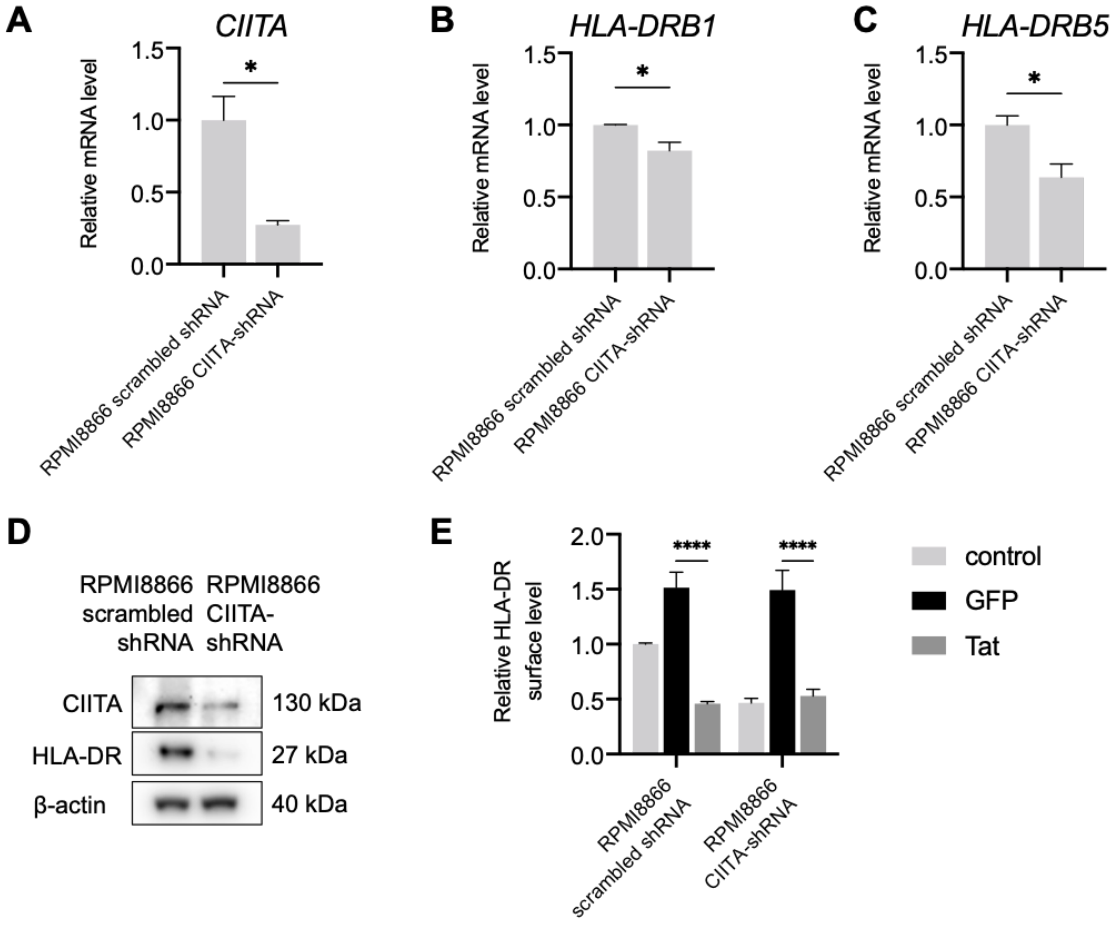

Supplementary figure 7. CIITA knockdown does not perturb the ability of HIV-1 Tat to downregulate HLA-DR expression in RPMI8866 cells. RPMI8866 cell lines that stably expressed scrambled shRNA or CIITA-shRNA were produced through lentiviral transduction with pLKO.1-shCIITA or pLKO.1-scrambled-shRNA and puromycin selection. Cells were then subjected to the second round of lentiviral transduction to produce RPMI8866 cell lines that stably expressed scrambled shRNA or CIITA-shRNA and EGFP or EGFP-Tat. (A-C) The level of *CIITA* (A), *HLA-DRB1* (B) and *HLA-DRB5* (C) mRNA expression in the obtained RPMI8866 cell lines that stably expressed

scrambled shRNA or CIITA-shRNA. The mRNA level of *CIITA*, *HLA-DRB1* or *HLA-DRB5* was normalized to *RPL32* and *GAPDH* expression as housekeeping genes; the normalization was done assuming the mean level of transcript in WT cells to be 1. * $p <$ 0.05, t-test. (D) The level of CIITA and HLA-DR protein expression in the obtained RPMI8866 cell lines that stably expressed scrambled shRNA or CIITA-shRNA. β-actin was used as a control of protein load. (E) The level of HLA-DR surface expression in RPMI8866 cell lines that stably expressed scrambled shRNA or CIITA-shRNA (control) and the same cell lines with stable expression of EGFP or Tat-EGFP as analyzed by flow cytometry. HLA-DR surface relative expression was calculated as the median fluorescence intensity in the sample normalized relative to the median fluorescence intensity in the control (RPMI8866 scrambled shRNA control), averaged data from at least three biologically independent experiments are shown. **** $p <$ 0.0001, two-way ANOVA, Tukey's posthoc test.

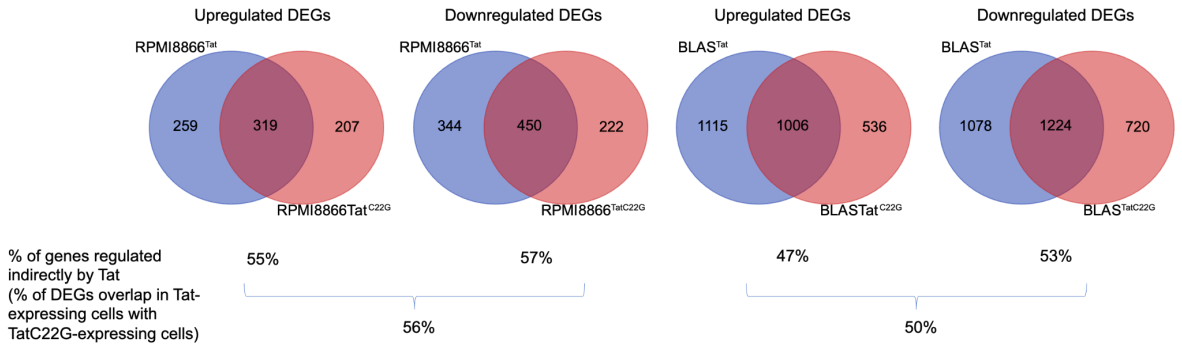

Supplementary figure 8. Venn diagrams demonstrating the overlap of upregulated and downregulated DEGs between RPMI8866^{Tat} *vs* RPMI8866 and RPMI8866^{TatC22G} *vs* RPMI8866, BLAS^{Tat} *vs* BLAS and BLAS^{TatC22G} *vs* BLAS.

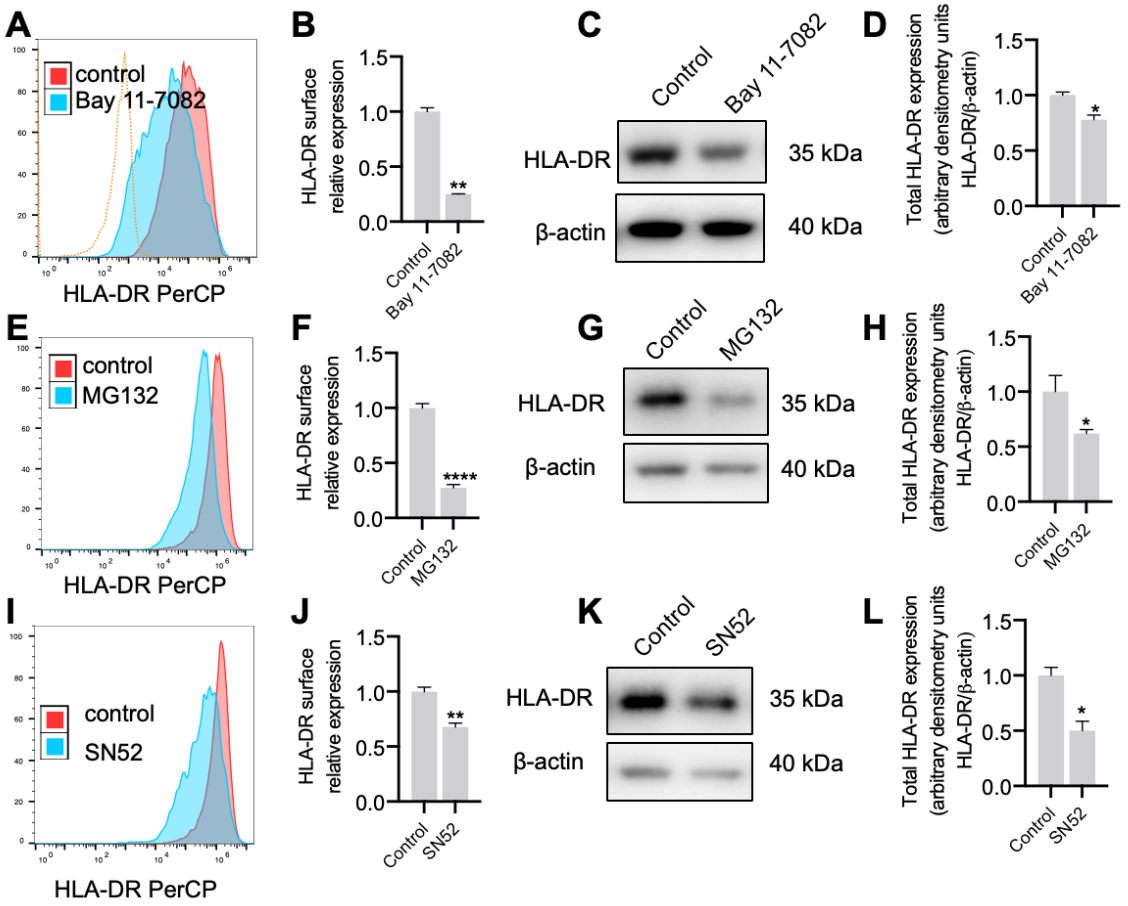

Supplementary figure 9. NF-κB pathway regulates HLA-DR expression in B cells. (A-D) BLAS cells were treated for 24 hours with 1 μM Bay 11-7082 or left untreated (control), HLA-DR expression was then analyzed by flow cytometry analysis and western blotting. (A) A representative histogram for flow cytometry analysis of HLA-DR surface staining in control BLAS cells (red) and cells, treated with 1 μM Bay 11-7082 (blue). Negative control sample is shown for comparison (orange dotted line). (B) HLA-DR surface relative expression was calculated as the median fluorescence intensity in the sample normalized relative to the median fluorescence intensity in the control, averaged data from at least three biologically independent experiments are shown. (C) Western blotting analysis of HLA-DR content in RPMI8866 cells. β-actin was used as a loading control. A reproducible result is presented. (D) Densitometry analysis of HLA-DR content normalized to β-actin.

(E-H) BLAS cells were treated for 6 hours with 20 μM MG132 or left untreated (control), HLA-DR expression was then analyzed by flow cytometry analysis and western blotting. (E) A representative histogram for flow cytometry analysis of HLA-DR surface staining in control BLAS cells (red) and cells, treated with 20 μM MG132 (blue). (F) HLA-DR surface relative expression was calculated as the median fluorescence intensity in the sample normalized relative to the median fluorescence intensity in the control, averaged data from at least three biologically independent experiments are shown. (G) Western blotting analysis of HLA-DR content in RPMI8866 cells. β-actin was used as a loading control. A reproducible result is presented. (H) Densitometry analysis of HLA-DR content normalized to β-actin. (I-L) BLAS cells were treated for 24 hours with 40 μg/ml SN52 or left untreated (control), HLA-DR expression was then analyzed by flow cytometry analysis and western blotting. (I) A representative histogram for flow cytometry analysis of HLA-DR surface staining in control BLAS cells (red) and cells, treated with 40 μg/ml SN52 (blue). (J) HLA-DR surface relative expression was calculated as the median fluorescence intensity in the sample normalized relative to the median fluorescence intensity in the control, averaged data from at least three biologically independent experiments are shown. (K) Western blotting analysis of HLA-DR content in RPMI8866 cells. β-actin was used as a loading control. A reproducible result is presented. (L) Densitometry analysis of HLA-DR content normalized to β-actin. Data are presented as mean ± SEM, * $p < 0.05$, ** $p < 0.01$, *** $p < 0.001$, t-test.

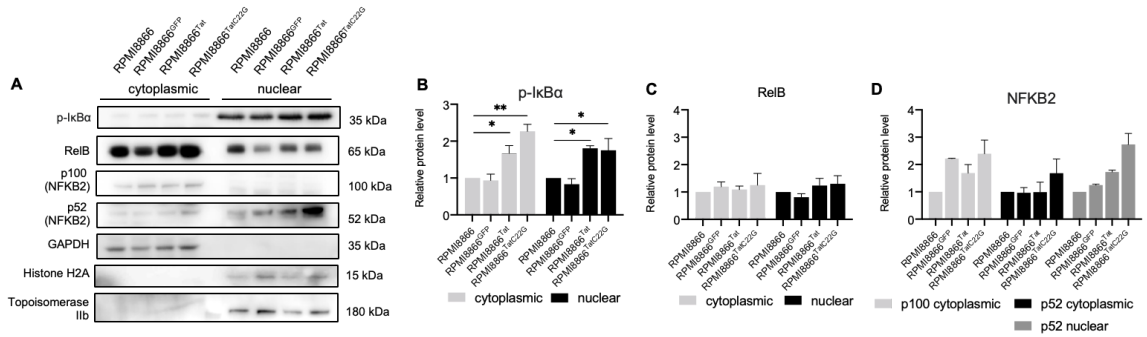

Supplementary figure 10. The effect of HIV-1 Tat expression on non-canonical NF-κB activation and IκBα phosphorylation B cells. (A) Western blotting analysis of p-IκBα, RelB, and NFKB2 (p100 and p52) cytoplasmic and nuclear content in RPMI8866, RPMI8866^{GFP}, RPMI8866^{Tat} and RPMI8866^{TatC22G} cells. GAPDH was used as a loading control for cytoplasmic extracts; histone H2A and topoisomerase IIb were used as loading controls for nuclear extracts. A reproducible result is presented. (B-D) Densitometry analysis of p-IκBα (B), RelB (C), NFKB2 (D) cytoplasmic and nuclear content normalized to respective cytosolic or nuclear control of protein load. Data are presented as mean ± SEM, * $p < 0.05$, ** $p < 0.01$, ANOVA, Tukey's post-hoc test.

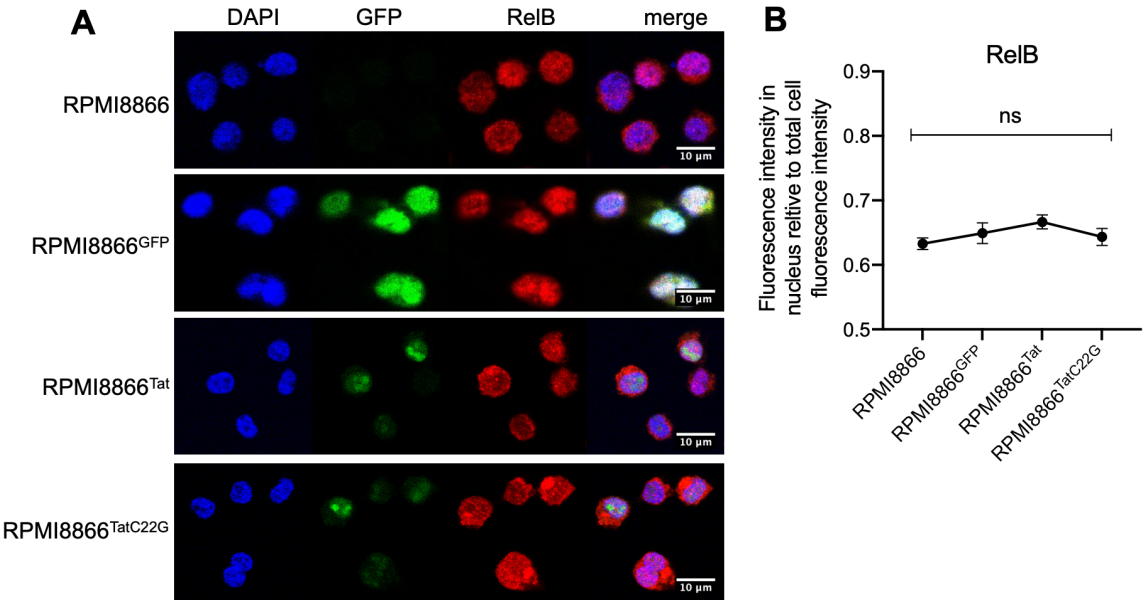

Supplementary figure 11. The effect of HIV-1 Tat expression on non-canonical NF-κB activation in B cells. (A) A representative confocal image of RPMI8866, RPMI8866^{GFP}, RPMI8866^{Tat} and RPMI8866^{TatC22G} cells, stained with antibodies to RelB (red). Nuclei were counterstained with DAPI (blue) and GFP fluorescence in cells expressing GFP, Tat-GFP or TatC22G-GFP was detected (green). Scale bar 10 μm. (B) The ratio of total fluorescence intensity of RelB in the nucleus divided by the respective total cellular fluorescence intensity for each cell. Data are presented as mean ± SEM, ns – non-significant, ANOVA.

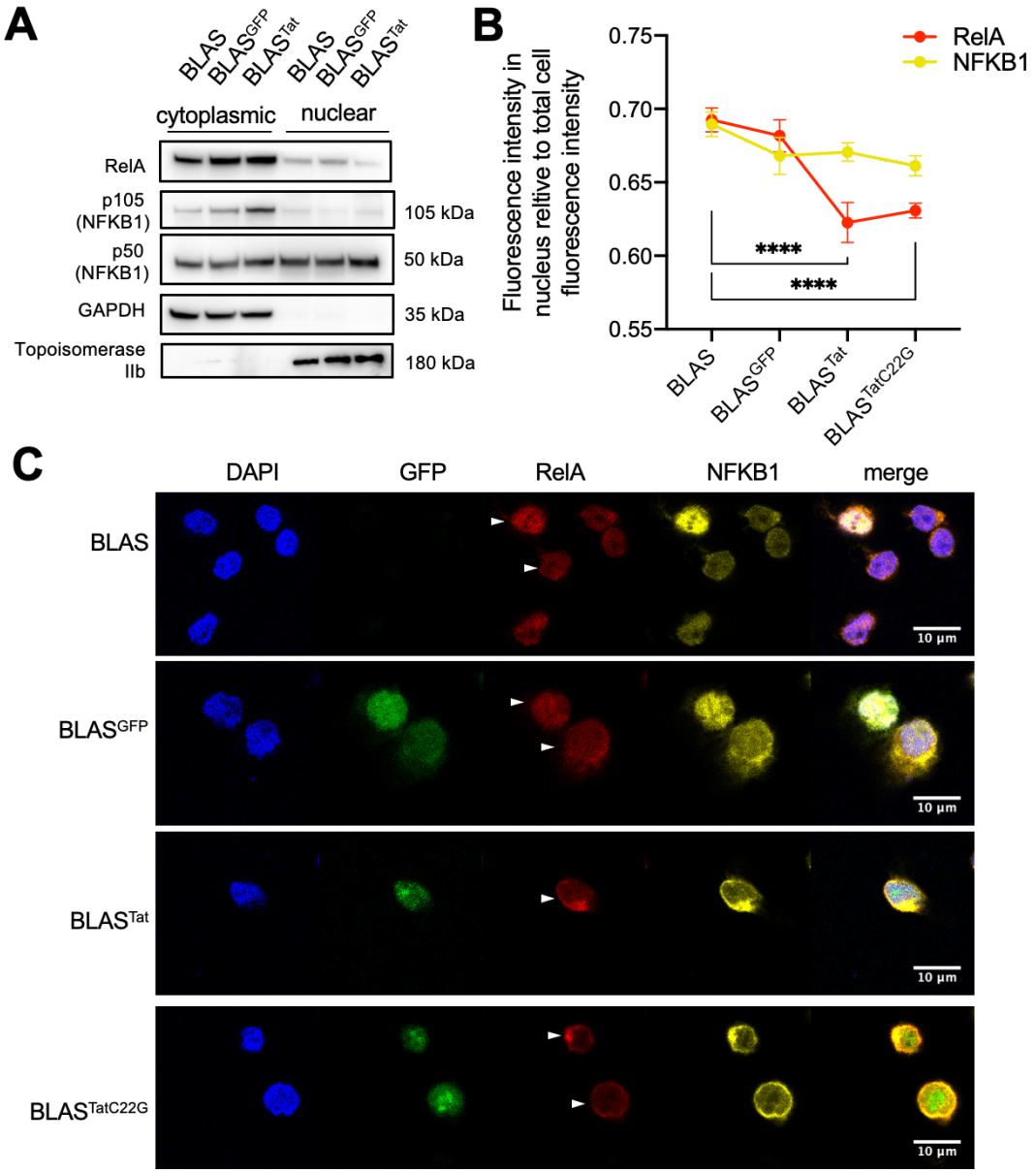

Supplementary figure 12. HIV-1 Tat expression decreased classical NF-κB activation in B cells. (A) Western blotting analysis of RelA cytoplasmic and nuclear content in BLAS, $BLAS^{GFP}$ and $BLAS^{Tat}$ cells. GAPDH was used as a loading control for cytoplasmic extracts; topoisomerase IIb was used as a loading control for nuclear extracts. A reproducible result is presented. (B-C) Immunofluorescent staining with antibodies to RelA and to NFKB1 (p105 and p50) in BLAS, $BLAS^{GFP}$, $BLAS^{Tat}$ and $BLAS^{TatC22G}$ cells. (B) The ratio of total fluorescence intensity of RelA (red) or NFKB1 (yellow) in the nucleus divided by the respective total cellular fluorescence intensity for each cell. (C) A representative confocal image of BLAS, $BLAS^{GFP}$, $BLAS^{Tat}$ and $BLAS^{TatC22G}$ cells, stained with antibodies to RelA (red) and to NFKB1 (p105 and p50, yellow). Nuclei were counterstained with DAPI (blue) and GFP fluorescence in cells expressing GFP, Tat-GFP or TatC22G-GFP was detected (green). White arrows indicate RelA sequestration in the nucleus or cytoplasm. Scale bar 10 μm. Data are presented as mean ± SEM, **** $p <$ 0.0001, ANOVA, Tukey's post-hoc test.

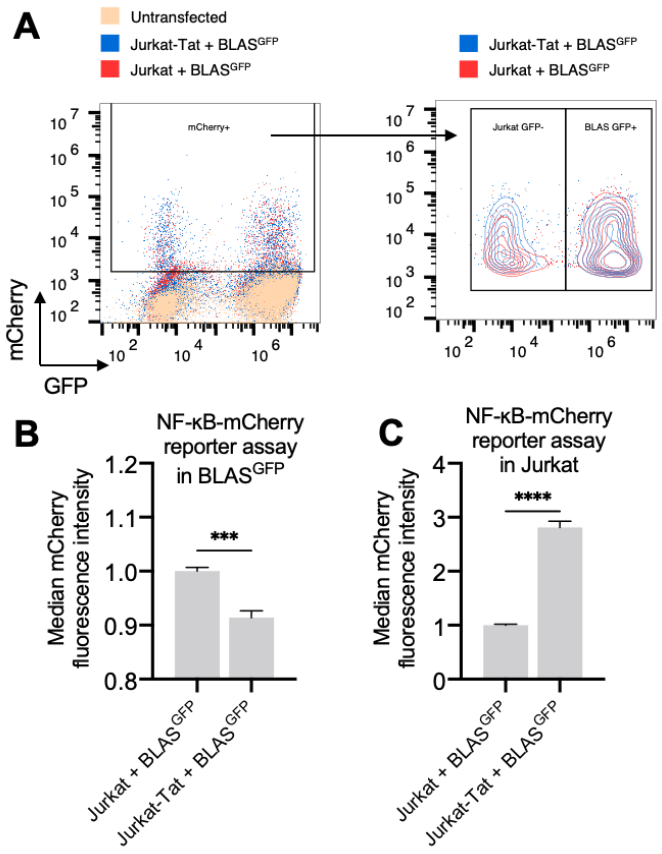

Supplementary figure 13. HIV-1 Tat chronic secretion from T cells decreased NF-κB activation in B cells in the co-culture model. Briefly, BLAS^{GFP} cells were mixed with Jurkat or Jurkat-Tat cells and co-cultivated for 7 days, followed by transfection with the NF-κB-mCherry reporter plasmid. NF-κB reporter activity was analysed 24 hours after transfection. (A) Gating strategy for flow cytometry analysis of NF-κB-mCherry reporter fluorescence in BLAS^{GFP} cells co-cultured with Jurkat (red) or Jurkat-Tat cells (blue). Untransfected co-cultured cells are shown as negative control (pale orange). (B) The activity of the NF-B pathway analysed by the reporter assay in BLAS^{GFP} cells co-cultured with Jurkat or Jurkat-Tat cells and co-cultivated for 7 days, followed by transfection with the NF-κB-mCherry reporter plasmid. (C) The activity of the NF-B pathway analysed by the reporter assay in Jurkat or Jurkat-Tat cells co-cultured with BLAS^{GFP} cells and co-cultivated for 7 days, followed by transfection with the NF-κB-mCherry reporter

plasmid. mCherry expression level was calculated as the median fluorescence intensity in the sample normalized relative to the median fluorescence intensity in the control cells, averaged data from at least three biologically independent experiments are shown. Data are presented as mean ± SEM, *** $p < 0.001$, **** $p < 0.0001$, t-test.

References

1. Sall FB, Shmakova A, Karpukhina A, et al. Epstein−Barr virus reactivation induces MYC-IGH spatial proximity and t(8;14) in B cells. Journal of Medical Virology 2023;95(3):e28633.
2. Kular L, Liu Y, Ruhrmann S, et al. DNA methylation as a mediator of HLA-DRB1*15:01 and a protective variant in multiple sclerosis. Nat Commun 2018;9(1):2397.
3. Ma J, Zhang J-K, Yang D, Ma X-X. Identification of novel prognosis-related genes in the endometrial cancer immune microenvironment. Aging (Albany NY) 2020;12(21):22152–22173.
4. Fiume G, Vecchio E, De Laurentiis A, et al. Human immunodeficiency virus-1 Tat activates NF-κB via physical interaction with IκB-α and p65. Nucleic Acids Res 2012;40(8):3548–3562.
5. Banerjee AS, Pal AD, Banerjee S. Epstein–Barr virus-encoded small non-coding RNAs induce cancer cell chemoresistance and migration. Virology 2013;443(2):294–305.

A potential consequence of reduced MHC class II expression, induced by HIV-1 Tat in B cells, is impaired antigen presentation, leading to a compromised ability to activate CD4+ T cells and initiate an effective immune response against pathogens, including HIV itself. It is known that despite its circulation in the blood and effective cell penetration, HIV-1 Tat is able to elicit an antibody-mediated immune response only in ~20% of people living with HIV (Tripiciano et al. 2021). HIV-1 Tat-mediated downregulation of MHC class II genes in B cells might contribute to the defects in B cell activation and antibody response. It highlights the need for research on Tat implications in HIV-associated clinical disorders and on potential therapeutic approaches to inhibit Tat secretion or penetration in B cells, for instance through the use of endocytosis inhibitors (Szewczyk-Roszczenko et al. 2023).

By contrasting the effects of HIV-1 Tat with its transactivation-deficient mutant (TatC22G), we discovered that approximately half of the genes are regulated in Tat's transactivation-dependent manner (i.e. only by Tat), while another half is regulated by Tat independently of its transactivation activity (i.e. by both Tat and TatC22G) in both cell lines used (RPMI8866 and BLAS) (**Figure 21A**). To explain this observation, we propose the following model (**Figure 21B**). Gene regulation by Tat only depends on the transcriptional activation function of Tat, i.e. involves Tat direct interaction with chromatin, transcription factors or Tat interaction with TAR-like elements. Tat direct action can lead to both transcription upregulation and downregulation (Reeder et al. 2015). Gene regulation by Tat and TatC22G does not depend on the transcriptional activation function of Tat but rather involves the protein-protein interaction of Tat with transcriptional factors (Jean et al. 2017), which can lead to their activation or inhibition. Finally, gene regulation by TatC22G only can be explained by the fact that the gene is regulated both directly and indirectly by Tat with a bidirectional effect, thus, these genes are not significantly deregulated by Tat, but when Tat transcriptional activation function is blocked, TatC22G can only interact with TFs, leading to significant changes in gene expression.

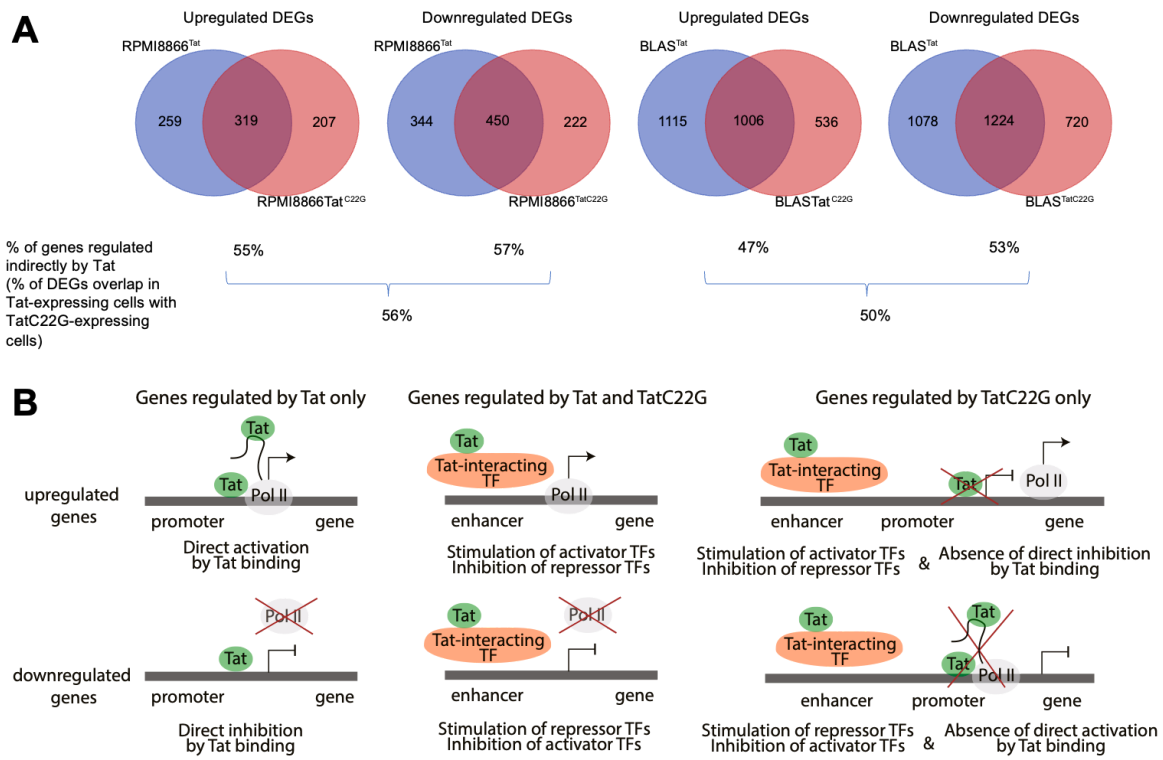

Figure 21. Proposed model for gene regulation by Tat and TatC22G in B cells. (A) Venn diagrams demonstrating the overlap of upregulated and downregulated DEGs between RPMI8866^{Tat} vs RPMI8866 and RPMI8866^{TatC22G} vs RPMI8866, BLAS^{Tat} vs BLAS and BLAS^{TatC22G} vs BLAS. (B) Proposed model for gene regulation by Tat and TatC22G. Gene regulation by Tat only relies on its transactivation activity and direct interactions with chromatin, transcription factors, or TAR-like elements, leading to both upregulation and downregulation. On the other hand, gene regulation by Tat and TatC22G is independent of Tat's transcriptional activation function. Instead, it might involve protein-protein interactions with transcription factors, leading to their activation or inhibition. TatC22G's unique regulation involves both direct and indirect actions of Tat, resulting in bidirectional effects. When Tat's transcriptional activation is blocked, TatC22G interacts only with transcription factors, causing significant changes in gene expression. DEGs, differentially expressed genes; Pol II, RNA-polymerase II; TF, transcription factor.

3.2.4 Comparative analysis of transcriptomes between Tat-expressing B cells and B cells from people living with HIV

To validate our model of ectopic HIV-1 Tat expression in B cells and its relation to B cell pathology in people living with HIV, we performed data mining and analysis of RNA-seq data of B cells isolated from lymph nodes of individuals living with HIV and HIV-uninfected individuals (Austin et al. 2019). We conducted an overlap analysis of deregulated genes in people living with HIV B cells (relative to B cells from non-infected individuals) with genes deregulated by Tat ectopic expression in two B cell lines, RPMI8866^{Tat} and BLAS^{Tat} (relative to wild-type B cell lines).

In the overlap analysis, we identified a total of three genes (*SLAMF1*, *TFEC*, and *DNAH7*) that were upregulated in B cells from people living with HIV, as well as

in both Tat-expressing B cell lines (**Figure 22A**). *SLAMF1* (Signaling Lymphocytic Activation Molecule Family Member 1, also known as CD150 and SLAM) promotes B cell proliferation and is known to be upregulated upon B cell activation (Punnonen et al. 1997), which reflects that dysregulated B cell activation during HIV infection might arise at least partially from the action of HIV-1 Tat. *TFEC* (Transcription Factor EC) is involved in transcriptional regulation and in B cells it has been associated with an immunoglobulin heavy-chain gene enhancer and was shown to be upregulated in memory B cells (Zhao et al. 1993). A total of 28 genes were found to be upregulated in both B cells from individuals living with HIV and RPMI8866^{Tat} B cells. Noteworthy genes in this subset included *STAT1*, *IL12B*, *TNFSF10* (TRAIL), *IFI6*, *IFI44L*, which have been implicated in B cell activation, inflammatory signalling, apoptosis and B cell lymphomas (Benjamin et al. 1996; Chen et al. 2016; Morgan & Tergaonkar 2022; Oshima et al. 2001). We observed an overlap of 39 upregulated genes in B cells from people living with HIV and Tat-expressing BLAS cells. This set included genes such as *TNFRSF9* (CD137), *PTK2* (encoding focal adhesion kinase), *HCK*, *EPHA4*, *DEK*, *PTCH1*, involved in B cell activation, proliferation, B cell receptor signalling and B cell lymphomas (Çalışkaner et al. 2017; Darling & Lamb 2019; Mlinaric-Rascan & Yamamoto 2001; Munshi et al. 2021; Zhao et al. 2013).

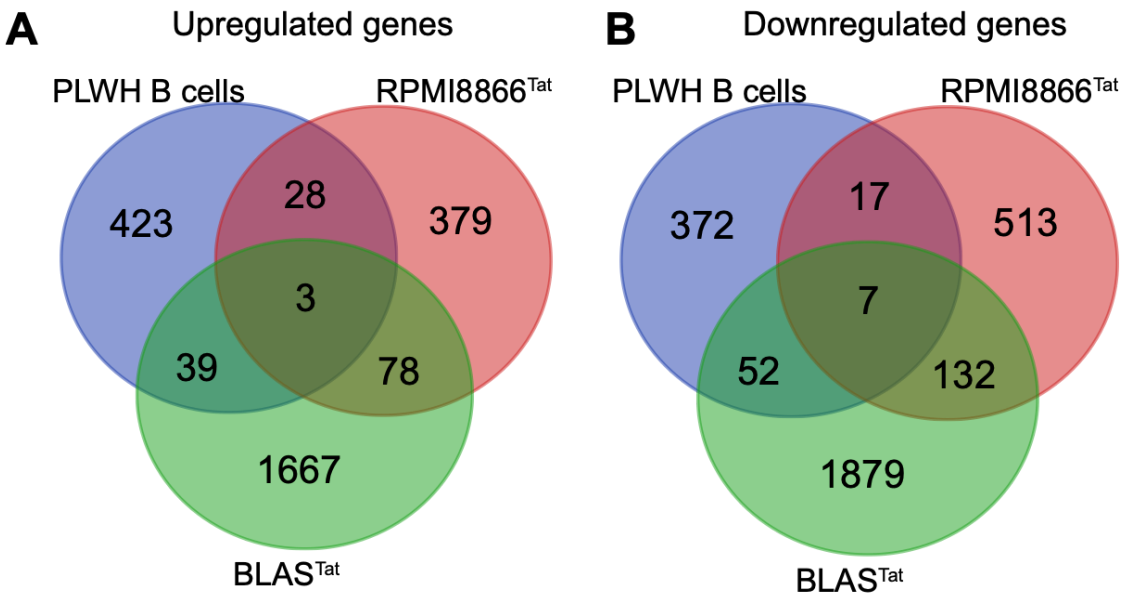

Figure 22. A comparison of transcriptomes of Tat-expressing B cells and B cells from people living with HIV. Venn diagrams demonstrating the overlap of upregulated (A) and downregulated (B) DEGs between PLWH B cells vs B cells from HIV-uninfected individuals, RPMI8866^{Tat} vs RPMI8866, and BLAS^{Tat} vs BLAS. DEGs, differentially expressed genes; PLWH, people living with HIV.

Among downregulated genes (**Figure 22B**), we identified seven genes that were consistently downregulated across all three subsets (B cells from people living with HIV, RPMI8866^{Tat} and BLAS^{Tat} cells), comprising *CXCR4*, *ANKRD6*,

SULF2, *NR4A1* (Nur77), *TIMD4*, *MYO5B*, and *PECAM1* (CD31). The downregulation of these genes may contribute to altered immune responses and cellular functions in B cells during HIV infection and Tat ectopic expression since they are implicated in B cell development, viability, antigen response, proliferation and apoptosis of B cell lymphoma cells (Jang et al. 2021; Li et al. 2020; Nie et al. 2004; Tan et al. 2019; Wong & Jackson 2004). Furthermore, we identified 17 genes that were commonly downregulated between B cells from people living with HIV and RPMI8866^{Tat} B cells. Among these genes were *BAMBI*, *SH3PXD2A*, *ZFYVE9*, *F13A1*, *SASH1*, *STK31*, *LY9* (CD229), *ESR2*, *ARHGEF10L*, *AKAP7*, *APLP2*, *VCL*, *VCAM1* (CD106), *SLC45A3*, *TNFSF9* (CD137 ligand), and *JUN*. These genes have been implicated in various processes, such as inflammation, B cell proliferation, activation, development and adhesion, potentially contributing to the perturbation of B cell functions (Blonska et al. 2015; de Salort et al. 2013; Roncador et al. 2022; Wong et al. 2020; Zhang et al. 2010). Finally, we observed an overlap of 52 genes that were commonly downregulated between B cells with Tat ectopic expression in BLAS and people living with HIV B cells. Genes among this set included *WASF1*, *EPN2*, *ITM2B*, *NFKB2*, *ZNF284*, *TNXB*, *CD6*, *TM6SF1*, *RIC3*, *CCDC144A*, *PITPNM2*, *ICAM2* (CD102), *TSPAN14*, *BLK*, *SLC23A1*, *LDLRAP1*, *KCNA3*, *SELPLG*, *CCDC17*, *UXS1*, *PTPRJ*, *HSBP1L1*, *CEACAM1*, *RBMS1*, *CD1C*, *CPNE2*, *LEF1*, *NFKBID*, *USP53*, *BEX4*, *LAMA5*, *LAMC1*, *CREB3L2*, *BTBD3*, *P4HA2*, *PTPRN2*, *SBF2*, *ZDHHC9*, *JUNB*, *WNT10A*, *TPK1*, *AEBP1*, *TUBG2*, *STARD9*, *ERN1*, *GAB1*, *NDFIP1*, *FBXW4P1*, *CMTM7*, *CCDC9*, *N4BP3*, and *IL11RA*. These genes may play crucial roles in the molecular pathways involved in B cell oncogenesis. Two of these genes are related to the NF-κB signalling pathway (*NFKB2, NFKBID*). *LEF1* and *BLK* are involved in B cell development, differentiation, proliferation and survival (Reya et al. 2000; Tandon et al. 2011; Texido et al. 2000). Intriguingly, *LEF1* depletion is associated with a decrease in the NF-κB signalling pathway (Zhang et al. 2021) and we observed a decrease in the NF-κB pathway activity in Tat-expressing B cells. Reciprocally, *LEF1* is an NF-κB transcriptional target (Yun et al. 2007). Finally, JunB is known to inhibit the proliferation and transformation of B cells (Szremska et al. 2003). *JUNB* gene is an NF-κB transcriptional target (Brown et al. 1995) and its downregulation in B cells from people living with HIV and Tat-expressing B cells might be a prerequisite for their oncogenic transformation.

To sum up, the commonalities in deregulated gene expression in B cells from people living with HIV and B cells with Tat ectopic expression support our hypothesis that B cell pathology in people living with HIV might be at least partially related to the chronic secretion of HIV-1 Tat protein by infected cells and its penetration in B cells. This provides valuable insights into potential mechanisms contributing to B cell oncogenesis in HIV-infected individuals.

3.2.5 Interaction between HIV-1 Tat and EBV Zta favours immune escape of B cells by suppressing HLA-ABC

Transcriptional activators Tat of HIV-1 and Zta of EBV possess many similar features: they are both transcriptional activators, they can be released from infected cells, penetrate other cells, where being transported into a nucleus regulate viral and host gene transcription (Germini et al. 2020; Habib et al. 2017; Rayne et al. 2010b; Rothe et al. 2010). HIV-1 Tat and EBV Zta can be hypothetically found simultaneously in blood, lymph nodes and other tissues in people living with HIV as their secretion was independently shown for people living with HIV in the case of Tat (Poggi et al. 2004) and people infected with EBV in case of Zta (Habib et al. 2017). Above, we have confirmed that HIV-1 Tat circulates in the blood of people living with HIV despite effective viral suppression and the absence of immune deficiency in the era of cART (**Figure 16**). Infection with EBV is highly widespread in the general population (90%) (Cohen 2000; Tsurumi et al. 2005), thus making coinfection with EBV in people living with HIV almost inevitable; this population also frequently presents EBV reactivation (**Figure 10**), nevertheless, to our knowledge, EBV Zta secretion by infected B cells and its presence in the blood of HIV-positive individuals was never analyzed before. We now analysed the presence of EBV Zta in the serum of people living with HIV using the ELISA assay described previously (Habib et al. 2017; Lupo et al. 2022).

The cohort consisted of 30 people living with HIV and 5 HIV-uninfected healthy controls. None of the healthy controls had detectable EBV Zta levels (**Figure 23A**). Among the group of people living with HIV, 7/30 (23%) individuals were found to have detectable levels of Zta, with values ranging from 0 to 488.7 ng/ml. The mean Zta concentration for all HIV-positive individuals was 21.84 ± 16.65 ng/ml, and the mean Zta concentration for HIV-positive individuals with detectable levels was 93.60 ± 67.99, compared to the mean value of 21.84 ± 16.65 for all people living with HIV (**Figure 23A**). To confirm this result, we used immunoprecipitation with anti-Zta antibodies in a serum sample with detectable EBV Zta. As a control, we employed a sample of healthy control serum with recombinant Zta added at a concentration of 50 ng/ml (**Figure 23B**). The immunoprecipitation results validated the presence of Zta in an individual with HIV. Notably, this individual also had detectable levels of HIV-1 Tat in the serum as identified using immunoprecipitation from serum with anti-Tat antibodies (**Figure 23B**). The finding suggests that EBV Zta can circulate in the blood of people living with HIV, warranting further investigation into its potential implication in B cell oncogenesis in this population.

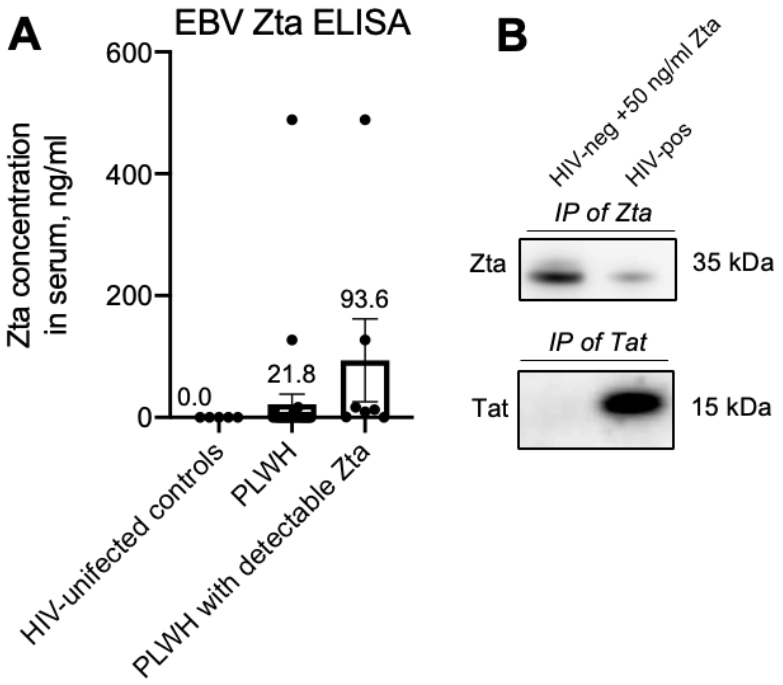

Figure 23. Zta presence in the serum of people living with HIV. (A) Quantification of soluble Zta using ELISA in serum samples from people living with HIV and healthy controls. (B) Healthy donor plasma (HIV-neg.) supplemented with recombinant Zta protein (50 ng/ml) and serum sample from an HIV-positive individual (HIV-pos) were immunoprecipitated using Protein G magnetic beads cross-linked with anti-Zta or anti-Tat antibodies. Immunoprecipitated (IP) fractions are analyzed by Western Blot staining for Zta and Tat. Abbreviations: PLWH, people living with HIV.

The investigation into the effect of the simultaneous presence of both HIV-1 Tat and EBV Zta in the serum of people living with HIV (**Figure 16, Figure 23**) could provide valuable insights into the complex interactions underlying the pathobiology of HIV-EBV combined infection. This study underscores the need for a comprehensive exploration of viral interactions to inform therapeutic strategies and improve the management of individuals living with HIV. HIV-1 Tat and EBV Zta interaction was never questioned before. It was however shown that HIV-1 Tat and EBV Zta can synergistically activate HIV-1 long terminal repeat (LTR): while with Tat and Zta only the LTR-driven LacZ expression increased 44- and 18-fold, the combination of HIV-1 Tat and EBV Zta caused a 214-fold increase in LTR-driven LacZ expression (Mallon et al. 1990). We hypothesized that HIV-1 Tat and EBV Zta can interact physically and/or functionally with each other in promoting oncogenesis in people living with HIV.

In this study, we extensively employed the YFP reconstitution technique, also known as bimolecular fluorescence complementation, which allows the study of protein-protein interaction and is based on fluorescence emergence after reconstitution of a functional fluorescent protein YFP upon coexpression of its N- and C-terminal fragments (YFP1 and YFP2, respectively), fused to interacting proteins of interest (Kudla & Bock 2016) (**Figure 24A**). To perform YFP

reconstitution analysis, we cloned Tat and Zta in pcDNA3-YFP1 and pcDNA3-YFP2 plasmids, kindly provided by the authors (Nyfeler et al. 2005). Plasmids encoded for a YFP split fragment, followed by a short peptide linker (GGGS)2 to allow structural flexibility for the interaction, ending by Tat or Zta sequence (**Figure 24B**). A hypothetical interaction of Tat and Zta conjugated to split YFP parts is depicted in **Figure 24A**.

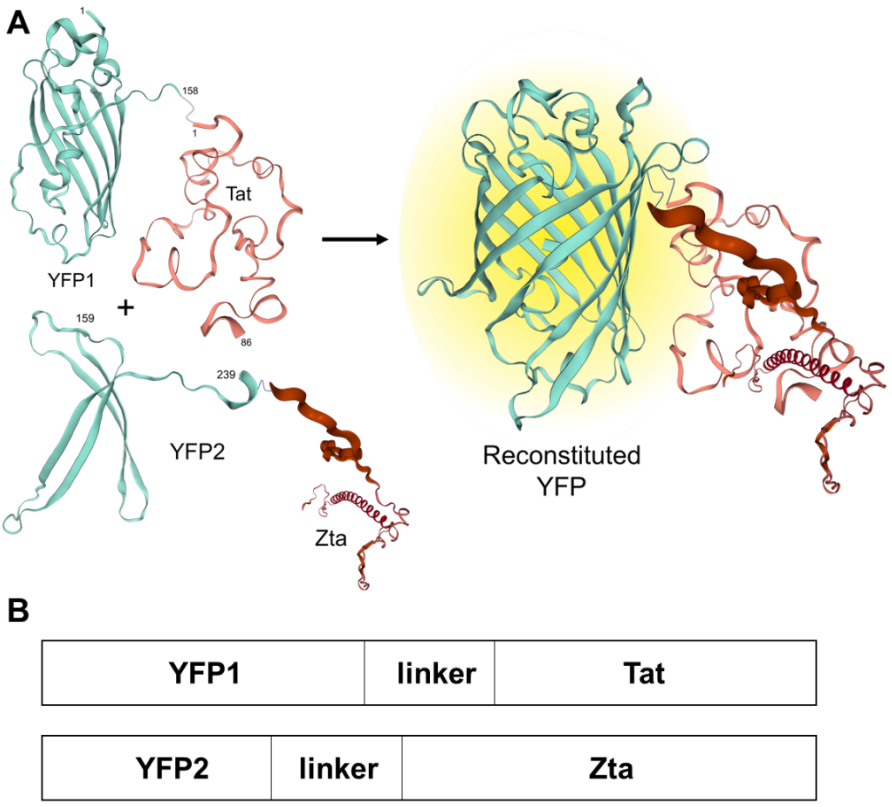

Figure 24. YFP reconstitution technique. (A) The scheme of the YFP reconstitution technique used in the current study. YFP split fragments 1 (amino acids 1–158) and 2 (amino acids 159–239) were fused to Tat and Zta proteins to study their interaction, which will bring YFP1 and YFP2 into close proximity and lead to reconstituted fluorescence. YFP and Tat 3D structures were imported from SWISS-MODEL Repository (Bienert et al. 2017), accession numbers A0A059PIR9, P04608; YFP split structures were modelled by SWISS-MODEL modelling workspace; Zta structure was predicted using (PS)2: Protein Structure Prediction Server (Huang et al. 2015b). (B) The modular composition of the fusion proteins used in this study.

In the current study (**Article 10**), we analysed the possible interaction of HIV-1 Tat and EBV Zta and its relation to oncogenesis in human B cells. We found that Tat and Zta directly bind each other in human B cells, T cells, and blood serum. Tat and Zta interaction was also observed in a serum sample from an HIV-positive individual. Through the YFP reconstitution assay, we determined that this binding mainly occurs within the nucleus, which suggests potential implications for the host genome. Using RNA-sequencing we found that combined Tat and Zta action in B cells differed from a simple combination of two proteins. A subset of genes, activated by Tat or Zta alone, that trigger an

immune response, and antigen presentation in B cells (heat shock proteins (HSPs)), remained unchanged when two proteins were combined.

The expression of HLA-ABC (MHC class I), a crucial element of the antigen processing and presentation pathway (Leone et al. 2013), was significantly decreased in B cells treated or transfected with Tat and Zta. This reduction in HLA-ABC levels appears to be associated with proteasomal degradation, rather than transcriptional downregulation. Moreover, the downregulation of HLA-ABC caused by Tat and Zta interaction provided a shield against recognition by cytotoxic T cells of B cells infected with EBV.

In summary, our study presents a conceptually novel finding: the direct interaction between two viral proteins from different viruses. The functional consequences of this interaction seem to be related to the evasion of the immune response in EBV-infected or transformed B cells.

Article 10. Research paper "Interaction between HIV-1 Tat and EBV Zta favours immune escape of B cells by downregulating HLA-ABC expression"

Interaction between HIV-1 Tat and EBV Zta favours immune escape of B cells by downregulating HLA-ABC expression

(manuscript in preparation)

Anna Shmakova[1,2], Anna Schwager (Karpukhina)[1,2], Ivan Tsimailo[1], Emile Clerf [1], Yana Kozhevnikova[1], Laurence Gerard[3], David Boutboul[3], Eric Oksenhendler[3], Diego Germini[1], Yegor Vassetzky[1,2]*

[1]CNRS, UMR 9018, Université Paris-Saclay, Institut Gustave Roussy, 94800 Villejuif, France;

[2]Koltzov Institute of Developmental Biology, 119334 Moscow, Russia;

[3]Service d'Immunopathologie Clinique, Hôpital St Louis, APHP, 75012 Paris, France.

*Corresponding author: yegor.vassetzky@cnrs.fr

Abstract

Both Human immunodeficiency virus (HIV) and Epstein Barr Virus (EBV) are associated with an increased risk of malignancies. HIV infection is associated with EBV reactivation and an increase in EBV viral loads in saliva and blood, and people living with HIV frequently develop EBV-associated B-cell malignancies. In this study, we aimed to investigate the involvement of HIV-1 and EBV co-existence in the development of B-cell malignancies. To do so, we focused our attention on the two viral transcriptional activators (HIV-1 Tat and EBV Zta) and analyzed their possible interaction since they both have cell-penetration domains and can be found simultaneously in the blood or cells of people living with HIV.

We investigated the interaction of two viral proteins using co-immunoprecipitation, *in vitro* binding, YFP reconstitution assay and FRET. We found that Tat and Zta directly bind each other in human B cells, T cells and blood serum. Tat and Zta interaction was also observed in a serum sample from an HIV-positive individual. YFP reconstitution demonstrated that this interaction occurred predominantly in the nucleus, indicating that it might affect the host genome. We further analyzed the effects of Tat and Zta on primary human B cells by RNA-sequencing and found that combined Tat and Zta action in B cells differed from a simple combination of two proteins. A subset of genes, activated by Tat or Zta alone, that trigger an immune response and antigen presentation in B cells, remained unchanged when two proteins were combined. B cells, treated or transfected with Tat and Zta, exhibited a substantial decrease in HLA-ABC (MHC class I) expression, a critical component of the antigen processing and presentation pathway. Our findings suggest that the reduction of total HLA-ABC levels in B cells upon Tat and Zta interaction might be linked to HLA-ABC proteasomal degradation. Furthermore, HLA-ABC downregulation induced by

Tat and Zta interaction conferred protection against cytotoxic T cell recognition of EBV-infected B cells.

To conclude, we demonstrated for the first time that HIV-1 Tat and EBV Zta interacted directly in B, T cells and blood serum, this interaction can be found in people with HIV. The functional effects of this interaction may be linked to immune evasion of EBV-infected or transformed B cells.

Introduction

Human immunodeficiency virus (HIV) and Epstein-Barr virus (EBV) cause chronic, currently incurable infections that have a major negative impact on the immune system and contribute to the development of cancer. Combined antiretroviral therapy (cART) provides complete suppression of HIV replication and immune recovery [1]; despite this fact, people living with HIV are still at higher risk of developing cancer [2–4]. Contrary to the HIV-negative population, people living with HIV are also more likely to be seropositive for EBV, experience EBV reactivation more frequently, and are at a higher risk of developing EBV-associated malignancies [5–7].

EBV infects 90% of the world population and has a strong association with human cancers (1-2% of human cancers) [8–10]. After primary infection, EBV establishes a life-long latency in B cells and a very stable virus-host relationship with the possibility to reactivate following specific stimuli [11]. EBV is an established etiological factor for diseases of B and epithelial cells: infectious mononucleosis, Burkitt lymphoma (BL), Hodgkin's lymphomas (HL), nasopharyngeal (NPC) and gastric carcinoma and post-transplant lymphoproliferative disorder (PTLD) [12]. EBV is also associated with diseases involving cells not directly targeted by the virus: breast and hepatocellular carcinoma, leiomyosarcoma, follicular dendritic sarcoma and T-cell malignancies [13].

EBV presence in people living with HIV (EBV and HIV combined infection) is a highly probable event [14–16] that largely contributes to the cancer burden. HIV infection is associated with EBV reactivation and increases EBV viral loads in saliva and blood [17–19]. EBV is involved in lymphomagenesis in people living with HIV: HIV-associated BL is EBV positive in 30-40% cases, classical HL – ~100% of EBV+ cases, diffuse large B-cell lymphoma (DLBCL) is EBV positive in 30-40% and HIV-associated B-lymphoproliferative disease consists of ~100% of EBV+ cases [18,20]. In humanized mice, EBV combined infection with HIV leads to increased tumour formation as compared to separate virus infection independently of CD8+ T cell response [21]. Immune deficiency cannot fully explain the increased incidence of certain EBV-related malignancies in people living with HIV, which remains still increased in the cART era [22-24]. These aspects point to a complex relationship between HIV and EBV, which is not straightforwardly linked to immunosuppression and lack of EBV control. A detailed understanding of the mechanisms and consequences of viral coexistence at the molecular level is required for novel strategies of targeted cancer therapy.

With this regard, we draw our attention to viral transactivator proteins with cell penetration capacities. It is known that viruses evolved different strategies to manipulate host cell defence programs [25,26]. Many of these strategies are governed by viral transcriptional activator proteins that above sustaining the transcription of viral genomes alter existing cellular programs in a way that promotes viral propagation [27]. Transcriptional activators Tat of HIV-1 and Zta of EBV possess many similar features: they are both transcriptional activators, they can exit infected cells, and penetrate other cells, where being transported into a nucleus regulate viral and host gene transcription [28–30]. HIV-1 Tat and EBV Zta can be hypothetically found simultaneously in blood, lymph nodes and other tissues in people living with HIV as their secretion was independently shown for people living with HIV in the case of Tat [31] and people infected with EBV in the case of Zta [32]. We hypothesized that they can interact physically and functionally with each other in promoting oncogenesis in people living with HIV.

HIV-1 Tat is a 12 kDa basic protein secreted by HIV-infected cells that can penetrate cells *via* its charged cell-penetration domain (CPD) [33], as well as the brain-blood barrier [34,35]. Circulating Tat is detectable in the blood serum at concentrations ranging from 2 ng/ml to 550 ng/ml [31]. Tat has also been detected in the cerebrospinal fluid of 36.8% of people living with HIV on cART (at concentrations ranging from 200 pg/ml to 6.5 ng/ml), and its secretion was shown to increase in four out of five patients after cART initiation, which indicates that Tat secretion is not inhibited by cART [36]. HIV-1 Tat protein binds both viral and host gene promoters, recruiting transcriptional factors (P-TEFb, TBP), which leads to increased viral transcript synthesis and facilitates viral propagation, meanwhile, it also causes disturbances in cellular gene expression, regulating hundreds of host genes [37–41]. EBV Zta (also known as ZEBRA, Z, or EB-1) is a 35 kDa protein, encoded by the *BZLF1* gene of EBV [28]. Zta is a key factor in switching from latency to lytic cycle during EBV reactivation [42,43]. Zta is a basic leucine zipper transcription factor [44] with a cell penetration domain [30] and a special affinity and selectivity for CpG-methylated binding sites [45–47]. There is growing evidence concerning Zta implication in EBV-driven oncogenesis. Zta is detected in serum samples from humanized mice developing lymphomas and correlates with tumour mass [48]. Zta high expression was shown in PTLD samples, HL, DLBCL, BL, nasopharyngeal carcinoma (NPC) and breast cancer [49–53].

In the current study, we analyzed the possible interaction of HIV-1 Tat and EBV Zta and its relation to oncogenesis in human B cells. We found that Tat and Zta directly bind each other in human B cells, T cells and blood serum. Tat and Zta interaction was also observed in a serum sample from an HIV-infected patient. Using RNA-sequencing we found that combined Tat and Zta action in B cells differed from a simple combination of two proteins. A subset of genes, activated by Tat or Zta alone, that trigger an immune response, antigen presentation in B cells remained unchanged when two proteins were combined. The cooperative interaction of Tat and Zta in B cells led to a notable decrease in the expression of HLA-ABC, a critical component of the antigen presentation pathway. This reduction compromised the susceptibility of EBV-infected B cells to cytotoxic T cell-mediated lysis.

We thus hypothesize that Tat and Zta interaction may provide an immune evasion for transformed B cells, which may contribute to B cell lymphoma development in people living with HIV.

Materials and methods

Antibodies, enzymes, recombinant proteins

The following antibodies were used in the work: mouse anti-Tat (Santa Cruz, cat. # sc-65912), mouse anti-Zta (kindly provided by Dr. Emmanuel Drouet, Université Grenoble Alpes), mouse anti-transthyretin (Santa Cruz, cat. # sc-377517), mouse anti-transferrin (Santa Cruz, cat. # sc-52256), rabbit anti-Galectin-9 (Proteintech, 17938-1-AP), mouse anti-HLA-ABC (Santa Cruz, cat. #sc-52810), mouse anti-β-actin (1:1000, control of protein load, #sc-81178, Santa Cruz), rabbit anti-GAPDH (1:1000, control of protein load, Cell Signaling Technology, cat. #2118), mouse anti-vinculin (1:1000, control of protein load, Sigma, cat. #SAB4200729), PE-Cy5 anti-HLA-DR (Biolegend, cat. #307608), PE-Cy5 anti-HLA-ABC (BD, cat. # 555554), APC CD3 (Biolegend, cat. #300312), goat anti-mouse IgG (Fc) F(ab)2 HRP Highly absorbed (Sigma, cat. # SAB3701029), goat anti-mouse IgG-HRP (Santa Cruz, cat. # sc-2005), donkey anti-rabbit IgG-HRP (Santa Cruz, cat. # sc-2313), AF647 Goat anti-mouse IgG H+L (Invitrogen, cat. # A21235). The following antibodies were obtained through the NIH HIV Reagent Program, Division of AIDS, NIAID, NIH: anti-HIV-1 Tat Monoclonal (15.1), ARP-1974, contributed by DAIDS/NIAID ; anti-HIV-1 HXB2 Tat Monoclonal (1D9), ARP-7377, contributed by Dr. Dag E. Helland. The following reagent was obtained through the NIH HIV Reagent Program, Division of AIDS, NIAID, NIH and Centre for AIDS Reagents, NIBSC, UK, supported by EURIPRED (EC FP7 INFRASTRUCTURES-2012 - INFRA-2012-1.1.5.: Grant Number 31266): Anti-Human Immunodeficiency Virus 1 (HIV-1) Tat Monoclonal (NT3 5A5.1), ARP-4374 (CFAR#3253), contributed by Dr. Jonathan Karn.

Restriction enzymes (XhoI cat. # FD0694, EcoRI cat. # FD0274, SalI cat. #FD0644, BamHI cat. # FD0054, AgeI cat. # ER1461, BglII cat. # ER0081), T4 DNA ligase (cat. # EL0011), Shrimp Alkaline Phosphatase (cat. # EF0511) were obtained from Thermo Fisher.

Zta recombinant protein was synthesized by a biological company BiologicsCorp, USA, from pET29a(+)-BZLF1 plasmid, encoding for His-tagged Zta. Tat recombinant protein was obtained through the NIH AIDS Research and Reagent Program, Division of AIDS, NIAID, NIH: HIV-1 IIIB Tat Recombinant Protein (cat. # 2222). Proteins were added to the cell medium or blood plasma at the indicated concentrations.

Blood plasma collection and primary B cell isolation

Whole blood samples from anonymous healthy donors of different sex and age were obtained from the “Etablissment Français du Sang”, Hôpital Saint-Louis, Paris, France in accordance with the French legislation (agreement number № 14/EFS/033). Blood plasma was collected after EDTA-treated blood samples centrifugation for 15 minutes at 2000g.

Blood samples from hospitalized HIV-infected patients who signed a written informed consent for the study were collected in Clinical Hospital № 67, Moscow, Russia in accordance with the Russian legislation or in Hôpital Saint-Louis, Paris, France in accordance with the French legislation. HIV status was analysed by immunoassay of anti-HIV-1/2 antibodies IgM and IgG and antigen p24 in venous blood samples. Positive tests were confirmed twice. Tat concentrations in sera from HIV-positive individuals were determined using both a dot blotting assay and an enzyme-linked immunosorbent assay as described previously [54].

PBMCs were purified by Pancoll (PAN biotech) density gradient centrifugation. B lymphocytes were obtained by negative cell selection using the MagniSort Human B cell Enrichment Kit (Thermo, cat. # 8804-6867-74) according to the manufacturer's protocol. For the RNA-sequencing experiment, primary B cells from four healthy donors were pooled.

Cell culture and cell treatments

Human cervical carcinoma cell line HeLa (American Type Culture Collection), Human Epstein-Barr virus (EBV)-transformed B lymphoblastoid cell line RPMI8866 (ECACC General Cell Collection), freshly EBV-transformed B lymphoblastoid cell line from healthy donor AS (BLAS, established by EBV (B95-8) immortalization of mature B cells and characterized by Genethon (Evry, France)), human immortalized T cell line Jurkat (American Type Culture Collection) and their derivatives were used in the study. RPMI8866 cell line with inducible expression of HIV-1 Tat protein (RPMI8866 Tat^{i} line) was produced as previously described [55] and was a kind gift from Dr. Eugene V. Sheval. Jurkat that stably expresses HIV-1 Tat (Jurkat-Tat) was obtained through the NIH HIV Reagent Program, Division of AIDS, NIAID, NIH, ARP-1399, contributed by Dr. Antonella Caputo, Dr. William Haseltine and Dr. Joseph Sodroski). M81 marmoset lymphoblastoid cell line with a spontaneous EBV lytic activity was a kind gift from Henri-Jacques Delecluse (DKFZ, Heidelberg, Germany). RPMI8866 and Jurkat derivatives with inducible expression of YFP, YFP-Tat, YFP-Zta or YFP1-Tat-P2A-YFP2-Zta were produced through lentiviral transduction as described below. The induction of YFP, YFP-Tat, YFP-Zta or YFP1-Tat-P2A-YFP2-Zta expression in these cell lines or of Tat in RPMI8866 Tat^{i} line was performed with doxycycline (Dox, Sigma, St. Louis, Missouri, USA) in the concentration of 1 µg/ml for 48 hours unless otherwise specified.

Lymphoblastoid B-cell lines RPMI8866, BLAS and their derivatives were cultured in RPMI 1640 medium supplemented with 10% FBS, 2% glucose, 2 mM L-Glutamine, 1 mM Pyruvate and 1× penicillin/streptomycin antibiotics (all from Gibco, Thermo Fisher Scientific, Waltham, Massachusetts, USA). Jurkat T cells were cultured in RPMI 1640 medium supplemented with 10% FBS, 1% D-glucose, 1M HEPES Buffer solution, 100 mM sodium pyruvate, 1x penicillin/streptomycin antibiotics (all from Gibco). Jurkat-Tat were cultured with the addition of 800 µg/ml G418 (Sigma-Aldrich, Burlington, MA, USA). HeLa cells were cultured in DMEM medium supplemented with 10% FBS and 1x

penicillin/streptomycin antibiotics (all from Gibco). Purified B-cells (plated 10^6/ml) were incubated in RPMI 1640 medium supplemented with 10% FBS and 1x penicillin/streptomycin antibiotics. All cells were cultured at 37°C in a humidified 5% CO_2 atmosphere.

For the experiments with ubiquitin-proteasomal pathway inhibition, RPMI8866 cells were transfected with YFP or YFP1-Tat + YFP2-Zta and 40 hours after transfection were treated with the following inhibitors for a total duration of 8 hours: MG-132 (50 μM), PYR-41 (20 μM), Pevonedistat (2 μM), Bay 11-7082 (20 μM), and NSC697923 (2 μM) (all from MedChemExpress, Monmouth Junction, NJ, USA). After the indicated times, cells were collected for total HLA-ABC expression analysis by flow cytometry. For the experiments with antiretroviral drugs and other inhibitors, Jurkat cells with inducible YFP1-Tat-P2A-YFP2-Zta expression were treated with Dox (1 μg/ml) concomitantly with abacavir (ABC, 6 μM), amprenavir (0.4 μM), atazanavir sulfate (5 nM), azidothymidine (AZT, 0.4 μM), emtricitabine (FTC, 0.64 μM), indinavir sulfate (100 nM), lamivudine (3TC, 15 μM), nevirapine (100 nM), rilpivirine (9.2 μM), saquinavir (30 nM), TAK-779 (200 nM), filgotinib (JAK1 inhibitor, 10 μM, AbMole BioScience), wortmannin (PI3K inhibitor, 20 μM, MedChemExpress), JNK inhibitor II (SP600125, 50 μM, Calbiochem), Akt inhibitor XI (20 μM, Calbiochem), and IKK-2 inhibitor V (10 μM, Calbiochem). Antiretroviral drugs were used at the concentrations that correspond to IC_{50} for virus inhibition as described previously [56] and obtained through the NIH HIV Reagent Program, Division of AIDS, NIAID, NIH. YFP fluorescence was analysed 24 hours after treatment by flow cytometry.

Cell counting was performed by mixing 1:1 cell suspension with Trypan blue, transferring to counting slides and analyzing on TC 20™ Automated Cell Counter.

Generation of EBV-specific cytotoxic T cell line

EBV-specific human cytotoxic T cells (CTLs) were derived as previously described [57]. Briefly, PBMCs from healthy donor AS (1×10^6/ml) were cocultured with autologous irradiated (4000 Rad) EBV-transformed BLAS (2.5×10^4/ml) in 24-well plates in RPMI 1640 medium supplemented with 10% human AB serum (Sigma) and 1x penicillin/streptomycin antibiotics. After 9 to 11 days, T cells (1×10^6/ml) were restimulated with irradiated BLAS (2.5×10^5/mL). Recombinant human IL-2 (50 ng/ml; Proteintech, cat. # HZ-1015) was added to the cultures at this time. T-cell lines were subsequently maintained by restimulation with irradiated BLAS every 14 days, with interim half-changes of fresh medium plus IL-2 every 3 to 4 days. After three to four restimulation cycles, T cell lines were typically >90% CD3+ by flow cytometric analysis. Phenotype analysis was performed by flow cytometry with immunofluorescent staining specific for CD3 (APC).

For cytotoxicity assays, the previously described non-radioactive method comparable with the conventional ^{51}Cr release assay was used [58] with modifications. Briefly, sensitive BLAS and control RPMI8866 target cells were labelled with 5- (and 6-)

carboxyfluorescein diacetate succinimidyl ester (CFSE, Biolegend, cat. #423801) as follows: 1×10^6 cells were washed once with PBS and resuspended in 1% FBS/PBS to a concentration 1×10^6 cells/ml. For sensitive targets (BLAS), 1 µl of 5 mM CFSE solution was added to 1 ml of cell suspension; for control targets (RPMI8866), 0.5 µl of 500 µM CFSE solution was added to 1 ml of cell suspension; cells were incubated for 4 min at room temperature under shading. After incubation, 9 ml of 5%FBS/PBS was added to stop the labelling reaction. Then, cells were washed once with 5%FBS/PBS and resuspended with 400 µl of RPMI 1640 medium supplemented with 10% human AB serum (Sigma) and 1× penicillin/streptomycin antibiotics at a final concentration (2.5×10^6 cells/ml). Cytotoxic T cell line effector cells were washed once with PBS and resuspended in RPMI 1640 medium supplemented with 10% human AB serum (Sigma) and 1× penicillin/streptomycin antibiotics to a final concentration of 1×10^6 cells/ml. For sensitive reactions, 5×10^4 BLAS target cells (20 µl) and various numbers of effector cells (0, 1.25×10^5, 2.5×10^5, 5×10^5) were mixed in a 48-well plate at a final volume of 520 µL to yield various effector/target (E/T) ratios (0:1, 2.5:1, 5:1, 10:1). For each sensitive reaction a respective control reaction was also separately prepared: 5×10^4 RPMI8866 target cells (20 µl) and the same number of effector cells were mixed in a 48-well plate at a final volume of 520 µL. The plate was centrifuged at 200g for 1 min and then incubated at 37°C for 4 h. After incubation, wells with sensitive target cells were mixed 1:1 with the respective control target cells with the same E/T ratio in one tube, washed once with PBS and fixed in 4% PFA/PBS for 10 minutes. The % of specific lysis was calculated as follows:

$$\%\ of\ specific\ lysis\ =\ \frac{a-b}{a-ab}\ *\ 100\%,$$

where a - the fraction of sensitive cells among target cells in E/T 0:1 sample, and b - the fraction of sensitive cells among target cells in E/T X:1 sample.

Lentivirus production and lentiviral transduction

HEK 293 T cells were used for lentivirus packaging and production. Cells were seeded in a T-175 flask 24 hours before transfection to achieve 80% confluency on the day of transfection. HEK 293 T cells were transfected with second-generation lentiviral packaging plasmid psPAX2 (Addgene, # 12260), VSV-G envelope expressing plasmid pMD2.G (Addgene, # 12259) and transfer plasmid (FUdeltaGW-rtTA, FUW-tetO-YFP, FUW-tetO-YFP-Tat, FUW-tetO-YFP-Zta, FUW-tetO-YFP1-Tat-P2A-YFP2-Zta) at 15:6:20 ratio using Turbofect transfection reagent (Thermo Fisher Scientific, USA) according to the manufacturer's instructions (20 µg of plasmid DNA and 40 µl of Turbofect transfection reagent were premixed in 2 ml of OptiMEM medium (Gibco) and added to 20 ml of DMEM/10% FBS cell medium in T-175 flask). Cell medium was changed to DMEM/0%FBS 24 hours after transfection and lentiviral supernatant was collected 48 hours after transfection, centrifuged to remove cell debris and filtered through a 0.45-µm filter.

RPMI8868- and Jurkat-derived cell lines that inducibly expressed YFP, YFP-Tat, YFP-Zta, or YFP1-Tat-P2A-YFP2-Zta were produced as follows. 2 × 10^6 cells (plated in six-well plates) diluted in 1 ml of normal medium were transduced with 1 ml of FUdeltaGW-rtTA lentiviral supernatant and 1 ml of lentiviral supernatant with one of the FUW-tetO constructs (FUW-tetO-YFP, FUW-tetO-YFP-Tat, FUW-tetO-YFP-Zta, FUW-tetO-YFP1-Tat-P2A-YFP2-Zta). To confirm YFP expression and establish cell lines, 72 hours after transduction cells were treated with Dox for 24 hours and YFP^+ cells were then sorted using ARIA Fusion-UV cell sorter (BD Biosciences). Cells were then maintained in the normal cell medium.

Cell transfection

HeLa cells were transfected with the use of Viafect transfection reagent (Promega) or Turbofect transfection reagent (Thermo Fisher Scientific, USA) following the manufacturer's instructions. RPMI8866 and Jurkat cells were electrotransfected by the protocol established in our laboratory previously [59]. Briefly, to electrotrasfect RPMI8866, we used the Cliniporator (Igea) with 4-mm electroporation cuvettes (Cell Projects); 8×10^6 cells were diluted in 400 µl of S-MEM medium, containing 50 µg of plasmid and 50% of water, and electrotransfected at 1300 V/cm, with eight 100 µs pulses at 1 Hz. Jurkat cells (4×10^6) were diluted in 100 µl of S-MEM medium, containing 50 µg of plasmid and 10% of water, and electrotransfected at 1300 V/cm, with twelve 100 µs pulses at 1 Hz in 1-mm electroporation cuvettes.

Flow cytometry analysis

YFP fluorescence was analysed using a fluorescence-activated cell sorter (FACS) BD Accuri C6 Plus Flow Cytometer (BD Biosciences, USA) or Cytofex (Beckman Coulter). YFP-positive cells were sorted using BD FACSAria Fusion-UV Cell Sorter (BD Biosciences, USA). The cell cycle was studied using propidium iodide (10 µg/ml) staining preceded by RNA digestion with RNAse A (100 µg/ml). For antibody staining of surface molecules, 0.3×10^6/test cells were harvested, washed with PBS and resuspended in 1% BSA/PBS. For intracellular staining, 0.8×10^6/test cells were harvested, washed with PBS and fixed and permeabilized using Cyto-Fast™ Fix/Perm Buffer Set (Biolegend, cat. # 426803) according to the manufacturer's instructions. For B cells (including BLAS and RPMI8866) Fc receptor binding was blocked by Fc block (Miltenyi Biotec Inc., cat. # 130-059-901) according to the manufacturer's instructions. Cells were then incubated on ice with fluorescently labelled antibodies for 30 minutes followed by 3 washings with PBS. Fluorescence was acquired using BD Accuri C6 Plus Flow Cytometer (BD Biosciences, USA) or Cytofex (Beckman Coulter) and the data were analyzed using FlowJo software (version 10.4), the same gating was applied to all samples within one experiment. If several fluorescent channels were analysed, the compensation was performed with single-stained controls.

Immunofluorescent staining, microscopy and image analysis

Adherent cells were directly cultured on coverslips, suspension cells were attached to coverslips covered with poly-D-lysine (Merck Millipore, cat. # A-003-E, 50 µg/ml). Cells were washed with PBS, fixed in 4% paraformaldehyde (Electron Microscopy Sciences, cat. # 15710). Cells were permeabilized with 2% Triton X-100 in case of intracellular staining. When analyzing HLA-ABC expression, cells were stained with anti-HLA-ABC (1:100) antibodies, followed by staining with secondary antibodies AF647 Goat anti-mouse IgG H+L (1:200) with or without permeabilization for total and surface staining, respectively. Nuclei were counterstained with Hoechst 33342 dye (Invitrogen, cat. # H3570). Coverslips were mounted on slides with Fluoroshield mounting medium with DAPI (Abcam, cat. # ab104139). All antibodies were diluted in 1% BSA in 1X PBS.

Live and fixed fluorescent images were acquired using an inverted phase contrast fluorescence microscope (Axio Observer Z1, Zeiss) and ZEN 2010 software or Leica TCS SP8 Multiphoton Confocal Microscope (Leica Microsystems). All images within the experiment were captured with the same laser intensity, gain and exposure settings.

To analyze surface HLA-ABC expression, confocal images were processed using a semi-automatic macro in Fiji that detected cellular regions of interest (ROIs) in the YFP channel and enlarged them by 3 units to create outside ROIs that encompassed HLA-ABC staining. The mean fluorescence intensity of HLA-ABC (HLA-ABC expression) in the outside ROIs was analysed for each image. The macro is available on request. At least five fields were analyzed per biological replicate and images from at least two independent experiments were analyzed.

Cell lysate preparation, SDS-PAGE and western blotting

Cells were harvested from culture dishes and collected by centrifugation for 10 min at 800g. Cell pellets were resuspended in NETN buffer (NaCl 150 mM, ethylenediaminetetraacetic acid (EDTA) 1 mM, Tris pH 7.5 50 mmol/L, NP40 0.5%, 1× protease inhibitor cocktail; Roche, Basel, Switzerland), sonicated for 10 seconds at 30% using a Vibra Cell sonicator (SONICS & MATERIALS, Inc., Newtown, CT, USA), incubated on ice for 30 minutes and centrifuged at 4°C at 12000g for 10 minutes. The supernatant was transferred into a new pre-cooled microcentrifuge tube and the cell pellet was discarded. When preparing cytoplasmic and nuclear extracts, cells and nuclei were lysed using NE-PER Nuclear and Cytoplasmic Extraction Reagents (ThermoFisher) according to the manufacturer's instructions. The lysates (whole cell, cytoplasmic or nuclear) (5 µl) were used for quantification of protein concentration by BCA assay (Thermo Fisher Scientific). Protein quantification was performed using the Pierce™ BCA Protein Assay Kit (Thermo Scientific) on the NanoDrop 2000C (Thermo Scientific). After measuring the concentration, cell lysates used for Western blotting were supplemented with 6× Laemmli buffer (LDS) and 0.1M DTT, then heated at 95°C for 10 min.

Cell lysates (20 µg) and prestained molecular weight markers (PageRuler™ Prestained Plus Protein Ladder, Thermo Scientific) were resolved on 12- or 15- well precast SDS-PAGE gels (4-12 %) (NuPage) in MOPS Running Buffer (NuPage). Proteins were

transferred onto 0.45 μm PVDF membrane (GE Healthcare, USA) in transfer buffer (0.025M Tris, 0.192M Glycine, 20% ethanol) at 90V at +4°C for 2h. Nonspecific binding was blocked in 5% non-fat dried milk in Tris-buffered saline, 0.1% Tween-20 (TBST) at room temperature for 1h.

Proteins were probed at +4°C overnight with the following primary antibodies: anti-Tat (1:200), anti-Zta (1:1000), anti-p53 (1:200), anti-Galectin-9 (1:1000), anti-GFP (1:1000), anti-transthyretin (1:1000), anti-transferrin (1:1000), anti-HLA-ABC (1:500), anti-GAPDH (1:1000, control of protein load), anti-vinculin (1:1000, control of protein load), anti-β-actin (1:1000, control of protein load). Membranes were washed with TBST, and incubated with appropriate peroxidase-conjugated secondary antibodies in 1:1000 dilution at room temperature for 1.5 h, followed by washing in TBST. Proteins were visualized using Immobilon Western Chemiluminescent HRP Substrate (Millipore) and ImageQuant LAS 4000 mini (GE Healthcare) for western blotting imaging and analysis. Densitometric analysis of blots at non-saturating exposures was performed using ImageJ.

Immunoprecipitation (IP) and co-immunoprecipitation (Co-IP)

IP and Co-IP were performed using magnetic beads: Dynabeads™ His-Tag (Novotex) or Dynabeads™ Protein G (Invitrogen), coupled with 10 μg of appropriate antibody, following manufacturer's instructions. Due to high immunoglobulin presence, for co-immunoprecipitation in blood plasma specific antibody was cross-linked to magnetic beads with the use of BS_3 crosslinking regent (Abcam, cat. # ab145612), following the manufacturer's instructions. Proteins were eluted from magnetic beads in NETN buffer supplemented with LDS and 0.1M DTT by shaking at 95°C for 10 min.

In vitro binding assay

In vitro binding assay was applied to study the direct interaction between purified Tat and Zta proteins. The procedure was performed according to the protocol described by [60]. In brief, Tat (the "bait" protein) was immobilized on AminoLink Coupling resin agarose beads (Thermo Scientific, cat. # 20381) and was covalently linked to agarose beads by reducing agent sodium cyanoborohydride. Tat-linked beads were blocked with BSA to prevent non-specific binding, while empty agarose beads blocked with BSA were used as BSA control beads. Zta (the "prey" protein) was kept in solution and incubated with agarose beads to allow binding. The concentration of the bait protein Tat was kept constant (3.1 μg/mL), while the concentration of the prey protein Zta was increased. After incubation, the beads were precipitated to separate unbound prey protein in solution from prey protein bound to the bait. The fraction of bound prey protein was analysed by Western Blot.

ELISA of Zta in serum samples

Zta concentration in serum samples was determined as described previously [32]. Briefly, the 96-well plates were coated with AZ69 capture antibodies overnight at +4°C, blocked in 10% FBS, 4% Gelofusin PBST for 1 hour at room temperature. Reference dilutions of

recombinant ZEBRA-FC CHO protein (standards) and serum samples were loaded onto the plate, incubated with PBST for 2 hours at room temperature. Next, the samples were incubated with a biotinylated AZ130 detection antibody for 1 hour at room temperature, followed by incubation with HRP-conjugated streptavidin for 30 minutes at room temperature and TMB for 10 minutes for revealing. The reaction was stopped by the addition of 0.1 M H_2SO_4 and 1 M Tris. The absorbance was measured at 450 nm by Plate reader Infinite 200 PRO (Tecan Life Sciences). The resulting Zta concentration was extrapolated from the standard curve based on Zta reference dilution. All samples were analysed in duplicates, the mean result is presented. All materials for ELISA of Zta were kindly provided by Dr. Emmanuel Drouet, Université Grenoble Alpes.

Plasmid cloning, synthesis, extraction

Plasmids pcDNA3-YFP1 and pcDNA3-YFP2 that encode for split-YFP fragments (YFP1 – residues 1-158; YFP2 – residues 159-239, GenBank: ABV26713.1), as well as plasmids pcDNA3-YFP1-ERGIC-53, pcDNA3-YFP2-ERGIC-53, pcDNA3-YFP1-MCFD2 and pcDNA3-YFP2-MCFD2 were a generous gift from the authors [61]. pcDNA3-CFP, FUW-tetO-hOKMS, FUdeltaGW-rtTA, mCherry2-C1 plasmids were purchased from Addgene (cat. #109330, 51543, 19780, 54563). pEYFP-C3 plasmid was a generous gift from Francesco Baschieri. pTagBFP-C was purchased from Evrogen, Russia (cat.# FP171). HIV-1 Tat sequence (GenBank: AAB59870.1, 86 residues) was synthesized by Eurofins Genomics, Germany, in pEXA128 plasmid (pEXA128-Tat). pcDNA3.1+/Tat101-flag(PEV280) plasmid was obtained through the NIH HIV Reagent Program, Division of AIDS, NIAID, NIH, ARP-10453, contributed by Dr. Eric Verdin. EBV (strain B95-8) Zta sequence (Sequence ID: P03206.2) was synthesized by VectorBuilder, USA, in pcDNA3(+)-YFP2 plasmid (pcDNA3(+)-YFP2-Zta). pET29a(+)-Zta was previously cloned in our laboratory by inserting the Zta sequence in pET29(+) plasmid between SalI and NdeI restriction sites. The resulting sequence encoded for a His-tagged Zta. An LTR-TurboRFP plasmid that contained the HIV-1 3' LTR fragment upstream to the promoter-less red fluorescent protein TurboRFP gene cloned in pTurboRFP-PRL plasmid (Evrogen, Moscow, Russia) was described previously [62] and was a kind gift from Dr. Eugene V. Sheval. Primers used for cloning were purchased from Eurofins Genomics, Germany (**Supplementary table 1**).

For all cloning reactions the target plasmid was first digested by one or multiple restriction enzymes, then its linearized form was isolated from agarose gel and dephosphorylated with shrimp alkaline phosphatase (SAP) (Fermentas, # EF0511). Tat short sequence (86 residues) was generated by XhoI digestion of pEXA128-Tat plasmid and was ligated in pcDNA3-YFP1 and pcDNA3-YFP2 plasmids at the XhoI site. Tat long sequence (101 residues, Tat101) was generated by PCR of pcDNA3.1+/Tat101-flag(PEV280) plasmid with primers that encode for the SalI restriction site. Of note, SalI and XhoI have compatible ends. After SalI digestion, Tat101 was inserted in pcDNA3-YFP1 plasmid at the XhoI site. To clone the Tat-CFP plasmid, the Tat sequence was amplified by PCR of pEXA128-Tat plasmid with the forward primer that encodes for the XhoI restriction site and the reverse primer that excludes stop-codon and encodes for the EcoRI restriction site.

To create a flexible $(GGGS)_2$ linker between Tat and CFP, nearly complementary oligonucleotides were purchased from Eurofins Genomics (Germany). Oligonucleotides were annealed, creating EcoRI and XhoI compatible sticky ends at 5' and 3' ends of forward oligonucleotide, respectively. Tat sequence, amplified without stop codon was digested by EcoRI and ligated with annealed oligonucleotides, then the ligation product was digested by XhoI and inserted in pcDNA3-CFP plasmid at XhoI site. To clone the YFP-Tat plasmid, the linker-Tat sequence was amplified by PCR of the YFP1-Tat plasmid with primers that encode for SalI restriction site and after SalI digestion was inserted in the pEYFPC3 plasmid at XhoI site. To clone the BFP-Tat plasmid, the Tat sequence was amplified by PCR of YFP1-Tat plasmid with primers that encode for XhoI restriction site and after XhoI digestion was inserted in pTagBFP-C plasmid at XhoI site.

Zta sequence generated by XhoI digestion of pcDNA3(+)-YFP2-Zta plasmid and was ligated in pcDNA3-YFP1 plasmid by XhoI site. To clone the Zta-CFP plasmid, the Zta sequence was amplified by PCR of the pcDNA3(+)-YFP2-Zta plasmid with forward primer that encodes for XhoI restriction site and reverse primer that excludes stop-codon and encodes for EcoRI restriction site. To create a flexible $(GGGS)_2$ linker between Zta and CFP, nearly complementary oligonucleotides were purchased from Eurofins Genomics. Oligonucleotides were annealed, creating EcoRI and XhoI compatible sticky ends at 5' and 3' ends of forward oligonucleotide, respectively. Zta sequence, amplified without stop codon was digested by EcoRI and ligated with annealed oligonucleotides, then the ligation product was digested by XhoI and inserted in pcDNA3-CFP plasmid at XhoI site. To clone the YFP-Zta plasmid, the linker-Zta sequence was amplified by PCR of YFP2-Zta plasmid with primers that encode for SalI restriction site and after SalI digestion was inserted in the pEYFPC3 plasmid at XhoI site. To clone the BFP-Zta plasmid, the Zta sequence was amplified by PCR of YFP2-Zta plasmid with primers that encode for XhoI restriction site and after XhoI digestion was inserted in pTagBFP-C plasmid at XhoI site. To clone the mCherry-Zta plasmid, the linker-Zta sequence was amplified by PCR of YFP2-Zta plasmid with primers that encode for SalI restriction site and after SalI digestion was inserted in the mCherry2-C1 plasmid at SalI site.

All obtained plasmid sequences were confirmed by PCR, restriction analysis and Sanger sequencing. The expression of Tat and Zta from the cloned plasmids was verified by Western blotting and immunofluorescent staining.

Tat and Zta sequences lacking key domains (**Supplementary figure 3**) were generated by PCR from YFP1-Tat and YFP2-Zta plasmids, respectively, with primers that encode for SalI restriction sites and BamHI restriction sites (in case of internal deletion) and after SalI digestion (or after BamHI digestion, fragment ligation followed by XhoI digestion) were inserted in pcDNA3-YFP1 and pcDNA3-YFP2 plasmids, digested by XhoI and dephosphorylated. Obtained plasmid sequences were confirmed by PCR, restriction analysis and Sanger sequencing.

To generate cells with inducible expression of fluorescent protein-fusion constructs (YFP, YFP-Tat, YFP-Zta, YFP1-Tat-P2A-YFP2-Zta), FuW-tetO-YFP, FuW-tetO-YFP-Tat,

FuW-tetO-YFP-Zta or FuW-tetO-YFP1-Tat-P2A-YFP2 plasmids were cloned. Initially, the FUW-tetO-hOKMS plasmid was digested with EcoRI to remove hOKMS, and a multiple cloning site (MCS) was inserted. For FUW-tetO-YFP1-Tat-P2A-YFP2-Zta, YFP1-Tat was amplified by PCR of pcDNA3-YFP1-Tat plasmid with a forward primer that encodes for AgeI restriction site and a reverse primer that encodes for SphI restriction site. To create a P2A linker between YFP1-Tat and YFP2-Zta, nearly complementary oligonucleotides were purchased from Eurofins Genomics. Oligonucleotides were annealed, creating SphI and BglII compatible sticky ends at 5' and 3' ends of forward oligonucleotide, respectively. YFP2-Zta was amplified by PCR of pcDNA3-YFP2-Zta plasmid with a forward primer that encodes for the BglII restriction site and a reverse primer that encodes for the BamHI restriction site. FUW-tetO-MCS was digested by AgeI and BamHI, and YFP1-Tat, P2A, and YFP2-Zta fragments were ligated. For FUW-tetO-YFP, FUW-tetO-YFP-Tat, and FUW-tetO-YFP-Zta, YFP, YFP-Tat, and YFP-Zta fragments obtained from the digestion of pEYFPC3, pEYFPC3-Tat, pEYFPC3-Zta plasmids with AgeI and BamHI were ligated into FUW-tetO-MCS plasmid digested with AgeI and BamHI. These cloning steps yielded plasmids for inducible protein expression, facilitating the investigation of protein interactions and functions in cells under controlled conditions. Obtained plasmid sequences were confirmed by PCR and Sanger sequencing.

Plasmids were transformed into *E. coli* Stellar™ competent cells (Takara Bio) by heat shock (42°C, 90 sec) and grown in LB medium. Plasmids were extracted with NucleoSpin Plasmid Mini, Midi and Maxi kits (Macherey-Nagel, Germany). DNA fragments from agarose gel were extracted with a NucleoSpin Gel extraction kit (Macherey-Nagel, Germany).

PCR

PCR was carried out using Powerup SYBR Green Mastermix (ThermoFisher), primers used for PCR are listed in **Supplementary table 1** and were purchased from Eurofins Genomics, Germany. The thermal cycling program was as follows: a 2-minute denaturation set at 50°C, a 2-minute denaturing step at 95°C followed by 40 amplification cycles consisting of 15 seconds denaturing at 95°C, 1 minute of annealing at 60°C and 1 minute of elongation at 72°C, followed by a final step 10-minute elongation at 72°C.

RNA extraction, sequencing, RNA-seq data processing and analysis

Purified B cells or BLAS cells were treated with Tat (250 ng/ml ~ 25 μM), Zta (1000 ng/ml ~ 37 μM) or Tat and Zta (at 250 ng/ml and 1000 ng/ml, respectively) or left untreated. The concentrations were chosen based on previous reports on the range of serum concentrations of Tat [31] and Zta [32]. 6 h and 48h later cells were collected and RNA was extracted using a NucleoSpin RNA isolation kit (Macherey-Nagel, Germany) following manufacturer's instructions. Each condition was performed and analyzed in quadruplicates. Total RNA from BLAS cell lines was also isolated using the NucleoSpin RNA kit following the manufacturer's instructions. Each condition was performed and analyzed in triplicates. The quantity and quality of total RNA were measured using

NanoDrop2000C Spectrophotometer (Thermo Fisher Scientific). The cDNA libraries were constructed and sequenced in Novogene, China. The raw sequencing reads were mapped to the human genome (assembly GRCh38.p10) using HISAT2 (version 2.0.5). Read counting was performed using featureCounts (ver 2.0.1) in a strand-specific mode. GENCODE v26 gene annotation (ALL) was used. Features with a low total count number (< N counts across all samples, where N is the number of replicates in each condition) were discarded. Differential expression analysis was performed using the DESeq2 R package (version 1.30.1). The genes meeting the criteria *p*-value adjusted (p_{adjusted}) by the Benjamini-Hochberg procedure < 0.05 were considered differentially expressed. No filter was applied to fold changes in gene expression, i. e. all statistically significant deregulated genes were taken into analysis, since unlike "classical" experiments when a transgene is ectopically expressed in all cells, we used more "physiological" experimental setup and it is probable that 100%-efficient cell penetration with viral proteins was not achieved.

Overrepresentation analysis (ORA) was performed with an R package clusterProfiler (version 4.4.4) [63] on a list of genes that overlapped between the following comparisons: Tat vs control and Zta vs control, excluding the genes deregulated by Tat + Zta vs control. Benjamini-Hochberg p.adjust cutoff of 0.05 and q-value cutoff of 0.05 were used to select statistically significant categories. KEGG databases were used for annotation.

RNA extraction, reverse transcription and qPCR

Total RNA was isolated using the NucleoSpin RNA kit (Macherey-Nagel, Düren, Germany) following the manufacturer's instructions. The quantity and quality of total RNA were measured using NanoDrop2000C Spectrophotometer (Thermo Fisher Scientific). 1.0 µg of total RNA was reverse-transcribed using Maxima™ H Minus cDNA Synthesis Master Mix (Thermo Scientific, USA). Quantitative PCR was carried out using Powerup SYBR Green Mastermix (ThermoFisher) on a StepOnePlus Real-Time PCR System machine (Applied Biosystems). The human cDNA primers (**Supplementary table 2**) were obtained from Eurofins Genomics, Germany. The thermal cycling program was as follows: a 2-minute denaturation step at 50°C, a 2-minute denaturation step at 95°C followed by 40 amplification cycles consisting of 15 seconds of denaturation at 95°C, 1 minute of annealing at 60°C and 1 minute of elongation at 72°C, followed by a final step 10-minute elongation at 72°C. qPCRs for each sample were performed in triplicates (technical replicates). A relative transcript level was calculated using the Pfaffl method [64] with the geometric averaging of the relative quantities of the *RPL32* and *GAPDH* reference genes as described previously [65,66]; normalization was done assuming as 1 the mean level of each transcript in the control group. The analysis of primer efficiency was performed by plotting the cycle threshold value (Ct) against the serial 1:10 dilution of the cDNA sample using the equation $E = 10^{-\frac{1}{\text{the slope value}}}$.

Statistical analysis

Data were analyzed using GraphPad Prism 9 software (GraphPad Software Inc.). The unit of analysis was a single biological replicate. Student's unpaired t-tests were used to

compare cell sizes between two groups. One-way analysis of variance (ANOVA), followed by Tukey's posthoc test, was used to determine differences between more than two groups that involved one factor. Two-way ANOVA, followed by Tukey's posthoc test, was used to determine differences between two or more groups that involved two factors. Data are presented as a mean ± standard error of the mean (SEM). The level of significance was set at $p < 0.05$.

Results and discussion

HIV-1 Tat and EBV Zta physically interact with each other

Since HIV-1 Tat and EBV Zta transcriptional activators can be secreted by infected T and B cells, respectively, we hypothesized that two proteins can be simultaneously found in B cells, T cells or blood plasma. To investigate our hypothesis about their physical interaction, we performed co-immunoprecipitation in B cell line (RPMI8866 lymphoblastoid cell line), T cell line (Jurkat) and blood plasma.

We used the modified RPMI8866 lymphoblastoid cell line inducibly expressing unconjugated HIV-1 Tat (RPMI8866 Tat^{i} cell line) previously produced in the laboratory [67]. Cells were treated for 24h with 1 µg/ml recombinant Zta protein and doxycycline (Dox) to induce Tat expression or left untreated. Cell lysates were immunoprecipitated for Tat using anti-Tat antibodies. We found that Zta was present in the Tat-immunoprecipitated fraction of RPMI8866 Tat^{i} + Dox + Zta cell lysates (**Figure 1A**). Galectin-9, normally expressed in various cell types, including those of B and T cell origin [68,69], was used as a negative control for the specificity of immunoprecipitation and was absent in all immunoprecipitated fractions. To analyse whether this phenomenon is observed in other cell types, we next studied the interaction of Tat and Zta in the T cell line Jurkat that expressed unconjugated Tat protein (Jurkat-Tat), the wild-type Jurkat cell line was used as a control. Cells were treated or not with 1 µg/ml recombinant Zta protein for 24h. Cell lysates were immunoprecipitated for Tat using anti-Tat antibodies and Zta was present in the Tat-immunoprecipitated fraction of Jurkat-Tat + Zta cell lysates (**Figure 1B**), corroborating the results observed in B cells. Galectin-9, a negative control, was absent in all immunoprecipitated fractions. To confirm the obtained results, a reverse co-immunoprecipitation was performed. This time, RPMI8866 wild-type cells were transfected with Tat (YFP-Tat) and/or Zta (mCherry-Zta) and 24 hours after transfection cell lysates were immunoprecipitated for Zta using anti-Zta antibodies. As expected, Tat (~40 kDa) was present in the Zta-immunoprecipitated fraction of RPMI8866 YFP-Tat + mCherry-Zta cell lysates (**Figure 1C**). Galectin-9 was not present in the immunoprecipitated fraction. Thus, we demonstrated for the first time the interaction between Tat and Zta in B and T cells and confirmed that the interaction was not perturbed by the conjugation of Tat and Zta to fluorescent proteins.

We then proceeded with the analysis of Tat and Zta interaction in human serum. To imitate the condition of HIV and EBV combined infection when both transcriptional activators can be secreted in blood, we added recombinant Tat and Zta proteins (at concentrations of

250 ng/ml and 1000 ng/ml, respectively) in healthy donor serum. After 2h incubation at room temperature, to let proteins bind with their interaction partners, a co-immunoprecipitation for Zta using anti-Zta antibodies was performed (**Supplementary figure 1A**). As expected, Zta was present in immunoprecipitated plasma fraction but was absent in non-immunoprecipitated serum flowthrough (FT). In accordance with previous results, Tat was also present only in the Zta-immunoprecipitated fraction of serum. A serum protein transthyretin of similar size as Tat (~15 kDa) was used as a negative control for the specificity of immunoprecipitation and was only present in non-immunoprecipitated serum fraction. A reverse coIP in serum with the use of different anti-Tat antibodies (1D9, 15.1, NT3) confirmed the obtained results (**Supplementary figure 1B**). We next questioned whether this interaction occurs in people living with HIV infected with EBV. We analyzed a serum sample from an HIV-positive individual, wherein EBV Zta presence was confirmed by ELISA (data not shown). A healthy donor serum (HIV-negative) with recombinant Tat and Zta proteins (at 250 ng/ml and 1000 ng/ml, respectively) added was used as a control. Both samples were incubated for 2h at room temperature to let proteins restore their protein-protein interactions, followed by immunoprecipitation with anti-Zta and anti-Tat antibodies (**Figure 1D**). Zta and Tat were present in respective immunoprecipitated fractions for Zta/Tat both in control and in an HIV-patient sample, indicating that immunoprecipitation of respective proteins was functional and, importantly, that serum from an HIV-positive patient contained both Tat and Zta proteins that interacted with each other. In agreement with previous results, Tat was present in the Zta-immunoprecipitated fraction of control and patient serum samples. A reverse coIP for Tat confirmed our observation: Zta was present in the Tat-immunoprecipitated fraction of control and patient serum. Serum proteins transthyretin (~15 kDa) and transferrin (~80 kDa, which is close to the mass of dimeric Zta) were used as a negative control for the specificity of immunoprecipitation and were only present in non-immunoprecipitated plasma fraction (FT). Of note, a longer form of Tat (presumably, 101 residues) can be observed in the HIV-positive sample. Thus, we confirmed the possibility of Tat and Zta interaction in people with HIV.

We next questioned whether this interaction was direct and not facilitated by other proteins. We examined the direct interaction between purified Tat and Zta proteins using an *in vitro* binding assay [60]. Equal amounts of purified Tat linked to AminoLink agarose beads or BSA control beads were incubated with increasing amounts of purified Zta. Bound proteins were analysed by SDS-PAGE and western blotting for Zta. We observed that incubation of beads with an increasing concentration of Zta in solution led to increased Zta binding to Tat-linked beads, but not to control BSA beads, where only a background binding was observed (**Figure 1E**). Thus, we can conclude that Zta binds directly and specifically to Tat and this binding does not require additional proteins. The dissociation constant (K_d) of the Tat-Zta complex was predicted to be 0.0642 ± 0.0224 μM (95% confidence interval 0.02938 to 0.1163 μM) (**Figure 1F**).

Having established the interaction between Tat and Zta in both *in vitro* and *ex vivo*, we aimed to elucidate the subcellular localization of this interaction. To achieve this, we

employed the yellow fluorescent protein (YFP) reconstitution technique, also known as bimolecular fluorescence complementation. This method explores protein-protein interactions by inducing fluorescence reconstitution upon the coexpression of N- and C-terminal fragments (YFP1 and YFP2, respectively) of the YFP, fused to the target proteins of interest [70]. We cloned Tat and Zta into pcDNA3-YFP1 and pcDNA3-YFP2 plasmids, respectively. These plasmids were encoded YFP split fragments, joined with proteins of interest by a short peptide linker (GGGS)2, promoting the requisite structural flexibility for the interaction (**Figure 1G**). HeLa, RPMI8866 and Jurkat cells were transfected with YFP1-Tat and YFP2-Zta plasmids and analysed by flow cytometry and microscopy. Co-transfection with YFP1-ERGIC-53 and YFP2-MCFD2 was used as a positive control since ERGIC-53 and MCFD2 were previously shown to interact [61]. In accordance with co-immunoprecipitation and *in vitro* binding assay data, we observed a reconstituted YFP fluorescence when YFP1-Tat and YFP2-Zta were coexpressed in HeLa, LCL RPMI 8866 and Jurkat cells (**Figure 1G, 1H**). Compared to HeLa cells, the percentage of YFP-positive cells was lower in RPMI8866 and Jurkat cells as they are notoriously harder to transfect [59]. The signal of YFP reconstituted fluorescence from Tat and Zta interaction was predominantly located in the cell nucleus, while nucleoli were depleted in the Tat-Zta signal (**Figure 1G, Supplementary figure 2A**). The co-transfection of YFP1-Tat or YFP2-Zta with YFP2-MCFD2 or YFP1-ERGIC-53 or YFP1-MCFD2 (negative controls [70]) in HeLa cells didn't result in a reconstituted YFP fluorescence, confirming the specificity of interaction (**Figure 1G, Supplementary figure 2B**), while YFP1-Zta and YFP2-Zta co-transfection in RPMI 8866 resulted in YFP-positive cells (**Supplementary figure 2C**), which indicates that Zta expression from these plasmids produced native Zta structure that forms homodimers [28]. We also used the YFP-reconstitution technique to verify that the long form of Tat, Tat101, which is more often present in HIV-positive individuals [71], can also interact with Zta. We cloned Tat101 in pcDNA3-YFP1 plasmid and transfected HeLa and RPMI8866 cells with YFP1-Tat + YFP2-Zta or YFP1-Tat101 + YFP2-Zta plasmid combinations. As expected, YFP reconstitution was observed in both cases in HeLa and RPMI8866 cells (**Supplementary figure 2D, 2E**). As in the case of YFP1-Tat + YFP2-Zta pannuclear pattern of fluorescence, omitting nucleolus, was observed (**Supplementary figure 2F**). Thus, both short (86 residues) and long (101 residues) forms of Tat can interact with Zta and the interaction takes place in the nucleus.

Since the YFP reconstitution technique allows for easy detection of cells, where Tat and Zta interact, it can be used to identify the domains of Tat and Zta interaction. We created a set of plasmids that encode for YFP1-Tat and YFP2-Zta, where Tat and Zta lack key domains (activation domain (AD), basic and glutamine-rich domain (BD-GRD) and exon 2 domain (Ex2) for Tat and transactivation domain (TAD), basic leucine zipper domain (bZIP), C-terminal domain (CT) for Zta) (**Supplementary figure 3A, 3B**). The different sets of 2 plasmids YFP1-Tat WT + YFP2-Zta mutated or YFP1-Tat mutated + YFP2-WT were transfected into HeLa and RPMI8866 cells. The percentage of YFP-positive cells was analyzed for each combination and was normalized to the percentage of YFP-positive cells in YFP1-Tat WT + YFP2-Zta WT control within each experiment. We observed a

significant decrease in YFP interaction with YFP1-Tat + YFP2-ZtaΔCT and YFP1-TatΔEx2+ YFP2-Zta both in HeLa and RPMI8866 cells, which demonstrated that the exon 2 of Tat and the C-terminal tail of Zta participate in Tat-Zta interaction (**Supplementary figure 3C-3F**).

The YFP reconstitution technique was also employed to investigate whether antiretroviral drugs might affect the interaction between Tat and Zta proteins (**Supplementary figure 4**). None of the tested antiretroviral drugs (ABC, amprenavir, atazanavir, AZT, FTC, 3TC, indinavir, nevirapine, rilpivirine, saquinavir, TAK-779) inhibited the interaction between Tat and Zta, as evidenced by the lack of a decrease in YFP fluorescence (**Supplementary figure 4**). Remarkably, the JAK1 inhibitor filgotinib significantly enhanced and stabilized the Tat-Zta interaction, as evidenced by increased YFP fluorescence (4.314 ± 0.24 in filgotinib-treated cells vs 1.000 ± 0.038 in control cells, $p < 0.0001$, ANOVA, Tukey's posthoc test, **Supplementary figure 4C**).

Finally, to substantiate our data on Tat and Zta interaction, we utilized the FRET approach. We cloned plasmids that encode Tat-CFP, Zta-CFP, YFP-Tat and YFP-Zta and transfected them in HeLa and RPMI 8866 cells. To detect FRET, we used the acceptor photobleaching technique (**Figure 1I**), which correlates the increase in donor fluorescence intensity after acceptor photobleaching with FRET efficiency [72]. FRET efficiencies were substantially higher in cells, transfected with Tat-CFP and YFP-Zta or Zta-CFP and YFP-Tat relative to negative controls (Tat-CFP+YFP, Zta-CFP+YFP, CFP+YFP-Tat or CFP+YFP-Zta) (**Figure 1J, 1K**), which confirms our previously described observations on Tat and Zta direct interaction.

To summarise, we described for the first time a direct interaction between HIV-1 Tat and EBV Zta, transcriptional activator proteins from different viruses, in B cells, T cells and blood serum.

The effect of Tat and Zta on B cells contrasts with the individual effect of each protein

After confirming the direct interaction of Tat and Zta through various methodologies and localizing this interaction predominantly within the cell nucleus, our investigation delved into the functional implications of the inter-viral protein-protein interaction. Given the shared associations of both HIV and EBV with B cell lymphomas, coupled with the potential for both proteins to be present in B cells, our focus turned to exploring their combined effect on B cells.

Firstly, primary B cells from healthy donors were isolated and subjected to treatments with recombinant Tat (250 ng/ml), recombinant Zta (1000 ng/ml), or a combination of both proteins (250 ng/ml Tat and 1000 ng/ml Zta) by their addition to cell medium. No differences in B cell cycling were observed upon Tat and/or Zta treatment of primary B cells (**Supplementary figure 5**). To identify alterations in gene expression profiles, RNA-sequencing analyses were conducted 6 and 48 hours after treatment with viral proteins. Differentially expressed genes (DEGs) were defined as genes with $p_{adjusted} < 0.05$

as compared to untreated B cells. The number of all differentially expressed genes and genes with |log2 fold change| > 0.4 are presented in **Figure 2A, 2B**. The RNA-sequencing analysis unveiled significant shifts in gene expression patterns in response to Tat and Zta treatments after 6 hours: Tat treatment upregulated 105 and downregulated 99 genes, while Zta treatment upregulated 644 and downregulated 580 genes, which included 116 genes commonly deregulated by both Tat and Zta, all in the same direction (upregulation or downregulation), highlighting a consistent regulatory influence on B cells shared by these viral proteins (**Figure 2C**). Most of these genes were protein-coding genes, although differentially expressed lncRNAs were also identified (**Supplementary figure 6A-6D**). For genes with |log2 Fold Change| > 0.4, comparable trends were seen. It is noteworthy that, although significant, the observed fold changes in gene expression were relatively modest, potentially influenced by the incomplete transport of viral proteins into B cells and their nuclei. The action Tat and Zta combined treatment drastically differed from the action of individual proteins, together they upregulated only 60 and downregulated only 72 genes (**Figure 2A, 2B**). A similar pattern was observed at 48 hours: Tat treatment upregulated 103 genes and downregulated 116, Zta treatment upregulated 39 and downregulated 30, while Tat and Zta combined treatment upregulated 15 and downregulated 16 genes. Given the notably higher number of DEGs at 6 hours, we proceeded with the analysis of the effects of the viral proteins at the 6-hour time point. A significant proportion of genes that were individually regulated by Tat and Zta ceased to be differentially expressed when both Tat and Zta were administered in combination (**Figure 2C**), indicating a potential interactive influence between these viral proteins. Interestingly, despite this apparent mutual inhibition upon Tat and Zta interaction, no decrease in LTR-driven transcription was observed upon Tat and Zta combination (**Supplementary figure 7A-7F**) as measured using HIV-1 3′-LTR-TurboRFP reporter plasmid as described previously [62]. The presence of Tat also didn't perturb Zta functioning as the key regulator of EBV reactivation (**Supplementary figure 7G-7H**).

To get insights into the regulatory impact of their interaction, a functional annotation of genes commonly deregulated by Tat and Zta individually, but no longer affected when both proteins were combined, was performed. We implemented overrepresentation analysis (ORA) and searched for activated and suppressed functional categories associated with these genes and defined by the Kyoto Encyclopedia of Genes and Genomes (KEGG [73]) database. The activated functional categories included lipid and atherosclerosis pathways, measles, legionellosis, longevity-regulating mechanisms, antigen processing and presentation, spliceosome activity, and endocytosis (**Figure 2D**). Conversely, the repressed functional categories included pathways related to cell signalling, such as JAK-STAT signalling, cytokine-cytokine receptor interactions, Th17 cell differentiation, inflammatory bowel disease, influenza A and rheumatoid arthritis (**Figure 2E**). The genes implicated in these functional processes were not deregulated by the Tat and Zta combination, suggesting a possible modulation of host-virus interactions with the Tat and Zta complex.

To corroborate these findings, we extended our analysis to freshly EBV-immortalized and proliferating B cells (BLAS). Similarly to primary B cells, we conducted an RNA-sequencing screen to investigate the effects of Tat (250 ng/ml), Zta (1000 ng/ml), or a combination of both proteins (250 ng/ml Tat and 1000 ng/ml Zta), administered to the BLAS cell medium for 6 or 48 hours. At 6 hours, Tat treatment led to the upregulation of 143 genes and downregulation of 129 genes, while Zta treatment upregulated 54 genes and downregulated 31 genes (**Figure 2F**). Again, the majority of these genes were protein-coding genes, and differentially expressed lncRNAs were also present (**Supplementary figure 6E-6H**). Remarkably, the combined treatment of Tat and Zta downregulated 3 genes and did not significantly upregulate any genes at this time point. In BLAS cells, more pronounced gene expression changes were observed at 48 hours. At the 48-hour interval, Tat treatment resulted in the upregulation of 585 genes and downregulation of 575 genes, whereas Zta treatment showed the upregulation of 1368 genes and downregulation of 2084 genes, which is in concordance with a pattern observed in primary B cells at 6 hours, where Zta treatment resulted in a more pronounced gene deregulation as compared to Tat. This included 1020 genes commonly deregulated by both Tat and Zta, all in the same direction (upregulation or downregulation) (**Figure 2H**).

Strikingly, the combined Tat and Zta treatment resulted in the deregulation of only 178 genes (75 upregulated and 103 downregulated, **Figure 2F**), which is again in agreement with a profile observed in primary B cells, where the combination of two proteins deregulated fewer genes than the individual action of viral proteins (**Figure 2A-2C**). Genes with |log2 Fold Change| > 0.4 showed comparable trends (**Figure 2G**). Among the genes that were commonly deregulated by both Tat and Zta when administered individually, a significant majority (930 out of 1020 genes) exhibited no differential expression in BLAS cells upon combined Tat and Zta treatment. This notable observation provides further support to the notion that the interaction between these two viral proteins may elicit effects on B cells, distinct from the singular impact of each protein acting independently.

When focusing on genes that were commonly deregulated by Tat and Zta individually in BLAS cells after 48 hours of treatment, we searched again for activated and suppressed functional categories associated with these genes as defined by the KEGG database. The activated functional categories included the MAPK, HIF-1, AGE-RAGE, FoxO, Erb signalling pathways, the lipid and atherosclerosis pathway and the endoplasmic reticulum protein processing pathway (**Figure 2I**). Conversely, a set of suppressed functional categories included pathways associated with neurodegenerative diseases, such as amyotrophic lateral sclerosis, Huntington's disease, and Parkinson's disease, oxidative phosphorylation, DNA replication and the proteasome pathway (**Figure 2J**). Together, these findings suggest that the interaction between Tat and Zta may lead to the interruption or modulation of specific pathways that would normally be activated by the individual actions of these two proteins.

The analysis of pathways that converged among primary B cells and BLAS cells revealed intriguing insights into the shared regulatory mechanisms influenced by Tat and Zta, but

not by their combination. In both cell types, activation of functional pathways related to protein processing was observed: antigen processing and presentation (in primary B cells) and protein processing in the endoplasmic reticulum (in BLAS cells) (**Supplementary figure 4I**), underscoring the activation of antigen processing and presentation upon Tat and Zta individual action on B cells, but not upon their combined action. Additionally, the lipid and atherosclerosis pathway was consistently activated by Tat and Zta in both primary and immortalized B cells, suggesting a potential impact of viral proteins on cellular lipid metabolism.

In summary, gene expression analyses revealed unique patterns of the transcriptomic changes when Tat and Zta were administered together, indicating their interactive influence. A subset of genes, activated by Tat or Zta alone remained unchanged when two proteins were combined. This "normalization to control" included the genes that may trigger an immune response in B cells - protein and antigen processing and presentation. The absence of a prominent transcriptome response upon Tat and Zta combination as well as "normalization" to control levels of many genes indicated that Tat and Zta interaction may provide an immune evasion for B cells, an important hallmark of malignancies [74].

Tat and Zta interaction decreased HLA-ABC (MHC I) expression in B cells

As we have seen by RNA-sequencing, several genes involved in antigen processing and presentation were normalized to the level of control untreated B or BLAS cells when treated simultaneously with Tat and Zta (**Supplementary figure 4I**), we thus hypothesized that Tat and Zta interaction might play a role in attenuating immune response in B cells. To answer this question, we analyzed the surface expression of HLA-ABC (MHC class I), a crucial component of the antigen presentation pathway, in BLAS cells treated with Tat, Zta alone or together for 48 hours (**Figure 3A**). The surface expression of HLA-ABC exhibited a substantial decrease in BLAS cells when treated simultaneously with Tat and Zta, as revealed by flow cytometry staining (0.617 ± 0.075 in Tat+Zta-treated cells vs 1.000 ± 0.020 in control, 1.262 ± 0.075 in Tat-treated cells and 1.148 ± 0.058 in Zta-treated cells, $p = 0.0006$, ANOVA, Tukey's posthoc test, **Figure 3A**). This effect was not observed with the treatment of BLAS cells with Tat or Zta individually (**Figure 3A**).

To confirm the dependence of HLA-ABC downregulation on Tat and Zta interaction, we transfected RPMI8866 cells, chosen for their better transfection efficiency, with YFP1-Tat and YFP2-Zta to specifically detect cells where Tat and Zta interact. As controls, we transfected RPMI8866 cells with YFP, YFP-Tat, or YFP-Zta, to ascertain that the observed decrease in HLA-ABC expression was not caused by YFP or individual action of Tat or Zta. The ratio of HLA-ABC fluorescence in YFP-positive cells (transfected) vs YFP-negative cells (untransfected) was analysed in each condition as an internal normalisation. Our results indicate a substantial reduction in HLA-ABC expression in cells where Tat and Zta interact, while no significant changes were observed in other conditions (0.666 ± 0.031 in cells transfected with YFP1-Tat+YFP2-Zta vs 1.016 ± 0.030 with YFP, 0.988 ± 0.043 with YFP-Tat and 0.915 ± 0.038 with YFP-Zta, $p < 0.0001$, ANOVA, Tukey's posthoc test, **Figure 3B**). To establish the specificity of the observed effect on

MHC class I, we analysed surface HLA-DR (MHC class II) levels in the same cells. No significant differences in HLA-DR surface levels were observed among cells transfected with YFP, YFP-Tat, YFP-Zta or YFP1-Tat+YFP2-Zta (**Figure 3C**), demonstrating the specificity of the influence of the Tat and Zta complex on the expression of MHC class I in B cells.

The downregulation of surface HLA-ABC might result from an overall decrease in HLA-ABC protein levels or from its potential relocalization from the cell plasma membrane, e.g. endoplasmic reticulum retention. To test this, we assessed the total HLA-ABC protein levels in RPMI8866 cells transfected with YFP, YFP-Tat, YFP-Zta, and YFP1-Tat+YFP2-Zta constructs. A consistent reduction in the total HLA-ABC protein levels in cells where Tat and Zta interacted was observed (0.470 ± 0.024 in cells transfected with YFP1-Tat+YFP2-Zta vs 1.042 ± 0.044 with YFP, 0.878 ± 0.011 with YFP-Tat and 0.799 ± 0.012 with YFP-Zta, $p < 0.0001$, ANOVA, Tukey's posthoc test, **Figure 3D**). We next decided to confirm that the observed HLA-ABC downregulation following RPMI8866 cell transfection with YFP1-Tat and YFP2-Zta was not an artefact of YFP reconstitution. RPMI8866 cells were transfected with BFP-Tat and YFP-Zta constructs (or BFP and YFP as a control) and the HLA-ABC total level in BFP+/YFP+ cells compared to BFP-/YFP- cells was analysed. The results revealed that transfection with BFP-Tat + YFP-Zta yielded a significantly lower HLA-ABC expression in RPMI8866 cells, contrasting with other conditions (0.645 ± 0.028 in cells transfected with BFP-Tat + YFP-Zta vs (BFP + YFP: 1.069 ± 0.078 with BFP + YFP, 1.055 ± 0.141 with BFP-Tat + YFP, 1.083 ± 0.050 BFP + YFP-Zta, $p = 0.0016$, ANOVA, Tukey's posthoc test, **Figure 3E**). These data indicate that the cooperative action of Tat and Zta upon their concomitant presence in B cells results in a reduction of total HLA-ABC protein levels.

In pursuit of corroborating our findings, we established an RPMI8866 cell line with doxycycline-inducible expression of YFP1-Tat-P2A-YFP2-Zta construct, enabling the detection of Tat and Zta interaction by YFP reconstitution. We utilized a P2A self-cleaving peptide that allowed equimolar expression of YFP1-Tat and YFP2-Zta proteins (**Supplementary figure 8A**). As a control, a similar RPMI8866 cell line with inducible expression of full-length YFP was generated. Subsequent analysis of HLA-ABC surface expression, conducted 48 hours after induction of YFP1-Tat-P2A-YFP2-Zta expression, was performed using immunofluorescent staining. The results demonstrated a nearly complete absence of HLA-ABC expression in cells where Tat and Zta interaction was detectable by YFP reconstitution (an image of two neighbouring cells with and without Tat and Zta interaction in the same field, **Figure 3F**). This effect was further confirmed at the total protein level of HLA-ABC (**Figure 3G**). In contrast, induction of YFP expression in RPMI8866 cells did not lead to a similar abolishment of HLA-ABC surface expression (**Figure 3F, 3H**). Similar results were observed on a total protein level of HLA-ABC analysed by western blotting in these cells (**Figure 3I, 3J**) as well as in Jurkat cells (**Supplementary figure 8B**). These results substantiate our previous findings about the role of Tat and Zta interaction in the downregulation of HLA-ABC expression.

Remarkably, despite the recognized roles of Tat and Zta as viral transcriptional activators, we did not observe decreased mRNA expression levels of *HLA-A*, *HLA-B*, or *HLA-C* in B cells upon Tat and Zta combined treatment and interaction. This observation held true in BLAS cells upon treatment with Tat and Zta recombinant proteins (**Figure 3K**), in YFP-positive RPMI8866 cells upon transfection with YFP1-Tat and YFP2-Zta (**Figure 3L**), and in RPMI8866 cells with inducible expression of the YFP1-Tat-P2A-YFP2-Zta construct (**Supplementary figure 8C**). We thus hypothesized that the reduction of total HLA-ABC levels in B cells upon Tat and Zta interaction might be linked to HLA-ABC proteasomal degradation. To explore this hypothesis, we used inhibitors of the ubiquitin-proteasomal system in RPMI8866 cells transfected with either YFP or YFP1-Tat + YFP2-Zta. 40 hours after transfection, cells were treated with MG132, PYR-41, Pevonedistat, Bay 11-7082, NSC697923, or DMSO as a control for a period of 8 hours, followed by the analysis of total HLA-ABC expression levels (**Figure 3M**). Normalization was performed by analyzing the ratio of HLA-ABC fluorescence in YFP-positive (transfected) cells versus YFP-negative (untransfected) cells. HLA-ABC was downregulated in RPMI8866 cells transfected YFP1-Tat + YFP2-Zta cells treated with DMSO (0.542 ± 0.044 in RPMI8866 cells transfected YFP1-Tat + YFP2-Zta vs 0.929 ± 0.052 in RPMI8866 cells transfected YFP, $p < 0.0001$, ANOVA, Tukey's posthoc test), aligning with earlier observations. MG132 treatment led to the restoration of HLA-ABC levels (0.892 ± 0.043 in RPMI8866 cells transfected YFP1-Tat + YFP2-Zta vs 0.896 ± 0.030 in RPMI8866 cells transfected YFP), establishing proteasomal involvement in the downregulation of HLA-ABC. Subsequent use of inhibitors targeting E1 activation (PYR-41 and Pevonedistat) revealed persistent HLA-ABC reduction (0.445 ± 0.088 with PYR-41 and 0.5032 ± 0.04793 with Pevonedistat in RPMI8866 cells transfected YFP1-Tat + YFP2-Zta vs 0.889 ± 0.022 with PYR-41 and 0.860 ± 0.016 with Pevonedistat in RPMI8866 cells transfected YFP), while inhibitors of E2 conjugation restored HLA-ABC levels to control (0.868 ± 0.039 with Bay 11-7082 and 0.8560 ± 0.136 with NSC697923 in RPMI8866 cells transfected YFP1-Tat + YFP2-Zta vs 0.909 ± 0.031 with Bay 11-7082 and 0.937 ± 0.029 with NSC697923 in RPMI8866 cells transfected YFP), highlighting E2 dependence in the proteasomal degradation mechanism. YFP-expressing cells exhibited consistent HLA-ABC levels across different inhibitor conditions.

Having established the involvement of the ubiquitin-proteasome pathway in the downregulation of HLA-ABC levels in B cells with Tat and Zta interaction, we verified whether the total cellular protein ubiquitination levels were increased upon Tat and Zta interaction. As shown in **Supplementary figure 8D**, the overall ubiquitin levels in cells expressing YFP1-Tat-P2A-Zta-YFP2 were not increased in comparison to cells expressing YFP, indicating that the increase in ubiquitin-dependent proteasomal degradation was specific for HLA-ABC.

To confirm that HLA-ABC downregulation induced by Tat and Zta interaction could compromise cytotoxic T cell response and contribute to B cell evasion from immune surveillance, we established a BLAS-reactive EBV-specific cytotoxic T cell line. Briefly, PBMCs from healthy donor AS were stimulated with autologous irradiated BLAS cells

which caused their in vitro expansion. Through five restimulation cycles, the cytotoxic cell line was >90% CD3+ by flow cytometric analysis (**Supplementary figure 9A**).

The cytotoxicity was assessed as the percentage of specific lysis. Briefly, sensitive target lymphoblastoid cells (BLAS, pre-treated or not with Tat and Zta for 48 hours at concentrations 250 ng/ml and 1000 ng/ml, respectively) and control target lymphoblastoid cells (RPMI8866) were differentially labelled with CFSE at two different concentrations to allow their differentiation between each other and with cytotoxic T cells (**Supplementary figure 9B**). The target cells (T, BLAS or RPMI8866) were combined with effector cells (E, cytotoxic T cell line) at various E/T ratios and incubated for 4 hours; the percentage of specific lysis was derived from the reduction in the population of sensitive target cells. BLAS cells that were pre-treated with Tat and Zta exhibited diminished susceptibility to cell lysis by cytotoxic T cells in comparison to control BLAS cells (**Figure 3N**). Specifically, at an E/T ratio of 2.5:1, the percentage of specific lysis was 10.67 ± 0.67 in BLAS cells + Tat and Zta, compared to 20.50 ± 3.50 in control BLAS cells, 31.67 ± 1.45 in BLAS cells + Tat, and 20.33 ± 0.33 in BLAS cells + Zta ($p = 0.0326$ for BLAS cells + Tat and Zta vs BLAS, two-way ANOVA, Tukey's posthoc test). These findings collectively underscore the compelling evidence that HLA-ABC expression downregulation induced by cooperative Tat and Zta interaction, potentially through targeted HLA-ABC proteasomal degradation, might contribute to the immune evasion of EBV-infected lymphoblastoid B cells.

Discussion

Combined antiretroviral therapy (cART) provides complete suppression of HIV replication and immune restoration [1]; despite this fact, people living with HIV are at higher risk of developing cancer, they have a more severe clinical course and lower survival rates compared to the non-infected population [2–4]. People living with HIV diagnosed with cancer experience excess mortality that exceeds the expected mortality from the simple combination of HIV and cancer [75]. Cancers in people living with HIV are traditionally divided into AIDS-defining cancers (ADCs: Kaposi's sarcoma, non-Hodgkin's B cell lymphomas (NHLs), invasive cervical cancer) and others, referred to as non-AIDS defining cancers (NADCs) [76]. The incidence of AIDS-defining cancers, though decreased in the cART era, is still largely elevated, while the incidence of non-AIDS-defining cancers is rising in the cART era and is expected to continue to rise [23,77]. B cell lymphomas in people living with HIV are more frequently associated with EBV, i.e. EBV is found in lymphoma cells of HIV-positive patients more frequently than in the same lymphoma subtypes in HIV-negative patients [78]. Understanding the reasons for these trends and finding the causative agents is a vital need and a rising challenge for public health [22].

Since HIV-associated B cell lymphomas affect cells not targeted by the virus, a direct oncogenic effect of HIV-1 could be mediated by viral proteins that have the property of being secreted by the infected cell and entering other non-infected cells [79]. With this regard, we draw our attention to viral transactivator proteins with cell penetration

capacities: HIV-1 Tat and EBV Zta. HIV-1 Tat and EBV Zta share several important features: both are transcriptional activators, both can be released from infected cells and penetrate other cells, where being transported into a nucleus regulate viral and host gene transcription [62,80–82]. Additionally, both proteins have oncogenic properties. HIV-1 Tat modulates cell cycling, DNA repair mechanisms, decreases apoptosis and promotes DNA damage [80,83–88]. It additionally promotes vascular permeability, worsens the oncogenic properties of cancer cells and accelerates tumour development in animal xenograft models [89,90]. The mechanisms of Zta contribution to cancer development include Zta-induced tumour-promoting inflammation, genome instability, immune evasion (e.g. transcriptional repression of *CIITA*, a main regulator of MHC class II genes), stimulation of growth and proliferation and resistance to apoptosis [28].

In this study, we investigated the potential physical interaction between HIV-1 Tat and EBV Zta. The findings presented here unveil a previously unrecognized direct interaction between two viral transcriptional activators, HIV-1 Tat and EBV Zta, in B cells, T cells, and human serum (**Figure 1**). The circulating Tat-Zta complex may be present in the blood of people living with HIV (**Figure 1D**). To our knowledge, this is the first demonstration of direct inter-viral protein-protein interaction. HIV proteins were previously implicated in indirect inter-viral interactions: HIV-1 Tat was shown to bind LINC00313, an endogenous lncRNA upregulated during Kaposi's sarcoma-associated herpesvirus (KSHV) lytic reactivation [91], while HIV p17 matrix protein was shown to up-regulate the EBV protein latent membrane protein (LMP)-1 in B cells [109].

Tat and Zta interaction occurred predominantly in the cell nucleus (**Figure 1G**), hinting at a potential involvement in the transcriptional regulation of host genes. To elucidate the combined effect of Tat and Zta on B cells, we performed RNA-sequencing analyses. We observed significant shifts in gene expression patterns in response to Tat and Zta individual treatments, with a notable number of commonly deregulated genes by two viral proteins. Strikingly, when Tat and Zta were administered in combination, many of these genes ceased to be differentially expressed, indicating a possible interactive influence between these viral proteins (**Figure 2C, 2H**). Of particular interest was the functional annotation of genes commonly deregulated by Tat and Zta individually but no longer affected when both proteins were combined. The ORA revealed activated functional categories associated with antigen processing and presentation, and protein processing (**Figure 2D, 2I**). This points to the possibility that the interaction between Tat and Zta could prevent or modify the activation of particular pathways that would otherwise be triggered by their independent actions. The mechanisms of Tat and Zta functioning upon interaction requires further investigation. It was previously shown that HIV-1 Tat and EBV Zta can synergistically activate HIV-1 long terminal repeat (LTR): while with Tat and Zta only the LTR-driven LacZ expression increased 44- and 18-fold, the combination of HIV-1 Tat and EBV Zta caused a 214-fold increase in LTR-driven LacZ expression [92]. Our data, however, contradict this observation as we do not observe any changes in Tat-induced LTR-driven transcription upon Zta presence (**Supplementary figure 7**). It is

plausible that upon interaction, Tat and Zta are no longer able to regulate their conventional targets in B cells.

We subsequently explored the implication of Tat and Zta interaction in the immune response evasion of B cells. We found that B cells, where Tat and Zta are present, downregulate the expression of HLA-ABC (**Figure 3**), a pivotal component of antigen presentation. Previously, HIV-1 Tat was implicated in repressing MHC class I promoter activity in HeLa cells [93]. Here we show that at least in B cells individual Tat action does not lead to a decrease in HLA-ABC expression (**Figure 3A-3E**). Our findings suggest that the reduction of total HLA-ABC levels in B cells upon Tat and Zta interaction might be linked to HLA-ABC proteasomal degradation (**Figure 3M**). This strategy is commonly employed by other viral proteins, e.g. EBV BDLF3 [94] or KSHV gene product K3[95].

HLA-ABC downregulation, induced by Tat and Zta complex, compromised the recognition of EBV-infected cells by cytotoxic T cells (**Figure 3N**). This may contribute to B cell evasion from immune surveillance, especially for B cells with reactivating EBV, where Zta is present in large quantities. EBV reactivation from latency is a rather rare event, possibly because Zta expression needs to overcome a certain threshold. When Zta expression is low, the transactivator protein will bind only high-affinity Zta response elements, while oriLyt (origin of replication) requires a higher Zta concentration for binding [47,96,97]. This threshold can be overcome by a positive feedback loop, whereby Zta stimulates its own expression [98]. EBV is mainly prevented from reactivating through efficient EBV-specific CD8+ cytotoxic T cellular response (reviewed in [99–101]). Lytic antigen-specific CD8+ T cells play a major role in controlling EBV reactivation by eliminating virus-producing cells at an early stage, since even during persistent EBV infection, most EBV-specific CD8+ T cells are directed against lytic epitopes [101]. People living with HIV more often present EBV reactivation even in the ear of cART [5,102] and this does not always correlate with immune suppression. Notably, cART interruption results in EBV DNA rebound despite the absence of a pronounced CD4+ T cell decrease [103]. We hypothesize that HIV-1 Tat penetration in reactivating B cells might lead to its binding to EBV Zta and a decrease in HLA-ABC surface expression, which would contribute to the escape of reactivating B cells from the immune response. Importantly, the presence of Tat in B cells didn't perturb EBV reactivation (**Supplementary figure 7G-7H**).

Impaired immune surveillance against EBV is a critical step towards lymphomagenesis in people living with HIV [104]. The impairment of EBV-specific T-cell immunity might permit EBV reactivation from latency and expansion of the pool of EBV-infected B cells; the latter increases the chances of a subsequent malignant transformation of EBV-infected B cells. For instance, in HIV-progressors the appearance of NHL is preceded by a decrease in EBV-specific CD8+ T cell response and an increase in the number of EBV-infected B cells [105]. Aberrant MHC expression and immune escape is a common feature of B cell lymphomas [106,107]. Interestingly, it was previously shown that the level of Zta-specific CD8+ T cells is decreased in long-term cART-treated people living with HIV as compared to HIV-uninfected individuals, while the level of EBNA1-specific CD8+ T cells didn’t

differ from HIV-uninfected individuals [108]. Additionally, no correlation was found between CD4+ and CD8+ T cell responses to Zta as opposed to a strong positive correlation between CD4+ and CD8+ T cell responses to EBNA-1 [108]. It is unlikely that this is due to lower levels of EBV reactivation in people living with HIV relative to uninfected individuals. This points to the hypothesis that there might be factors, other than immune deficiency and decreased CD4+ T cell help, implicated in the dysregulation of EBV-specific immune response in people living with HIV. One such factor might be HIV-1 Tat and EBV Zta interaction.

In summary, this study reveals a direct interaction between two viral proteins, HIV-1 Tat and EBV Zta, in B cells, T cells, and human serum, shedding light on potential factors contributing to the elevated cancer risk in people with HIV. Together, Tat and Zta downregulate HLA-ABC expression in B cells, impairing the recognition of EBV-infected B cells by cytotoxic T cells. Downregulation of HLA expression is a common mechanism of immune escape of various tumour and virus-infected cells. This finding underscores the intricate interplay between viral proteins from different viruses that infect different cell types.

References

1. HIV-CAUSAL Collaboration; Ray, M.; Logan, R.; Sterne, J.A.C.; Hernández-Díaz, S.; Robins, J.M.; Sabin, C.; Bansi, L.; van Sighem, A.; de Wolf, F.; et al. The Effect of Combined Antiretroviral Therapy on the Overall Mortality of HIV-Infected Individuals. *AIDS* **2010**, *24*, 123–137, doi:10.1097/QAD.0b013e3283324283.
2. Powles, T.; Robinson, D.; Stebbing, J.; Shamash, J.; Nelson, M.; Gazzard, B.; Mandelia, S.; Møller, H.; Bower, M. Highly Active Antiretroviral Therapy and the Incidence of Non–AIDS-Defining Cancers in People With HIV Infection. *Journal of Clinical Oncology* **2009**, *27*, 884–890, doi:10.1200/JCO.2008.19.6626.
3. Coghill, A.E.; Shiels, M.S.; Suneja, G.; Engels, E.A. Elevated Cancer-Specific Mortality among HIV-Infected Patients in the United States. *Journal of clinical oncology : official journal of the American Society of Clinical Oncology* **2015**, *33*, 2376–2383, doi:10.1200/JCO.2014.59.5967.
4. Marcus, J.L.; Chao, C.; Leyden, W.A.; Xu, L.; Yu, J.; Horberg, M.A.; Klein, D.; Towner, W.J.; Quesenberry, C.P.; Abrams, D.I.; et al. Survival among HIV-Infected and HIV-Uninfected Individuals with Common Non-AIDS-Defining Cancers. *Cancer Epidemiology Biomarkers & Prevention* **2015**, *24*, 1167–1173, doi:10.1158/1055-9965.EPI-14-1079.
5. Sallah, N.; Miley, W.; Labo, N.; Carstensen, T.; Fatumo, S.; Gurdasani, D.; Pollard, M.O.; Dilthey, A.T.; Mentzer, A.J.; Marshall, V.; et al. Distinct Genetic Architectures and Environmental Factors Associate with Host Response to the Γ2-Herpesvirus Infections. *Nat Commun* **2020**, *11*, 3849, doi:10.1038/s41467-020-17696-2.
6. Yan, Y.; Ren, Y.; Chen, R.; Hu, J.; Ji, Y.; Yang, J.; Shen, J.; Hu, L.; Pei, H.; Wang, J.; et al. Evaluation of Epstein-Barr Virus Salivary Shedding in HIV/AIDS Patients and HAART Use: A Retrospective Cohort Study. *Virologica Sinica* **2018**, *33*, 227–233, doi:10.1007/s12250-018-0028-z.
7. Quesnel, A.; Pozzetto, B.; Touraine, F.; Moja, P.; Lucht, F.; De The, G.; Touraine, J.L.; Gaudin, O.; Genin, C. Antibodies to Epstein-Barr Virus and Cytomegalovirus in Relation to CD4 Cell Number in Human Immunodeficiency Virus 1 Infection. *J Med Virol* **1992**, *36*, 60–64, doi:10.1002/jmv.1890360112.
8. Cohen, J.I. Epstein–Barr Virus Infection. *New England Journal of Medicine* **2000**, *343*, 481–492, doi:10.1056/NEJM200008173430707.
9. Tsurumi, T.; Fujita, M.; Kudoh, A. Latent and Lytic Epstein-Barr Virus Replication Strategies. *Reviews in Medical Virology* 2005, *15*, 3–15.
10. Cohen, J.I.; Fauci, A.S.; Varmus, H.; Nabel, G.J. Epstein-Barr Virus: An Important Vaccine Target for Cancer Prevention. In Proceedings of the Science Translational Medicine; American Association for the Advancement of Science, November 2 2011; Vol. 3, p. 107.
11. Murata, T. Regulation of Epstein-Barr Virus Reactivation from Latency. *Microbiology and Immunology* 2014, *58*, 307–317.
12. Pattle, S.B.; Farrell, P.J. The Role of Epstein–Barr Virus in Cancer. *Expert Opinion on Biological Therapy* **2006**, *6*, 1193–1205, doi:10.1517/14712598.6.11.1193.
13. Kutok, J.L.; Wang, F. Spectrum of Epstein-Barr Virus-Associated Diseases. *Annual review of pathology* **2006**, *1*, 375–404, doi:10.1146/annurev.pathol.1.110304.100209.
14. Gianella, S.; Moser, C.; Vitomirov, A.; McKhann, A.; Layman, L.; Scott, B.; Caballero, G.; Lada, S.; Bosch, R.J.; Hoenigl, M.; et al. Presence of Asymptomatic CMV and EBV DNA in Blood of Persons with HIV Starting Antiretroviral Therapy

Are Associated with Non-AIDS Clinical Events. *AIDS* **2020**, *34*, 849–857, doi:10.1097/QAD.0000000000002484.
15. O'Sullivan, C.E.; Peng, R.; Cole, K.S.; Montelaro, R.C.; Sturgeon, T.; Jenson, H.B.; Ling, P.D. Epstein-Barr Virus and Human Immunodeficiency Virus Serological Responses and Viral Burdens in HIV-Infected Patients Treated with HAART. *J Med Virol* **2002**, *67*, 320–326, doi:10.1002/jmv.10080.
16. Ouedraogo, D.E.; Bollore, K.; Viljoen, J.; Foulongne, V.; Reynes, J.; Cartron, G.; Vendrell, J.-P.; Van de Perre, P.; Tuaillon, E. Comparison of EBV DNA Viral Load in Whole Blood, Plasma, B-Cells and B-Cell Culture Supernatant. *Journal of Medical Virology* **2014**, *86*, 851–856, doi:10.1002/jmv.23858.
17. Ling, P.D.; Vilchez, R.A.; Keitel, W.A.; Poston, D.G.; Peng, R.S.; White, Z.S.; Visnegarwala, F.; Lewis, D.E.; Butel, J.S. Epstein-Barr Virus DNA Loads in Adult Human Immunodeficiency Virus Type 1-Infected Patients Receiving Highly Active Antiretroviral Therapy. *Clinical Infectious Diseases* **2003**, *37*, 1244–1249, doi:10.1086/378808.
18. Yan, Y.; Ren, Y.; Chen, R.; Hu, J.; Ji, Y.; Yang, J.; Shen, J.; Hu, L.; Pei, H.; Wang, J.; et al. Evaluation of Epstein-Barr Virus Salivary Shedding in HIV/AIDS Patients and HAART Use: A Retrospective Cohort Study. *Virologica Sinica* **2018**, *33*, 227–233, doi:10.1007/s12250-018-0028-z.
19. Rahman, M.A.; Kingsley, L.A.; Atchison, R.W.; Belle, S.; Breinig, M.C.; Ho, M.; Rinaldo, C.R. Reactivation of Epstein-Barr Virus during Early Infection with Human Immunodeficiency Virus. *Journal of Clinical Microbiology* **1991**, *29*, 1215–1220, doi:10.1128/jcm.29.6.1215-1220.1991.
20. Shannon-Lowe, C.; Rickinson, A.B.; Bell, A.I. Epstein-Barr Virus-Associated Lymphomas. *Philosophical Transactions of the Royal Society B: Biological Sciences* 2017, *372*.
21. McHugh, D.; Myburgh, R.; Caduff, N.; Spohn, M.; Kok, Y.L.; Keller, C.W.; Murer, A.; Chatterjee, B.; Rühl, J.; Engelmann, C.; et al. EBV Renders B Cells Susceptible to HIV-1 in Humanized Mice. *Life Science Alliance* **2020**, *3*, doi:10.26508/LSA.202000640.
22. Shmakova, A.; Germini, D.; Vassetzky, Y. HIV‐1, HAART and Cancer: A Complex Relationship. *International Journal of Cancer* **2020**, *146*, 2666–2679, doi:10.1002/ijc.32730.
23. Hernández-Ramírez, R.U.; Shiels, M.S.; Dubrow, R.; Engels, E.A. Cancer Risk in HIV-Infected People in the USA from 1996 to 2012: A Population-Based, Registry-Linkage Study. *The Lancet HIV* **2017**, *4*, e495–e504, doi:10.1016/S2352-3018(17)30125-X.
24. Biggar, R.J.; Chaturvedi, A.K.; Goedert, J.J.; Engels, E.A. AIDS-Related Cancer and Severity of Immunosuppression in Persons with AIDS. *Journal of the National Cancer Institute* **2007**, *99*, 962–972, doi:10.1093/jnci/djm010.
25. Xu, F.; Zhao, C.; Li, Y.; Li, J.; Deng, Y.; Shi, T. Exploring Virus Relationships Based on Virus-Host Protein-Protein Interaction Network. *BMC Systems Biology* **2011**, *5*, S11, doi:10.1186/1752-0509-5-S3-S11.
26. Agol, V.I.; Gmyl, A.P. Viral Security Proteins: Counteracting Host Defences. *Nature Reviews Microbiology* 2010, *8*, 867–878.
27. Liu, X.; Hong, T.; Parameswaran, S.; Ernst, K.; Marazzi, I.; Weirauch, M.T.; Fuxman Bass, J.I. Human Virus Transcriptional Regulators. *Cell* **2020**, *182*, 24–37, doi:10.1016/j.cell.2020.06.023.
28. Germini, D.; Sall, F.B.; Shmakova, A.; Wiels, J.; Dokudovskaya, S.; Drouet, E.; Vassetzky, Y. Oncogenic Properties of the Ebv Zebra Protein. *Cancers* 2020, *12*,

1–26.
29. Kurnaeva, M.A.; Sheval, E.V.; Musinova, Y.R.; Vassetzky, Y.S. Tat Basic Domain: A "Swiss Army Knife" of HIV-1 Tat? *Reviews in Medical Virology* **2019**, *in press*, doi:10.1002/rmv.2031.
30. Rothe, R.; Liguori, L.; Villegas-Mendez, A.; Marques, B.; Grunwald, D.; Drouet, E.; Lenormand, J.L. Characterization of the Cell-Penetrating Properties of the Epstein-Barr Virus ZEBRA Trans-Activator. *Journal of Biological Chemistry* **2010**, *285*, 20224–20233, doi:10.1074/jbc.M110.101550.
31. Poggi, A.; Carosio, R.; Fenoglio, D.; Brenci, S.; Murdaca, G.; Setti, M.; Indiveri, F.; Scabini, S.; Ferrero, E.; Zocchi, M.R. Migration of Vδ1 and Vδ2 T Cells in Response to CXCR3 and CXCR4 Ligands in Healthy Donors and HIV-1-Infected Patients: Competition by HIV-1 Tat. *Blood* **2004**, *103*, 2205–2213, doi:10.1182/blood-2003-08-2928.
32. Habib, M.; Buisson, M.; Lupo, J.; Agbalika, F.; Socié, G.; Germi, R.; Baccard, M.; Imbert-Marcille, B.-M.; Dantal, J.; Morand, P.; et al. Lytic EBV Infection Investigated by Detection of Soluble Epstein-Barr Virus ZEBRA in the Serum of Patients with PTLD. *Scientific Reports* **2017**, *7*, 10479, doi:10.1038/s41598-017-09798-7.
33. Musinova, Y.R.; Sheval, E. V.; Dib, C.; Germini, D.; Vassetzky, Y.S. Functional Roles of HIV-1 Tat Protein in the Nucleus. *Cellular and Molecular Life Sciences* **2016**, *73*, 589–601, doi:10.1007/s00018-015-2077-x.
34. Banks, W.A.; Robinson, S.M.; Nath, A. Permeability of the Blood-Brain Barrier to HIV-1 Tat. *Experimental Neurology* **2005**, *193*, 218–227, doi:10.1016/j.expneurol.2004.11.019.
35. Li, S.; Hou, H.; Mori, T.; Sawmiller, D.; Smith, A.; Tian, J.; Wang, Y.; Giunta, B.; Sanberg, P.R.; Zhang, S.; et al. Swedish Mutant APP-Based BACE1 Binding Site Peptide Reduces APP β-Cleavage and Cerebral Aβ Levels in Alzheimer's Mice. *Scientific Reports* **2015**, *5*, doi:10.1038/srep11322.
36. Henderson, L.J.; Johnson, T.P.; Smith, B.R.; Reoma, L.B.; Santamaria, U.A.; Bachani, M.; Demarino, C.; Barclay, R.A.; Snow, J.; Sacktor, N.; et al. Presence of Tat and Transactivation Response Element in Spinal Fluid despite Antiretroviral Therapy. *AIDS* **2019**, *33 Suppl 2*, S145–S157, doi:10.1097/QAD.0000000000002268.
37. Marban, C.; Su, T.; Ferrari, R.; Li, B.; Vatakis, D.; Pellegrini, M.; Zack, J.A.; Rohr, O.; Kurdistani, S.K. Genome-Wide Binding Map of the HIV-1 Tat Protein to the Human Genome. *PLoS ONE* **2011**, *6*, e26894, doi:10.1371/journal.pone.0026894.
38. Mancebo, H.S.Y.; Lee, G.; Flygare, J.; Tomassini, J.; Luu, P.; Zhu, Y.; Peng, J.; Blau, C.; Hazuda, D.; Price, D.; et al. P-TEFb Kinase Is Required for HIV Tat Transcriptional Activation in Vivo and in Vitro. *Genes and Development* **1997**, *11*, 2633–2644, doi:10.1101/gad.11.20.2633.
39. Raha, T.; Cheng, S.W.G.; Green, M.R. HIV-1 Tat Stimulates Transcription Complex Assembly through Recruitment of TBP in the Absence of TAFs. *PLoS Biology* **2005**, *3*, e44, doi:10.1371/journal.pbio.0030044.
40. Reeder, J.E.; Kwak, Y.-T.T.; McNamara, R.P.; Forst, C. V.; D'Orso, I.; D'Orso, I. HIV Tat Controls RNA Polymerase II and the Epigenetic Landscape to Transcriptionally Reprogram Target Immune Cells. *eLife* **2015**, *4*, e08955, doi:10.7554/eLife.08955.
41. Romani, B.; Engelbrecht, S.; Glashoff, R.H. Functions of Tat: The Versatile Protein of Human Immunodeficiency Virus Type 1. *The Journal of general virology* **2010**, *91*, 1–12, doi:10.1099/vir.0.016303-0.

42. Countryman, J.; Miller, G. Activation of Expression of Latent Epstein-Barr Herpesvirus after Gene Transfer with a Small Cloned Subfragment of Heterogeneous Viral DNA. *Proceedings of the National Academy of Sciences of the United States of America* **1985**, *82*, 4085–4089, doi:10.1073/pnas.82.12.4085.
43. Feederle, R.; Kost, M.; Baumann, M.; Janz, A.; Drouet, E.; Hammerschmidt, W.; Delecluse, H.J. The Epstein-Barr Virus Lytic Program Is Controlled by the Co-Operative Functions of Two Transactivators. *EMBO Journal* **2000**, *19*, 3080–3089, doi:10.1093/emboj/19.12.3080.
44. Petosa, C.; Morand, P.; Baudin, F.; Moulin, M.; Artero, J.B.; Müller, C.W. Structural Basis of Lytic Cycle Activation by the Epstein-Barr Virus ZEBRA Protein. *Molecular Cell* **2006**, *21*, 565–572, doi:10.1016/j.molcel.2006.01.006.
45. Dickerson, S.J.; Xing, Y.; Robinson, A.R.; Seaman, W.T.; Gruffat, H.; Kenney, S.C. Methylation-Dependent Binding of the Epstein-Barr Virus BZLF1 Protein to Viral Promoters. *PLoS Pathogens* **2009**, *5*, doi:10.1371/journal.ppat.1000356.
46. Flower, K.; Thomas, D.; Heather, J.; Ramasubramanyan, S.; Jones, S.; Sinclair, A.J. Epigenetic Control of Viral Life-Cycle by a DNA-Methylation Dependent Transcription Factor. *PLoS ONE* **2011**, *6*, 25922, doi:10.1371/journal.pone.0025922.
47. Bergbauer, M.; Kalla, M.; Schmeinck, A.; Göbel, C.; Rothbauer, U.; Eck, S.; Benet-Pagés, A.; Strom, T.M.; Hammerschmidt, W. CpG-Methylation Regulates a Class of Epstein-Barr Virus Promoters. *PLoS Pathogens* **2010**, *6*, doi:10.1371/journal.ppat.1001114.
48. Ma, S.-D.; Yu, X.; Mertz, J.E.; Gumperz, J.E.; Reinheim, E.; Zhou, Y.; Tang, W.; Burlingham, W.J.; Gulley, M.L.; Kenney, S.C. An Epstein-Barr Virus (EBV) Mutant with Enhanced BZLF1 Expression Causes Lymphomas with Abortive Lytic EBV Infection in a Humanized Mouse Model. *Journal of Virology* **2012**, *86*, 7976–7987, doi:10.1128/jvi.00770-12.
49. Xue, S.A.; Labrecque, L.G.; Lu, Q.L.; Ong, S.K.; Lampert, I.A.; Kazembe, P.; Molyneux, E.; Broadhead, R.L.; Borgstein, E.; Griffin, B.E. Promiscuous Expression of Epstein-Barr Virus Genes in Burkitt's Lymphoma from the Central African Country Malawi. *International Journal of Cancer* **2002**, *99*, 635–643, doi:10.1002/ijc.10372.
50. Cohen, M.; Vistarop, A.G.; Huaman, F.; Narbaitz, M.; Metrebian, F.; De Matteo, E.; Preciado, M.V.; Chabay, P.A. Epstein-Barr Virus Lytic Cycle Involvement in Diffuse Large B Cell Lymphoma. *Hematological Oncology* **2018**, *36*, 98–103, doi:10.1002/hon.2465.
51. Xue, S.-A.; Lu, Q.-L.; Poulsom, R.; Karran, L.; Jones, M.D.; Griffin, B.E. Expression of Two Related Viral Early Genes in Epstein-Barr Virus-Associated Tumors. *Journal of Virology* **2000**, *74*, 2793–2803, doi:10.1128/jvi.74.6.2793-2803.2000.
52. Huang, J.; Chen, H.; Hutt-Fletcher, L.; Ambinder, R.F.; Hayward, S.D. Lytic Viral Replication as a Contributor to TheDetection of Epstein-Barr Virus in BreastCancer. *Journal of Virology* **2003**, *77*, 13267–13274, doi:10.1128/jvi.77.24.13267-13274.2003.
53. Ramayanti, O.; Juwana, H.; Verkuijlen, S.A.M.W.; Adham, M.; Pegtel, M.D.; Greijer, A.E.; Middeldorp, J.M. Epstein-Barr Virus MRNA Profiles and Viral DNA Methylation Status in Nasopharyngeal Brushings from Nasopharyngeal Carcinoma Patients Reflect Tumor Origin. *International Journal of Cancer* **2017**, *140*, 149–162, doi:10.1002/ijc.30418.
54. Germini, D.; Tsfasman, T.; Klibi, M.; El-Amine, R.; Pichugin, A.; Iarovaia, O. V; Bilhou-Nabera, C.; Subra, F.; Bou Saada, Y.; Sukhanova, A.; et al. HIV Tat Induces

a Prolonged MYC Relocalization next to IGH in Circulating B-Cells. *Leukemia* **2017**, *31*, 2515–2522, doi:10.1038/leu.2017.106.
55. Gorbacheva, M.A.; Tikhomirova, M.A.; Potashnikova, D.M.; Akbay, B.; Sheval, E.V.; Musinova, Y.R. Production of Stable Cell Lines on the Basis of the Cultured RPMI 8866 B-Cells with Constant and Inducible Expression of the Human Immunodeficiency Virus Tat Protein. *Russian Journal of Developmental Biology* **2019**, *50*, 275–280, doi:10.1134/s1062360419050060.
56. Shmakova, A.; Lomov, N.; Viushkov, V.; Tsfasman, T.; Kozhevnikova, Y.; Sokolova, D.; Pokrovsky, V.; Syrkina, M.; Germini, D.; Rubtsov, M.; et al. Cell Models with Inducible Oncogenic Translocations Allow to Evaluate the Potential of Drugs to Favor Secondary Translocations. *Cancer Commun (Lond)* **2022**, *43*, 154–158, doi:10.1002/cac2.12370.
57. Levitsky, V.; Frisan, T.; Masucci, M. Generation of Polyclonal EBV-Specific CTL Cultures and Clones. *Methods Mol Biol* **2001**, *174*, 203–208, doi:10.1385/1-59259-227-9:203.
58. Nakagawa, Y.; Watari, E.; Shimizu, M.; Takahashi, H. One-Step Simple Assay to Determine Antigen-Specific Cytotoxic Activities by Single-Color Flow Cytometry. *Biomed Res* **2011**, *32*, 159–166, doi:10.2220/biomedres.32.159.
59. Canoy, R.J.; André, F.; Shmakova, A.; Wiels, J.; Lipinski, M.; Vassetzky, Y.; Germini, D. Easy and Robust Electrotransfection Protocol for Efficient Ectopic Gene Expression and Genome Editing in Human B Cells. *Gene Therapy* **2020**, doi:10.1038/s41434-020-00194-x.
60. Lapetina, S.; Gil-Henn, H. A Guide to Simple, Direct, and Quantitative in Vitro Binding Assays. *Journal of Biological Methods* **2017**, *4*, 62, doi:10.14440/jbm.2017.161.
61. Nyfeler, B.; Michnick, S.W.; Hauri, H.P. Capturing Protein Interactions in the Secretory Pathway of Living Cells. *Proceedings of the National Academy of Sciences of the United States of America* **2005**, *102*, 6350–6355, doi:10.1073/pnas.0501976102.
62. Kurnaeva, M.A.; Zalevsky, A.O.; Arifulin, E.A.; Lisitsyna, O.M.; Tvorogova, A.V.; Shubina, M.Y.; Bourenkov, G.P.; Tikhomirova, M.A.; Potashnikova, D.M.; Kachalova, A.I.; et al. Molecular Coevolution of Nuclear and Nucleolar Localization Signals inside the Basic Domain of HIV-1 Tat. *Journal of Virology* **2022**, *96*, e01505-21, doi:10.1128/JVI.01505-21.
63. Wu, T.; Hu, E.; Xu, S.; Chen, M.; Guo, P.; Dai, Z.; Feng, T.; Zhou, L.; Tang, W.; Zhan, L.; et al. ClusterProfiler 4.0: A Universal Enrichment Tool for Interpreting Omics Data. *Innovation (Camb)* **2021**, *2*, 100141, doi:10.1016/j.xinn.2021.100141.
64. Pfaffl, M.W. A New Mathematical Model for Relative Quantification in Real-Time RT-PCR. *Nucleic Acids Res* **2001**, *29*, e45, doi:10.1093/nar/29.9.e45.
65. Vandesompele, J.; De Preter, K.; Pattyn, F.; Poppe, B.; Van Roy, N.; De Paepe, A.; Speleman, F. Accurate Normalization of Real-Time Quantitative RT-PCR Data by Geometric Averaging of Multiple Internal Control Genes. *Genome Biol* **2002**, *3*, research0034.1-research0034.11.
66. Hellemans, J.; Mortier, G.; De Paepe, A.; Speleman, F.; Vandesompele, J. QBase Relative Quantification Framework and Software for Management and Automated Analysis of Real-Time Quantitative PCR Data. *Genome Biol* **2007**, *8*, R19, doi:10.1186/gb-2007-8-2-r19.
67. Gorbacheva, M.A.; Tikhomirova, M.A.; Potashnikova, D.M.; Akbay, B.; Sheval, E. V.; Musinova, Y.R. Production of Stable Cell Lines on the Basis of the Cultured RPMI 8866 B-Cells with Constant and Inducible Expression of the Human

Immunodeficiency Virus Tat Protein. *Russian Journal of Developmental Biology* **2019**, *50*, 275–280, doi:10.1134/s1062360419050060.
68. Giovannone, N.; Liang, J.; Antonopoulos, A.; Geddes Sweeney, J.; King, S.L.; Pochebit, S.M.; Bhattacharyya, N.; Lee, G.S.; Dell, A.; Widlund, H.R.; et al. Galectin-9 Suppresses B Cell Receptor Signaling and Is Regulated by I-Branching of N-Glycans. *Nature Communications* **2018**, *9*, 3287, doi:10.1038/s41467-018-05770-9.
69. Chabot, S.; Kashio, Y.; Seki, M.; Shirato, Y.; Nakamura, K.; Nishi, N.; Nakamura, T.; Matsumoto, R.; Hirashima, M. Regulation of Galectin-9 Expression and Release in Jurkat T Cell Line Cells. *Glycobiology* **2002**, *12*, 111–118, doi:10.1093/glycob/12.2.111.
70. Kudla, J.; Bock, R. Lighting the Way to Protein-Protein Interactions: Recommendations on Best Practices for Bimolecular Fluorescence Complementation Analyses. *Plant Cell* 2016, *28*, 1002–1008.
71. Mele, A.R.; Marino, J.; Dampier, W.; Wigdahl, B.; Nonnemacher, M.R. HIV-1 Tat Length: Comparative and Functional Considerations. *Frontiers in Microbiology* **2020**, *11*, 444, doi:10.3389/FMICB.2020.00444.
72. Ishikawa-Ankerhold, H.C.; Ankerhold, R.; Drummen, G.P.C. Advanced Fluorescence Microscopy Techniques—FRAP, FLIP, FLAP, FRET and FLIM. *Molecules* **2012**, *17*, 4047, doi:10.3390/MOLECULES17044047.
73. Kanehisa, M.; Goto, S. KEGG: Kyoto Encyclopedia of Genes and Genomes. *Nucleic Acids Res* **2000**, *28*, 27–30, doi:10.1093/nar/28.1.27.
74. de Charette, M.; Houot, R. Hide or Defend, the Two Strategies of Lymphoma Immune Evasion: Potential Implications for Immunotherapy. *Haematologica* 2018, *103*, 1256–1268.
75. Coghill, A.E.; Pfeiffer, R.M.; Shiels, M.S.; Engels, E.A. Excess Mortality among HIV-Infected Individuals with Cancer in the United States. *Cancer epidemiology, biomarkers & prevention : a publication of the American Association for Cancer Research, cosponsored by the American Society of Preventive Oncology* **2017**, *26*, 1027–1033, doi:10.1158/1055-9965.EPI-16-0964.
76. Berretta, M.; Di Francia, R.; Stanzione, B.; Facchini, G.; LLeshi, A.; De Paoli, P.; Spina, M.; Tirelli, U. New Treatment Strategies for HIV-Positive Cancer Patients Undergoing Antiblastic Chemotherapy. *Expert Opinion on Pharmacotherapy* **2016**, *17*, 2391–2403, doi:10.1080/14656566.2016.1252332.
77. Shiels, M.S.; Islam, J.Y.; Rosenberg, P.S.; Hall, H.I.; Jacobson, E.; Engels, E.A. Projected Cancer Incidence Rates and Burden of Incident Cancer Cases in HIV-Infected Adults in the United States Through 2030. *Annals of Internal Medicine* **2018**, *168*, 866, doi:10.7326/M17-2499.
78. Arvey, A.; Ojesina, A.I.; Pedamallu, C.S.; Ballon, G.; Jung, J.; Duke, F.; Leoncini, L.; De Falco, G.; Bressman, E.; Tam, W.; et al. The Tumor Virus Landscape of AIDS-Related Lymphomas. *Blood* **2015**, *125*, e14–e22, doi:10.1182/blood-2014-11-599951.
79. Isaguliants, M.; Bayurova, E.; Avdoshina, D.; Kondrashova, A.; Chiodi, F.; Palefsky, J.M. Oncogenic Effects of HIV-1 Proteins, Mechanisms Behind. *Cancers (Basel)* **2021**, *13*, 305, doi:10.3390/cancers13020305.
80. Germini, D.; Tsfasman, T.; Klibi, M.; El-Amine, R.; Pichugin, A.; Iarovaia, O.V.; Bilhou-Nabera, C.; Subra, F.; Bou Saada, Y.; Sukhanova, A.; et al. HIV Tat Induces a Prolonged MYC Relocalization next to IGH in Circulating B-Cells. *Leukemia* **2017**, *31*, 2515–2522, doi:10.1038/leu.2017.106.
81. Rayne, F.; Debaisieux, S.; Yezid, H.; Lin, Y.-L.; Mettling, C.; Konate, K.; Chazal,

N.; Arold, S.T.; Pugnière, M.; Sanchez, F.; et al. Phosphatidylinositol-(4,5)-Bisphosphate Enables Efficient Secretion of HIV-1 Tat by Infected T-Cells. *EMBO J* **2010**, *29*, 1348–1362, doi:10.1038/emboj.2010.32.

82. Rothe, R.; Liguori, L.; Villegas-Mendez, A.; Marques, B.; Grunwald, D.; Drouet, E.; Lenormand, J.L. Characterization of the Cell-Penetrating Properties of the Epstein-Barr Virus ZEBRA Trans-Activator. *Journal of Biological Chemistry* **2010**, *285*, 20224–20233, doi:10.1074/jbc.M110.101550.
83. Colombrino, E.; Rossi, E.; Ballon, G.; Terrin, L.; Indraccolo, S.; Chieco-Bianchi, L.; De Rossi, A. Human Immunodeficiency Virus Type 1 Tat Protein Modulates Cell Cycle and Apoptosis in Epstein–Barr Virus-Immortalized B Cells. *Experimental Cell Research* **2004**, *295*, 539–548, doi:10.1016/j.yexcr.2004.01.018.
84. Cantaluppi, V.; Biancone, L.; Boccellino, M.; Doublier, S.; Benelli, R.; Carlone, S.; Albini, A.; Camussi, G. HIV Type 1 Tat Protein Is a Survival Factor for Kaposi's Sarcoma and Endothelial Cells. *AIDS Research and Human Retroviruses* **2001**, *17*, 965–976, doi:10.1089/088922201750290087.
85. Nunnari, G.; Smith, J.A.; Daniel, R. HIV-1 Tat and AIDS-Associated Cancer: Targeting the Cellular Anti-Cancer Barrier? *Journal of Experimental & Clinical Cancer Research* **2008**, *27*, 3, doi:10.1186/1756-9966-27-3.
86. Nyagol, J.; Leucci, E.; Onnis, A.; De Falco, G.; Tigli, C.; Sanseverino, F.; Torriccelli, M.; Palummo, N.; Pacenti, L.; Santopietro, R.; et al. The Effects of HIV-1 Tat Protein on Cell Cycle during Cervical Carcinogenesis. *Cancer biology & therapy* **2006**, *5*, 684–690.
87. Valyaeva, A.A.; Tikhomirova, M.A.; Potashnikova, D.M.; Bogomazova, A.N.; Snigiryova, G.P.; Penin, A.A.; Logacheva, M.D.; Arifulin, E.A.; Shmakova, A.A.; Germini, D.; et al. Ectopic Expression of HIV-1 Tat Modifies Gene Expression in Cultured B Cells: Implications for the Development of B-Cell Lymphomas in HIV-1-Infected Patients. *PeerJ* **2022**, *10*, e13986, doi:10.7717/peerj.13986.
88. El-Amine, R.; Germini, D.; Zakharova, V.V.; Tsfasman, T.; Sheval, E.V.; Louzada, R.A.N.; Dupuy, C.; Bilhou-Nabera, C.; Hamade, A.; Najjar, F.; et al. HIV-1 Tat Protein Induces DNA Damage in Human Peripheral Blood B-Lymphocytes via Mitochondrial ROS Production. *Redox Biology* **2018**, *15*, 97–108, doi:10.1016/j.redox.2017.11.024.
89. Huynh, D.; Vincan, E.; Mantamadiotis, T.; Purcell, D.; Chan, C.-K.; Ramsay, R. Oncogenic Properties of HIV-Tat in Colorectal Cancer Cells. *Current HIV research* **2007**, *5*, 403–409.
90. Toschi, E.; Barillari, G.; Sgadari, C.; Bacigalupo, I.; Cereseto, A.; Carlei, D.; Palladino, C.; Zietz, C.; Leone, P.; Stürzl, M.; et al. Activation of Matrix-Metalloproteinase-2 and Membrane-Type-1-Matrix-Metalloproteinase in Endothelial Cells and Induction of Vascular Permeability In Vivo by Human Immunodeficiency Virus-1 Tat Protein and Basic Fibroblast Growth Factor. *Molecular Biology of the Cell* **2001**, *12*, 2934–2946, doi:10.1091/mbc.12.10.2934.
91. Yang, W.-S.; Lin, T.-Y.; Chang, L.; Yeh, W.W.; Huang, S.-C.; Chen, T.-Y.; Hsieh, Y.-T.; Chen, S.-T.; Li, W.-C.; Pan, C.-C.; et al. HIV-1 Tat Interacts with a Kaposi's Sarcoma-Associated Herpesvirus Reactivation-Upregulated Antiangiogenic Long Noncoding RNA, LINC00313, and Antagonizes Its Function. *J Virol* **2020**, *94*, e01280-19, doi:10.1128/JVI.01280-19.
92. Mallon, R.; Borkowski, J.; Albin, R.; Pepitoni, S.; Schwartz, J.; Kieff, E. The Epstein-Barr Virus BZLF1 Gene Product Activates the Human Immunodeficiency Virus Type 1 5' Long Terminal Repeat. *J Virol* **1990**, *64*, 6282–6285, doi:10.1128/JVI.64.12.6282-6285.1990.

93. Howcroft, T.K.; Strebel, K.; Martin, M.A.; Singer, D.S. Repression of MHC Class I Gene Promoter Activity by Two-Exon Tat of HIV. *Science* **1993**, *260*, 1320–1322, doi:10.1126/science.8493575.
94. Quinn, L.L.; Williams, L.R.; White, C.; Forrest, C.; Zuo, J.; Rowe, M. The Missing Link in Epstein-Barr Virus Immune Evasion: The BDLF3 Gene Induces Ubiquitination and Downregulation of Major Histocompatibility Complex Class I (MHC-I) and MHC-II. *J Virol* **2015**, *90*, 356–367, doi:10.1128/JVI.02183-15.
95. Hewitt, E.W.; Duncan, L.; Mufti, D.; Baker, J.; Stevenson, P.G.; Lehner, P.J. Ubiquitylation of MHC Class I by the K3 Viral Protein Signals Internalization and TSG101-Dependent Degradation. *EMBO J* **2002**, *21*, 2418–2429, doi:10.1093/emboj/21.10.2418.
96. Buschle, A.; Mrozek-Gorska, P.; Krebs, S.; Blum, H.; Cernilogar, F.; Schotta, G.; Pich, D.; Straub, T.; Hammerschmidt, W. Epstein-Barr Virus Inactivates the Transcriptome and Disrupts the Chromatin Architecture of Its Host Cell in the First Phase of Lytic Reactivation. *bioRxiv* **2019**, 573659, doi:10.1101/573659.
97. Buschle, A.; Hammerschmidt, W. Epigenetic Lifestyle of Epstein-Barr Virus. *Seminars in Immunopathology* 2020, *42*, 131–142.
98. Flemington, E.; Speck, S.H. Autoregulation of Epstein-Barr Virus Putative Lytic Switch Gene BZLF1. *Journal of Virology* **1990**, *64*.
99. Rickinson, A.B.; Long, H.M.; Palendira, U.; Münz, C.; Hislop, A.D. Cellular Immune Controls over Epstein-Barr Virus Infection: New Lessons from the Clinic and the Laboratory. *Trends Immunol* **2014**, *35*, 159–169, doi:10.1016/j.it.2014.01.003.
100. Hislop, A.D.; Taylor, G.S.; Sauce, D.; Rickinson, A.B. Cellular Responses to Viral Infection in Humans: Lessons from Epstein-Barr Virus. *Annual Review of Immunology* **2007**, *25*, 587–617, doi:10.1146/annurev.immunol.25.022106.141553.
101. Taylor, G.S.; Long, H.M.; Brooks, J.M.; Rickinson, A.B.; Hislop, A.D. The Immunology of Epstein-Barr Virus-Induced Disease. *Annu Rev Immunol* **2015**, *33*, 787–821, doi:10.1146/annurev-immunol-032414-112326.
102. Burbelo, P.D.; Ching, K.H.; Morse, C.G.; Alevizos, I.; Bayat, A.; Cohen, J.I.; Ali, M.A.; Kapoor, A.; Browne, S.K.; Holland, S.M.; et al. Altered Antibody Profiles against Common Infectious Agents in Chronic Disease. *PLoS One* **2013**, *8*, e81635, doi:10.1371/journal.pone.0081635.
103. Petrara, M.R.; Freguja, R.; Gianesin, K.; Zanchetta, M.; De Rossi, A. Epstein-Barr Virus-Driven Lymphomagenesis in the Context of Human Immunodeficiency Virus Type 1 Infection. *Front Microbiol* **2013**, *4*, 311, doi:10.3389/fmicb.2013.00311.
104. Righetti, E.; Ballon, G.; Ometto, L.; Cattelan, A.M.; Menin, C.; Zanchetta, M.; Chieco-Bianchi, L.; De Rossi, A. Dynamics of Epstein-Barr Virus in HIV-1-Infected Subjects on Highly Active Antiretroviral Therapy. *AIDS* **2002**, *16*, 63–73, doi:10.1097/00002030-200201040-00009.
105. Kersten, M.J.; Klein, M.R.; Holwerda, A.M.; Miedema, F.; van Oers, M.H. Epstein-Barr Virus-Specific Cytotoxic T Cell Responses in HIV-1 Infection: Different Kinetics in Patients Progressing to Opportunistic Infection or Non-Hodgkin's Lymphoma. *J Clin Invest* **1997**, *99*, 1525–1533.
106. Nijland, M.; Veenstra, R.N.; Visser, L.; Xu, C.; Kushekhar, K.; van Imhoff, G.W.; Kluin, P.M.; van den Berg, A.; Diepstra, A. HLA Dependent Immune Escape Mechanisms in B-Cell Lymphomas: Implications for Immune Checkpoint Inhibitor Therapy? *Oncoimmunology* **2017**, *6*, e1295202, doi:10.1080/2162402X.2017.1295202.
107. de Charette, M.; Houot, R. Hide or Defend, the Two Strategies of Lymphoma

Immune Evasion: Potential Implications for Immunotherapy. *Haematologica* **2018**, *103*, 1256–1268, doi:10.3324/haematol.2017.184192.
108. Piriou, E.; Jansen, C.A.; van Dort, K.; De Cuyper, I.; Nanlohy, N.M.; Lange, J.M.A.; van Oers, M.H.J.; Miedema, F.; van Baarle, D. Reconstitution of EBV Latent but Not Lytic Antigen-Specific CD4+ and CD8+ T Cells after HIV Treatment with Highly Active Antiretroviral Therapy. *J Immunol* **2005**, *175*, 2010–2017, doi:10.4049/jimmunol.175.3.2010.
109. Martorelli, D.; Muraro, E.; Mastorci, K.; Dal Col, J.; Faè, D.A.; Furlan, C.; Giagulli, C.; Caccuri, F.; Rusnati, M.; Fiorentini, S.; et al. A Natural HIV P17 Protein Variant Up-Regulates the LMP-1 EBV Oncoprotein and Promotes the Growth of EBV-Infected B-Lymphocytes: Implications for EBV-Driven Lymphomagenesis in the HIV Setting. *Int J Cancer* **2015**, *137*, 1374–1385, doi:10.1002/ijc.29494.

Figures and figure legends

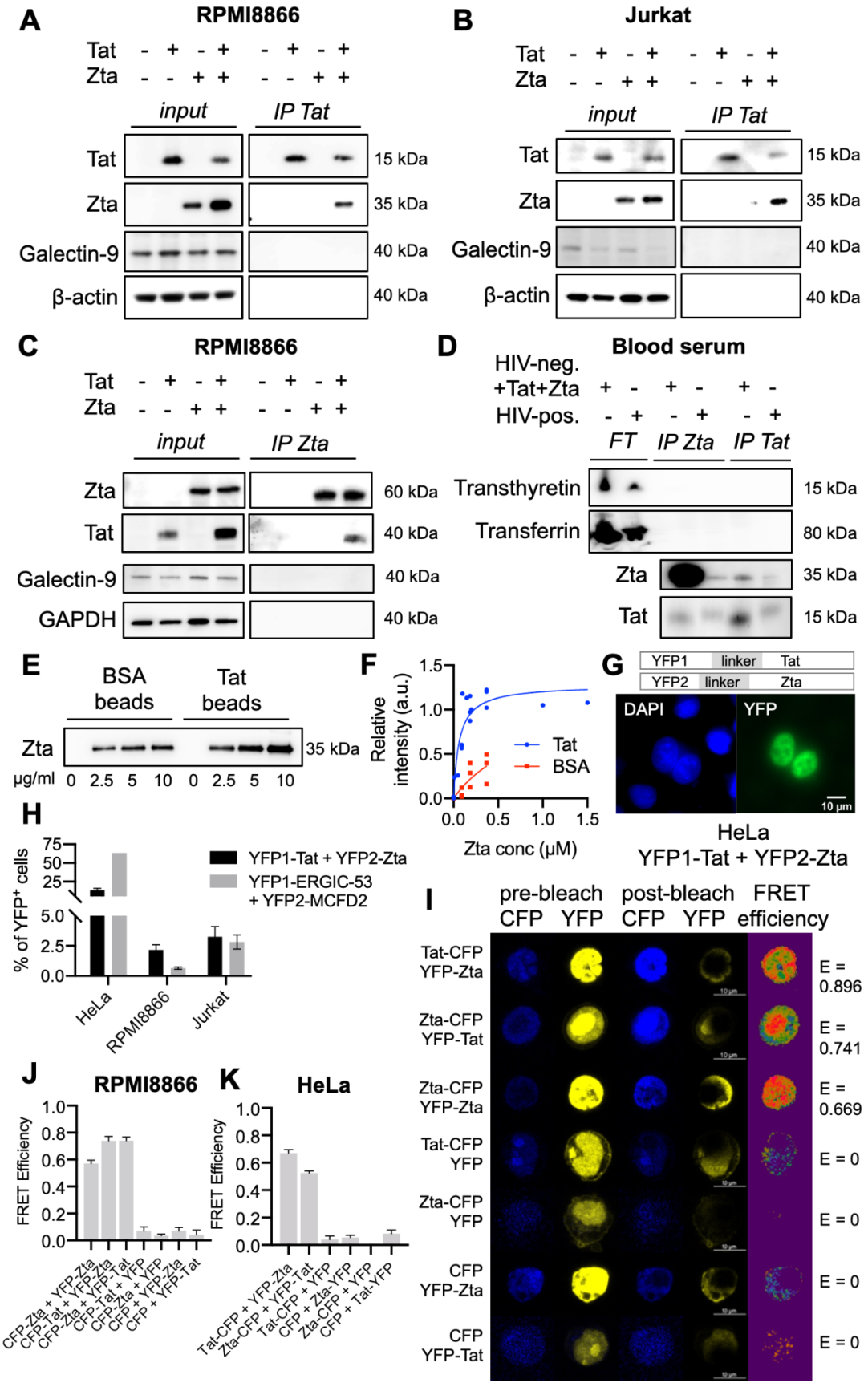

Figure 1. HIV-1 Tat and EBV Zta physically interact in B cells, T cells and human serum. **(A)** Immunoprecipitation of Tat in B cells. The RPMI8866 lymphoblastoid cell line inducibly expressing unconjugated HIV-1 Tat (RPMI8866 Tat^{i} cell line) upon treatment with Doxycycline (Tat) was treated or not with 1 μg/ml recombinant Zta protein. Cell lysates were subjected to immunoprecipitation using anti-Tat antibodies. Input and immunoprecipitated fractions were analysed by western blotting staining for Tat, Zta, Galectin 9 (negative control) and β-actin (control of protein load). **(B)** Immunoprecipitation of Tat in T cells. The Jurkat-Tat cell line expressing unconjugated Tat and the wild-type Jurkat T cell line were treated or not with 1 μg/ml recombinant Zta protein for 24 hours. Cell lysates were immunoprecipitated using anti-Tat antibodies. Input and immunoprecipitated fractions were analysed by western blotting staining for Tat, Zta, Galectin 9 (negative control) and β-actin (control of protein load). **(C)** Immunoprecipitation of Zta in B cells. The RPMI8866 lymphoblastoid cells were transfected with YFP-Tat (Tat) and/or mCherry-Zta (Zta), followed by immunoprecipitation of Zta using anti-Zta antibodies after 24 hours. Input and immunoprecipitated fractions were analysed by western blotting staining for Tat, Zta, Galectin 9 (negative control) and GAPDH (control of protein load). (**D)** A healthy donor (HIV-negative) serum sample supplemented with Tat and Zta (at 250 ng/ml and 1000 ng/ml, respectively, HIV-neg. + Tat + Zta) and a serum sample from an HIV-positive individual (HIV-pos.) were immunoprecipitated using Protein G magnetic beads cross-linked with anti-Zta or anti-Tat antibodies. Immunoprecipitated (IP) and non-immunoprecipitated flowthrough (FT) fractions were analysed by Western blotting staining for Zta, Tat, transferrin (negative control) and transthyretin (negative control). **(E, F)** Analysis of Tat and Zta interaction by an in vitro binding assay. Equal amounts of recombinant HIV-1 Tat protein linked to AminoLink agarose beads or BSA control agarose beads were incubated with increasing amounts of recombinant Zta protein. **(E)** Bound protein was separated on SDS-PAGE gel and bound Zta was then analysed by Western blotting staining. A representative image is shown. **(F)** The non-linear fit of Zta binding to Tat (densitometry analysis of western blotting band intensity of bound Zta) against Zta concentration in solution with one site-specific binding model. Zta binding at concentration 0.2 μM was set as 1 (fraction bound). **(G, H)** Tat and Zta interaction analysed by YFP reconstitution. **(G)** The modular composition of the fusion proteins used in this study (above). A representative image of HeLa cells after transfection with YFP1-Tat and YFP2-Zta plasmids, nuclei were counterstained with DAPI, scale bar 10 μm (below). **(H)** The percentage of YFP-positive cells in HeLa, RPMI8866 or Jurkat cells transfected with YFP1-Tat + YFP2-Zta or YFP1-ERGIC-53 and YFP2-MCFD2 (positive control) as analysed by flow cytometry. **(I-K)** The analysis of Tat and Zta interaction by FRET with acceptor photobleaching method. (I) Representative images of RPMI8866 cells, transfected with different combinations of CFP, YFP, Tat-CFP and YFP-Zta. Scale bar 10 μm. **(J-K)** FRET efficiencies for each combination in HeLa **(J)** and RPMI8866 **(K)** cells. Data are presented as mean ± SEM.

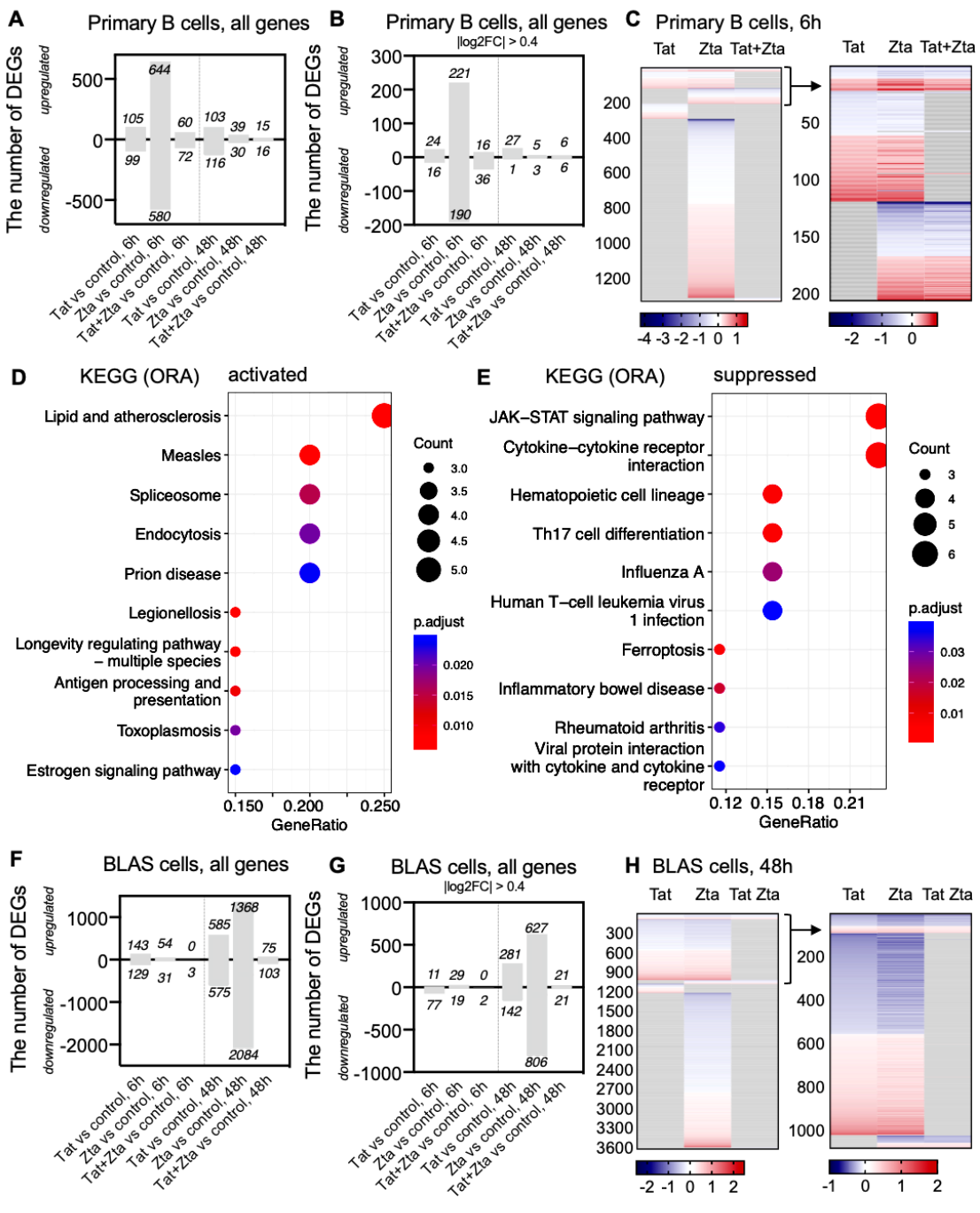
A
Primary B cells, all genes
The number of DEGs
upregulated
downregulated
Tat vs control, 6h
Zta vs control, 6h
Tat+Zta vs control, 6h
Tat vs control, 48h
Zta vs control, 48h
Tat+Zta vs control, 48h
B
Primary B cells, all genes
|log2FC| > 0.4
C
Primary B cells, 6h
Tat
Zta
Tat+Zta
D
KEGG (ORA)
activated
Lipid and atherosclerosis
Measles
Spliceosome
Endocytosis
Prion disease
Legionellosis
Longevity regulating pathway – multiple species
Antigen processing and presentation
Toxoplasmosis
Estrogen signaling pathway
GeneRatio
Count
p.adjust
E
KEGG (ORA)
suppressed
JAK–STAT signaling pathway
Cytokine–cytokine receptor interaction
Hematopoietic cell lineage
Th17 cell differentiation
Influenza A
Human T–cell leukemia virus 1 infection
Ferroptosis
Inflammatory bowel disease
Rheumatoid arthritis
Viral protein interaction with cytokine and cytokine receptor
F
BLAS cells, all genes
G
BLAS cells, all genes
|log2FC| > 0.4
H
BLAS cells, 48h
I
KEGG (ORA)
activated
MAPK signaling pathway
Lipid and atherosclerosis
Protein processing in endoplasmic reticulum
HIF–1 signaling pathway
Measles
AGE–RAGE signaling pathway in diabetic complications
Neurotrophin signaling pathway
FoxO signaling pathway
ErbB signaling pathway
Small cell lung cancer
J
KEGG (ORA)
suppressed
Amyotrophic lateral sclerosis
Pathways of neurodegeneration – multiple diseases
Huntington disease
Alzheimer disease
Parkinson disease
Prion disease
Oxidative phosphorylation
DNA replication
Proteasome
Glycosaminoglycan biosynthesis – chondroitin sulfate / dermatan sulfate

Figure 2. Tat and Zta regulate gene expression in B cells. **(A-E)** RNA-sequencing of primary B cells treated with Tat (at 250 ng/ml), Zta (1000 ng/ml) or Tat and Zta together (at 250 ng/ml and 1000 ng/ml, respectively) for 6 hours and 48 hours. **(A)** The number of all differentially expressed genes (DEGs) in B cells treated with Tat, Zta or Tat and Zta in comparison vs untreated B cells. **(B)** The number of all DEGs with |log2 fold change| > 0.4 in B cells treated with Tat, Zta or Tat and Zta in comparison vs untreated B cells. **(C)** A heatmap of subsets of significantly deregulated genes in primary B cells treated with Tat, Zta or Tat and Zta for 6h. The colour code is used to illustrate the direction of expression modulation: upregulation (red) and downregulation (blue). Gray stands for unchanged gene expression relative to untreated control B cells. **(D)** Overrepresentation analysis of upregulated DEGs, overlapping between Tat and Zta vs untreated control in primary B cells after 6 hours of treatment, excluding the DEGs deregulated by combined Tat and Zta action vs untreated control. The top 10 significantly overrepresented KEGG functional categories are shown. **(E)** Overrepresentation analysis of downregulated DEGs, overlapping between Tat and Zta vs untreated control in primary B cells after 6 hours of treatment, excluding the DEGs deregulated by combined Tat and Zta action vs untreated control. The top 10 significantly overrepresented KEGG functional categories are shown. **(F-J)** RNA-sequencing of BLAS cells treated with Tat (at 250 ng/ml), Zta (1000 ng/ml) or Tat and Zta together (at 250 ng/ml and 1000 ng/ml, respectively) for 6 hours and 48 hours. **(F)** The number of all differentially expressed genes (DEGs) in BLAS cells treated with Tat, Zta or Tat and Zta in comparison vs untreated BLAS cells. **(G)** The number of all DEGs with |log2 fold change| > 0.4 in BLAS cells treated with Tat, Zta or Tat and Zta in comparison vs untreated BLAS cells. **(H)** A heatmap of subsets of significantly deregulated genes in BLAS cells treated with Tat, Zta or Tat and Zta for 48h. The colour code is used to illustrate the direction of expression modulation: upregulation (red) and downregulation (blue). Gray stands for unchanged gene expression relative to untreated control BLAS cells. **(I)** Overrepresentation analysis of upregulated DEGs, overlapping between Tat and Zta vs untreated control in BLAS cells after 48 hours of treatment, excluding the DEGs deregulated by combined Tat and Zta action vs untreated control. The top 10 significantly overrepresented KEGG functional categories are shown. **(J)** Overrepresentation analysis of downregulated DEGs, overlapping between Tat and Zta vs untreated control in BLAS cells after 48 hours of treatment, excluding the DEGs deregulated by combined Tat and Zta action vs untreated control. The top 10 significantly overrepresented KEGG functional categories are shown.

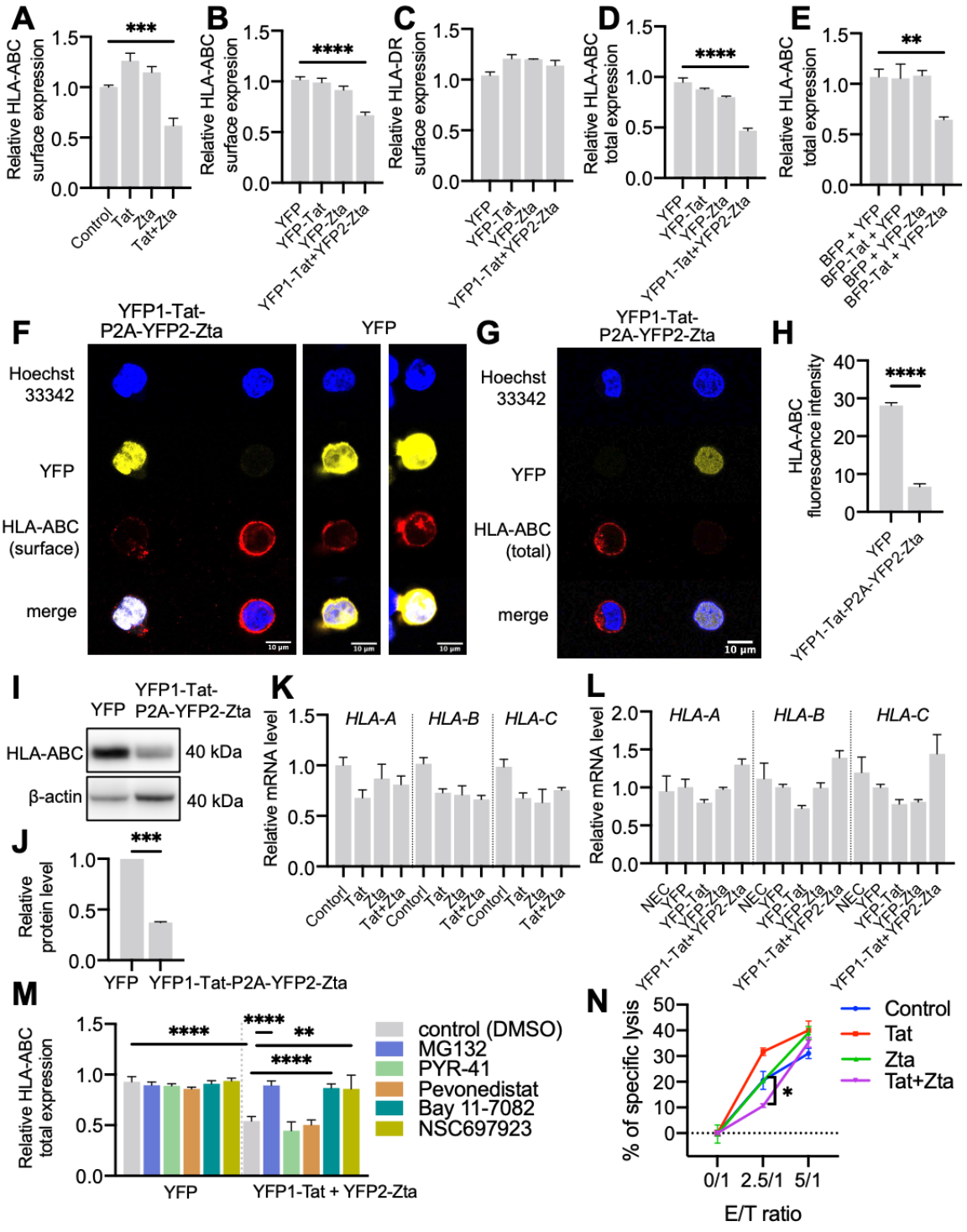

Figure 3. Tat and Zta interaction decreased total HLA-ABC protein level in lymphoblastoid B cells. **(A)** The level of HLA-ABC surface expression in BLAS cells treated for 48 hours with Tat (250 ng/ml), Zta (1000 ng/ml) or Tat and Zta together (at the same concentrations). Non-treated cells were used as a control. **(B)** The level of HLA-ABC surface expression 48 hours after transfection of RPMI8866 with YFP, YFP-Tat, YFP-Zta, YFP1-Tat+YFP2-Zta as analyzed by flow cytometry. The ratio of HLA-ABC surface expression in YFP+ population relative to YFP- population was

analysed. **(C)** The level of HLA-DR surface expression 48 hours after transfection of RPMI8866 with YFP, YFP-Tat, YFP-Zta, YFP1-Tat+YFP2-Zta as analyzed by flow cytometry. The ratio of HLA-ABC surface expression in YFP+ population relative to YFP- population was analysed. **(D)** The level of HLA-ABC total expression 48 hours after transfection of RPMI8866 with YFP, YFP-Tat, YFP-Zta, YFP1-Tat+YFP2-Zta as analyzed by flow cytometry. The ratio of HLA-ABC surface expression in YFP+ population relative to YFP- population was analysed. **(E)** The level of HLA-ABC total expression 48 hours after transfection of RPMI8866 with BFP + YFP, BFP-Tat + YFP, BFP + YFP-Zta, BFP-Tat + YFP-Zta as analyzed by flow cytometry. HLA-ABC total level in BFP+/YFP+ cells compared to BFP-/YFP- cells was analysed. **(F)** A representative confocal image of the level of HLA-ABC surface expression in inducible RPMI8866 cell lines expressing YFP1-Tat-P2A-YFP2-Zta or YFP analysed by immunofluorescent staining. **(G)** A representative confocal image of the total level of HLA-ABC expression in the inducible RPMI8866 cell lines expressing YFP1-Tat-P2A-YFP2-Zta analysed by immunofluorescent staining. **(H)** The mean fluorescence intensity of surface HLA-ABC around the cell surface as defined by YFP channel in inducible RPMI8866 cell lines expressing YFP1-Tat-P2A-YFP2-Zta or YFP. **(I)** Western blotting analysis of HLA-ABC content in inducible RPMI8866 cell lines expressing YFP1-Tat-P2A-YFP2-Zta or YFP. β-actin was used as a loading control. A reproducible result is presented. **(G)** Densitometry analysis of HLA-ABC content normalized to β-actin in inducible RPMI8866 cell lines expressing YFP1-Tat-P2A-YFP2-Zta or YFP. **(K)** The levels of *HLA-A*, *HLA-B*, and *HLA-C* mRNA in BLAS cells treated for 48 hours with Tat (250 ng/ml), Zta (1000 ng/ml) or Tat and Zta together (at the same concentrations). Non-treated cells were used as a control. The mRNA level was normalized to *GAPDH* expression as a housekeeping gene; the normalization was done assuming the mean level of transcript in control cells to be 1. **(L)** The levels of *HLA-A*, *HLA-B*, and *HLA-C* mRNA in RPMI8866 cells 48 hours after transfection with YFP, YFP-Tat, YFP-Zta, YFP1-Tat+YFP2-Zta. YFP-positive cells were sorted for analysis. Non-electrotransfected control (NEC) RPMI8866 cells were also analysed. The mRNA level was normalized to *GAPDH* expression as a housekeeping gene; the normalization was done assuming the mean level of transcript in cells expressing YFP to be 1. **(M)** The level of HLA-ABC total expression as analyzed by flow cytometry in RPMI8866 cells 48 hours after transfection with YFP or YFP1-Tat+YFP2-Zta, cells were treated or not for 8 hours with the indicated inhibitors of the ubiquitin-proteasomal system. The ratio of HLA-ABC surface expression in YFP+ population relative to YFP- population was analysed. **(N)** Percentage of specific lysis of BLAS cells pre-treated or not for 48 hours with Tat (250 ng/ml), Zta (1000 ng/ml) or Tat and Zta together (at the same concentrations) and co-cultivated with BLAS-reactive EBV-specific cytotoxic T cell line at various E/T ratios for 4h. Data are presented as mean ± SEM, * $p < 0.05$, ** $p < 0.01$, *** $p < 0.001$, **** $p < 0.0001$, (A-E, K-M) ANOVA, Tukey's posthoc test, (H, J) t-test, (N) two-way ANOVA, Tukey's posthoc test.

Supplementary figures

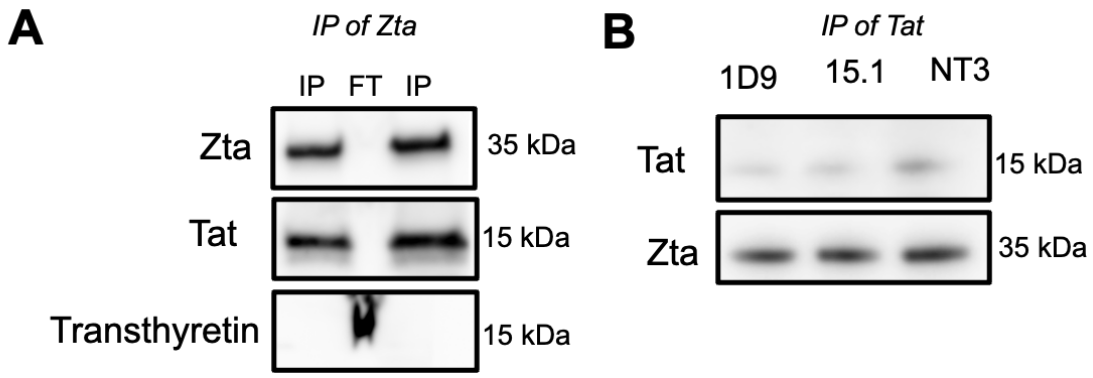

Supplementary figure 1. Tat and Zta interaction analysed by co-immunoprecipitation from human serum. **(A)** Healthy donor serum was supplemented with Tat and Zta (at 250 ng/ml and 1000 ng/ml, respectively), incubated for 2h at room temperature and immunoprecipitated for Zta using Protein G magnetic beads cross-linked with anti-Zta antibodies. Immunoprecipitated (IP) and non-immunoprecipitated flowthrough (FT) fractions are analysed by Western blotting staining for Zta, Tat and transthyretin. **(B)** Healthy donor serum was supplemented with Tat and Zta (both at 250 ng/ml), incubated for 2h at room temperature and immunoprecipitated for Tat using Protein G magnetic beads cross-linked with different anti-Tat antibodies (1D9, 15.1, NT3, all from the NIH HIV Reagent Program, Division of AIDS, NIAID, NIH and Centre for AIDS Reagents). Immunoprecipitated (IP) fractions were analysed by Western blotting staining for Tat and Zta.

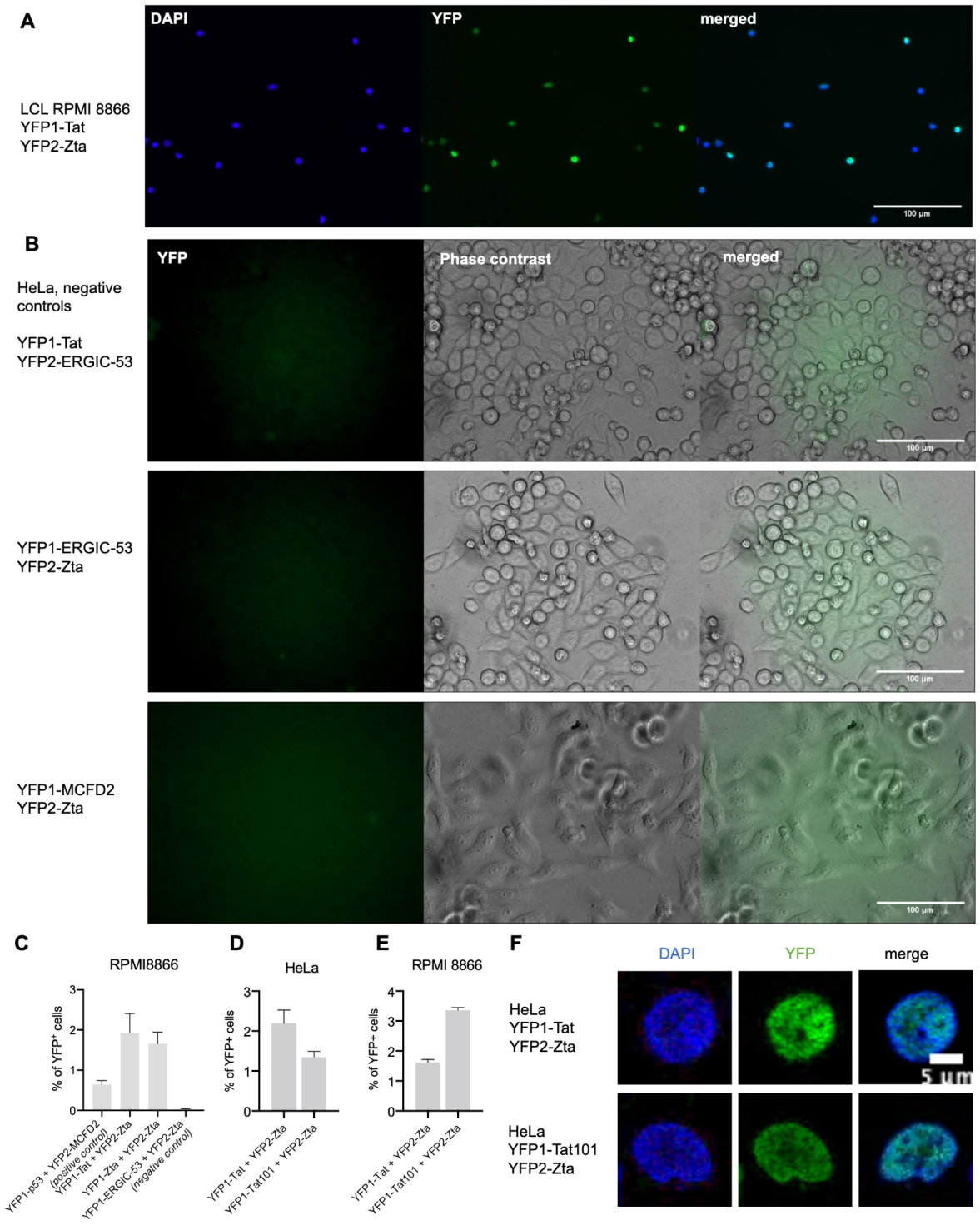

Supplementary figure 2. YFP reconstitution analysis in cells expressing the indicated split YFP constructs. **(A)** A representative image of RPMI8866 cells after transfection with YFP1-Tat and YFP2-Zta plasmids; nuclei were counterstained with DAPI. Scale bar 100 µm. **(B)** A representative image of HeLa cells transfected with YFP1-Tat&YFP2-ERGIC-53, YFP1-ERGIC-53&YFP2-Zta, YFP1-MCFD2&YFP2-Zta (negative controls). Scale bar 100 µm. **(C)** The percentage of YFP-positive cells evaluated in RPMI8866 cells transfected with different split YFP constructs by flow cytometry

analysis. **(D-F)** Both Tat short (86 residues) and Tat long (101 residues) interact with Zta as analyzed by YFP reconstitution. **(D)** The percentage of YFP-positive cells evaluated in HeLa cells transfected with YFP1-Tat + YFP2-Zta or YFP1-Tat101 + YFP2-Zta plasmid combinations by flow cytometry analysis. **(E)** The percentage of YFP-positive cells evaluated in RPMI8866 cells transfected with YFP1-Tat + YFP2-Zta or YFP1-Tat101 + YFP2-Zta plasmid combinations by flow cytometry analysis. **(F)** A representative image of HeLa cells after transfection with YFP1-Tat / YFP1-Tat101 and YFP2-Zta plasmids, nuclei were counterstained with DAPI. Scale bar 5 μm. Data are represented as means ± SEM.

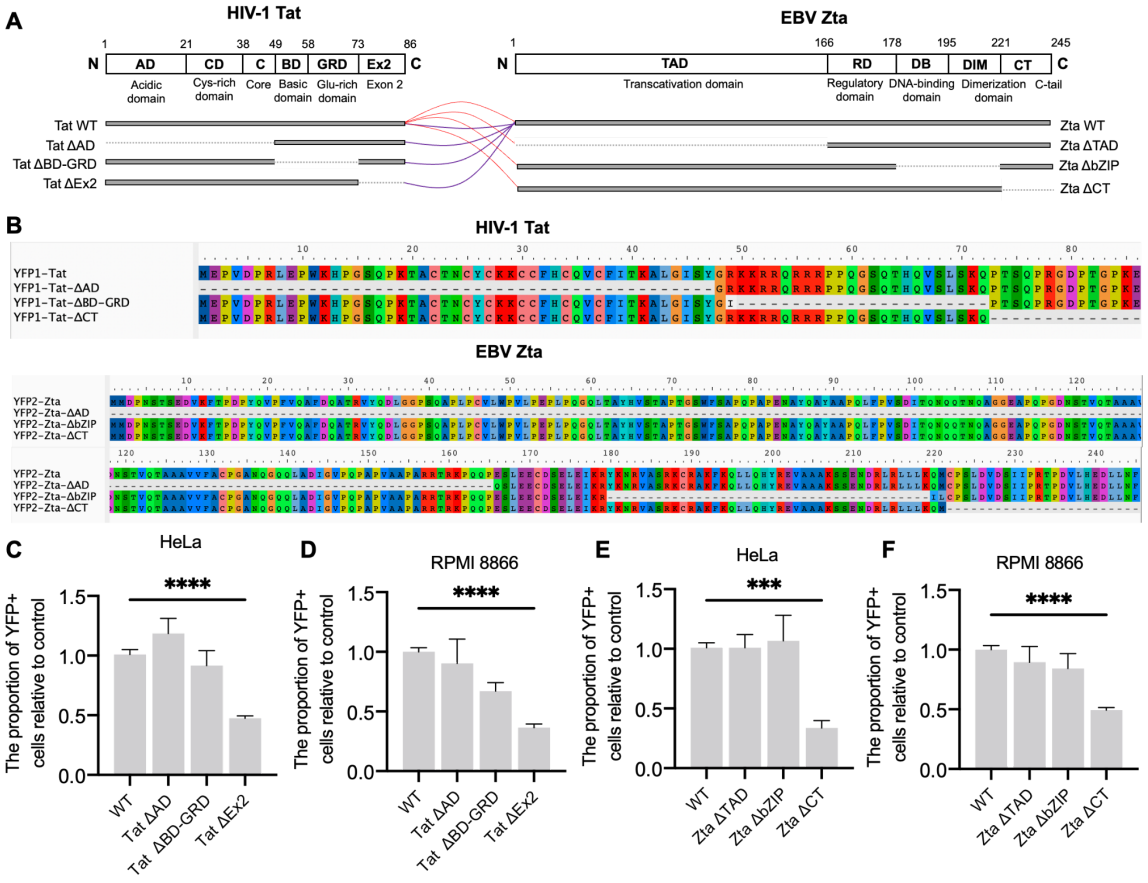

Supplementary figure 3. The analysis of domains of interaction between HIV-1 Tat and EBV Zta by YFP reconstitution technique. **(A)** The schematic structure of Tat and Zta and protein sequences of mutated their variants, lacking key domains. **(B)** Amino acid sequences of proteins, encoded by cloned YFP1/YFP2 plasmids with confirmed sequence. **(C-F)** HeLa and RPMI 8866 cells were transfected with different sets of two plasmids YFP1-Tat mutated + YFP2-Zta WT **(C, D)** or YFP1-Tat WT + YFP2-Zta mutated (**E, F**). The mean ± SEM percentage of YFP-positive cells normalized to the percentage of YFP-positive cells in YFP1-Tat WT + YFP2-Zta WT control within each experiment is presented. At least 3 independent biological experiments were performed. *** $p < 0.001$, **** $p < 0.0001$, ANOVA, Tukey post-hoc.

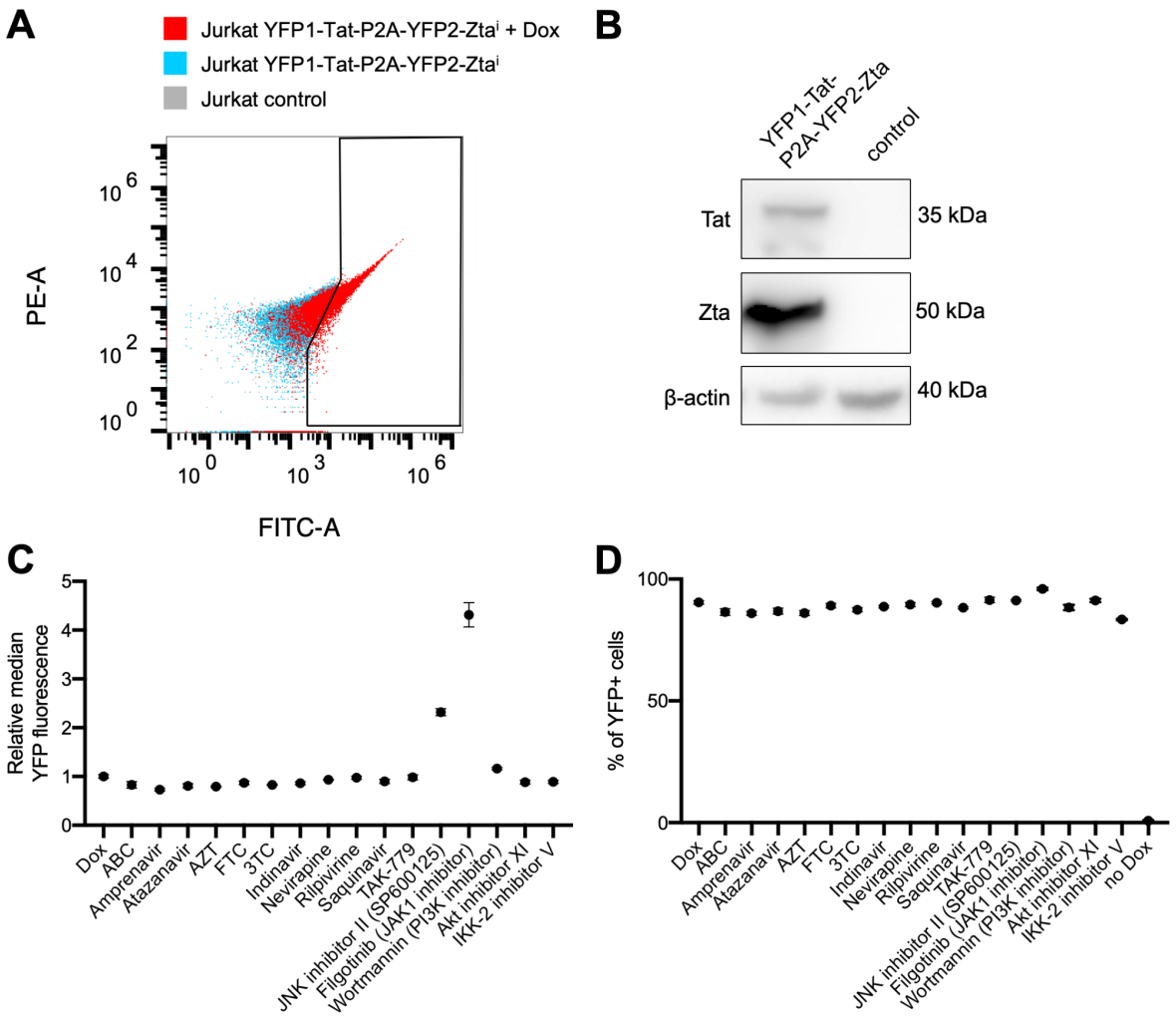

Supplementary figure 4. The effect of antiretroviral drugs and other inhibitors on Tat and Zta interaction assessed by YFP reconstitution assay. **(A)** A representative flow cytometry dot plot of Jurkat T cell line with inducible expression of YFP1-Tat-P2A-YFP2-Zta with (red) and without (blue) doxycycline (Dox) treatment for 24 hours, wild-type Jurkat cells were used as a control (grey). **(B)** Western blotting analysis of YFP1-Tat and YFP2-Zta expression and efficient YFP1-Tat-P2A-YFP2-Zta cleavage in Jurkat cell line with inducible expression of YFP1-Tat-P2A-YFP2-Zta after doxycycline treatment for 24 hours. As a reference, the control Jurkat cell line was analysed. β-actin was used as a loading control. **(C, D)** Jurkat T cells were treated with antiretroviral drugs and other inhibitors simultaneously with the induction of YFP1-Tat-P2A-YFP2-Zta expression by Dox treatment for 24 hours. The median YFP fluorescence intensity relative to Dox-treated cells **(C)** and the percentage of YFP-positive cells were analysed **(D)**. Data are presented as mean ± SEM.

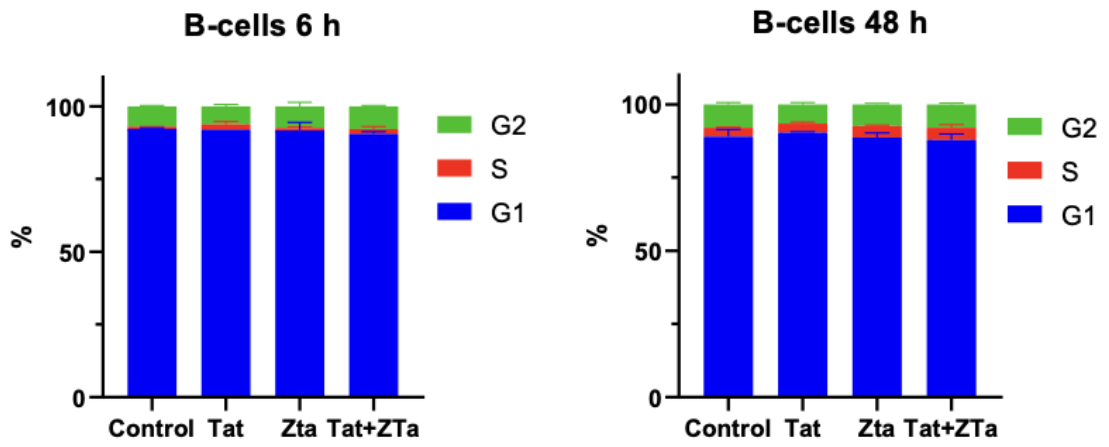

Supplementary figure 5. The analysis of cell cycling in primary B cells treated with Tat, Zta, or Tat and Zta for various time periods. Percentages of cells in the G1, S, and G2 cycle phases are represented as mean ± SEM.

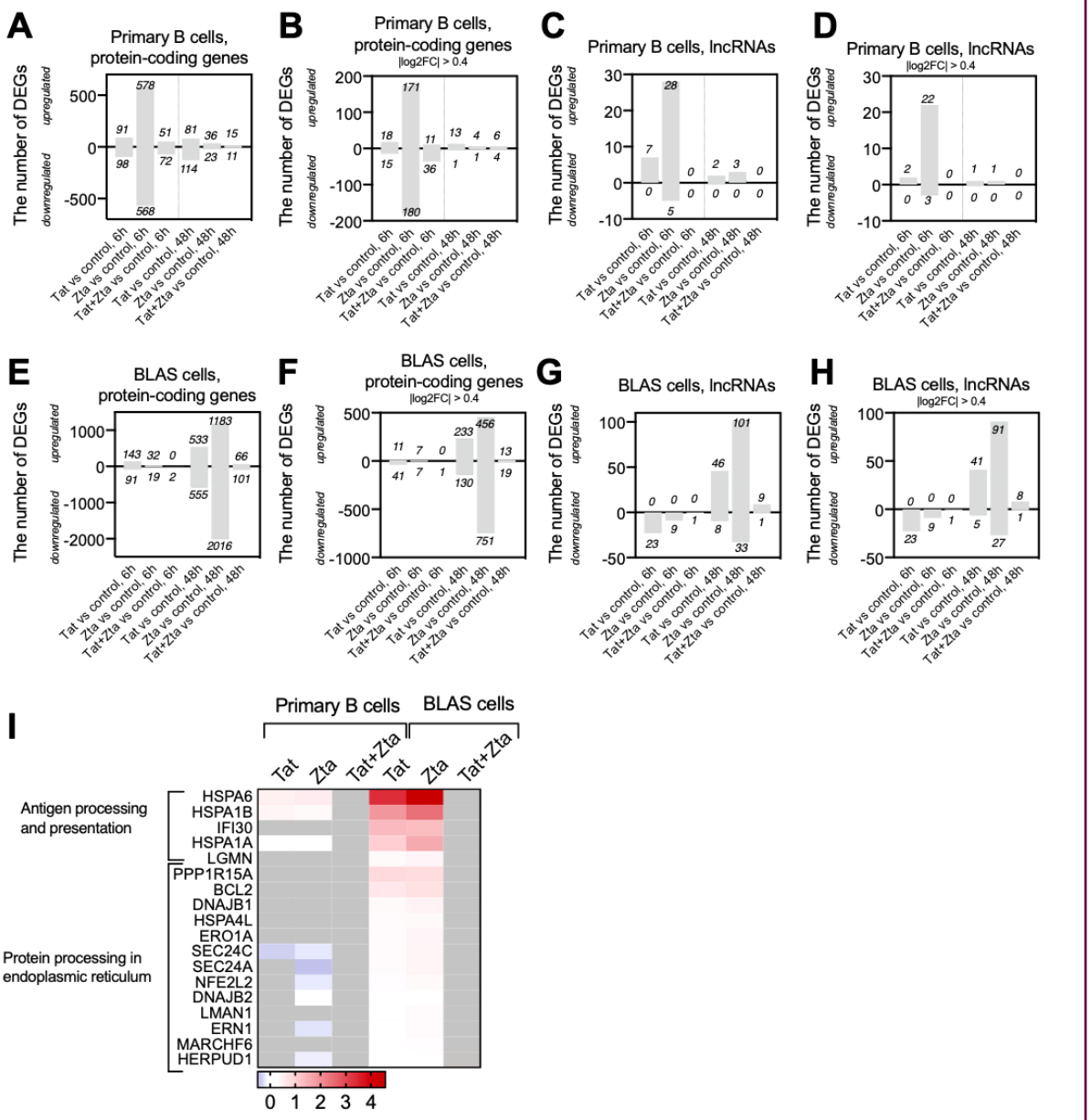

Supplementary figure 6. Tat and Zta regulate gene expression in B cells. **(A-D)** RNA-sequencing of primary B cells treated with Tat (at 250 ng/ml), Zta (1000 ng/ml) or Tat and Zta together (at 250 ng/ml and 1000 ng/ml, respectively) for 6 hours and 48 hours. **(A)** The number of protein-coding differentially expressed genes (DEGs) in B cells treated with Tat, Zta or Tat and Zta in comparison vs untreated B cells. **(B)** The number of protein-coding DEGs with |log2 fold change| > 0.4 in B cells treated with Tat, Zta or Tat and Zta in comparison vs untreated B cells. **(C)** The number of DEGs encoding long non-coding RNAs (lncRNAs) in B cells treated with Tat, Zta or Tat and Zta in comparison vs untreated B cells. **(D)** The number of DEGs encoding lncRNAs with |log2 fold change| > 0.4 in B cells treated with Tat, Zta or Tat and Zta in comparison vs untreated B cells. **(E-H)** RNA-sequencing of freshly EBV-transformed B cells (BLAS) treated with Tat (at 250 ng/ml), Zta (1000 ng/ml) or Tat and Zta together (at 250 ng/ml and 1000 ng/ml, respectively) for 6 hours and 48 hours. **(E)** The number of protein-coding DEGs in BLAS

cells treated with Tat, Zta or Tat and Zta in comparison vs untreated BLAS cells. **(F)** The number of protein-coding DEGs with |log2 fold change| > 0.4 in BLAS cells treated with Tat, Zta or Tat and Zta in comparison vs untreated BLAS cells. **(G)** The number of DEGs encoding long non-coding RNAs (lncRNAs) in BLAS cells treated with Tat, Zta or Tat and Zta in comparison vs untreated BLAS cells. **(H)** The number of DEGs encoding lncRNAs with |log2 fold change| > 0.4 in BLAS cells treated with Tat, Zta or Tat and Zta in comparison vs untreated BLAS cells. **(I)** A heatmap of significantly deregulated genes from antigen processing and presentation and protein processing in endoplasmic reticulum KEGG functional categories in primary B cells treated with Tat, Zta or Tat and Zta and BLAS cells treated with Tat, Zta or Tat and Zta for 48h. The colour code is used to illustrate the direction of expression modulation: upregulation (red) and downregulation (blue). Gray stands for unchanged gene expression relative to untreated control B cells or BLAS cells.

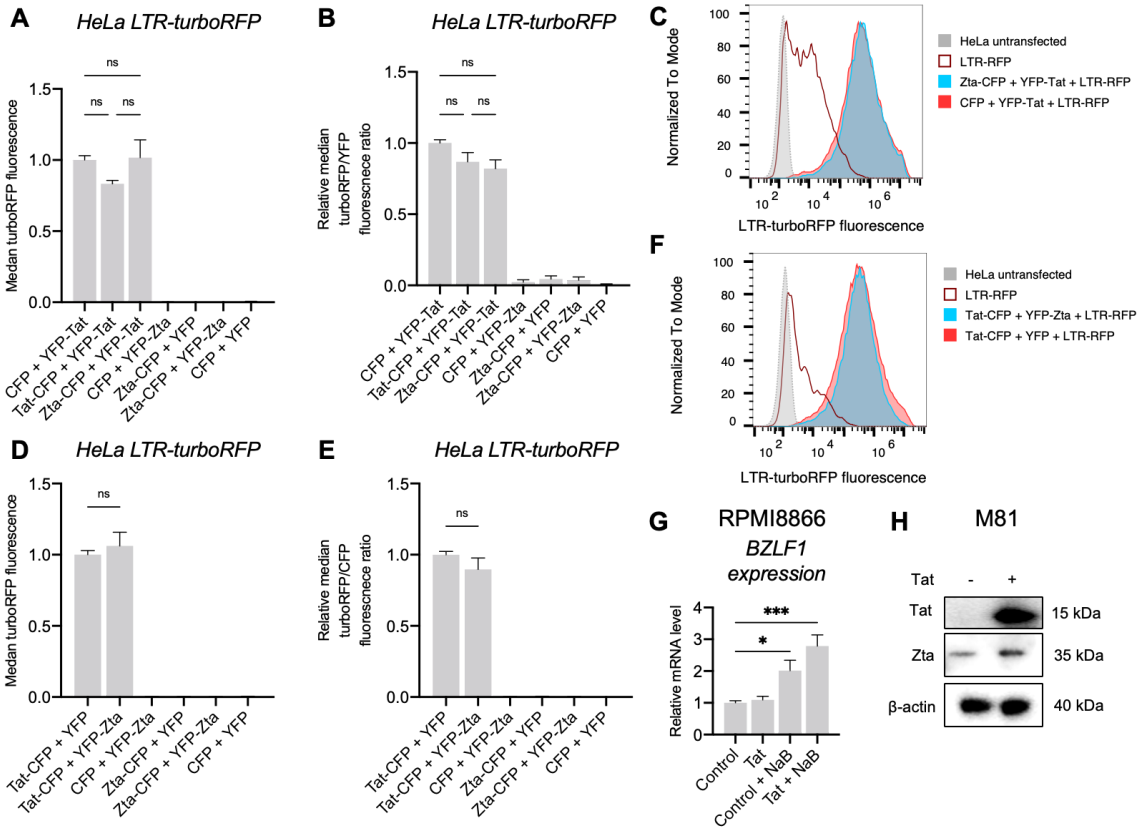

Supplementary figure 7. The effect of Zta on Tat-activated LTR-driven transcription and the effect of Tat on EBV reactivation. **(A-F)** HeLa cells were transfected with the different combinations of plasmids encoding CFP, Tat-CFP, Zta-CFP, YFP, YFP-Tat, YFP-Zta and LTR-turboRFP; turboRFP fluorescence was analysed 24 hours after transfection. **(A)** The level of turboRFP fluorescence in HeLa cells transfected with LTR-turboRFP and combinations of plasmids that involved YFP-Tat (with CFP, Tat-CFP or Zta-CFP). The combinations of plasmids without Tat (CFP, YFP, Zta-CFP or YFP-Tat) were used as a control. The level of turboRFP fluorescence was by several magnitudes higher in cells transfected with Tat. TurboRFP fluorescence was calculated as the median fluorescence

intensity in the sample normalized relative to the median fluorescence intensity in the control (HeLa cells transfected with CFP + YFP-Tat), averaged data from at least three biologically independent experiments are shown. **(B)** The level of turboRFP fluorescence in HeLa cells transfected with LTR-turboRFP and combinations of plasmids that involved YFP-Tat (with CFP, Tat-CFP or Zta-CFP) normalized to YFP fluorescence (to control for the expression level of Tat). Relative TurboRFP fluorescence was calculated as the ratio of median fluorescence intensity of turboRFP in the sample normalized to the median fluorescence intensity of YFP in the same sample and normalised to the same ratio in the control (HeLa cells transfected with CFP + YFP-Tat), averaged data from at least three biologically independent experiments are shown. **(C)** A representative flow cytometry histogram of LTR-driven turboRFP fluorescence in HeLa cells transfected with LTR-turbRFP alone (red contour) or in combination with CFP + YFP-Tat (red) or Zta-CFP + YFP-Tat (blue). Untransfected HeLa cells are shown for comparison (grey). **(D)** The level of turboRFP fluorescence in HeLa cells transfected with LTR-turboRFP and combinations of plasmids that involved Tat-CFP (with YFP, YFP-Tat or YFP-Zta). The combinations of plasmids without Tat (CFP, YFP, Zta-CFP or YFP-Tat) were used as a control. TurboRFP fluorescence was calculated as the median fluorescence intensity in the sample normalized relative to the median fluorescence intensity in the control (HeLa cells transfected with CFP + YFP-Tat), averaged data from at least three biologically independent experiments are shown. **(E)** The level of turboRFP fluorescence in HeLa cells transfected with LTR-turboRFP and combinations of plasmids that involved Tat-CFP (with YFP, YFP-Tat or YFP-Zta) normalized to CFP fluorescence (to control for the expression level of Tat). Relative TurboRFP fluorescence was calculated as the ratio of median fluorescence intensity of turboRFP in the sample normalized to the median fluorescence intensity of CFP in the same sample and normalised to the same ratio in the control (HeLa cells transfected with Tat-CFP + YFP), averaged data from at least three biologically independent experiments are shown. **(F)** A representative flow cytometry histogram of LTR-driven turboRFP fluorescence in HeLa cells transfected with LTR-turbRFP alone (red contour) or in combination with Tat-CFP + YFP (red) or Tat-CFP + YFP-Zta (blue). Untransfected HeLa cells are shown for comparison (grey). **(G)** RPMI8866 Tat^{i} cells were treated for 48h with sodium butyrate (NaB) to reactivate EBV with or without concomitant induction of HIV-1 Tat expression by doxycycline treatment. *BZLF1* mRNA expression was used as the marker of EBV reactivation. **(H)** M81 cells show with spontaneous EBV lytic activity were treated or not with recombinant Tat protein (250 ng/ml) and Zta protein expression was used as the marker of EBV reactivation. Data are represented as mean ± SEM. ns, not-significant, * $p < 0.05$, *** $p < 0.001$, ANOVA, Tukey's post-hoc.

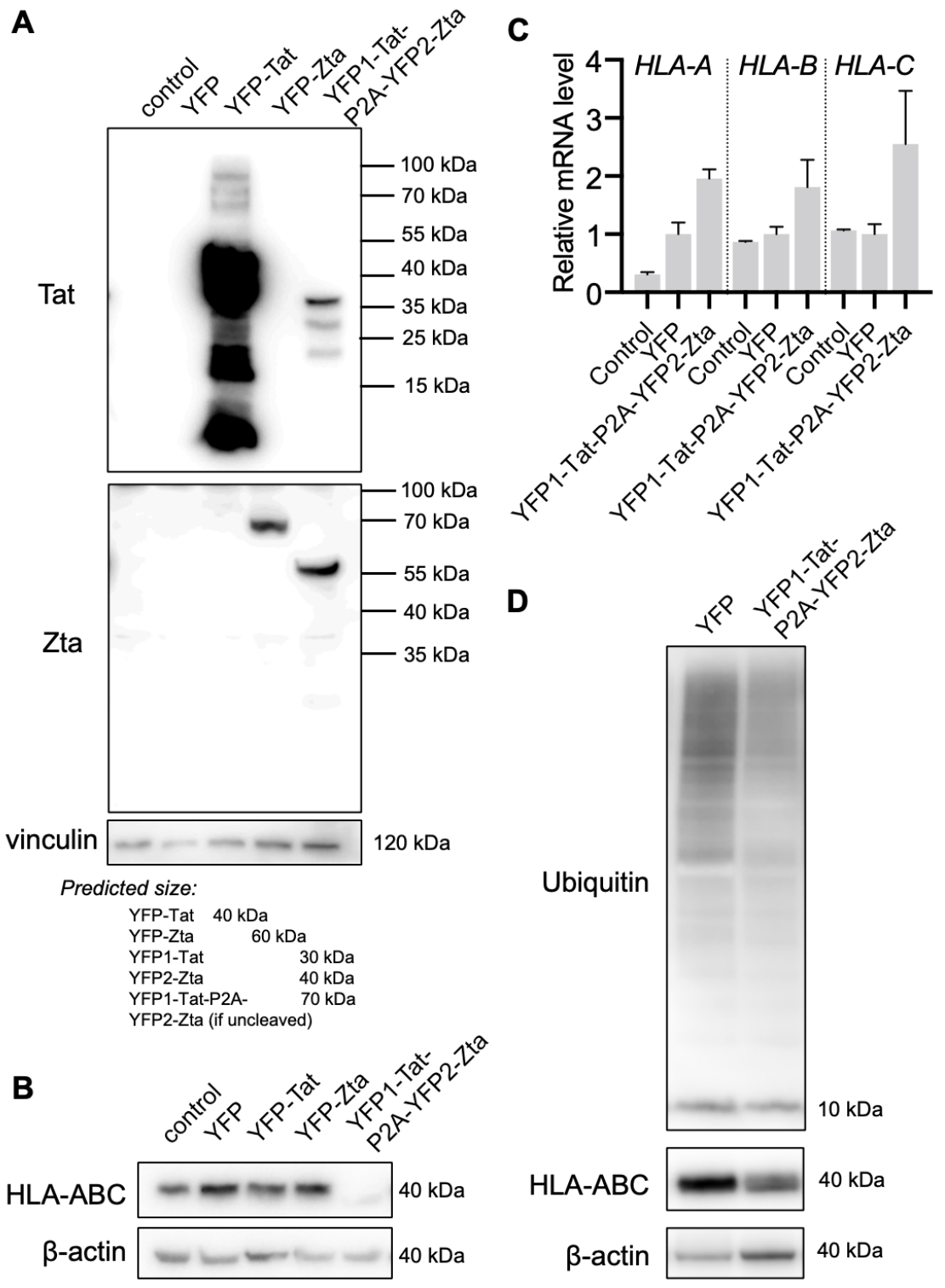

Supplementary figure 8. HLA-ABC expression analysis in cells with inducible expression of YFP and YFP1-Tat-P2A-YFP2-Zta. **(A)** Western blotting analysis of YFP1-Tat and YFP2-Zta expression and efficient YFP1-Tat-P2A-YFP2-Zta cleavage in RPMI8866 cell lines with inducible expression of YFP1-Tat-P2A-YFP2-Zta. As a reference, control RPMI8866 cell and RPMI8866 cell lines with inducible expression of YFP, YFP-Tat and YFP-Zta are shown. The predicted mass of fusion proteins is indicated below. Vinculin was used as a loading control. **(B)** Western blotting analysis of HLA-ABC

content in Jurkat cell lines with inducible expression of YFP, YFP-Tat, YFP-Zta or YFP1-Tat-P2A-YFP2-Zta 48 hours after the induction of respective proteins by doxycycline. β-actin was used as a loading control. A reproducible result is presented. **(C)** The levels of *HLA-A*, *HLA-B*, *HLA-C* mRNA in RPMI8866 cells 48 hours after the induction of YFP or YFP1-Tat-P2A-YFP2-Zta expession. Wild-type RPMI8866 cells (control) were also analysed. The mRNA level was normalized to *RPL32* and *GAPDH* expression as housekeeping genes; the normalization was done assuming the mean level of transcript in cells expressing YFP to be 1. Data are represented as mean ± SEM. **(D)** Western blotting analysis of ubiquitin and HLA-ABC content in inducible RPMI8866 cell lines expressing YFP1-Tat-P2A-YFP2-Zta or YFP (48 hours after the induction of respective proteins by doxycycline). β-actin was used as a loading control. A reproducible result is presented.

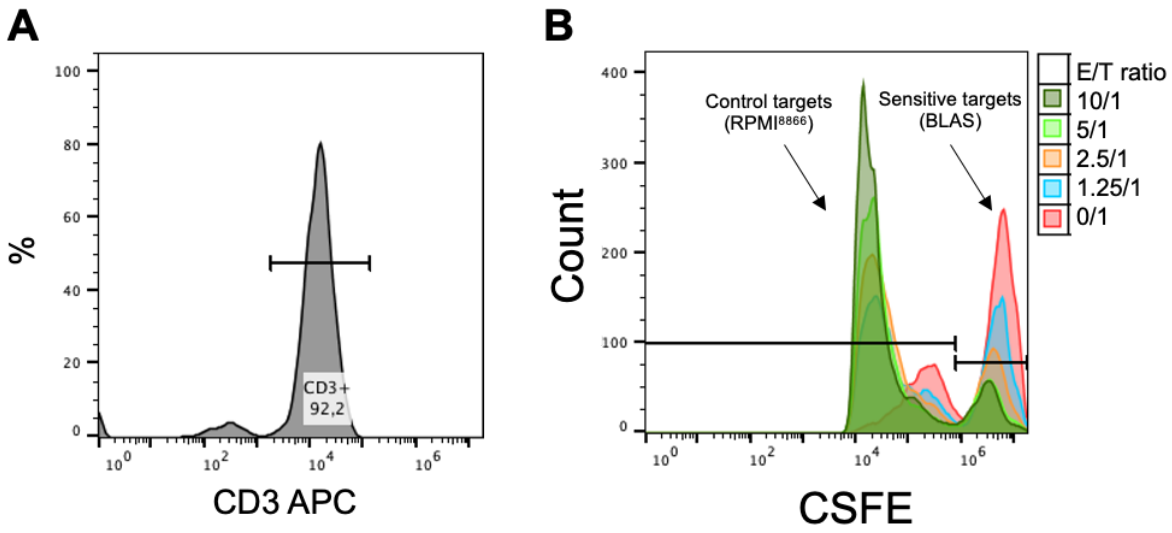

Supplementary figure 9. The characterisation of BLAS-reactive EBV-specific cytotoxic T cell line. **(A)** Representative flow cytometry histogram plots showing CD3 APC antibody staining of BLAS-reactive EBV-specific cytotoxic T cell line. **(B)** Representative histograms for flow cytometry analysis of CFSE fluorescence in the target cell population (CFSE positive gating) after co-cultivating with BLAS-reactive EBV-specific cytotoxic T cell line at various E/T ratios for 4h, two populations are visualized: $CFSE^{low}$, which are control target cells RPMI886, and $CFSE^{high}$, which are sensitive target cells BLAS that gradually decrease with the increasing E/T ratio.

Supplementary tables

Supplementary table 1. Primers and oligonucleotides used in the study for cloning.

Primer	**Sequence 5'→3'**
delta AD XhoI F (Tat)	GCATCTCGAGGTGGCAGGAAGAAGCGG
delta AD XhoI F (Zta)	AACACTCGAGAATCGCTGGAGGAATG
delta AD XhoI R (Tat)	AGATGCATGCTCGAGCTATTCCTTC
delta BD F (Tat)	CTATCAAAGGATCCAAGGCAGTCAGACTCAT
delta BD-GRD BamHI F (Tat)	CAAAGGATCCCCACCTCCCAACCCCGG
delta BD-GRD BamHI R (Tat)	TTCTGGATCCCATAGGAGATGCCTAAG
delta BD-GRD XhoI R (Tat)	CATGCTCGAGCTATTCCTTCG
delta bZIP BamHI F (Tat)	TGAAGGATCCTGTGCCCAAGCCTGGA
delta bZIP BamHI R (Tat)	TTCTGGATCCGCTTTATTTCTAGTTCAG
delta C term R (Zta)	AAGTCGACTTACATCTGCTTCAACAGGAGG
delta Ex2 R (Tat)	AAGTCGACTATTGCTTTGATAGAGAAACTTG
delta GRD R (Tat)	CGCTTCTGGATCCGAGGAGGTCTTCGTCGCT
delta TAD XhoI R (Zta)	CATGCTCGAGATTTAGGTGACAC
Linker SalI F	ACCACGTTGTCGACGGTGGCGGTGGC
Linker EcoRI F	AATTCGGTGGCGGTGGCTCTGGAGGTGGTGGGTCGC
Linker SalI F	ACGTTGTCGACGGTGGCGGTGGC
Linker XhoI R	TCGAGCGACCCACCACCTCCAGAGCCACCGCCACCG
pcDNA-YFP1/2 F	GTGGCTCTGGAGGTGGTG
pcDNA-YFP1/2 R	GGCAAACAACAGATGGCTGG
pcDNA3-CFP F	GCCAGTGTGCTGGAATTCTGC
pcDNA3-CFP R	GCTCCTCGCCCTTGCTCA
Tat 101 end stop+SalI R	CATGGTCGACCTAATCGAATGGATCTGTCTCTGTC
Tat end SalI R	AGATGCATGGTCGACCTATTCCTTCGG
Tat w/o stop F	GTAGCTCGAGGTATGGAGCCAG
Tat w/o stop R	CTACGAATTCTTCCTTCGGGCCTGTCGG
YFP F	GCTCGAGGTATGGTGAGCAAGGGCGAG
YFP link R	ACCTCGAGGGACCCACCACCTCCAGAG
Zta end SalI R	GCATGGTCGACATTTAGGTGACAC
Zta w/o stop F	GTAGCTCGAGGTATGATGGACCC
Zta w/o stop R	CTACGAATTCGAAATTTAAGAGATCCTCGTGTAAAACATCTGGTG

MCS EcoRI F	AATTCACCGGTCTAGAGCTAGCTTCGAATGTACAGGATCCG
MCS EcoRI R	AATTCGGATCCTGTACATTCGAAGCTAGCTCTAGACCGGTG
YFP1-Tat SphI R	AAAAAAGCATGCTTCCTTCGGGCCTGTC
YFP1-Tat AgeI F	AAAAAAACCGGTAAGCTTATGGTGAGCAAGG
P2A F	CGGAAGCGGAGCTACTAACTTCAGCCTGCTGAAGCAGGCTGGAGACGTGGAGGAGAACCCTGGACCTA
P2A R	GATCTAGGTCCAGGGTTCTCCTCCACGTCTCCAGCCTGCTTCAGCAGGCTGAAGTTAGTAGCTCCGCTTCCGCATG
YFP2-Zta BglII F	AAAAAAAGATCTATGAAGAACGGCATCAAGG
YFP2-Zta BamHI R	AAAAAAGGATCCGGGCCCTCTAGACTC

Supplementary table 2. Primers used for qPCR.

Primer	**Sequence 5'→3'**	**Primer efficiency**
RPL32 F	CATCTCCTTCTCGGCATCA	2.023
RPL32 R	AACCCTGTTGTCAATGCCTC	
GAPDH F	CTGCACCACCAACTGCTTAG	2.010
GAPDH R	AGGTCCACCACTGACACGTT	
HLA-A F	CGACGCCGCGAGCCAGA	1.822
HLA-A R	GCGATGTAATCCTTGCCGTCGTAG	
HLA-B F	GACGGCAAGGATTACATCGCCCTGAA	1.851
HLA-B R	CACGGGCCGCCTCCCACT	
HLA-C F	GGAGACACAGAAGTACAAGCG	2.072
HLA-C R	CGTCGTAGGCGGACTGGTCATA	
BZLF1 F	CGCCTCCTGTTGAAGCAGAT	
BZLF1 R	AAATTTAAGAGATCCTCGTGTAAAACATC	

Tat and Zta interaction induced proteasomal degradation of HLA-ABC in B cells, decreasing the total levels of HLA-ABC protein. Ubiquitylation of host factors by viral proteins plays a crucial role in manipulating the host cellular machinery to facilitate viral replication and evade immune responses. Viral proteins have evolved to exploit the host ubiquitin-proteasome system, e.g. by co-opting host ubiquitin-ligases or mimicking their activities. The ubiquitylation of host factors can lead to various consequences, such as altered protein stability, subcellular localization, and interaction with other cellular components. As a result, viral proteins perturb key cellular processes, subvert antiviral defences, and promote viral replication and spread. For instance, an immediate-early protein of human herpes simplex virus 1 ICP0 serves as both a transcriptional activator and ubiquitin ligase and it was shown that ICP0 induces ubiquitylation of host transcription factor E2FBP1 that inhibits ICP0 transcription (Fukuyo et al. 2011). MHC proteasomal degradation is commonly induced by viral proteins, e.g. EBV BDLF3 (Quinn et al. 2015) or KSHV gene product K3 (Hewitt et al. 2002). An indirect confirmation of our data comes from the observation that B cells, co-infected with HIV and EBV *in vitro*, are less susceptible to cytotoxic T-cell lysis.

We can not exclude that downregulation or loss of MHC expression in B cells might lead to their recognition by NK cells according to the 'missing self' hypothesis (Ljunggren & Kärre 1990; Shifrin et al. 2014). Viruses, however, employ different strategies to counteract NK cell responses. Notably, Tat can trigger the apoptosis of NK cells through the activation of ERK1/c-Jun signalling, activation of AP-1, and the production of TGFβ, which reduces the expression of anti-apoptotic transcripts Bcl-xL and Bcl-2, ultimately inducing apoptosis in NK cells (Poggi & Zocchi 2006; Zocchi et al. 2005). Furthermore, Tat hinders NK cell lytic activity (Poggi et al. 2002; Tasca et al. 2003). It is suggested that Tat may obstruct L-type calcium channels in NK cells, impeding their degranulation process and thereby impairing their cytotoxic activity (Zocchi et al. 1998). EBV-infected cells, including those during lytic EBV infection, also have the ability to evade NK cell responses (Jochum et al. 2012; Williams et al. 2015). Moreover, the number of "EBV-reactive" NK cells ($CD56^{dim}CD16^{-}$ subtype, primed for cytotoxic functions) decreases with age, suggesting that NK cell-mediated control over EBV infection (primary or reactivation) might be partially lost in the older population (Azzi et al. 2014; Taylor et al. 2015).

In the current study, we mainly focused on the effects of the Tat and Zta complex, rather than on the individual action of each protein. We should note, however, that both Tat and Zta, when administered alone, had profound effects on B cell transcriptomes. Both upregulation and downregulation of genes after Tat or Zta treatment were identified in B cells, consistent with the notion that these viral proteins can both downregulate and upregulate the expression of their target host genes (Germini et al. 2020; Ramasubramanyan

et al. 2015; Reeder et al. 2015; Valyaeva et al. 2022). Interestingly, in B cells almost half of Zta-deregulated genes were downregulated both at 6 hours and 48 hours, while in BLAS cells at 48h the majority of deregulated genes (60%) were downregulated. The decrease of cellular transcription is in agreement with a previously reported rapid and large reduction of chromatin accessibility and transcription due to Zta action in Raji Burkitt's lymphoma cells (B cell origin) as identified by ATAC-seq and RNA-seq (Buschle et al. 2019). However, in other work, RNA-seq of Akata Burkitt's lymphoma cells (B cell origin) ectopically expressing Zta revealed a prevalence (74%) of upregulated genes (Ramasubramanyan et al. 2015). As it was previously mentioned, Zta has a special affinity and selectivity for CpG-methylated binding sites (Bergbauer et al. 2010; Dickerson et al. 2009; Flower et al. 2011). Upon binding to such promotors, Zta recruits chromatin remodelers (e.g. INO80), unwinding DNA and depleting it from repressive chromatin marks, which results in transcription induction (Buschle & Hammerschmidt 2020; Schaeffner et al. 2019). We can hypothesize that genes initially suppressed by DNA methylation may be further activated by Zta binding during its more prolonged action. Moreover, the protein level of Zta is also important, since when it is ectopically expressed, Zta binds to most of its DNA binding sites, while when the protein concentration is low, only the high-affinity binding site will be occupied (Bergbauer et al. 2010; Buschle & Hammerschmidt 2020; Buschle et al. 2019). These factors may explain a significant data discrepancy between datasets.

Zta action on primary B cells at 6h with regard to cell death or survival mediators was ambiguous: we observed an upregulation of a pro-survival BAFF receptor (*TNFRSF13C*); downregulation of pro-apoptotic tumour necrosis factor receptor 1 (*TNFRSF1A*); upregulation of a TACI (*TNFRSF13B*), involved in B cell apoptosis (Figgett et al. 2013); downregulation of CD137 (*TNFRSF9*), that promotes B cell survival and proliferation (Zhang et al. 2010); upregulation of pro-apoptotic death receptor 3 (*TNFRSF25*); upregulation of an immune system regulator HVEM (*TNFSF14*), which is lost in ~20% of HL, DLBCL and FL (Boice et al. 2016; Cheung et al. 2010; Launay et al. 2012). In agreement with previous reports (Zeidler et al. 1997), we also found that several genes responsible for immune evasion are targeted Zta action in B cells: we registered downregulation of the transporter protein 1 (*TAP1*) associated with antigen presentation; downregulation of *CD86*, coding for a co-stimulator of T cell activation by B cells; downregulation of intercellular adhesion molecule 1 (*ICAM1* or CD54), crucial for immune synapse. Oppositely to what was reported before (Morrison et al. 2001; Zeidler et al. 1997; Zuo et al. 2011), we found a rapid upregulation of MHCI and MHCII associated genes after 6h of B cell treatment with Zta: *HLA-A, HLA-F, HLA-DMA, HLA-DMB, HLA-DPB1, HLA-DRB1* and *CD74*, the invariant chain of MHC II critical for antigen presentation. Interestingly, apart *HLA-DMA* and *CD74*, all the genes remained unchanged in B cells treated with Tat and Tat&Zta for 6h. Programmed death-ligand 1 (PD-L1,

CD274) and Fas ligand (*FASLG*) were downregulated upon Zta action at 6h. These changes may reflect a first-line cellular defence against viruses and viral proteins.

Tat and Zta combination only, but not single protein action, induced IL-12, which can exhaust T cell response in B cell malignancies (Yang et al. 2012) and IL-17A, which promotes the growth of B cell lymphoma (Ferretti et al. 2015).

3.2.6 Comparison of our data with published Tat and Zta transcriptomes in T and B cells

Aiming to reveal shared or distinct regulatory patterns, we undertake a comparative analysis of our data on transcriptomes of B cells treated with Tat and Zta proteins with previously published Tat and Zta transcriptomes in T and B cells. We compared the results of our transcriptome analysis in B cells, treated with Tat, with the transcriptome and genome mapping analysis of Jurkat T cells ectopically expressing Tat previously published (Reeder et al. 2015) (**Figure 25**). When comparing deregulated genes in Tat-treated B cells at 6h with Tat-Jurkat cells, we identified 30 common deregulated genes (32% of all deregulated genes in B cells) and only 14 of them had the same sense of deregulation (**Figure 25A**). For Tat-treated B cells at 48h, we identified 51 common deregulated genes (23% of all deregulated genes in B cells) with previously reported data and 47 of them had the same sense of deregulation. These data indicate that Tat action significantly differs from one cell type to another. According to (Reeder et al. 2015), around 23% of all deregulated genes under Tat action in Jurkat T cells are directly targeted by Tat binding to respective promotors, with almost equal distribution between upregulated (Tat stimulated genes) and downregulated (Tat downregulated genes). Our analysis identified upregulation of 1 Tat-stimulated gene (*EVL*) and downregulation of 2 Tat downregulated genes (*CDK6*, *DYNC1H1*) at 6h. At 48h of Tat treatment, we observed upregulation of 2 Tat-stimulated genes (*ATM* and *CD96*) and downregulation of 8 Tat downregulated genes (*RPS2, RPS12, EIF5A, RPS2, NPM1, MRPL1, HMGA1*) (**Figure 25B**). Overall, common direct target genes are only 1.5% and 4.6% of all deregulated genes in B cells 6h and 48h after Tat treatment, respectively. It may indicate that the Tat genome mapping profile is largely different in B cells as compared to T cells.

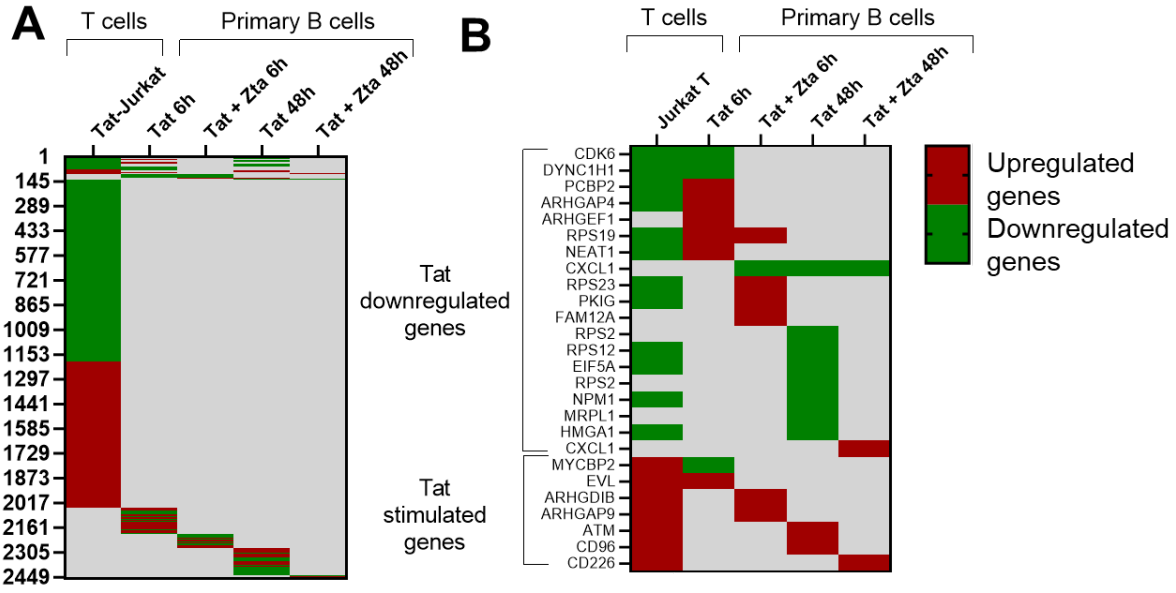

Figure 25. Transcriptome comparison of T cells, expressing Tat, and B cells, treated with Tat. (A) Subsets of significantly deregulated genes identified by RNA-sequencing analysis in Tat-expressing Jurkat T cells (Tat-Jurkat) (Reeder et al. 2015) and in primary B cells treated with Tat or Tat and Zta for 6h and 48h. The colour code is used to illustrate the sense of expression changes: upregulation (red) and downregulation (green). Gray stands for unchanged gene expression. (B) subsets of significantly deregulated genes that can be direct target genes, regulated by Tat binding. Upregulated direct target genes, identified in original work in Tat-Jurkat cells, are denoted as Tat stimulated genes, while downregulated direct target genes are denoted as Tat downregulated genes. The data about significantly deregulated genes, log2 fold changes and Tat directly targeted genes were kindly provided by authors (Reeder et al. 2015).

We next compared the results of our transcriptomic analysis in B cells, treated with Zta, with the transcriptome and genome mapping analysis of Akata cells ectopically expressing Zta (Ramasubramanyan et al. 2015) (**Figure 26**). Surprisingly, the profile of deregulated genes differed significantly between datasets. When comparing deregulated genes in Zta-treated B cells at 6h with Zta-Akata cells, we identified 165 common deregulated genes (25% of all deregulated genes in B cells) and only 19 of them had the same sense of deregulation (**Figure 26A**). For Zta-treated B cells at 48h, we identified 7 common deregulated genes (10% of all deregulated genes in B cells) with previously reported data and 5 of them had the same sense of deregulation. These data discrepancies may depend on the time of Zta action and EBV status.

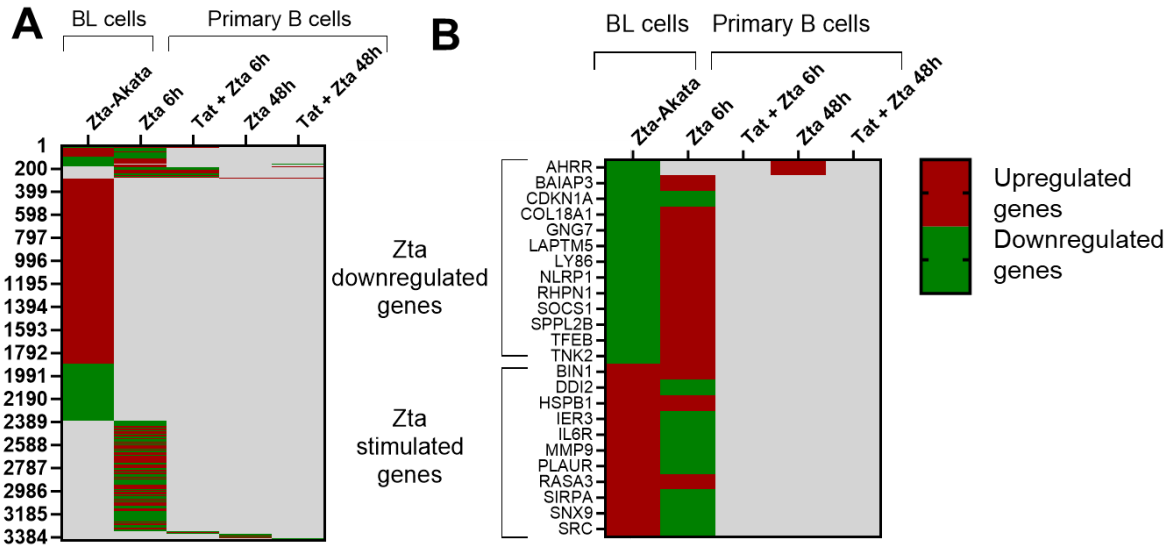

Figure 26. Transcriptome comparison of Akata B cells, expressing Zta, and B cells, treated with Zta. (A) subsets of significantly deregulated genes identified by RNA-sequencing analysis in Akata Burkitt's lymphoma (BL) cells (B cell origin) ectopically expressing Zta (Zta-Akata) (Ramasubramanyan et al. 2015) and in primary B cells treated with Zta or Tat and Zta for 6h and 48h. The colour code is used to illustrate the sense of expression changes: upregulation (red) and downregulation (green). Gray stands for unchanged gene expression. (B) subsets of significantly deregulated genes that can be direct target genes, regulated by Zta binding. Upregulated direct target genes, identified in original work in Zta-Akata cells, are denoted as Zta stimulated genes, while downregulated direct target genes are denoted as Zta downregulated genes. The data about significantly deregulated genes and Zta directly targeted genes were imported from original work data (Ramasubramanyan et al. 2015).

According to (Ramasubramanyan et al. 2015), around 13% of all deregulated genes under Zta action in Akata BL cells are directly targeted by Zta binding to respective promotors, with 74% of them being upregulated (Zta stimulated genes) and 26% downregulated (Zta downregulated genes). Our analysis identified upregulation of 3 Zta-stimulated genes (*BIN1, HSPB1, RASA3*) and downregulation of 1 Zta downregulated gene (*CDKN1A*) at 6h. However, most of the changes in Zta stimulated and downregulated direct genes at 6h were of the opposite sense (**Figure 26B**). At 48h of Zta treatment, no Zta downregulated or stimulated genes were identified. We also searched for the genes that were identified as associated with Zta binding but without significant expression changes (Ramasubramanyan et al. 2015) and found 121 genes that could be directly targeted by Zta. Overall, common direct target genes regardless of the direction of expression changes are only 1.1% and 11.6% of all deregulated genes in B cells 6h and 48h after Zta treatment, respectively. It may indicate that fast Zta action is significantly different from more prolonged Zta exposure in B cells.

4 Materials and methods

4.1 Antibodies, enzymes, recombinant proteins

The following antibodies were used in the work:

- Primary, unconjugated:

mouse anti-Tat (Santa Cruz, cat. # sc-65912), mouse anti-Zta (kindly provided by Dr. Emmanuel Drouet, Université Grenoble Alpes), mouse anti-transthyretin (Santa Cruz, cat. # sc-377517), mouse anti-transferrin (Santa Cruz, cat. # sc-52256), rabbit anti-p53 (Santa Cruz, cat. # sc-47698), rabbit anti-phospho-p53 (Ser15) antibodies (Cell Signaling Technology, cat. # 9284), rabbit anti-His-Tag (Abcam, cat. # ab9018), mouse anti-GFP (Roche, cat. # 11814460001), rabbit anti-Galectin-9 (Proteintech, 17938-1-AP), rabbit anti-calnexin (Invitrogen, cat. # PA5-34754), mouse anti-p65 (RelA) (Santa Cruz, cat. # sc-8008), rabbit anti-NF-κB1 (Proteintech, 14220-1-AP), mouse anti-HLA-DR (1:1000; Santa Cruz, cat. # sc-6262), mouse anti-IκBα (1:1000, Santa Cruz, cat. # sc-371), rabbit anti-pIκBα (1:1000, R&D Systems, cat. # AF4809), rabbit anti-RelB (1:1000, Proteintech, cat. # 25027-1-AP), rabbit anti-NFKB2 (p100, p52, 1:1000, Proteintech, cat. # 15503-1-AP), IgM monoclonal antibody (SA-DA4) (eBioscience, Invitrogen, cat. # 14-9998-82), mouse anti-BMRF1 (Sigma, cat. # MAB8186), mouse anti-Cas 9 (1:200, Santa Cruz, cat. # sc-517386), mouse anti-CD40 (Sigma, cat. # WH0000958M1), rabbit anti-histone H2AX phospho-Ser139 (γH2AX) (Active Motif, cat. # 39118 or BioLegend, cat. #613412), rat anti-cisplatin modified DNA [CP9/19] (Abcam, cat. #ab103261), rabbit anti-α-tubulin (Santa Cruz, cat. # sc-398103), rabbit anti-actin (Sigma, cat. # A2103), mouse anti-β-actin (1:1000, control of protein load in whole cell extracts, Santa Cruz, #sc-81178), mouse anti-vinculin (1:1000, control of protein load in whole cell exptracts, Sigma, cat. #SAB4200729), rabbit anti-GAPDH (1:1000, control of protein load in cytoplasmic extracts, Cell Signaling Technology, cat. #2118), rabbit anti-H2A (1:1000, control of protein load in nuclear extracts, Abcam, cat. # ab116677), rabbit anti-topoisomerase IIb (1:1000, control of protein load in nuclear extracts, Santa Cruz, cat. # sc-13059).

The following antibodies were obtained through the NIH HIV Reagent Program, Division of AIDS, NIAID, NIH: anti-HIV-1 Tat Monoclonal (15.1), ARP-1974, contributed by DAIDS/NIAID ; anti-HIV-1 HXB2 Tat Monoclonal (1D9), ARP-7377, contributed by Dr. Dag E. Helland. The following reagent was obtained through the NIH HIV Reagent Program, Division of AIDS, NIAID, NIH and Centre for AIDS Reagents, NIBSC, UK, supported by EURIPRED (EC FP7 INFRASTRUCTURES-2012, INFRA-2012-1.1.5.: Grant Number 31266). www.euripred.eu/: Anti-Human Immunodeficiency Virus 1 (HIV-1) Tat

Monoclonal (NT3 5A5.1), ARP-4374 (CFAR#3253), contributed by Dr. Jonathan Karn.

- Primary, conjugated:

FITC anti-CD23 (BD, cat. # 561146), FITC anti-CD8 (Biolegend, cat. #344704), PE anti-CD19 (Biolegend, cat. # 302208), PE-Cy5 anti-HLA-DR (Biolegend, cat. #307608), PE-Cy5 anti-HLA-ABC (BD, cat. # 555554), APC anti-CD3 (Biolegend, cat. # 300312), PerCP anti-IFNγ (Biolegend, cat. #502524), PerCP anti-CD4 (Biolegend, cat. #300528), APC anti-CD4 (Biolegend, cat. #300514), PerCP Mouse IgG1, κ isotype control (Biolegend, cat. # 400148), APC Mouse IgG2a, κ isotype control (Biolegend, cat. #400220).

- Secondary, conjugated:

goat anti-mouse IgG (Fc) F(ab)2 HRP Highly absorbed (Sigma, cat. # SAB3701029), goat anti-mouse IgG-HRP (Santa Cruz, cat. # sc-2005), donkey anti-rabbit IgG-HRP (Santa Cruz, cat. # sc-2313), goat-anti-rat IgG-HRP (Sigma-Aldrich, cat. # AP136P), unconjugated rabbit anti-mouse (Sigma, cat. # M7023), AF488 Goat anti-rabbit IgG H+L (Thermo, cat. # A-11034), AF546 Goat anti-rabbit IgG H+L (Invitrogen, cat. # A11010), AF633 goat anti-rabbit (Invitrogen, cat. # A21070), AF647 Goat anti-mouse IgG H+L (Invitrogen, cat. # A21235).

Restriction enzymes (XhoI cat. # FD0694, EcoRI cat. # FD0274, NdeI cat. # FD0583, XbaI cat. # FD0684, SalI cat. #FD0644, BamHI cat. # FD0054, AgeI cat. # ER1461, BglII cat. # ER0081), T4 DNA ligase (cat. # EL0011), Shrimp Alkaline Phosphatase (cat. # EF0511) were obtained from Thermo Fisher.

Tat recombinant protein was obtained through the NIH AIDS Research and Reagent Program, Division of AIDS, NIAID, NIH: HIV-1 IIIB Tat Recombinant Protein (cat. # 2222). Proteins were added to the cell medium or blood plasma at the indicated concentrations. Zta recombinant protein was synthesized by a biological company BiologicsCorp, USA, from pET29a(+)-BZLF1 plasmid, encoding for His-tagged Zta (see below). The protein was 90% pure and endotoxin-free. The SilverQuest™ Silver-stained SDS-PAGE and the western blots of the recombinant Zta protein were conducted to confirm its purity (**Figure 27**).

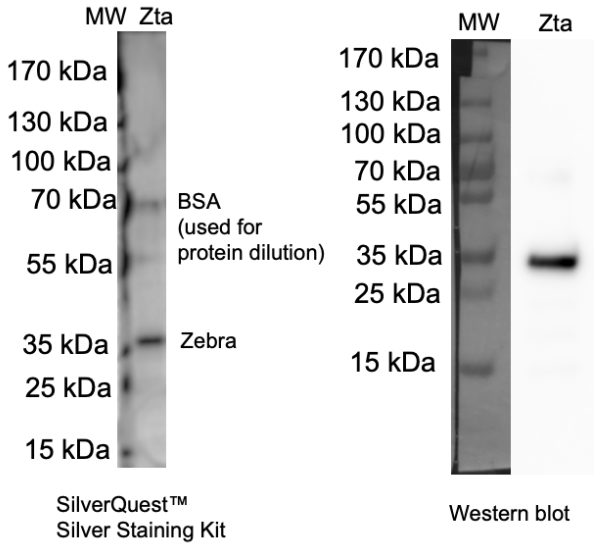

Figure 27. The confirmation of the purity of recombinant Zta protein. SDS-PAGE of the recombinant Zta protein (250 ng). The left panel, a gel stained with a SilverQuest™ Silver Staining Kit (Thermo); the right panel, a representative image of Zta staining by Western blot using anti-Zta monoclonal antibodies.

We additionally tested Zta cell penetration into cells, since Zta is known to have a cell-penetration domain (Mahot et al. 2005; Rothe et al. 2010). Zta was labelled with tetramethylrhodamine tetramethylrhodamine (TRITC)-5-(and 6)-isothiocyanate (ThermoFisher, cat. # 46112) following the manufacturer's instructions. Briefly, lyophilised Zta protein was dissolved in conjugation buffer (0.1 Sodium Carbonate/Bicarbonate, pH 9.0 adjusted with HCl) to obtain a concentration of 5 mg/ml. TRITC isothiocyanate was dissolved in DMSO to achieve a concentration of 40 mg/ml. Next, 110 µg of Zta (22 µl) was mixed with 40 µg of TRITC (1 µl of 40 mg/ml) to achieve a molar ratio of 1:25. A control sample for TRITC was run using 1 µl of 40 mg/ml in 22 µl of Conjugation Buffer. The mixture was then incubated for 2 hours at room temperature while shaking in the dark. After incubation, the reaction mixture was diluted 1:10 with conjugation buffer and filtered through a 10 K filter at 12,000 g for 15 minutes to remove excess dye. The upper part was recovered by turning the filter and centrifuging it at 1000 g for 2 minutes. Finally, the molarity and labelling efficiency of Zta were calculated using the "Calculate dye: protein (F/P) molar ratios TECH TIP #31" from Thermo. 1×10^5 HeLa cells were plated in 500 µl of the normal medium in each of the chambers of a Labtek Chambered Borosilicate 4 Chamber Coverglass System and were allowed to attach overnight. HeLa cells were then incubated with 1 µg/ml of the TRITC-labelled recombinant Zta protein added to the culture medium. ~100% of cells were transduced by Zta already after 1h of incubation and it localized preferentially in the nucleus, as expected (**Figure 28**).

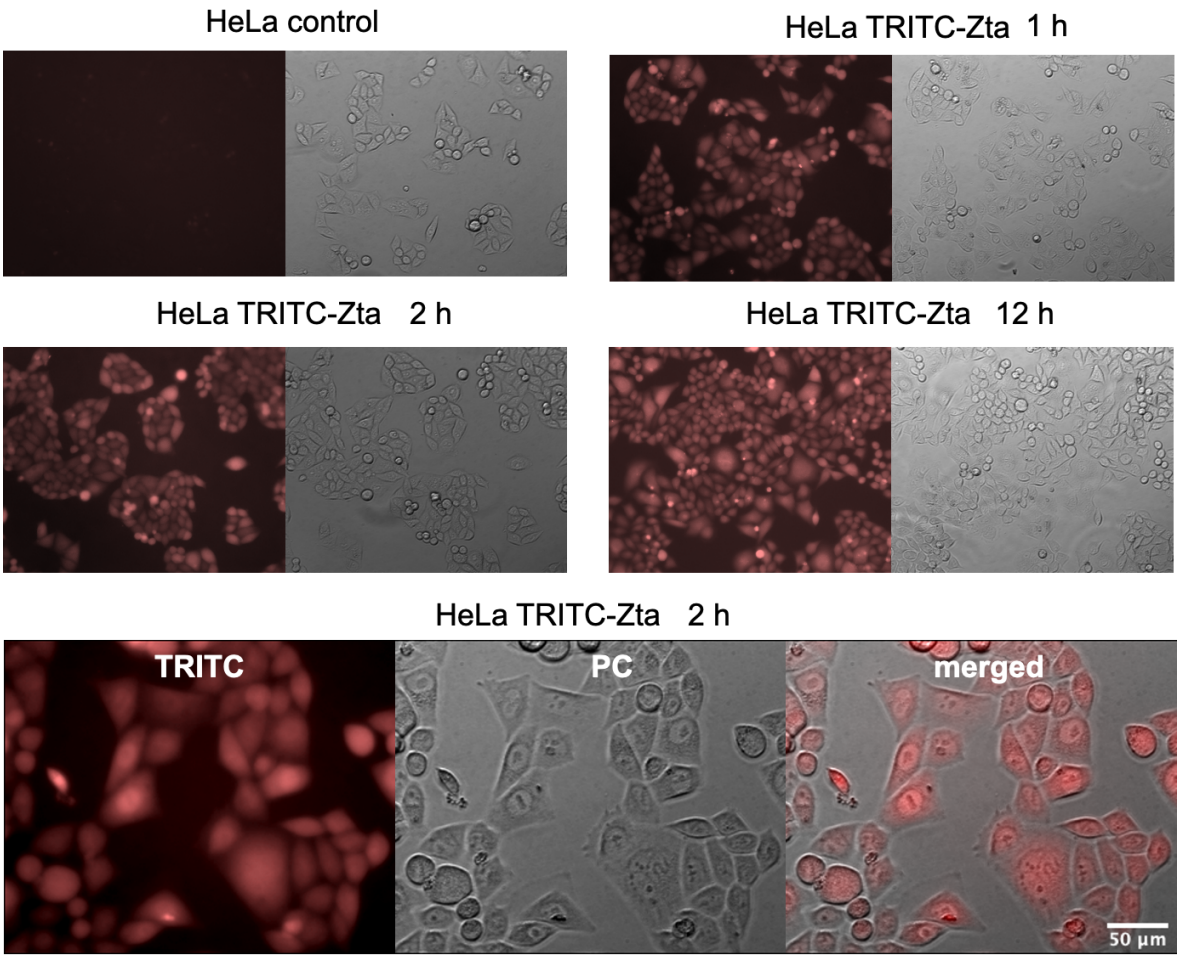

Figure 28. The penetration of Zta in the cells. HeLa cells treated with 1 µg/ml recombinant Zta protein labeled with the TRITC fluorescent dye. The penetration of Zta into cells was detectable after two hours of incubation. PC, phase contrast; scale bar, 50 µm.

4.2 Blood plasma collection and primary B cell isolation

Whole blood samples from anonymous healthy donors of different sex and age were obtained from the “Etablissment Français du Sang”, Hôpital Saint-Louis, Paris, France in accordance with the French legislation (agreement number № 14/EFS/033). Blood plasma was collected after EDTA-treated blood samples centrifugation for 15 minutes at 2000g. Blood samples from hospitalized HIV-infected patients who signed a written informed consent for the study were collected in Clinical Hospital № 67, Moscow, Russia in accordance with the Russian legislation or in Hôpital Saint-Louis, Paris, France in accordance with the French legislation. HIV status was analysed by immunoassay of anti-HIV-1/2 antibodies IgM and IgG and antigen p24 in venous blood samples. Positive tests were confirmed twice. Tat concentrations in sera from HIV-positive individuals were determined using both a dot blotting assay and an enzyme-linked immunosorbent assay as described previously (Germini et al. 2017b).

PBMCs were purified by Pancoll (PAN biotech) density gradient centrifugation. B lymphocytes were obtained by negative cell selection using the MagniSort Human B cell Enrichment Kit (Thermo, cat. # 8804-6867-74) according to the manufacturer's protocol. For the RNA-sequencing experiment primary B cells from four healthy donors were pooled.

4.3 Cell lines, cell culture and cell treatments

Human cervical carcinoma cell line HeLa (American Type Culture Collection), Human Epstein-Barr virus (EBV)-transformed B lymphoblastoid cell line RPMI8866 (ECACC General Cell Collection), freshly EBV-transformed B lymphoblastoid cell lines from healthy donors AS, YaK, IT (BLAS, BLYaK, BLIT, established by EBV (B95-8) immortalization of mature B cells and characterized by Genethon (Evry, France)), human immortalized T cell line Jurkat (American Type Culture Collection) and Jurkat that stably expresses HIV-1 Tat (Jurkat-Tat, obtained through the NIH HIV Reagent Program, Division of AIDS, NIAID, NIH, ARP-1399, contributed by Dr. Antonella Caputo, Dr. William Haseltine and Dr. Joseph Sodroski), human EBV-negative Burkitt's lymphoma cell line Ramos (obtained through the NIH HIV Reagent Program, Division of AIDS, NIAID, ARP-9938, contributed by Drs. Li Wu and Vineet N. Kewal Ramani), monocytic THP-1 cell line (American Type Culture Collection), neuroblastoma SH-SY5Y cell line (American Type Culture Collection), human embryonic kidney (HEK) 293T cell line (American Type Culture Collection) and their derivatives were used in the study. RPMI8866^{GFP}, RPMI8866^{Tat}, RPMI8866^{TatC22G}, BLAS^{GFP}, BLAS^{Tat}, BLAS^{TatC22G} cell lines that stably express EGFP, EGFP-Tat or EGFP-TatC22G (Tat defective in transactivation) as well as RPMI8866 cell line inducibly expressing Tat (Tat^{i}) were a kind gift from Eugene Sheval and produced as described previously (Gorbacheva et al. 2019).

Ramos^{Tat} and THP-1^{Tat} cell lines that stably EGFP-Tat or EGFP-TatC22G (Tat defective in transactivation) were produced through lentiviral transduction as described below. RPMI8866 cells with stable integration of HIV-1 3′-LTR-TurboRFP reporter were obtained through RPMI8866 electrotransfection with HIV-1 3′-LTR-TurboRFP plasmid and subsequent selection with G418 (800 μg/ml, Sigma-Aldrich, Burlington, MA, USA) for at least 8 weeks, following selection, cells were confirmed to be 100% weakly positive for TurboRFP. RPMI8866 cell lines that stably expressed scrambled shRNA or CIITA-shRNA were produced through lentiviral transduction with pLKO.1-shCIITA or pLKO.1-scrambled-shRNA as described below and subsequent selection with 1 μg/ml puromycin for at least five weeks. Cells were maintained in normal RPMI8866 cell medium with 1 μg/ml puromycin and subjected to the second round of lentiviral transduction to produce RPMI8866 cell lines that stably expressed scrambled shRNA or CIITA-shRNA and EGFP or EGFP-Tat.

Lymphoblastoid B-cell lines RPMI8866, Ramos, BLAS, BLIT, BLYaK, a monocytic THP-1 cell line and their derivatives were cultured in RPMI 1640 medium supplemented with 10% FBS, 2% glucose, 2 mM L-Glutamine, 1 mM Pyruvate and 1× penicillin/streptomycin antibiotics (all from Gibco, Thermo Fisher Scientific, Waltham, Massachusetts, USA). Jurkat T cells were cultured in RPMI 1640 medium supplemented with 10% FBS, 1% D-glucose, 1M HEPES Buffer solution, 100 mM sodium pyruvate, 1x penicillin/streptomycin antibiotics (all from Gibco). Jurkat-Tat were cultured with the addition of 800 µg/ml G418 (Sigma-Aldrich, Burlington, MA, USA). HeLa, SH-SY5Y, and HEK cells were cultured in DMEM medium supplemented with 10% FBS and 1x penicillin/streptomycin antibiotics (all from Gibco). Purified B-cells (plated 10^6/ml) were incubated in RPMI 1640 medium supplemented with 10% FBS and 1x penicillin/streptomycin antibiotics. All cells were cultured at 37°C in a humidified 5% CO_2 atmosphere.

The induction of HIV-1 Tat expression in RPMI8866 Tat^i cells was performed with doxycycline (Sigma, St. Louis, Missouri, USA) in the concentration of 1 µg/ml for 16 hours unless otherwise specified (RPMI8866 Tat^i + Dox); cells from the same line without Tat induction with doxycycline served as control (RPMI8866 Tat^i control). For the experiments with NF-κB pathway inhibition, RPMI8866 and BLAS cells were treated for 24 hours with 1 µM Bay 11-7082 (MedChemExpress, Monmouth Junction, NJ, USA), for 24 hours with 40 µg/ml SN52 (MedChemExpress), or for 6 hours with 20 µM MG132 (Selleckchem, Houston, TX, US). After the indicated times, cells were collected for HLA-DR expression analysis by flow cytometry or western blotting. For the experiments of endocytosis inhibition, co-cultured Jurkat and BLAS-GFP cells (mixed 1:1 at day 0) were treated with 100 µM genistein (MedChemExpress) at day 3. For the experiments with a fluorescently-labelled Tat-derived cell-penetrating peptide GRKKRRQRRRPPQ-Cy5 (Tat CPP-Cy5, SB-PEPTIDE, Saint Egreve, France), SH-SY5Y cells were seeded in 4-chamber Labtek plates (0.0925×10^6 cells / well in 500 µl of DMEM medium supplemented with 10% FBS and 1× penicillin/streptomycin). On the day of assay, the cell medium was changed to a fresh one and cells were pre-treated or not (control) with 100 µM genistein (MedChemExpress, cat. # HY-14596) for one hour and then 1 µM Tat CPP-Cy5 was added to cell medium. After 30 minutes of incubation with Tat CPP-Cy5, cells were washed three times with PBS and then fixed in 4% paraformaldehyde (Electron Microscopy Sciences, cat. # 15710) for 10 minutes followed by another three washes with PBS and nuclear counterstaining with cell-permeant nuclear dye Hoechst 33342 (1 µg/ml, Invitrogen, cat. #H3570). For the experiments with nuclear export inhibition, RPMI8866 cells were treated for 2 hours with 5 ng/ml Lemptomycin B (LMB) from Streptomyces sp. (Sigma-Aldrich, L2913). Cells were then washed with PBS and fixed in 4% paraformaldehyde (Electron Microscopy Sciences, cat. # 15710) for 10 minutes followed by immunofluorescent staining as described below. For the

experiments with ubiquitin-proteasomal pathway inhibition, RPMI8866 cells were transfected with YFP or YFP1-Tat + YFP2-Zta and 40 hours after transfection were treated with the following inhibitors for a total duration of 8 hours: MG-132 (50 μM), PYR-41 (20 μM), Pevonedistat (2 μM), Bay 11-7082 (20 μM), and NSC697923 (2 μM) (all from MedChemExpress, Monmouth Junction, NJ, USA). After the indicated times, cells were collected for total HLA-ABC expression analysis by flow cytometry. For the experiments with antiretroviral drugs and other inhibitors, Jurkat cells with inducible YFP1-Tat-P2A-YFP2-Zta expression were treated with Dox (1 μg/ml) concomitantly with abacavir (ABC, 6 μM), amprenavir (0.4 μM), atazanavir sulfate (5 nM), azidothymidine (AZT, 0.4 μM), emtricitabine (FTC, 0.64 μM), indinavir sulfate (100 nM), lamivudine (3TC, 15 μM), nevirapine (100 nM), rilpivirine (9.2 μM), saquinavir (30 nM), TAK-779 (200 nM), filgotinib (JAK1 inhibitor, 10 μM, AbMole BioScience), wortmannin (PI3K inhibitor, 20 μM, MedChemExpress), JNK inhibitor II (SP600125, 50 μM, Calbiochem), Akt inhibitor XI (20 μM, Calbiochem), and IKK-2 inhibitor V (10 μM, Calbiochem). Antiretroviral drugs were used at the concentrations that correspond to IC_{50} for virus inhibition as described previously [56] and obtained through the NIH HIV Reagent Program, Division of AIDS, NIAID, NIH. YFP fluorescence was analysed 24 hours after treatment by flow cytometry.

Cell counting was performed by mixing 1:1 cell suspension with Trypan blue, transferring to counting slides and analyzing on TC 20™ Automated Cell Counter.

4.4 Generation of EBV-specific cytotoxic CD8+ T cell lines

EBV-specific human cytotoxic T cells (CTLs) were derived as previously described (Levitsky et al. 2001). Briefly, PBMCs from healthy donor AS (1×10^6/ml) were cocultured with autologous irradiated (4000 Rad) EBV-transformed BLAS (2.5×10^4/ml) in 24-well plates in RPMI 1640 medium supplemented with 10% human AB serum (Sigma) and 1x penicillin/streptomycin antibiotics. After 9 to 11 days, T cells (1×10^6/ml) were restimulated with irradiated BLAS (2.5×10^5/mL). Recombinant human IL-2 (50 ng/ml; Proteintech, cat. # HZ-1015) was added to the cultures at this time. T-cell lines were subsequently maintained by restimulation with irradiated BLAS every 14 days, with interim half-changes of fresh medium plus IL-2 every 3 to 4 days. After three to four restimulation cycles, T cell lines were typically >85% $CD8^+$ by flow cytometric analysis. $CD8^+$ T cells were further isolated (to >98% purity) by positive selection with anti-CD8 Beads (Proteintech).

Phenotype analysis was performed by flow cytometry with immunofluorescent staining specific for CD3 (APC).

4.5 Generation of EBV-specific CD4+ T cell line and the analysis of their reactivity

EBV-specific polyclonal human CD4+ T cell line was derived as previously described (Long et al. 2009) with modifications. Briefly, PBMCs from healthy donor AS were depleted in CD8+ T cells using human CD8 magnetic beads (Proteintech, cat. # MS0044-100) following the manufacturer's instructions. CD8-depleted PBMCs (1×10^6/ml) were then co-cultured with autologous irradiated (40 Gy) EBV-transformed BLAS (2.5×10^4/ml) at 40:1 responder-to-stimulator ratio in 24-well plates in RPMI 1640 medium supplemented with 10% human AB serum (Sigma) and 1× penicillin/streptomycin antibiotics. After 9 to 11 days, T cells (1×10^6/ml) were restimulated with irradiated BLAS (2.5×10^5/ml) at 4:1 responder-to-stimulator ratio. Recombinant human IL-2 (50 ng/ml; Proteintech, cat. # HZ-1015) was added to the cultures at this time. T-cell lines were subsequently maintained by restimulation with irradiated BLAS every 14 days, with interim half-changes of fresh medium plus IL-2 every 3 to 4 days. After seven restimulation cycles, the T cell line was >90% CD4+ by flow cytometric analysis (**Figure 29**). Phenotype analysis was performed by flow cytometry with immunofluorescent staining specific for CD3 (APC), CD8 (FITC), and CD4 (PerCP).

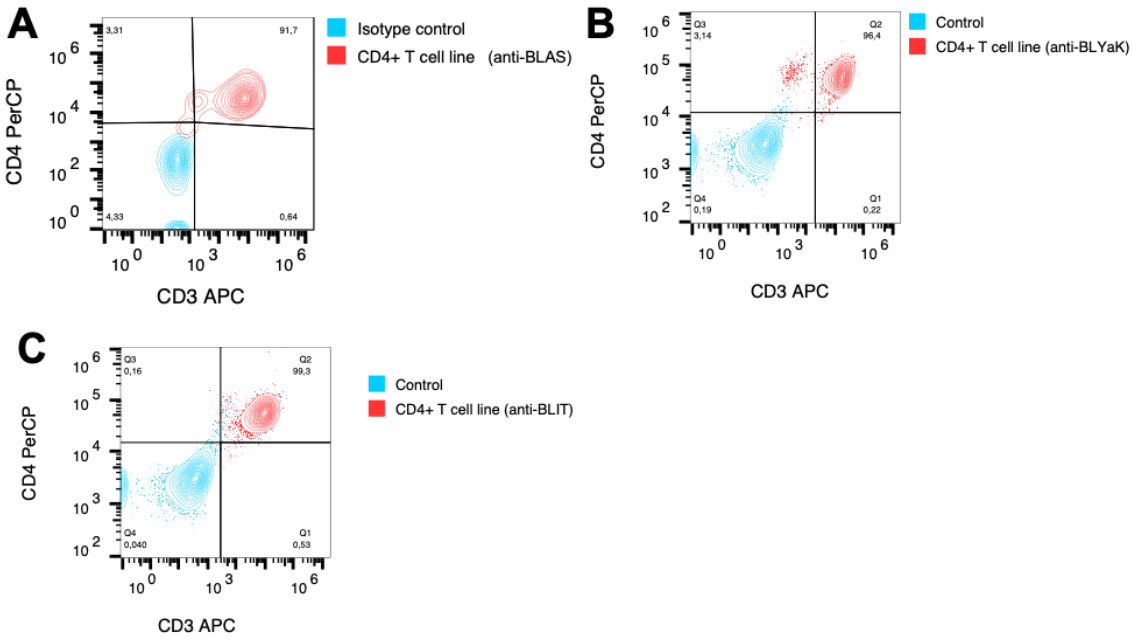

Figure 29. Representative flow cytometry contour plots showing CD3 and CD4 and respective isotype control antibody staining of BLAS-reactive (A), BLYaK-reactive (B) and BLIT-reactive (C) EBV-specific CD4+ T cell lines.

For IFNγ production analysis, the generated CD4+ T cell line or PBMCs (5×10^5/well) from autologous donor were co-cultured with BLAS, BLAS^{GFP}, BLAS^{Tat} or BLAS^{TatC22G} (1.25×10^4/well) at 40:1 E/T ratio for 18 hours in 48-well plates in

RPMI 1640 medium supplemented with 10% human AB serum (Sigma) and 1× penicillin/streptomycin antibiotics followed by CD4 and IFNγ staining as described below.

For cytotoxicity assays, the previously described non-radioactive method comparable with the conventional ^{51}Cr release assay was used (Nakagawa et al. 2011) with modifications. Briefly, sensitive BLAS and control RPMI8866 target cells were labelled with 5- (and 6-) carboxyfluorescein diacetate succinimydyl ester (CFSE, Biolegend, cat. #423801) as follows: 1×10^6 cells were washed once with PBS and resuspended in 1% FBS/PBS to a concentration 1×10^6 cells/ml. For sensitive targets (BLAS), 1 µl of 5 mM CFSE solution was added to 1 ml of cell suspension; for control targets (RPMI8866), 0.5 µl of 500 µM CFSE solution was added to 1 ml of cell suspension; cells were incubated for 4 min at room temperature under shading. After incubation, 9 ml of 5%FBS/PBS was added to stop the labelling reaction. Then, cells were washed once with 5%FBS/PBS and resuspended with 400 µl of RPMI 1640 medium supplemented with 10% human AB serum (Sigma) and 1× penicillin/streptomycin antibiotics at a final concentration (2.5×10^6 cells/ml). CD4+ T cell line effector cells were washed once with PBS and resuspended in RPMI 1640 medium supplemented with 10% human AB serum (Sigma) and 1× penicillin/streptomycin antibiotics to a final concentration of 1×10^6 cells/ml. For sensitive reactions, 5×10^4 BLAS target cells (20 µl) and various numbers of effector cells (0, 1.25×10^5, 2.5×10^5, 5×10^5) were mixed in a 48-well plate at a final volume of 520 µL to yield various effector/target (E/T) ratios (0:1, 2.5:1, 5:1, 10:1). For each sensitive reaction a respective control reaction was also separately prepared: 5×10^4 RPMI8866 target cells (20 µl) and the same number of effector cells were mixed in a 48-well plate at a final volume of 520 µL. The plate was centrifuged at 200g for 1 min and then incubated at 37°C for 4 h. After incubation, wells with sensitive target cells were mixed 1:1 with the respective control target cells with the same E/T ratio in one tube, washed once with PBS and fixed in 4% PFA/PBS for 10 minutes. The % of specific lysis was calculated as follows:

$$\%\ of\ specific\ lysis\ =\ \frac{a,b}{a,ab}\ *\ 100\%,$$

where a, the fraction of sensitive cells among target cells in E/T 0:1 sample, and b, the fraction of sensitive cells among target cells in E/T X:1 sample. The derivation of the % of specific lysis formula is explained in **Figure 30**.

Typical output of flow cytometry analysis:

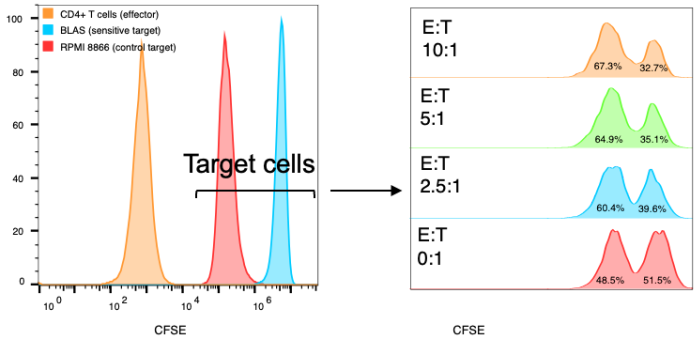

Fraction of sensitive cells:

0.327	b_{10}
0.351	b_5
0.396	$b_{2.5}$
0.515	a

Let a be a fraction of sensitive cells among target cells in E/T 0:1 sample, b be the fraction of sensitive cells among target cells in E/T 10:1 sample, x be the total number of sensitive target cells before the cytotoxic lysis, y be the total number of control target cells before the cytotoxic lysis, and z be the total number of sensitive target cells lysed by the cytotoxic lysis.

Knowing that control and target cells were mixed at the same quantity for all samples, then the fraction of sensitive cells among target cells in E/T 0:1 sample can be expressed as the fraction of sensitive target cells before the cytotoxic lysis and the fraction of sensitive cells among target cells in E/T 10:1 sample can be expressed as the fraction of sensitive target cells after the cytotoxic lysis:

$$a = \frac{x}{x+y} \text{ and } b = \frac{x-z}{x-z+y}$$

Then the percentage of specific lysis can be expressed as the total number of sensitive target cells lysed by the cytotoxic lysis relative to the the total number of sensitive target cells before the cytotoxic lysis:

$$\%\ of\ specific\ lysis = \frac{z}{x} * 100\%$$

If we express x and z through a and b and substitute it in the above formula, it turns out that:

$$a = \frac{x}{x+y} \Rightarrow$$
$$(x+y)a = x \Rightarrow$$
$$xa + ya = x \Rightarrow$$
$$ya = x(1-a) \Rightarrow$$
$$y = \frac{x(1-a)}{a}$$

$$b = \frac{x-z}{x-z+y} \Rightarrow$$
$$b(x-z+y) = x-z \Rightarrow$$
$$bx - bz + by = x - z \Rightarrow$$
$$z - bz = x - bx - by \Rightarrow$$
$$z(1-b) = x(1-b) - by \Rightarrow$$
$$z = x - \frac{b}{1-b} * y \Rightarrow$$
$$z = x - \frac{b}{1-b} * \frac{x(1-a)}{a} \Rightarrow$$
$$z = x\left(1 - \frac{b}{1-b} * \frac{1-a}{a}\right)$$

$$\frac{z}{x} = \frac{x\left(1 - \frac{b}{1-b} * \frac{1-a}{a}\right)}{x} \Rightarrow$$
$$\frac{z}{x} = 1 - \frac{b}{1-b} * \frac{1-a}{a} \Rightarrow$$
$$\frac{z}{x} = \frac{(1-b)a - b(1-a)}{(1-b)a} \Rightarrow$$
$$\frac{z}{x} = \frac{a - ab - b + ab}{a - ab} \Rightarrow$$
$$\frac{z}{x} = \frac{a-b}{a-ab}$$

Thus, the $\%\ of\ specific\ lysis = \frac{a-b}{a-ab} * 100\%$

and for the above example at E/T 10:1 $\%\ of\ specific\ lysis = \frac{0.515-0.327}{0.515-0.515*0.327} * 100\% = 54\%$, which can be illustrated like this:

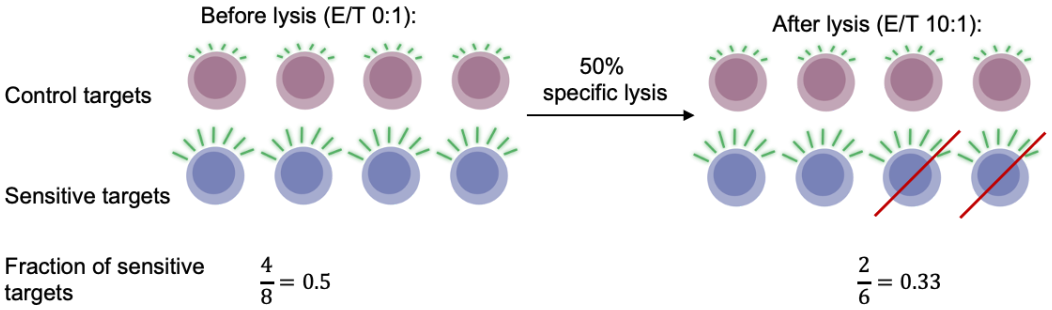

Figure 30. The derivation of the % of specific lysis formula used in the study.

4.6 Generation of RPMI8866-based cell lines with inducible translocations

RPMI8866 cells were co-electrotransfected with the Puro-Cas9-gRNAs plasmid, containing puromycin resistance, Tet-inducible Cas9 and gRNAs genes, and homology arms for AAVS1 site, AAVS1-Neo-M2rtTA plasmid containing neomycin resistance and tetracycline transactivator (TA) genes and homology arms for AAVS1 site (Addgene, #60843) and two TALEN plasmids for cutting in the safe-harbour AAVS1 site (AAVS1-TALEN-L+ AAVS1-TALEN-R) (Addgene # 59025 and # 59026) using a protocol developed in our laboratory (Canoy et al. 2020). RPMI8866 cells with inducible Cas9 expression and gRNAs to MYC and IGH (iMYC-IGH cell line) or AML1 and ETO loci (iAML1-ETO cell line) were created. The cells were maintained in the RPMI 1640 medium, supplemented with 10% certified tetracycline-free fetal bovine serum (Takara, Japan), 100 U/ml penicillin, 100 μg/ml streptomycin, and 800 µg/ml G418 antibiotic for 10 days. The cells were subsequently transferred into the medium with 0.3 µg/ml puromycin (Sigma-Aldrich, USA) and were cultured for 4 days. Resistant cells were cloned via finite dilution technique in a 96-well plate. Clones and bulk lines were grown with and without 1 μg/ml doxycycline (Dox) for 48h and then tested for the presence of specific translocations.

4.7 Drug treatment of RPMI8866-based cell lines with inducible translocations

Cytotoxic activity of the drugs and cell survival was evaluated by cell counting using TC 20^{TM} Automated Cell Counter and methylthiazolyltetrazolium (MTT) test as described earlier (van Meerloo et al. 2011). Briefly, cells were seeded at equal densities and treated with different drugs. After treatment (48 hours for the iMYC-IGH line and 96 hours for the iAML1-ETO line, which corresponds to the peak of detected translocations) 100 µl of cell suspension was incubated with 0.1 mg of MTT (5 mg/ml, Merck Millipore, USA) for 2 hours at 37°C in the dark and then lysed in 100 µl of lysing buffer (25 mM HCl, 2% acetic acid, 3% DMF, 5% SDS, pH 4.7). The absorbance at 570 nm was measured using a plate reader Infinite F200 PRO (Life Sciences, Tecan, Germany). Each sample was tested in two technical replicates and the mean absorbance was taken into consideration. The cell survival was calculated relative to non-treated cells.

To assess the effect of various drugs on translocation formation, drugs were added to the cell medium simultaneously with the induction of Cas9 expression (Dox treatment). Since the peak of translocation frequency was 48 hours for iMYC-IGH cell line and 96 hours for iAML1-ETO cell line (data not shown), iMYC-IGH cells were treated for 48 hours, iAML1-ETO cells were treated for 96 hours. After indicated times cells were collected, DNA was

extracted and tested for the presence of specific translocations by qPCR. In each experiment negative control (non-treated with Dox cells) and cells treated with Dox only were present. The frequency of translocations in drug+Dox-treated cells was normalized to the frequency of translocations in Dox-treated cells within the same experiment in at least 3 biological replicates. The list of drugs and their concentrations is presented in **Table 7**. Antiretroviral therapy (ART) drugs were used at the concentrations that correspond to IC_{50} for virus inhibition, chemotherapeutic drugs were used at the concentrations that correspond to IC_{10} to ensure that cells survive the treatment. ART drugs were obtained through the NIH HIV Reagent Program, Division of AIDS, NIAID, NIH. Chemotherapeutic agents were purchased from Accord, Sigma, Veropharm, Teva, Bristol-Myers Squibb, EBEWE PHARMA, AstraZeneca, Sanofi (**Table 7**).

Table 7. Treatments of RPMI8866-based cell lines with inducible translocations. Abbreviations: 3TC, lamivudine; ABC, abacavir; ATM, Ataxia telangiectasia, mutated; AZT, azidothymidine; FTC, emtricitabine; Hsp, heat-shock protein; NRTI, nucleoside analogue reverse-transcriptase inhibitors; NNRTI, non-nucleoside reverse transcriptase inhibitors; PARP, poly (ADP-ribose) polymerase; PI, protease inhibitors.

Drug	Company	Mechanism of action	Working concentration
ART			
Abacavir (ABC)	NIH ARP	NRTI	6 μM
Amprenavir	NIH ARP	PI	0.4 μM
Atazanavir sulfate	NIH ARP	PI	5 nM
AZT	NIH ARP	NRTI	0.4 μM
Emtricitabine (FTC)	NIH ARP	NRTI	0.64 μM
Indinavir sulfate	NIH ARP	PI	100 nM
Lamivudine (3TC)	NIH ARP	NRTI	15 μM
Nevirapine	NIH ARP	NNRTI	100 nM
Rilpivirine	NIH ARP	NNRTI	9.2 μM
Saquinavir	NIH ARP	PI	30 nM
TAK-779	NIH ARP	CCR5 antagonist	200 nM
Chemotherapy			
Carboplatin	Accord	DNA crosslinks and lesions	For iMYC-IGH: 15 μM For iAML-ETO: 270 nM
Cisplatin	Accord	DNA crosslinks and lesions	For iMYC-IGH: 0.1 μM For iAML-ETO:

			24 nM
Cytarabine	Sigma	Antimetabolite and nucleoside analog	0.01 nM
Docetaxel	Accord	Microtubule suppression	0.1 nM
Doxorubicin	Teva	DNA intercalation, topoisomerase II inhibitor	3 nM
Etoposide	Teva	Topoisomerase II inhibitor	2 nM
Fluorouracil	Accord	Antimetabolite, thymidylate synthase inhibitor	3 μM
Ifosfamide	Veropharm	Alkylating agent and nitrogen mustard	35.6 μM
Irinotecan	Veropharm	Topoisomerase I inhibitor	15.5 nM
Methotrexate	EBEWE PHARMA	Antimetabolite of the antifolate type	2.9 nM
Mitoxantrone	Accord	Topoisomerase II inhibitor	5 nM
Olaparib	AstraZeneca	PARP inhibitor	3 μM
Oxaliplatin	Sanofi	DNA crosslinks and lesions	7 nM
Paclitaxel	Bristol-Myers Squibb	Cytoskeletal drug (tubulin)	4.7 pM
Inhibitors			
Mirin	Calbiochem	MRE11 inhibitor	25 μM
NU7026	Sigma Aldrich	DNA-PK inhibitor	20 μM
17-AAG	Apexbio	Hsp90 inhibitor	10 μM
L67	Sigma Aldrich	DNA ligase I and III inhibitor	25 μM
KU-55933	Sigma Aldrich	ATM inhibitor	10 μM

4.8 Analysis of RPMI8866 Tat^{i} cell sensitivity to cisplatin, oxaliplatin and doxorubicin

MTT test was performed to evaluate the viability of RPMI8866 Tat^{i} cells with or without induction of HIV-1 Tat expression as described previously (Shmakova et al. 2022a). Cells were seeded in complete medium in 96-well plates at 0.1×10^{6} / 100 µl concentration; the expression of HIV-1 Tat was induced by doxycycline treatment for 16 hours, followed by treatment with either cisplatin (Mylan), oxaliplatin (Accord) or doxorubicin (Teva) in different concentrations. For survival experiments, we used the following concentrations: 0, 1, 5, 10, 20, 30, 40, 50, 100, 200 or 300 µM of cisplatin; 0, 0.05, 0.1, 0.5, 1, 5, 10 or 50 µM of oxaliplatin; 0, 0.1, 0.2, 0.3, 0.4, 0.5, 1, 2, 5, 10 or 20 µM of doxorubicin. 24 hours after the treatment cells were incubated with 0.1 mg of MTT (Merck Millipore, Burlington, MA, USA) for 2 hours at 37 °C and then lysed in 100 µL per well of lysing buffer (25 mM HCl, 2% acetic acid, 3% DMF, 5% SDS, pH 4.7) at room temperature overnight. The next day the absorbance at 570 nm was measured using a plate reader Infinite F200 PRO (Life Sciences, Tecan, Grodig, Austria). Acquired data was analyzed using Excel software. For all experiments, six technical repeats of each dose were analyzed for each of at least three biological replicates.

For apoptosis tests, RPMI8866 Tat^{i} cells were treated or not with doxycycline for 16 hours to induce HIV-1 Tat expression, and then treated with 0, 10, 50, 100 or 300 µM of cisplatin, 0, 0.1, 1, 10 or 100 µM of oxaliplatin or 0, 0.2, 20, or 200 µM of doxorubicin for 24 hours. 0.5×10^{6} cells were collected by centrifugation for 5 minutes at 800g, washed with PBS and resuspended in 300 µL of Annexin buffer (100 mM Hepes pH 7.4, 150 mM NaCl, and 2.5 mM $CaCl_2$). 3 µL of APC Annexin V (Biolegend, cat. #640941) and 3 µL of propidium iodide (PI) (Sigma-Aldrich, cat. #P4170-10MG) were added to each sample and incubated for 5 minutes in the dark. Fluorescence was acquired using BD Accuri C6 Plus Flow Cytometer (BD Biosciences, USA), and the data were analyzed using FlowJo software (version 10.4), the same gating was applied to all samples within one experiment, the compensation was performed with single-stained controls. For all experiments, two technical repeats of each dose were analyzed for each of at least three biological replicates.

4.9 Cell transfection

HeLa cells were transfected with the use of Viafect transfection reagent (Promega) or Turbofect transfection reagents (ThermoFisher) following the manufacturer's instructions. RPMI8866 and Jurkat cells were electrotransfected by the protocol established in our laboratory previously (Canoy et al. 2020) with the parameters listed in **Table 8**. Briefly, we used the CliniporatorTM (Igea) with 4-mm or 1-mm electroporation cuvettes (Cell

Projects). For 4-mm electroporation cuvettes, 8×10^6 cells were diluted in 200 µl of Minimum Essential Medium Eagle with Spinner Modification (S-MEM, Sigma Aldrich) and 200 µl of water containing 50 µg of plasmid, and electrotransfected at 1300 V/cm (520V), with 100 µs pulses at 1 Hz. For 1-mm electroporation cuvettes, $4*10^6$ cells were diluted in 90 µl of S-MEM medium and 10 µl of water containing 50 µg of plasmid, and electrotransfected at 1300 V/cm (130 V) with 100 µs pulses at 1 Hz. When transfecting with YFP-split fragments the ratio 1:1 was used; to assess transfection efficiency in hard-to-transfect LCL cells, mCherry plasmid (Addgene, cat. #54563) was co-electrotransfected, with the ratio YFP1:YFP2:mCherry = 1:1:0.5.

Table 8. Electrotransfection conditions for different cell lines used in the study.

Cell line	Cuvette size	Cell quantity	Voltage	Number of pulses	Pulse frequency
RPMI8866	4-mm	8×10^6	520 V	8	100 µs at 1 Hz
Ramos	4-mm	8×10^6	520 V	8	100 µs at 1 Hz
BLAS	4-mm	8×10^6	520 V	4	100 µs at 1 Hz
THP-1	4-mm	8×10^6	520 V	4	100 µs at 1 Hz
Jurkat	1-mm	4×10^6	130 V	12	100 µs at 1 Hz

4.10 Lentivirus production and lentiviral transduction

HEK 293 T cells were used for lentivirus packaging and production. Cells were seeded in a T-175 flask 24 hours before transfection to achieve 80% confluency on the day of transfection. HEK 293 T cells were transfected with second-generation lentiviral packaging plasmid psPAX2 (Addgene, # 12260), VSV-G envelope expressing plasmid pMD2.G (Addgene, # 12259) and transfer plasmid (EGFP, EGFP-Tat, EGFP-TatC22G, pLKO.1-scrambled-shRNA or pLKO.1-shCIITA1, FUdeltaGW-rtTA, FUW-tetO-YFP, FUW-tetO-YFP-Tat, FUW-tetO-YFP-Zta, FUW-tetO-YFP1-Tat-P2A-YFP2-Zta) at 15:6:20 ratio using Turbofect transfection reagent (Thermo Fisher Scientific, USA) according to the manufacturer's instructions (20 µg of plasmid DNA and 40 µl of Turbofect transfection reagent were premixed in 2 ml of OptiMEM medium (Gibco) and added to 20 ml of DMEM/10% FBS cell medium in T-175 flask). Cell medium was changed to DMEM/0%FBS 24 hours after transfection and lentiviral supernatant was collected 48 hours after transfection, centrifuged to remove cell debris and filtered through a 0.45-µm filter.

RPMI8866^{GFP}, RPMI8866^{Tat}, RPMI8866^{TatC22G}, BLAS^{GFP}, BLAS^{Tat}, BLAS^{TatC22G}, Ramos^{Tat} and THP-1^{Tat} cell lines that stably expressed enhanced green fluorescent protein (EGFP), EGFP-Tat or EGFP-TatC22G (Tat defective in transactivation) were produced through lentiviral transduction as described previously (Valyaeva et al. 2022). Briefly, 2 × 10^6 cells (plated in six-well plates) diluted in 1 ml of normal medium were transduced with 1 ml of lentiviral supernatant, GFP expression was confirmed 72 hours after transduction and GFP$^+$ cells were sorted using ARIA Fusion-UV cell sorter (BD Biosciences). RPMI8866 cell lines that stably expressed scrambled shRNA or CIITA-shRNA were produced through lentiviral transduction of 2 × 10^6 cells with 1 ml of lentiviral supernatant and subsequent selection with 1 μg/ml puromycin for at least five weeks. Cells were maintained in normal RPMI8866 cell medium with 1 μg/ml puromycin and subjected to the second round of lentiviral transduction to produce RPMI8866 cell lines that stably expressed scrambled shRNA or CIITA-shRNA and EGFP or EGFP-Tat as described above. RPMI8868- and Jurkat-derived cell lines that inducibly expressed YFP, YFP-Tat, YFP-Zta, or YFP1-Tat-P2A-YFP2-Zta were produced as follows. 2 × 10^6 cells (plated in six-well plates) diluted in 1 ml of normal medium were transduced with 1 ml of FUdeltaGW-rtTA lentiviral supernatant and 1 ml of lentiviral supernatant with one of the FUW-tetO constructs (FUW-tetO-YFP, FUW-tetO-YFP-Tat, FUW-tetO-YFP-Zta, FUW-tetO-YFP1-Tat-P2A-YFP2-Zta). To confirm YFP expression and establish cell lines, 72 hours after transduction cells were treated with Dox for 24 hours and YFP$^+$ cells were then sorted using ARIA Fusion-UV cell sorter (BD Biosciences). Cells were then maintained in a normal cell medium.

4.11 Flow cytometry analysis

YFP fluorescence was analysed using a fluorescence-activated cell sorter (FACS) BD Accuri C6 Plus Flow Cytometer (BD Biosciences, USA). YFP-positive cells were sorted using BD FACSAria Fusion-UV Cell Sorter (BD Biosciences, USA). The cell cycle was studied using propidium iodide (10 μg/ml) staining preceded by RNA digestion with RNAse A (100 μg/ml). The level of apoptosis was analysed using Annexin V – Cy5.5 (BD, cat. #559935) and propidium iodide staining following the manufacturer's instructions. Early apoptotic cells were defined as Annexin V-positive and PI-negative, while Annexin V-positive and PI-positive cells were considered late apoptotic. For antibody staining of surface molecules, 0.3 × 10^6 cells/test were harvested, washed with PBS and resuspended in 1% BSA/PBS. For intracellular staining of HLA-ABC, CD4 and IFNγ 0.8 × 10^6 cells/test were harvested, washed with PBS and fixed and permeabilized using Cyto-Fast™ Fix/Perm Buffer Set (Biolegend, cat. # 426803) according to the manufacturer's instructions. For B cells (including LCL) Fc receptor binding was blocked by Fc block (Miltenyi Biotec Inc., cat. # 130-059-901) according to the manufacturer's instructions. Cells were then

incubated on ice with fluorescently labelled antibodies for 30 minutes followed by 3 washings with PBS. Fluorescence was acquired using BD Accuri C6 Plus Flow Cytometer (BD Biosciences, USA) and the data were analyzed using FlowJo software (version 10.4), the same gating was applied to all samples within one experiment. If several fluorescent channels were analysed, the compensation was performed with single-stained controls. Representative graphs of the gating strategy are shown in **Figure 31**.

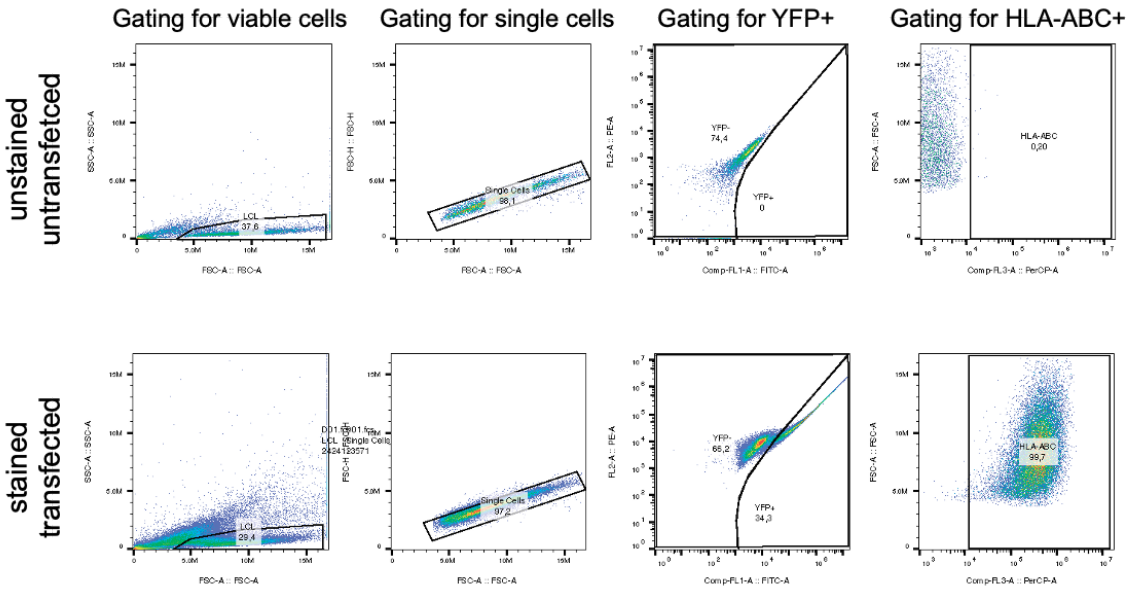

Figure 31. Flow cytometry gating strategy as shown on RPMI8866 cells (untransfected and unstained) and RPMI8866 cells transfected with YFP and stained with PE-Cy5 anti-HLA-ABC antibodies. LCL, lymphoblastoid cells, YFP, yellow fluorescent protein.

4.12 Immunofluorescent staining and microscopy

Adherent cells were directly cultured on coverslips, suspension cells were attached to coverslips covered with poly-D-lysine (Merck Millipore, cat. # A-003-E, 100 µg/ml). Cells were washed with PBS, and fixed in 4% paraformaldehyde (Electron Microscopy Sciences, cat. # 15710). Cells were permeabilized with 2% Triton X-100 in case of intracellular staining. Nonspecific binding was blocked with 10% normal goat serum (JacksonImmunoResearch cat. #005-000-121) in 1% bovine serum albumin (BSA)/PBS at 37℃ for 1h. When analyzing HLA-ABC expression and its colocalization with ER, cells were stained with anti-HLA-ABC (1:100) and anti-calnexin (1:500) antibodies, followed by staining with secondary antibodies AF488 Goat anti-rabbit IgG H+L (1:200) and AF647 Goat anti-mouse IgG H+L (1:200). When analyzing RelA and NF-κB1 expression and localization, cells were stained with anti-p65 (1:100) and anti-NF-κB1 (1:200) antibodies, followed by staining with secondary antibodies AF546 Goat anti-rabbit IgG H+L (1:200) and AF647 Goat anti-mouse IgG H+L (1:200). When analyzing HLA-DR

expression, cells were first stained with PE-Cy5 anti-HLA-DR antibody (1:10) without permeabilization, followed by their fixation and permeabilization to allow nuclear counterstaining. When analyzing γH2AX presence, cells were stained with anti-H2A.X Phospho (Ser139) antibody (1:200), followed by staining with secondary antibodies Alexa Fluor 647 Goat anti-mouse IgG H+L (1:200). When analyzing RelA localization upon LMB treatment, cells were stained with anti-RelA (1:100) and anti-actin (1:200) antibodies (since RelA was almost entirely translocated to the nucleus upon LMB treatment, we stained for actin to mark cytoplasm), followed by staining with secondary antibodies AF546 Goat anti-rabbit IgG H+L (1:200) and AF647 Goat anti-mouse IgG H+L (1:200). When counterstaining nuclei without cell permeabilisation, Hoechst 33342 dye was used (Invitrogen, cat. # H3570). Coverslips were mounted on slides with Fluoroshield mounting medium with DAPI (Abcam, cat. # ab104139) or without DAPI (Vector, cat. # H-1000). All antibodies were diluted in 1% BSA in 1× PBS.

In the case of Tat and Zta staining, heat-induced antigen retrieval (HIAR) was performed in Sodium Citrate Buffer at 95°C for 10 minutes. Non-specific staining was blocked by incubation in 5% normal goat serum, 1% BSA, 0.1 % saponin in 1X PBS. The immunofluorescent staining protocol was adopted from (Vendeville et al. 2004). Cells were incubated with primary mouse anti-Tat or mouse anti-Zta antibodies (1:100), followed by incubation with secondary unconjugated rabbit anti-mouse antibodies (1:400) and then AF488 Goat anti-rabbit IgG H+L (1:200). All antibodies were diluted in 1% BSA, 0.1% Saponin in 1X PBS. Coverslips were mounted on slides with Fluoroshield mounting medium with DAPI (Abcam, cat. # ab104139). All antibodies were diluted in 1% BSA in 1X PBS.

Live and fixed fluorescent images were acquired using an inverted phase contrast fluorescence microscope (Axio Observer Z1, Zeiss) and ZEN 2010 software or Leica TCS SP8 Multiphoton Confocal Microscope (Leica Microsystems). All images within the experiment were captured with the same laser intensity, gain and exposure settings.

4.13 3D-fluorescence in situ hybridization (FISH)

Hybridization and staining of human chromosome loci 8q24 (*MYC* gene locus, RP11-440N18 red) and 14q32 (*IGH* gene locus, RP11-346I20 green) were performed using “RainbowFISH'' probes (Empire Genomics, Buffalo, NY, USA). 3D-FISH was performed as previously described (Germini et al. 2017a; Sall et al. 2023). Briefly, polylysine-coated coverslips were prepared by applying polylysine solution (Merck Millipore, cat. # A-003-E, 0.1 mg/ml in water) on the coverslips. Cell attachment to the slips was achieved by resuspending cells in RPMI 1640 medium without FBS (Gibco) to obtain 0.5 × 10^6 cells in 70 µl per coverslip, which were then allowed to attach at 37°C with 5% CO2 for 30

minutes. For fixation, non-attached cells were washed with 0.3 × PBS and the attached cells were fixed in 4% paraformaldehyde (Electron Microscopy Sciences) in 0.3 × PBS for 10 minutes at room temperature. The fixed cells were then washed three times for 5 minutes with 1 × PBS. Post-fixation treatment involved treating the cells with 2% Triton X-100 (Sigma-Aldrich) in 1 × PBS for 10 minutes, followed by incubation with 20% glycerol (Sigma-Aldrich) in 1 × PBS overnight at 4°C. The cells were subjected to congelation/de-congelation in liquid nitrogen (four times) by dipping the coverslip successively in 20% glycerol and then in liquid nitrogen, allowing the nitrogen to dry between dips. After congelation/de-congelation, the cells were washed three times for 5 minutes each with 1 × PBS. Next, the cells were treated with 0.1 M HCl (Sigma-Aldrich) for 20 minutes at room temperature, followed by washing two times for 5 minutes each with 2 × SSC (Saline-Sodium Citrate Buffer, ThermoFisher). The cells were then incubated with RNase A (200 µg/ml, ThermoFisher) in 2 × SSC for 1 hour at 37°C in a humid chamber. After RNase treatment, the cells were washed three times for 5 minutes each with 2 × SSC. For equilibration, the cells were then treated with 50% formamide (Sigma-Aldrich) in 2 × SSC overnight at 4°C. During the hybridization step, 50 µl of 70% formamide (in 2 × SSC) was put in the middle of glass slides, the coverslips with the attached cells were placed on a glass slide (cells in contact with the formamide) and were heated to 80°C for 5 minutes. The hybridization mix (1 µl of each probe and up to 10 µl of hybridization buffer (Empire Genomics) per two coverslips) was prepared in the dark and heated to 80°C for 5 minutes. Then, one coverslip with cells facing up was placed on a glass slide, 10 µl of hybridization mix was added, and the other coverslip with cells facing down was turned on to create a sandwich. The sandwich was closed with glue, placed in a humid chamber in the dark at 37°C, and incubated for 72 hours. After hybridization, the glue was removed, and each coverslip was placed in 50% formamide at 37°C for 5 minutes. The coverslips were then washed two times for 5 minutes each with 2 × SSC at room temperature, followed by three washes for 5 minutes each with 1 × PBS at room temperature. The mounting was done by placing a drop of Vectashield mounting medium with DAPI (Vector Laboratories, Burlingame, CA, USA, to counterstain nuclei) on a glass slide and placing a coverslip with cells facing down on top. The coverslip was sealed with nail polish to prevent air from entering, and the slides were either immediately analyzed using a fluorescence microscope or stored in the dark at 4°C in the refrigerator. For additional antibody staining (immuno-FISH), the following steps were performed after the FISH procedure described above: the slides were saturated with 1% BSA (Sigma-Aldrich) in 1 × PBS for 30 minutes at 37°C in humid chamber, incubated with primary antibodies (1 hour at 37°C in humid chamber), washed three times with 1 × PBS for 5 minutes each, incubated with appropriate secondary antibodies (1 hour at 37°C in humid chamber),

washed three times with 1 × PBS 1 for 5 minutes each, and finally, the coverslips were mounted on glass slides.

Multiphoton SP8 confocal microscope (Leica Microsystems, Berlin, Germany) with a 63× oil immersion objective was used for 3D-FISH image acquisition. Z-stacks were acquired using a frame size of 1024 × 1024, and 0.5 µm z-steps, with sequential multitrack scanning using the 405, 488, 543, and 633 nm laser wavelengths. For *MYC-IGH* colocalization, Imaris software (Bitplane) was used. The colocalization rate corresponded to the percentage of cells where at least one *MYC* locus was located 1 μm or less from one *IGH* locus. The cutoff distance of 1 μm between signal centres was chosen based on the average diameter of the signals representing each gene locus (1 μm), considering that when the signals touched or came into close proximity, they were within a 1 μm physical distance.

4.14 Image analysis

To analyze the total and nuclear fluorescence intensity of RelA and NFKB1, confocal images were processed using a semi-automatic macro in Fiji (ImageJ version 2.1.0/1.53c, Java version 1.8.0). Briefly, to create nuclear and total cell masks, the nuclear regions of interest (ROIs) were detected on the images with the DAPI-staining, and the total cellular ROIs were detected on the images with the RelA-staining; in both cases, the threshold method "Huang dark" implemented in Fiji was used. ROIs on image borders were excluded form the analysis. The masks were split to detect single nuclei and single cells. The area, circularity and X and Y centre coordinates of detected ROIs were measured, and total fluorescence intensity (integrated density in Fiji) in nuclear and cellular ROIs was measured in RelA and NFKB1 channels. An algorithm in R (version 4.2.1) was created to process the results. Nuclear ROIs with area <10 µm^2 (debris) or >55 µm^2 (doublets), irregular nuclei (ROIs circularity < 0.3), cellular ROIs with area <20 µm^2 or >95 µm^2 and circularity < 0.3 were automatically removed. A provisional cellular radius (r_{cell}) was calculated as follows: $r_{cell} = \sqrt{\frac{Area}{\pi}}$; nuclear ROIs that met the condition $(Xnuc, Xcell)^2 + (Ynuc, Ycell)^2 < r_{cell}^2$ were matched with respective cellular ROIs; unmatched nuclear or cellular ROIs or cellular ROIs where >1 nuclei matched were removed from the analysis (**Figure 32**). The total fluorescence intensity in the nuclear ROI was then divided by the respective total fluorescence intensity in the total cellular ROI for each cell. At least five fields were analysed per biological replicate and images from at least two independent experiments were analysed. The plugin is available on request.

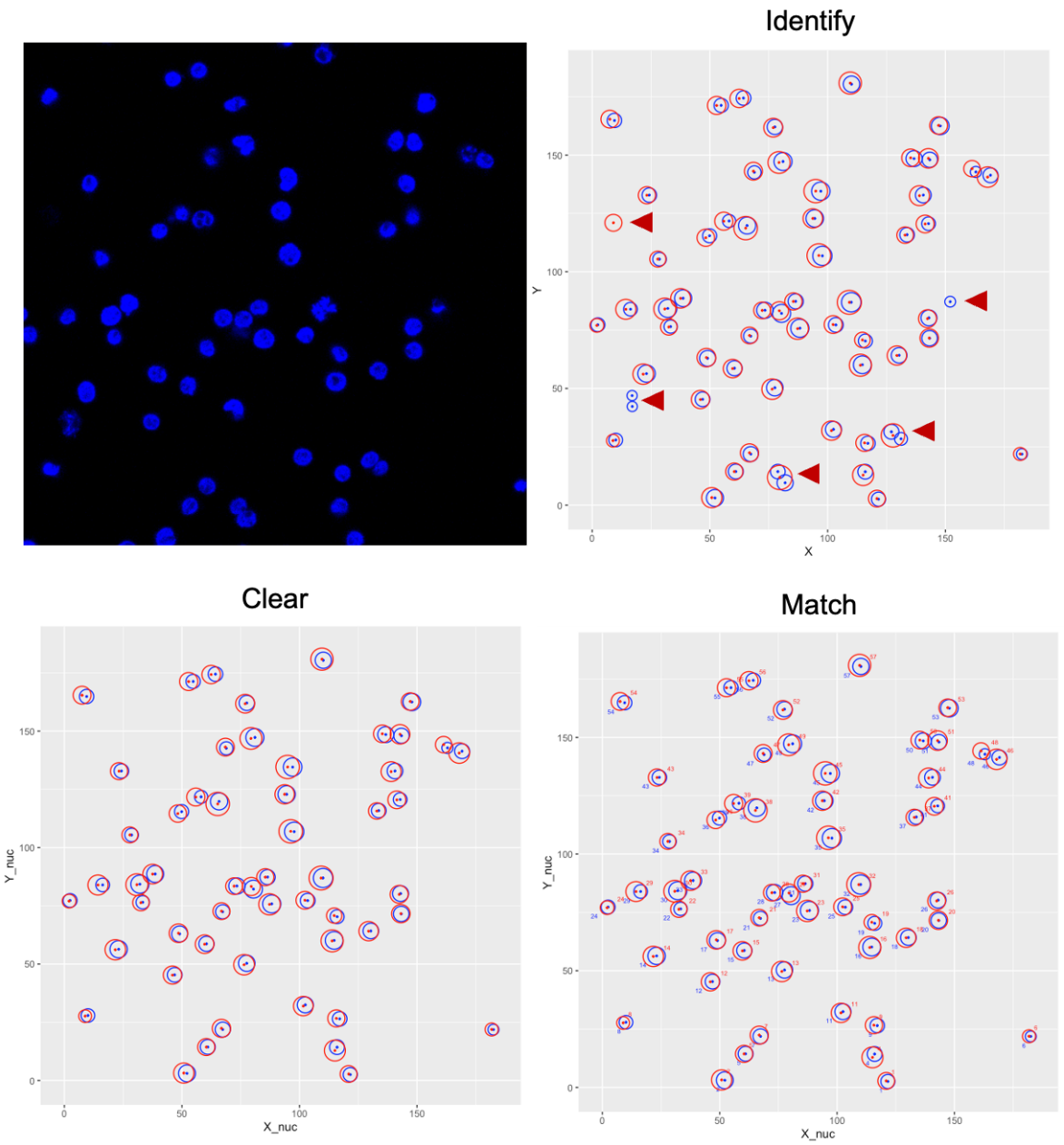

Figure 32. The illustration of the functioning of a plugin developed for matching nuclear and cellular ROIs. Briefly, the algorithm in R (version 4.2.1) processed the results of Fiji analysis of nuclear and cellular ROIs, a provisional cellular radius was calculated and nuclear centres that were inside the cellular area were matched with each other. Unmatched nuclear or cellular ROIs, as well as cellular ROIs where more than one nucleus matched, were excluded from the analysis. Nuclear and total cellular borders are shown arbitrarily, the real dimensions are not ideal circles. The plugin is available on request. Abbreviations: ROIs, regions of interest.

To analyze surface HLA-DR expression, confocal images were processed using a semi-automatic macro in Fiji that detected nuclear and outside ROIs. The mean fluorescence intensity of GFP fluorescence (Tat expression) in the nuclear ROI and mean fluorescence intensity of HLA-DR in the outside ROI were analysed for each cell individually. The cells were then categorized into two distinct groups: "Tat^{low}" and "Tat^{high}" according to the expression of Tat in

each nucleus (a cut-off value of median Tat expression across the cell population was chosen in such a way that 50% of cells were below it and 50% of cells were above).

To analyse the nuclear penetration of Tat CPP-Cy5, confocal images were processed using a semi-automatic macro in Fiji that detected nuclear ROIs on the images with the Hoechst 33342-staining as described above. Mean Cy5 fluorescence intensity in the nuclear ROI was analysed for each cell individually.

To analyze the nuclear fluorescence intensity of γH2AX, confocal images were processed using a semi-automatic macro in Fiji (ImageJ version 2.1.0/1.53c, Java version 1.8.0). Briefly, to create nuclear cell masks, the nuclear regions of interest (ROIs) were detected on the images with the DAPI-staining, the "Moments" threshold method implemented in Fiji was used. The masks were split to detect single nuclei. The area and circularity of detected ROIs were measured, and mean fluorescence intensity in nuclear ROIs was measured in the γH2AX channel. Nuclear ROIs with area <10 μm^2 (debris) or >60 μm^2 (doublets), irregular nuclei (ROIs circularity <0.3) were removed. At least five fields were analysed per biological replicate and images from at least two independent experiments were analysed. The plugin is available on request.

To analyze surface HLA-ABC expression, confocal images were processed using a semi-automatic macro in Fiji that detected cellular regions of interest (ROIs) in the YFP channel and enlarged them by 3 units to create outside ROIs that encompassed HLA-ABC staining. The mean fluorescence intensity of HLA-ABC (HLA-ABC expression) in the outside ROIs was analysed for each image. The macro is available on request. At least five fields were analyzed per biological replicate and images from at least two independent experiments were analyzed.

4.15 Cell lysate preparation

Cells were harvested from culture dishes and collected by centrifugation for 10 min at 800g. Cell pellets were resuspended in NETN buffer (NaCl 150 mM, ethylenediaminetetraacetic acid (EDTA) 1 mM, Tris pH 7.5 50 mmol/L, NP40 0.5%, 1× protease inhibitor cocktail; Roche, Basel, Switzerland), sonicated for 10 seconds at 30% using a Vibra Cell sonicator (SONICS & MATERIALS, Inc., Newtown, CT, USA), incubated on ice for 30 minutes and centrifuged at 4°C at 12000g for 10 minutes. The supernatant was transferred into a new pre-cooled microcentrifuge tube and the cell pellet was discarded. When preparing cytoplasmic and nuclear extracts, cells and nuclei were lysed using NE-PER Nuclear and Cytoplasmic Extraction Reagents (ThermoFisher) according to the manufacturer's instructions. The lysates (whole cell, cytoplasmic or nuclear) (5 µl) were used for quantification of protein

concentration by BCA assay (Thermo Fisher Scientific). Protein quantification was performed using the Pierce™ BCA Protein Assay Kit (Thermo Scientific) on the NanoDrop 2000C (Thermo Scientific). After measuring the concentration, cell lysates used for Western blot were supplemented with 6× Laemmli buffer (LDS) and 0.1M DTT, then heated at 95°C for 10 min.

4.16 Western Blot

Cell lysates (20 µg) and prestained molecular weight markers (PageRuler™ Prestained Plus Protein Ladder, Thermo Scientific) were resolved on 12- or 15-well precast SDS-PAGE gels (4-12 %) (NuPage) in MOPS Running Buffer (NuPage). Proteins were transferred onto 0.45 µm PVDF membrane (GE Healthcare, USA) in transfer buffer (0.025M Tris, 0.192M Glycine, 20% ethanol) at 90V at +4°C for 2h. Nonspecific binding was blocked in 5% non-fat dried milk in Tris-buffered saline, 0.1% Tween-20 (TBST) at room temperature for 1h.

Proteins were probed at +4°C overnight with the following primary antibodies: anti-Tat (1:200), anti-Zta (1:1000), anti-p53 (1:200), anti-Galectin-9 (1:1000), anti-GFP (1:1000), anti-transthyretin (1:1000), anti-transferrin (1:1000), anti-β-actin (1:1000, control of protein load). Membranes were washed with TBST, and incubated with appropriate peroxidase-conjugated secondary antibodies in 1:1000 dilution at room temperature for 1.5 h, followed by washing in TBST. Proteins were visualized using Immobilon Western Chemiluminescent HRP Substrate (Millipore) and ImageQuant LAS 4000 mini (GE Healthcare) for western blotting imaging and analysis. Densitometric analysis of blots at non-saturating exposures was performed using Fiji (ImageJ).

4.17 Immunoprecipitation and co-immunoprecipitation (Co-IP)

IP and Co-IP were performed using magnetic beads: Dynabeads™ His-Tag (Novotex) or Dynabeads™ Protein G (Invitrogen), coupled with 10 µg of appropriate antibody, following manufacturer's instructions. Due to high immunoglobulin presence, for co-immunoprecipitation in blood plasma specific antibody was cross-linked to magnetic beads with the use BS_3 crosslinking regent (Abcam, cat. # ab145612), following the manufacturer's instructions. Proteins were eluted from magnetic beads in NETN buffer supplemented with LDS and 0.1M DTT by shaking at 95°C for 10 min.

4.18 *In vitro* binding assay

In vitro binding assay was applied to study the direct interaction between purified Tat and Zta proteins. The procedure was performed according to the protocol described by (Lapetina & Gil-Henn 2017). In brief, Tat (the "bait" protein) was immobilized on AminoLink Coupling resin agarose beads

(Thermo Scientific, cat. # 20381) and was covalently linked to agarose beads by reducing agent sodium cyanoborohydride. Tat-linked beads were blocked with BSA to prevent non-specific binding, while empty agarose beads blocked with BSA were used as BSA control beads. Zta (the "prey" protein) was kept in solution and incubated with agarose beads to allow binding. The concentration of the bait protein Tat was kept constant (3.1 µg/mL), while the concentration of the prey protein Zta was increased (0; 2.5; 5; 10 µg/ml). After incubation, the beads were precipitated to separate unbound prey protein in solution from prey protein bound to the bait. The fraction of bound prey protein was analysed by Western Blot.

4.19 HIV-1 Tat ELISA in human serum samples

HIV-1 Tat concentration in human serum samples was determined as described previously (Rayne et al. 2016). Briefly, the 96-well plates (Sarstedt, ref 82.1581200) were coated with rabbit polyclonal anti-Tat-Loret antibodies (HXB2 J90, kindly provided by Dr. Bruno Beaumelle) at a dilution of 1:1000 in a 0.2M carbonate buffer (pH 9.6). After incubation overnight at 4°C, the plates were washed twice in PCBST (0.015 M Na_2HPO4, 0.015 M sodium citrate, 0.140 M NaCl, 0.05% Tween-20) and saturated with 8% milk in PBST (PBS/0.05% Tween-20) for 2 hours at room temperature, followed by three washes with PCBST. Reference dilutions of recombinant Tat protein (standards) and serum samples were loaded onto the plate (100 µl/well) and incubated for 4 hours at room temperature. The plates were then washed five times with PCBST and incubated overnight at 4°C with mouse monoclonal anti-Tat antibodies (Santa-Cruz, sc65912) diluted 1:100 in 8% milk in PCBST. The plates were then washed five times with PCBST and incubated for 2.5 hours at room temperature with peroxidase-conjugated goat anti-mouse antibodies (Santa-Cruz, sc65912) diluted 1:2000 in 8% milk in PBST, followed by five washes with PCBST. The signal was revealed by adding 3,3′,5,5′ Tetramethylbenzidine (TMB, Sigma T8665-100ML, 100 µl/well) for 20 minutes and the reaction was stopped using 0.5 M H_2SO_4 (50 µl/well). The absorbance at 450 nm was measured using a Tecan luminometer (Tecan Life Sciences). The HIV-1 Tat protein concentration in the samples was determined based on the absorbance values from the standard linear curve. All materials for ELISA of HIV-1 Tat were kindly provided by Dr. Bruno Beaumelle, CPBS, University of Montpellier.

4.20 HIV p24 ELISA in human serum samples

Capsid protein p24 (encoded by the *gag* gene) is the most abundant viral antigen and its detection in serum is an established marker of HIV infection, HIV replication, disease progression, and therapy efficacy in the clinical surveillance of people living with HIV (Brinkhof et al. 2006; Garcia et al. 2011;

Passaes et al. 2021; Schüpbach 2002; Schüpbach et al. 2000). HIV-1 p24 concentration in human serum samples was determined using an HIV Antigen mAB ELISA kit (Innotest, cat. # 80564) following the manufacturer's instructions. Briefly, a conjugate working solution 1 and reference dilutions of p24 antigen (standards) or human serum samples were loaded onto the plate (100 µl/well) and incubated for 1 hour at 37 °C. The plates were washed 5 times with wash solution and a conjugate working solution 2 was added, followed by incubation for 30 minutes at 37 °C and washing 5 times with wash solution. The signal was revealed by adding TMB substrate solution for 30 minutes and the reaction was stopped using 0.5 M H_2SO_4 (50 µl/well). The absorbance at 450 nm was measured using a Tecan luminometer (Tecan Life Sciences). The p24 antigen concentration in the samples was determined based on the absorbance values from the standard linear curve. All materials for ELISA of p24 were kindly provided by Dr. Bruno Beaumelle, CPBS, University of Montpellier.

4.21 EBV Zta ELISA in human serum samples

EBV Zta concentration in human serum samples was determined as described previously (Habib et al. 2017). Briefly, the 96-well plates were coated with AZ69 capture antibodies overnight at +4°C, blocked in 10% FBS, 4% Gelofusin PBST for 1 hour at room temperature. Reference dilutions of recombinant Zta-FC CHO protein (standards) and serum samples were loaded onto the plate, and incubated for 2 hours at room temperature. Next, the samples were incubated with a biotinylated AZ130 detection antibody for 1 hour at room temperature, followed by incubation with HRP-conjugated streptavidin for 30 minutes at room temperature and TMB for 10 minutes for revealing. The reaction was stopped by the addition of 0.1 M H_2SO_4 and 1 M Tris. The absorbance was measured at 450 nm by Plate reader Infinite 200 PRO (Tecan Life Sciences). The resulting Zta concentration was extrapolated from the standard curve based on Zta reference dilution. All samples were analysed in duplicates, the mean result is presented. All materials for ELISA of Zta were kindly provided by Dr. Emmanuel Drouet, Université Grenoble Alpes.

4.22 Plasmid cloning, synthesis, extraction

Plasmids pcDNA3-YFP1 and pcDNA3-YFP2 that encode for split-YFP fragments (YFP1 – amino acids 1-158; YFP2 – amino acids 159-239, GenBank: ABV26713.1), as well as plasmids pcDNA3-YFP1-ERGIC-53, pcDNA3-YFP2-ERGIC-53, pcDNA3-YFP1-MCFD2 and pcDNA3-YFP2-MCFD2 were a generous gift from authors (Nyfeler et al. 2005). pcDNA3-CFP, FUW-tetO-hOKMS, FUdeltaGW-rtTA, mCherry2-C1 plasmids were purchased from Addgene (cat. #109330, 51543, 19780, 54563). pEYFP-C3 plasmid was a generous gift from Francesco Baschieri. pTagBFP-C and pTagGFP2-C were

purchased from Evrogen, Russia (cat.# FP171, cat.# FP191). HIV-1 Tat sequence (GenBank: AAB59870.1, 86 amino acids) was synthesized by Eurofins Genomics, Germany, in pEXA128 plasmid (pEXA128-Tat). pcDNA3.1+/Tat101-flag(PEV280) plasmid was obtained through the NIH HIV Reagent Program, Division of AIDS, NIAID, NIH, ARP-10453, contributed by Dr. Eric Verdin. EBV (strain B95-8) Zta sequence (Sequence ID: P03206.2) was synthesized by VectorBuilder, USA, in pcDNA3(+)-YFP2 plasmid (pcDNA3(+)-YFP2-Zta). pET29a(+)-Zta was previously cloned in our laboratory by inserting Zta sequence in pET29(+) plasmid between SalI and NdeI restriction sites. The resulting sequence encoded for a His-tagged Zta. An LTR-TurboRFP plasmid that contained the HIV-1 3' LTR fragment upstream to the promoter-less red fluorescent protein TurboRFP gene cloned in pTurboRFP-PRL plasmid (Evrogen, Moscow, Russia) was described previously (Kurnaeva et al. 2022) and was a kind gift from Eugene V. Sheval. Primers used for cloning were purchased from Eurofins Genomics, Germany (**Table 9**).

Table 9. Primers and oligonucleotides used in the study for cloning.

Primer	Sequence 5’→3’
BZLF1-b F	AAATTTAAGAGATCCTCGTGTAAAACATC
BZLF1-b R	CGCCTCCTGTTGAAGCAGAT
delta AD XhoI F (Tat)	GCATCTCGAGGTGGCAGGAAGAAGCGG
delta AD XhoI F (Zta)	AACACTCGAGAATCGCTGGAGGAATG
delta AD XhoI R (Tat)	AGATGCATGCTCGAGCTATTCCTTC
delta BD F (Tat)	CTATCAAAGGATCCAAGGCAGTCAGACTCAT
delta BD-GRD BamHI F (Tat)	CAAAGGATCCCCACCTCCCAACCCCGG
delta BD-GRD BamHI R (Tat)	TTCTGGATCCCATAGGAGATGCCTAAG
delta BD-GRD XhoI R (Tat)	CATGCTCGAGCTATTCCTTCG
delta bZIP BamHI F (Tat)	TGAAGGATCCTGTGCCCAAGCCTGGA
delta bZIP BamHI R (Tat)	TTCTGGATCCGCTTTATTTCTAGTTCAG
delta C term R (Zta)	AAGTCGACTTACATCTGCTTCAACAGGAGG
delta Ex2 R (Tat)	AAGTCGACTATTGCTTTGATAGAGAAACTTG
delta GRD R (Tat)	CGCTTCTGGATCCGAGGAGGTCTTCGTCGCT
delta TAD XhoI R (Zta)	CATGCTCGAGATTTAGGTGACAC
Link SalI F L	ACCACGTTGTCGACGGTGGCGGTGGC
Linker EcoRI F	AATTCGGTGGCGGTGGCTCTGGAGGTGGTGGG TCGC
Linker SalI F	ACGTTGTCGACGGTGGCGGTGGC
Linker XhoI R	TCGAGCGACCCACCACCTCCAGAGCCACCGCCA CCG
Minimal promoter F	CCGGTTAGAGGGTATATAATGGAAGCTCGACTT CCAGA
Minimal promoter R	CCGGTCTGGAAGTCGAGCTTCCATTATATACCCT CTAA

NFκB RE 1 F	CATGTTGGGGACTTTCCGCTGGGGACTTTCCGCTGGG
NFκB RE 2 F	GACTTTCCGCTGGGGACTTTCCGCTGGGGACTTTCCGCGCTAG
NFκB RE 1 R	AGTCCCCAGCGGAAAGTCCCCAGCGGAAAGTCCCCAA
NFκB RE 2 R	CGCGGAAAGTCCCCAGCGGAAAGTCCCCAGCGGAA
pcDNA-YFP1/2 F	GTGGCTCTGGAGGTGGTG
pcDNA-YFP1/2 R	GGCAAACAACAGATGGCTGG
pcDNA3-CFP F	GCCAGTGTGCTGGAATTCTGC
pcDNA3-CFP R	GCTCCTCGCCCTTGCTCA
shRNA CIITA F	CCGGCATACGTGATGCGCTACTTTGCTCGAGCAAAGTAGCGCATCACGTATGTTTTTG
shRNA CIITA R	AATTCAAAAACATACGTGATGCGCTACTTTGCTCGAGCAAAGTAGCGCATCACGTATG
scrambled shRNA F	CCGGCCTAAGGTTAAGTCGCCCTCGCTCGAGCGAGGGCGACTTAACCTTAGGTTTTTG
scrambled shRNA R	AATTCAAAAACCTAAGGTTAAGTCGCCCTCGCTCGAGCGAGGGCGACTTAACCTTAGG
SV40pA R	GAAATTTGTGATGCTATTGC
Tat 101 end stop+SalI R	CATGGTCGACCTAATCGAATGGATCTGTCTCTGTC
Tat check F	GATCCTAGACTAGAGCCCTGGAAGC
Tat end SalI R	AGATGCATGGTCGACCTATTCCTTCGG
Tat screen R	TGTTATGAAACAAACTTGGCAATGAAAGCAACA
Tat w/o stop F	GTAGCTCGAGGTATGGAGCCAG
Tat w/o stop R	CTACGAATTCTTCCTTCGGGCCTGTCGG
YFP F	GCTCGAGGTATGGTGAGCAAGGGCGAG
YFP link R	ACCTCGAGGGACCCACCACCTCCAGAG
Zta 1 low	GGCTGTTGTGGTTTCCGTGTG
Zta 1 up	TCAGCTGTTCCCAGTCTCCGA
Zta end SalI R	GCATGGTCGACATTTAGGTGACAC
Zta w/o stop F	GTAGCTCGAGGTATGATGGACCC
Zta w/o stop R	CTACGAATTCGAAATTTAAGAGATCCTCGTGTAAAACATCTGGTG
MCS EcoRI F	AATTCACCGGTCTAGAGCTAGCTTCGAATGTACAGGATCCG
MCS EcoRI R	AATTCGGATCCTGTACATTCGAAGCTAGCTCTAGACCGGTG
YFP1-Tat SphI R	AAAAAAGCATGCTTCCTTCGGGCCTGTC
YFP1-Tat AgeI F	AAAAAAACCGGTAAGCTTATGGTGAGCAAGG

P2A F	CGGAAGCGGAGCTACTAACTTCAGCCTGCTGAAGCAGGCTGGAGACGTGGAGGAGAACCCTGGACCTA
P2A R	GATCTAGGTCCAGGGTTCTCCTCCACGTCTCCAGCCTGCTTCAGCAGGCTGAAGTTAGTAGCTCCGCTTCCGCATG
YFP2-Zta BglII F	AAAAAAAGATCTATGAAGAACGGCATCAAGG
YFP2-Zta BamHI R	AAAAAAGGATCCGGGCCCTCTAGACTC

For all cloning reactions the target plasmid was first digested by restriction enzyme, then its linearized form was isolated from agarose gel and dephosphorylated with shrimp alkaline phosphatase (SAP) (Fermentas, # EF0511). Tat short sequence (86 amino acids) was generated by XhoI digestion of pEXA128-Tat plasmid and was ligated in pcDNA3-YFP1 and pcDNA3-YFP2 plasmids at the XhoI site. Tat long sequence (101 amino acids, Tat101) was generated by PCR of pcDNA3.1+/Tat101-flag(PEV280) plasmid with primers that encode for the SalI recognition site. Of note, SalI and XhoI have compatible ends. After SalI digestion, Tat101 was inserted in pcDNA3-YFP1 plasmid at the XhoI site. To clone the Tat-CFP plasmid, the Tat sequence was amplified by PCR of pEXA128-Tat plasmid with the forward primer that encodes for the XhoI recognition site and the reverse primer that excludes the stop-codon and encodes for EcoRI recognition site. To create a flexible $(GGGS)_2$ linker between Tat and CFP, nearly complementary oligonucleotides were purchased from Eurofins Genomics. Oligonucleotides were annealed, creating EcoRI and XhoI compatible sticky ends at 5’ and 3’ ends of forward oligonucleotide, respectively. Tat sequence, amplified without stop codon was digested by EcoRI and ligated with annealed oligonucleotides, then the ligation product was digested by XhoI and inserted in pcDNA3-CFP plasmid at XhoI site. To clone the YFP-Tat plasmid, the linker-Tat sequence was amplified by PCR of YFP1-Tat plasmid with primers that encode for SalI recognition site and after SalI digestion was inserted in pEYFPC3 plasmid at the XhoI site (pEYFPC3-Tat). To clone BFP-Tat and GFP2-Tat plasmid, the Tat sequence was amplified by PCR of YFP1-Tat plasmid with primers that encode for XhoI recognition site and after XhoI digestion was inserted in pTagBFP-C and pTagGFP2-C plasmids at XhoI site. Importantly, fusion with a fluorescent protein did not perturb Tat's transactivation capacity as assessed by HIV-1 3′-LTR-TurboRFP reporter as described previously (Kurnaeva et al. 2022) in RPMI8866 cells with stable integration of HIV-1 3′-LTR- TurboRFP reporter (**Figure 33**).

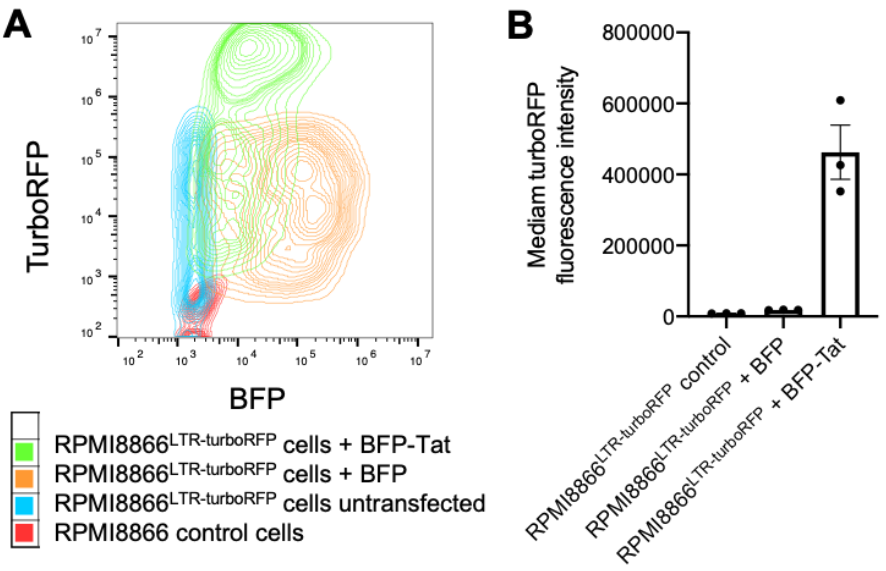

Figure 33. The analysis of the transactivation capacity of BFP-Tat in RPMI8866 cells stably expressing HIV-1 3′-LTR-TurboRFP reporter and transfected with BFP or BFP-Tat. (A) A representative contour plot graph of flow cytometry analysis of BFP and TurboRFP fluorescence. (B) The median fluorescence intensity of TurboRFP in nontransfected RPMI8866 cells and BFP^+ RPMI8866 cells transfected with BFP or BFP-Tat, data are presented as mean ± SEM.

Zta sequence generated by XhoI digestion of pcDNA3-YFP2-Zta was ligated in pcDNA3-YFP1 plasmid by XhoI site. To clone the Zta-CFP plasmid, the Zta sequence was amplified by PCR of pcDNA3-YFP2-Zta plasmid with forward primer that encodes for XhoI recognition site and reverse primer that excludes stop-codon and encodes for EcoRI recognition site. To create a flexible $(GGGS)_2$ linker between Zta and CFP, nearly complementary oligonucleotides were purchased from Eurofins Genomics. Oligonucleotides were annealed, creating EcoRI and XhoI compatible sticky ends at 5′ and 3′ ends of forward oligonucleotide, respectively. Zta sequence, amplified without stop codon was digested by EcoRI and ligated with annealed oligonucleotides, then the ligation product was digested by XhoI and inserted in pcDNA3-CFP plasmid at XhoI site. To clone the YFP-Zta plasmid, the linker-Zta sequence was amplified by PCR of YFP2-Zta plasmid with primers that encode for SalI recognition site and after SalI digestion was inserted in pEYFPC3 plasmid at XhoI site (pEYFPC3-Zta). To clone BFP-Zta and GFP2-Zta plasmid, the Zta sequence was amplified by PCR of pcDNA3-YFP2-Zta plasmid with primers that encode for XhoI recognition site and after XhoI digestion was inserted in pTagBFP-C and pTagGFP2-C plasmids at XhoI site. To clone the mCherry-Zta plasmid, the linker-Zta sequence was amplified by PCR of YFP2-Zta plasmid with primers that encode for SalI restriction site and after SalI digestion was inserted in the mCherry2-C1 plasmid at SalI site.

All obtained plasmid sequences were confirmed by PCR (**Figure 34A**), restriction analysis and Sanger sequencing with primers

5’-GTGGCTCTGGAGGTGGTG-3’ and 5’-GGCAAACAACAGATGGCTGG-3’ (data not shown). The expression of Tat and Zta from the cloned plasmids was verified by Western Blot (**Figure 34B**) and immunofluorescent staining (**Figure 34C**).

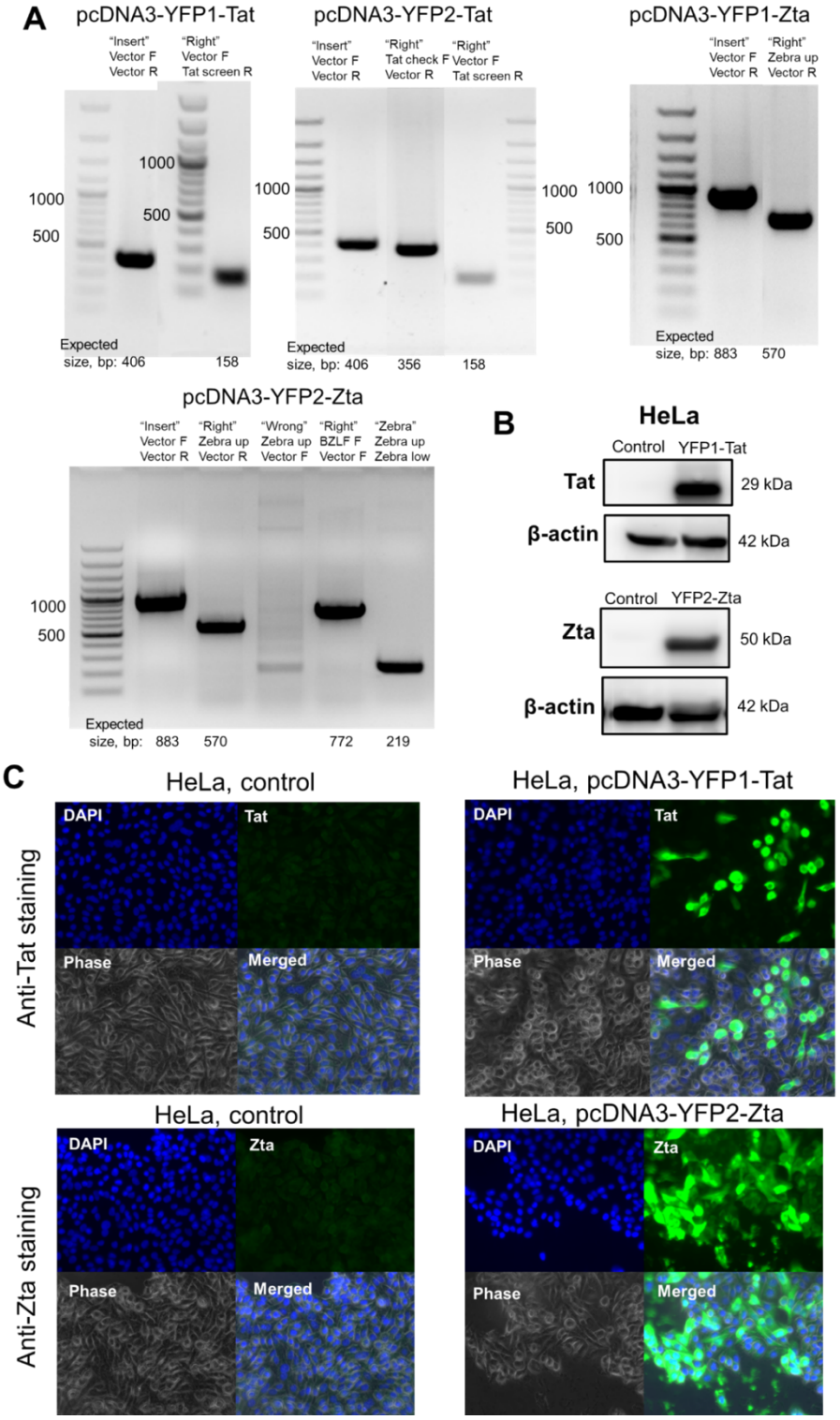

Figure 34. Confirmation of Tat and Zta successful cloning in pcDNA3-YFP1 and pcDNA3-YFP2 plasmids by PCR (A), Western blot (B) and immunofluorescent staining (C). (A) PCR of selected colonies was performed to confirm the insert (“insert”, with Vector F + R primers) of Tat and Zta sequence in pcDNA3-YFP1 and pcDNA3-YFP2 plasmids. The expected size of PCR product for plasmid without insert is 137 bp, for plasmid

with the insert of full-length Tat is 406 bp, and for plasmid with the insert of full-length Zta is 883 bp. All selected colonies had an insert. The right orientation was confirmed with the use of one primer annealing to vector backbone (Vector F or R) and another primer annealing to insert (Tat screen R, Tat check F, Zebra up, BZLF F). All selected colonies had the right orientation of the insert. The sequence was also confirmed by Sanger sequencing with Vector F+R primers. (B) the expression of Tat and Zta from pcDNA3-YFP1-Tat and pcDNA3-YFP2-Zta plasmids was checked by Western blot staining for Tat and Zta. B-actin was used as a control of protein load. The bands of YFP1-Tat (~29 kDa) and YFP2-Zta (~50 kDa) were only observed in transfected HeLa cells. (C) the expression of Tat and Zta from pcDNA3-YFP1-Tat and pcDNA3-YFP2-Zta plasmids was checked by immunofluorescent staining using antibodies against Tat and Zta under permeabilizing conditions. Nuclei were counterstained with DAPI. Tat and Zta staining were observed only in transfected HeLa cells.

Tat and Zta sequences lacking key domains were generated by PCR from YFP1-Tat and YFP2-Zta plasmids, respectively, with primers that encode for SalI recognition sites and BamHI recognition sites (in case of internal deletion) and after SalI digestion (or after BamHI digestion, fragment ligation followed by XhoI digestion) were inserted in pcDNA3-YFP1 and pcDNA3-YFP2 plasmids, digested by XhoI and dephosphorylated. The obtained plasmid sequence was confirmed by PCR, restriction analysis (**Figure 35**) and Sanger sequencing with primers 5'-GTGGCTCTGGAGGTGGTG-3' and 5'-GGCAAACAACAGATGGCTGG-3' (data not shown).

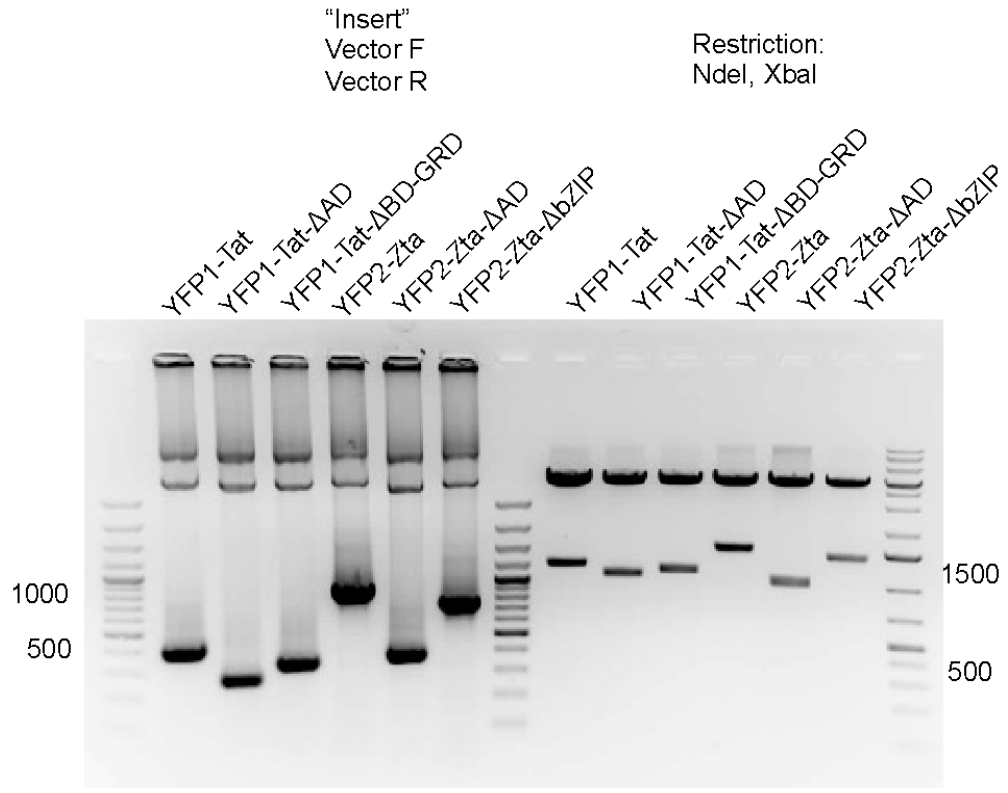

Expected size, bp: 406 265 337 883 376 754 4947 4947 4947 4947 4947 4947
1209 1068 1140 1477 1019 1397

Figure 35. Confirmation of Tat and Zta mutants successful cloning in pcDNA3-YFP1 and pcDNA3-YFP2 plasmids by PCR and restriction analysis. A – PCR of selected colonies was performed to confirm the insert ("insert", with Vector F + R primers) of Tat and Zta mutant sequence in pcDNA3-YFP1 and pcDNA3-YFP2 plasmids. The expected sizes of the PCR products for plasmids are listed below each line. All selected colonies had an insert, which was confirmed by Sanger Sequencing.

gRNAs targeting *MYC*, *IGH*, *ETO* and *AML1* genes were designed using the online CRISPR Design tool (Zhang Lab, MIT) (**Table 10**) and cloned into the phU6-gRNA plasmid (Addgene #53188, (Kabadi et al. 2014)) digested by the BstV2I restriction enzyme. gRNAs efficacy was confirmed by the ENIT method based on the detection of translocations formed as a result of tested gRNA and nuclease of known specificity and efficacy as described previously (Germini et al. 2017a). gRNA genes from phU6-gRNA plasmids were amplified by PCR and were subsequently cloned into Puro-Cas9 donor plasmid (Addgene #58409, (González et al. 2014)) with puromycin resistance gene in the SalI restriction site. Plasmids were assembled using a Gibson Assembly Master Mix kit (NEB, USA). Primers for insert amplification were designed according to the NEB Gibson Assembly protocol. PCR products were purified using NucleoSpin® Gel or PCR Clean-up PCR kit (Macherey-Nagel, Germany).

Table 10. gRNA sequences used in (Shmakova et al. 2022b).

Target loci	Sequence 5′→3′	Position
AML1 (RUNX1)	GACTCCCCCATGTACCCCTA	intron 5
ETO (RUNX1T1)	GATGTAAGAGGAAGCAGCTT	intron 1
IGH	GAGAACATACCAAGCCCCAC	4.8 kb upstream IGH constant μ locus
MYC	TGCACCTCGGACGCTCCTGC	1.4 kb upstream 1 exon

A NF-κB-mCherry reporter plasmid consisted of five repeats of the NF-κB response elements (5′-TGGGGACTTTCCGC-3′), a minimal promoter (5′-TAGAGGGTATATAATGGAAGCTCGACTTCCAG-3′) and red fluorescent protein mCherry2 as a reporter gene. The construct was cloned into mCherry2-C1 plasmid (Addgene, # 54563) through the removal of CMV enhancer and CMV promoter fragments. For this, the plasmid was digested by the PciI and BmtI restriction enzymes (New England Biolabs) and dephosphorylated using shrimp alkaline phosphatase (Fermentas) prior to ligation. Single-stranded DNA oligos encoding NF-κB response elements and minimal promoter sequences were purchased from Eurofins Genomics, Germany (**Table 9**), annealed, phosphorylated using T4 polynucleotide kinase (Thermo Fisher Scientific) and sequentially ligated into the mCherry2-C1 plasmid upstream to the mCherry2 gene using T4 DNA ligase (Thermo Fisher Scientific): NF-κB

response elements were inserted at the PciI and BmtI restriction sites, the minimal promoter was inserted at the AgeI restriction site (Thermo Fisher Scientific). The sequence of the resulting plasmid was confirmed using Sanger sequencing. To confirm the functionality of the created NF-κB-mCherry reporter plasmid, RPMI8866 cells were electrotransfected with the NF-κB-mCherry reporter plasmid as described above and phorbol myristate acetate (PMA, also known as 12-O-tetradecanoylphorbol 13-acetate (TPA), 1-3 μg/ml, Sigma Aldrich), an activator of NF-κB pathway (Holden et al. 2008), was added to cells 24 h after electrotransfection; mCherry fluorescence was evaluated 48 h after electrotransfection. The expression of mCherry2 was detectable when this plasmid was transfected into RPMI8888 cells, and it increased noticeably after NF-κB activation with PMA (**Figure 36**).

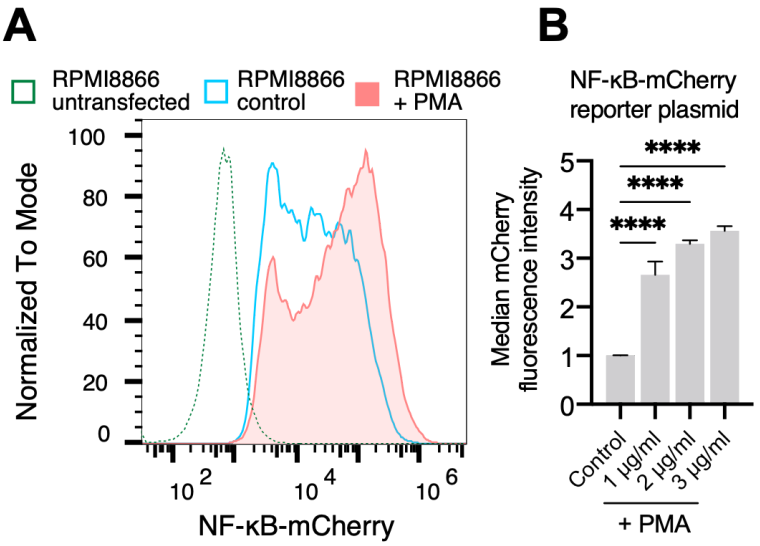

Figure 36. Confirmation of the functionality of the created NF-κB-mCherry reporter plasmid. (A) A representative histogram for flow cytometry analysis of RPMI8866 cells transfected with the NF-κB-mCherry reporter plasmid and treated (red) or not (blue) with 1 μg/ml PMA for 24 h. Untransfected RPMI8866 cells served as negative control (green dotted line). (B) The effect of different concentrations of PMA on mCherry expression in RPMI8866 cells after transfection with the NF-κB-mCherry reporter plasmid calculated as the median fluorescence intensity in the sample normalized relative to the median fluorescence intensity in the control (untreated RPMI8866 cells after transfection with the NF-κB-mCherry reporter plasmid), averaged data from at least three biologically independent experiments are shown. Data are presented as mean ± SEM, **** $p < 0.0001$, ANOVA, Tukey's post-hoc test.

shRNA targeting the human CIITA gene was designed using the GPP Web Portal (the RNAi Consortium, https://portals.broadinstitute.org/gpp/public/, date of accession 13.03.2023). Scrambled shRNA sequence was imported from Addgene plasmid #1864, (Sarbassov et al. 2005). shRNAs were cloned into the pLKO.1 plasmid with puromycin resistance gene (Addgene, #8453, (Stewart et

al. 2003)) as described previously (Shmakova et al. 2023). Briefly, single-stranded DNA oligos encoding shRNA sequences were purchased from Eurofins Genomics, Germany (**Table 9**), annealed, phosphorylated using T4 polynucleotide kinase (Thermo Fisher Scientific) and ligated into the pLKO.1 plasmid using T4 DNA ligase (Thermo Fisher Scientific). The plasmid was digested by the AgeI and EcoRI restriction enzymes (New England Biolabs) and dephosphorylated using shrimp alkaline phosphatase (Fermentas) prior to ligation. The sequence of resulting plasmids encoding CIITA shRNA (pLKO.1-shCIITA) or scrambled shRNA (pLKO.1-scrambled-shRNA) was confirmed using Sanger sequencing.

To generate cells with inducible expression of fluorescent protein-fusion constructs (YFP, YFP-Tat, YFP-Zta, YFP1-Tat-P2A-YFP2-Zta), FuW-tetO-YFP, FuW-tetO-YFP-Tat, FuW-tetO-YFP-Zta or FuW-tetO-YFP1-Tat-P2A-YFP2 plasmids were cloned. Initially, the FUW-tetO-hOKMS plasmid was digested with EcoRI to remove hOKMS, and a multiple cloning site (MCS) was inserted. For FUW-tetO-YFP1-Tat-P2A-YFP2-Zta, YFP1-Tat was amplified by PCR of pcDNA3-YFP1-Tat plasmid with a forward primer that encodes for AgeI restriction site and a reverse primer that encodes for SphI restriction site. To create a P2A linker between YFP1-Tat and YFP2-Zta, nearly complementary oligonucleotides were purchased from Eurofins Genomics. Oligonucleotides were annealed, creating SphI and BglII compatible sticky ends at 5' and 3' ends of forward oligonucleotide, respectively. YFP2-Zta was amplified by PCR of of pcDNA3-YFP2-Zta plasmid with a forward primer that encodes for the BglII restriction site and a reverse primer that encodes for the BamHI restriction site. FUW-tetO-MCS was digested by AgeI and BamHI, and YFP1-Tat, P2A, and YFP2-Zta fragments were ligated. For FUW-tetO-YFP, FUW-tetO-YFP-Tat, and FUW-tetO-YFP-Zta, YFP, YFP-Tat, and YFP-Zta fragments obtained from the digestion of pEYFPC3, pEYFPC3-Tat, pEYFPC3-Zta plasmids with AgeI and BamHI were ligated into FUW-tetO-MCS plasmid digested with AgeI and BamHI. These cloning steps yielded plasmids for inducible protein expression, facilitating the investigation of protein interactions and functions in cells under controlled conditions. Obtained plasmid sequences were confirmed by PCR and Sanger sequencing.

Plasmids were transformed into E. coli Stellar™ competent cells (Takara Bio) by heat shock (42°C, 90 sec) and grown in LB medium. Plasmids were extracted with NucleoSpin Plasmid Mini, Midi and Maxi kits (Macherey-Nagel, Germany). DNA fragments from agarose gel were extracted with a NucleoSpin Gel extraction kit (Macherey-Nagel, Germany).

4.23 PCR

PCR was carried out using Powerup SYBR Green Mastermix (ThermoFisher), primers used for PCR are listed in **Table 11** and were purchased from Eurofins

Genomics, Germany. The thermal cycling program was as follows: a 2-minute denaturation set at 50°C, a 2-minute denaturing step at 95°C followed by 40 amplification cycles consisting of 15 seconds denaturing at 95°C, 1 minute of annealing at 60°C and 1 minute of elongation at 72°C, followed by a final step 10-minute elongation at 72°C.

Table 11. Primers used for PCR and qPCR.

Primer	Sequence 5′→3′
ACTB F	GCATGGGTCAGAAGGAT
ACTB R	CCAATGGTGATGACCTG
BZLF1-b F	AAATTTAAGAGATCCTCGTGTAAAACATC
BZLF1-b R	CGCCTCCTGTTGAAGCAGAT
GAPDH F cDNA	CTGCACCACCAACTGCTTAG
GAPDH R cDNA	AGGTCCACCACTGACACGTT
HIV Tat F	CTAGACTAGAGCCCTGGAAGCA
HIV Tat R	TGAGGAGGTCTTCGTCGCT
HLA-A F	CGACGCCGCGAGCCAGA
HLA-A R	GCGATGTAATCCTTGCCGTCGTAG
HLA-B F	GACGGCAAGGATTACATCGCCCTGAA
HLA-B R	CACGGGCCGCCTCCCACT
HLA-C F	GGAGACACAGAAGTACAAGCG
HLA-C R	CGTCGTAGGCGGACTGGTCATA
HLA-DQA1 F	CAACATCACATGGCTGAGCA
HLA-DQA1 R	TGCTCCACCTTGCAGTCATAA
HLA-DQB1 F	TCTCCCCATCCAGGACAGAG
HLA-DRB1 R	ACCACTCACAGAACAGACCAGGAG
HLA-DRB1ex1 F	GGGTGGAGGGGTTCATAGTT
HLA-DRB1ex1 R	CTCCAGGGAGCTTCAGACAC
HLA-DRB5 F	CACAGTGGAATGGAGAGCACAGTC
HLA-DRB5 R	GAGCAGGCCCAGCACAAAGC
HLA-E F	CCTACGACGGCAAGGA
HLA-E R	CCCTTCTCCAGGTATTTGTG
HLA-F F	GGCAGAGGAATATGCAGAGGAGTT
HLA-F R	TCTGTGTCCTGGGTCTGTT
HSPA1A+B F	GCGAGGCGGACAAGAAGAA
HSPA1A+B R	GATGGGGTTACACACCTGCT
HSPA6 F	GATGTGTCGGTTCTCTCCATTG
HSPA6 R	CTTCCATGAAGTGGTTCACGA
RPL32 F	CATCTCCTTCTCGGCATCA
RPL32 R	AACCCTGTTGTCAATGCCTC
Cas9 F	CCGAAGAGGTCGTGAAGAAG
Cas9 R	GCCTTATCCAGTTCGCTCAG
TA F	AAATCAGCTCGCGTTCCTGT

TA R	CGCTTTCGCACTTTAGCTGT
GAPDH F2	CAAGGTCATCCATGACAACTTTG
GAPDH R2	GTCCACCACCCTGTTGCTGTAG
MYC T R (translocation primer)	GCGTTCAGGTTTGCGAAAGTA
IGH T R (translocation primer)	TCCCCTCCCTTCTGAGTCTGC
MYC no T (~6.8 kbp downstream the breakpoint)	AAGGTCAGAGTCTGGATCAC
MYC R (~6.8 kbp downstream the breakpoint)	TAACTACCTTGGGGGCCTTT
ETO F	TGCATGAACATAAACAGGCACTC
AML1 R	GAAGCTCACCAGATAGGCTGTA
GAPDH F gDNA	CCCATCACCATCTTCCAGGAG
GAPDH R gDNA	GTTGTCATGGATGACCTTGGC
ACTB F gDNA	GCCAGCTGCAAGCCTTGG
ACTB R gDNA	GCCACTGGGCCTCCATTC
EBER1 F gDNA	AGGACCTACGCTGCCCTA
EBER1 R gDNA	AAAACATGCGGACCACCA
BLLF1 F	AGAATCTGGGCTGGGACGTT
BLLF1 R	ACATGGAGCCCGGACAAG
HLA-DRB1 i F ChIP	GCTGGAGAACAGGACAGGAC
HLA-DRB1 i R ChIP	TTACCCAACCCAGGAGCAAG
HLA-DRB5 i F ChIP	TGCTTTACTGCTATCACCCTGT
HLA-DRB5 i R ChIP	CCACTCCCACTTCCCAAACC
HLA-DRB5 ii F ChIP	GTGTCACTGTCAGCTTTGCC
HLA-DRB5 ii R ChIP	TGGTCCTGTCCTGTTCTCCA
ACTB F ChIP	GCCAGCTGCAAGCCTTGG
ACTB R ChIP	GCCACTGGGCCTCCATTC

4.24 RNA extraction, sequencing, RNA-seq data processing and analysis

Purified B cells were treated with Tat (250 ng/ml ~ 25 μM), Zta (1000 ng/ml ~ 37 μM) or Tat and Zta (at 250 ng/ml and 1000 ng/ml, respectively) or left untreated. The concentrations were chosen based on previous reports on the range of serum concentrations of Tat (Poggi et al. 2004) and Zta (Habib et al. 2017). 6 h and 48h after treatment cells were collected and RNA was extracted

using NucleoSpin RNA isolation kit (Macherey-Nagel, Germany) following manufacturer's instructions. Each condition was performed and analysed in quadruplicates. Tat and Zta cellular penetration in primary B cells was confirmed by Western blot analysis (**Figure 37**).

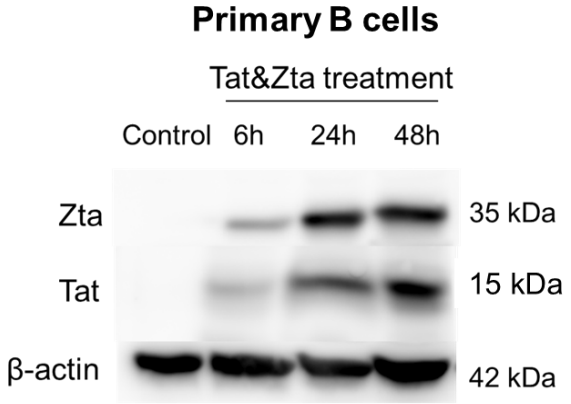

Figure 37. A Western blot analysis of Tat and Zta accumulation in B cells. Primary B cells were treated with Tat and Zta (at 250 ng/ml and 1000 ng/ml, respectively) for 6, 24h and 48h by addition of recombinant proteins in cell medium. Untreated B cells were used as a control. After the time indicated, cells were collected, and washed three times with PBS to avoid collecting proteins present in the medium and Western blot staining for Tat, Zta and β-actin (control of protein load) was performed.

Total RNA from BLAS cell lines was isolated using the NucleoSpin RNA kit following the manufacturer's instructions. Each condition was performed and analysed in triplicates.

The quantity and quality of total RNA were measured using a NanoDrop2000C Spectrophotometer (Thermo Fisher Scientific). The cDNA libraries were constructed and sequenced in Novogene, China. The raw sequencing reads were mapped to the human genome (assembly GRCh38.p10) using HISAT2 (version 2.0.5). Read counting was performed using featureCounts (ver 2.0.1) in a strand-specific mode. GENCODE v26 gene annotation (ALL) was used. Features with a low total count number (< N counts across all samples, where N is the number of replicates in each condition) were discarded. Differential expression analysis was performed using the DESeq2 R package (version 1.30.1). For BLAS cell lines, the genes meeting the criteria p value adjusted (p.adjust) by the Benjamini-Hochberg procedure < 0.05, $|\log_2$ fold change$|$ > 0.5 were considered differentially expressed. Raw RNA-seq data for BLAS cell lines as well as processed data (gene counts) are deposited in GEO with accession number GSE212499. For B cells, differentially expressed genes were filtered by adjusted P value < 0.05. No filter was applied to fold changes in gene expression, i. e. all statistically significant deregulated genes were taken into analysis, since unlike "classical" experiments when a transgene is ectopically expressed in all cells, we used more "physiological" experimental

setup and it is probable that 100%-efficient cell and nuclear penetration with viral proteins was not achieved (**Figure 38**).

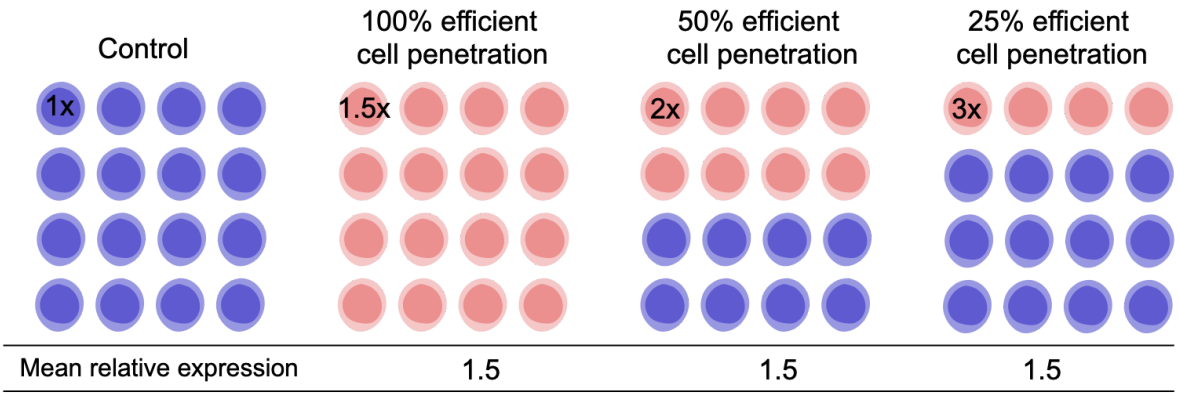

Figure 38. Cell penetration efficiency might affect gene expression levels in the bulk population. A hypothetical model where varying fold changes in gene expression (1.5X, 2X, 3X) and varying degrees of cell penetration efficiency by viral proteins might result in the same fold changes for a bulk population.

Overrepresentation analysis (ORA) was performed with an R package clusterProfiler (version 4.4.4) (Wu et al. 2021) on a list of genes that overlapped between the following comparisons: RPMI8866^{Tat} vs RPMI8866 and BLAS^{Tat} vs BLAS. Benjamini-Hochberg p.adjust cutoff of 0.05 and q-value cutoff of 0.05 were used to select statistically significant categories, redundant terms were removed with the simplify() function of the same package (cutoff parameter of 0.7). The GO biological process and KEGG databases were used for annotation. Transcription factor (TF)-target enrichment was performed based on the TRRUST TF-target database (2019) (Han et al. 2018) *via* an R-based interface accessing the Enrichr server (Kuleshov et al. 2016) with a p.adjust cutoff of 0.05.

clusterProfiler R package (version 4.4.4) was used to conduct gene set enrichment analysis (GSEA) on a pre-ranked list of genes ordered by the stat column of DESeq2 results. Gene sets of biological processes and pathways were obtained from the Gene Ontology resource (R package org.Hs.eg.db, version 3.15.0) (The Gene Ontology Consortium, 2017) and the Kyoto Encyclopedia of Genes and Genomes (KEGG) database (release 104.0) (Kanehisa & Goto 2000). An adjusted p-value cutoff of 0.05 was used to select statistically significant activated or suppressed pathways; redundant terms were removed with the simplify() function of the same package (cutoff parameter of 0.7).

For the RPMI8866 cell lines, raw sequencing data were downloaded from GSE182538 (Valyaeva et al. 2022) and processed as described above. For RNA-seq data from B cells isolated from lymph nodes of people living with HIV and HIV-uninfected individuals were obtained from GSE119234 (Austin et al.

2019) and processed as described above. Deregulated genes were identified using appropriate statistical methods. For BLAS cell lines, the genes meeting the criteria p value adjusted (p.adjust) by the Benjamini-Hochberg procedure < 0.05, $|\log_2$ fold change$| > 0.5$ were considered differentially expressed.

4.25 RNA extraction, reverse transcription and quantitative PCR (qPCR)

Total RNA was isolated using the NucleoSpin RNA kit (Macherey-Nagel, Düren, Germany) following the manufacturer's instructions. The quantity and quality of total RNA were measured using a NanoDrop2000C Spectrophotometer (Thermo Fisher Scientific). 1.0 µg of total RNA was reverse-transcribed using Maxima™ H Minus cDNA Synthesis Master Mix (Thermo Scientific, USA). Quantitative PCR was carried out using Powerup SYBR Green Mastermix (ThermoFisher) on a StepOnePlus Real-Time PCR System machine (Applied Biosystems). The human cDNA primers (**Table 11**) were obtained from Eurofins Genomics, Germany. The thermal cycling program was as follows: a 2-minute denaturation step at 50°C, a 2-minute denaturation step at 95°C followed by 40 amplification cycles consisting of 15 seconds of denaturation at 95°C, 1 minute of annealing at 60°C and 1 minute of elongation at 72°C, followed by a final step 10-minute elongation at 72°C. qPCRs for each sample were performed in triplicates (technical replicates). A relative transcript level was calculated using the Pfaffl method (Pfaffl 2001) with *Rpl32* as a reference gene; normalization was done assuming as 1 the mean level of each transcript in the control group. The analysis of primer efficiency was performed by plotting the cycle threshold value (Ct) against the serial 1:10 dilution of the cDNA sample using the equation $E = 10^{-\frac{1}{the\ slope\ value}}$.

4.26 qPCR for translocation quantification

Genomic DNA was extracted using the Nucleospin® Tissue kit (Macherey-Nagel) according to the manufacturer's protocol. To detect MYC-IGH translocation qPCR amplification was performed with StepOnePlus Real-Time PCR System (Applied Biosystems) using the PowerUp SYBR Green Master Mix (Thermo Scientific) with the following cycling conditions: 1 cycle of 50°C (2min), 95°C (2min); 40 cycles 95°C (15s), annealing at 60°C or 64°C (1min), 72°C (1min); 1 cycle 72°C (10min). 500 ng of genomic DNA was used for the reaction, all reactions were performed in triplicates. Primers surrounding the translocation breakpoint were designed to detect MYC-IGH translocation (MYC T R and IGH T R); primers that target MYC region ~6.8 kbp away from the translocation breakpoint (MYC noT F and Myc no T R) were used as a control of DNA load. Primer sequences are listed in **Table 11**. The $2^{-\Delta\Delta Ct}$ method was used for the quantification of the translocation rate.

To detect AML1-ETO translocation qPCR amplification was performed using the TaqMan probe with the following cycling conditions: 1 cycle of 95°C (5min); 40 cycles including melting at 95°C (30s), annealing at 58°C (1min), elongation at 72°C (15 s); 1 µg of genomic DNA measured by Qubit Fluorometer was used in 25 µl reaction, all reactions were performed in triplicates. Primers surrounding the translocation breakpoint were designed to detect AML1-ETO translocation (AML1_R and ETO_F) and TaqMan probe (FAM—CCCAGCAGAATAGGCCCACTGGAGCCCA—BHQ1). pUC18-based plasmid containing AML1-ETO PCR product was created for the quantification of translocation rate and for the amplification efficiency determination with the standard curve method.

4.27 DNA extraction and dot blot for cisplatin-specific DNA damage

To analyze the accumulation of cisplatin-induced DNA damage, RPMI8866 Tat[i] cells were seeded at a concentration 1×10^6 cells/ml, treated or not with doxycycline for 16 hours to induce HIV-1 Tat expression, then treated with 50 µM or 300 µM of cisplatin and incubated for 2 and 4 hours. 3×10^6 cells were pelleted by centrifugation for 5 minutes at 800g, washed with phosphate-buffered saline (PBS, Sigma) and pelleted again. To collect chromatin fraction, cell pellets were resuspended in 150 µL of cold MNAse buffer (20 mM Tris pH 7.5, 2.5 mM $CaCl_2$, 5 mM NaCl) with protease inhibitor cocktail and subjected to lysis by freezing them at −80 °C overnight. After defrosting, lysed cells were centrifuged for 5 minutes at 16000g at 4℃ and the supernatant was removed. To release chromatin-bound proteins and shear chromatin, pellets were treated with 2U of micrococcal nuclease (MNase) from Staphylococcus aureus (Sigma-Aldrich, USA, cat. #N3755) in 100 µL of MNase buffer and incubated on ice for 10 minutes. Samples were then centrifuged for 5 minutes at 16000g at 4℃, and pellets were washed with 100 µL of 10X TBS buffer (200 mM Tris, 1500 mM NaCl) followed by washing with 200 µL of 1X TBS buffer; supernatants from three centrifugations were combined to obtain chromatin fraction.

To isolate DNA from chromatin fraction, phenol-chloroform extraction was used. Briefly, 150 µL of chromatin fraction was treated with 2 µL of RNAse A 10mg/mL (ThermoFisher Scientific, cat. #EN0531) for 1 hour at 37℃, followed by treatment with 150 µl of Proteinase K 5 mg/ml (Macherey-Nagel, cat. #740506) in Proteinase Buffer (10 mM Tris pH 8; 20 mM EDTA pH 8; 10 mM NaCl, 1% SDS) for 1 hour at 56℃. Samples were supplemented with 300 µL of Phenol-Chloroform-Isoamyl solution (25:24:1, Biosolve Chemicals, France) and centrifuged for 5 minutes at 16000g; the upper phase was transferred to the new tube. After the addition of 1 volume of chloroform, samples were centrifuged and the upper phase was separated with the addition of 10% of 3

M Sodium acetate buffer solution and 3 volumes of cold 100% ethanol. Samples were incubated on dry ice for 40 minutes and then centrifuged for 30 minutes at 16000g at 4°C. The supernatant was aspirated and 1 mL of cold 70% ethanol was added to the pellet, followed by centrifugation for 20 minutes at 16000g. After aspiration of ethanol, pellets were dried and dissolved in 12 µL of water. DNA concentration was measured on a NanoDrop 2000C Spectrophotometer (Thermo Scientific, USA). Some protocols recommend DNA denaturation before loading on a membrane (Bonin & Dotti 2011; Park & Kang 2015), we found, however, that denaturation (in 0.4 M NaOH for 10 min at 95 °C, followed by neutralization with 2 M NH_4OAc) decreased the specificity of our analysis and led to some background signal in control samples (not treated with cisplatin) and to detection of oxaliplatin-induced DNA adducts (**Figure 39**). We, thus, proceed without DNA denaturation to detect cisplatin-specific DNA damage.

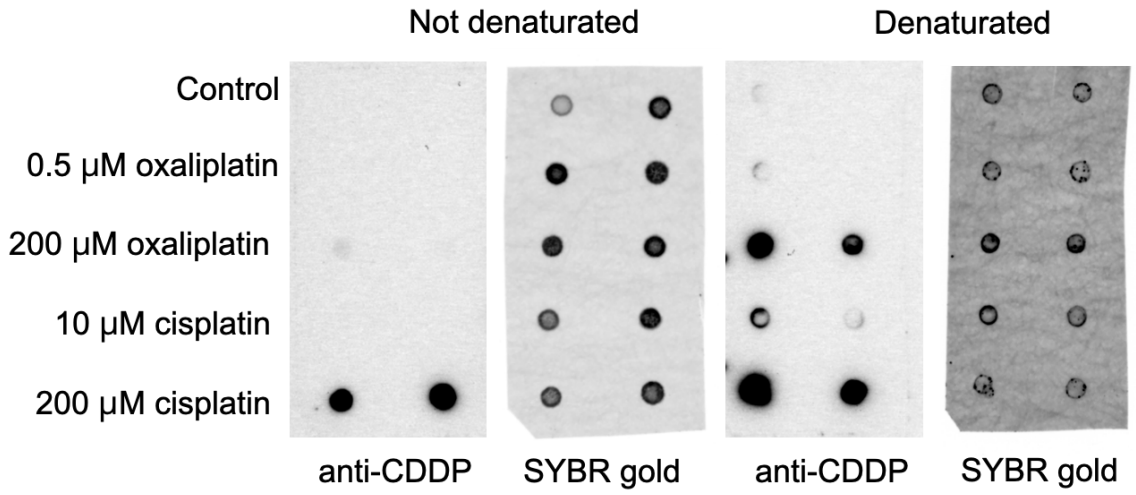

Figure 39. The effect of DNA denaturation on the detection of cisplatin-specific DNA damages. Dot blot analysis of cisplatin-modified DNA levels in RPMI8866 cells after treatment with 0.5 µM oxaliplatin, 200 µM oxaliplatin, 10 µM cisplatin or 200 µM cisplatin. Non-treated cells were used as a control. The same DNA samples were left not denaturated or denaturated with 0.4 M NaOH for 10 min at 95 °C, followed by neutralization with 2 M NH_4OAc. SYBR gold was used as DNA loading control.

Each sample was diluted to the concentration of 100 ng/µL and 3 µL of each sample was loaded on 0.45 µm nylon membrane (Amersham Hybond-N+, GE Healthcare, cat. #RPN203B). The membrane was dried and crosslinked with 254-nm UV, 120 mJ/cm2 on UV Stratalinker 2400™ (Stratagene). Then the membrane was incubated in 1:10000 SYBR Gold (Invitrogen, cat. #S11494) in TBST for 30 minutes in the dark and washed with 20% ethanol for 20 minutes. ImageQuant LAS 4000 mini (GE Healthcare, USA) was used to detect DNA loading. The membrane was then blocked in 5% milk in TBST for 30 minutes at room temperature and incubated for 2 hours at room temperature in primary rat antibodies to cisplatin-modified DNA [CP9/19] (Abcam, cat. #ab103261).

The membrane was then washed 3 times for 5 minutes in TBST and incubated for 2 hours at room temperature with secondary goat-anti-rat antibodies HRP conjugate (Sigma-Aldrich, cat. # AP136P). After washing 3 times for 5 minutes in TBST, the membrane was revealed using Immobilon Western Chemiluminescent HRP Substrate (Millipore, USA) and ImageQuant LAS 4000 mini (GE Healthcare, USA). Images were analyzed using ImageJ software.

4.28 Chromatin immunoprecipitation quantitative real-time PCR (ChIP-qPCR)

Chromatin immunoprecipitation (ChIP) was performed as described previously (Holliday et al. 2021). Briefly, to perform ChIP-qPCR, 2 × 10^7 RPMI8866, RPMI8866^{GFP} and RPMI8866^{Tat} cells were collected, centrifuged (800g, 5 min), and resuspended in 10 ml of culture medium. Formaldehyde (37%) was added drop-wise to a final concentration of 1%, followed by gentle rotation for 10 minutes at room temperature for cross-linking. The fixation was halted by adding glycine (2.5 M) to a final concentration of 125 mM and incubating with rotation for 5 minutes at room temperature. After washing the cells three times with ice-cold PBS, the cell pellet was resuspended in 1 ml of cytoplasm lysis buffer (10mM Tris-HCl pH 8, 150mM NaCl, 0.5mM EDTA, 0.5% NP-40, 1× protease inhibitor cocktail, 0.5mM PMSF) and dounced 10 times in dounce homogenizer. The nuclei were then pelleted, and the supernatant (cytoplasm) was removed. The nuclei were resuspended in 350 µl of nuclear lysis buffer (50mM Tris-HCl pH 8, 10mM EDTA, 1% SDS, 1× protease inhibitor cocktail, 1mM PMSF). The chromatin was sonicated using a Covaris sonicator, and specific parameters (Power Peak: 200; Duty Factor: 20; Cycles/Burst: 200; 20 min) were set to achieve an average fragment size of 200-1000 bp (**Figure 40**). After sonication, debris was pelleted by centrifugation for 10 min, 4°C, 15000 g, and the supernatant was transferred to a new tube. A 25 µl aliquot was taken to determine DNA concentration and fragment size. For DNA concentration and fragment size determination, 20 µl of 2M NaCl, 145 µl of water, and 3 µl of RNase A (10 mg/ml) were added to the aliquot, followed by overnight incubation at 65°C. On the next day, 3 µl of proteinase K (20 mg/ml) was added, and the mixture was incubated with shaking at 60°C for 1 hour. DNA was purified using a PCR clean-up kit (Marchery-Nagel, Germany). For immunoprecipitation, a pre-clearing step was performed by adding 10 µl of Protein G Dynabeads (Invitrogen) to the 20 µg of sonicated chromatin and incubating for 2 hours with gentle rotation at 4°C. ChIP was carried out overnight at 4°C with 5 µl of the rabbit monoclonal anti-RelA antibody (Cell Signalling, cat. #8242) or 5 µl of normal rabbit IgG antibody (Cell Signalling, cat. #2729) and 10 µg of chromatin per reaction in ChIP buffer (16.7 mM Tris-HCl pH 8, 167 mM NaCl, 1.2 mM EDTA, 0.01% SDS, 1.1% Triton X-100, supplemented with protease inhibitors). An aliquot of the chromatin sample

(200 ng, 2%) was kept as a ChIP input. The next day, the bead/chromatin mixture was placed on a magnetic rack, and the supernatant was removed. The beads were washed successively with Low-salt Wash Buffer (150 mM NaCl, 20 mM Tris-HCl pH 8, 2 mM EDTA, 0.1% SDS, 1% Triton X-100, supplemented with protease inhibitors), High-salt Wash Buffer (500 mM NaCl, 20 mM Tris-HCl pH 8, 2 mM EDTA, 0.1% SDS, 1% Triton X-100), LiCl Wash Buffer (250 mM LiCl, 10 mM Tris HCl pH 8, 1 mM EDTA, 1% Nonidet P-40, 1% Na-Deoxycholate), and twice with TE Wash Buffer (10 mM Tris HCl pH 8, 1 mM EDTA). DNA was eluted with 200 µl of ChIP elution buffer (100 mM sodium bicarbonate, 1% SDS). ChIP input and the eluted DNA were incubated with 8 µl of 5M NaCl and 3 µl of RNase A (10 mg/ml) at 65°C with shaking overnight, followed by the addition of 3 µl of proteinase K (20 mg/ml) and incubation with shaking at 60°C for 1 hour. DNA purification using a PCR clean-up kit (Marchery-Nagel, Germany) was performed and DNA concentration was measured with a Nanodrop. For qPCR analysis, 5% of the immunoprecipitated and input DNA were used.

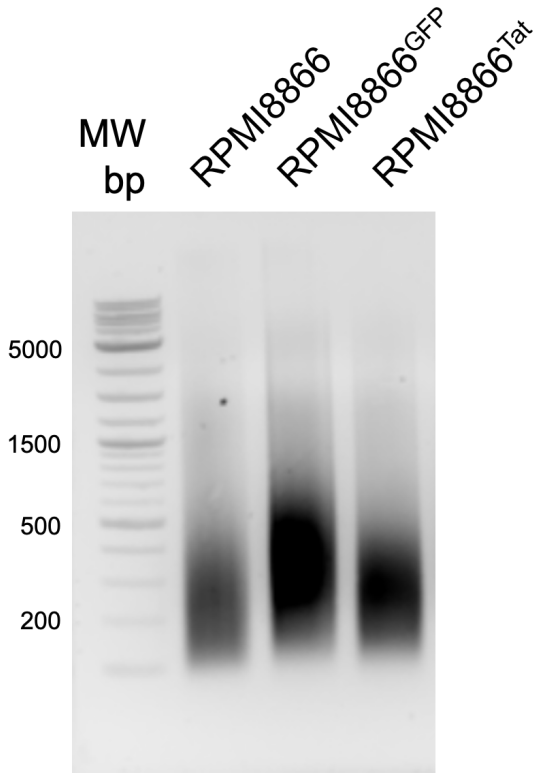

Figure 40. Chromatin sonication analysis by agarose gel electrophoresis. MW, molecular weights.

RelA binding to *HLA-DRB1* and *HLA-DRB5* promoter sequences was measured by qPCR with StepOnePlus™ Real-Time PCR System (Applied Biosystems) using PowerUp SYBR Green Master Mix (Thermo Scientific) with the following program: a 2-minute denaturation step at 50°C, a 2-minute denaturation step at 95°C followed by 40 amplification cycles consisting of 15 seconds denaturation at 95°C, 1 minute of annealing at 60°C and 1 minute of elongation at 72°C, followed by a final step 10-minute elongation at 72°C. For

qPCR analysis, 5% of the immunoprecipitated and input DNA were used. The human genomic DNA primers for ChIP-qPCR (**Table 11**) were obtained from Eurofins Genomics, Germany. Primers for *HLA-DRB1* and *HLA-DRB5* promoter sequences were chosen based on data of RelA binding from ReMap 2022 (4th release, https://remap.univ-amu.fr/, accession date: 12 January 2023), a database of transcriptional regulators peaks derived from curated ChIP-seq, ChIP-exo, DAP-seq experiments in human (Hammal et al. 2022). Primers for *ACTB* were imported from (Fiume et al. 2012), *ACTB* PCR product sequence did not overlap with RelA peaks from ReMap 2022 and served as a control. For each sample, values were normalized to input DNA and reported as % of input.

4.29 Statistical analysis

Data were analyzed using GraphPad Prism 9 software (GraphPad Software Inc.). The unit of analysis was a single biological replicate. Student's unpaired t-tests were used to compare cell sizes between two groups. One-way analysis of variance (ANOVA), followed by Tukey's post-hoc test, was used to determine differences between more than two groups that involved one factor. Two-way ANOVA, followed by Tukey's post-hoc post-hoc test, was used to determine differences between two or more groups that involved two factors. For the correlation analysis, the Spearman correlation was performed. Data are presented as a mean ± standard error of the mean (SEM). The level of significance was set at $p < 0.05$.

CONCLUSIONS

People living with HIV are at higher risk of developing EBV-associated B cell lymphomas (Hernández-Ramírez et al. 2017), which, in the era of cART, cannot be fully attributed to immune suppression. This observation raises important questions about the specific mechanisms through which HIV infection may contribute to the development of these malignancies. By understanding the underlying biological factors and molecular pathways involved, I aimed to shed light on the complex interplay between HIV, EBV and B cell lymphomagenesis, which may pave the way for novel therapeutic strategies and targeted interventions to mitigate lymphoma risk in people living with HIV.

The development of B cell lymphomas is a complex process influenced by various factors. One of the main contributors to B cell lymphomagenesis, a "hallmark" of cancer, is genome instability (Hanahan 2022; Hanahan & Weinberg 2011). An increased risk of B cell lymphomas in people living with HIV despite cART has prompted us to investigate the potential implications of antiretroviral therapy in the process of B cell lymphomagenesis. We developed CRISPR/Cas9-based experimental human B cell-based models to study the generation of t(8;14) *MYC-IGH* translocation, characteristic of Burkitt's lymphoma - a common B cell neoplasm in people living with HIV. We revealed that antiretroviral drugs, notably abacavir, emtricitabine, and the CCR5 antagonist TAK-779, exhibit a concerning propensity to increase the frequency of *MYC-IGH* chromosomal translocations, potentially contributing to the development of Burkitt's lymphoma in individuals living with HIV. Further epidemiological studies are needed to investigate the association between cancer incidence and the use of specific cART drugs and their dosages in people living with HIV.

We have also shown that even asymptomatic HIV-positive individuals with complete HIV viral suppression are prone to EBV reactivation. Using the same CRISPR/Cas9-based experimental system, we demonstrated that EBV reactivation increases the frequency of *MYC-IGH* translocation. The results of our study revealed that EBV reactivation induced DNA damage in the *MYC* locus and increased the spatial proximity between *MYC* and *IGH* loci in B cells. This increased proximity was associated with a higher risk of chromosomal translocation involving *MYC* and *IGH*, which might also contribute to the risk of Burkitt's lymphoma in individuals living with HIV.

Any dysregulation in DNA damage sensing and repair response can lead to genomic instability and may increase the risk of B cell lymphomas. I demonstrated that people living with HIV with effective viral suppression have detectable levels of a viral protein, HIV-1 Tat, circulating in the blood. Due to its cell-penetration capacity, HIV-1 Tat might penetrate B cells. My results

demonstrate that exposure of B cells to HIV-1 Tat suppressed the expression of multiple genes involved in DNA sensing and repair pathways in B cells. Consequently, Tat-expressing B cells displayed impaired DNA damage sensing and repair when exposed to the DNA-damaging agents. These cells exhibited an increase in cisplatin-specific DNA adducts and a decrease in the levels of key markers involved in DNA damage recognition and repair, such as γH2AX and the phosphorylated form of p53. Despite the impairment of DNA repair pathways, B cells exposed to Tat maintained their viability, suggesting that they survive at the same level as control cells even in the presence of accumulated DNA lesions. These findings highlight the potential role of HIV-1 Tat in promoting genome instability and DNA damage in B cells, which could contribute to the development of B-cell lymphomas in people living with HIV.

Immune evasion is another "hallmark of cancer" (Hanahan 2022; Hanahan & Weinberg 2011) and it plays a critical role in the development and progression of B cell lymphomas, particularly in the context of chronic viral infections such as HIV and EBV. I demonstrated that the chronic secretion of HIV-1 Tat by infected cells might decrease the expression of MHC class II molecules HLA-DR on B cells by inhibiting the activation of the NF-κB pathway. The impaired expression of HLA-DR molecules led to reduced recognition of EBV-transformed B cells by CD4+ T cells, suggesting that Tat-induced HLA-DR downregulation could foster immune evasion mechanisms for infected or transformed B cells. The causal relationship between HIV-1 Tat and B cell lymphomas in people living with HIV remains to be established with *in vivo* studies.

Finally, I observed that another circulating viral protein - EBV Zta - was present in the blood of people living with HIV. We discovered that HIV-1 Tat and EBV Zta interact directly in B, T cells and blood serum, and this interaction can be found in people living with HIV. To our knowledge, these data serve as the first demonstration of a direct inter-viral protein-protein interaction. Functionally, the combined action of Tat and Zta in B cells went beyond a simple combination of two individual proteins, triggering unique alterations in gene expression. Most notably, their interaction resulted in the reduction of the protein expression of HLA-ABC, integral to antigen presentation, which provided the protection for EBV-infected B cells against cytotoxic T cell recognition and the mechanism of immune evasion by EBV-infected or transformed B cells in the context of HIV and EBV combined infections.

In conclusion, the intricate relationship between HIV and EBV presents a multifaceted landscape for understanding the aetiology of B cell malignancies in individuals living with HIV in the era of cART. Beyond the traditional scope of immune suppression, this study has unveiled novel potential mechanisms that might contribute to the increased risk of lymphomas in this population. The coexistence of HIV-1 Tat and EBV Zta in the blood of individuals living with HIV

sheds light on a direct interplay between these viral proteins, potentially influencing immune evasion and oncogenesis. Antiretroviral drugs, while crucial for viral control, may paradoxically promote chromosomal translocations associated with Burkitt's lymphoma. The same effect can be associated with EBV reactivation in B cells. Moreover, the persistent presence of HIV-1 Tat may exacerbate genome instability and DNA damage in B cells, potentially driving lymphomagenesis. By elucidating these intricate interactions and mechanisms, we gain insights into the development of EBV-associated B cell lymphomas in the context of HIV infection. These findings highlight the importance of exploring viral partnerships, genome stability, and immune evasion as integral factors in lymphoma pathogenesis, ultimately guiding the design of innovative therapeutic strategies to mitigate malignancy risk and improve the health outcomes of individuals living with HIV.

Major publications related to the topic of PhD thesis

1. Canoy R.J.[†], **Shmakova A.**[†], Karpukhina A., Lomov N., Tiukacheva E., André F., Germini D., Vassetzky Y. Breakage first drives generation of chromosomal translocations upon targeted induction of double-stranded breaks in different cell types. *NAR Cancer*. 2023. V. 5, № 3, P. zcad049. doi: 10.1093/narcan/zcad049. (Research paper)

[†]Both authors contributed equally to this work

2. Szewczyk-Roszczenko O.K., Roszczenko P., **Shmakova A.**, Finiuk N., Holota S., Lesyk R., Bielawska A., Vassetzky Y., Bielawski K. The chemical inhibitors of endocytosis: from mechanisms to potential clinical applications. *Cells*. 2023. V. 12(18), P. 2312. doi:10.3390/cells12182312. (Review)

3. Sall F.B., **Shmakova A.**, Tsfasman T., Lomov N., Toure A.O., Lipinski M., Wiels J., Germini D., Vassetzky Y. Epstein-Barr Virus reactivation induces *MYC-IGH* spatial proximity and t(8;14) in B cells. *Journal of Medical Virology*. 2023. V. 95, №. 3, P. e28633. doi: 10.1002/jmv.28633. (Research paper)

4. **Shmakova A.**[†], Lomov N.[†], Vyushkov V., Tsfasman T., Germini D., Kozhevnikova Y., Sokolova D., Pokrovsky V., Rubtsov M., Vassetzky Y. Cell model with inducible oncogenic translocations allows to evaluate the potential of drugs to favor secondary translocations. *Cancer Communications.* 2023. V. 43, № 1, P. 154-158. doi: 10.1002/cac2.12370. (Research paper)

[†]Both authors contributed equally to this work

5. Canoy R.J., André F., **Shmakova A.**, Wiels J., Lipinski M., Vassetzky Y., Germini D. Easy and robust electrotransfection protocol for efficient ectopic gene expression and genome editing in human B cells. *Gene Therapy*. 2023. V. 30, P. 167–171 doi: 10.1038/s41434-020-00194-x. (Research paper)

6. **Shmakova A.**, Vassetzky Y. LncRNA: a new danger for genome integrity. *International Journal of Cancer*. 2022. V. 152, P. 1288–1289. doi: 10.1002/ijc.34397. (Editorial)

7. Canoy R.J., **Shmakova A.**, Karpukhina A., Shepelev M., Germini D., Vassetzky Y. Factors That Affect the Formation of Chromosomal Translocations in Cells. *Cancers*. 2022. V. 14, № 20, P. 5110. doi: 10.3390/cancers14205110. (Review)

8. Valyaeva A., Tikhomirova M., Potashnikova D., Bogomazova A., Snigiryova G., Penin A., Logacheva M., Arifulin E., **Shmakova A.**, Germini D., Kachalova A., Saidova A., Zharikova A., Musinova Y., Mironov A., Vassetzky Y., Sheval E. Ectopic expression of HIV-1 Tat modifies gene expression in cultured B cells: Implications for the development of B-cell lymphomas in HIV-1-infected patients. *PeerJ*, 2022. V. 18, № 10, P. e13986. doi: 10.7717/peerj.13986. (Research paper)

9. **Shmakova A.***, Shmakova O., Karpukhina A., Vasetsky Y.* CRISPR/Cas: History and Perspectives. *Russian Journal of Developmental Biology*. 2022. V. 53, P. 272–282. doi: 10.1134/S1062360422040075. (Review)

* corresponding authors

10. Germini D., Sall F.B.[†], **Shmakova A.**[†], Wiels J., Dokudovskaya S., Drouet E., Vassetzky Y. Oncogenic Properties of the EBV ZEBRA Protein. *Cancers*. 2020. V. 12, № 6, P.1479. doi: 10.3390/cancers12061479. (Review)

[†]Both authors contributed equally to this work

11. Akbay B., **Shmakova A.**, Vassetzky Y., Dokudovskaya S. Modulation of mTORC1 Signaling Pathway by HIV-1. *Cells*. 2020, V. 9, P. 1090. doi:10.3390/cells9051090. (Review)

12. **Shmakova A.**, Germini D., Vassetzky Y. HAART, HIV-1 and cancer: a complex relationship. *International Journal of Cancer*, 2020, V. 146, № 10, P. 2666-2679, doi: 10.1002/ijc.32730. (Review)

Participation in the conferences

1. Journée scientifique HerPAs-2023 (30 June 2023) Villejuf, Institut Gustave Roussy, “L’interaction entre EBV Zta et VIH-1 Tat cause l'évasion immunitaire dans les cellules B par la dégradation de HLA-ABC” (oral presentation)

2. Réunion DYNAVIR (29 June 2023), Paris, Institut Cochin, "Degradation of HLA-ABC and Immune Evasion in B Cells Induced by the Interaction of EBV Zta and HIV-1 Tat" (oral presentation)

3. 27th Wilhelm Bernhard Workshop on the Cell Nucleus (19, 23 June 2023) Prague, Institute of Molecular Genetics of the Czech Academy of Sciences, "The interaction of two viral nuclear transcription factors HIV-1 Tat and EBV Zta induces immune evasion of EBV-infected B cells" (oral presentation)

4. XXVes Journées Francophones de Virologie (17-18 April 2023), Paris, Institut Pasteur, "L'interaction entre EBV Zta et VIH-1 Tat induit la dégradation de HLA-ABC et l'évasion immunitaire dans les cellules B" (poster presentation)

5. XXVes Journées Francophones de Virologie (17-18 April 2023), Paris, Institut Pasteur, "L'action chronique de VIH-1 Tat induit une régulation négative de HLA-DR dans les cellules B : un mécanisme d'échappement immunitaire des lymphomes chez les personnes vivant avec le VIH" (poster presentation)

6. Cell Symposium: Viruses in health and disease (19-21 March 2023), Sitges, "EBV Zta and HIV-1 Tat interaction-induced HLA-ABC degradation and immune evasion in B cells" (poster presentation)

7. Cell Symposium: Viruses in health and disease (19-21 March 2023), Sitges, "HLA-DR downregulation by chronic action of HIV-1 Tat in B cells" (poster presentation)

8. «Computational biology and artificial intelligence for personalized medicine» («Information technologies for personalized medicine» (2-4 August 2022), Virtual, FSBI «National Medical Research Center of Endocrinology» of the Ministry of Health of Russia, "Cell models with inducible oncogenic translocations allow to evaluate the potential of drugs to favor secondary translocations" (poster presentation)

9. Journée scientifique HerPAs-2022 (27 June 2022) Gif-sur-Yvette, I2BC, "L'interaction entre Tat du VIH et Zta de l'EBV provoque une évasion immunitaire des cellules B infectées par l'EBV" (oral presentation)

10. CSHL Meeting Retroviruses (23-28 May 2022) Cold Spring Harbor Meeting, Virtual, "The role of HIV-1 Tat in HLA-DR expression regulation in B cells" (poster presentation)

11. ANRS AC41 Work In Progress (WIP) meeting « Interactions hôte/virus » (22-23 March 2022) ANRS, Virtual, "HIV-1 Tat induces HLA-DR downregulation in B cells" (oral presentation)

12. «Computational biology and artificial intelligence for personalized medicine» («Information technologies for personalized medicine» (23 September 2021), Virtual, FSBI «National Medical Research Center of Endocrinology» of the Ministry of Health of Russia, "Implications of interaction between HIV-1 Tat and EBV Zta for lymphomagenesis" (poster presentation)

13. Journée scientifique HerPAs-2021 (10 June 2021) Association HerPAs, Virtual, “The tole of EBV Zta interaction with HIV-1 Tat in B cell oncogenesis” (oral presentation)

14. Cell biology meeting (1 June 2021), Assosiation jeunes chercheures, Villejuif, Institut Gustave Roussy, “HIV-1 Tat and EBV Zta: the role of inter-viral protein-protein interaction in B cell oncogenesis” (oral presentation)

15. CSHL Meeting Retroviruses (18 May 2021) Cold Spring Harbor Meeting, Virtual, “Inter-viral protein-protein interaction of HIV-1 Tat and EBV Zta” (poster presentation)

16. ANRS AC41 Work In Progress (WIP) meeting « Interactions hôte/virus » (18-19 March 2021) ANRS, Virtual, “HIV-1 Tat and EBV Zta interact upon co-infection” (oral presentation)

Annexes

In the review **Article 11**, I discussed the history of CRISPR/Cas9 discovery and its potential applications as well as ethical problems related to the use of CRISPR/Cas for genome editing in human embryos.

Article 11. Review "CRISPR/Cas: History and Perspectives"

ISSN 1062-3604, Russian Journal of Developmental Biology, 2022, Vol. 53, No. 4, pp. 272–282. © The Author(s), 2022. This article is an open access publication.
Russian Text © The Author(s), 2022, published in Ontogenez, 2022, Vol. 53, No. 4, pp. 287–300.

REVIEWS

CRISPR/Cas: History and Perspectives

A. A. Shmakova[a, b, *], O. P. Shmakova[c], A. A. Karpukhina[a], and Y. S. Vassetzky[a, **]

[a] *Koltsov Institute of Developmental Biology, Russian Academy of Sciences, Moscow, 119334 Russia*

[b] *Laboratory of Molecular Endocrinology, Federal State Budgetary Institution National Medical Research Center of Cardiology Named after Academician E.I. Chazov of the Ministry of Health of the Russian Federation, Moscow, 121552 Russia*

[c] *Adolescent Psychiatry Research Unit, Federal State Budgetary Scientific Institution Mental Health Research Center, Moscow, 115522 Russia*

**e-mail: anyashm@gmail.com*

***e-mail: vassetzky@gmail.com*

Received March 2, 2022; revised April 16, 2022; accepted April 18, 2022

Abstract—Discovery of the CRISPR/Cas system revolutionized biology and biomedicine in the 21st century. Here we discuss the milestones in the development of CRISPR/Cas genome editing technology, from the history of discovery to current developments, including medical applications. Technical and ethical problems associated with the use of CRISPR/Cas for editing human embryonic genomes are also discussed.

Keywords: CRISPR, Cas, genome editing, history of science

DOI: 10.1134/S1062360422040075

INTRODUCTION

Discovery of the system of clustered regularly interspaced short palindromic repeats (CRISPR) in prokaryotic genomes and the Cas proteins (CRISPR associated proteins) is one of the most groundbreaking events in modern biology. CRISPR are DNA regions in the prokaryote genome consisting of identical short repeats (30–40 bp) separated by unique spacer sequences of the same length; CRISPR-associated Cas proteins are located in the vicinity of these regions (Hille and Charpentier, 2016). Short palindromic repeats are quite common: CRISPR regions are found in the genomes of 50% of all known bacteria and 90% of archaea (Grissa et al., 2007; Hille et al., 2018); this may indicate their extreme importance for prokaryotes. In 2020, Emmanuelle Charpentier and Jennifer Doudna were awarded the Nobel Prize in Chemistry for their work on development of the CRISPR/Cas system for genome editing.

CRISPR/Cas research has progressed from the discovery of unusual and inexplicable repeats found by researchers in the genomes of various bacteria and archaea to the description of CRISPR/Cas involvement in prokaryotic acquired immunity and the use of this knowledge for targeted eukaryotic genome editing and other aims. Using CRISPR/Cas-based tools, researchers made breakthroughs in clinical trials and biotechnology companies have launched gene therapy trials for a range of diseases. The technology continues to develop rapidly, with great promise for further work in biology, medicine, bioengineering, biochemistry and other sciences. This review describes the history of CRISPR/Cas discovery and the use of the CRISPR/Cas technique for fundamental and applied research.

DISCOVERY AND DEVELOPMENT OF THE CRISPR/Cas METHOD FOR GENOME EDITING

The first unusual repetitive sequences were described in 1987 in the genome of *Escherichia coli* (*E. coli*) by a group of Japanese scientists led by Yoshizumi Ishino, who discovered that the 3' end of the gene *Iap*, whose products are responsible for the isoenzymatic conversion of alkaline phosphatase, contained "five highly homologous sequences of 29 nucleotides arranged as direct repeats with 32 nucleotides as spacing" (Ishino et al., 1987). They found no biological explanation for the presence and function of these repeats, and this work did not receive much attention from colleagues either: until 2007, Ishino's publication was cited 1–2 times a year.

The unusual repetitive sequences in prokaryotic genomes interested the Spanish researcher Francisco Mojica, who discovered them in the genome of the archaea *Haloferax mediterranei* in 1993 (Mojica et al., 1993); at that time, the scientist was only 30 years old. In 1995, Mojica and co-authors described in detail these "tandem repeats" as they called them, in the genomes of *Haloferax mediterranei* and *H. volcanii*: a 30 bp sequence with dyad symmetry repeated in tandem with insertions of unique sequences of 33–39 bp

and extending over long stretches, 1.4 kb in the *H. mediterranei* chromosome and ~3 kb in the *H. volcanii* chromosome (Mojica et al., 1995). To understand the role of this DNA region, the Mojica's group decided to introduce an extra copy of this DNA region into *H. volcanii* by transformation with a recombinant plasmid containing a 1.1 bp fragment of tandem repeats. This resulted in a significant decrease of cell viability and unequal distribution of the genome among daughter cells (Mojica et al., 1995). The first hypothesis about the biological role of tandem repeats in prokaryotic genomes proposed their participation in the chromosome segregation during mitosis. Around the same time, similar repeats were described in the genomes of *Mycobacterium tuberculosis* (Groenen et al., 1993), *Streptococcus* (Hoe et al., 1999), cyanobacteria *Anabaena* sp. (Masepohlet al., 1996), *Shigella dysenteriae, Salmonella typhimurium* (Nakata et al., 1989) and other bacterial species. It has been proposed that these repeats might be involved in chromosomal rearrangements, recombination, or were landing sites for regulatory proteins (Nakata et al., 1989; Groenen et al., 1993), but these assumptions were not tested experimentally.

After defending his PhD thesis in 1995, Francisco Mojica worked as a postdoc at Oxford University and then, driven by his interest in cryptic repeats, he returned to Spain where he tried to set up his own research group to study "tandem repeats." At the time, he could not obtain research grants and was severely restricted in funding his work and building the infrastructure of his own laboratory (Mojica and Rodriguez-Valera, 2016). Despite the difficulties, the scientist continued his research. Mojica refocused on *E. coli* as a model organism, but reproduction of the experiments he had conducted earlier on *H. volcanii* did not yield the expected results: no clear phenotype of *E. coli* genome segregation defects was observed when an additional copy of the "tandem repeat" was introduced into its genome. Mojica's second hypothesis was that tandem repeats served as reference points for DNA binding to cellular structures (e.g. cell membrane proteins or soluble proteins). However, no repeat-binding proteins were found in *E. coli* cell extracts. The third assumption was that the repeats could affect the three-dimensional structure of DNA, but this was not confirmed: analysis of plasmid DNA showed that the introduction of the repeat arrays had no effect on its topology (Mojica and Rodriguez-Valera, 2016).

Francisco Mojica did not give up on his ambition to find the functions of the mystery repeats. Gradual advances in sequencing technology made it easier to find such structures in the genomes of other organisms and Mojica's colleague, César Díez-Villaseñor, created software to search for repetitive regions in prokaryote genomes. By 2000, Mojica's lab systematized the data on genomic repeats in 9 species of archaea and 10 species of bacteria and gave them a name: Short Regularly Spaced Repeats (SRSR; an acronym that also indicates alternation of spacers and repeats, because it can also be decoded as: Spacer-Repeat-Spacer-Repeat) (Mojica et al., 2000). This highly important work for science was published in a Micro-Correspondence two-page format (a consolation to modern scientists who are asked to shorten their papers by journal editors).

The group of Dutch microbiologist Ruud Jansen, who described tandem repeats in *Mycobacterium tuberculosis* and other prokaryotic species, named them SPIDR (SPacers Interspersed Direct Repeats) (Jansen et al., 2002a). To avoid further confusion in the rapidly growing subject, Mojica and Jansen jointly decided to replace the names: direct repeats, tandem repeats, SRSR, SPIDR and other variations of the names, with a simple, "crispy" (as R. Jansen himself aptly put it) and the name we know today, CRISPR (Fig. 1). In 2002, Jansen and colleagues also identified protein-coding genes located in the vicinity of the repeat loci which they named as CRISPR-associated (Cas) proteins (Jansen et al., 2002b).

Although the role of genomic repeats remained a mystery to scientists at that time, the widespread distribution of repeat sequences in various prokaryote species indicated their undoubted importance and fundamental cellular role. Having discovered Cas proteins, Jansen suggested that they were involved in DNA metabolism or regulation of gene expression in a genomic region functionally related to the CRISPR locus, as they had a structure similar to DNA helicases or exonucleases (Jansen et al., 2002b).

However, the final key to unraveling the functions of the CRISPR/Cas system was the discovery of the origin of unique intermediate spacers. The role of these sequences has long been a mystery. Francisco Mojica initially did not give them much importance, he wrote: "the name itself (spacer) hints at an irrelevant role in the repeats just separating the palindromes" (Mojica and Rodriguez-Valera, 2016). In the early 2000s, his research group continued to work on CRISPR repeats in *E. coli*. They routinely amplified CRISPR loci using PCR, sequenced them and compared them with sequences in publicly available nucleotide databases. And then one day the scientists were lucky: one of the queries yielded a matching sequence, they found that the sequence of the spacer is homologous to a piece of the genome of the *E. coli* bacteriophage. Gradually, Mojica accumulated data on other spacers that had similarities to sequences in bacteriophages or in conjugative plasmids (Mojica et al., 2005). It turned out that bacteriophages whose sequences were found in CRISPR spacers were unable to infect a spacer host cell but infected closely related strains lacking this spacer (Mojica et al., 2005). An eureka moment occurred and Mojica was the first to make the correct assumption that the role of the CRISPR system is to acquire immunity against for-

Asunto: Re: Acronym
Fecha: Wed, 21 Nov 2001 16:39:06 +0100
De: "Ruud Jansen" <R.Jansen@vet.uu.nl>
Empressa: Diergeneeskunde
A: "Francisco J. Martínez Mojica" <fmojica@ua.es>

Dear Francis
What a great acronym is CRISPR.
I feel that every letter that was removed in the alternatives made it less crispy so I prefer the snappy CRISPR over SRSR and SPIDR.
Also not unimportnat is the fact that in MedLine CRISPR is a unique entry, which is not true for some of the shorter acronyms.

Fig. 1. Email sent by R. Jansen to F. Mojica regarding the name of regularly spaced CRISPR repeats. Source: Mojica and Garrett, 2013.

eign DNA and that the locus itself is a "compartment for storing DNA chunks of invaders" (Mojica et al., 2005; Mojica and Rodriguez-Valera, 2016). It is worth mentioning again the difficulties of recognition that the authors of this revolutionary discovery encountered when trying to publish their findings (Lander, 2016). We cite these facts not in order to disappoint the reader in the objectivity of modern scientific publishing houses, although this would not be unreasonable in this case, but rather to console those scientists to whom this story gives hope of subsequent recognition of their work regardless of the initially negative reaction of the scientific community to their discovery. Realizing the importance of his scientific conclusion, Mojica submitted his article to *Nature*. In November 2003, the editors of *Nature* rejected the paper without even sending it to the reviewers: for unknown reasons, the editor stated that the idea for the paper was already known. In January 2004, the *Proceedings of the National Academy of Sciences* (*PNAS*) also decided that the paper lacked the 'novelty and importance' to send it for review. *Molecular Microbiology* and *Nucleic Acids Research* were the next journals to reject Mojica's manuscript. Desperate and worried that he may be outrun, Mojica sent the article to the *Journal of Molecular Evolution* where after a year (!) of reviews the article was finally published on February 1, 2005. Mojica recalled this period as follows: "Imagine you have something you know it's big in your hands and there's the possibility that another article that takes the originality of your work is published. I remember sending mail every month to the editor, saying 'please tell me if you're going to publish or not so we can submit to another journal'. I was in absolute despair" (Fernández, 2019).

In March and August 2005, two independent research groups from France described similar findings in *Yersinia pestis* and *Streptococcus* (Bolotin et al., 2005; Pourcel et al., 2005). The study of such an unusual model organism, *Y. pestis*, the causative agent of plague, was explained by the fact that the research group, headed by Gilles Vergnaud, was commissioned by the French Ministry of Defense and was developing methods to trace the source of potential biological weapons. Their unique collection of *Y. pestis* was obtained during the 1964–1966 Vietnam plague outbreak (Lander, 2016). Similarly to Mojica, Vergnaud faced the reluctance of journals to publish the patterns found: his paper was rejected by *PNAS*, *Journal of Bacteriology*, *Nucleic Acids Research and Genome Research* before finally being published in *Microbiology* on March 1, 2005.

The second French research group included our former compatriots, Alexander Bolotin and Alexei Sorokin, who studied streptococci in Paris. According to Sergei Kiselev, professor of the Vavilov Institute of General Genetics recalls, Bolotin "was approached by a large yogurt company at the time with a request to find out why they were no longer able to kill unwanted bacteria in the sourdough. Producers always used special viruses to suppress their life activity, but at some point bacteriophages stopped killing bacteria" (Vedeneeva, 2020). Bolotin was the first to describe the now famous *Streptococcus* nuclease Cas9 protein which was named Cas5 or Csn1 at that time (Bolotin et al., 2005). In the course of their work, Bolotin and collaborators noticed that the spacers had a common sequence at the end: the protospacer adjacent motif (PAM) necessary for target recognition (Bolotin et al., 2005).

Interestingly, both the biological weapons and yogurt studies led to similar scientific conclusions. Both groups confirmed Mojica's hypothesis on the role of CRISPR in the formation of acquired immunity in bacteria. In 2006, a group of US researchers (from ex-USSR), Kira S. Makarova, Nick V. Grishin, Svetlana A. Shabalina, Yuri I. Wolf, Eugene V. Koonin

analyzed all prokaryotic genomes available at that time and found several gene clusters corresponding to Cas proteins (Makarova et al., 2006). The researchers classified Cas into protein families and described their potential functional and structural features. Assuming that the CRISPR/Cas immune defense system operates on the principle of RNA interference, they analyzed the similarity of Cas proteins to proteins of the RNA interference system, but found no similarities. They nevertheless made a number of assumptions about the mechanism of CRISPR/Cas operation and how new spacers can be acquired.

Without direct experimental confirmation, these findings only supported the hypothesis but did not prove it unequivocally. However, the proof of the beautiful hypothesis of acquired immunity in prokaryotes did not wait long: in 2007 Philip Horvath's group in France demonstrated that after virus infection, bacteria integrated new spacers derived from phage genomic sequences; and removing or adding certain spacers modified prokaryotic cell phage resistance (Barrangou et al., 2007). They showed that Cas9 was a key protein required for the process by which the CRISPR system inactivated the invading phage (Barrangou et al., 2007). Once again, the discovery was facilitated by a request from the food industry: the authors of the article were at the time working for Danish food ingredient manufacturer Danisco (now DuPont) and were sequencing the genomes of bacteria used as starter cultures in the dairy industry to produce yogurt and cheese. They also sequenced bacteriophages that infect and destroy dairy cultures (Nair, 2017). Remarkably, since 2011 DuPont yogurt and cheese cultures have been 'vaccinated' against bacteriophages naturally using CRISPR (Nair, 2017). In 2008, John van der Oost's group, together with Kira S. Makarova and Eugene V. Kunin showed that it is the small RNA (CRISPR RNA, crRNA) transcribed from the CRISPR locus that binds to Cas proteins and guides towards the target DNA for immune protection (Brouns et al., 2008). The same year, Luciano Marraffini and Eric Sontheimer described the defense mechanism of bacteria against plasmid DNA (Marraffini and Sontheimer, 2008). They elegantly demonstrated that the target molecule of Cas proteins is DNA and not RNA. They were also the first to suggest that the CRISPR/Cas system could be used outside bacteria as a molecular tool: "From a practical point of view, the ability to direct specific targeted degradation of DNA containing any given target sequence of 24–48 nucleotides can have significant functional utility, especially if the system can function outside its native bacterial or archaeal context.... The main difference between a restriction-modification system and CRISPR interference is that the latter can be programmed with a suitable effector crRNA" (Marraffini and Sontheimer, 2008).

Now the CRISPR topic has finally received the attention it deserved. New discoveries have appeared with snowballing speed: S. Moineau's group (Garneau et al., 2010) found that the Cas-crRNA complex cuts foreign DNA 3 nucleotides above the PAM; K.S. Makarova and colleagues developed a classification of CRISPR/Cas systems (Makarova et al., 2011); Francisco Mojica in 2010 described in detail how the *E. coli* CRISPR system is turned on and off and suggested a mechanism of the system (Mojica and Díez-Villaseñor, 2010). The final solution to the puzzle of the CRISPR/Cas9-driven natural immunity mechanism was found in 2011 by Emmanuelle Charpentier's group: in addition to sgRNA, there was a second small RNA, which the authors called transactivating CRISPR RNA (tracrRNA). The latter was discovered by next-generation sequencing, the benefit of tracrRNA being the third most abundant transcriptome after rRNA and tRNA. Researchers showed that tracrRNA formed a duplex with sgRNA and it is this duplex that directed Cas9 to its DNA targets (Deltcheva et al., 2011).

Once the mechanism of CRISPR/Cas was finally decrypted, the scientific research immediately switched to the practical application of this system, as scientists understood the enormous potential of the discovered mechanism. The study of CRISPR/Cas began to take place away from the host bacteria: the CRISPR/Cas was used as a targeted tool for targeted DNA cutting. In 2011, Lithuanian biochemist Virginijus Šikšnis, a graduate student in chemistry at Moscow State University, was able to transfer a functional CRISPR/Cas from *S. thermophilus* and express it in *E. coli*. This confirmed that the CRISPR/Cas system is capable of working autonomously and all its necessary elements (Cas9, crRNA and tracrRNA) were already known (Sapranauskas et al., 2011). In 2012, his group characterised the structure of Cas9 in detail, identified its nuclease domains, showed that crRNA can be shortened to 20 nucleotides, and that Cas9 targets could be changed by replacing crRNA (Gasiunas et al., 2012). The authors showed that the Cas9/crRNA/tracrRNA complex can cleave target DNA in vitro. Šikšnis submitted his paper to *Cell* on April 6, 2012, and the journal rejected the paper without peer review six days later, then he sent it to *PNAS* on May 21, where it was published on September 4 (Lander, 2016).

A technological breakthrough was provided by Emmanuelle Charpentier (E. Charpentier) and Jennifer A. Doudna, who reported that crRNA and tracrRNA can be combined together to form a single synthetic guide RNA (sgRNA); this is currently the technology used by researchers who now need only two elements to program the targeted cutting of DNA: a Cas9 nuclease and a single guide RNA that guides the nuclease (Jinek et al., 2012). Like Šikšnis, Charpentier and Doudna demonstrated that Cas9 could cut purified DNA in vitro, and that the latter could be programmed by specially designed sgRNAs. Their work was submitted to *Science* on June 8 and published on June 28, 2012. Around the same time, Doudna filed a

patent application for the CRISPR/Cas9 gene editing system.

Finally, in 2013, Feng Zhang, who had previously worked on TALEN (transcription activator-like effectors) programmable nucleases, was the first to successfully adapt CRISPR/Cas9 for genome editing in eukaryotic cells (Cong et al., 2013). He applied CRISPR/Cas9 to target editing of different genome loci in human and murine cells (Cong et al., 2013). Around the same time, similar results were published by George M. Church's laboratory (Mali et al., 2013). After publication, Feng Zhang also applied for a patent in his own name and was able to obtain one before Doudna.

NOBEL PRIZE

CRISPR is considered nowadays the most important discovery in molecular biology since PCR, entailing the creation of the latest and most successful genetic engineering technology. Understanding the importance of this discovery, researchers and people interested in science have been wondering when the Nobel Prize for CRISPR/Cas would be awarded. Many feared that the technology was expected to make some sort of practical advance in order to finally be awarded the prize.

The 2020 Nobel Prize in Chemistry went to Emmanuelle Charpentier and Jennifer Doudna for developing the CRISPR/Cas9 gene editing technique. Firstly, this is of course a choice in favor of applied rather than basic science, as if the prize had been awarded for the discovery of CRISPR/Cas, it would certainly have been worth celebrating the merits of Francisco Mojica. Nevertheless, the wording of the Nobel Committee unequivocally speaks specifically of "method development." Secondly, a maximum of three people can be awarded the Nobel Prize for a single discovery, and awarding it to the two female researchers Charpentier and Doudna can be regarded as a kind of statement of the Nobel Committee. Before the award, part of the scientific community thought it would go to Charpentier, Doudna and Zhang (less frequently Šikšnis was named third), as those who had made major contributions to the application of CRISPR/Cas for genome editing in vitro and in vivo, in prokaryotic and eukaryotic cells.

Overall, in the era of collectivism in science, the justification of awarding Nobel Prizes to two or three people is increasingly questioned, as many discoveries are the achievement of a dozen scientists and their research teams.

CURRENT DEVELOPMENTS USING CRISPR/Cas

One of the industrial sectors most interested in CRISPR/Cas is agriculture. Targeted editing of plant genomes is actively used to increase yields in fruit and grain crops, give them resistance to disease and changing weather conditions, and other desirable traits. For example, editing genes related to cytokine signaling has significantly increased yields in rice and wheat (Cong et al., 2013; Wang et al., 2014). Mutation of *CLV* (Rodríguez-Leal et al., 2017) and *ENO* (Yuste-Lisbona et al., 2020) genes responsible for meristem size has increased tomato yields. Using CRISPR/Cas technology, a variety of wheat with a reduced gluten content and 85% less immunogenicity has been created as it is important for people with celiac disease to control their dietary intake of gluten in wheat products. This result would have been almost impossible to achieve by classical crossbreeding methods, as gluten group proteins are scattered in about a hundred loci in the wheat genome (Sánchez-León et al., 2018).

Most genetically modified plants are still under development and are not used for mass cultivation, but there are many exceptions. By now, more than a hundred CRISPR/Cas-derived plant varieties have been officially approved. These include, for example, soybean with increased oleic acid content due to a mutation in the omega-6 fatty acid desaturase gene and wheat that is resistant to powdery mildew by editing the *MLO* gene locus that suppresses the plant's defense mechanisms against fungal infections (Wang et al., 2014).

Another promising area for the use of CRISPR/Cas in living organisms is editing the genomes of vectors of infectious and parasitic diseases to reduce their populations, or their ability to transmit a particular disease: for example, research is ongoing to induce sterility in malaria mosquitoes, which could lead to a significant reduction in malaria vector populations (North et al., 2020). This approach could help control disease transmission and protect ecosystems from species that are dangerous to humans.

Genetic engineering using CRISPR/Cas also offers unique medical applications; for example, the use of CRISPR/Cas technology solves transplant compatibility problems and other problems associated with the use of porcine organs in humans. These include the problem of porcine endogenous retroviruses pathological to humans. George Church's lab successfully applied CRISPR/Cas9 to inactivate all 62 copies of retroviruses in pig cells (Yang et al., 2015); this incidentally set a record for the number of modified loci in a single experiment.

Muhammad Mohiuddin form the University of Maryland, USA is working on immunocompatibility problems between pig organs and the human body in heart xenotransplant. His group has created pigs with a knockout of three genes responsible for carbohydrate antigen synthesis and human rejection of the pig heart (*GGTA1KO,* β*4GalNT2KO, CMAHKO*), a growth hormone receptor gene (*GHR*) knockout to inhibit pig heart growth in the human body, and the addition of six human genes: two anti-inflammatory (*hCD47,*

hHO-1), two genes that promote normal blood clotting (*hTBM, hEPCR*), and two complement system regulator genes (*hCD46, hDAF*) (Goerlich et al., 2021). Heart transplant from genetically modified pigs has been tested in baboons and has shown good results (Goerlich et al., 2021). Thanks to the work of Mohiuddin's team, the high-profile achievement of this year was the world's first heart transplant of a genetically modified pig to a human on January 7, 2022 by M. Mohiuddin's team (Reardon, 2022; Jee, 2022).

In 2021, the results of *ex vivo* clinical trials using CRISPR/Cas9 in human cells were published. Haydar Frangoul's group performed haematopoietic stem cell editing to knockout the *BCL11A* enhancer in two patients with sickle cell anaemia and β-thalassaemia (monogenic diseases caused by mutations in the gene encoding the β-subunit of haemoglobin) (Frangoul et al., 2021). *BCL11A* is a repressor of haemoglobin γ-subunit (HbF) and its knockout results in increased *HbF* expression, which increases survival in patients with sickle cell anaemia and β-thalassaemia. Autologous haematopoietic stem cell transplantation of *ex vivo* corrected cells resulted in an increase in blood HbF concentration and relief of disease symptoms (Kaiser, 2020; Frangoul et al., 2021).

Currently, research on the CRISPR/Cas technology develops in several directions, including the development of effective ways to deliver CRISPR/Cas components into cells (as DNA, RNA or ribonucleoproteins) using biological (viruses, virus-like particles, cellular penetration peptides), chemical (liposomes, nanoparticles) and physical methods (electroporation, sonoporation, microinjection) (Taha et al., 2022); as well as the development of approaches aimed at improving the on-target and reducing the off-target mutagenic activity of Cas proteins (Nidhi et al., 2021). To minimize off-target editing, various software programs are being developed aimed at *in silico* prediction of off-target activity and selection of optimal and specific sgRNAs; chemically modified sgRNAs with higher specificity are used; improved variants of Cas are selected and constructed (Naeem et al., 2020).

A number of scientific groups in Russia are actively engaged in CRISPR/Cas research. Konstantin Severinov's laboratory from SkolTech is engaged in the prediction and functional characterisation of the new CRISPR-Cas system. Sergey Shmakov from this team has created a semi-automated search system that detects novel CRISPR/Cas systems (Shmakov et al., 2019). Using this software, members of Severinov's laboratory found and characterized the C2c2 protein (now Cas13a), unique in that it cuts RNA rather than DNA (Abudayyeh et al., 2016). Yana Fedorova from the same laboratory described a compact Cas9 orthologue with all the same functional features but reduced in size, making it easier to deliver to cells (Fedorova et al., 2020). Suren Zakiyan's Epigenetics of Development Laboratory from the Institute of Cytology and Genetics in Novosibirsk is successfully working on the creation of cellular models of various human neurodegenerative diseases (Medvedev et al., 2021), muscular dystrophies (Medvedev et al., 2021), including Huntington's disease (Morozova et al., 2018; Malankhanova et al., 2020), amyotrophic lateral sclerosis (Ustyantseva et al., 2019), and spinal muscular atrophy (Valetdinova et al., 2017) using CRISPR/Cas9 system. Maxim Karagyaur from the Laboratory of Biochemistry and Molecular Medicine at the Faculty of Fundamental Medicine, Moscow State University has been using the CRISPR/Cas technology to knockout genes of interest, to regulate gene expression at the epigenetic level, to model single-nucleotide polymorphisms to create cellular and tissue models to study tissue development and regeneration (Karagyaur et al., 2018; Rysenkova et al., 2018; Tyurin-Kuzmin et al., 2018; Dyikanov et al., 2019; Slobodkina et al., 2020; Rusanov et al., 2020). Other interesting works by Russian scientists include the development of a method for rapid sorting of cells with genetic modifications after CRISPR/Cas9 action based on a short peptide expression (Zotova et al., 2019) and the use of CRISPR/Cas9 to simultaneously create double-stranded breaks in different chromosomal locations to study the mechanisms of chromosomal translocations (Shmakova et al., 2019; Canoy and Vassetzky, 2021). Thus, the use of CRISPR/Cas genome editing technology in various fields and in different organisms, provides unique industrial and medical opportunities to improve the quality of life.

USING CRISPR/Cas TO EDIT GERMLINE DNA

Since the CRISPR/Cas system is a convenient tool for genome editing, almost immediately after the description of its use in eukaryotic cells, studies began on the possibility of its application to human embryos, both for the correction of pathological mutations and for fundamental studies of early human embryonic development. The effectiveness of this approach, off-target mutagenicity, the editing efficacy (embryo mosaicism), and the possibility of subsequent embryo development have been studied (Ormond et al., 2017; Lea and Niakan, 2019). The sources of embryos in such works were unclaimed embryos from in vitro fertilisation procedures (Fogarty et al., 2017). It appears that knockout models in mice do not always accurately reflect the role of the genes under study in human embryonic development (Fogarty et al., 2017). Despite many attempts, accurate targeted editing of embryos (through DNA repair by homologous recombination mechanism) remains low, with deletions or insertions occurring after double-strand breaks in most cases, while mechanisms of early embryonic DNA repair remain poorly understood (Ma et al., 2017). For this reason, the use of CRISPR/Cas to correct pathological mutations in embryos is difficult. At

the same time, the use of CRISPR/Cas for targeted mutagenesis and gene knockout also poses certain risks: apparently, double-stranded breaks introduced by Cas9 at a single locus result in deletions that can extend over several thousand bases, including in embryonic and progenitor cells (Kosicki et al., 2018).

Despite significant progress in the field, there are a number of concerns about the clinical use of CRISPR/Cas in humans: questions about both the safety of the method and the ethics of its application are increasingly being raised. A precedent has been set in the case of He Jiankui, a researcher at Southern University of Science and Technology in Shenzhen (China), who used CRISPR/Cas to modify the genome of human embryos. Providing in vitro fertilisation services, He Jiankui's group suggested that a couple in which the husband was infected with HIV should make a genetic modification to the *CCR5* gene in the embryos that would lead to the cells being resistant to HIV infection (Regalado, 2019). The natural CCR5Δ32 mutation is found in Europe and Western Asia, where its average frequency is around 10%, and homozygotes for the mutant allele do have resistance to HIV (Novembre et al., 2005; Lopalco, 2010). According to He Jiankui, who announced his experiment in November 2018, the genome editing was successful and resulted in the birth of healthy twin girls Lulu and Nana (Cyranoski and Ledford, 2018). It is worth noting that neither the plan nor the results of this work have been fully published or peer-reviewed by the scientific community. On November 29, 2018, Chinese authorities suspended He Jiankui's scientific activities and he was prosecuted for violating Chinese laws on human experimentation and for providing unlicensed medical care; in December 2019, the scientist was sentenced to three years in prison and a fine of three million yuan.

He Jiankui, in an attempt to publish the results of his high-profile experiment, submitted an article titled "Twin births after genome editing for HIV resistance" to *Nature* and *JAMA*, both journals rejected the article (Regalado, 2019). Interestingly, He Jiankui's co-authors included Michael Deem, a scientist at Rice University (Houston, USA). Despite claims that he did not consent to the publication of the data, an internal review was initiated against Deem, the results of which are classified, but as of 2021 he is no longer employed by Rice University.

He Jiankui's study has been heavily criticised by scientists for several reasons:

(1) The claims made in the article were not supported by the data provided. Although the article stated that they were trying to replicate a frequent variant of the CCR5Δ32 mutation, in fact they were not: other mutations have been introduced into the *CCR5* gene, whose role in providing HIV resistance had not even been studied in vitro. The never-published article did not provide evidence that the genetic manipulation did lead to HIV resistance, although this could have been tested before the embryos were implanted. Moreover, analysing the sequencing data cited in the article, one could see an extended region of multiple uninterpretable peaks in the sequencing data of the *CCR5* gene (Regalado, 2019), suggesting that the embryos were mosaic, i.e. different cells had different mutations in this region, whose role was also unexplored.

(2) The parents of the twins may have been poorly informed about the nature of the experiment or may have agreed to the experiment under pressure. There are established protocols for in vitro fertilisation in HIV+ parents that reduce the risks of infection to the embryo or foetus to zero. In this regard, the genome modification procedure offered no medical benefit but introduced unnecessary risks that the couple may not have been aware of. Moreover, in China, HIV-positive people do not have access to fertility treatment and in vitro fertilisation, indicating that the couple may have been forced to experiment because it gave them the only chance of having a child.

(3) The claimed medical benefit of CCR5 deletion is questionable. Even if CRISPR is effective in making people resistant to HIV, it is unlikely to be widely used, especially in places where HIV epidemics are unfolding, such as southern Africa, due to its complexity, cost, need for constant monitoring and a variety of other reasons. It will probably take many decades of widespread use of genetic editing using CRISPR (assuming it is effective) to halt the HIV epidemic. Public health initiatives, education and widespread access to antiretrovirals are more logical and effective solutions to control the HIV epidemic.

(4) The side-effects of applying human genome editing are poorly understood and researchers led by He Jiankui have begun creating genetically modified live humans before they have fully grasped the implications of their edits. CRISPR/Cas technology is not 100% specific to a given gene and the insertion of a nuclease with sgRNA can lead to off-target mutations elsewhere in the genome. He Jiankui's team tested selected 3–5 cells from embryos at an early stage before implantation for off-target mutations and found a single nucleotide insertion in a non-coding region of the genome in one embryo. A key problem here, however, is that sequencing for mutations involves lysing the cells and isolating the DNA, meaning that the cells tested cannot be further used for fertilisation and may be different from the embryo from which they were taken. Conversely, embryos that gave rise to twins could not be fully screened for off-target mutations in each of the cells. For example, the use of CRISPR/Cas9 on sheep embryos together with pre-implantation screening and selection of embryos with the desired mutation nevertheless leads to mosaicism in half of the fetuses (Vilarino et al., 2018). A recent study applying CRISPR/Cas9 to correct the EYS gene in human embryos found that on-target and off-target

cutting of Cas9 can lead to complete or partial chromosomal losses (Zuccaro et al., 2020).

In conclusion, it must be reiterated that the genetic modification of human embryos should be regarded as a high-risk procedure and the mass introduction of CRISPR/Cas technology will require legislation to ensure that the technology is not used in violation of ethical rules.

In addition to editing of the human embryo genome, one can edit human germline cells (sperm and egg cells). The introduction of CRISPR/Cas9 into oocytes together with spermatogonial cells (as part of in vitro fertilization) has been proposed to improve editing efficiency and reduce the risk of embryo mosaicism (Ma et al., 2017), although there are rather few experimental developments in human germ cell editing. Genetic modification of spermatogonial stem cells has been tested in mice (Wu et al., 2015) and pigs (Webster et al., 2021).

Ethical and social guidelines regarding clinical editing of the human embryonic genome have been set out by the American National Academies of Sciences, Engineering and Medicine and the English Nuffield Council on Bioethics (National Academies of Sciences, 2017; Nuffield Council on Bioethics, 2018). In 2019, a call for a global moratorium on clinical use of germline DNA editing (in sperm, eggs or embryos) to create genetically modified children on technological, scientific, medical and ethical grounds was published by several leading scientists, including Emmanuel Charpentier, Eric Lander and Feng Zhang (Lander et al., 2019). In 2020, the Geneva Statement on the need for a course correction in the editing of the human inherited genome was issued (Andorno et al., 2020). Its authors insist that a global public consensus is required before any steps towards reproductive editing of the human genome can be initiated. The authors have included an explanation to the general public about the current misunderstandings surrounding genome editing, the mainstreaming of social issues, including equity, and the development of criteria for empowering the public to influence decision-making in this area.

CONCLUSIONS

Until 20 years ago, the CRISPR/Cas system was only known to a narrow circle of scientists working on the subject. The mysterious system of repeats and spacers was of interest only to a few microbiologists working with bacteria or archaea and did not seem like a major scientific breakthrough. Today, the technique has become the subject of intense scrutiny by the entire scientific community, including both specialists and historians of science, philosophers discussing ethical issues that have arisen, as well as the general public. CRISPR/Cas studies are actively receiving grant support, and articles are willingly published on it. It is worth remembering that only the undying interest of the discoverers (especially Francisco Mojica) has brought us to the level of knowledge where we are today.

Researchers in almost every biochemistry, molecular biology or cytology lab now use CRISPR/Cas for genome editing. The rapid development of the technique has brought society to a turning point: the possibility of editing human genomes has opened up before us. Nevertheless, the risks also exist. Is the technology completely safe for humans because of possible off-target effects? How can possible criminal and anti-human use of the technique be ruled out? The inability to test the side effects of CRISPR/Cas at the early stages of embryonic development raises an important moral and ethical issue: who will be responsible if a child is born with genetic abnormalities?

Other pressing questions arise: can CRISPR/Cas be used for non-lethal, treatable diseases? Can CRISPR/Cas be used at a population level? Will the introduction of this cutting-edge and expensive technology further divide the poor from the rich, giving the latter more advantages? Finally, could CRISPR/Cas be used en masse to “improve” human genetics?

It would seem that not so long ago, fantasy literature described how human phenotypic traits could be altered on demand, right down to the choice of eye or hair colour. Now it seems that this possibility is much less fantastic. But while eye and hair colour are polygenic traits that are difficult or even impossible to change using CRISPR/Cas, editing single genes seems like a solvable scientific task. The precedent of editing the *CCR5* gene has caused deep reflection among an informed public, because in addition to the described resistance to HIV, the CCR5 mutation has been associated with improved memory and learning ability (Zhou et al., 2016). Will prospective parents want to improve the cognitive abilities of their unborn children through genome editing? All these important questions remain to be answered in the near future, and it is best to do so before embarking on human genome editing.

FUNDING

This work was supported by the Ministry of Science and Higher Education of the Russian Federation (075-15-2020-773) and the Basic Research Programme of the Institute of Developmental Biology of the Russian Academy of Sciences (0088-2021-0007).

COMPLIANCE WITH ETHICAL STANDARDS

The authors declare that there is no conflicts of interest.

This paper does not describe research performed by the authors involving humans or using animals as subjects.

OPEN ACCESS

This article is licensed under a Creative Commons Attribution 4.0 International License, which permits use, sharing, adaptation, distribution and reproduction in any medium or format, as long as you give appropriate credit to the original author(s) and the source, provide a link to the Creative Commons license, and indicate if changes were made. The images or other third party material in this article are included in the article's Creative Commons license, unless indicated otherwise in a credit line to the material. If material is not included in the article's Creative Commons license and your intended use is not permitted by statutory regulation or exceeds the permitted use, you will need to obtain permission directly from the copyright holder. To view a copy of this license, visit http://creativecommons.org/licenses/by/4.0/.

REFERENCES

Barrangou, R., Fremaux, C., Deveau, H., et al., CRISPR provides acquired resistance against viruses in prokaryotes, *Science*, 2007, vol. 315, no. 5819, pp. 1709–1712.

Bolotin, A., Quinquis, B., Sorokin, A., et al., Clustered regularly interspaced short palindrome repeats (CRISPRs) have spacers of extrachromosomal origin, *Microbiology*, 2005, vol. 151, no. 8, pp. 2551–2561.

Brouns, S.J.J., Jore, M.M., Lundgren, M., et al., Small CRISPR RNAs guide antiviral defense in prokaryotes, *Science*, 2008, vol. 321, no. 5891, pp. 960–964.

Canoy, R.J. and Vassetzky, Y.S., Factors that affect chromosomal translocations in cells, *Doctoral Dissertation*, Paris: Université Paris-Saclay, 2021.

Cong, L., Ran, F.A., Cox, D., et al., Multiplex genome engineering using CRISPR/Cas systems, *Science*, 2013, vol. 339, no. 6121, pp. 819–823.

Cyranoski, D. and Ledford, H., How the genome-edited babies revelation will affect research. www.nature.com/articles/d41586-018-07559-8. Accessed January 23, 2022.

Deltcheva, E., Chylinski, K., Sharma, C.M., et al., CRISPR RNA maturation by trans-encoded small RNA and host factor RNase III, *Nature*, 2011, vol. 471, no. 7340, pp. 602–607.

Dyikanov, D.T., Vasiluev, P.A., Rysenkova, K.D., et al., Optimization of CRISPR/Cas9 technology to knock out genes of interest in aneuploid cell lines, *Tissue Eng., Part C*, 2019, vol. 25, no. 3, pp. 168–175.

Fedorova, I., Vasileva, A., Selkova, P., et al., PpCas9 from *Pasteurella pneumotropica*—a compact Type II-C Cas9 ortholog active in human cells, *Nucleic Acids Res.*, 2020, vol. 48, no. 21, pp. 12297–12309.

Fernández, C.R., www.labiotech.eu/interview/francis-mojica-crispr-interview/. Accessed February 5, 2022.

Fogarty, N.M.E., McCarthy, A., Snijders, K.E., et al., Genome editing reveals a role for OCT4 in human embryogenesis, *Nature*, 2017, vol. 550, no. 7674, pp. 67–73.

Frangoul, H., Altshuler, D., Cappellini, M.D., et al., CRISPR-Cas9 gene editing for sickle cell disease and β-thalassemia, *N. Engl. J. Med.*, 2021, vol. 384, no. 3, pp. 252–260.

Garneau, J.E., Dupuis, M.-E., Villion, M., et al., The CRISPR/Cas bacterial immune system cleaves bacteriophage and plasmid DNA, *Nature*, 2010, vol. 468, no. 7320, pp. 67–71.

Gasiunas, G., Barrangou, R., Horvath, P., et al., Cas9-crRNA ribonucleoprotein complex mediates specific DNA cleavage for adaptive immunity in bacteria, *Proc. Natl. Acad. Sci. U. S. A.*, 2012, vol. 109, no. 39, pp. E2579–E2586.

Goerlich, C.E., Griffith, B., Hanna, P., et al., The growth of xenotransplanted hearts can be reduced with growth hormone receptor knockout pig donors, *J. Thorac. Cardiovasc. Surg.*, 2021, article ID S0022-5223(21)01261–7.

Grissa, I., Vergnaud, G., and Pourcel, C., The CRISPRdb database and tools to display CRISPRs and to generate dictionaries of spacers and repeats, *BMC Bioinf.*, 2007, vol. 8, no. 1, p. 172.

Groenen, P.M., Bunschoten, A.E., van Soolingen, D., et al., Nature of DNA polymorphism in the direct repeat cluster of *Mycobacterium tuberculosis*; application for strain differentiation by a novel typing method, *Mol. Microbiol.*, 1993, vol. 10, no. 5, pp. 1057–1065.

Hille, F. and Charpentier, E., CRISPR-Cas: biology, mechanisms and relevance, *Philos. Trans. R. Soc., B*, 2016, vol. 371, no. 1707, article ID 20150496.

Hille, F., Richter, H., Wong, S.P., et al., The biology of CRISPR-Cas: backward and forward, *Cell*, 2018, vol. 172, no. 6, pp. 1239–1259.

Hoe, N.P., Nakashima, K., Lukomski, S., et al., Rapid selection of complement-inhibiting protein variants in group A *Streptococcus* epidemic waves, *Nat. Med.*, 1999, vol. 5, no. 8, pp. 924–929.

Ishino, Y., Shinagawa, H., Makino, K., et al., Nucleotide sequence of the iap gene, responsible for alkaline phosphatase isozyme conversion in *Escherichia coli*, and identification of the gene product, *J. Bacteriol.*, 1987, vol. 169, no. 12, pp. 5429–5433.

Jansen, R., Embden, J.D.A., Gaastra, W., et al., Identification of a novel family of sequence repeats among prokaryotes, *OMICS*, 2002a, vol. 6, no. 1, pp. 23–33.

Jansen, R., Embden, J.D.A., Gaastra, W., et al., Identification of genes that are associated with DNA repeats in prokaryotes, *Mol. Microbiol.*, 2002b, vol. 43, no. 6, pp. 1565–1575.

Jee, C., A gene-edited pig's heart has been transplanted into a human for the first time. www.technologyreview.com/2022/01/11/1043374/gene-edited-pigs-heart-transplant/. Accessed January 31, 2022.

Jinek, M., Chylinski, K., Fonfara, I., et al., A programmable dual-RNA-guided DNA endonuclease in adaptive bacterial immunity, *Science*, 2012, vol. 337, no. 6096, pp. 816–821.

Kaiser, J., CRISPR and another genetic strategy fix cell defects in two common blood disorders. https://www.science.org/content/article/crispr-and-another-genetic-strategy-fix-cell-defects-two-common-blood-disorders. Accessed February 18, 2022.

Karagyaur, M.N., Rubtsov, Y.P., Vasiliev, P.A., et al., Practical recommendations for improving efficiency and accuracy of the CRISPR/Cas9 genome editing system, *Biochemistry* (Moscow), 2018, vol. 83, no. 6, pp. 629–642.

Kosicki, M., Tomberg, K., and Bradley, A., Repair of double-strand breaks induced by CRISPR-Cas9 leads to large deletions and complex rearrangements, *Nat. Biotechnol.*, 2018, vol. 36, no. 8, pp. 765–771.

Lander, E.S., The heroes of CRISPR, *Cell*, 2016, vol. 164, no. 1, pp. 18–28.

Lander, E.S., Baylis, F., Zhang, F., et al., Adopt a moratorium on heritable genome editing, *Nature*, 2019, vol. 567, no. 7747, pp. 165–168.

Lea, R. and Niakan, K., Human germline genome editing, *Nat. Cell. Biol.*, 2019, vol. 21, no. 12, pp. 1479–1489.

Lopalco, L., CCR5: from natural resistance to a new anti-HIV strategy, *Viruses*, 2010, vol. 2, no. 2, pp. 574–600.

Ma, H., Marti-Gutierrez, N., Park, S.-W., et al., Correction of a pathogenic gene mutation in human embryos, *Nature*, 2017, vol. 548, no. 7668, pp. 413–419.

Makarova, K.S., Grishin, N.V., Shabalina, S.A., et al., A putative RNA-interference-based immune system in prokaryotes: computational analysis of the predicted enzymatic machinery, functional analogies with eukaryotic RNAi, and hypothetical mechanisms of action, *Biol. Direct.*, 2006, vol. 1, p. 7.

Makarova, K.S., Haft, D.H., Barrangou, R., et al., Evolution and classification of the CRISPR–Cas systems, *Nat. Rev. Microbiol.*, 2011, vol. 9, no. 6, pp. 467–477.

Malankhanova, T., Sorokin, M., Medvedev, S., et al., Introducing an expanded trinucleotide repeat tract into the human genome for Huntington's disease modeling in vitro, *Curr. Protoc. Hum. Genet.*, 2020, vol. 106, no. 1. e 100.

Mali, P., Yang, L., Esvelt, K.M., et al., RNA-guided human genome engineering via Cas9, *Science*, 2013, vol. 339, no. 6121, pp. 823–826.

Marraffini, L.A. and Sontheimer, E.J., CRISPR interference limits horizontal gene transfer in staphylococci by targeting DNA, *Science*, 2008, vol. 322, no. 5909, pp. 1843–1845.

Masepohl, B., Görlitz, K., and Böhme, H., Long tandemly repeated repetitive (LTRR) sequences in the filamentous *Cyanobacterium anabaena* sp. PCC 7120, *Biochim. Biophys. Acta*, 1996, vol. 1307, no. 1, pp. 26–30.

Medvedev, S.P., Malankhanova, T.B., Valetdinova, K.R., et al., Creation and research of cell models of hereditary neurodegenerative diseases using directed genome editing, *Neurochem. J.*, 2021, vol. 15, no. 4, pp. 353–358.

Mojica, F.J.M. and Díez-Villaseñor, C., The on-off switch of CRISPR immunity against phages in *Escherichia coli*, *Mol. Microbiol.*, 2010, vol. 77, no. 6, pp. 1341–1345.

Mojica, F. and Garrett, R., Discovery and seminal developments in the CRISPR field, in *CRISPR-Cas Systems: RNA-Mediated Adaptive Immunity in Bacteria and Archaea*, Barrangou, R. and van der Oost, J., Eds., Springer VS, 2013, pp. 1–31.

Mojica, F.J.M. and Rodriguez-Valera, F., The discovery of crispr in archaea and bacteria, *FEBS J.*, 2016, vol. 283, no. 17, pp. 3162–3169.

Mojica, F.J., Juez, G., and Rodríguez-Valera, F., Transcription at different salinities of *Haloferax mediterranei* sequences adjacent to partially modified PstI sites, *Mol. Microbiol.*, 1993, vol. 9, no. 3, pp. 613–621.

Mojica, F.J., Ferrer, C., Juez, G., et al., Long stretches of short tandem repeats are present in the largest replicons of the archaea *Haloferax mediterranei* and *Haloferax volcanii* and could be involved in replicon partitioning, *Mol. Microbiol.*, 1995, vol. 17, no. 1, pp. 85–93.

Mojica, F.J., Díez-Villaseñor, C., Soria, E., et al., Biological significance of a family of regularly spaced repeats in the genomes of archaea, bacteria and mitochondria, *Mol. Microbiol.*, 2000, vol. 36, no. 1, pp. 244–246.

Mojica, F.J.M., Díez-Villaseñor, C., García-Martínez, J., et al., Intervening sequences of regularly spaced prokaryotic repeats derive from foreign genetic elements, *J. Mol. Evol.*, 2005, vol. 60, no. 2, pp. 174–182.

Morozova, K.N., Suldina, L.A., Malankhanova, T.B., et al., Introducing an expanded CAG tract into the *huntingtin* gene causes a wide spectrum of ultrastructural defects in cultured human cells, *PLoS One*, 2018, vol. 13, no. 10, article ID e0204735.

Naeem, M., Majeed, S., Hoque, M.Z., et al., Latest developed strategies to minimize the off-target effects in CRISPR-Cas-mediated genome editing, *Cells*, 2020, vol. 9, no. 7, p. 1608.

Nair, P., QnAs with rodolphe barrangou, *Proc. Natl. Acad. Sci. U. S. A.*, 2017, vol. 114, no. 28, pp. 7183–7184.

Nakata, A., Amemura, M., and Makino, K., Unusual nucleotide arrangement with repeated sequences in the *Escherichia coli* K-12 chromosome, *J. Bacteriol.*, 1989, vol. 171, no. 6, pp. 3553–3556.

National Academies of Sciences, Engineering, and Medicine, National Academy of Medicine; National Academy of Sciences, Committee on Human Gene Editing: Scientific, Medical, and Ethical Considerations, *Human Genome Editing: Science, Ethics, and Governance*, Washington (DC): National Academies Press, 2017. PMID: 28796468.

Nidhi, S., Anand, U., Oleksak, P., et al., Novel CRISPR–Cas systems: an updated review of the current achievements, applications, and future research perspectives, *Int. J. Mol. Sci.*, 2021, vol. 22, no. 7, p. 3327.

North, A.R., Burt, A., and Godfray, H.C.J., Modelling the suppression of a malaria vector using a CRISPR-Cas9 gene drive to reduce female fertility, *BMC Biol.*, 2020, vol. 18, no. 1, p. 98.

Novembre, J., Galvani, A.P., and Slatkin, M., The geographic spread of the CCR5 Δ32 HIV-resistance allele, *PLoS Biol.*, 2005, vol. 3, no. 11, article ID e339.

Nuffield Council on Bioethics, *Genome Editing and Human Reproduction: Social and Ethical Issues*, London: Nuffield Council on Bioethics, 2018.

Ormond, K.E., Mortlock, D.P., Scholes, D.T., et al., Human germline genome editing, *Am. J. Hum. Genet.*, 2017, vol. 101, no. 2, pp. 167–176.

Pourcel, C., Salvignol, G., and Vergnaud, G., CRISPR elements in *Yersinia pestis* acquire new repeats by preferential uptake of bacteriophage DNA, and provide additional tools for evolutionary studies, *Microbiology*, 2005, vol. 151, part 3, pp. 653–663.

Reardon, S., First pig-to-human heart transplant: what can scientists learn?, *Nature*, 2022, vol. 601, no. 7893, pp. 305–306.

Regalado, A., China's CRISPR babies: Read exclusive excerpts from the unseen original research. https://

www.technologyreview.com/2019/12/03/131752/chinas-crispr-babies-read-exclusive-excerpts-he-jiankui-paper/. Accessed January 23, 2022.

Rodríguez-Leal, D., Lemmon, Z.H., Man, J., et al., Engineering quantitative trait variation for crop improvement by genome editing, *Cell*, 2017, vol. 171, no. 2, pp. 470– 480. e8.

Rusanov, A., Kozhin, P., Romashin, D., et al., Impact of p53 modulation on interactions between p53 family members during HaCaT keratinocytes differentiation, *Bull Russ. State Med. Univ.*, 2020.

Rysenkova, K.D., Semina, E.V., Karagyaur, M.N., et al., CRISPR/Cas9 nickase mediated targeting of urokinase receptor gene inhibits neuroblastoma cell proliferation, *Oncotarget*, 2018, vol. 9, no. 50, pp. 29414–29430.

Sánchez-León, S., Gil-Humanes, J., Ozuna, C.V., et al., Low-gluten, nontransgenic wheat engineered with CRISPR/Cas9, *Plant Biotechnol. J.*, 2018, vol. 16, no. 4, pp. 902–910.

Sapranauskas, R., Gasiunas, G., Fremaux, C., et al., The *Streptococcus thermophilus* CRISPR/Cas system provides immunity in *Escherichia coli, Nucleic Acids Res.*, 2011, vol. 39, no. 21, pp. 9275–9282.

Shmakov, S.A., Faure, G., Makarova, K.S., et al., Systematic prediction of functionally linked genes in bacterial and archaeal genomes, *Nat. Protoc.*, 2019, vol. 14, no. 10, pp. 3013–3031.

Shmakova, A.A., Germini, D., and Vassetzky, Y.S., Exploring the features of Burkitt's lymphoma-associated t(8;14) translocations generated via a CRISPR/Cas9-based system, *Biopolymers Cell*, 2019, vol. 35, no. 3, pp. 232–233.

Slobodkina, E.A., Karagyaur, M.N., Balabanian, V.Yu., et al., Gene' therapy in regenerative medicine: recent achievements and current areas of investigations, *Genes Cells*, 2020, vol. 15, no. 1, pp. 6–16.

Taha, E.A., Lee, J., and Hotta, A., Delivery of CRISPR-Cas tools for in vivo genome editing therapy: trends and challenges, *J. Controlled Release*, 2022, vol. 342, pp. 345–361.

Tyurin-Kuzmin, P.A., Karagyaur, M.N., Rubtsov, Y.P., et al., CRISPR/Cas9-mediated modification of the extreme C-terminus impairs PDGF-stimulated activity of Duox2, *Biol. Chem.*, 2018, vol. 399, no. 5, pp. 437–446.

Ustyantseva, E.I., Medvedev, S.P., Vetchinova, A.S., et al., A platform for studying neurodegeneration mechanisms using genetically encoded biosensors, *Biochemistry* (Moscow), 2019, vol. 84, no. 3, pp. 299–309.

Valetdinova, K.R., Ovechkina, V.S., Grigorieva, E.V., et al., Using the CRISPR/CAS9 system for studying the cell model of spinal myodystrophy, *Genes Cells*, 2017, vol. 12, no. 3.

Vedeneeva, N., Nobel Prize in Chemistry 2020: Who changed the code of a hen? https://www.mk.ru/science/2020/10/07/nobel-po-khimii-2020-kto-izmenil-kod-zhizni-kuricynesushki.html. Accessed January 23, 2022.

Vilarino, M., Suchy, F.P., Rashid, S.T., et al., Mosaicism diminishes the value of pre-implantation embryo biopsies for detecting CRISPR/Cas9 induced mutations in sheep, *Transgenic Res.*, 2018, vol. 27, no. 6, pp. 525–537.

Wang, Y., Cheng, X., Shan, Q., et al., Simultaneous editing of three homoeoalleles in hexaploid bread wheat confers heritable resistance to powdery mildew, *Nat. Biotechnol.*, 2014, vol. 32, no. 9, pp. 947–951.

Webster, D., Bondareva, A., Solin, S., et al., Targeted gene editing in porcine spermatogonia, *Front. Genet.*, 2021, vol. 11.

Wu, Y., Zhou, H., Fan, X., et al., Correction of a genetic disease by CRISPR-Cas9-mediated gene editing in mouse spermatogonial stem cells, *Cell Res.*, 2015, vol. 25, no. 1, pp. 67–79.

Yang, L., Güell, M., Niu, D., et al., Genome-wide inactivation of porcine endogenous retroviruses (PERVs), *Science*, 2015, vol. 350, no. 6264, pp. 1101–1104.

Yuste-Lisbona, F.J., Fernandez-Lozano, A., Pineda, B., et al., ENO regulates tomato fruit size through the floral meristem development network, *Proc. Natl. Acad. Sci. U. S. A.*, 2020, vol. 117, no. 14, pp. 8187–8195.

Zhou, M., Greenhill, S., Huang, S., et al., CCR5 is a suppressor for cortical plasticity and hippocampal learning and memory, *eLife*, 2016, vol. 5, article ID e20985.

Zotova, A., Pichugin, A., Atemasova, A., et al., Isolation of gene-edited cells via knock-in of short glycophosphatidylinositol-anchored epitope tags, *Sci. Rep.*, 2019, vol. 9, no. 1, p. 3132.

Zuccaro, M.V., Xu, J., Mitchell, C., et al., Allele-specific chromosome removal after Cas9 cleavage in human embryos, *Cell*, 2020, vol. 183, no. 6, pp. 1650–1664. Article ID e15.

Chromosomal translocations are a major cause of cancer, and they are often cell-type-specific. This means that different translocations occur in different types of cells. It is not well understood why this is the case, but it could be due to either the occurrence of particular translocations in specific cell types or the adaptive survival advantage conferred by translocations only in specific cells.

In **Article 12**, we experimentally addressed this question by inducing DSBs at specific gene loci that often participate in oncogenic translocations in different cell types. We found that any translocation could potentially arise in any cell type. Among different factors that could affect the frequency of the translocations, we found that the only factor that correlated with the translocation frequency was the spatial proximity between gene loci after the DSB induction. This supports the "breakage-first" model, which states that broken chromosomal ends are free to move in the nuclear space and that they may meet after the break to generate translocations. Interestingly, only oncogenic translocations persisted upon a two-month culture, suggesting that whether the cell with the translocation would persist in a cell population depends on the cell type-specific selective survival advantage that the chromosomal translocation confers to the cell.

Overall, the results of the study suggest that chromosomal translocations can be generated in any type of cell, but whether the cell with the translocation will persist depends on the cell type-specific selective survival advantage that the translocation confers.

I contributed to this paper by performing experiments on loci colocalisation before and after DSBs with the use of different inhibitors, performing experiments for paper revision, data analysis, manuscript reviewing and editing and creating illustrations and figures.

Article 12. Research paper "Specificity of cancer-related chromosomal translocations is linked to proximity after the DNA double-strand break and subsequent selection"

Published online 23 September 2023

NAR Cancer, 2023, Vol. 5, No. 3 **1**
https://doi.org/10.1093/narcan/zcad049

Specificity of cancer-related chromosomal translocations is linked to proximity after the DNA double-strand break and subsequent selection

Reynand Jay Canoy[1,2,†], Anna Shmakova[1,3,4,†], Anna Karpukhina[1,4], Nikolai Lomov[5], Eugenia Tiukacheva[1,4], Yana Kozhevnikova[1], Franck André[1], Diego Germini[1,*] and Yegor Vassetzky[1,4,*]

[1]UMR 9018, CNRS, Univ. Paris-Sud, Université Paris Saclay, Institut Gustave Roussy, F-94805 Villejuif, France, [2]Institute of Human Genetics, National Institutes of Health, University of the Philippines Manila, 1000 Manila, The Philippines, [3]Laboratory of Molecular Endocrinology, Institute of Experimental Cardiology, Federal State Budgetary Organization 'National Cardiology Research Center' of the Ministry of Health of the Russian Federation, 127994 Moscow, Russia, [4]Koltzov Institute of Developmental Biology, 117334 Moscow, Russia and [5]Department of Molecular Biology, Faculty of Biology, Lomonosov Moscow State University, 119991 Moscow, Russia

Received March 17, 2023; Revised August 01, 2023; Editorial Decision August 30, 2023; Accepted September 14, 2023

ABSTRACT

Most cancer-related chromosomal translocations appear to be cell type specific. It is currently unknown why different chromosomal translocations occur in different cells. This can be due to either the occurrence of particular translocations in specific cell types or adaptive survival advantage conferred by translocations only in specific cells. We experimentally addressed this question by double-strand break (DSB) induction at *MYC*, *IGH*, *AML* and *ETO* loci in the same cell to generate chromosomal translocations in different cell lineages. Our results show that any translocation can potentially arise in any cell type. We have analyzed different factors that could affect the frequency of the translocations, and only the spatial proximity between gene loci after the DSB induction correlated with the resulting translocation frequency, supporting the 'breakage-first' model. Furthermore, upon long-term culture of cells with the generated chromosomal translocations, only oncogenic *MYC–IGH* and *AML–ETO* translocations persisted over a 60-day period. Overall, the results suggest that chromosomal translocation can be generated after DSB induction in any type of cell, but whether the cell with the translocation would persist in a cell population depends on the cell type-specific selective survival advantage that the chromosomal translocation confers to the cell.

GRAPHICAL ABSTRACT

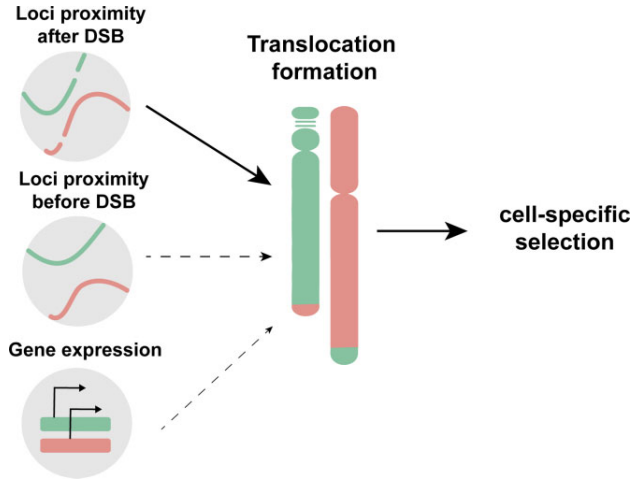

INTRODUCTION

Chromosomal translocations are hallmarks of many cancers (1). More than 50% of leukemias and almost all lymphomas exhibit or are directly caused by chromosomal translocations (2–5). Functional consequences of chromosomal translocations include aberrant expression of otherwise normal genes, expression of fusion genes and/or large-scale changes in the nuclear organization (6–9).

Many of the known chromosomal translocations appear to be cell type specific (3). For example, the *MYC–IGH* translocation has only been observed in B cells and not in

*To whom correspondence should be addressed. Tel: +33 1 42 11 45 26; Email: germinidiego@gmail.com
Correspondence may also be addressed to Yegor Vassetzky. Tel: +33 1 42 11 62 83; Fax: +33 1 42 11 54 94; Email: yegor.vassetzky@cnrs.fr
†The authors wish it to be known that, in their opinion, the first two authors should be regarded as Joint First Authors.

© The Author(s) 2023. Published by Oxford University Press on behalf of NAR Cancer.
This is an Open Access article distributed under the terms of the Creative Commons Attribution-NonCommercial License (http://creativecommons.org/licenses/by-nc/4.0/), which permits non-commercial re-use, distribution, and reproduction in any medium, provided the original work is properly cited. For commercial re-use, please contact journals.permissions@oup.com

other cell types. Why do different chromosomal translocations occur in different cells? Is this due to the fact that some translocations are more likely to occur in specific cell types due to cell-specific characteristics or do translocations occur in a similar manner in all cells, but they confer a selective advantage in a specific cell type? The generation of chromosomal translocation involves two major steps: the formation of specific double-strand breaks (DSBs) and their erroneous repair via nonhomologous end joining (NHEJ) (10). Cell-specific traits that may potentially affect translocation formation include preferential occurrence of DSBs at specific loci in specific cell types [e.g. due to chromatin state or the activity of intrinsic DNA-cutting enzymes (9,11)] and/or predetermined factors that affect DNA repair [e.g. transcriptional activity, loci spatial proximity, the activity of specific repair factors or even cell-specific expression of chromosomal aberrations stimulating long noncoding RNAs (lncRNAs) (12)]. While previous studies have extensively explored the occurrence of cell-specific DSBs, less is known about the risk factors that interfere with translocation-prone DSB repair once they are already formed in a particular cell type. Chromatin state, DSB movement and DNA damage sensing and repair mechanisms influence the generation of chromosomal translocations at this step (9). The presence of specific transcripts [e.g. lncRNAs that share homology regions for two different loci (12,13)] or certain drugs (14) can also affect the formation of chromosomal rearrangements. Understanding these risk factors is crucial for developing targeted interventions to prevent the occurrence of translocations and the development of related diseases such as cancer.

Studying randomly induced and/or naturally occurring chromosomal translocations poses challenges and serious limitations. First, translocations are rare events, for certain types of translocations literally a single event occurs in the whole organism, and cells with translocations can survive and proliferate only if translocation provides a proliferative advantage in a cell population. Second, the localization of breakpoints in naturally occurring translocations varies from kilobases to hundreds of kilobases, which requires sophisticated techniques to detect them [e.g. long-range polymerase chain reaction (PCR), fluorescence *in situ* hybridization (FISH), deep sequencing, etc.] (15,16). With the advancement of gene-editing tools that can produce DSBs at specific loci, the generation of cell lines with specific chromosomal translocations became possible (14,17–22). The CRISPR/Cas9 tool generates DSBs in both euchromatin and heterochromatin regions (23–27), which facilitates the study of factors that affect the formation of translocations across different cell types. Here, we devised a CRISPR/Cas9-based experimental strategy to induce DSBs in one cell within several specific loci that are commonly involved in oncogenic chromosomal rearrangements (*MYC*, *IGH*, *AML*, *ETO*) with the aim to stimulate the formation of chromosomal translocations between these loci. Using this strategy, we investigated different factors associated with the frequency of generated chromosomal translocations in human cells of different developmental origins. We analyzed the translocation frequencies with respect to the transcription activity, nuclear radial position and spatial proximity of the gene loci targeted by CRISPR/Cas9 and demonstrated that in all of the considered cell types the most prominent factor affecting the chromosomal translocations was the spatial proximity between the potential partner loci after the DSB induction. The colocalization of potential partner loci after the DSB induction was dependent on DNA-dependent protein kinase (DNA-Pk) activity. Our results demonstrated that virtually any type of chromosomal translocation can arise in any cell type after the induction of DSBs, but the persistence of cells with these translocations is dependent on the specific survival advantage conferred by the translocation in that cell type. This highlights the complexity of chromosomal translocations in cancer cells and underscores the importance of considering the selective survival advantage of chromosomal translocations in different cell types, adding a new dimension to our understanding of the process.

MATERIALS AND METHODS

Cell culture

All cells were handled in aseptic techniques and were kept in a humidified incubator at 37°C with 5% CO_2 until use. They were maintained in their respective cell culture growth medium and were passed at least once a week. For the recipes of the growth medium, see Supplementary Data. Cell treatments are listed in Supplementary Table S1.

gRNA design, cloning and testing

All guide RNA (gRNA) binding sites were generated from CRISPOR gRNA design online tool (http://crispor.tefor.net/) (28) and were inserted into the phU6 gRNA plasmids (Addgene #53188). gRNA and Cas9 plasmids (Addgene #57818) were transformed into DH5α competent cells via heat shock and were then subsequently clonally expanded for plasmid extraction (Machery-Nagel NucleoBond Xtra Midi or Maxi kit). gRNA efficiency was tested following the procedures provided in TIDE (29) and ENIT (30) protocols. For the sequences of the gRNA binding sites, see Supplementary Table S2.

Electrotransfection

Cells were electrotransfected following the protocol for hard-to-transfect cells in (31). Briefly, 4–8 × 10^6 cells were electrotransfected with 50 μg total plasmid, 60% of which is Cas9 and the remaining 40% consists of gRNA plasmids. After 2 days, electrotransfection efficiency was checked using Accuri™ C6 Flow Cytometer (BD Biosciences). Depending on the intended number of electrotransfected cells, the electrotransfection reactions were scaled up.

Western blot

Western blot analysis was performed following the protocol in (32) using the following antibodies: Cas9 antibody (7A9-3A3) (anti-mouse, Santa Cruz Biotechnology, sc-517386), GAPDH (anti-mouse, Cell Signaling Technology, 2118) and anti-mouse peroxidase-conjugated secondary antibodies (Jackson ImmunoResearch, 315035003).

PCR and qPCR

Total DNA was extracted using NucleoSpin Tissue DNA purification kit (Macherey-Nagel) following the manufacturer's protocol. Total RNA was extracted using NucleoSpin RNA II purification kit (Macherey-Nagel) and was then converted to complementary DNA (cDNA) using Maxima H Minus cDNA Synthesis Master Mix (Thermo Fisher Scientific) following the manufacturer's protocol. PCR amplification was performed using PowerUp SYBR Green Master Mix (Thermo Scientific) following the manufacturer's protocol. For the PCR primers used, see Supplementary Tables S3 and S4.

Translocation frequency was calculated using the Pfaffl method (33) to correct for the observed varying amplification efficiencies of each primer pair (Supplementary Figure S2F). The calculated frequencies were then adjusted to the respective transfection efficiencies measured 2 days after electrotransfection, right before cell collection, using the Accuri™ C6 Flow Cytometer (BD Biosciences).

3D-FISH

3D-FISH was performed following the protocols in (18) using the following probes: AML (Empire Genomics, RP11-1056O16 blue), ETO (Empire Genomics, RP11-643O11 orange), MYC (Empire Genomics, RP11-440N18 red) and IGH (Empire Genomics, RP11-346I20 green). For image acquisition and analysis, see Supplementary Data.

Statistical analysis

All experiments were performed with at least two biological replicates and two technical replicates. Statistical analyses were performed using GraphPad Prism 9.1.0.221 and R Studio. For comparisons between the two groups, an unpaired *t*-test was done. For comparisons involving more than two groups, one-way analysis of variance (ANOVA) and Tukey's honest significant difference as the post-hoc test were performed. For the correlation analysis, the Spearman correlation between the translocation frequency and the predictors (gene expression/loci proximity before DSB/loci proximity after DSB) was performed.

RESULTS

Experimental strategy for analysis of CRISPR/Cas9-induced chromosomal translocations

With the aim to identify factors affecting the generation of chromosomal translocations across cell types, we developed a CRISPR/Cas9-based strategy to induce DSBs in one cell within several chromosomes. This would potentially generate several different chromosomal translocations upon erroneous repair of these DSBs via NHEJ (Figure 1A and Supplementary Figure S1A). The frequencies of induced chromosomal translocations were measured by quantitative PCR (qPCR) and compared in one cell type and between different cell types. We selected four loci for DSB induction: the *RUNX1T1* (formerly known as *ETO*) gene on chromosome 8q21, the upstream region of the *MYC* gene on chromosome 8q24, the immunoglobulin heavy chain (*IGH*) gene locus on chromosome 14q32 and the *RUNX1* (formerly known as *AML*) gene on chromosome 21q22. These gene loci are involved in clinically relevant oncogenic translocations: t(8;21) between *AML* and *ETO* in acute myeloid leukemia and t(8;14) between *MYC* and *IGH* in Burkitt's lymphoma.

The gRNAs were designed (Supplementary Table S2) to target the above loci and cloned into phU6 plasmids. gRNA efficiency was tested by TIDE (29) as described in the 'Materials and Methods' section and gRNAs with similar efficiencies were chosen to avoid a bias of different CRISPR/Cas9 cutting efficiencies (Supplementary Figure S2A). The cells were then electrotransfected with the Cas9-expressing plasmid to determine the Cas9 expression kinetics. The Cas9 expression started to peak 48 h after the electrotransfection (Supplementary Figure S2B). We then tested the cell survival and apoptosis after electrotransfection (Supplementary Figure S2C and D).

We designed PCR primers (Supplementary Tables S3 and S4) to detect resulting translocations. Supplementary Figure S2E shows a representative image of an agarose gel electrophoresis of PCR-amplified *MYC–IGH* translocations after electrotransfection with Cas9 and gRNAs targeting the *MYC* and *IGH*, *AML–ETO* translocations after electrotransfection with Cas9 and gRNAs targeting the *AML* and *ETO*, *IGH–ETO* translocations after electrotransfection with Cas9 and gRNAs targeting the *IGH* and *ETO*, and *AML–IGH* translocations after electrotransfection with Cas9 and gRNAs targeting the *AML* and *IGH*. The amplification efficiencies of each primer pair (Supplementary Figure S2F) were taken into account when calculating the translocation frequency (see the 'Materials and Methods' section). The translocation frequency started peaking 48 h post-transfection (Supplementary Figure S3); therefore, we selected the 48 h post-electrotransfection as the collection time point for the next experiments to avoid the effect of positive or negative selection of translocations upon subsequent cell divisions.

We used inhibitors of specific repair pathways to determine the pathway of the translocation formation in our model. We added the inhibitors of either MRE11 involved in both classical and alternative NHEJ (mirin) or DNA-Pk involved in the canonical NHEJ pathway (NU7026). We observed that treatment with NU7026 led to a 2.4-fold increase ($P = 0.0056$) in the translocation rate (Figure 1B), suggesting that translocations are mainly due to the alternative NHEJ repair as already proposed by others (34).

Simultaneous induction of DSBs results in cell type-specific translocation frequencies

To analyze the appearance of chromosomal translocations in different cell types, we induced DSBs in cell lines of different developmental origin and ploidy: RPMI8866 (lymphoid, B cell, diploid with three to four copies of chromosome 8), Jurkat (lymphoid, T cell, diploid), K562 [myeloid, nearly triploid (35)], MRC5 (lung fibroblast, diploid) and Hek-293 (embryonic kidney, epithelial, hypotriploid). These cell lines were electrotransfected with plasmids encoding for Cas9 and gRNA combinations targeting two sets of gene loci: *MYC*, *IGH* and *AML* (MIA) or

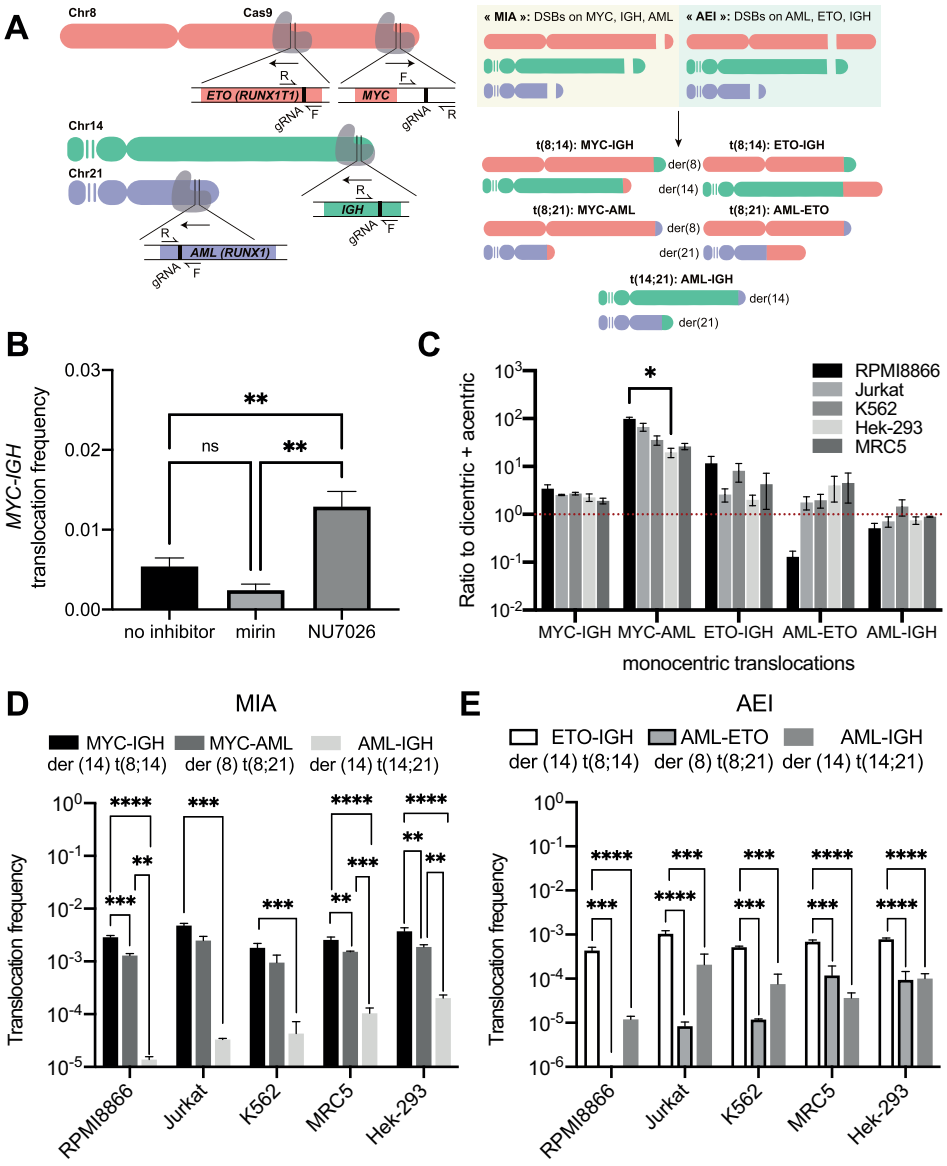

Figure 1. Translocations generated in different cells after the simultaneous induction of three DSBs on chromosomes 8, 14 and 21. (**A**) Positions of sites targeted by gRNA in the *ETO* (8q21.3), *MYC* (8q24.12), *IGH* (14q32.33) and *AML* (21q22.12) gene loci (left panel) and the resulting potential unicentric chromosomal translocations after targeting *MYC*, *IGH* and *AML* loci (MIA) or *AML*, *ETO* and *IGH* loci (AEI) (right panel). (**B**) *MYC*–*IGH* translocation frequency after inhibition of NHEJ repair components. Six hours after electrotransfection with gRNA and Cas9 plasmids, cells were treated with either mirin (an inhibitor of MRE11) or NU7026 (an inhibitor of DNA-Pk). The number of biological replicates $n = 4$–5. (**C**) Ratio of the combined translocation frequencies of the two monocentric derivative chromosomes with respect to the combined translocation frequencies of the dicentric and acentric derivative chromosomes. The data are shown on a $\log_{10}$ scale. Translocations were induced in RPMI8866, Jurkat, K562, MRC5 and Hek-293 cells via electrotransfection with gRNA and Cas9 plasmids, targeting *MYC*, *IGH* and *AML* loci or *AML*, *ETO* and *IGH* loci and the resulting translocation frequencies were measured 2 days later by qPCR with a subset of primers that target monocentric (two pairs for each translocation), dicentric or acentric derivative chromosomes. Then, the frequencies of monocentric chromosomes were added and divided by the sum of frequencies of the dicentric and acentric derivative chromosomes, providing the resulting ratio. In almost all cases, the ratio was >1, indicating that the generation of monocentric derivative chromosomes was favored over dicentric and acentric ones. The number of biological replicates $n = 2$–7. (**D**, **E**) Frequencies of translocations induced by DSBs. RPMI8866, Jurkat, K562, MRC5 and Hek-293 cells were electrotransfected with gRNA and Cas9 plasmids, targeting MIA (D) or AEI (E). After 2 days, electrotransfected cells were collected for DNA extraction and translocations were detected using qPCR with translocation-specific PCR primers. The translocation frequencies were calculated as described in the 'Materials and Methods' section. Only the unicentric derivative chromosomes with the highest frequency compared to their reciprocal counterparts are shown in the graphs. Means ± standard errors of the mean (SEMs) of at least two biological and two technical replicates are shown. One-way ANOVA with Tukey's honest significant difference post-hoc test was performed to compare the translocation frequencies within each cell type: $^{**}P \leq 0.01$, $^{***}P \leq 0.001$ and $^{****}P \leq 0.0001$.

AML, *ETO* and *IGH* (AEI). DNA was collected 48 h later and all possible resulting translocations were quantified using qPCR as described in the 'Materials and Methods' section. In theory, each chromosome pair can form three types of translocations: unicentric (with one centromere; most cancer-related translocations are unicentric), dicentric (with two centromeres) and acentric (without centromeres). The latter two types of translocations are usually lost in the course of cell divisions; therefore, we concentrated on unicentric translocations.

In almost all translocations in all cell types, the combined translocation frequencies of the monocentric derivative chromosomes were higher compared to the combined dicentric and acentric derivative chromosomes after induction of three DSBs (Figure 1C), suggesting that the formation of monocentric derivative chromosomes is already favored early on. The *MYC–IGH* translocation had the highest frequency after MIA DSB induction (2–5×10^{-3} translocations/cell) compared to the *MYC–AML* and *AML–IGH* translocations (1–2×10^{-3} and 0.01–0.2×10^{-3} translocations/cell, respectively) (Figure 1D and Supplementary Figure S4A–E). After AEI DSB induction, the *ETO–IGH* translocation had the highest frequency ($0.4–1 \times 10^{-3}$ translocations/cell) compared to the *AML–IGH* and *AML–ETO* translocations ($0.01–0.2 \times 10^{-3}$ and $0.008–0.1 \times 10^{-3}$ translocations/cell, respectively) (Figure 1E and Supplementary Figure S4F–J). Of the five cell types, Jurkat exhibited the highest translocation frequencies after induction of either MIA or AEI DSBs. The oncogenic *MYC–IGH* translocation had the highest frequency after MIA DSB induction (Figure 1D), while another oncogenic *AML–ETO* translocation had the lowest frequency after AEI DSB induction (Figure 1E), although it was relatively high in the myeloid K562 and epithelial Hek-293 cells (0.01×10^{-3} and 0.1×10^{-3}, respectively). Interestingly, the translocation frequencies involving the *MYC* locus were two to four times higher than those of the other translocations in all cell types. Another important conclusion is that while the studied cell lines had different ploidies, relative frequencies of translocations were similar across the cell lines with few exceptions.

Transcriptional activity and nuclear radial distribution of gene loci do not correlate with the translocation formation after DSB induction

We next tried to identify factors that could account for the observed translocation frequencies. Actively transcribed loci, loci with an open chromatin configuration or loci located close to each other may have higher propensities to form translocations (36–39). *MYC–IGH* and *AML–ETO* translocations will now serve as examples of our results, but all the described analyses were performed for all possible translocations.

We first correlated the frequencies of the *MYC–IGH* and *AML–ETO* translocations in different cell types (Figure 2A and B) with the transcriptional activity of the involved genes determined by quantitative reverse transcription PCR (Figure 2C) and no positive correlation was observed ($R_s = 0.24$, Figure 2D). Higher transcriptional activity did not always mean higher translocation rate. For example, both *MYC* and *IGH* were actively transcribed in the RPMI8866 cells, and *IGH* was minimally or not transcribed in other cell types, but this did not affect the frequency of the *MYC–IGH* translocation that remained high. On the contrary, the *AML–ETO* translocation was generated at a very low frequency in K562 cells (Figure 2B) even though the *AML* and *ETO* genes were actively transcribed (Figure 2C). The *ETO–IGH* translocation in Jurkat was still generated (Figure 1E) though neither *ETO* nor *IGH* was actively transcribed (Figure 2C).

Radial positions reflect the localization of gene loci within the nucleus. Peripheral regions of the nucleus are often heterochromatin-rich and transcriptionally repressed, while central regions are transcriptionally active. We determined the nuclear radial positions of the four gene loci before the DSB induction using 3D-FISH. The *MYC*, *IGH*, *AML* and *ETO* loci were positioned near the center of the nucleus and had a roughly similar radial distribution before (Figure 2E) and after DSB induction (Figure 2F). Thus, this factor could not solely account for the variability of translocation frequencies between different gene loci across the studied cell lines in our system.

The breakage-first model accounts for translocation formation after DSB induction

As translocations are produced by NHEJ, a proximity-based mechanism (40), we next studied whether the loci involved in the translocations were proximal in the cell nuclei. We have measured the distance between fluorescent signals corresponding to the studied loci. As each 3D-FISH signal was ~1 μm in diameter, two signals were considered to be proximal (colocalized) when the distance between their centers was no more than 1 μm, since at this distance, spots partially or completely overlapped. The spatial proximity between the gene loci was expressed as the percentage of cells where the two loci were colocalized. Surprisingly, before the occurrence of DSB, we did not observe a positive correlation between gene proximity and translocation rate ($R_s = 0.32$; $P = 0.0331$) (Figure 3C). As DSBs are known to induce mobility of the damaged gene loci [reviewed in (41)], we also measured gene proximity after the DSB induction. We observed a significant increase of gene loci proximity after DSB induction in the case of *MYC–IGH* and *ETO–IGH* pairs in all considered cell types (Figure 3A and D, and Supplementary Figure S5A–F) and the translocations between these very gene loci were also the most frequent (Figure 3B and E). A representative image shows the positions of *MYC* and *IGH* loci before and after the DSB induction (Figure 3G). It is noteworthy that colocalization of gene loci was a predisposing factor for their translocation but did not necessarily mean that they were translocated (e.g. *AML–ETO* were colocalized in 4.4 ± 0.3% of RPMI8866 cells after DSBs, but no translocations between these loci were observed; Figure 3D and E). Overall, we observe colocalization between loci at a much higher rate than translocations; this shows that colocalization alone is not sufficient to induce translocations. The inverse is also true, as in the case of *MYC–AML* translocation, where the loci were not found to colocalize at a detectable rate and yet the translocation was still formed (Figure 3A and B). When we took into

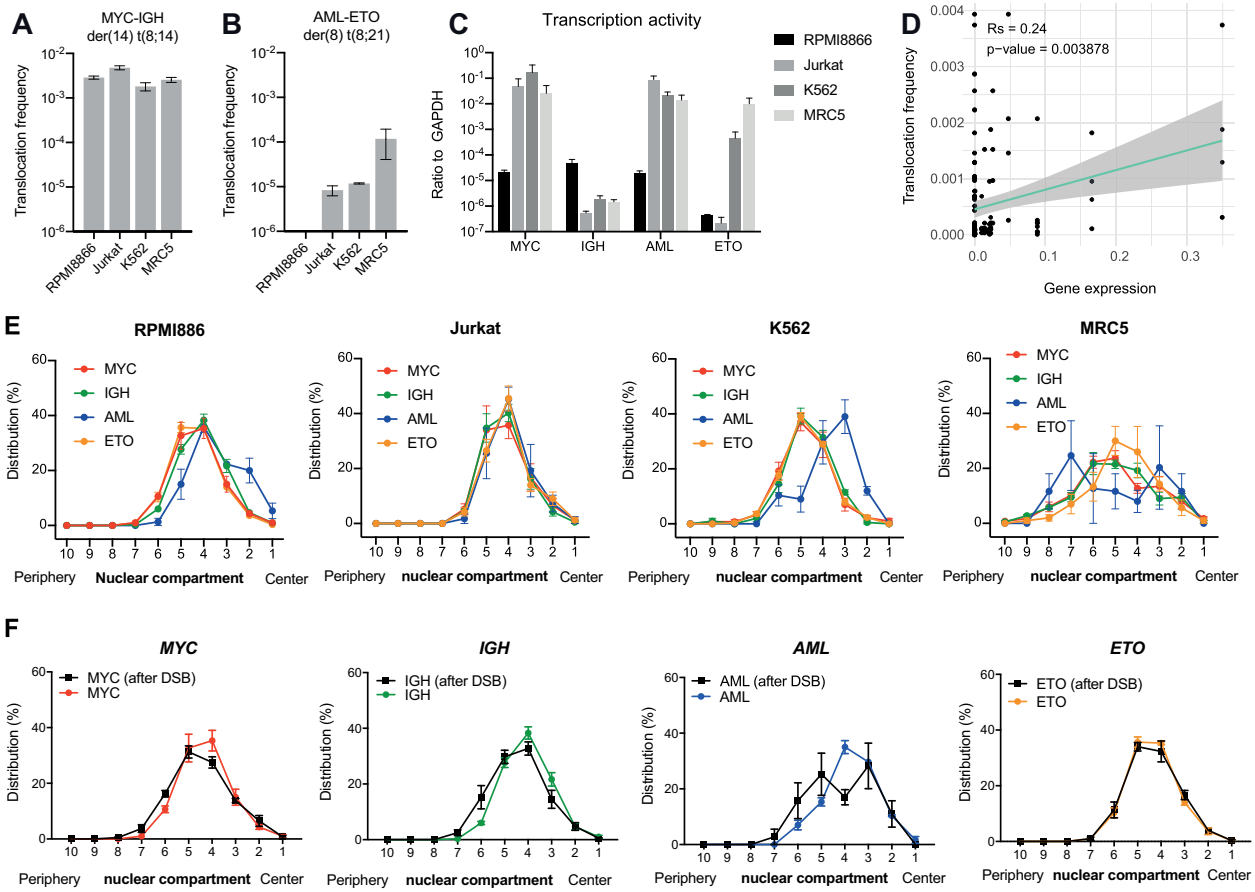

Figure 2. Transcriptional activity and nuclear radial position of gene loci do not correlate with their translocation frequency. Frequencies of the *MYC–IGH* (**A**) and *AML–ETO* (**B**) translocations across the cell lines. RPMI8866, Jurkat, K562 and MRC5 cells were electrotransfected with gRNAs and Cas9 plasmids targeting MIA (A) or AEI (B). Forty-eight hours after electrotransfection, cells were collected for DNA extraction and translocations were detected using qPCR with translocation-specific PCR primers. The translocation frequencies were calculated. Means ± SEMs are shown representing the results of two to four biological and two technical replicates. (**C**) Transcriptional activity of the *MYC*, *IGH, AML* and *ETO* genes in the studied cell lines. RNA was extracted from cells and relative fold gene expression with respect to the housekeeping gene *GAPDH* was calculated from Ct values obtained from the qPCR results as described in the 'Materials and Methods' section. Means ± SEMs of two to three biological and two technical replicates are shown. (**D**) Correlation plot for the gene expression and observed translocation frequencies. The Spearman correlation coefficient ($R_s = 0.24$) and its corresponding *P*-value (0.003878) are shown. The green line represents the linear regression fit and the gray area represents the 95% confidence intervals. (**E**) Radial position of the gene loci in the nuclear space of RPMI8866, Jurkat, K562 and MRC5 cells analyzed by 3D-FISH. (**F**) Radial position in the nuclear space of *MYC*, *IGH*, *AML* and *ETO* before and after DSB induction in RPMI8866. For the nuclear radial position before DSB induction, non-electrotransfected cells were collected and processed for 3D-FISH. For the nuclear radial position after DSB induction, RPMI8866 (16×10^6 cells) were electrotransfected with Cas9 and gRNA-expressing plasmids targeting either MIA or AEI. Two days after electrotransfection, cells were sorted for GFP, as the electrotransfected Cas9 plasmid also codes for GFP. The sorted cells were then processed for 3D-FISH. The images were acquired using a confocal microscope and analyzed using the Bitplane Imaris software. Each gene locus was mapped within the nucleus with respect to the 10 concentric compartments with the equal volume numbered from the center to the periphery of the nucleus. Data are presented as means ± SEMs of three to four biological replicates. For each technical replicate, at least 100 cells were analyzed.

consideration all detected translocations in all studied cell types, we could reveal a positive correlation ($R_s = 0.55$; $P = 0.0001$) between the proximity after the DSB and the translocation frequency (Figure 3F), indicating that translocation formation was affected by the spatial proximity between gene loci after the DSB induction. In multiple linear regression of different factors that could affect translocation frequency, which also took into account the cell type, only the proximity after the DSB showed a significant association with the translocation frequency ($P = 0.012$, Table 1).

To identify factors that affected loci movement after DSB induction, we used several inhibitors: NU7026 (an inhibitor of DNA-Pk), L67 (a DNA ligase I and III inhibitor) and KU-55933 (ATM inhibitor). We found that loci proximity after the DSB induction increased significantly in the presence of NU7026 (Figure 3H), which indicates that DNA-Pk-dependent signaling prevents loci relocation upon DSB.

Different survival outcomes of cells with chromosomal translocations

Our results show that any translocation can potentially arise in all types of cells; at the same time, the majority of described cancer-related chromosomal translocations

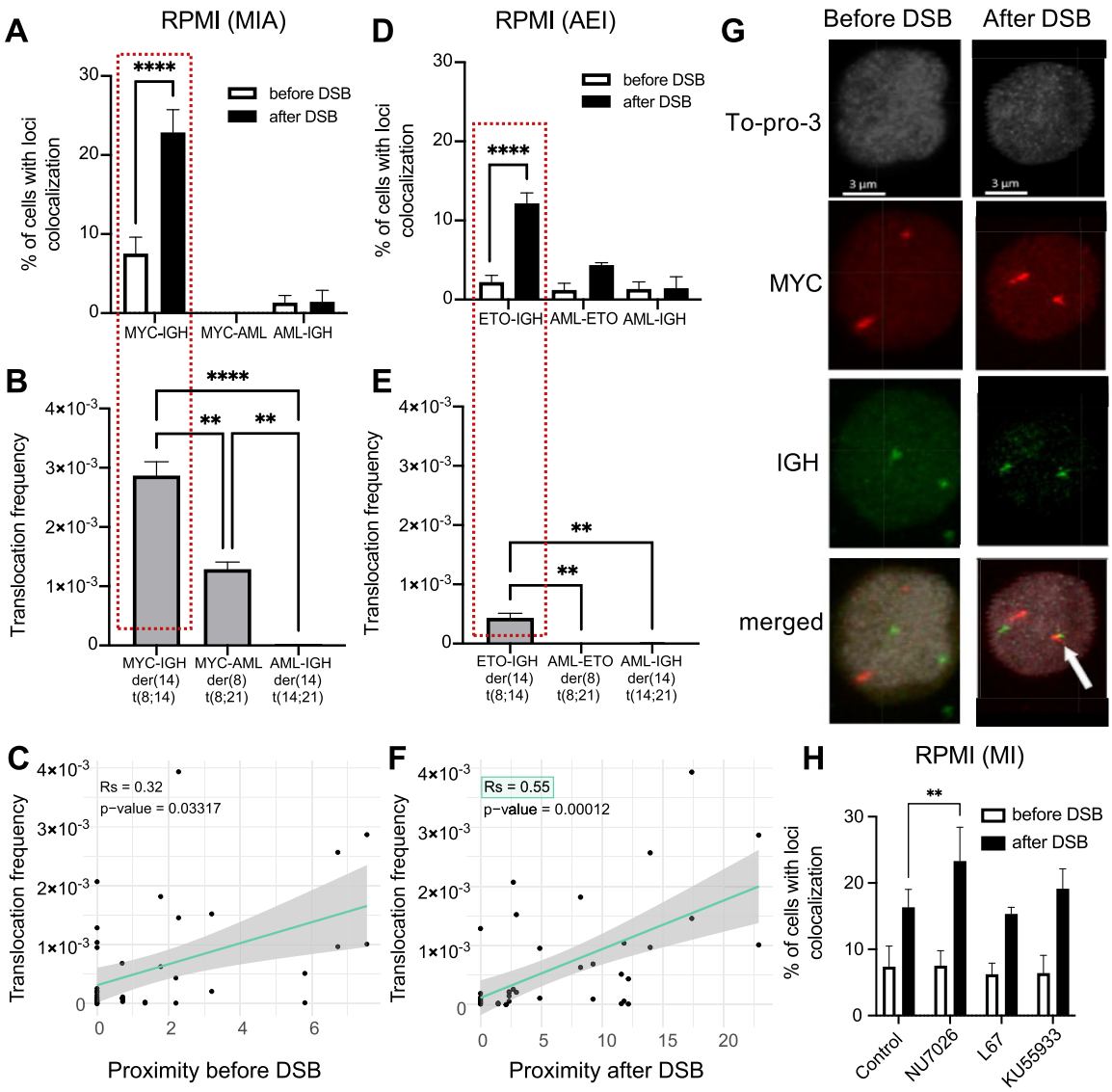

Figure 3. Spatial proximity between gene loci before and after DSB induction in RPMI8866. Spatial proximity between gene loci before and after DSB induction in MIA (**A**) and AEI (**D**) in RPMI8866. Non-electrotransfected cells ($1–2 \times 10^5$) (before DSB) and sorted cells (after DSB) ($1–2 \times 10^5$) that were electrotransfected with gRNAs and Cas9 plasmids 2 days prior were collected and processed for 3D-FISH. The slides were scanned using a confocal microscope and 3D-FISH images were analyzed in Bitplane Imaris software. The percentage of cells with the target gene loci pair located at 1 μm or less (colocalized) was calculated. The number of replicates $n = 2–8$. Translocation frequencies after DSB induction in MIA (**B**) and AEI (**E**) in RPMI8866. Only the unicentric derivative chromosomes with the highest frequency are shown. The number of replicates $n = 3$. Scatter plots of translocation frequency versus before DSB proximity (**C**) and after DSB proximity (**F**). The Spearman correlation coefficient (Rs) and its corresponding *P*-value are shown. (**G**) Representative 3D-FISH image of RPMI8866 cells before (left column) and after DSB induction (right column). The nuclei were stained with To-Pro-3 and are represented in the images as gray. Meanwhile, the *MYC* and *IGH* loci were stained with specific fluorescent probes and are represented in red and green, respectively. Colocalization between *MYC* and *IGH* is pointed out in the merged image by a white arrow. Scale bar = 3 μm. (**H**) Spatial proximity between gene loci before and after DSB induction in *MYC* and *IGH* (MI) in RPMI8866; cells were treated with NU7026 (an inhibitor of DNA-Pk), L67 (a DNA ligase I and III inhibitor), KU-55933 (ATM inhibitor) or left untreated (control). The number of replicates $n = 3–7$. For each replicate, at least 100 cells were analyzed. For all plotted values of each graph, one-way ANOVA was performed. For each comparison, the statistical significance is shown: $^{**}P \leq 0.01$ and $^{****}P \leq 0.0001$.

Table 1. Multiple linear regression of different factors involved in translocation formation. *P*-value < 0.05 is denoted in bold

	Translocation frequency		
Predictors	Estimates	95% CI	*P*-value
Cell type			
Jurkat	−0.00	−0.07 to 0.06	0.968
K562	−0.03	−0.10 to 0.04	0.385
MRC5	0.00	−0.05 to 0.06	0.869
RPMI8866	−0.01	−0.06 to 0.04	0.620
Loci proximity before DSB	0.00	−0.01 to 0.02	0.586
Loci proximity after DSB	0.01	0.00–0.01	**0.012**
Gene 1 expression	0.33	−0.24 to 0.89	0.251
Gene 2 expression	0.89	−0.36 to 2.14	0.156

Number of observations = 44; $R^2/R^2_{adjusted} = 0.621/0.537$; genes 1 and 2, genes involved in chromosomal translocation; 95% CI, 95% confidence intervals.

are cell type specific (3,42). This may be due to the selective advantage the translocation provides to only specific types of cells. To test this, we analyzed how the generated chromosomal translocations would be retained in different cell lines upon long-term culture. Cells transfected with CRISPR/Cas9 and gRNAs were cultured for 60 days with regular weekly passages. Translocation persistence was different in different cell types (Figure 4A–E and Supplementary Figure S6A–J). The proportion of cells bearing *MYC–IGH* translocation increased >50 times on Day 60 and attained over 10% of the total cell population as compared to Day 2 in RPMI8866 cells suggesting that *MYC–IGH* translocation could be a subject of positive selection in RPMI8866 cells. In other cell lines, *MYC–IGH* translocation either did not increase significantly or eventually decreased by Day 60. It should be noted that *IGH* is actively transcribed only in B cells and its translocation with *MYC* can lead to *MYC* overexpression in B cells (43). In addition, *MYC* expression was much lower in RPMI8866 cells prior to translocations as compared to other cell types (Figure 2C). On the other hand, the *AML–ETO* translocation was found to persist after long-term culture in MRC5 cells only (Supplementary Figure S6F–J) although still at a low frequency. These results point out that the generated chromosomal translocations either confer cell type-dependent survival advantages or are progressively eliminated from the cell population.

DISCUSSION

Why are certain chromosomal translocations observed in specific cell types? Several studies addressed this question before. They found that genes that are proximally positioned in the nuclear space, have a higher transcriptional activity or have an accessible chromatin configuration tend to have a higher propensity to form translocations in a specific cell type (22,44–52). Initial studies on chromosomal translocation formation utilized naturally occurring chromosomal translocations, as in the case of B-cell lymphomas, and then correlated their formation with the nuclear spatial position and transcription activity of the involved genes in normal cells (44,45). Naturally occurring chromosomal translocations are, however, significantly dependent on DSBs that occur in specific gene loci in these cells. More recently, stimulated chromosomal translocations were investigated after experimental induction of DSBs, either by programmed nucleases or by ionizing radiation. The resulting chromosomal translocations were tracked using live cell microscopy to characterize the spatial and dynamic properties of translocation formation (46). Variants of massively parallel sequencing (47,48) in combination with chromosome capture techniques (4C or Hi-C) (49–52) were also used to detect the generated translocations genome-wide to demonstrate the role of spatial proximity between gene loci and DSBs, gene transcription activity, chromatin configuration and nuclear organization in translocation formation. From these studies, the factors that appear to contribute significantly to translocation formation are the spatial proximity between the gene loci and their transcription activity (46–49,51). Translocation breakpoints were also found to be close to the transcription start sites (47–49).

Chromosomal translocations are products of erroneous repair of DSBs (9,53). The error-prone NHEJ repair pathway illegitimately joins two broken chromosomal ends from nonhomologous chromosomes (54). As NHEJ is a proximity-based repair, the physical proximity of the partner loci is a prerequisite to translocation formation (37). In this context, two models are proposed to explain the formation of chromosomal translocations (55). The 'contact-first' model proposes that the broken chromosomal ends are immobile or have limited movement in the nuclear space and that translocation occurs to those that are initially close to each other (colocalize prior to and at the time of DSB) (55). This is supported by the occurrence of chromosomal translocations involving gene loci that were already proximal, such as *RET* and *H4* (56), *ABL* and *BCR* (57), and *PML* and *RARA* (58) loci, or gene loci that have moved closer to each other before the chromosomal breakage occurred, e.g. *MYC* and *IGH* loci upon B-lymphocyte activation (18,22,44,45,59). The 'breakage-first' model postulates that broken chromosomal ends can freely move around the nuclear space and that the meeting of the two ends may lead to translocation formation. In this scenario, there is a higher likelihood for translocation to occur if DSB movement and colocalization increase. This DSB movement can be directed, stochastic or both [reviewed in (41)]. DSB mobility was observed in the case of multiple DSBs induced by alpha particles or ionizing radiation (60,61).

To experimentally test these conclusions, we induced several DSBs in specific loci of one cell and compared the frequency of resulting chromosomal translocations between these loci in different cell types using the CRISPR/Cas9 system (Figure 1). The advantage of this system is that CRISPR/Cas9 induces DSBs in both euchromatin and heterochromatin regions (although Cas9 can be less efficient in heterochromatin regions) (23,24,26,27). Additionally, the repair of DSBs after Cas9 cleavage is error-prone, which prevents recutting of the same locus (62). The observed translocations were likely produced by the alternative NHEJ pathway as inhibition of DNA-Pk, an important component of the canonical NHEJ, resulted in a significant increase of translocation frequency (Figure 1B). This result is in agreement with previous studies that reported that in rodent and human cells chromosome

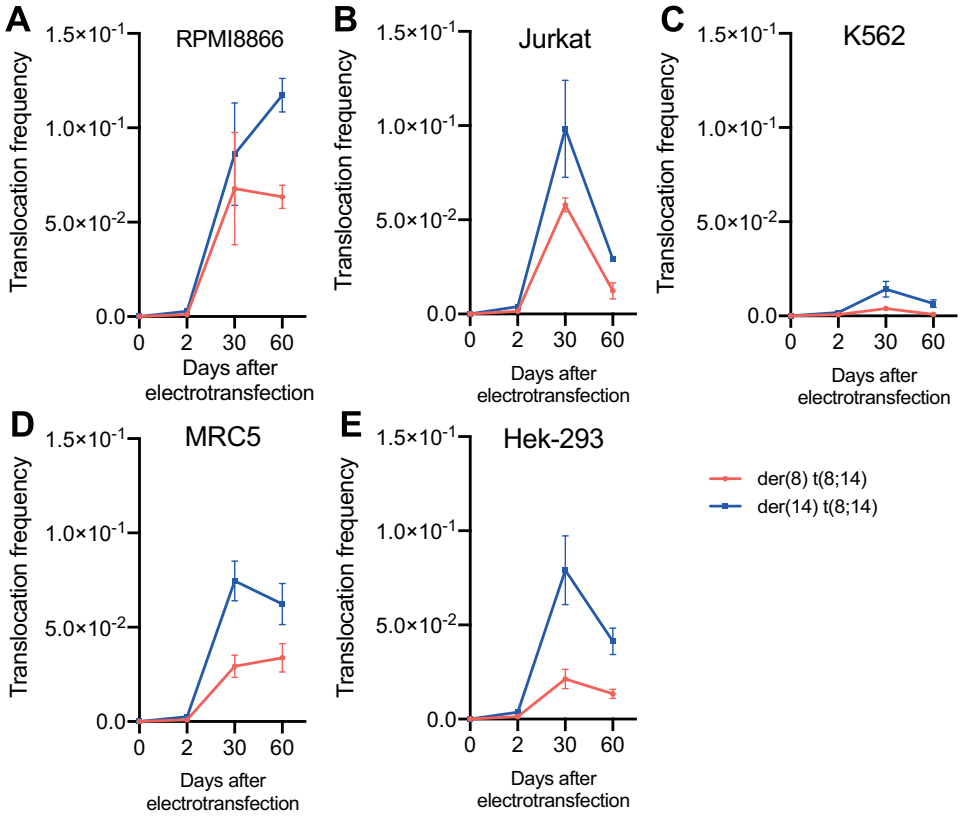

Figure 4. *MYC–IGH* translocation frequency after long-term culture. RPMI8866 (**A**), Jurkat (**B**), K562 (**C**), MRC5 (**D**) and Hek-293 (**E**) cells (24–32 × 10^6) were electrotransfected with gRNA, targeting *MYC, IGH* and *AML*, and Cas9 plasmids. Two days later, the electrotransfected cells were split into two parts. The first part was collected to determine the *MYC–IGH* translocation frequency. The second part was sorted and then cultured for 60 days with regular weekly passage. Cells were collected 30 and 60 days after electrotransfection to determine the *MYC–IGH* translocation frequency. Both of the reciprocal (der8, red line; der14, blue line) *MYC–IGH* translocations are shown. Data represent means ± SEMs of two independent biological experiments and two technical replicates.

translocations are mainly formed by the alternative NHEJ pathway (46,63–67). Nonetheless, a subset of chromosomal translocations may be generated through the canonical NHEJ pathway (68,69). The increased frequency of translocations when canonical NHEJ is abrogated can be explained by the slow kinetics of DNA repair via alternative NHEJ, which is ∼10-fold slower than canonical NHEJ; this permits the free movement of unrepaired DNA ends, increasing the chance to meet their translocation partner in the nuclear space (70). Likewise, we observed that inhibiting DNA-Pk increased *MYC–IGH* colocalization after the DSB (Figure 3H). The accumulation of DSB clustering upon DNA-Pk inhibition was also recently described by Zagelbaum *et al.* (68).

Interestingly, all possible combinations of translocations can be generated in almost any cell type, albeit with different frequencies (Supplementary Figure S4A–J), although the generation of monocentric derivative chromosomes was favored over dicentric and acentric ones (Figure 1C). The mechanism of this preferential formation of unicentric derivative chromosomes early after DNA repair deserves a separate study. It can be noted that *MYC–IGH* translocation frequency was higher compared to the *MYC–AML* translocation frequency in all cell lines (Figure 1D), while the ratio of monocentric versus dicentric and acentric chromosomes was much lower for *MYC–IGH* compared to *MYC–AML* in these cells (Figure 1C). From these data, it seems that pro-oncogenic *MYC* and *IGH* breaks tend to be 'incorrectly' repaired to a greater extent than others, i.e. more often form translocated and dicentric/acentric derivatives. We hypothesize that the DSB in *IGH* loci, located in the subtelomeric region of chromosome 14, produces a relatively small and motile chromosomal fragment of 1 Mb that can migrate larger distances more readily to meet its translocation partner compared to a larger *AML* fragment (12 Mb): both *MYC–IGH* (t8;14) and *ETO–IGH* (t8;14) translocation frequencies are higher than *MYC–AML* (t8;21) and *ETO–AML* (t8;21) translocation frequencies (Figure 1D and Supplementary Figure S1E).

The cell lines that we used were diploid, except for K562 (nearly triploid) and Hek-293 (hypotriploid). Although the cell lines had different numbers of induced DSBs, the resulting translocation frequency profiles were similar among them (Table 1), indicating that the ploidy did not play a significant role in the pattern of chromosomal translocations after simultaneous induction of DSBs.

Once DSBs are formed, shared transcription factories (71), as well as spatial positioning (72), are the potential factors influencing DSB repair and thus they could affect translocation frequency. In our system, however, the frequency of translocations was not affected by the nuclear radial position or transcription activity of the participating gene loci (Figure 2 and Table 1), but rather by their spatial proximity after the DSB induction (Figure 3 and Table 1). This favors the 'breakage-first' hypothesis of translocation formation. An increase in *MYC–IGH* and *ETO–IGH* colocalization frequencies, but not in *MYC–AML* or *ETO–AML* colocalization frequencies, after the respective DSBs (Figure 3A and D) corroborates the higher motility of a shorter chromosomal fragment (*IGH*) proposed above. Different loci, however, may behave differently regarding translocation frequency and colocalization after DSB induction; e.g. colocalizing *AML* and *ETO* loci did not translocate in RPMI8866 cells (Figure 3D and E), while *MYC* and *AML* were not found to colocalize at a detectable rate and yet the translocation was still formed (Figure 3A and B). The mobility of DSBs was previously described (41,61,73), and it may serve either to facilitate the search of a recombination partner (39,74) or to join common DNA repair centers (60,75). DSBs were found to cluster in DNA damage repair foci in yeasts and mammalian cells (60,75,76). However, in mammalian cells DSB clustering was mostly observed for multiple DSBs (67,68,75). An increase in chromatin movement following DSBs can result in chromosomal translocations (46).

Regarding the role of transcription, it is important to acknowledge that while we observe no significant positive correlation between basal transcriptional activity and translocation frequency in between cell line comparisons, this may not concern the changes in gene expression within one cell line and their potential influence on translocation frequency. Whether changes in gene transcriptional activity or distance from DSB to transcription start sites might affect translocation frequencies requires further exploration. Similarly, while our data did not show a significant effect of nuclear radial position on translocation frequency, we acknowledge that this may be influenced by other factors and may vary depending on the specific loci and cell types.

We next tested the persistence of the observed chromosomal translocations upon long-term culture and found that it was different in different cell types (Figure 4A–E and Supplementary Figure S6A–J). Two months after DSB induction, the proportion of cells bearing *MYC–IGH* translocation continued to increase only in RPMI8866 cells (Figure 4A), while the *AML–ETO* translocation was found to persist after long-term culture in MRC5 cells only (Supplementary Figure S6I). These results point out that the generated oncogenic chromosomal translocations confer cell type-dependent survival advantages. The persistence of chromosomal translocations may also depend on whether both derivative chromosomes are present and no genetic material is lost. That is what we supposedly observed in the case of the *MYC–IGH* translocation in RPMI8866 cells, where both derivative chromosomes were present (Figure 4A). A more precise evaluation of potential genetic material loss during such selection requires further investigation. This finding adds to the ongoing discussion on the role of selection in the formation of cancer cells (77) and provides new evidence for the importance of considering the selective survival advantage of chromosomal translocations in different cell types.

We should also mention the limitations of our system, which provides a valid approximation but does not fully recapitulate all aspects of natural carcinogenesis in primary cells. With CRISPR/Cas9, we deliberately create several simultaneous DSBs; however, 'naturally occurring' DSBs can arise spontaneously and not necessarily at the same time, and their origins are diverse, encompassing external factors, e.g. irradiation, and various cellular activities, such as gene transcription, DNA replication and oxidative metabolism (31). Certain chromosomal translocations are caused by DNA-damaging enzymes (RAGs, AID, topoisomerases I and II). These enzymes are sensitive to chromatin organization, transcription and/or DNA sequence. Other chromosomal translocations are induced by random factors that are less strongly dependent on the chromatin context. These include ionizing radiation, oxidative stress, etc. As CRISPR/Cas9 is less sensitive to chromatin structure, it better reproduces the latter situation, although this does not invalidate our conclusions on translocation formation. A potential contributor to the choice of repair pathway, and thus translocation formation, is the cell cycle (78,79), which was not directly addressed in the current study. Further use of our experimental model will allow us to unravel other patterns in the generation of chromosomal translocations. The results on the persistence of the observed chromosomal translocations upon long-term culture might be limited by the fact that we used already proliferating cells; thus, the potential survival or growth rate advantages of chromosomal translocations on different cell types might not be fully estimated.

To conclude, we devised an experimental system to study the factors that drive the formation of chromosomal translocations between four distinct gene loci and five cell types; all the possible combinations of translocations can be generated in almost any cell type, albeit with different frequencies. The frequency of translocations correlates only with the spatial proximity of the partner loci after the DSB induction supporting the 'breakage-first' model for translocation formation. Upon long-term culture, only oncogenic *MYC–IGH* and *AML–ETO* chromosomal translocations conferred cell type-dependent survival advantages.

DATA AVAILABILITY

The data underlying this article are available in the article and in its online supplementary material.

SUPPLEMENTARY DATA

Supplementary Data are available at NAR Cancer Online.

ACKNOWLEDGEMENTS

The authors express their gratitude to Tudor Manoliu and Yann Lecluse, Gustave Roussy Cancer Campus, Plateforme Imagerie et Cytométrie—UMS 23/3655—Université Paris Saclay, Villejuif, France, for their technical help.

Authors' contributions: R.J.C. performed the experiments, analyzed and interpreted data, and wrote the original draft; A.S. and A.K. performed the experiments, analyzed and interpreted data, and wrote the paper (review and editing); N.L., E.T., Y.K. and F.A. performed the experiments; D.G. and Y.V. designed research, analyzed data and wrote the paper (review and editing). All authors read and approved the final manuscript.

FUNDING

Ministry of Science and Higher Education of the Russian Federation [075-15-2020-773]; CHED-PhilFrance Scholarship Programme (to R.J.C.).

Conflict of interest statement. The authors declare that they have no conflict of interest.

REFERENCES

1. Wilch,E.S. and Morton,C.C. (2018) Historical and clinical perspectives on chromosomal translocations. In: Zhang,Y. (ed). *Advances in Experimental Medicine and Biology*. Springer, Singapore, pp. 1–14.
2. Lobato,M.N., Metzler,M., Drynan,L., Forster,A., Pannell,R. and Rabbitts,T.H. (2008) Modeling chromosomal translocations using conditional alleles to recapitulate initiating events in human leukemias. *JNCI Monogr.*, **2008**, 58–63.
3. Mitelman,F., Johansson,B. and Mertens,F. (2021) In: *Mitelman Database of Chromosome Aberrations and Gene Fusions in Cancer*. https://mitelmandatabase.isb-cgc.org.
4. Nakano,K. and Takahashi,S. (2018) Translocation-related sarcomas. *Int. J. Mol. Sci.*, **19**, 3784.
5. Nambiar,M. and Raghavan,S.C. (2011) How does DNA break during chromosomal translocations?*Nucleic Acids Res.*, **39**, 5813–5825.
6. Bohlander,S.K., Kakadiya,P.M. and Coysh,A. (2019) Chromosome rearrangements and translocations. In: Boffetta, P. and Hainaut,P. (eds.) *Encyclopedia of Cancer*, 3rd edn. Academic Press, Oxford, pp. 389–404.
7. Pannunzio,N.R. and Lieber,M.R. (2018) Concept of DNA lesion longevity and chromosomal translocations. *Trends Biochem. Sci.*, **43**, 490–498.
8. Zheng,H. and Xie,W. (2019) The role of 3D genome organization in development and cell differentiation. *Nat. Rev. Mol. Cell Biol.*, **20**, 535–550.
9. Canoy,R.J., Shmakova,A., Karpukhina,A., Shepelev,M., Germini,D. and Vassetzky,Y. (2022) Factors that affect the formation of chromosomal translocations in cells. *Cancers*, **14**, 5110.
10. Lieber,M.R. (2010) The mechanism of double-strand DNA break repair by the nonhomologous DNA end-joining pathway. *Annu. Rev. Biochem.*, **79**, 181–211.
11. Liu,M., Duke,J.L., Richter,D.J., Vinuesa,C.G., Goodnow,C.C., Kleinstein,S.H. and Schatz,D.G. (2008) Two levels of protection for the B cell genome during somatic hypermutation. *Nature*, **451**, 841–845.
12. Shmakova,A. and Vassetzky,Y. (2023) lncRNA: a new danger for genome integrity. *Int. J. Cancer*, **152**, 1288–1289.
13. Demin,D.E., Murashko,M.M., Uvarova,A.N., Stasevich,E.M., Shyrokova,E.Y., Gorlachev,G.E., Zaretsky,A., Korneev,K.V., Ustiugova,A.S., Tkachenko,E.A. *et al.* (2023) Adversary of DNA integrity: a long non-coding RNA stimulates driver oncogenic chromosomal rearrangement in human thyroid cells. *Int. J. Cancer*, **152**, 1452–1462.
14. Shmakova,A.A., Lomov,N., Viushkov,V., Tsfasman,T., Kozhevnikova,Y., Sokolova,D., Pokrovsky,V., Syrkina,M., Germini,D., Rubtsov,M. *et al.* (2023) Cell models with inducible oncogenic translocations allow to evaluate the potential of drugs to favor secondary translocations. *Cancer Commun.*, **43**, 154–158.
15. Kovalchuk,A.L., Ansarah-Sobrinho,C., Hakim,O., Resch,W., Tolarová,H., Dubois,W., Yamane,A., Takizawa,M., Klein,I., Hager,G.L. *et al.* (2012) Mouse model of endemic Burkitt translocations reveals the long-range boundaries of Ig-mediated oncogene deregulation. *Proc. Natl Acad. Sci. U.S.A.*, **109**, 10972–10977.
16. Busch,K., Keller,T., Fuchs,U., Yeh,R.-F., Harbott,J., Klose,I., Wiemels,J., Novosel,A., Reiter,A. and Borkhardt,A. (2007) Identification of two distinct MYC breakpoint clusters and their association with various IGH breakpoint regions in the t(8;14) translocations in sporadic Burkitt-lymphoma. *Leukemia*, **21**, 1739–1751.
17. Brunet,E., Simsek,D., Tomishima,M., DeKelver,R., Choi,V.M., Gregory,P., Urnov,F., Weinstock,D.M. and Jasin,M. (2009) Chromosomal translocations induced at specified loci in human stem cells. *Proc. Natl Acad. Sci. U.S.A.*, **106**, 10620–10625.
18. Germini,D., Tsfasman,T., Klibi,M., El-Amine,R., Pichugin,A., Iarovaia,O.V., Bilhou-Nabera,C., Subra,F., Bou Saada,Y., Sukhanova,A. *et al.* (2017) HIV Tat induces a prolonged MYC relocalization next to IGH in circulating B-cells. *Leukemia*, **31**, 2515–2522.
19. Piganeau,M., Ghezraoui,H., De Cian,A., Guittat,L., Tomishima,M., Perrouault,L., René,O., Katibah,G.E., Zhang,L., Holmes,M.C. *et al.* (2013) Cancer translocations in human cells induced by zinc finger and TALE nucleases. *Genome Res.*, **23**, 1182–1193.
20. Vanoli,F. and Jasin,M. (2017) Generation of chromosomal translocations that lead to conditional fusion protein expression using CRISPR–Cas9 and homology-directed repair. *Methods*, **121–122**, 138–145.
21. Vanoli,F., Tomishima,M., Feng,W., Lamribet,K., Babin,L., Brunet,E. and Jasin,M. (2017) CRISPR–Cas9-guided oncogenic chromosomal translocations with conditional fusion protein expression in human mesenchymal cells. *Proc. Natl Acad. Sci. U.S.A.*, **114**, 3696–3701.
22. Sall,F.B., Shmakova,A., Karpukhina,A., Tsfasman,T., Lomov,N., Canoy,R.J., Boutboul,D., Oksenhendler,E., Toure,A.O., Lipinski,M. *et al.* (2023) Epstein–Barr virus reactivation induces MYC–IGH spatial proximity and t(8;14) in B cells. *J. Med. Virol.*, **95**, e28633.
23. Jain,S., Shukla,S., Yang,C., Zhang,M., Fatma,Z., Lingamaneni,M., Abesteh,S., Lane,S.T., Xiong,X., Wang,Y. *et al.* (2021) TALEN outperforms Cas9 in editing heterochromatin target sites. *Nat. Commun.*, **12**, 606.
24. Mitrentsi,I. and Soutoglou,E. (2021) CRISPR/Cas9-induced breaks in heterochromatin, visualized by immunofluorescence. *Methods Mol. Biol.*, **2153**, 439–445.
25. Schep,R., Brinkman,E.K., Leemans,C., Vergara,X., van der Weide,R.H., Morris,B., van Schaik,T., Manzo,S.G., Peric-Hupkes,D., van den Berg,J. *et al.* (2021) Impact of chromatin context on Cas9-induced DNA double-strand break repair pathway balance. *Mol. Cell*, **81**, 2216–2230.
26. Kallimasioti-Pazi,E.M., Thelakkad Chathoth,K., Taylor,G.C., Meynert,A., Ballinger,T., Kelder,M.J.E., Lalevée,S., Sanli,I., Feil,R. and Wood,A.J. (2018) Heterochromatin delays CRISPR–Cas9 mutagenesis but does not influence the outcome of mutagenic DNA repair. *PLoS Biol.*, **16**, e2005595.
27. Friskes,A., Koob,L., Krenning,L., Severson,T.M., Koeleman,E.S., Vergara,X., Schubert,M., van den Berg,J., Evers,B., Manjón,A.G. *et al.* (2022) Double-strand break toxicity is chromatin context independent. *Nucleic Acids Res.*, **50**, 9930–9947.
28. Concordet,J.-P. and Haeussler,M. (2018) CRISPOR: intuitive guide selection for CRISPR/Cas9 genome editing experiments and screens. *Nucleic Acids Res.*, **46**, W242–W245.
29. Brinkman,E.K., Chen,T., Amendola,M. and Van Steensel,B. (2014) Easy quantitative assessment of genome editing by sequence trace decomposition. *Nucleic Acids Res.*, **42**, e168.
30. Germini,D., Saada,Y.B., Tsfasman,T., Osina,K., Robin,C., Lomov,N., Rubtsov,M., Sjakste,N., Lipinski,M. and Vassetzky,Y. (2017) A one-step PCR-based assay to evaluate the efficiency and precision of genomic DNA-editing tools. *Mol. Ther. Methods Clin. Dev.*, **5**, 43–50.
31. Canoy,R.J., André,F., Shmakova,A., Wiels,J., Lipinski,M., Vassetzky,Y. and Germini,D. (2023) Easy and robust electrotransfection protocol for efficient ectopic gene expression and genome editing in human B cells. *Gene Ther.*, **30**, 167–171.
32. Akbay,B., Germini,D., Bissenbaev,A.K., Musinova,Y.R., Sheval,E.V., Vassetzky,Y. and Dokudovskaya,S. (2021) HIV-1 Tat activates Akt/mTORC1 pathway and AICDA expression by

downregulating its transcriptional inhibitors in B cells. *Int. J. Mol. Sci.*, **22**, 1588.
33. Pfaffl,M.W. (2001) A new mathematical model for relative quantification in real-time RT-PCR. *Nucleic Acids Res.*, **29**, e45.
34. Brunet,E. and Jasin,M. (2018) Induction of chromosomal translocations with CRISPR–Cas9 and other nucleases: understanding the repair mechanisms that give rise to translocations. In: Zhang,Y. (ed.) *Chromosome Translocation, Advances in Experimental Medicine and Biology*. Springer, Singapore, pp. 15–25.
35. Naumann,S., Reutzel,D., Speicher,M. and Decker,H.J. (2001) Complete karyotype characterization of the K562 cell line by combined application of G-banding, multiplex-fluorescence *in situ* hybridization, fluorescence *in situ* hybridization, and comparative genomic hybridization. *Leuk. Res.*, **25**, 313–322.
36. Lin,C.-Y., Shukla,A., Grady,J.P., Fink,J.L., Dray,E. and Duijf,P.H.G. (2018) Translocation breakpoints preferentially occur in euchromatin and acrocentric chromosomes. *Cancers*, **10**, 13.
37. Misteli,T. (2010) Higher-order genome organization in human disease. *Cold Spring Harb. Perspect. Biol.*, **2**, a000794.
38. Osborne,C.S. (2014) Molecular pathways: transcription factories and chromosomal translocations. *Clin. Cancer Res.*, **20**, 296–300.
39. Miné-Hattab,J. and Chiolo,I. (2020) Complex chromatin motions for DNA repair. *Front. Genet.*, **11**, 800.
40. Pannunzio,N.R., Watanabe,G. and Lieber,M.R. (2018) Nonhomologous DNA end-joining for repair of DNA double-strand breaks. *J. Biol. Chem.*, **293**, 10512–10523.
41. Iarovaia,O.V., Rubtsov,M., Ioudinkova,E., Tsfasman,T., Razin,S.V. and Vassetzky,Y.S. (2014) Dynamics of double strand breaks and chromosomal translocations. *Mol. Cancer*, **13**, 249.
42. Mitelman,F., Johansson,B. and Mertens,F. (2007) The impact of translocations and gene fusions on cancer causation. *Nat. Rev. Cancer*, **7**, 233–245.
43. Saleh,K., Michot,J.-M., Camara-Clayette,V., Vassetsky,Y. and Ribrag,V. (2020) Burkitt and Burkitt-like lymphomas: a systematic review. *Curr. Oncol. Rep.*, **22**, 33.
44. Osborne,C.S., Chakalova,L., Mitchell,J.A., Horton,A., Wood,A.L., Bolland,D.J., Corcoran,A.E. and Fraser,P. (2007) Myc dynamically and preferentially relocates to a transcription factory occupied by Igh. *PLoS Biol.*, **5**, e192.
45. Roix,J.J., McQueen,P.G., Munson,P.J., Parada,L.A. and Misteli,T. (2003) Spatial proximity of translocation-prone gene loci in human lymphomas. *Nat. Genet.*, **34**, 287–291.
46. Roukos,V., Voss,T.C., Schmidt,C.K., Lee,S., Wangsa,D. and Misteli,T. (2013) Spatial dynamics of chromosome translocations in living cells. *Science*, **341**, 660–664.
47. Chiarle,R., Zhang,Y., Frock,R.L., Lewis,S.M., Molinie,B., Ho,Y.-J., Myers,D.R., Choi,V.W., Compagno,M., Malkin,D.J. *et al.* (2011) Genome-wide translocation sequencing reveals mechanisms of chromosome breaks and rearrangements in B cells. *Cell*, **147**, 107–119.
48. Klein,I.A., Resch,W., Jankovic,M., Oliveira,T., Yamane,A., Nakahashi,H., Di Virgilio,M., Bothmer,A., Nussenzweig,A., Robbiani,D.F. *et al.* (2011) Translocation-capture sequencing reveals the extent and nature of chromosomal rearrangements in B lymphocytes. *Cell*, **147**, 95–106.
49. Hakim,O., Resch,W., Yamane,A., Klein,I., Kieffer-Kwon,K.-R., Jankovic,M., Oliveira,T., Bothmer,A., Voss,T.C., Ansarah-Sobrinho,C. *et al.* (2012) DNA damage defines sites of recurrent chromosomal translocations in B lymphocytes. *Nature*, **484**, 69–74.
50. Rocha,P.P., Micsinai,M., Kim,J.R., Hewitt,S.L., Souza,P.P., Trimarchi,T., Strino,F., Parisi,F., Kluger,Y. and Skok,J.A. (2012) Close proximity to Igh is a contributing factor to AID-mediated translocations. *Mol. Cell*, **47**, 873–885.
51. Zhang,Y., McCord,R.P., Ho,Y.-J., Lajoie,B.R., Hildebrand,D.G., Simon,A.C., Becker,M.S., Alt,F.W. and Dekker,J. (2012) Spatial organization of the mouse genome and its role in recurrent chromosomal translocations. *Cell*, **148**, 908–921.
52. Aymard,F., Aguirrebengoa,M., Guillou,E., Javierre,B.M., Bugler,B., Arnould,C., Rocher,V., Iacovoni,J.S., Biernacka,A., Skrzypczak,M. *et al.* (2017) Genome-wide mapping of long-range contacts unveils clustering of DNA double-strand breaks at damaged active genes. *Nat. Struct. Mol. Biol.*, **24**, 353–361.
53. Roukos,V. and Misteli,T. (2014) The biogenesis of chromosome translocations. *Nat. Cell Biol.*, **16**, 293–300.
54. Lieber,M.R., Gu,J., Lu,H., Shimazaki,N. and Tsai,A.G. (2010) Nonhomologous DNA end joining (NHEJ) and chromosomal translocations in humans. In: Nasheuer,H.-P. (ed). *Genome Stability and Human Diseases, Subcellular Biochemistry*. Springer Netherlands, Dordrecht, pp. 279–296.
55. Meaburn,K.J., Misteli,T. and Soutoglou,E. (2007) Spatial genome organization in the formation of chromosomal translocations. *Semin. Cancer Biol.*, **17**, 80–90.
56. Nikiforova,M.N., Stringer,J.R., Blough,R., Medvedovic,M., Fagin,J.A. and Nikiforov,Y.E. (2000) Proximity of chromosomal loci that participate in radiation-induced rearrangements in human cells. *Science*, **290**, 138–141.
57. Lukášová,E., Kozubek,S., Kozubek,M., Kjeronská,J., Rýznar,L., Horáková,J., Krahulcová,E. and Horneck,G. (1997) Localisation and distance between ABL and BCR genes in interphase nuclei of bone marrow cells of control donors and patients with chronic myeloid leukaemia. *Hum. Genet.*, **100**, 525–535.
58. Neves,H., Ramos,C., da Silva,M.G., Parreira,A. and Parreira,L. (1999) The nuclear topography of ABL, BCR, PML, and RARα genes: evidence for gene proximity in specific phases of the cell cycle and stages of hematopoietic differentiation. *Blood*, **93**, 1197–1207.
59. Boxer,L.M. and Dang,C.V. (2001) Translocations involving c-myc and c-myc function. *Oncogene*, **20**, 5595–5610.
60. Aten,J.A., Stap,J., Krawczyk,P.M., Oven,C.H., Hoebe,R.A., Essers,J. and Kanaar,R.. (2004) Dynamics of DNA double-strand breaks revealed by clustering of damaged chromosome domains. *Science*, **303**, 92–95.
61. Krawczyk,P.M., Borovski,T., Stap,J., Cijsouw,T., Cate,R., Medema,J.P., Kanaar,R., Franken,N.A.P. and Aten,J.A. (2012) Chromatin mobility is increased at sites of DNA double-strand breaks. *J. Cell Sci.*, **125**, 2127–2133.
62. Brinkman,E.K., Chen,T., de Haas,M., Holland,H.A., Akhtar,W. and van Steensel,B. (2018) Kinetics and fidelity of the repair of Cas9-induced double-strand DNA breaks. *Mol. Cell*, **70**, 801–813.e6.
63. Soni,A., Siemann,M., Pantelias,G.E. and Iliakis,G. (2015) Marked contribution of alternative end-joining to chromosome-translocation-formation by stochastically induced DNA double-strand-breaks in G2-phase human cells. *Mutat. Res. Genet. Toxicol. Environ. Mutagen.*, **793**, 2–8.
64. Zhang,Y. and Jasin,M. (2011) An essential role for CtIP in chromosomal translocation formation through an alternative end-joining pathway. *Nat. Struct. Mol. Biol.*, **18**, 80–84.
65. Boboila,C., Jankovic,M., Yan,C.T., Wang,J.H., Wesemann,D.R., Zhang,T., Fazeli,A., Feldman,L., Nussenzweig,A., Nussenzweig,M. *et al.* (2010) Alternative end-joining catalyzes robust IgH locus deletions and translocations in the combined absence of ligase 4 and Ku70. *Proc. Natl Acad. Sci. U.S.A.*, **107**, 3034–3039.
66. Simsek,D. and Jasin,M. (2010) Alternative end-joining is suppressed by the canonical NHEJ component Xrcc4–ligase IV during chromosomal translocation formation. *Nat. Struct. Mol. Biol.*, **17**, 410–416.
67. Caron,P., Choudjaye,J., Clouaire,T., Bugler,B., Daburon,V., Aguirrebengoa,M., Mangeat,T., Iacovoni,J.S., Álvarez-Quilón,A., Cortés-Ledesma,F. *et al.* (2015) Non-redundant functions of ATM and DNA-PKcs in response to DNA double-strand breaks. *Cell Rep.*, **13**, 1598–1609.
68. Zagelbaum,J., Schooley,A., Zhao,J., Schrank,B.R., Callen,E., Zha,S., Gottesman,M.E., Nussenzweig,A., Rabadan,R., Dekker,J. *et al.* (2023) Multiscale reorganization of the genome following DNA damage facilitates chromosome translocations via nuclear actin polymerization. *Nat. Struct. Mol. Biol.*, **30**, 99–106.
69. Ghezraoui,H., Piganeau,M., Renouf,B., Renaud,J. - B., Sallmyr,A., Ruis,B., Oh,S., Tomkinson,A.E., Hendrickson,E.A., Giovannangeli,C. *et al.* (2014) Chromosomal translocations in human cells are generated by canonical nonhomologous end-joining. *Mol. Cell*, **55**, 829–842.
70. Lieber,M.R. (2010) NHEJ and its backup pathways: relation to chromosomal translocations. *Nat. Struct. Mol. Biol.*, **17**, 393–395.
71. Osborne,C.S., Chakalova,L., Brown,K.E., Carter,D., Horton,A., Debrand,E., Goyenechea,B., Mitchell,J.A., Lopes,S., Reik,W. *et al.* (2004) Active genes dynamically colocalize to shared sites of ongoing transcription. *Nat. Genet.*, **36**, 1065–1071.

72. Tsouroula,K., Furst,A., Rogier,M., Heyer,V., Maglott-Roth,A., Ferrand,A., Reina-San-Martin,B. and Soutoglou,E. (2016) Temporal and spatial uncoupling of DNA double strand break repair pathways within mammalian heterochromatin. *Mol. Cell*, **63**, 293–305.
73. Kruhlak,M.J., Celeste,A., Dellaire,G., Fernandez-Capetillo,O., Müller,W.G., McNally,J.G., Bazett-Jones,D.P. and Nussenzweig,A. (2006) Changes in chromatin structure and mobility in living cells at sites of DNA double-strand breaks. *J. Cell Biol.*, **172**, 823–834.
74. Miné-Hattab,J. and Rothstein,R. (2012) Increased chromosome mobility facilitates homology search during recombination. *Nat. Cell Biol.*, **14**, 510–517.
75. Neumaier,T., Swenson,J., Pham,C., Polyzos,A., Lo,A.T., Yang,P., Dyball,J., Asaithamby,A., Chen,D.J., Bissell,M.J. *et al.* (2012) Evidence for formation of DNA repair centers and dose-response nonlinearity in human cells. *Proc. Natl Acad. Sci. U.S.A.*, **109**, 443–448.
76. Lisby,M., Rothstein,R. and Mortensen,U.H. (2001) Rad52 forms DNA repair and recombination centers during S phase. *Proc. Natl Acad. Sci. U.S.A.*, **98**, 8276–8282.
77. Vendramin,R., Litchfield,K. and Swanton,C. (2021) Cancer evolution: Darwin and beyond. *EMBO J.*, **40**, e108389.
78. Jasin,M. and Rothstein,R. (2013) Repair of strand breaks by homologous recombination. *Cold Spring Harb. Perspect. Biol.*, **5**, a012740.
79. Kakarougkas,A. and Jeggo,P.A. (2014) DNA DSB repair pathway choice: an orchestrated handover mechanism. *Br. J. Radiol.*, **87**, 20130685.

© The Author(s) 2023. Published by Oxford University Press on behalf of NAR Cancer.
This is an Open Access article distributed under the terms of the Creative Commons Attribution-NonCommercial License (http://creativecommons.org/licenses/by-nc/4.0/), which permits non-commercial re-use, distribution, and reproduction in any medium, provided the original work is properly cited. For commercial re-use, please contact journals.permissions@oup.com

Supplementary Information for

Specificity of cancer-related chromosomal translocations is linked to proximity after the DNA double-strand break and subsequent selection

Reynand Jay Canoy[1,2 †], Anna Shmakova[1,3 †], Anna Karpukhina[1,4], Nikolai Lomov[5], Eugenia Tiukacheva[1], Yana Kozhevnikova[1], Franck André[1], Diego Germini[1*] and Yegor Vassetzky[1,4*]

[1]UMR 9018, CNRS, Univ. Paris-Sud, Université Paris Saclay, Institut Gustave Roussy, F-94805 Villejuif, France
[2]Institute of Human Genetics, National Institutes of Health, University of the Philippines Manila, 1000 Manila, Philippines
[3]Laboratory of Molecular Endocrinology, Institute of Experimental Cardiology, Federal State Budgetary Organization National Cardiology Research Center Ministry of Health of the Russian Federation, Moscow, Russia
[4]Koltzov Institute of Developmental Biology, 117334 Moscow, Russia
[5]Lomonosov Moscow State University, Moscow, Russia

[†]Joint Authors

*Corresponding authors:
Diego Germini germinidiego@gmail.com
Yegor Vassetzky yegor.vassetzky@cnrs.fr

Table of contents:

Supplementary text
Figures S1 to S7
Tables S1 to S4
SI References

Supplementary Information

Cell culture

RPMI8866, Jurkat, K562 and MRC5 cells were grown in RPMI Medium 1640 base medium supplemented with 10% fetal bovine serum, 100 U/mL penicillin, 100 µg/mL streptomycin and 1.25 mg plasmocin. On the other hand, Hek-293 cells were cultivated in a similar medium composition except for the base medium which was DMEM. For RPMI8866, the medium was further supplemented with components to have a final composition of 2 mM L-Glutamine, 1 mM sodium pyruvate and 20 mM glucose. For Jurkat cells, the medium was further supplemented with components to have a final composition of 1 mM sodium pyruvate, 4.5 g/L glucose and 2.4 g/L HEPES. For K562 cells, the medium was further supplemented with components to have a final composition of 10 mM sodium pyruvate and 2 mM L-Glutamine. All cell culture components were from ThermoFisher Scientific except for Plasmocin which was from Invivogen. The list of inhibitors used for cell treatment and their concentrations is presented in **Supplementary Table 1.**

gRNA design, cloning and testing

Several gRNAs were designed to target specific regions in *AML*, *ETO*, *MYC* and *IGH* gene using the online gRNA design tool (http://crispor.tefor.net/) (1). In the selection tool, the hg38 build of the human genome was used to identify potential gRNA binding sites with NGG as the Protospacer Adjacent Motif (PAM). As a result, the following gRNA sequences were generated from the online gRNA design tool (**Supplementary Table 2**).

The designed gRNAs were all cloned into the phU6-gRNA plasmid backbone (Addgene plasmid #53188) (2) by restriction digest and ligation at the BbSI restriction site. The digestion produces an overhang at the restriction site and so CACC and AAAC nucleotides had to be added to the gRNA sequence and to its reverse complement, respectively, before oligos were synthesized. The resulting plasmids were transformed into DH5α cells for clonal expansion. The transformed DH5α cells were then subsequently extracted of plasmids using either NucleoSpin Plasmid Mini Kit (Machery-Nagel, 740588.250), NucleoBond Xtra Midi kit (Machery-Nagel, 740410.50) or NucleoBond Xtra Maxi kit (Machery-Nagel, 740414.10) following manufacturer's instructions.

The gRNA plasmids were tested if they could generate chromosomal translocation using the ENIT protocol (3). Briefly, each gRNA was paired with a TALEN endonuclease (targeting either *MYC* in chromosome 8 or *IGH* in chromosome 14). The gRNA, Cas9 and TALEN plasmids were then transfected on HeLa cells using Viafect™ Transfection Reagent (Promega, E4982) and the transfected cells were collected after two days for DNA extraction. An endpoint PCR was performed on the extracted DNA using translocation-specific primers (**Supplementary Table 3**), testing all possible translocations (**Supplementary Table 4**). A positive PCR amplicon with the expected size on the agarose gel would signify that the gRNA was effective in inducing DSBs. In addition, the gRNA plasmids were also tested for their efficiency using the TIDE protocol (4). Briefly, the 300-700 bp region surrounding the gRNA binding site was amplified using an end-point PCR. After PCR product purification, the purified products were sent for Sanger sequencing at Eurofins Genomics in Cologne, Germany. The obtained *ab1* files from the sequencing results were analyzed against an untransfected control using the TIDE online analysis platform (http://shinyapps.datacurators.nl/tide/) (4). The analysis estimates the spectrum and frequency of small indels generated by CRISPR/Cas9 where an overall efficiency is calculated to estimate the efficiency of the gRNA in inducing DSBs. gRNA efficiency values were normalized to the average percentage of transfected cells. gRNAs with similar efficiencies were chosen to avoid bias of different CRISPR/Cas9 cutting efficiencies (**Fig. S2A**). Out of three gRNAs tested for *MYC* locus, two were discarded as they did not show the same efficiency as the other ones.

Electrotransfection

The cells were transfected with plasmids encoding for gRNA and Cas9 (Addgene plasmid #57818) using the Cliniporator™ (Igea) following the electrotransfection protocol in (5). Briefly, 4-8 x 10^6 cells with electrotransfected with 50 µg total plasmid, 60% of which is Cas9 and the remaining 40% are gRNA plasmids. Of the total volume of electrotransfection mixture, 10% or 50% was composed of the Spinners Modification of Minimum Essential Medium Eagle (Sigma, M8167-500ML) and the rest were the plasmids dissolved in nuclease-free water. Either 1 mm or 4 mm electroporation cuvettes (Cell Projects, EP201 and EP202) were used. Two days after, the electrotransfection efficiency was checked using the Accuri™ C6 Flow Cytometer (BD Biosciences). Depending on the intended number of electrotransfected cells, the electrotransfection reactions were scaled up by increasing the number of electroporation reactions.

DNA and RNA extraction

The DNA and RNA were extracted from cells using NucleoSpin Tissue Mini Kit for DNA from cells and tissues (Machery-Nagel, 740952.250) and NucleoSpin RNA Mini Kit for RNA Purification (Machery-Nagel, 740955.50), respectively, following manufacturer's instructions. The extracted DNA and RNA were quantified using the NanoDrop™ 2000c (Thermo Fisher Scientific) spectrophotometer.

PCR, qPCR and cDNA synthesis reactions and conditions

All PCR and qPCR reactions were prepared using PowerUp™ SYBR™ Green Master Mix (Applied Biosystems, A25778) with a composition for a 1x reaction (12.5 µL) of: 6.25 µL of PCR mastermix, 0.5 µL of 10 µM forward primer, 0.5 µL of 10 µM reverse primer and 5.25 µL DNA/cDNA in nuclease-free water. For RNA samples, the extracted RNA was converted to complementary DNA (cDNA) using the Maxima H Minus First Strand cDNA Synthesis Kit (Thermo Fisher Scientific, K1651) following the manufacturer's instructions.
The regular PCR reactions were performed using the GeneAmp PCR System 9700 (Applied Biosystems). Meanwhile, the qPCR reactions were performed using the StepOnePlus Real-Time PCR System (Applied Biosystems).

The PCR and qPCR conditions were set with initial activation at 50°C for 2 minutes and at 95°C for two minutes; followed by 40 cycles of denaturation at 95°C for 15 seconds, annealing at 60°C for 60 seconds and extension at 72°C for 60-90 seconds; then with final extension at 72°C for 10 minutes; and were then kept at 4°C until needed for downstream procedures. For qPCR reactions, measurements were taken during the extension phase. If needed, melt-curve analysis was performed after the final extension following the settings available in the qPCR machine. The primers for PCR and qPCR reactions are listed in **Supplementary Table 3**.

Translocation frequency was calculated using the Pfaffl Method (6) with *GAPDH* as a reference gene to correct for the observed varying amplification efficiencies of each primer pair (**Fig. S2D**). The analysis of primer efficiency was performed by plotting the cycle threshold value (Ct) against the serial 1:10 dilution of the DNA sample using the equation $E = 10^{-\frac{1}{the\ slope\ value}}$. The translocation frequency was calculated as follows: $N\ of\ translocations\ per\ 1\ cell\ (translocation\ frequency) = = N\ of\ reference\ genes\ per\ 1\ cell * \frac{E_{reference}\hat{}(Ct\ reference)}{E_{translocation}\hat{}(Ct\ translocation)})$. N of reference genes per 1 cell was assumed to be 2 for diploid cells and 3 for triploid cells. The calculated frequencies were then adjusted to the respective transfection efficiencies measured two days after electrotransfection, right before cell collection, using the Accuri™ C6 Flow Cytometer (BD Biosciences).

Protein extraction and Western blotting

The proteins were extracted from cells washed with 1x PBS. The washed cells were resuspended in NETN buffer (150 mM NaCl, 1 mM EDTA, 50 mM Tris-HCl, pH 7.5 and 0.5% Nonidet P-40) with protease inhibitors (Roche, 04693159001) and phosphatase inhibitors (Roche, 04906837001) for 30 minutes on ice. The cell lysates were then sonicated at 30% amplitude for 15 seconds. The sonicated cell lysates were then centrifuged at 16000 g in 4°C for 30 minutes. After centrifugation, the supernatant was decanted as the protein sample. The extracted proteins were then quantified using the BCA Protein Assay Kit (Thermo Fisher Scientific, 23227) according to the manufacturer's protocol. After quantification, the protein samples were denatured and normalized to 50 µg per 20 µL total volume (1 µL DTT, 5 µL LDS and 14 µL protein sample in NETN buffer) at 90°C for 10 minutes.

The denatured protein samples (20 µg) were run on 4–12% Bis-Tris gel (Thermo Fisher Scientific, NP0323) in MOPS-SDS buffer (Thermo Fisher Scientific, NP0001) at 80 V for 30 minutes and at 120 V for 60 minutes. The separated proteins were then transferred into a PVDF membrane (Millipore, IPVH00010) at 90 V at 4°C for 2 hours. The membrane with the transferred proteins was then blocked with 5% milk at room temperature for one hour. Depending on the size of the target protein, the blocked membrane was cut and incubated with the respective primary antibody (resuspended in 5% BSA) at 4°C overnight. After overnight incubation, the membranes were then rinsed with a wash buffer (0.05 M Tris, 0.15 M NaCl, pH 7.6) containing 0.1% Tween 20. The washed membranes were then incubated in the corresponding secondary antibody which was either anti-mouse or anti-rabbit secondary peroxidase-conjugated antibodies at room temperature for two hours. After incubation, the membranes were rinsed three times with the wash buffer and then target proteins were then revealed using the SuperSignal West Pico chemiluminescent substrate(Thermo Fisher Scientific. 34580) for 1-5 minutes. Then the proteins on the membrane were visualized using the ImageQuant LAS 4000 Mini system (GE Healthcare).

The following are the antibodies that were used: anti-Cas9 Antibody (7A9-3A3) (mouse, Santa Cruz Biotechnology, sc-517386), anti-GAPDH (rabbit, Cell Signaling Technology, 2118), anti-β-actin (mouse, Santa Cruz Biotechnology, sc-81178), anti-mouse peroxidase-conjugated secondary antibodies (Jackson ImmunoResearch, 315035003).

3D-FISH

The cells (1-2 x 10^5) were collected and resuspended in 50 µL RPMI Medium 1640 (Gibco, 21875-034) on a coverslip with poly-lysine and incubated in 37°C for 15-30 minutes. After incubation, the slips were washed with 1X PBS and then fixed with 4% PFA (Electron Microscopy Sciences, 15710) at room temperature for 10 minutes. Then the slips were washed with 1X PBS three times. After washing, the slips were treated with 2% Triton X-100 (Sigma, T8532-500mL) in 1X PBS for 10 minutes. After that, the slips were soaked in 20% glycerol (Euromedex, EU35500) in 1X PBS at room temperature for one hour or at 4°C overnight.

After soaking in glycerol, the slips were flash-frozen in liquid nitrogen for 3-5 seconds three times. For each time, the slips were soaked in 20% glycerol before flash freezing. After this, the slips were washed in 1X PBS three times and soaked in 0.1 M HCl (Sigma-Aldrich, 30721-2.5L-GL) at room temperature for one hour. Then the slips were washed in 2X SSC (Euromedex, EU0300-C) two times and then treated with 200 µg/mL RNase (Thermo Scientific, EN0531)) in 2X SSC in a humidified chamber at 37°C for one hour. After this, the slips were washed with 2X SSC three times. Then the slips were soaked in 50% formamide (Sigma, F9037-500mL) in 2X SSC at room temperature for at least two hours or at 4°C overnight.

After soaking in formamide, 50 µL 70% formamide was added to each slide while preparing the hybridization mix. Then two slides were put together to form a “sandwich” with the hybridization mix as its “filling”. The sandwich slides were then incubated in a humidified chamber at 37°C for 48-72 hours.

After hybridization, the slips were washed with 50% formamide at 37°C, 2x SSC twice and then with 1X PBS three times (each wash was for 5 minutes). Then the slips were mounted on a microscope slide with a mounting medium containing To-pro-3 (Life Technologies, T3605). The slides were scanned using the Microscope Multiphoton SP8 Confocal (Leica). The images were then analyzed using the Bitplane Imaris Analysis Software (Oxford Instruments).

The following are the probes that were used: AML (Empire Genomics, RP11-1056O16 blue), ETO (Empire Genomics, RP11-643O11 orange), MYC (Empire Genomics, RP11-440N18 red), and IGH (Empire Genomics, RP11-346I20 green).

Image acquisition and analysis

The Multiphoton SP8 confocal microscope (Leica Microsystems, Berlin, Germany) with a 63X oil immersion objective was used for image acquisition. Z-stacks were acquired using a frame size of 1024 × 1024, and 0.5 µm z-steps, with sequential multitrack scanning using the 405, 488, 543, 633 nm laser wavelengths. The image analysis (nuclear radial position and colocalization) was done following the protocol in (7). Briefly, the colocalization rate corresponded to the percentage of cells where the center of one locus was located 1 μm or less from the center of another locus. The cutoff distance of 1 μm between signal centers was chosen based on the average diameter of the signals representing each gene locus (1 μm), considering that when the signals touched or came into close proximity, they were within a 1 μm physical distance. On the other hand, the radial position was determined as a percent distribution of the loci position in any of the 10 concentric nuclear equal volumes, from the periphery to the center.

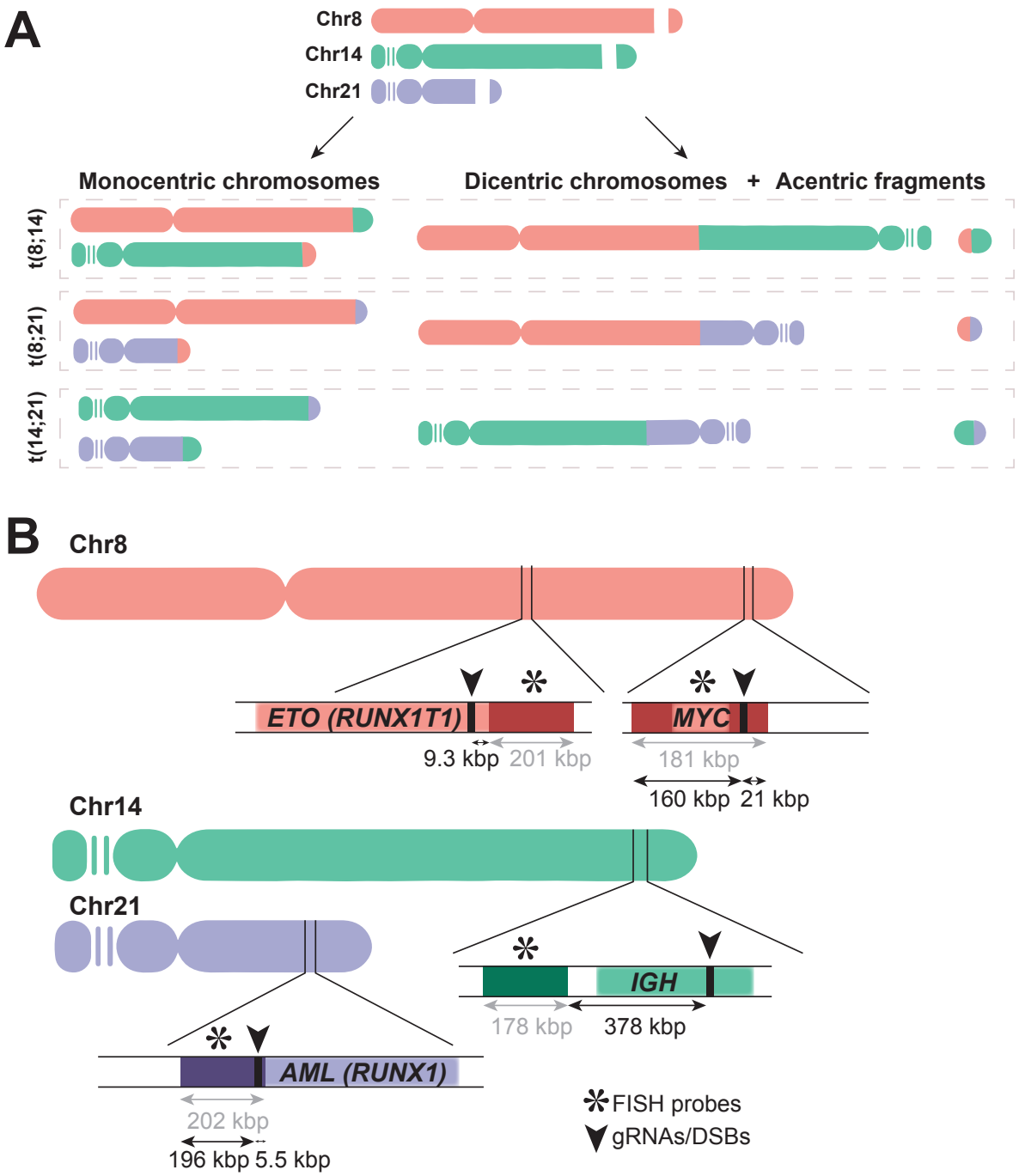

Fig. S1. Possible chromosomal translocations after induction of DSBs and FISH probe positions relative to DSBs. (A) Reciprocal translocation after induction of DSBs in heterologous chromosomes can result in the formation of monocentric derivative chromosomes (lower part, left), if the chromosomes exchange their smaller broken parts. Likewise, the bigger parts of the broken chromosomes can join together, forming a dicentric derivative chromosome with two centromeres, and small broken parts join together forming an acentric derivative chromosome without a centromere (lower part, right). In this figure, all possible chromosomal translocations after precise double-strand break (DSB) induction in chromosomes 8, 14 and 21 are shown. (B) The positions of Fluorescence In Situ Hybridization (FISH) probes (asterisks and shaded rectangles) relative to guide RNAs (gRNAs) target sites where DSBs were induced (arrowheads and black traits). The sizes of FISH probes for each locus are shown in gray; the distance to gRNAs/DSBs is shown in black. If a gRNA site was situated within a FISH probe, the distances to each end of the FISH probe are shown.

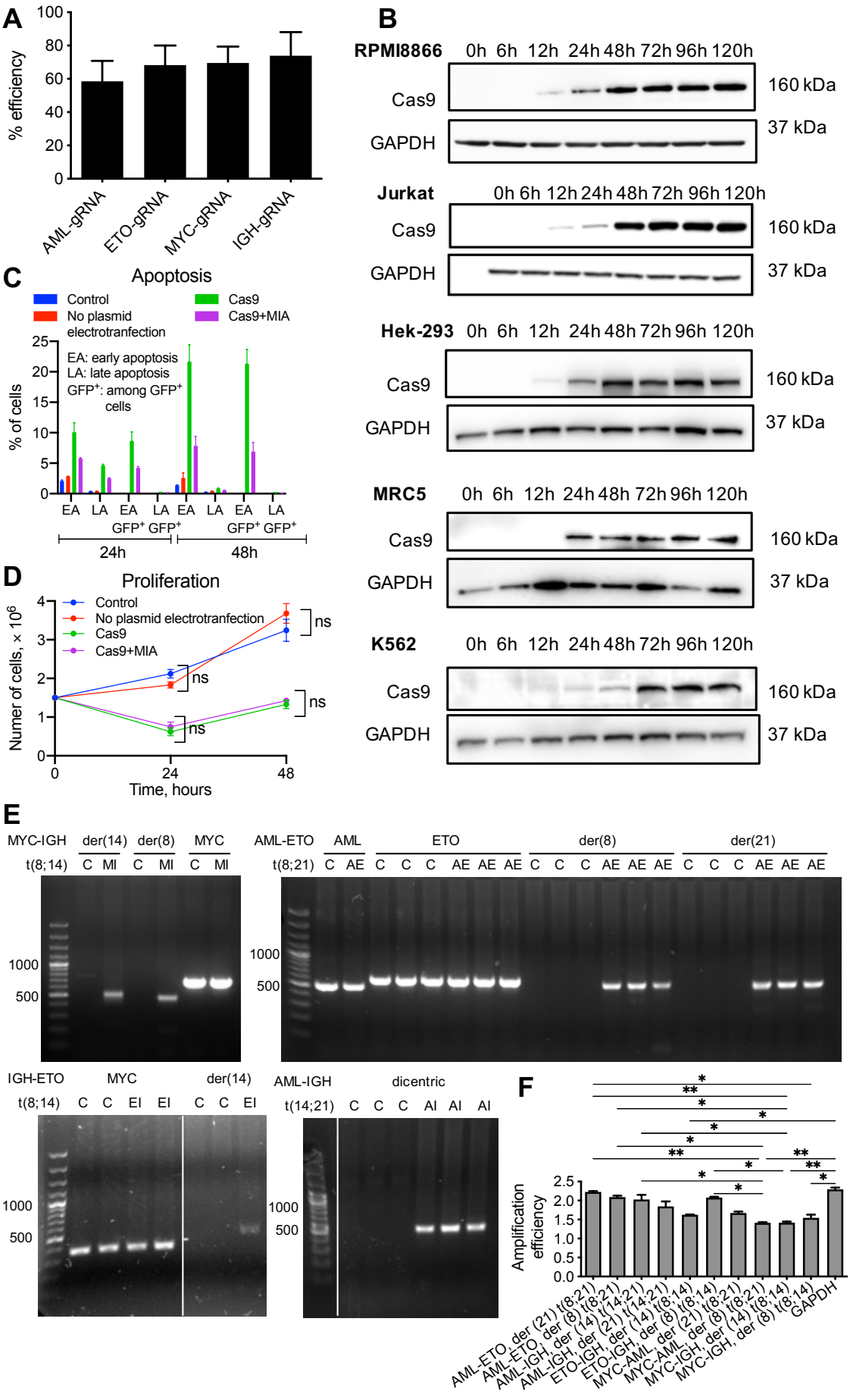
A
% efficiency
AML-gRNA
ETO-gRNA
MYC-gRNA
IGH-gRNA
B
RPMI8866
Jurkat
Hek-293
MRC5
K562
0h 6h 12h 24h 48h 72h 96h 120h
Cas9
GAPDH
160 kDa
37 kDa
C
Apoptosis
Control
No plasmid electrotranfection
Cas9
Cas9+MIA
EA: early apoptosis
LA: late apoptosis
GFP+: among GFP+ cells
% of cells
24h
48h
D
Proliferation
Numer of cells, x 10^6
Time, hours
ns
E
MYC-IGH
AML-ETO
IGH-ETO
AML-IGH
F
Amplification efficiency
GAPDH

Fig. S2. Experimental strategy to induce simultaneous DSBs and detect the resulting chromosomal translocations. (**A**) The efficiency of the designed gRNAs to induce DSBs in RPMI8866 cells was evaluated by TIDE. 48h after electrotransfection with the gRNA and Cas9 plasmids, DNA was extracted from cells and 300-700 bp sequence regions surrounding the gRNA sites were amplified. The obtained sequences were compared to those from the control cells. gRNA efficiency was normalized to transfection efficiency. No significant (ns) difference in cutting efficiency was found among the four gRNAs using the one-way ANOVA test ($p>0.05$), the number of replicates n = 3-16. (**B**) Representative western blot of Cas9 protein expression at indicated time points after electrotransfection of RPMI8866, Jurkat, Hek-293, MRC5, K562 with the Cas9-expressing plasmid. GAPDH was used as the loading control. (**C**) Percentage of K562 cells undergoing apoptosis and (**D**) proliferation of K562 cells 24 and 48 hours after electrotransfection. The number of biological replicates n = 4. (**E**) Detection of CRISPR/Cas9-induced translocations by PCR. Representative agarose gel electrophoresis of the PCR amplicons obtained from the PCR primers specific for either *MYC-IGH*; *AML-ETO, IGH-ETO* or *AML-IGH* translocations. RPMI8866 cells were electrotransfected with plasmids coding for Cas9 and gRNA targeting the *MYC*, *IGH, AML* or *ETO* loci and collected 48h later for DNA extraction and PCR amplification. C - untransfected control; MI - transfection with gRNA targeting the *MYC* and *IGH*; AE - transfection with gRNA targeting the *AML* and *ETO; EI* - transfection with gRNA targeting the *ETO* and *IGH*; *AI* - transfection with gRNA targeting the *AML* and *IGH*. The white lines indicate where the lanes were cut from the same immunoblot image and pieced together to allow for a direct comparison. (**F**) Amplification efficiencies of all the PCR primers used in this study. Cells were electrotransfected with gRNA and Cas9 plasmids and collected 48h later for DNA extraction. Amplification efficiencies were determined by performing qPCR reactions on the extracted DNA samples in four 10-fold dilutions. The average Ct values from each of the four template concentrations were plotted against the log sample quantity to calculate the line slope. The amplification efficiency was calculated using the formula $E = 10^{-1/slope}$. The calculated amplification efficiencies were found to be significantly different from each other (p=0.0003). To take into account the primer efficiency, the translocation frequency was computed with respect to the actual amplification efficiencies of the target and reference PCR primer pairs (6). One-way analysis of variance (ANOVA) with Tukey's post-hoc test was performed, and the statistical significance is shown: $P \leq 0.05$ (*), $P \leq 0.01$ (**), the number of replicates n = 2-4.

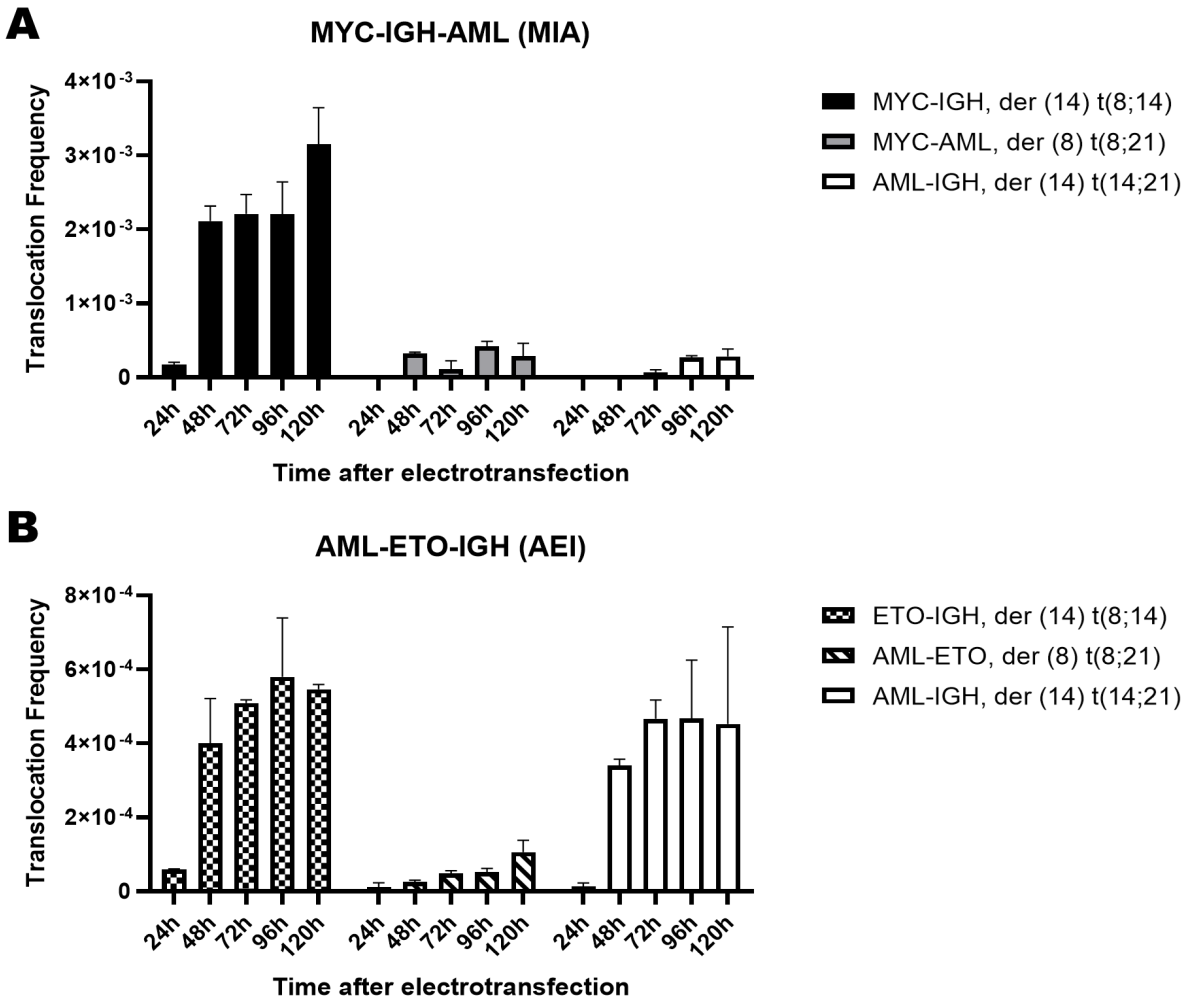

Fig. S3. Translocation frequency at different time points. RPMI8866 (40 x 10^6 cells) were electrotransfected with Cas9 and gRNA plasmids targeting *MYC-IGH-AML* (MIA) **(A)** or *AML-ETO-IGH* **(B)**. Electrotransfected cells were collected at different time points for DNA extraction and then the translocations were detected using qPCR. Only the unicentric derivative chromosomes with the highest frequency compared to their reciprocal counterparts are shown in the graphs. Mean±SEM of at least two biological and two technical replicates are shown.

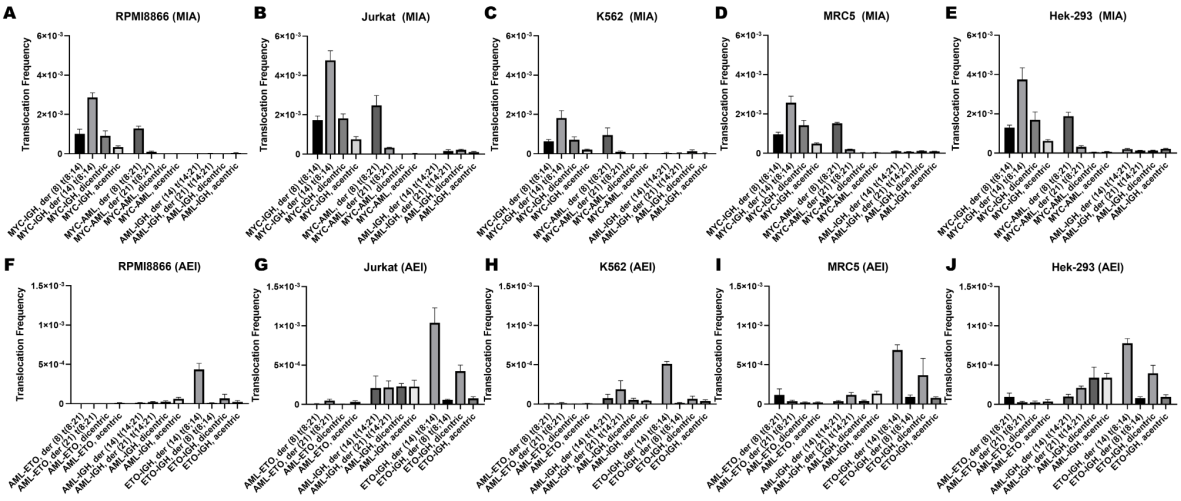

Fig. S4. Chromosomal translocations formed after simultaneous induction of three DSBs. RPMI8866 (**A** and **F**), Jurkat (**B** and **G**), K562 (**C** and **H**), MRC5 (**D** and **I**) and Hek-293 (**E** and **J**) cells (4-8x10^6) were electrotransfected with Cas9- and gRNA-encoding plasmids that target *MYC, IGH* and *AML* (MIA) (**A-F**) or *AML, ETO* and *IGH* (AEI) (**F-J**). Two days later, the transfection efficiency was determined using a flow cytometer. After that, the cells were collected for DNA extraction and the translocation frequencies were determined using qPCR with translocation-specific primers. The calculated translocation frequencies were then adjusted according to their respective transfection efficiencies. Means±standard errors of the mean (SEM) of at least two biological and two technical replicates are shown.

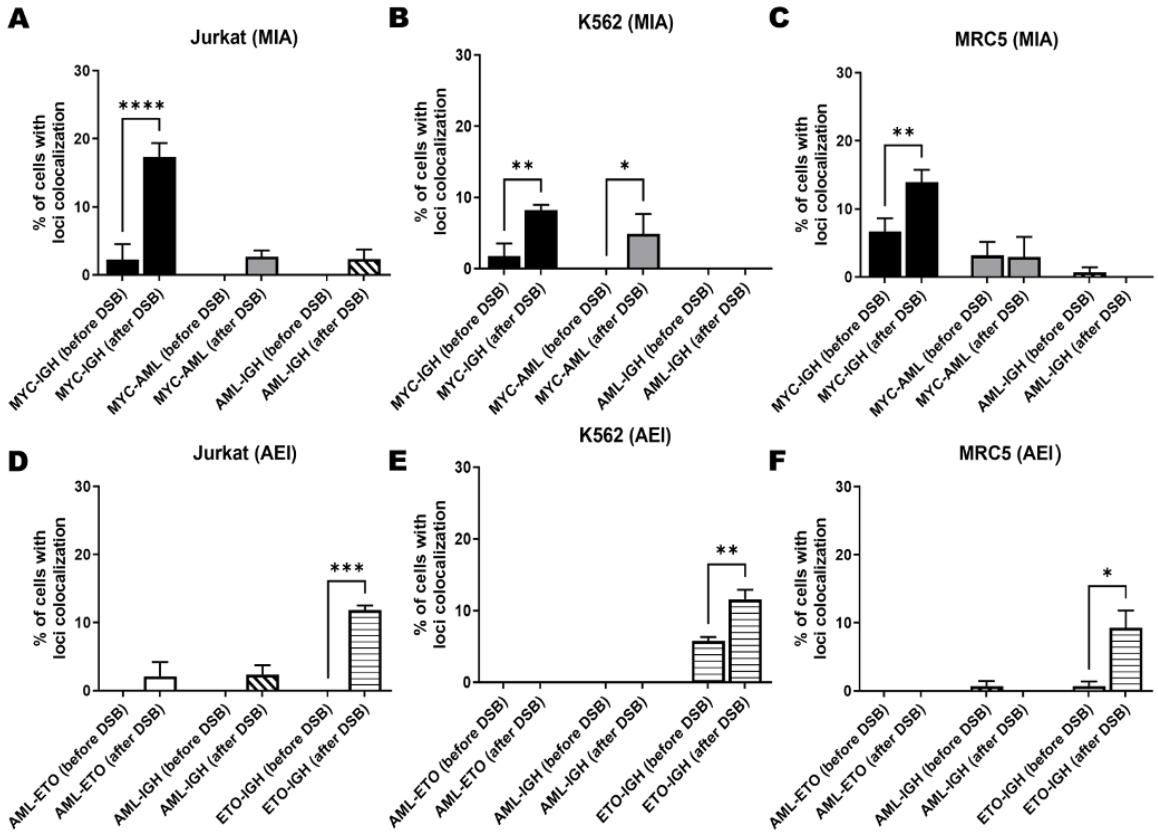

Fig. S5. Spatial proximity between gene loci before and after DSB induction in Jurkat, K562 and MRC5. Spatial proximity between gene loci before and after DSB induction of *MYC*, *IGH* and *AML* (MIA) (**A-C**) and of *AML*, *ETO* and *IGH* (AEI) (**D-F**) in Jurkat (**A, D**), K562 (**B, E**) and MRC5 (**C, F**) cells. Non-electrotransfected cells (1-2 x 10^5) (before DSB) and sorted cells (after DSB) (1-2 x 10^5) that were electrotransfected with gRNAs and Cas9 plasmids two days prior, were collected and processed for 3D-FISH. The slides were scanned using a confocal microscope and 3D-FISH images were analyzed in Bitplane Imaris software. The percentage of cells with the target gene loci pair located at a distance of 1 µm or less (colocalized) was calculated. At least two biological and at least two technical replicates were analyzed. For all plotted values of each graph, a one-way analysis of variance (ANOVA) was performed. For each comparison, the statistical significance is shown: $P \leq 0.05$ (*), $P \leq 0.01$ (**), $P \leq 0.001$ (***), and $P \leq 0.0001$ (****).

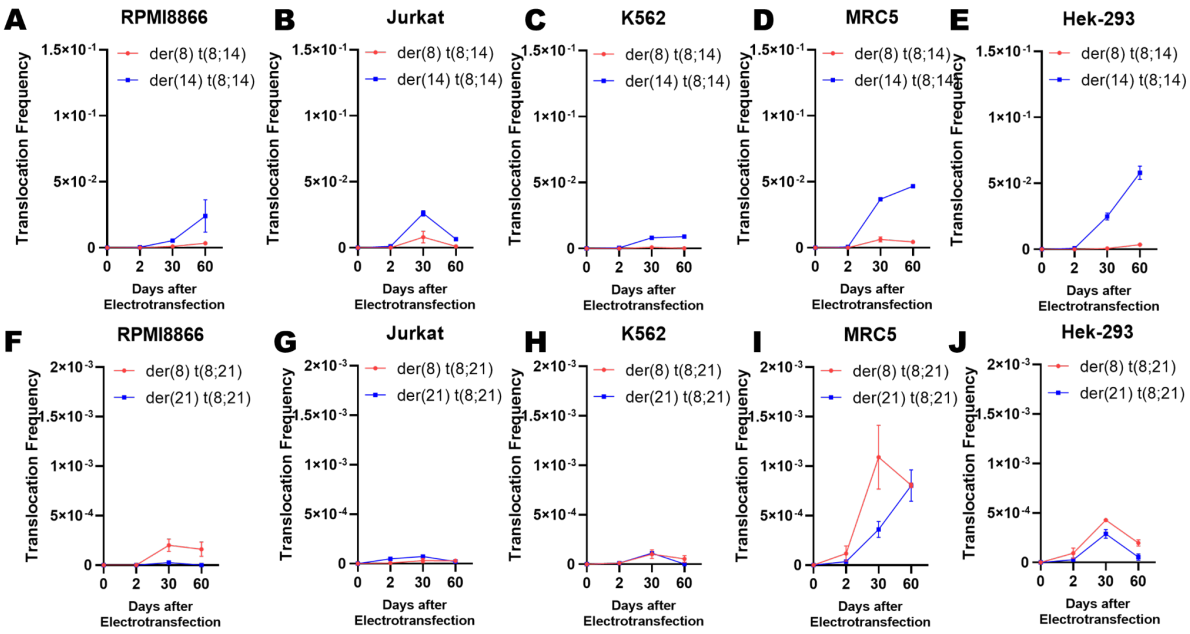

Fig. S6. *ETO-IGH* and *AML-ETO* translocation frequencies after long term culture of electrotransfected cells. RPMI8866 (**A, F**), Jurkat (**B, G**), K562 (**C, H**), MRC5 (**D, I**) and Hek-293 (**E, J**) (24-32 x 10^6 cells) were electrotransfected with Cas9 and gRNA plasmids, targeting *MYC-IGH-AML* (MIA) or *AML-ETO-IGH* (AEI). Two days later, the electrotransfected cells were splitted into two parts. The first part was collected to determine the *ETO-IGH* (**A-E**) and *AML-ETO* (**F-J**) translocation frequencies. The second part was sorted and then cultured for 60 days with regular weekly passage. Cells were collected after 30 and 60 days from electrotransfection to determine the *ETO-IGH* and *AML-ETO* translocation frequencies. Both of the reciprocal translocations are shown. Data represent mean±SEM of two independent biological experiments and two technical replicates.

Supplementary Table 1. Cell treatments.

Inhibitor	Company	Mechanism of action	Working concentration
Mirin	Calbiochem	MRE11 inhibitor	25 μM
NU7026	Sigma Aldrich	DNA-PK inhibitor	20 μM
L67	Sigma Aldrich	DNA ligase I and III inhibitor	25 μM
KU-55933	Sigma Aldrich	ATM inhibitor	10 μM

Supplementary Table 2. Designed gRNAs. + indicates that the gRNA is downstream of the transcription start site; - indicates that the gRNA is upstream of the transcription start site. kbp, kilobase pairs.

Target gene	gRNA binding site (5' to 3')	Distance to transcription start site
AML	GACTCCCCCATGTACCCCTA	+214 kbp
ETO	GATGTAAGAGGAAGCAGCTT	-10 kbp
MYC	TATCCCTTAAAGCGCTGACG	+8.6 kbp
IGH	GAGAACATACCAAGCCCCAC	-4.8 kbp to IGHM +2.1 kbp to IGHJ6

Supplementary Table 3. Primers used for PCR amplification

Target	Sequence (5’ to 3’)	Purpose
AML-F1	CTTCCTGGTGACGGTTGTTT	Translocation PCR (qPCR)
AML-R1	GAACGGCTGTTCCTTACTGC	
ETO-F1	CTTGGGTGGAAGCTGGTAAA	
ETO-R1	AGCCCATTAATGCTATCAGACC	
MYC-n-F1	CCAAACTGGTTGGAGACGAC	
MYC-n-R1	GACTTGGGGACAGCCATTTA	
IGH-out-F3	GCTGCTGCATTTGCTTCTCT	

IGH-out-R3	TTGCTCTAGAAGTGGCAGCA	
GAPDH-DNA-F	GCTGGCACCACTACTTCAGAG	
GAPDH-DNA-R	GCCAACAGCAGATAGCCTAGG	
AML-gex-F1	CTGCTCCGTGCTGCCTAC	Gene expression profile (qRT-PCR)
AML-gex-R1	AGCCATCACAGTGACCAGAGT	
ETO-gex-F1	ACGAACAGCTGCTTCTGGAT	
ETO-gex-R1	TGCTTGGATGTTCTGAGTGC	
MYC-gex-F1	AAACACAAACTTGAACAGCTAC	
MYC-gex-R1	ATTTGAGGCAGTTTACATTATGG	
IGH-gex-F1	CTGGCTGGGATTCGTGTAGT	
IGH-gex-F2	TGTGTTTCCGGATTTTGTGA	
GAPDH-cDNA-F	CTGCACCACCAACTGCTTAG	
GAPDH-cDNA-R	AGGTCCACCACTGACACGTT	

Supplementary Table 4. Primer pairs used to detect different translocations.

#	Primer pair	Approximate length (bp)	Derivative chromosome type	Derivative centromere
AEI-1	AML-F1 ETO-R1	514	monocentric	ETO (der 8)
AEI-2	AML-R1 ETO-F1	463	monocentric	AML (der 21)
AEI-3	AML-F1 ETO-F1	471	acentric	acentric
AEI-4	AML-R1 ETO-R1	506	dicentric	dicentric

AEI-5	AML-F1 IGH-out-R3	432	monocentric	IGH (der 14)
AEI-6	AML-R1 IGH-out-F3	481	monocentric	AML (der 21)
AEI-7	AML-F1 IGH-out-F3	489	acentric	acentric
AEI-8	AML-R1 IGH-out-R3	424	dicentric	dicentric
AEI-9	ETO-F1 IGH-out-R3	457	monocentric	IGH (der 14)
AEI-10	ETO-R1 IGH-out-F3	557	monocentric	ETO (der 8)
AEI-11	ETO-F1 IGH-out-F3	514	acentric	acentric
AEI-12	ETO-R1 IGH-out-R3	500	dicentric	dicentric
MIA-1	MYCn-F1 IGH-out-R3	413	dicentric	dicentric
MIA-2	MYCn-R1 IGH-out-F3	446	acentric	acentric
MIA-3	MYCn-F1 IGH-out-F3	470	monocentric	MYC (der 8)
MIA-4	MYCn-R1 IGH-out-R3	389	monocentric	IGH (der 14)
MIA-5	MYCn-F1 AML-R1	419	dicentric	dicentric
MIA-6	MYCn-R1 AML-F1	403	acentric	acentric
MIA-7	MYCn-F1 AML-F1	427	monocentric	MYC (der 8)
MIA-8	MYCn-R1 AML-R1	395	monocentric	AML (der 21)
MIA-9	IGH-out-F3 AML-R1	481	monocentric	AML (der 21)
MIA-10	IGH-out-R3 AML-F1	432	monocentric	IGH (der 14)
MIA-11	IGH-out-F3 AML-F1	489	acentric	acentric

MIA-12	IGH-out-R3 AML-R1	424	dicentric	dicentric

References

1. Haeussler,M., Schönig,K., Eckert,H., Eschstruth,A., Mianné,J., Renaud,J.-B., Schneider-Maunoury,S., Shkumatava,A., Teboul,L., Kent,J., *et al.* (2016) Evaluation of off-target and on-target scoring algorithms and integration into the guide RNA selection tool CRISPOR. *Genome Biol.*, **17**, 148.
2. Kabadi,A.M., Ousterout,D.G., Hilton,I.B. and Gersbach,C.A. (2014) Multiplex CRISPR/Cas9-based genome engineering from a single lentiviral vector. *Nucleic Acids Res.*, **42**.
3. Germini,D., Bou Saada,Y., Tsfasman,T., Osina,K., Robin,C., Lomov,N., Rubtsov,M., Sjakste,N., Lipinski,M. and Vassetzky,Y. (2017) A One-Step PCR-Based Assay to Evaluate the Efficiency and Precision of Genomic DNA-Editing Tools. *Mol. Ther. Methods Clin. Dev.*, **5**, 43–50.
4. Brinkman,E.K., Chen,T., Amendola,M. and van Steensel,B. (2014) Easy quantitative assessment of genome editing by sequence trace decomposition. *Nucleic Acids Res.*, **42**, e168.
5. Canoy,R.J., André,F., Shmakova,A., Wiels,J., Lipinski,M., Vassetzky,Y. and Germini,D. (2020) Easy and robust electrotransfection protocol for efficient ectopic gene expression and genome editing in human B cells. *Gene Ther.*, 10.1038/s41434-020-00194-x.
6. Pfaffl,M.W. (2001) A new mathematical model for relative quantification in real-time RT–PCR. *Nucleic Acids Res.*, **29**, e45–e45.
7. Germini,D., Tsfasman,T., Klibi,M., El-Amine,R., Pichugin,A., Iarovaia,O.V., Bilhou-Nabera,C., Subra,F., Bou Saada,Y., Sukhanova,A., *et al.* (2017) HIV Tat induces a prolonged MYC relocalization next to IGH in circulating B-cells. *Leukemia*, **31**, 2515–2522.

References

Abrahams M-R, Joseph SB, Garrett N, Tyers L, Moeser M, et al. 2019. The replication-competent HIV-1 latent reservoir is primarily established near the time of therapy initiation. *Sci Transl Med*. 11(513):eaaw5589

Adamson AL, Kenney S. 2001. Epstein-Barr Virus Immediate-Early Protein BZLF1 Is SUMO-1 Modified and Disrupts Promyelocytic Leukemia Bodies. *Journal of Virology*. 75(5):2388–99

Agol VI, Gmyl AP. 2010. Viral security proteins: Counteracting host defences. *Nature Reviews Microbiology*. 8(12):867–78

Ahn JH, Brignole EJ, Hayward GS. 1998. Disruption of PML subnuclear domains by the acidic IE1 protein of human cytomegalovirus is mediated through interaction with PML and may modulate a RING finger-dependent cryptic transactivator function of PML. *Mol Cell Biol*. 18(8):4899–4913

Aid M, Dupuy FP, Moysi E, Moir S, Haddad EK, et al. 2018. Follicular CD4 T Helper Cells As a Major HIV Reservoir Compartment: A Molecular Perspective. *Front Immunol*. 9:895

Akbay B, Germini D, Bissenbaev AK, Musinova YR, Sheval EV, et al. 2021. HIV-1 Tat Activates Akt/mTORC1 Pathway and AICDA Expression by Downregulating Its Transcriptional Inhibitors in B Cells. *Int J Mol Sci*. 22(4):1588

Akbay B, Shmakova A, Vassetzky Y, Dokudovskaya S. 2020. Modulation of mTORC1 Signaling Pathway by HIV-1. *Cells*. 9(5):E1090

Al Tabaa Y, Tuaillon E, Bollore K, Foulongne V, Petitjean G, et al. 2009. Functional Epstein-Barr virus reservoir in plasma cells derived from infected peripheral blood memory B cells. *Blood*. 113(3):604–11

Alaggio R, Amador C, Anagnostopoulos I, Attygalle AD, Araujo IB de O, et al. 2022. The 5th edition of the World Health Organization Classification of Haematolymphoid Tumours: Lymphoid Neoplasms. *Leukemia*. 36(7):1720–48

Alanazi A, Ivanov A, Kumari N, Lin X, Wang S, et al. 2021. Targeting Tat–TAR RNA Interaction for HIV-1 Inhibition. *Viruses*. 13(10):2004

Albini A, Benelli R, Presta M, Rusnati M, Ziche M, et al. 1996a. HIV-tat protein is a heparin-binding angiogenic growth factor. *Oncogene*. 12(2):289–97

Albini A, Soldi R, Giunciuglio D, Giraudo E, Benelli R, et al. 1996b. The angiogenesis induced by HIV-1 tat protein is mediated by the Flk-1/KDR receptor on vascular endothelial cells. *Nat Med*. 2(12):1371–75

Altavilla G, Caputo A, Lanfredi M, Piola C, Barbanti-Brodano G, Corallini A. 2000. Enhancement of chemical hepatocarcinogenesis by the HIV-1 tat gene. *The American journal of pathology*. 157(4):1081–89

Altavilla G, Caputo A, Trabanelli C, Brocca Cofano E, Sabbioni S, et al. 2004. Prevalence of liver tumours in HIV-1 tat-transgenic mice treated with urethane. *European journal of cancer (Oxford, England : 1990)*.

40(2):275–83
Altavilla G, Trabanelli C, Merlin M, Caputo A, Lanfredi M, et al. 1999. Morphological, Histochemical, Immunohistochemical, and Ultrastructural Characterization of Tumors and Dysplastic and Non-Neoplastic Lesions Arising in BK Virus/tat Transgenic Mice. *The American Journal of Pathology*. 154(4):1231–44
Alter G, Altfeld M. 2009. NK cells in HIV-1 infection: Evidence for their role in the control of HIV-1 infection. *J Intern Med*. 265(1):29–42
Altfeld M, Fadda L, Frleta D, Bhardwaj N. 2011. DCs and NK cells: critical effectors in the immune response to HIV-1. *Nature Reviews Immunology*. 11(3):176–86
Alves de Souza Rios L, Mapekula L, Mdletshe N, Chetty D, Mowla S. 2021. HIV-1 Transactivator of Transcription (Tat) Co-operates With AP-1 Factors to Enhance c-MYC Transcription. *Front Cell Dev Biol*. 9:693706
Amon W, Farrell PJ. 2005. Reactivation of Epstein-Barr virus from latency. *Reviews in Medical Virology*. 15(3):149–56
Amoroso R, Fitzsimmons L, Thomas WA, Kelly GL, Rowe M, Bell AI. 2011. Quantitative Studies of Epstein-Barr Virus-Encoded MicroRNAs Provide Novel Insights into Their Regulation. *Journal of Virology*. 85(2):996
Annovazzi L, Mellai M, Schiffer D. 2017. Chemotherapeutic Drugs: DNA Damage and Repair in Glioblastoma. *Cancers (Basel)*. 9(6):57
Antel K, Levetan C, Mohamed Z, Louw VJ, Oosthuizen J, et al. 2019. The determinants and impact of diagnostic delay in lymphoma in a TB and HIV endemic setting. *BMC Cancer*. 19(1):384
Arvey A, Ojesina AI, Pedamallu CS, Ballon G, Jung J, et al. 2015. The tumor virus landscape of AIDS-related lymphomas. *Blood*. 125(20):e14–22
Aten JA, Stap J, Krawczyk PM, van Oven CH, Hoebe RA, et al. 2004. Dynamics of DNA double-strand breaks revealed by clustering of damaged chromosome domains. *Science*. 303(5654):92–95
Attia S, Egger M, Müller M, Zwahlen M, Low N. 2009. Sexual transmission of HIV according to viral load and antiretroviral therapy: systematic review and meta-analysis. *AIDS*. 23(11):1397
Austin JW, Buckner CM, Kardava L, Wang W, Zhang X, et al. 2019. Overexpression of T-bet in HIV infection is associated with accumulation of B cells outside germinal centers and poor affinity maturation. *Science Translational Medicine*. 11(520):eaax0904
Azzi T, Lünemann A, Murer A, Ueda S, Béziat V, et al. 2014. Role for early-differentiated natural killer cells in infectious mononucleosis. *Blood*. 124(16):2533–43
Babcock GJ, Decker LL, Freeman RB, Thorley-Lawson DA. 1999. Epstein-Barr Virus–Infected Resting Memory B Cells, Not Proliferating Lymphoblasts, Accumulate in the Peripheral Blood of Immunosuppressed Patients. *J Exp Med*. 190(4):567–76
Baeten JM, Kahle E, Lingappa JR, Coombs RW, Delany-Moretlwe S, et al. 2011.

Genital HIV-1 RNA Quantity Predicts Risk of Heterosexual HIV-1 Transmission. *Sci Transl Med*. 3(77):77ra29

Bagashev A, Sawaya BE. 2013. Roles and functions of HIV-1 Tat protein in the CNS: an overview. *Virol J*. 10:358

Bailly J, Jenkins N, Chetty D, Mohamed Z, Verburgh ER, Opie JJ. 2022. Plasmablastic lymphoma: An update. *International Journal of Laboratory Hematology*. 44(S1):54–63

Balfour HH Jr, Sifakis F, Sliman JA, Knight JA, Schmeling DO, Thomas W. 2013. Age-Specific Prevalence of Epstein–Barr Virus Infection Among Individuals Aged 6–19 Years in the United States and Factors Affecting Its Acquisition. *The Journal of Infectious Diseases*. 208(8):1286–93

Banga R, Procopio FA, Noto A, Pollakis G, Cavassini M, et al. 2016. PD-1+ and follicular helper T cells are responsible for persistent HIV-1 transcription in treated aviremic individuals. *Nat Med*. 22(7):754–61

Bangs SC, McMichael AJ, Xu X-N. 2006. Bystander T cell activation – implications for HIV infection and other diseases. *Trends in Immunology*. 27(11):518–24

Banks WA, Robinson SM, Nath A. 2005. Permeability of the blood-brain barrier to HIV-1 Tat. *Experimental Neurology*. 193(1):218–27

Barboric M, Yik JHN, Czudnochowski N, Yang Z, Chen R, et al. 2007. Tat competes with HEXIM1 to increase the active pool of P-TEFb for HIV-1 transcription. *Nucleic Acids Res*. 35(6):2003–12

Barillari G, Gendelman R, Gallo RC, Ensoli B. 1993. The Tat protein of human immunodeficiency virus type 1, a growth factor for AIDS Kaposi sarcoma and cytokine-activated vascular cells, induces adhesion of the same cell types by using integrin receptors recognizing the RGD amino acid sequence. *Proc Natl Acad Sci U S A*. 90(17):7941–45

Barillari G, Sgadari C, Fiorelli V, Samaniego F, Colombini S, et al. 1999a. The Tat protein of human immunodeficiency virus type-1 promotes vascular cell growth and locomotion by engaging the alpha5beta1 and alphavbeta3 integrins and by mobilizing sequestered basic fibroblast growth factor. *Blood*. 94(2):663–72

Barillari G, Sgadari C, Palladino C, Gendelman R, Caputo A, et al. 1999b. Inflammatory cytokines synergize with the HIV-1 Tat protein to promote angiogenesis and Kaposi's sarcoma via induction of basic fibroblast growth factor and the alpha v beta 3 integrin. *J Immunol*. 163(4):1929–35

Bekker V, Scherpbier H, Beld M, Piriou E, van Breda A, et al. 2006. Epstein-Barr virus infects B and non-B lymphocytes in HIV-1-infected children and adolescents. *J Infect Dis*. 194(9):1323–30

Ben Haij N, Leghmari K, Planès R, Thieblemont N, Bahraoui E. 2013. HIV-1 Tat protein binds to TLR4-MD2 and signals to induce TNF-α and IL-10. *Retrovirology*. 10(1):123

Benjamin D, Sharma V, Kubin M, Klein JL, Sartori A, et al. 1996. IL-12 expression in AIDS-related lymphoma B cell lines. *The Journal of*

Immunology. 156(4):1626–37
Benleulmi MS, Matysiak J, Robert X, Miskey C, Mauro E, et al. 2017. Modulation of the functional association between the HIV-1 intasome and the nucleosome by histone amino-terminal tails. *Retrovirology*. 14(1):54
Bergbauer M, Kalla M, Schmeinck A, Göbel C, Rothbauer U, et al. 2010. CpG-methylation regulates a class of Epstein-Barr virus promoters. *PLoS Pathogens*. 6(9):
Berretta M, Di Francia R, Stanzione B, Facchini G, LLeshi A, et al. 2016. New treatment strategies for HIV-positive cancer patients undergoing antiblastic chemotherapy. *Expert Opinion on Pharmacotherapy*. 17(18):2391–2403
Besson C, Lancar R, Prevot S, Brice P, Meyohas M-C, et al. 2015. High Risk Features Contrast With Favorable Outcomes in HIV-associated Hodgkin Lymphoma in the Modern cART Era, ANRS CO16 LYMPHOVIR Cohort. *Clin Infect Dis*. 61(9):1469–75
Bienert S, Waterhouse A, de Beer T, Tauriello G, Studer G, et al. 2017. The SWISS-MODEL Repository: new features and functionalities. *Nucleic acids research*. 45:D313–19
Birx DL, Redfield RR, Tosato G. 1986. Defective regulation of Epstein-Barr virus infection in patients with acquired immunodeficiency syndrome (AIDS) or AIDS-related disorders. *N Engl J Med*. 314(14):874–79
Blackford AN, Jackson SP. 2017. ATM, ATR, and DNA-PK: The Trinity at the Heart of the DNA Damage Response. *Molecular Cell*. 66(6):801–17
Blonska M, Zhu Y, Chuang HH, You MJ, Kunkalla K, et al. 2015. Jun-regulated genes promote interaction of diffuse large B-cell lymphoma with the microenvironment. *Blood*. 125(6):981–91
Blumberg RS, Paradis TJ, Crawford D, Byington RE, Hirsch MS, Schooley RT. 1987. Effects of human immunodeficiency virus (HIV) on the cytotoxic response to Epstein Barr virus (EBV) transformed B lymphocytes. *AIDS Res Hum Retroviruses*. 3(3):303–15
Boboila C, Alt FW, Schwer B. 2012. Classical and alternative end-joining pathways for repair of lymphocyte-specific and general DNA double-strand breaks. *Adv Immunol*. 116:1–49
Boboila C, Jankovic M, Yan CT, Wang JH, Wesemann DR, et al. 2010. Alternative end-joining catalyzes robust IgH locus deletions and translocations in the combined absence of ligase 4 and Ku70. *Proc Natl Acad Sci U S A*. 107(7):3034–39
Bodescot M, Perricaudet M. 1986. Epstein-Barr virus mRNAs produced by alternative splicing. *Nucleic Acids Res*. 14(17):7103–14
Boerma EG, Siebert R, Kluin PM, Baudis M. 2009. Translocations involving 8q24 in Burkitt lymphoma and other malignant lymphomas: a historical review of cytogenetics in the light of todays knowledge. *Leukemia*. 23(2):225–34
Boice M, Salloum D, Mourcin F, Sanghvi V, Amin R, et al. 2016. Loss of the

HVEM Tumor Suppressor in Lymphoma and Restoration by Modified CAR-T Cells. *Cell*. 167(2):405-418.e13

Bonin S, Dotti I. 2011. General Protocol for Dot-Blot. In *Guidelines for Molecular Analysis in Archive Tissues*, ed. G Stanta, pp. 115–16. Berlin, Heidelberg: Springer

Bosch Príncep R, Lejeune M, Salvadó Usach MT, Jaén Martínez J, Pons Ferré LE, Alvaro Naranjo T. 2005. Decreased number of granzyme B+ activated CD8+ cytotoxic T lymphocytes in the inflammatory background of HIV-associated Hodgkin's lymphoma. *Ann Hematol*. 84(10):661–66

Bouwman RD, Palser A, Parry CM, Coulter E, Rasaiyaah J, et al. 2014. Human immunodeficiency virus Tat associates with a specific set of cellular RNAs. *Retrovirology*. 11:53

Brandt CD, Sison AV, Rakusan TA, Saxena ES, Kaufman TE, et al. 1998. Epstein-Barr virus DNA in the blood of infants, young children, and adults by age and HIV status. *J Acquir Immune Defic Syndr Hum Retrovirol*. 17(1):69–72

Brigati C, Giacca M, Noonan DM, Albini A. 2003. HIV Tat, its TARgets and the control of viral gene expression. *FEMS Microbiology Letters*. 220(1):57–65

Brinkhof MWG, Böni J, Steiner F, Tomasik Z, Nadal D, Schüpbach J. 2006. Evaluation of p24-based antiretroviral treatment monitoring in pediatric HIV-1 infection: prediction of the CD4+ T-cell changes between consecutive visits. *J Acquir Immune Defic Syndr*. 41(5):557–62

Brinkman EK, Chen T, de Haas M, Holland HA, Akhtar W, van Steensel B. 2018. Kinetics and Fidelity of the Repair of Cas9-Induced Double-Strand DNA Breaks. *Mol Cell*. 70(5):801-813.e6

Brinkman K, ter Hofstede HJ, Burger DM, Smeitink JA, Koopmans PP. 1998. Adverse effects of reverse transcriptase inhibitors: mitochondrial toxicity as common pathway. *AIDS (London, England)*. 12(14):1735–44

Brown JA, Pack LR, Fowler JD, Suo Z. 2011. Pre-steady-state kinetic analysis of the incorporation of anti-HIV nucleotide analogs catalyzed by human X- and Y-family DNA polymerases. *Antimicrobial agents and chemotherapy*. 55(1):276–83

Brown RT, Ades IZ, Nordan RP. 1995. An acute phase response factor/NF-kappa B site downstream of the junB gene that mediates responsiveness to interleukin-6 in a murine plasmacytoma. *J Biol Chem*. 270(52):31129–35

Burbelo PD, Ching KH, Morse CG, Alevizos I, Bayat A, et al. 2013. Altered Antibody Profiles against Common Infectious Agents in Chronic Disease. *PLoS One*. 8(12):e81635

Burdick RC, Li C, Munshi M, Rawson JMO, Nagashima K, et al. 2020. HIV-1 uncoats in the nucleus near sites of integration. *Proc Natl Acad Sci U S A*. 117(10):5486–93

Burighel N, Ghezzi S, Nozza S, Del Bianco P, Lazzarin A, et al. 2006. Differential dynamics of Epstein-Barr virus in individuals infected with human

immunodeficiency virus-1 receiving intermittent interleukin-2 and antiretroviral therapy. *Haematologica*. 91(2):244–47

Busch K, Keller T, Fuchs U, Yeh R-F, Harbott J, et al. 2007. Identification of two distinct MYC breakpoint clusters and their association with various IGH breakpoint regions in the t(8;14) translocations in sporadic Burkitt-lymphoma. *Leukemia*. 21(8):1739–51

Buschle A, Hammerschmidt W. 2020. Epigenetic lifestyle of Epstein-Barr virus. *Seminars in Immunopathology*. 42(2):131–42

Buschle A, Mrozek-Gorska P, Krebs S, Blum H, Cernilogar F, et al. 2019. Epstein-Barr virus inactivates the transcriptome and disrupts the chromatin architecture of its host cell in the first phase of lytic reactivation. *bioRxiv*. 573659

Byrne CM, Johnston C, Orem J, Okuku F, Huang M-L, et al. 2021. Examining the dynamics of Epstein-Barr virus shedding in the tonsils and the impact of HIV-1 coinfection on daily saliva viral loads. *PLoS Comput Biol*. 17(6):e1009072

Cafaro A, Tripiciano A, Picconi O, Sgadari C, Moretti S, et al. 2019. Anti-Tat Immunity in HIV-1 Infection: Effects of Naturally Occurring and Vaccine-Induced Antibodies Against Tat on the Course of the Disease. *Vaccines (Basel)*. 7(3):

Çalışkaner ZO, Çakar T, Özçelik E, Özdilek A, Kim AS, et al. 2017. DEK protein level is a biomarker of CD138positive normal and malignant plasma cells. *PLoS One*. 12(5):e0178025

Campbell GR, Loret EP. 2009. What does the structure-function relationship of the HIV-1 Tat protein teach us about developing an AIDS vaccine? *Retrovirology*. 6(1):50

Campbell-Yesufu OT, Gandhi RT. 2011. Update on Human Immunodeficiency Virus (HIV)-2 Infection. *Clin Infect Dis*. 52(6):780–87

Canoy RJ, André F, Shmakova A, Wiels J, Lipinski M, et al. 2020. Easy and robust electrotransfection protocol for efficient ectopic gene expression and genome editing in human B cells. *Gene Therapy*

Canoy RJ, Shmakova A, Karpukhina A, Lomov N, Tiukacheva E, et al. 2023. Specificity of cancer-related chromosomal translocations is linked to proximity after the DNA double-strand break and subsequent selection. *NAR Cancer*. 5(3):zcad049

Canoy RJ, Shmakova A, Karpukhina A, Shepelev M, Germini D, Vassetzky Y. 2022. Factors That Affect the Formation of Chromosomal Translocations in Cells. *Cancers (Basel)*. 14(20):5110

Cantaluppi V, Biancone L, Boccellino M, Doublier S, Benelli R, et al. 2001. HIV Type 1 Tat Protein Is a Survival Factor for Kaposi's Sarcoma and Endothelial Cells. *AIDS Research and Human Retroviruses*. 17(10):965–76

Cao Y, Xie L, Shi F, Tang M, Li Y, et al. 2021. Targeting the signaling in Epstein–Barr virus-associated diseases: mechanism, regulation, and clinical study. *Sig Transduct Target Ther*. 6(1):1–33

Carmichael A, Jin X, Sissons P, Borysiewicz L. 1993. Quantitative analysis of the human immunodeficiency virus type 1 (HIV-1)-specific cytotoxic T lymphocyte (CTL) response at different stages of HIV-1 infection: differential CTL responses to HIV-1 and Epstein-Barr virus in late disease. *J Exp Med*. 177(2):249–56

Caron P, Choudjaye J, Clouaire T, Bugler B, Daburon V, et al. 2015. Non-redundant Functions of ATM and DNA-PKcs in Response to DNA Double-Strand Breaks. *Cell Reports*. 13(8):1598–1609

Caseiro MM, Nelson M, Diaz RS, Gathe J, de Andrade Neto JL, et al. 2012. Vicriviroc plus optimized background therapy for treatment-experienced subjects with CCR5 HIV-1 infection: Final results of two randomized phase III trials. *Journal of Infection*. 65(4):326–35

Castillo JJ, Bibas M, Miranda RN. 2015. The biology and treatment of plasmablastic lymphoma. *Blood*. 125(15):2323–30

Chaganti S, Heath EM, Bergler W, Kuo M, Buettner M, et al. 2009. Epstein-Barr virus colonization of tonsillar and peripheral blood B-cell subsets in primary infection and persistence. *Blood*. 113(25):6372–81

Chaillon A, Gianella S, Dellicour S, Rawlings SA, Schlub TE, et al. 2020a. HIV persists throughout deep tissues with repopulation from multiple anatomical sources. *J Clin Invest*. 130(4):1699–1712

Chaillon A, Nakazawa M, Rawlings SA, Curtin G, Caballero G, et al. 2020b. Subclinical Cytomegalovirus and Epstein-Barr Virus Shedding Is Associated with Increasing HIV DNA Molecular Diversity in Peripheral Blood during Suppressive Antiretroviral Therapy. *J Virol*. 94(19):e00927-20

Chang HC, Samaniego F, Nair BC, Buonaguro L, Ensoli B. 1997. HIV-1 Tat protein exits from cells via a leaderless secretory pathway and binds to extracellular matrix-associated heparan sulfate proteoglycans through its basic region. *AIDS*. 11(12):1421–31

Chapman JR, Bouska AC, Zhang W, Alderuccio JP, Lossos IS, et al. 2021. EBV-positive HIV-associated diffuse large B cell lymphomas are characterized by JAK/STAT (STAT3) pathway mutations and unique clinicopathologic features. *Br J Haematol*. 194(5):870–78

Chaudhuri J, Basu U, Zarrin A, Yan C, Franco S, et al. 2007. Evolution of the immunoglobulin heavy chain class switch recombination mechanism. *Adv Immunol*. 94:157–214

Chavez L, Calvanese V, Verdin E. 2015. HIV Latency Is Established Directly and Early in Both Resting and Activated Primary CD4 T Cells. *PLoS Pathog*. 11(6):e1004955

Chen B. 2019. Molecular Mechanism of HIV-1 Entry. *Trends Microbiol*. 27(10):878–91

Chen J, Sathiyamoorthy K, Zhang X, Schaller S, Perez White BE, et al. 2018. Ephrin receptor A2 is a functional entry receptor for Epstein-Barr virus. *Nat Microbiol*. 3(2):172–80

Chen T-T, Tsai M-H, Kung JT, Lin K-I, Decker T, Lee C-K. 2016. STAT1 regulates marginal zone B cell differentiation in response to inflammation and infection with blood-borne bacteria. *J Exp Med*. 213(13):3025–39

Chen X, Cheng L, Jia X, Zeng Y, Yao S, et al. 2009. Human immunodeficiency virus type 1 Tat accelerates Kaposi sarcoma-associated herpesvirus Kaposin A-mediated tumorigenesis of transformed fibroblasts in vitro as well as in nude and immunocompetent mice. *Neoplasia (New York, N.Y.)*. 11(12):1272–84

Cheung KJJ, Johnson NA, Affleck JG, Severson T, Steidl C, et al. 2010. Acquired TNFRSF14 mutations in follicular lymphoma are associated with worse prognosis. *Cancer Research*. 70(22):9166–74

Chiozzini C, Collacchi B, Nappi F, Bauer T, Arenaccio C, et al. 2014. Surface-bound Tat inhibits antigen-specific CD8+ T-cell activation in an integrin-dependent manner. *AIDS*. 28(15):2189–2200

Chipitsyna G, Slonina D, Siddiqui K, Peruzzi F, Skorski T, et al. 2004. HIV-1 Tat increases cell survival in response to cisplatin by stimulating Rad51 gene expression. *Oncogene*. 23(15):2664–71

Chomont N, El-Far M, Ancuta P, Trautmann L, Procopio FA, et al. 2009. HIV reservoir size and persistence are driven by T cell survival and homeostatic proliferation. *Nat Med*. 15(8):893–900

Christ F, Debyser Z. 2013. The LEDGF/p75 integrase interaction, a novel target for anti-HIV therapy. *Virology*. 435(1):102–9

Christensen-Quick A, Massanella M, Frick A, Rawlings SA, Spina C, et al. 2019. Subclinical Cytomegalovirus DNA Is Associated with CD4 T Cell Activation and Impaired CD8 T Cell CD107a Expression in People Living with HIV despite Early Antiretroviral Therapy. *J Virol*. 93(13):e00179-19

Chun TW, Engel D, Berrey MM, Shea T, Corey L, Fauci AS. 1998. Early establishment of a pool of latently infected, resting CD4(+) T cells during primary HIV-1 infection. *Proc Natl Acad Sci U S A*. 95(15):8869–73

Cirino TJ, McLaughlin JP. 2021. Mini review: Promotion of substance abuse in HIV patients: Biological mediation by HIV-1 Tat protein. *Neurosci Lett*. 753:135877

Ciuffi A, Llano M, Poeschla E, Hoffmann C, Leipzig J, et al. 2005. A role for LEDGF/p75 in targeting HIV DNA integration. *Nat Med*. 11(12):1287–89

Clark E, Nava B, Caputi M. 2017. Tat is a multifunctional viral protein that modulates cellular gene expression and functions. *Oncotarget*. 8(16):27569–81

Coghill AE, Pfeiffer RM, Shiels MS, Engels EA. 2017. Excess Mortality among HIV-Infected Individuals with Cancer in the United States. *Cancer epidemiology, biomarkers & prevention : a publication of the American Association for Cancer Research, cosponsored by the American Society of Preventive Oncology*. 26(7):1027–33

Coghill AE, Shiels MS, Suneja G, Engels EA. 2015. Elevated cancer-specific mortality among HIV-infected patients in the United States. *Journal of*

clinical oncology : official journal of the American Society of Clinical Oncology. 33(21):2376–83

Coghill AE, Suneja G, Rositch AF, Shiels MS, Engels EA. 2019. HIV Infection, Cancer Treatment Regimens, and Cancer Outcomes Among Elderly Adults in the United States. *JAMA Oncol*. 5(9):e191742

Cohen J, Torres C. 2017. HIV-associated cellular senescence: A contributor to accelerated aging. *Ageing Research Reviews*. 36:117–24

Cohen JI. 2000. Epstein–Barr Virus Infection. *New England Journal of Medicine*. 343(7):481–92

Cohen JI, Fauci AS, Varmus H, Nabel GJ. 2011. Epstein-Barr virus: An important vaccine target for cancer prevention. *Science Translational Medicine*. 3(107):107

Cohen M, Vistarop AG, Huaman F, Narbaitz M, Metrebian F, et al. 2018. Epstein-Barr virus lytic cycle involvement in diffuse large B cell lymphoma. *Hematological Oncology*. 36(1):98–103

Cohn LB, Chomont N, Deeks SG. 2020. The Biology of the HIV-1 Latent Reservoir and Implications for Cure Strategies. *Cell Host Microbe*. 27(4):519–30

Collins DR, Gaiha GD, Walker BD. 2020. CD8+ T cells in HIV control, cure and prevention. *Nat Rev Immunol*. 20(8):471–82

Colombrino E, Rossi E, Ballon G, Terrin L, Indraccolo S, et al. 2004. Human immunodeficiency virus type 1 Tat protein modulates cell cycle and apoptosis in Epstein–Barr virus-immortalized B cells. *Experimental Cell Research*. 295(2):539–48

Corallini A, Altavilla G, Pozzi L, Bignozzi F, Negrini M, et al. 1993. Systemic expression of HIV-1 tat gene in transgenic mice induces endothelial proliferation and tumors of different histotypes. *Cancer research*. 53(22):5569–75

Corallini A, Campioni D, Rossi C, Albini A, Possati L, et al. 1996. Promotion of tumour metastases and induction of angiogenesis by native HIV-1 Tat protein from BK virus/tat transgenic mice. *AIDS (London, England)*. 10(7):701–10

Corpet A, Kleijwegt C, Roubille S, Juillard F, Jacquet K, et al. 2020. PML nuclear bodies and chromatin dynamics: catch me if you can! *Nucleic Acids Research*. 48(21):11890–912

Countryman J, Miller G. 1985. Activation of expression of latent Epstein-Barr herpesvirus after gene transfer with a small cloned subfragment of heterogeneous viral DNA. *Proceedings of the National Academy of Sciences of the United States of America*. 82(12):4085–89

Crespan E, Garbelli A, Amoroso A, Maga G. 2011. Exploiting the nucleotide substrate specificity of repair DNA polymerases to develop novel anticancer agents. *Molecules (Basel, Switzerland)*. 16(9):7994–8019

Dahl KE, Burrage T, Jones F, Miller G. 1990. Persistent nonproductive infection of Epstein-Barr virus-transformed human B lymphocytes by human

immunodeficiency virus type 1. *J Virol*. 64(4):1771–83
Dalla-Favera R, Bregni M, Erikson J, Patterson D, Gallo RC, Croce CM. 1982. Human c-myc onc gene is located on the region of chromosome 8 that is translocated in Burkitt lymphoma cells. *Proc Natl Acad Sci U S A*. 79(24):7824–27
Dalod M, Dupuis M, Deschemin JC, Sicard D, Salmon D, et al. 1999. Broad, intense anti-human immunodeficiency virus (HIV) ex vivo CD8(+) responses in HIV type 1-infected patients: comparison with anti-Epstein-Barr virus responses and changes during antiretroviral therapy. *J Virol*. 73(9):7108–16
Darling TK, Lamb TJ. 2019. Emerging Roles for Eph Receptors and Ephrin Ligands in Immunity. *Front Immunol*. 10:1473
De Falco G, Bellan C, Lazzi S, Claudio P, La Sala D, et al. 2003. Interaction between HIV-1 Tat and pRb2/p130: a possible mechanism in the pathogenesis of AIDS-related neoplasms. *Oncogene*. 22(40):6214–19
De Paschale M, Clerici P. 2012. Serological diagnosis of Epstein-Barr virus infection: Problems and solutions. *World J Virol*. 1(1):31–43
de Salort J, Cuenca M, Terhorst C, Engel P, Romero X. 2013. Ly9 (CD229) Cell-Surface Receptor is Crucial for the Development of Spontaneous Autoantibody Production to Nuclear Antigens. *Frontiers in Immunology*. 4:225
De Scheerder M-A, Vrancken B, Dellicour S, Schlub T, Lee E, et al. 2019. HIV Rebound Is Predominantly Fueled by Genetically Identical Viral Expansions from Diverse Reservoirs. *Cell Host Microbe*. 26(3):347-358.e7
Debaisieux S, Lachambre S, Gross A, Mettling C, Besteiro S, et al. 2015. HIV-1 Tat inhibits phagocytosis by preventing the recruitment of Cdc42 to the phagocytic cup. *Nature Communications*. 6(1):6211
Debaisieux S, Rayne F, Yezid H, Beaumelle B. 2012. The Ins and Outs of HIV-1 Tat. *Traffic*. 13(3):355–63
Deeks SG, Overbaugh J, Phillips A, Buchbinder S. 2015. HIV infection. *Nat Rev Dis Primers*. 1(1):1–22
Delecluse HJ, Anagnostopoulos I, Dallenbach F, Hummel M, Marafioti T, et al. 1997. Plasmablastic lymphomas of the oral cavity: a new entity associated with the human immunodeficiency virus infection. *Blood*. 89(4):1413–20
Demin DE, Murashko MM, Uvarova AN, Stasevich EM, Shyrokova EY, et al. 2022. Adversary of DNA integrity: a long non-coding RNA stimulates driver oncogenic chromosomal rearrangement in human thyroid cells. *Int J Cancer*. in press:
Deng L, Ammosova T, Pumfery A, Kashanchi F, Nekhai S. 2002. HIV-1 Tat Interaction with RNA Polymerase II C-terminal Domain (CTD) and a Dynamic Association with CDK2 Induce CTD Phosphorylation and Transcription from HIV-1 Promoter *. *Journal of Biological Chemistry*. 277(37):33922–29

Dharan A, Bachmann N, Talley S, Zwikelmaier V, Campbell EM. 2020. Nuclear pore blockade reveals that HIV-1 completes reverse transcription and uncoating in the nucleus. *Nat Microbiol*. 5(9):1088–95

Di Noia JM, Neuberger MS. 2007. Molecular mechanisms of antibody somatic hypermutation. *Annu Rev Biochem*. 76:1–22

Dickerson SJ, Xing Y, Robinson AR, Seaman WT, Gruffat H, Kenney SC. 2009. Methylation-dependent binding of the epstein-barr virus BZLF1 protein to viral promoters. *PLoS Pathogens*. 5(3):

Doitsh G, Cavrois M, Lassen KG, Zepeda O, Yang Z, et al. 2010. Abortive HIV Infection Mediates CD4 T Cell Depletion and Inflammation in Human Lymphoid Tissue. *Cell*. 143(5):789–801

Doitsh G, Galloway NL, Geng X, Yang Z, Monroe KM, et al. 2014. Pyroptosis drives CD4 T-cell depletion in HIV-1 infection. *Nature*. 505(7484):509–14

Doitsh G, Greene WC. 2016. Dissecting How CD4 T Cells Are Lost During HIV Infection. *Cell Host & Microbe*. 19(3):280–91

Dorothea M, Xie J, Yiu SPT, Chiang AKS. 2023. Contribution of Epstein-Barr Virus Lytic Proteins to Cancer Hallmarks and Implications from Other Oncoviruses. *Cancers (Basel)*. 15(7):2120

Dorsett Y, Robbiani DF, Jankovic M, Reina-San-Martin B, Eisenreich TR, Nussenzweig MC. 2007. A role for AID in chromosome translocations between c-myc and the IgH variable region. *The Journal of Experimental Medicine*. 204(9):2225–32

D'Orso I, Frankel AD. 2010. RNA-mediated displacement of an inhibitory snRNP complex activates transcription elongation. *Nat Struct Mol Biol*. 17(7):815–21

Doucas V, Ishov AM, Romo A, Juguilon H, Weitzman MD, et al. 1996. Adenovirus replication is coupled with the dynamic properties of the PML nuclear structure. *Genes Dev*. 10(2):196–207

Dunmire SK, Verghese PS, Balfour HH. 2018. Primary Epstein-Barr virus infection. *J Clin Virol*. 102:84–92

El-Amine R, Germini D, Zakharova VV, Tsfasman T, Sheval EV, et al. 2018. HIV-1 Tat protein induces DNA damage in human peripheral blood B-lymphocytes via mitochondrial ROS production. *Redox Biology*. 15:97–108

Ellwanger JH, Kulmann-Leal B, Ziliotto M, Chies JAB. 2023. HIV Infection, Chromosome Instability, and Micronucleus Formation. *Viruses*. 15(1):155

Engelman A, Cherepanov P. 2012. The structural biology of HIV-1: mechanistic and therapeutic insights. *Nat Rev Microbiol*. 10(4):279–90

Engels EA, Biggar RJ, Hall HI, Cross H, Crutchfield A, et al. 2008. Cancer risk in people infected with human immunodeficiency virus in the United States. *International Journal of Cancer*. 123(1):187–94

Ensoli B, Barillari G, Salahuddin SZ, Gallo RC, Wong-Staal F. 1990. Tat protein of HIV-1 stimulates growth of cells derived from Kaposi's sarcoma lesions of AIDS patients. *Nature*. 345(6270):84–86

Ensoli B, Buonaguro L, Barillari G, Fiorelli V, Gendelman R, et al. 1993. Release, uptake, and effects of extracellular human immunodeficiency virus type 1 Tat protein on cell growth and viral transactivation. *J Virol*. 67(1):277–87

Eshleman SH, Laeyendecker O, Kammers K, Chen A, Sivay MV, et al. 2019. Comprehensive Profiling of HIV Antibody Evolution. *Cell Rep*. 27(5):1422-1433.e4

Estes JD, Kityo C, Ssali F, Swainson L, Makamdop KN, et al. 2017. Defining total-body AIDS-virus burden with implications for curative strategies. *Nat Med*. 23(11):1271–76

Everett RD. 2001. DNA viruses and viral proteins that interact with PML nuclear bodies. *Oncogene*. 20(49):7266–73

Everett RD, Rechter S, Papior P, Tavalai N, Stamminger T, Orr A. 2006. PML contributes to a cellular mechanism of repression of herpes simplex virus type 1 infection that is inactivated by ICP0. *J Virol*. 80(16):7995–8005

Faller E, Kakal J, Kumar R, Macpherson P. 2009. IL-7 and the HIV Tat protein act synergistically to down-regulate CD127 expression on CD8 T cells. *Int Immunol*. 21(3):203–16

Faller EM, McVey MJ, Kakal JA, MacPherson PA. 2006. Interleukin-7 receptor expression on CD8 T-cells is downregulated by the HIV Tat protein. *J Acquir Immune Defic Syndr*. 43(3):257–69

Faller EM, McVey MJ, MacPherson PA. 2014. IL-7 Receptor Recovery on CD8 T-Cells Isolated from HIV+ Patients Is Inhibited by the HIV Tat Protein. *PLOS ONE*. 9(7):e102677

Faller EM, Sugden SM, McVey MJ, Kakal JA, MacPherson PA. 2010. Soluble HIV Tat protein removes the IL-7 receptor alpha-chain from the surface of resting CD8 T cells and targets it for degradation. *J Immunol*. 185(5):2854–66

Fan H, Kim SC, Chima CO, Israel BF, Lawless KM, et al. 2005. Epstein-Barr viral load as a marker of lymphoma in AIDS patients. *J Med Virol*. 75(1):59–69

Faust TB, Li Y, Bacon CW, Jang GM, Weiss A, et al. 2018. The HIV-1 Tat protein recruits a ubiquitin ligase to reorganize the 7SK snRNP for transcriptional activation. *eLife*. 7:e31879

Feederle R, Kost M, Baumann M, Janz A, Drouet E, et al. 2000. The Epstein-Barr virus lytic program is controlled by the co-operative functions of two transactivators. *EMBO Journal*. 19(12):3080–89

Fellner MD, Durand K, Correa RM, Redini L, Yampolsky C, et al. 2007. Circulating Epstein–Barr virus (EBV) in HIV-infected patients and its relation with primary brain lymphoma. *International Journal of Infectious Diseases*. 11(2):172–78

Ferrell D, Giunta B. 2014. The impact of HIV-1 on neurogenesis: Implications for HAND. *Cell Mol Life Sci*. 71(22):4387–92

Ferrer M, Clerté C, Chamontin C, Basyuk E, Lainé S, et al. 2016. Imaging HIV-1

RNA dimerization in cells by multicolor super-resolution and fluctuation microscopies. *Nucleic Acids Res*. 44(16):7922–34

Ferretti E, Di Carlo E, Ognio E, Guarnotta C, Bertoni F, et al. 2015. Interleukin-17A promotes the growth of human germinal center derived non-Hodgkin B cell lymphoma. *OncoImmunology*. 4(10):

Fields J, Dumaop W, Elueteri S, Campos S, Serger E, et al. 2015a. HIV-1 Tat Alters Neuronal Autophagy by Modulating Autophagosome Fusion to the Lysosome: Implications for HIV-Associated Neurocognitive Disorders. *Journal of Neuroscience*. 35(5):1921–38

Fields JA, Dumaop W, Crews L, Adame A, Spencer B, et al. 2015b. Mechanisms of HIV-1 Tat Neurotoxicity via CDK5 Translocation and Hyper-Activation: Role in HIV-Associated Neurocognitive Disorders. *Curr HIV Res*. 13(1):43–54

Figgett WA, Fairfax K, Vincent FB, Le Page MLA, Katik I, et al. 2013. The TACI Receptor Regulates T-Cell-Independent Marginal Zone B Cell Responses through Innate Activation-Induced Cell Death. *Immunity*. 39:573–83

Fittipaldi A, Ferrari A, Zoppé M, Arcangeli C, Pellegrini V, et al. 2003. Cell membrane lipid rafts mediate caveolar endocytosis of HIV-1 Tat fusion proteins. *J Biol Chem*. 278(36):34141–49

Fiume G, Vecchio E, De Laurentiis A, Trimboli F, Palmieri C, et al. 2012. Human immunodeficiency virus-1 Tat activates NF-κB via physical interaction with IκB-α and p65. *Nucleic Acids Res*. 40(8):3548–62

Flemington E, Speck SH. 1990. Autoregulation of Epstein-Barr virus putative lytic switch gene BZLF1. *Journal of Virology*. 64(3):

Fletcher CV, Staskus K, Wietgrefe SW, Rothenberger M, Reilly C, et al. 2014. Persistent HIV-1 replication is associated with lower antiretroviral drug concentrations in lymphatic tissues. *Proc Natl Acad Sci U S A*. 111(6):2307–12

Flower K, Thomas D, Heather J, Ramasubramanyan S, Jones S, Sinclair AJ. 2011. Epigenetic control of viral Life-Cycle by a DNA-Methylation dependent transcription factor. *PLoS ONE*. 6(10):25922

Frankel AD, Pabo CO. 1988. Cellular uptake of the tat protein from human immunodeficiency virus. *Cell*. 55(6):1189–93

Freed EO. 2015. HIV-1 assembly, release and maturation. *Nat Rev Microbiol*. 13(8):484–96

Frit P, Barboule N, Yuan Y, Gomez D, Calsou P. 2014. Alternative end-joining pathway(s): Bricolage at DNA breaks. *DNA Repair*. 17:81–97

Fukuyo Y, Horikoshi N, Ishov AM, Silverstein SJ, Nakajima T. 2011. The Herpes Simplex Virus Immediate-Early Ubiquitin Ligase ICP0 Induces Degradation of the ICP0 Repressor Protein E2FBP1. *J Virol*. 85(7):3356–66

Gallastegui E, Millán-Zambrano G, Terme J-M, Chávez S, Jordan A. 2011. Chromatin Reassembly Factors Are Involved in Transcriptional Interference Promoting HIV Latency. *J Virol*. 85(7):3187–3202

Garber ME, Wei P, KewalRamani VN, Mayall TP, Herrmann CH, et al. 1998. The

interaction between HIV-1 Tat and human cyclin T1 requires zinc and a critical cysteine residue that is not conserved in the murine CycT1 protein. *Genes Dev*. 12(22):3512–27

Garcia MN, dos Ramos Farias MS, Avila MM, Rabinovich RD. 2011. Presence of p24-antigen associated to erythrocyte in HIV-positive individuals even in patients with undetectable plasma viral load. *PLoS One*. 6(1):e14544

Gasser O, Bihl FK, Wolbers M, Loggi E, Steffen I, et al. 2007a. HIV Patients Developing Primary CNS Lymphoma Lack EBV-Specific CD4+ T Cell Function Irrespective of Absolute CD4+ T Cell Counts. *PLoS Med*. 4(3):e96

Gasser O, Wolbers M, Steffen I, Hirsch HH, Battegay M, et al. 2007b. Increased Epstein–Barr virus-specific antibody-levels in HIV-infected individuals developing primary central nervous system lymphoma. *AIDS*. 21(12):1664–66

Geretti AM, Dings MEM, van Els CACM, van Baalen CA, Wijnholds FJ, et al. 1996. Human Immunodeficiency Virus Type 1 (HIV-1)- and Epstein-Barr Virus-Specific Cytotoxic T Lymphocyte Precursors Exhibit Different Kinetics in HIV-1-Infected Persons. *The Journal of Infectious Diseases*. 174(1):34–45

Germini D, Bou Saada Y, Tsfasman T, Osina K, Robin C, et al. 2017a. A One-Step PCR-Based Assay to Evaluate the Efficiency and Precision of Genomic DNA-Editing Tools. *Mol Ther Methods Clin Dev*. 5:43–50

Germini D, Sall FB, Shmakova A, Wiels J, Dokudovskaya S, et al. 2020. Oncogenic properties of the ebv zebra protein. *Cancers*. 12(6):1–26

Germini D, Tsfasman T, Klibi M, El-Amine R, Pichugin A, et al. 2017b. HIV Tat induces a prolonged MYC relocalization next to IGH in circulating B-cells. *Leukemia*. 31(11):2515–22

Ghezraoui H, Piganeau M, Renouf B, Renaud J-B, Sallmyr A, et al. 2014. Chromosomal Translocations in Human Cells Are Generated by Canonical Nonhomologous End-Joining. *Molecular Cell*. 55(6):829–42

Gianella S, Anderson CM, Var SR, Oliveira MF, Lada SM, et al. 2016. Replication of Human Herpesviruses Is Associated with Higher HIV DNA Levels during Antiretroviral Therapy Started at Early Phases of HIV Infection. *J Virol*. 90(8):3944–52

Gianella S, Moser C, Vitomirov A, McKhann A, Layman L, et al. 2020. Presence of Asymptomatic CMV and EBV DNA in Blood of Persons with HIV Starting Antiretroviral Therapy are Associated with Non-AIDS Clinical Events. *AIDS*. 34(6):849–57

Gibson TM, Morton LM, Shiels MS, Clarke CA, Engels EA. 2014. Risk of non-Hodgkin lymphoma subtypes in HIV-infected people during the HAART era: a population-based study. *AIDS (London, England)*. 28(15):2313–18

Global Health Observatory data repository. 2022. *Antiretroviral therapy coverage*. WHO. https://apps.who.int

Godon A, Moreau A, Talmant P, Baranger-Papot L, Geneviève F, et al. 2003. Is

t(14;18)(q32;q21) a constant finding in follicular lymphoma? An interphase FISH study on 63 patients. *Leukemia*. 17(1):255–59

Goldblum N, Daefler S, Llana T, Ablashi D, Josephs S, Salahuddin Z. 1990. Susceptibility to HIV-1 infection of a human B-lymphoblastoid cell line, DG75, transfected with subgenomic DNA fragments of Epstein-Barr virus. *Dev Biol Stand*. 72:309–13

González F, Zhu Z, Shi Z-D, Lelli K, Verma N, et al. 2014. An iCRISPR platform for rapid, multiplexable, and inducible genome editing in human pluripotent stem cells. *Cell Stem Cell*. 15(2):215–26

Gonzalo-Gil E, Ikediobi U, Sutton RE. 2017. Mechanisms of Virologic Control and Clinical Characteristics of HIV+ Elite/Viremic Controllers. *Yale J Biol Med*. 90(2):245–59

Gopal S, Patel MR, Yanik EL, Cole SR, Achenbach CJ, et al. 2013. Temporal trends in presentation and survival for HIV-associated lymphoma in the antiretroviral therapy era. *Journal of the National Cancer Institute*. 105(16):1221–29

Gorbacheva MA, Tikhomirova MA, Potashnikova DM, Akbay B, Sheval E V., Musinova YR. 2019. Production of Stable Cell Lines on the Basis of the Cultured RPMI 8866 B-Cells with Constant and Inducible Expression of the Human Immunodeficiency Virus Tat Protein. *Russian Journal of Developmental Biology*. 50(5):275–80

Gottlieb GS, Raugi DN, Smith RA. 2018. 90-90-90 for HIV-2? Ending the HIV-2 epidemic by enhancing care and clinical management of patients infected with HIV-2. *Lancet HIV*. 5(7):e390–99

Griffin E, Krantz E, Selke S, Huang M-L, Wald A. 2008. Oral mucosal reactivation rates of herpesviruses among HIV-1 seropositive persons. *J Med Virol*. 80(7):1153–59

Grulich AE, van Leeuwen MT, Falster MO, Vajdic CM. 2007. Incidence of cancers in people with HIV/AIDS compared with immunosuppressed transplant recipients: a meta-analysis. *Lancet*. 370(9581):59–67

Guech-Ongey M, Simard EP, Anderson WF, Engels EA, Bhatia K, et al. 2010. AIDS-related Burkitt lymphoma in the United States: what do age and CD4 lymphocyte patterns tell us about etiology and/or biology? *Blood*. 116(25):5600–5604

Gulick RM, Su Z, Flexner C, Hughes MD, Skolnik PR, et al. 2007. Phase 2 study of the safety and efficacy of vicriviroc, a CCR5 inhibitor, in HIV-1-Infected, treatment-experienced patients: AIDS clinical trials group 5211. *J Infect Dis*. 196(2):304–12

Haas A, Rehr M, Graw F, Rusert P, Bossart W, et al. 2010. HIV-1 replication activates CD4+ T cells with specificities for persistent herpes viruses. *EMBO Molecular Medicine*. 2(6):231–44

Habib M, Buisson M, Lupo J, Agbalika F, Socié G, et al. 2017. Lytic EBV infection investigated by detection of Soluble Epstein-Barr virus ZEBRA in the serum of patients with PTLD. *Scientific Reports*. 7(1):10479

Haij NB, Planès R, Leghmari K, Serrero M, Delobel P, et al. 2015. HIV-1 Tat Protein Induces Production of Proinflammatory Cytokines by Human Dendritic Cells and Monocytes/Macrophages through Engagement of TLR4-MD2-CD14 Complex and Activation of NF-κB Pathway. *PLOS ONE*. 10(6):e0129425

Hammal F, de Langen P, Bergon A, Lopez F, Ballester B. 2022. ReMap 2022: a database of Human, Mouse, Drosophila and Arabidopsis regulatory regions from an integrative analysis of DNA-binding sequencing experiments. *Nucleic Acids Research*. 50(D1):D316–25

Hammerschmidt W, Sugden B. 2013. Replication of Epstein–Barr Viral DNA. *Cold Spring Harb Perspect Biol*. 5(1):a013029

Han H, Cho J-W, Lee S, Yun A, Kim H, et al. 2018. TRRUST v2: an expanded reference database of human and mouse transcriptional regulatory interactions. *Nucleic Acids Research*. 46(D1):D380–86

Hanahan D. 2022. Hallmarks of Cancer: New Dimensions. *Cancer Discovery*. 12(1):31–46

Hanahan D, Weinberg RA. 2011. Hallmarks of Cancer: The Next Generation. *Cell*. 144(5):646–74

He N, Liu M, Hsu J, Xue Y, Chou S, et al. 2010. HIV-1 Tat and host AFF4 recruit two transcription elongation factors into a bifunctional complex for coordinated activation of HIV-1 transcription. *Mol Cell*. 38(3):428–38

He N, Zhou Q. 2011. New Insights into the Control of HIV-1 Transcription: When Tat Meets the 7SK snRNP and Super Elongation Complex (SEC). *J Neuroimmune Pharmacol*. 6(2):260–68

Henderson LJ, Johnson TP, Smith BR, Reoma LB, Santamaria UA, et al. 2019. Presence of Tat and transactivation response element in spinal fluid despite antiretroviral therapy. *AIDS*. 33 Suppl 2:S145–57

Henrich TJ, Hobbs KS, Hanhauser E, Scully E, Hogan LE, et al. 2017. Human Immunodeficiency Virus Type 1 Persistence Following Systemic Chemotherapy for Malignancy. *J Infect Dis*. 216(2):254–62

Herbein G, Gras G, Khan KA, Abbas W. 2010. Macrophage signaling in HIV-1 infection. *Retrovirology*. 7:34

Hernández DM, Valderrama S, Gualtero S, Hernández C, López M, et al. 2018. Loss of T-Cell Multifunctionality and TCR-Vβ Repertoire Against Epstein-Barr Virus Is Associated With Worse Prognosis and Clinical Parameters in HIV+ Patients. *Frontiers in Immunology*. 9:

Hernández-Ramírez RU, Qin L, Lin H, Leyden W, Neugebauer RS, et al. 2019. Association of immunosuppression and HIV viraemia with non-Hodgkin lymphoma risk overall and by subtype in people living with HIV in Canada and the USA: a multicentre cohort study. *Lancet HIV*. 6(4):e240–49

Hernández-Ramírez RU, Shiels MS, Dubrow R, Engels EA. 2017. Cancer risk in HIV-infected people in the USA from 1996 to 2012: a population-based, registry-linkage study. *The Lancet HIV*. 4(11):e495–504

Herndier BG, Sanchez HC, Chang KL, Chen YY, Weiss LM. 1993. High prevalence of Epstein-Barr virus in the Reed-Sternberg cells of HIV-associated Hodgkin's disease. *Am J Pathol*. 142(4):1073–79

Herrmann CH, Rice AP. 1993. Specific interaction of the human immunodeficiency virus Tat proteins with a cellular protein kinase. *Virology*. 197(2):601–8

Herrmann CH, Rice AP. 1995. Lentivirus Tat proteins specifically associate with a cellular protein kinase, TAK, that hyperphosphorylates the carboxyl-terminal domain of the large subunit of RNA polymerase II: candidate for a Tat cofactor. *J Virol*. 69(3):1612–20

Hewitt EW, Duncan L, Mufti D, Baker J, Stevenson PG, Lehner PJ. 2002. Ubiquitylation of MHC class I by the K3 viral protein signals internalization and TSG101-dependent degradation. *EMBO J*. 21(10):2418–29

Hirose T, Ninomiya K, Nakagawa S, Yamazaki T. 2023. A guide to membraneless organelles and their various roles in gene regulation. *Nat Rev Mol Cell Biol*. 24(4):288–304

Hislop AD, Taylor GS, Sauce D, Rickinson AB. 2007. Cellular Responses to Viral Infection in Humans: Lessons from Epstein-Barr Virus. *Annual Review of Immunology*. 25(1):587–617

HIV-CAUSAL Collaboration, Ray M, Logan R, Sterne JAC, Hernández-Díaz S, et al. 2010. The effect of combined antiretroviral therapy on the overall mortality of HIV-infected individuals. *AIDS*. 24(1):123–37

Hladik F, McElrath MJ. 2008. Setting the stage: host invasion by HIV. *Nat Rev Immunol*. 8(6):447–57

Holden NS, Squires PE, Kaur M, Bland R, Jones CE, Newton R. 2008. Phorbol ester-stimulated NF-kappaB-dependent transcription: roles for isoforms of novel protein kinase C. *Cell Signal*. 20(7):1338–48

Holliday H, Khoury A, Swarbrick A. 2021. Chromatin immunoprecipitation of transcription factors and histone modifications in Comma-Dβ mammary epithelial cells. *STAR Protoc*. 2(2):100514

Honjo T, Kinoshita K, Muramatsu M. 2002. Molecular mechanism of class switch recombination: linkage with somatic hypermutation. *Annu Rev Immunol*. 20:165–96

Howcroft TK, Strebel K, Martin MA, Singer DS. 1993. Repression of MHC class I gene promoter activity by two-exon Tat of HIV. *Science*. 260(5112):1320–22

Huang H, Santoso N, Power D, Simpson S, Dieringer M, et al. 2015a. FACT Proteins, SUPT16H and SSRP1, Are Transcriptional Suppressors of HIV-1 and HTLV-1 That Facilitate Viral Latency. *J Biol Chem*. 290(45):27297–310

Huang J, Chen H, Hutt-Fletcher L, Ambinder RF, Hayward SD. 2003. Lytic Viral Replication as a Contributor to theDetection of Epstein-Barr Virus in BreastCancer. *Journal of Virology*. 77(24):13267–74

Huang L, Bosch I, Hofmann W, Sodroski J, Pardee AB. 1998. Tat protein induces

human immunodeficiency virus type 1 (HIV-1) coreceptors and promotes infection with both macrophage-tropic and T-lymphotropic HIV-1 strains. *J Virol*. 72(11):8952–60

Huang L, Li CJ, Pardee AB. 1997. Human immunodeficiency virus type 1 TAT protein activates B lymphocytes. *Biochem Biophys Res Commun*. 237(2):461–64

Huang TT, Hwang JK, Chen CH, Chu CS, Lee CW, Chen CC. 2015b. (PS)2: Protein structure prediction server version 3.0. *Nucleic Acids Research*. 43(W1):W338–42

Hutto C, Zhou Y, He J, Geffin R, Hill M, et al. 1996. Longitudinal studies of viral sequence, viral phenotype, and immunologic parameters of human immunodeficiency virus type 1 infection in perinatally infected twins with discordant disease courses. *J Virol*. 70(6):3589–98

Huynh D, Vincan E, Mantamadiotis T, Purcell D, Chan C-K, Ramsay R. 2007. Oncogenic properties of HIV-Tat in colorectal cancer cells. *Current HIV research*. 5(4):403–9

Hwang JP, Granwehr BP, Torres HA, Suarez-Almazor ME, Giordano TP, et al. 2015. HIV Testing in Patients With Cancer at the Initiation of Therapy at a Large US Comprehensive Cancer Center. *J Oncol Pract*. 11(5):384–90

Iarovaia OV, Rubtsov M, Ioudinkova E, Tsfasman T, Razin SV, Vassetzky YS. 2014. Dynamics of double strand breaks and chromosomal translocations. *Mol Cancer*. 13:249

Iliakis G, Murmann T, Soni A. 2015. Alternative end-joining repair pathways are the ultimate backup for abrogated classical non-homologous end-joining and homologous recombination repair: Implications for the formation of chromosome translocations. *Mutat Res Genet Toxicol Environ Mutagen*. 793:166–75

Imamichi H, Dewar RL, Adelsberger JW, Rehm CA, O'Doherty U, et al. 2016. Defective HIV-1 proviruses produce novel protein-coding RNA species in HIV-infected patients on combination antiretroviral therapy. *Proc Natl Acad Sci U S A*. 113(31):8783–88

Imamichi H, Smith M, Adelsberger JW, Izumi T, Scrimieri F, et al. 2020. Defective HIV-1 proviruses produce viral proteins. *Proc Natl Acad Sci U S A*. 117(7):3704–10

Isaguliants M, Bayurova E, Avdoshina D, Kondrashova A, Chiodi F, Palefsky JM. 2021. Oncogenic Effects of HIV-1 Proteins, Mechanisms Behind. *Cancers (Basel)*. 13(2):305

Ishov AM, Maul GG. 1996. The periphery of nuclear domain 10 (ND10) as site of DNA virus deposition. *J Cell Biol*. 134(4):815–26

Ishov AM, Sotnikov AG, Negorev D, Vladimirova OV, Neff N, et al. 1999. Pml Is Critical for Nd10 Formation and Recruits the Pml-Interacting Protein Daxx to This Nuclear Structure When Modified by Sumo-1. *J Cell Biol*. 147(2):221–34

Ito M, Ishida T, He L, Tanabe F, Rongge Y, et al. 1998. HIV type 1 Tat protein

inhibits interleukin 12 production by human peripheral blood mononuclear cells. *AIDS Res Hum Retroviruses*. 14(10):845–49

Ivanov A, Lin X, Ammosova T, Ilatovskiy AV, Kumari N, et al. 2018. HIV-1 Tat phosphorylation on Ser-16 residue modulates HIV-1 transcription. *Retrovirology*. 15(1):39

Izmailova E, Bertley FMN, Huang Q, Makori N, Miller CJ, et al. 2003. HIV-1 Tat reprograms immature dendritic cells to express chemoattractants for activated T cells and macrophages. *Nat Med*. 9(2):191–97

Jain P, Wang ML. 2022. Mantle cell lymphoma in 2022-A comprehensive update on molecular pathogenesis, risk stratification, clinical approach, and current and novel treatments. *Am J Hematol*. 97(5):638–56

Jain S, Shukla S, Yang C, Zhang M, Fatma Z, et al. 2021. TALEN outperforms Cas9 in editing heterochromatin target sites. *Nat Commun*. 12(1):606

Jang J-W, Thuy PX, Lee J-W, Moon E-Y. 2021. CXCR4 promotes B cell viability by the cooperation of nuclear factor (erythroid-derived 2)-like 2 and hypoxia-inducible factor-1α under hypoxic conditions. *Cell Death Dis*. 12(4):1–12

Jasin M, Rothstein R. 2013. Repair of Strand Breaks by Homologous Recombination. *Cold Spring Harb Perspect Biol*. 5(11):a012740

Jean MJ, Power D, Kong W, Huang H, Santoso N, Zhu J. 2017. Identification of HIV-1 Tat-Associated Proteins Contributing to HIV-1 Transcription and Latency. *Viruses*. 9(4):E67

Jiang Y, Chai L, Fasae MB, Bai Y. 2018. The role of HIV Tat protein in HIV-related cardiovascular diseases. *J Transl Med*. 16(1):121

Jiao X, Velasco-Velázquez MA, Wang M, Li Z, Rui H, et al. 2018. CCR5 Governs DNA Damage Repair and Breast Cancer Stem Cell Expansion. *Cancer Res*. 78(7):1657–71

Joab I, Triki B, de Saint Martin J, Perricaudet M, Nicolas JC. 1991. Detection of Anti-Epstein-Barr Virus trans-Activator (ZEBRA) Antibodies in Sera from Patients with Human Immunodeficiency Virus. *The Journal of Infectious Diseases*. 163(1):53–56

Jochum S, Moosmann A, Lang S, Hammerschmidt W, Zeidler R. 2012. The EBV Immunoevasins vIL-10 and BNLF2a Protect Newly Infected B Cells from Immune Recognition and Elimination. *PLOS Pathogens*. 8(5):e1002704

Johannsen EC, Kaye KM. 2020. Epstein-Barr Virus (Infectious Mononucleosis, Epstein-Barr Virus–Associated Malignant Diseases, and Other Diseases) - ClinicalKey. In *Mandell, Douglas, and Bennett's Principles and Practice of Infectious Diseases*, pp. 1872–90. Elsevier

Kabadi AM, Ousterout DG, Hilton IB, Gersbach CA. 2014. Multiplex CRISPR/Cas9-based genome engineering from a single lentiviral vector. *Nucleic Acids Research*. 42(19):

Kajiwara N, Nomura N, Ukaji M, Yamamoto N, Kohara M, et al. 2020. Cell-penetrating peptide-mediated cell entry of H5N1 highly pathogenic avian influenza virus. *Scientific Reports*. 10(1):18008

Kanakry JA, Hegde AM, Durand CM, Massie AB, Greer AE, et al. 2016. The clinical significance of EBV DNA in the plasma and peripheral blood mononuclear cells of patients with or without EBV diseases. *Blood*. 127(16):2007–17

Kanehisa M, Goto S. 2000. KEGG: kyoto encyclopedia of genes and genomes. *Nucleic Acids Res*. 28(1):27–30

Kao SY, Calman AF, Luciw PA, Peterlin BM. 1987. Anti-termination of transcription within the long terminal repeat of HIV-1 by tat gene product. *Nature*. 330(6147):489–93

Katano H, Sato Y, Hoshino S, Tachikawa N, Oka S, et al. 2007. Integration of HIV-1 caused STAT3-associated B cell lymphoma in an AIDS patient. *Microbes Infect*. 9(14–15):1581–89

Kelly G, Bell A, Rickinson A. 2002. Epstein-Barr virus-associated Burkitt lymphomagenesis selects for downregulation of the nuclear antigen EBNA2. *Nat Med*. 8(10):1098–1104

Kelly GL, Long HM, Stylianou J, Thomas WA, Leese A, et al. 2009. An Epstein-Barr virus anti-apoptotic protein constitutively expressed in transformed cells and implicated in burkitt lymphomagenesis: the Wp/BHRF1 link. *PLoS Pathog*. 5(3):e1000341

Keramat F, Basir HRG, Ahmadpour S, Moradi A. 2019. Seroprevalence of Epstein-Barr Virus in HIV-Infected Patients, A Case Control Study. *J Kermanshah Univ Med Sci*. 23(2):

Kerr JR. 2019. Epstein-Barr virus (EBV) reactivation and therapeutic inhibitors. *Journal of Clinical Pathology*. 72(10):651–58

Kersten MJ, Klein MR, Holwerda AM, Miedema F, van Oers MH. 1997. Epstein-Barr virus-specific cytotoxic T cell responses in HIV-1 infection: different kinetics in patients progressing to opportunistic infection or non-Hodgkin's lymphoma. *J Clin Invest*. 99(7):1525–33

Kersten MJ, Van Gorp J, Pals ST, Boon F, Van Oers MH. 1998. Expression of Epstein-Barr virus latent genes and adhesion molecules in AIDS-related non-Hodgkin's lymphomas: correlation with histology and CD4-cell number. *Leuk Lymphoma*. 30(5–6):515–24

Khan N, Lakpa KL, Halcrow PW, Afghah Z, Miller NM, et al. 2019. BK channels regulate extracellular Tat-mediated HIV-1 LTR transactivation. *Sci Rep*. 9:12285

Khanolkar A, Yagita H, Cannon MJ. 2001. Preferential utilization of the perforin/granzyme pathway for lysis of Epstein-Barr virus-transformed lymphoblastoid cells by virus-specific CD4+ T cells. *Virology*. 287(1):79–88

Kim BO, Liu Y, Zhou BY, He JJ. 2004. Induction of C chemokine XCL1 (lymphotactin/single C motif-1 alpha/activation-induced, T cell-derived and chemokine-related cytokine) expression by HIV-1 Tat protein. *J Immunol*. 172(3):1888–95

Kimura H, Ito Y, Suzuki R, Nishiyama Y. 2008. Measuring Epstein-Barr virus (EBV) load: the significance and application for each EBV-associated

disease. *Rev Med Virol*. 18(5):305–19
Koczor CA, Lewis W. 2010. Nucleoside reverse transcriptase inhibitor toxicity and mitochondrial DNA. *Expert Opinion on Drug Metabolism & Toxicology*. 6(12):1493–1504
Kolson DL, Collman R, Hrin R, Balliet JW, Laughlin M, et al. 1994. Human immunodeficiency virus type 1 Tat activity in human neuronal cells: uptake and trans-activation. *J Gen Virol*. 75 (Pt 8):1927–34
Korioth F, Maul GG, Plachter B, Stamminger T, Frey J. 1996. The nuclear domain 10 (ND10) is disrupted by the human cytomegalovirus gene product IE1. *Exp Cell Res*. 229(1):155–58
Kostense S, Otto SA, Knol GJ, Manting EH, Nanlohy NM, et al. 2002. Functional restoration of human immunodeficiency virus and Epstein-Barr virus-specific CD8+ T cells during highly active antiretroviral therapy is associated with an increase in CD4+ T cells. *European Journal of Immunology*. 32(4):1080–89
Kovalchuk AL, Ansarah-Sobrinho C, Hakim O, Resch W, Tolarová H, et al. 2012. Mouse model of endemic Burkitt translocations reveals the long-range boundaries of Ig-mediated oncogene deregulation. *Proceedings of the National Academy of Sciences*. 109(27):10972–77
Krawczyk PM, Borovski T, Stap J, Cijsouw T, ten Cate R, et al. 2012. Chromatin mobility is increased at sites of DNA double-strand breaks. *J Cell Sci*. 125(Pt 9):2127–33
Kruhlak MJ, Celeste A, Dellaire G, Fernandez-Capetillo O, Müller WG, et al. 2006. Changes in chromatin structure and mobility in living cells at sites of DNA double-strand breaks. *J Cell Biol*. 172(6):823–34
Kudla J, Bock R. 2016. Lighting the way to protein-protein interactions: Recommendations on best practices for bimolecular fluorescence complementation analyses
Kuleshov MV, Jones MR, Rouillard AD, Fernandez NF, Duan Q, et al. 2016. Enrichr: a comprehensive gene set enrichment analysis web server 2016 update. *Nucleic Acids Res*. 44(W1):W90-97
Kulkarni A, Kurle S, Shete A, Ghate M, Godbole S, et al. 2017. Indian Long-term Non-Progressors Show Broad ADCC Responses with Preferential Recognition of V3 Region of Envelope and a Region from Tat Protein. *Front. Immunol.* 8:
Kundu RK, Sangiorgi F, Wu LY, Pattengale PK, Hinton DR, et al. 1999. Expression of the human immunodeficiency virus-Tat gene in lymphoid tissues of transgenic mice is associated with B-cell lymphoma. *Blood*. 94(1):275–82
Kurnaeva MA, Sheval EV, Musinova YR, Vassetzky YS. 2019. Tat basic domain: a “Swiss army knife” of HIV-1 Tat? *Reviews in Medical Virology*. in press:
Kurnaeva MA, Zalevsky AO, Arifulin EA, Lisitsyna OM, Tvorogova AV, et al. 2022. Molecular Coevolution of Nuclear and Nucleolar Localization Signals inside the Basic Domain of HIV-1 Tat. *Journal of Virology*. 96(1):e01505-21

Kutok JL, Wang F. 2006. Spectrum of Epstein-Barr virus-associated diseases. *Annual review of pathology*. 1(1):375–404

Lafrenie RM, Wahl LM, Epstein JS, Hewlett IK, Yamada KM, Dhawan S. 1996. HIV-1-Tat protein promotes chemotaxis and invasive behavior by monocytes. *J Immunol*. 157(3):974–77

Lallemand-Breitenbach V, de Thé H. 2010. PML Nuclear Bodies. *Cold Spring Harb Perspect Biol*. 2(5):a000661

Lapetina S, Gil-Henn H. 2017. A guide to simple, direct, and quantitative in vitro binding assays. *Journal of Biological Methods*. 4(1):62

Launay E, Pangault C, Bertrand P, Jardin F, Lamy T, et al. 2012. High rate of TNFRSF14 gene alterations related to 1p36 region in de novo follicular lymphoma and impact on prognosis

Laux G, Perricaudet M, Farrell PJ. 1988. A spliced Epstein-Barr virus gene expressed in immortalized lymphocytes is created by circularization of the linear viral genome. *EMBO J*. 7(3):769–74

Lazzi S, Bellan C, De Falco G, Cinti C, Ferrari F, et al. 2002. Expression of RB2/p130 tumor-suppressor gene in AIDS-related non-Hodgkin's lymphomas: implications for disease pathogenesis. *Hum Pathol*. 33(7):723–31

Lee AWM, Lee VHF, Ng W-T, Strojan P, Saba NF, et al. 2021. A systematic review and recommendations on the use of plasma EBV DNA for nasopharyngeal carcinoma. *European Journal of Cancer*. 153:109–22

Lee J-H, Paull TT. 2021. Cellular functions of the protein kinase ATM and their relevance to human disease. *Nat Rev Mol Cell Biol*. 22(12):796–814

Lefevre EA, Krzysiek R, Loret EP, Galanaud P, Richard Y. 1999. Cutting edge: HIV-1 Tat protein differentially modulates the B cell response of naive, memory, and germinal center B cells. *J Immunol*. 163(3):1119–22

Legoff J, Amiel C, Calisonni O, Fromentin D, Rajoely B, et al. 2004. Early impairment of CD8+ T cells immune response against Epstein-Barr virus (EBV) antigens associated with high level of circulating mononuclear EBV DNA load in HIV infection. *J Clin Immunol*. 24(2):125–34

Leone P, Shin E-C, Perosa F, Vacca A, Dammacco F, Racanelli V. 2013. MHC Class I Antigen Processing and Presenting Machinery: Organization, Function, and Defects in Tumor Cells. *JNCI: Journal of the National Cancer Institute*. 105(16):1172–87

Levin LI, Munger KL, O'Reilly EJ, Falk KI, Ascherio A. 2010. Primary infection with the Epstein-Barr virus and risk of multiple sclerosis. *Ann Neurol*. 67(6):824–30

Levitsky V, Frisan T, Masucci M. 2001. Generation of polyclonal EBV-specific CTL cultures and clones. *Methods Mol Biol*. 174:203–8

Lewis W, Copeland WC, Day BJ. 2001. Mitochondrial dna depletion, oxidative stress, and mutation: mechanisms of dysfunction from nucleoside reverse transcriptase inhibitors. *Laboratory investigation; a journal of technical methods and pathology*. 81(6):777–90

Li CJ, Friedman DJ, Wang C, Metelev V, Pardee AB. 1995a. Induction of apoptosis in uninfected lymphocytes by HIV-1 Tat protein. *Science*. 268(5209):429–31

Li CJ, Wang C, Friedman DJ, Pardee AB. 1995b. Reciprocal modulations between p53 and Tat of human immunodeficiency virus type 1. *Proc Natl Acad Sci U S A*. 92(12):5461–64

Li JZ, Aga E, Bosch RJ, Pilkinton M, Kroon E, et al. 2022. Time to Viral Rebound After Interruption of Modern Antiretroviral Therapies. *Clin Infect Dis*. 74(5):865–70

Li JZ, Etemad B, Ahmed H, Aga E, Bosch RJ, et al. 2016. The Size of the Expressed HIV Reservoir Predicts Timing of Viral Rebound after Treatment Interruption. *AIDS*. 30(3):343–53

Li Q, Spriggs MK, Kovats S, Turk SM, Comeau MR, et al. 1997. Epstein-Barr virus uses HLA class II as a cofactor for infection of B lymphocytes. *J Virol*. 71(6):4657–62

Li Y, Zhang P-Y, Yang Z-W, Ma F, Li F-X. 2020. TIMD4 exhibits regulatory capability on the proliferation and apoptosis of diffuse large B-cell lymphoma cells via the Wnt/β-catenin pathway. *The Journal of Gene Medicine*. 22(8):e3186

Lieber MR. 2010a. The mechanism of double-strand DNA break repair by the nonhomologous DNA end-joining pathway. *Annu Rev Biochem*. 79:181–211

Lieber MR. 2010b. NHEJ and Its Backup Pathways: Relation to Chromosomal Translocations. *Nat Struct Mol Biol*. 17(4):393–95

Lieber MR, Gu J, Lu H, Shimazaki N, Tsai AG. 2010. Nonhomologous DNA End Joining (NHEJ) and Chromosomal Translocations in Humans. *Subcell Biochem*. 50:279–96

Lin J-J, Bhattacharjee MJ, Yu C-P, Tseng YY, Li W-H. 2019. Many human RNA viruses show extraordinarily stringent selective constraints on protein evolution. *PNAS*. 116(38):19009–18

Ling PD, Vilchez RA, Keitel WA, Poston DG, Peng RS, et al. 2003. Epstein-Barr Virus DNA Loads in Adult Human Immunodeficiency Virus Type 1-Infected Patients Receiving Highly Active Antiretroviral Therapy. *Clinical Infectious Diseases*. 37(9):1244–49

Lisco A, Munawwar A, Introini A, Vanpouille C, Saba E, et al. 2012. Semen of HIV-1–Infected Individuals: Local Shedding of Herpesviruses and Reprogrammed Cytokine Network. *J Infect Dis*. 205(1):97–105

Lista MJ, Jousset A-C, Cheng M, Saint-André V, Perrot E, et al. 2023. DNA topoisomerase 1 represses HIV-1 promoter activity through its interaction with a guanine quadruplex present in the LTR sequence. *Retrovirology*. 20:10

Liu S, Borras AM, Liu P, Suske G, Speck SH. 1997. Binding of the ubiquitous cellular transcription factors Sp1 and Sp3 to the ZI domains in the Epstein-Barr virus lytic switch BZLF1 gene promoter. *Virology*.

228(1):11–18
Liu X, Hong T, Parameswaran S, Ernst K, Marazzi I, et al. 2020. Human Virus Transcriptional Regulators. *Cell*. 182:24–37
Liu Y, Chen C, Yen C, Tung C, Chen C, et al. 2018. Human immunodeficiency virus Tat-TIP30 interaction promotes metastasis by enhancing the nuclear translocation of Snail in lung cancer cell lines. *Cancer Sci*. 109(10):3105–14
Ljunggren HG, Kärre K. 1990. In search of the "missing self": MHC molecules and NK cell recognition. *Immunol Today*. 11(7):237–44
Llano M, Saenz DT, Meehan A, Wongthida P, Peretz M, et al. 2006. An essential role for LEDGF/p75 in HIV integration. *Science*. 314(5798):461–64
Loghavi S, Alayed K, Aladily TN, Zuo Z, Ng S-B, et al. 2015. Stage, age, and EBV status impact outcomes of plasmablastic lymphoma patients: a clinicopathologic analysis of 61 patients. *J Hematol Oncol*. 8:65
Long HM, Zuo J, Leese AM, Gudgeon NH, Jia H, et al. 2009. CD4+ T-cell clones recognizing human lymphoma-associated antigens: generation by in vitro stimulation with autologous Epstein-Barr virus–transformed B cells. *Blood*. 114(4):807–15
López C, Burkhardt B, Chan JKC, Leoncini L, Mbulaiteye SM, et al. 2022. Burkitt lymphoma. *Nat Rev Dis Primers*. 8(1):1–26
Lu J, Sharma LK, Bai Y. 2009. Implications of mitochondrial DNA mutations and mitochondrial dysfunction in tumorigenesis. *Cell Research*. 19(7):802–15
Luo Q, Pfeiffer RM, Noone A-M, Horner M-J, Engels EA, Shiels MS. 2022. Years of life lost to cancer among the United States HIV population, 2006-2015. *AIDS*. 36(9):1279–86
Lupo J, Germi R, Lancar R, Algarte-Genin M, Hendel-Chavez H, et al. 2019. Epstein-Barr virus biomarkers have no prognostic value in HIV-related Hodgkin lymphoma in the modern combined antiretroviral therapy era. *AIDS*. 33(6):993–1000
Lupo J, Germi R, Lancar R, Algarte-Genin M, Hendel-Chavez H, et al. 2021. Prospective evaluation of blood Epstein–Barr virus DNA load and antibody profile in HIV-related non-Hodgkin lymphomas. *AIDS*. 35(6):861–68
Lupo J, Wielandts A-S, Buisson M, Consortium C, Habib M, et al. 2022. High Predictive Value of the Soluble ZEBRA Antigen (Epstein-Barr Virus Trans-Activator Zta) in Transplant Patients with PTLD. *Pathogens*. 11(8):928
Luzzi A, Morettini F, Gazaneo S, Mundo L, Onnis A, et al. 2014. HIV-1 Tat induces DNMT over-expression through microRNA dysregulation in HIV-related non Hodgkin lymphomas. *Infectious Agents and Cancer*. 9(1):41
Ma S-D, Yu X, Mertz JE, Gumperz JE, Reinheim E, et al. 2012. An Epstein-Barr Virus (EBV) Mutant with Enhanced BZLF1 Expression Causes Lymphomas with Abortive Lytic EBV Infection in a Humanized Mouse

Model. *Journal of Virology*. 86(15):7976–87
Macchi B, Mastino A. 2002. Pharmacological and biological aspects of basic research on nucleoside-based reverse transcriptase inhibitors. *Pharmacological research*. 46(6):473–82
MacMahon EM, Glass JD, Hayward SD, Mann RB, Becker PS, et al. 1991. Epstein-Barr virus in AIDS-related primary central nervous system lymphoma. *Lancet*. 338(8773):969–73
Mah L-J, El-Osta A, Karagiannis TC. 2010. γH2AX: a sensitive molecular marker of DNA damage and repair. *Leukemia*. 24(4):679–86
Mahot S, Fender P, Vivès RR, Caron C, Perrissin M, et al. 2005. Cellular uptake of the EBV transcription factor EB1/Zta. *Virus Res*. 110(1–2):187–93
Mallon R, Borkowski J, Albin R, Pepitoni S, Schwartz J, Kieff E. 1990. The Epstein-Barr virus BZLF1 gene product activates the human immunodeficiency virus type 1 5' long terminal repeat. *J Virol*. 64(12):6282–85
Mancebo HSY, Lee G, Flygare J, Tomassini J, Luu P, et al. 1997. P-TEFb kinase is required for HIV Tat transcriptional activation in vivo and in vitro. *Genes and Development*. 11(20):2633–44
Manic G, Maurin-Marlin A, Laurent F, Vitale I, Thierry S, et al. 2013. Impact of the Ku Complex on HIV-1 Expression and Latency. *PLoS One*. 8(7):e69691
Marban C, Su T, Ferrari R, Li B, Vatakis D, et al. 2011. Genome-wide binding map of the HIV-1 Tat protein to the human genome. *PLoS ONE*. 6(11):e26894
Marchiò S, Alfano M, Primo L, Gramaglia D, Butini L, et al. 2005. Cell surface-associated Tat modulates HIV-1 infection and spreading through a specific interaction with gp120 viral envelope protein. *Blood*. 105(7):2802–11
Marcus JL, Chao C, Leyden WA, Xu L, Yu J, et al. 2015. Survival among HIV-Infected and HIV-Uninfected Individuals with Common Non-AIDS-Defining Cancers. *Cancer Epidemiology Biomarkers & Prevention*. 24(8):1167–73
Maréchal A, Zou L. 2013. DNA Damage Sensing by the ATM and ATR Kinases. *Cold Spring Harb Perspect Biol*. 5(9):a012716
Marks MA, Rabkin CS, Engels EA, Busch E, Kopp W, et al. 2013. Markers of microbial translocation and risk of AIDS-related lymphoma. *AIDS*. 27(3):469–74
Martin LP, Hamilton TC, Schilder RJ. 2008. Platinum Resistance: The Role of DNA Repair Pathways. *Clinical Cancer Research*. 14(5):1291–95
Martín P, Gomez-Lozano N, Montes S, Salas C, Provencio M, Bellas C. 2011. Epstein-Barr virus in the germinal centres of adenopathies affected by classic Hodgkin lymphoma. *Histopathology*. 59(2):349–52
Matysiak J, Lesbats P, Mauro E, Lapaillerie D, Dupuy J-W, et al. 2017. Modulation of chromatin structure by the FACT histone chaperone complex regulates HIV-1 integration. *Retrovirology*. 14(1):39

Maul GG, Ishov AM, Everett RD. 1996. Nuclear domain 10 as preexisting potential replication start sites of herpes simplex virus type-1. *Virology*. 217(1):67–75

Maul GG, Yu E, Ishov AM, Epstein AL. 1995. Nuclear domain 10 (ND10) associated proteins are also present in nuclear bodies and redistribute to hundreds of nuclear sites after stress. *J Cell Biochem*. 59(4):498–513

McHugh D, Myburgh R, Caduff N, Spohn M, Kok YL, et al. 2020. EBV renders B cells susceptible to HIV-1 in humanized mice. *Life Science Alliance*. 3(8):

McNeely M, Hendrix J, Busschots K, Boons E, Deleersnijder A, et al. 2011. In vitro DNA tethering of HIV-1 integrase by the transcriptional coactivator LEDGF/p75. *J Mol Biol*. 410(5):811–30

McShane AN, Malinova D. 2022. The Ins and Outs of Antigen Uptake in B cells. *Frontiers in Immunology*. 13:

Menon M, Budhwar R, Shukla RN, Bankar K, Vasudevan M, Ranga U. 2020. The Signature Amino Acid Residue Serine 31 of HIV-1C Tat Potentiates an Activated Phenotype in Endothelial Cells. *Front Immunol*. 11:529614

Miné-Hattab J, Chiolo I. 2020. Complex Chromatin Motions for DNA Repair. *Front Genet*. 11:800

Miné-Hattab J, Rothstein R. 2012. Increased chromosome mobility facilitates homology search during recombination. *Nat Cell Biol*. 14(5):510–17

Mitrentsi I, Soutoglou E. 2021. CRISPR/Cas9-Induced Breaks in Heterochromatin, Visualized by Immunofluorescence. *Methods Mol Biol*. 2153:439–45

Miyashita EM, Yang B, Babcock GJ, Thorley-Lawson DA. 1997. Identification of the site of Epstein-Barr virus persistence in vivo as a resting B cell. *J Virol*. 71(7):4882–91

Mlinaric-Rascan I, Yamamoto T. 2001. B cell receptor signaling involves physical and functional association of FAK with Lyn and IgM. *FEBS Lett*. 498(1):26–31

Mohamed G, Vrzalikova K, Cader FZ, Vockerodt M, Nagy E, et al. 2014. Epstein–Barr virus, the germinal centre and the development of Hodgkin's lymphoma. *J Gen Virol*. 95(Pt 9):1861–69

Mohiuddin IS, Kang MH. 2019. DNA-PK as an Emerging Therapeutic Target in Cancer. *Frontiers in Oncology*. 9:

Moir S, Fauci AS. 2017. B-cell responses to HIV infection. *Immunol Rev*. 275(1):33–48

Molle D, Maiuri P, Boireau S, Bertrand E, Knezevich A, et al. 2007. A real-time view of the TAR:Tat:P-TEFb complex at HIV-1 transcription sites. *Retrovirology*. 4(1):36

Monroe JE, Calender A, Mulder C. 1988. Epstein-Barr virus-positive and -negative B-cell lines can be infected with human immunodeficiency virus types 1 and 2. *J Virol*. 62(9):3497–3500

Montagnier L, Gruest J, Chamaret S, Dauguet C, Axler C, et al. 1984. Adaptation of Lymphadenopathy Associated Virus (LAV) to Replication in

EBV-Transformed B Lymphoblastoid Cell Lines. *Science*. 225(4657):63–66
Montgomery ND, Randall C, Painschab M, Seguin R, Kaimila B, et al. 2019. High pretreatment plasma Epstein-Barr virus (EBV) DNA level is a poor prognostic marker in HIV-associated, EBV-negative diffuse large B-cell lymphoma in Malawi. *Cancer Med*. 9(2):552–61
Montrose K, Yang Y, Sun X, Wiles S, Krissansen GW. 2013. Xentry, a new class of cell-penetrating peptide uniquely equipped for delivery of drugs. *Sci Rep*. 3:
Morgan D, Tergaonkar V. 2022. Unraveling B cell trajectories at single cell resolution. *Trends in Immunology*. 43(3):210–29
Morlat P, Roussillon C, Henard S, Salmon D, Bonnet F, et al. 2014. Causes of death among HIV-infected patients in France in 2010 (national survey): trends since 2000. *AIDS*. 28(8):1181–91
Morris SR, Zhao M, Smith DM, Vargas MV, Little SJ, Gianella S. 2017. Longitudinal Viral Dynamics in Semen During Early HIV Infection. *Clin Infect Dis*. 64(4):428–34
Morrison TE, Mauser A, Wong A, Ting JPY, Kenney SC. 2001. Inhibition of IFN-γ signaling by an Epstein-Barr virus immediate-early protein. *Immunity*. 15(5):787–99
Müller TG, Zila V, Peters K, Schifferdecker S, Stanic M, et al. 2021. HIV-1 uncoating by release of viral cDNA from capsid-like structures in the nucleus of infected cells. *eLife*. 10:e64776
Muncunill J, Baptista M-J, Hernandez-Rodríguez Á, Dalmau J, Garcia O, et al. 2019. Plasma Epstein-Barr Virus Load as an Early Biomarker and Prognostic Factor of Human Immunodeficiency Virus-related Lymphomas. *Clin Infect Dis*. 68(5):834–43
Mundo L, Del Porro L, Granai M, Siciliano MC, Mancini V, et al. 2020. Frequent traces of EBV infection in Hodgkin and non-Hodgkin lymphomas classified as EBV-negative by routine methods: expanding the landscape of EBV-related lymphomas. *Mod Pathol*. 33(12):2407–21
Muniz L, Egloff S, Ughy B, Jády BE, Kiss T. 2010. Controlling cellular P-TEFb activity by the HIV-1 transcriptional transactivator Tat. *PLoS Pathog*. 6(10):e1001152
Munshi M, Liu X, Kofides A, Tsakmaklis N, Demos MG, et al. 2021. A New Role for the SRC Family Member HCK As a Driver of BCR/SYK Signaling in MYD88 Mutated Lymphomas. *Blood*. 138:3512
Münz C. 2019. Latency and lytic replication in Epstein–Barr virus-associated oncogenesis. *Nat Rev Microbiol*. 17(11):691–700
Murata T. 2014. Regulation of Epstein-Barr virus reactivation from latency
Musinova YR, Sheval E V., Dib C, Germini D, Vassetzky YS. 2016. Functional roles of HIV-1 Tat protein in the nucleus. *Cellular and Molecular Life Sciences*. 73(3):589–601
Nakagawa Y, Watari E, Shimizu M, Takahashi H. 2011. One-step simple assay to determine antigen-specific cytotoxic activities by single-color flow

cytometry. *Biomed Res*. 32(2):159–66
Ne E, Palstra R-J, Mahmoudi T. 2018. Transcription: Insights From the HIV-1 Promoter. *Int Rev Cell Mol Biol*. 335:191–243
Nekhai S, Jeang K-T. 2006. Transcriptional and post-transcriptional regulation of HIV-1 gene expression: role of cellular factors for Tat and Rev. *Future Microbiol*. 1(4):417–26
Nekhai S, Jeang K-T. 2009. Human Immunodeficiency Virus Type 1 Tat and Rev as Potential Targets for Drug Development. In *Antiviral Research*, pp. 97–111. John Wiley & Sons, Ltd
Neumaier T, Swenson J, Pham C, Polyzos A, Lo AT, et al. 2012. Evidence for formation of DNA repair centers and dose-response nonlinearity in human cells. *Proc Natl Acad Sci U S A*. 109(2):443–48
Nickoloff JA, De Haro LP, Wray J, Hromas R. 2008. Mechanisms of leukemia translocations. *Curr Opin Hematol*. 15(4):338–45
Nicoli F, Finessi V, Sicurella M, Rizzotto L, Gallerani E, et al. 2013. The HIV-1 Tat protein induces the activation of CD8+ T cells and affects in vivo the magnitude and kinetics of antiviral responses. *PLoS One*. 8(11):e77746
Nie Y, Waite J, Brewer F, Sunshine M, Littman D, Zou Y. 2004. The role of CXCR4 in maintaining peripheral B cell compartments and humoral immunity. *The Journal of experimental medicine*. 200(9):
Noy A. 2019. Optimizing treatment of HIV-associated lymphoma. *Blood*. 134(17):1385–94
Nunnari G, Smith JA, Daniel R. 2008. HIV-1 Tat and AIDS-associated cancer: targeting the cellular anti-cancer barrier? *Journal of Experimental & Clinical Cancer Research*. 27(1):3
Nussenzweig A, Nussenzweig MC. 2010. Origin of chromosomal translocations in lymphoid cancer. *Cell*. 141(1):27–38
Nyagol J, Leucci E, Onnis A, De Falco G, Tigli C, et al. 2006. The effects of HIV-1 Tat protein on cell cycle during cervical carcinogenesis. *Cancer biology & therapy*. 5(6):684–90
Nyamweya S, Hegedus A, Jaye A, Rowland-Jones S, Flanagan KL, Macallan DC. 2013. Comparing HIV-1 and HIV-2 infection: Lessons for viral immunopathogenesis. *Reviews in Medical Virology*. 23(4):221–40
Nyfeler B, Michnick SW, Hauri HP. 2005. Capturing protein interactions in the secretory pathway of living cells. *Proceedings of the National Academy of Sciences of the United States of America*. 102(18):6350–55
Ogembo JG, Kannan L, Ghiran I, Nicholson-Weller A, Finberg RW, et al. 2013. Human complement receptor type 1/CD35 is an Epstein-Barr Virus receptor. *Cell Rep*. 3(2):371–85
Olive PL, Banáth JP. 2009. Kinetics of H2AX phosphorylation after exposure to cisplatin. *Cytometry Part B: Clinical Cytometry*. 76B(2):79–90
Olivero OA. 2007. Mechanisms of genotoxicity of nucleoside reverse transcriptase inhibitors. *Environmental and Molecular Mutagenesis*. 48(3–4):215–23

Olszewski AJ, Fallah J, Castillo JJ. 2016. Human immunodeficiency virus-associated lymphomas in the antiretroviral therapy era: Analysis of the National Cancer Data Base. *Cancer*. 122(17):2689–97

Opi S, Péloponèse J-M, Esquieu D, Campbell G, de Mareuil J, et al. 2002. Tat HIV-1 primary and tertiary structures critical to immune response against non-homologous variants. *J Biol Chem*. 277(39):35915–19

Osborne CS, Chakalova L, Mitchell JA, Horton A, Wood AL, et al. 2007. Myc Dynamically and Preferentially Relocates to a Transcription Factory Occupied by Igh. *PLoS Biol*. 5(8):e192

Oshima K, Yanase N, Ibukiyama C, Yamashina A, Kayagaki N, et al. 2001. Involvement of TRAIL/TRAIL-R interaction in IFN-alpha-induced apoptosis of Daudi B lymphoma cells. *Cytokine*. 14(4):193–201

O'Sullivan CE, Peng R, Cole KS, Montelaro RC, Sturgeon T, et al. 2002. Epstein-Barr virus and human immunodeficiency virus serological responses and viral burdens in HIV-infected patients treated with HAART. *J Med Virol*. 67(3):320–26

Ott M, Geyer M, Zhou Q. 2011. The Control of HIV Transcription: Keeping RNA Polymerase II on Track. *Cell Host Microbe*. 10(5):426–35

Ouedraogo DE, Bollore K, Viljoen J, Foulongne V, Reynes J, et al. 2014. Comparison of EBV DNA viral load in whole blood, plasma, B-cells and B-cell culture supernatant. *Journal of Medical Virology*. 86(5):851–56

Park J-M, Kang T-H. 2015. DNA Slot Blot Repair Assay. *Bio-protocol*. 5(8):e1453

Passaes C, Delagreverie HM, Avettand-Fenoel V, David A, Monceaux V, et al. 2021. Ultrasensitive Detection of p24 in Plasma Samples from People with Primary and Chronic HIV-1 Infection. *J Virol*. 95(14):e00016-21

Pattle SB, Farrell PJ. 2006. The role of Epstein–Barr virus in cancer. *Expert Opinion on Biological Therapy*. 6(11):1193–1205

Perkins ND, Edwards NL, Duckett CS, Agranoff AB, Schmid RM, Nabel GJ. 1993. A cooperative interaction between NF-kappa B and Sp1 is required for HIV-1 enhancer activation. *EMBO J*. 12(9):3551–58

Petosa C, Morand P, Baudin F, Moulin M, Artero JB, Müller CW. 2006. Structural basis of lytic cycle activation by the Epstein-Barr virus ZEBRA protein. *Molecular Cell*. 21(4):565–72

Petrara MR, Cattelan AM, Sasset L, Freguja R, Carmona F, et al. 2017. Impact of monotherapy on HIV-1 reservoir, immune activation, and co-infection with Epstein-Barr virus. *PLoS One*. 12(9):e0185128

Petrara MR, Freguja R, Gianesin K, Zanchetta M, De Rossi A. 2013. Epstein-Barr virus-driven lymphomagenesis in the context of human immunodeficiency virus type 1 infection. *Front Microbiol*. 4:311

Pfaffl MW. 2001. A new mathematical model for relative quantification in real-time RT-PCR. *Nucleic Acids Res*. 29(9):e45

Pham VV, Salguero C, Khan SN, Meagher JL, Brown WC, et al. 2018. HIV-1 Tat interactions with cellular 7SK and viral TAR RNAs identifies dual structural mimicry. *Nat Commun*. 9(1):4266

Piriou E, Jansen CA, van Dort K, De Cuyper I, Nanlohy NM, et al. 2005a. Reconstitution of EBV latent but not lytic antigen-specific CD4+ and CD8+ T cells after HIV treatment with highly active antiretroviral therapy. *J Immunol*. 175(3):2010–17

Piriou E, van Dort K, Nanlohy NM, van Oers MHJ, Miedema F, van Baarle D. 2005b. Loss of EBNA1-specific memory CD4+ and CD8+ T cells in HIV-infected patients progressing to AIDS-related non-Hodgkin lymphoma. *Blood*. 106(9):3166–74

Piriou ER, van Dort K, Nanlohy NM, Miedema F, van Oers MH, van Baarle D. 2004. Altered EBV viral load setpoint after HIV seroconversion is in accordance with lack of predictive value of EBV load for the occurrence of AIDS-related non-Hodgkin lymphoma. *J Immunol*. 172(11):6931–37

Piriou ER, van Dort K, Nanlohy NM, van Oers MH, Miedema F, van Baarle D. 2005c. Novel method for detection of virus-specific CD41+ T cells indicates a decreased EBV-specific CD4+ T cell response in untreated HIV-infected subjects. *Eur J Immunol*. 35(3):796–805

Planès R, BenMohamed L, Leghmari K, Delobel P, Izopet J, Bahraoui E. 2014. HIV-1 Tat protein induces PD-L1 (B7-H1) expression on dendritic cells through tumor necrosis factor alpha- and toll-like receptor 4-mediated mechanisms. *J Virol*. 88(12):6672–89

Poggi A, Carosio R, Fenoglio D, Brenci S, Murdaca G, et al. 2004. Migration of Vδ1 and Vδ2 T cells in response to CXCR3 and CXCR4 ligands in healthy donors and HIV-1-infected patients: Competition by HIV-1 Tat. *Blood*. 103(6):2205–13

Poggi A, Carosio R, Spaggiari GM, Fortis C, Tambussi G, et al. 2002. NK Cell Activation by Dendritic Cells Is Dependent on LFA-1-Mediated Induction of Calcium-Calmodulin Kinase II: Inhibition by HIV-1 Tat C-Terminal Domain. *The Journal of Immunology*. 168(1):95–101

Poggi A, Zocchi MR. 2006. HIV-1 Tat triggers TGF-beta production and NK cell apoptosis that is prevented by pertussis toxin B. *Clin Dev Immunol*. 13(2–4):369–72

Post JJ, Chan MK, Whybin LR, Shi Q, Rawlinson WD, et al. 2011. Positive Epstein–Barr virus and cytomegalovirus IgM assays in primary HIV infection. *Journal of Medical Virology*. 83(8):1406–9

Powles T, Robinson D, Stebbing J, Shamash J, Nelson M, et al. 2009. Highly Active Antiretroviral Therapy and the Incidence of Non–AIDS-Defining Cancers in People With HIV Infection. *Journal of Clinical Oncology*. 27(6):884–90

Punnonen J, Cocks BG, Carballido JM, Bennett B, Peterson D, et al. 1997. Soluble and membrane-bound forms of signaling lymphocytic activation molecule (SLAM) induce proliferation and Ig synthesis by activated human B lymphocytes. *J Exp Med*. 185(6):993–1004

Quesnel A, Pozzetto B, Touraine F, Moja P, Lucht F, et al. 1992. Antibodies to Epstein-Barr virus and cytomegalovirus in relation to CD4 cell number in

human immunodeficiency virus 1 infection. *J Med Virol*. 36(1):60–64
Quinn LL, Williams LR, White C, Forrest C, Zuo J, Rowe M. 2015. The Missing Link in Epstein-Barr Virus Immune Evasion: the BDLF3 Gene Induces Ubiquitination and Downregulation of Major Histocompatibility Complex Class I (MHC-I) and MHC-II. *J Virol*. 90(1):356–67
Raha T, Cheng SWG, Green MR. 2005. HIV-1 Tat Stimulates Transcription Complex Assembly through Recruitment of TBP in the Absence of TAFs. *PLoS Biology*. 3(2):e44
Rahimian P, He JJ. 2016. Exosome-associated release, uptake, and neurotoxicity of HIV-1 Tat protein. *J Neurovirol*. 22(6):774–88
Rahman M, Kingsley L, Breinig M, Ho M, Armstrong, et al. 1989. Enhanced antibody responses to Epstein-Barr virus in HIV-infected homosexual men. *The Journal of infectious diseases*. 159(3):
Rahman MA, Kingsley LA, Atchison RW, Belle S, Breinig MC, et al. 1991. Reactivation of Epstein-Barr virus during early infection with human immunodeficiency virus. *Journal of Clinical Microbiology*. 29(6):1215–20
Ramasubramanyan S, Osborn K, Al-Mohammad R, Naranjo Perez-Fernandez IB, Zuo J, et al. 2015. Epstein-Barr virus transcription factor Zta acts through distal regulatory elements to directly control cellular gene expression. *Nucleic Acids Research*. 43(7):3563–77
Ramayanti O, Juwana H, Verkuijlen SAMW, Adham M, Pegtel MD, et al. 2017. Epstein-Barr virus mRNA profiles and viral DNA methylation status in nasopharyngeal brushings from nasopharyngeal carcinoma patients reflect tumor origin. *International Journal of Cancer*. 140(1):149–62
Ramiro AR, Jankovic M, Eisenreich T, Difilippantonio S, Chen-Kiang S, et al. 2004. AID is required for c-myc/IgH chromosome translocations in vivo. *Cell*. 118(4):431–38
Ramos JC, Sparano JA, Chadburn A, Reid EG, Ambinder RF, et al. 2020. Impact of Myc in HIV-associated non-Hodgkin lymphomas treated with EPOCH and outcomes with vorinostat (AMC-075 trial). *Blood*. 136(11):1284–97
Ranjbar S, Rajsbaum R, Goldfeld AE. 2006. Transactivator of transcription from HIV type 1 subtype E selectively inhibits TNF gene expression via interference with chromatin remodeling of the TNF locus. *J Immunol*. 176(7):4182–90
Rayne F, Debaisieux S, Bonhoure A, Beaumelle B. 2010a. HIV-1 Tat is unconventionally secreted through the plasma membrane. *Cell Biol Int*. 34(4):409–13
Rayne F, Debaisieux S, Tu A, Chopard C, Tryoen-Toth P, Beaumelle B. 2016. Detecting HIV-1 Tat in Cell Culture Supernatants by ELISA or Western Blot. *Methods Mol Biol*. 1354:329–42
Rayne F, Debaisieux S, Yezid H, Lin Y-L, Mettling C, et al. 2010b. Phosphatidylinositol-(4,5)-bisphosphate enables efficient secretion of HIV-1 Tat by infected T-cells. *EMBO J*. 29(8):1348–62
Reeder JE, Kwak Y-T, McNamara RP, Forst CV, D'Orso I. 2015. HIV Tat controls

RNA Polymerase II and the epigenetic landscape to transcriptionally reprogram target immune cells. *eLife*. 4:e08955

Regad T, Chelbi-Alix MK. 2001. Role and fate of PML nuclear bodies in response to interferon and viral infections. *Oncogene*. 20(49):7274–86

Reya T, O'Riordan M, Okamura R, Devaney E, Willert K, et al. 2000. Wnt Signaling Regulates B Lymphocyte Proliferation through a LEF-1 Dependent Mechanism. *Immunity*. 13(1):15–24

Richard Y, Amiel C, Jeantils V, Mestivier D, Portier A, et al. 2010. Changes in Blood B Cell Phenotypes and Epstein-Barr Virus Load in Chronically Human Immunodeficiency Virus—Infected Patients before and after Antiretroviral Therapy. *The Journal of Infectious Diseases*. 202(9):1424–34

Richardson C, Jasin M. 2000. Coupled homologous and nonhomologous repair of a double-strand break preserves genomic integrity in mammalian cells. *Mol Cell Biol*. 20(23):9068–75

Rickinson AB, Long HM, Palendira U, Münz C, Hislop AD. 2014. Cellular immune controls over Epstein-Barr virus infection: new lessons from the clinic and the laboratory. *Trends Immunol*. 35(4):159–69

Righetti E, Ballon G, Ometto L, Cattelan AM, Menin C, et al. 2002. Dynamics of Epstein-Barr virus in HIV-1-infected subjects on highly active antiretroviral therapy. *AIDS*. 16(1):63–73

Robbiani DF, Nussenzweig MC. 2013. Chromosome Translocation, B Cell Lymphoma, and Activation-Induced Cytidine Deaminase. *Annual Review of Pathology: Mechanisms of Disease*. 8(1):79–103

Robertson P, Beynon S, Whybin R, Brennan C, Vollmer-Conna U, et al. 2003. Measurement of EBV-IgG anti-VCA avidity aids the early and reliable diagnosis of primary EBV infection. *J Med Virol*. 70(4):617–23

Robinson M, Schor S, Barouch-Bentov R, Einav S. 2018. Viral journeys on the intracellular highways. *Cell Mol Life Sci*. 75(20):3693–3714

Robinson WH, Steinman L. 2022. Epstein-Barr virus and multiple sclerosis. *Science*. 375(6578):264–65

Rocha CRR, Silva MM, Quinet A, Cabral-Neto JB, Menck CFM. 2018. DNA repair pathways and cisplatin resistance: an intimate relationship. *Clinics*. 73:e478s

Roche PA, Furuta K. 2015. The ins and outs of MHC class II-mediated antigen processing and presentation. *Nat Rev Immunol*. 15(4):203–16

Rodriguez-Alfageme C, Chen Z, Sonoda G, Testa JR, Damiani RD, Astrin SM. 1998. B cells malignantly transformed by human immunodeficiency virus are polyclonal. *Virology*. 252(1):34–38

Romani B, Engelbrecht S, Glashoff RH. 2010. Functions of Tat: the versatile protein of human immunodeficiency virus type 1. *The Journal of general virology*. 91(Pt 1):1–12

Roncador G, Puñet-Ortiz J, Maestre L, Rodríguez-Lobato LG, Jiménez S, et al. 2022. CD229 (Ly9) a Novel Biomarker for B-Cell Malignancies and Multiple Myeloma. *Cancers*. 14(9):2154

Rosemarie Q, Sugden B. 2020. Epstein-Barr Virus: How Its Lytic Phase Contributes to Oncogenesis. *Microorganisms*. 8(11):

Roth GA, Abate D, Abate KH, Abay SM, Abbafati C, et al. 2018. Global, regional, and national age-sex-specific mortality for 282 causes of death in 195 countries and territories, 1980–2017: a systematic analysis for the Global Burden of Disease Study 2017. *The Lancet*. 392(10159):1736–88

Rothe R, Liguori L, Villegas-Mendez A, Marques B, Grunwald D, et al. 2010. Characterization of the cell-penetrating properties of the Epstein-Barr virus ZEBRA trans-activator. *Journal of Biological Chemistry*. 285(26):20224–33

Roukos V, Voss TC, Schmidt CK, Lee S, Wangsa D, Misteli T. 2013. Spatial dynamics of chromosome translocations in living cells. *Science*. 341(6146):660–64

Roy CN, Khandaker I, Oshitani H. 2015. Evolutionary Dynamics of Tat in HIV-1 Subtypes B and C. *PLOS ONE*. 10(6):e0129896

Ruggiero E, Richter SN. 2023. Targeting G-quadruplexes to achieve antiviral activity. *Bioorg Med Chem Lett*. 79:129085

Ruiz AP, Ajasin DO, Ramasamy S, DesMarais V, Eugenin EA, Prasad VR. 2019. A Naturally Occurring Polymorphism in the HIV-1 Tat Basic Domain Inhibits Uptake by Bystander Cells and Leads to Reduced Neuroinflammation. *Scientific Reports*. 9(1):3308

Rusnati M, Coltrini D, Oreste P, Zoppetti G, Albini A, et al. 1997. Interaction of HIV-1 Tat protein with heparin. Role of the backbone structure, sulfation, and size. *J Biol Chem*. 272(17):11313–20

Sall FB, El Amine R, Markozashvili D, Tsfasman T, Oksenhendler E, et al. 2019. HIV-1 Tat protein induces aberrant activation of AICDA in human B-lymphocytes from peripheral blood. *J Cell Physiol*. 234(9):15678–85

Sall FB, Germini D, Kovina AP, Ribrag V, Wiels J, et al. 2018. Effect of Environmental Factors on Nuclear Organization and Transformation of Human B Lymphocytes. *Biochemistry (Mosc)*. 83(4):402–10

Sall FB, Shmakova A, Karpukhina A, Tsfasman T, Lomov N, et al. 2023. Epstein−Barr virus reactivation induces MYC-IGH spatial proximity and t(8;14) in B cells. *Journal of Medical Virology*. 95(3):e28633

Sallah N, Miley W, Labo N, Carstensen T, Fatumo S, et al. 2020. Distinct genetic architectures and environmental factors associate with host response to the γ2-herpesvirus infections. *Nat Commun*. 11(1):3849

Sample J, Liebowitz D, Kieff E. 1989. Two related Epstein-Barr virus membrane proteins are encoded by separate genes. *J Virol*. 63(2):933–37

Sarbassov DD, Guertin DA, Ali SM, Sabatini DM. 2005. Phosphorylation and regulation of Akt/PKB by the rictor-mTOR complex. *Science*. 307(5712):1098–1101

Saylor D, Dickens AM, Sacktor N, Haughey N, Slusher B, et al. 2016. HIV-associated neurocognitive disorder — pathogenesis and prospects for treatment. *Nat Rev Neurol*. 12(4):234–48

Schaeffner M, Mrozek-Gorska P, Buschle A, Woellmer A, Tagawa T, et al. 2019. BZLF1 interacts with chromatin remodelers promoting escape from latent infections with EBV. *Life Science Alliance*. 2(2):

Scheidegger P, Weiglhofer W, Suarez S, Console S, Waltenberger J, et al. 2001. Signalling properties of an HIV-encoded angiogenic peptide mimicking vascular endothelial growth factor activity. *Biochem J*. 353(Pt 3):569–78

Schepers A, Pich D, Hammerschmidt W. 1993. A transcription factor with homology to the AP-1 family links RNA transcription and DNA replication in the lytic cycle of Epstein-Barr virus. *EMBO J*. 12(10):3921–29

Scherer M, Stamminger T. 2016. Emerging Role of PML Nuclear Bodies in Innate Immune Signaling. *J Virol*. 90(13):5850–54

Schommers P, Hentrich M, Hoffmann C, Gillor D, Zoufaly A, et al. 2015. Survival of AIDS-related diffuse large B-cell lymphoma, Burkitt lymphoma, and plasmablastic lymphoma in the German HIV Lymphoma Cohort. *British Journal of Haematology*. 168(6):806–10

Schröder ARW, Shinn P, Chen H, Berry C, Ecker JR, Bushman F. 2002. HIV-1 Integration in the Human Genome Favors Active Genes and Local Hotspots. *Cell*. 110(4):521–29

Schüpbach J. 2002. Measurement of HIV-1 p24 antigen by signal-amplification-boosted ELISA of heat-denatured plasma is a simple and inexpensive alternative to tests for viral RNA. *AIDS Rev*. 4(2):83–92

Schüpbach J, Tomasik Z, Nadal D, Ledergerber B, Flepp M, et al. 2000. Use of HIV-1 p24 as a sensitive, precise and inexpensive marker for infection, disease progression and treatment failure. *Int J Antimicrob Agents*. 16(4):441–45

Scott RS. 2017. Epstein–Barr virus: a master epigenetic manipulator. *Current Opinion in Virology*. 26:74–80

Secchiero P, Zella D, Capitani S, Gallo RC, Zauli G. 1999. Extracellular HIV-1 tat protein up-regulates the expression of surface CXC-chemokine receptor 4 in resting CD4+ T cells. *J Immunol*. 162(4):2427–31

Sedore SC, Byers SA, Biglione S, Price JP, Maury WJ, Price DH. 2007. Manipulation of P-TEFb control machinery by HIV: recruitment of P-TEFb from the large form by Tat and binding of HEXIM1 to TAR. *Nucleic Acids Res*. 35(13):4347–58

Shannon-Lowe C, Rickinson AB, Bell AI. 2017. Epstein-barr virus-associated lymphomas

Shen X, Tomaras GD. 2011. Alterations of the B-Cell Response by HIV-1 Replication. *Curr HIV/AIDS Rep*. 8(1):23–30

Shepherd AJ, Boyd JE, Hogg CL, Aw D, James K. 1992. Susceptibility of human monoclonal antibody-producing B cell lines to infection by human immunodeficiency virus. *Hum Antibodies Hybridomas*. 3(4):168–76

Shibata A, Conrad S, Birraux J, Geuting V, Barton O, et al. 2011. Factors determining DNA double-strand break repair pathway choice in G2 phase. *EMBO J*. 30(6):1079–92

Shibata A, Moiani D, Arvai AS, Perry J, Harding SM, et al. 2014. DNA Double-Strand Break Repair Pathway Choice Is Directed by Distinct MRE11 Nuclease Activities. *Molecular Cell*. 53(1):7–18

Shiels MS, Islam JY, Rosenberg PS, Hall HI, Jacobson E, Engels EA. 2018. Projected Cancer Incidence Rates and Burden of Incident Cancer Cases in HIV-Infected Adults in the United States Through 2030. *Annals of Internal Medicine*. 168(12):866

Shifrin N, Raulet DH, Ardolino M. 2014. NK cell self tolerance, responsiveness and missing self recognition. *Semin Immunol*. 26(2):138–44

Shmakova A, Germini D, Vassetzky Y. 2020. HIV-1, HAART and cancer: A complex relationship. *International Journal of Cancer*. 146(10):2666–79

Shmakova A, Klimovich P, Rysenkova K, Popov V, Gorbunova AS, et al. 2022a. Urokinase Receptor uPAR Downregulation in Neuroblastoma Leads to Dormancy, Chemoresistance and Metastasis. *Cancers*. 14(4):994

Shmakova A, Lomov N, Viushkov V, Tsfasman T, Kozhevnikova Y, et al. 2022b. Cell models with inducible oncogenic translocations allow to evaluate the potential of drugs to favor secondary translocations. *Cancer Commun (Lond)*. 43(1):154–58

Shmakova A, Popov V, Romanov I, Khabibullin N, Sabitova N, et al. 2023. Urokinase System in Pathogenesis of Pulmonary Fibrosis: A Hidden Threat of COVID-19. *Int J Mol Sci*. 24(2):1382

Shmakova A, Vassetzky Y. 2023. lncRNA: A new danger for genome integrity. *International Journal of Cancer*. 152(7):1288–89

Shojania S, O'Neil JD. 2006. HIV-1 Tat is a natively unfolded protein: the solution conformation and dynamics of reduced HIV-1 Tat-(1-72) by NMR spectroscopy. *J Biol Chem*. 281(13):8347–56

Shun M-C, Botbol Y, Li X, Di Nunzio F, Daigle JE, et al. 2008. Identification and characterization of PWWP domain residues critical for LEDGF/p75 chromatin binding and human immunodeficiency virus type 1 infectivity. *J Virol*. 82(23):11555–67

Siliciano JD, Kajdas J, Finzi D, Quinn TC, Chadwick K, et al. 2003. Long-term follow-up studies confirm the stability of the latent reservoir for HIV-1 in resting CD4+ T cells. *Nat Med*. 9(6):727–28

Silva APF da, Giron LB, Silva SR da, Barbosa AN, Almeida RAM de B, Oliveira DE de. 2015. Human gammaherpesviruses viraemia in HIV infected patients. *Journal of Clinical Pathology*. 68(9):726–32

Simard EP, Engels EA. 2010. Cancer as a cause of death among people with AIDS in the United States. *Clin Infect Dis*. 51(8):957–62

Simsek D, Jasin M. 2010. Alternative end-joining is suppressed by the canonical NHEJ component Xrcc4–ligase IV during chromosomal translocation formation. *Nat Struct Mol Biol*. 17(4):410–16

Skalsky RL, Cullen BR. 2015. EBV Noncoding RNAs. *Curr Top Microbiol Immunol*. 391:181–217

Sloan RD, Wainberg MA. 2011. The role of unintegrated DNA in HIV infection.

Retrovirology. 8(1):52

Slyker JA, Casper C, Tapia K, Richardson B, Bunts L, et al. 2013. Clinical and Virologic Manifestations of Primary Epstein-Barr Virus (EBV) Infection in Kenyan Infants Born to HIV-Infected Women. *J Infect Dis*. 207(12):1798–1806

Smatti MK, Yassine HM, AbuOdeh R, AlMarawani A, Taleb SA, et al. 2017. Prevalence and molecular profiling of Epstein Barr virus (EBV) among healthy blood donors from different nationalities in Qatar. *PLoS One*. 12(12):e0189033

Smith DM, Nakazawa M, Freeman ML, Anderson CM, Oliveira MF, et al. 2016. Asymptomatic CMV Replication During Early Human Immunodeficiency Virus (HIV) Infection Is Associated With Lower CD4/CD8 Ratio During HIV Treatment. *Clin Infect Dis*. 63(11):1517–24

Smith MZ, Bastidas S, Karrer U, Oxenius A. 2013. Impact of antigen specificity on CD4+ T cell activation in chronic HIV-1 infection. *BMC Infect Dis*. 13:100

So-Armah K, Benjamin LA, Bloomfield GS, Feinstein MJ, Hsue P, et al. 2020. HIV and cardiovascular disease. *The Lancet HIV*. 7(4):e279–93

Sobhian B, Laguette N, Yatim A, Nakamura M, Levy Y, et al. 2010. HIV-1 Tat assembles a multifunctional transcription elongation complex and stably associates with the 7SK snRNP. *Mol Cell*. 38(3):439–51

Soni A, Siemann M, Pantelias GE, Iliakis G. 2015. Marked contribution of alternative end-joining to chromosome-translocation-formation by stochastically induced DNA double-strand-breaks in G2-phase human cells. *Mutation Research/Genetic Toxicology and Environmental Mutagenesis*. 793:2–8

Speck SH, Chatila T, Flemington E. 1997. Reactivation of Epstein-Barr virus: regulation and function of the BZLF1 gene. *Trends Microbiol*. 5(10):399–405

Srivastava DK, Tendler CL, Milani D, English MA, Licht JD, Wilson SH. 2001. The HIV-1 transactivator protein Tat is a potent inducer of the human DNA repair enzyme beta-polymerase. *AIDS*. 15(4):433–40

Stevens SJC, Blank BSN, Smits PHM, Meenhorst PL, Middeldorp JM. 2002. High Epstein–Barr virus (EBV) DNA loads in HIV-infected patients: correlation with antiretroviral therapy and quantitative EBV serology. *AIDS*. 16(7):993–1001

Stewart SA, Dykxhoorn DM, Palliser D, Mizuno H, Yu EY, et al. 2003. Lentivirus-delivered stable gene silencing by RNAi in primary cells. *RNA*. 9(4):493–501

Stiff T, O'Driscoll M, Rief N, Iwabuchi K, Löbrich M, Jeggo PA. 2004. ATM and DNA-PK function redundantly to phosphorylate H2AX after exposure to ionizing radiation. *Cancer Res*. 64(7):2390–96

Stracker TH, Petrini JHJ. 2011. The MRE11 complex: starting from the ends. *Nat Rev Mol Cell Biol*. 12(2):90–103

Strowig T, Gurer C, Ploss A, Liu Y-F, Arrey F, et al. 2009. Priming of protective T cell responses against virus-induced tumors in mice with human immune system components. *J Exp Med*. 206(6):1423–34

Sükösd Z, Andersen ES, Seemann SE, Jensen MK, Hansen M, et al. 2015. Full-length RNA structure prediction of the HIV-1 genome reveals a conserved core domain. *Nucleic Acids Res*. 43(21):10168–79

Sun Y, Huang Y-C, Xu Q-Z, Wang H-P, Bai B, et al. 2006. HIV-1 Tat depresses DNA-PK(CS) expression and DNA repair, and sensitizes cells to ionizing radiation. *Int J Radiat Oncol Biol Phys*. 65(3):842–50

Suñé C, García-Blanco MA. 1995. Sp1 transcription factor is required for in vitro basal and Tat-activated transcription from the human immunodeficiency virus type 1 long terminal repeat. *J Virol*. 69(10):6572–76

Swerdlow S, Campo E, Harris N, Jaffe E, Pileri S, et al. 2017. *WHO Classification of Tumours of Haematopoietic and Lymphoid Tissues*. 4th ed.

Szewczyk-Roszczenko OK, Roszczenko P, Shmakova A, Finiuk N, Holota S, et al. 2023. The Chemical Inhibitors of Endocytosis: From Mechanisms to Potential Clinical Applications. *Cells*. 12(18):2312

Szremska AP, Kenner L, Weisz E, Ott RG, Passegué E, et al. 2003. JunB inhibits proliferation and transformation in B-lymphoid cells. *Blood*. 102(12):4159–65

Takahashi Y, Lallemand-Breitenbach V, Zhu J, de Thé H. 2004. PML nuclear bodies and apoptosis. *Oncogene*. 23(16):2819–24

Tan C, Mueller JL, Noviski M, Huizar J, Lau D, et al. 2019. Nur77 Links Chronic Antigen Stimulation to B Cell Tolerance by Restricting the Survival of Self-Reactive B Cells in the Periphery. *J Immunol*. 202(10):2907–23

Tandon B, Peterson L, Gao J, Nelson B, Ma S, et al. 2011. Nuclear overexpression of lymphoid-enhancer-binding factor 1 identifies chronic lymphocytic leukemia/small lymphocytic lymphoma in small B-cell lymphomas. *Modern Pathology*. 24(11):1433–43

Tanner J, Weis J, Fearon D, Whang Y, Kieff E. 1987. Epstein-Barr virus gp350/220 binding to the B lymphocyte C3d receptor mediates adsorption, capping, and endocytosis. *Cell*. 50(2):203–13

Tantale K, Garcia-Oliver E, Robert M-C, L'Hostis A, Yang Y, et al. 2021. Stochastic pausing at latent HIV-1 promoters generates transcriptional bursting. *Nat Commun*. 12(1):4503

Tasca S, Tambussi G, Nozza S, Capiluppi B, Zocchi MR, et al. 2003. Escape of monocyte-derived dendritic cells of HIV-1 infected individuals from natural killer cell-mediated lysis. *AIDS*. 17(16):2291–98

Tavalai N, Stamminger T. 2008. New insights into the role of the subnuclear structure ND10 for viral infection. *Biochimica et Biophysica Acta (BBA) - Molecular Cell Research*. 1783(11):2207–21

Taylor BS, Sobieszczyk ME, McCutchan FE, Hammer SM. 2008. The Challenge of HIV-1 Subtype Diversity. *N Engl J Med*. 358(15):1590–1602

Taylor GS, Long HM, Brooks JM, Rickinson AB, Hislop AD. 2015. The immunology of Epstein-Barr virus-induced disease. *Annu Rev Immunol*. 33:787–821

Texido G, Su I, Mecklenbräuker I, Saijo K, Malek SN, et al. 2000. The B-Cell-Specific src-Family Kinase Blk Is Dispensable for B-Cell Development and Activation. *Molecular and Cellular Biology*. 20(4):1227–33

Thierry S, Thierry E, Subra F, Deprez E, Leh H, et al. 2016. Opposite transcriptional regulation of integrated vs unintegrated HIV genomes by the NF-κB pathway. *Sci Rep*. 6(1):25678

Thorley-Lawson DA. 2001. Epstein-Barr virus: exploiting the immune system. *Nat Rev Immunol*. 1(1):75–82

Tirelli U, Errante D, Dolcetti R, Gloghini A, Serraino D, et al. 1995. Hodgkin's disease and human immunodeficiency virus infection: clinicopathologic and virologic features of 114 patients from the Italian Cooperative Group on AIDS and Tumors. *J Clin Oncol*. 13(7):1758–67

Tisi MC, Cupelli E, Santangelo R, Maiolo E, Alma E, et al. 2016. Whole blood EBV-DNA predicts outcome in diffuse large B-cell lymphoma. *Leuk Lymphoma*. 57(3):628–34

Toschi E, Barillari G, Sgadari C, Bacigalupo I, Cereseto A, et al. 2001. Activation of Matrix-Metalloproteinase-2 and Membrane-Type-1-Matrix-Metalloproteinase in Endothelial Cells and Induction of Vascular Permeability In Vivo by Human Immunodeficiency Virus-1 Tat Protein and Basic Fibroblast Growth Factor. *Molecular Biology of the Cell*. 12(10):2934–46

Tozzi V, Britton S, Ehrnst A, Lenkei R, Strannegård O. 1989. Persistent productive HIV infection in EBV-transformed B lymphocytes. *J Med Virol*. 27(1):19–24

Tremblay M, Fitz-Gibbon L, Wainberg MA. 1988. Heterogeneity of HIV-1 replication and antigen expression in EBV-transformed B cell lines. *Leukemia*. 2(12 Suppl):233S-240S

Tremblay M, Meloche S, Sekaly RP, Wainberg MA. 1990. Complement receptor 2 mediates enhancement of human immunodeficiency virus 1 infection in Epstein-Barr virus-carrying B cells. *J Exp Med*. 171(5):1791–96

Tremblay M, Wainberg MA. 1989. Susceptibility of EBV-carrying B cell lines to infection by HIV-1: variability of production of progeny virus and expression of viral antigens. *Cancer Lett*. 48(2):95–103

Tripiciano A, Picconi O, Moretti S, Sgadari C, Cafaro A, et al. 2021. Anti-Tat immunity defines CD4+ T-cell dynamics in people living with HIV on long-term cART. *EBioMedicine*. 66:103306

Tsai DE, Luskin MR, Kremer BE, Chung AK, Arnoldi S, et al. 2015. A pilot trial of quantitative Epstein-Barr virus polymerase chain reaction in patients undergoing treatment for their malignancy: potential use of Epstein-Barr virus polymerase chain reaction in multiple cancer types.

Leuk Lymphoma. 56(5):1530–32
Tsibris AMN, Paredes R, Chadburn A, Su Z, Henrich TJ, et al. 2009. Lymphoma diagnosis and plasma Epstein-Barr virus load during vicriviroc therapy: results of the AIDS Clinical Trials Group A5211. *Clin Infect Dis*. 48(5):642–49
Tsurumi T, Fujita M, Kudoh A. 2005. Latent and lytic Epstein-Barr virus replication strategies
Ul-Haq I, Dalla Pria A, Suardi E, Pinato DJ, Froeling F, et al. 2018. Blood Epstein–Barr virus DNA does not predict outcome in advanced HIV-associated Hodgkin lymphoma. *Med Oncol*. 35(4):53
Urbinati C, Nicoli S, Giacca M, David G, Fiorentini S, et al. 2009. HIV-1 Tat and heparan sulfate proteoglycan interaction: a novel mechanism of lymphocyte adhesion and migration across the endothelium. *Blood*. 114(15):3335–42
Valyaeva AA, Tikhomirova MA, Potashnikova DM, Bogomazova AN, Snigiryova GP, et al. 2022. Ectopic expression of HIV-1 Tat modifies gene expression in cultured B cells: implications for the development of B-cell lymphomas in HIV-1-infected patients. *PeerJ*. 10:e13986
van Baarle D, Hovenkamp E, Callan MF, Wolthers KC, Kostense S, et al. 2001. Dysfunctional Epstein-Barr virus (EBV)-specific CD8(+) T lymphocytes and increased EBV load in HIV-1 infected individuals progressing to AIDS-related non-Hodgkin lymphoma. *Blood*. 98(1):146–55
van der Kuyl AC, Vink M, Zorgdrager F, Bakker M, Wymant C, et al. 2018. The evolution of subtype B HIV-1 tat in the Netherlands during 1985-2012. *Virus Res*. 250:51–64
van Leeuwen MT, Vajdic CM, Middleton MG, McDonald AM, Law M, et al. 2009. Continuing declines in some but not all HIV-associated cancers in Australia after widespread use of antiretroviral therapy. *AIDS (London, England)*. 23(16):2183–90
van Meerloo J, Kaspers GJL, Cloos J. 2011. Cell sensitivity assays: the MTT assay. *Methods Mol Biol*. 731:237–45
Vaughan J, Perner Y, Mayne E, Wiggill T. 2021. Plasmablastic lymphoma in Johannesburg, South Africa, in the era of widescale antiretroviral therapy use. *HIV Med*. 22(3):225–30
Vendeville A, Rayne F, Bonhoure A, Bettache N, Montcourrier P, Beaumelle B. 2004. HIV-1 Tat enters T cells using coated pits before translocating from acidified endosomes and eliciting biological responses. *Mol Biol Cell*. 15(5):2347–60
Vidrih JA, Walensky RP, Sax PE, Freedberg KA. 2001. Positive Epstein-Barr virus heterophile antibody tests in patients with primary human immunodeficiency virus infection. *Am J Med*. 111(3):192–94
Vockerodt M, Yap L-F, Shannon-Lowe C, Curley H, Wei W, et al. 2015. The Epstein-Barr virus and the pathogenesis of lymphoma. *J Pathol*. 235(2):312–22

Vogel J, Cepeda M, Enk A, Ngo L, Jay G. 1995. The hiv tat gene is a promoter of epidermal skin tumors. *International journal of oncology*. 7(4):727–33

Vos T, Lim SS, Abbafati C, Abbas KM, Abbasi M, et al. 2020. Global burden of 369 diseases and injuries in 204 countries and territories, 1990–2019: a systematic analysis for the Global Burden of Disease Study 2019. *The Lancet*. 396(10258):1204–22

Wagner HJ, Bein G, Bitsch A, Kirchner H. 1992. Detection and quantification of latently infected B lymphocytes in Epstein-Barr virus-seropositive, healthy individuals by polymerase chain reaction. *Journal of Clinical Microbiology*. 30(11):2826–29

Wang X, Duan Z, Yu G, Fan M, Scharff MD. 2018. Human Immunodeficiency Virus Tat Protein Aids V Region Somatic Hypermutation in Human B Cells. *mBio*. 9(2):e02315-17

Wei P, Garber ME, Fang SM, Fischer WH, Jones KA. 1998. A novel CDK9-associated C-type cyclin interacts directly with HIV-1 Tat and mediates its high-affinity, loop-specific binding to TAR RNA. *Cell*. 92(4):451–62

Weissman JD, Brown JA, Howcroft TK, Hwang J, Chawla A, et al. 1998. HIV-1 tat binds TAFII250 and represses TAFII250-dependent transcription of major histocompatibility class I genes. *Proc Natl Acad Sci U S A*. 95(20):11601–6

Westendorp MO, Frank R, Ochsenbauer C, Stricker K, Dhein J, et al. 1995. Sensitization of T cells to CD95-mediated apoptosis by HIV-1 Tat and gp120. *Nature*. 375(6531):497–500

WHO fact sheet. 2022. *HIV/AIDS*. https://www.who.int/. www.who.int

Williams LR, Quinn LL, Rowe M, Zuo J. 2015. Induction of the Lytic Cycle Sensitizes Epstein-Barr Virus-Infected B Cells to NK Cell Killing That Is Counteracted by Virus-Mediated NK Cell Evasion Mechanisms in the Late Lytic Cycle. *Journal of Virology*. 90(2):947–58

Williams SA, Kwon H, Chen L-F, Greene WC. 2007. Sustained Induction of NF-κB Is Required for Efficient Expression of Latent Human Immunodeficiency Virus Type 1. *Journal of Virology*. 81(11):6043–56

Woisetschlaeger M, Yandava CN, Furmanski LA, Strominger JL, Speck SH. 1990. Promoter switching in Epstein-Barr virus during the initial stages of infection of B lymphocytes. *Proc Natl Acad Sci U S A*. 87(5):1725–29

Woldemeskel BA, Kwaa AK, Blankson JN. 2020. Viral reservoirs in elite controllers of HIV-1 infection: Implications for HIV cure strategies. *EBioMedicine*. 62:

Wong HY, Prasad A, Gan SU, Chua JJE, Schwarz H. 2020. Identification of CD137-Expressing B Cells in Multiple Sclerosis Which Secrete IL-6 Upon Engagement by CD137 Ligand. *Frontiers in Immunology*. 11:

Wong M, Jackson D. 2004. Regulation of B cell activation by PECAM-1: implications for the development of autoimmune disorders. *Current pharmaceutical design*. 10(2):155–61

Wu T, Hu E, Xu S, Chen M, Guo P, et al. 2021. clusterProfiler 4.0: A universal enrichment tool for interpreting omics data. *Innovation (Camb)*. 2(3):100141

Xiao H, Neuveut C, Tiffany HL, Benkirane M, Rich EA, et al. 2000. Selective CXCR4 antagonism by Tat: implications for in vivo expansion of coreceptor use by HIV-1. *Proc Natl Acad Sci U S A*. 97(21):11466–71

Xie L, Zhao T, Cai J, Su Y, Wang Z, Dong W. 2016. Methotrexate induces DNA damage and inhibits homologous recombination repair in choriocarcinoma cells. *Onco Targets Ther*. 9:7115–22

Xing L, Kieff E. 2011. cis-Acting effects on RNA processing and Drosha cleavage prevent Epstein-Barr virus latency III BHRF1 expression. *J Virol*. 85(17):8929–39

Xu F, Zhao C, Li Y, Li J, Deng Y, Shi T. 2011. Exploring virus relationships based on virus-host protein-protein interaction network. *BMC Systems Biology*. 5(SUPPL. 3):S11

Xu Z, Pone EJ, Al-Qahtani A, Park S-R, Zan H, Casali P. 2007. Regulation of aicda expression and AID activity: relevance to somatic hypermutation and class switch DNA recombination. *Crit Rev Immunol*. 27(4):367–97

Xue B, Mizianty MJ, Kurgan L, Uversky VN. 2012. Protein intrinsic disorder as a flexible armor and a weapon of HIV-1. *Cell. Mol. Life Sci.* 69(8):1211–59

Xue SA, Labrecque LG, Lu QL, Ong SK, Lampert IA, et al. 2002. Promiscuous expression of Epstein-Barr virus genes in Burkitt's lymphoma from the central African country Malawi. *International Journal of Cancer*. 99(5):635–43

Xue S-A, Lu Q-L, Poulsom R, Karran L, Jones MD, Griffin BE. 2000. Expression of Two Related Viral Early Genes in Epstein-Barr Virus-Associated Tumors. *Journal of Virology*. 74(6):2793–2803

Yan Y, Ren Y, Chen R, Hu J, Ji Y, et al. 2018. Evaluation of Epstein-Barr Virus Salivary Shedding in HIV/AIDS Patients and HAART Use: A Retrospective Cohort Study. *Virologica Sinica*. 33(3):227–33

Yang X, Gold MO, Tang DN, Lewis DE, Aguilar-Cordova E, et al. 1997. TAK, an HIV Tat-associated kinase, is a member of the cyclin-dependent family of protein kinases and is induced by activation of peripheral blood lymphocytes and differentiation of promonocytic cell lines. *Proc Natl Acad Sci U S A*. 94(23):12331–36

Yang ZZ, Grote DM, Ziesmer SC, Niki T, Hirashima M, et al. 2012. IL-12 upregulates TIM-3 expression and induces T cell exhaustion in patients with follicular B cell non-Hodgkin lymphoma. *Journal of Clinical Investigation*. 122(4):1271–82

Yarchoan R, Uldrick TS. 2018. HIV-Associated Cancers and Related Diseases. *N Engl J Med*. 378(11):1029–41

Ye BH, Chaganti S, Chang CC, Niu H, Corradini P, et al. 1995. Chromosomal translocations cause deregulated BCL6 expression by promoter substitution in B cell lymphoma. *EMBO J*. 14(24):6209–17

Ye BH, Lista F, Lo Coco F, Knowles DM, Offit K, et al. 1993. Alterations of a zinc finger-encoding gene, BCL-6, in diffuse large-cell lymphoma. *Science*. 262(5134):747–50

Yu F, Li Q, Chen X, Liu J, Li L, et al. 2020. X4-Tropic Latent HIV-1 Is Enriched in Peripheral Follicular Helper T Cells and Is Correlated with Disease Progression. *J Virol*. 94(2):e01219-19

Yun K, Choi YD, Nam JH, Park Z, Im S-H. 2007. NF-κB regulates Lef1 gene expression in chondrocytes. *Biochemical and Biophysical Research Communications*. 357(3):589–95

Zagelbaum J, Schooley A, Zhao J, Schrank BR, Callen E, et al. 2023. Multiscale reorganization of the genome following DNA damage facilitates chromosome translocations via nuclear actin polymerization. *Nat Struct Mol Biol*. 30(1):99–106

Zalani S, Holley-Guthrie E, Kenney S. 1996. Epstein-Barr viral latency is disrupted by the immediate-early BRLF1 protein through a cell-specific mechanism. *Proc Natl Acad Sci U S A*. 93(17):9194–99

Zauli G, Davis BR, Re MC, Visani G, Furlini G, La Placa M. 1992. tat protein stimulates production of transforming growth factor-beta 1 by marrow macrophages: a potential mechanism for human immunodeficiency virus-1-induced hematopoietic suppression. *Blood*. 80(12):3036–43

Zauli G, Gibellini D, Caputo A, Bassini A, Negrini M, et al. 1995. The human immunodeficiency virus type-1 Tat protein upregulates Bcl-2 gene expression in Jurkat T-cell lines and primary peripheral blood mononuclear cells. *Blood*. 86(10):3823–34

Zauli G, Gibellini D, Celeghini C, Mischiati C, Bassini A, et al. 1996. Pleiotropic effects of immobilized versus soluble recombinant HIV-1 Tat protein on CD3-mediated activation, induction of apoptosis, and HIV-1 long terminal repeat transactivation in purified CD4+ T lymphocytes. *J Immunol*. 157(5):2216–24

Zeidler R, Eissner G, Meissner P, Uebel S, Tampé R, et al. 1997. Downregulation of TAP1 in B Lymphocytes by Cellular and Epstein-Barr Virus–Encoded Interleukin-10. *Blood*. 90(6):2390–97

Zeitler M, Steringer JP, Müller H-M, Mayer MP, Nickel W. 2015. HIV-Tat Protein Forms Phosphoinositide-dependent Membrane Pores Implicated in Unconventional Protein Secretion. *J Biol Chem*. 290(36):21976–84

Zhang G, Miao F, Liu K, Wu J, Xu J. 2021. Downregulation of LEF1 Impairs Myeloma Cell Growth Through Modulating CYLD/NF-κB Signaling. *Technology in Cancer Research & Treatment*. 20:15330338211034270

Zhang H, Li Y, Wang H-B, Zhang A, Chen M-L, et al. 2018a. Ephrin receptor A2 is an epithelial cell receptor for Epstein-Barr virus entry. *Nat Microbiol*. 3(2):1–8

Zhang P, Monteiro da Silva G, Deatherage C, Burd C, DiMaio D. 2018b. Cell-Penetrating Peptide Mediates Intracellular Membrane Passage of Human Papillomavirus L2 Protein to Trigger Retrograde Trafficking. *Cell*.

174(6):1465-1476.e13
Zhang T, Shen Y, Chen Y, Hsieh J-T, Kong Z. 2015. The ATM inhibitor KU55933 sensitizes radioresistant bladder cancer cells with DAB2IP gene defect. *Int J Radiat Biol*. 91(4):368–78
Zhang X, Voskens CJ, Sallin M, Maniar A, Montes CL, et al. 2010. CD137 Promotes Proliferation and Survival of Human B Cells. *The Journal of Immunology*. 184(2):787–95
Zhang Y, Jasin M. 2011. An essential role for CtIP in chromosomal translocation formation through an alternative end-joining pathway. *Nat Struct Mol Biol*. 18(1):80–84
Zhao GQ, Zhao Q, Zhou X, Mattei MG, de Crombrugghe B. 1993. TFEC, a basic helix-loop-helix protein, forms heterodimers with TFE3 and inhibits TFE3-dependent transcription activation. *Mol Cell Biol*. 13(8):4505–12
Zhao S, Zhang H, Xing Y, Natkunam Y. 2013. CD137 ligand is expressed in primary and secondary lymphoid follicles and in B-cell lymphomas: diagnostic and therapeutic implications. *Am J Surg Pathol*. 37(2):250–58
Zhao X, Fan Y, Vann PH, Wong JM, Sumien N, He JJ. 2020. Long-term HIV-1 Tat Expression in the Brain Led to Neurobehavioral, Pathological, and Epigenetic Changes Reminiscent of Accelerated Aging. *Aging Dis*. 11(1):93–107
Zheng L, Yang Y, Guocai L, Pauza CD, Salvato MS. 2007. HIV Tat protein increases Bcl-2 expression in monocytes which inhibits monocyte apoptosis induced by tumor necrosis factor-alpha-related apoptosis-induced ligand. *Intervirology*. 50(3):224–28
Zheng P, Guo Y, Niu Q, Levy DE, Dyck JA, et al. 1998. Proto-oncogene PML controls genes devoted to MHC class I antigen presentation. *Nature*. 396(6709):373–76
Zhou Q, Yik JHN. 2006. The Yin and Yang of P-TEFb regulation: implications for human immunodeficiency virus gene expression and global control of cell growth and differentiation. *Microbiol Mol Biol Rev*. 70(3):646–59
Zimmermann J, Hammerschmidt W. 1995. Structure and role of the terminal repeats of Epstein-Barr virus in processing and packaging of virion DNA. *J Virol*. 69(5):3147–55
Zocchi MR, Contini P, Alfano M, Poggi A. 2005. Pertussis Toxin (PTX) B Subunit and the Nontoxic PTX Mutant PT9K/129G Inhibit Tat-Induced TGF-β Production by NK Cells and TGF-β-Mediated NK Cell Apoptosis. *The Journal of Immunology*. 174(10):6054–61
Zocchi MR, Rubartelli A, Morgavi P, Poggi A. 1998. HIV-1 Tat inhibits human natural killer cell function by blocking L-type calcium channels. *J Immunol*. 161(6):2938–43
Zuo J, Thomas WA, Haigh TA, Fitzsimmons L, Long HM, et al. 2011. Epstein-Barr Virus Evades CD4+ T Cell Responses in Lytic Cycle through BZLF1-mediated Downregulation of CD74 and the Cooperation of vBcl-2. *PLoS Pathogens*. 7(12):e1002455

Title: Factors that contribute to B cell oncogenesis in people living with HIV

Keywords: HIV, EBV, HIV-1 Tat, EBV Zta, chromosomal translocations, immune evasion

Abstract: People living with HIV are at higher risk of developing B cell lymphomas, particularly those associated with EBV. However, the specific mechanisms behind this increased risk are not fully understood. In this study, I investigated factors beyond immune deficiency that may contribute to B cell lymphomagenesis in individuals with HIV.

I examined the impact of specific antiretroviral drugs on chromosomal translocations in B cells using a CRISPR/Cas9-based model, identifying some drugs as potential contributors to lymphomagenesis. Additionally, I studied EBV reactivation, a common phenomenon in people living with HIV, finding that it promotes proximity between potential translocation partners, *MYC* and *IGH* loci, and chromosomal translocations, increasing the likelihood of Burkitt's lymphoma.

Moreover, I explored how HIV-1 Tat, a viral transcriptional activator protein with cell-penetration capacities, disrupts DNA damage sensing and repair in B cells and downregulates MHC class II expression, potentially fostering an environment favourable for lymphomagenesis. Finally, I investigated the interaction between HIV-1 Tat and EBV Zta, showing that they directly interact in B cells and serum of people living with HIV. This interaction leads to immune evasion by downregulating MHC class I molecules in B cells.

This study provides important insights into the complex interplay between HIV, EBV, and B cell lymphomagenesis. Understanding these mechanisms may guide the development of new therapeutic strategies to reduce lymphoma risk in individuals with HIV.

Titre : Facteurs qui contribuent à l'oncogenèse des lymphocytes B chez les personnes vivant avec le VIH

Mots clés : VIH, EBV, VIH-1 Tat, EBV Zta, translocations chromosomiques, évasion immunitaire

Résumé : Les personnes vivant avec le VIH sont plus à risque de développer des lymphomes à cellules B, en particulier ceux associés à l'EBV. Dans cette étude, j'ai étudié des facteurs au-delà de l'immunodéficience qui peuvent contribuer à la lymphomagenèse des cellules B chez les personnes vivant avec le VIH.

J'ai examiné l'impact de médicaments antirétroviraux spécifiques sur les translocations chromosomiques dans les lymphocytes B à l'aide du modèle basé sur CRISPR/Cas9, en identifiant certains médicaments comme contributeurs potentiels à la lymphomagenèse. De plus, j'ai étudié la réactivation de l'EBV, un phénomène courant chez les personnes vivant avec le VIH, constatant qu'elle favorise la proximité entre les partenaires potentiels de translocation, *MYC* et *IGH*, et les translocations chromosomiques, augmentant la probabilité de lymphome de Burkitt.

J'ai ensuite exploré comment Tat du VIH-1, une protéine virale activatrice de la transcription dotée de capacités de pénétration cellulaire, perturbe la détection et la réparation des dommages à l'ADN et régule à la baisse l'expression du CMH de classe II dans les cellules B, favorisant potentiellement un environnement propice à la lymphomagenèse. Enfin, j'ai étudié l'interaction entre Tat du VIH-1 et Zta de l'EBV, montrant qu'ils interagissent directement dans les cellules B et le sérum des personnes vivant avec le VIH, réduisant les molécules du CMH de classe I et favorisant l'évasion immunitaire dans les cellules B.

Cette étude éclaire l'interaction complexe entre le VIH, l'EBV et la lymphomagenèse à cellules B, pouvant guider de nouvelles thérapies pour réduire le risque de lymphome.